NASA Conference Publication 3221
Part 2

Eleventh Workshop for Computational Fluid Dynamic Applications in Rocket Propulsion

Compiled by
R.W. Williams
George C. Marshall Space Flight Center
Marshall Space Flight Center, Alabama

Proceedings of a workshop held at
NASA George C. Marshall Space Flight Center
Huntsville, Alabama
April 20–22, 1993

National Aeronautics and
Space Administration
Office of Management
Scientific and Technical
Information Program
1993

TABLE OF CONTENTS

TABLE OF CONTENTS (Continued)

TABLE OF CONTENTS (Continued)

TABLE OF CONTENTS (Continued)

TABLE OF CONTENTS (Continued)

TABLE OF CONTENTS (Continued)

HEAT TRANSFER IN ROCKET ENGINE COMBUSTION CHAMBERS AND NOZZLES

P. G. Anderson, G. C. Cheng and R. C. Farmer

SECA, Inc.
Huntsville, AL

Abstract

Complexities of liquid rocket engine heat transfer which involve the injector faceplate and regeneratively and film cooled walls are being investigated by computational analysis. A conjugate heat transfer analysis will be used to describe localized heating phenomena associated with particular injector configurations and coolant channels and film coolant dumps. These components are being analyzed, and the analyses verified with appropriate test data. Finally, the component analyses will be synthesized into an overall flowfield/heat transfer model. The FDNS code is being used to make the component analyses. Particular attention is being given to the representation of the thermodynamic properties of the fluid streams and to the method of combining the detailed models to represent overall heating. Unit flow models of specific coaxial injector elements have been developed and will be described.

Since test data from the NLS development program are not available, new validation heat transfer data has been sought. Suitable data was obtained from a Rocketdyne test program on a model hydrocarbon/oxygen engine. Simulations of this test data will be presented.

Recent interest in the hybrid motor have established the need for analyses of ablating solid fuels in the combustion chamber. Analysis of a simplified hybrid motor will also be presented.

HEAT TRANSFER IN ROCKET ENGINE COMBUSTION CHAMBERS AND NOZZLES

P. G. Anderson, R. C. Farmer and G. C. Cheng
SECA, Inc.

OBJECTIVE

To develop and verify a conjugate heat transfer CFD model to describe regenerative cooling of the main combustion chamber and nozzle of a launch vehicle class liquid rocket engine.

APPROACH

To analyze and verify the critical subprocesses which occur in the combustion chamber and synthesize all such processes into an overall heat transfer design tool.

HEAT TRANSFER ANALYSIS OF INJECTOR ELEMENTS

- PROVIDE FLUID PROPERTIES OF FUEL AND OXIDIZER AT OUTLET OF MAIN INJECTOR AND BAFFLE ELEMENTS
- ANALYSIS OF INJECTORS FROM LOX DOME TO ELEMENT OUTLETS
- ELEMENT EXTERNAL ENVIRONMENTS OBTAINED FROM FLOW ANALYSES
  - HOT EXHAUST GAS REGION
  - REGION BETWEEN INJECTOR PLATES
- OXYGEN FROM DOME AND COOLANT HYDROGEN ABOVE CRITICAL
  - NOT IDEAL GAS
  - HMBS EQUATIONS INCORPORATED INTO FDNS CODE
- GRIDS
  - AXISYMMETRIC
  - MAIN INJECTOR - 10962 NODES
  - BAFFLE INJECTOR - 10404 NODES

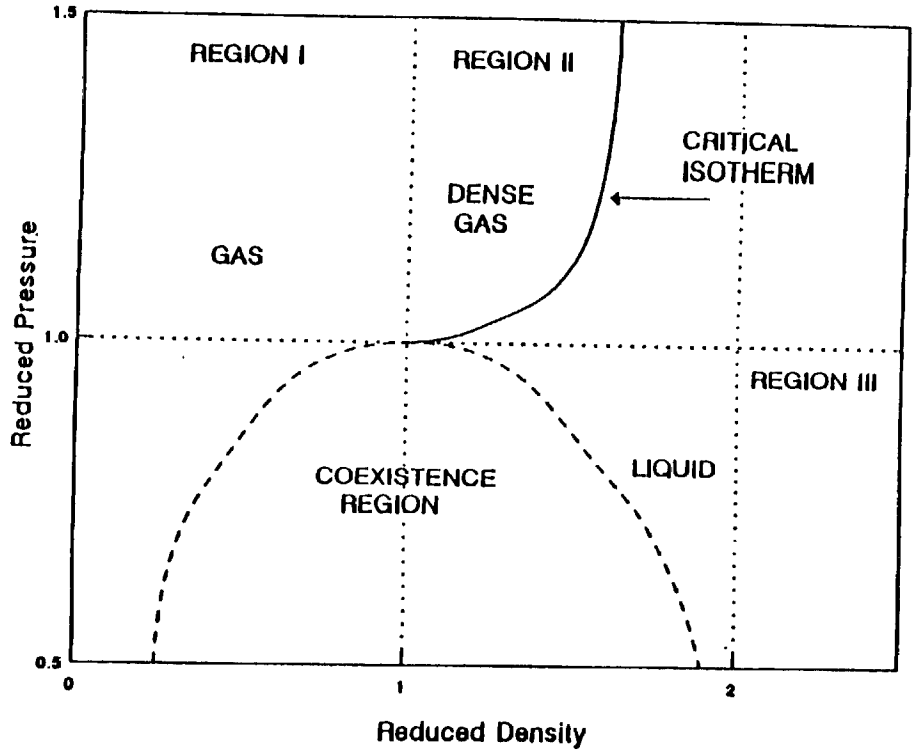

For each region

$$\frac{P}{P_{crit}} = \sum_{j=1}^{4} t^{j-2} \sum_{i=1}^{6} B_{ij}\, \rho^{i-2} + A(t)$$

$$\frac{H-H_o}{RT} = Z_c \int_a^b \left[\frac{P}{t} - \left(\frac{\delta p}{\delta t}\right)_\rho\right] \rho^{-2}\, d\rho + Z_c \frac{P}{\rho t} + C(t)$$

Also , P_v, ρ_L, H_o are functions of t and ρ_v is a function of t and P_v

MAIN INJECTOR ELEMENT (PARTIAL GRID)

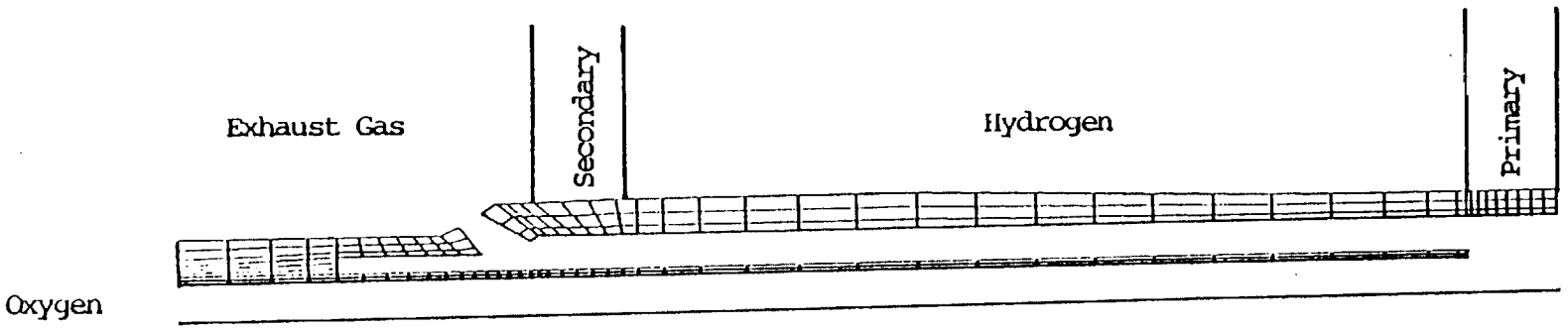

BAFFLE ELEMENT (PARTIAL GRID)

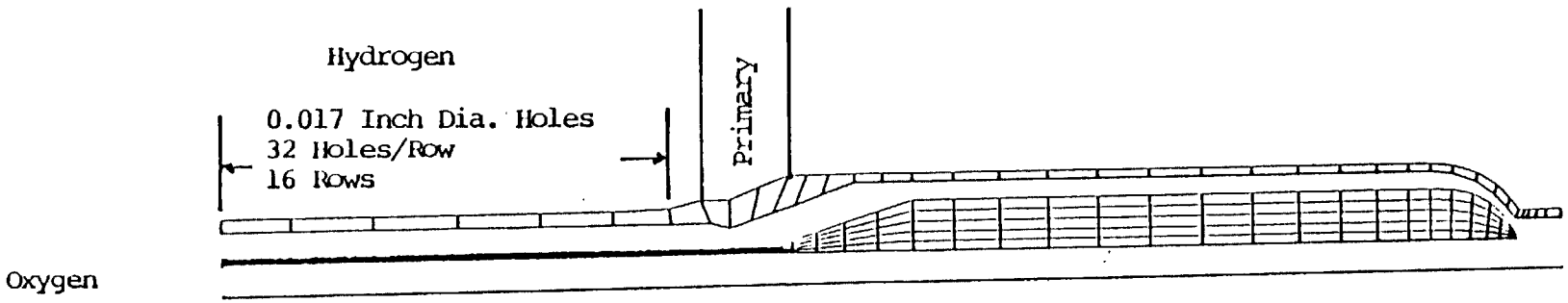

BOUNDARY CONDITIONS

- MASS FLOW RATE BALANCE FOR INLETS AND OUTLETS
- EXTERNAL SKIN TEMPERATURES COMPUTED EACH ITERATION USING QUASI-ONE DIMENSIONAL HEAT BALANCE BASED ON NUSSELT NUMBER FOR CROSSFLOW IN TUBE BANKS (HEAT AND MASS TRANSFER, WHITE, PP 353-355)
  - AVERAGED IN-LINE AND STAGGERED RESULTS
  - EXTERNAL FLUID TEMPERATURES OBTAINED FROM PREVIOUS ANALYSES BY SECA
- CONDUCTION IN WALLS CALCULATED BY FDNS

MODIFICATIONS TO FDNS

PRESSURE-BASED VERSION	DENSITY-BASED VERSION
• SOLVE MOMENTUM CONSERVATION FOR VELOCITIES	• SAME
• SOLVE ENERGY CONSERVATION FOR ENTHALPY	• SOLVE ENERGY CONSERVATION FOR TEMPERATURE
• SOLVE SPECIES CONTINUITY FOR SPECIES MASS FRACTIONS	• SOLVE SPECIES CONTINUITY FOR SPECIES DENSITIES
• SOLVE PRESSURE-CORRECTION EQUATION FOR PRESSURE	• DENSITY = SUM OF SPECIES DENSITIES
• USE HMBS MODEL TO OBTAIN DENSITY AND TEMPERATURE (ITERATIVE PROCEDURE HAS CONVERGENCE PROBLEMS IN 2D)	• USE HMBS MODEL TO OBTAIN PRESSURE AND ENTHALPY

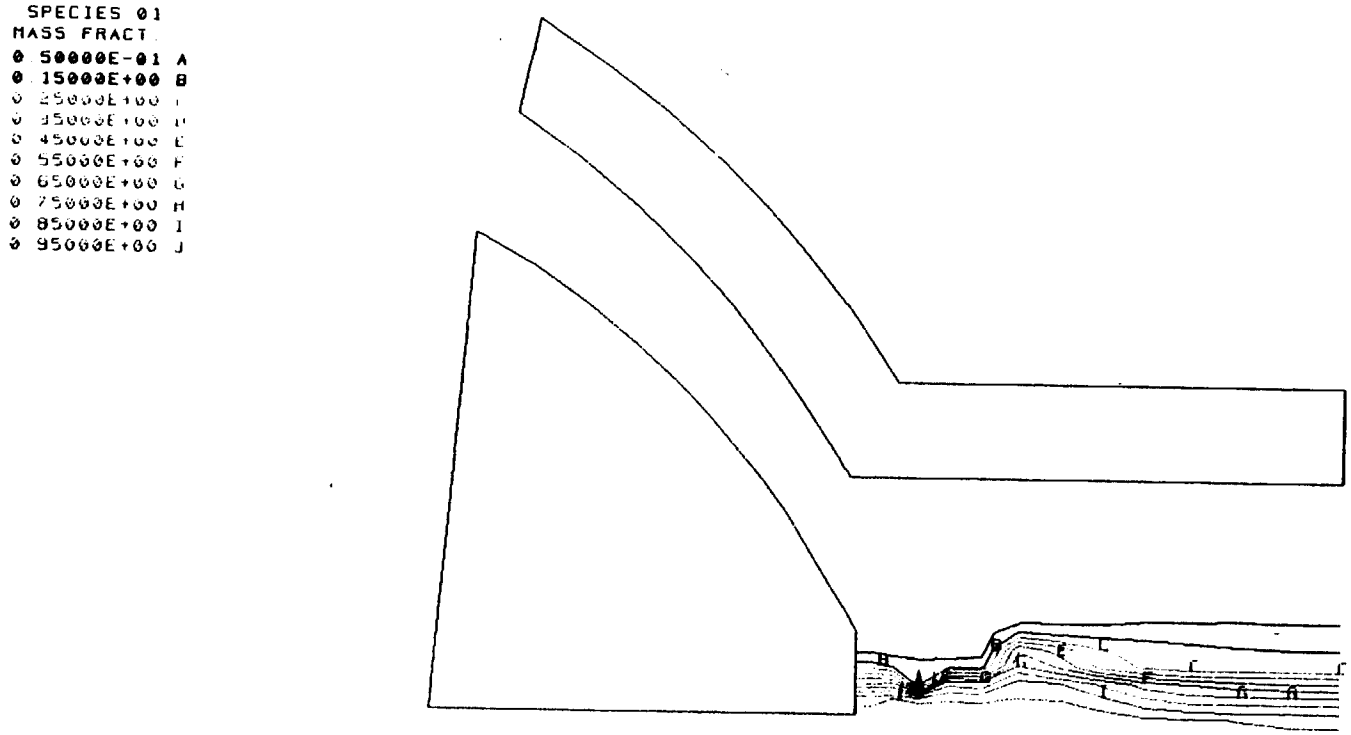

OXYGEN MASS FRACTION IN BAFFLE ELEMENT EXIT

VELOCITY VECTORS IN BAFFLE ELEMENT EXIT

ORIGINAL PAGE IS
OF POOR QUALITY

TEMPERATURE IN BAFFLE ELEMENT EXIT

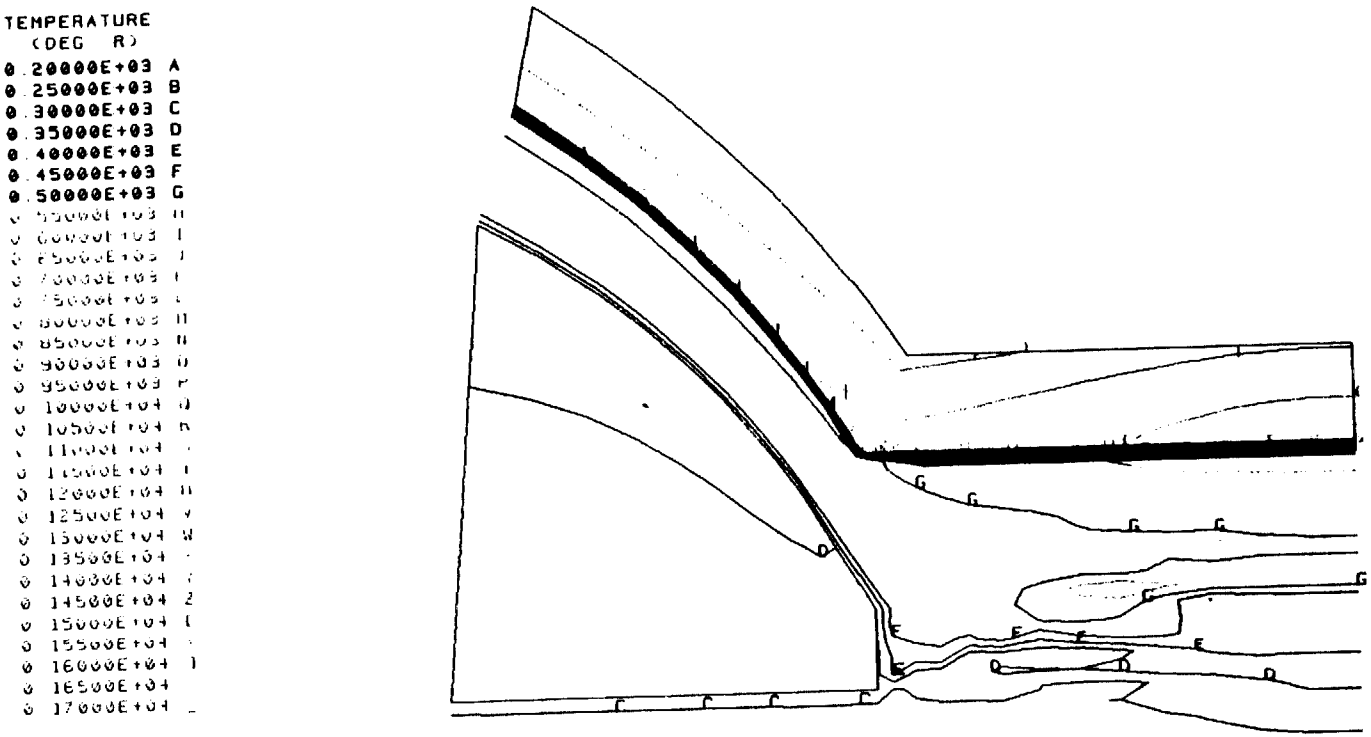

TEMPERATURE IN BAFFLE ELEMENT EXIT

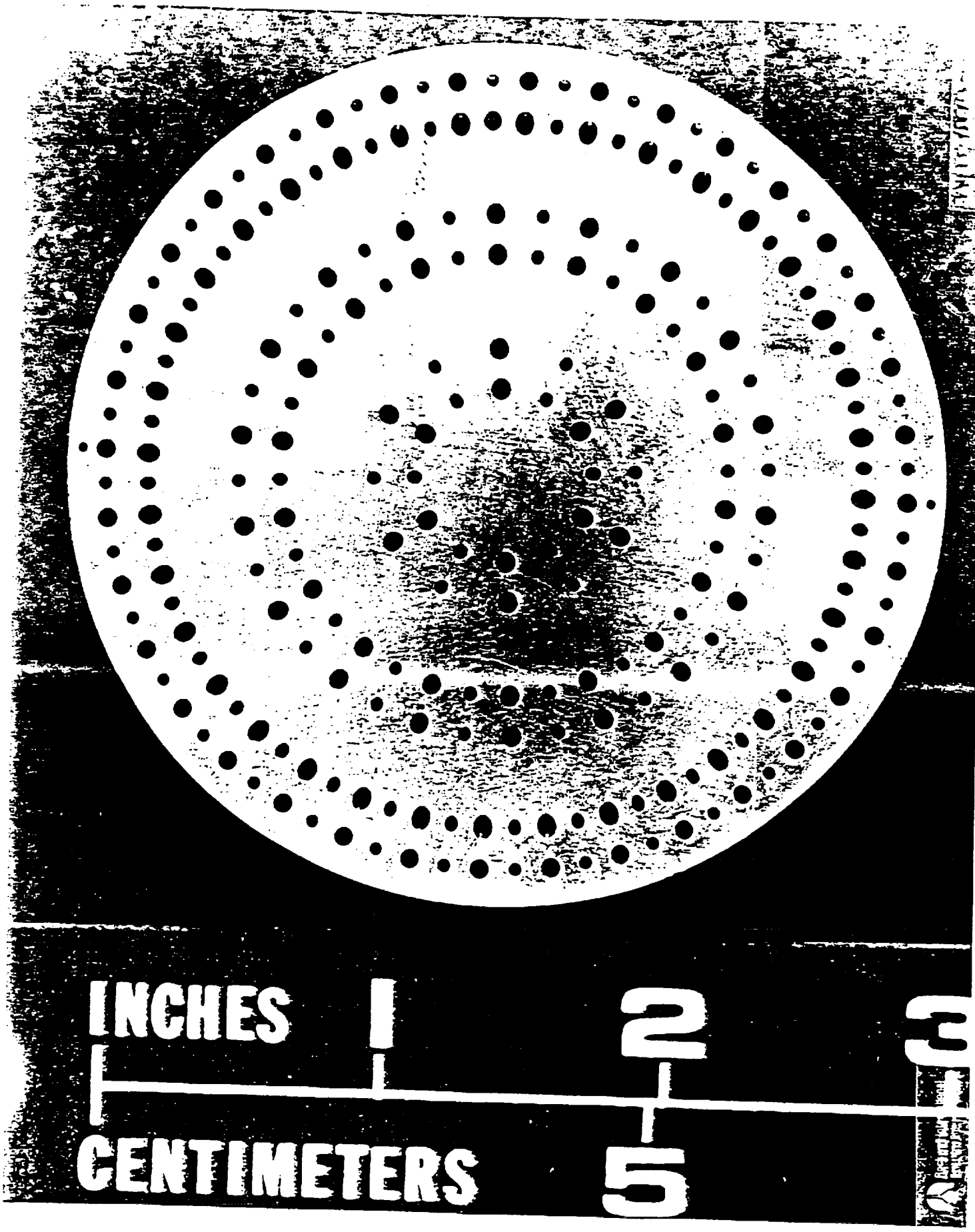
INCHES
1
2
3
CENTIMETERS
5

1XZ41.11/2C/E9.C1D

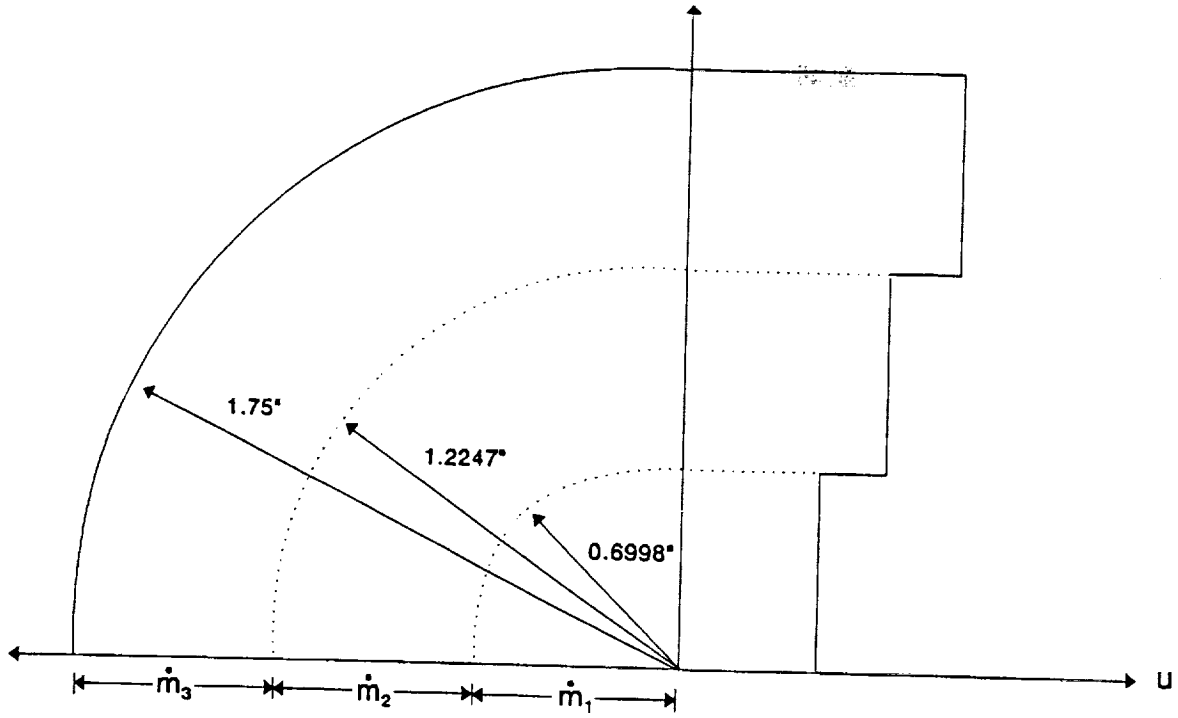

(a) Uniform O/F Distribution

($\dot{m}_1$ = 4.45 lb/sec, $\dot{m}_2$ = 13.35 lb/sec, $\dot{m}_3$ = 26.7 lb/sec)

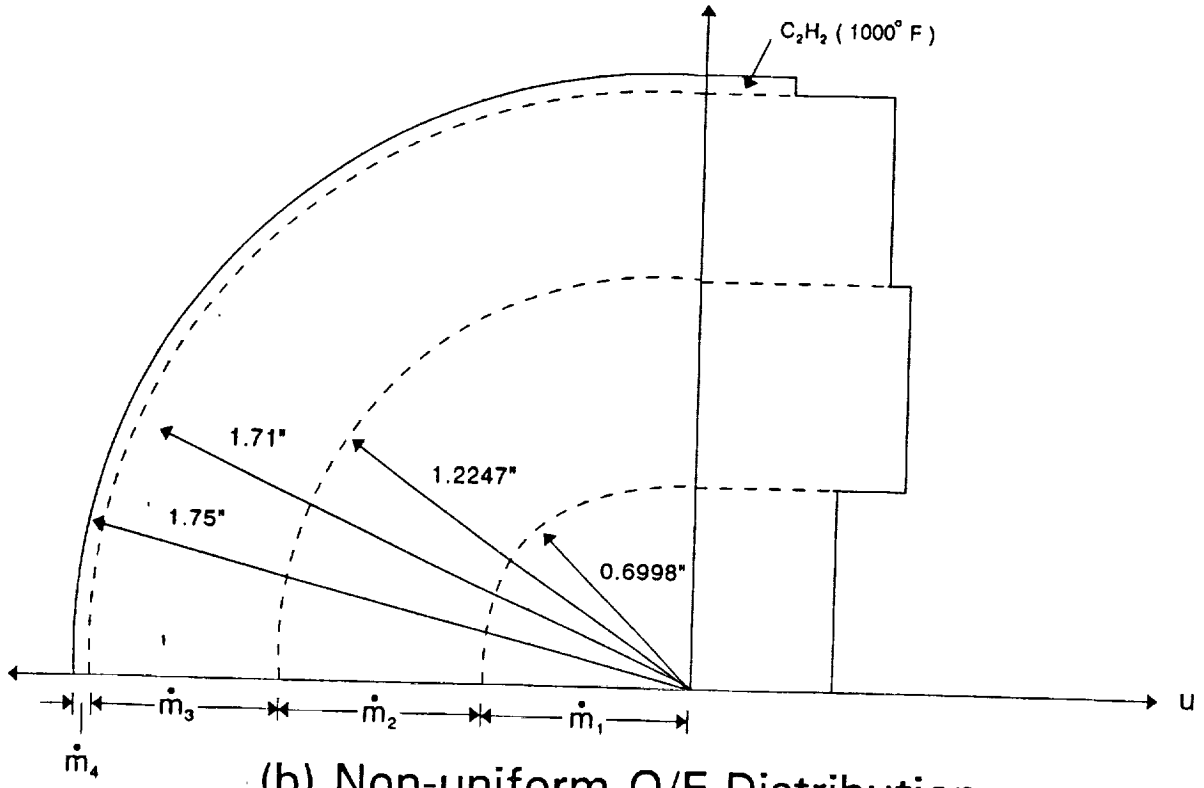

(b) Non-uniform O/F Distribution

($\dot{m}_1$ = 4.45 lb/sec, $\dot{m}_2$ = 13.35 lb/sec, $\dot{m}_3$ = 23.13 lb/sec, $\dot{m}_4$ = 3.57 lb/sec)

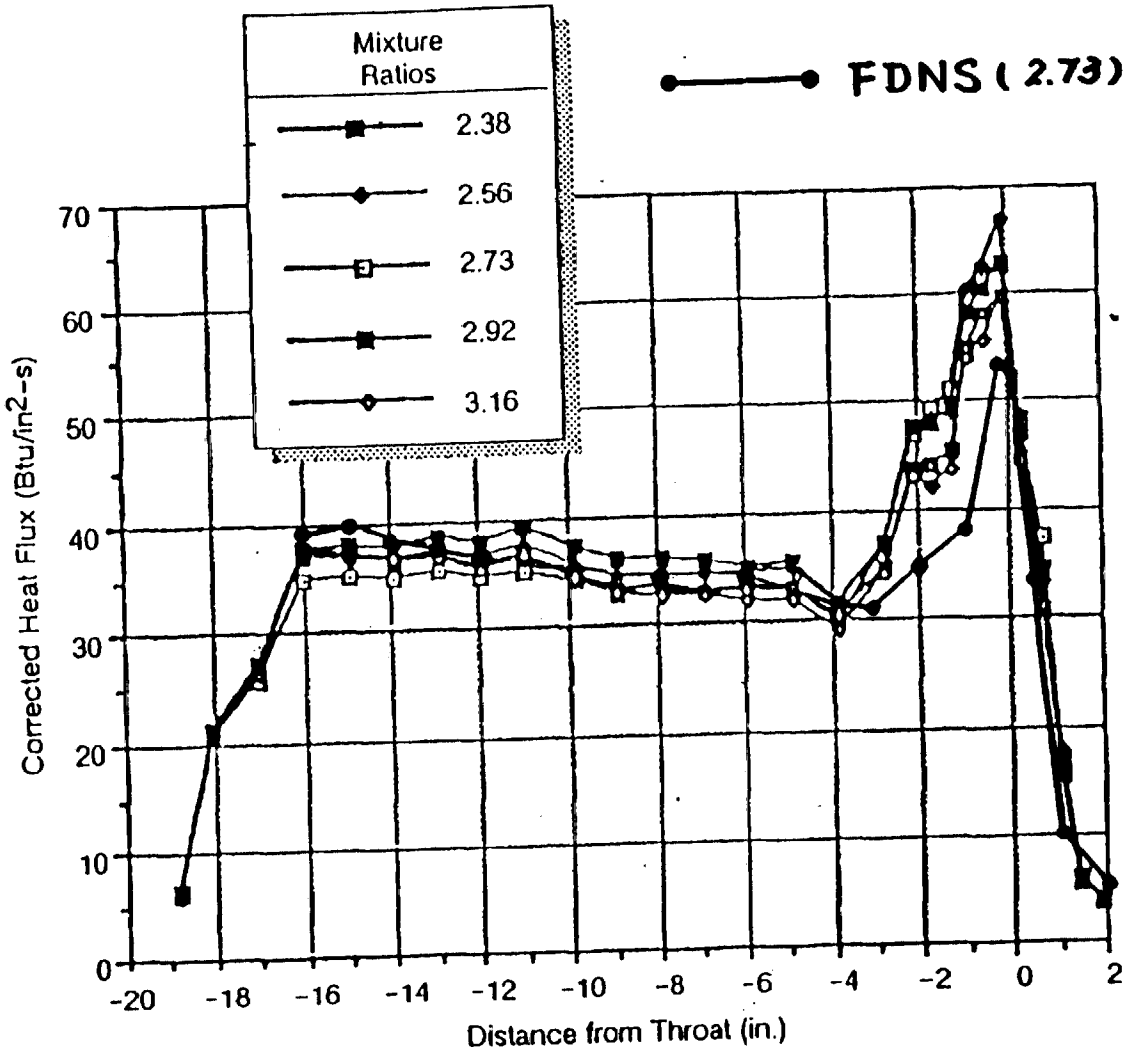

Heat Flux Distribution for the Original Configuration of Rocketdyne's Circumferential Fan Injector

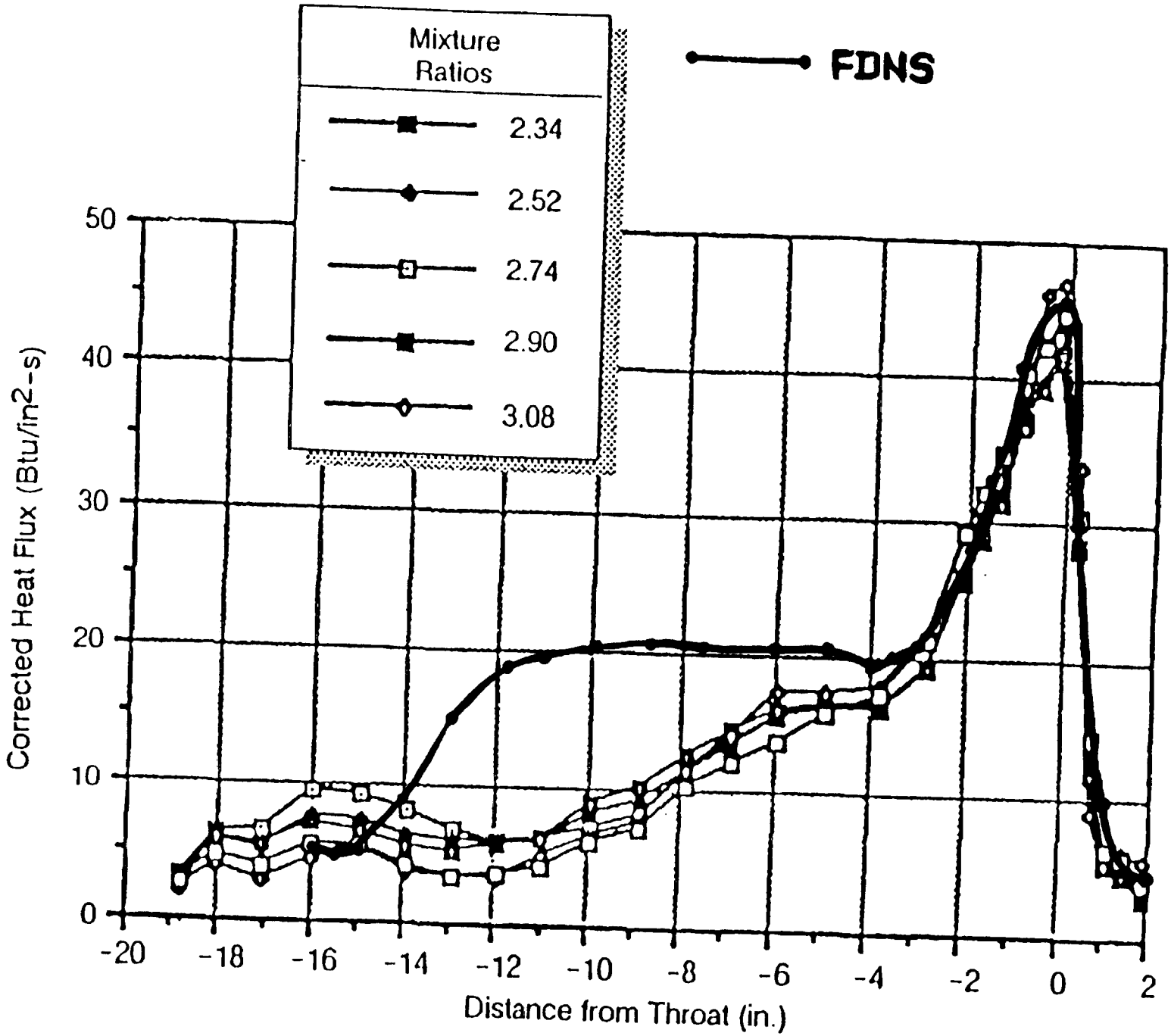
Mixture Ratios
2.34
2.52
2.74
2.90
3.08
FDNS
Corrected Heat Flux (Btu/in2-s)
50
40
30
20
10
0
-20
-18
-16
-14
-12
-10
-8
-6
-4
-2
0
2
Distance from Throat (in.)

Table 1

SUMMARY OF OXIDIZER AND FUEL INLET BOUNDARY CONDITIONS FOR THE HYBRID ROCKET MOTOR NUMERICAL SIMULATION

Oxidizer Mass flow Rate	620 lb/sec
Oxidizer Inlet Pressure	500 psi
Oxidizer Inlet Temperature	300 °K
Oxidizer Inlet Reynolds Number	1.76×10^{7} ft $^{-1}$
Fuel Regression Rate	0.088 in/sec
Fuel Injection Density	1.7034 lb/ft^3
Fuel Injection Temperature	820 °K
Solid Fuel Density	57.553 lb/ft^3
Overall O/F Ratio	2

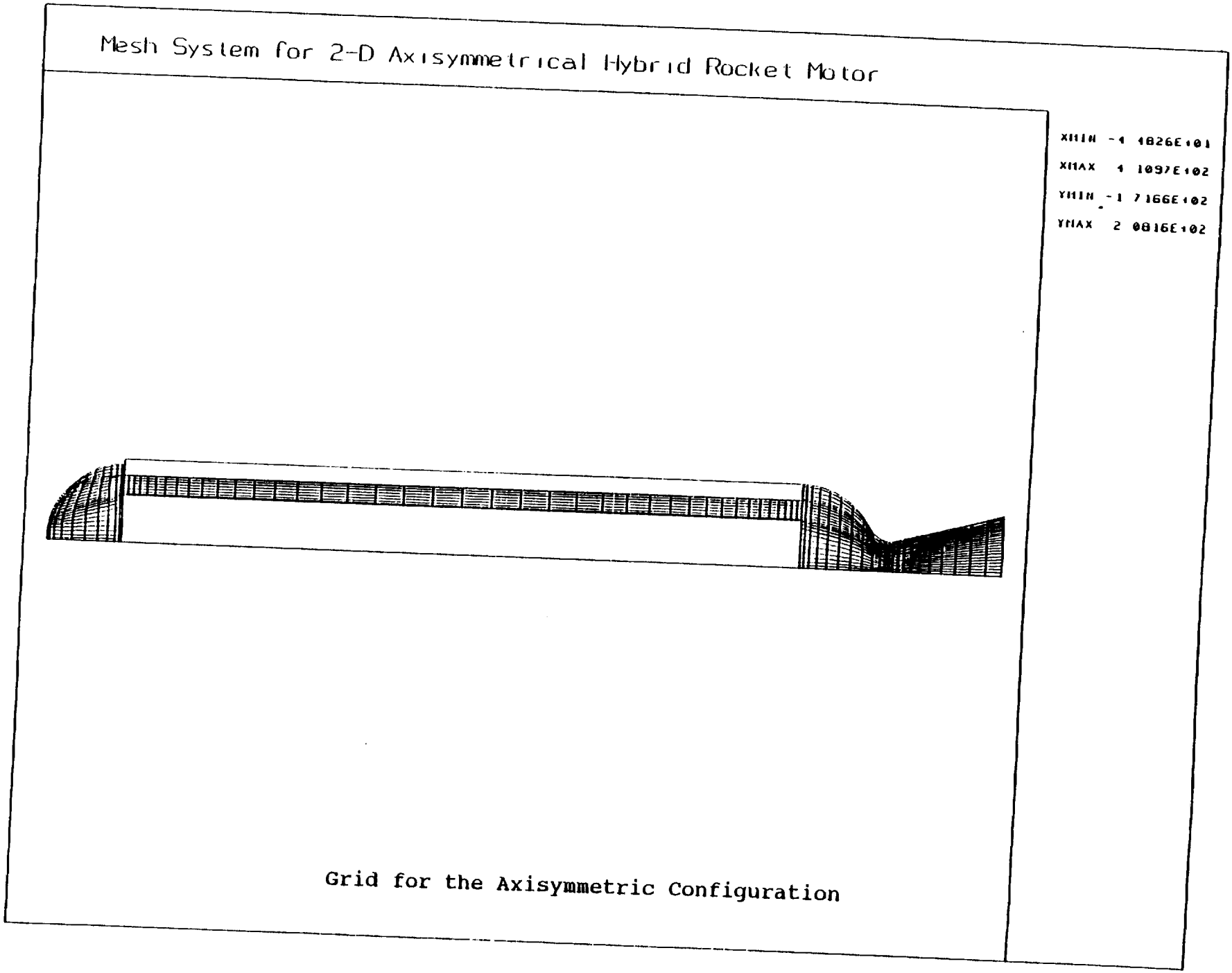

Grid for the Axisymmetric Configuration

Temperature in the axisymmetric hybrid rocket motor (deg. K)

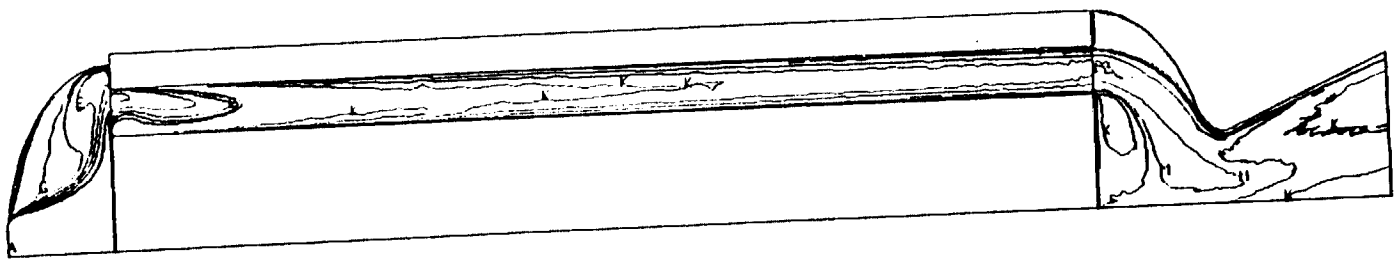

XMIN: -4.4826E+01
XMAX: 4.1097E+02
YMIN: -9.6724E+01
YMAX: 1.3322E+02

FMIN: 3.0000E+02
FMAX: 4.2259E+03
DELF: 3.0000E+02

CONTOUR LEVELS:

ID	VALUES
A	3.0000E+02
B	6.0000E+02
C	9.0000E+02
D	1.2000E+03
E	1.5000E+03
F	1.7999E+03
G	2.0999E+03
K	3.2999E+03
L	3.5999E+03
M	3.9000E+03
N	4.1999E+03

Axisymmetric Hybrid Configuration

Temperature in the head-end region (degree K)

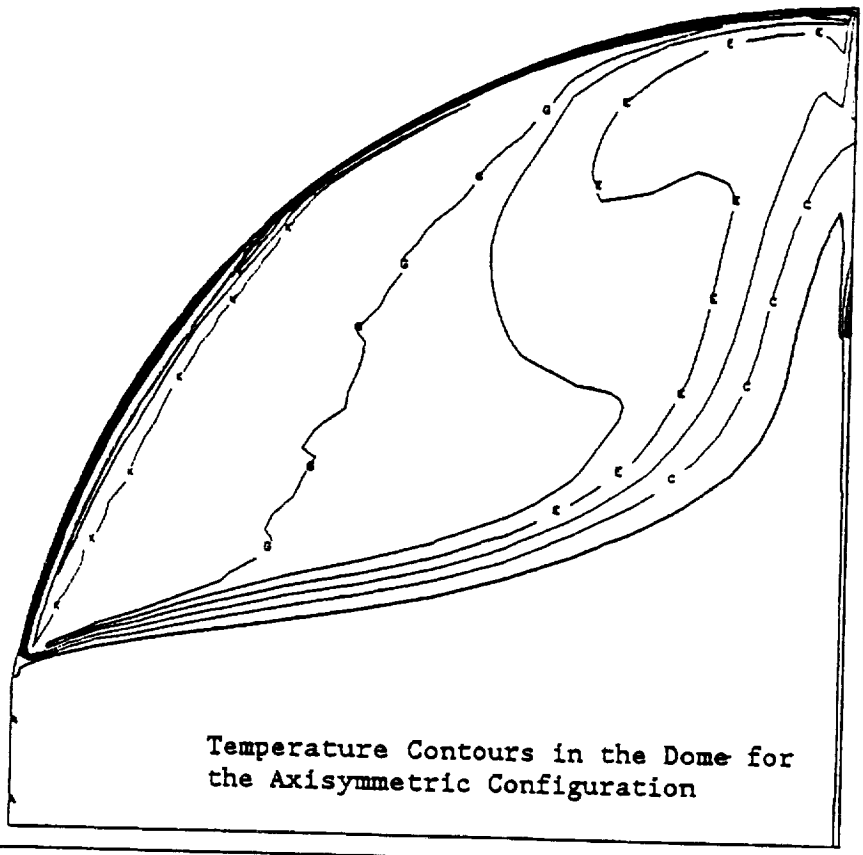

XMIN -3.8722E+01
XMAX 4.7478E+00
YMIN -8.8249E-01
YMAX 3.5362E+01

FMIN 3.0000E+02
FMAX 4.2239E+03
DELF 3.0000E+02

CONTOUR LEVELS:

ID	VALUES
A	3.0000E+02
B	8.0000E+02
C	9.0000E+02
D	1.2000E+03
E	1.5000E+03
F	1.7999E+03
G	2.0999E+03
K	3.2999E+03
L	3.5999E+03
M	3.9000E+03
N	4.1999E+03

Temperature Contours in the Dome for the Axisymmetric Configuration

H2O mass fraction in the head-end region

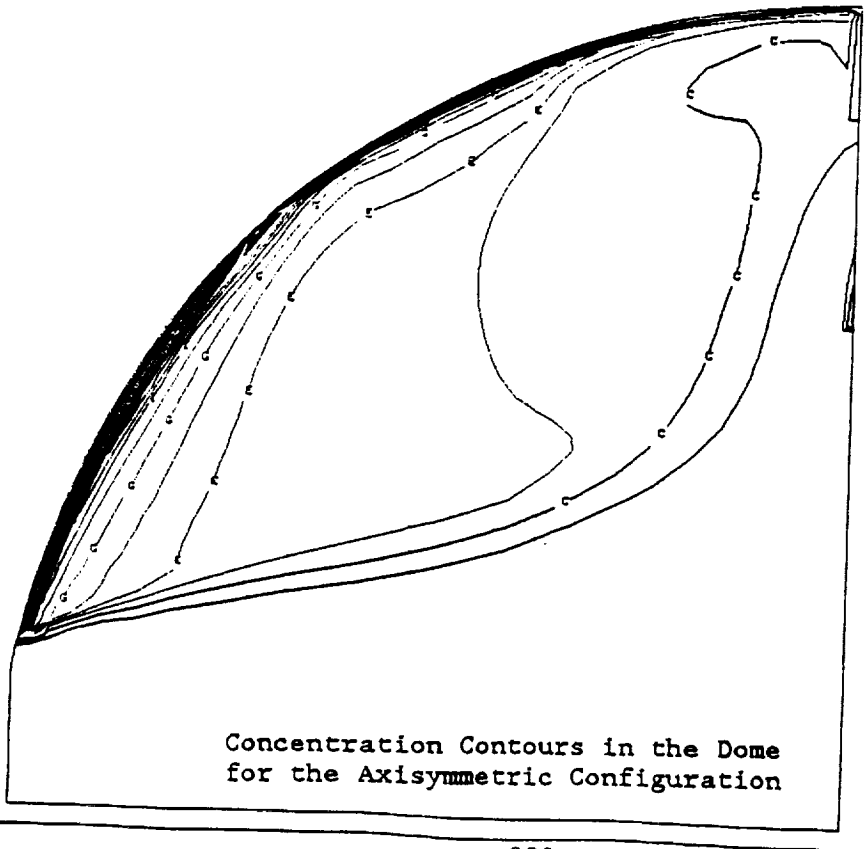

XMIN -3.8722E+01
XMAX 4.7478E+00
YMIN -8.8249E-01
YMAX 3.5362E+01

FMIN 0.0000E+00
FMAX 2.1017E-01
DELF 1.0000E-02

CONTOUR LEVELS:

ID	VALUES
A	0.0000E+00
B	1.0000E-02
C	1.9999E-02
D	2.9999E-02
E	3.9999E-02
F	4.9999E-02
G	5.9999E-02
H	7.0000E-02
I	7.9999E-02
J	9.0000E-02
K	9.9999E-02
P	1.4999E-01
Q	1.9999E-01
R	1.7000E-01
S	1.7999E-01
T	1.9000E-01
U	1.9999E-01
V	2.0999E-01

Concentration Contours in the Dome for the Axisymmetric Configuration

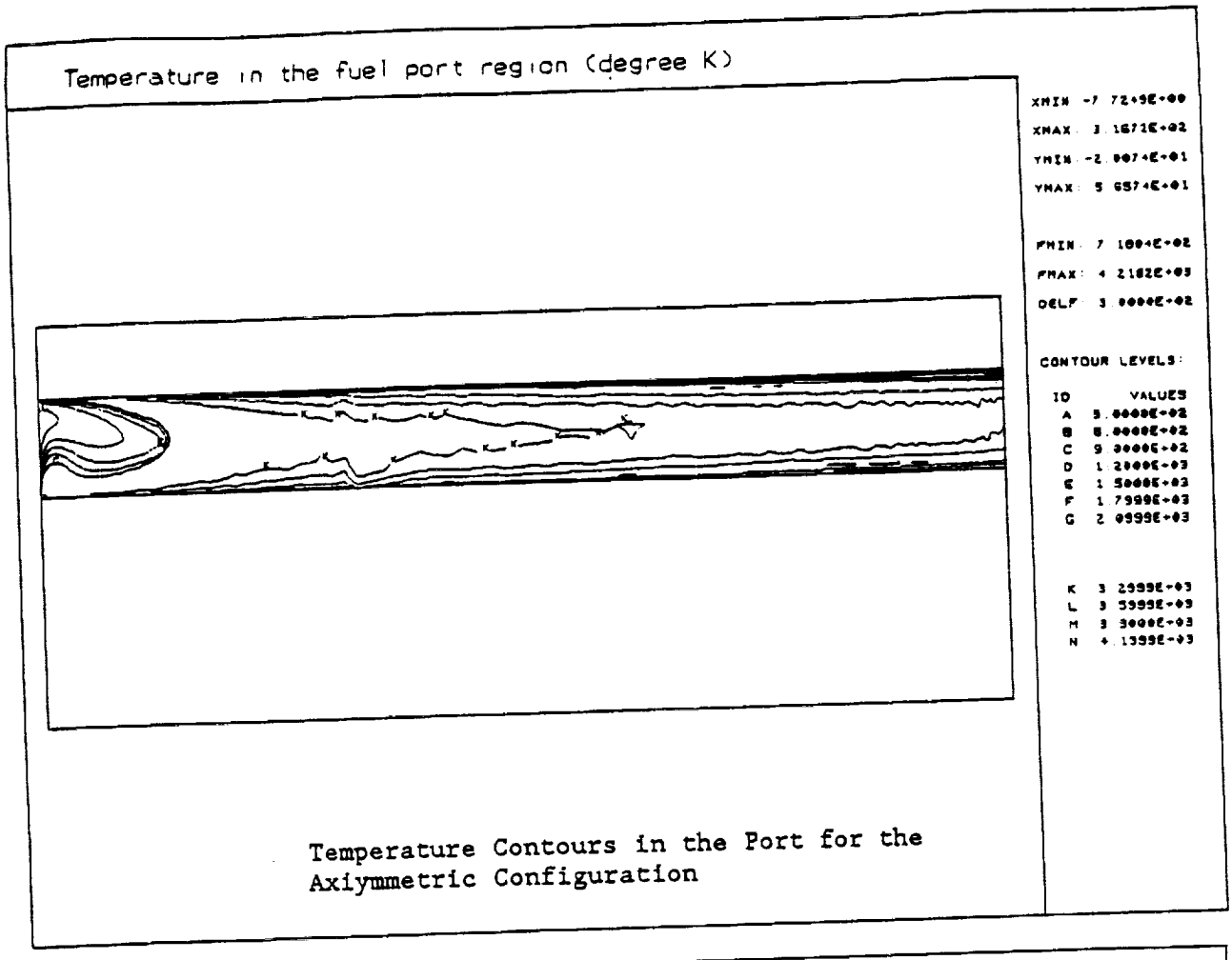

Temperature Contours in the Port for the Axiymmetric Configuration

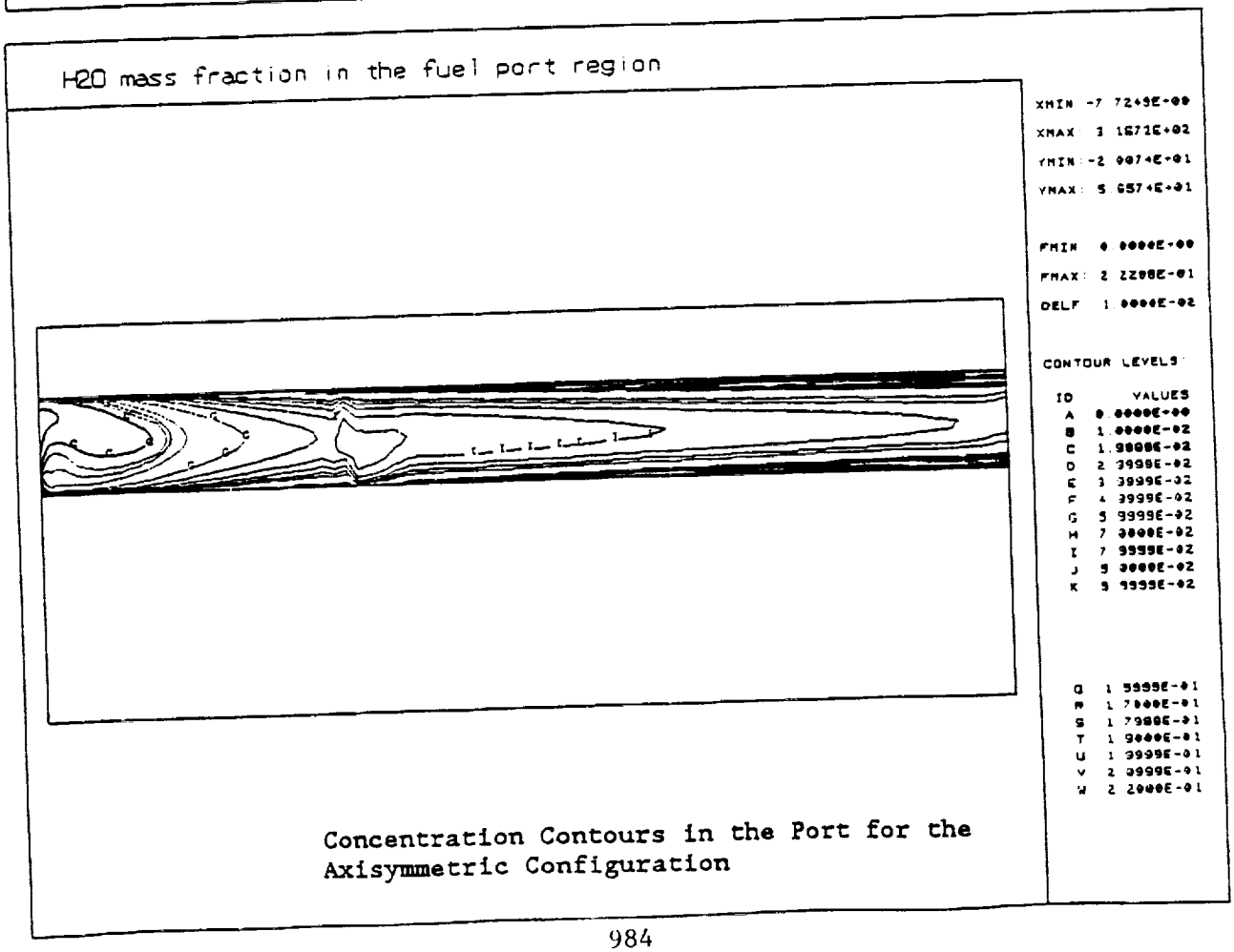

Concentration Contours in the Port for the Axisymmetric Configuration

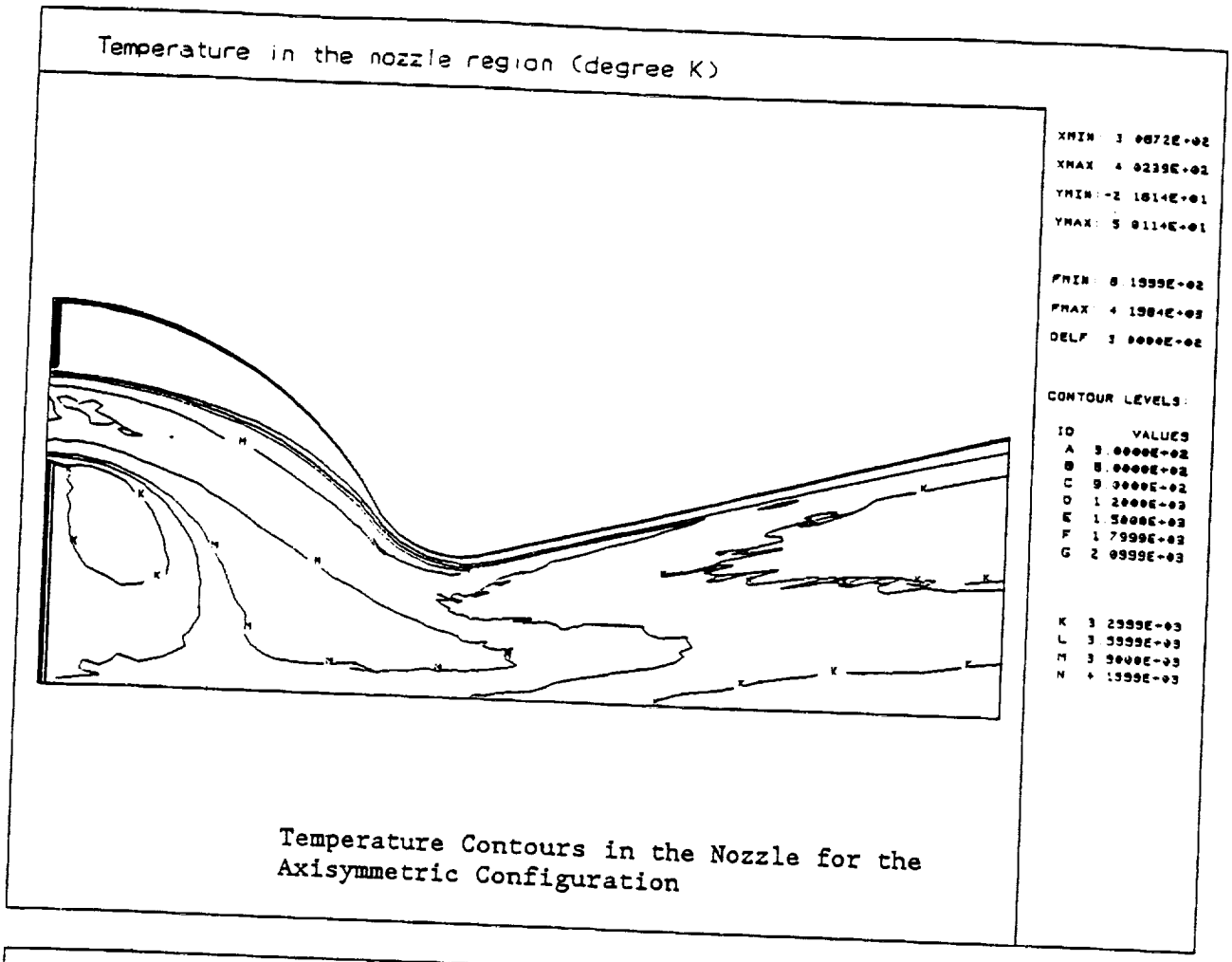

Temperature Contours in the Nozzle for the Axisymmetric Configuration

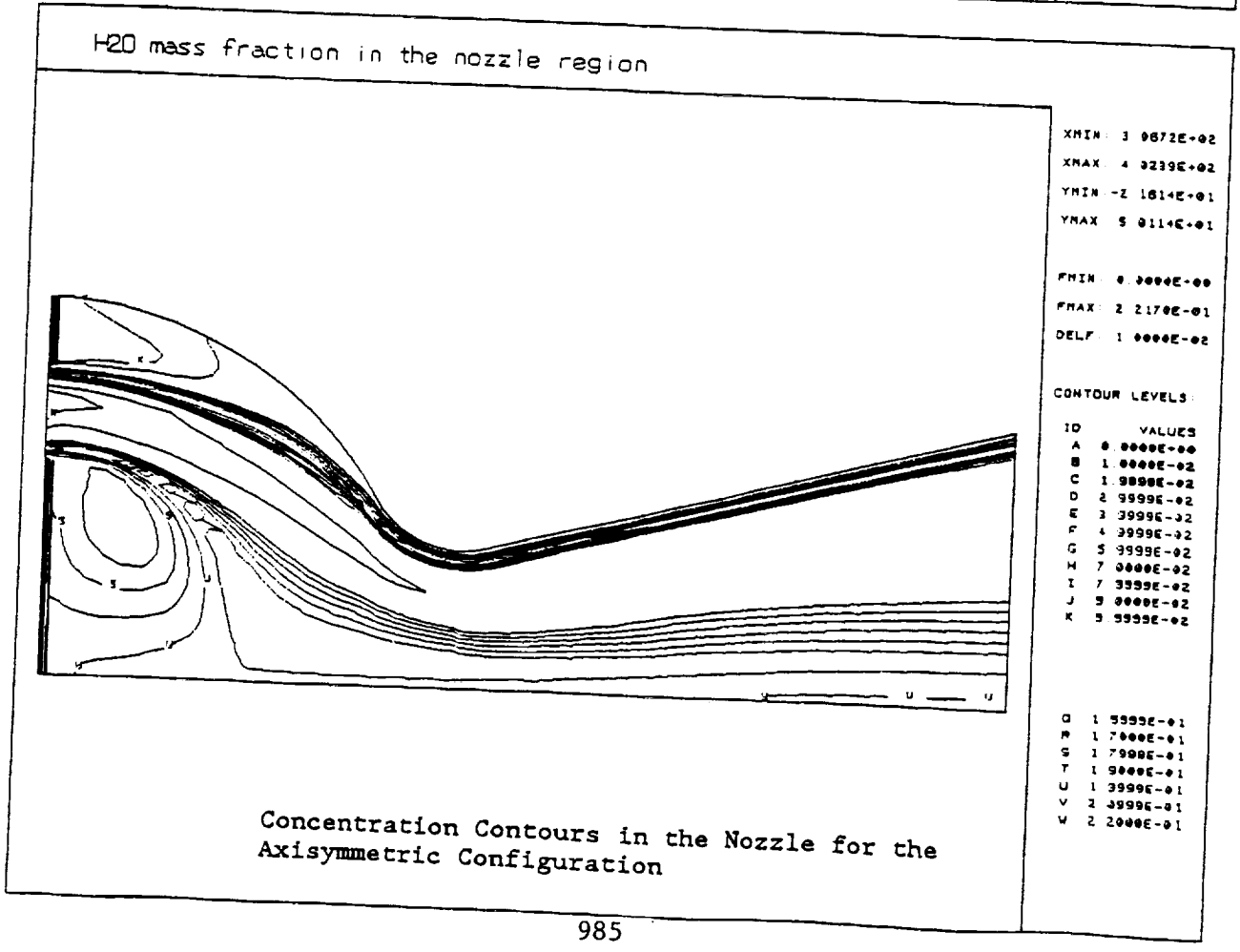

Concentration Contours in the Nozzle for the Axisymmetric Configuration

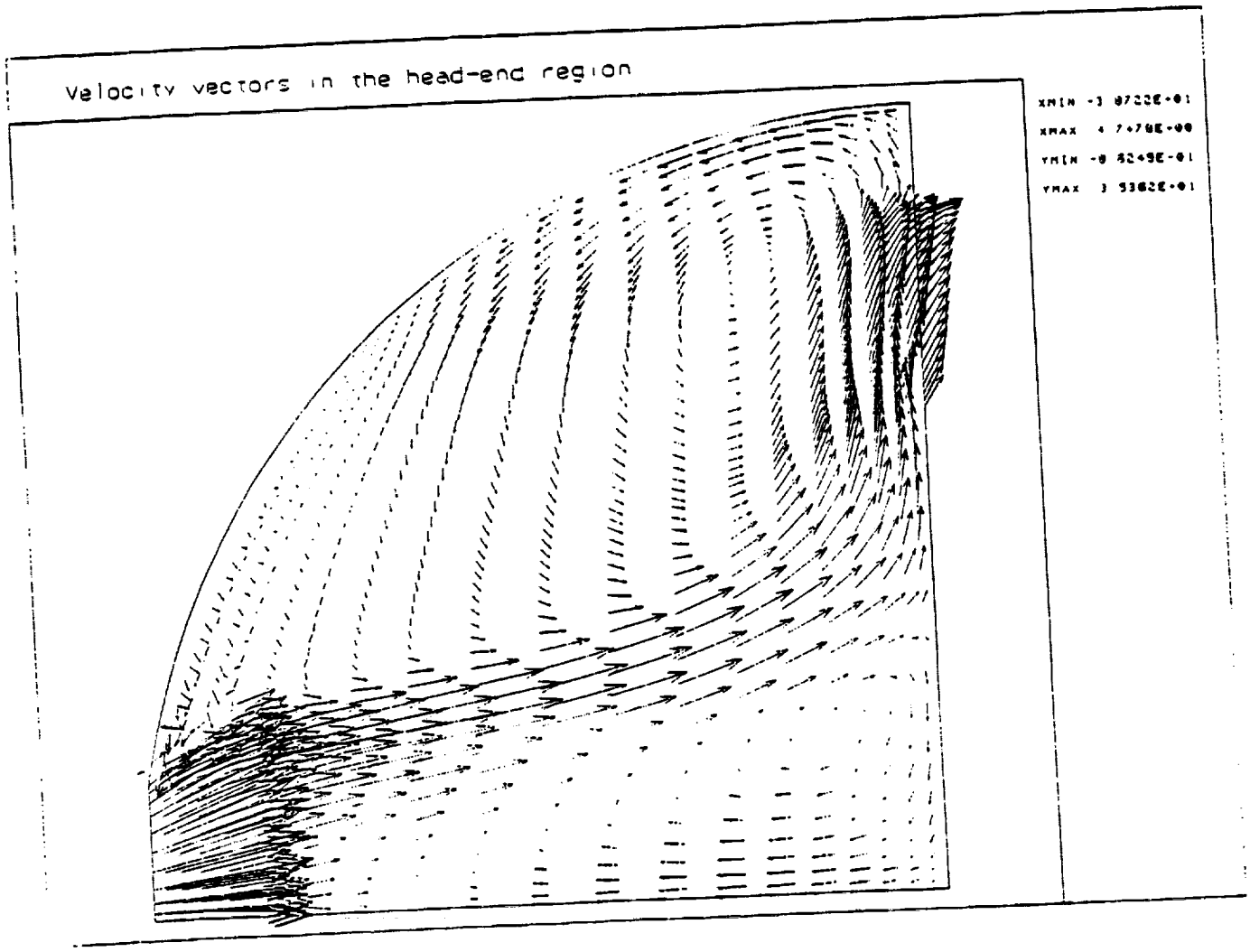

Velocity Vectors in the Heat - End of the Axisymmetric Configuration

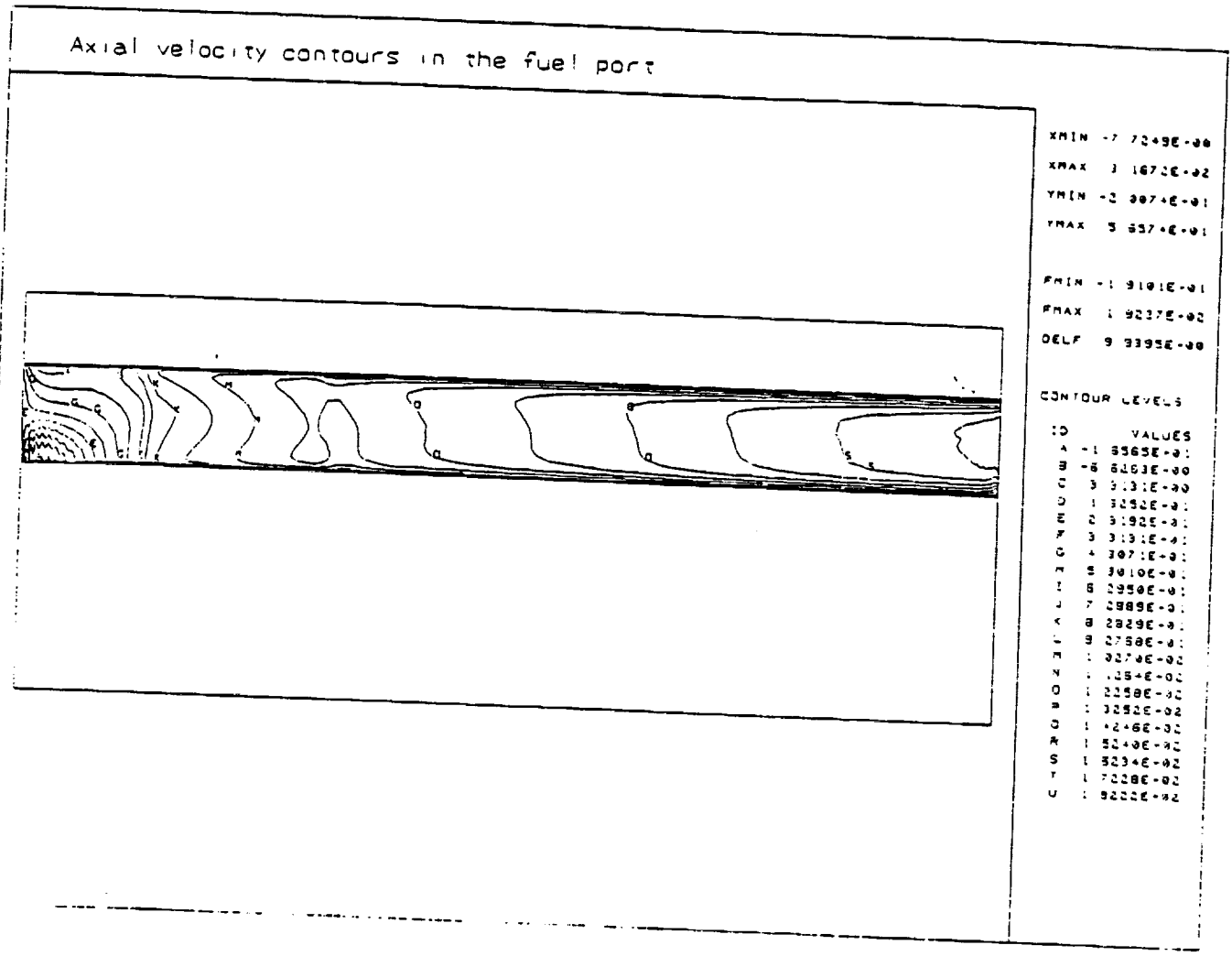

Axial Velocity Contours in the Port of the Axisymmetric Configuration

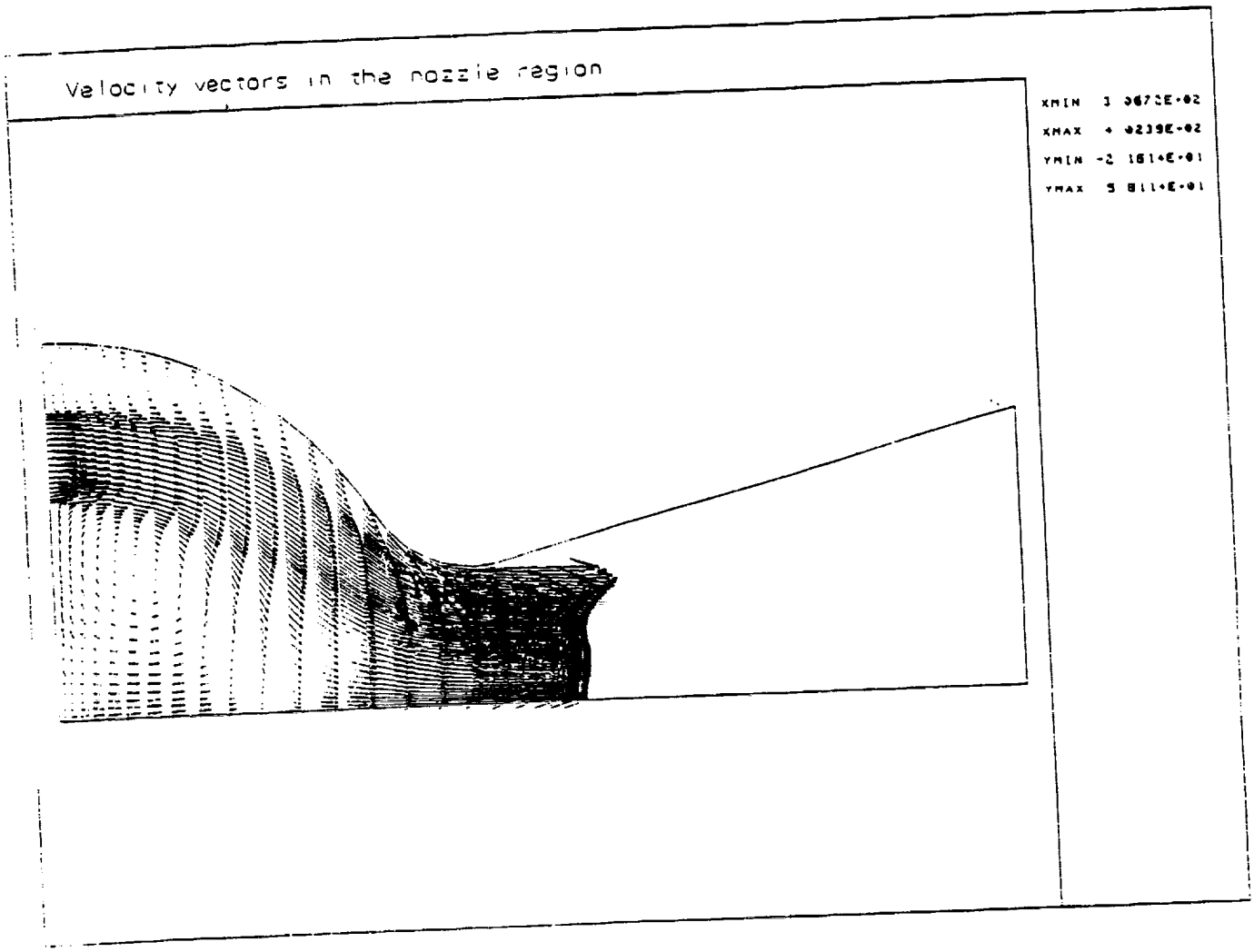

Velocity Vectors in the Aft-End of the Axisymmetric Configuration

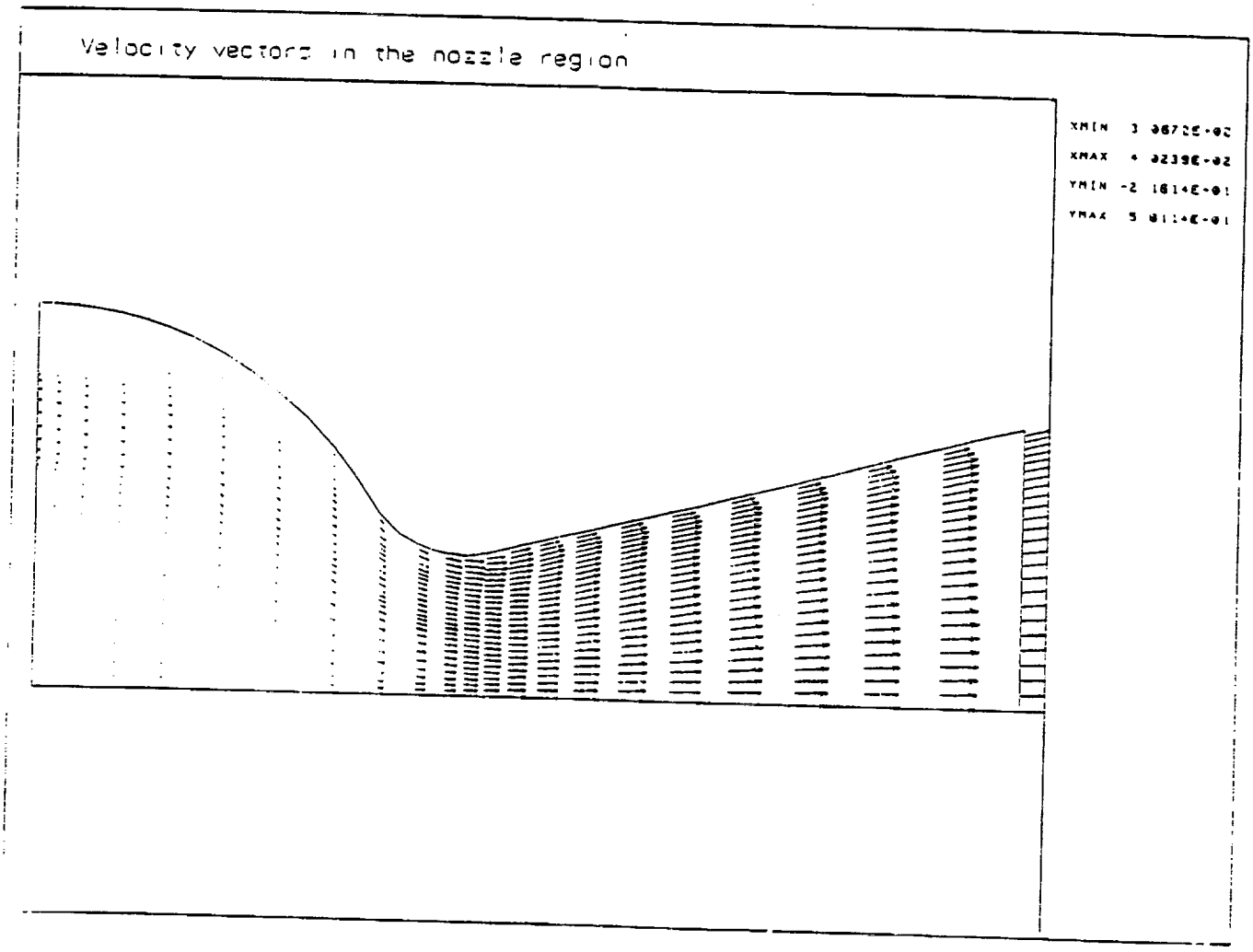

Velocity Vectors in the Nozzle of the Axisymmetric Configuration

CONCLUSIONS

- Conjugate heat transfer of single injector elements is efficiently treated with the density based version of the FDNS code for any fluid state.
- Heat transfer to combustion chamber walls is accurately simulated with the FDNS code.
- The head-end, port, and aft sections of a hybrid motor are well simulated with respect to finite-rate combustion and turbulent mixing processes.

RADIATION/CONVECTION COUPLING IN ROCKET MOTORS AND PLUMES

R. C. Farmer
A. J. Saladino

SECA, Inc.
Huntsville, AL

Abstract

The three commonly used propellant systems; H2/O2, RP-1/O2, and solid propellants; primarily radiate as: molecular emitters, non-scattering small particles, and scattering larger particles, respectively. Present technology has accepted the uncoupling of the radiation analysis from that of the flowfield. This approximation becomes increasingly inaccurate as one considers plumes, interior rocket chambers, and nuclear rocket propulsion devices. This study will develop a hierarchy of methods which will address radiation/convection coupling in all of the aforementioned propulsion systems.

The nature of the radiation/convection coupled problem is that the divergence of the radiative heat flux must be included in the energy equation and that the local, volume-averaged intensity of the radiation must be determined by a solution of the radiative transfer equation (RTE). The intensity is approximated by solving the RTE along several lines of sight (LOS) for each point in the flowfield. Such a procedure is extremely costly; therefore, further approximations are needed. Modified differential approximations are being developed for this purpose. It is not obvious which order of approximations are required for a given rocket motor analysis. Therefore, LOS calculations have been made for typical rocket motor operating conditions in order to select the type approximations required. The results of these radiation calculations, and the interpretation of these intensity predictions are presented herein.

The study is still in progress. The inclusion of the selected radiation model into a coupled CFD solution will be reported at a later date.

RADIATION/CONVECTION COUPLING IN ROCKET MOTORS & PLUMES

R. C. Farmer

A. J. Saladino

SECA, INC.

Presentation for:

Workshop for CFD Applications in Rocket Propulsion

April 20-22, 1993

NASA/MSFC, MSFC, AL

OBJECTIVE:

Develop a radiation/convection coupled analysis of rocket motors & plumes

Tasks:

1 - Characterize radiation for various type motors

2 - Develop radiation/convection coupling methodology

PARAMETERS AFFECTING RADIATION

H_2/O_2 Propellant System

- Radiator H_2O vapor
- Requires spectral integration

HC/O_2 Propellant System

- Radiators soot, H_2O, CO_2
- Requires soot concentration prediction

SRM

- Radiators Al_2O_3 particles, H_2O, CO_2, HCl
- Requires
  - Predicting particle size distributions
  - Predicting particle temperatures
  - Specifying optical property data

Internal Surface Characteristics

- Not well known
- Assume reflectivity of 0.2

Radiation Analyses

Molecular Radiators

- Narrow Band Models
- Wide Band Models
- Mean of all Bands

Particle Radiators

- Small particles - like soot emit & absorb but do not scatter
- large particles - like Al_2O_3 emit, absorb, & scatter non-isotropically.

Evaluations made with line-of-sight (LOS) calculation for typical motors.

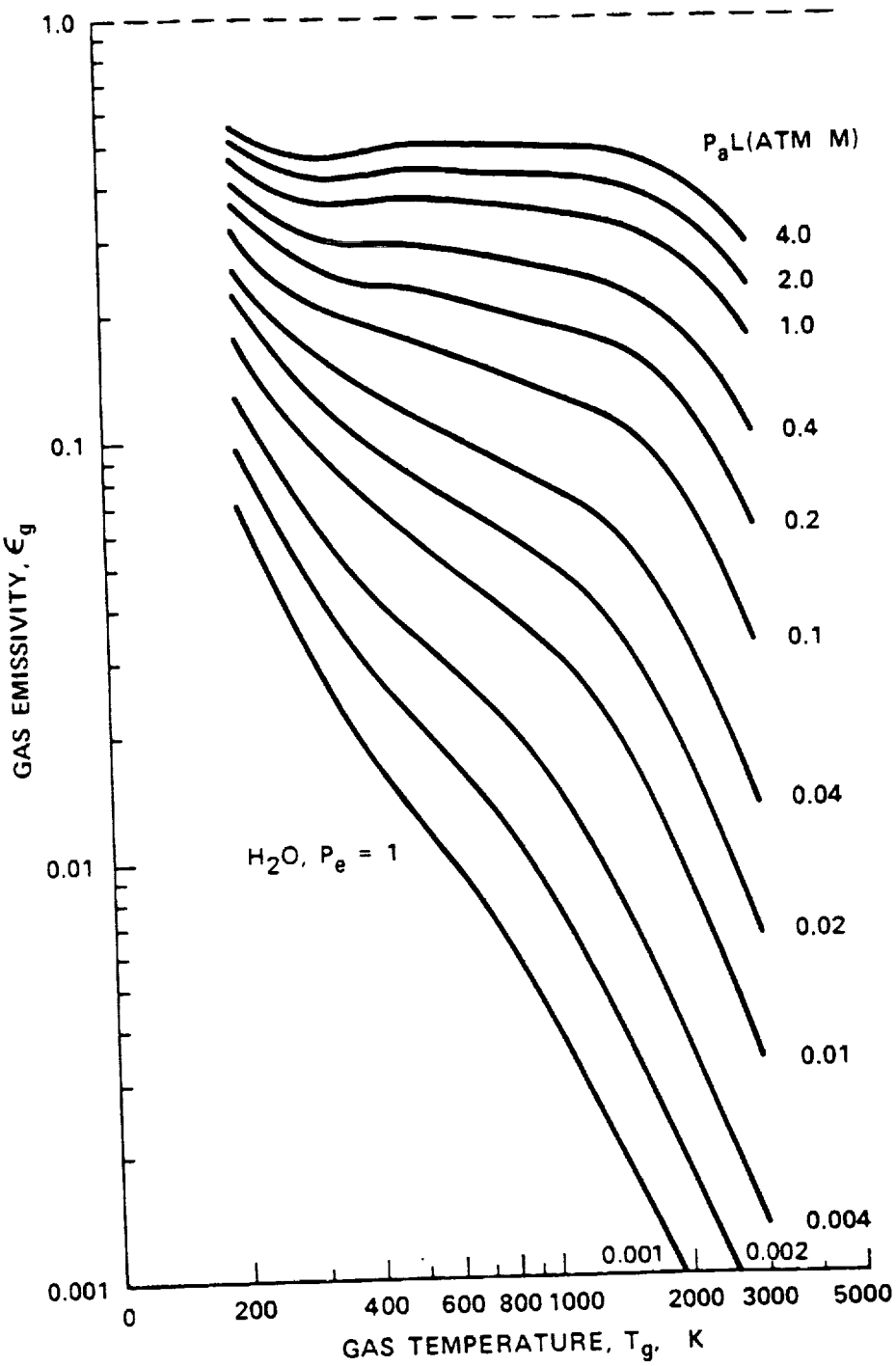

Total emissivity of H_2O.

Wide band model correlation parameters for various gases

Band Location λ [μm]	(δ_k)	Pressure Parameters n	b	Correlation Parameters α_0 [$cm^{-1}/(g/m^2)$]	γ_0	ω_0 [cm^{-1}]
H_2O	$m = 3$, $\eta_1 = 3652\,cm^{-1}$, $\eta_2 = 1595\,cm^{-1}$, $\eta_3 = 3756\,cm^{-1}$, $g_k = (1, 1, 1)$					
71 μm[a]	$\eta_c = 140\,cm^{-1}$ (Rotational) (0,0,0)	1	$8.6\sqrt{\frac{T_0}{T}} + 0.5$	44,205	0.14311	69.3
6.3 μm	$\eta_c = 1600\,cm^{-1}$ (0,1,0)	1	$8.6\sqrt{\frac{T_0}{T}} + 0.5$	41.2	0.09427	56.4
2.7 μm	$\eta_c = 3760\,cm^{-1}$ (0,2,0)			0.2		
	(1,0,0) (0,0,1)	1	$8.6\sqrt{\frac{T_0}{T}} + 0.5$	2.3 23.4	0.13219[b,c]	60.0[b]
1.87 μm	$\eta_c = 5350\,cm^{-1}$ (0,1,1)	1	$8.6\sqrt{\frac{T_0}{T}} + 1.5$	3.0	0.08169	43.1
1.38 μm	$\eta_c = 7250\,cm^{-1}$ (1,0,1)	1	$8.6\sqrt{\frac{T_0}{T}} + 1.5$	2.5	0.11628	32.0
CO_2	$m = 3$, $\eta_1 = 1351\,cm^{-1}$, $\eta_2 = 666\,cm^{-1}$, $\eta_3 = 2396\,cm^{-1}$, $g_k = (1, 2, 1)$					
15 μm	$\eta_c = 667\,cm^{-1}$ (0,1,0)	0.7	1.3	19.0	0.06157	12.7
10.4 μm	$\eta_c = 960\,cm^{-1}$ (−1,0,1)	0.8	1.3	2.47×10^{-9}	0.04017	13.4
9.4 μm	$\eta_c = 1060\,cm^{-1}$ (0,−2,1)	0.8	1.3	2.48×10^{-9}	0.11888	10.1
4.3 μm	$\eta_u = 2410\,cm^{-1}$ (0,0,1)	0.8	1.3	110.0	0.24723	11.2
2.7 μm	$\eta_c = 3660\,cm^{-1}$ (1,0,1)	0.65	1.3	4.0	0.13341	23.5
2.0 μm	$\eta_c = 5200\,cm^{-1}$ (2,0,1)	0.65	1.3	0.060	0.39305	34.5

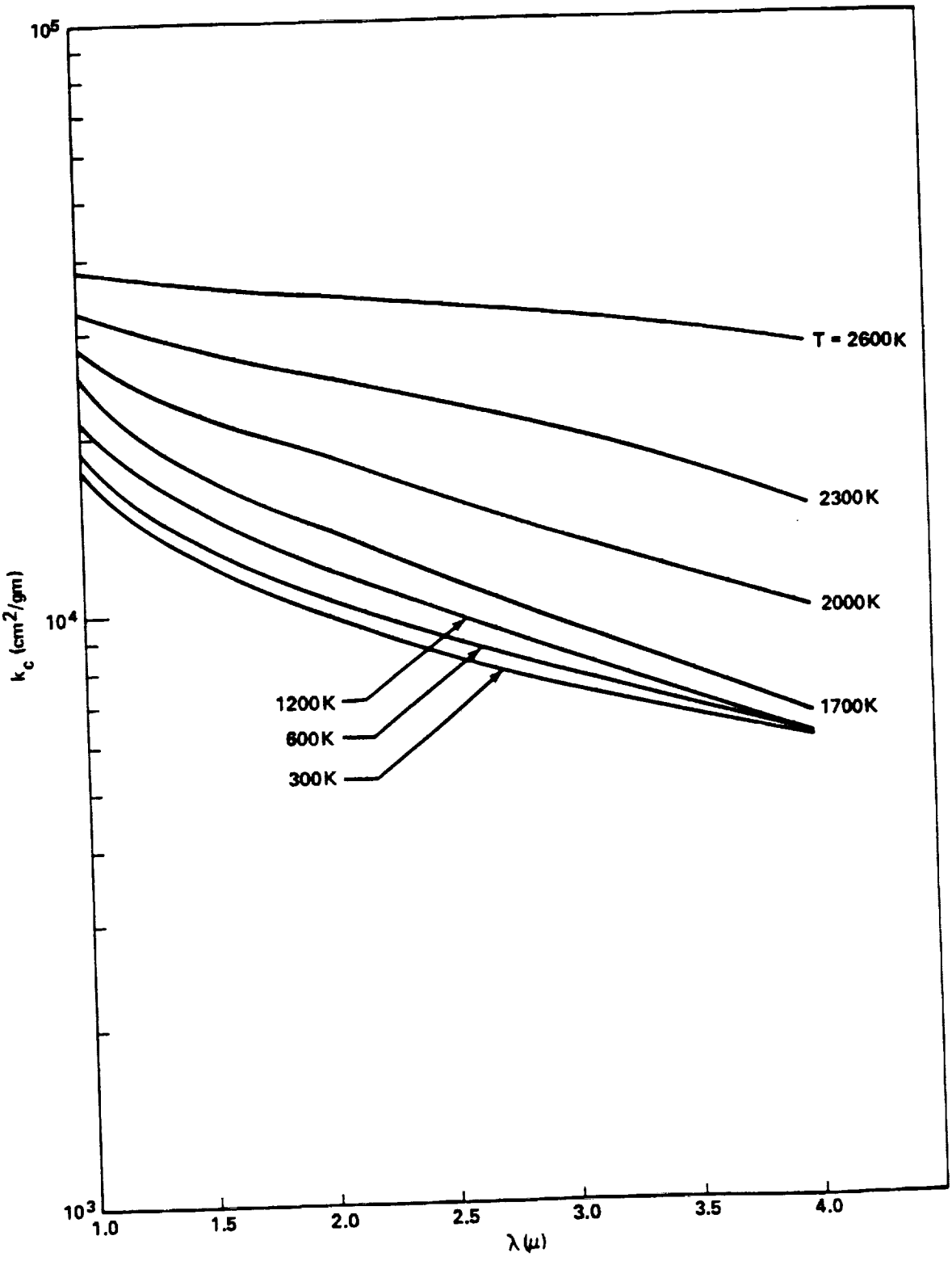

Experimentally Determined Carbon Absorption Coefficients
(from Radiation Handbook)

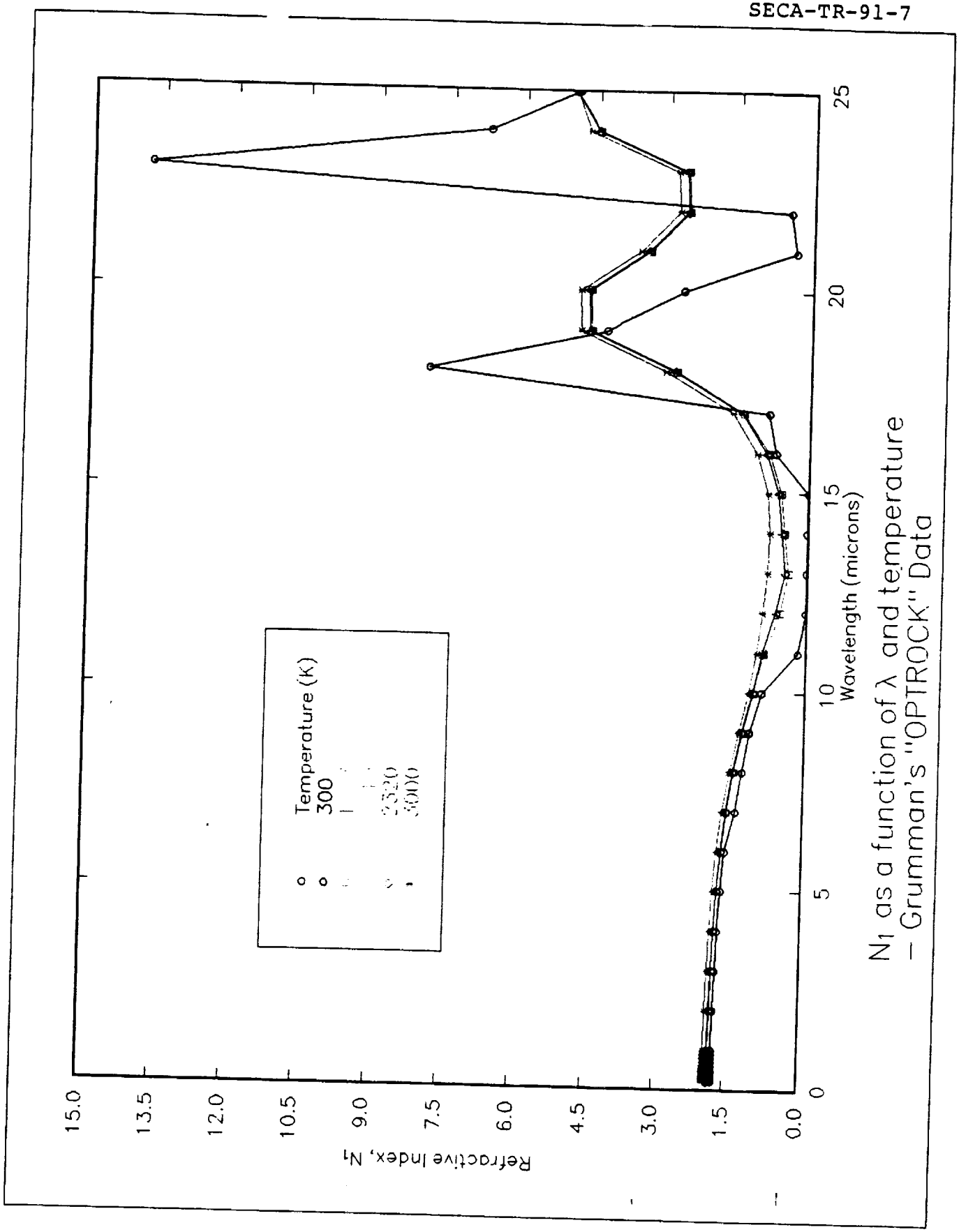
N1 as a function of λ and temperature
– Grumman's "OPTROCK" Data
Refractive Index, N1
Wavelength (microns)
Temperature (K)
300
0.0
1.5
3.0
4.5
6.0
7.5
9.0
10.5
12.0
13.5
15.0
0
5
10
15
20
25

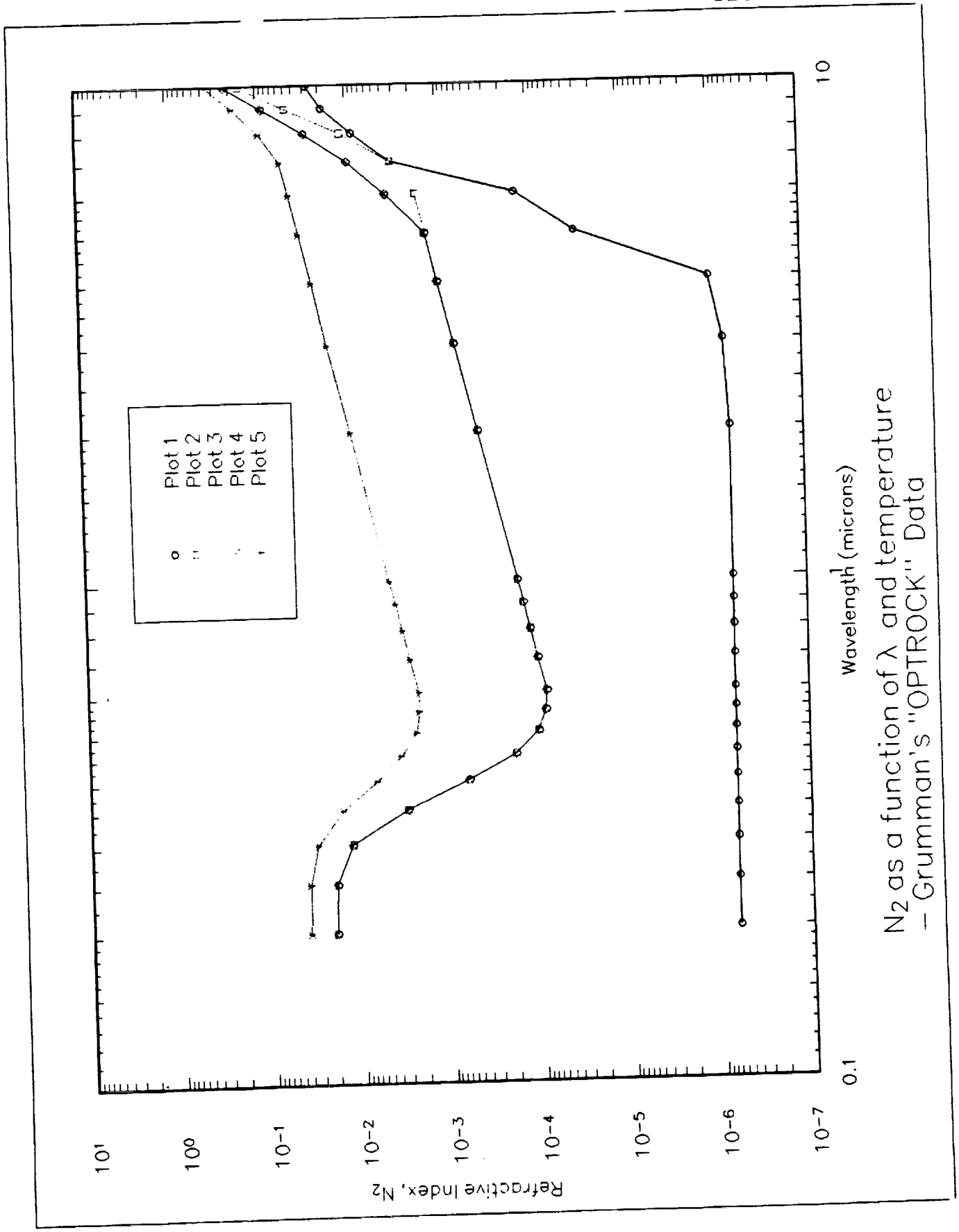
Plot 1
Plot 2
Plot 3
Plot 4
Plot 5
Refractive Index, N_2
10^1
10^0
10^{-1}
10^{-2}
10^{-3}
10^{-4}
10^{-5}
10^{-6}
10^{-7}
0.1
1
10
Wavelength (microns)
N_2 as a function of λ and temperature
– Grumman's "OPTROCK" Data

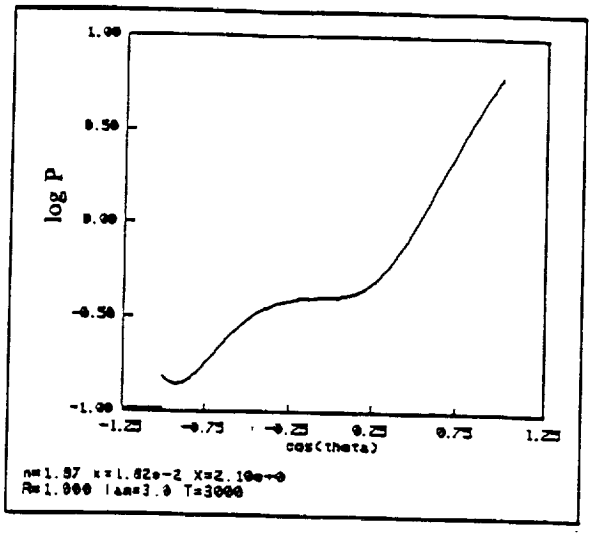

PHASE FUNCTION AS DETERMINED BY MIE THEORY CALCULATION

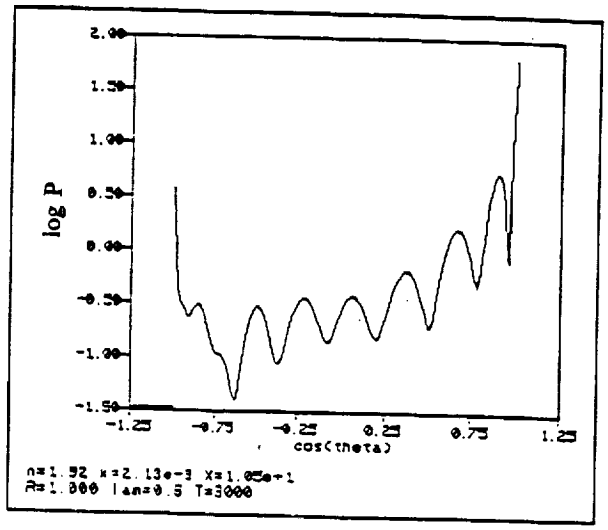

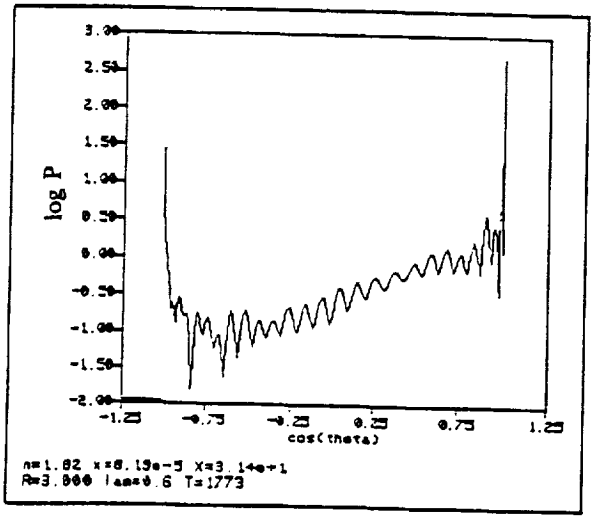

Optical properties: n,κ
Particle Radius: R
Wavelength: lam
Temperature: T
Particle Size
Parameter: $X=2\pi R/\lambda$

Al_2O_3 RADIATION PROPERTIES

r, (μm)	Wave Number	σ_e, (cm^2)	Albedo	s_b	b_b	b_2	T(K)	
1.0E-3	400	6.181E-19	5.565E-10	.14352	.21295	.49999	3000	OS
		6.181E-19	5.565E-10	.1439	.2120	.5065		OM
3	5000	6.7430E-7	.98982	.073316	.061334	.087562	2320	RS
		5.956E-7	.9905	.07461	.06874	.14723		RM
3	10000	6.3054E-7	.99193	.059637	.053251	.070317	2320	RS
		6.618E-7	.9924	.05366	.05025	.10287		RM
3	3333	6.841E-7	.98754	.08270	.07050	.11115	2320	RS
		8.103E-7	.9831	.06509	.08108	.17645		RM
3	10000	6.723E-7	.98954	.07248	.060389	.085913	1773	RS
		6.752E-7	1.000	.05096	.05813	.11004		RM
3	10000	6.843E-7	.81057	.06522	.04385	.060442	3000	RS
		6.445E-7	.8666	.05318	.03896	.09529		RM

OS Original Al_2O_3 Optical Properties in SIRRM

OM Original Al_2O_3 Optical Property Data With MIE Code

RS OPTROCK Properties in SIRRM

RM OPTROCK Properties Calculated With A MIE Code

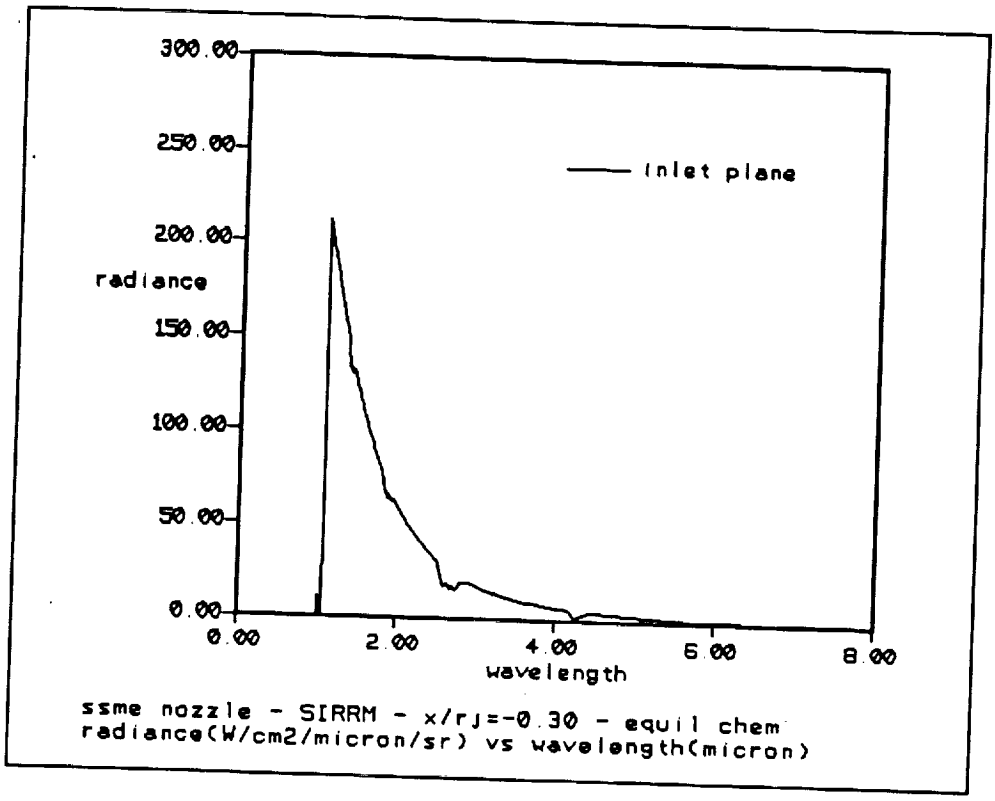
300.00
250.00
200.00
radiance
150.00
100.00
50.00
0.00
0.00
2.00
4.00
6.00
8.00
wavelength
inlet plane
ssme nozzle - SIRRM - x/rj=-0.30 - equil chem
radiance(W/cm2/micron/sr) vs wavelength(micron)

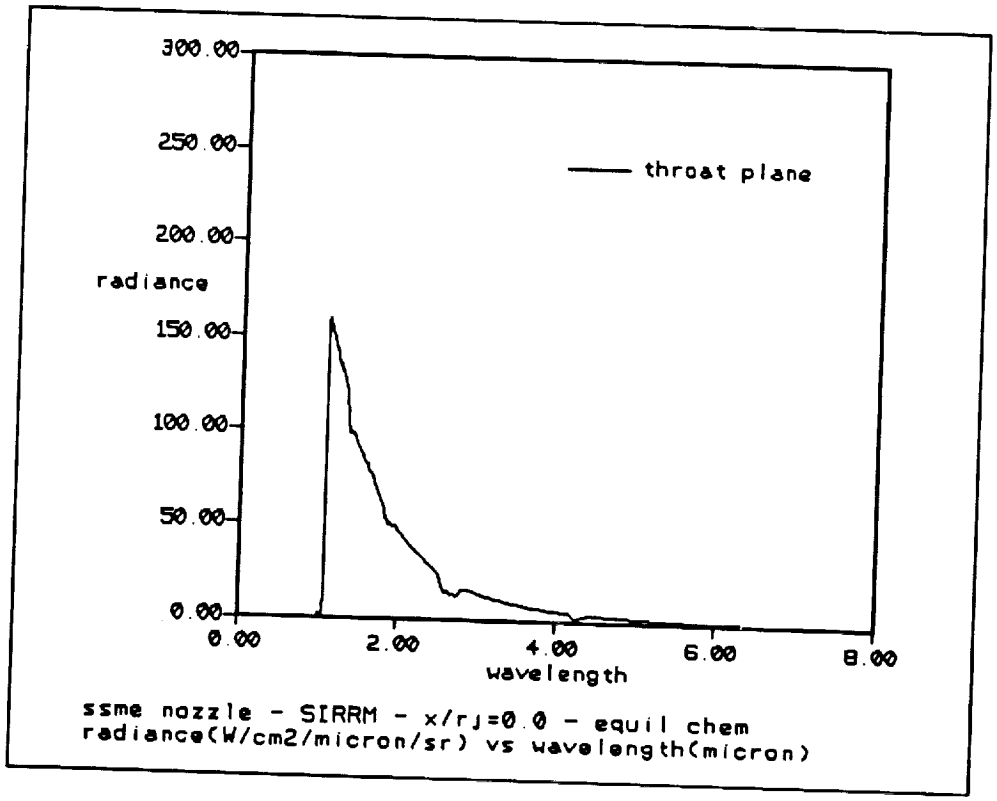
300.00
250.00
200.00
radiance
150.00
100.00
50.00
0.00
0.00
2.00
4.00
6.00
8.00
wavelength
throat plane
ssme nozzle - SIRRM - x/rj=0.0 - equil chem
radiance(W/cm2/micron/sr) vs wavelength(micron)

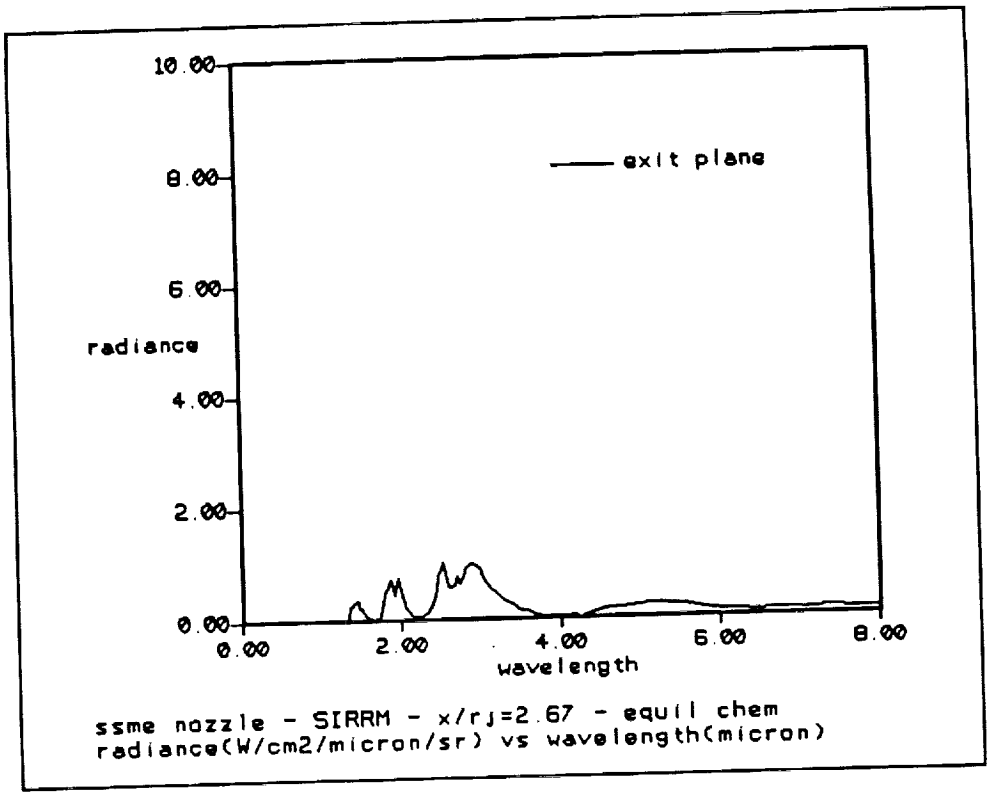

ssme nozzle - SIRRM - x/rj=2.67 - equil chem
radiance(W/cm2/micron/sr) vs wavelength(micron)

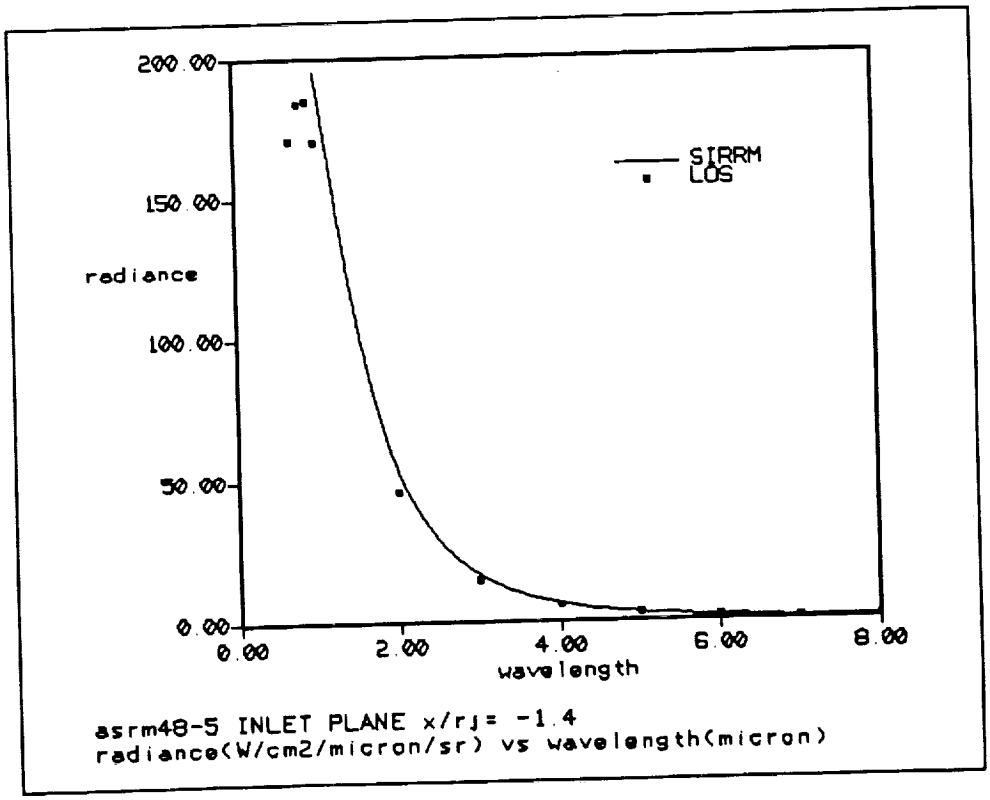

asrm48-5 INLET PLANE x/rj= -1.4
radiance(W/cm2/micron/sr) vs wavelength(micron)

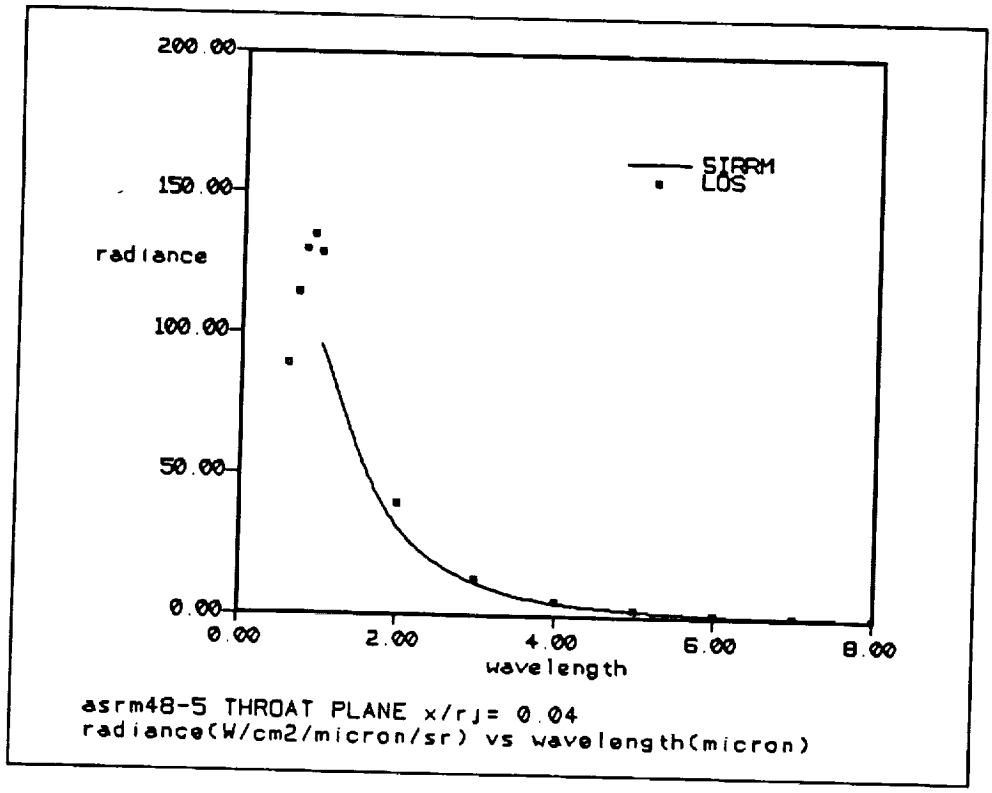

asrm48-5 THROAT PLANE x/rj= 0.04
radiance(W/cm2/micron/sr) vs wavelength(micron)

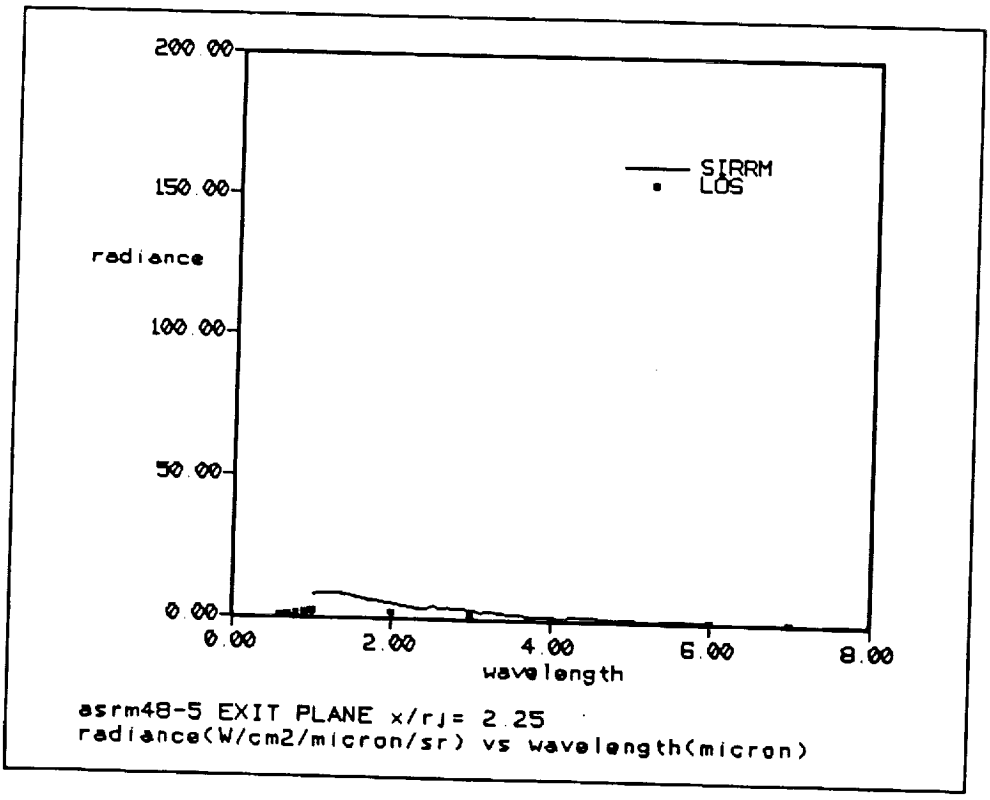

asrm48-5 EXIT PLANE x/rj= 2.25
radiance(W/cm2/micron/sr) vs wavelength(micron)

TOTAL GAS RADIATION - cal/cm^2-s

SSME				
	Mean	Wide	Narrow	σT^4
CHAMBER P=194.4 atm T=3626.02K L=43.98 cm P_w= 134.5 atm	234	90.7	124	234
THROAT P=115 atm T=3450K L=25.42 cm P_w= 81.1 atm	192	65.8	98.4	192
EXIT P=0.1943 atm T=1279K L=230.436 cm P_w= 0.15 atm	0.692	0.621	0.63	3.62

TOTAL GAS RADIATION - cal/cm^2-s

ASRM 48-5			
	Mean	Wide	σT^4
CHAMBER P=43 atm T=3513K L=105.184 cm P_w= 5.76 atm P_c= 0.57 atm	91.1	51.4	206
THROAT P=25 atm T=3230K L=24.918 cm P_w= 3.40 atm P_c= 0.33 atm	21.6	22.1	147
EXIT P=1.04 atm T=2200 K L=67.95 cm P_w= 0.14 atm P_c= 0.014 atm	2.48	2.53	31.7

Al_2O_3 PARTICLE RADIATION - cal/cm^2-s		
	LOS	σT^4
CHAMBER	182	206.3
THROAT	95.0	156.8
EXIT	12.5	39.1

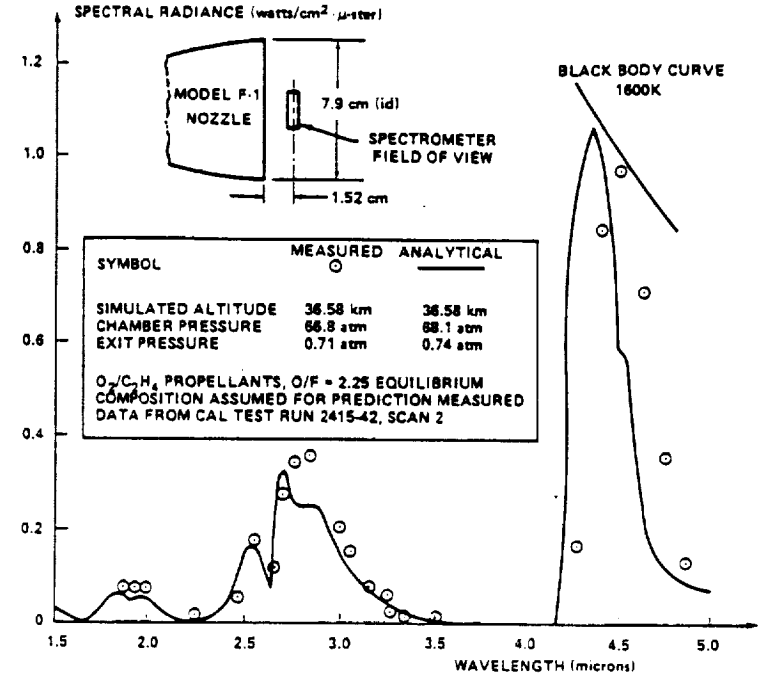

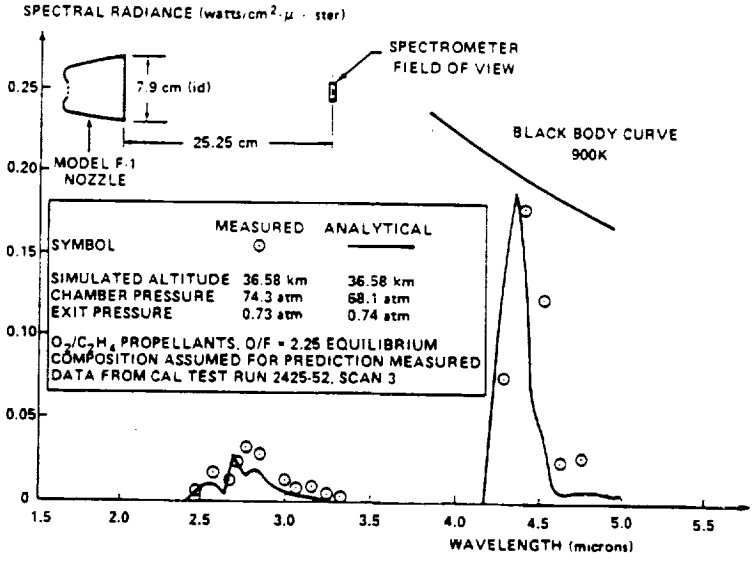

Plume Radiation from a Small Scale F-1 Engine
(Reardon, Radiation Handbook)

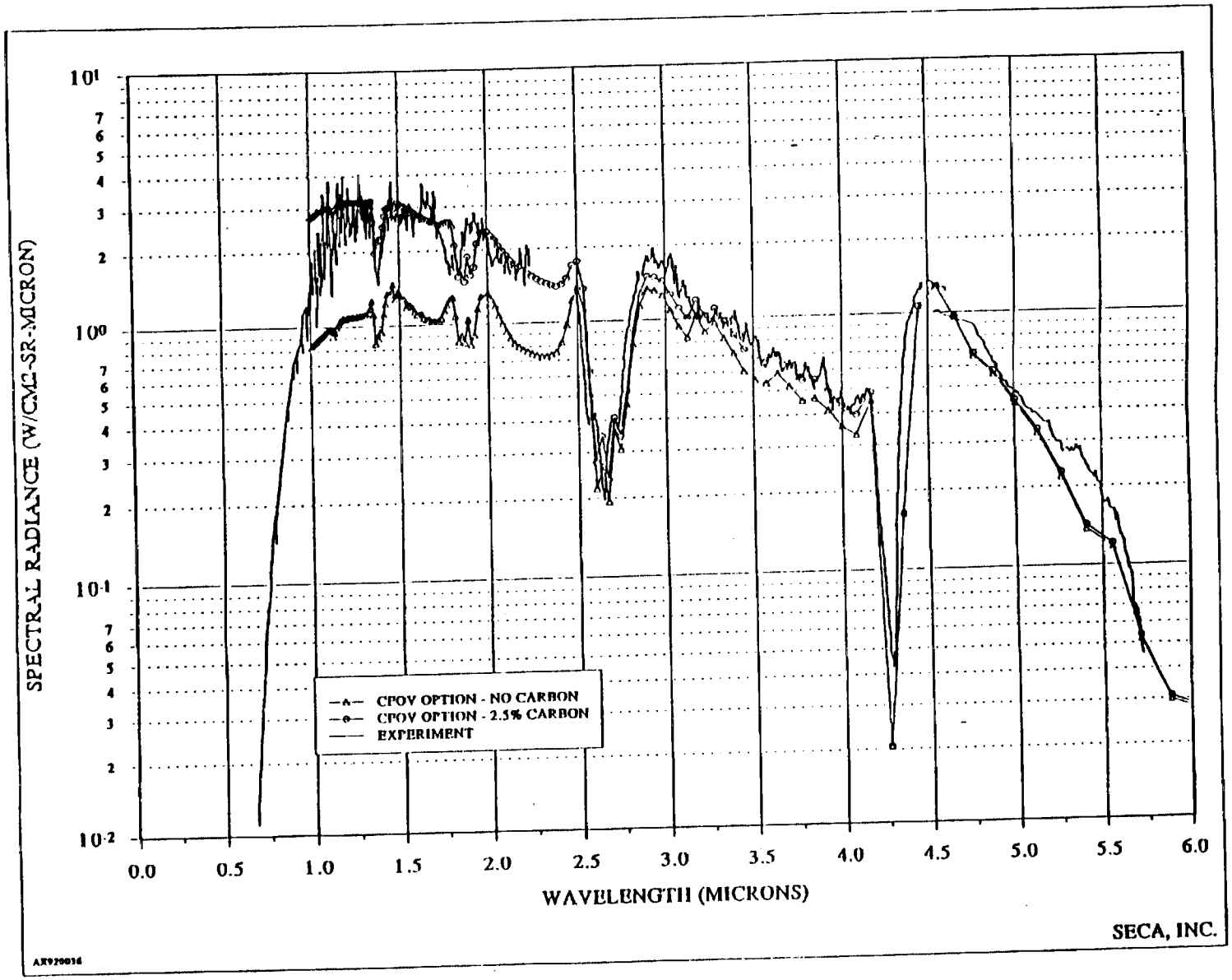

RSRM48-1 SIRRM-II Predicted Plume Radiance at X/R_j = 2.24

TRENDS IN Al_2O_3 PARTICLE SIZE FOR SRM

(from Netzer's experiments)

- Chamber near propellant surface - 130 μm
- Chamber at nozzle entrance - 4-17 μm
- Converging Nozzle Section - particles breakup
- Diverging Nozzle Section - particles agglomerate
- Plume Nearfield - multi-modal PSD w/large particles near centerline
- Plume Farfield - small particles

PRESENT PLUME RADIATION METHODOLOGY

- Flowfields - Standard Axisymmetric Models (RAMP2, SPF/2, SPF/3)
- Radiation - SIRRM, Reverse Monte Carlo
- Particle Size Based on MNASA 48" Measurements of Sambamurthi
- Improve Particle-Gas Heat Transfer Method of Moylan

RADIATION/CONVECTION COUPLING

Transport Equation Solver: the FDNS-EL Code

Energy Equation contains:

$$\nabla \cdot \vec{q}_r = \int_0^\infty \kappa_\lambda [4\pi I_{\lambda b}\{T\} - \int_{4\pi} I_\lambda \{\vec{r},\ \vec{\Omega}\} d\,\vec{\Omega}] d\lambda$$

The last term in this equation requires an evaluation of the intensity in all directions at each point in the flowfield.

The intensity is obtained from the Radiative Transfer Equation (RTE):

$$\vec{\Omega} \cdot \nabla I_\lambda \{\vec{r},\ \vec{\Omega}\} = \kappa_\lambda\, I_{\lambda b}\{T\} - (\kappa_\lambda + \sigma_\lambda) I_\lambda \{\vec{r}, \vec{\Omega}\}$$

$$+ \frac{\sigma_\lambda}{4\pi} \int_{4\pi} P\{\vec{r},\ \vec{\Omega}' - \vec{\Omega}\} I_\lambda \{\vec{r},\ \vec{\Omega}'\}\, d\Omega'$$

FORMAL SOLUTION TO RTE

$$I\{\vec{r},\ \vec{\Omega}\} = I\{\vec{r}',\ \vec{\Omega}\}\ e^{-\tau}$$

$$+ \int_{o}^{\tau} e^{-\kappa t} \left[\kappa I_b\{\vec{r}\} + \frac{\sigma}{4\pi} \int_{4\pi} I\{\vec{r},\ \vec{\Omega}\}\ P\{\vec{r},\ \vec{\Omega}' - \vec{\Omega}\} d\vec{\Omega}' \right] dt$$

(Subscript λ is suppressed for clarity, but intensity is still monochromatic)

Solutions have been obtained by:

- **the PIM method** (Tan)
  - numerical evaluation of the integral terms.
- **the YIX method** (Tan & Howell)
  - uses piecewise-constant interpolation and stores intermediate integral evaluations to improve the PIM method.

SOLUTIONS TO THE RTE USING SPHERICAL HARMONICS

(P_N - Approximation)

The P_1 - Approximation (ODA) requires solutions of PDE's to evaluate the integrated form of the RTE rather than integral equations:

1. Express the intensity as a generalized Fourier Series using Legendre Polynomials.

2. Express the Phase Function with Legendre Polynominals

$$P\{\vec{r},\ \vec{\Omega}'-\vec{\Omega}\} = 1+A_1\,\vec{r}\cdot(\vec{\Omega}'-\vec{\Omega})$$

Requires solution to:

$$\nabla_\tau \cdot \left(\frac{1}{(1-A_1\omega/3)}\nabla_\tau G\right) = -3(1-\omega)(4\pi I_b - G)$$

If $A_1\omega$ is constant, this is an elliptic PDE. When solved,

$$\vec{q} = -\left(\frac{1}{3-A_1\omega}\right)\nabla_\tau G$$

G is incident radiation at a point

$$G\{r\} = \int_{4\pi} I\{\vec{r},\ \vec{\Omega}'\}\,d\Omega'$$

$$I\{\vec{r},\ \vec{\Omega}\} = \frac{1}{4\pi}[G\{\vec{r}\} + 3\vec{q}\{\vec{r}\}\cdot\vec{\Omega}]$$

Limitation: For N=1 or 3, accurate for only optically thick media.

THE MODIFIED DIFFERENTIAL APPROXIMATION

The MDA generalizes P_1 solution to treat arbitrary optical thickness.

Let surface & media contribute to intensity:

$$I\{\vec{r},\ \vec{s}\} = I_w\{\vec{r},\ \vec{s}\} + I_m\{\vec{r},\ \vec{s}\}$$

Solution requires evolution of:

$$G_w\{\vec{r}\} = \frac{1}{\pi}\int_{4\pi} J_w\{\vec{r}_w\}\, e^{-\tau_s}\, d\Omega$$

$$\vec{q}_w\{\vec{r}\} = \frac{1}{\pi}\int_{4\pi} J_w\{\vec{r}_w\}\, e^{-\tau_s}\, \vec{s}\, d\Omega$$

$$J_i = \epsilon_i\, \pi I_{bi} + (1-\epsilon_i)\sum_{j=1}^{N} J_i e^{-\tau_{ij}} F_{i\to j}$$

$$\nabla_\tau\, G_m = A_1\, \omega\, (\vec{q}_w + \vec{q}_m) - 3\, \vec{q}_m$$

$$\nabla_\tau \cdot \vec{q}_m = (1-\omega) 4\pi I_b + \omega\, (G_w + G_m) - G_m$$

THE IMPROVED DIFFERENTIAL APPROXIMATION

The IDA has the same solution features as the MDA but is more computationally efficient.

Solution requires:

The ODA, i.e. the P_1 solution, and also:

$$J_w\{\vec{r}\} = \epsilon\pi I_{bw}\{\vec{r}\} + (1-\epsilon)\int_A \left[J_w\{\vec{r}'\}e^{-\tau_s} + \pi S^*\{\vec{r}-s_o\hat{s},\ \hat{s}\}(1-e^{\tau_s})\right]\frac{\cos\theta\cos\theta'}{\pi S^2}dA$$

$$G\{\vec{r}\} = \int_A [J_w\{\vec{r}'\}e^{-\tau_s} + \pi S^*\{\vec{r}-s_o\hat{s},\ \hat{s}\}(1-e^{-\tau_s})\frac{\cos\theta' dA}{\pi S^2}$$

$$q\{\vec{r}\} = \int_A [J_w\{\vec{r}'\}e^{-\tau_s} + \pi S^*\{\vec{r}-s_o\hat{s},\ \hat{s}\}(1-e^{-\tau_s})]\,\hat{s}\,\frac{\cos\theta' dA}{\pi S^2}$$

SOLUTIONS TO THE RTE USING THE METHOD OF DISCRETE COORDINATES

Solves a number of LOS's to obtain:

$$G\{\vec{r}\} = \sum_{i=1}^{n} w_i I_i\{\vec{r}\}$$

$$\vec{q}\{\vec{r}\} = \sum_{i=1}^{n} w_i I_i\{\vec{r}\}\vec{s}_i$$

w_i's are weighting functions which must sum to the surface of a unit sphere.

Radiation/convection coupled solution has been reported for a 2-D sooty, ethylene flame in which 12 LOS's were used to evaluate each grid point (Kaplan, NRL)

CONCLUSIONS

1. For H_2/O_2 motors -
   - use narrow band models for H_2O
   - within chamber use $\epsilon = 0.95$ between 1-4μm

2. For SRM motors -
   - use narrow band models for CO_2 & H_2O
   - use linear anisotropic scattering model for Al_2O_3 particles
   - within chamber use $\epsilon = 0.97$ between 0.6-8μm

3. For HC/O_2 motors -
   - reasonable prediction of soot concentration is needed

4. Radiation/convection coupling
   - use FDNS (or FDNS-EL) for flowfield
   - use ODA in chamber & converging nozzle
   - use IDA in diverging nozzle & plume

IGES TRANSFORMER AND NURBS IN GRID GENERATION

by
TZU-YI YU , Bharat K. Soni
NSF/ERC For Computational Field Simulation
Mississippi State University, MS39762

ABSTRACT

In the field of Grid Generation and the CAD/CAM , there are numerous geometry output formats which require the designer to spend a great deal of time manipulating geometrical entities in order to achieve a useful sculptured geometrical description for grid generation. Also in this process , there is a danger of loosing fidelity of the geometry under consideration. This stresses the importance of a standard geometry definition for the communication link between varing CAD/CAM and grid system . The IGES (Initial Graphics Exchange Specification) (Ref1) file is a widely used communication between CAD/CAM and the analysis tools . The scientists at NASA Research Centers - including NASA Ames,NASA Langley, NASA Lewis and NASA Marshall - have recognized this importance and therefore, in 1992 they formed the committee of the "NASA-IGES" which is the subset of the standard IGES . This committee stresses the importance and encourage the CFD community to use the standard IGES file for the interface between the CAD/CAM and CFD analysis . Also two of the IGES entities -- the NURBS Curve (Entity 126) and NURBS Surface (Entity 128) -- which have many useful geometric properties -- like the convex hull property , local control property and affine invariance, also widely utilized analytical geometries can be accurately represented using NURBS. This is improtant in today grid generation tools because of the emphasis of the interactive design.

To satisfy the geometry transformation between the CAD/CAM system and Grid Generation field , the CAGI-- Computer Aided Geometry Design is developed , which include the Geometry Transformation , Geometry Manipulation and Geometry Generation as well as the user interface . A self explanatory pictorial views of CAGI modules and links is shown in Figure 1 .

This paper will present the successful development IGES file transformer and application of NURBS definition (Ref 3) in the grid generation (Ref 4,5) .

IGES TRANSFORMER AND NURBS

IN

GRID GENERATION

1022

Graduate Student : Tzu – Yi YU

Advisor : Dr. Bharat K. Soni

Sponsor :NASA/Marshall Space Flight Center

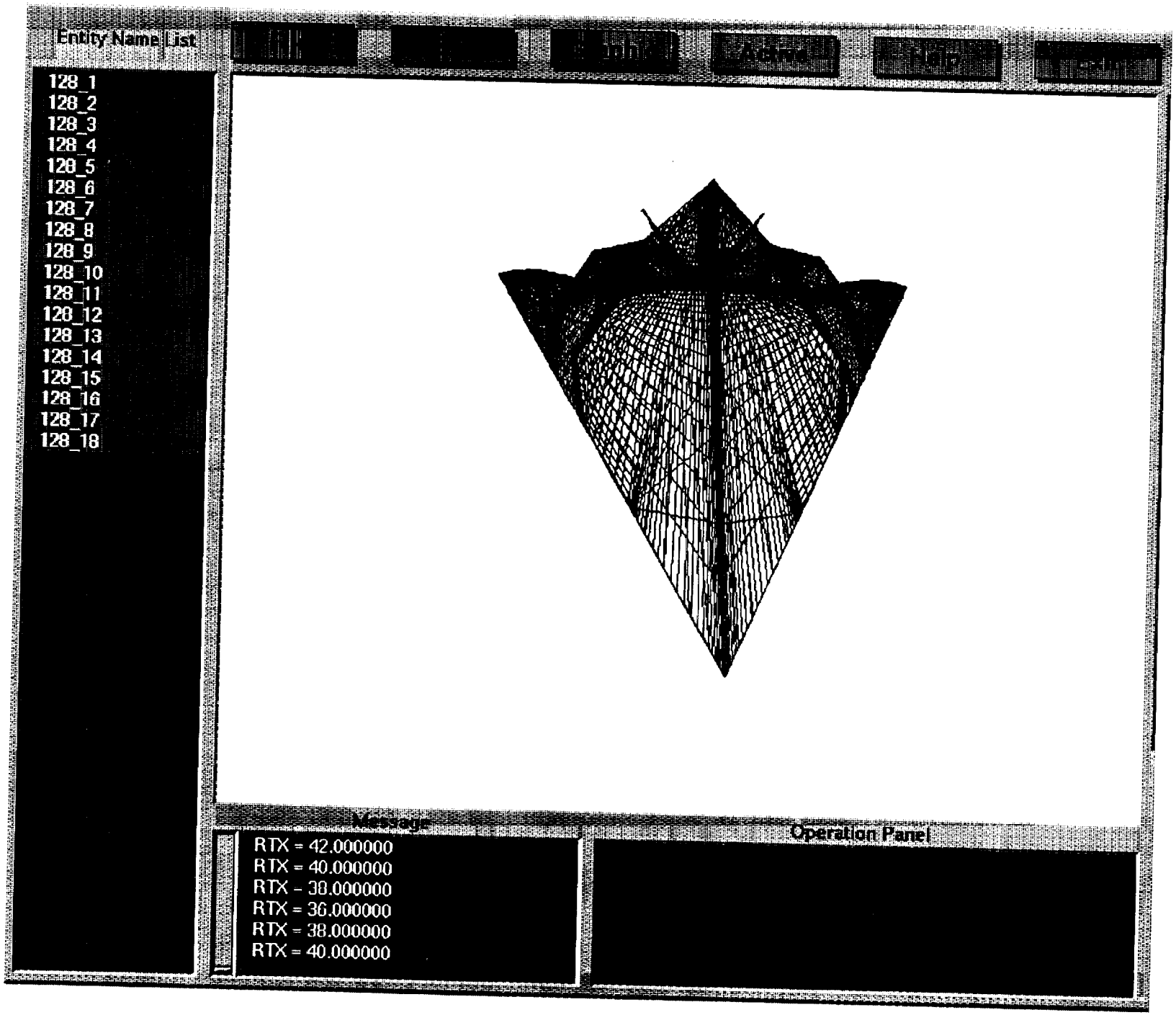
Entity Name List
128_1
128_2
128_3
128_4
128_5
128_6
128_7
128_8
128_9
128_10
128_11
128_12
128_13
128_14
128_15
128_16
128_17
128_18
Message
RTX = 42.000000
RTX = 40.000000
RTX = 38.000000
RTX = 36.000000
RTX = 38.000000
RTX = 40.000000
Operation Panel

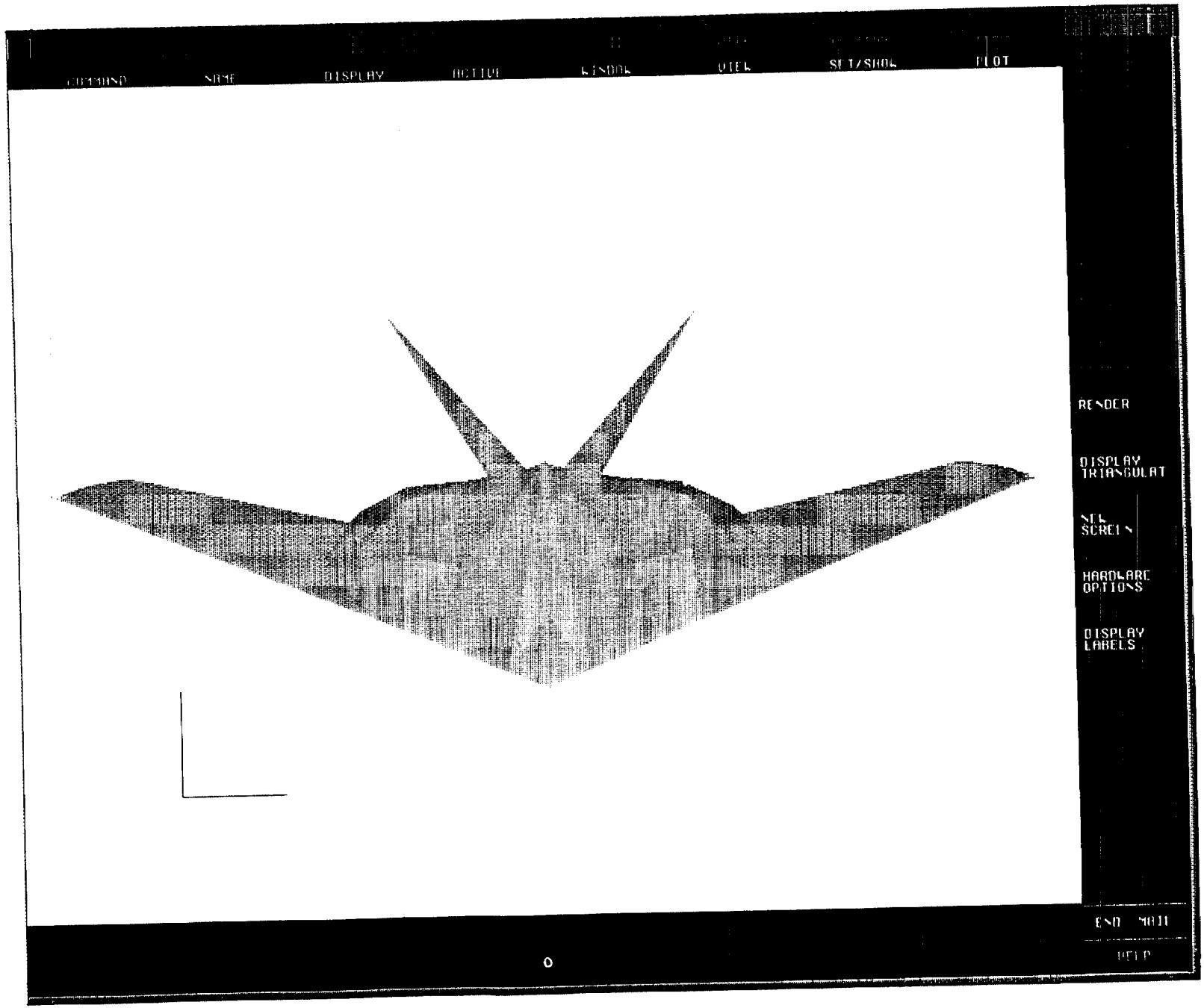
COMMAND
NAME
DISPLAY
ACTIVE
WINDOW
VIEW
SET/SHOW
PLOT
RENDER
DISPLAY TRIANGULAT
SEE SCREEN
HARDWARE OPTIONS
DISPLAY LABELS
END MAIN
HELP
0

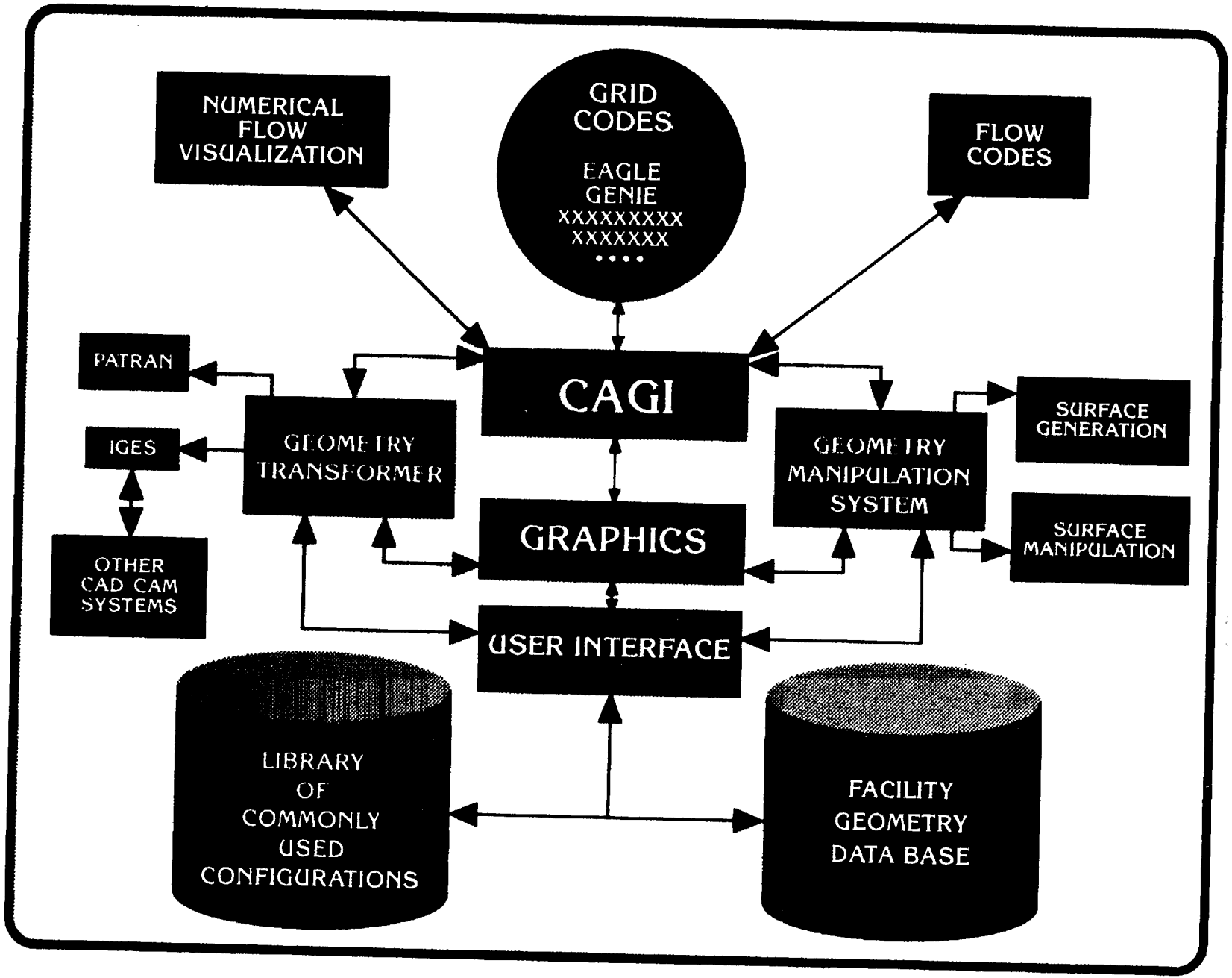
NUMERICAL FLOW VISUALIZATION
GRID CODES
EAGLE
GENIE
XXXXXXXXX
XXXXXXX
• • • •
FLOW CODES
PATRAN
IGES
OTHER CAD CAM SYSTEMS
GEOMETRY TRANSFORMER
CAGI
GRAPHICS
USER INTERFACE
GEOMETRY MANIPULATION SYSTEM
SURFACE GENERATION
SURFACE MANIPULATION
LIBRARY OF COMMONLY USED CONFIGURATIONS
FACILITY GEOMETRY DATA BASE

MOTIVATION :

- Follow the National Standard and set the communication between CAD/CAM and the Grid Generation Tools
- Apply the NURBS definition to Grid Generation

STRATEGY :

- Develop the integrated computer program — CAGI : Computer Aided Grid Interface

WHY IGES ?

. . . IGES - - ->

Initial Graphics Exchange Specification

. . . . . National Standard

. . . . . All-inclusive

NASA IGES

Entity Type Number	Entype Type	CAGI	NASA-IGES
100	Circular Arc	*	**
102	Composite Curve	*	**
104	Conic Arc	*	**
106	Copious Data	*	**
108	Plane	*	**
110	Line	*	**
112	Parametric Spline Curve	*	
114	Parametric Spline Surface	*	
116	Point	*	**
118	Ruled Surface	*	
120	Surface of Revolution	*	
122	Tabulated Cylinder	*	
124	Transformation Matrix	*	**
125	Flash		
126	Rational B-Spline Curve	*	**
128	Rational B-Spline Surface	*	**
130	Offset Curve		
140	Offset Surface		
141	Boundary		**
142	Curve on a Parametric Surface		**
143	Bounded Surface		**
144	Trimmed Parametric Surface		

Entity Type Number	Entype Type	CAGI NURB	NASA-NURB-ONLY
100	Circular Arc	*	
102	Composite Curve		**
104	Conic Arc	*	
106	Copious Data		
108	Plane		
110	Line	*	
112	Parametric Spline Curve	*	
114	Parametric Spline Surface	*	
116	Point		
118	Ruled Surface		
120	Surface of Revolution	*	
122	Tabulated Cylinder		
124	Transformation Matrix	*	**
125	Flash		
126	Rational B-Spline Curve	*	**
128	Rational B-Spline Surface	*	**
130	Offset Curve		
140	Offset Surface		
141	Boundary		**
142	Curve on a Parametric Surface	*	**
143	Bounded Surface		**
144	Trimmed Parametric Surface		

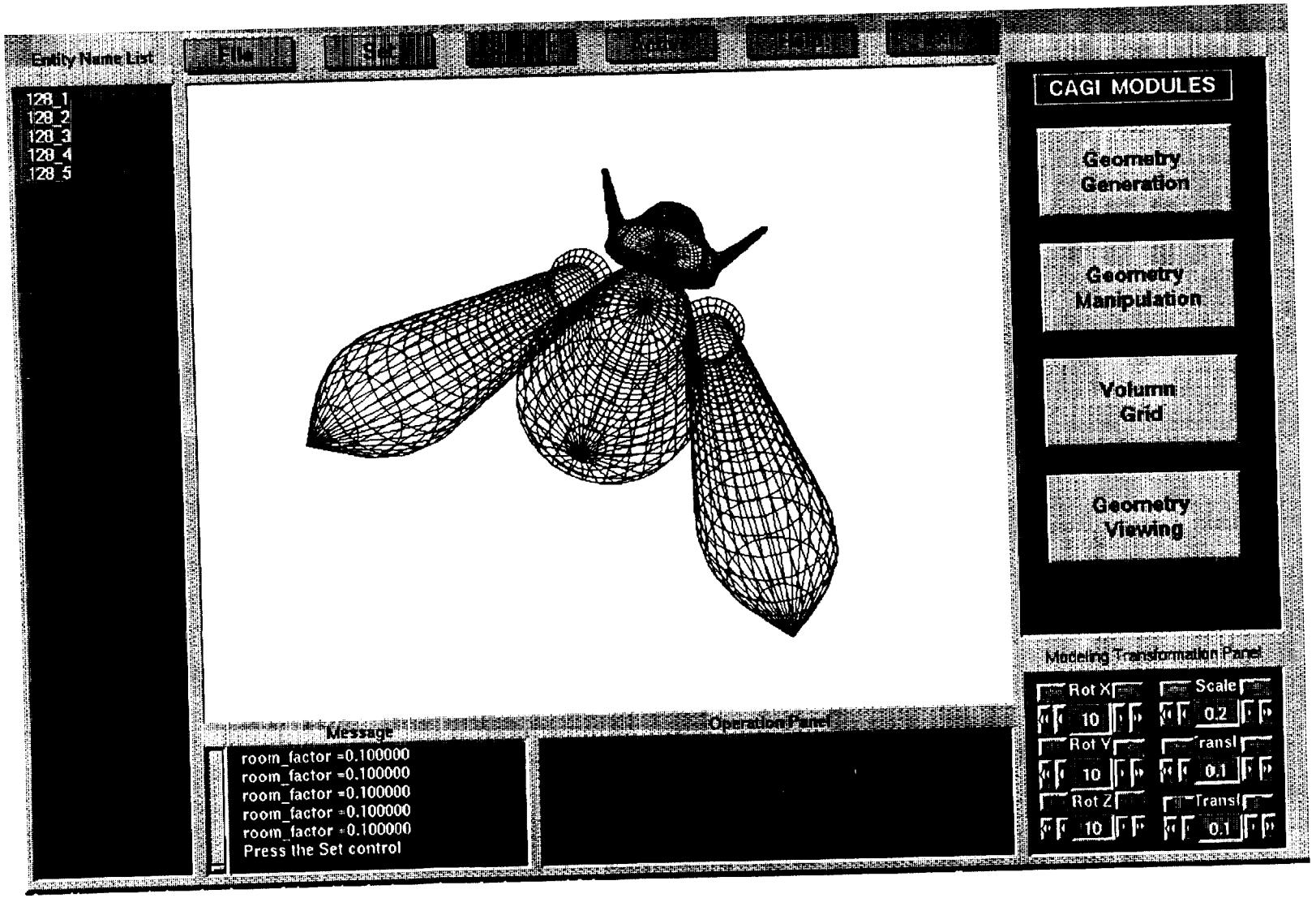
Entity Name List
128_1
128_2
128_3
128_4
128_5
CAGI MODULES
Geomatry Generation
Geometry Manipulation
Volumn Grid
Geometry Viewing
Modeling Transformation Panel
Rot X
10
Rot Y
10
Rot Z
10
Scale
0.2
Transl
0.1
Transl
0.1
Message
room_factor =0.100000
room_factor =0.100000
room_factor =0.100000
room_factor =0.100000
room_factor =0.100000
Press the Set control
Operation Panel

CAGI MODULES
Wing_sur.1
Body_sur.1
Strut_sur.1
Strut_sur.2
Prim_sur.1
Prim_sur.2
Cowl_sur.1
Cowl_sur.2
Scale
Transl
Transl
0.0
0.0
0.0
CAGI has been set up
Reading IAT IGES
Translate IGES file Complete

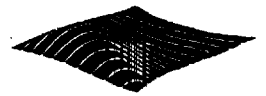

Geometry Generation :

- Point , Line , Parametric Curve , Bezier Curve

  NURBS Curve

  TFI , NURBS Surface , Bezier Surface

  Surface of Revolution

Geometry Manipulation :

- Picking , Changing the definition of NURBS

  Redistuibute the existing geometry

Geometry Generation :

- Point , Line , Parametric Curve , Bezier Curve
  NURBS Curve

  TFI , NURBS Surface , Bezier Surface

  Surface of Revolution

Geometry Manipulation :

- Picking , Changing the definition of NURBS

  Redistuibute the existing geometry

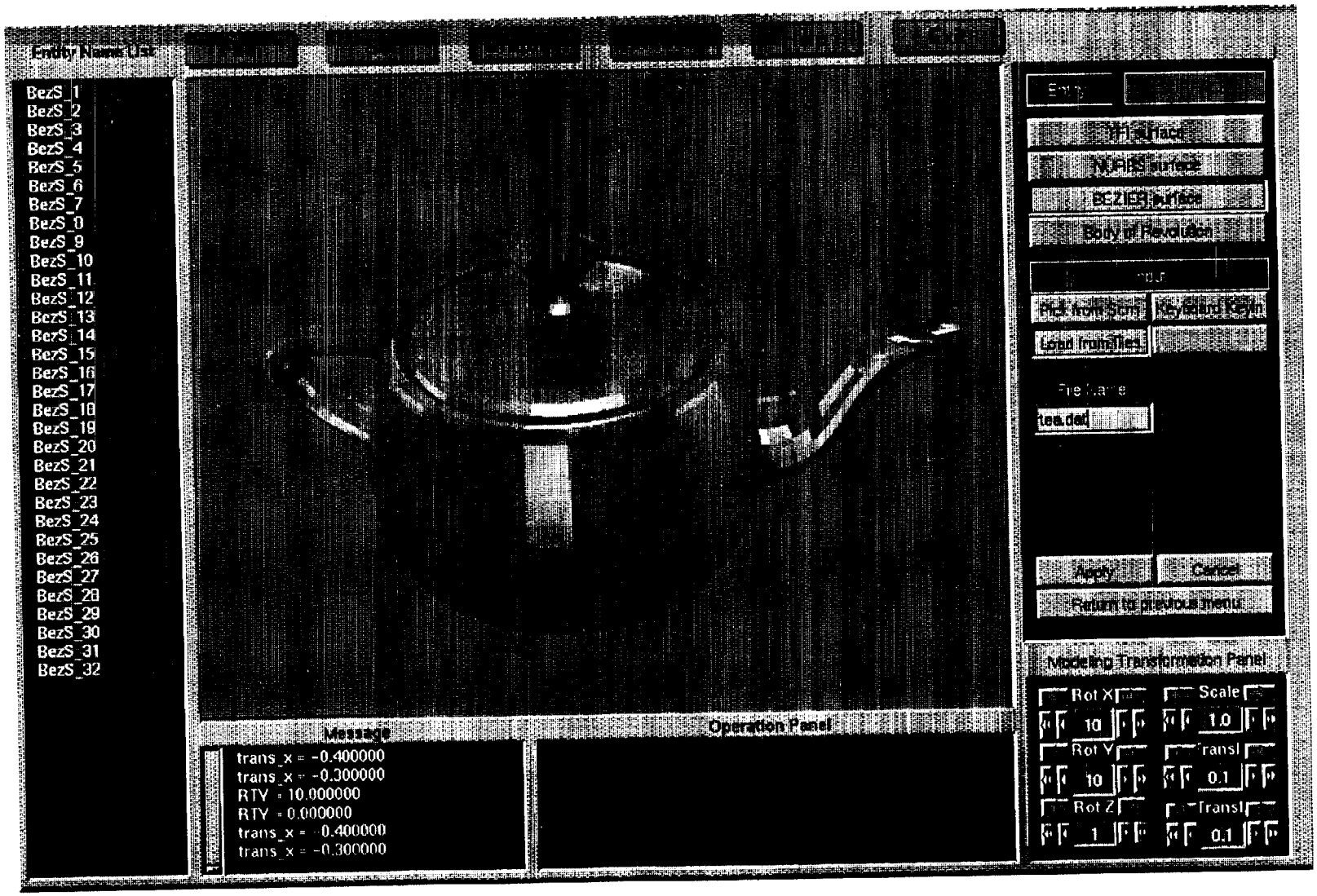
BezS_1
BezS_2
BezS_3
BezS_4
BezS_5
BezS_6
BezS_7
BezS_8
BezS_9
BezS_10
BezS_11
BezS_12
BezS_13
BezS_14
BezS_15
BezS_16
BezS_17
BezS_18
BezS_19
BezS_20
BezS_21
BezS_22
BezS_23
BezS_24
BezS_25
BezS_26
BezS_27
BezS_28
BezS_29
BezS_30
BezS_31
BezS_32
Operation Panel
trans_x = -0.400000
trans_x = -0.300000
RTV = 10.000000
RTV = 0.000000
trans_x = -0.400000
trans_x = -0.300000
Modeling Transformation Panel
Rot X
10
Scale
1.0
Rot Y
10
Transl
0.1
Rot Z
1
Transl
0.1

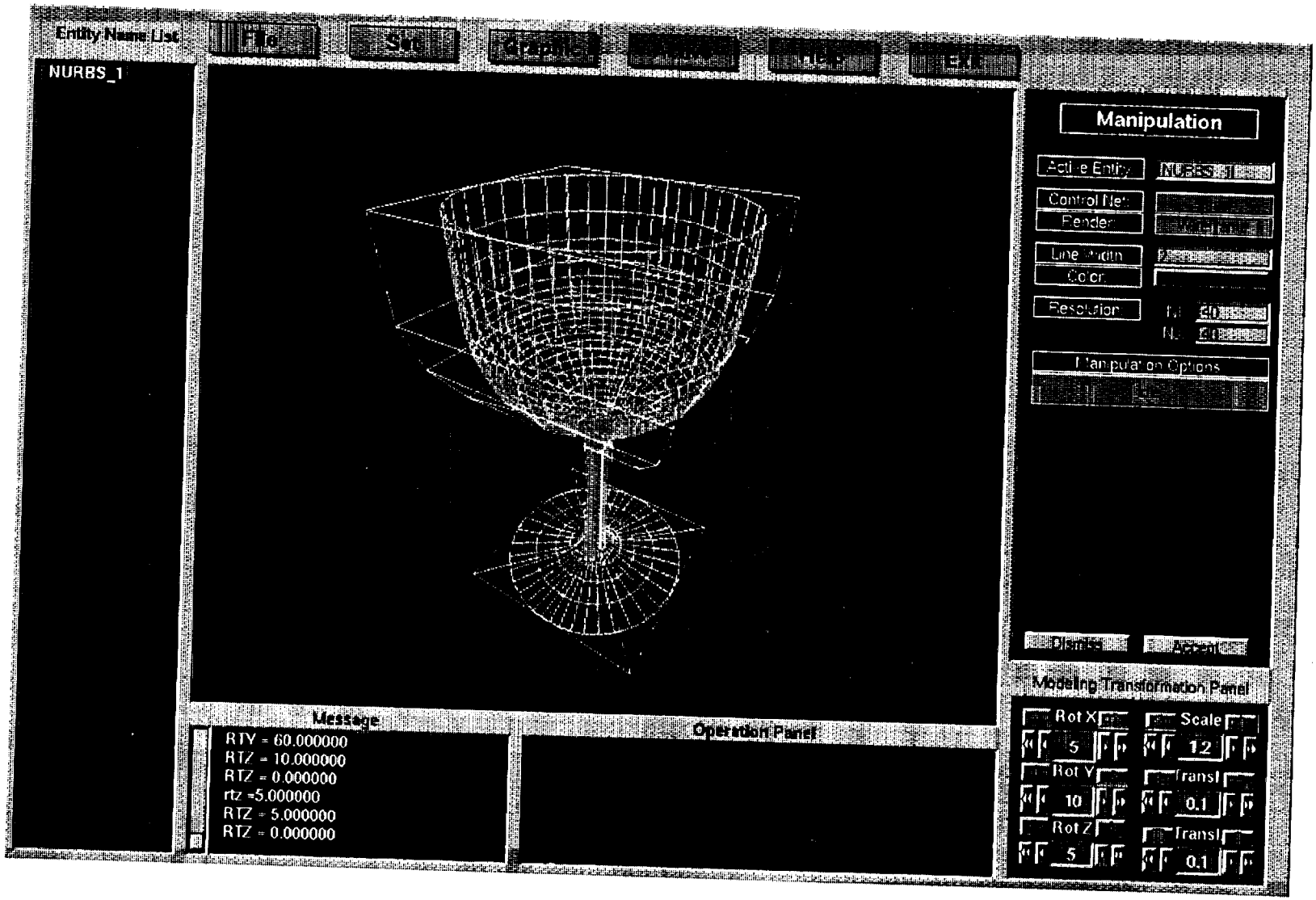
Entity Name List
File
Edit
NURBS_1
Manipulation
Active Entity
Control Net
Render
Line Width
Color
Resolution
Manipulation Options
Dismiss
Accept
Modeling Transformation Panel
Rot X
5
Rot Y
10
Rot Z
5
Scale
12
Transl
0.1
Transl
0.1
Message
RTY = 60.000000
RTZ = 10.000000
RTZ = 0.000000
rtz =5.000000
RTZ = 5.000000
RTZ = 0.000000
Operation Panel

• NURBS Curve

> Entity type = 126

$$C(t) = \frac{\sum_{i=0}^{K} W(i)P(i)b_i(t)}{\sum_{i=0}^{K} W(i)b_i(t)}$$

W(i) : the weights

P(i) : the control points

b_i (t) : the basis functions

$$b_{i,k}(t) = \frac{(t - T(i))b_{i,k-1}(t)}{T(i+k-1) - T(i)} + \frac{(T(i+k) - t)b_{i+1,k-1}(t)}{T(i+k) - T(i+1)}$$

where subscript k is the order of the curve

and $b_{i,1}(t) = 1$ if $T(i) \le t < T(i+1)$

$= 0$ otherwise

$M = k - 1$, $N = K - M + 1$

knot sequence :

T(-M) .... T(0) .... T(N+M)

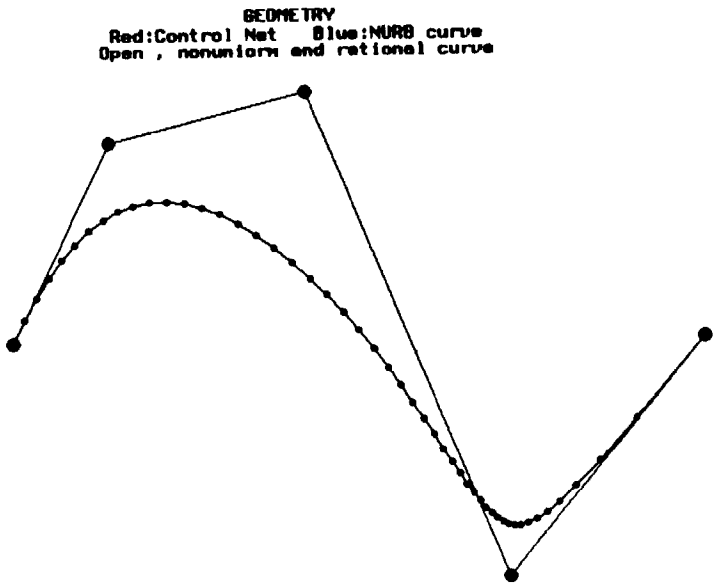
GEOMETRY
Red:Control Net Blue:NURB curve
Open , nonuniform and rational curve

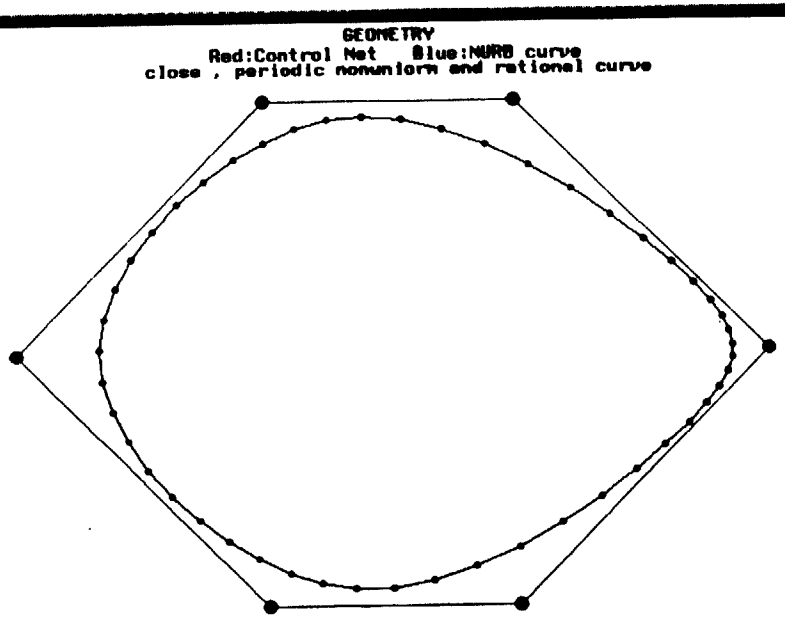
GEOMETRY
Red:Control Net Blue:NURB curve
close , periodic nonuniform and rational curve

• NURBS Surface

> Entity type = 128

$$S(s,t) = \frac{\sum_{i=0}^{K1}\sum_{j=0}^{K2} W(i,j)P(i,j)b_i(s)b_j(t)}{\sum_{i=0}^{K1}\sum_{j=0}^{K2} W(i,j)b_i(s)b_j(t)}$$

W(i,j) = weights

P(i,j) = control points

$b_i(s)$, $b_j(t)$: the basis functions in

$$b_{i,k1}(s) = \frac{(s - S(i))b_{i,k1-1}(s)}{S(i+k1-1) - S(i)} + \frac{(S(i+k1) - s)b_{i+1,k1-1}(s)}{S(i+k1) - S(i+1)}$$

M1 = k1 –1 , N1 = K1–M1+1

where *k1* is the order of the surface in I direction

and $b_{i,1}(s)$ = 1 if $S(i) \le s < S(i+1)$

= 0 otherwise

knot sequence :

S(-M1) . . .S(0) . . . S(N1+M1)

$$b_{i,k2}(t) = \frac{(t - T(i))b_{i,k2-1}(t)}{T(i+k2-1) - T(i)} + \frac{(T(i+k2) - t)b_{i+1,k2-1}(t)}{T(i+k2) - T(i+1)}$$

M2 = *k2* – 1 , N2 = K2 – M2 +1

where *k2* is the order of the surface in J direction

and $b_{i,1}(t)$ = 1 if $T(i) \le t < T(i+1)$

= 0 otherwise

knot sequence :

T(-M2) . . . T(0) . . . T(N2+M2)

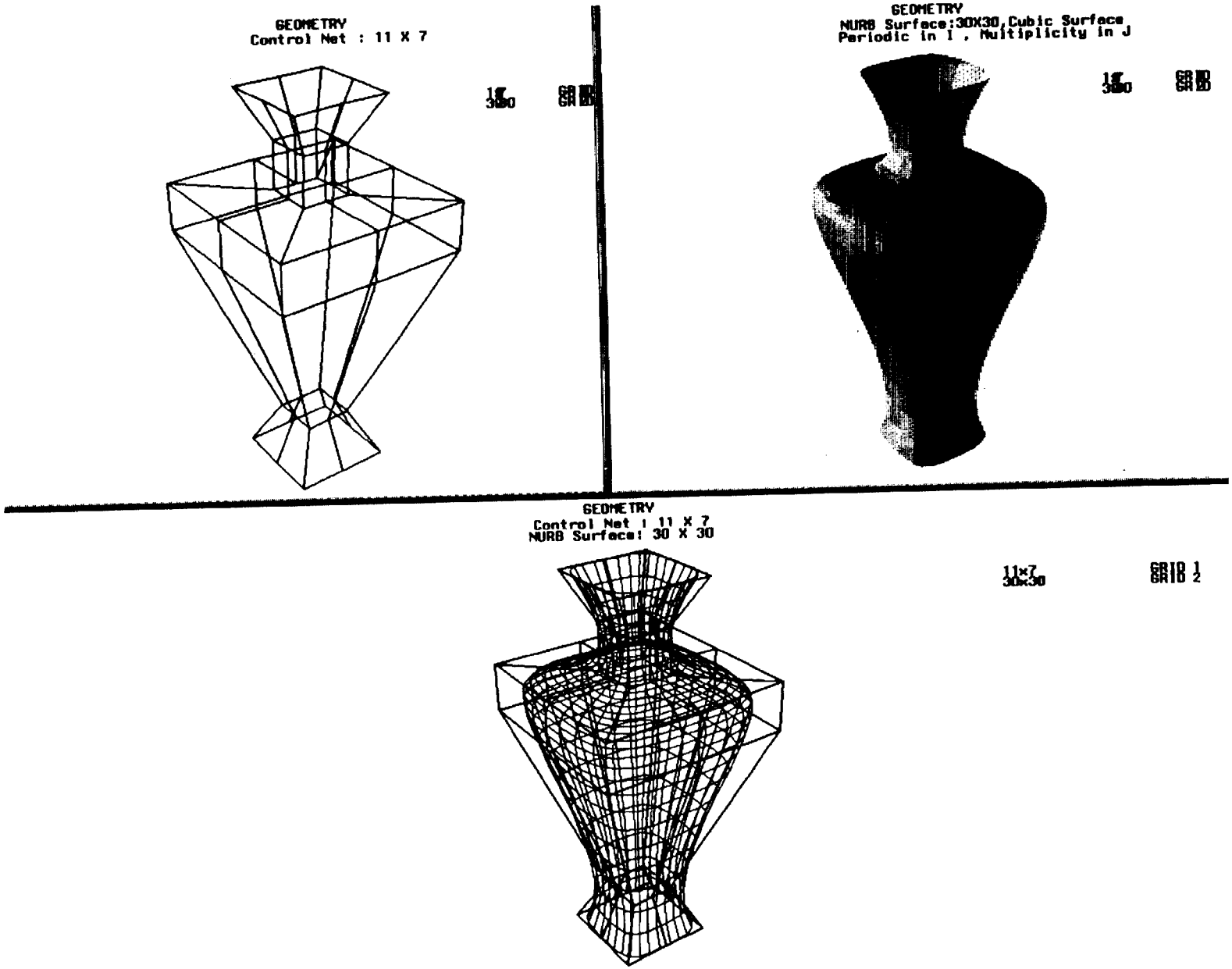
GEOMETRY
Control Net : 11 X 7
GEOMETRY
NURB Surface:30X30,Cubic Surface
Periodic in I , Multiplicity in J
GEOMETRY
Control Net : 11 X 7
NURB Surface: 30 X 30
11x7
30x30
GRID 1
GRID 2

• NURBS Volume

$$V(s,t,w) = \frac{\sum_{i=0}^{K1}\sum_{j=0}^{K2}\sum_{k=0}^{K3} W(i,j,k)P(i,j,k)b_i(s)b_j(t)b_k(u)}{\sum_{i=0}^{K1}\sum_{j=0}^{K2}\sum_{k=0}^{K3} W(i,j,k)b_i(s)b_j(t)b_k(u)}$$

W(i,j,k) = the weights of the control volume

P(i,j,k) = the control points of the volume

$b_i(s), b_j(t), b_k(u)$: the basis functions in I J K direction

$$b_{i,k1}(s) = \frac{(s - S(i))b_{i,k1-1}(s)}{S(i+k1-1) - S(i)} + \frac{(S(i+k1) - s)b_{i+1,k1-1}(s)}{S(i+k1) - S(i+1)}$$

M1 = k1 –1 , N1 = K1–M1+1

where *k1* is the order of the volume in I direction

and $b_{i,1}(s) = 1$ if $S(i) \le s < S(i+1)$

$= 0$ otherwise

knot sequence :

S(–M1) . . .S(0) . . . S(N1+M1)

$$b_{i,k2}(t) = \frac{(t - T(i))b_{i,k2-1}(t)}{T(i+k2-1) - T(i)} + \frac{(T(i+k2) - t)b_{i+1,k2-1}(t)}{T(i+k2) - T(i+1)}$$

M2 = *k2* – 1 , N2 = K2 – M2 +1

where *k2* is the order of the volume in J direction

and $b_{i,1}(t) = 1$ if $T(i) \le t < T(i+1)$

$= 0$ otherwise

knot sequence :

T(–M2) . . . T(0) . . . T(N2+M2)

$$b_{i,k3}(u) = \frac{(u - U(i))b_{i,k3-1}(u)}{U(i+k3-1) - U(i)} + \frac{(U(i+k3) - u)b_{i+1,k3-1}(u)}{U(i+k3) - U(i+1)}$$

M3 = *k3* – 1 , N3 = K3 –M3 + 1

where *k3* is the order of the volume in K direction

and $b_{i,1}(u) = 1$ if $U(i) \le u < U(i+1)$

$= 0$ otherwise

knot sequence :

U(–M3) ... U(0) . . . U(N2+M2)

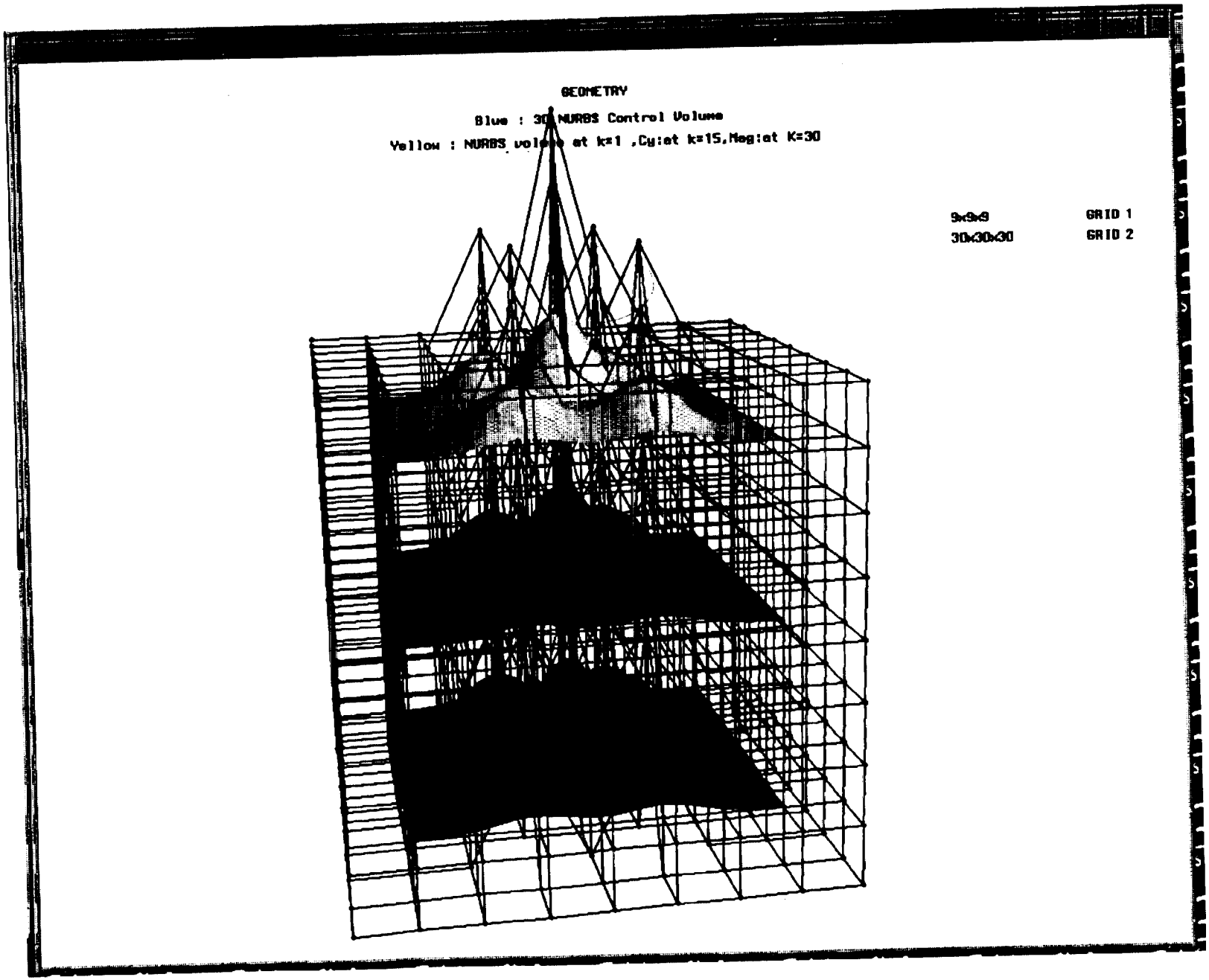
GEOMETRY
Blue : 30 NURBS Control Volume
Yellow : NURBS volume at k=1 ,Cy:at k=15,Mag:at K=30
9x9x9 GRID 1
30x30x30 GRID 2

- **WHY NURBS**
  - **Local control**
  - **stable**
  - **describe the analytic geometry**
  - **flexible and efficient data structure**

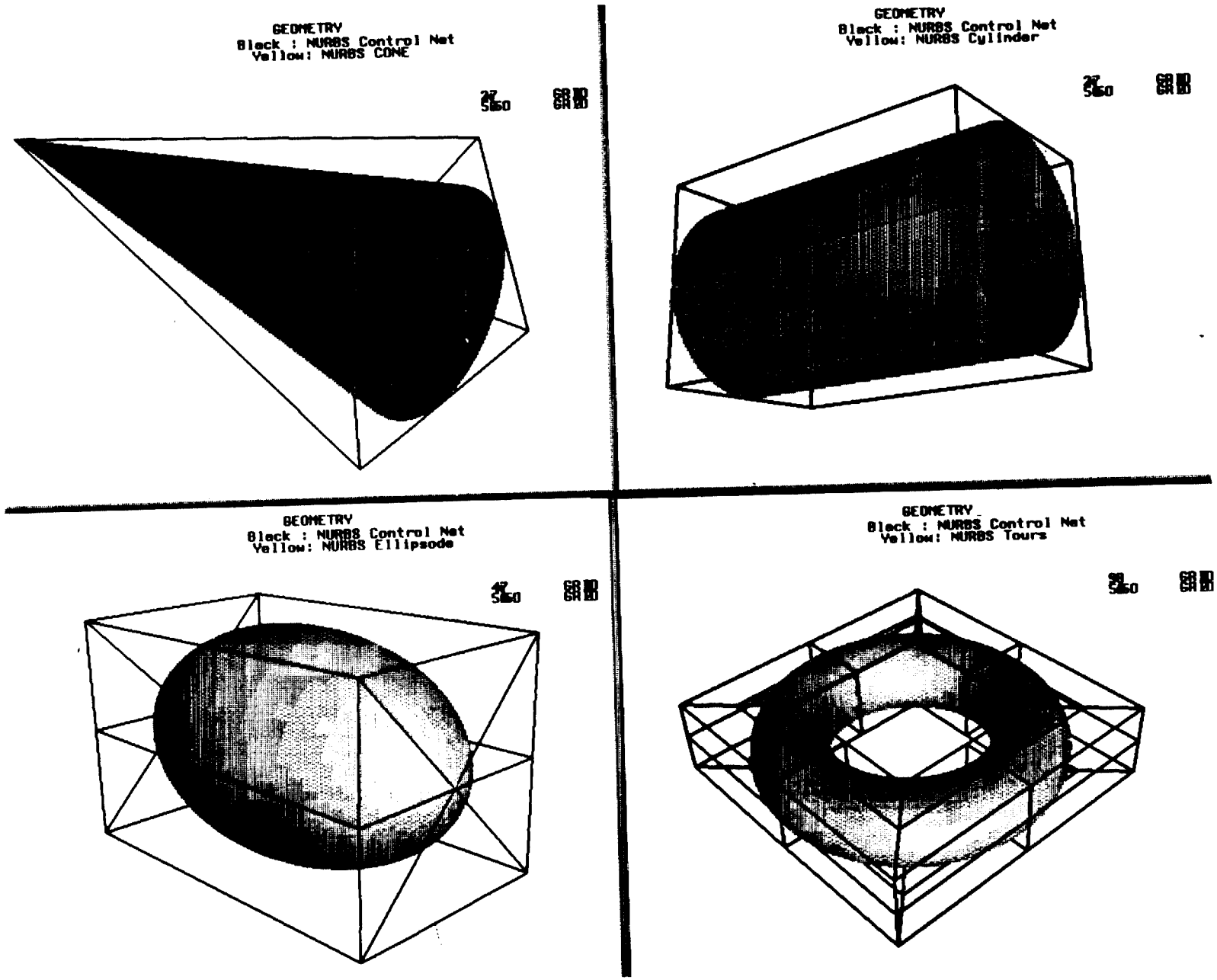
GEOMETRY
Black : NURBS Control Net
Yellow: NURBS CONE
GEOMETRY
Black : NURBS Control Net
Yellow: NURBS Cylinder
GEOMETRY
Black : NURBS Control Net
Yellow: NURBS Ellipsode
GEOMETRY
Black : NURBS Control Net
Yellow: NURBS Tours

GEOMETRY
GEOMETRY
GEOMETRY

• Inverse Approach

>. Given input curve $X_0 , X_1 \ldots .. X_L$
determine the control points $d_{-1} , d_0 , \ldots . d_L$

>. Knot sequence : by chord length or centripetal

$$\begin{bmatrix} 1 & & & & \\ \alpha_1 & \beta_1 & \gamma_1 & & \\ & \alpha_2 & \beta_2 & \gamma_2 & \\ & & \ddots & \ddots & \ddots \\ & & \alpha_{L-1} & \beta_{L-1} & \gamma_{L-1} \\ & & & 0 & 1 \end{bmatrix} \begin{bmatrix} d_0 \\ d_1 \\ d_2 \\ \vdots \\ d_{L-1} \\ d_L \end{bmatrix} = \begin{bmatrix} r_0 \\ r_1 \\ r_2 \\ \vdots \\ r_{L-1} \\ r_L \end{bmatrix}$$

$$\begin{bmatrix} \beta_0 & \gamma_0 & & & \alpha_0 \\ \alpha_1 & \beta_1 & \gamma_1 & & \\ & \alpha_2 & \beta_2 & \gamma_2 & \\ & & \ddots & \ddots & \ddots \\ & & \alpha_{L-2} & \beta_{L-2} & \gamma_{L-2} \\ \gamma_0 & & & \alpha_{L-1} & \beta_{L-1} \end{bmatrix} \begin{bmatrix} d_0 \\ d_1 \\ d_2 \\ \vdots \\ d_{L-2} \\ d_{L-1} \end{bmatrix} = \begin{bmatrix} r_0 \\ r_1 \\ r_2 \\ \vdots \\ r_{L-2} \\ r_{L-1} \end{bmatrix}$$

$$\alpha_i = \frac{\Delta_i^2}{\Delta_{i-2} + \Delta_{i-1} + \Delta_i} \qquad \beta_i = \frac{\Delta_i(\Delta_{i-2} + \Delta_{i-1})}{\Delta_{i-2} + \Delta_{i-1} + \Delta_i} + \frac{\Delta_{i-1}(\Delta_i + \Delta_{i+1})}{\Delta_{i-1} + \Delta_i + \Delta_{i+1}} \qquad \gamma_i = \frac{\Delta_{i-1}^2}{\Delta_{i-1} + \Delta_i + \Delta_{i+1}}$$

r_0 , r_L could be arbitrarily set

$r_i = (\Delta_{i-1} + \Delta_i)x_i$

and we set $\Delta_{-1} = \Delta_L = 0$

$\Delta_{-1} = \Delta_{L-1} , \Delta_{-2} = \Delta_{L-2}$

$r_i = (\Delta_{i-1} + \Delta_i)x_i$

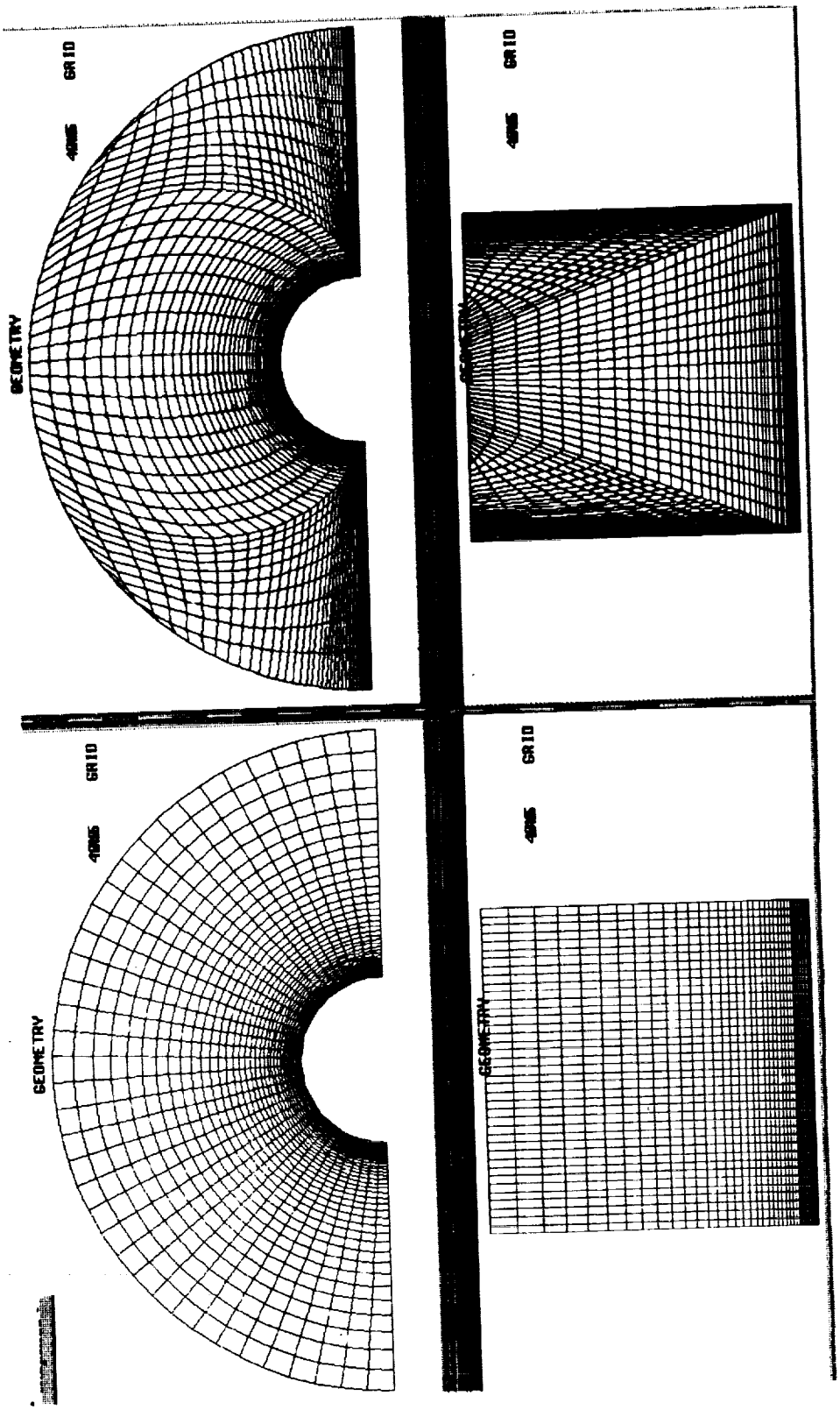

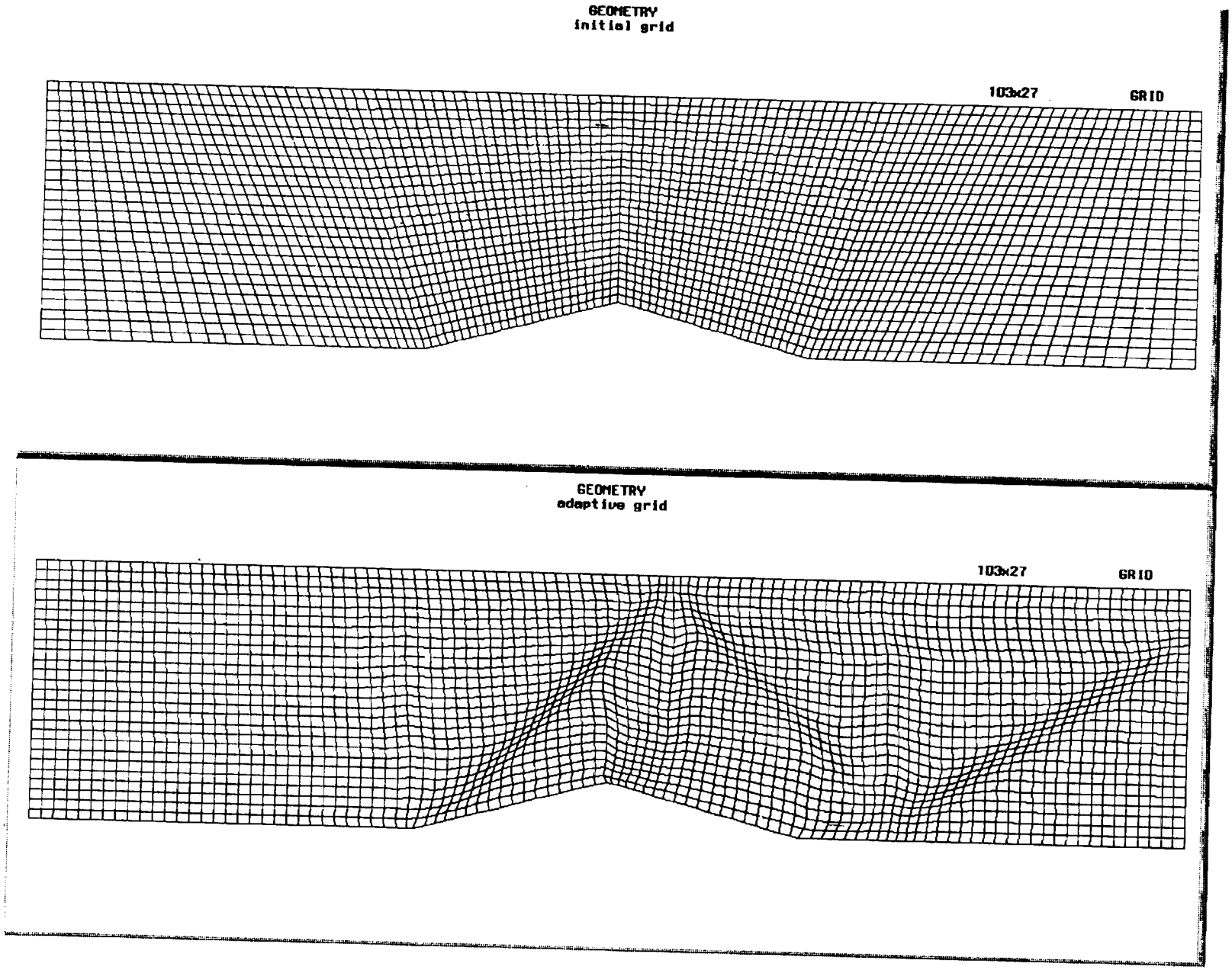
GEOMETRY
initial grid
103x27
GRID
GEOMETRY
adaptive grid
103x27
GRID

Conclusion :

- Importance of Geometry Transformation between different system
- NURBS provide robust Geometry data structure

Future Work :

- Geometry Generation / Manipulation
- IGES Entities with NURBS form

References

1. Initial Graphics Exchange Specification (IGES) Version 5.1 , distributed by the National Computer Graphics Association (NCGA) , Technical Services and Standards , IPO Administrator , 2722 Merrilee Drive , Suite 200, Fairfax, VA 22031.

2. Matthew W. Blake , Project Leader ,"NASA Geometry Specification for Computational Fluid Dynamics (draft)" ,CFD workshop for software System for Surface Modeling and Grid Generation at NASA Langley, April 28 , 1992 .

3. Farin, Gerald, *Curves and Surfaces for Computer Aided Geometric Design : A Practical Guide*, third Edition,

4. Yu,T.Y., "IGES Transformer and NURBS in Grid Generation ", Master's thesis , Mississippi State University, August 1992 .

5. Soni, B. K., "Grid Generation for Internal Flow Configurations", *Journal of Computers and Mathematics with Applications, 1991.*

6. Bartels/Beatty/Barsky:" An Introduction to Splines for the Use in Computer Graphics and Geometric Modeling" Morgan Kaufmann Publishers , 1987 .

7. Yamaguchi:"Curves and Surfaces for Computer Aided Geometric Design" , Springer-Verlag , 1988.

Criteria for Evaluation of Grid Generation Systems

Edward, P. Ascoli, Steven L. Barson, Michele E. DeCroix, and Wayne W. Hsu

Rockwell International, Rocketdyne Division

Workshop for Computational Fluid Dynamic Applications in Rocket Propulsion

April 20-22, 1993
NASA Marshall Space Flight Center

Abstract

Many CFD grid generation systems are in use nationally, but few comparative studies have been performed to quantify their relative merits. A study was undertaken to systematically evaluate and select the best CFD grid generation codes available. Detailed evaluation criteria were established as the basis for the evaluation conducted. Descriptions of thirty four separate criteria, grouped into eight general categories are provided. Benchmark test cases, developed to test basic features of selected codes, are described in detail. Scoring guidelines were generated to establish standards for measuring code capabilities, ensure uniformity of ratings, and minimize personal bias among the three code evaluators. Ten candidate codes were identified from government, industry, universities, and commercial software companies. A three phase evaluation was conducted. In Phase 1, ten codes identified were screened through conversations with code authors and other industry experts. Seven codes were carried forward into a Phase 2 evaluation in which all codes were scored according to the predefined criteria. Two codes emerged as being significantly better than the others; RAGGS and GRIDGEN. Finally, these two codes were carried forward into a Phase 3 evaluation in which complex 3-D multizone grids were generated to verify capability.

CRITERIA FOR EVALUATION OF GRID GENERATION SYSTEMS

Edward P. Ascoli
Steven L. Barson
Michele E. DeCroix
Wayne W. Hsu

Rockwell International, Rocketdyne Division

Workshop for Computational Fluid Dynamic Applications in Rocket Propulsion

April 20-22, 1993
NASA Marshall Space Flight Center

EVALUATION OF GRID GENERATION SYSTEMS

- **BACKGROUND**
  - MANY GRID GENERATION CODES CURRENTLY AVAILABLE
  - VARIOUS SYSTEMS EMPLOY DIFFERENT APPROACHES AND CODE FEATURES
  - NEED EXISTS TO CONDUCT SYSTEMATIC REVIEW OF GRID GENERATION CODES CURRENTLY AVAILABLE

- **OBJECTIVES**
  - IDENTIFY CANDIDATE GRID GENERATION CODES
  - SYSTEMATICALLY EVALUATE IDENTIFIED CODES
  - INTEGRATE BEST CODES WITH ROCKETDYNE ADVANCED COMPUTATIONAL ENGINEERING SYSTEM (RACES) FOR INCREASED PRODUCTIVITY

APPROACH

- **DETAILED EVALUATION CRITERIA ESTABLISHED**
- **BENCHMARK CASES DEVELOPED**
- **SCORING GUIDELINES GENERATED**
- **CANDIDATE CODES IDENTIFIED**
- **THREE PHASE EVALUATION CONDUCTED**
  - PHASE 1 - SCREEN POTENTIAL CODES
  - PHASE 2 - PRELIMINARY EVALUATION
  - PHASE 3 - FINAL EVALUATION

EVALUATION CRITERIA

- **34 SEPARATE CRITERIA DEFINED**

- **GROUPED INTO 8 GENERAL CATEGORIES**
  - GEOMETRY DEFINITION
  - SURFACE / VOLUME GRIDS
  - GRID TYPES SUPPORTED
  - GRID CONTROL
  - USABILITY
  - SUPPORT SERVICES
  - PORTABILITY
  - COSTS

EVALUATION CRITERIA

GEOMETRY DEFINITION

- **GEOMETRY DEFINITION CATEGORY INCLUDES:**
  - ABILITY TO I/O VARIOUS FORMATS (e.g., CAD/CAE VIA DIRECT, IGES, OTHERS)
  - CREATION CAPABILITY WITHIN GRID GENERATION CODE
  - SURFACE ACCURACY (AS CREATED, AS IMPORTED)

- **KEY CRITERIA (HIGHEST WEIGHTING)**
  - IGES INPUT (9/10)
    - POINTS
    - LINES
    - SURFACES
  - INTERNAL GEOMETRY CREATION CAPABILITY (5/10)

1060

EVALUATION CRITERIA

SURFACE / VOLUME GRID

- **SURFACE / VOLUME GRID CATEGORY INCLUDES:**
  - ACCURACY ISSUES
    - CONSTRUCTION OF ENTITIES ON GEOMETRIC SURFACE
    - POINTS ON GEOMETRIC SURFACE
  - RANGE OF METHODOLOGIES AVAILABLE AND THEIR EFFECTIVENESS
    - ALGEBRAIC
    - ELLIPTIC
    - HYPERBOLIC

- **KEY CRITERIA (HIGHEST WEIGHTING)**
  - METHODOLOGIES AVAILABLE
    - ALGEBRAIC (10/10)
    - ELLIPTIC (9/10)

EVALUATION CRITERIA

GRID TYPES SUPPORTED

- **GRID TYPES SUPPORTED CATEGORY INCLUDES:**
  - MULTIZONE
  - PERIODIC
  - H-TYPE
  - C- AND O-TYPES
  - FAN (DEGENERATE CELLS)
  - 2-D AND 3-D

- **KEY CRITERIA (HIGHEST WEIGHTING)**
  - MULTIZONE (10/10)
  - H-TYPE (1010)
  - 2-D AND 3-D (10/10)

EVALUATION CRITERIA

GRID CONTROL

- **GRID CONTROL CATEGORY INCLUDES:**
  - CLUSTERING OPTIONS (e.g., LINEAR, GEOMETRIC, EXPONENTIAL, etc.)
  - LOCAL CONTROL
    - EDITING
    - INTERACTIVE
    - SMOOTHING

- **KEY CRITERION (HIGHEST WEIGHTING)**
  - CLUSTERING (10/10)

EVALUATION CRITERIA

USABILITY

- **USABILITY CATEGORY INCLUDES:**
  - LEARNABILITY
  - USER INTERFACE
  - EASY TO MODIFY (PARAMETRICS)
  - SPECIALIZE (TEMPLATES)
  - SAVE INTERMEDIATE STATE
  - GRID DIAGNOSTICS
  - ERROR HANDLING
  - SIZE LIMITATIONS

- **KEY CRITERIA (HIGHEST WEIGHTING)**
  - USER INTERFACE (10/10)
  - LEARNABILITY (10/10)
  - SAVE INTERMEDIATE STATE (10/10)

EVALUATION CRITERIA

SUPPORT SERVICES

- **SUPPORT SERVICES CATEGORY INCLUDES:**
  - SUPPORT SERVICES AVAILABLE (e.g., DOCUMENTATION, TRAINING, HOT LINE, etc.)
  - SOURCE CODE AVAILABILITY
  - AUTHOR/VENDOR RESPONSIVENESS

- **KEY CRITERIA (HIGHEST WEIGHTING)**
  - SUPPORT SERVICES AVAILABLE (10/10)
  - SOURCE CODE AVAILABILITY (10/10)
  - AUTHOR/VENDOR RESPONSIVENESS (10/10)

EVALUATION CRITERIA

PORTABILITY

- **PORTABILITY CATEGORY INCLUDES:**
  - RANGE OF COMPUTING PLATFORMS SUPPORTED
  - NOTE: ALL CODES EXCEPT PATRAN REQUIRE SGI
    - GL OR OPEN GL
    - FEW OPTIONS

- **KEY CRITERION (HIGHEST WEIGHTING)**
  - PORTABILITY (5/10)
  - NOT A DISTINGUISHING FACTOR

EVALUATION CRITERIA

COSTS

- **COSTS CATEGORY INCLUDES:**
  - SOURCE CODE AND ANNUAL MAINTENANCE
  - TRAINING
  - CONSULTING

- **KEY CRITERION (HIGHEST WEIGHTING)**
  - SOURCE CODE AND ANNUAL MAINTENANCE (10/10)

BENCHMARK CASES DEVELOPED

- **SERIES OF TEST CASES DEVISED TO TEST BASIC CODE FEATURES**
  - MANY SIMPLE CASES
  - ISOLATE SINGLE GRID GENERATION ISSUE
  - TYPICAL OF PROBLEMS ENCOUNTERED DURING CFD GRID GENERATION
  - THREE SETS OF 2-D CASES, ONE SET OF 3-D CASES
- **ALL CODES TESTED THROUGH EXECUTION OF BENCHMARK CASES**
- **AS MANY CASES EXECUTED AS PRACTICAL FOR EACH CODE**
  - CODE LIMITATIONS
  - LIMITED LEARNING VALUE
  - TIME LIMITATIONS

BENCHMARK CASES - SET 1

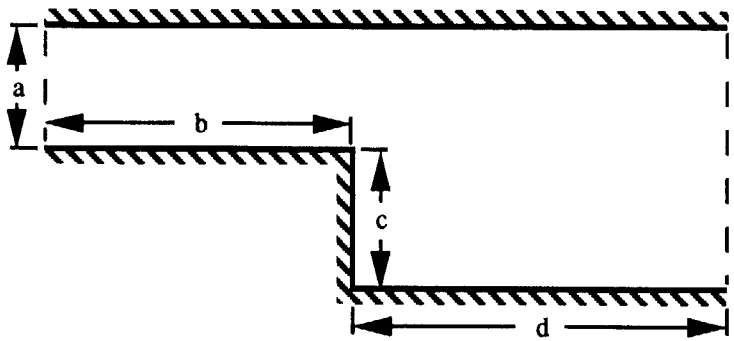

GEOMETRY 1: a=b=c=d=1
GEOMETRY 2: a=0.25, b=c=d=1
GEOMETRY 3: a=b=1, c=4, d=1

SUBSET	GEOMETRY	TOPOLOGY	GRID TYPE	CLUSTERING
A	1, 2, 3	SINGLE ZONE	H	NONE
B	1, 2, 3	SINGLE ZONE	A+ELLIPTIC	NONE
C	1, 2, 3	SINGLE ZONE	H	2-3 OPTIONS
D	1, 2, 3	SINGLE ZONE	A+ELLIPTIC	1 OPTION-FINE GRID
E	1	SINGLE ZONE	H-FAN-H	NONE
F	1	SINGLE ZONE	H-FAN-H	1 OPTION
G	1	MULTI-ZONE	H-H	NONE
H	1	MULTI-ZONE	H-H	ALL OPTIONS
I	1	MULTI-ZONE	E+ELLIPTIC	NONE
J	1	MULTI-ZONE	E+ELLIPTIC	1 OPTION-FINE GRID

BENCHMARK CASES - SET 1 (CONT'D)

TOPOLOGY 1: H-GRID

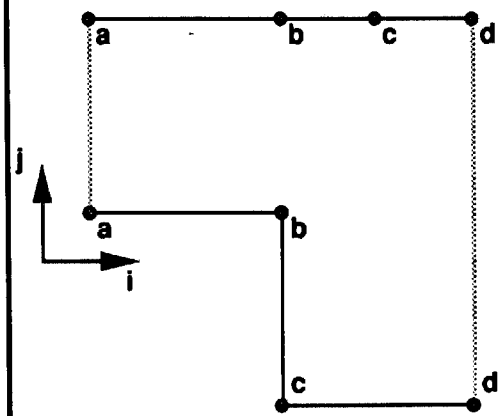

GEOM 1:
imax = 30, jmax = 20+18+20
(1740 grid points)

GEOM 2:
imax = 30, jmax = 20+18+20
(1740 grid points)

GEOM 3:
imax = 30, jmax = 10+38+10
(1740 grid points)

TOPOLOGY 2: H-FAN-H

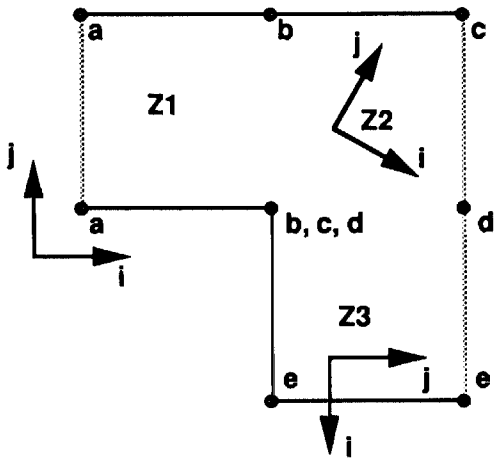

GEOM 1 Z1: imax = 41, jmax = 41
Z2: imax = 41, jmax = 41
Z3: imax = 41, jmax = 41
(5043 grid points)

GEOM 2 Z1: imax = 41, jmax = 11
Z2: imax = 31, jmax = 11
Z3: imax = 41, jmax = 11
(1243 grid points)

GEOM 3 Z1: imax = 41, jmax = 41
Z2: imax = 41, jmax = 41
Z3: imax = 161, jmax = 41
(9963 grid points)

TOPOLOGY 3: H-H

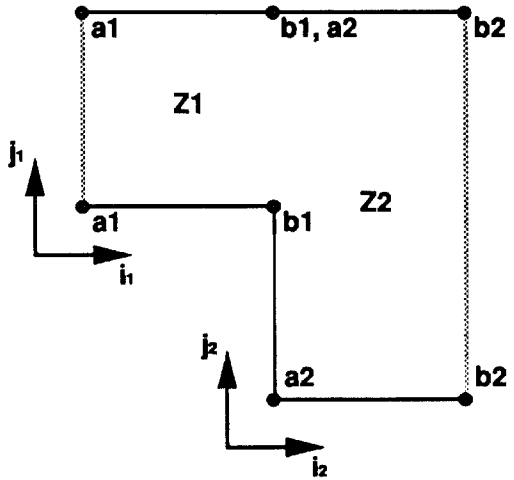

GEOM 1
Z1: imax = 41, jmax = 41
Z2: imax = 41, jmax = 81
(5002 grid points)

GEOM 2
Z1: imax = 41, jmax = 11
Z2: imax = 41, jmax = 51
(2542 grid points)

GEOM 3
Z1: imax = 41, jmax = 41
Z2: imax = 41, jmax = 161
(8282 grid points)

BENCHMARK CASES - SET 2

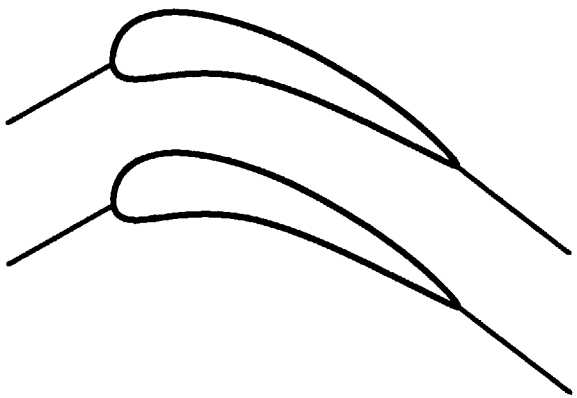

GEOMETRY 1 - REACTION TYPE

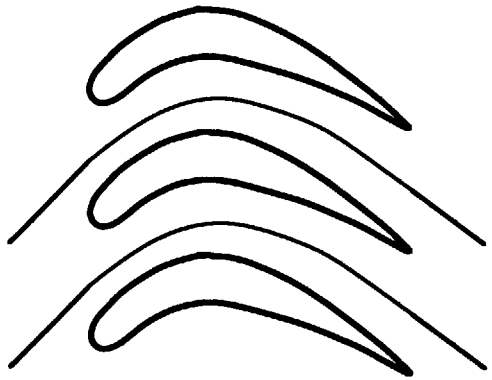

GEOMETRY 2 - IMPULSE TYPE

SUBSET	GEOMETRY	TOPOLOGY	GRID TYPE	CLUSTERING
A	1	SINGLE ZONE - PASSAGE	H-PERIODIC	NONE
B	1	SINGLE ZONE - PASSAGE	H-PERIODIC	1-2 OPTIONS
C	2	MULTI-ZONE OBSTRUCTION	H-O	NONE
D	2	MULTI-ZONE OBSTRUCTION	H-C	NONE
E	2	MULTI-ZONE OBSTRUCTION	H-O OR H-C	1-2 OPTIONS

BENCHMARK CASES - SET 2 (CONT'D)

TOPOLOGY 1: H-GRID, PERIODIC

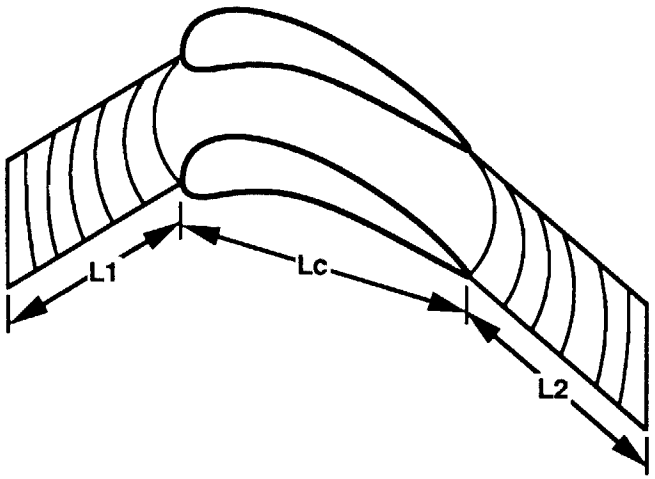

GEOM 1: imax = 100+100+100, jmax = 50

TOPOLOGY 2&3: C & O - GRIDS, PERIODIC

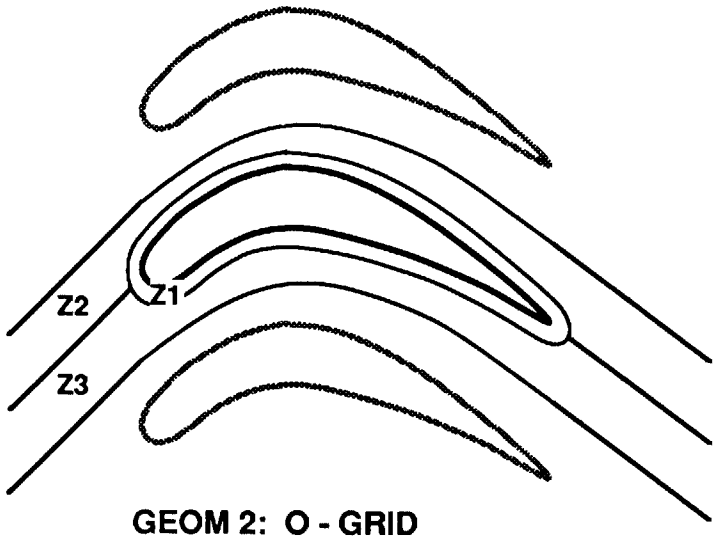

GEOM 2: O - GRID

Z1: imax = 200, jmax = 11
Z2: imax = 300, jmax = 25
Z3: imax = 300, jmax = 25

GEOM 2: C - GRID

Z1: imax = 200, jmax = 11
Z2: imax = 300, jmax = 25
Z3: imax = 300, jmax = 25

BENCHMARK CASES - SET 3

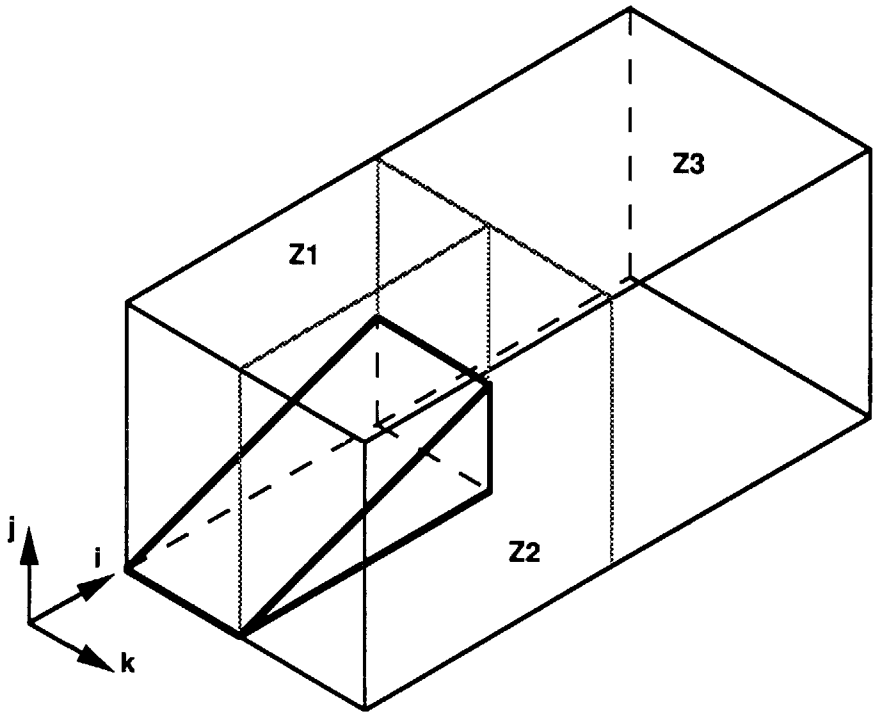

$W_{wedge} = 0.25$
$L_{wedge} = 1.0$

$\alpha_{wedge} = 15°$
$H_{wedge} = 0.2679$

$H_{Z1} = H_{Z2} = H_{Z3} = 1.0$
$W_{Z1} = W_{WEDGE} = 0.25$
$W_{Z2} = 0.75,\ W_{Z3} = 1.0$
$L_{Z1} = L_{Z2} = L_{Z3} = 1.0$

ZONE 1: imax = 21, jmax = 16, kmax = 6
ZONE 2: imax = 21, jmax = 21, kmax = 16
ZONE 3: imax = 21, jmax = 21, kmax = 21

(2016 + 7056 + 9261 = 18333 grid points)

SUBSET	GEOMETRY	TOPOLOGY	GRID TYPE	CLUSTERING
A	1	MULTI-ZONE	H-FAN	NONE
B	1	MULTI-ZONE	H-FAN	1-2 OPTIONS

BENCHMARK CASES - SET 4

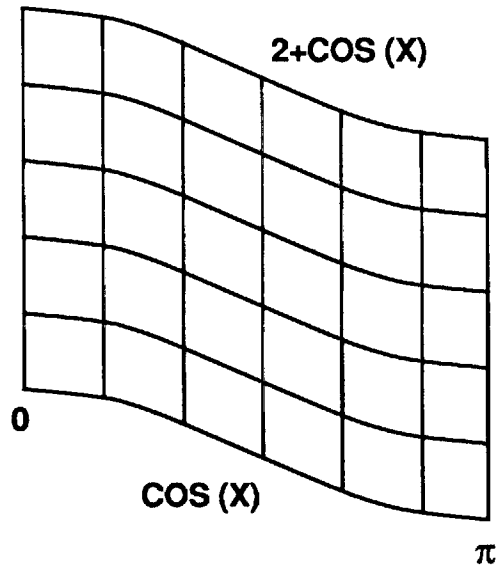

GEOMETRY:

TOP: $2+\cos(X)$, $0 \le X \le \pi$
BOTTOM: $\cos(X)$, $0 \le X \le \pi$

$H = 5$

GRIDS

1: $i_{max} = 10$, $j_{max} = 10$
2: $i_{max} = 100$, $j_{max} = 100$
3: $i_{max} = 1000$, $j_{max} = 1000$

SUBSET	GRID	TOPOLOGY	GRID TYPE	CLUSTERING
A	1	SINGLE ZONE	H	NONE
B	1	SINGLE ZONE	H + ELLIPTIC	NONE
C	2	SINGLE ZONE	H	NONE
D	2	SINGLE ZONE	H + ELLIPTIC	NONE
E	3	SINGLE ZONE	H	NONE
F	3	SINGLE ZONE	H + ELLIPTIC	NONE

Rockwell International
Rocketdyne Division

SCORING GUIDELINES DEVELOPED

- **OBJECTIVES**
  - ESTABLISH STANDARDS FOR SCORING CODE CAPABILITIES
  - ENSURE UNIFORMITY OF RATINGS (SHARED WORKLOAD)
  - MINIMIZE PERSONAL BIAS

- **APPROACH**
  - REVIEW EACH CRITERION
  - CONSIDER POSSIBLE RANGE OF ATTRIBUTES
  - ASSIGN SCORES ACCORDINGLY USING POINT SYSTEM

SCORING GUIDELINES

EXAMPLES

- **GEOMETRY DEFINITION, INPUT FORMATS, CAD**
  - ACCEPTS IGES FORMAT = 7 PTS
  - EACH ADDITIONAL CAD STANDARD = +1 PT
  - MAXIMUM SCORE = 10 PTS

- **SCORING**
  - ICEM: ACCEPTS IGES AND 2 EUROPEAN CAD STANDARDS (SCORE = 7 + 1 + 1 = 9 PTS)
  - RAGGS: ACCEPTS IGES ONLY (SCORE = 7 PTS)

SCORING GUIDELINES

EXAMPLES (CONT'D)

- **SURFACE/VOLUME GRIDS, METHODOLOGIES, ALGEBRAIC**
  - BASIC LINEAR INTERPOLATION = 1 PT
  - BASIC TRANSFINITE INTERPOLATION (TFI) = 4 PTS
  - ADVANCED TFI = 7 PTS
  - ADDITIONAL POINTS FOR EXTENT OF CONTROL AND DEGREE OF AUTOMATION
  - MAXIMUM SCORE = 10 PTS
- **SCORING**
  - PATRAN: BASIC LINEAR INTERPOLATION AND SOME ADDITIONAL CONTROL FEATURES (SCORE = 1 + 1 = 2 PTS)
  - EAGLEVIEW, ICEM, IGB, RAGGS: TFI (SCORE = 7 PTS)
  - GRIDGEN: TFI AND EXTENSIVE OPTIONS (SCORE = 7 + 2 = 9 PTS)

CANDIDATE CODES IDENTIFIED

- **GRID GENERATION CODES CONSIDERED FROM MANY SOURCES**
  - GOVERNMENT
  - INDUSTRY
  - UNIVERSITY
  - COMMERCIAL

- **10 CODES IDENTIFIED AS CANDIDATES FOR EVALUATION**
  - EAGLE (MSU)
  - EAGLEVIEW MSU)
  - GENIE (MSU)
  - GRAPE (NASA AMES)
  - GRIDGEN (GD/MDA/NASA)
  - ICEM (CDC)
  - IGB (NASA LEWIS)
  - PATRAN (PDA)
  - RAGGS (RI NAA)
  - TIGER (MSU)

CODE EVALUATION

PHASE 1 PRE-SCREEN

- **OBJECTIVES**
  - IDENTIFY MOST PROMISING CODES
  - REDUCE LIST OF CODES TO PRACTICAL SIZE
  - IDENTIFY PHASE 2 EVALUATION CODES

- **APPROACH: SURVEY CODE AUTHORS AND INDUSTRY EXPERTS**
  - GENERAL CAPABILITY (IGES, GEOMETRY, ALGORITHMS)
  - UNIQUE ASPECTS
  - USE IN, AND ACCEPTANCE BY COMMUNITY
  - NEAR-TERM UPGRADES PLANNED (IGES, INTERACTIVE)
  - USABILITY (SCRIPTS, BATCH VS INTERACTIVE)
  - AVAILABILITY (FOR EVALUATION)
  - DOCUMENTATION AND TRAINING AVAILABLE

CODE EVALUATION

PHASE 1 PRE-SCREEN RESULTS (CONT'D)

- **CODES RANKED BASED ON TECHNICAL CAPABILITY AND OTHER CONSIDERATIONS***

1. **GRIDGEN**
2. **RAGGS**
3. **CDC**
4. / **5.** EAGLE / **EAGLEVIEW**
6. **GENIE**
7. **PATRAN**
8. **IGB**
9. GRAPE
10. TIGER

* **OTHER CONSIDERATIONS**

- BENCHMARK CODES
  - NASA MSFC EXPERIENCE WITH GENIE
  - ROCKETDYNE EXPERIENCE WITH PATRAN AND IGB
- AVAILABILITY DURING PLANNED EVALUATION TIMEFRAME
- AVAILABLE VERSIONS "FROZEN" FOR PHASE 2 EVALUATION

1080

PHASE 2 - PRELIMINARY EVALUATION MATRIX DEVELOPED

- **CRITERIA GROUPED INTO LOGICAL CATEGORIES**
- **WEIGHTING FACTORS ASSIGNED**
  - EACH CRITERION WEIGHS EQUALLY
  - FACTOR RANGE FROM 1-10
    - 1 - LOW IMPORTANCE
    - 10 - HIGH IMPORTANCE
- **SPREADSHEET DEVELOPED TO AUTOMATE EVALUATION**
  - SCORING GUIDELINES APPLIED
  - EACH CODE SCORED FROM 1-10 BASED ON CAPABILITY IN EACH AREA
- **AVAILABLE VERSIONS "FROZEN" FOR PHASE 2 EVALUATION**

PHASE 2 - PRELIMINARY EVALUATION MATRIX
(Page 1 of 2)

CRITERIA	WEIGHT	CDC	EAGLE-VIEW	IGB	GENIE	GRIDGEN	PATRAN	RAGGS
GEOMETRY DEFINITION								
• INPUT FORMATS	9.000	9	0	0	0	0	9	7
• CAD	6.000	6	4	1	6	6	6	6
• OTHER	2.000	10	2	1	1	2	10	1
• OUTPUT CAPABILITY	5.000	10	5	0	5	5	9	5
• CREATION CAPABILITY								
• ACCURACY OF SURFACE		NA	NA	NA	NA	NA	NA	NA
• AS CREATED (IN GG)		NA	NA	NA	NA	NA	NA	NA
• AS TRANSLATED (TO GG)								
SURFACE / VOLUME GRIDS		NA	NA	NA	NA	NA	NA	NA
• ACCURACY (PTS. ON SURFACE)								
• METHODOLOGIES	10.000	7	7	7	7	9	2	7
• ALGEBRAIC	9.000	6	0	7	9	10	1	8
• ELLIPTIC	2.000	0	0	0	0	0	0	0
• HYPERBOLIC								
GRID TYPES SUPPORTED								
• MULTIZONE	10.000	5	5	1	3	6	1	6
• PERIODIC	6.000	5	5	10	5	5	1	5
• H	10.000	7	5	7	5	5	3	5
• C AND/OR O	6.000	4	4	0	4	5	4	4
• FAN (DEGENERATE CELLS)	6.000	7	5	0	5	5	1	5
• 2D/3D	10.000	10	3	5	7	10	10	10

PHASE 2 - PRELIMINARY EVALUATION MATRIX
(Page 2 of 2)

CRITERIA	WEIGHT	CDC	EAGLE-VIEW	IGB	GENIE	GRIDGEN	PATRAN	RAGGS
GRID CONTROL								
• CLUSTERING	10.000	4	3	2	5	7	2	9
• LOCAL CONTROL	5.000	0	0	7	7	9	7	5
USABILITY								
• LEARNABILITY	10.000	3	2	4	4	6	3	5
• USER INTERFACE	10.000	6	7	4	1	5	3	8
• MODIFY (PARAMETRICS)	4.000	6	5	5	5	1	5	1
• SPECIALIZE (TEMPLATE)	4.000	2	5	9	5	1	4	1
• SESSION HISTORY	8.000	6	9	5	7	0	7	0
• SAVE INTERMEDIATE STATE	10.000	5	4	4	4	5	7	5
• GRID DIAGNOSTICS	7.000	5	0	4	4	3	4	2
• ERROR HANDLING	8.000	4	1	4	2	8	4	3
• SIZE LIMITATIONS	8.000	5	8	7	7	9	2	8
VENDOR SUPPORT								
• SERVICES	10.000	7	5	6	1	8	9	7
• SOURCE CODE	10.000	0	7	6	5	9	0	8
• RESPONSIVE TO NEEDS	10.000	6	7	9	2	7	5	10
PORTABILITY	5.000	2	1	1	1	2	10	1
COST OF SERVICES								
• CODE/MAINTENANCE	10.000	1	10	10	10	10	7	10
• TRAINING	6.000	1	5	7	7	5	7	10
• CONSULTING	6.000	5	5	10	10	5	5	10
TOTALS		1180.0	1036.0	1135.0	1106.0	1395.0	1072.0	1442.0

PHASE 2 - PRELIMINARY EVALUATION

SUMMARY

- **SEVEN CODES RANKED ACCORDING TO PHASE 2 EVALUATION**

RANK	CODE	SCORE
1.	RAGGS	1442
2.	GRIDGEN	1395
3.	ICEM (CDC)	1180
4.	IGB *	1135
5.	GENIE	1106
6.	PATRAN	1072
7.	EAGLEVIEW	1036

- **SCORE DIFFERENCES OF 50-100 POINTS AND GREATER CONSIDERED TO BE SIGNIFICANT**

* **IGB WORKS WELL FOR INTENDED PURPOSE, BUT IS NOT A GENERAL USE CODE**

PHASE 2 - PRELIMINARY EVALUATION

CONCLUSIONS

- **TOP THREE GRID GENERATION CODES WORTHY OF CONSIDERATION**
- **SELECTION DEPENDS ON FUNCTIONAL REQUIREMENTS**
- **RAGGS AND GRIDGEN ARE BOTH GOOD GENERIC CFD GRID GENERATION SYSTEMS**
  - RAGGS PRIMARY ADVANTAGES
    - ABILITY TO IMPORT IGES FILES
    - MORE INTERACTIVE GRAPHICAL USER INTERFACE
  - GRIDGEN PRIMARY ADVANTAGES
    - MORE MATURE, ROBUST, WELL DOCUMENTED CODE
    - EXTENSIVE GRID GENERATION ALGORITHMS, OPTIONS
- **ICEM CODE PRIMARY STRENGTH IN EXTENSIVE CAD IMPORT/EXPORT CAPABILITY**
  - LIMITED GRID GENERATION FEATURES
  - THIRD PARTY CODE (NO SOURCE CODE, SIGNIFICANT COST)

PHASE 3 - FINAL EVALUATION COMPLETED

- **TOP TWO CODES (RAGGS, GRIDGEN) FROM PRELIMINARY (PHASE 2) EVALUATION CARRIED FORWARD TO FINAL EVALUATION (PHASE 3)**

- **COMPLEX 3-D CASE SELECTED TO VERIFY PHASE 2 RESULTS**
  - NLS 1.5 STAGE BASE REGION GEOMETRY
    - 8 ZONES
    - 638,000 GRID POINTS IN ONE QUADRANT
  - FULLY GENERATED WITH RAGGS
  - PARTIALLY GENERATED WITH GRIDGEN (SUFFICIENT FOR COMPARISON)

- **SPREADSHEET REVISED TO EXTEND EVALUATION**
  - COMPARISONS EXPANDED
  - MOST RECENT VERSIONS EVALUATED
  - RELATIVE ADJUSTMENTS MADE TO SCORES

PHASE 3 - FINAL EVALUATION MATRIX
(Page 1 of 2)

CRITERIA	WEIGHT	GRIDGEN	RAGGS
GEOMETRY DEFINITION			
• INPUT FORMATS			
• CAD	9.000	5	7
• OTHER	6.000	6	6
• OUTPUT CAPABILITY	2.000	2	1
• CREATION CAPABILITY	5.000	5	5
• ACCURACY OF SURFACE			
• AS CREATED (IN GG)		NA	NA
• AS TRANSLATED (TO GG)		NA	NA
SURFACE / VOLUME GRIDS			
• ACCURACY (PTS. ON SURFACE)		NA	NA
• METHODOLOGIES			
• ALGEBRAIC	10.000	8	9
• ELLIPTIC	9.000	9	9
• HYPERBOLIC	2.000	0	0
GRID TYPES SUPPORTED			
• MULTIZONE	10.000	6	7
• PERIODIC	6.000	5	5
• H	10.000	5	5
• C AND/OR O	6.000	5	4
• FAN (DEGENERATE CELLS)	6.000	5	5
• 2D/3D	10.000	10	10

PHASE 3 - FINAL EVALUATION MATRIX
(Page 2 of 2)

CRITERIA	WEIGHT	GRIDGEN	RAGGS
GRID CONTROL			
• CLUSTERING	10.000	8	9
• LOCAL CONTROL	5.000	9	9
USABILITY			
• LEARNABILITY	10.000	6	5
• USER INTERFACE	10.000	6	8
• MODIFY (PARAMETRICS)	4.000	1	3
• SPECIALIZE (TEMPLATE)	4.000	1	3
• SESSION HISTORY	8.000	0	6
• SAVE INTERMEDIATE STATE	10.000	5	5
• GRID DIAGNOSTICS	7.000	6	2
• ERROR HANDLING	8.000	8	4
• SIZE LIMITATIONS	8.000	9	8
VENDOR SUPPORT			
• SERVICES	10.000	8	7
• SOURCE CODE	10.000	9	8
• RESPONSIVE TO NEEDS	10.000	7	10
PORTABILITY	5.000	2	1
COST OF SERVICES			
• CODE/MAINTENANCE	10.000	10	10
• TRAINING	6.000	5	10
• CONSULTING	6.000	5	10
TOTALS		1462.0	1573.0

PHASE 3 - FINAL EVALUATION

SUMMARY AND CONCLUSIONS

- **SIGNIFICANT CHANGES IN LATEST VERSIONS**
  - RAGGS
    - HAS ENHANCED TFI OPTIONS, AUTOMATION
    - MORE AUTOMATED MULTIZONE CAPABILITY (FACE/SEGMENT SORTERS)
    - EXTENDED LOCAL CONTROL OPTIONS
    - EXTENDED HELP FACILITY
    - "SHORTCUT" SINGLE KEY COMMANDS
    - IMPROVED PARAMETRIC AND TEMPLATE CAPABILITIES
    - NEW SESSION HISTORY CAPABILITY
  - GRIDGEN v8.0
    - NOW ACCEPTS IGES INPUT
    - ADDITIONAL CLUSTERING OPTIONS
    - TRANSITIONING TOWARD MORE UNIFIED APPROACH
    - REAL TIME COLOR CODED GRID DIAGNOSTICS

PHASE 3 - FINAL EVALUATION

SUMMARY AND CONCLUSIONS (CONT'D)

- **RELATIVE RANKINGS OF TOP TWO CODES REMAINS UNCHANGED**

RANK	CODE	SCORE
1.	RAGGS	1573
2.	GRIDGEN	1462

- **RAGGS AND GRIDGEN BOTH CAPABLE OF GENERATING COMPLEX 3-D GRIDS**

STRUCTURED ADAPTIVE GRID GENERATION USING ALGEBRAIC METHODS

by

Jiann-Cherng Yang, Bharat K. Soni

NSF/ERCCFS

Mississippi State University, MS39762

and

R. P. Roger, Stephen C. Chan

Teledyne Brown Engineering, Huntsville, AL 35807

ABSTRACT

The accuracy of the numerical algorithm depends not only on the formal order of approximation but also on the distribution of grid points in the computational domain. Grid adaptation is a procedure which allows optimal grid redistribution as the solution progresses. It offers the prospect of accurate flow field simulations without the use of execessively time, computationally expensive, grid.

Grid adaptive schemes are divided into two basic categories: differentiall and algebraic. The differential method is based on a variational approach where a function which contains a measure of grid smoothness, orthogonality and volume variation is minimized by using a variational principle. This approach provideds a solid mathematical basis for the adaptive method, but the Euler-Lagrange equations must be solved in addition to the original governing equations. On the other hand, the algebraic method requires much less computational effort, but the grid may not be smooth. The algebraic techniques are based on devising an algorithm where the grid movement is governed by estimates of the local error in the numerical solution. This is achieved by requiring the points in the large error regions to attract other points and points in the low error region to repel other points.

The development of a fast, efficient, and robust algebraic adaptive algorithm for structured flow simulation applications is presented. This development is accomplished in a three step process. The first step is to define an adaptive weighting mesh (distribution mesh) [1][2] on the basis of the equidistribution law applied to the flow field solution. The second, and probably the most crucial step, is to redistribute grid points in the computational domain according to the aforementioned weighting mesh. The third and the last step is to reevalute the flow property by an appropriate search/interpolate scheme at the new grid locations.

The adaptive weighting mesh provides the information on the desired concentration of points to the grid redistribution scheme. The evaluation of the weighting mesh is accomplished by utilizing the weight function representing the solution variation and the equidistribution law [3]. The selection of the weight function plays a key role in grid adaptation [4] A new weight function utilizing a properly weighted boolean sum of various flowfield characteristics is defined. The redistribution scheme is developed utilizing Non-Uniform Rational B-Splines (NURBS) representation [5]. The application of NURBS representation results in a well distributed smooth grid by maintaining the fidelity of the geometry associated with boundary curves. Several algebraic methods are applied to smooth and/or nearly orthogonalize the grid lines. Elliptic solver is utilized to smooth the grid lines if there are grid crossing.

Various computational examples of practical interest are presented to demonstrate the success of these methods. (1) Single wedge case. (2) Cylinder case. (3) Airfoil NACA 0012 case. (4) Viscous missile case. (5) Slot cooled seeker window case. (6) Moving shock in converge inlet case. (7) 3-D single wedge case. (8) 3-D viscous cone case. (9) 3-D f15 body and wing case. (10) 3-D helicopter propeller shock prediction case. In case (1),(2),(4),(5),(6),(7),(8),and(9), PARC2D and PARC3D [6] are used as the flow simulation code. In case (3), UBI [7] is used as the flow simulation code, and compare to Peter M. Goorjian's solution [8]. In case (10), MSUTC [9] is used as the flow simulation code.

MISSISSIPPI STATE UNIVERSITY / National Science Foundation

STRUCTURED ADAPTIVE GRID GENERATION USING ALGEBRAIC METHOD

by

Jiann-Cherng Yang, Bharat K. Soni

ENGINEERING RESEARCH CENTER FOR
COMPUTATIONAL FIELD SIMULATION
COMPLEX GEOMETRY / COMPLEX PHYSICS

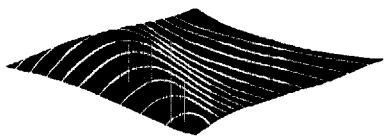

and

R. P. Roger, Stephen C. Chan

Teledyne Brown Engineering, Huntsville, AL

WHY?

More Accurate Simulated Solution

HOW?

1. Add More Grid Points

2. Move Grid Points

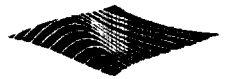

TWO CATEGORIES OF ADAPTIVE GRID SYSTEM

. Differential Method

. Slow
. Smooth
. Orthogonal

. Algebraic Method

. Fast
. Unsmooth
. Unorthogonal

. Weight function

$$W = \{\ 1 + [\sum_{j=1}^{N} \lambda_j\ (\ \alpha_j q_j \oplus \beta_j k_j\ )]\ wtf\ \}\ disf$$

$$\sum_{j=1}^{N} \lambda_j = 1\ ,\quad 0 \le \alpha_j \le 1\ ,\quad 0 \le \beta_j \le 1$$

where $W = W_s$ *or* W_r (*In* ξ *or* η *Direction*)

$q = q_s$ *or* q_r (*Gradient*)

$k = k_s$ *or* k_r (*Curvature*)

wtf = *weight factor*

disf = *distribution factor*

$$\alpha_j q_j \oplus \beta_j k_j = \alpha_j q_j + \beta_j k_j - (\alpha_j + \beta_j - 1) q_j k_j$$

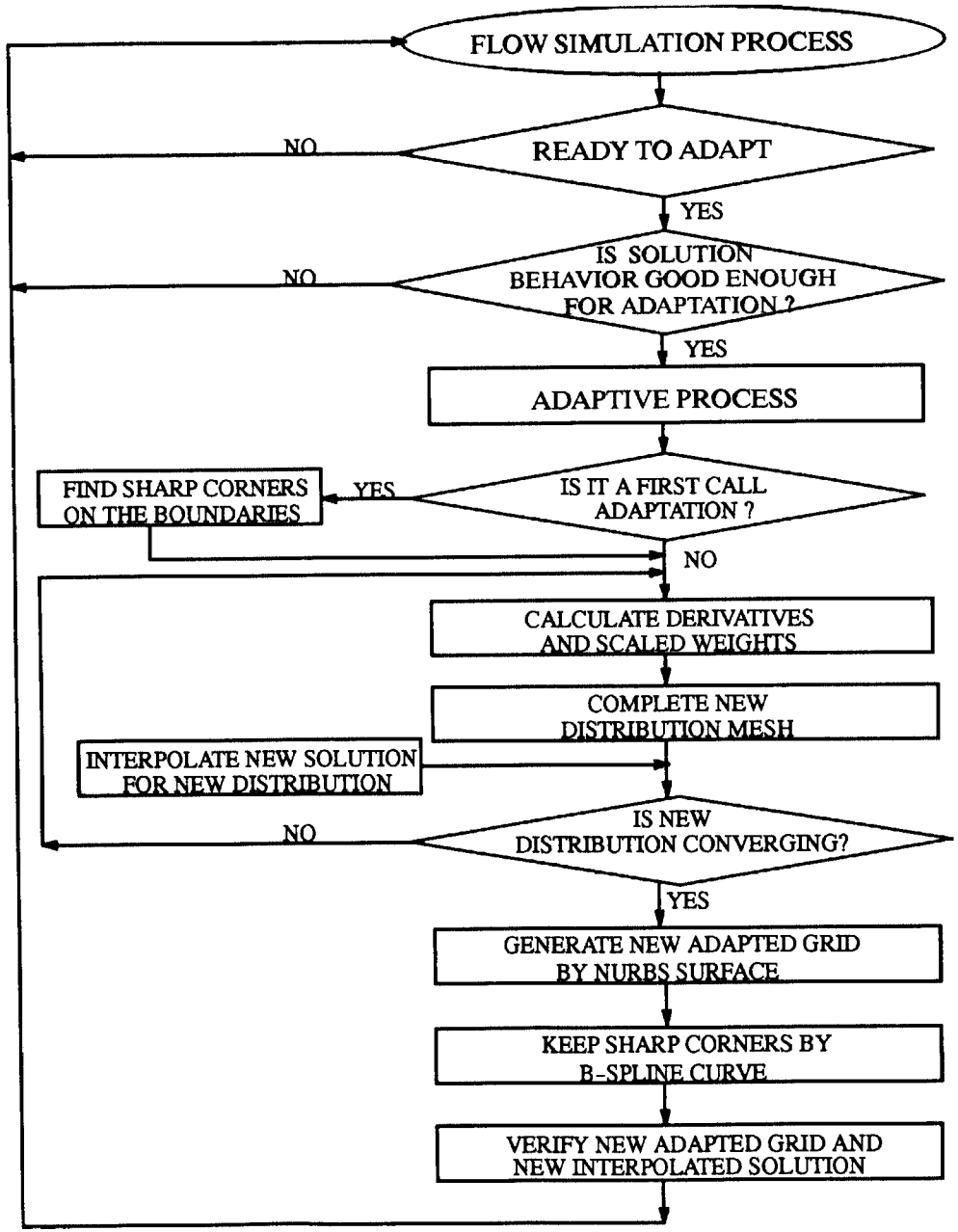

ENGINEERING RESEARCH CENTER FOR
COMPUTATIONAL FIELD SIMULATION
COMPLEX GEOMETRY / COMPLEX PHYSICS

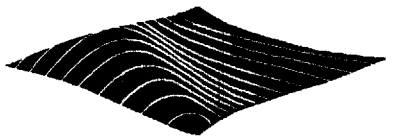

Figure 1.
Algorithm for Algebraic Adaptive Grid Generation System

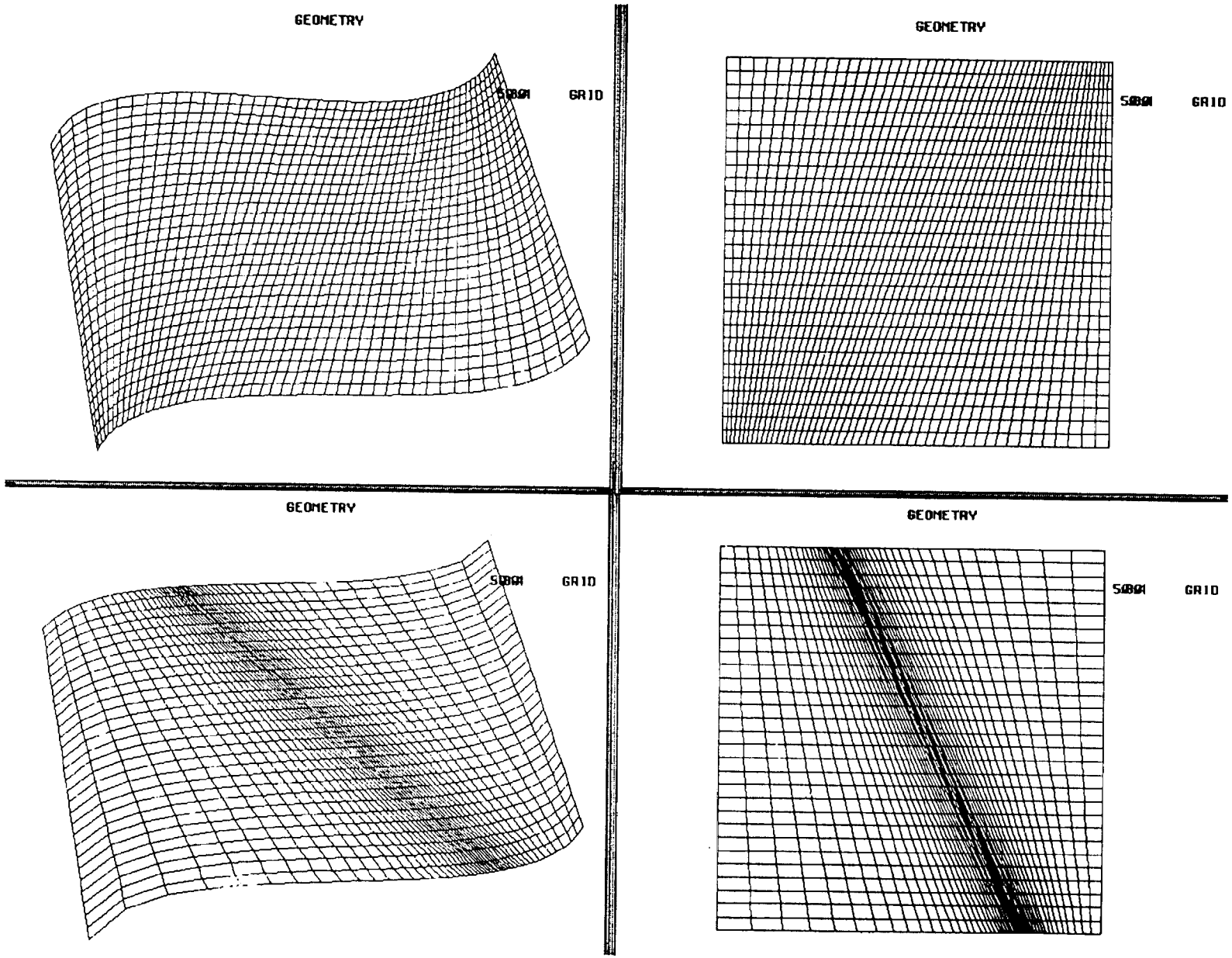

Figure 1.

Use NURBS surface to generate smooth grid.

Single Wedge Case

Grid Size : 80 X 50

Mach = 1.9

Flow Solver Applied : PARC2D

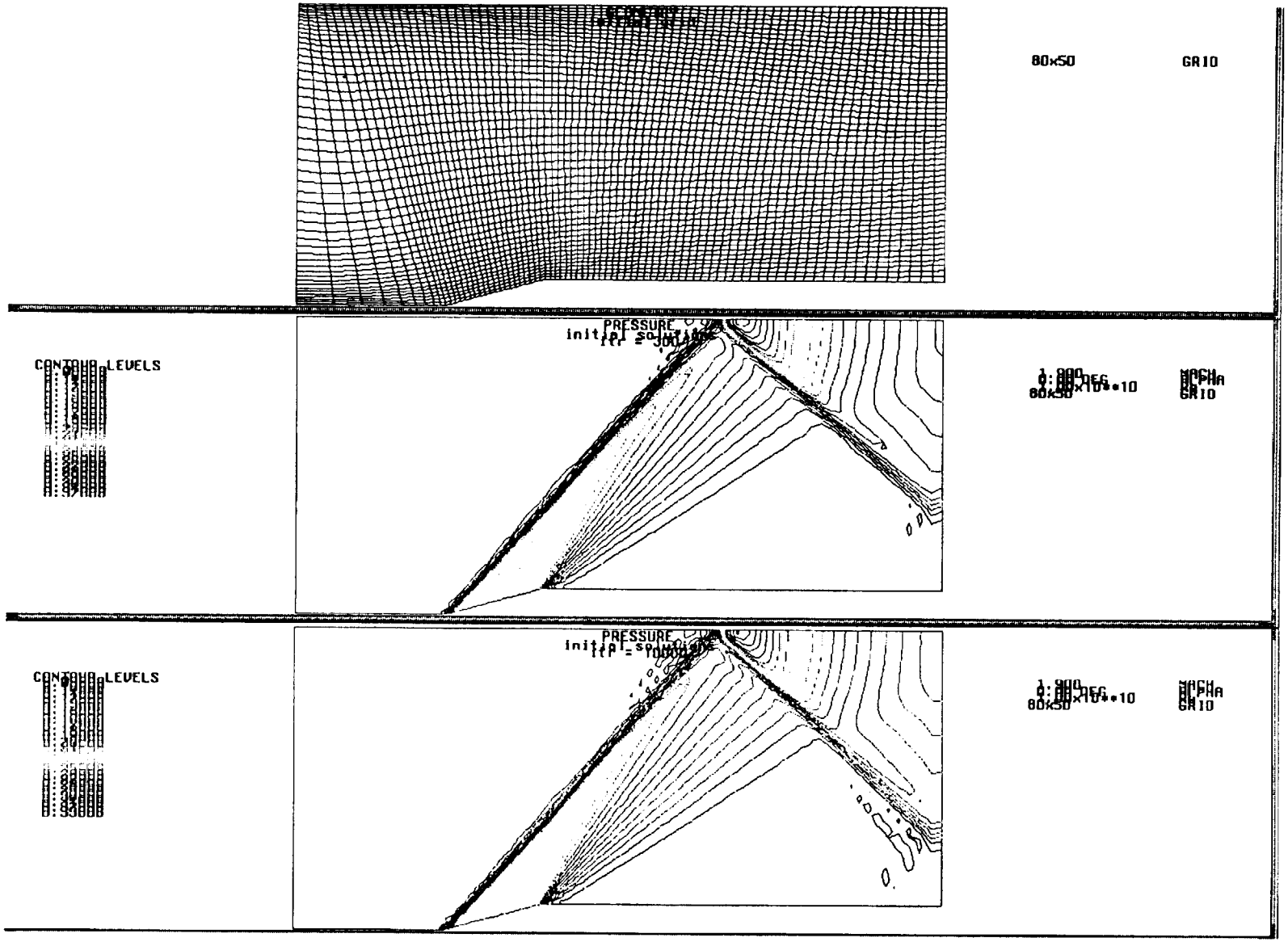

Figure 2.

Single wedge initial grids & solutions after 300 & 10000 iterations.

Figure 3.

Single wedge grid adaptation process.

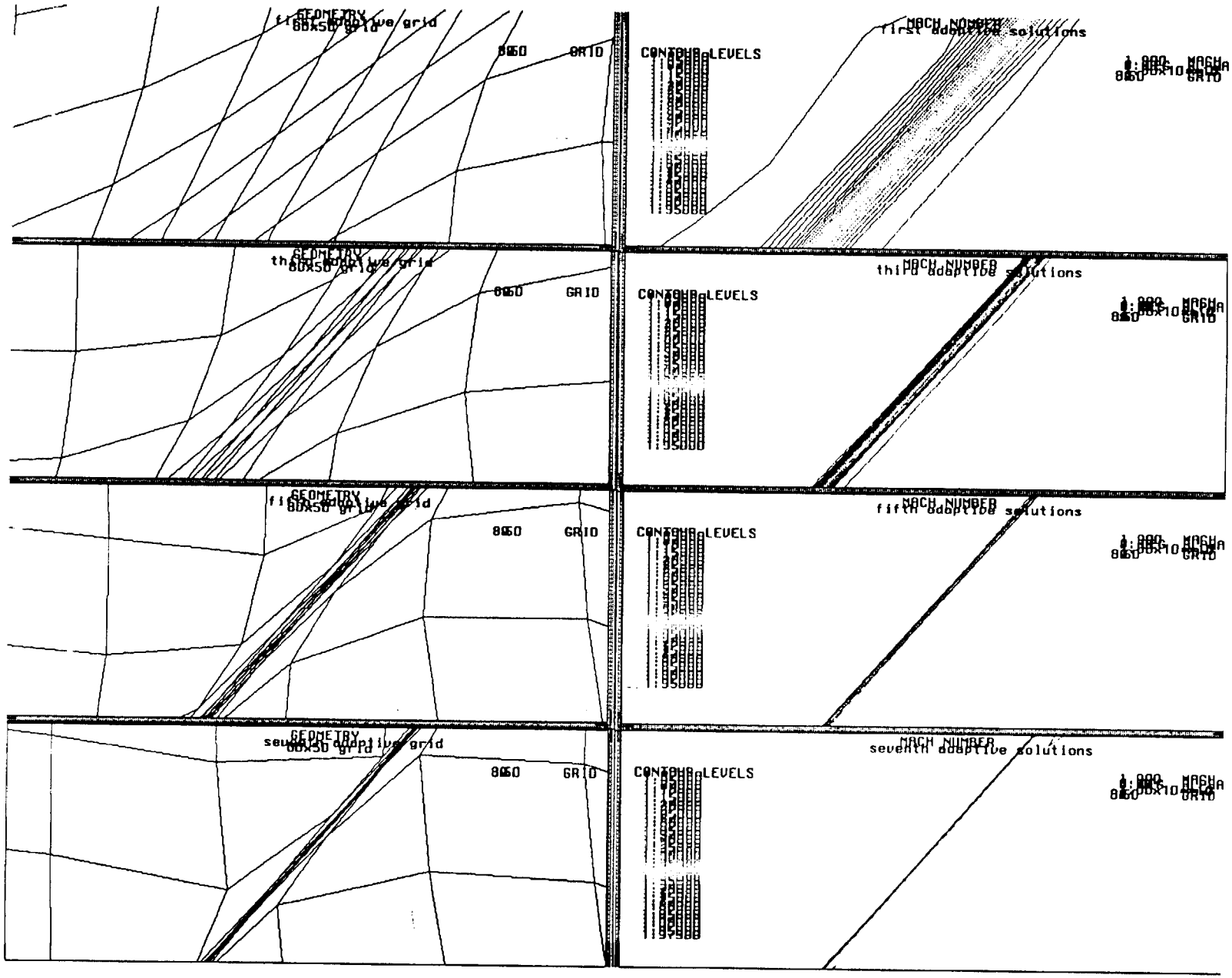

Figure 4.

Single wedge, closer Mach number contour look near shock region.

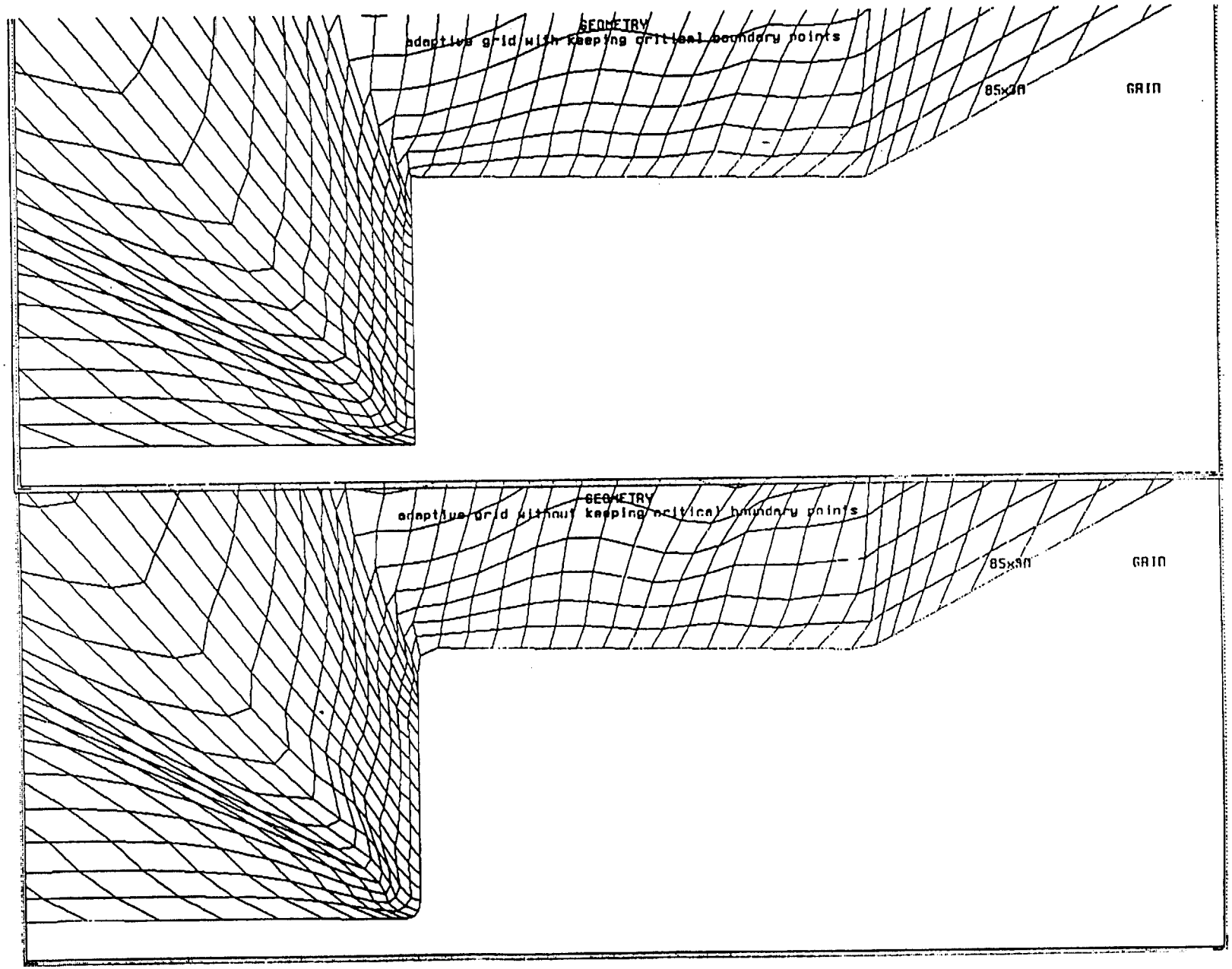

Figure 5.

Use B–Spline curve to keep sharp corners.

Cylinder Case

Grid Size : 80 X 100

Mach = 3.0

Flow Solver Applied : PARC2D

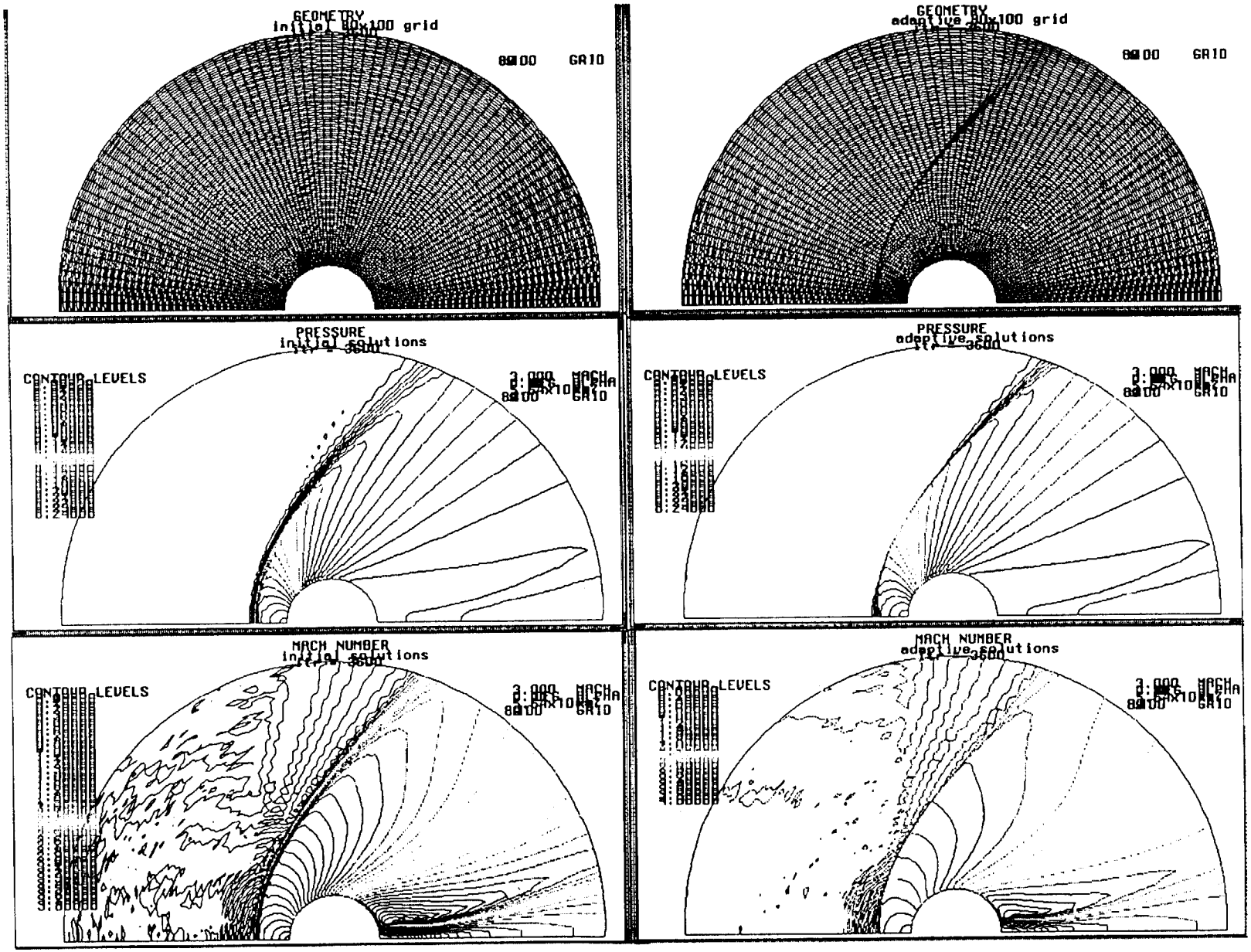

Initial grid simulation

Adaptive grid simulation

Figure 6.

Flow around cylinder initial/adaptive cases.

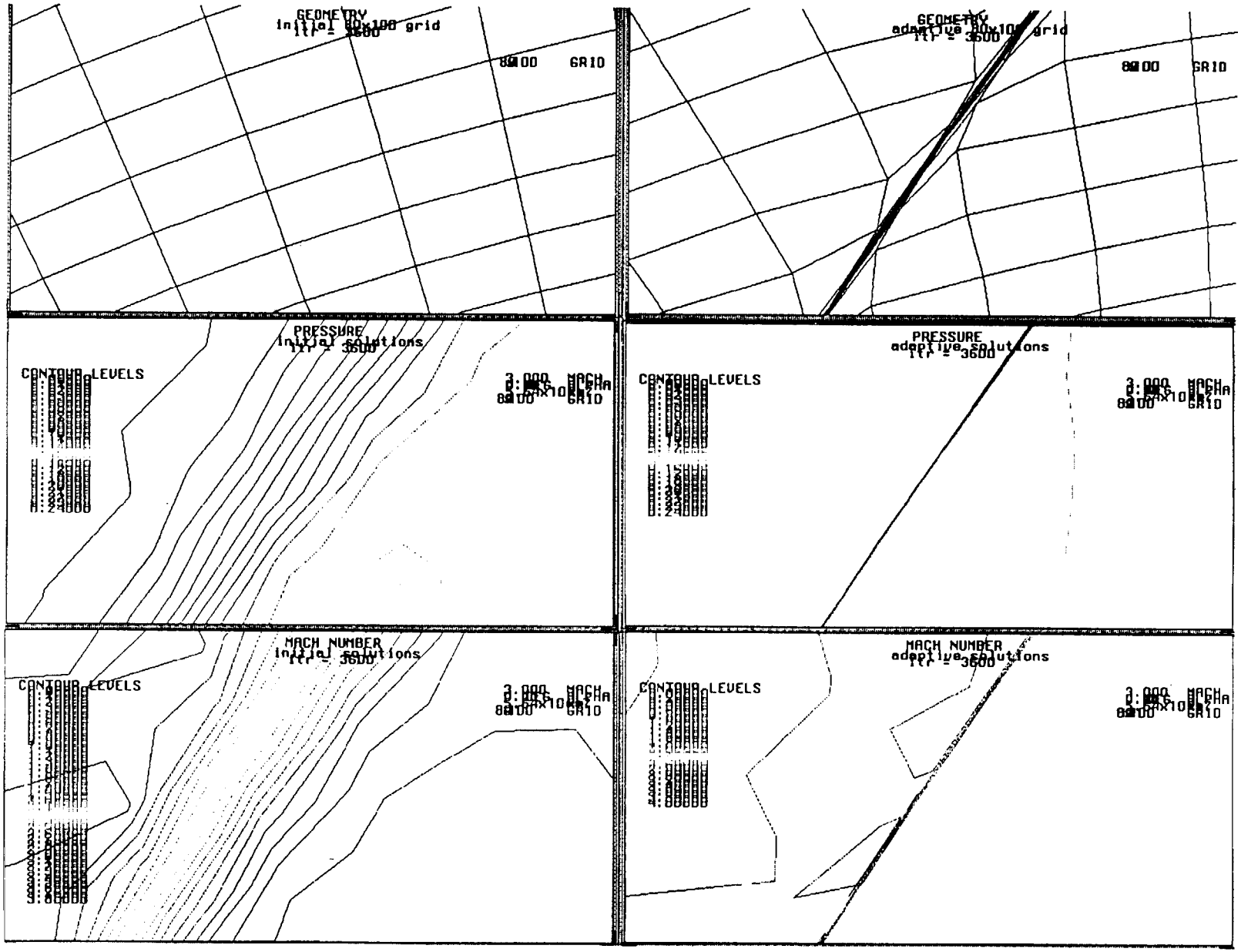

Figure 7.

Flow around cylinder, closer look near shock region.

Airfoil NACA0012 Case

Grid Size : 120 X 100

Mach = 0.8, α = 1.25

Flow Solver Applied : UBI

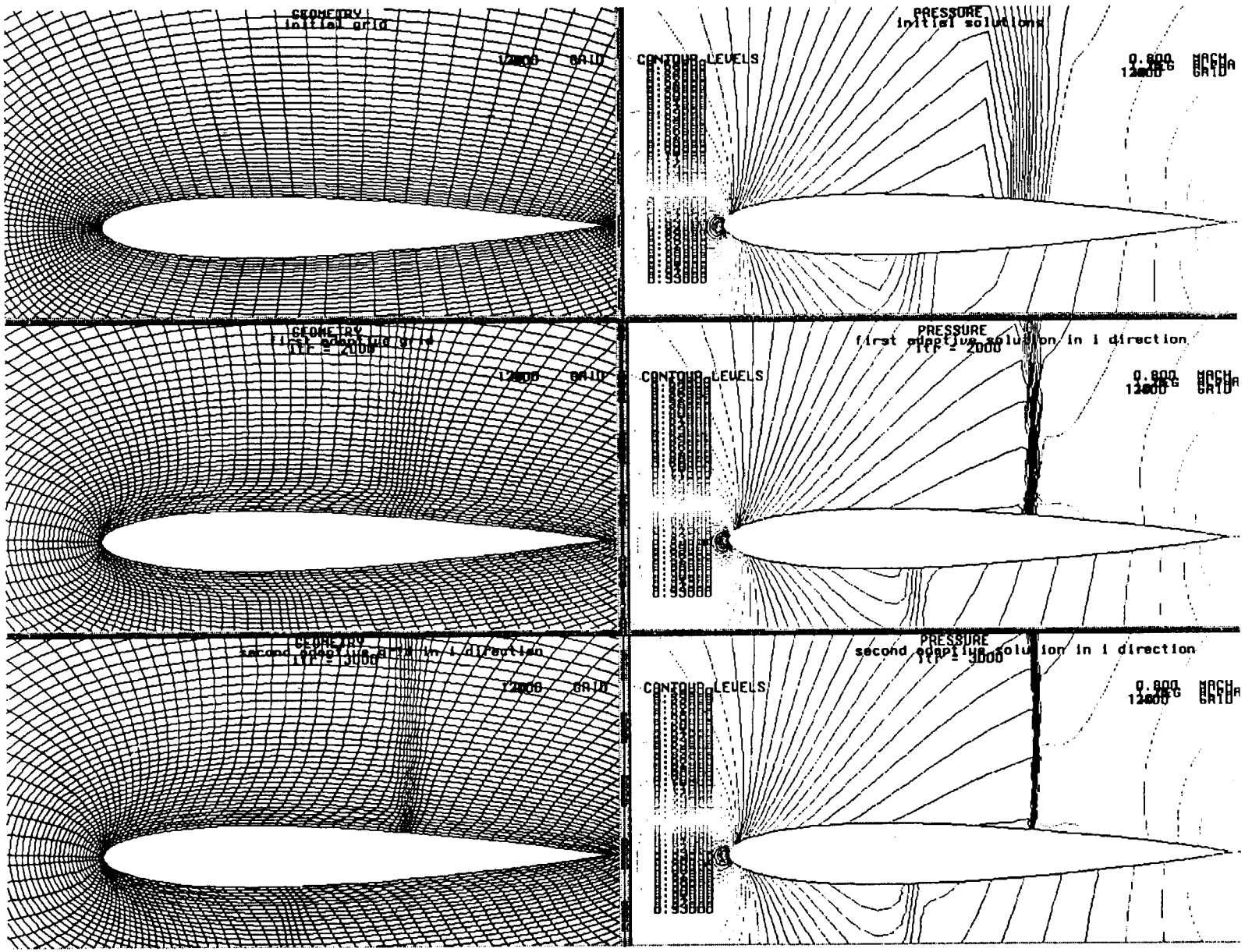

Figure 8.

Airfoil NACA0012 case non-adaptive/adaptive grid/solution,

Mach = 0.8, $\alpha = 1.25$.

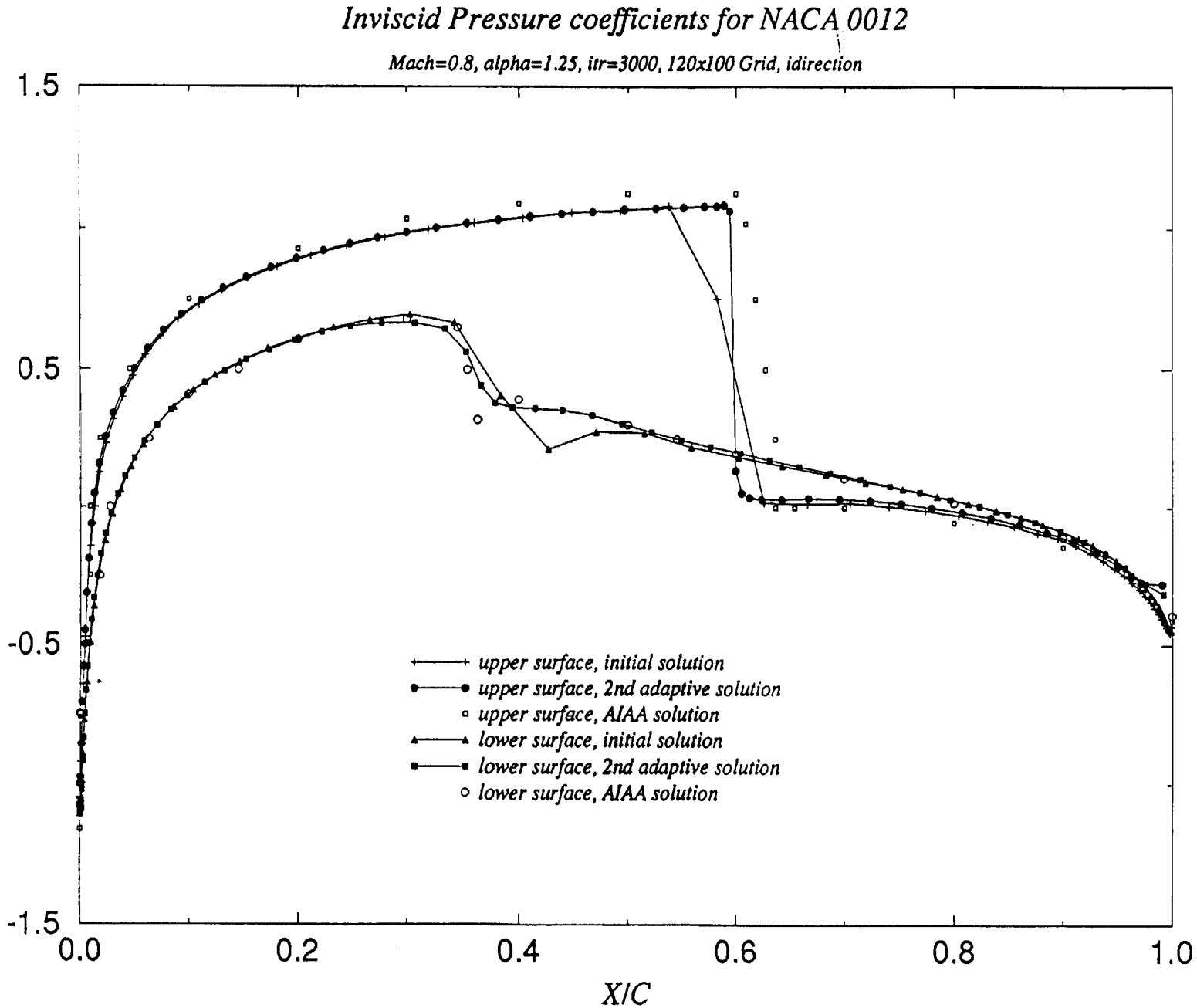

Figure 9.

Airfoil NACA0012 case Cp vs x/c plot, Mach = 0.8, α = 1.25.

Viscous Missile Case

Grid Size : 105 X 50

Mach = 3.0, Re = 4.9558×10^6

Flow Solver Applied : PARC2D

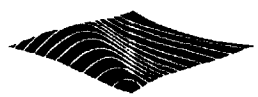

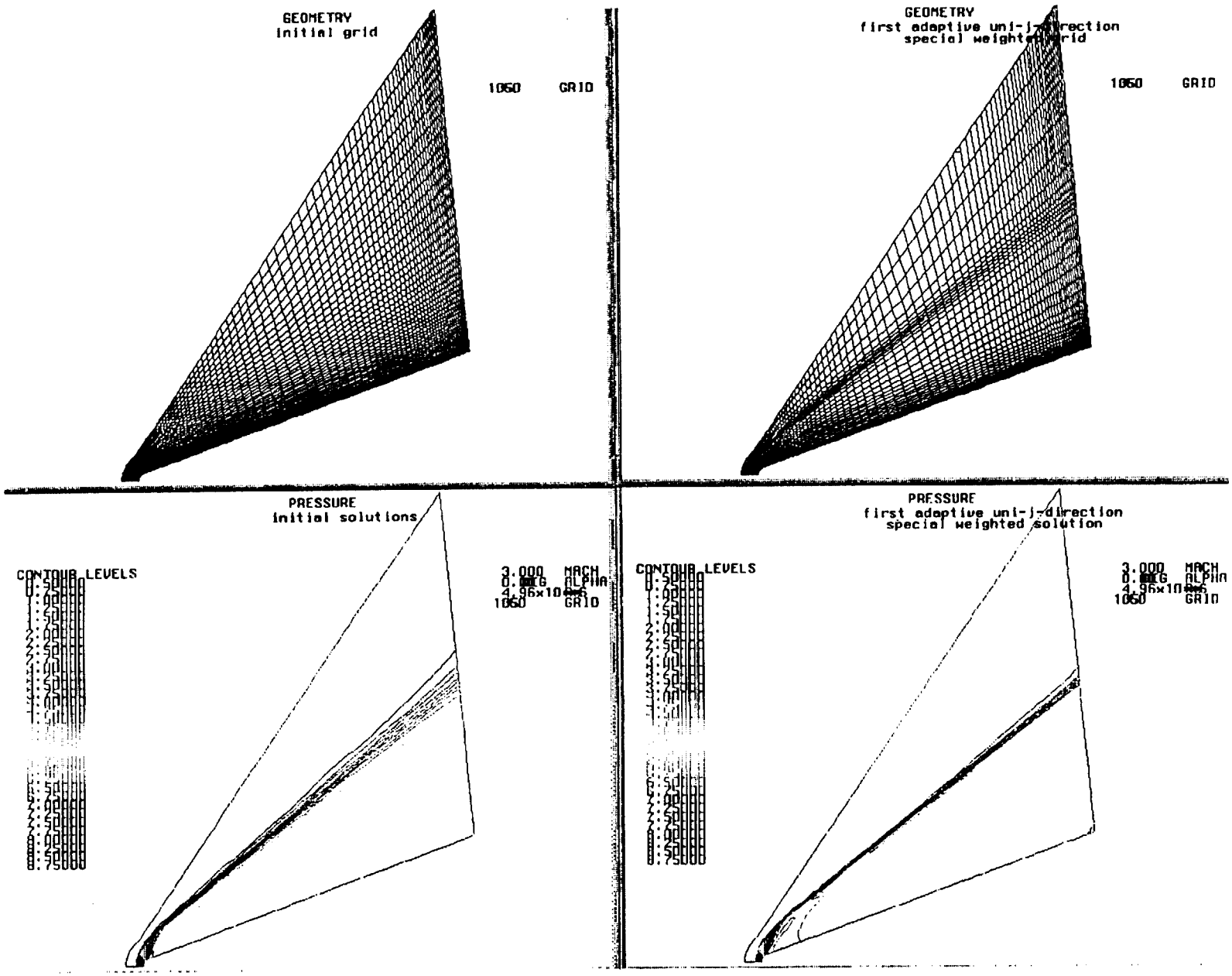

Figure 10.

Viscous missile case, whole field view.

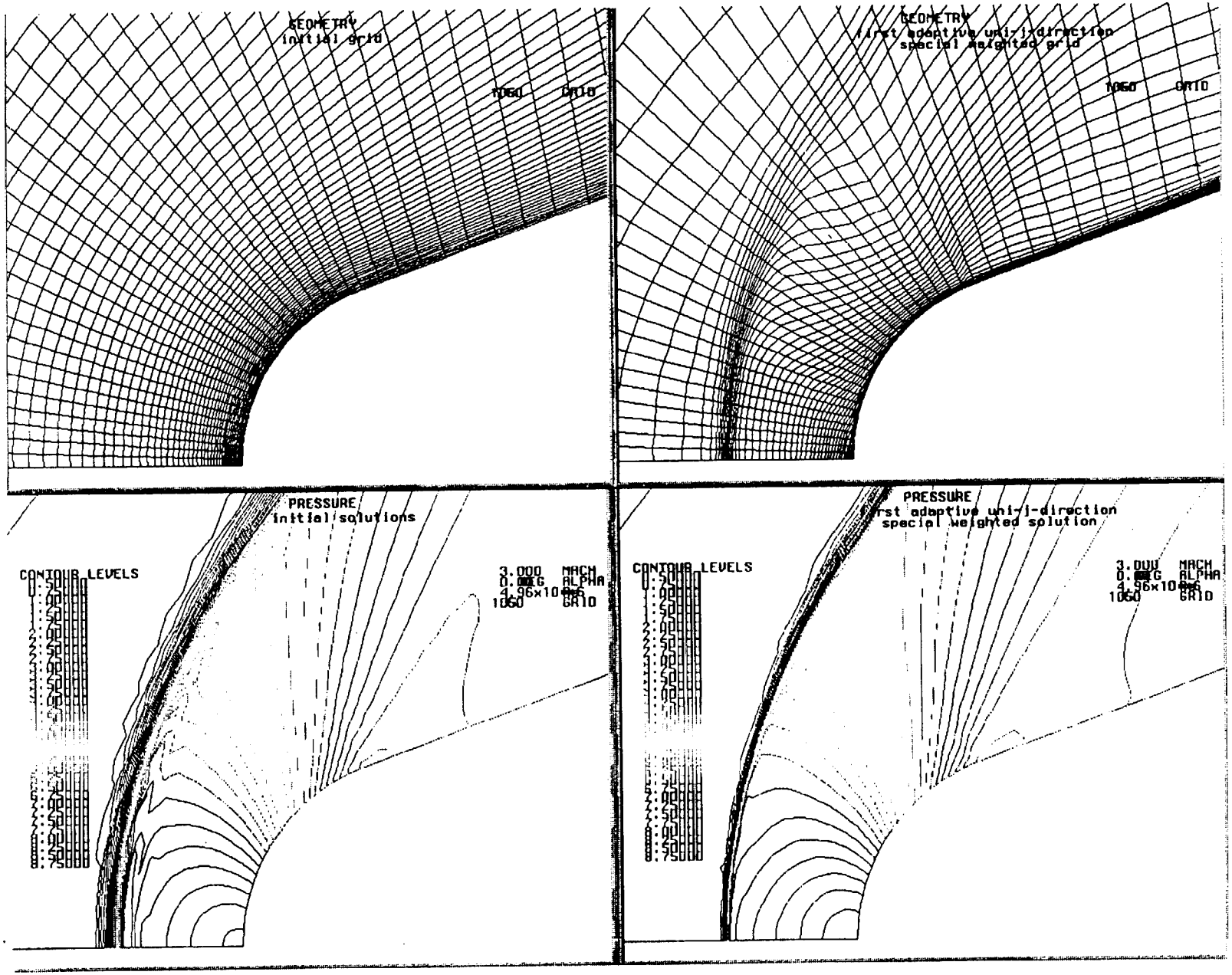

Figure 11.

Viscous missile case, bow shock in front of leading edge.

Slot Cooled Seeker Window

Grid Size : 381 X 109

Mach = 5.0, Re = 3.141×10^5

Flow Solver Applied : PARC2D

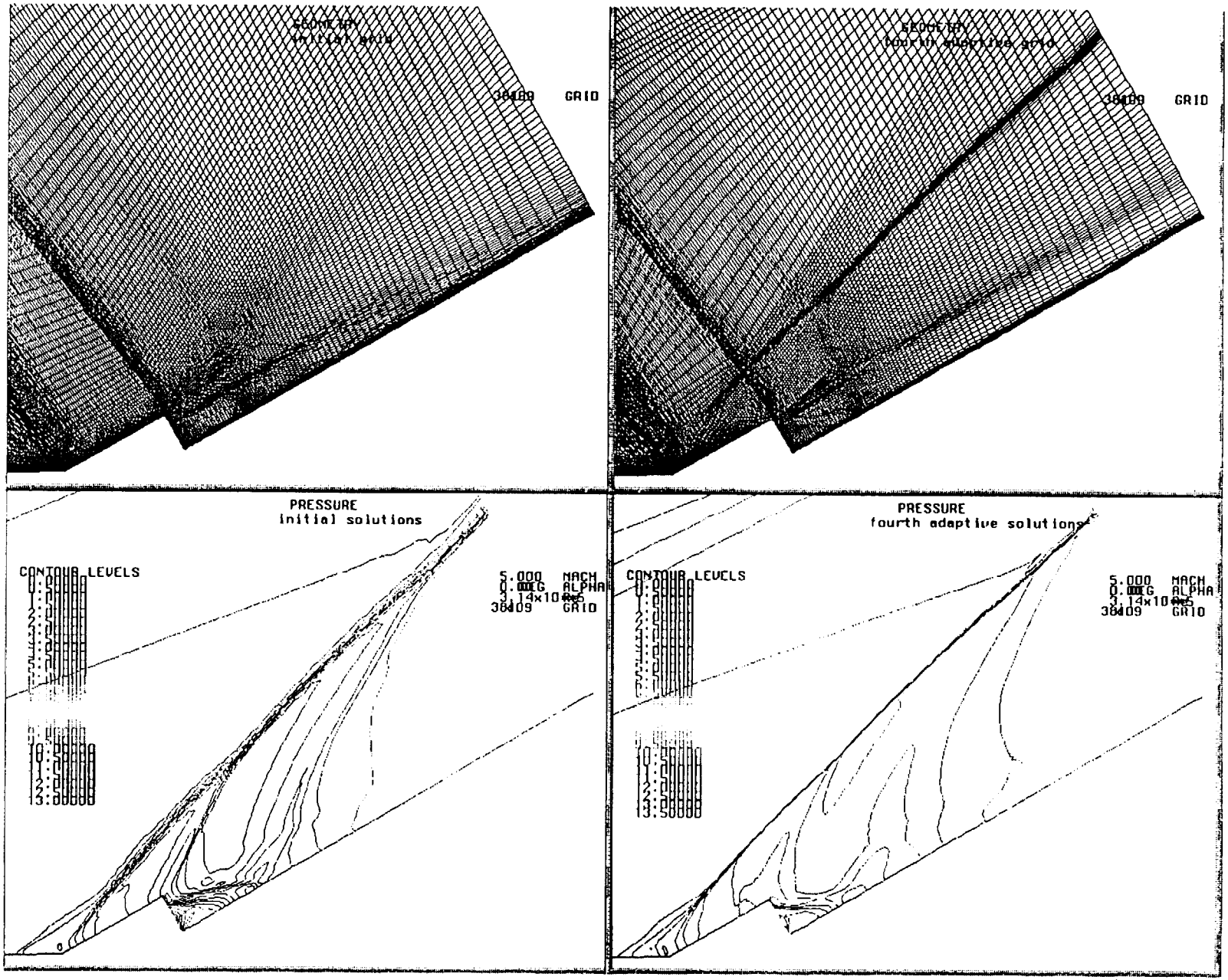

Figure 12.

Slot cooled seeker window case, oblique shock above deflection corner.

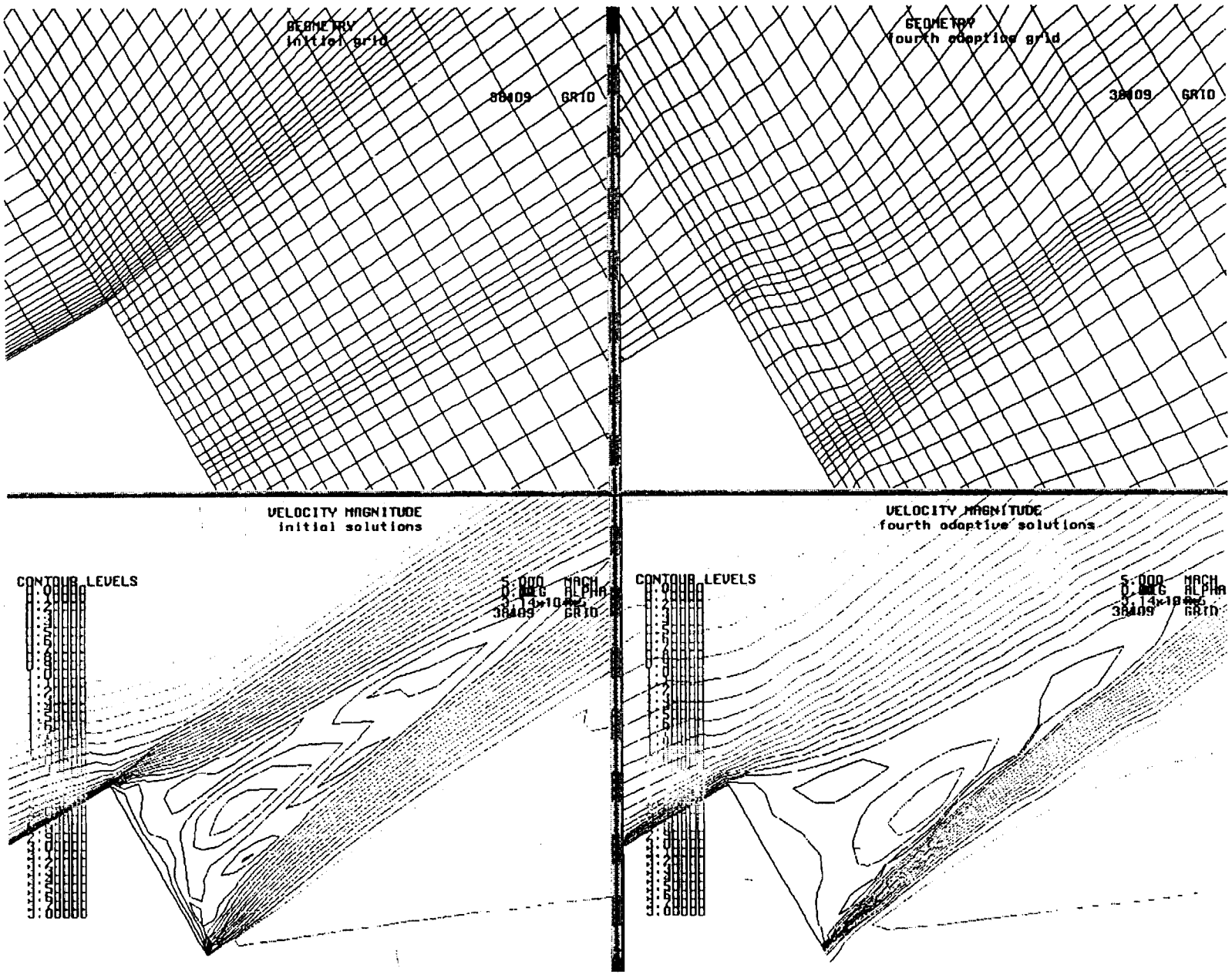

Figure 13.

Slot cooled seeker window case, velocity contour near interceptor.

Moving Shock in Converge Inlet

Grid Size : 200 X 40

Mach = 3.0

Flow Solver Applied : PARC2D

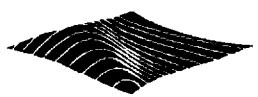

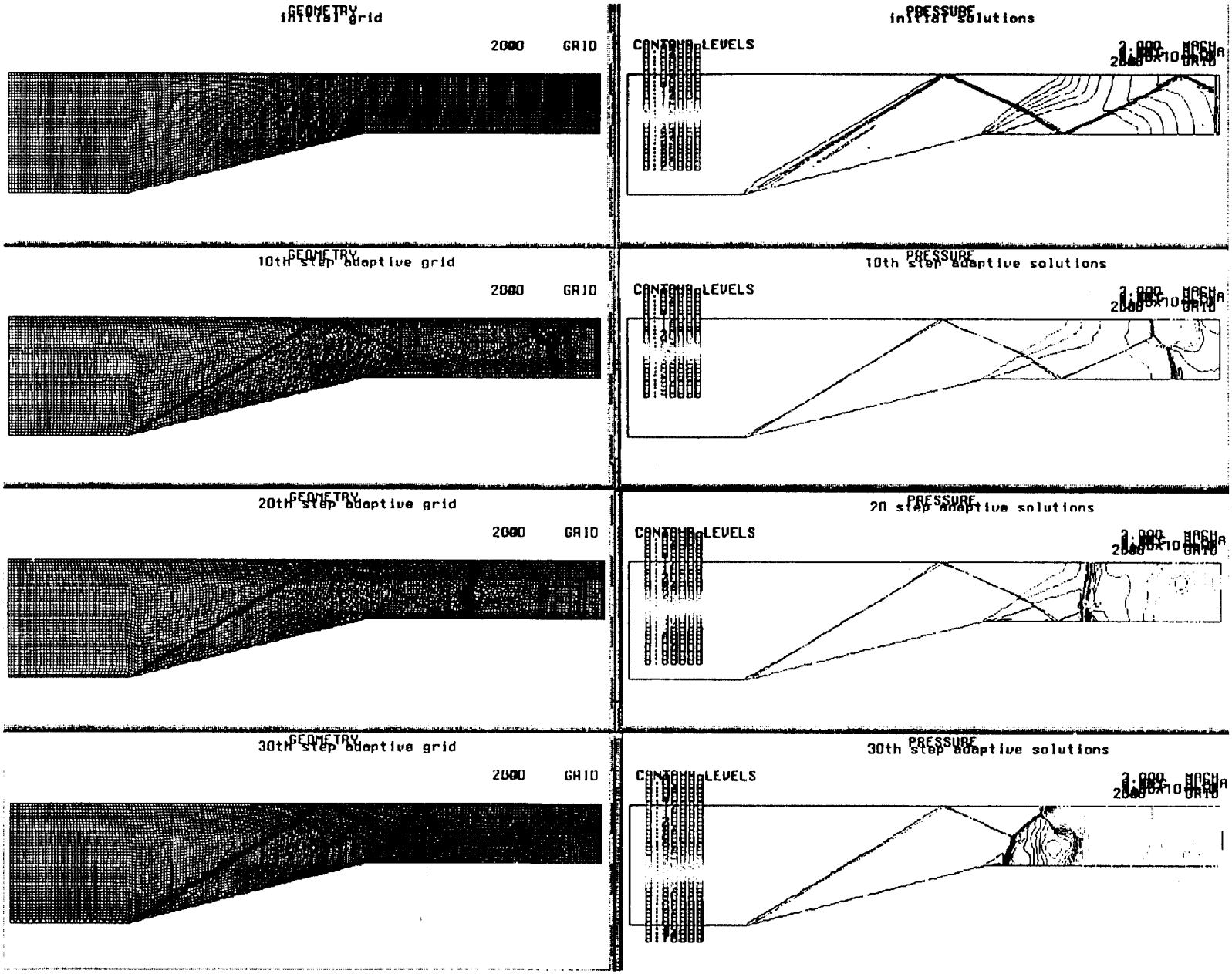

Figure 14.

Adaptive grid for the moving shock in the converge inlet.

3-D Single Wedge Case

Grid Size : 80 X 50 X 11

Mach = 1.9

Flow Solver Applied : PARC3D

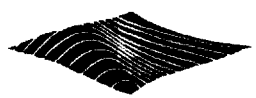

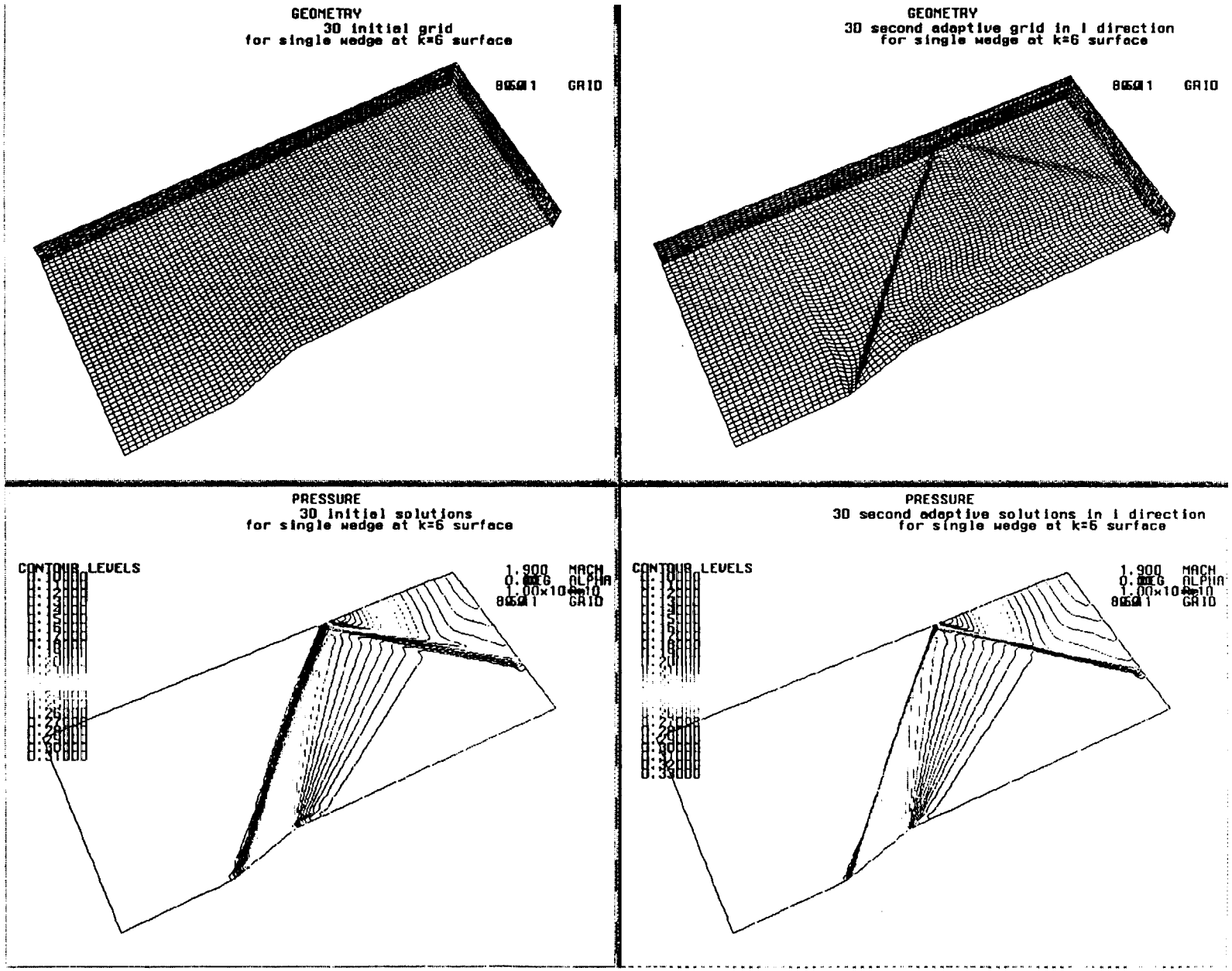

Figure 15.

3–D Single wedge, comparison of initial and adaptive grid & solution.

3-D Viscous Cone Case

Grid Size : 105 X 50 X 20

Mach = 3.0, Re = 4.9558×10^6

Flow Solver Applied : PARC3D

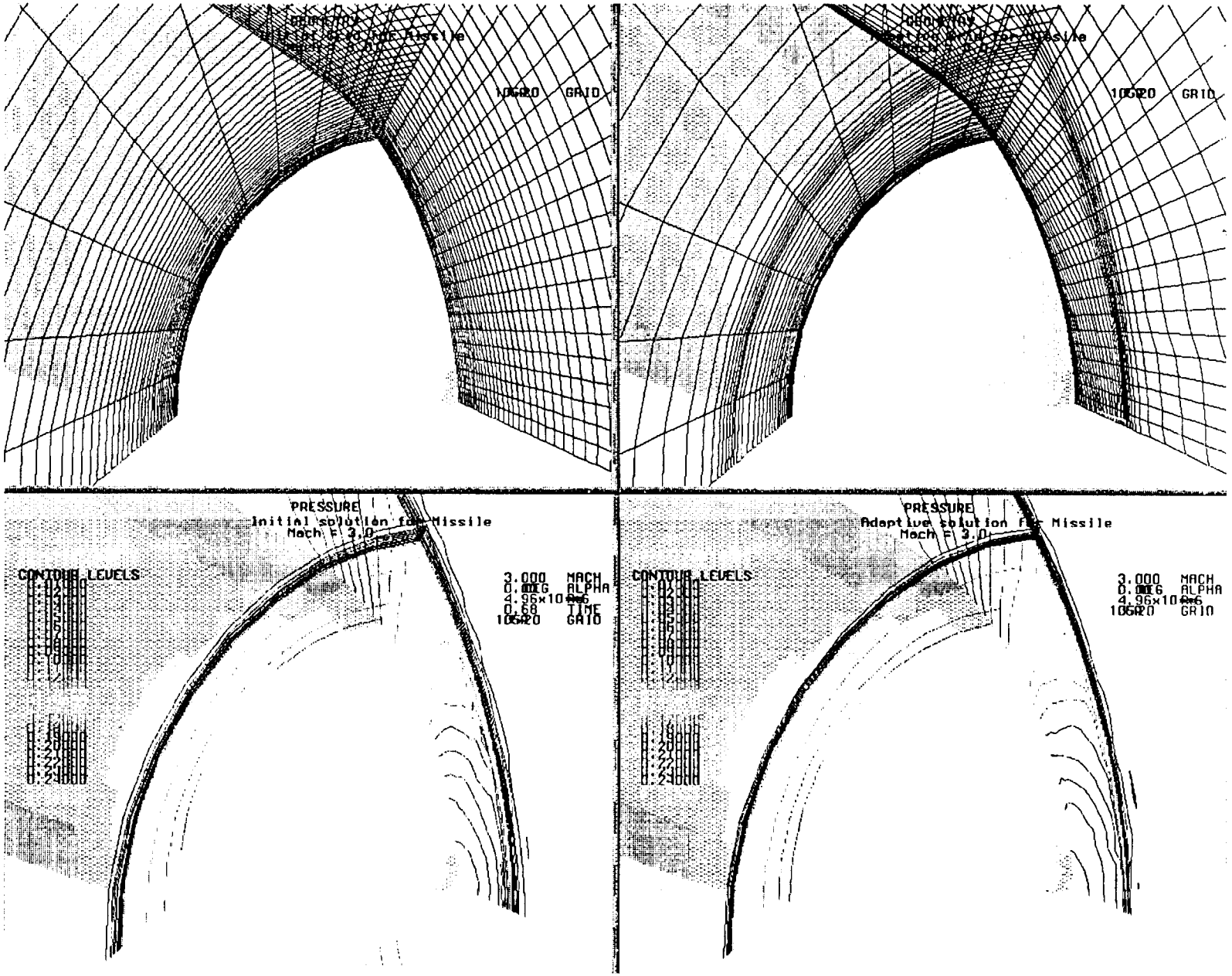

Figure 16.

3–D viscous cone case, bow shock in front of cone head.

3-D F-15 Body and Wing

Grid Size : 173 X 42 X 80

Mach = 1.5

Flow Solver Applied : PARC3D

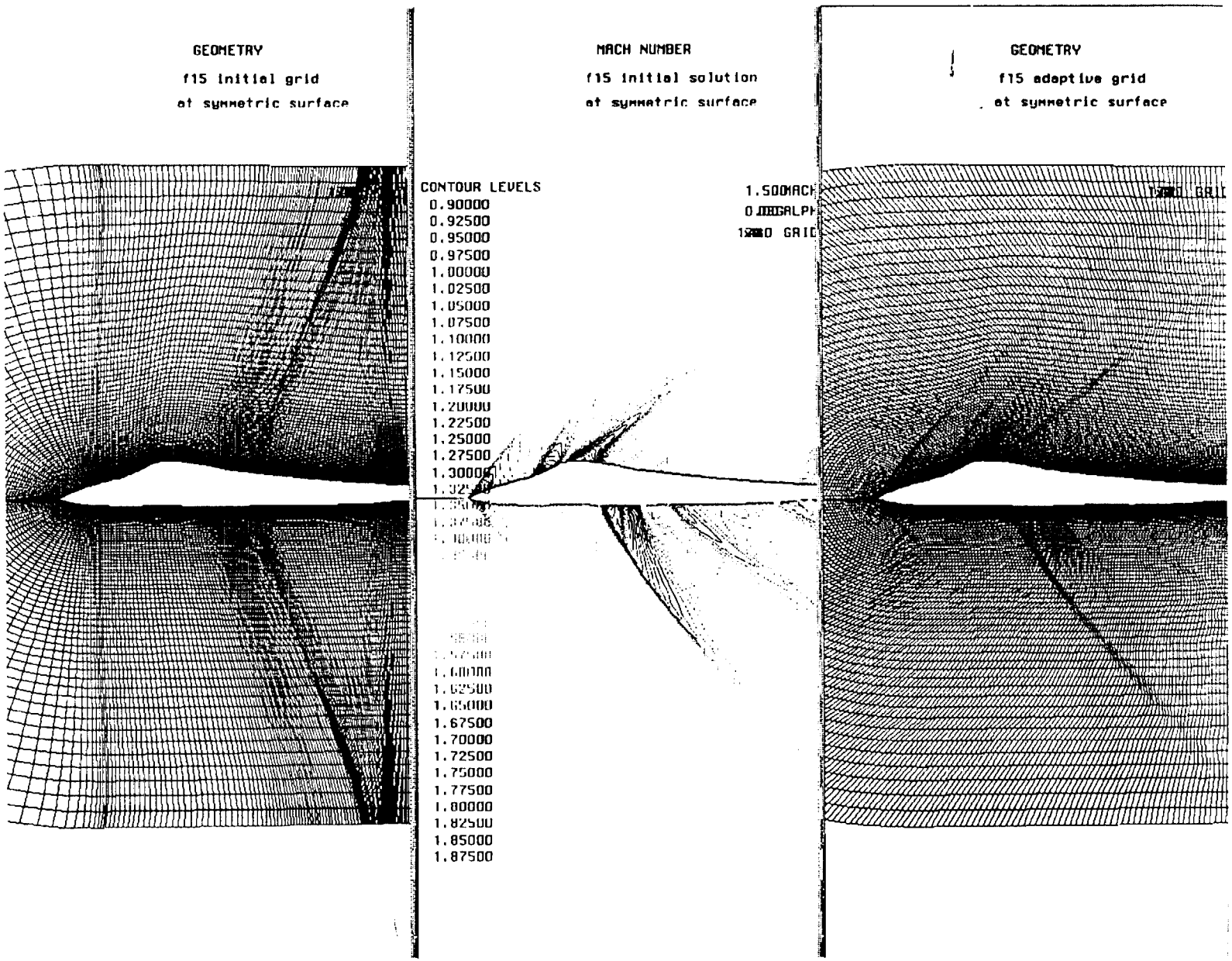

Figure 17.

3-D F-15 body and wing case, symmetric surface.

Helicopter Propeller Shock Prediction

Grid Size : Block 1 : 26 X 31 X 91

Block 2 : 26 X 31 X 91

Flow Solver Applied : MSUTC

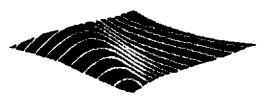

Figure 18.

3-D initial and adaptive grid for helicopter propeller.

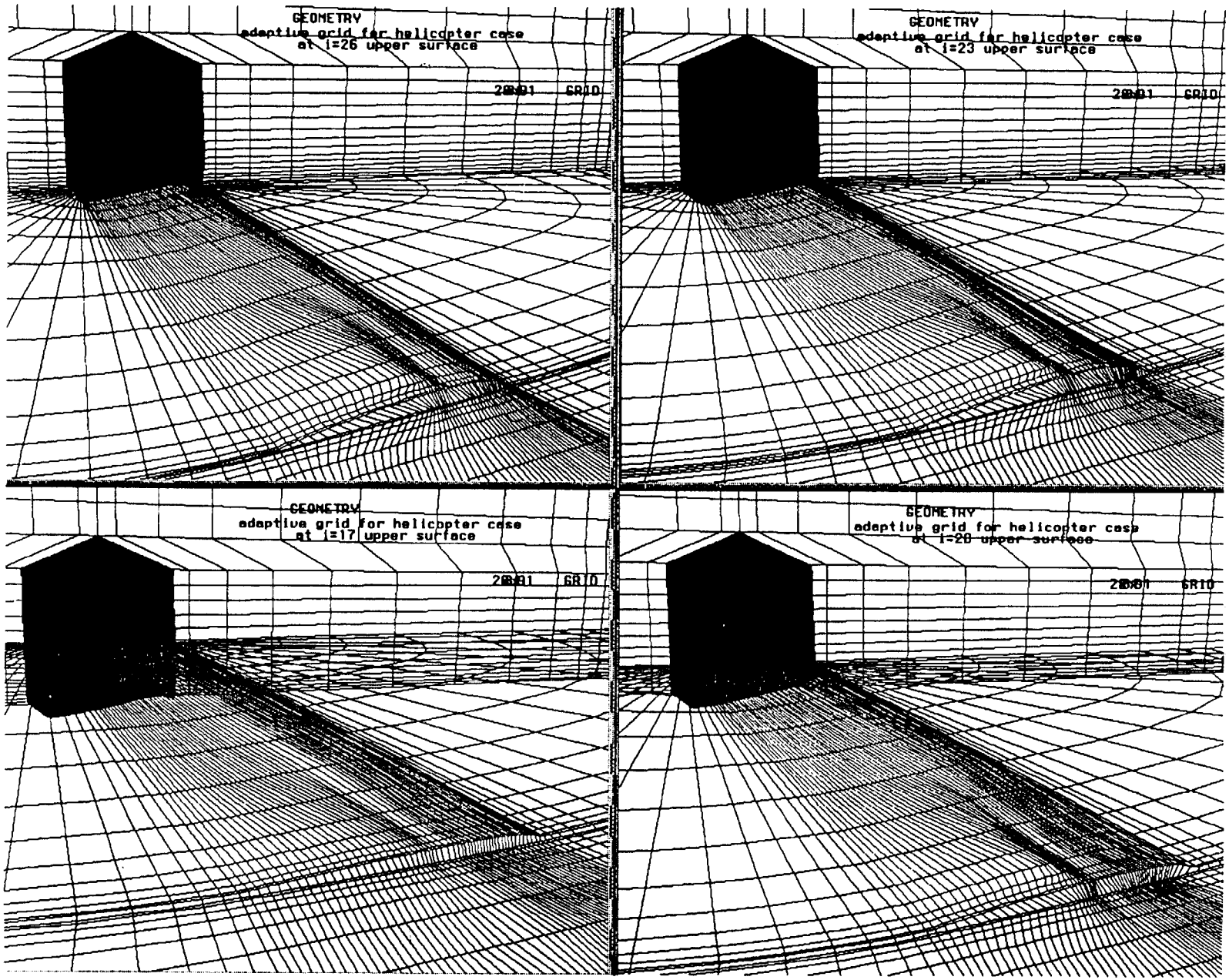

Figure 19.

3-D adaptive grid surfaces above the helicopter propeller.

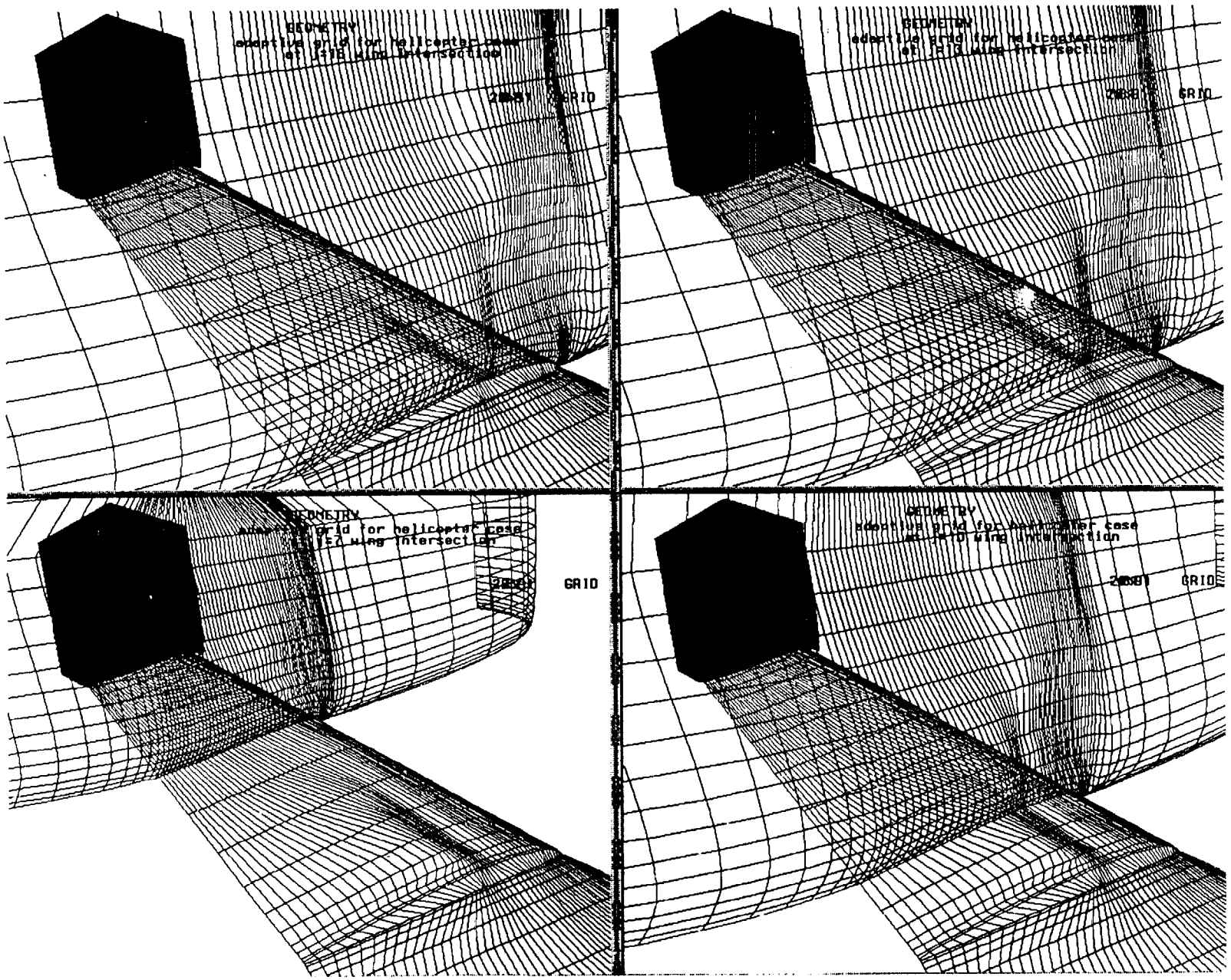

Figure 20.

3–D adaptive grid surfaces for the helicopter propeller intersection.

CONCLUSION

- Algebraic Structured Adaptive Grid Generation is fast
- NURBS makes the grid more smooth
- Boolean sum allows an appropriate weight to the flow characteristics
- More other flow characteristics can be added to the weight function

References

[1] Soni, B. K., "GENIE: GENeration of Computational Geometry–Grids for Internal Flow Configurations", *proceedings of Numerical Grid Generation in Computational Fluid Mechanics '88,* Miami, FL, 1988.

[2] Soni, B. K., "Grid Generation for Internal Flow Configurations", *Journal of Computers and Mathematics with Applications, 1991.*

[3] Thompson, J. F., "A Survey of Dynamically–Adaptive Grids in The Numerical Solution of Partial Differential Equations", *Applied Numerical Mathematics 1,* p. 3, North–Holland, 1985.

[4] Connett, W. C., Agarwal, R. K., and Schwartz, A. L., "An Adaptive Grid–Generation Scheme for Flow Field Calculations", AIAA–87–0199.

[5] Yu,T.Z. , "IGES Transformer and NURBS in Grid Generation", Master's thesis , Mississippi State University. August 1992 .

[6] G. K. Cooper and J.R. Sirbaugh, Sverdrup Technology, Inc., *PARC Code : Theory and Usage. Arnold Engineering Development Center, Arnold Air Force Base, Tennessee, 1989.*

[7] Abdollah Arabshahi and D. L. Whitfield, "A Multiblock Approach to Solving the Three–Dimensional Unsteady Euler Equations about a Wing–Pylon–Store Configuration", AIAA Atmospheric Flight Mechanics Conference, Aug. 14–16, 1989, Boston, Mass., 89–3401–CP.

[8] Peter M. Goorjian and Shigeru Obayashi, "Higher–Order Accuracy for Upwind Methods by Using the Compatibity Equations", AIAA Journal Vol. 31, No. 2, Feb. , 1993.

[9] J. P. Chen and D. L. Whitfield, "Navier–Stokes Calculations for the Unsteady Flowfield of Turbomachinery", 31st Aerospace Sciences Meeting & Exhibit, Jan. 11–14, 1993, Reno, NV, AIAA–93–0676.

An abstract for presentation at
Workshop for Computational Fluid Dynamics Applications in Rocket Propulsion
April 20-22, 1993
NASA/MSFC

A GENERIC EFFICIENT ADAPTIVE GRID SCHEME FOR ROCKET PROPULSION MODELING

J. D. Mo
Mechanical Engineering Department
Memphis State University
Memphis, TN 38152

Alan S. Chow
Combustion Science Branch
NASA/Marshall Space Flight Center
Huntsville, Al 35812

Abstract

The objective of this research is to develop an efficient, time-accurate numerical algorithm to discretize the Navier-Stokes equations for the predictions of internal one-, two-dimensional and axisymmetric flows. A generic, efficient, elliptic adaptive grid generator is implicitly coupled with the Lower-Upper factorization scheme in the development of ALUNS computer code. The calculations of one-dimensional shock tube wave propagation and two-dimensional shock wave capture, wave-wave interactions, shock wave-boundary interactions show that the developed scheme is stable, accurate and extremely robust. The adaptive grid generator produced a very favorable grid network by a grid speed technique. This generic adaptive grid generator is also applied in the PARC and FDNS codes and the computational results for solid rocket nozzle flowfield and crystal growth modeling by those codes will be presented in the conference, too. This research work is being supported by NASA/MSFC.

ORGANIZATION: COMBUSTION PHYSICS BR.	MARSHALL SPACE FLIGHT CENTER WORKSHOP FOR CFD APPLICATIONS IN ROCKET PROPULSION	NAME: ALAN S. CHOW
CHART NO.: No. 1		DATE: APRIL 21, 1993

A GENERIC EFFICIENT ADAPTIVE GRID SCHEME FOR ROCKET PROPULSION MODELING

Alan S. Chow
NASA/Marshall Space Flight Center
Huntsville, AL 35812

J. D. Mo
Memphis State University
Memphis, TN 38152

NASA/MSFC
Workshop for CFD Applications in Rocket Propulsion
April 20-22, 1993

MOTIVATION

* **Time-dependent sharp gradient region**
  -shock wave propagation
  -shedding vortex
* **Moving boundary**
  -time-dependent geometrical boundary
  (solid rocket chamber, etc.)
  -time-dependent free surface
* **Unknown sharp region for steady solution**
  -shock capture
  -boundary layer

OBJECTIVES

- To develop an adaptive grid generator
  - -efficient
  - -robust
  - -easy to be embodied in computer codes
  - -numerically stable with most schemes

Table of Contents

Elliptic PDEs for Grid Generation

$$\zeta_{xx} + \zeta_{yy} = P$$

$$\eta_{xx} + \eta_{yy} = Q$$

where P and Q are the control functions, and they could be

$$P = P_g + P_w + \ldots\ldots$$
$$Q = Q_g + Q_w + \ldots\ldots$$

CASE 1. SHOCK TUBE

P_1 (high pressure) P_2 (low pressure)

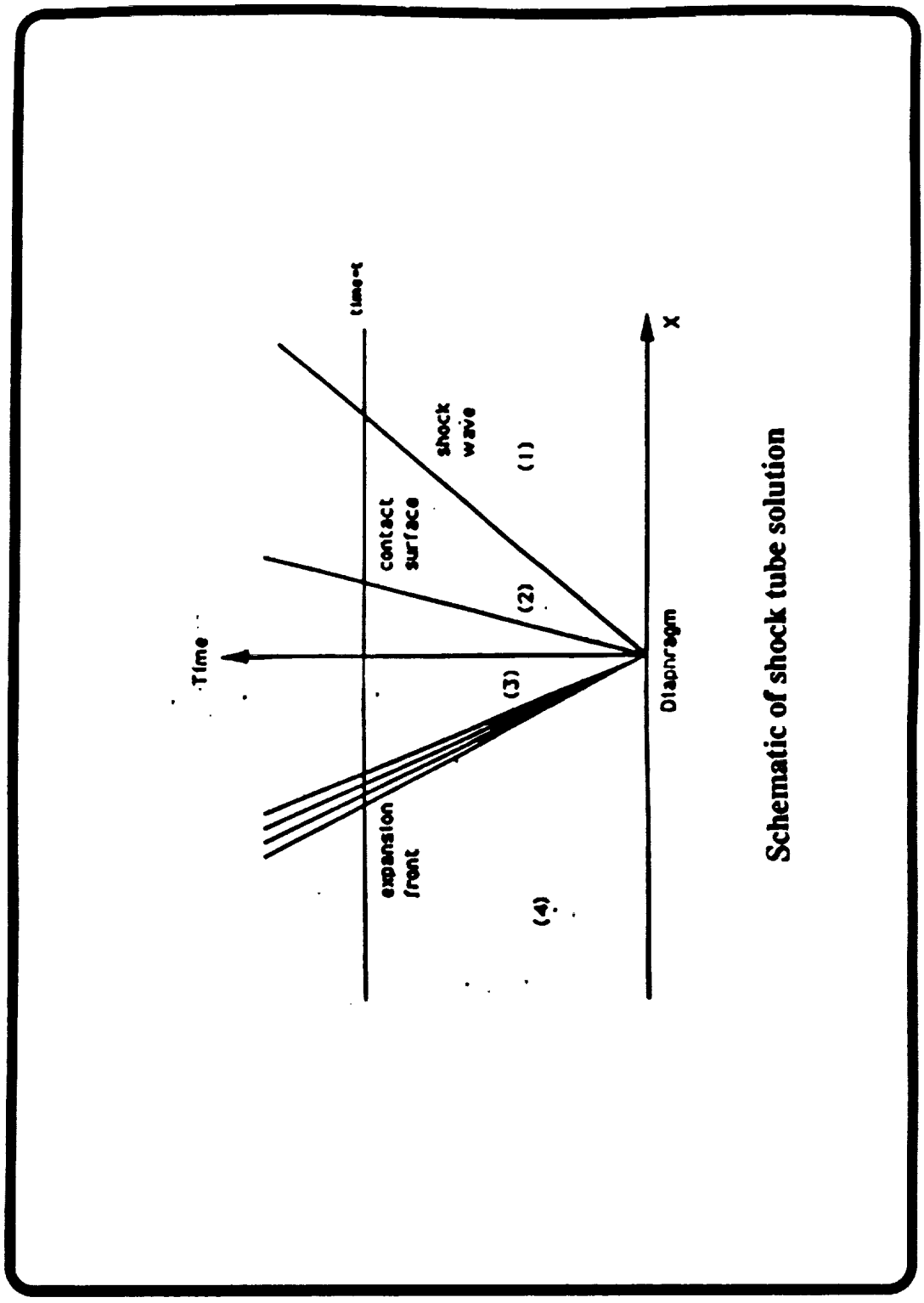

Schematic of shock tube solution

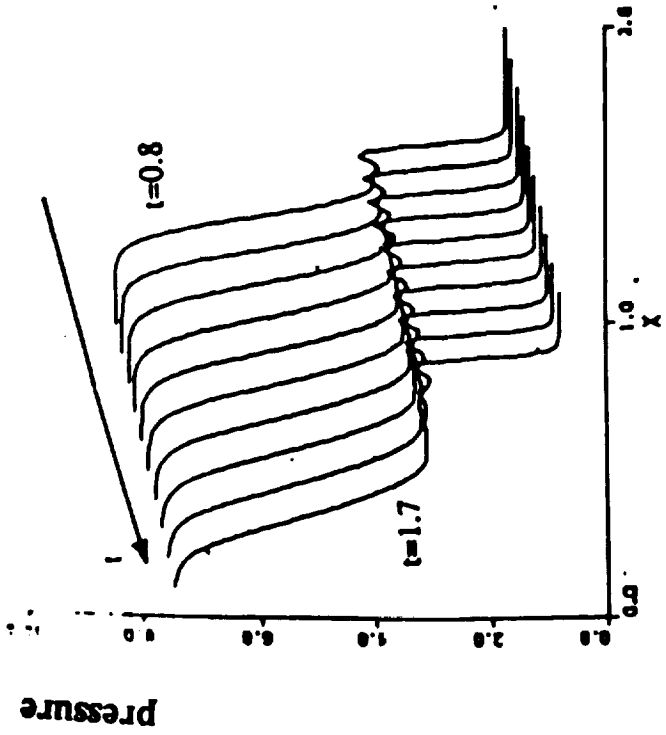

Shock tube pressure solution

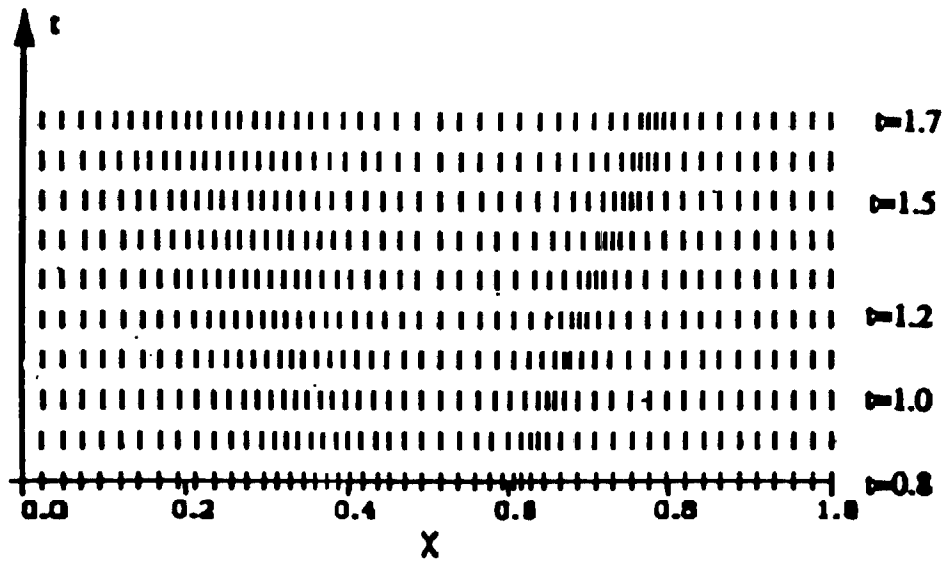

Time-accurate adaptive grid in one-dimensional shock tube simulation

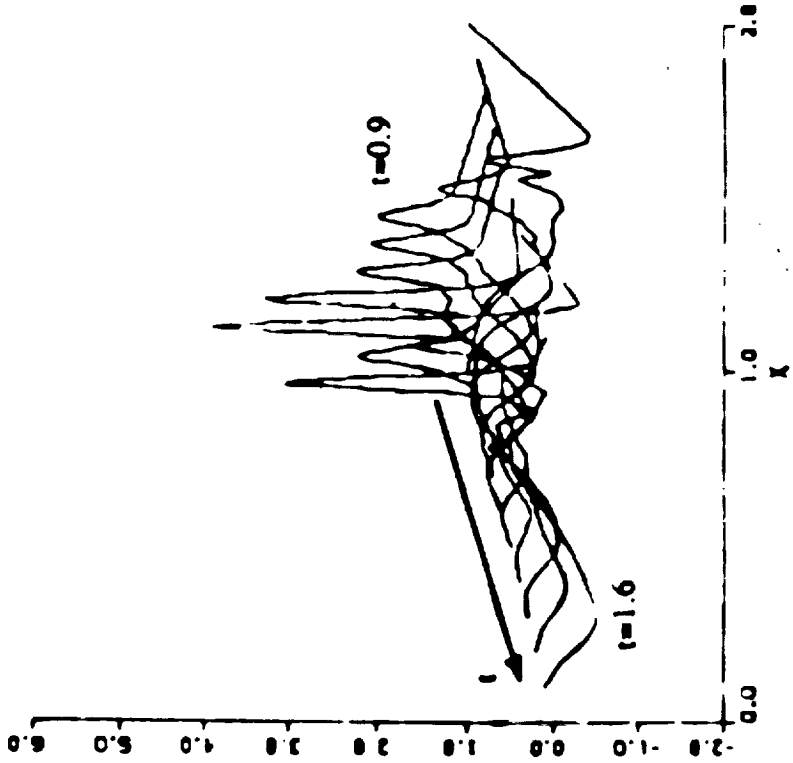

Adaptive grid speed in shock tube solution

CASE 2. SUPERSONIC RAMP INLET

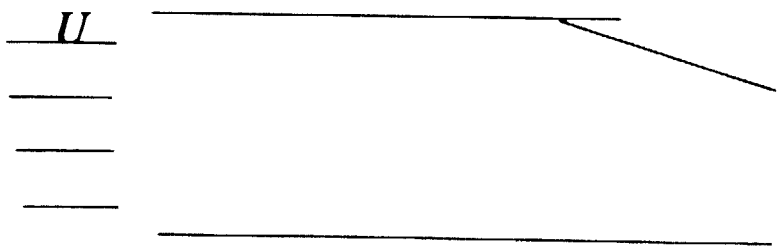

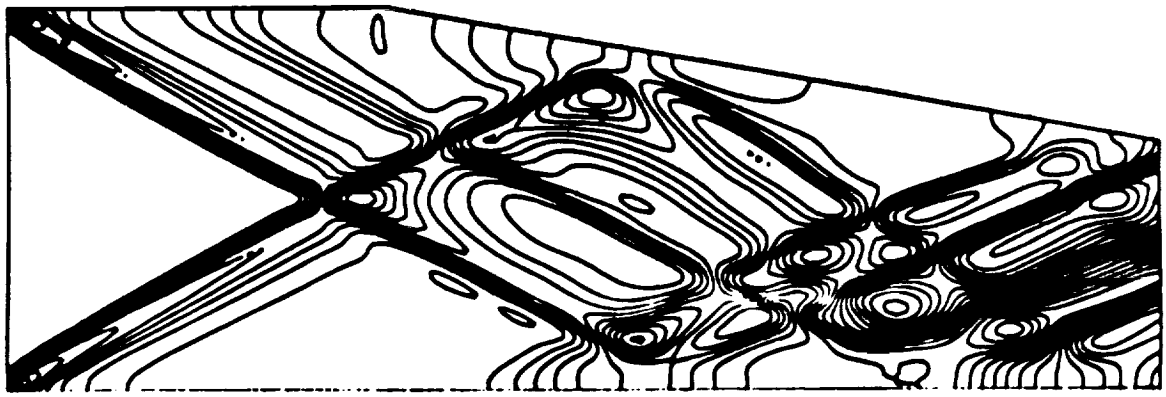

Pressure contour plot inside a two-dimensional duct.

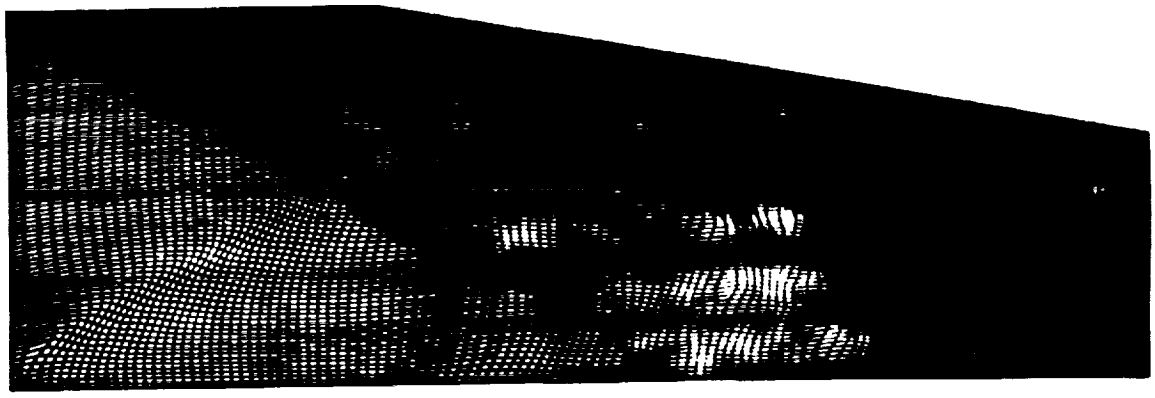

Adapted grid of a two-dimensional duct.

CASE 3. CAVITY FLOW SIMULATION

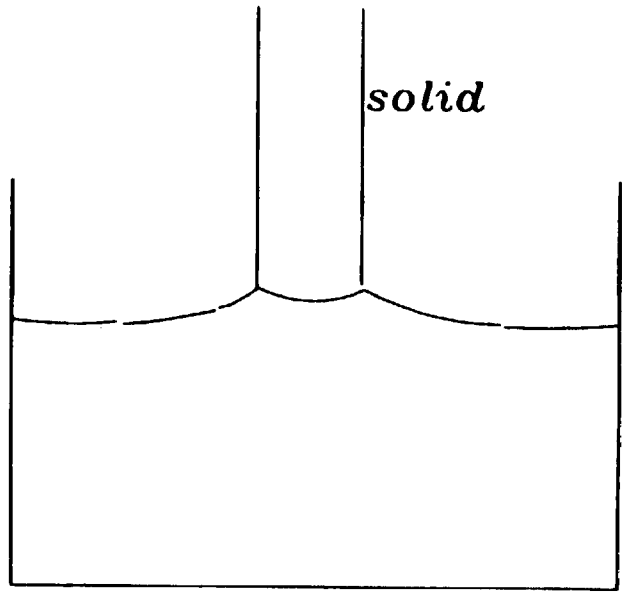

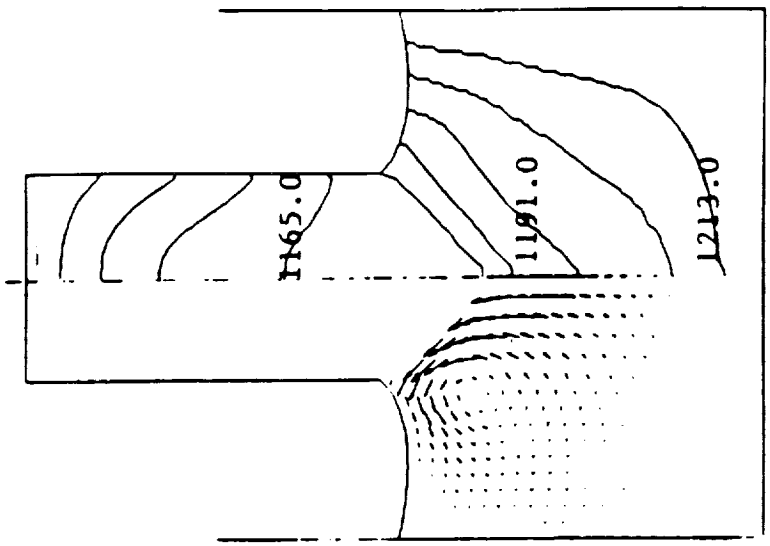

Flow field and isotherms

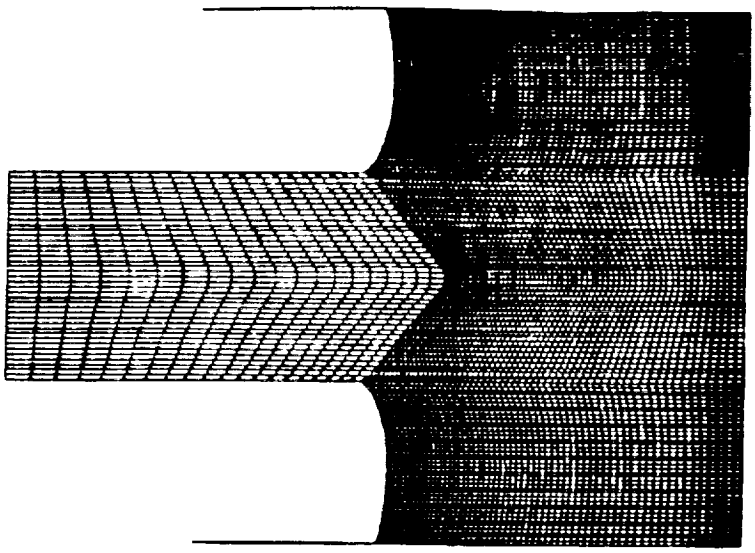

Computational grids

CASE 4. SOLID ROCKET NOZZLE FLOW MODELING

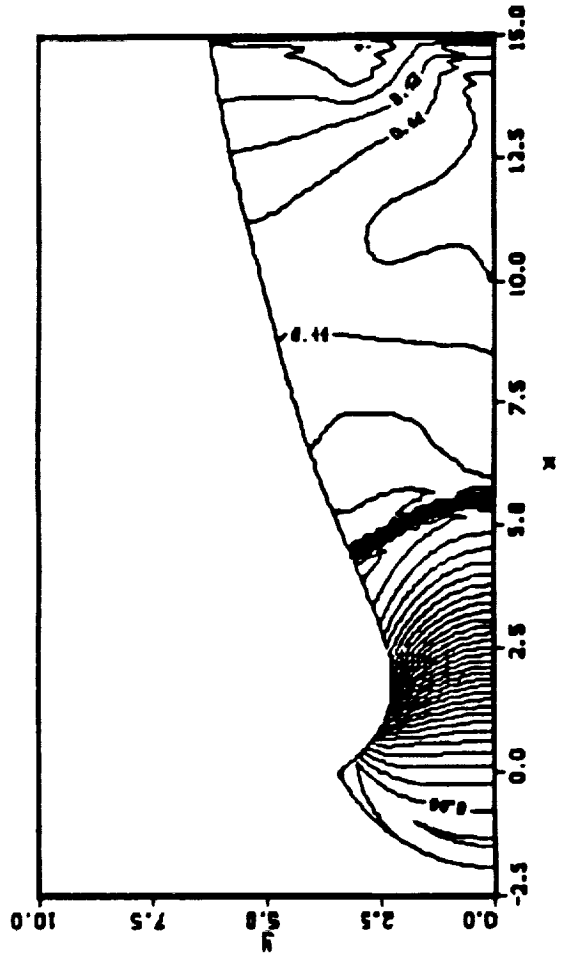

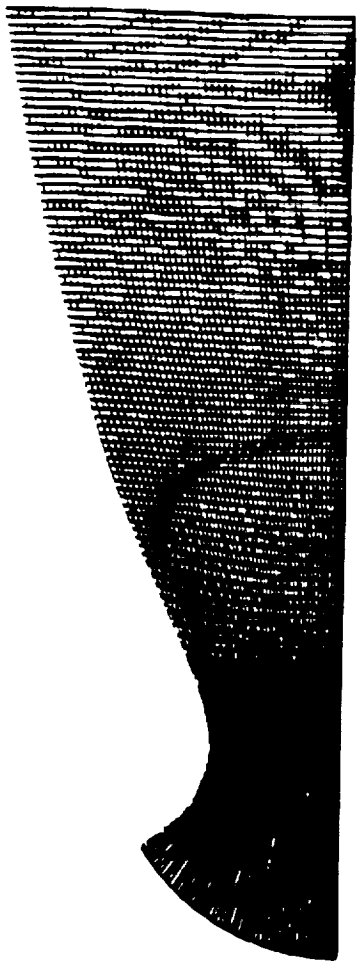

(b) An adapted grid

CONCLUSIONS

* Versatile grid generator
* Robust to general schemes (LU,FDNS,PARC)
* Efficient and compact

TIGER: A User–Friendly Interactive Grid Generation System For Complicated Turbomachinery And Axis–Symmetric Configurations

1149

Ming H. Shih

Bharat K. Soni

NSF Engineering Research Center For
Computational Field Simulation
Mississippi State University

Sponsor: NASA Lewis Research Center

April 21, 1993 CFD Workshop

Abstract

The issue of time efficiency in grid generation is addressed by developing a user–friendly graphical interface for interactive/automatic construction of structured grids around complex turbomachinery/axis–symmetric configurations. The accuracy of geometry modeling and its fidelity is accomplished by adapting the Non–Uniform Rational B–Spline (NURBS) representation.

A customized interactive grid generation code, TIGER[1–6], has been developed to facilitate the grid generation process for complicated internal, external, and internal–external turbomachinery fields simulations. The FORMS Library[7] is utilized to build user–friendly graphical interface (Figure 1). The algorithm allows a user to redistribute grid points interactively on curves/surfaces using NURBS formulation[8] with accurate geometry definition. TIGER's features include multi–block, multi–duct/shroud, multi–blade row, uneven blade count, and patched/overlapping block interfaces. It has been applied to generate grids for various complicated turbomachinery geometries (Figure 2), as well as to rocket and missile configurations (Figure 3).

Objectives

To develop an interactive grid generation system with user-friendly graphical user interface (GUI) customized for complicated turbomachinery configurations.

- **Accurate and Efficient**
- **Cost Effective (Labor time in overall grid generation)**
- **Timely for Engineering Design**

Features

- Compatible with various major industry formats for blade/shroud/duct/hub definition
- Multi–block, multi–blade row, multi–level duct/splitter uneven blade count
- CH/HH topologies with automatic domain mapping
- Journal capability
- External, internal, external–internal flow fields
- Automatic/default grid generation
- Interactive/iterative spacing specification
- User interaction for grid manipulation

Approach

- Originally developed as a module in GENIE
- Rewritten both in C and Frotran77 for better algorithm
- GUI with FORMS Library
- NURBS curve/surface for point re–distribution
- Bezier curve for grid line design/manipulation
- Weighted TFI for both surface/volume grid interpolation
- Elliptic system for surface/volume grid generation

TIGER System

O Grid Module:

Automatic/Default grid generation
User–Interactions:

- **RULER**
- **FRAME**
- **3D Manipulation**

O GVU Module:

Allows any block number, any number of patches in each block
Gouraund shading/Wireframe rendering
General Configurations

O ToolBox Module:

Converts various alien formats for geometry definition
2D LE/TE circle fitting

Applications

- **External flow fields:**

Hamilton Standard SR–7	(10 min)	**GE counter–rotating Propfan**	(15 min)
Naval CCOSC Torpedo	(1 hour)	**Various Missile Configurations**	

- **Internal flow fields:**

Rotor–67	(20 min)
Feul Inducer	(Have not yet tested with TIGER–II)

- **External–Internal flow fields:**

NASA Pressure Ration 1.15 Ducted Fan	(1~2 hours)
Pratt & Whitney Advanced Ducted Propfan (ADP)	(1~2 hours)
GE Energy Efficiency Engine Mockup	(1~2 hours with fan only)

Future Developments

- **Grid Module:**
  - Mixed Grid Topologies (CO/CC/HO/HC)
  - 2D capability
  - Tip Clearance Modeling
- **Flow Module:**
  - Flow Solver Coupling (Whitfield/Janus/Chen/Taylor)
  - Common I/O, Data Structure
- **Visualization Module:**
  - Flow Solution Visualization (Contour/Vector/Particle Trace)
  - Flow Solver BC/IC Setup Panel
- **ToolBox Module:**
  - Rotor Tip Cutter (Spherical)
  - 3D Blade LE/TE Circle Fitting
  - CAD Interface (CAGI)

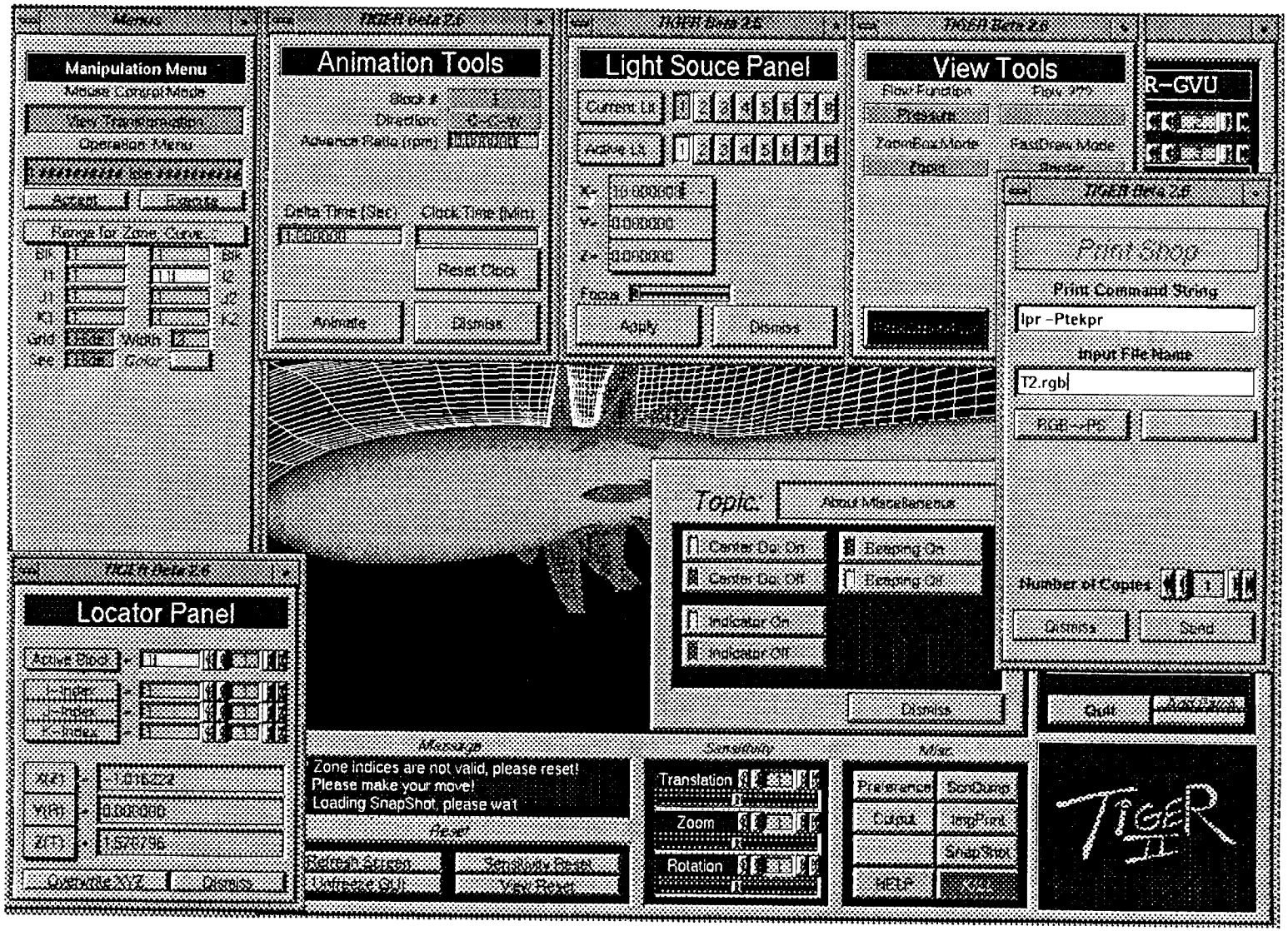

Figure 1. Tiger Graphical User Interface

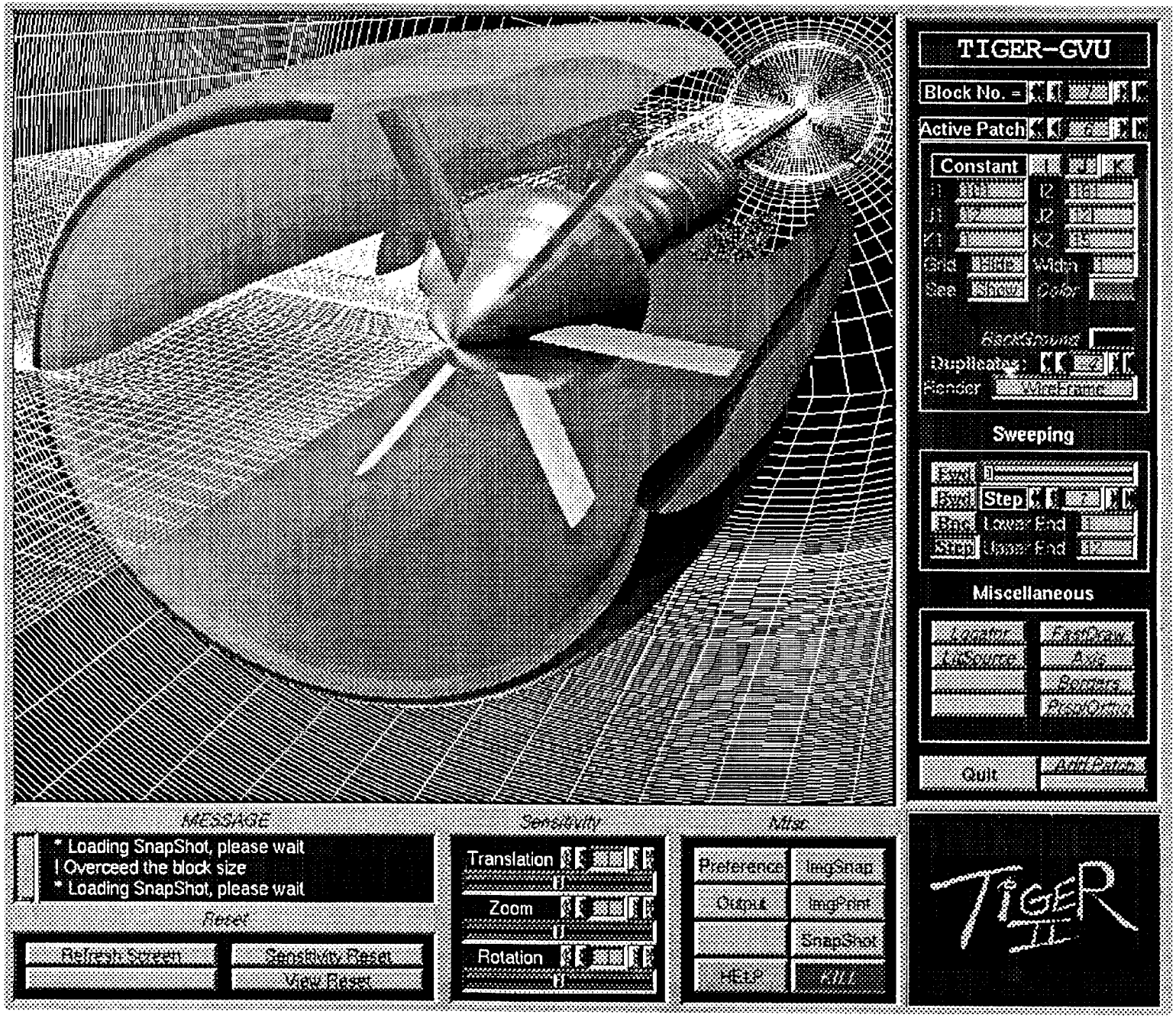

Figure 2. Engine Mockup

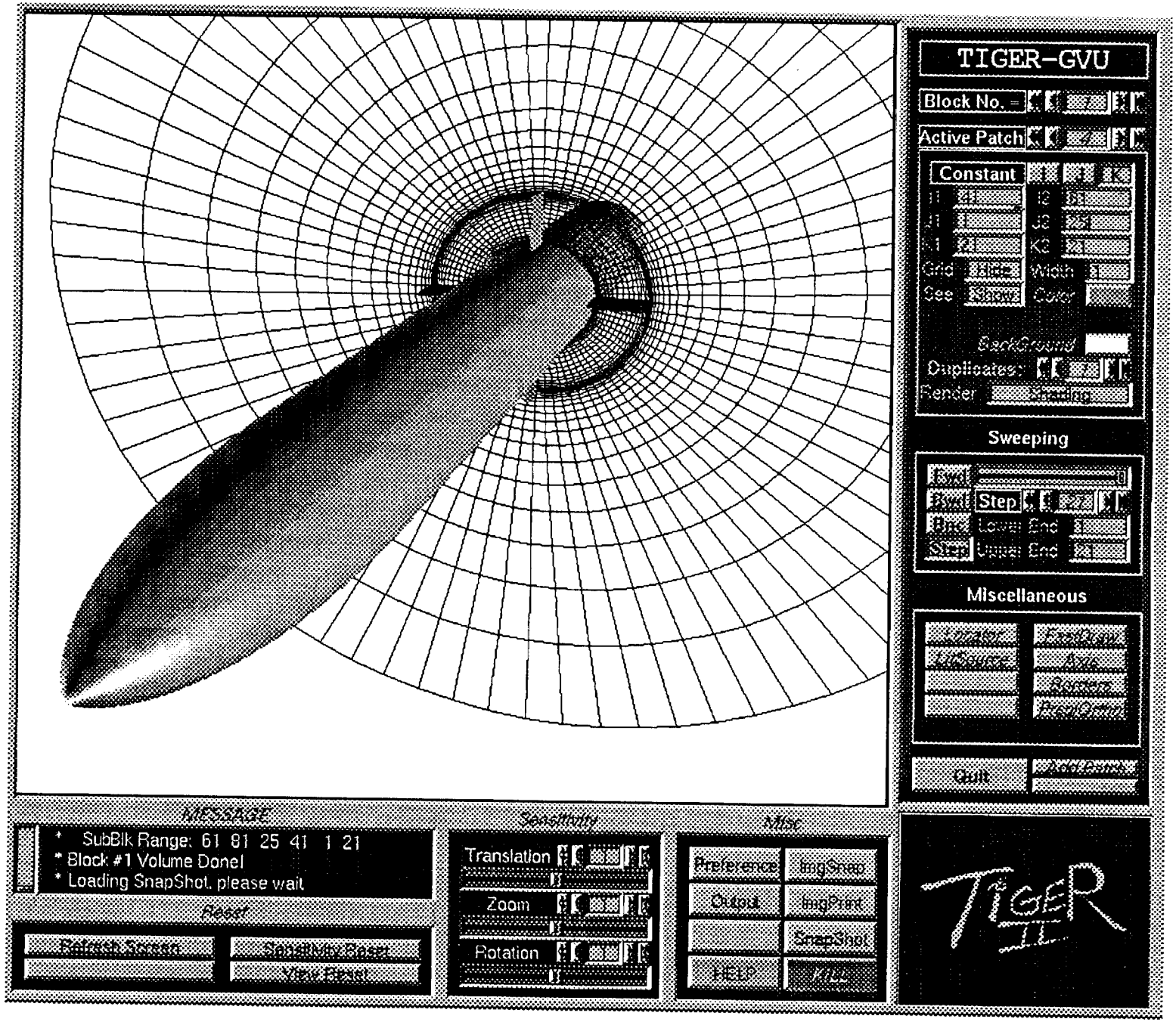

Figure 3. Missile Configuration

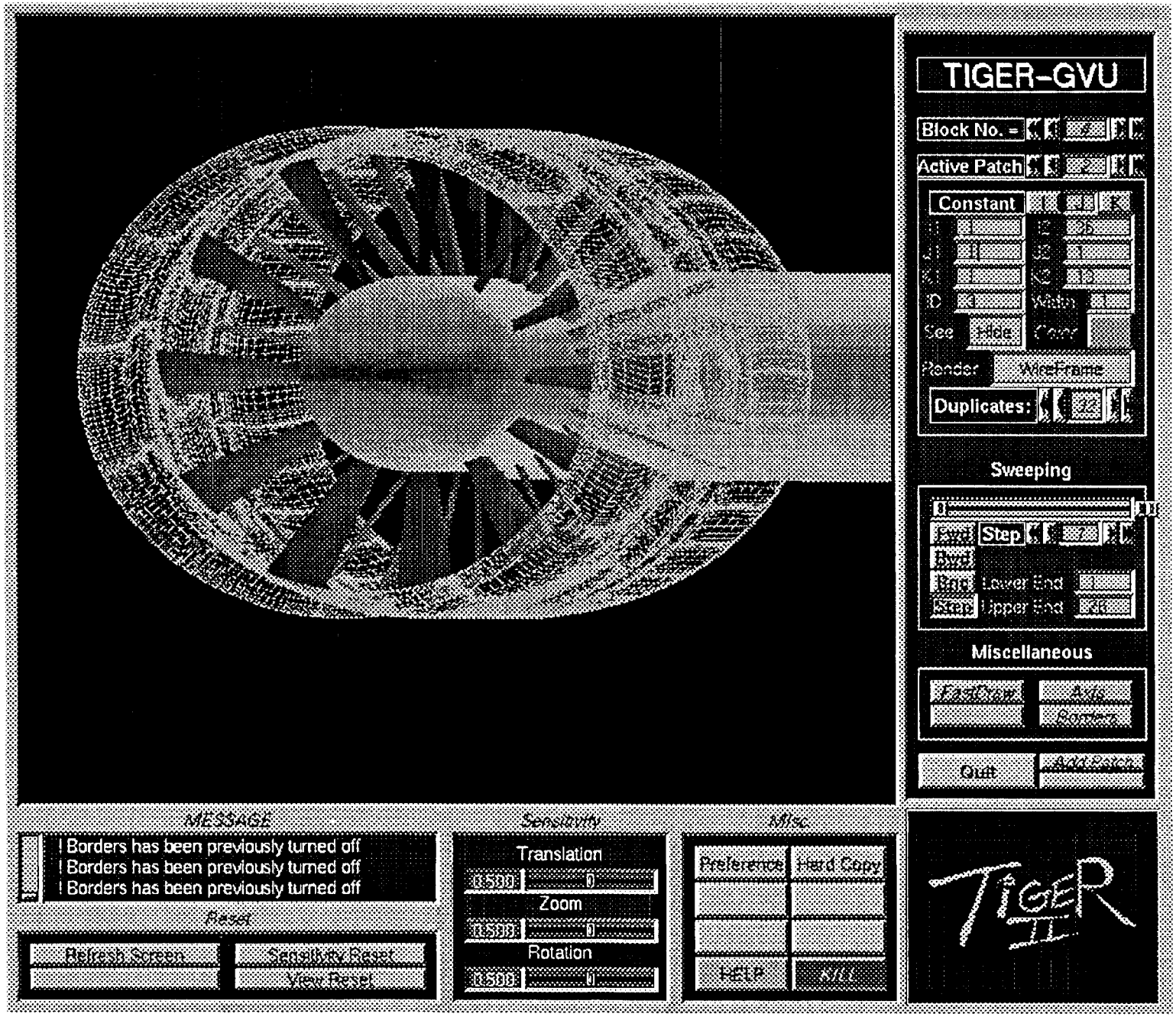

Figure 4. NASA Pressure Ratio 1.15 Ducted Fan

References

1. Shih, M.H. and Soni, B.K., "Grid Generation for 3D Turbomachinery Confiturations", AIAA-92-3671, AIAA/SAE/ASME/ASEE 28th Joint Propulsion Conference, Nashville, TN, July 1992.
2. Shih, M.H. and Soni, B.K., "Geometry Modeling and Multi-Block Grid Generation For Turbomachinery Configurations", Proceedings of the NASA Workshop on Software Systems for Surface Modeling and Grid Generation, Hampton, VA, April 1992.
3. Soni, B.K., Thompson, J.F., Stokes, M., and Shih, M.H., "*GENIE*$^{++}$, *EAGLEView and TIGER: General and Special Purpose Graphically Interactive Grid Systems*", 30th Aerospace Sciences Meeting & Exhibit, AIAA-92-0071, Reno, Nevada, January 1992.
4. Soni, B.K. and Shih, M.H., "TIGER: Turbomachinery Interactive Grid GenERation", Proceedings of the Third International Conference of Numerical Grid Generation in CFD, Barcelona, Spain, June 1991.
5. Soni, B.K. and Shih, M.H., "TURBOGRID: Turbomachinery Applications of Grid Generation", 26th AIAA/SAE/ASME Joint Propulsion Conference, AIAA-90-2242, Orlando, Florida, July 1990.
6. Shih, M.H., "TIGER: Turbomachinery Interactive Grid genERation", Master's Thesis, Mississippi State University, December 1989.
7. Overmars, M.H., "FORMS: A Graphical User Interface Toolkit for Silicon Graphics Workstations", Department of Computer Science, Utrecht University, Utrecht, Netherlands, 1991.
8. Yu, T.Y., "IGES Transformer And NURBS In Grid Generation", Master's Thesis, Mississippi State University, August 1992.

Towards A Generalized Computational Fluid Dynamics Technique for all Mach Numbers

R. W. Walters, D. C. Slack and A. G. Godfrey

Statement of the Problem

Currently there exists no single unified approach for efficiently and accurately solving computational fluid dynamics (CFD) problems across the Mach number regime, from truly low speed incompressible flows to hypersonic speeds. There are several CFD codes that have evolved into sophisticated prediction tools with a wide variety of features including multi-block capabilities, generalized chemistry and thermodynamics models among other features. However, as these codes evolve, the demand placed on the end user also increases simply because of the myriad of features that are incorporated into these codes. In order for a user to be able to solve a wide range of problems, several codes may be needed requiring the user to be familiar with the intricacies of each code and their rather complicated input files. Moreover, the cost of training users and maintaining several codes becomes prohibitive.

Objective of the Work

The objective of the current work is to extend the compressible, characteristic-based, thermochemical nonequilibrium Navier-Stokes code GASP to very low speed flows and simultaneously improve convergence at all speeds. Before this work began, the practical speed range of GASP was Mach numbers on the order of 0.1 and higher. In addition, a number of new techniques have been developed for more accurate physical and numerical modeling.

Approach Used

The primary focus has been on the development of optimal preconditioning techniques for the Euler and the Navier-Stokes equations with general finite-rate chemistry models and both equilibrium and nonequilibrium thermodynamics models. We began with the work of Van Leer, Lee, and Roe for inviscid, one-dimensional perfect gases and extended their approach to include three-dimensional reacting flows. The basic steps required to accomplish this task were a transformation to steam-aligned coordinates, the formulation of the preconditioning matrix, incorporation into both explicit and implicit temporal integration schemes, and modification of the numerical flux formulae. In addition, we improved the convergence rate of the implicit time integration schemes in GASP through the use of inner iteration strategies and the use of the GMRES (General Minimized RESisual) which belongs to the class of algorithms referred to as Krylov subspace iteration. Finally, we significantly improved the practical utility of GASP through the addition of mesh sequencing, a technique in which computations begin on a coarse grid and get interpolated onto successively finer grids.

Conclusions Relevant to Rocket Propulsion

The fluid dynamic problems of interest to the propulsion community involve complex flow physics spanning different velocity regimes and possibly involving chemical reactions. This class of problems results in widely disparate time scales causing numerical *stiffness*. Even in the absence of chemical reactions, eigenvalue stiffness manifests itself at transonic and very low speed flows which can be quantified by the large condition number of the system and evidenced by slow convergence rates. This results in the need for thorough numerical analysis and subsequent implementation of sophisticated numerical techniques for these difficult yet practical problems. As a result of this work, we have been able to extend the range of applicablity of compressible codes to very low speed inviscid flows (M=.001) and reacting flows. Our work now centers on the extension to viscous flows.

Towards a Generalized Computational Fluid Dynamics Technique for all Mach Numbers

R. W. Walters, D. C. Slack, and A. G. Godfrey

Workshop for CFD Applications in Rocket Propulsion
Marshall Space Flight Center
April 20-22, 1993

AeroSoft

Outline

- Phase I Objectives
- Recent improvements and enhancements
- Results
- Phase II Objectives and schedule

Source Code File Structure

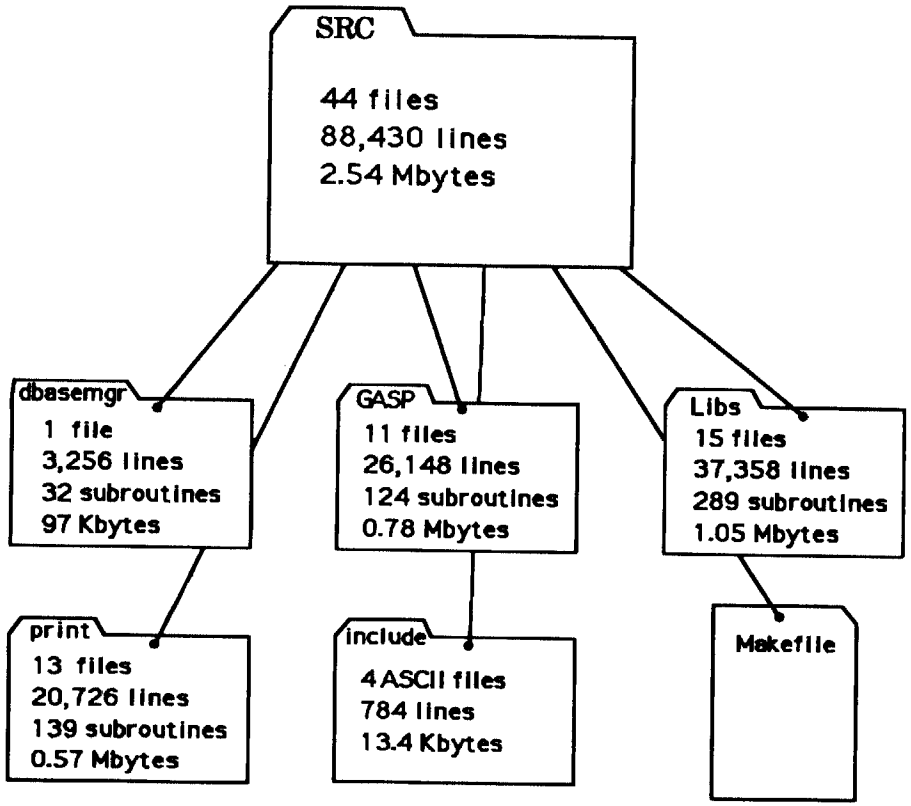

AeroSoft

GASP 2.0

GASP Version 2.2 Extended Features

Basic Features

- Solves steady and unsteady 3-D, Reynolds-Averaged, Navier-Stokes Equations (RANS) and subsets:
  - Thin-layer Navier-Stokes (TLNS)
  - Parabolized Navier-Stokes (PNS)
  - Euler equations
- Fully conservative, cell-centered, upwind, finite volume code
  - 3D, 2D, axisymmetric
  - Multiple grids
- Explicit & implicit time integration of primitive variables
- Finite-rate, frozen, & equilibrium chemistry, mixtures
- Equilibrium and nonequilibrium thermodynamics models

Fluxes and Jacobians

- Roe, Van Leer, and Steger-Warming flux splittings
- Approximate Roe linearization, complete Van Leer Jacobian
- Full flux with Vigneron technique and complete linearization

Chemistry

- Fully coupled finite-rate chemistry
- Species and Reaction databases for thermochemical properties
  - stand alone database manager
- Extended rate equations curve fits
- Complete reaction sets for existing chemistry models

Thermodynamics

- Equilibrium and non-equilibrium thermodynamics models
- NASA LeRC extended curve fit option
- Equilibrium curve fits
  - Tannehill TGAS routines
  - Liu and Vinokur curve fits

Time Integration

- m-stage Runge-Kutta integration
- 3-Factor Approximate Factorization (AF)
- 2-Factor AF/Relaxation in third direction
  - supports all (i,j,k) combinations
- Option to freeze LU elements

AeroSoft

GASP Version 2.2 Extended Features

Boundary Conditions
- User-selectable list of explicit and implicit boundary conditions:
  - Inflow/Outflow
  - Solid surface
  - Zonal boundaries

Turbulence Models
- Fully-coupled two-equation models
  - Characteristic-based treatment of the convective terms
  - Sarkar's compressibility correction
- Baldwin-Lomax algebraic model in any two logical directions
  - Option for Goldberg's backflow model

Graphical User Interface
- Implemeted as a FAST module
- Contains On-line documentation
- Performs consistency and error checks
- Graphical display of boundary conditions
- Constructs syntactically correct input

Mesh Sequencing
- Requires a single input deck per zone
- Refinement may be performed in any or all of the logical directions (i,j,k)
- Restart files contain solutions on all grids for convergence studies

Space-Marching
- Valid for many:
  - supersonic, inviscid flows (Euler)
  - high speed viscous flows (PNS)
- March in any logical (i,j,k) direction
- Use the same grid for PNS, TLNS, and RANS calculations

Post-Processing
- Integrated quantities, e.g. lift & drag
- Improvements & enhancements to the GASP 1.x output utilities
- Support for PLOT3D, FAST, and TECPLOT TM
- English and SI units

AeroSoft

Phase I Objectives

- Preconditioning for Inviscid Flows
- Mesh Sequencing
- GMRES and Jacobi inner iterations
- 3 Factor AF, Jacobi & Gauss Seidel solvers
- Documentation

Inner Iterations

- Improve Update Vector Δq
- Approaches Exact Solution of Linear Problem
- Relatively Inexpensive
- Most Useful with Block Jacobi Time Integration

Ramllc Blunt Body

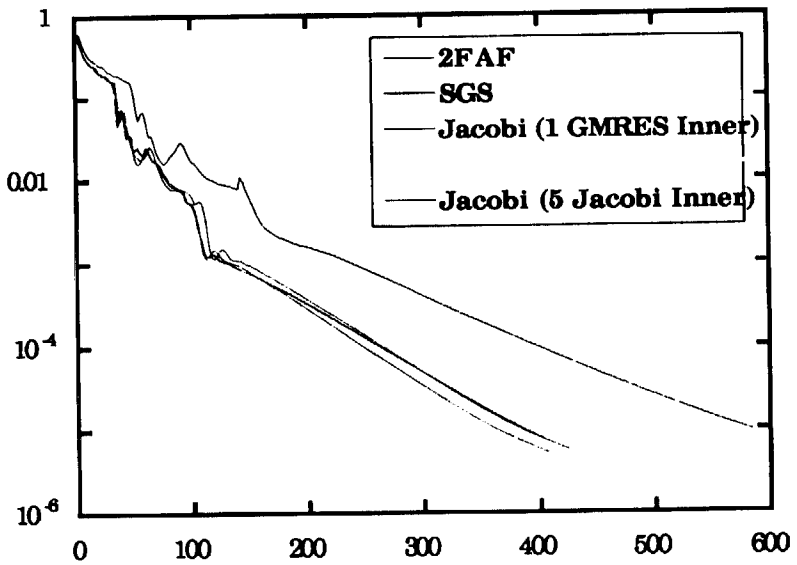

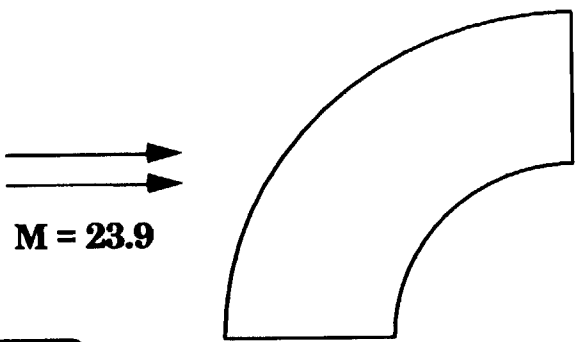

AeroSoft

GASP 2.0

Transonic Flow over Circular Arc

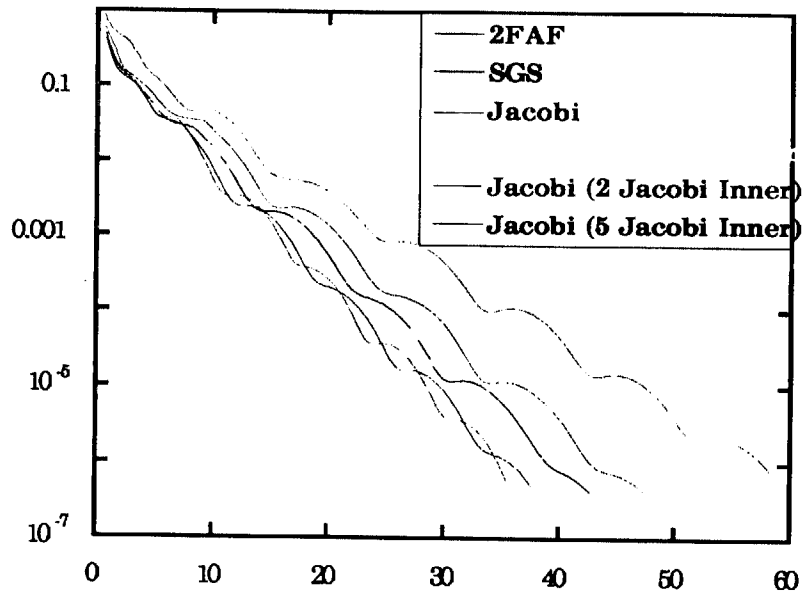

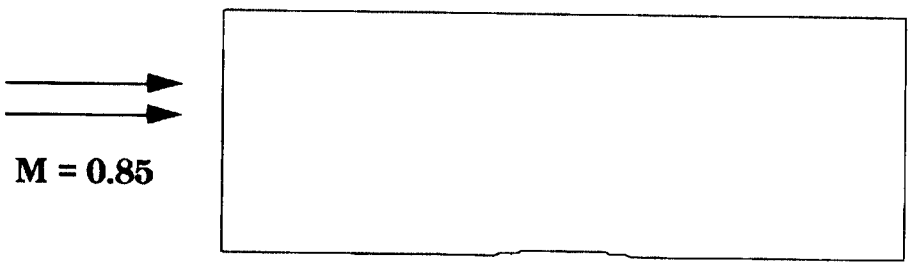

AeroSoft

GASP 2.0

Basic Steps in Preconditioning Analysis

- Transformation of governing equations to stream-aligned coordinates
- Formulation of the Preconditioning Matrix
- Incorporation into explicit and implicit time integration schemes
- Modification of the numerical flux formula (Roe's scheme)

Preconditioned 2-D Euler Equations

Euler equations: $$\frac{\partial Q}{\partial t} = -P \left(\frac{\partial F}{\partial x} + \frac{\partial G}{\partial y} \right)$$

Steady state: $$\frac{\partial Q}{\partial t} = 0$$ **implies** $R(q) = 0.$

Fourier Footprints

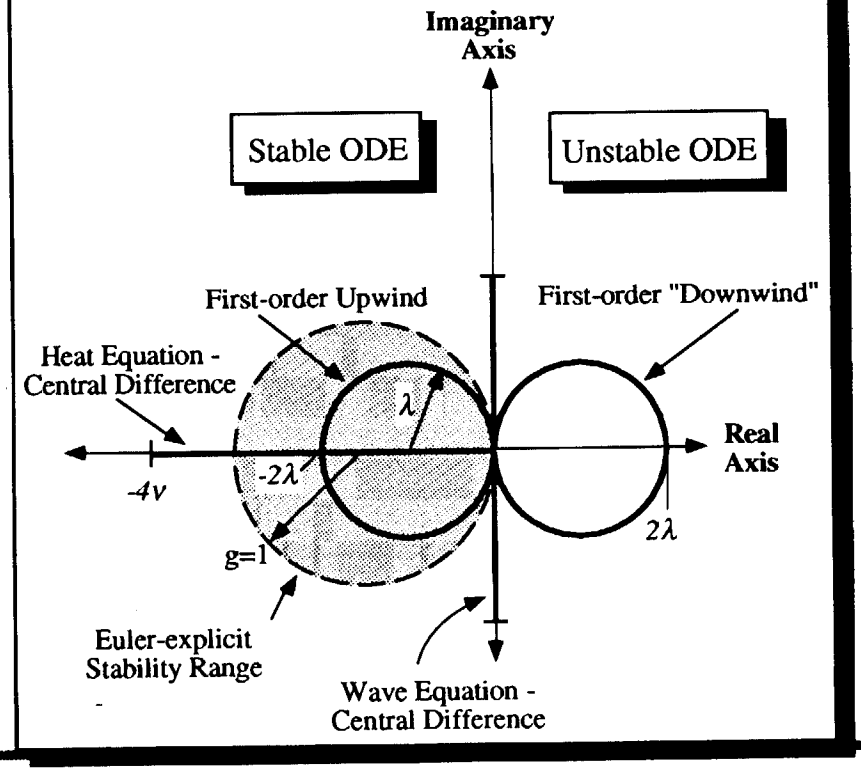

AeroSoft

Viscous Preconditioning

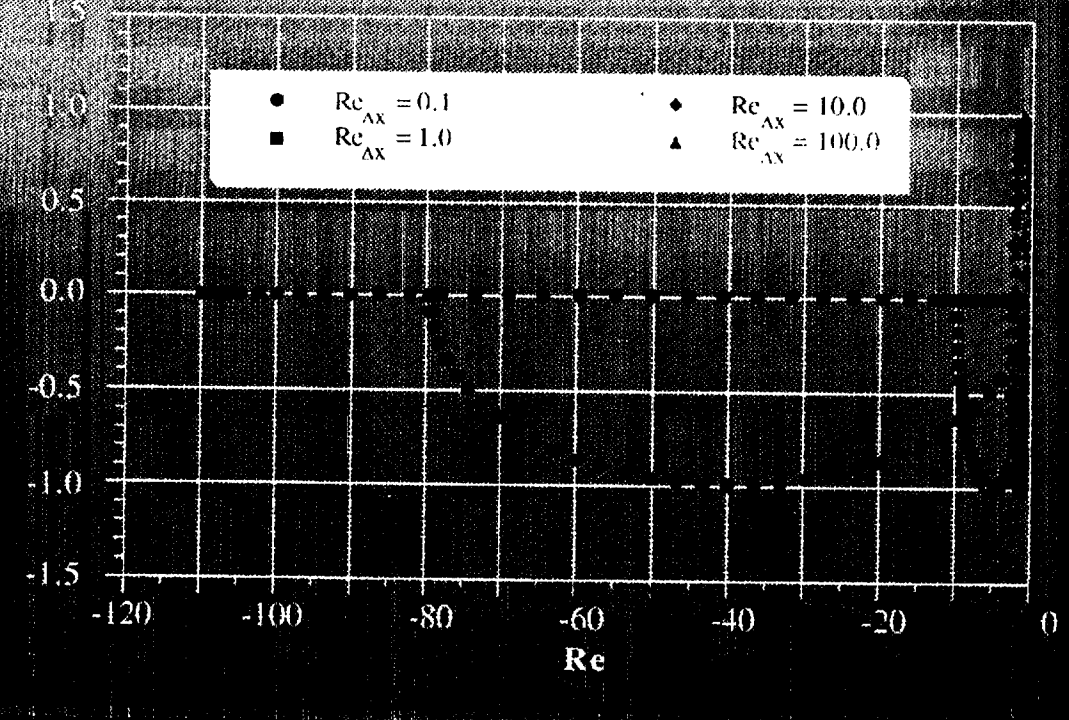

Inviscid 1-D *P* with $\tau = 1$

A Viscous Pre. Matrix

$$P = (|A| + \frac{2A}{Re})^{-1}$$

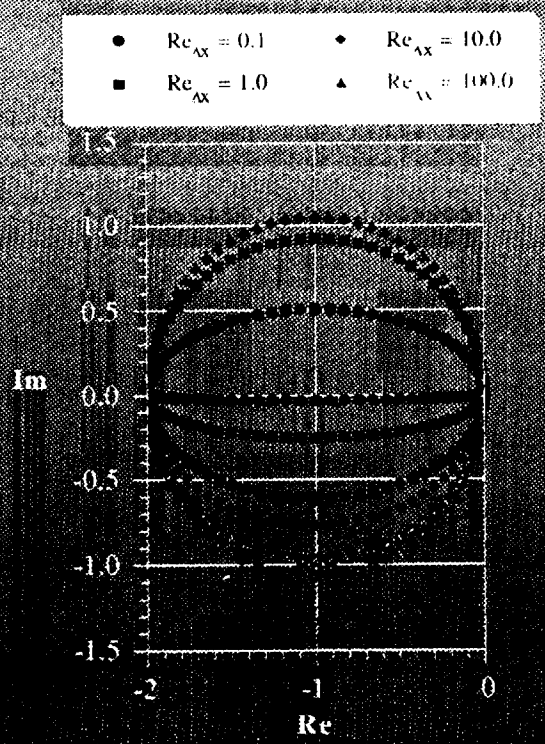

GASP Version 2.2 *New* Features

- **Improved turbulence modeling**
  - All algebraic and Two-equation models more accurate
    See Figure 1.
  - New k-ε minimization routine
  - Sarkar's compressibility correction
  - Goldberg's backflow extension to the Baldwin-Lomax model
- **Graphical User Interface - Version 1.1**
  - FAST™ Module (requires Silicon Graphics workstation)
- **New limiters**
  - Venkat's limiter with the improved convergence property
    See Figure 2. Reference AIAA-93-0880
  - The highly compressive Superbee limiter
  - Characteristic-based limiting option for all limiters

GASP Version 2.2 *New* Features

- **Improved implementation of the Vigneron Technique**
  See Figure 3. Reference AIAA-92-0189
- **New Binary Conversion Utility**
  - Convert Grid and Solution 'C' Binary files between architectures
    Cray, IEEE
- **Miscellaneous Improvements**
  - Entropy fix for Roe's numerical flux function
  - Extended Residual file format
  - CFL / Time Step ramping
- **Revised User Manual**
  - New chapter on theoretical formulation
  - Revised Quick Reference Cards

AeroSoft

Recent Improvements Made to Turbulence Models

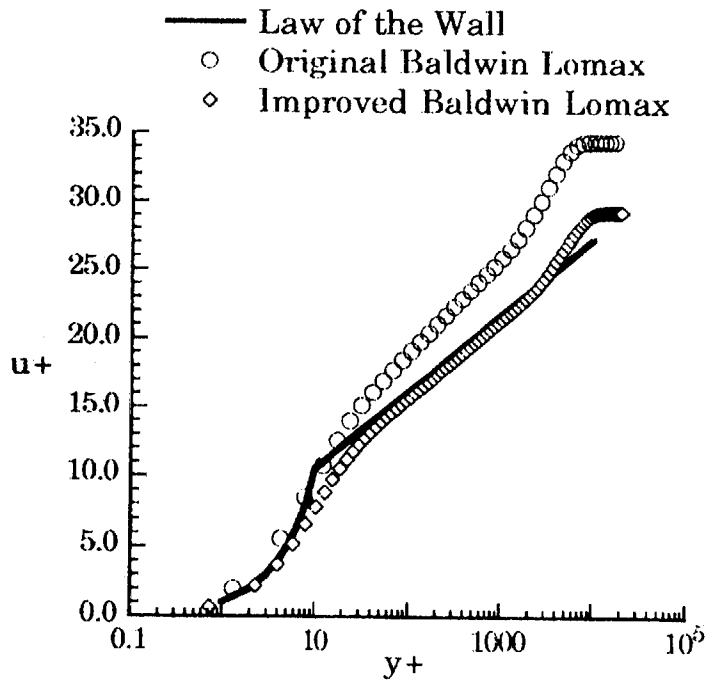

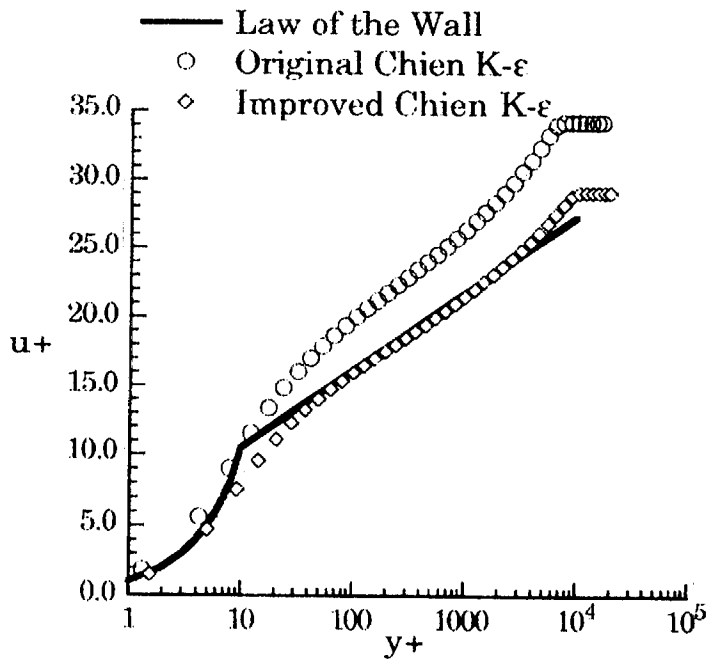

NASA

AeroSoft

Mach 6.5, Flow Over a Flat Plate, Comparison to Data

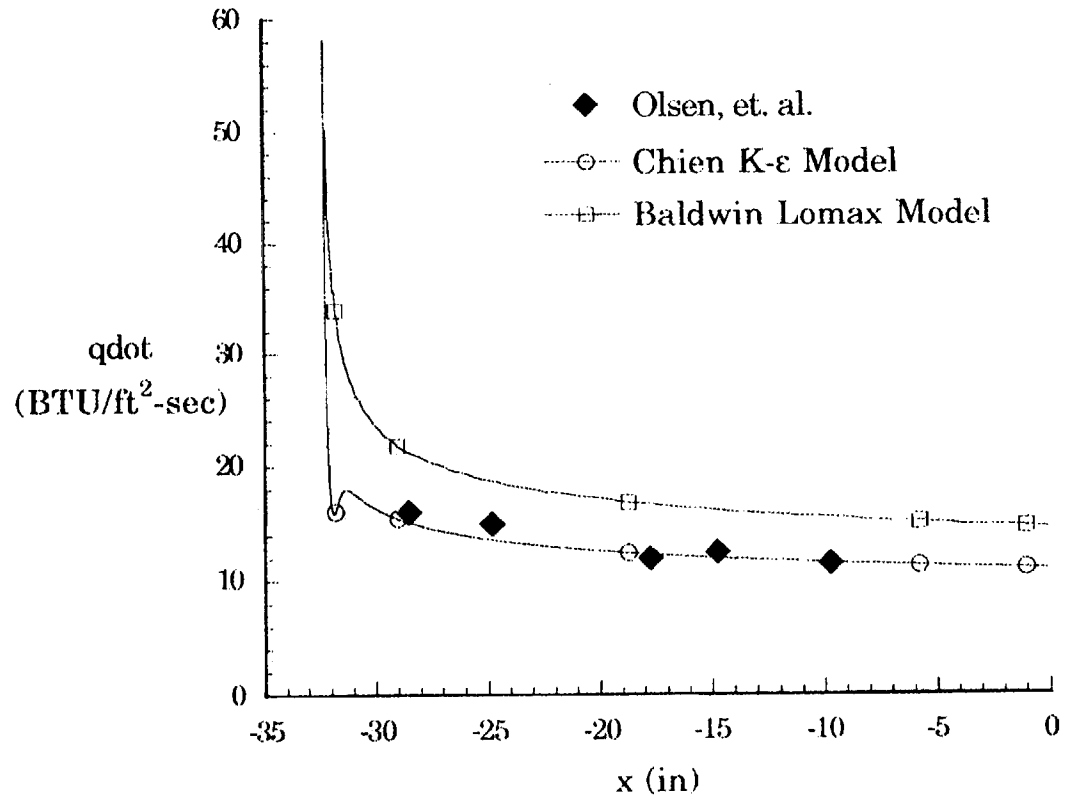

NASA

AeroSoft

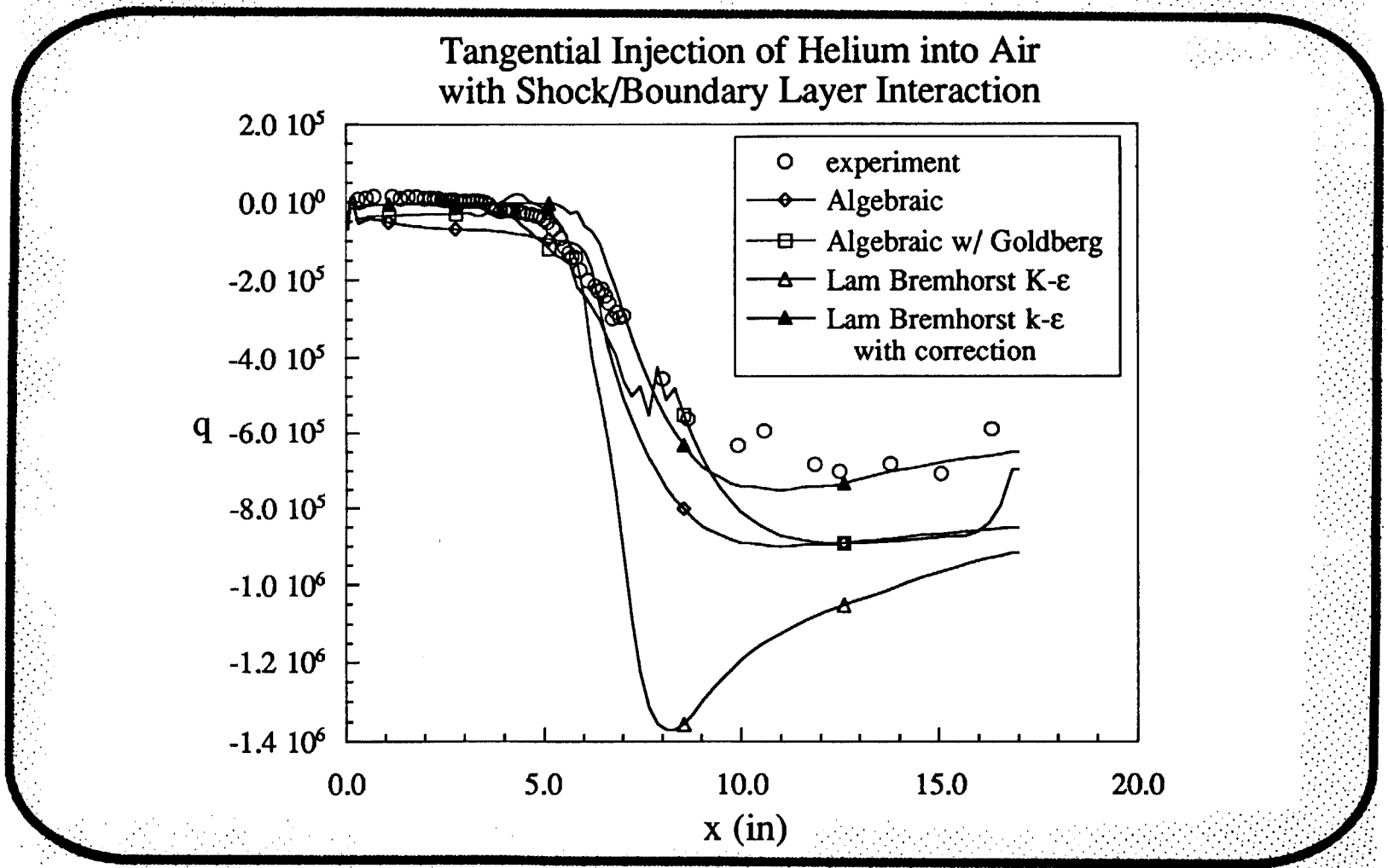
Tangential Injection of Helium into Air
with Shock/Boundary Layer Interaction
2.0 10^5
0.0 10^0
-2.0 10^5
-4.0 10^5
q -6.0 10^5
-8.0 10^5
-1.0 10^6
-1.2 10^6
-1.4 10^6
0.0
5.0
10.0
15.0
20.0
x (in)
experiment
Algebraic
Algebraic w/ Goldberg
Lam Bremhorst K-ε
Lam Bremhorst k-ε
with correction

AeroSoft

Limiter comparison for the Shock Reflection problem

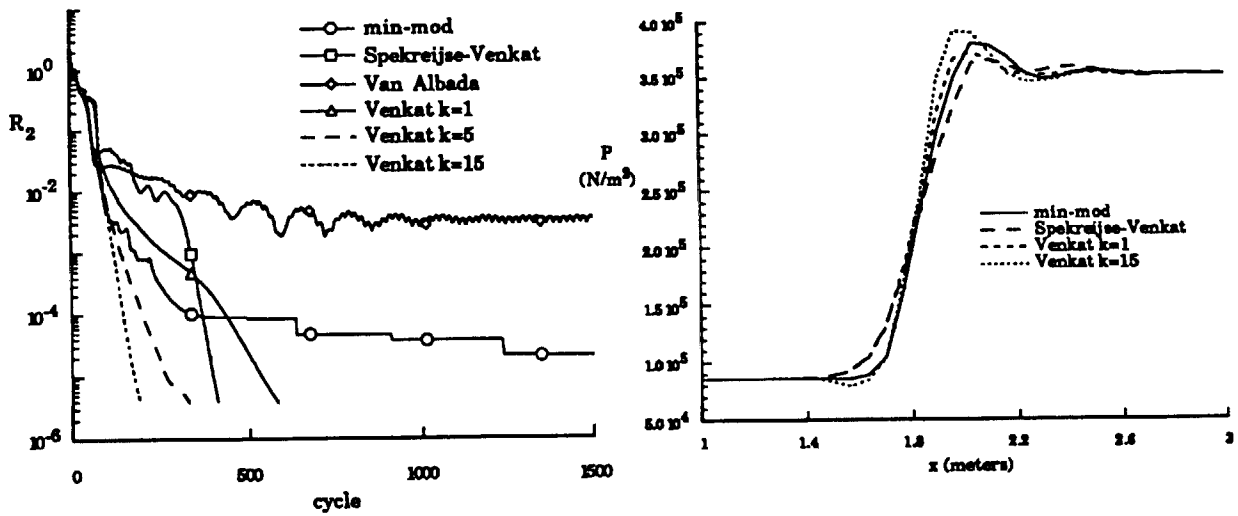

AeroSoft

Improved PNS results for the Mach 2 flow over a flate plate

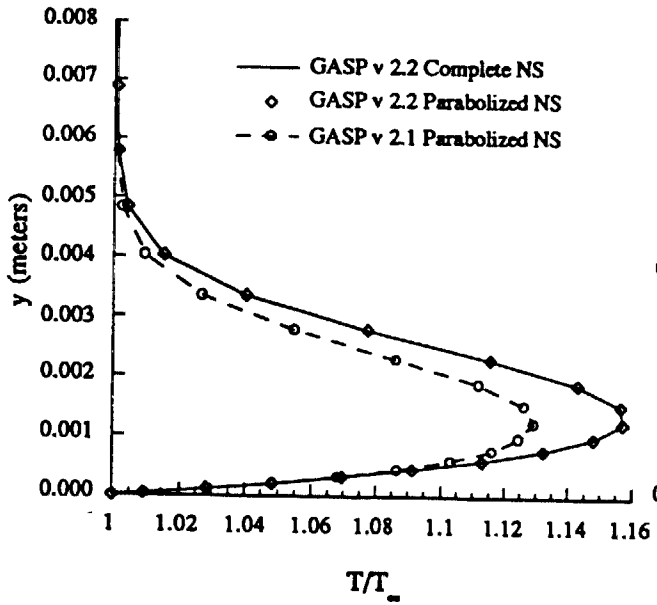

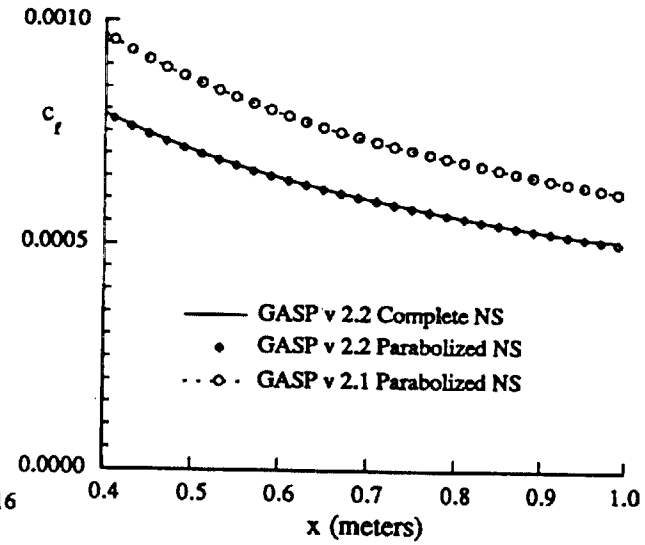

AeroSoft

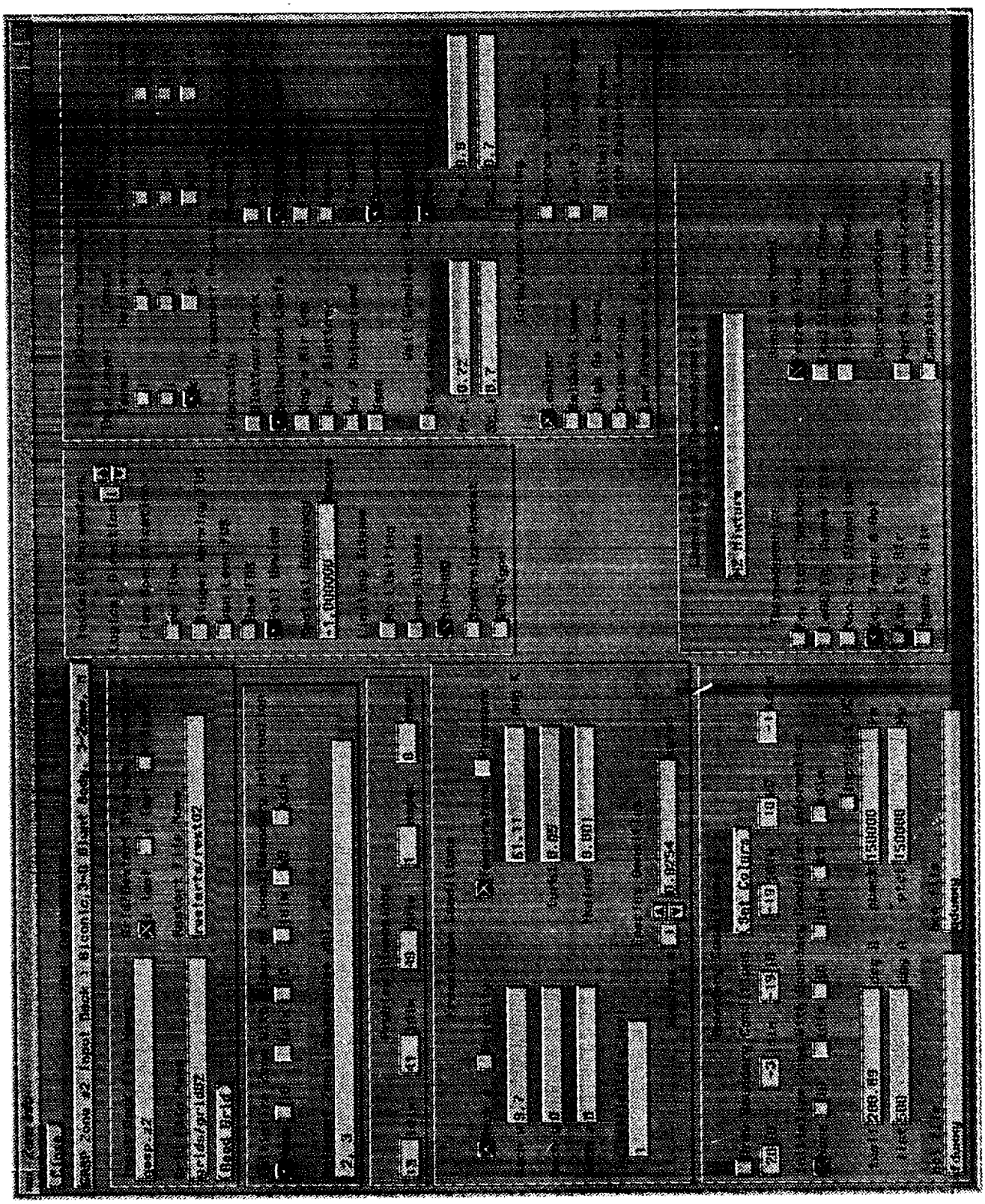

Support for GASP v2 GUI

- **Use of Motif User Interface as well as FAST**
  - Motif GUI supported on many Unix platforms
  - Motif widget set offers features not found in FAST
- **Support for pointwise boundary conditions**
  - Create boundary condition specification file graphically
- **Refinement of the zonal boundary definition**
  - Current implementation guarantees proper range
  - New implementation will also guarantee proper orientation

Support for GASP v2 GUI (cont.)

- **Refinement of the mesh sequencing definition**
  - Rules checking will be extended to include pointwise boundary conditions and zonal boundaries
- **Access to the GASP thermo-chemical database**
  - Interface will be able to calculate all freestream quantities
  - Interface will only allow the selection of valid chemistry models subject to current database.

Expected *GASP* v3.0 Features

- **More General Zonal Interpolation**
  - Allow for mesh point discontinuities at zonal boundaries
  - Correct fluxes to maintain global conservation
- **Improved Time Integration Algorithms**
  - Multi-Grid
  - Preconditioning
  - Inner Iteration techniques
  - Dual Time Stepping
- **Extended Mesh Sequencing**
  - More capabilities for multi-zone problems
  - Make it compatible to run with Multi-Grid

Expected GASPv3.0 Features

- **Chemistry Modeling**
  - Option for loosely OR fully coupled chemistry
  - New equilibrium chemistry solution technique
    - Law of mass action
    - Steffenson acceleration for Newton's method
- **Turbulence Modeling**
  - Option for loosely OR fully coupled turbulence
  - Possible new models
    - Wilcox's k-ω model
- **Implicit Boundary Conditions**
  - Library of linearized boundary conditions built-in

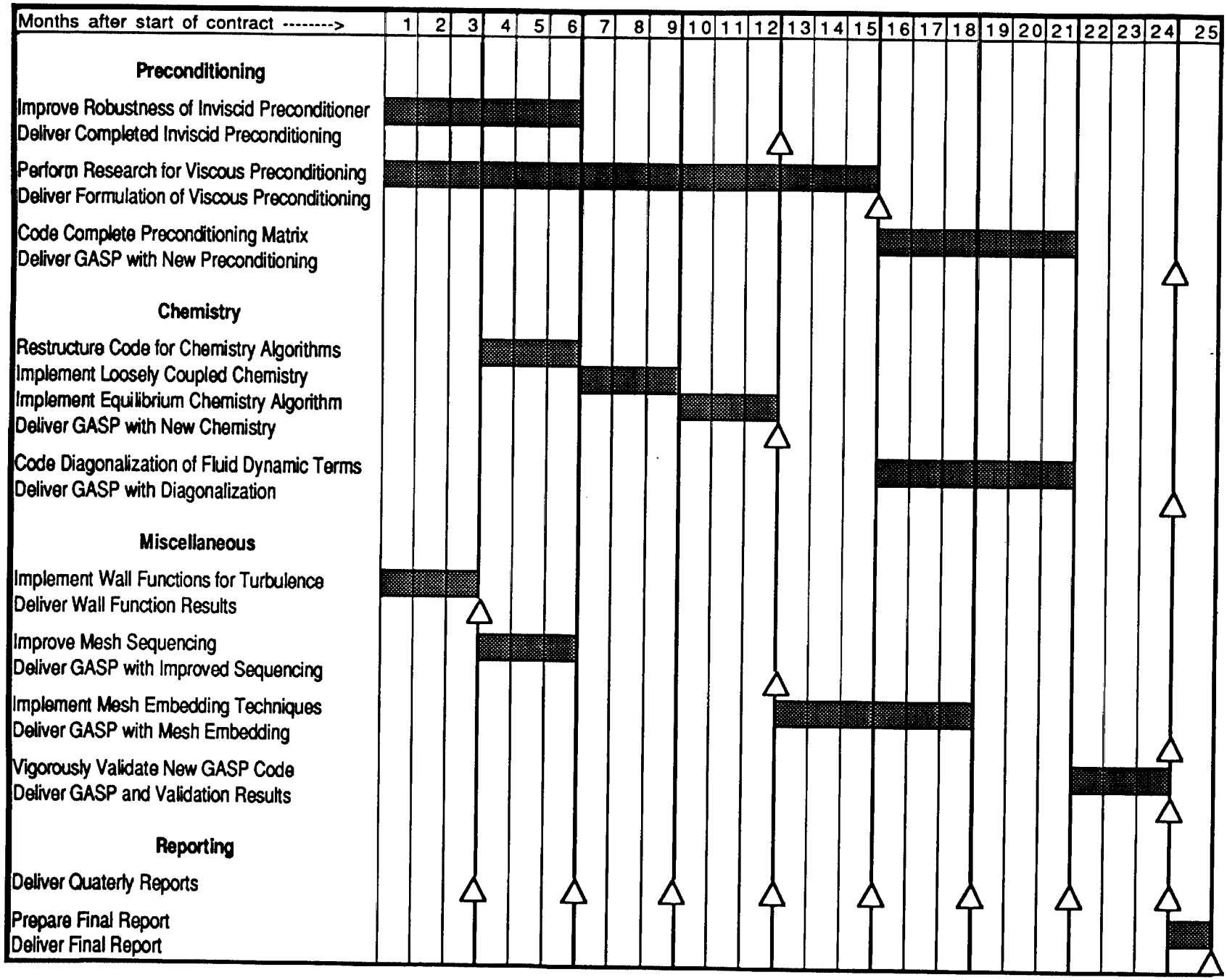

Table 1: AeroSoft Phase II Timetable

Unstructured Flow Solver Technology

- **The Best of GASP**
  - Generalized thermodynamics and chemistry models
  - Finite volume, flux splitting algorithms
  - Full Navier-Stokes physical model with appropriate turbulence models
  - Space marching, including PNS
  - Multi-zone capabilities

Unstructured Flow Solver Technology (cont.)

- **The Best of Current Unstructured Flow Solver Technology**
  - k-exact reconstruction for higher-order spatial accuracy and accurate modeling of viscous terms
  - Implicit relaxation methods for efficient time integration
  - Support for multiple control volume types including triangles, quadrilaterals, tetrahedra, prisms, and hexahedra

3-D Space Marching Discretization 2

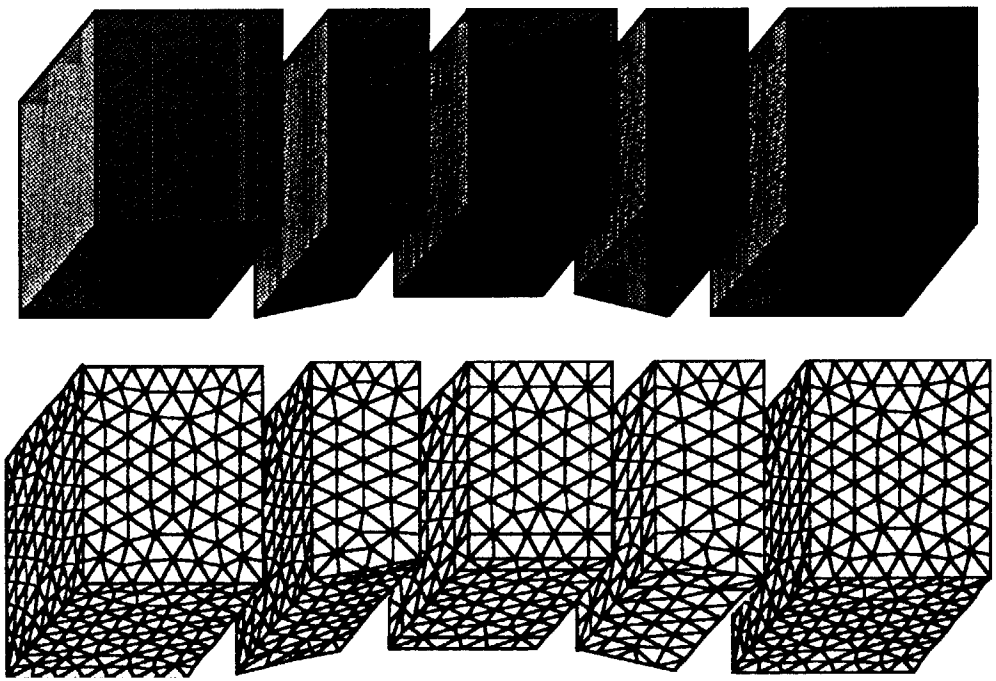

AeroSoft

Unstructured Technology

Pressure Contours

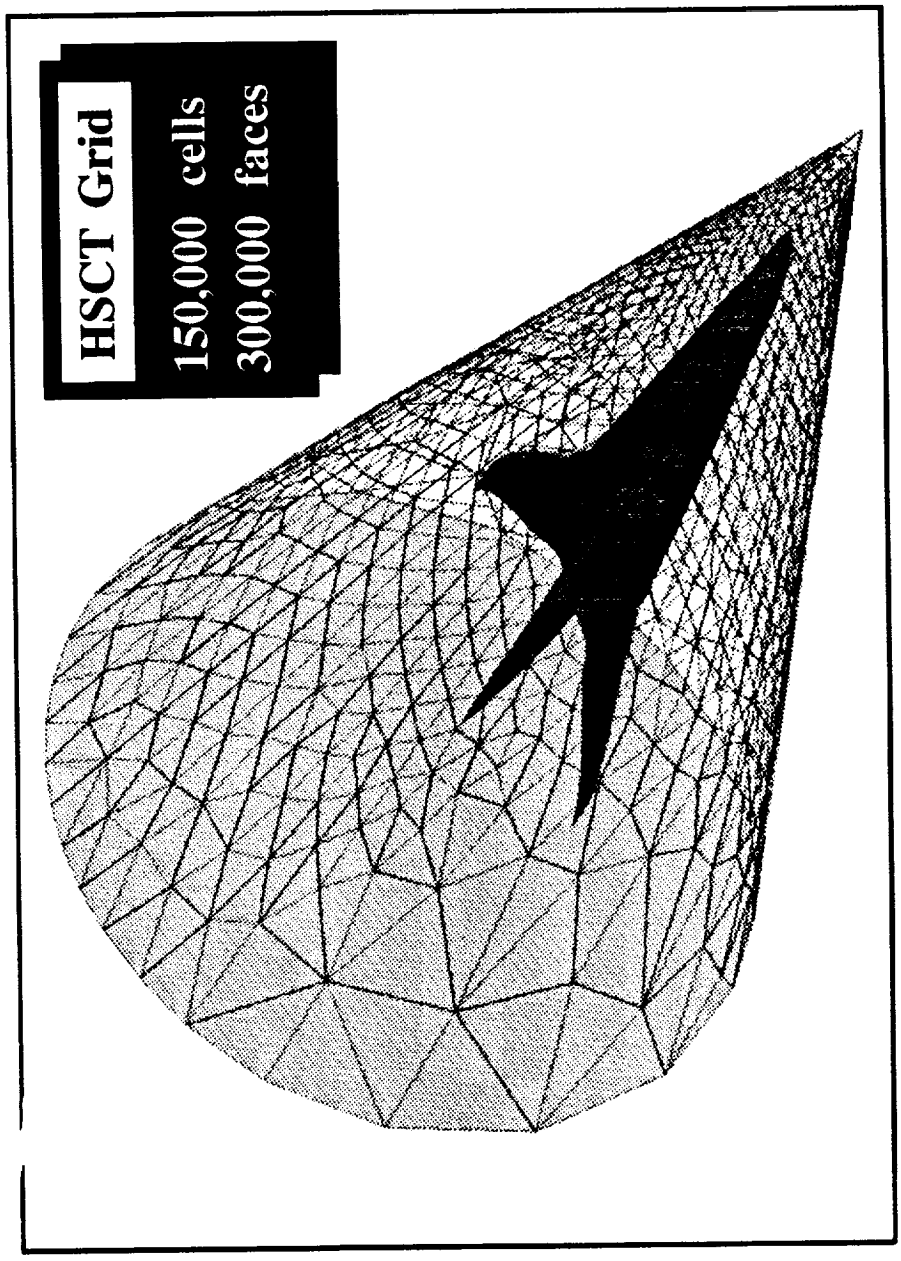
HSCT Grid
150,000 cells
300,000 faces

PRECONDITIONING FOR THE NAVIER-STOKES EQUATIONS WITH FINITE-RATE CHEMISTRY

Andrew G. Godfrey
Aero Thermo Technology
6703 Odyssey Drive, Suite 303
Huntsville, Alabama 35806

ABSTRACT

The extension of Van Leer's preconditioning procedure to generalized finite-rate chemistry is discussed. Application to viscous flow is begun with the proper preconditioning matrix for the one-dimensional Navier-Stokes equations. Eigenvalue stiffness is resolved and convergence-rate acceleration is demonstrated over the entire Mach-number range from nearly stagnant flow to hypersonic. Specific benefits are realized at the low and transonic flow speeds typical of complete propulsion-system simulations. The extended preconditioning matrix necessarily accounts for both thermal and chemical non-equilibrium. Numerical analysis reveals the possible theoretical improvements from using a preconditioner for all Mach number regimes. Numerical results confirm the expectations from the numerical analysis. Representative test cases include flows with previously troublesome embedded high-condition-number areas.

Van Leer, Lee, and Roe recently developed an optimal, analytic preconditioning technique to reduce eigenvalue stiffness over the full Mach-number range. By multiplying the flux-balance residual with the preconditioning matrix, the acoustic wave speeds are scaled so that all waves propagate at the same rate, an essential property to eliminate inherent eigenvalue stiffness. This session discusses a synthesis of the thermo-chemical non-equilibrium flux-splitting developed by Grossman and Cinnella and the characteristic wave preconditioning of Van Leer into a powerful tool for implicitly solving two and three-dimensional flows with generalized finite-rate chemistry.

For finite-rate chemistry, the state vector of unknowns is variable in length. Therefore, the preconditioning matrix extended to generalized finite-rate chemistry must accommodate a flexible system of moving waves. Fortunately, no new kind of wave appears in the system. The only existing waves are entropy and vorticity waves, which move with the fluid, and acoustic waves, which propagate in Mach-number dependent directions. The non-equilibrium vibrational energies and species densities in the unknown state vector act strictly as convective waves. The essential concept for extending the preconditioning to generalized chemistry models is determining the differential variables which symmetrize the flux Jacobians. The extension is then straight-forward.

This algorithm research effort will be released in a future version of the production-level computational code coined the General Aerodynamic Simulation Program (GASP), developed by Walters, Slack and McGrory.

Preconditioning for the Navier-Stokes Equations with Finite-Rate Chemistry

Dr. Andrew G. Godfrey

What's Preconditioning?

Preconditioning ...

- **reformulates the governing equations so that all wave fronts propagate at the same rate.**
- **scales the acoustic waves to reduce stiffness .**
- **accelerates convergence for all Mach numbers.**
- **maintains hyperbolic influence of the governing equations.**

Singular Systems

- Solution to a linear system

$$A\,x = b$$

$$Ax - b = R$$

- Condition Number, $k(A) = \|A\|\,\|A^{-1}\|$

$$\frac{\|\partial x\|}{\|x\|} = k(A)\,\frac{\|\partial R\|}{\|R\|}$$

- Compressible Euler equations decouple at low speed.

Preconditioned Structures

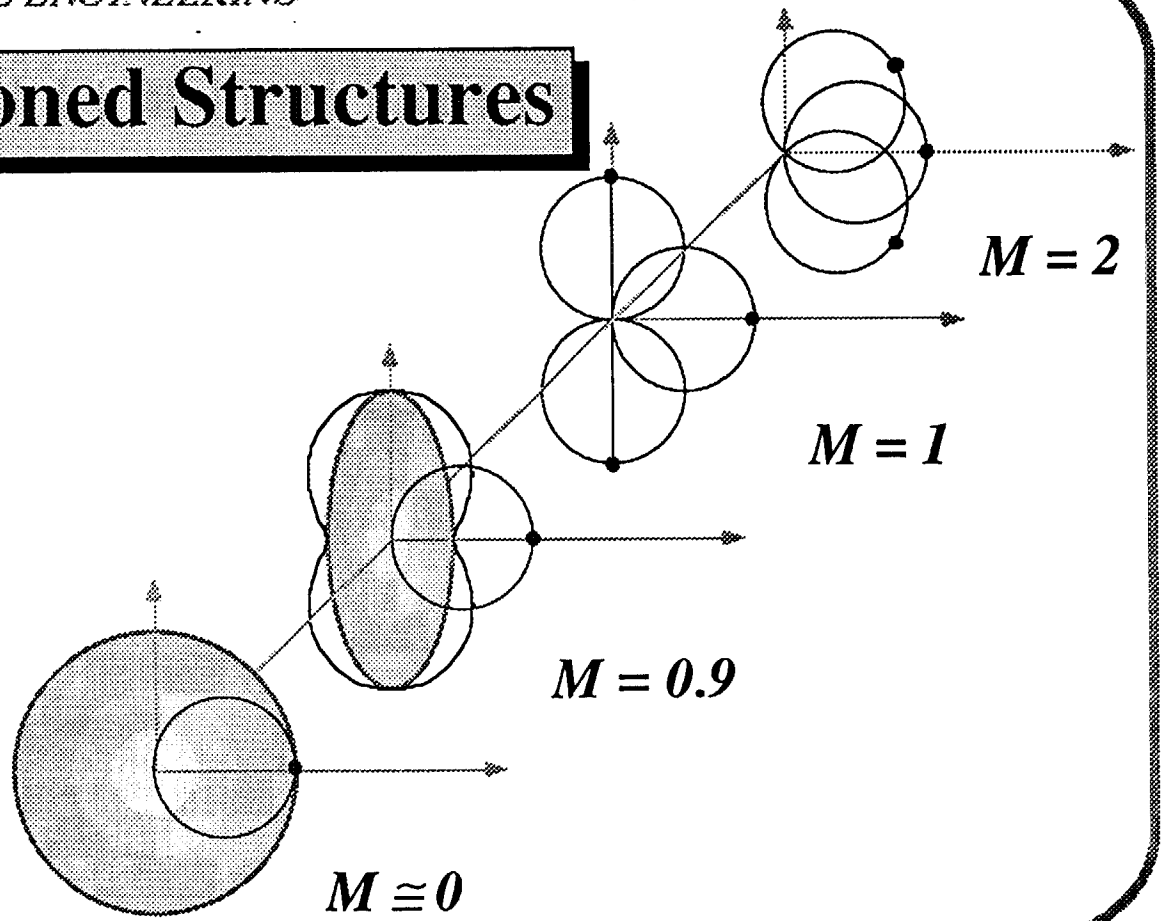

Euler Wave Structures

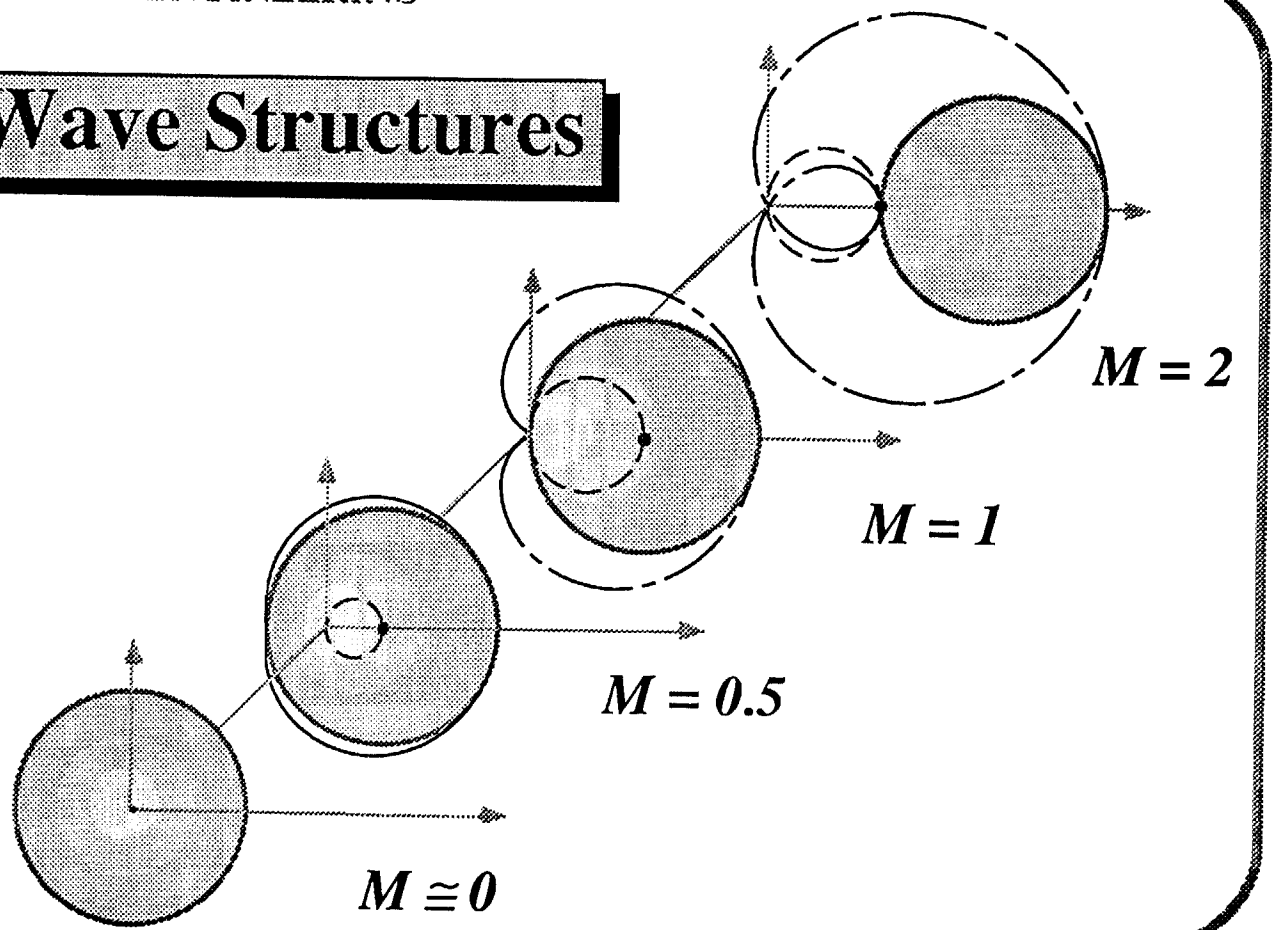

WITHOUT Preconditioning

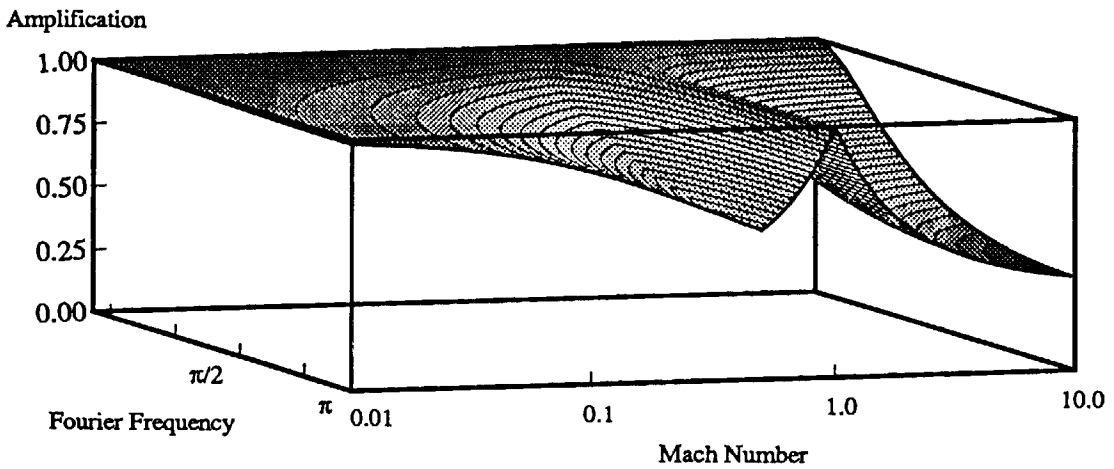

WITH Preconditioning

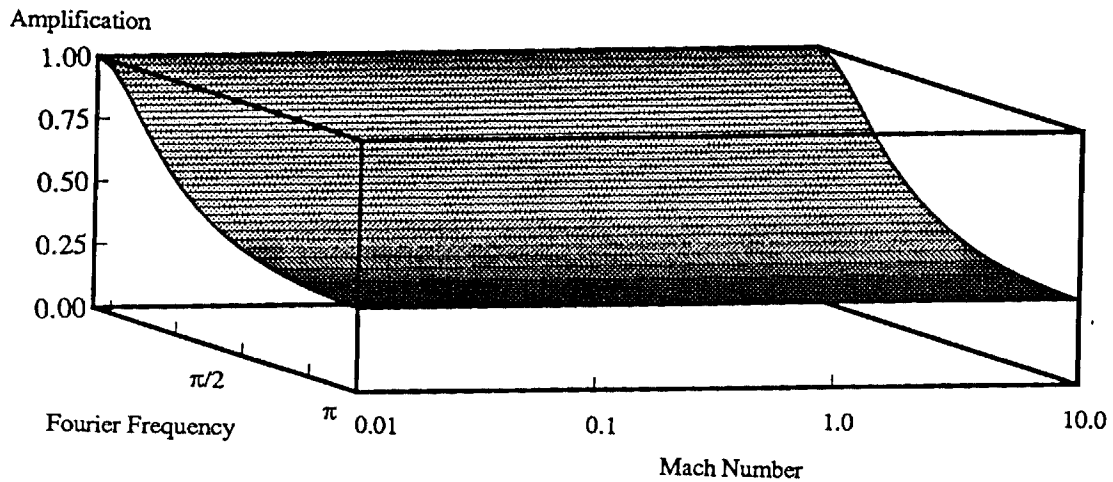

Low-Speed Channel Flow

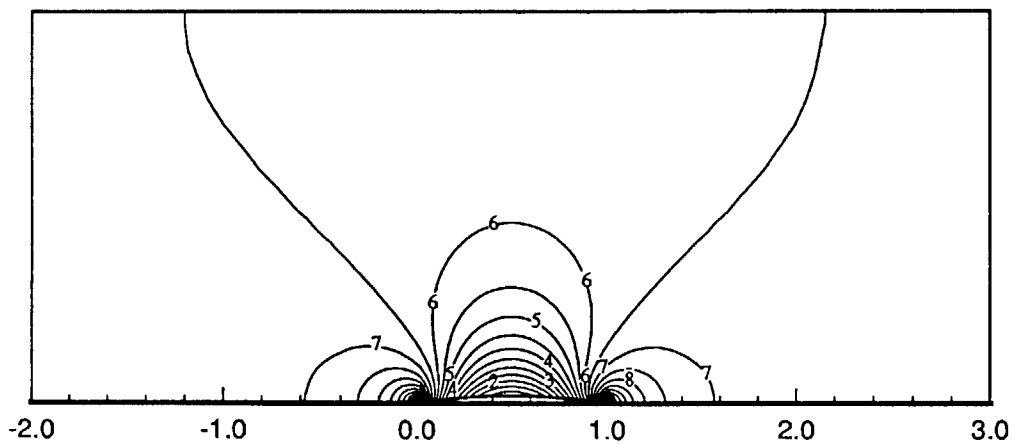

Level	Cp
D	0.245
C	0.206
B	0.168
A	0.130
9	0.092
8	0.054
7	0.016
6	-0.022
5	-0.060
4	-0.098
3	-0.136
2	-0.174
1	-0.213

M=0.001 WITH Preconditioning

Low-Speed Channel Flow

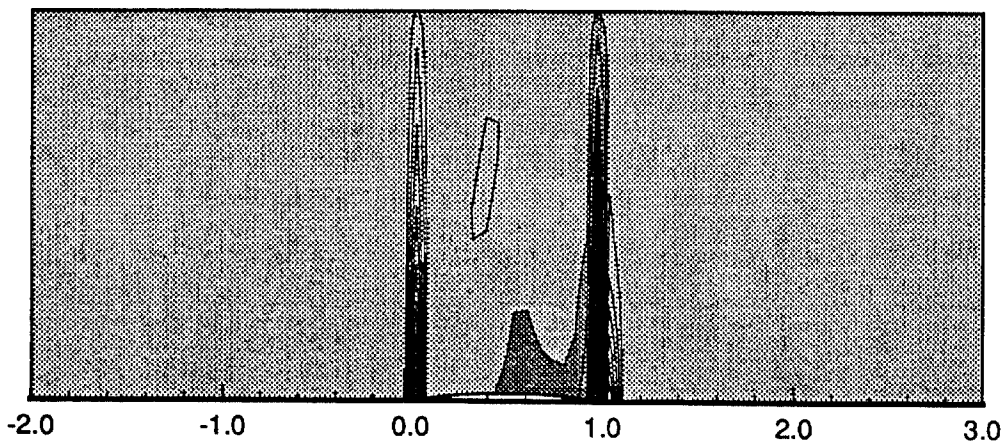

M=0.001 WITHOUT Preconditioning

Axi-Symmetric Nozzle

$$r(x) = \frac{L}{4}\left[1+\sin\left(\frac{\pi x}{2L}\right)\right]$$

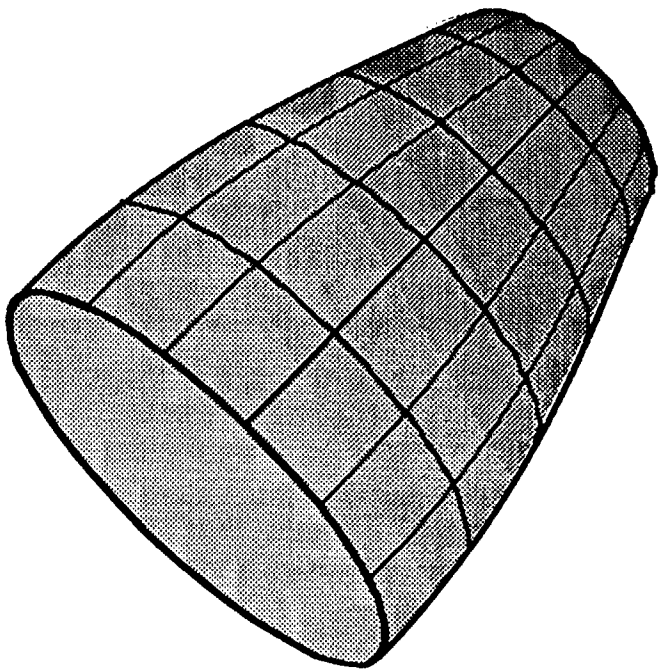

AEROSPACE ENGINEERING

Residual History - Finite Rate

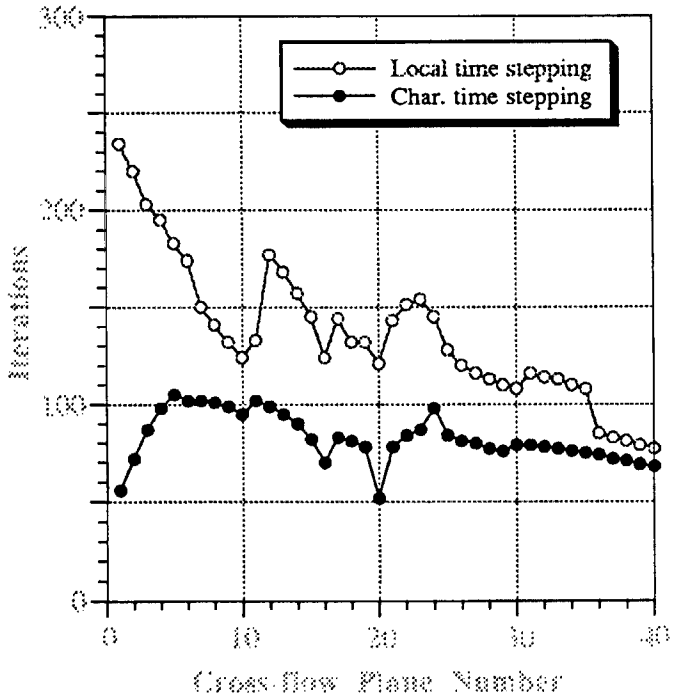

Pressure Damping

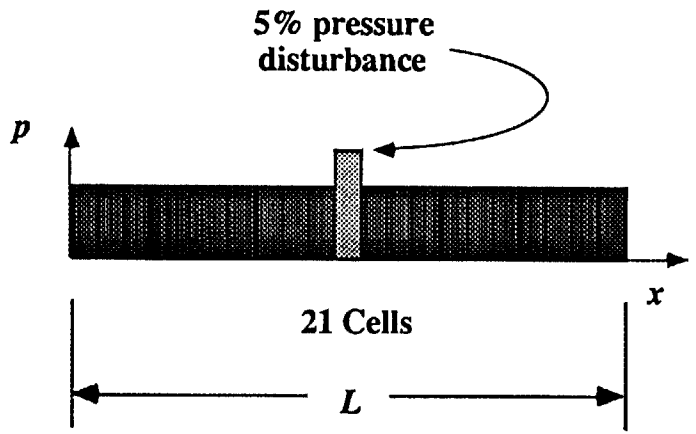

$M_\infty = 0.1$
$T_\infty = 400\ °K$
$\rho_\infty = 0.7068\ kg/m^3$

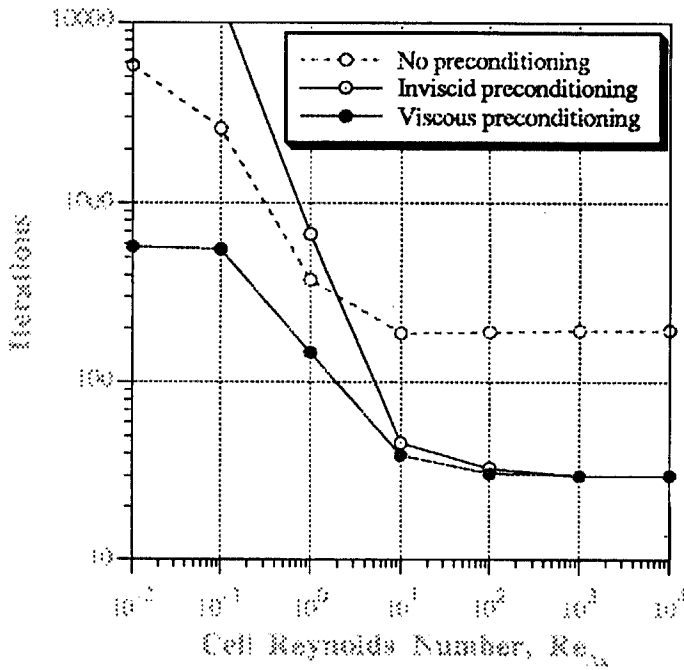

Future Work

- Boundary condition stiffness.
  Discretize characteristic variables.
- Smoothing of singular preconditioning matrix.
  Stagnation points.
- Multi-dimensional Navier-Stokes equations
  Laminar airfoils and separation bubbles.

A Numerical Procedure for Analysis of Finite Rate Reacting Flows

H.M. Shang and Y.S. Chen
Engineering Sciences, Inc., Huntsville, AL

Z.J. Chen and C.P. Chen
University of Alabama in Huntsville, AL

T.S. Wang
NASA MSFC, Huntsville, AL

ABSTRACT

Combustion processes in rocket propulsion systems are characterized by the existence of multiple, vastly differing time and length scales, as well as flow-speeds at wide variation of Mach numbers. The chemical kinetics processes in the highly active reaction zone are characterized by much more smaller scales compared to fluid convective and diffusive time scales. An operator splitting procedure for transient finite rate chemistry problems has been developed using a pressure based method, which can be applied to all speed flows without difficulties. The splitting of chemical kinetics terms formed the fluid-mechanical terms of the species equation ameliorated the difficulties associated with the disparate time scales and stiffness in the set of equations which describes highly exothermic combustion. A combined efficient ordinary differential equations (O.D.E.) solver was used to integrate the effective chemical source terms over the residence time at each grid cell. One and two dimensional reacting flow situations were carried out to demonstrate and verify the current procedure. Different chemical kinetics with different degrees of nonlinearity have also been incorporated to test the robustness and generality of the proposed method.

A NUMERICAL PROCEDURE FOR ANALYSIS OF FINITE RATE REACTING FLOWS

H.M. Shang and Y.S. Chen
Engineering Sciences, Inc.

Z.J. Chen and C.P. Chen
University of Alabama in Huntsville

T.S. Wang
NASA Marshall Space Flight Center

Presented At 11th Workshop for CFD Applications
in Rocket Propulsion -- NASA MSFC
April 20-22,1993

OBJECTIVE

- DEVELOP AN EFFICIENT ALGORITHM FOR FINITE RATE CHEMICAL REACTING FLOWS AT ALL-SPEED
- VALIDATE THE METHODOLOGY AT STEADY AND TRANSIENT FLOWS

BACKGROUND

- ENGINE COMBUSTOR IGNITION PROCESSES
- SHOCK-INDUCED COMBUSTION AND DETONATION
- IGNITION DELAY AND COMBUSTION EFFICIENCY
- SSME AND HYPERSONIC VEHICLE PROPULSION, etc.

NUMERICAL ISSUES

- FAST CHEMISTRY OF H2-O2 SYSTEM
- VERY SMALL CHEMICAL TIME SCALE COMPARE TO FLUID DYNAMICS TIME SCALE
- A SET OF STIFF NON-LINEAR PARTIAL DIFFERENTIAL EQUATIONS
- EXPENSIVE CPU TIME EVEN FOR TWO-DIMENSIONAL STUDY

NUMERICAL APPROACH

FINITE RATE CHEMISTRY MODEL

- **GENERAL SYSTEM OF CHEMICAL REACTION IN TERMS OF MASS FRACTION:**

$$\sum_i \upsilon_{ij} M_i = \sum_i \upsilon'_{ij} M'_i$$

$$\dot{\omega}_i = M_{Wi} \sum_j (\upsilon'_{ij} - \upsilon_{ij}) \left[K_{fj} \prod_i \left(\frac{\rho \alpha_i}{M_{Wi}}\right)^{\upsilon_{ij}} - K_{bj} \prod_i \left(\frac{\rho \alpha_i}{M_{Wi}}\right)^{\upsilon'_{ij}} \right]$$

- **SPECIES CONTINUITY EQUATION:**

$$\frac{\partial (\rho \alpha_i)}{\partial t} + \frac{\partial (\rho u_j \alpha_i)}{\partial x_j} = \frac{\partial}{\partial x_j} \left(\frac{\mu_{eff}}{\sigma_\alpha} \frac{\partial \alpha_i}{\partial x_j} \right) + \dot{\omega}_i$$

NUMERICAL APPROACH (cont.)

ODE SOLVER

- **DEFINE FLUID PARTICLE RESIDENCE TIME**

$$\Delta t_f = \left(\frac{u}{\Delta x} + \frac{v}{\Delta y} + \frac{w}{\Delta z} \right)^{-1}$$

- **INTEGRATE CHEMICAL KINETICS OVER** $\Delta t_c = \min(\Delta t_f, \Delta t)$ **WITH "DEBDF" ODE SOLVER**
- **CALCULATE CHEMICAL SOURCE TERM** $\dot{\omega}_i = \rho \frac{\alpha_i^* - \alpha_i^n}{\Delta t_c}$
- **OPERATOR-SPLITTING/POINT-IMPLICIT SCHEME**
- **AVOID TO SOLVE A SET OF NONLINEAR STIFF PDE EQUATIONS**

NUMERICAL APPROACH (cont.)

PENALTY FUNCTION (PF)

- **TIME STEP LIMITER FOR SPECIES EQUATIONS:**

$$\Delta t_s = \left[\rho(\Delta\alpha_i)_{assigned} / \dot{\omega}_i \right]_{\min}$$

- **ELEMENT BALANCE CONSTRAINTS:**

$$\sum_i \alpha_i = 1.0 \qquad and \qquad 0.0 \le \alpha_i \le 1.0$$

- **DEVISE A PENALTY FUNCTION** $P = \min(P_i)$

$$P_i = \frac{1.0 - \alpha_i^k}{\alpha_i^* - \alpha_i^k} \quad for \quad \alpha_i^* - \alpha_i^k > 0.0 \quad or \quad P_i = \frac{-\alpha_i^k}{\alpha_i^* - \alpha_i^k} \quad for \quad \alpha_i^* - \alpha_i^k < 0.0$$

- **ADJUST MASS FRACTION:** $\alpha_i^{k+1} = \alpha_i^k + (\alpha_i^* - \alpha_i^k) \cdot P$

- **ONLY FOR STEADY STATE CALCULATIONS**

NUMERICAL APPROACH (cont.)

NUMERICAL METHOD

- PRESSURE BASED FINITE DIFFERENCE NAVIER-STOKES FLOW SOLVER (FDNS)
- TIME-ACCURATE SOLUTION PROCEDURE
- HIGH ORDER CHAKRAVARTHY-OSHER (C-O) TVD SCHEME
- STANDARD & EXTENDED k-ε TURBULENCE MODELS WITH COMPRESSIBILITY CORRECTIONS
- CONJUGATE GRADIENT SQUARE (CGS) AND ADI SOLVER

VALIDATION

1. IGNITION DELAY

2. ONE-DIMENSIONAL DETONATION

3. SSME NOZZLE FLOW (PREMIXED)

4. BURROWS AND KURKOV DIFFUSION FLAME

VALIDATION (cont.)

1. IGNITION DELAY

- TO CHECK OUT THE CHEMICAL KINETICS MODELS, ODE SOLVER AND IMPLEMENTATION OF OPERATOR-SPLITTING SCHEME
- TEST CONDITIONS:
  STOICHIOMETRIC MIXTURE OF H2+AIR
  N2 IS CHEMICALLY INERT
  P_∞ = 101,325 Pa; U_∞ = 2,689 m/s; T_∞ = 1,000 K
- CHEMICAL KINETICS MODELS:
  2-STEP REACTION MODEL OF ROGERS AND CHINITZ
  9-STEP REACTION MODEL OF ANON

VALIDATION (cont.)

1. IGNITION DELAY (cont.)

- **ODE SOLVER IN TIME DOMAIN:**

$$\rho \frac{d\alpha_i}{dt} = \omega_i$$

- **OPERATOR-SPLITTING IN SPATIAL DOMAIN:**

$$\rho u \frac{d\alpha_i}{dx} = \omega_i$$

- **CONSTANT P, ρ AND U**
- **THE IGNITION DELAY SHOULD BE SAME BY USING BOTH METHODS WITH** $x = u \cdot t$
- **CAREFUL CALIBRATION**
- **CONSISTENT RESULTS**

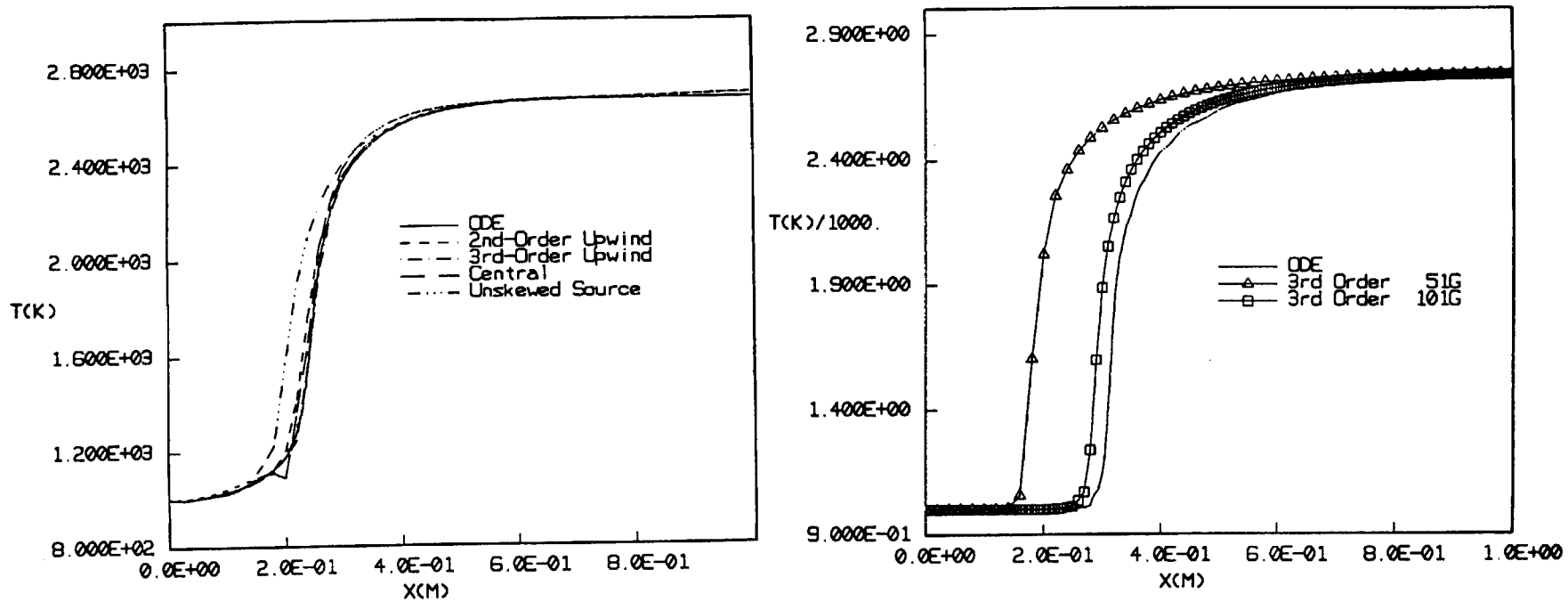

(a) 2-step reaction, 51 grids **(b) 9-step reaction**

Fig. 1 Temperature profiles in one-dimensional ignition delay calculation.

VALIDATION (cont.)

2. ONE-DIMENSIONAL DETONATION

- STOICHIOMETRIC MIXTURE OF H2 AND O2
  P_1 = 101,325 Pa; U_1 = 0.0 m/s; T_1 = 298 K;
  L=2.0 m; 201 UNIFORM GRIDS
- 9-STEP REACTION MODEL OF ANON
- HOT-SPOT AT X=0.0 m AND TIME=0.0 ms

	DT=2μs	DT=1μs	DATA
Vw* (m/s)	2,950	3,000	2,819
P (MPa)	1.405	1.335	1.80
T (K)	3,617	3,592	3,583

* DETONATION WAVE SPEED

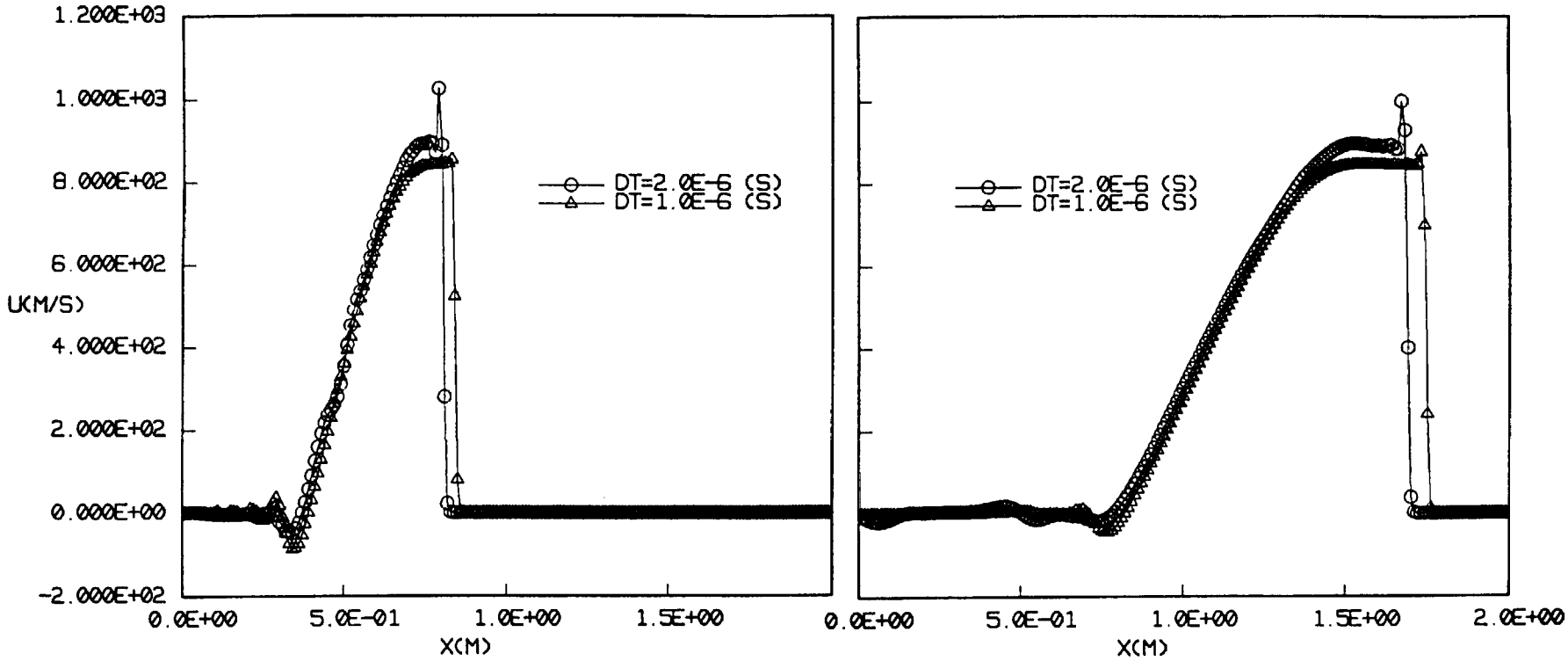

(a) Time=300μs **(b) Time=600μs**

Fig. 2 Velocity profiles at different times for one-dimensional detonation.

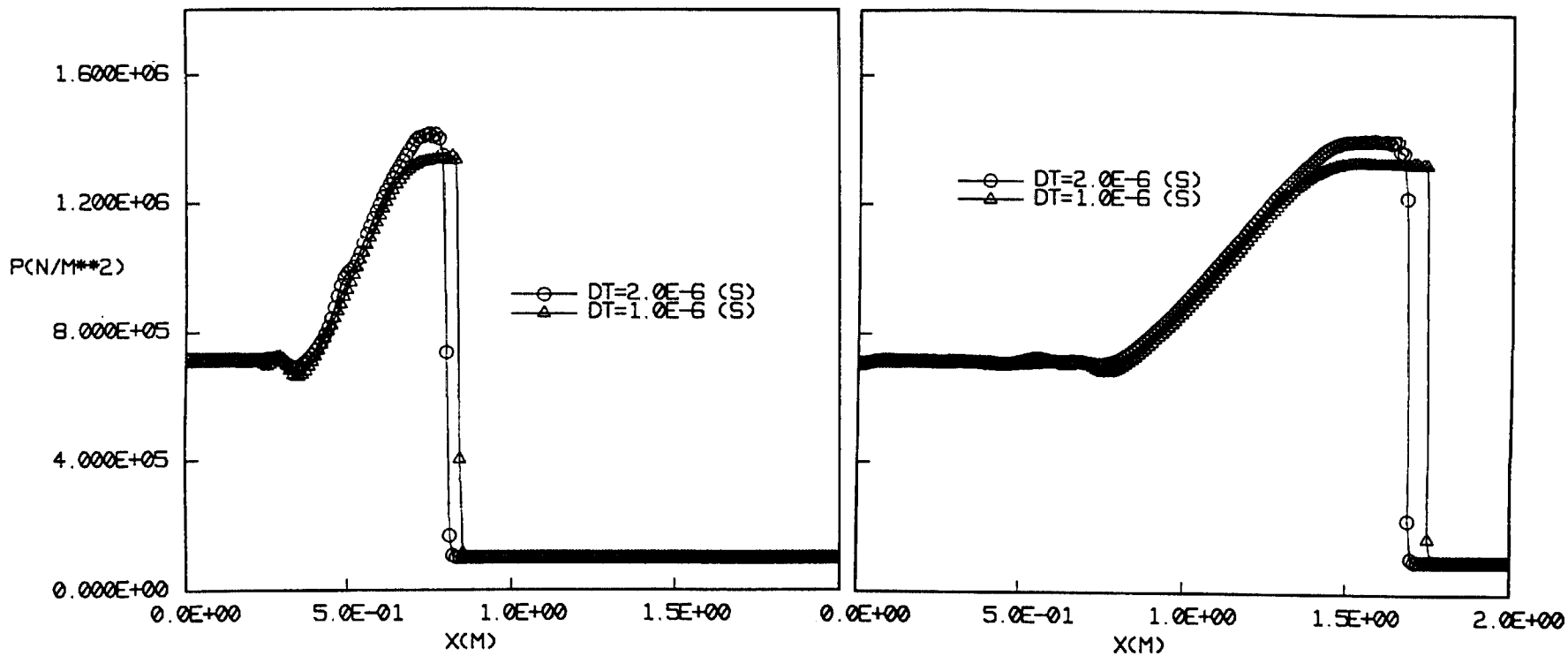

(a) Time=300μs **(b) Time=600μs**

Fig. 3 Pressure profiles at different times for one-dimensional detonation.

VALIDATION (cont.)

3. SSME NOZZLE FLOW (PREMIXED)

- SSME NOZZLE AT 100-PERCENT POWER LEVEL
- 9-STEP REACTION MODEL OF ANON
- 101X71 NON-UNIFORM GRIDS
- k-ε TURBULENCE MODEL

1229

	ITER	Ma**	Isp (s)	POINT STEP (μs)***
PF	1000	6.10	452.2	1,000
ODE	100*	6.09	452.2	28,000

*RESTART FROM PF; **AT CENTER LINE OF EXIT; *** IBM RISC/6000.

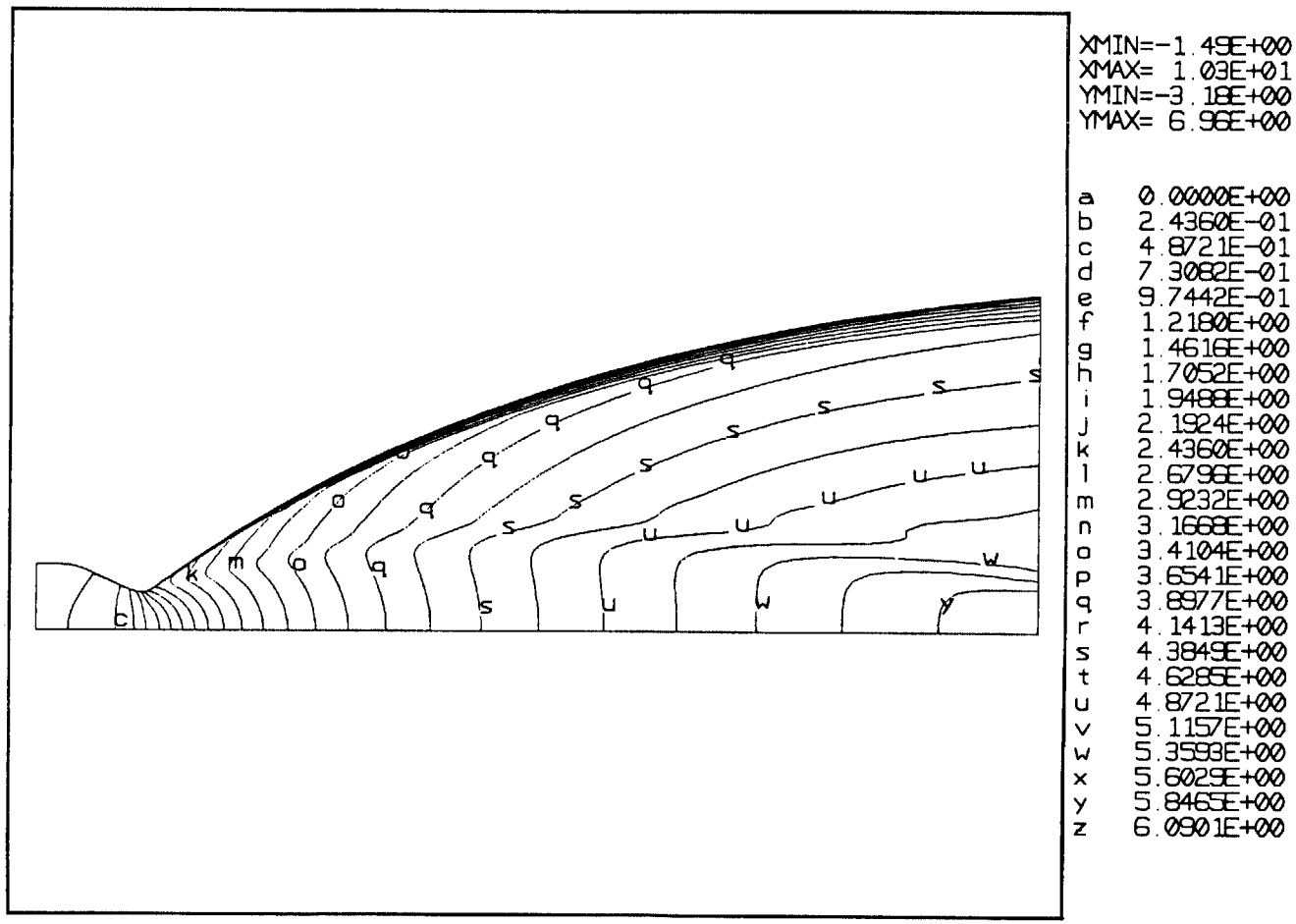

Prediction of the Mach number contour for SSME nozzle with ODE solver

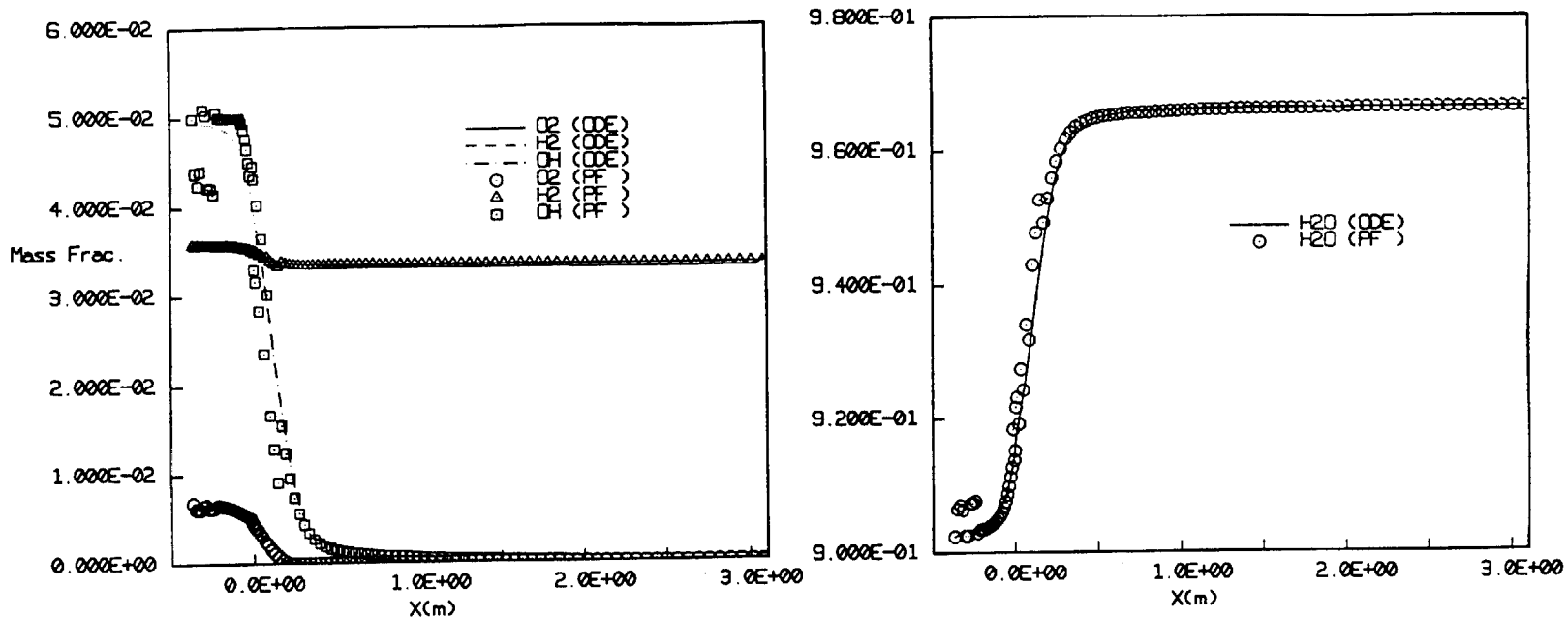

Fig. 4 Mass fraction profiles for SSME nozzle flow along the center line.

VALIDATION (cont.)

4. BURROWS AND KURKOV DIFFUSION FLAME

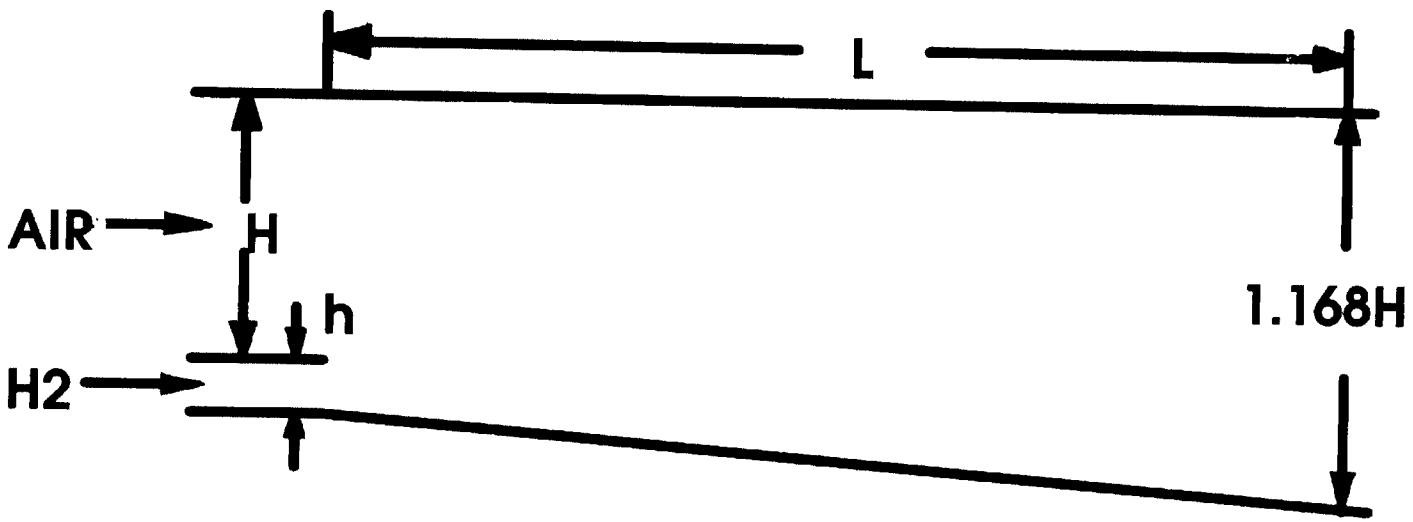

h=0.004m H=0.08976m L=0.356m

VALIDATION (cont.)

4. BURROWS AND KURKOV DIFFUSION FLAME (cont.)

	HYDROGEN JET	AIR STREAM VITIATED	AIR STREAM NON VITIATED
MACH NUMBER	1.00	2.44	2.44
TEMPERATURE, T, K	254	1270	1150
VELOCITY, U, m/s	1216	1764	1679
PRESSURE, P, MPa	0.1	0.1	0.1
MASS FRACTION:			
H2	1.00	0	0.000
O2	0	0.258	0.000
N2	0	0.486	0.744
H2O	0	0.256	0.256

- COMPUTATIONAL EFFICIENCY (RESIDUALS DROP 3 ORDER):
  - ODE: 300 TIME-STEP ITERATIONS, 3 HOUR CPU TIME*
  - PF: 900 TIME-STEP ITERATIONS, 0.8 HOUR CPU TIME*

*CPU TIME BASED ON IBM RISC/600

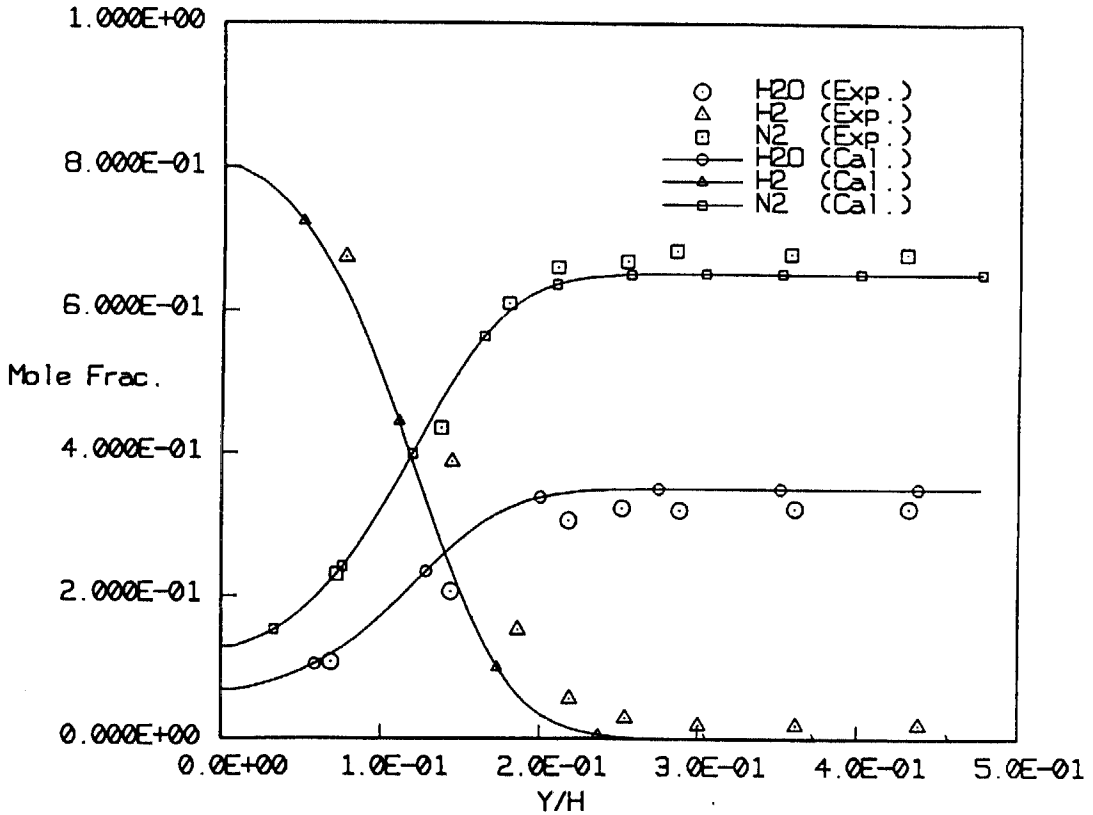

Fig. 5 Mole fraction profiles at x=35.6cm for Burrows and Kurkov's non-reacting case.

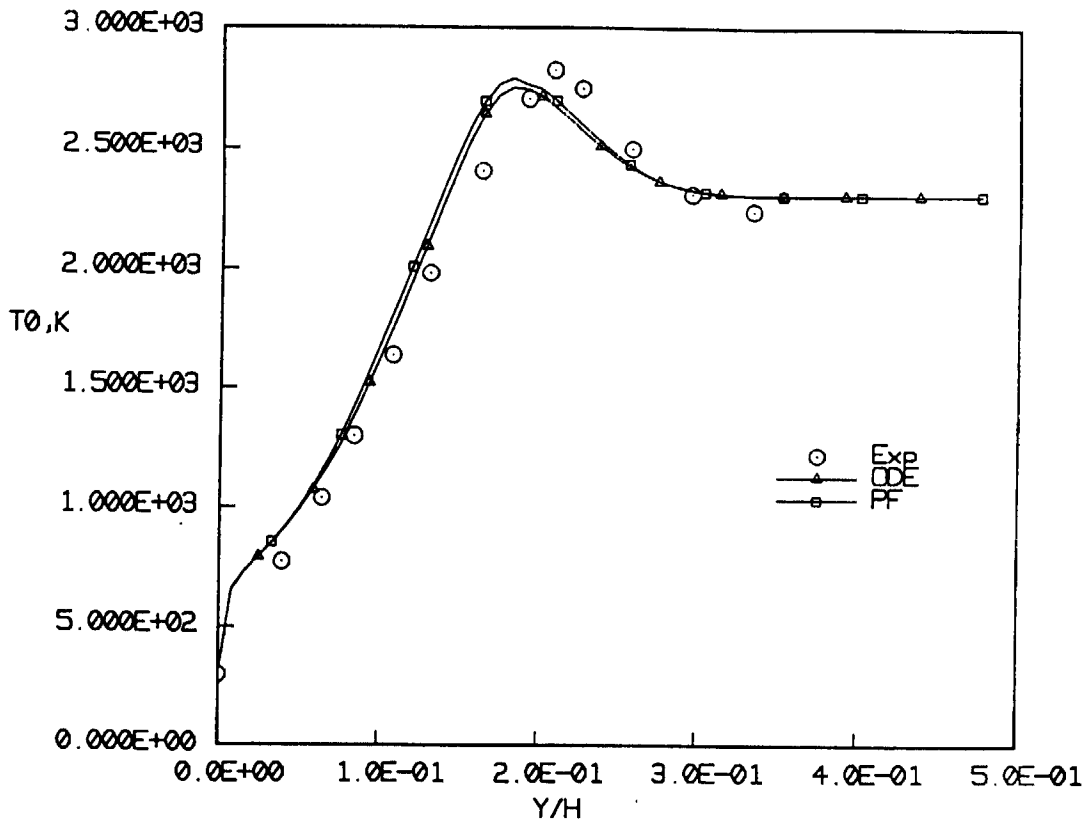

Fig. 6 Total temperature profiles at x=35.6cm for Burrows and Kurkov's reacting case.

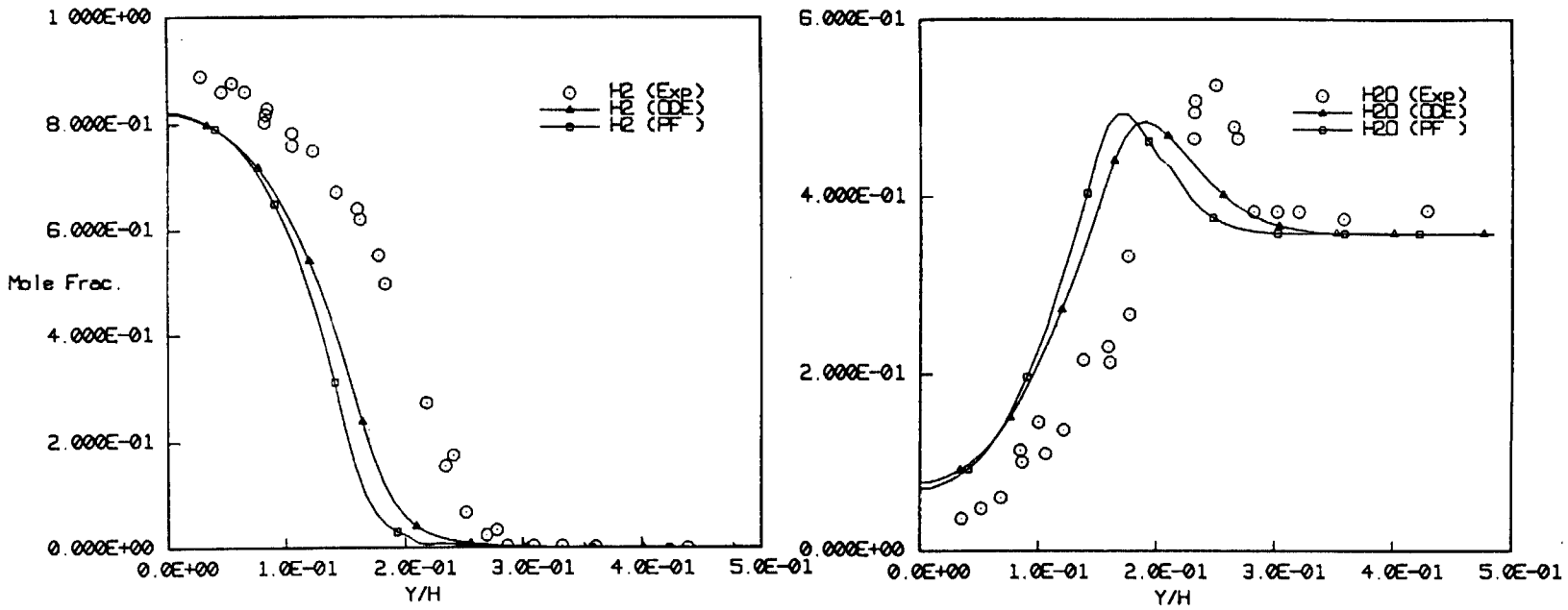

Fig. 7a Mole fraction profiles at x=35.6cm for Burrows and Kurkov's reacting case.

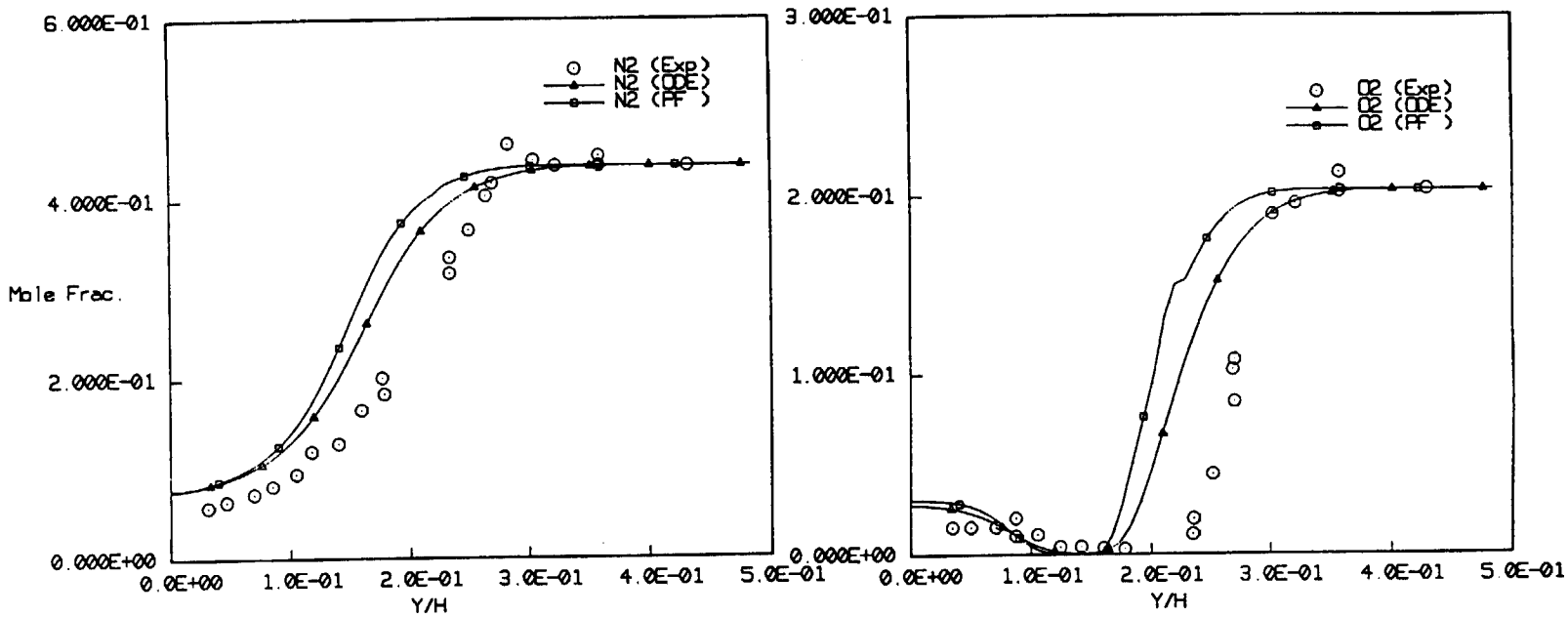

Fig. 7b Mole fraction profiles at x=35.6cm for Burrows and Kurkov's reacting case.

CONCLUSION

- SUCCESSFUL IMPLEMENTATION OF 'DEBDF' ODE SOLVER AND CHEMICAL KINETICS
- PENALTY FUNCTION -- EFFICIENT; BUT MASS FRACTION OSCILLATION IN SOME CASES
- ODE SOLVER -- CAN BE APPLIED TO TRANSIENT CALCULATIONS
- EFFICIENCY CAN BE ACHIEVED BY THE COMBINATION OF PENALTY FUNCTION AND ODE SOLVER IN STEADY STATE CASE
- CONTINUE TO INVESTIGATE TIME ACCURATE FLAME PROPAGATION CALCULATION
- INCORPORATE SPRAY COMBUSTION MODELS

- Abstract -

Workshop for Computational Fluid Dynamic Applications in Rocket Propulsion

Three-Dimensional Navier-Stokes Analysis and Redesign of an Imbedded Bellmouth Nozzle in a Turbine Cascade Inlet Section

P. W. Giel, J. R. Sirbaugh
Sverdrup Technology, Inc.
NASA LeRC Group
2001 Aerospace Parkway
Brook Park, OH 44142
(216) 826-6686

Verification of proposed turbopump blading performance will involve evaluation of candidate blades in cascade test facilities. It is necessary to be able to predict the flow fields within these cascades for the results to be applicable to actual engine environments. This work presents the results of a study to predict the flow field for the NASA Lewis Transonic Turbine Blade Cascade Facility, which is similar to those used to evaluate rocket propulsion turbines. A pitchwise non-uniform total pressure distribution was observed at the blade row leading edge plane. A CFD analysis was used to show that the cause of the flow non-uniformity was a pair of vortices that originated in an embedded bellmouth inlet. Further CFD analysis was used to verify that a redesigned inlet section resulted in a flow with acceptable uniformity.

A computational analysis was chosen because physical accessibility to the inlet section was limited, and because a computational approach also allows one to examine design changes cheaper and more quickly than an experimental approach would. The PARC code, a general purpose, three-dimensional, Navier-Stokes code with multi-block solution capability, was chosen for the present study. Results are presented detailing the computational requirements needed to accurately predict flows of this nature.

Calculations of the original geometry showed total pressure loss regions consistent in strength and in location to experimental measurements. An examination of the results shows that the distortions are caused by a pair of vortices that originate as a result of the interaction of the flow with the imbedded bellmouth. Computations were performed for an inlet geometry which eliminated the imbedded bellmouth by bridging the region between it and the upstream wall. This analysis indicated that eliminating the imbedded bellmouth eliminates the troublesome pair of vortices, resulting in a flow with much greater pitchwise uniformity.

Transonic Turbine Blade Cascade Inlet Analysis

Three-Dimensional Navier-Stokes Analysis and Redesign of an Imbedded Bellmouth Nozzle in a Turbine Cascade Inlet Section

Paul Giel, Sverdrup Technology, Inc.
NASA LeRC Group

Jim Sirbaugh,

Isaac Lopez, U.S. Army Aviation Systems Command

Jim Van Fossen NASA Lewis Research Center

April 1993

Transonic Turbine Blade Cascade Inlet Analysis – Outline of Presentation

- Motivation and objectives
- Computational methods and models
  - geometry and grids
  - boundary conditions
  - computational time and convergence
- Results of computations
- Proposed geometry modifications
- Ongoing and future work
  - 8:1 upstream contraction section
  - off–design incidence case

Transonic Turbine Blade Cascade Inlet Analysis – Overall View of Cascade Inlet Section

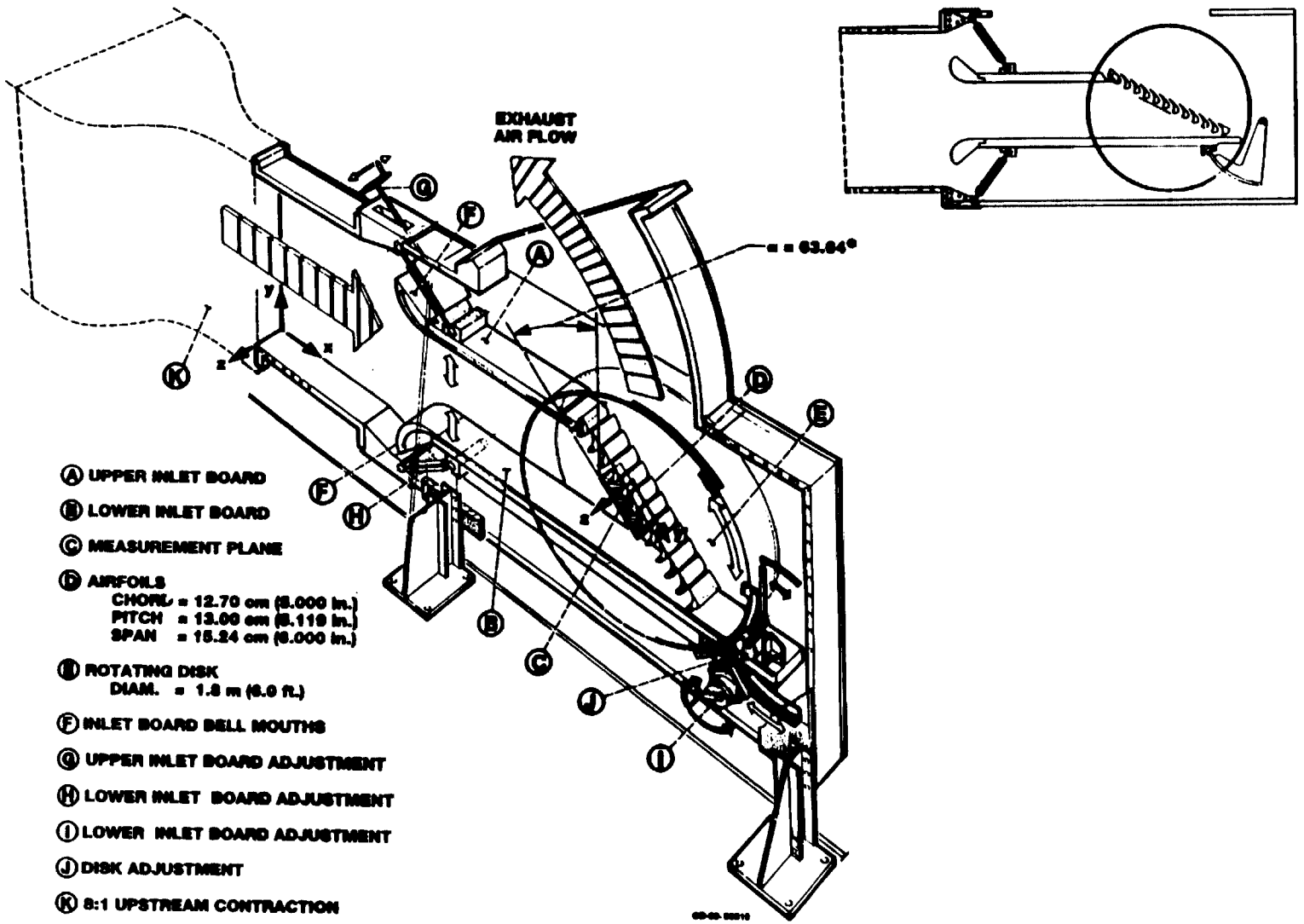

Transonic Turbine Blade Cascade Inlet Analysis – Preliminary Experimental Measurements

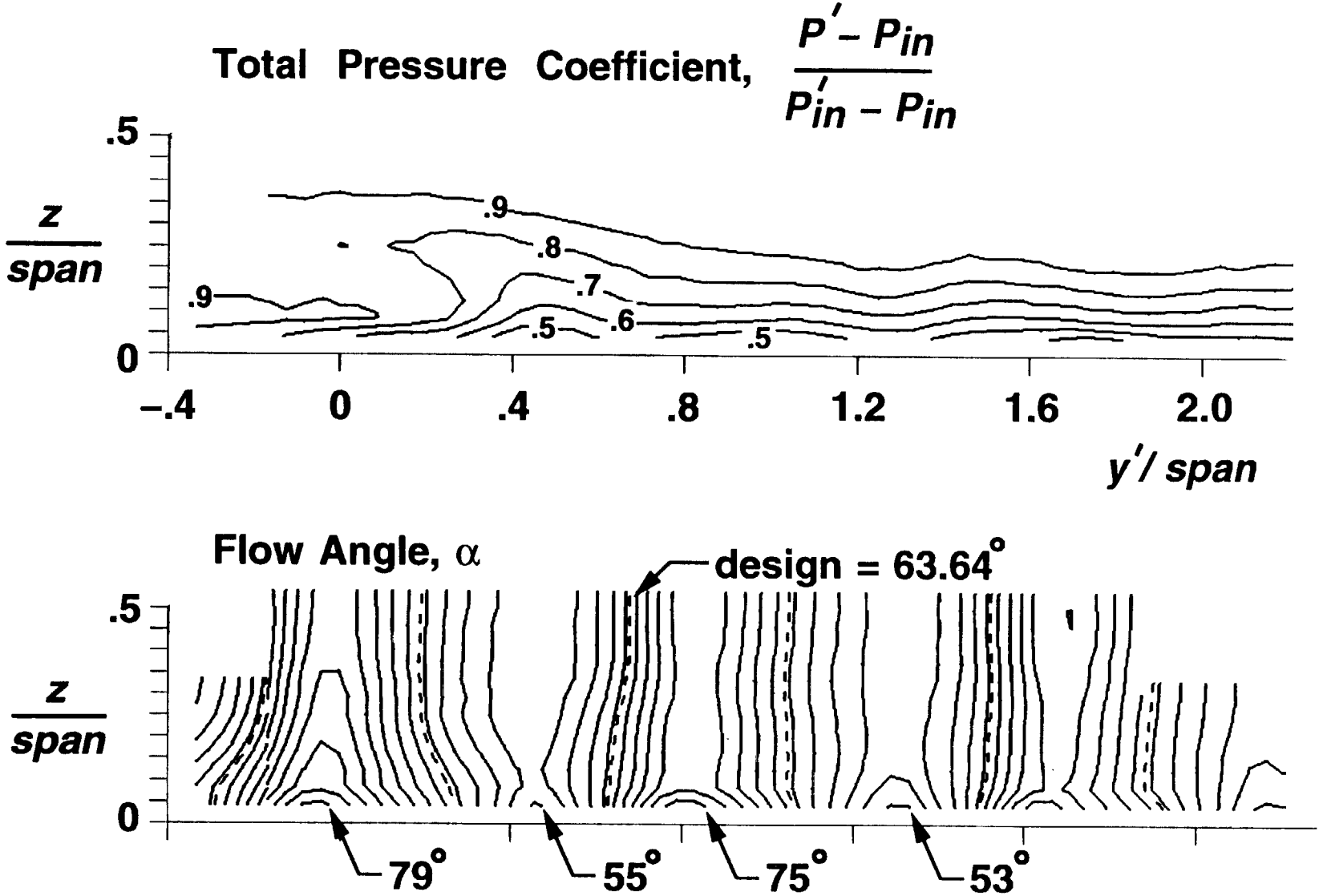

Transonic Turbine Blade Cascade Inlet Analysis – Code Descriptions

- PARC code, NASA Lewis version 7.2
  - General purpose Reynolds Averaged Navier–Stokes solver
  - Multi–block solution capability
  - Second–order accurate finite–differences
  - Blended second– and fourth–difference artificial dissipation
  - Beam & Warming solution algorithm
  - Baldwin–Lomax algebraic turbulence model used
  - No laminar–to–turbulent transition model used
- RVC3D
  - Turbomachinery Reynolds Averaged Navier–Stokes solver
  - Second–order accurate finite–differences
  - Blended second– and fourth–difference artificial dissipation
  - Four–stage Runge–Kutta solution algorithm
  - Baldwin–Lomax or Cebeci–Smith algebraic turbulence models

Transonic Turbine Blade Cascade Inlet Analysis – Original Geometry and Grids

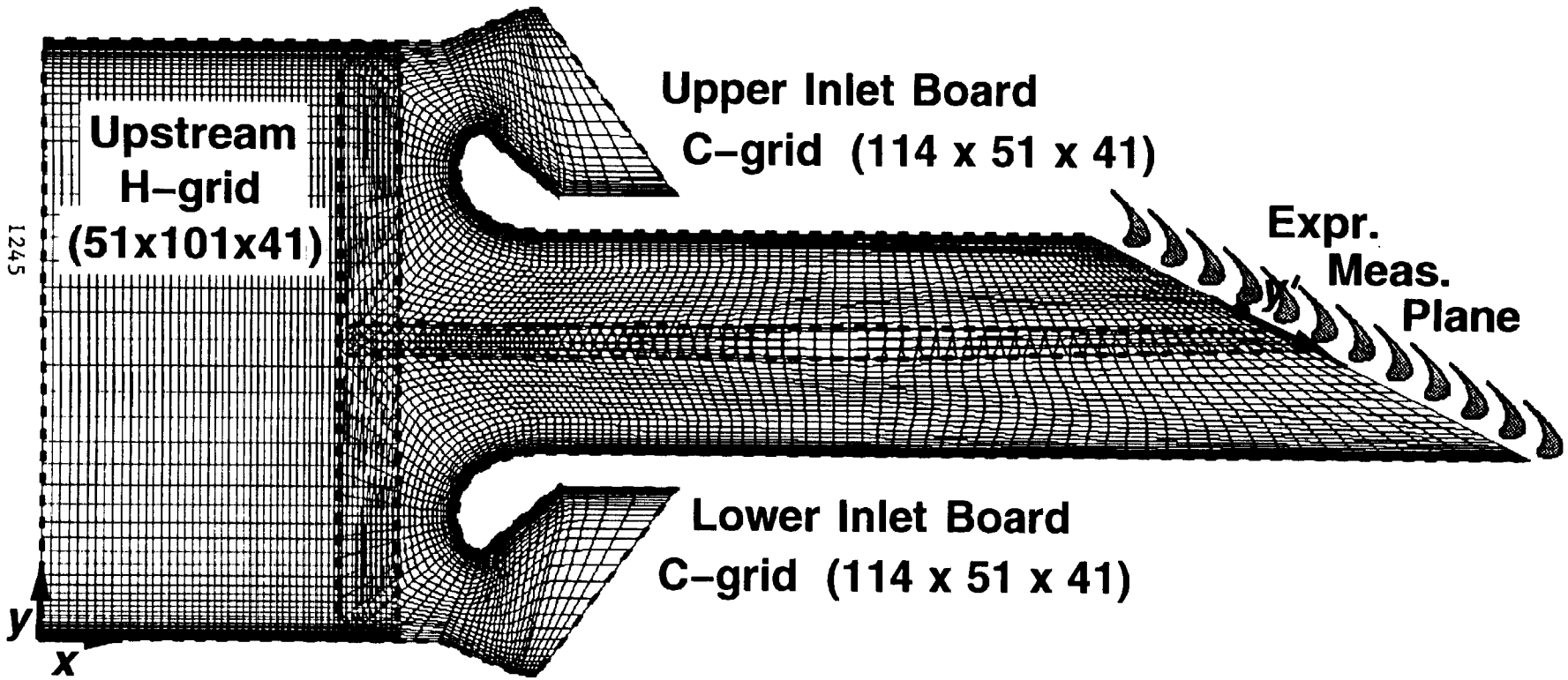

Transonic Turbine Blade Cascade Inlet Analysis – Calculations of Original Geometry (uniform exit)

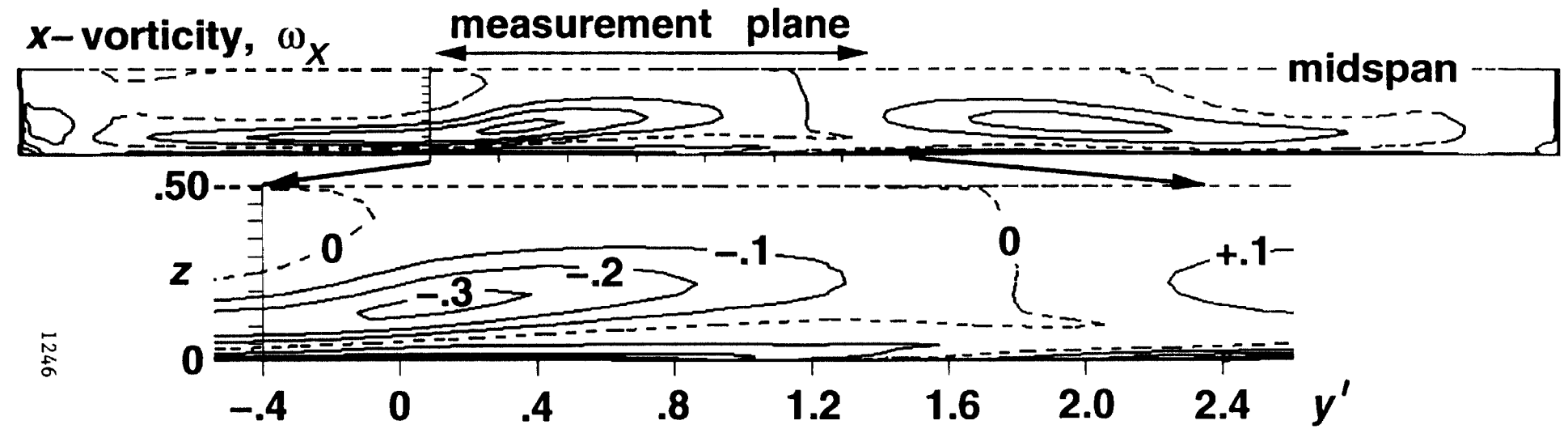

1246

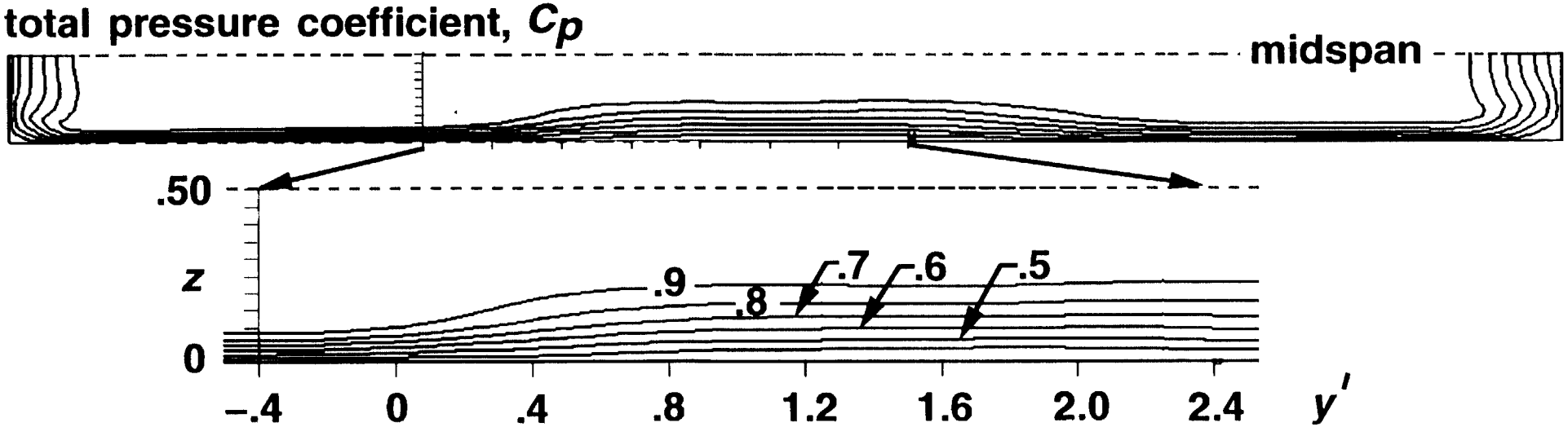

Transonic Turbine Blade Cascade Inlet Analysis – RVC3D Isolated Blade Calculations – Loading

$Re_{C_x} = 0.497 \times 10^6$; $\alpha_{in} = 63.64°$ (design);
$\delta_{hub} = 1.8$ in.; $\delta_{tip} = 1.0$ in.; subsonic exit - $M_{exit} = 0.9$

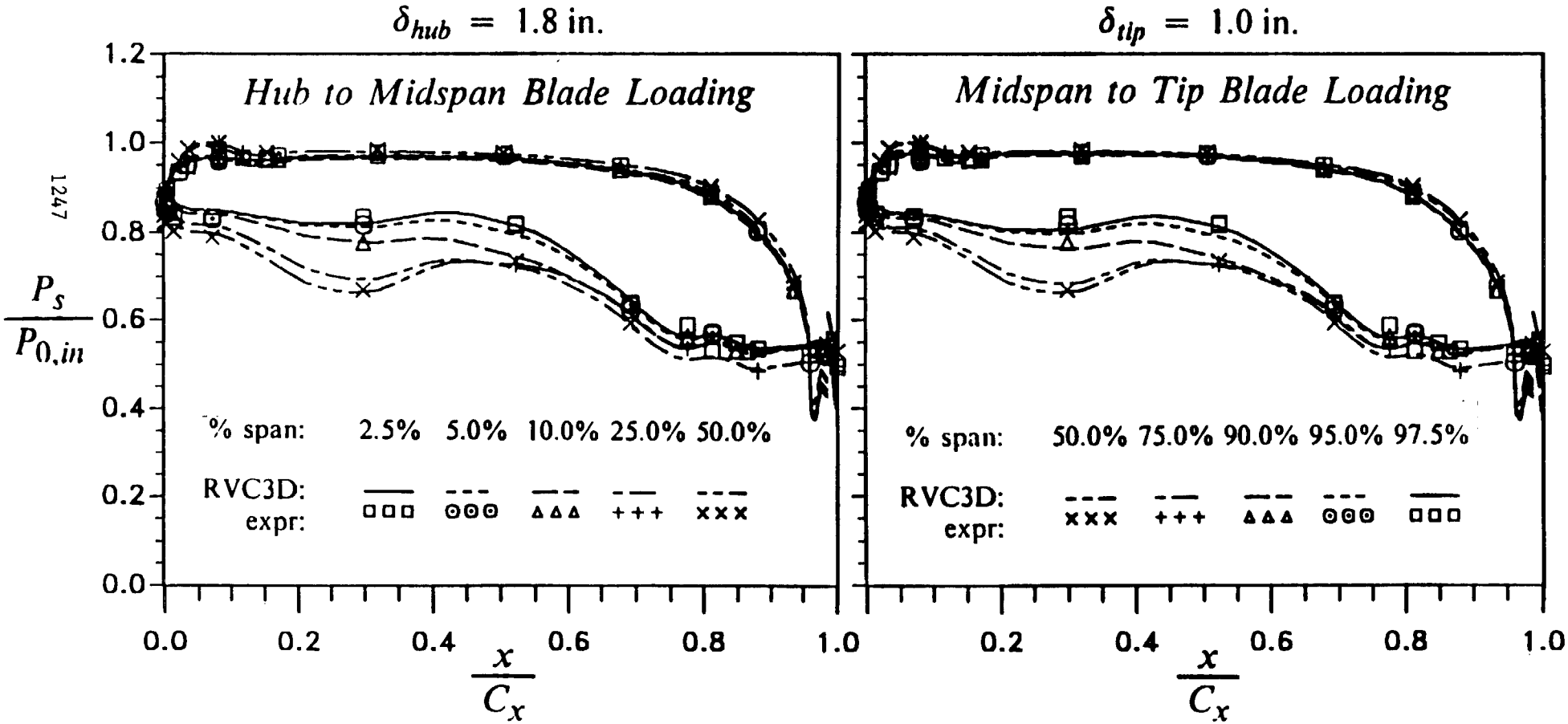

Transonic Turbine Blade Cascade Inlet Analysis – Non–uniform Exit Pressure Boundary Condition

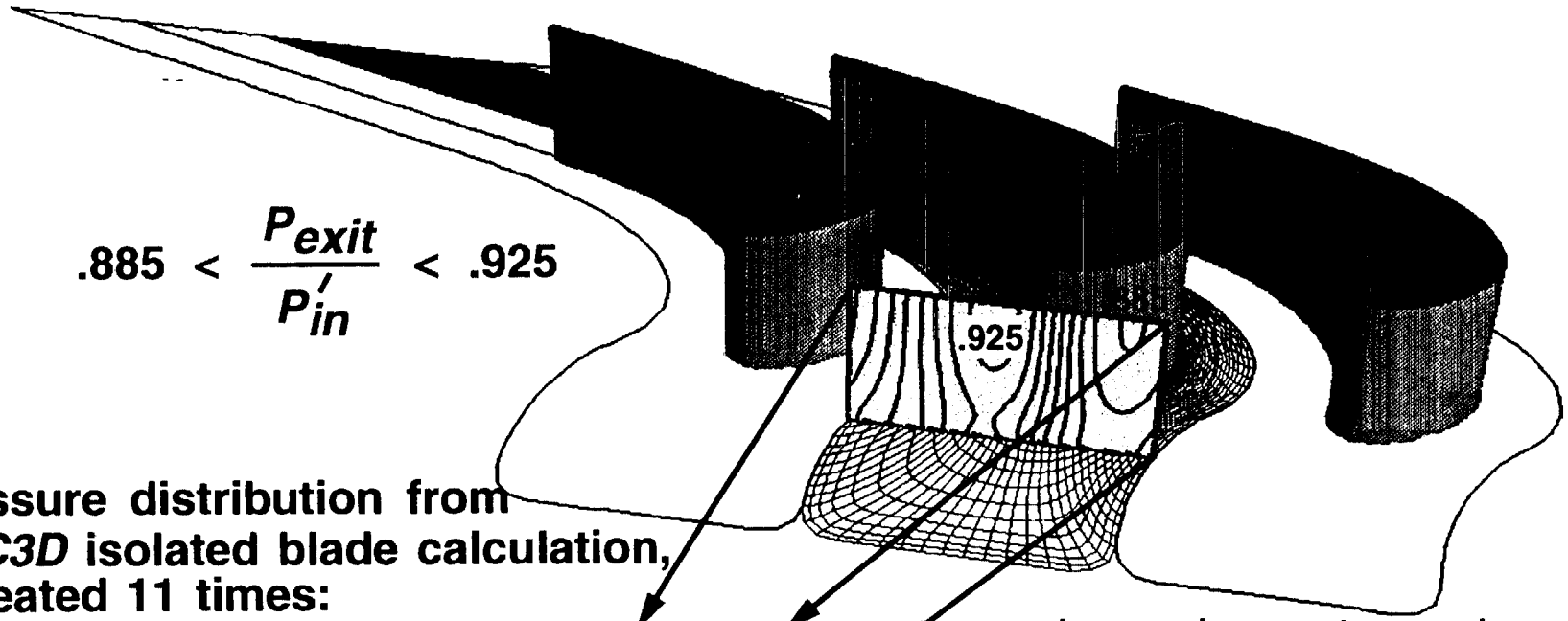

1248

Pressure distribution from *RVC3D* isolated blade calculation, repeated 11 times:

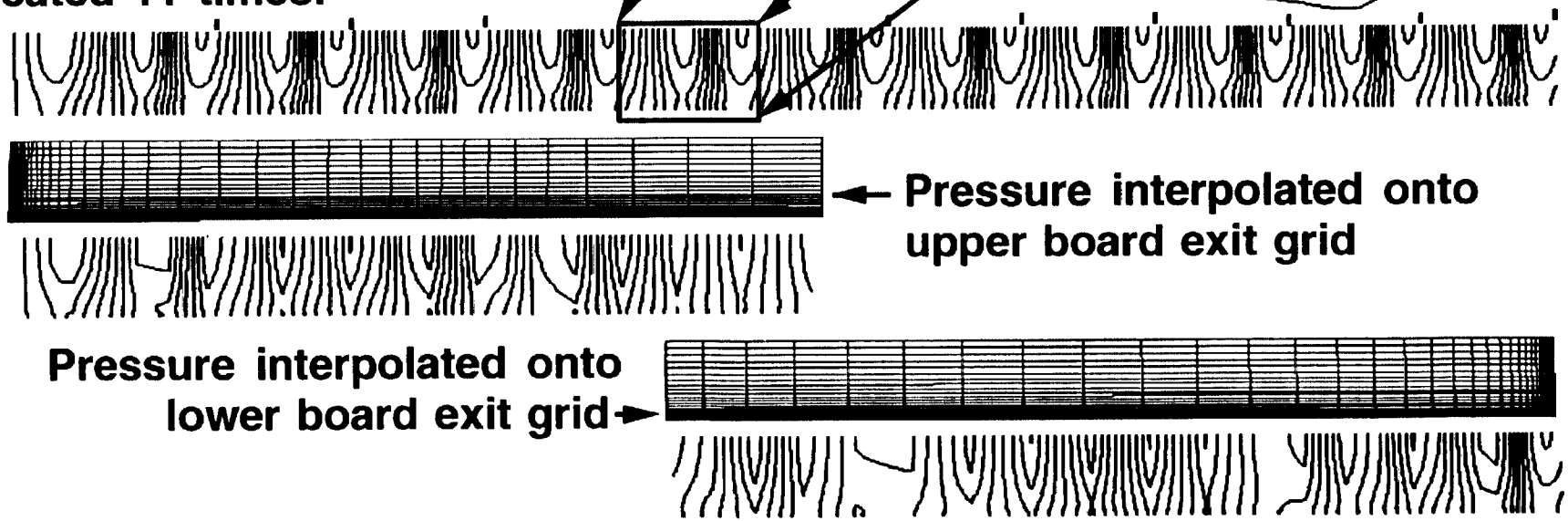

Transonic Turbine Blade Cascade Inlet Analysis – Calculations of Original Geometry (non–uniform exit)

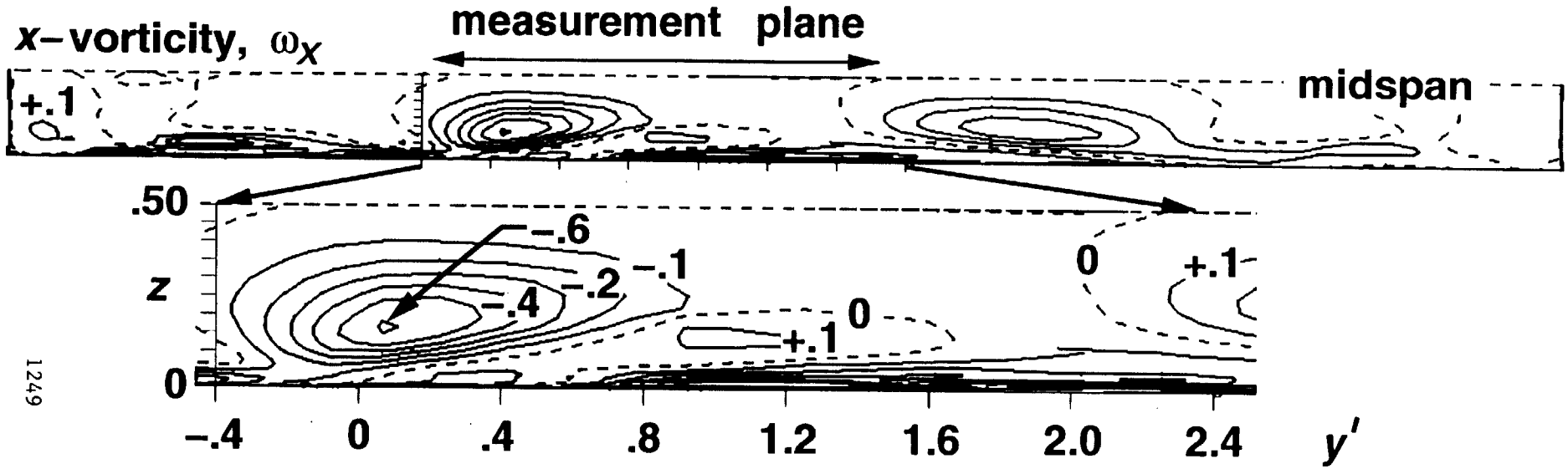

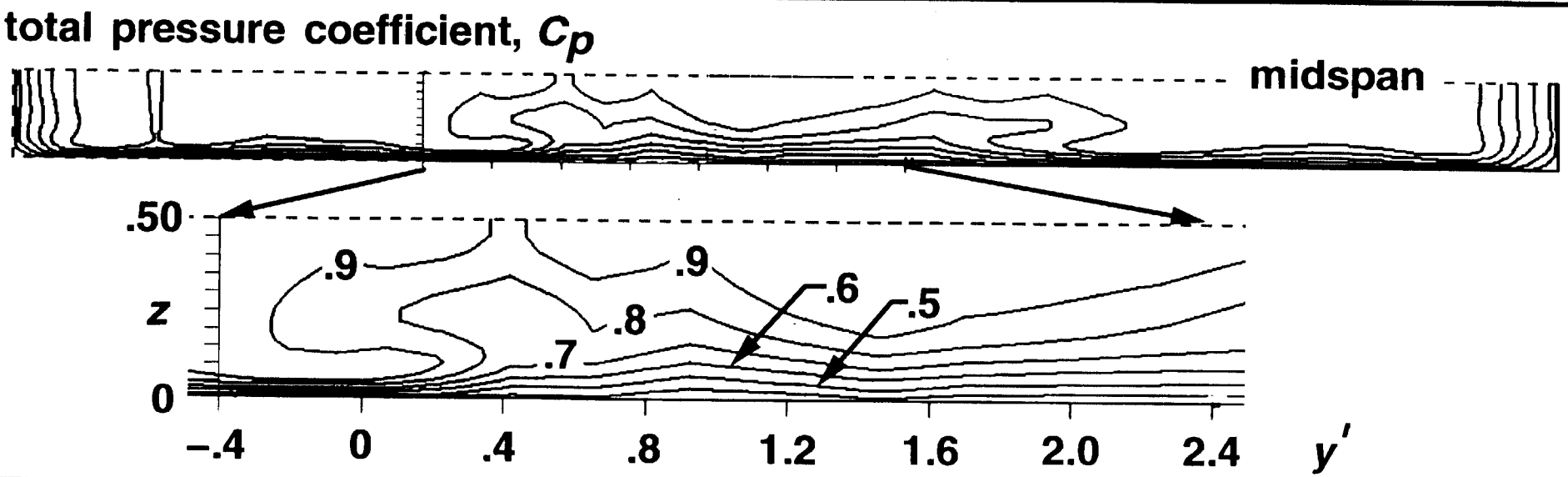

1249

Transonic Turbine Blade Cascade Inlet Analysis – Calculations of Original Geometry (non–uniform exit)

- contours of total pressure coefficient
- particles released from midspan
- design inlet flow angle

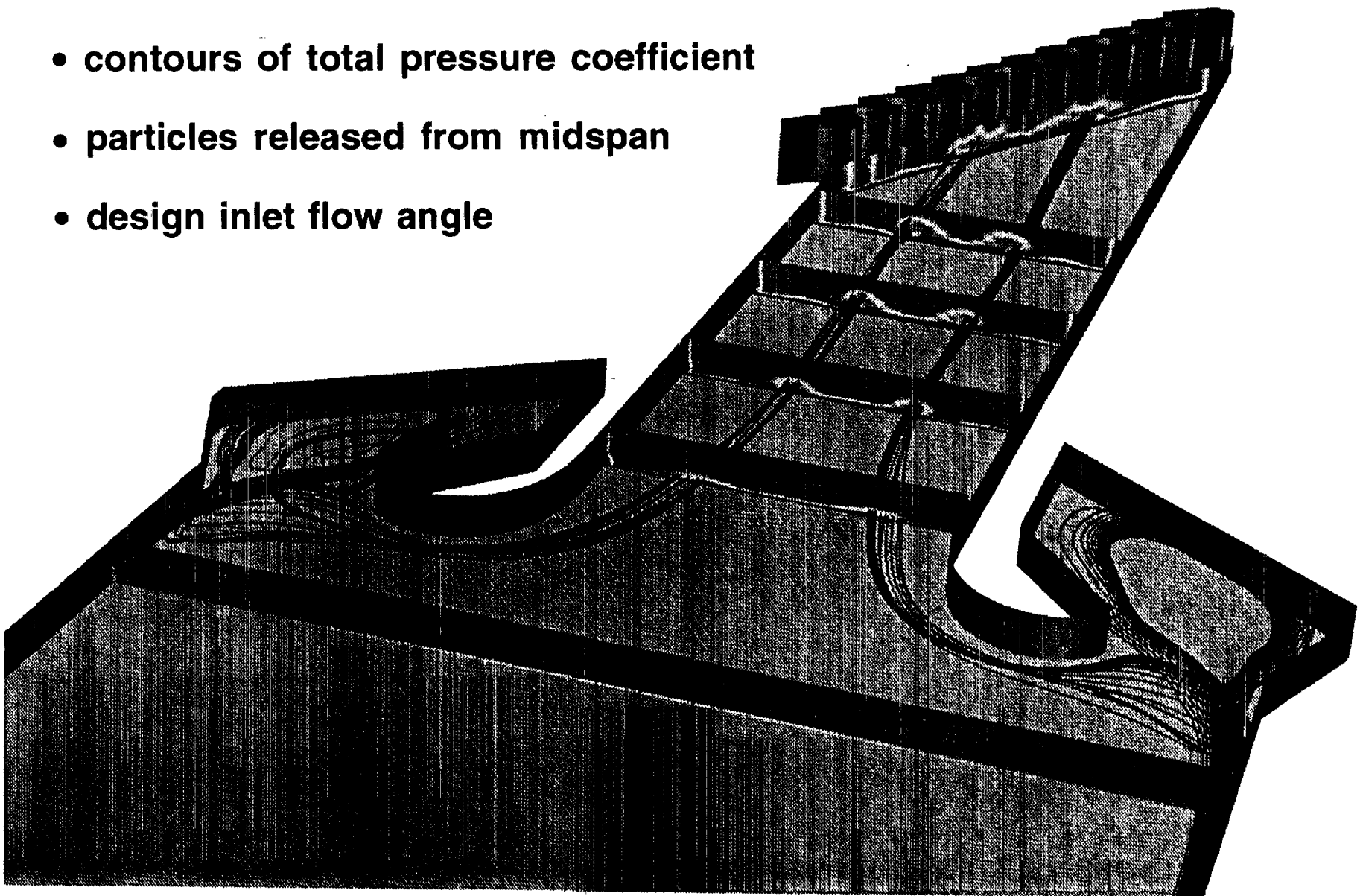

Transonic Turbine Blade Cascade Inlet Analysis – Calculations of Original Geometry (non–uniform exit)

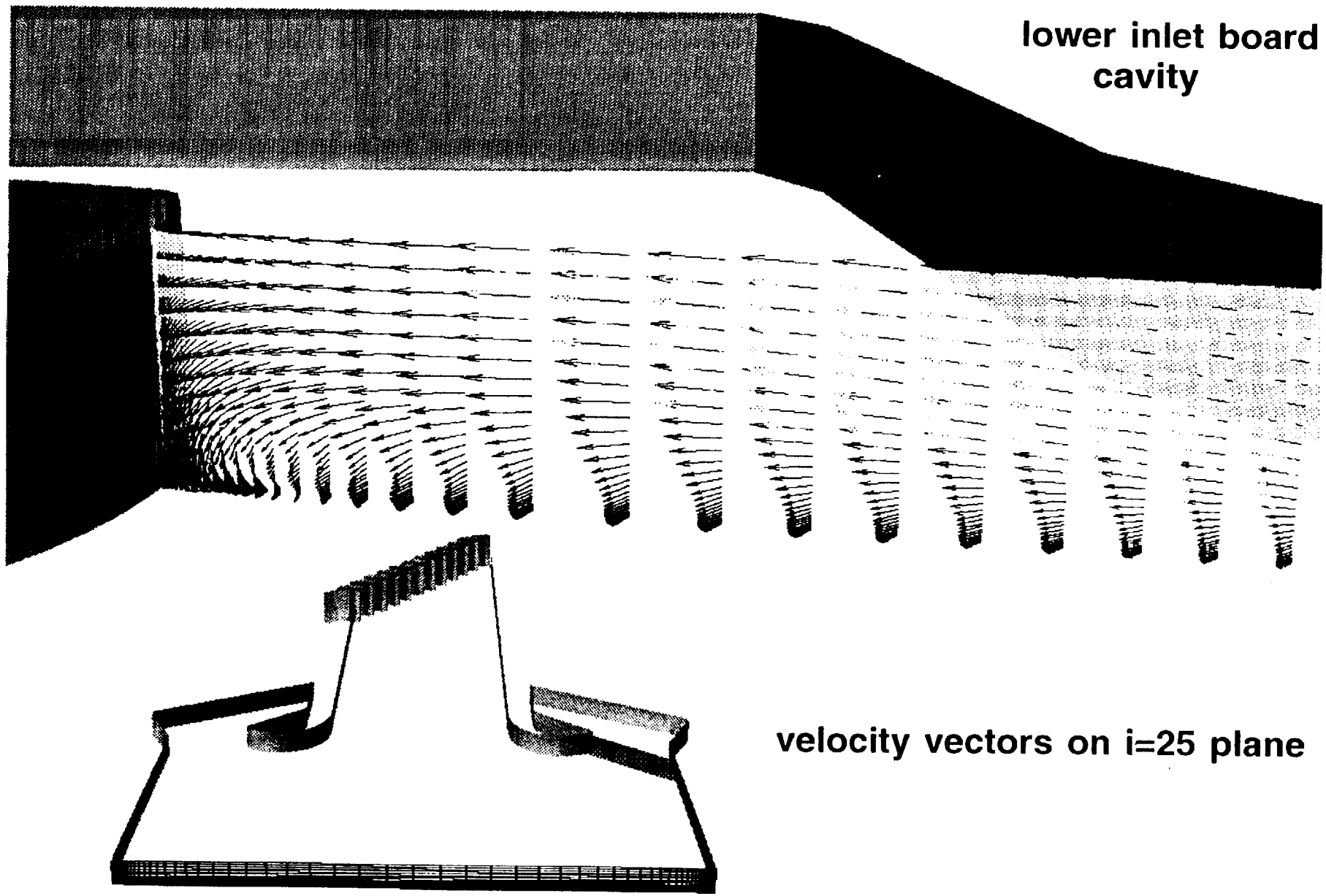

Transonic Turbine Blade Cascade Inlet Analysis – Modified Geometry and Grids

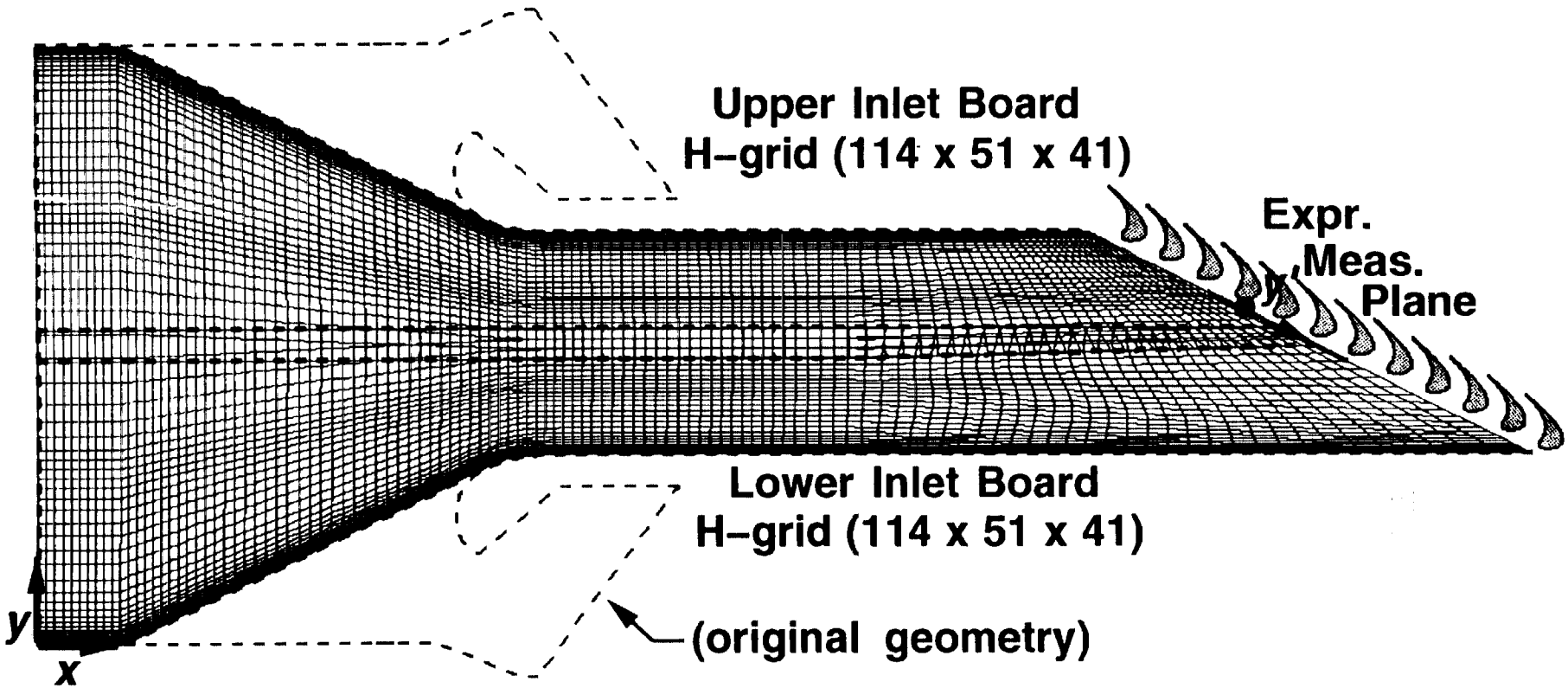

Transonic Turbine Blade Cascade Inlet Analysis – Calculations of Modified Geometry (non–uniform exit)

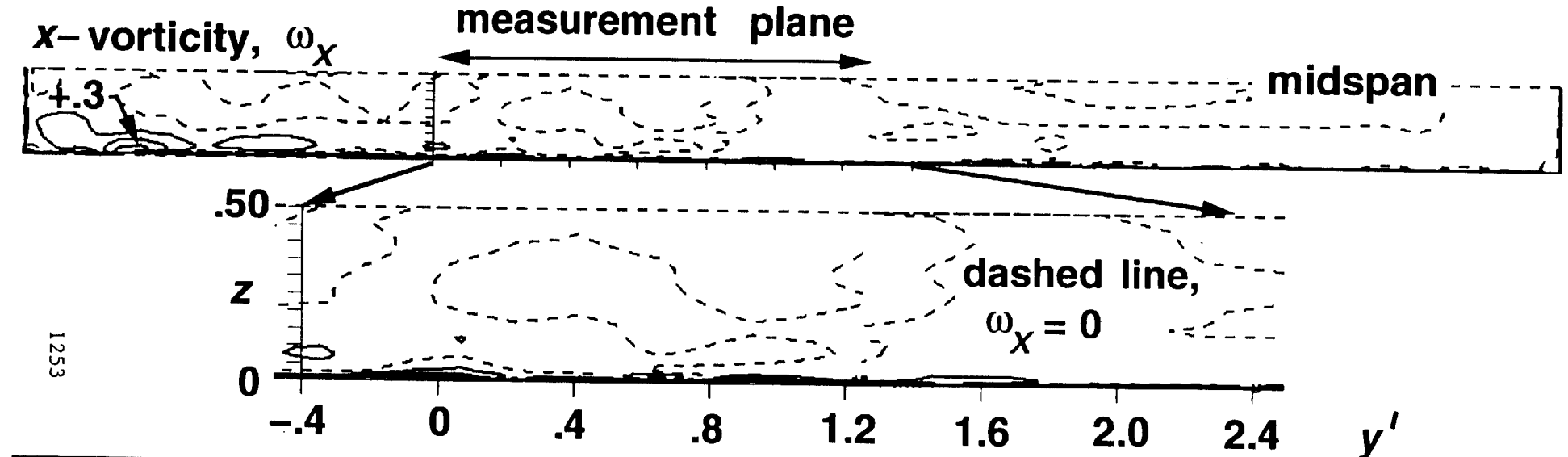

1253

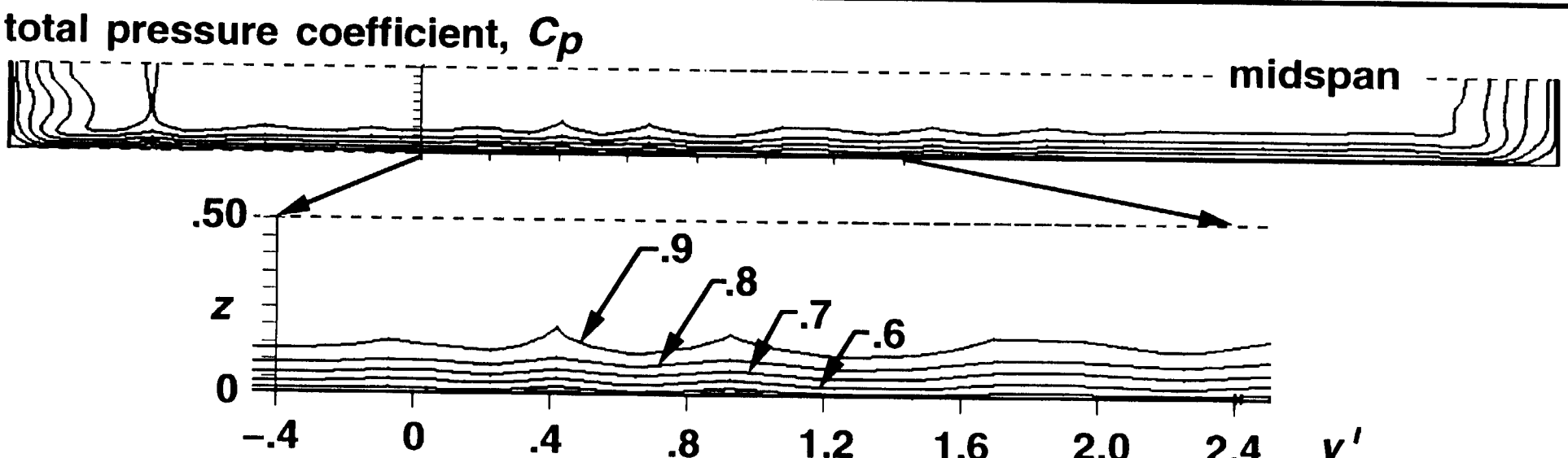

Transonic Turbine Blade Cascade Inlet Analysis – Upstream 8:1 Contraction; geometry and grid

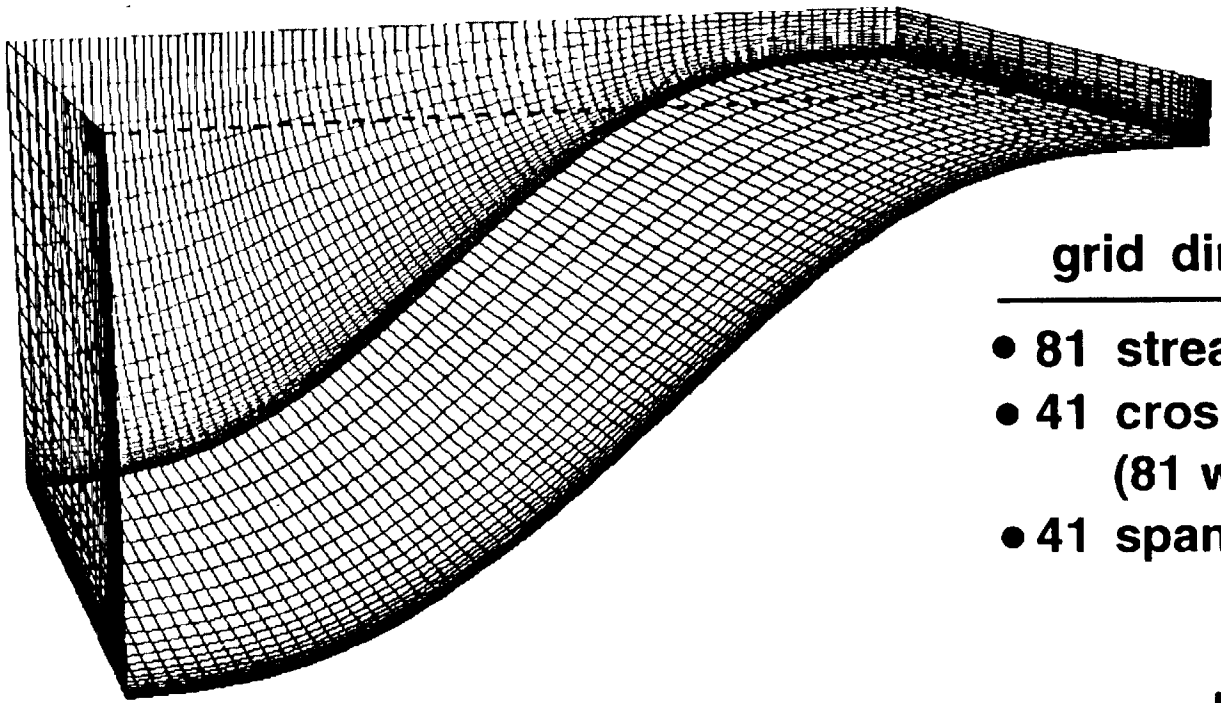

grid dimensions

- 81 streamwise
- 41 cross–channel
  (81 when doubled)
- 41 spanwise

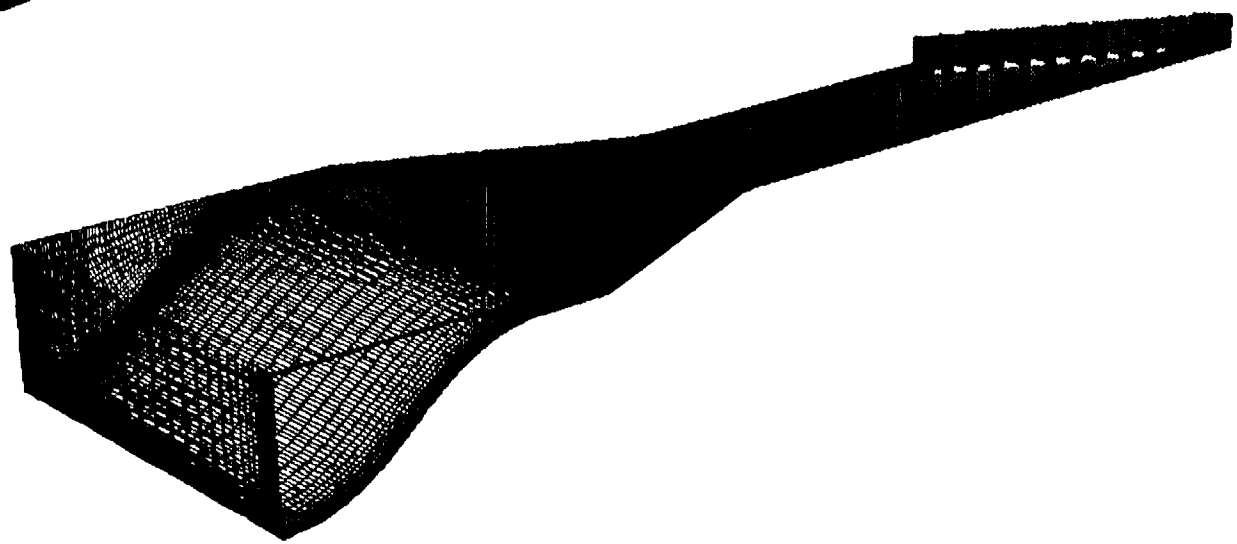

Transonic Turbine Blade Cascade Inlet Analysis – Upstream 8:1 Contraction; preliminary results

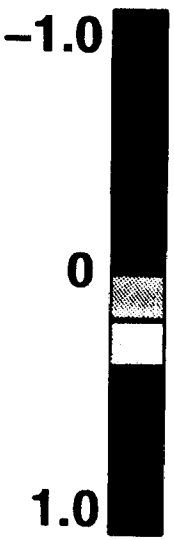

x–vorticity, ω_x

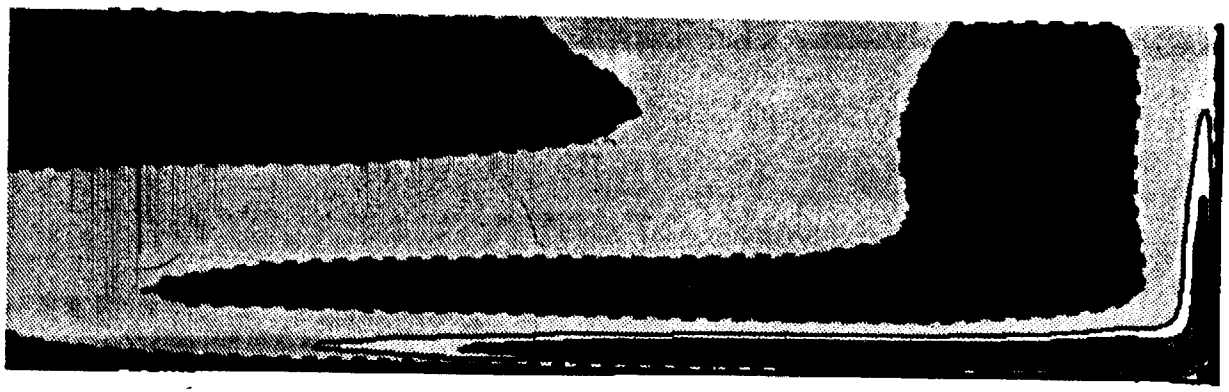

1255

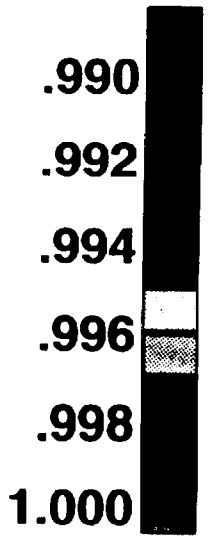

total pressure ratio, P'/P'_{in}

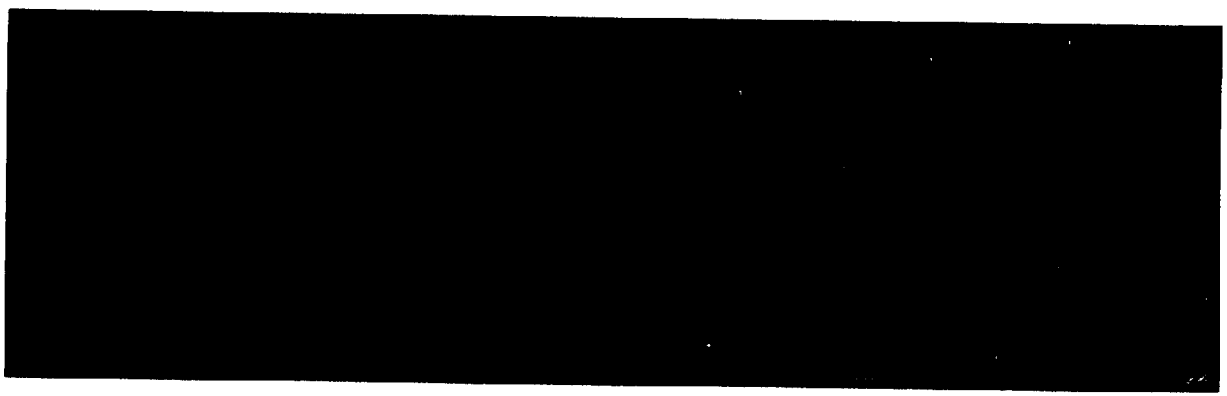

Transonic Turbine Blade Cascade Inlet Analysis –

Calculations of Modified Geometry with Upstream 8:1 Contraction (non–uniform exit)

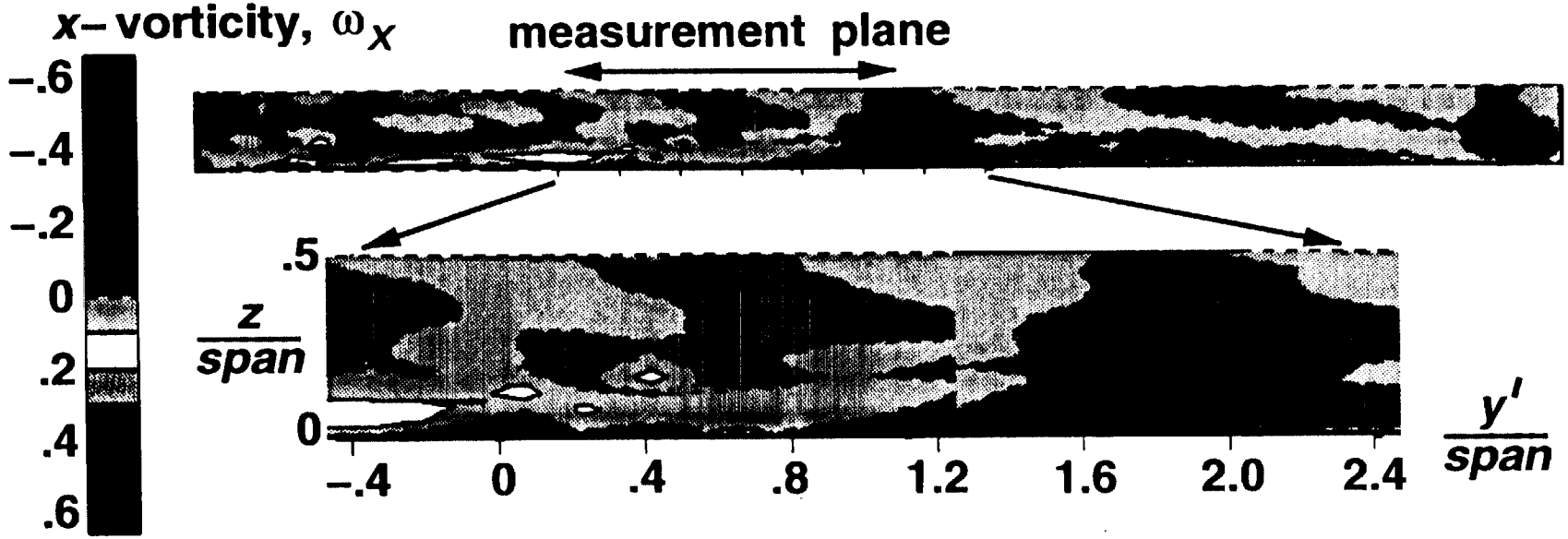

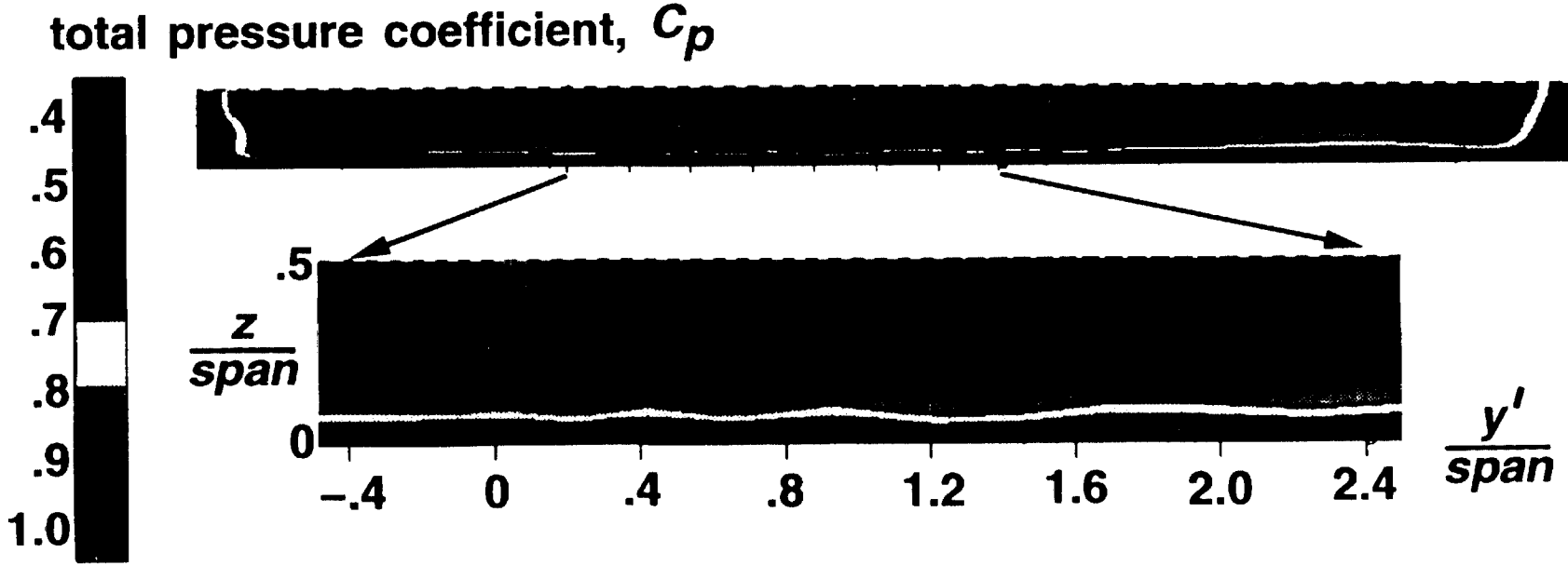

Transonic Turbine Blade Cascade Inlet Analysis – Summary of Results

Experimental data from original geometry:

total pressure coefficient,

$$\frac{P' - P_{in}}{P'_{in} - P_{in}}$$

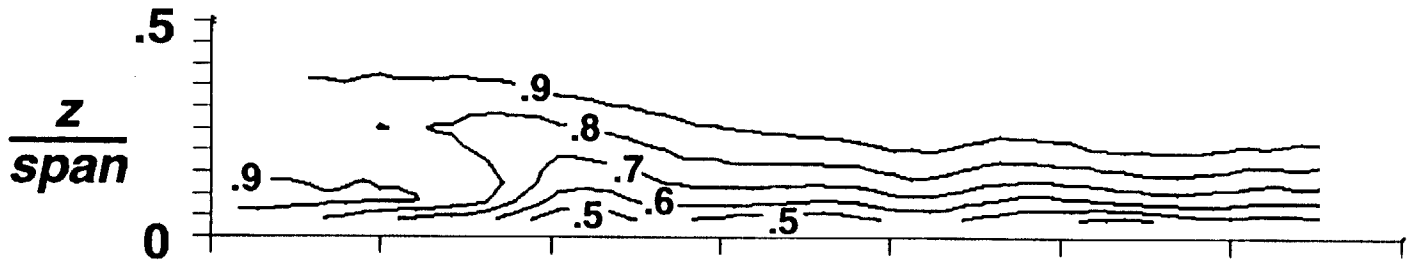

Calculation of original geometry:

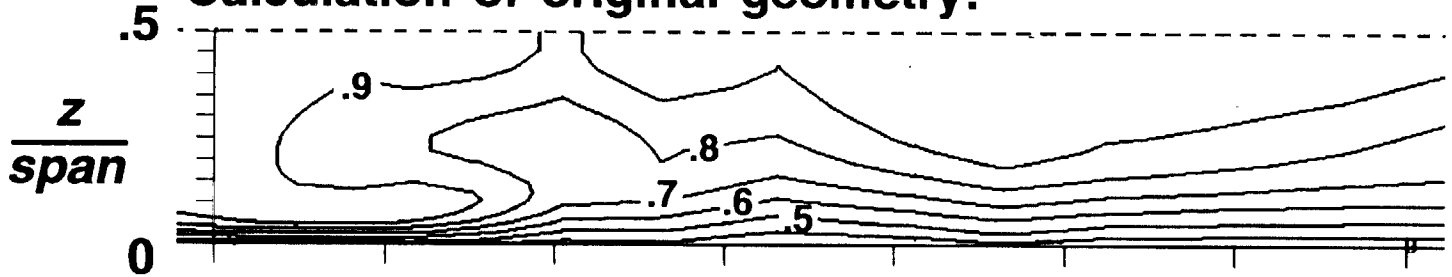

Calculation of modified geometry:

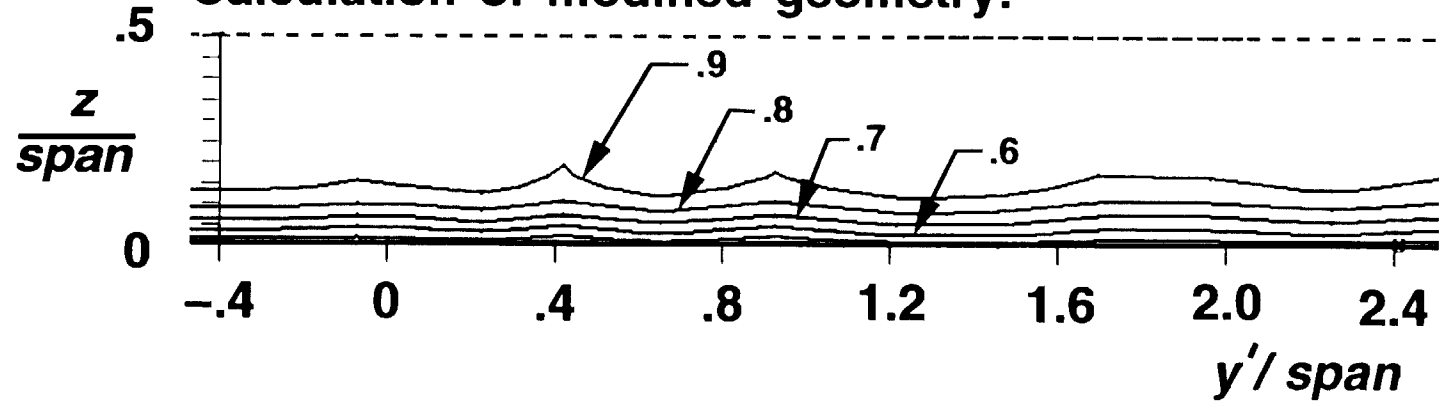

Abstract

Prediction of Incidence and Surface Roughness Effects on Turbine Performance

R. J. Boyle
NASA Lewis Research Center
Cleveland, OH 44135

The results of a Navier-Stokes analysis for predicting the change in turbine efficiency due to a change in either incidence or surface roughness is discussed. It was experimentally determined by Boynton, Tabibzadeh, and Hudson that polishing the SSME high pressure fuel turbine blades improved turbine efficiency by about 2 points over a wide range of operating conditions. These conditions encompassed the range of incidence seen by the turbine blading during flight. It is also necessary to be able to predict turbine performance at various operating points for future rocket turbopump applications. The code RVCQ3D, developed by Rod Chima, was used to determine the effects of changes in incidence angle on turbine blade row efficiency. The midspan Navier-Stokes results were used in conjunction with an inviscid flow analysis code to predict the efficiency of the two stage SSME over a wide range of operating conditions for smooth and rough turbine blades. The use of the Navier-Stokes analysis to predict changes in turbine efficiency due to variation in incidence angles was found to be superior to other incidence loss correlations available in the literature. The sensitivity of the Navier-Stokes results to grid parameters is discussed.

The effects of the surface roughness were accounted for using the Cebeci-Chang rough wall turbulence model. This model was implimented in the code RVCQ3D. The implimentation of this model for predicting the change in efficiency is also discussed.

PREDICTION OF INCIDENCE and SURFACE ROUGHNESS EFFECTS ON TURBINE PERFORMANCE

R. J. Boyle

NASA Lewis Research Center
Cleveland, OH 44135

OBJECTIVES

- IMPROVE TURBINE PERFORMANCE PREDICTION CAPABILITY
  - INCIDENCE EFFECTS
  - SURFACE ROUGHNESS EFFECTS

MOTIVATION

- INCIDENCE EFFECTS IMPORTANT
  - DURING ENGINE START
  - WHEN ENGINE IS THROTTLED

1262

- ROUGHNESS EFFECTS IMPORTANT
  - WHEN PROTECTIVE COATINGS ARE USED

INCIDENCE and SURFACE ROUGHNESS ?

- DIFFERENT QUESTIONS BUT SIMILAR APPROACHES

- RELATIVE CHANGE IMPORTANT

  RELATIVE GRID SENSITIVITY

  RELATIVE LOSS LEVEL

COMPUTATIONAL APPROACH

- USE INVISCID AND VISCOUS ANALYSES
- RELATIVELY QUICK ANALYSIS NEEDED

  MANY CASES NEEDED TO VERIFY APPROACH

- INVISCID - MTSB - QUASI-3D
- VISCOUS - RVCQ3D - MIDSPAN

MTSB - INVISCID + LOSSES

- FLOW ANALYSIS
  - HUB-TO-SHROUD - MERIDL
  - BLADE-TO-BLADE - TSONIC
- LOSS ANALYSIS
- BOUNDARY LAYER - BLAYER
  - PROFILE
  - ENDWALL
- CORRELATIONS
  - TIP CLEARANCE
  - SECONDARY FLOW
  - INCIDENCE

VISCOUS SOLVER

- MIDSPAN - BLADE-TO-BLADE ANALYSIS
- EXISTING SOLVER - RVCQ3D
  - EXPLICIT
  - TIME MARCHING
  - RESIDUAL SMOOTHING
- TURBULENCE MODEL
  - MIXING LENGTH
  - MODIFIED FOR ROUGHNESS EFFECTS
    - CEBECI-CHANG MODEL

INCIDENCE

- COMPARE NAVIER-STOKES INCIDENCE LOSS MODEL WITH EMPIRICAL CORRELATIONS
- EMPIRICAL MODELS
  - GLASSMAN'S
  - MOUSTAPHA et al.
  - TRAN et al. - SSME HPFT
- NAVIER-STOKES DERIVED CORRELATION
  - CURVE FIT MIDSPAN NAVIER-STOKES RESULTS & USE IN PLACE OF EMPIRICAL MODEL IN PERFORMANCE CALCULATION (MTSB)

INCIDENCE LOSS COMPARISONS

- MSFC BLOWDOWN TEST - 2 STAGE TURBINE

  SSME HPFT - U/V_{IDEAL} = 0.37(DESIGN)

  $0.25 < U/V_{IDEAL} < 0.65$

1268

- LEWIS 30in DIA TURBINES - 1 & 2 STAGES

  DESIGN POINTS - NO INCIDENCE EFFECTS

  40% SPEED LINE vs PRESSURE RATIO

DOES ONE CORRELATION FIT ALL CASES?

- COMPARISON WITH DIFFERENT TURBINES TESTS:

  UNIVERSALITY OF NAVIER-STOKES DERIVED INCIDENCE LOSS CORRELATION

- SSME HPFT - LOW PRESSURE RATIO

- 30 in DIAMETER TURBINES

  HIGH PRESSURE RATIO

  TRANSONIC FLOW CONDITIONS

SENSITIVITY OF ROTOR LOSS TO GRID PARAMETERS

Grid	y_1^+	$\bar{e}$
145×54	0.6	0.0509
291×54	0.6	0.0423
291×70	0.6	0.0438
291×54	1.2	0.0375
291×54	0.3	0.0321
291×70	0.3	0.0441
MTSB		0.0351

EFFICIENCY FOR SMOOTH BLADED SSME HPFT

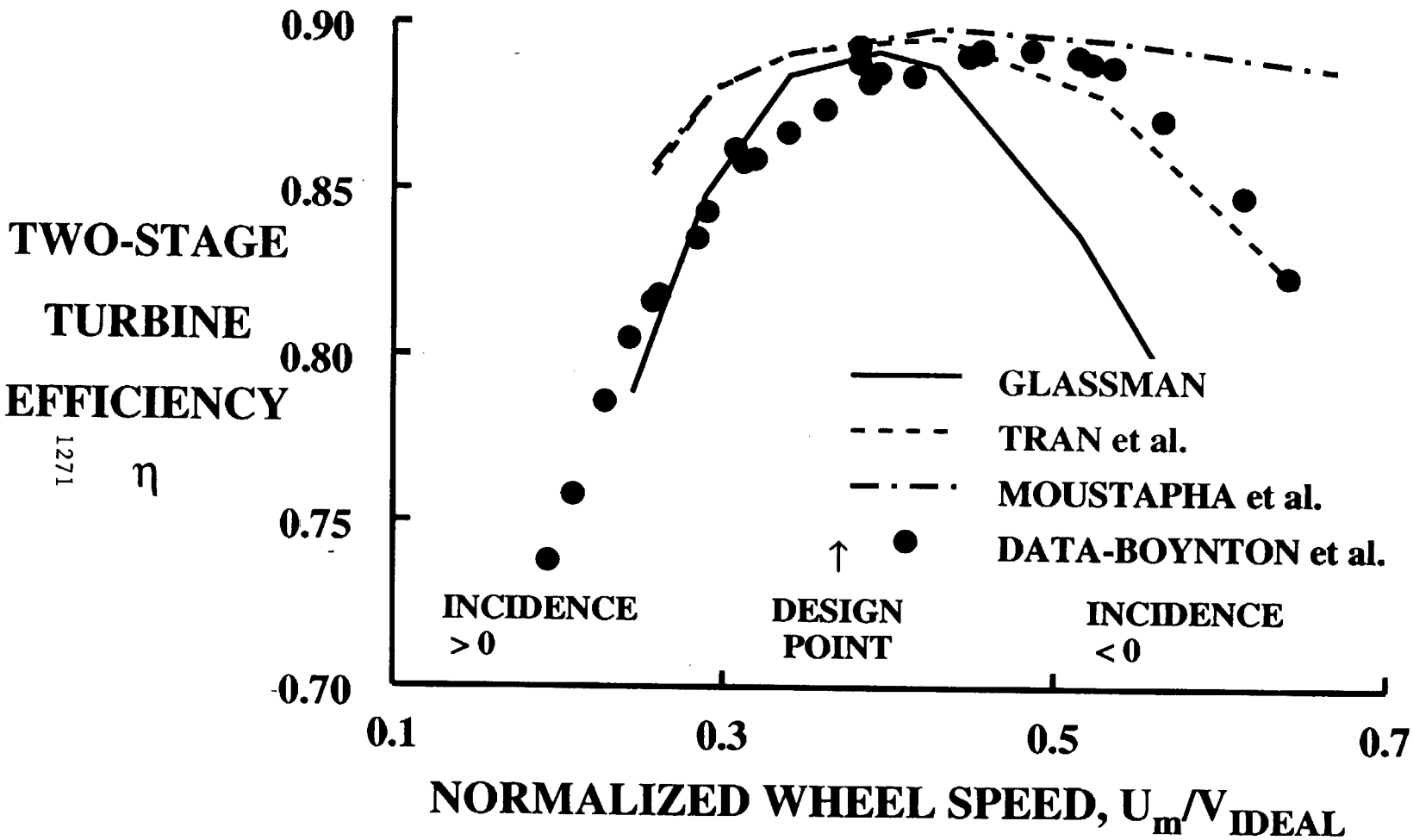

EFFICIENCY FOR SMOOTH BLADEDED SSME HPFT

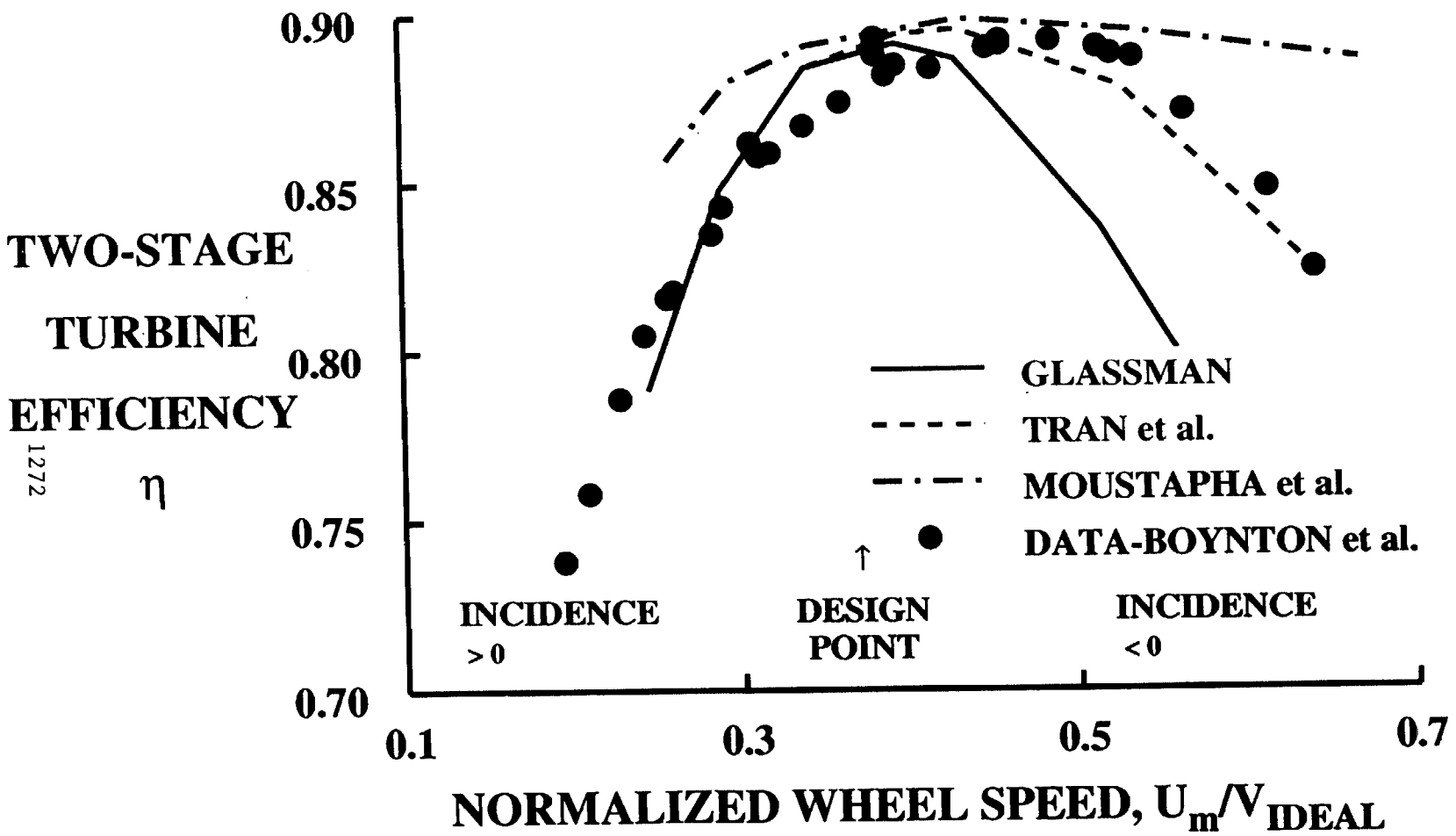

LOSS PREDICTIONS - NAVIER-STOKES & CORRELATIONS

SSME HPFT FIRST STAGE ROTOR

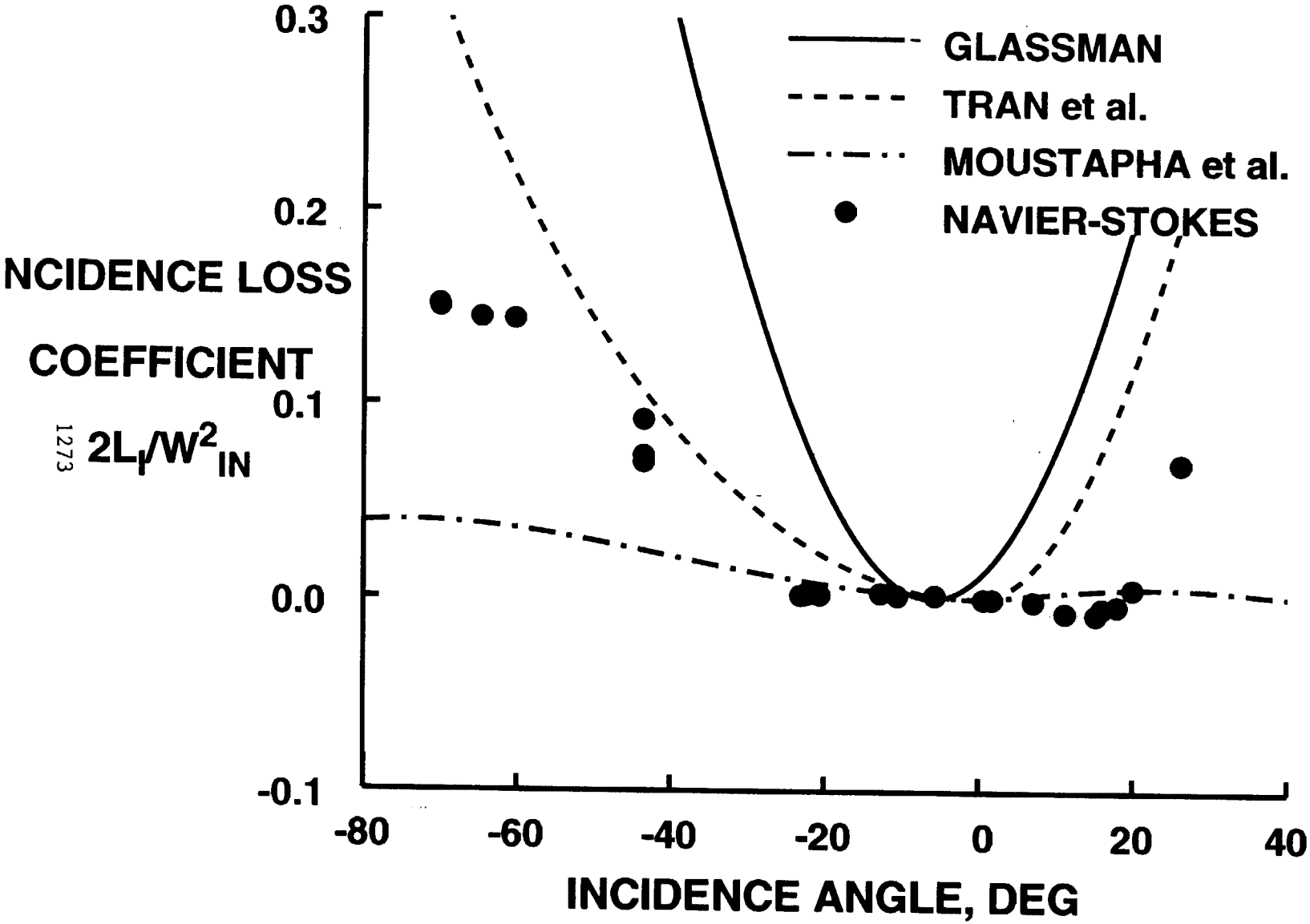

1273

LOSS PREDICTIONS - NAVIER-STOKES & CORRELATIONS
SSME HPFT SECOND STAGE STATOR

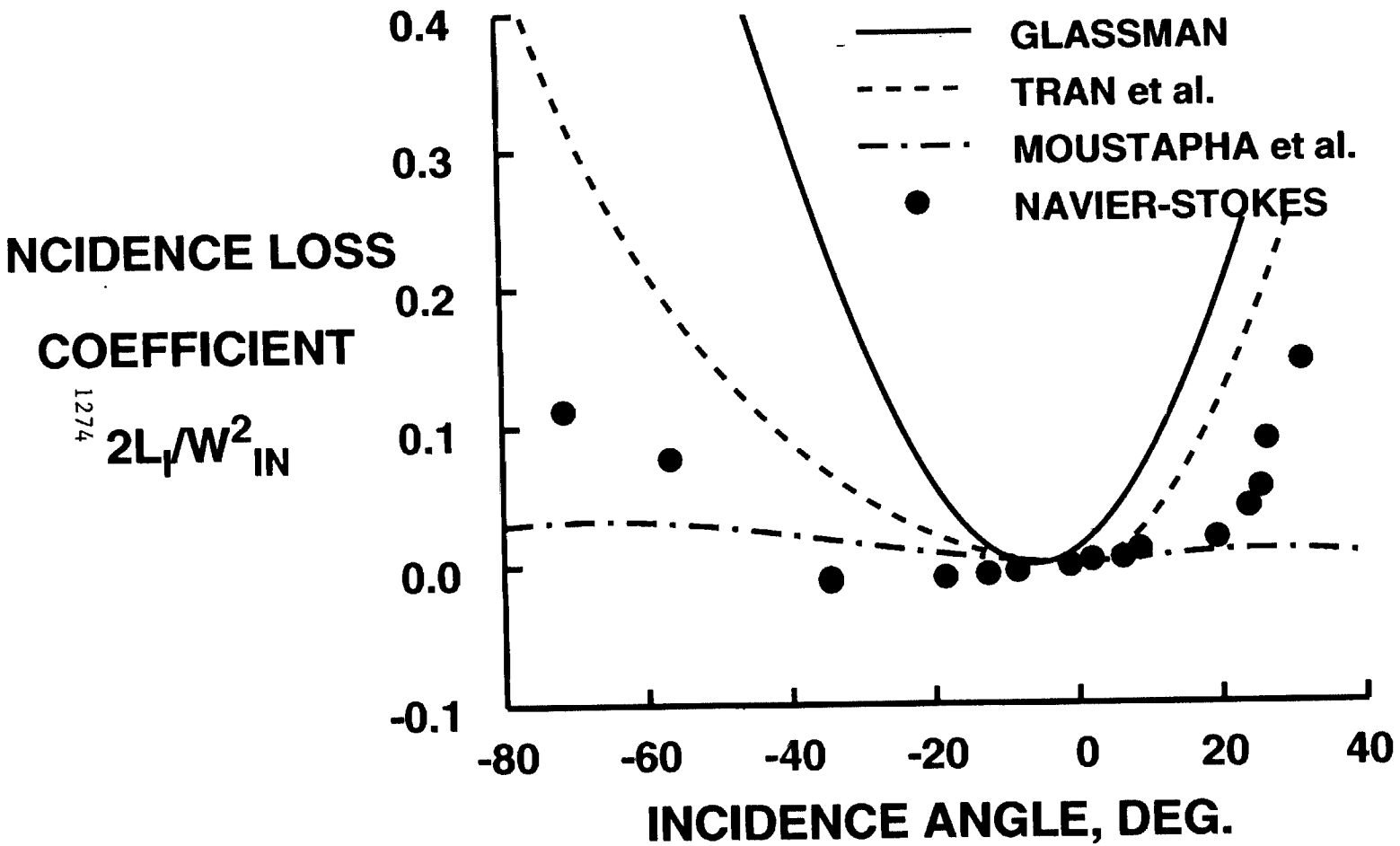

EFFECT OF OPTIMUM INCIDENCE ANGLE ON LOSS

SSME FIRST STAGE ROTOR

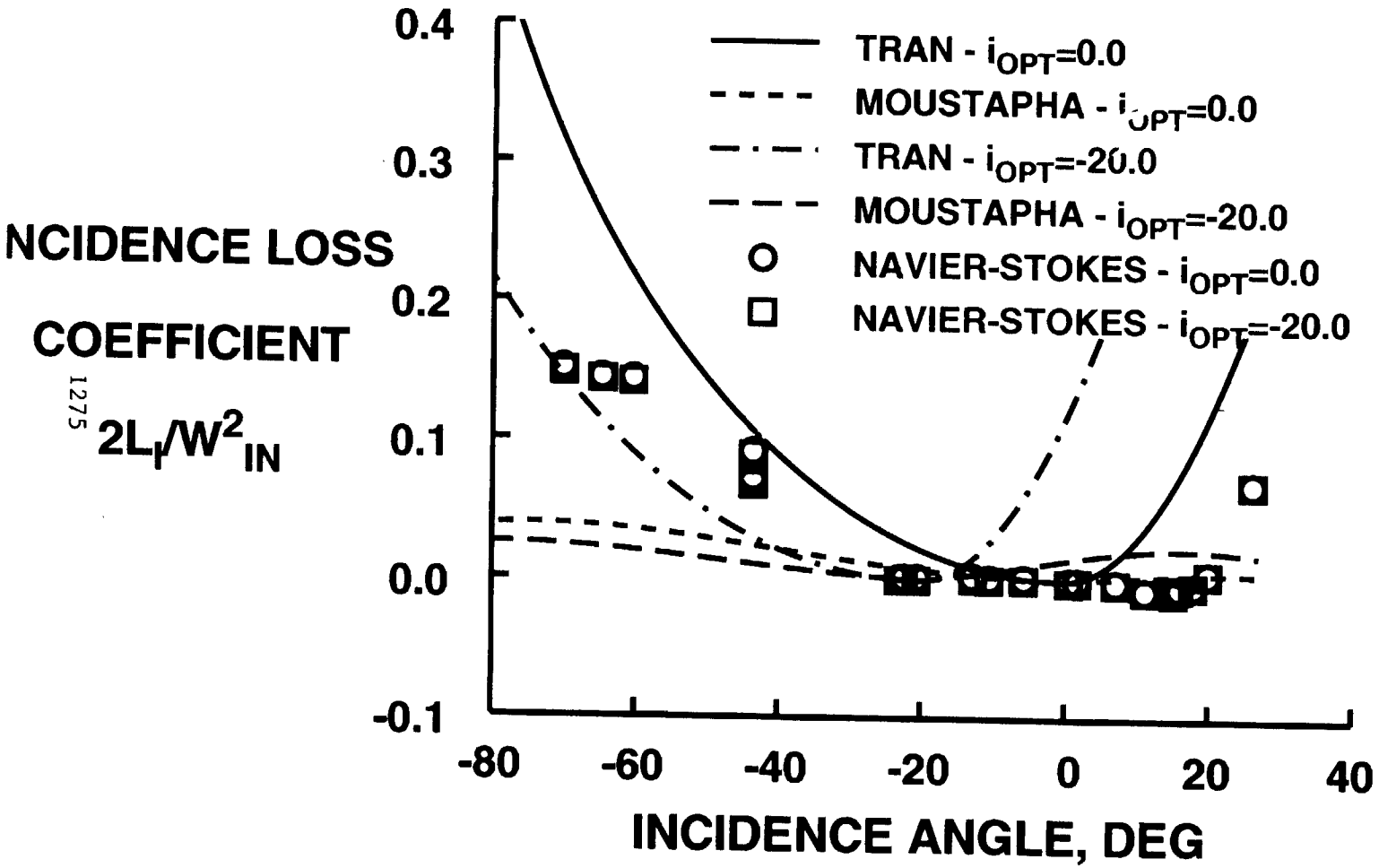

EFFECT OF OPTIMUM INCIDENCE ANGLE ON LOSS

SSME HPFT SECOND STAGE STATOR

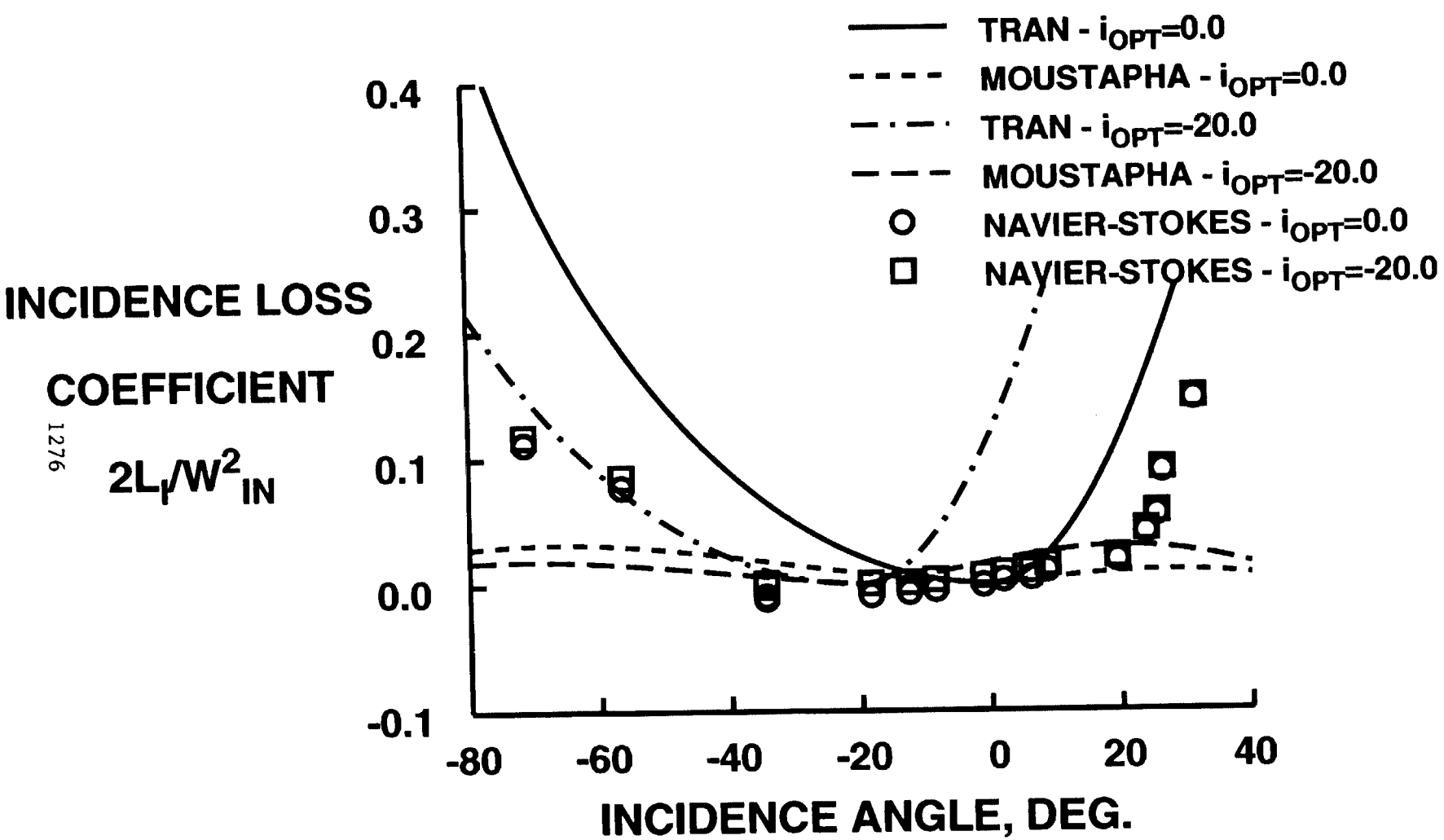

1276

EFFICIENCY OF SMOOTH BLADED SSME HPFT
NAVIER-STOKES DERIVED INCIDENCE LOSS MODEL

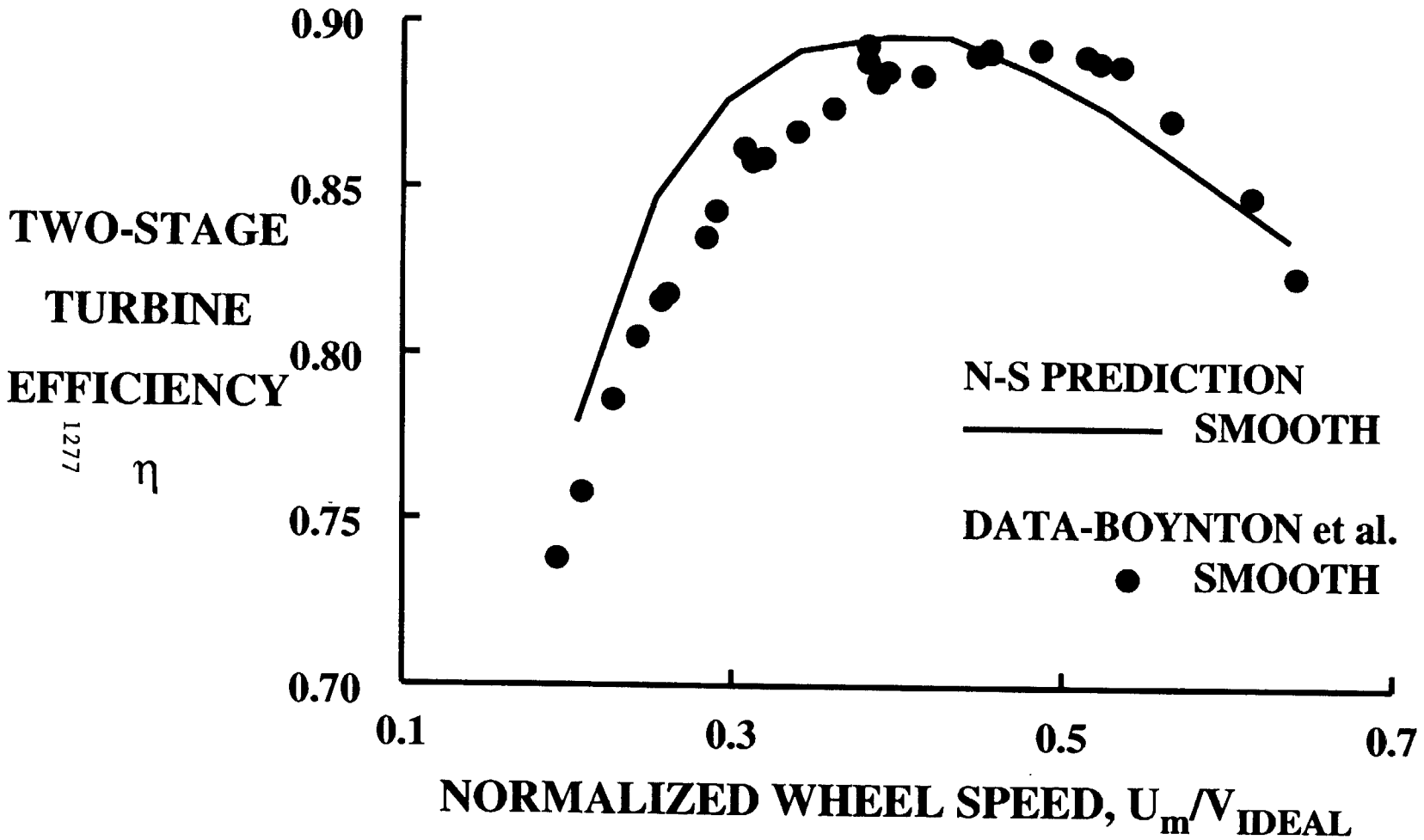

EFFICIENCY FOR SINGLE STAGE 30in TURBINE - 40% SPEED

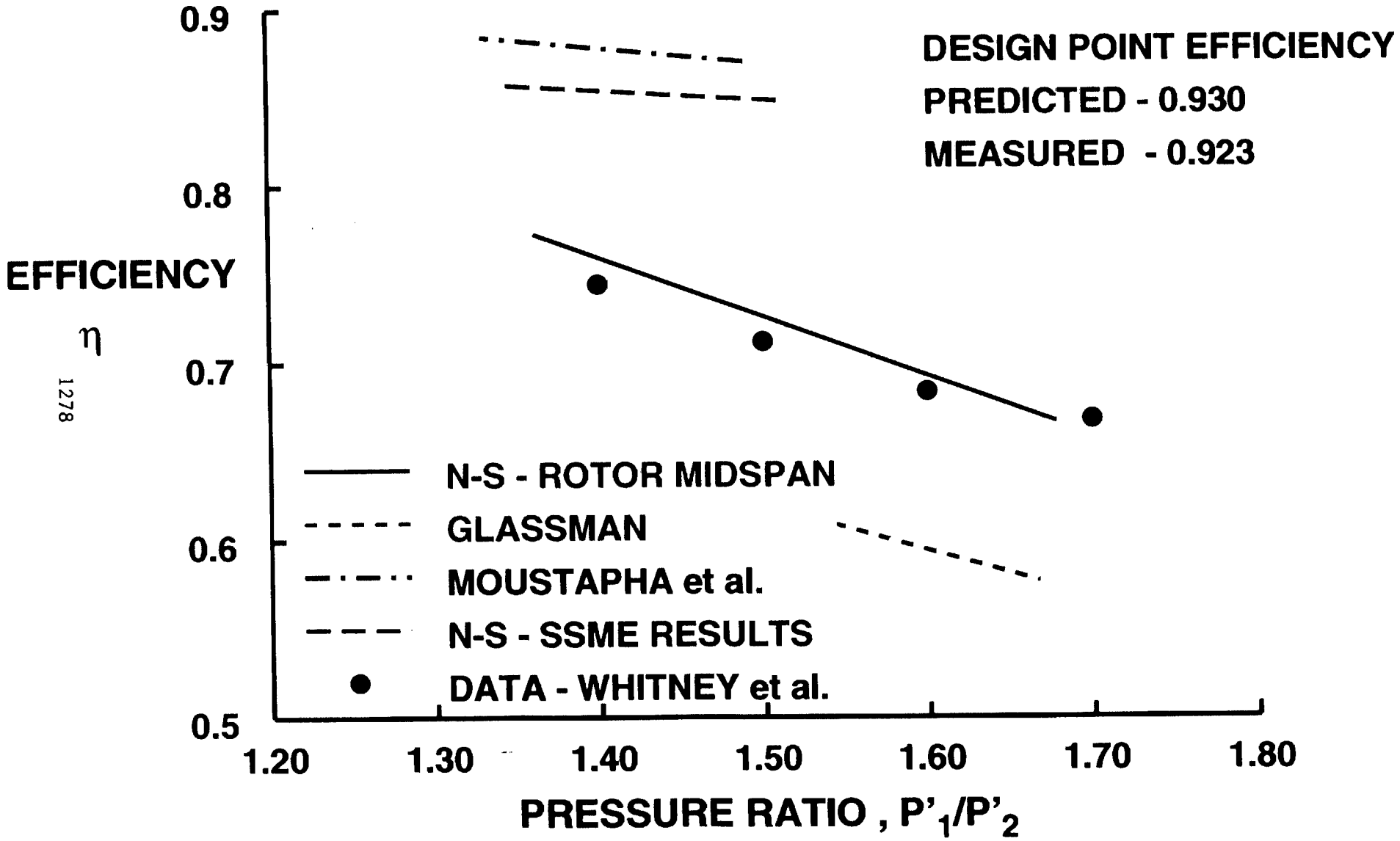

EFFICIENCY FOR TWO STAGE 30in TURBINE - 40% SPEED

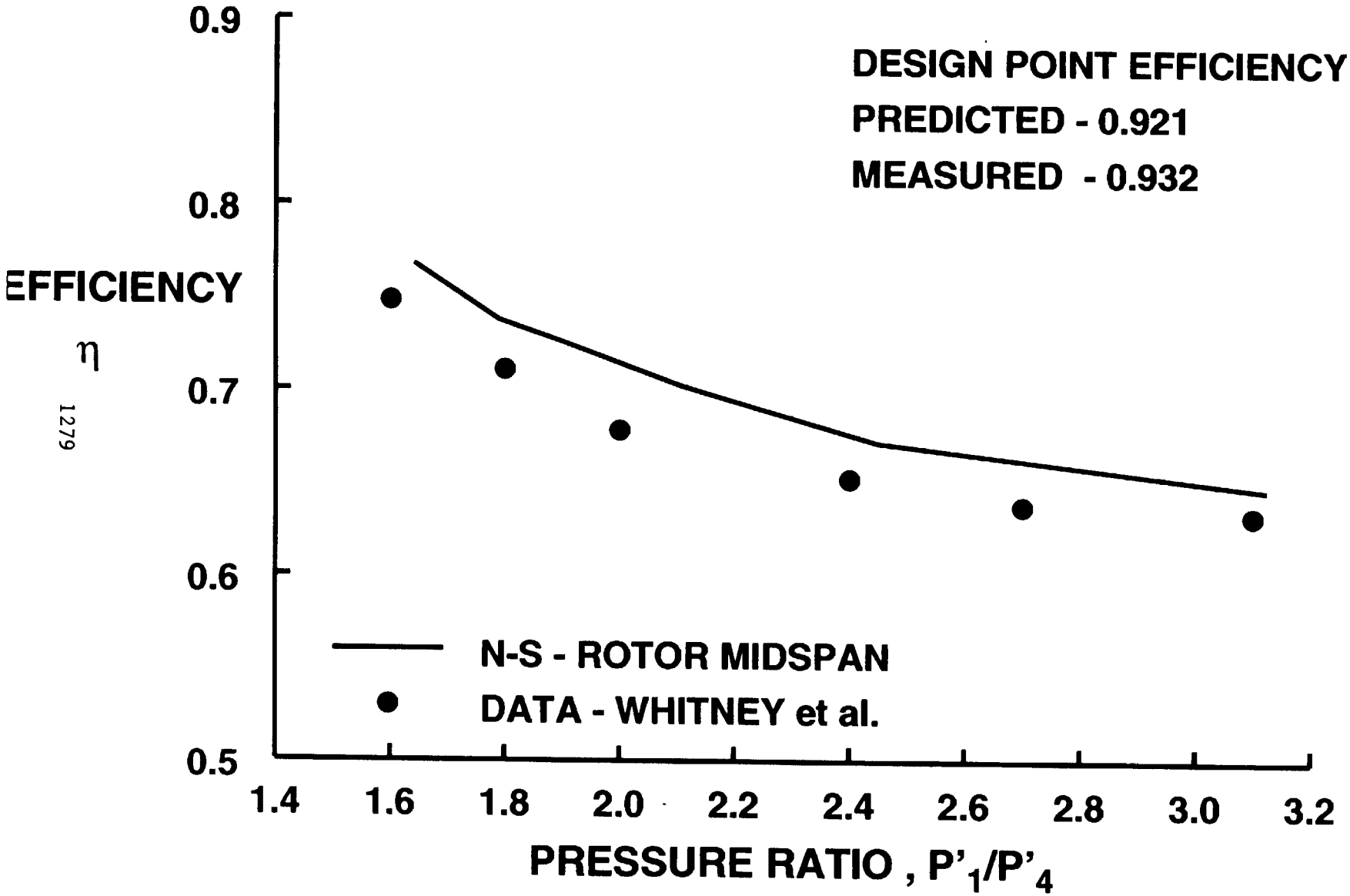

1279

INCIDENCE LOSS CONCLUSIONS

- INCIDENCE LOSS WELL PREDICTED BY NAVIER-STOKES MIDSPAN ANALYSIS
- NAVIER-STOKES APPROACH DOES NOT RELY ON A PRIORI KNOWLEDGE OF OPTIMUM INCIDENCE ANGLE
- BEST AGREEMENT WHEN USING NAVIER-STOKES RESULTS FOR SIMILAR CONFIGURATION

  NOT A SIGNIFICANT DISADVANTAGE

- IMPROVED INCIDENCE LOSS CORRELATION VIA VARIATION OF NAVIER-STOKES PARAMETERS

  NOT ALWAYS CONVENIENT IN EXPERIMENTS

SURFACE ROUGHNESS

- CEBECI-CHANG ROUGHNESS MODEL IMPLEMENTED IN MIDSPAN NAVIER-STOKES CODE

  MIXING LENGTH TURBULENT EDDY VISCOSITY MODEL FOR BOTH SMOOTH AND ROUGH SURFACES

  INCREASE IN MIXING LENGTH TO ACCOUNT FOR ROUGHNESS

  INCREASE IS A FUNCTION OF ROUGHNESS HEIGHT AND DENSITY

- NEAR WALL DAMPING (A^+) PART OF TURBULENT EDDY VISCOSITY MODEL

EFFECT OF GRID AND SURFACE ROUGHNESS ASSUMPTIONS ON EFFICIENCY

h =15 micrometers

Grid	y_1^+	K	A^+	$\bar{e}_{2D}$	$\Delta\eta$
291×54	0.3	0.0	26.0	0.0321	
		0.0	1.0	0.0483	0.011
		0.3	26.0	0.0348	0.002
		0.3	1.0	0.0550	0.015
		0.7	1.0	0.0656	0.022
		1.0	26.0	0.0455	0.009
		1.0	1.0	0.0703	0.025
291×54	0.6	0.0	26.0	0.0423	
		0.0	1.0	0.0570	0.010
		0.3	26.0	0.0449	0.002
		0.3	1.0	0.0654	0.015
		0.7	1.0	0.0726	0.020
		1.0	26.0	0.0546	0.008
		1.0	1.0	0.0767	0.023

Grid	y_1^+	K	A^+	$\bar{e}_{2D}$	$\Delta\eta$
291×54	1.2	0.0	26.0	0.0375	
		0.0	1.0	0.0531	0.010
		0.3	26.0	0.0402	0.002
		0.3	1.0	0.0586	0.014
		0.7	1.0	0.0686	0.021
		1.0	26.0	0.0502	0.008
		1.0	1.0	0.0730	0.024
291×70	0.3	0.0	26.0	0.0441	
		0.0	1.0	0.0564	0.008
		0.3	26.0	0.0462	0.001
		0.3	1.0	0.0623	0.012
		0.7	1.0	0.0720	0.019
		1.0	26.0	0.0581	0.009
		1.0	1.0	0.0760	0.021
Experimental					0.021

EFFICIENCY FOR SMOOTH AND ROUGH BLADED HPFT

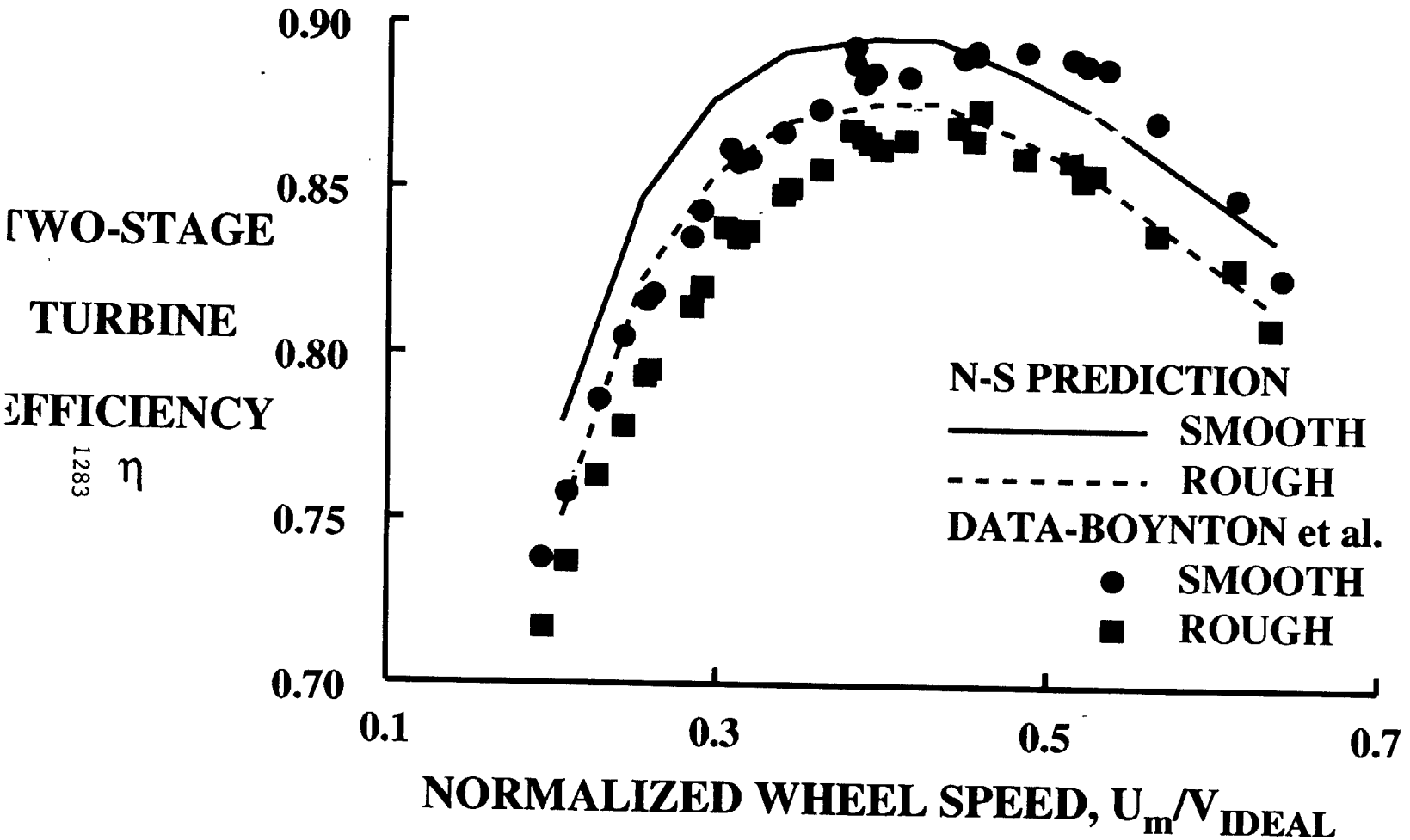

SURFACE ROUGHNESS CONCLUSIONS

- CEBECI-CHANG ROUGHNESS MODEL PREDICTS CHANGE IN TURBINE PERFORMANCE DUE TO ROUGHNESS

  $\Delta \eta$ = 2 POINTS

- USABLE FOR RANGE OF INCIDENCES

- TURBULENCE MODEL NEEDS IMPROVEMENT

  INCONSISTENCY BETWEEN ASSUMPTIONS NEEDED FOR ACCURATE LOSS & HEAT TRANSFER PREDICTIONS

OVERALL CONCLUSIONS

- MIDSPAN NAVIER-STOKES ANALYSIS USEFUL FOR PREDICTING OFF-DESIGN POINT PERFORMANCE AND ROUGHNESS EFFECTS

- MIDSPAN NAVIER-STOKES CODE(RVCQ3D) & PERFORMANCE CODE(MTSB) TOGETHER GIVE ACCURATE TURBINE EFFICIENCY PREDICTION

Abstract of a proposed presentation at the Workshop
for CFD Applications in Rocket Propulsion to be held
at NASA Marshall Space Flight Center, AL, April 20-22, 1993.

Three-dimensional unsteady flow calculations in an advanced Gas Generator turbine

Akil A. Rangwalla
MCAT Institute, Moffett Field, CA

Abstract

This paper deals with the application of a three-dimensional, unsteady Navier-Stokes code for predicting the unsteady flow in a single stage of an advanced gas generator turbine. The numerical method solves the three-dimensional thin-layer Navier-Stokes equations, using a system of overlaid grids, which allow for relative motion between the rotor and stator airfoils. Results in the form of time averaged pressures and pressure amplitudes on the airfoil surfaces will be shown. In addition, instantaneous contours of pressure, mach number etc. will be presented in order to provide a greater understanding of the inviscid as well as the viscous aspects of the flowfield. Also, relevant secondary flow features such as cross-plane velocity vectors and total pressure contours will be presented. Prior work in two-dimensions has indicated that for the advanced designs, the unsteady interactions can play a significant role in turbine performance. These interactions affect not only the stage efficiency but can substantially alter the time-averaged features of the flow. This work is a natural extension of the work done in two-dimensions and hopes to address some of the issues raised by the two-dimensional calculations. These calculations are being performed as an integral part of an actual design process and demonstrate the value of unsteady rotor-stator interaction calculations in the design of turbomachines.

THREE-DIMENSIONAL UNSTEADY FLOW CALCULATIONS FOR AN ADVANCED GAS GENERATOR TURBINE
(Preliminary results)

Akil A. Rangwalla
MCAT Institute

APPLIED COMPUTATIONAL FLUIDS BRANCH
NASA AMES RESEARCH CENTER

Scope

Perform three-dimensional unsteady computations for the single stage Gas Generator Oxidizer Turbine

Provide results to the Turbine Stage Design Team such as

- Time averaged and unsteady pressure envelopes
- Unsteady secondary flow features

OXIDIZER TURBINE BASELINE DESIGN

Full Scale Turbine Flowpath

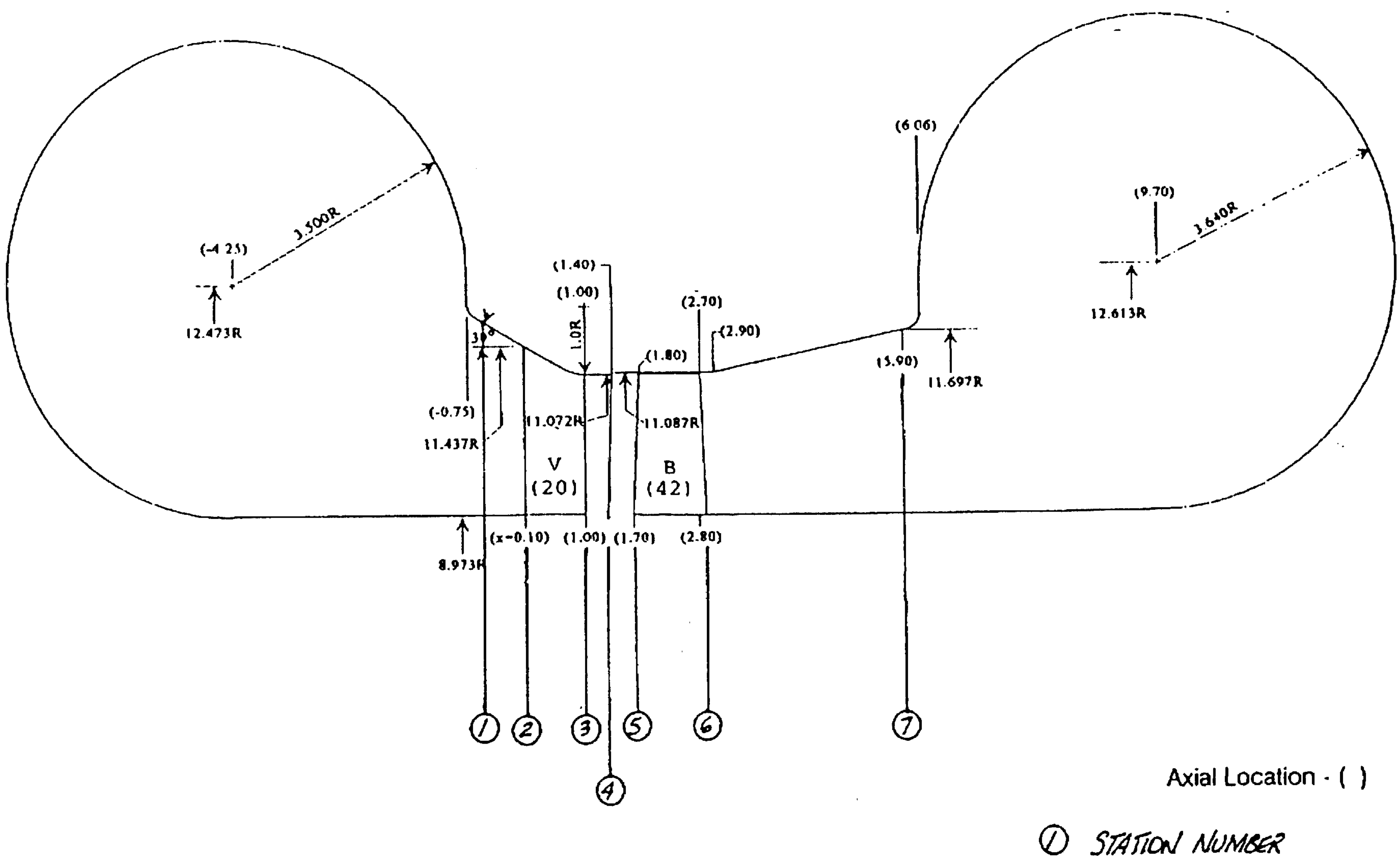

ORIGINAL PAGE IS
OF POOR QUALITY

Background

Design requirements of next generation turbines are

- High specific work per stage
- Low weight and small size
- High efficiency
- Durability

Background contd...

These design requirements imply

- High turning angles per stage
- Unconventional airfoil shapes
- Small axial gaps
- Large unsteady interactions

Effects of unsteady interactions on turbine performance still in the process of evaluation

Need a more powerful predictive capability

- Model as much of the flow physics
- Issues of accuracy

Background contd...

UNSTEADY ROTOR-STATOR INTERACTION CODES HAVE BEEN DEVELOPED AT NASA AMES

- HAVE DEMONSTRATED THE ABILITY OF PREDICTING FLOW QUANTITIES SUCH AS
  - TIME AVERAGED PRESSURE DISTRIBUTIONS ON AIRFOIL SURFACES.
  - PRESSURE AMPLITUDES AND PHASE ON THE SURFACE OF THE AIRFOILS.
  - TIME AVERAGED TOTAL PRESSURE DEFECTS IN WAKES.

- THESE CODES HAVE ATTAINED A LEVEL OF MATURITY TO WARRANT THEIR USE IN THE DESIGN PROCESS OF A TURBOMACHINE

Computational Details

TIME-ACCURATE SOLUTIONS TO THE 3D THIN-LAYER NAVIER-STOKES EQUATIONS.

HIGH-ORDER, UPWIND, FINITE-DIFFERENCE ALGORITHM USED

ALGORITHM SET IN ITERATIVE, FACTORED AND IMPLICIT FRAMEWORK

FLOWFIELD DISCRETIZED USING A SYSTEM OF OVERLAID GRIDS

ROTOR GRIDS MOVE RELATIVE TO STATOR GRIDS

TURBULENT EDDY VISCOSITY COMPUTED USING BALDWIN-LOMAX MODEL

Boundary conditions

- Inlet total pressure input as a function of radius
- Reimann variable as a function of radius
- Flow angles
- Exit static pressure input as a function of radius

Study of accuracy

A STUDY OF ACCURACY WAS INITIATED IN TWO-DIMENSIONS

MOTIVATIONS FOR THIS STUDY WERE

- DEVOLOPMENT OF A HYBRID STRUCTURED/UNSTRUCTURED CODE
  - FOR UNSTRUCTURED CODES, INCORPORATING HIGH ORDER TERMS MAY NOT BE STRAIGHTFORWARD
  - GRID ADAPTATION IS SIMPLER FOR UNSTRUCTURED SOLVERS
- NONLINEAR ROTOR-STATOR INTERACTIONS

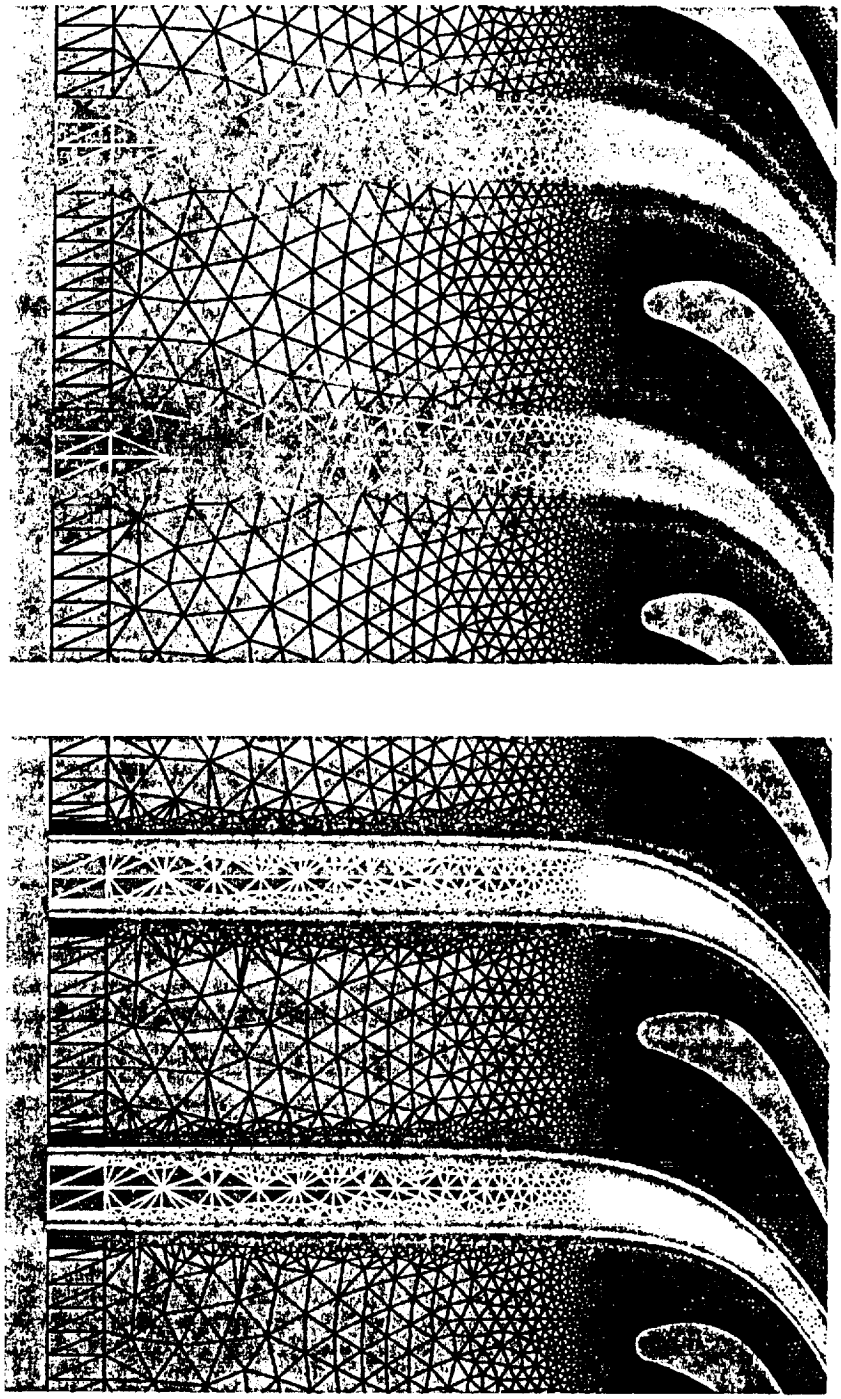

Figure Hot-streak calculation: original and adapted grids for the stator

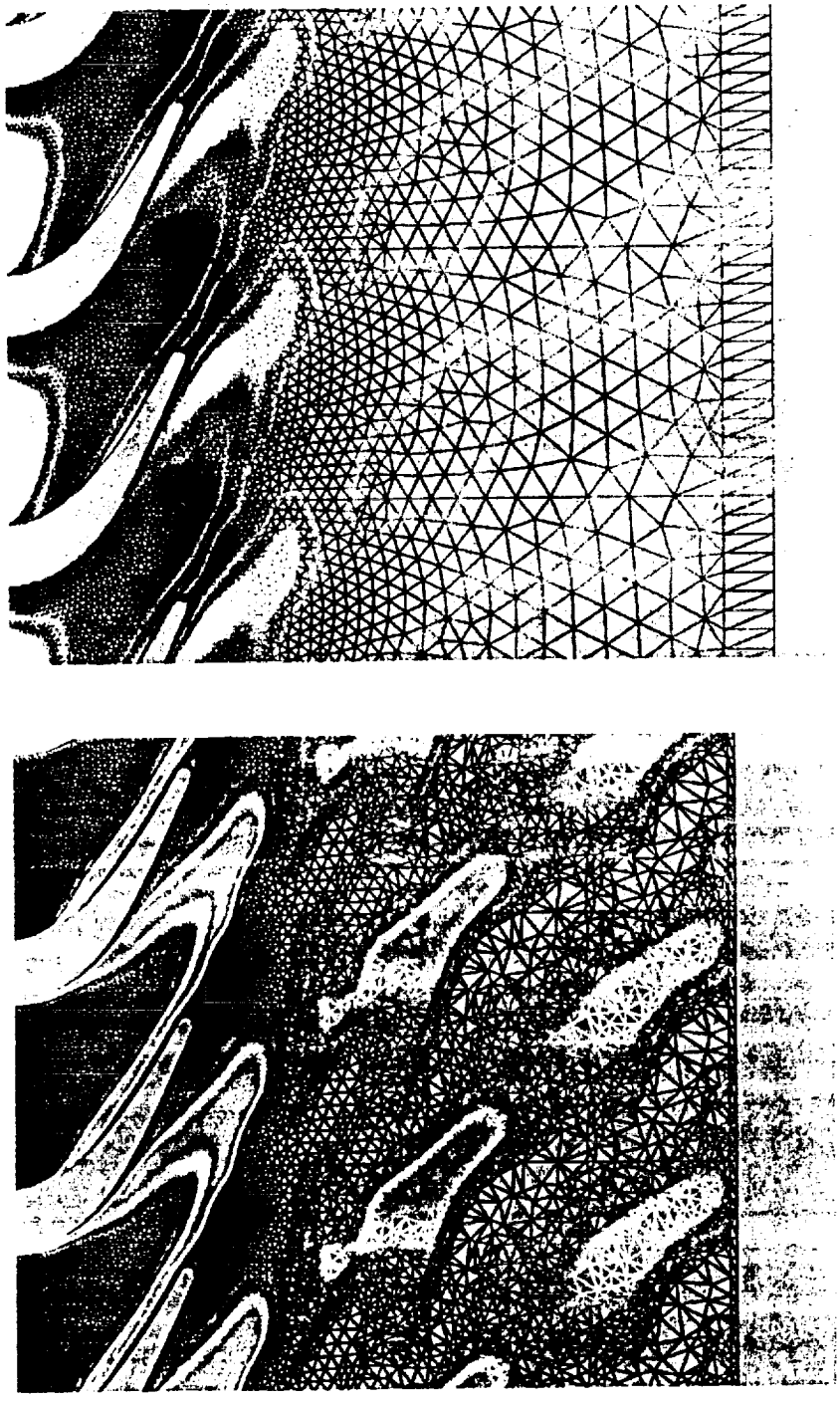

Figure Hot-streak calculation: original and adapted grids for the rotor

PRESSURE CONTOURS IN THE GGG BY A HYBRID STRUCTURED/UNSTRUCTURED SOLVER (FIRST-ORDER ACCURATE)
THE INTERACTION SHOCK IS NOT PREDICTED

PRESSURE CONTOURS IN THE GGG BY A HYBRID STRUCTURED/UNSTRUCTURED SOLVER (SECOND-ORDER ACCURATE)

AN INTERACTION SHOCK IS PREDICTED

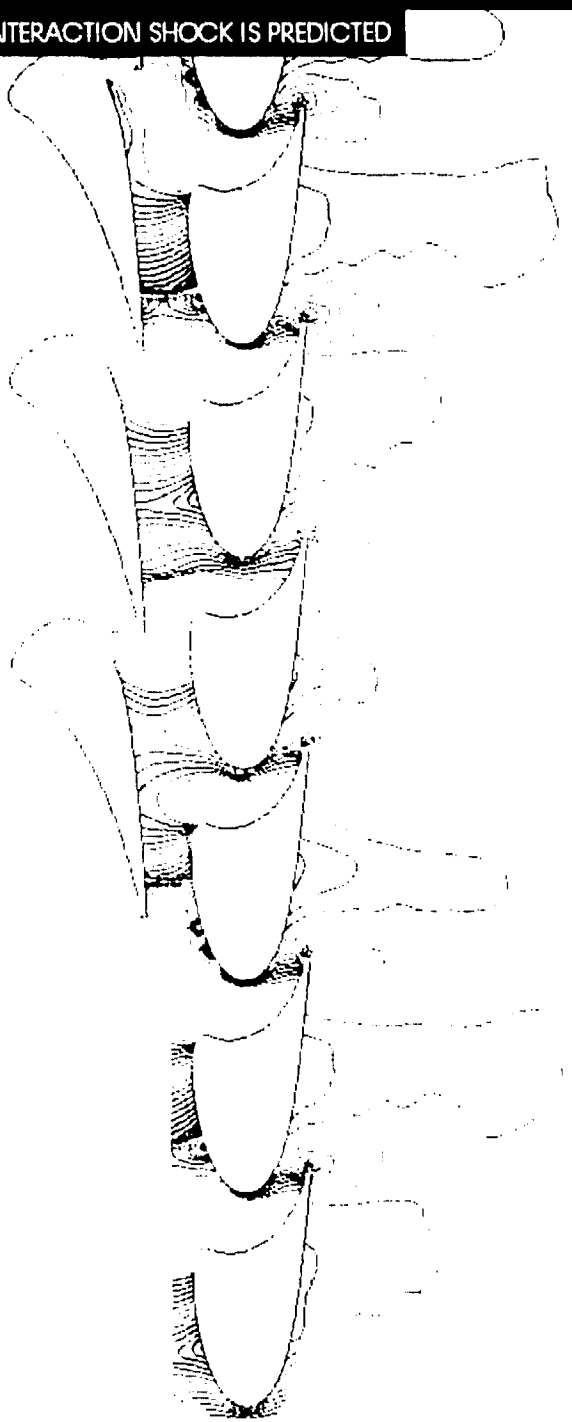

MACH CONTOURS OBTAINED FROM A STRUCTURED METHOD (STAGE-2)

Preliminary 3D Results for the GGOT

Results are preliminary because

- Solution has not completely converged to a time periodic state
- Grid is coarse (in radial direction)

Geometry Rescaling

Turbine Geometry

Number of stator blades	$= 20$
Number of rotor blades	$= 42$

Rescaled Geometry

Number of stator blades	$= 21$
Number of rotor blades	$= 42$

SURFACE GRID FOR THE GGOT

Every other gridline shown

Turbine operating conditions

INLET MACH NO.	0.46
INLET REYNOLDS NO.	2600000/*inch*
RPM	7880
INLET TOTAL PRESSURE	542.77 PSIA
EXIT STATIC PRESSURE	200.00 PSIA
INLET TOTAL TEMPERATURE	1307.02° *R*

INSTANTANEOUS MACH NUMBERS IN THE GGOT

PRESSURE VARIATION ON STATOR

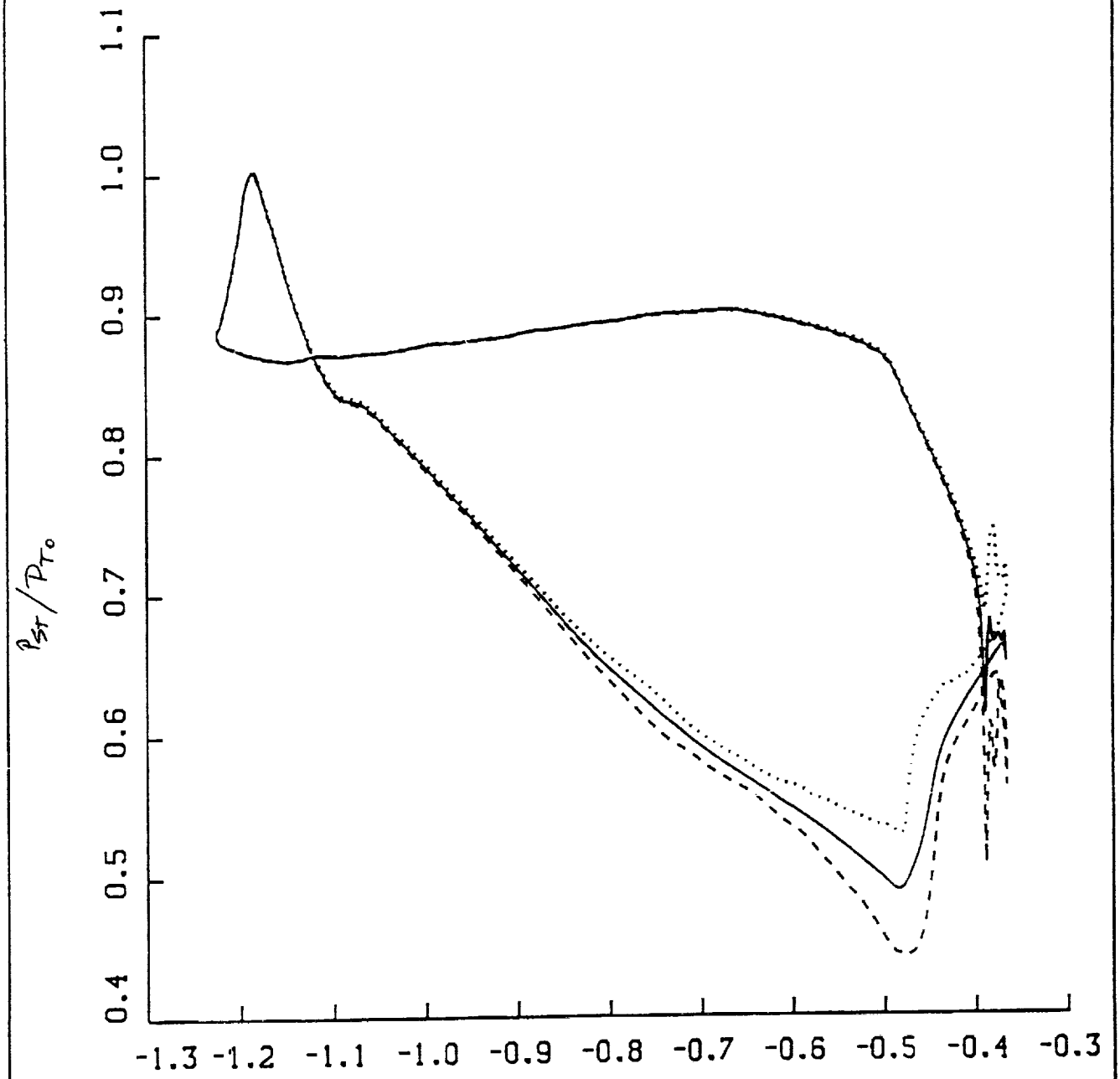

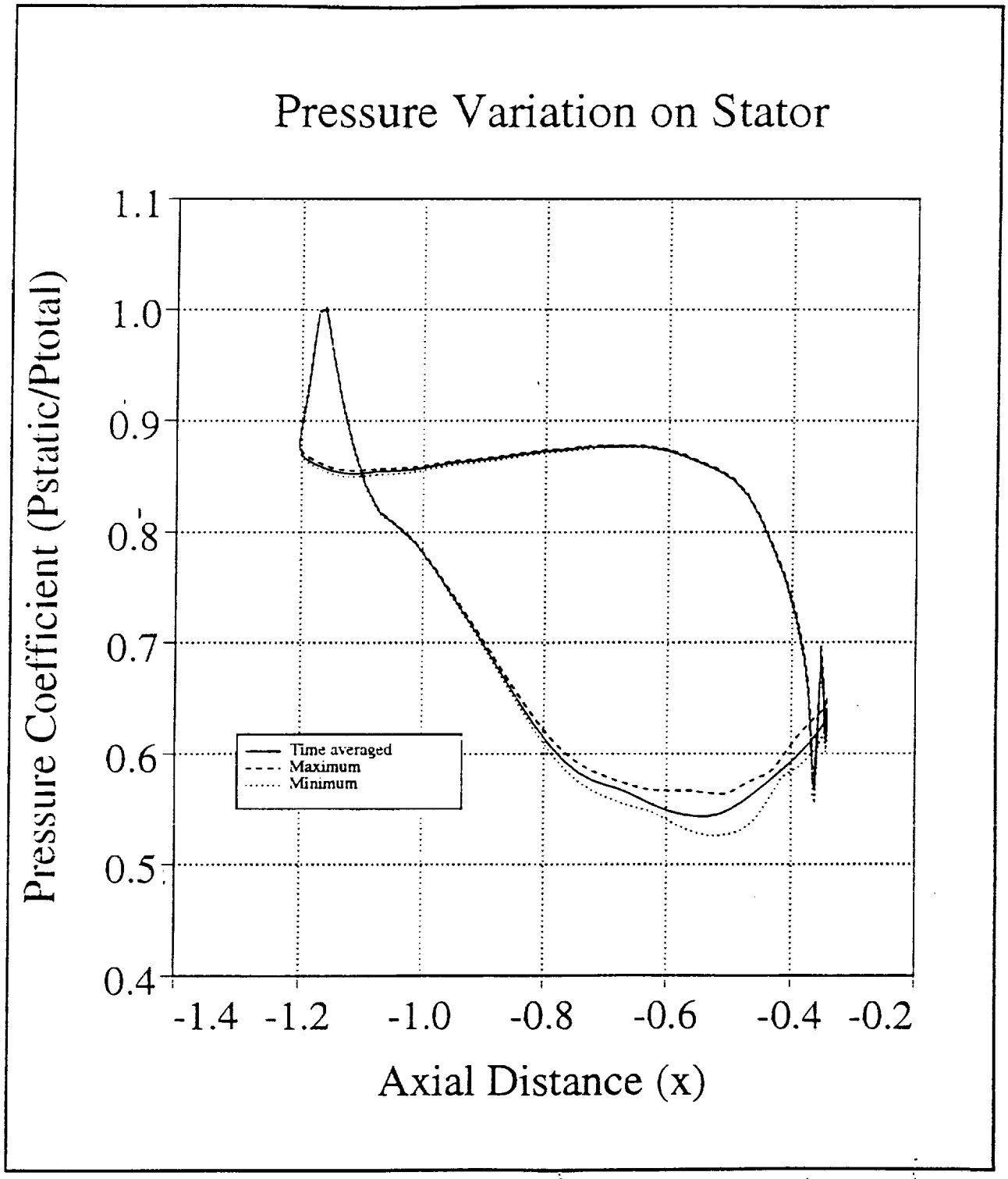
Pressure Variation on Stator
Pressure Coefficient (Pstatic/Ptotal)
1.1
1.0
0.9
0.8
0.7
0.6
0.5
0.4
-1.4
-1.2
-1.0
-0.8
-0.6
-0.4
-0.2
Axial Distance (x)
Time averaged
Maximum
Minimum

MID PLANE

PRESSURE VARIATION ON ROTOR

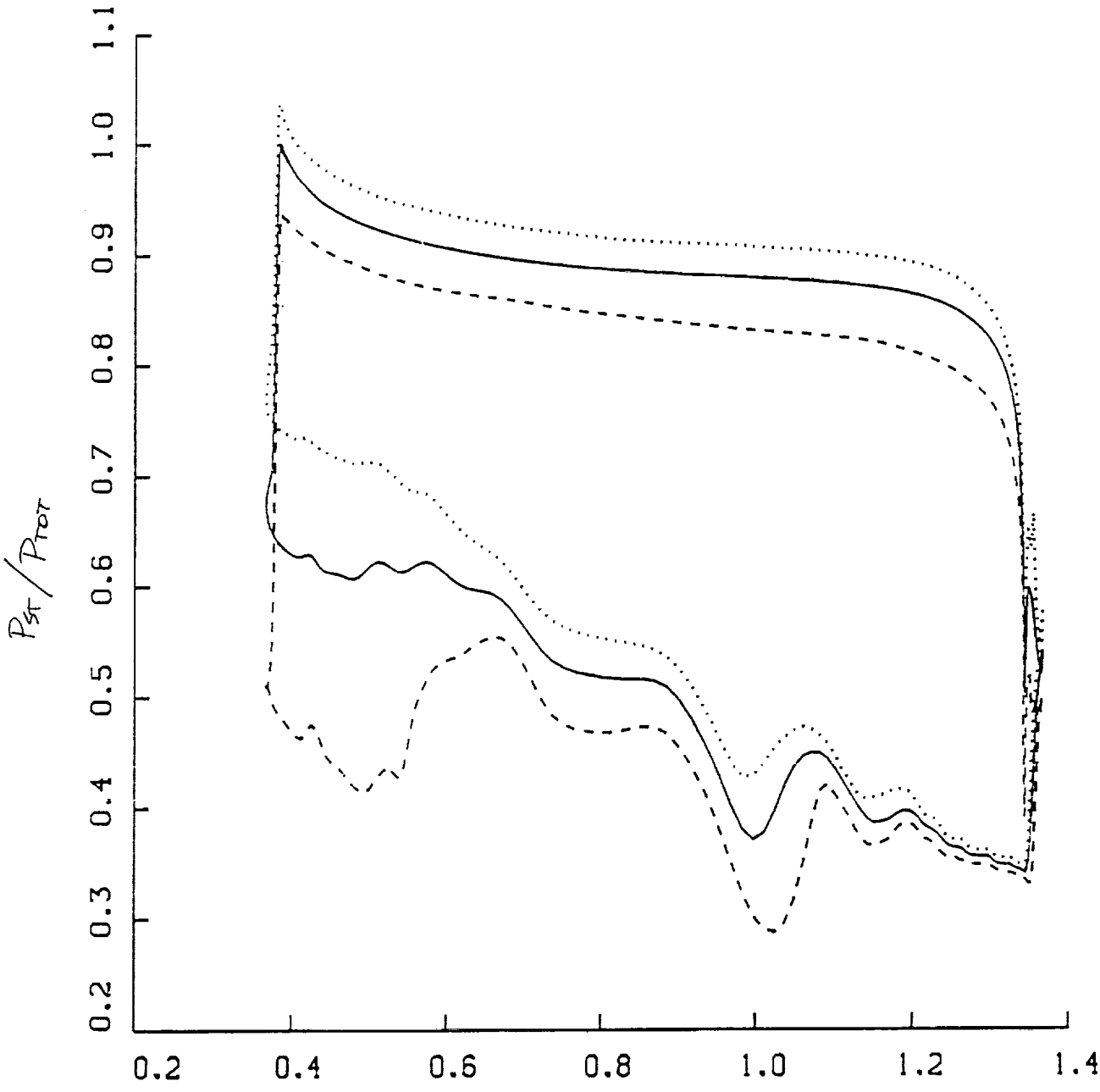

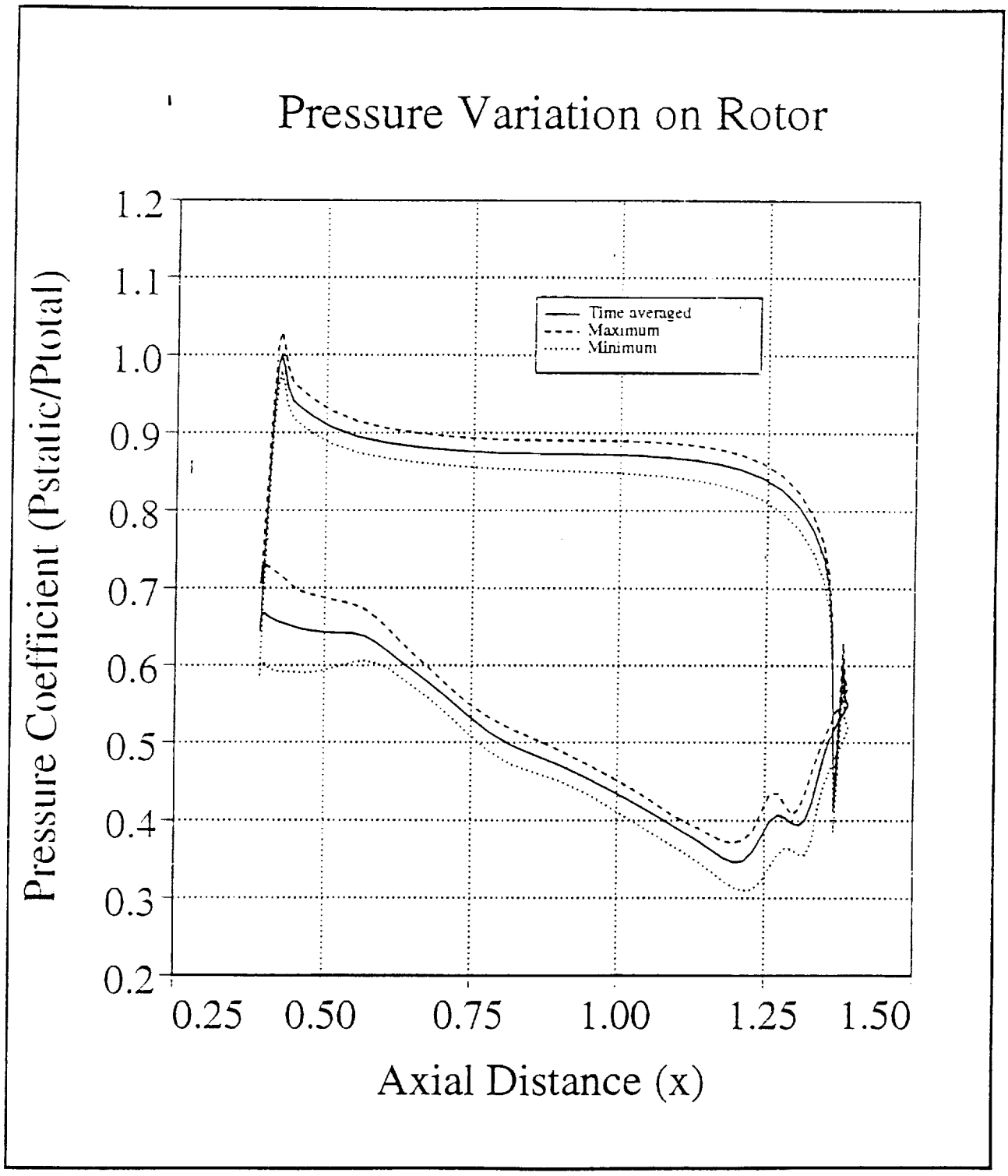
Pressure Variation on Rotor
Pressure Coefficient (Pstatic/Ptotal)
1.2
1.1
1.0
0.9
0.8
0.7
0.6
0.5
0.4
0.3
0.2
Time averaged
Maximum
Minimum
0.25
0.50
0.75
1.00
1.25
1.50
Axial Distance (x)

MID PLANE

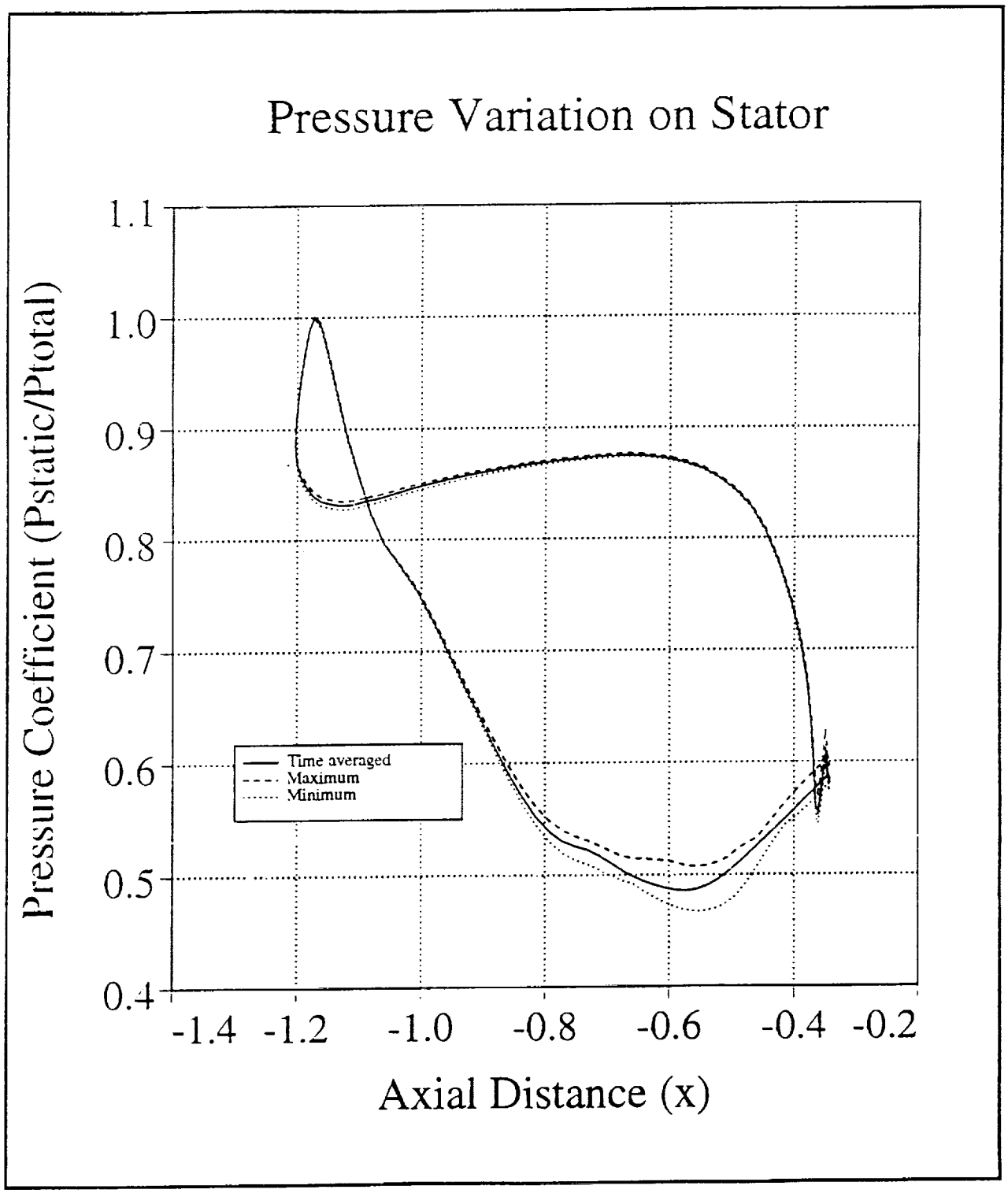
Pressure Variation on Stator
Pressure Coefficient (Pstatic/Ptotal)
1.1
1.0
0.9
0.8
0.7
0.6
0.5
0.4
-1.4
-1.2
-1.0
-0.8
-0.6
-0.4
-0.2
Axial Distance (x)
Time averaged
Maximum
Minimum

HUB

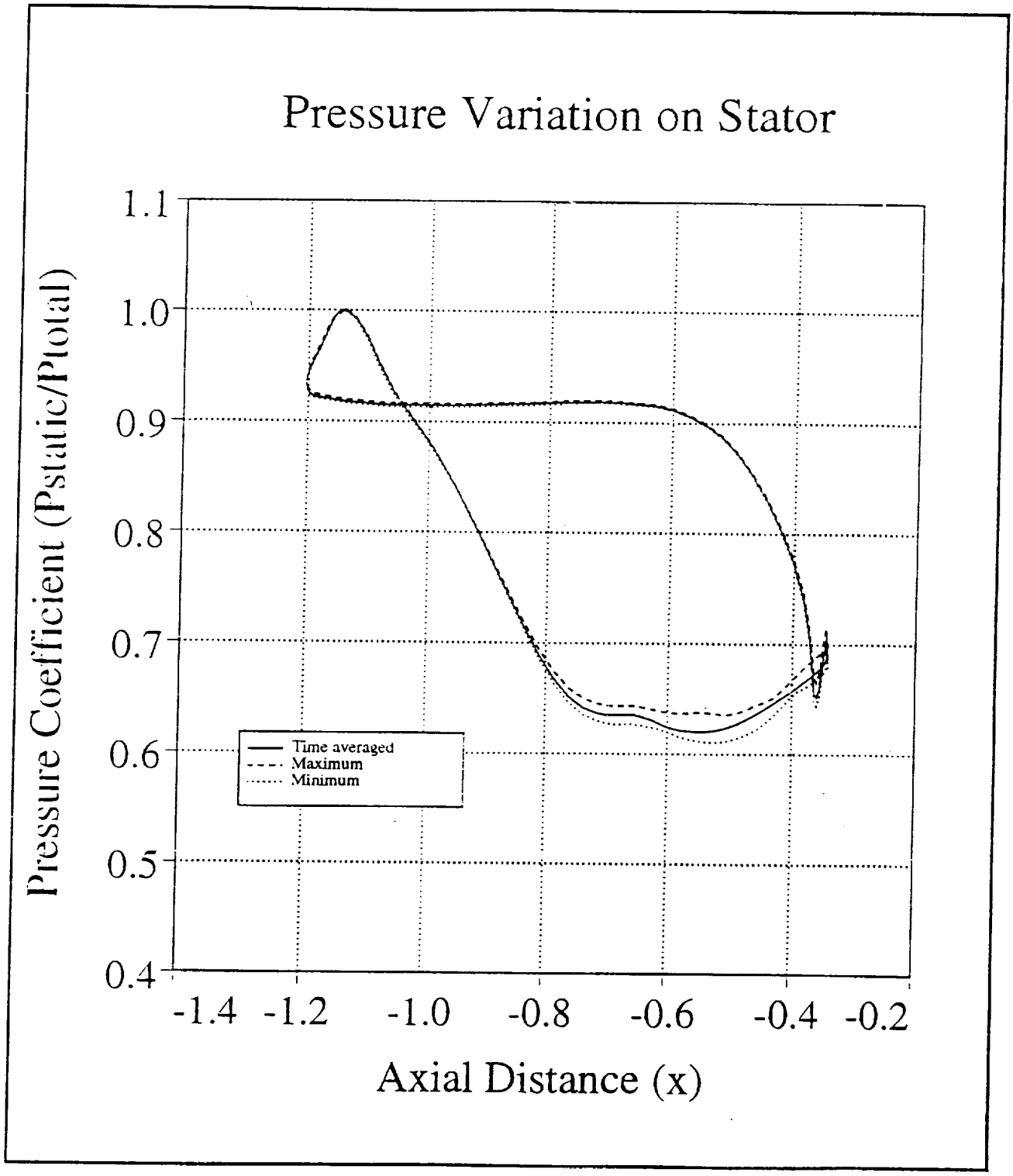
Pressure Variation on Stator
Pressure Coefficient (Pstatic/Ptotal)
1.1
1.0
0.9
0.8
0.7
0.6
0.5
0.4
-1.4
-1.2
-1.0
-0.8
-0.6
-0.4
-0.2
Axial Distance (x)
Time averaged
Maximum
Minimum

CASING

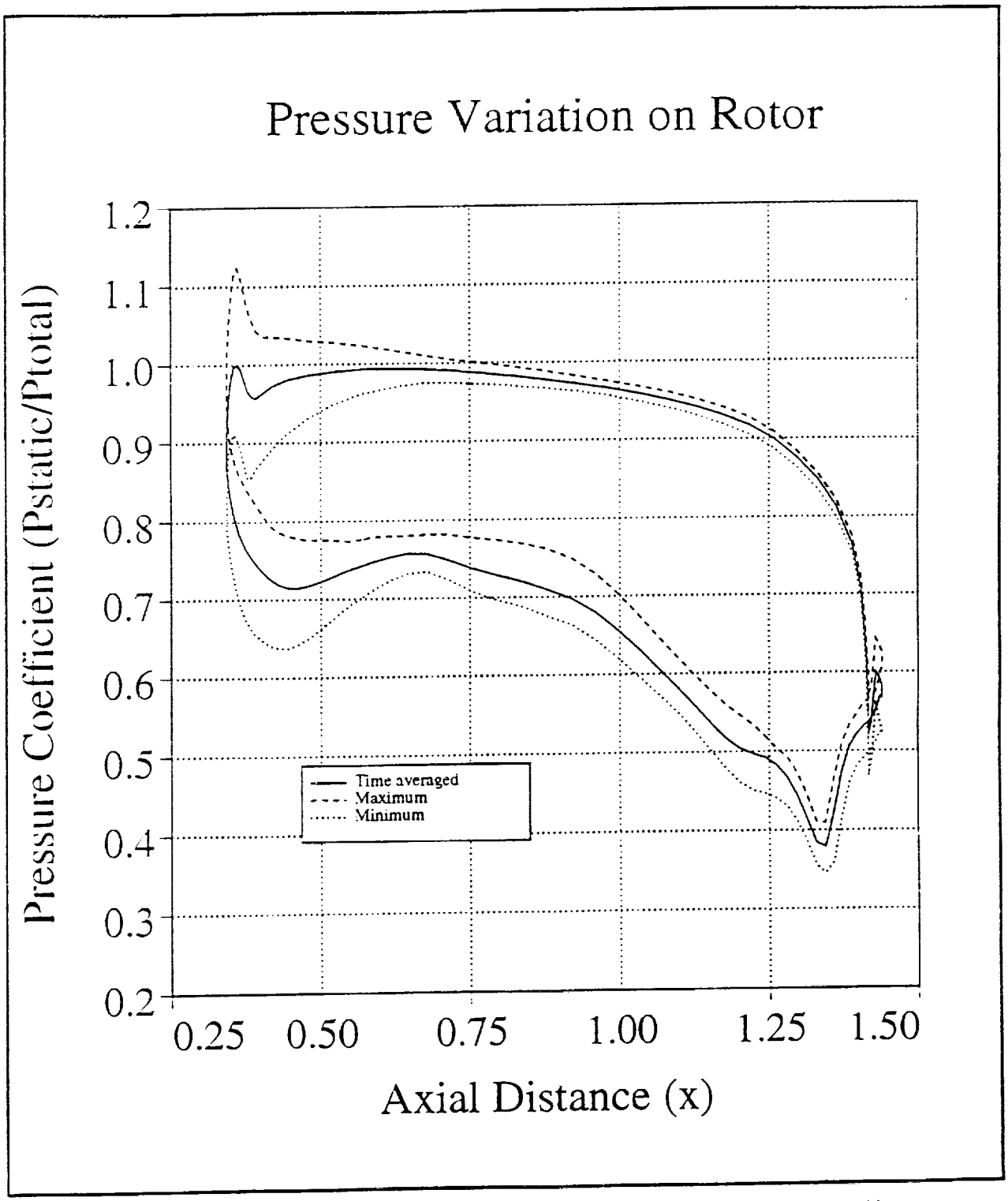
Pressure Variation on Rotor
Pressure Coefficient (Pstatic/Ptotal)
1.2
1.1
1.0
0.9
0.8
0.7
0.6
0.5
0.4
0.3
0.2
0.25
0.50
0.75
1.00
1.25
1.50
Axial Distance (x)
Time averaged
Maximum
Minimum

HUB

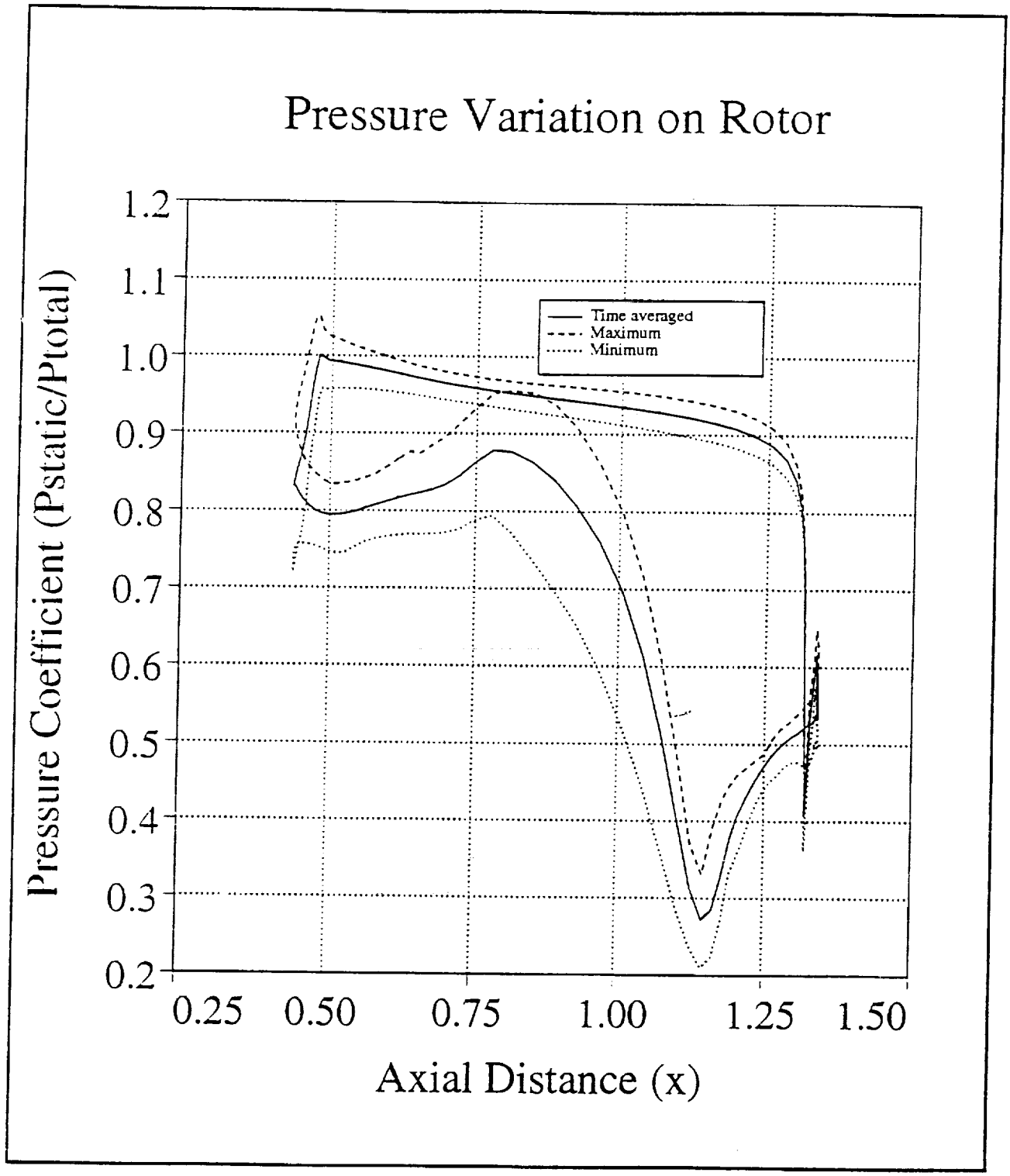
Pressure Variation on Rotor
Pressure Coefficient (Pstatic/Ptotal)
1.2
1.1
1.0
0.9
0.8
0.7
0.6
0.5
0.4
0.3
0.2
Time averaged
Maximum
Minimum
0.25
0.50
0.75
1.00
1.25
1.50
Axial Distance (x)

TIP

MACH CONTOURS AT 20% SPAN

MACH CONTOURS AT 40% SPAN

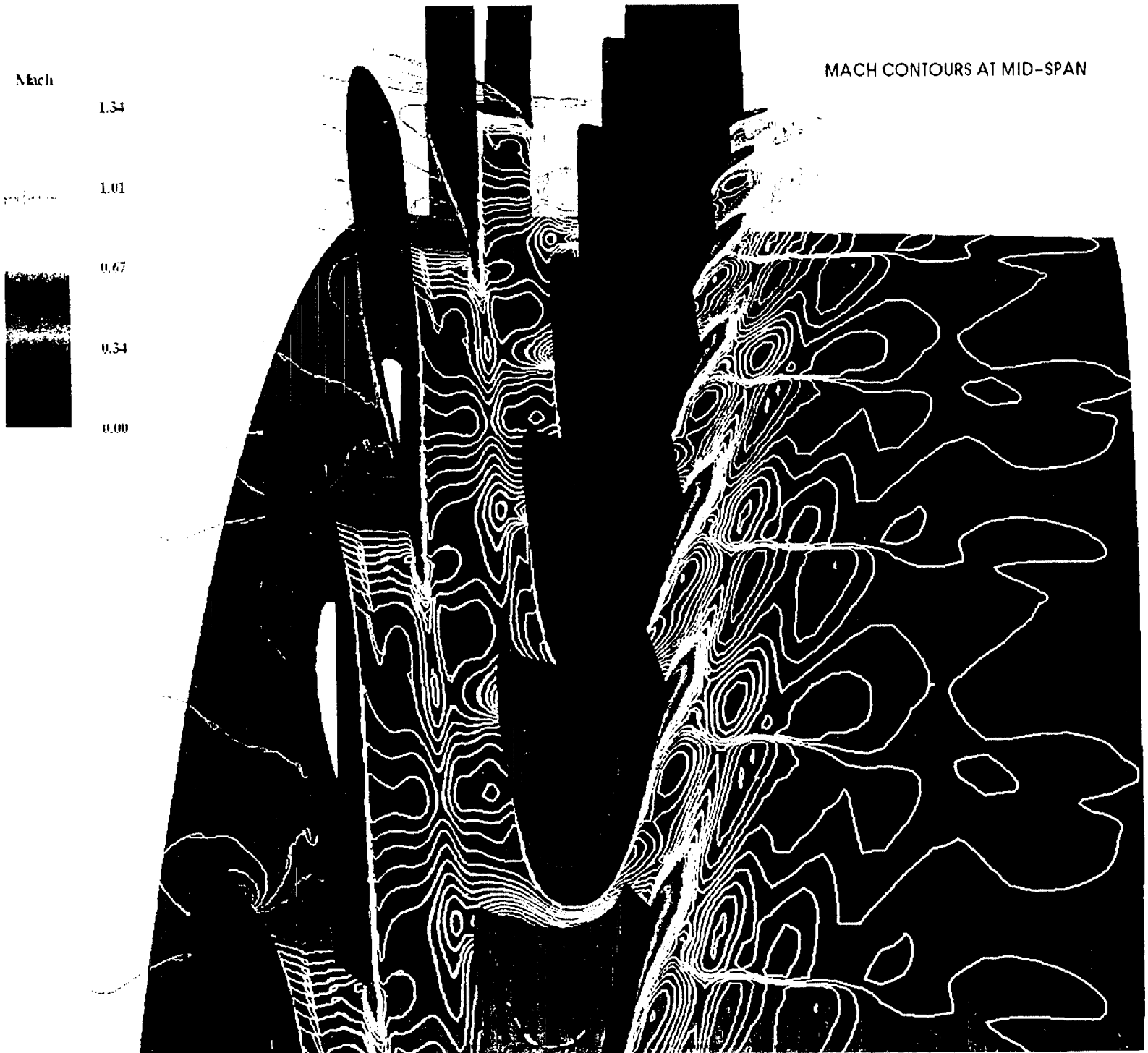
Mach
1.34
1.01
0.67
0.34
0.00
MACH CONTOURS AT MID-SPAN

Summary and conclusion

A COARSE GRID CALCULATION FOR THE GGOT IS NEARING COMPLETION

- THERE ARE SIMILARITIES AS WELL AS DIFFERENCES WITH THE CORRESPONDING TWO-DIMENSIONAL SOLUTIONS
  - ISSUES OF ACCURACY
  - TWO-DIMENSIONAL MODELLING (STREAM-TUBE CONTRACTION)
- FLOW FIELD SOLUTIONS WILL SERVE AS A GOOD STARTING SOLUTION FOR A FINER GRID CALCULATION ON THE C-90
- INPUT FROM THE DESIGN TEAM AS TO WHAT ASPECT OF THE FLOW FIELD NEEDS TO BE INVESTIGATED FURTHER

NUMERICAL SIMULATION OF STEADY AND UNSTEADY VISCOUS FLOW IN TURBOMACHINERY USING PRESSURE BASED ALGORITHM

B. LAKSHMINARAYANA, Y. HO and A. BASSON

The Pennsylvania State University
Department of Aerospace Engineering
University Park, PA 16802

The objective of this research is to simulate steady and unsteady viscous flows, including rotor/stator interaction and tip clearance effects in turbomachinery.

The numerical formulation for steady flow developed here includes an efficient grid generation scheme, particularly suited to computational grids for the analysis of turbulent turbomachinery flows and tip clearance flows, and a semi-implicit, pressure-based computational fluid dynamics scheme that directly includes artificial dissipation, and is applicable to both viscous and inviscid flows. The values of these artificial dissipation is optimized to achieve accuracy and convergency in the solution. The numerical model is used to investigate the structure of tip clearance flows in a turbine nozzle. The structure of leakage flow is captured accurately, including blade-to-blade variation of all three velocity components, pitch and yaw angles, losses and blade static pressures in the tip clearance region. The simulation also includes evaluation of such quantities of leakage mass flow, vortex strength, losses, dominant leakage flow regions and the spanwise extent affected by the leakage flow. It is demonstrated, through optimization of grid size and artificial dissipation, that the tip clearance flow field can be captured accurately.

The above numerical formulation was modified to incorporate time accurate solutions. An inner loop iteration scheme is used at each time step to account for the non-linear effects. The computation of unsteady flow through a flat plate cascade subjected to a transverse gust revels that the choice of grid spacing and the amount of artificial dissipation is critical for accurate prediction of unsteady phenomena. The rotor-stator interaction problem is simulated by starting the computation upstream of the stator, and the upstream rotor wake is specified from the experimental data. The results show that the stator potential effects have appreciable influence on the upstream rotor wake. The predicted unsteady wake profiles are compared with the available experimental data and the agreement is good. the numerical results are interpreted to draw conclusions on the unsteady wake transport mechanism in the blade passage.

NUMERICAL SIMULATION OF STEADY AND UNSTEADY FLOW IN TURBOMACHINERY USING PRESSURE BASED ALGORITHM

B. Lakshminarayana, Y.-H. Ho and A.H. Basson

The Pennsylvania State University

• This work is sponsored by ONR, with J. Fein as the technical monitor.
• A. H. Basson was supported by University of Stellanbosch, South Africa

OUTLINE

- OBJECTIVE
- INTRODUCTION
- NUMERICAL METHOD AND TURBULENCE MODEL
- VALIDATION OF 3D STEADY AND 2D UNSTEADY FLOW
- 3D STEADY FLOW IN THE END WALL AND TIP CLEARANCE REGION OF A TURBINE
- 2D UNSTEADY VISCOUS FLOW OVER AN AIRFOIL
- 2D UNSTEADY VISCOUS FLOW IN A TURBOMACHINERY BLADEROW DUE TO UPSTREAM ROTOR WAKE
- CONCLUSIONS

OBJECTIVE

- **To develop efficient, accurate codes and turbulence models for the prediction of steady and unsteady flow field in turbomachinery, including rotor/stator interaction, noise prediction, and tip clearance effects**

NUMERICAL METHOD

- **Incompressible flow equations**

$$\frac{\partial u_i}{\partial x_i} = 0$$

$$\frac{\partial u_i}{\partial t} + \frac{\partial u_i u_j}{\partial x_j} = -\frac{1}{\rho}\left\{\frac{\partial p}{\partial x_j} + \frac{\partial}{\partial x_j}\left[\mu\left(\frac{\partial u_j}{\partial x_i} + \frac{\partial u_i}{\partial x_j}\right) + \rho\,\overline{u_i' u_j'}\right]\right\}$$

- **3D steady flow**
  - **A SIMPLE type relaxation algorithm is used in steady state flow computation**
  - **The pressure field is coupled (smooth) by the 4th order dissipation scheme**
  - **Validate for inviscid flow computation**

NUMERICAL METHOD (CONTD.)

- 2D unsteady flow
  - A predictor-corrector time-marching algorithm (one predictor step and two corrector steps, Ho and Lakshminarayana (1991), Issa (1985))
  - An iteration scheme has been incorporated to enhance the coupling between the momentum and turbulence equations
- A control volume approach and a non-staggered grid system are used in the numerical solution of the equations
- A two-equation low Reynolds number turbulence model is implemented to account for turbulence effects at high Reynolds number

NUMERICAL METHOD (CONTD.)

- **Discretization procedure**
  - **Backward differencing for temporal discretization**
  - **Convection and diffusive term is discretized by: (1). upwind scheme (2) 2nd order + 4th order artificial dissipation (Basson and Lakshminarayana, 1992)**
  - **Cross derivative terms treated explicitly**
  - **Source terms treated explicitly**
- **Role of pressure**
  - **Pressure affects the velocity field through the momentum equations**
  - **Pressure is coupled with velocity field indirectly through the continuity equation**
  - **Substitute the discretized momentum equations into the continuity equation for derivation of pressure equation to ensure consistency**

VALIDATION/TEST CASES

- **Unsteady flow through a flat plate cascade**
  - Reduced frequency ($\omega C/2U$) = 0.5, 1.0, 2.5, 5.0, 7.5, and 15.0
  - Incidence = 0 and 5 degrees.
  - Pitch/Chord (S/C) = 1.0, Stagger angle = 0°
  - Reynolds No. =3.4 x 10^5 and 1.0 x 10^6, Gust Strength (V_g/U) = 0.02.
  - Good agreement (both amplitude and phase) with Whitehead's analysis

- **Unsteady flow through a C4 cascade**
  - Reduced frequency ($\omega C/2U$) = 1.0, 5.0, 7.5, and 15.0
  - Incidence = 0 and 5 degrees.
  - Pitch/Chord (S/C) = 1.0, Stagger angle = 0°
  - Reynolds No. = 3.4 x 10^5 and 1.0 x 10^6, Gust Strength (V_g/U) = 0.02 and 0.15.
  - Practical blade geometry reduces the unsteady response of the blade compared to the flat plate cascade

VALIDATION/TEST CASES (CONTD.)

- **Unsteady flow through a compressor cascade (Satyanarayana, 1976)**
  - **Reduced frequency ($\omega C/2U$) = 0.042**
  - **Pitch/Chord (S/C) = 0.707, Stagger angle = 45°**
  - **Reynolds No. =1.6 x 10^5, Gust Strength (V_g/U) = 0.082**
  - **Good agreement between measured and predicted steady and unsteady pressure and wakes.**
- **Unsteady flow through a compressor cascade (Stauter et al., 1990)**
  - **Reduced frequency ($\omega C/2U$) = 8.48**
  - **Pitch/Chord (S/C) = 0.964, Stagger angle = 34.2°**
  - **Reynolds No. =2.5 x 10^5, Gust Strength (V_g/U) = 0.25**
  - **Good agreement between measured and predicted steady and unsteady pressure and wakes.**
- **Unsteady flow over an airfoil**
- **Tip clearance flow through a turbine cascade**

VALIDATION/TEST CASES (CONTD.)

Unsteady response function of a flat plate cascade and a C4 cascade

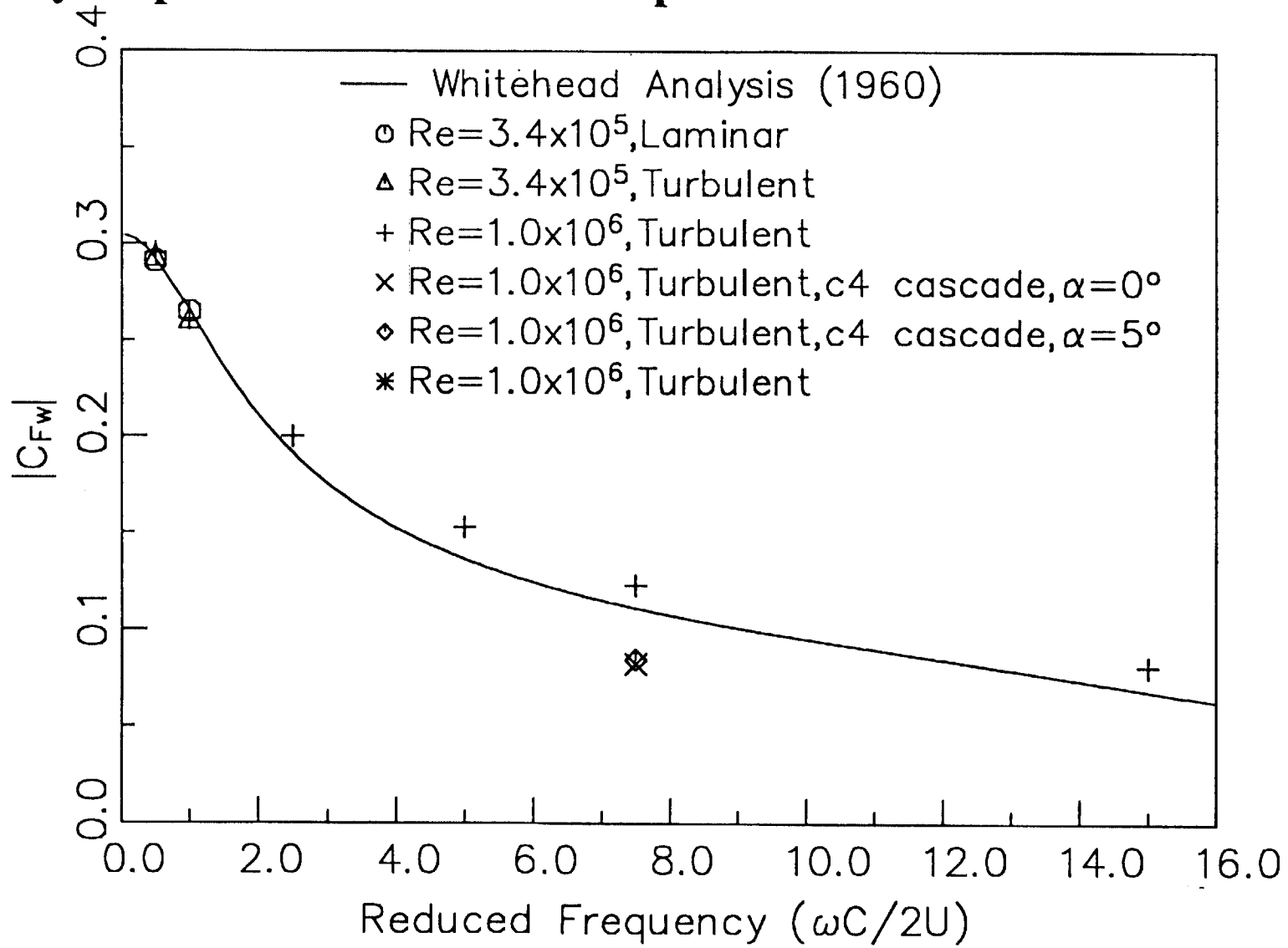

UNSTEADY FLOW IN A TURBOMACHINERY BLADEROW DUE TO UPSTREAM ROTOR WAKE

Time mean static pressure and pressure envelope of a compressor stator.

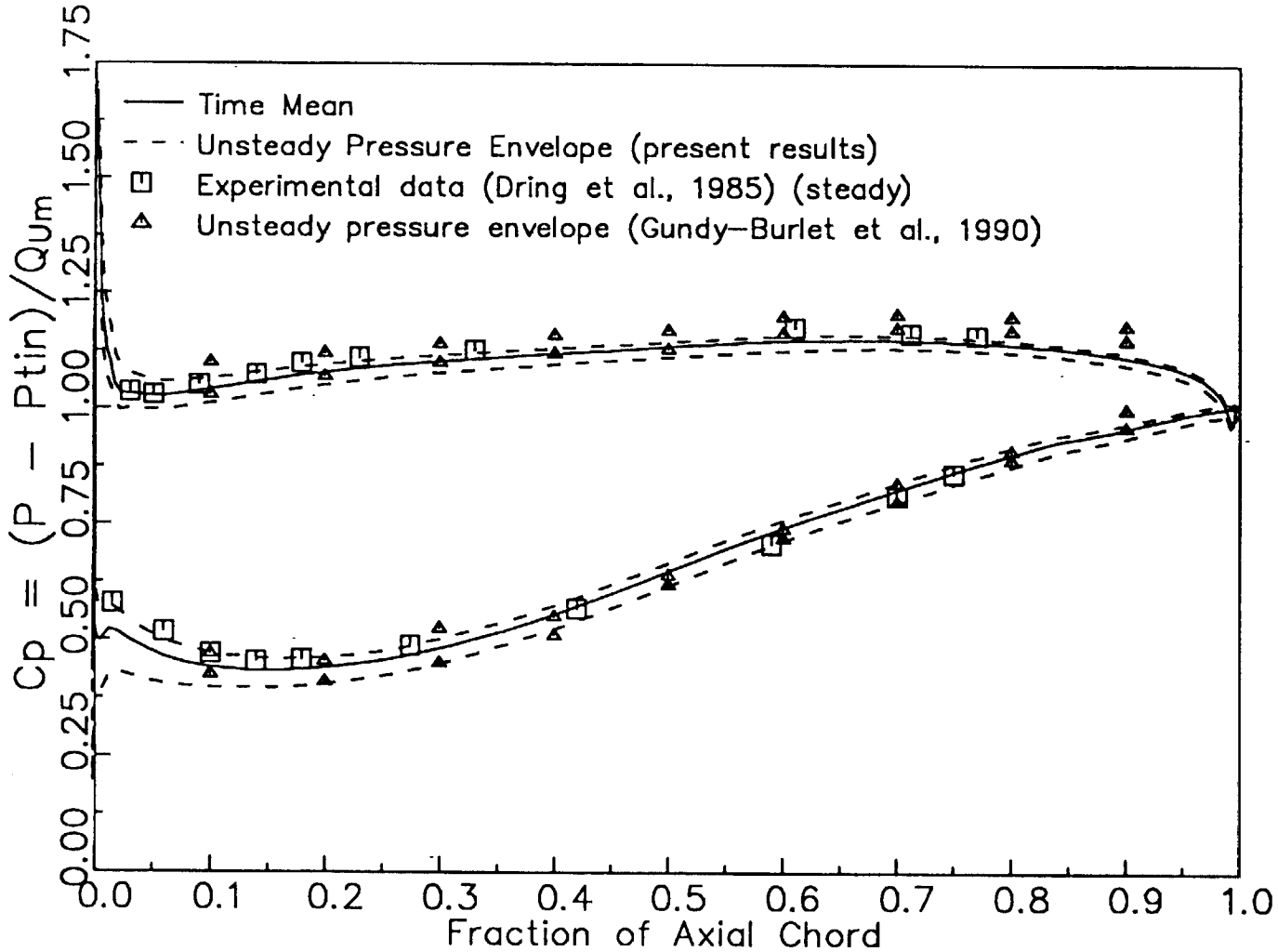

UNSTEADY FLOW IN A TURBOMACHINERY BLADEROW DUE TO UPSTREAM ROTOR WAKE

Time-dependent rotor wake profile at 20% stator axial chord upstream of the stator blade

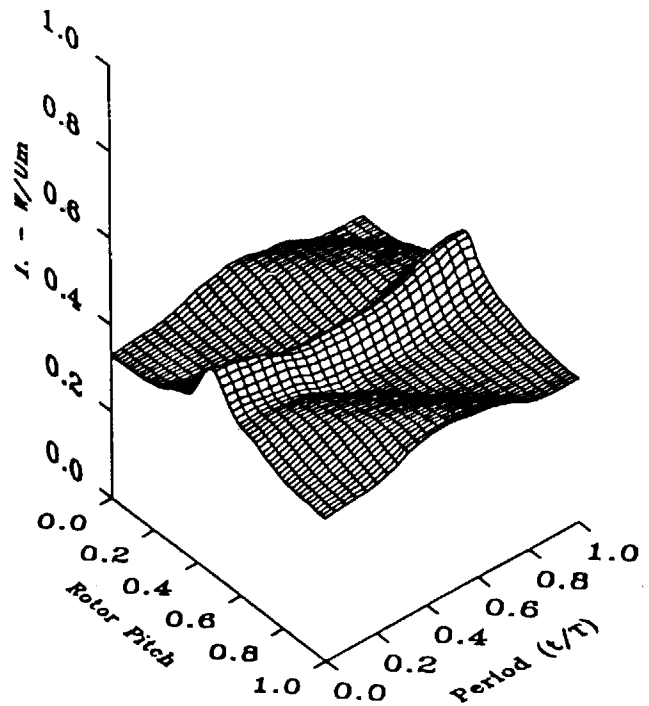

Computation

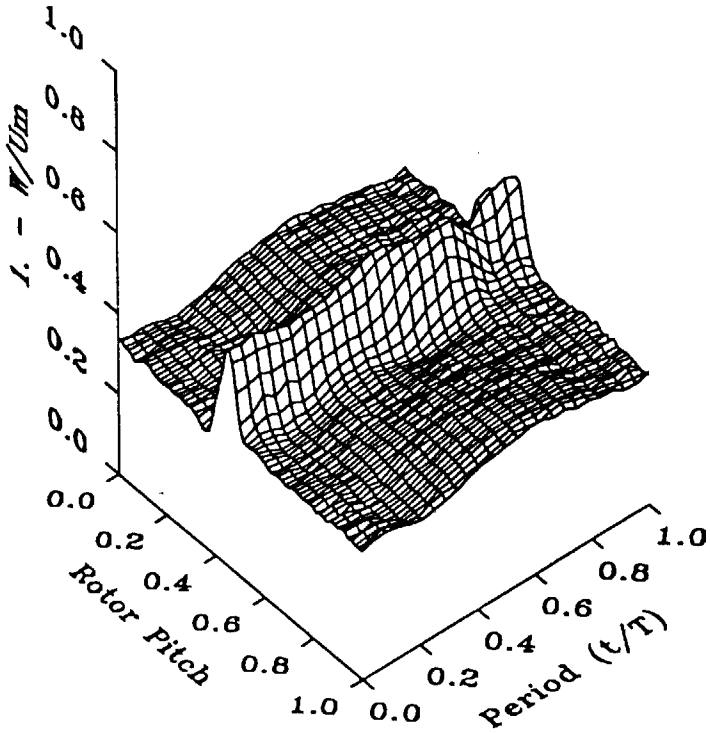

Experiment (Stauter et al., 1990)

UNSTEADY FLOW THROUGH A COMPRESSOR DUE TO UPSTREAM ROTOR WAKES

The fluctuating velocity (the difference between instantaneous and time-mean velocity) vectors inside a stator (t/T=0.25).

0.3 Um **(The largest vector at the inlet)**

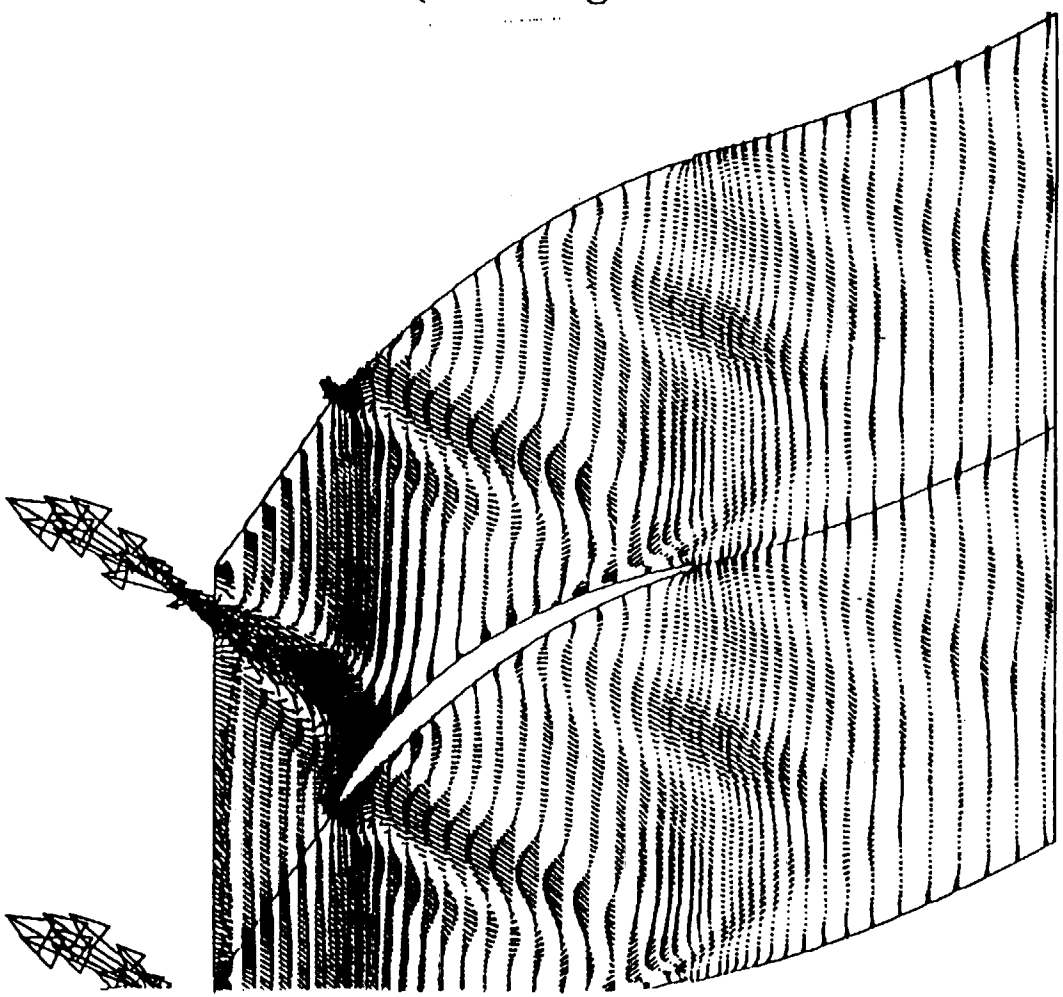

UNSTEADY VISCOUS OVER AN AIRFOIL

- The unsteadiness is generated by two flapping foils oscillating about one chord upstream the tested foil
- Reduced frequency ($\omega C/2U$)=3.76
- Incidence = 1.34 degrees
- Reynolds No. = 3.78×10^6
- Total no of grid points : 27537 (201×137)
- Reference : D. Keenan et. al., MIT

every second grid line is shown

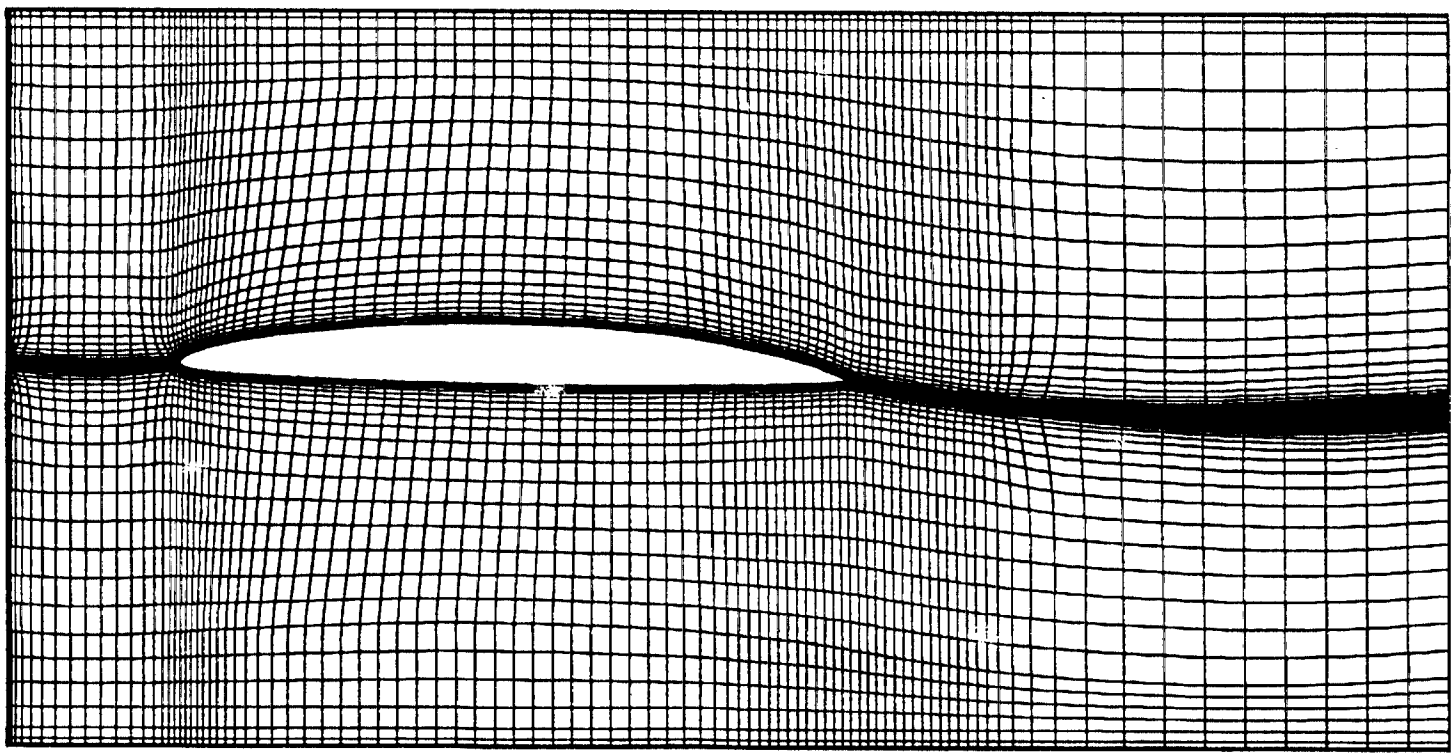

UNSTEADY VISCOUS OVER AN AIRFOIL

Amplitude of Cp for harmonic n=1

Solid lines = calculations, Dash lines = measurements (Keenan, 1992)

Suction Surface

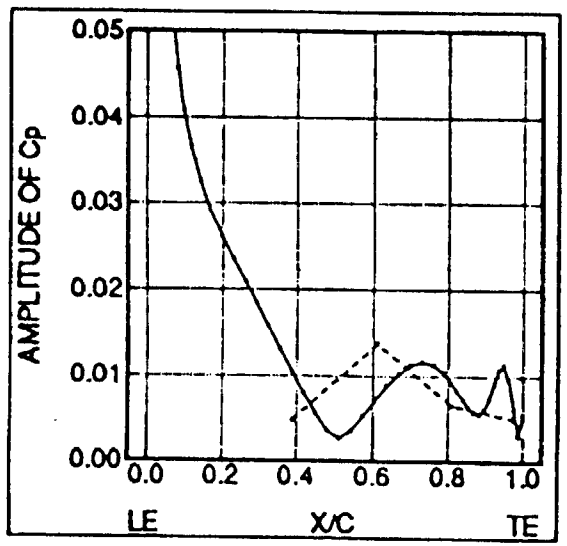

Pressure Surface

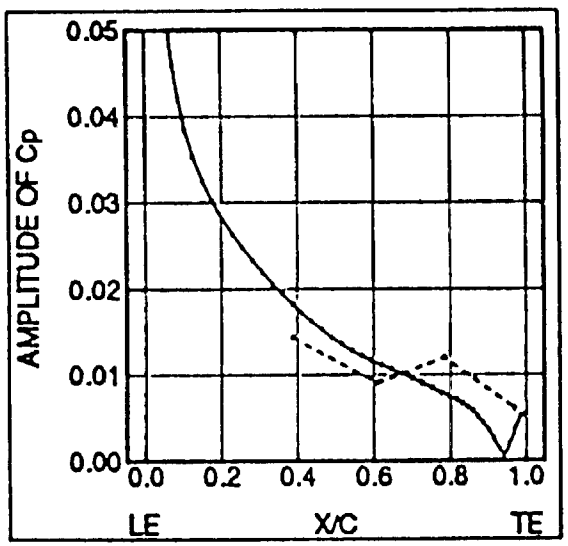

UNSTEADY VISCOUS OVER AN AIRFOIL

Phase of Cp for harmonic n=1

Solid lines = calculations, Dash lines = measurements (Keenan, 1992)

Suction Surface

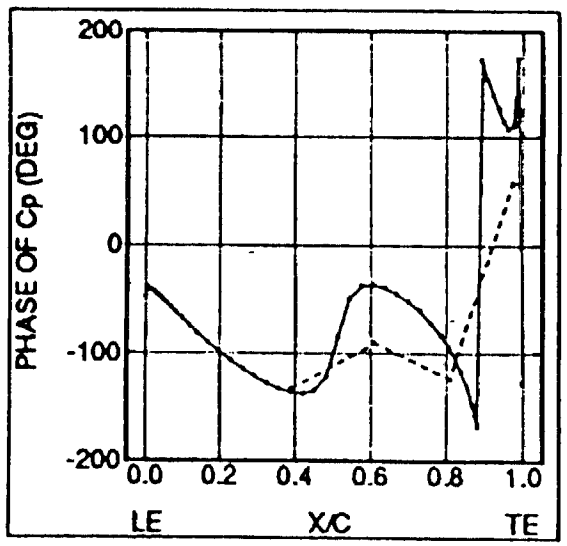

Pressure Surface

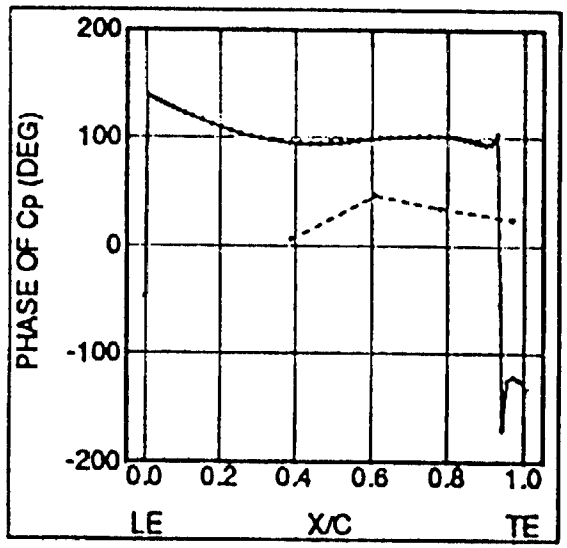

TIME HISTORY OF Cp

LAKSHMINARAYANA AND HO

Solid lines = calculations Dashed lines = measurements

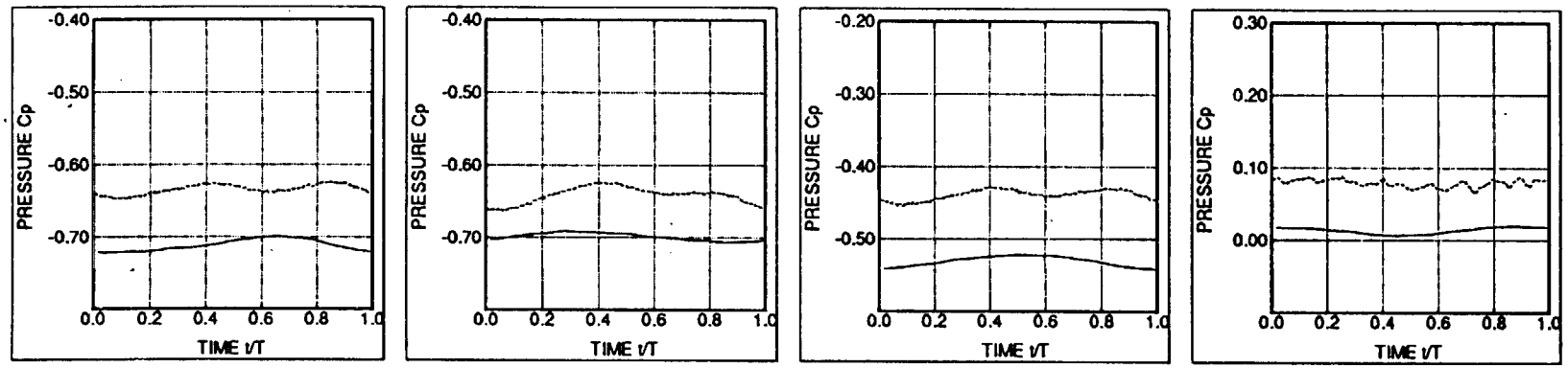

X/C=0.388 X/C=0.612 X/C=0.810 X/C=0.972

SUCTION SIDE

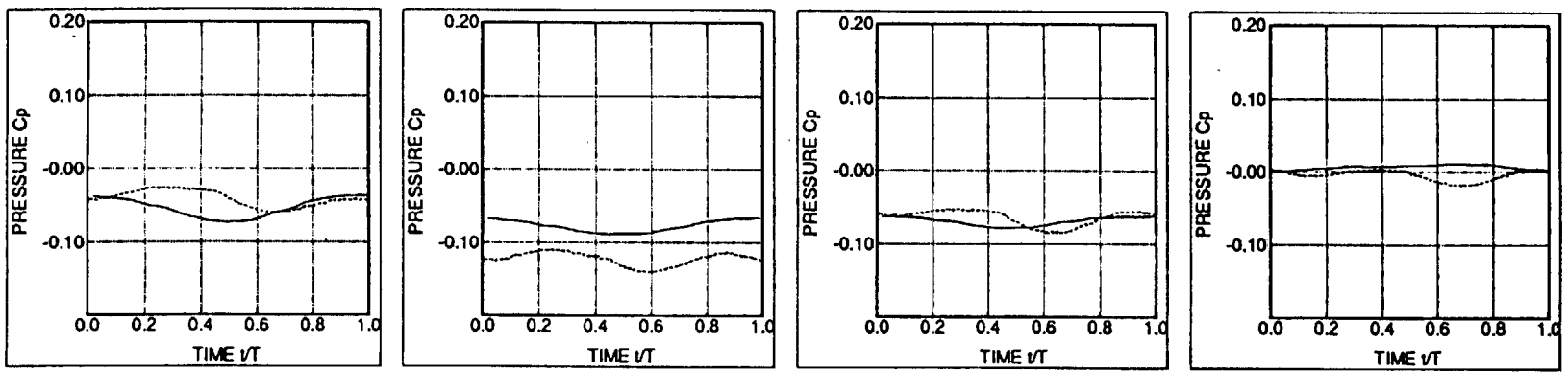

X/C=0.389 X/C=0.611 X/C=0.784 X/C=0.972

PRESSURE SIDE

AMPLITUDE OF VELOCITY FOR HARMONIC n=1

Solid lines = calculations Dashed lines = measurements

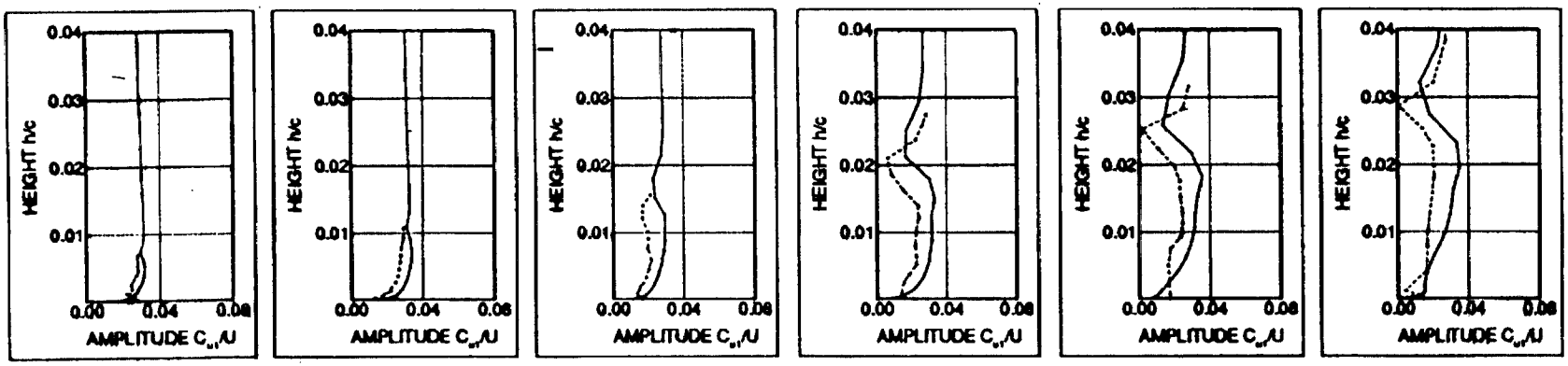

X/C=0.388 X/C=0.612 X/C=0.900 X/C=0.972 X/C=0.990 X/C=1.000

SUCTION SIDE

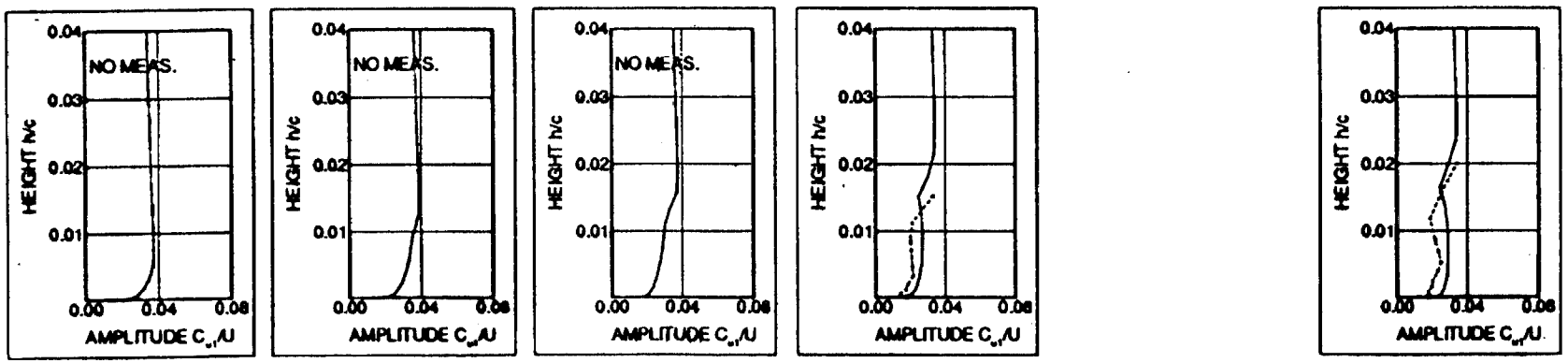

X/C=0.389 X/C=0.611 X/C=0.784 X/C=0.972 X/C=1.000

PRESSURE SIDE

PHASE OF VELOCITY FOR HARMONIC n=1

Solid lines = calculations

Dashed lines = measurements

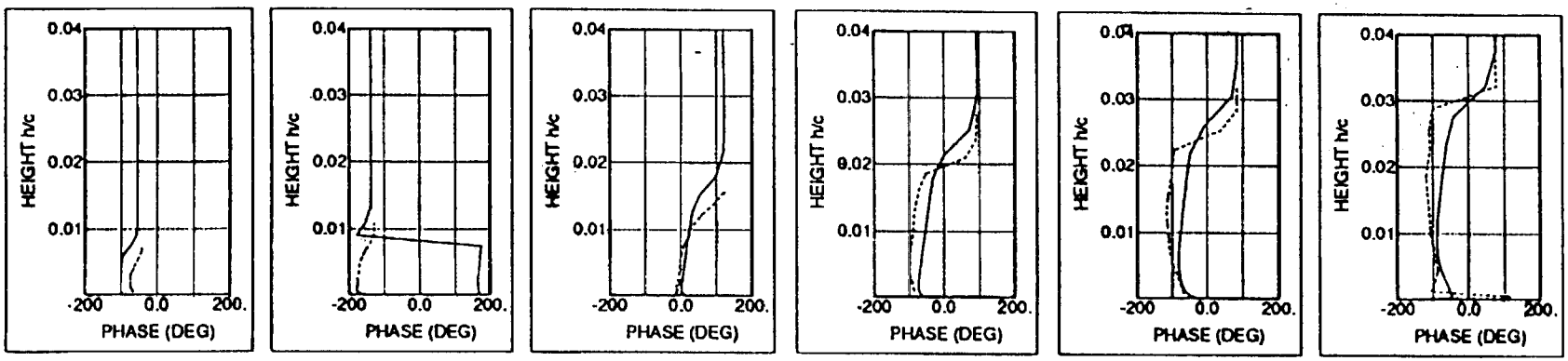

X/C=0.388 X/C=0.612 X/C=0.900 X/C=0.972 X/C=0.990 X/C=1.000

SUCTION SIDE

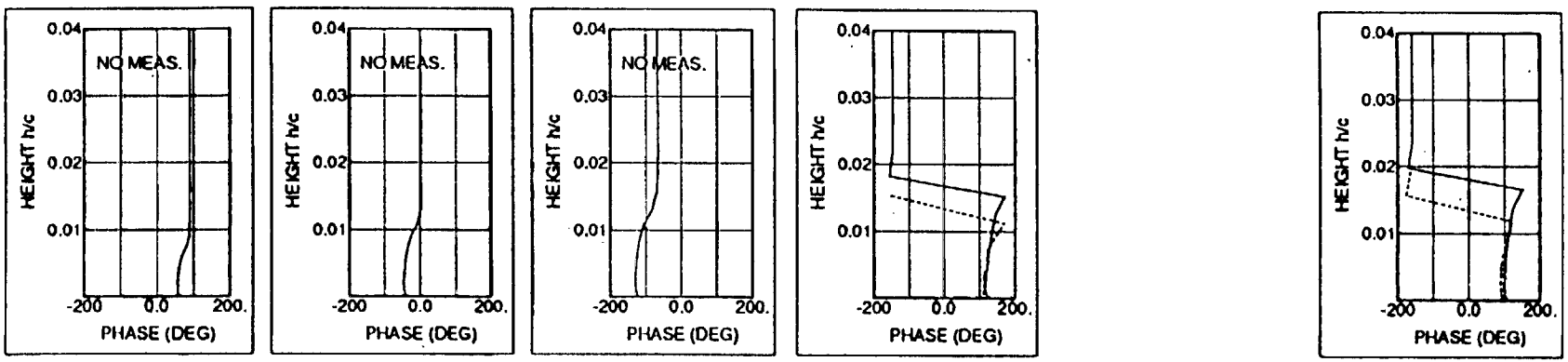

X/C=0.389 X/C=0.611 X/C=0.784 X/C=0.972 X/C=1.000

PRESSURE SIDE

TIP CLEARANCE MODELLING

3D STEADY FLOW IN THE TIP CLEARANCE REGION FLOW OF A TURBINE

- **Turbine Cascade experimental data : Bindon (1986, 1987, 1990)**
  - **C = 0.186 m**
  - **S/C = 0.7**
  - **τ/C = 2.5 %**
  - **Re = 4.7 x 10^5**
  - **$\alpha_1 = 0°$, $\alpha_2 = 68°$**
  - **Grid : 81 x 57 x 57, with 41 x 21 x 15 in the tip gap**

3D STEADY FLOW IN THE TIP CLEARANCE REGION FLOW OF A TURBINE

- Grid Methodology
  - Combined algebraic and elliptic approach.
  - Interior generated by elliptic generator- solved iteratively by Minimum residual method, while updating source terms and coefficients after each iteration.
  - Apply elliptic smoothing to interface to remove discontinuities, but the grid spacing normal to surface is altered. Restore grid spacing normal to surface.
  - Imbedded H grid topology; Three smaller H grids imbedded into large grid; No discontinuities in grid at blade tip; actual tip geometry mapped into computation domain; good tip gap resolution

EMBEDDED H-GRID TOPOLOGY

Grid Below Tip Gap

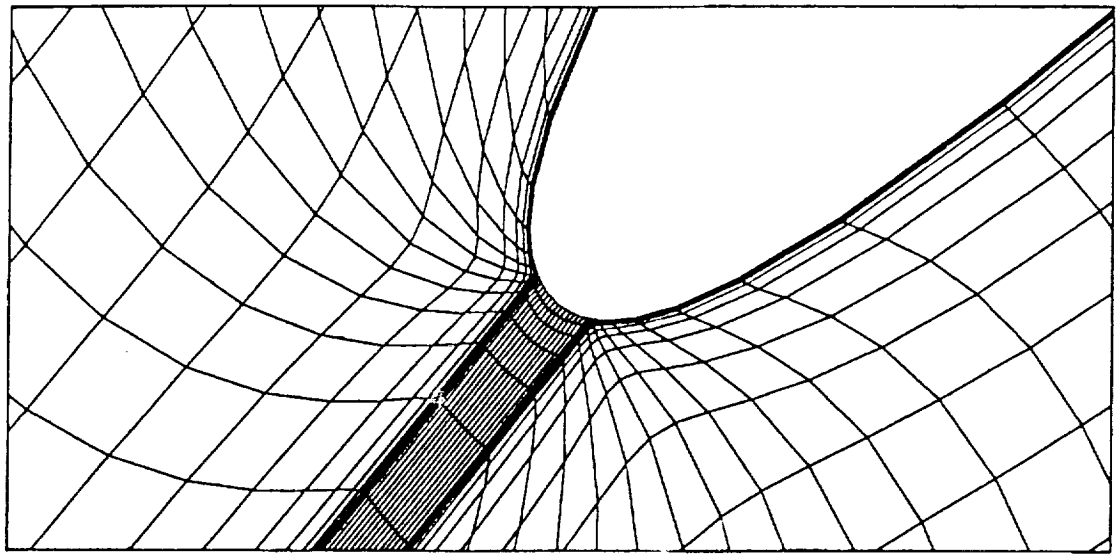

Grid Inside Gap

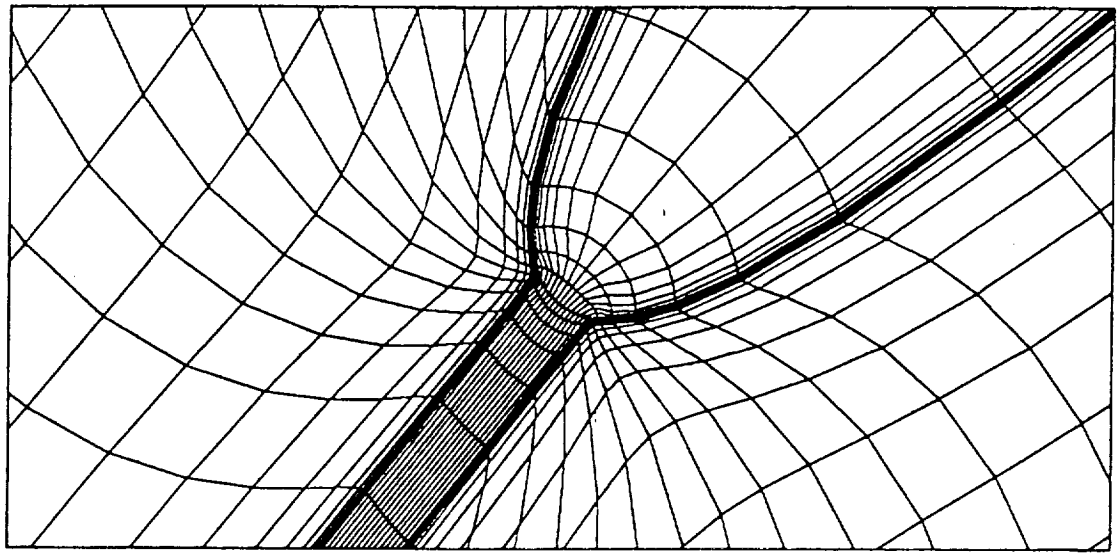

COMPARISON OF MEASURED AND PREDICTED PITCHWISE FLOW ANGLES

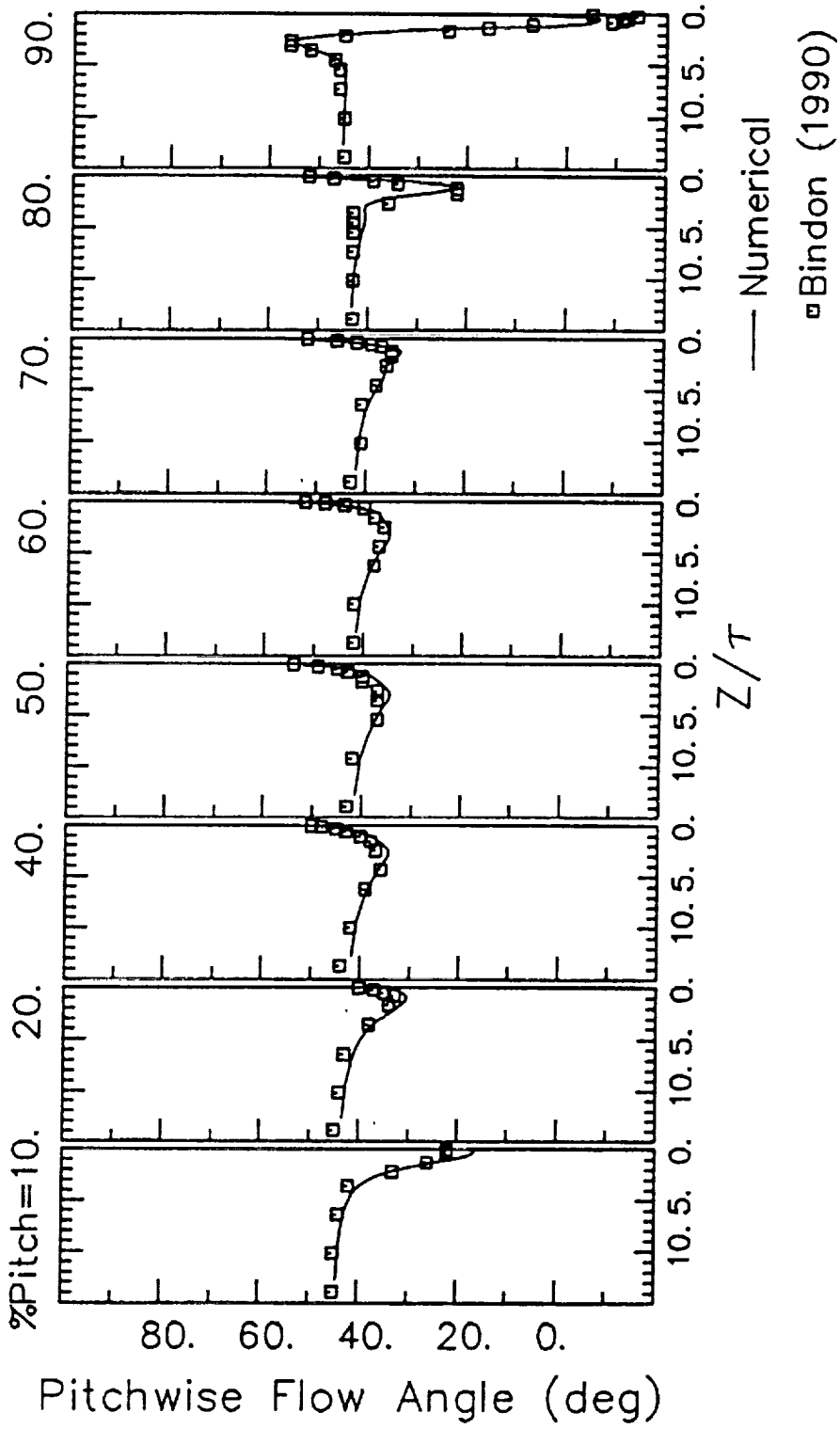

COMPARISON OF MEASURED AND PREDICTED PITCHWISE FLOW ANGLES

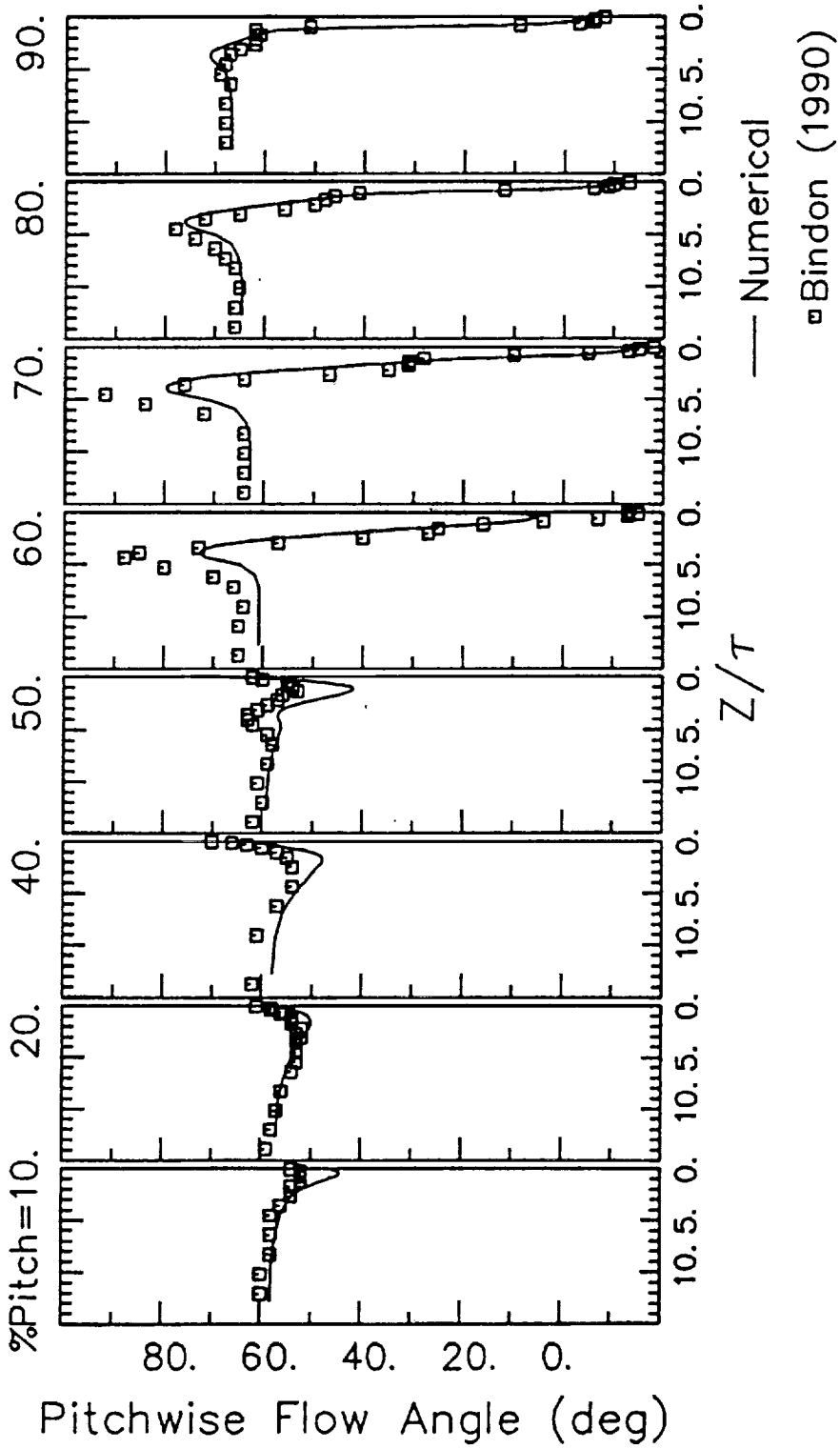

COMPARISON OF MEASURED AND COMPUTED SPANWISE FLOW ANGLES (POSITIVE ANGLE WHEN FLOW DIRECTED TOWARDS ENDWALL)

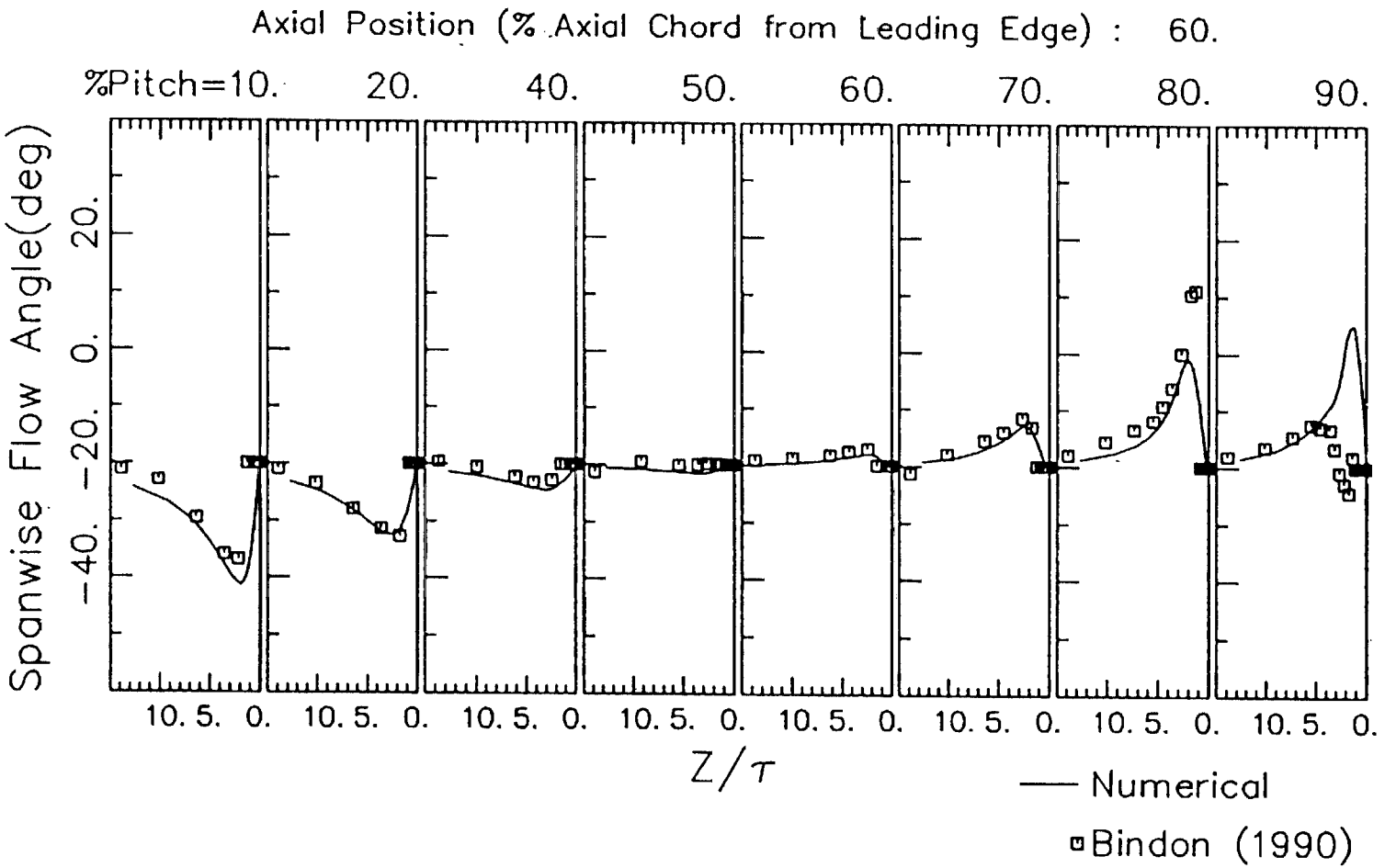

COMPARISON OF MEASURED AND COMPUTED SPANWISE FLOW ANGLES (POSITIVE ANGLE WHEN FLOW DIRECTED TOWARDS ENDWALL)

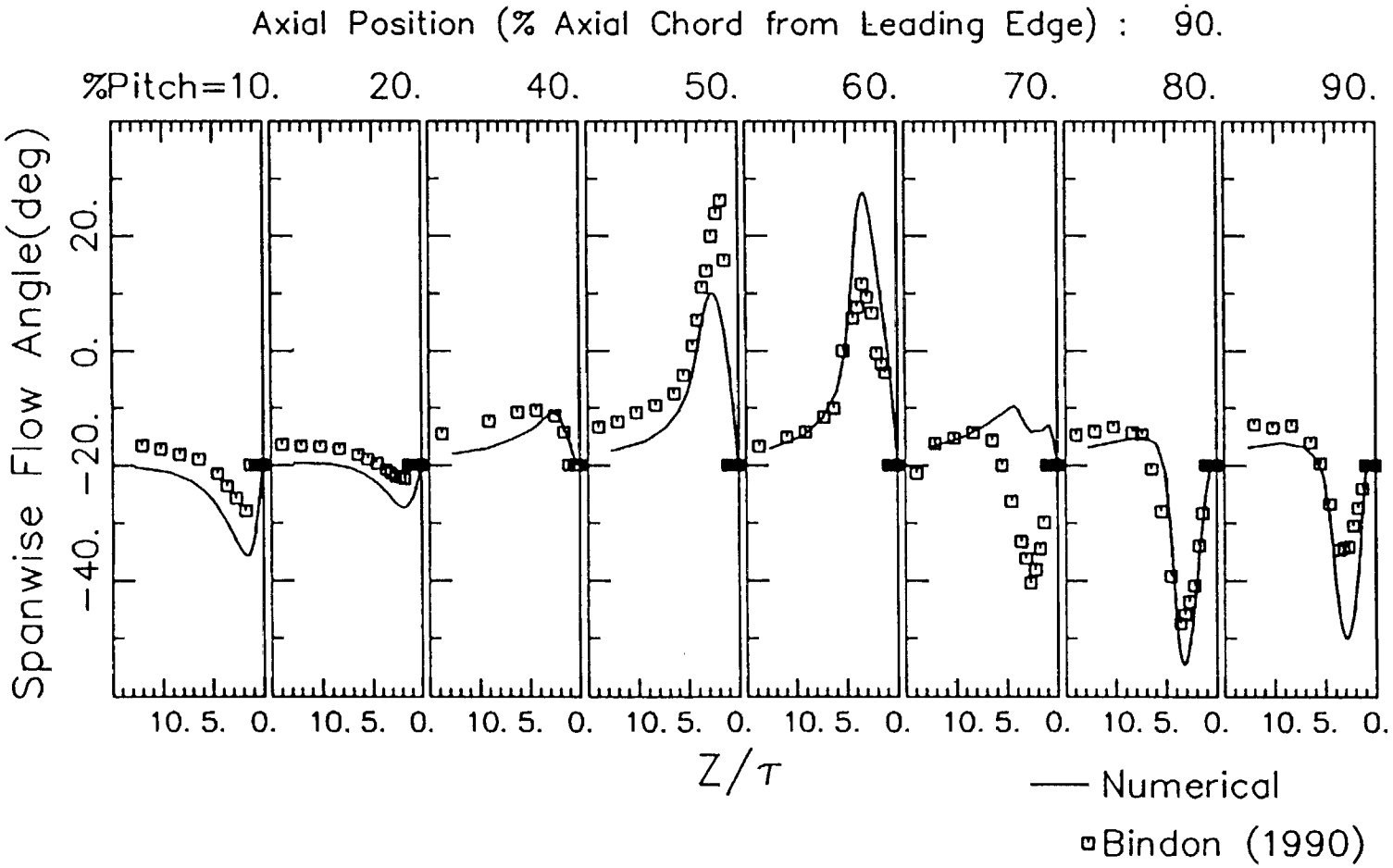

CONTOURS OF LOSS COEFFICIENT (ζ_L) PREDICTED AND MEASURED

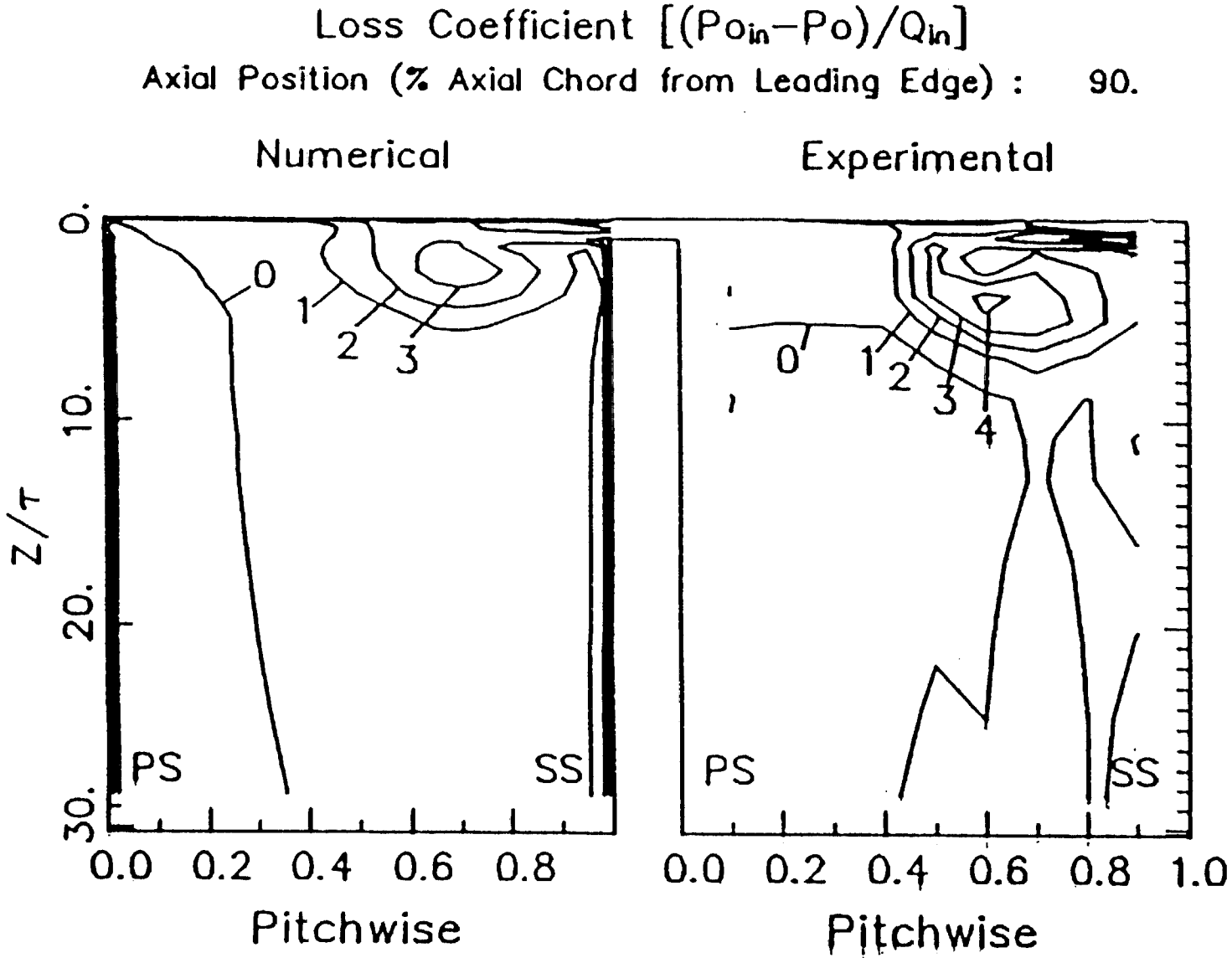

AXIAL DEVELOPMENT OF MASS AVERAGED LOSS COEFFICIENT ($\bar{\zeta}_L$)

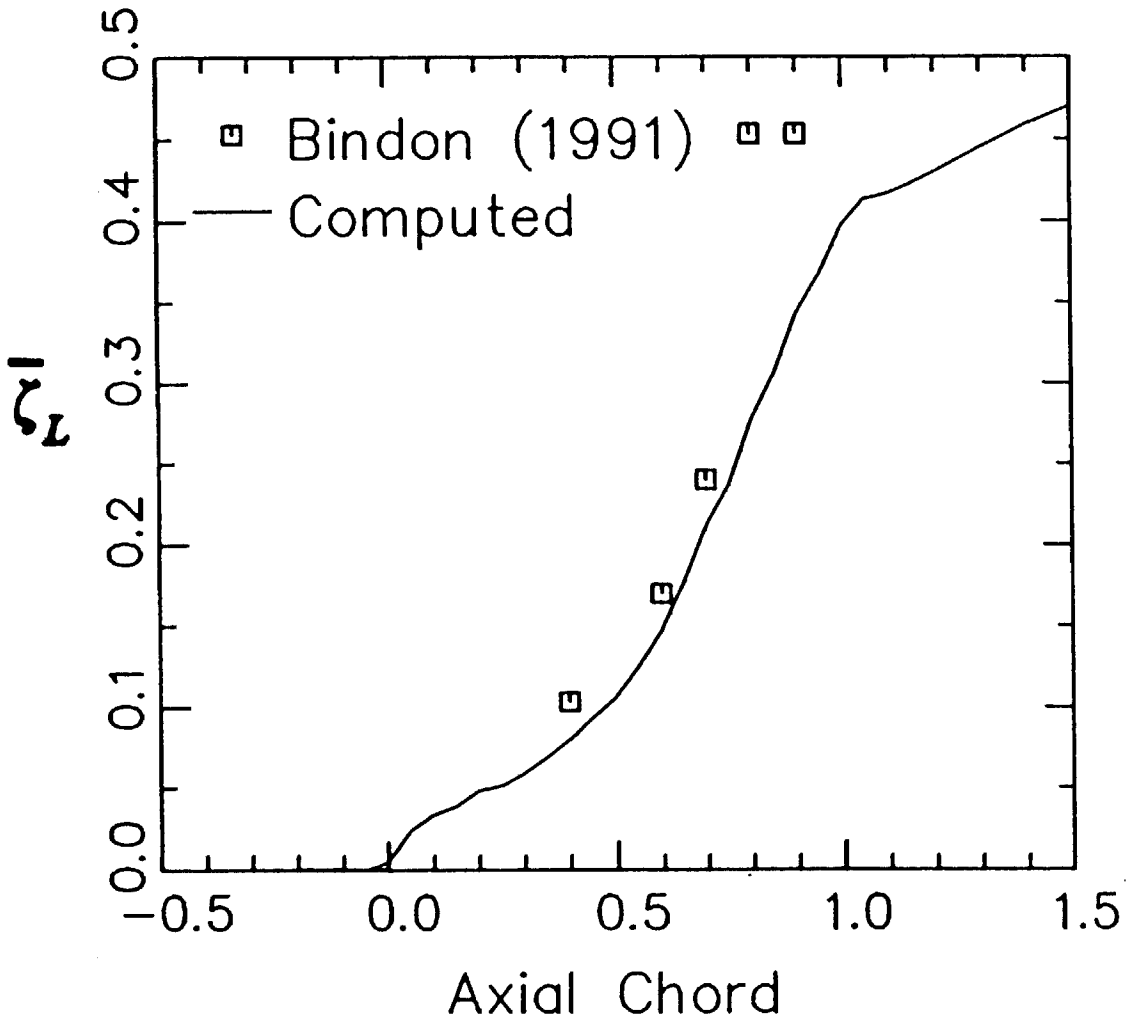

CONTOURS OF PRESSURE COEFFICIENT (c_p)

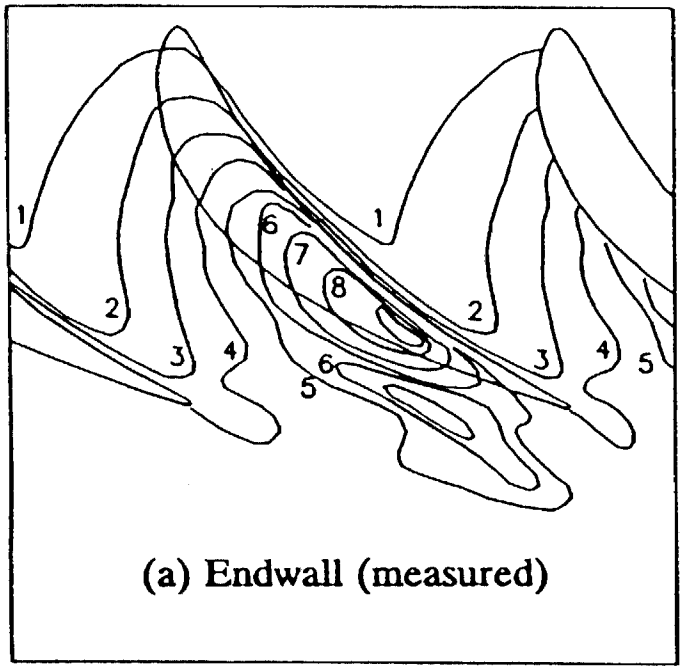

(a) Endwall (measured)

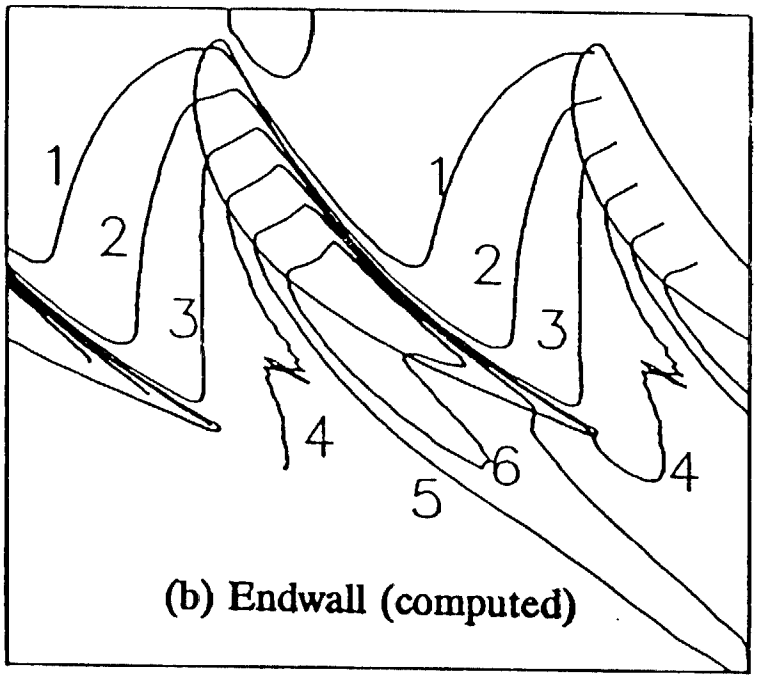

(b) Endwall (computed)

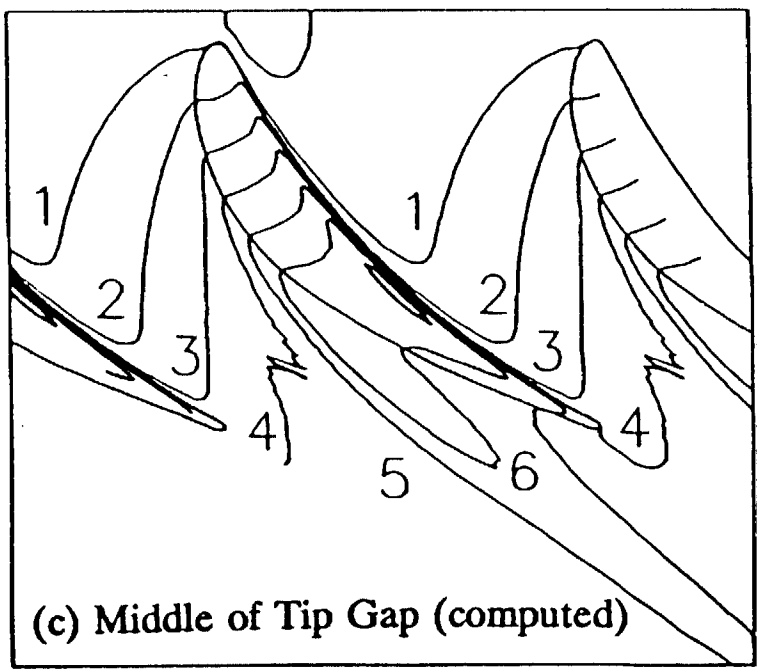

(c) Middle of Tip Gap (computed)

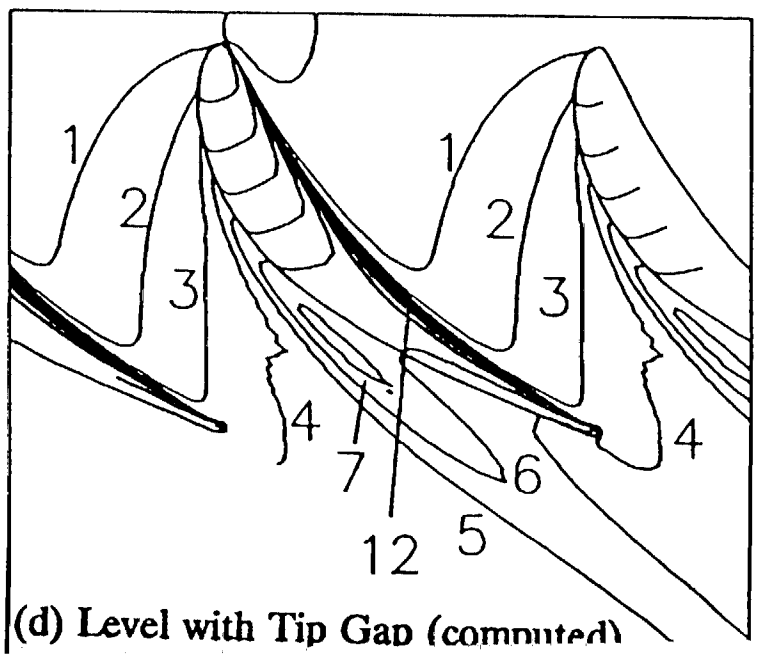

(d) Level with Tip Gap (computed)

VELOCITY VECTORS AT CONSTANT SPANWISE POSITIONS PROJECTED ON TO A BLADE-TO-BLADE (XY) PLANE

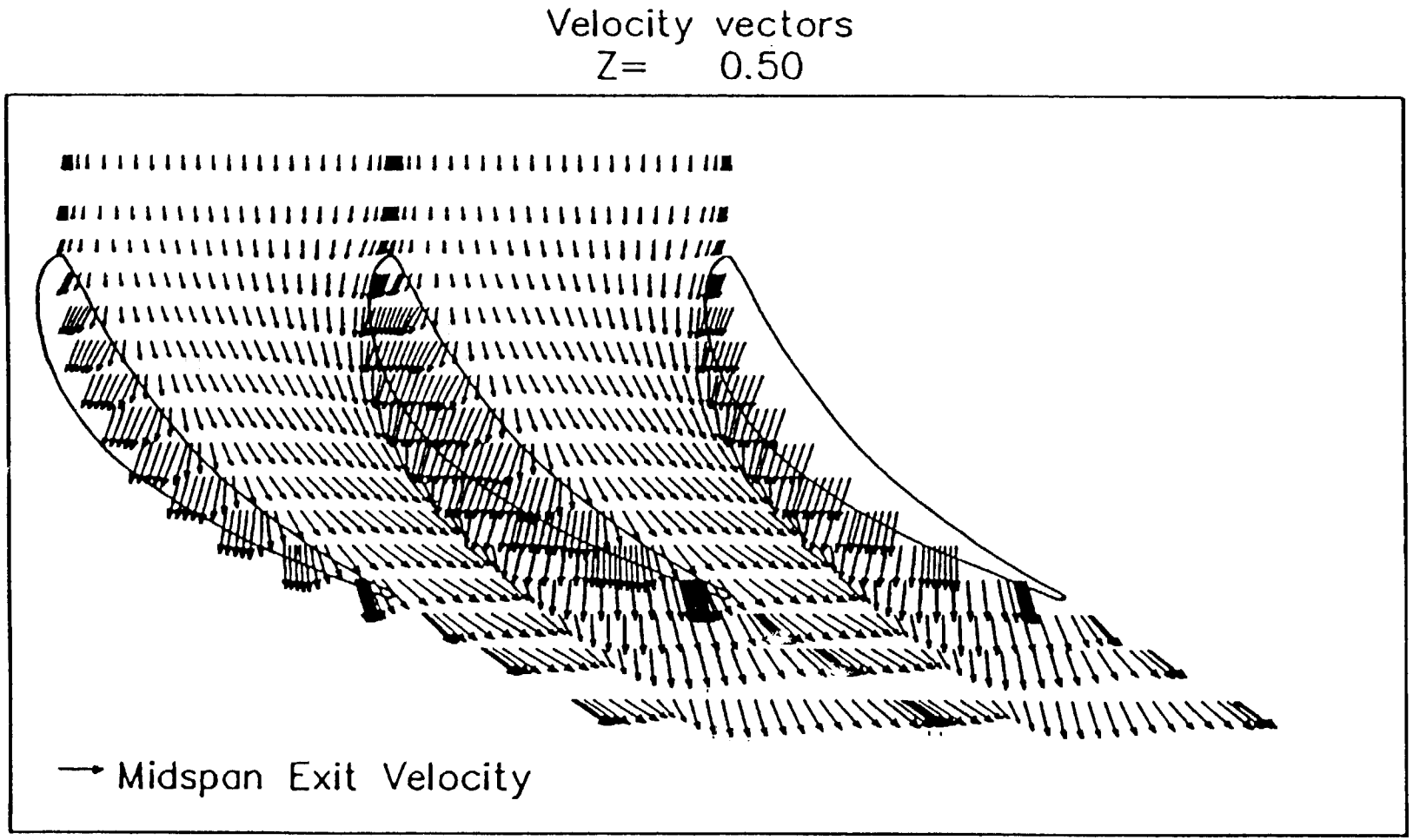

VELOCITY VECTORS AT CONSTANT SPANWISE POSITIONS PROJECTED ON TO A BLADE-TO-BLADE (XY) PLANE

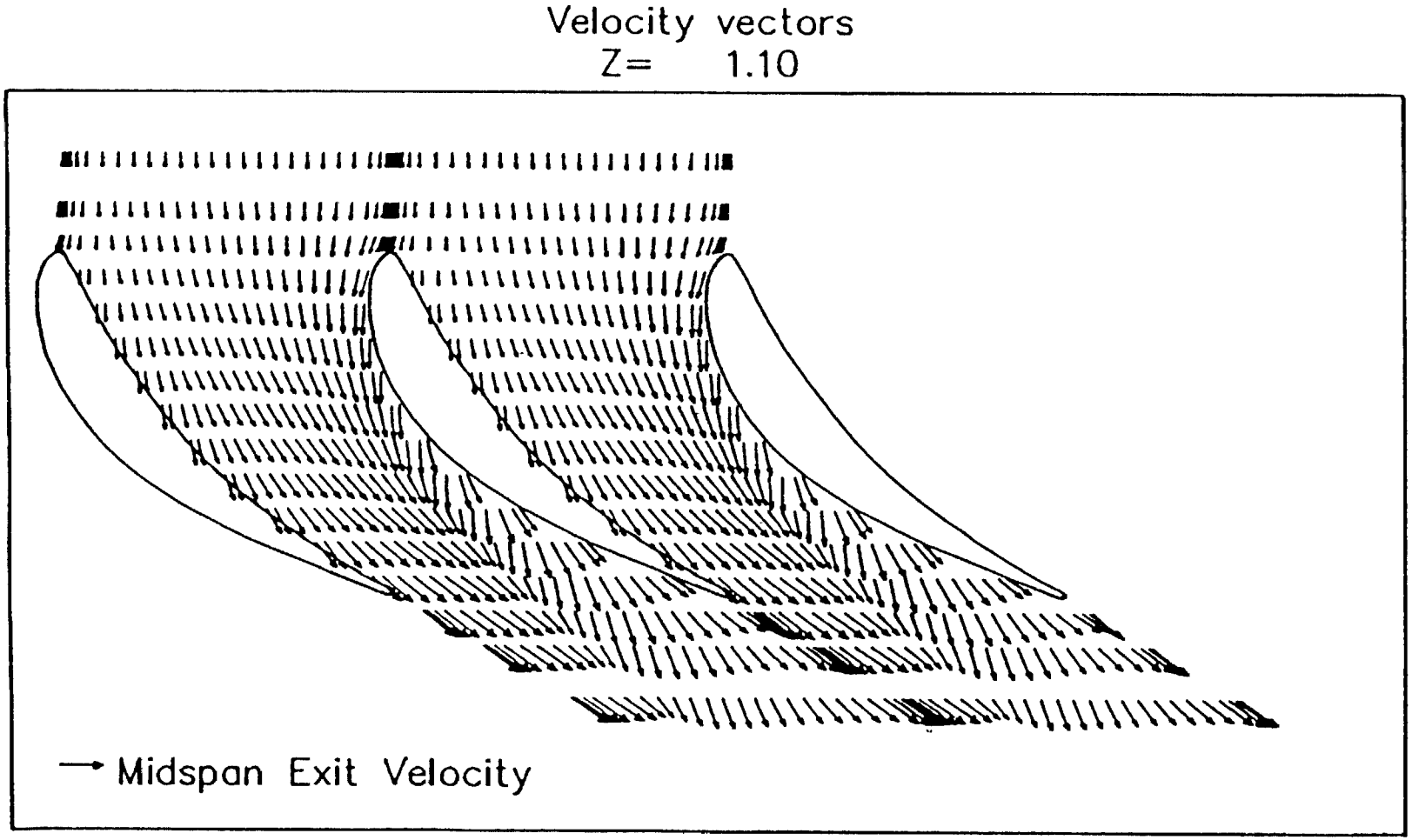

VELOCITY VECTORS AT CONSTANT SPANWISE POSITIONS PROJECTED ON TO A BLADE-TO-BLADE (XY) PLANE

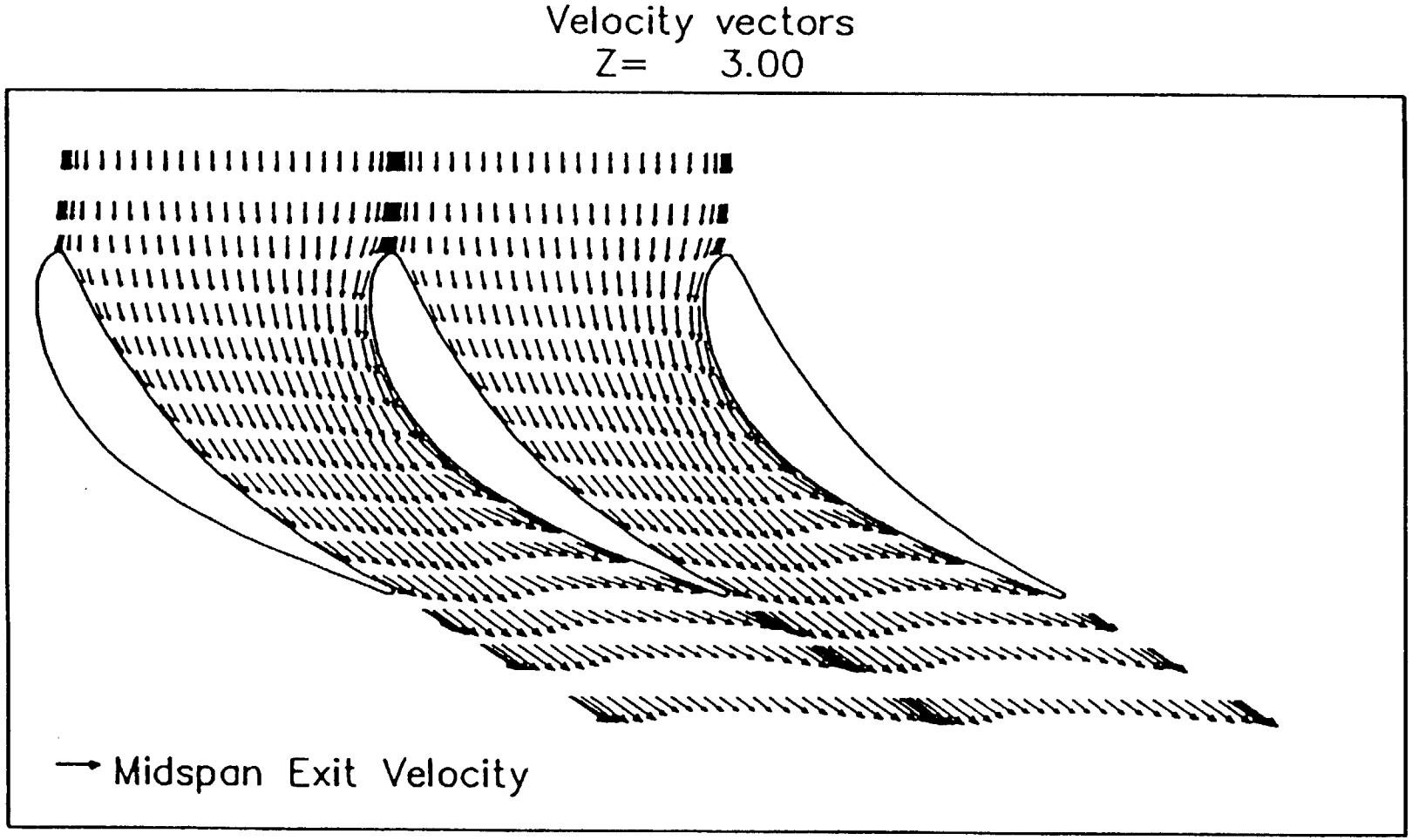

COMPUTED SECONDARY VORTICITY VECTORS

$$\left[\left(\nabla x \left(\underline{V} - \underline{V}_{midspan} \right) \right) \right]$$

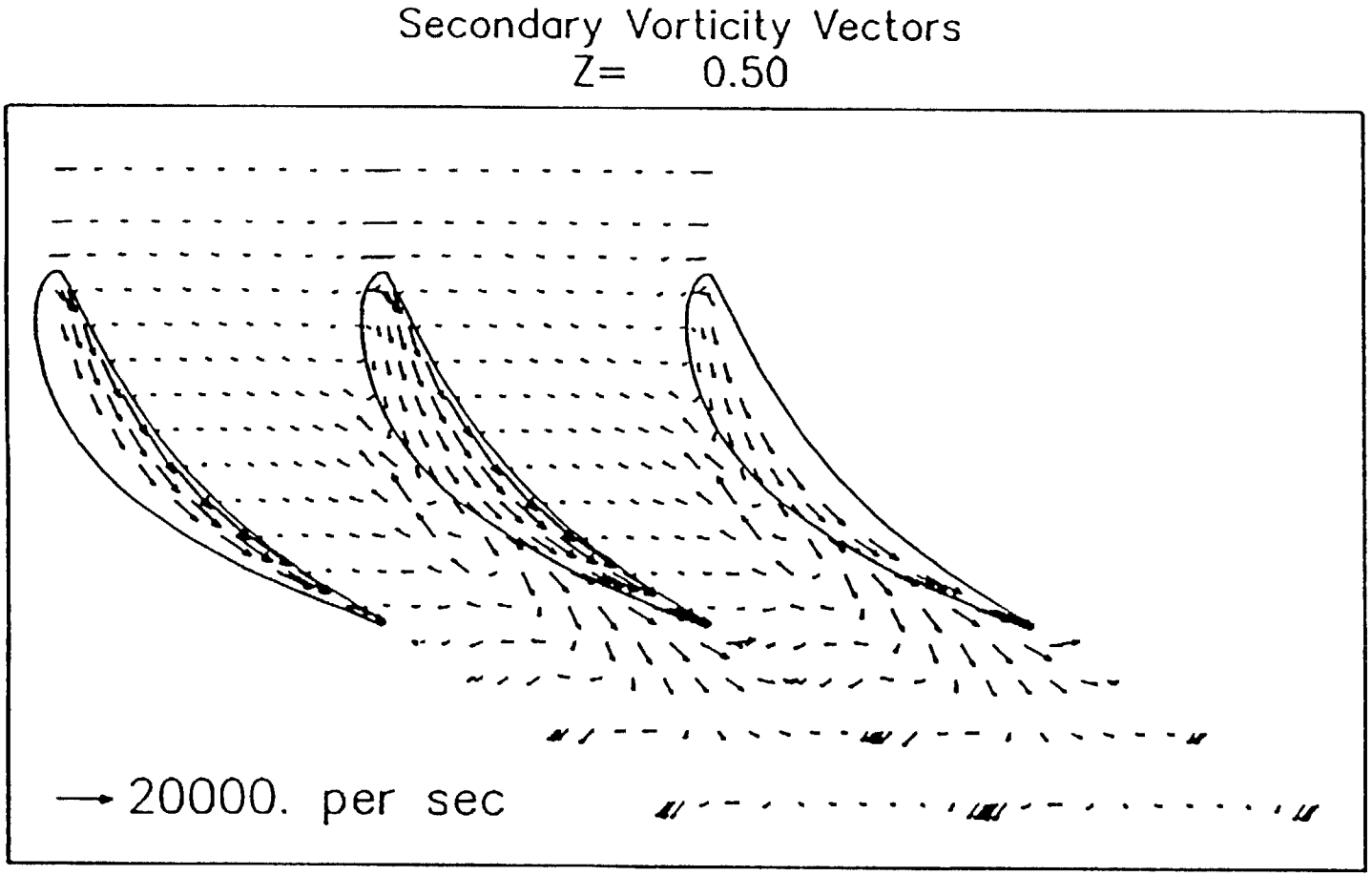

COMPUTED SECONDARY VORTICITY VECTORS

$$\left[\left(\nabla x \left(\underline{V} - \underline{V}_{midspan} \right) \right) \right]$$

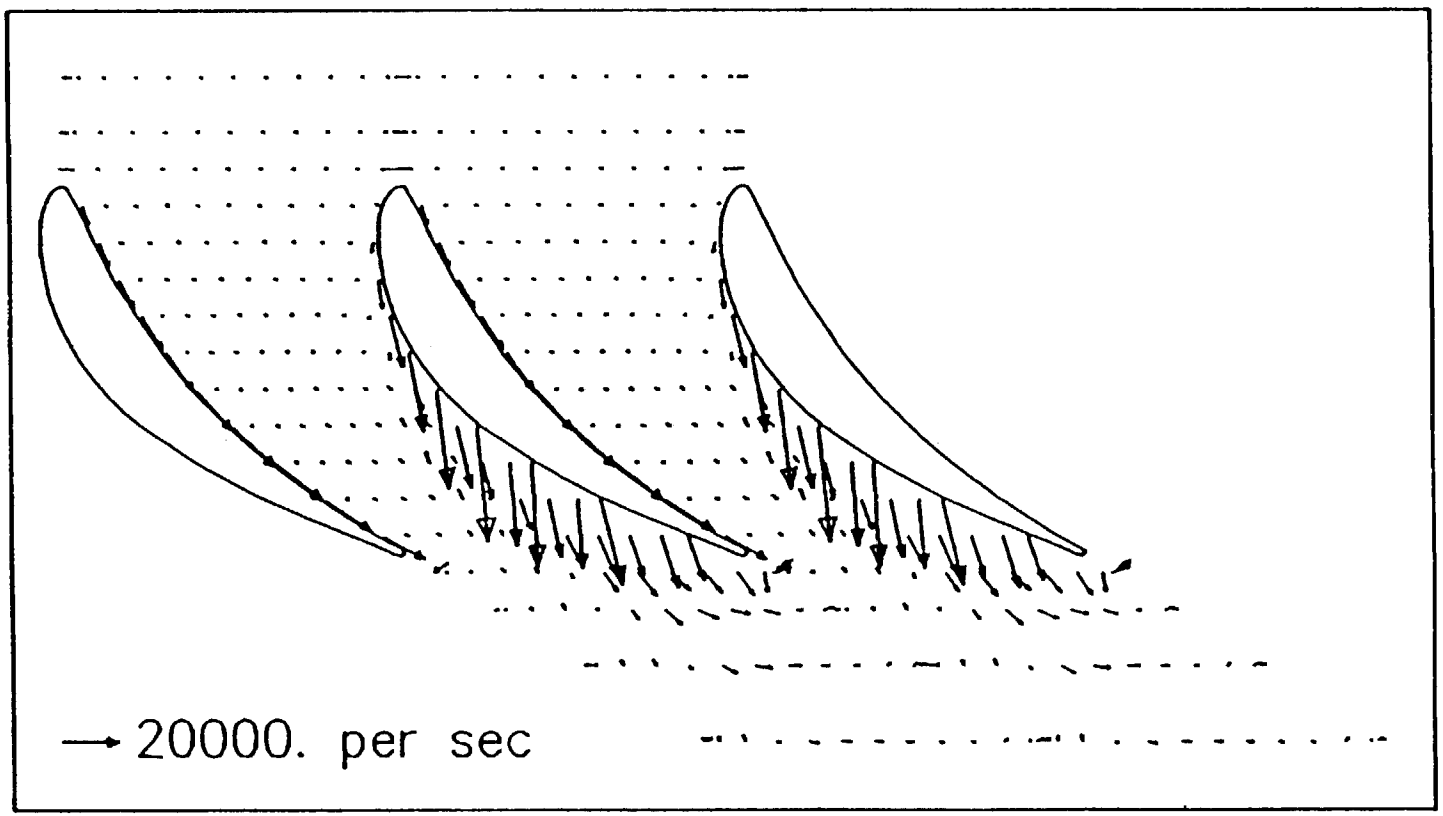

CONCLUSIONS

- **Geometric series distribution scheme**

  Good control over the boundary points

- **Algebraic-elliptic grid generation scheme**

  Good control over clustering

  Good control over orthogonality

  Enhanced stability of elliptic generation

- **Embedded H-grid**

  Single block discretization for tip clearance cases

  No Modification of blade tip shape required

  Retains H-grid connectivity pattern

- **Effect of artificial dissipation**

  Numerical accuracy vs. convergence rate

  Minimum artificial dissipation should be used

- **Modelling of tip clearance flows**

  Major physical phenomena captured

  Location of leakage vortex, pitchwise and spanwise angles, losses, static pressures predicted accurately

CONCLUSIONS

- **2D unsteady flow computation**
  - **For the rotor-stator interaction simulation case, the decay of rotor wake and the time-mean pressures agree very well with the experimental data. The potential effect of downstream stator on the rotor wake is captured very well.**
  - **The rotor wake decays through out the stator passage. The wake defect becomes insignificant after passing through the stator passage.**
  - **The interaction between the wake and the freestream induces two vortices on either side of rotor wake inside the stator passage. This causes the wake to smear out as it is transported downstream inside the stator passage.**
  - **For the unsteady flow over an airfoil case, the boundary layer velocity profiles and blade pressure agree with the measurements, including the magnitude and phase angle.**

GGOT TOTAL PRESSURE LOSS CONTROL CONCEPT EVALUATION

R. F. BLUMENTHAL
AEROJET PROPULSION DIVISION
SACRAMENTO, CA

Total pressure loss is one of the most important parameters in the design of a turbine. This parameter effects not only the turbine performance, but consequently the engine power balance and engine performance. Computational Fluid Dynamics (CFD) can be an effective tool in predicting turbine total pressure loss, and also for performing sensitivity studies to achieve an optimal design with respect to pressure loss. In the present study, the AEROVISC code was used to predict the total pressure loss in the Turbine Technology Team Gas Generator Oxidizer Turbine (GGOT).

The objectives in this study are two-fold. It is first necessary to determine an optimal methodology in predicting total pressure loss. The type of grid, grid density and distribution are parameters which may effect the loss prediction. Also, the effect of using a standard K-ε turbulence model with wall functions versus a two-layer turbulence model needs to be investigated. The use of grid embedding to resolve areas with high flow gradients needs to be explored. The second objective of the study is to apply the optimal methodology toward evaluating different tip leakage control concepts.

The approach taken in this study was as follows:

1) A nominal baseline case was run (baseline grid with standard wall functions)

   a) Grid parametrics were performed on grid density

   b) Grid embedding was applied to the rotor leading and trailing edges, and in the tip region.

   c) Evaluation of a two-layer turbulence model (in progress)

Each of the above cases were assessed in terms of total pressure loss in comparison with the baseline case, and in terms of the difference in secondary flow resolution in comparison with the baseline case.

2) The optimal methodology from Step 1 is applied towards evaluating different tip leakage control concepts which will include

   a) Hollow rotor

   b) Hollow rotor with partitions (labyrinth seal approach)

   c) Hollow rotor with partitions and suction-side rotor slots (to reduce fluid impingement angle)

As this work is still in progress, conclusions are not available at this time.

GENCORP AEROJET

Propulsion Division

GGOT TOTAL PRESSURE LOSS CONTROL CONCEPT EVALUATION

R. F. BLUMENTHAL
AEROJET PROPULSION DIVISION

APRIL 22, 1993

OXIDIZER TURBINE BASELINE DESIGN

Full Scale Turbine Flowpath

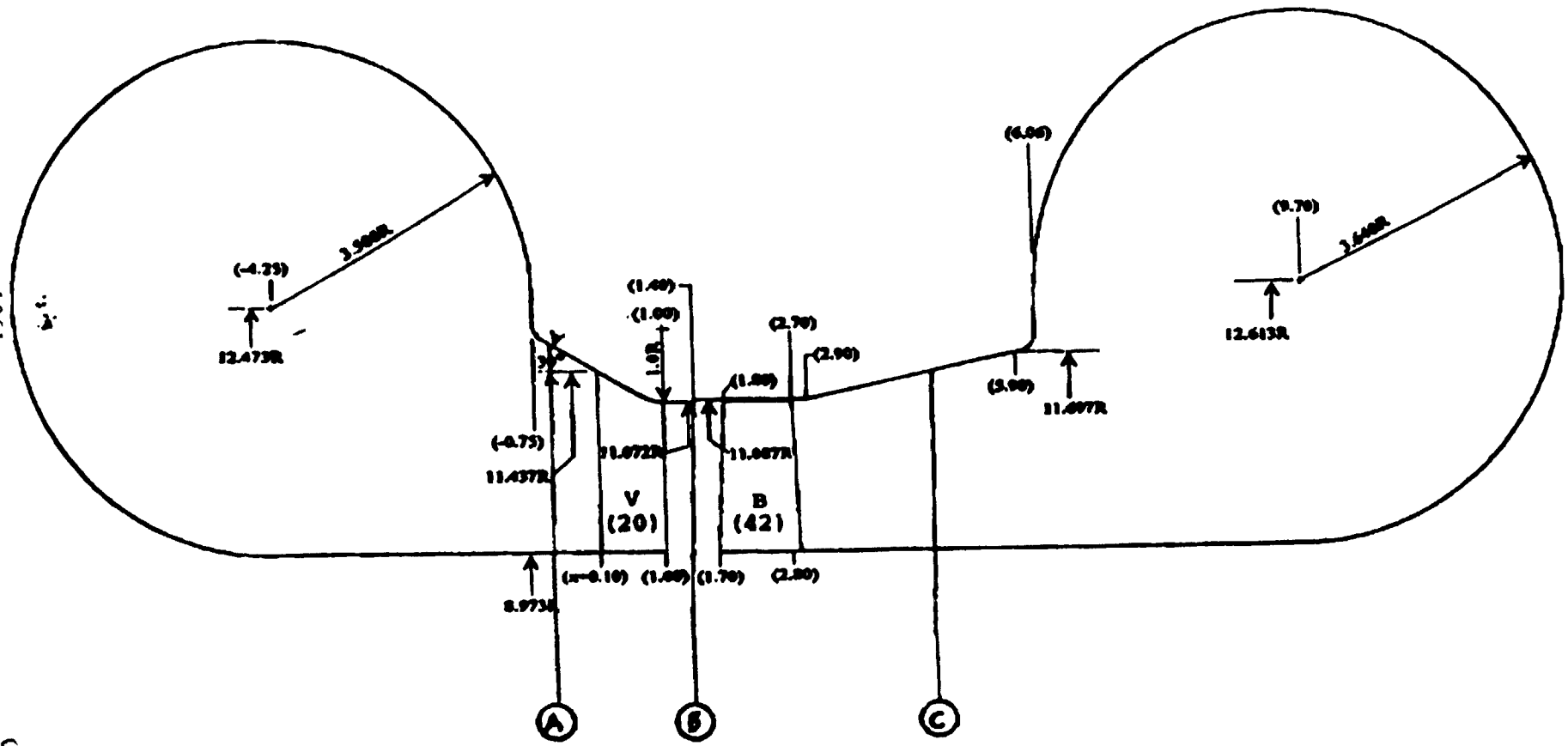

Axial Location - ( )

(A) STATION LETTER

1361

ORIGINAL PAGE IS
OF POOR QUALITY

GENCORP AEROJET

Propulsion Division

GGOT TOTAL PRESSURE LOSS CONTROL CONCEPT EVALUATION

OBJECTIVE : EVALUATE TIP LEAKAGE CONTROL CONCEPTS WHICH REDUCE TIP LEAKAGE AND TOTAL PRESSURE LOSS

APPROACH : 1.) PERFORM GRID DEPENDENCY STUDY

RUN NOMINAL BASELINE CASE WITH BASELINE GRID USING AEROVISC CODE AND STANDARD LOG-LAW WALL FUNCTION

a.) PERFORM GRID PARAMETERICS ON GRID DENSITY
b.) EVALUATE MERITS OF GRID EMBEDDING
c.) EVALUATE TWO-LAYER TURBULENCE MODEL

2.) EVALUATE TIP TREATMENT CONCEPTS , INCORPORATING OPTIMAL METHODOLOGY/PROCEDURE FROM STEP 1

GenCorp Aerojet

Propulsion Division

GGOT ROTOR CFD MODEL

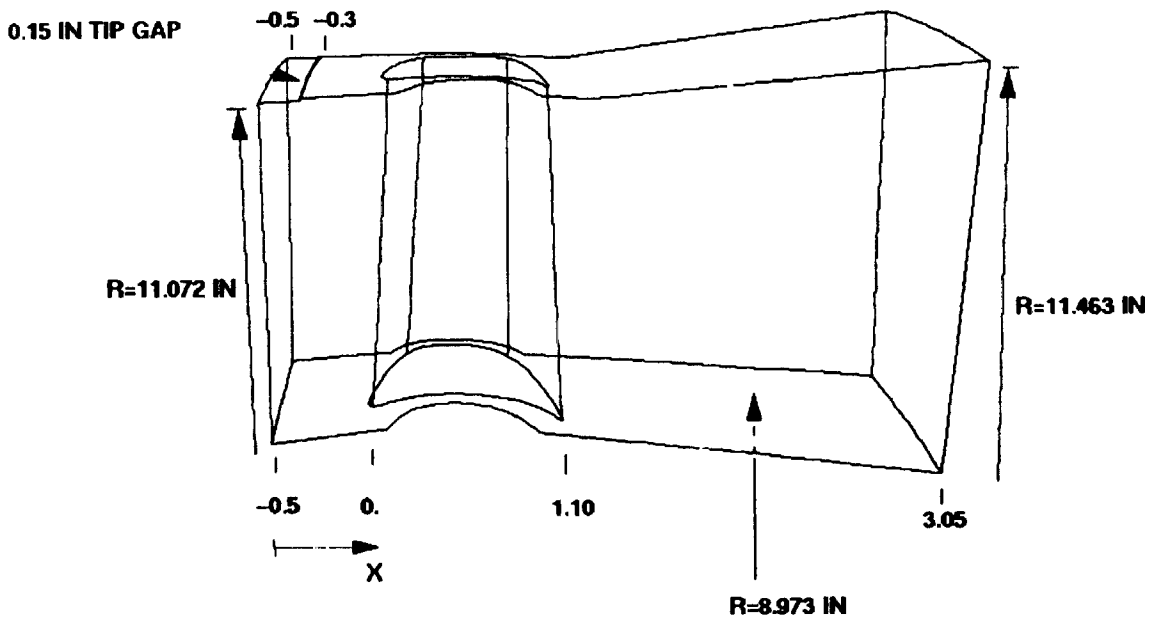

GENCORP AEROJET

Propulsion Division

GGOT TOTAL PRESSURE LOSS/ GRID DEPENDENCY STUDY

APPLIED BOUNDARY CONDITIONS

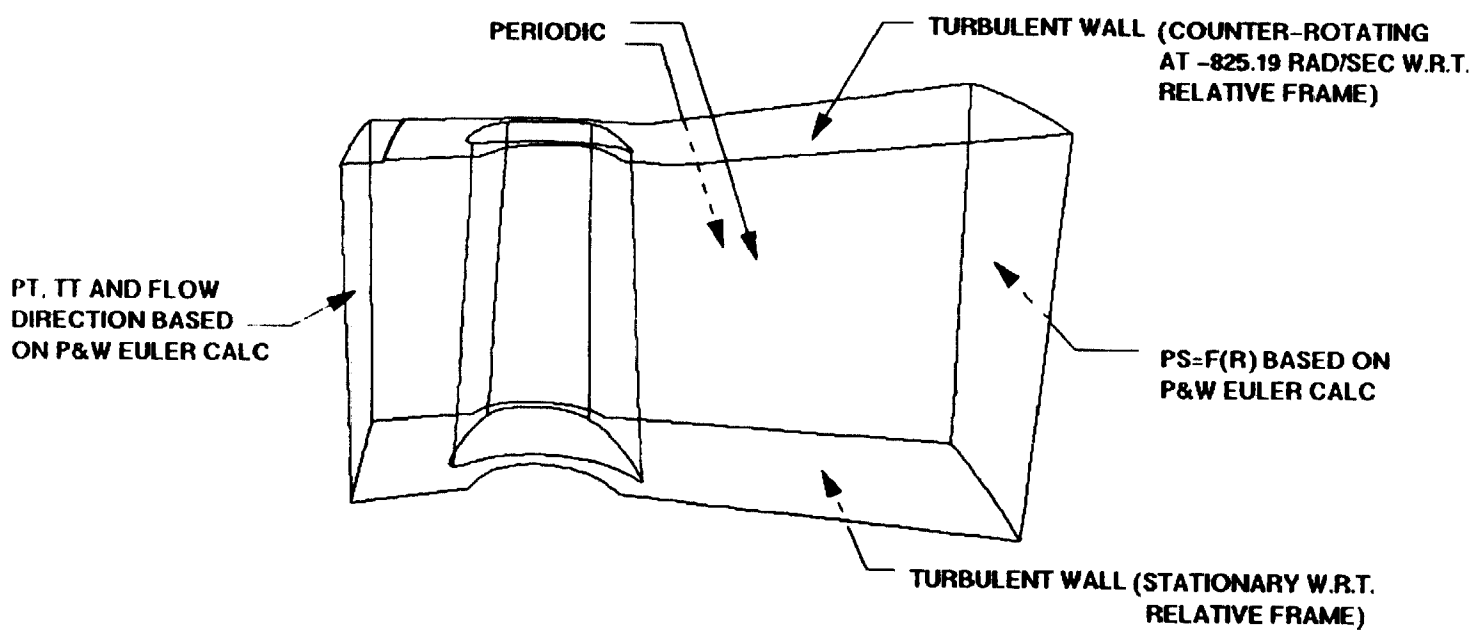

GENCORP AEROJET

Propulsion Division

GGOT TOTAL PRESSURE LOSS/ GRID DEPENDENCY STUDY

GRID PARAMETRIC APPROACH AND RESULTS

- BASELINE GGOT ROTOR GRID (82 x 41 x 24 w/ 5 GRIDS IN TIP GAP RADIAL DIRECTION)
- GRID PARAMETERICS PERFORMED BY INCREASING GRID COUNT UNIFORMLY IN EACH PARAMETRIC DIRECTION (AXIAL, CIRCUMFERENTIAL, RADIAL). THREE CASES IN EACH DIRECTION WERE RUN, FOR A TOTAL OF TEN CASES (INCLUDING THE BASELINE).
- ALL CASES WERE RUN UNTIL A SIMILAR CONVERGENCE LEVEL WAS ACHIEVED

GENCORP AEROJET

GGOT TOTAL PRESSURE LOSS/ GRID DEPENDENCY STUDY

Propulsion Division

BASELINE ROTOR GRID

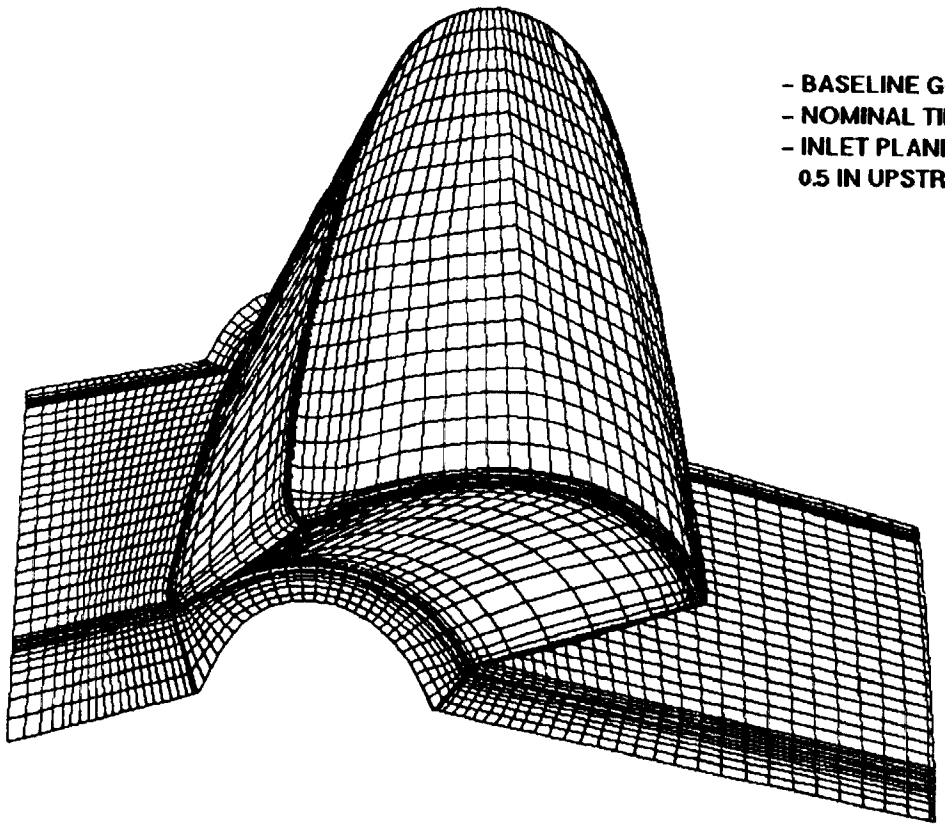

- BASELINE GRID (82 x 41 x 24)
- NOMINAL TIP GAP=0.015 IN
- INLET PLANE AXIAL LOCATION 0.5 IN UPSTREAM OF LEADING EDGE

GENCORP AEROJET

Propulsion Division

GGOT TOTAL PRESSURE LOSS/ GRID DEPENDENCY STUDY

GRID PARAMETRIC APPROACH AND RESULTS

	CASE	I-DIR	J-DIR	K-DIR	TIP GAP	TOTAL
	BASELINE	82	41	24	5	80688
AXIAL DIR (I)	CASE 1A	106	41	24	5	104304
	CASE 1B	131	41	24	5	128904
	CASE 1C	237	41	24	5	233208
CIRCUM. DIR (J)	CASE 2A	82	53	24	5	104304
	CASE 2B	82	67	24	5	131856
	CASE 2C	82	120	24	5	236160
RADIAL DIR (K)	CASE 3A	82	41	3(	6	100860
	CASE 3B	82	41	3(	7	121032
	CASE 3C	82	41	72	13	242064

GENCORP AEROJET

Propulsion Division

GGOT TOTAL PRESSURE LOSS/ GRID DEPENDENCY STUDY

GRID PARAMETRIC APPROACH AND RESULTS (PRELIMINARY)

CASE	PT REL (INLET) [PSI]	PT REL (EXIT) [PSI]	DPT REL [PSI]	PLOSS= DPT REL/PT REL (INLET)	PLOSS/ PLOSS BASE
BASE	457.498	365.800	91.698	0.2004	1.0000
CASE 1A	459.075	368.364	90.711	0.1976	0.9859
CASE 1B	459.446	368.627	90.819	0.1977	0.9862
CASE 2A	458.853	367.871	90.982	0.1983	0.9893
CASE 2B	458.978	367.607	91.371	0.1991	0.9932
CASE 3A	455.961	367.574	88.387	0.1939	0.9672
CASE 3B	456.026	367.613	88.413	0.1939	0.9673

NOTE: ALL PRESSURES ARE BASED ON MASS-AVERAGED VALUES

EXIT STATIC PRESSURE USED FOR PRELIMINARY PARAMETERICS
BASED ON STATIC PRESSURE SPECIFIED AT ONE NODE IN EXIT PLANE
(PS=215.5 PSI AT CENTER OF EXIT PLANE)

GENCORP AEROJET

Propulsion Division

GGOT TOTAL PRESSURE LOSS/ GRID DEPENDENCY STUDY

GRID PARAMETRIC APPROACH AND RESULTS

CASE	PT REL (INLET) [PSI]	PT REL (EXIT) [PSI]	DPT REL [PSI]	PLOSS= DPT REL/PT REL (INLET)	PLOSS/ PLOSS BASE
BASE	456.352	375.839	80.513	0.1764	1.0000
CASE 1C	456.987	373.528	83.459	0.1826	1.0351
CASE 2C	456.788	375.805	80.983	0.1773	1.0051
CASE 3C	456.890	376.620	80.270	0.1757	0.9960

NOTE: ALL PRESSURES ARE BASED ON MASS-AVERAGED VALUES

EXIT STATIC PRESSURE BASED ON RADIAL PRESSURE DISTRIBUTION PROVIDED BY P&W FROM EULER CALC

GENCORP AEROJET

BASELINE RESULTS

Propulsion Division

VELOCITIES IN MID-GAP REGION (K=22)

HIGH TIP FLOW VELOCITIES COUPLED WITH LARGE IMPINGEMENT ANGLE INFLUENCE MAINSTREAM FLOW AT SOME DISTANCE DOWNSTREAM OF ROTOR

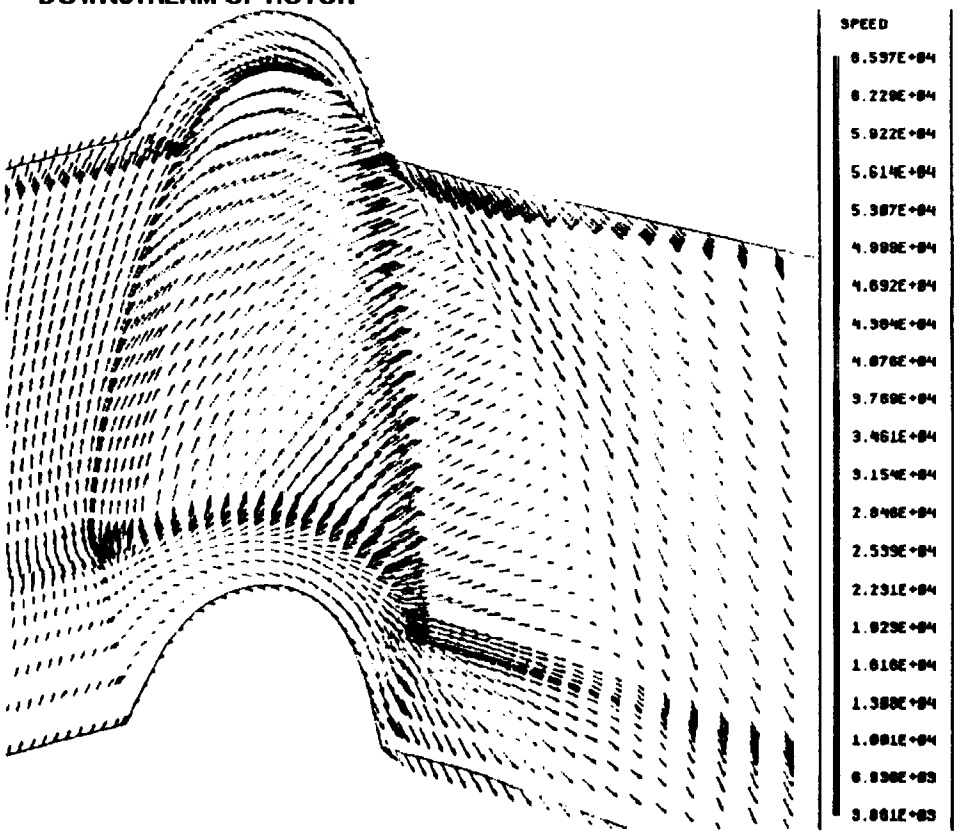

STREAKLINES AT TIP SHOW DEVELOPING PASSAGE VORTEX
(PARTICLES RELEASED IN MID-GAP REGION)

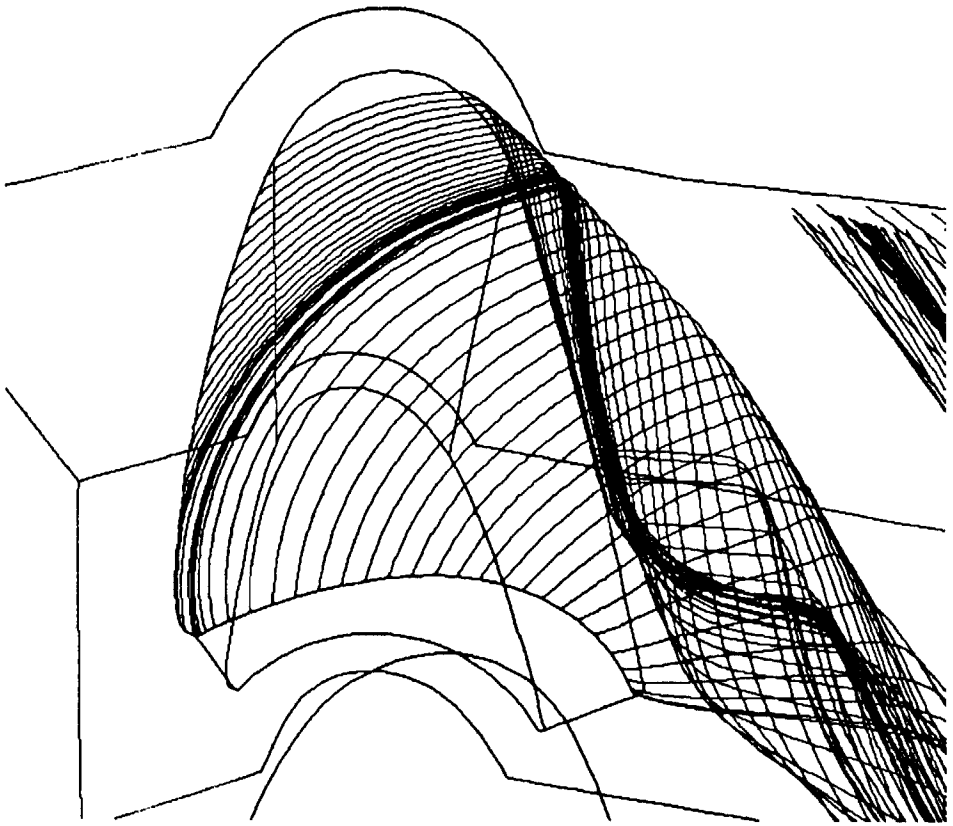

GENCORP AEROJET

BASELINE RESULTS

Propulsion Division

RELATIVE TOTAL PRESSURE LOSS DUE TO TIP GAP FLOW
HIGH LOSS GRADIENT EXISTS NEAR TIP

PTR=(PTOT REL(INLET AVE) PTOT REL)/PTOT REL(INLET AVE

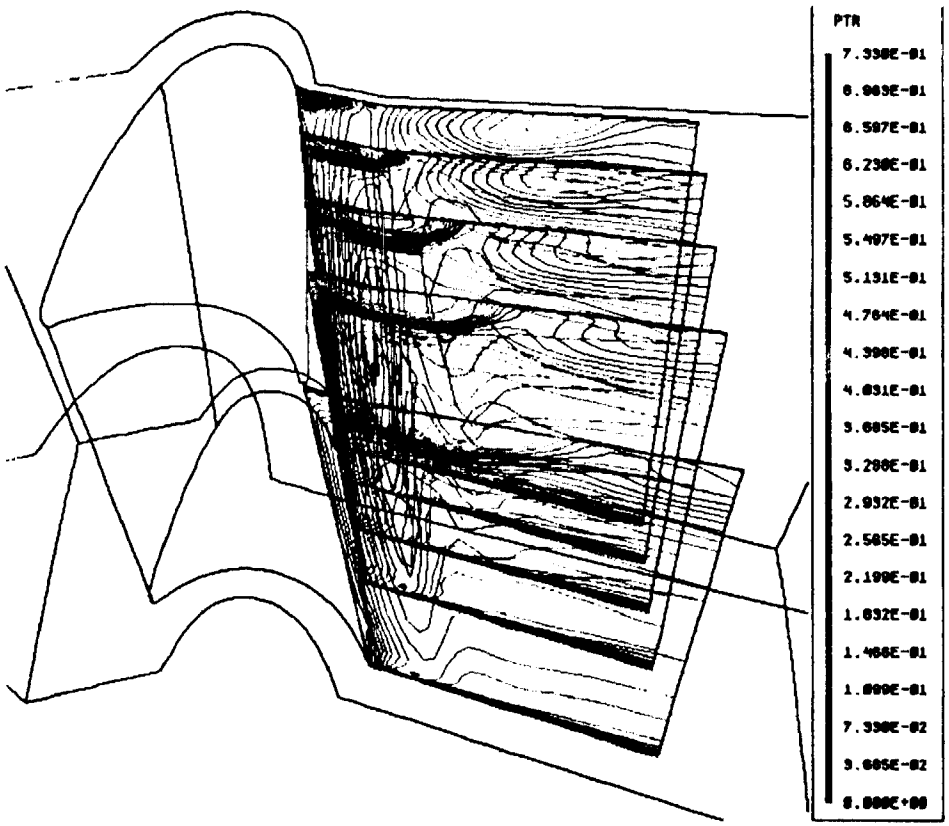

GENCORP AEROJET

BASELINE RESULTS

Propulsion Division

VELOCITY CONTOURS SHOW EFFECT OF TIP LEAKAGE ON MAINSTREAM FLOW
CONSIDERABLE FLOW DECELERATION OCCURS

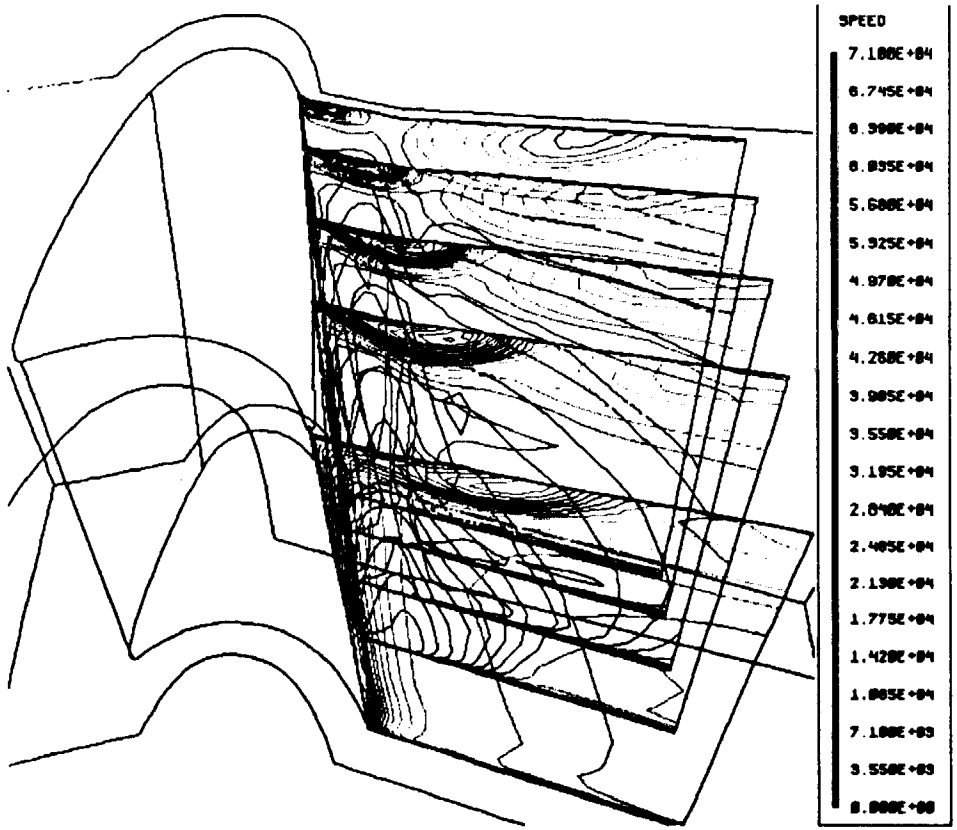

GENCORP AEROJET

GGOT TOTAL PRESSURE LOSS/ GRID DEPENDENCY STUDY

Propulsion Division

LEADING EDGE EMBEDDING – (31 x 25 x 70)
(EMBEDDED GRIDS EXTEND FROM HUB TO TIP ENDWALL)

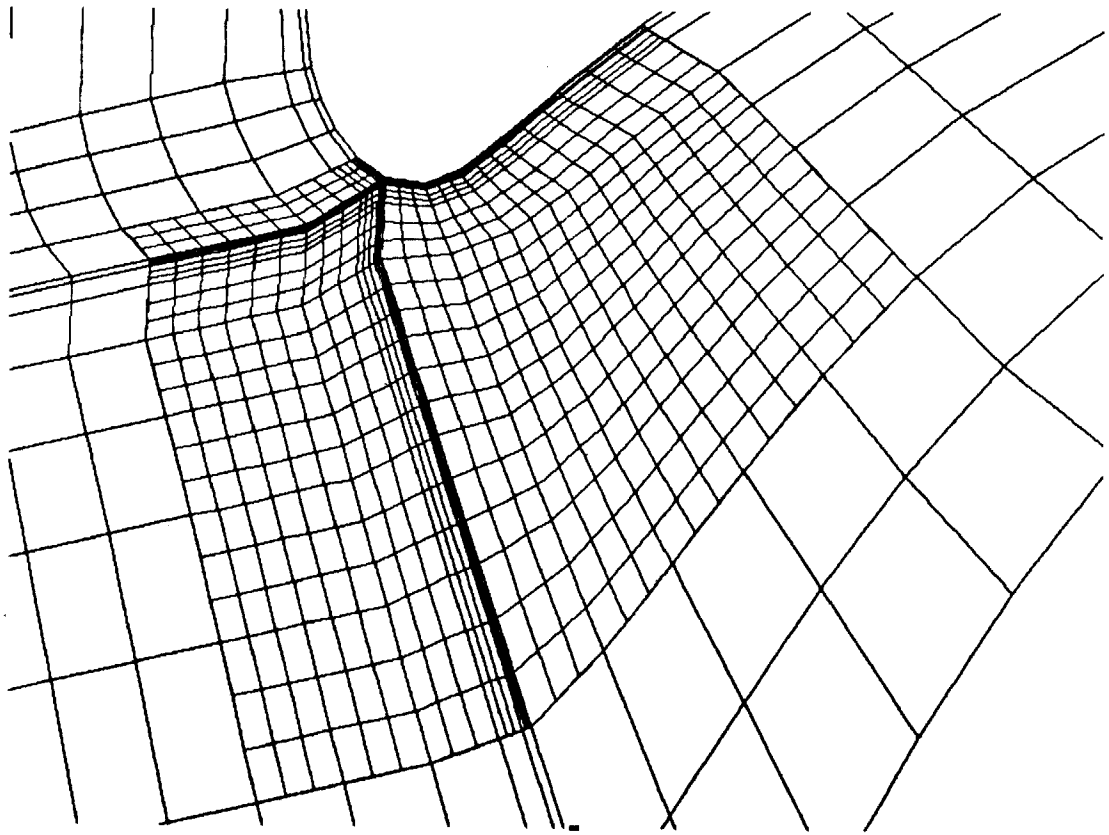

GENCORP AEROJET

Propulsion Division

GGOT TOTAL PRESSURE LOSS/ GRID DEPENDENCY STUDY

GRID EMBEDDING AT TRAILING EDGE (22 x 43 x 70)
(EMBEDDED GRIDS EXTEND FROM HUB TO TIP ENDWALL)

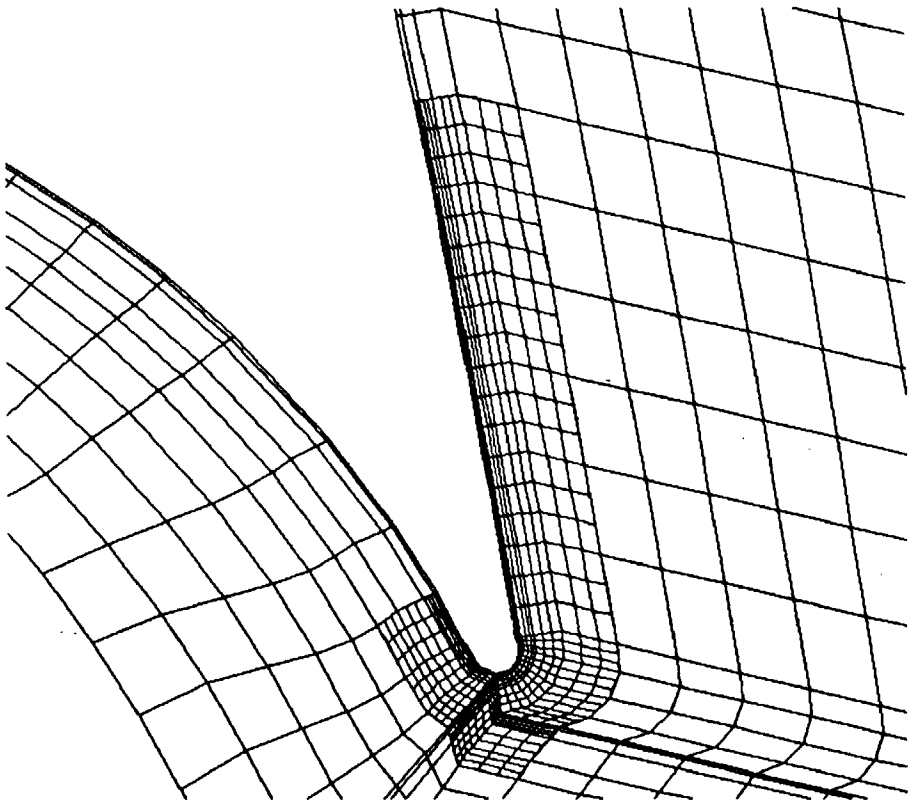

GenCorp Aerojet

Propulsion Division

GGOT TOTAL PRESSURE LOSS/ GRID DEPENDENCY STUDY

GRID EMBEDDING IN THE TIP GAP REGION (103 x 91 x 13)
(EMBEDDED GRIDS EXTEND FROM ROTOR TIP TO ENDWALL)

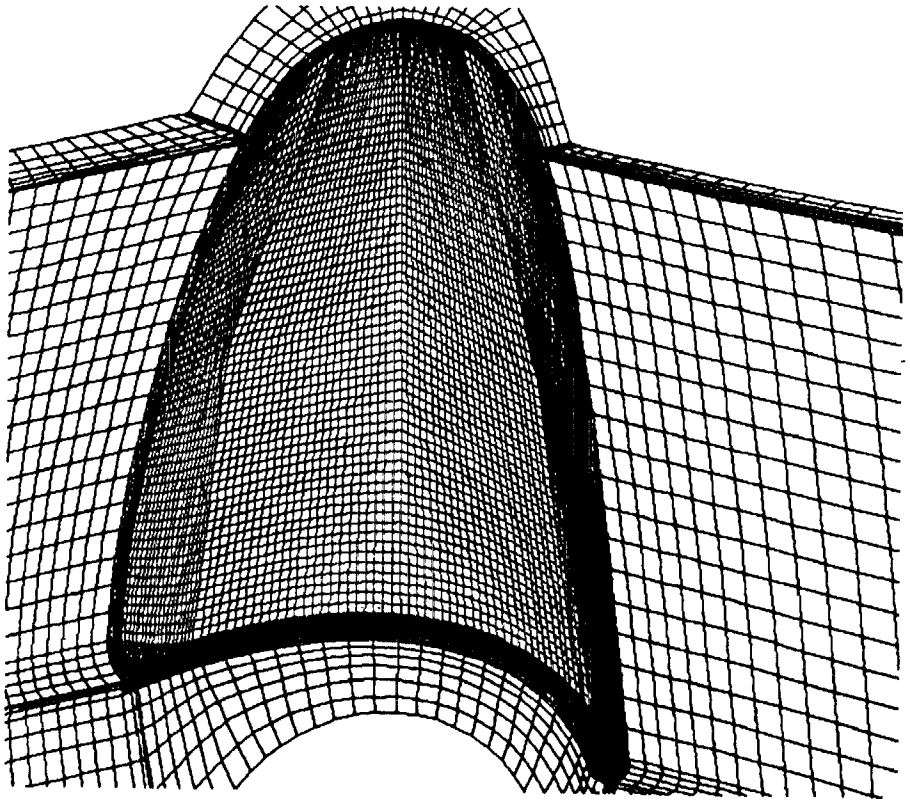

GENCORP AEROJET

GGOT TOTAL PRESSURE LOSS/ GRID DEPENDENCY STUDY

Propulsion Division

BASELINE GRID STREAKLINES NEAR LEADING EDGE (K=2)
GRID LACKS RESOLUTION NEEDED TO RESOLVE SADDLEPOINT

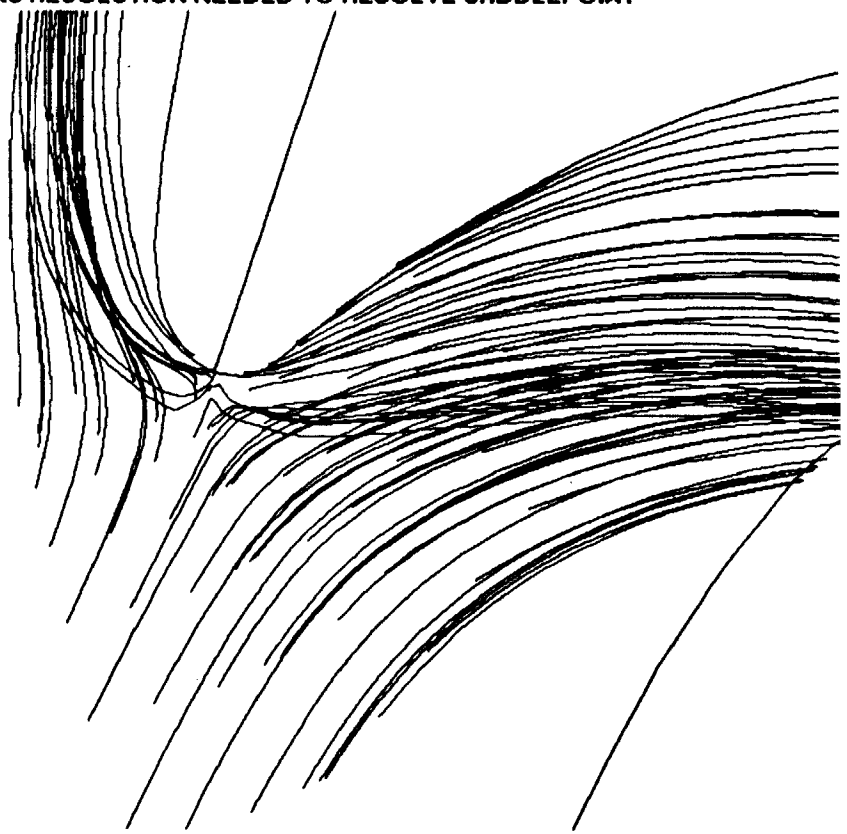

GENCORP AEROJET

GGOT TOTAL PRESSURE LOSS/ GRID DEPENDENCY STUDY

Propulsion Division

GRID EMBEDDING AT LEADING EDGE IS USEFUL IN DEFINING IMPORTANT FLOW FEATURES SUCH AS THE SADDLEPOINT OF THE LIMITING STREAMLINES AT THE HUB

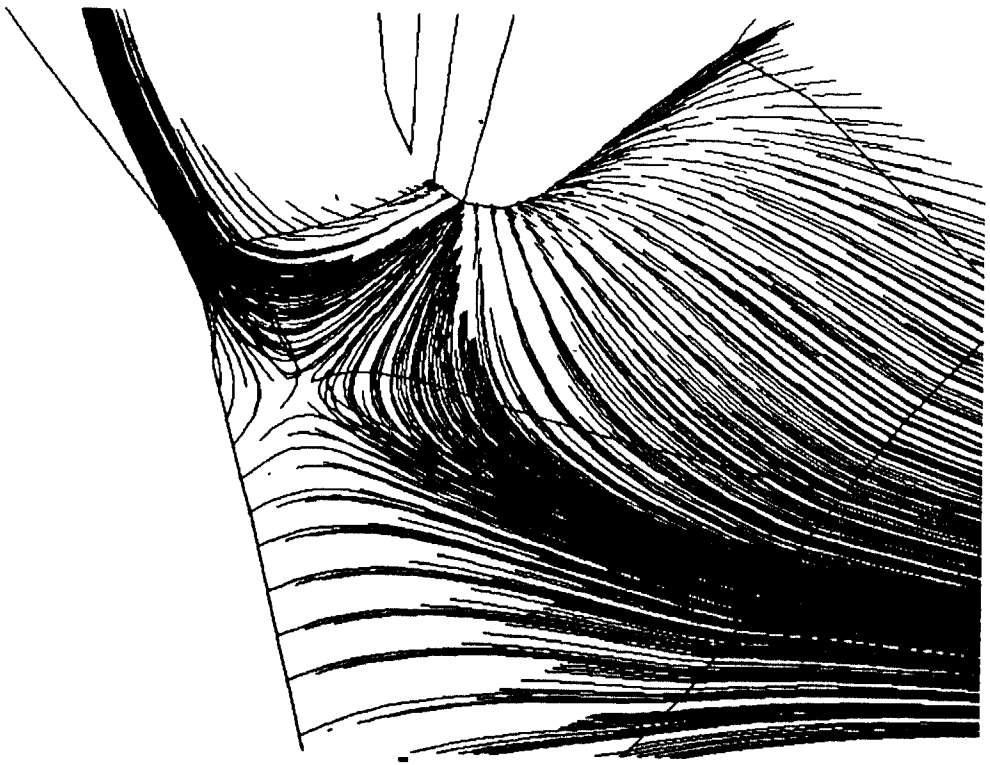

GENCORP AEROJET

GGOT TOTAL PRESSURE LOSS/ GRID DEPENDENCY STUDY

Propulsion Division

BASELINE RESULTS (PRELIMINARY)
RELATIVE TOTAL PRESSURE LOSS AT MIDGAP (K=22)
PTR=[PT_REL(IN AVE) - PT_REL]/PT_REL(IN AVE)

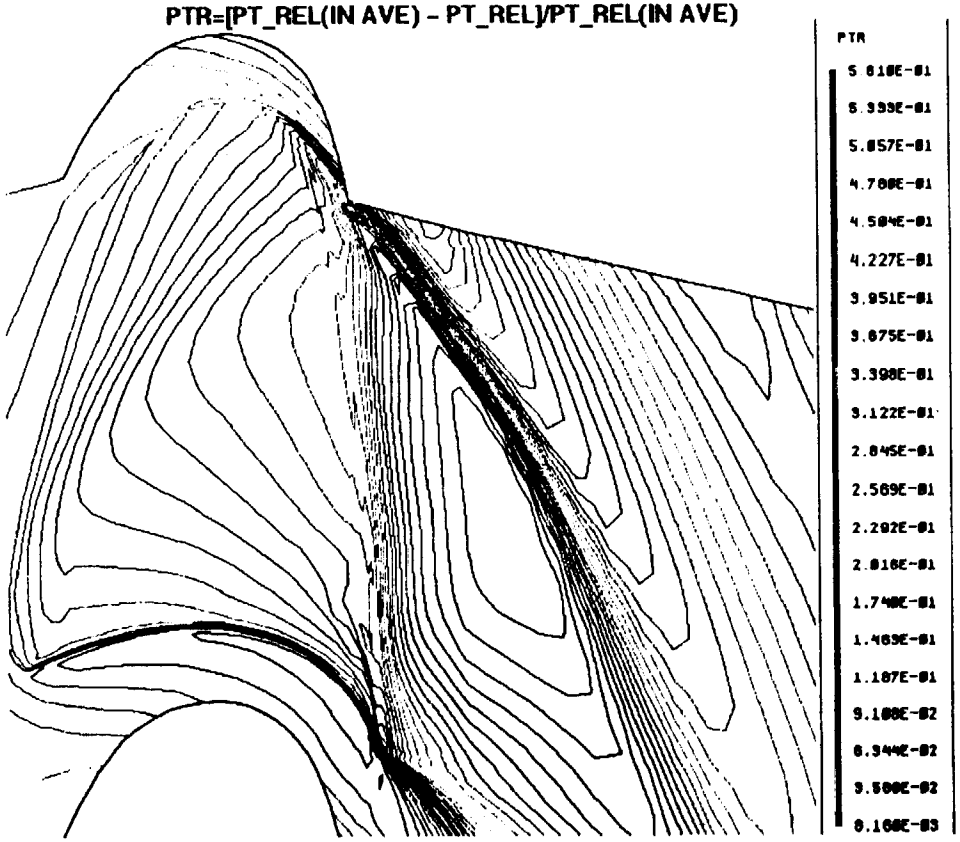

GenCorp Aerojet

GGOT TOTAL PRESSURE LOSS/ GRID DEPENDENCY STUDY

Propulsion Division

GRID EMBEDDING IN TIP GAP
RELATIVE TOTAL PRESSURE LOSS AT MIDGAP (K=22)
PTR=[PT_REL(IN AVE) - PT_REL]/PT_REL(IN AVE)

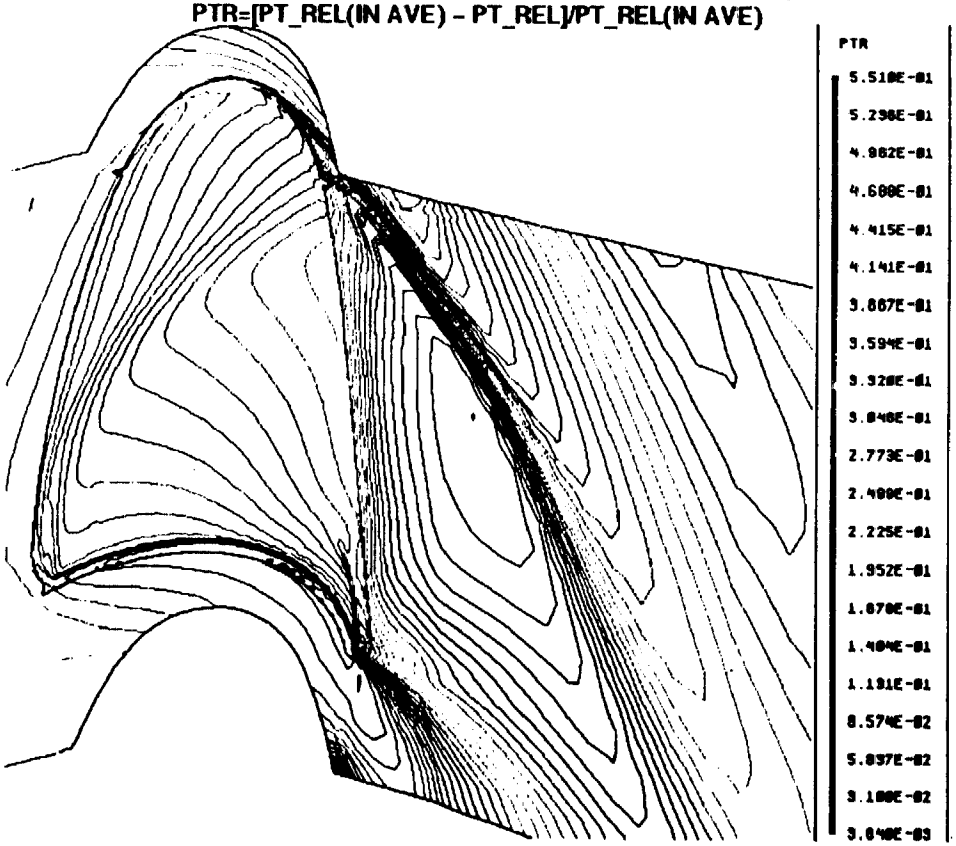

GENCORP AEROJET

GGOT TOTAL PRESSURE LOSS/ GRID DEPENDENCY STUDY

Propulsion Division

TRAILING EDGE GRID EMBEDDING NEAR HUB PLANE (K=2)
EMBEDDING HELPS TO RESOLVE SUCTION SIDE RECIRC

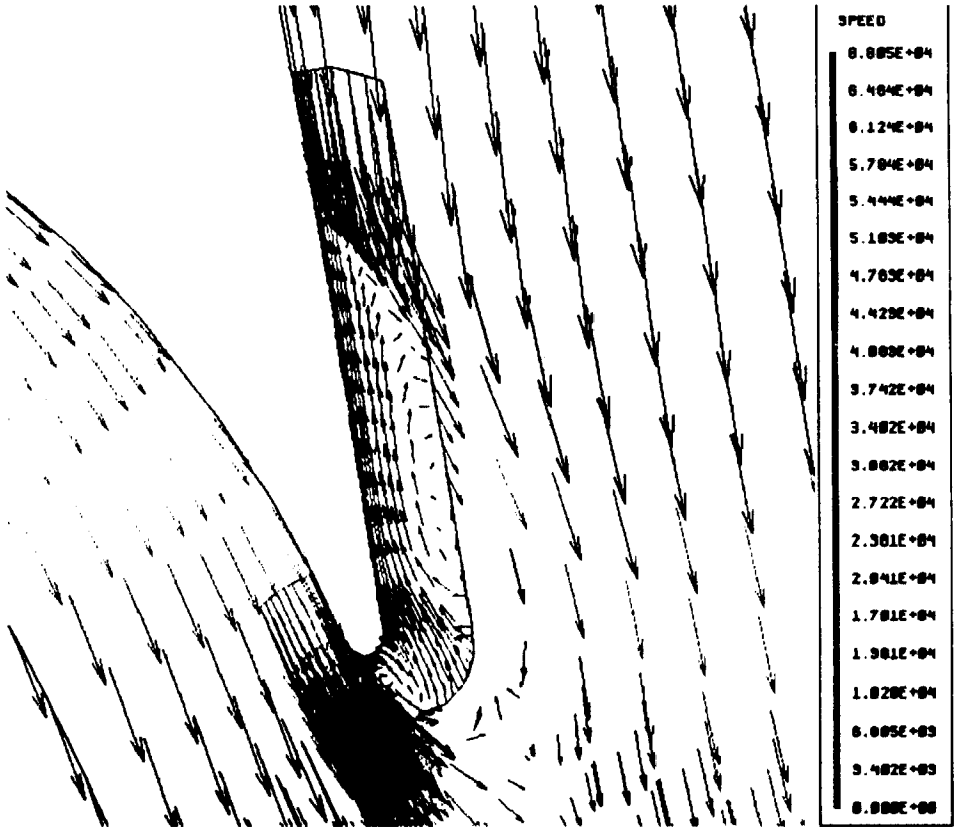

GENCORP AEROJET

Propulsion Division

GGOT TOTAL PRESSURE LOSS/ GRID DEPENDENCY STUDY

BASELINE TRAILING EDGE GRID NEAR HUB PLANE (K=2)

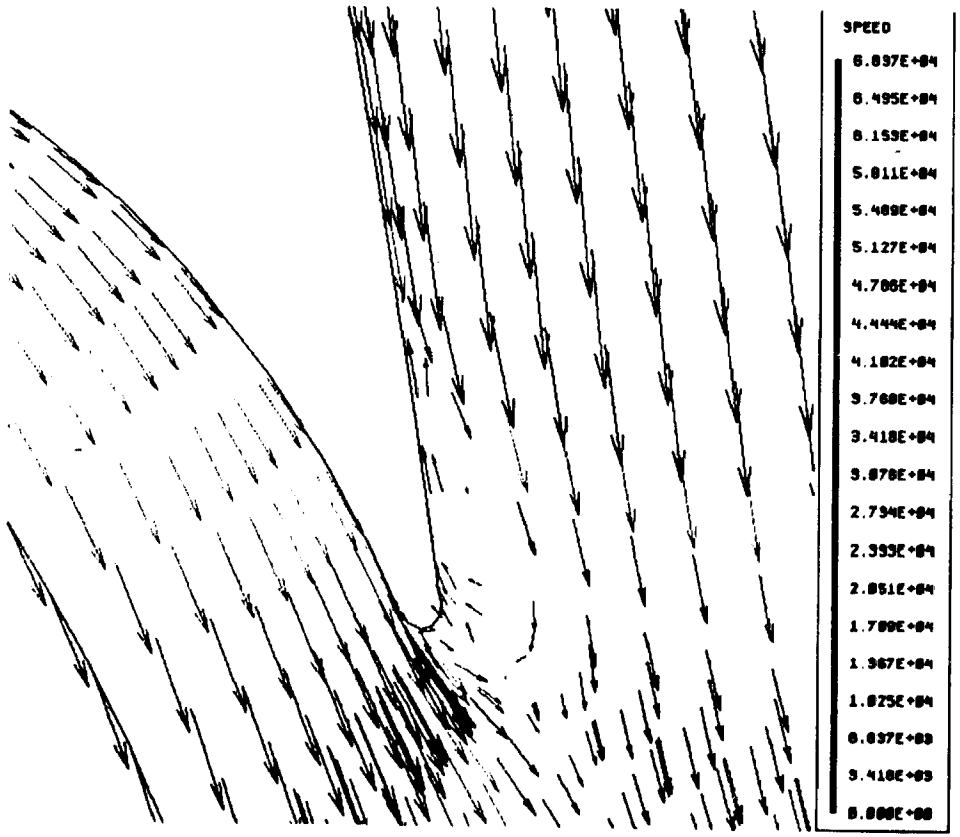

GENCORP AEROJET

Propulsion Division

GGOT TOTAL PRESSURE LOSS/ GRID DEPENDENCY STUDY

GRID EMBEDDING RESULTS

CASE	PT REL (INLET) [PSI]	PT REL (EXIT) [PSI]	DPT REL [PSI]	PLOSS= DPT REL/PT REL (INLET)	PLOSS/ PLOSS BASE
BASE	457.498	365.800	91.698	0.2004	1.0000
LEADING EDGE	458.104	369.822	88.282	0.1927	0.9614
TIP GAP	458.554	370.401	88.152	0.1922	0.9589
TRAILING EDGE	458.292	369.162	89.130	0.1945	0.9704

NOTE: ALL PRESSURES ARE BASED ON MASS-AVERAGED VALUES

EXIT STATIC PRESSURE USED FOR PRELIMINARY PARAMETERICS
BASED ON STATIC PRESSURE SPECIFIED AT ONE NODE IN EXIT PLANE
(PS=215.5 PSI AT CENTER OF EXIT PLANE)

GENCORP AEROJET

GGOT TOTAL PRESSURE LOSS/ -GRID DEPENDENCY STUDY

Propulsion Division

TWO-LAYER TURBULENCE MODEL

RESULTS PRESENTED THUS FAR ARE BASED ON THE STANDARD K-E TURBULENCE MODEL WHICH EMPLOYS WALL FUNCTIONS TO MODEL THE VISCOUS NEAR-WALL LAYER. THE ADVANTAGE OF THIS APPROACH IS THAT THE WALL FUNCTION ELIMINATES THE NECESSITY OF NUMERICALLY RESOLVING THE LARGE GRADIENTS IN THE THIN NEAR-WALL REGION, THUS CONSERVING COMPUTER RESOURCES. THE DISADVANTAGE IS THAT CERTAIN ASSUMPTIONS MUST BE MADE WHICH MAY NOT BE ACCURATE IN ALL FLOW SITUATIONS, ESPECIALLY WHERE THERE ARE SEPERATED FLOWS.

THE TWO-LAYER TURBULENCE MODEL EMPLOYS THE STANDARD TWO-EQUATION K-E MODEL AWAY FROM THE NEAR WALL REGION, AND USES A ONE-EQUATION TURBULENCE MODEL IN THE NEAR-WALL REGION. IN ORDER TO CORRECTLY APPLY THE TWO-LAYER MODEL, NODES MUST BE CLUSTERED NEAR THE WALLS SUCH THAT THE DAMPING FUNCTIONS fmu AND feps (USED TO CALCULATE TURBULENT VISCOSITY AND DISSIPATION RATE) CAN BE RESOLVED. IT IS RECOMMENDED THAT AT LEAST 5 NODES BE IN THE REGION YPLUS < 5 AND AT LEAST 15 NODES IN THE REGION YPLUS < 100.

STATUS: MODEL IS CURRENTLY RUNNING. CONVERGENCE DIFFICULTIES HAVE BEEN ENCOUNTERED, PROBABLY RELATED TO HIGH ASPECT RATIOS (~ 25000 AT BLADE SURFACE AT MID-SPAN). SOLUTIONS BEING EXAMINED INCLUDE INCREASING NODE COUNT IN RADIAL DIRECTION, RUNNING CODE IN DOUBLE PRECISION.

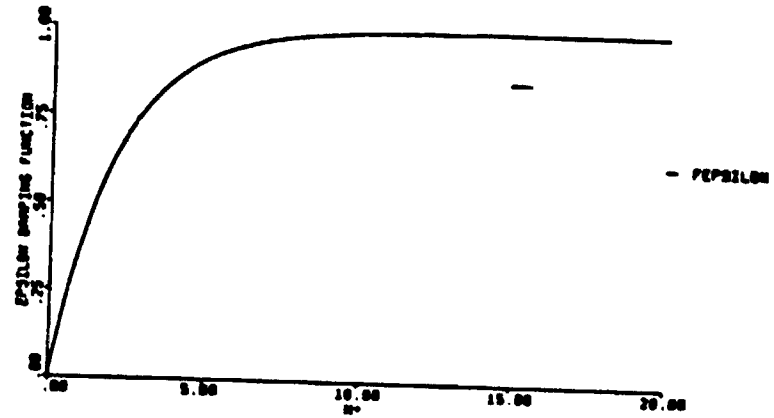

Figure 39: f_ϵ versus n^+

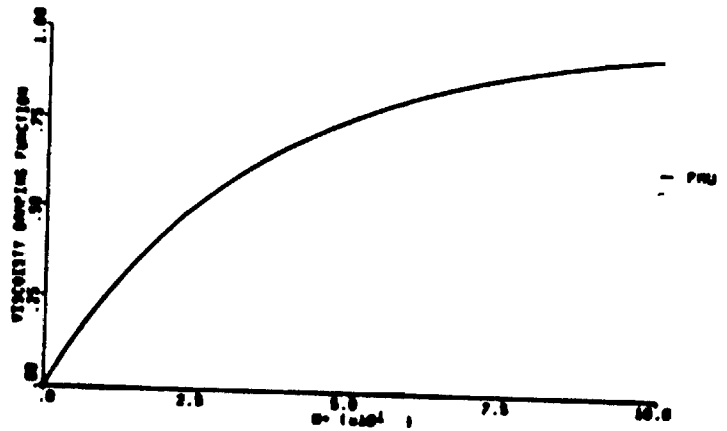

Figure 40: f_μ versus n^+

GENCORP AEROJET

GGOT TOTAL PRESSURE LOSS/ GRID DEPENDENCY STUDY

Propulsion Division

TWO-LAYER TURBULENCE MODEL

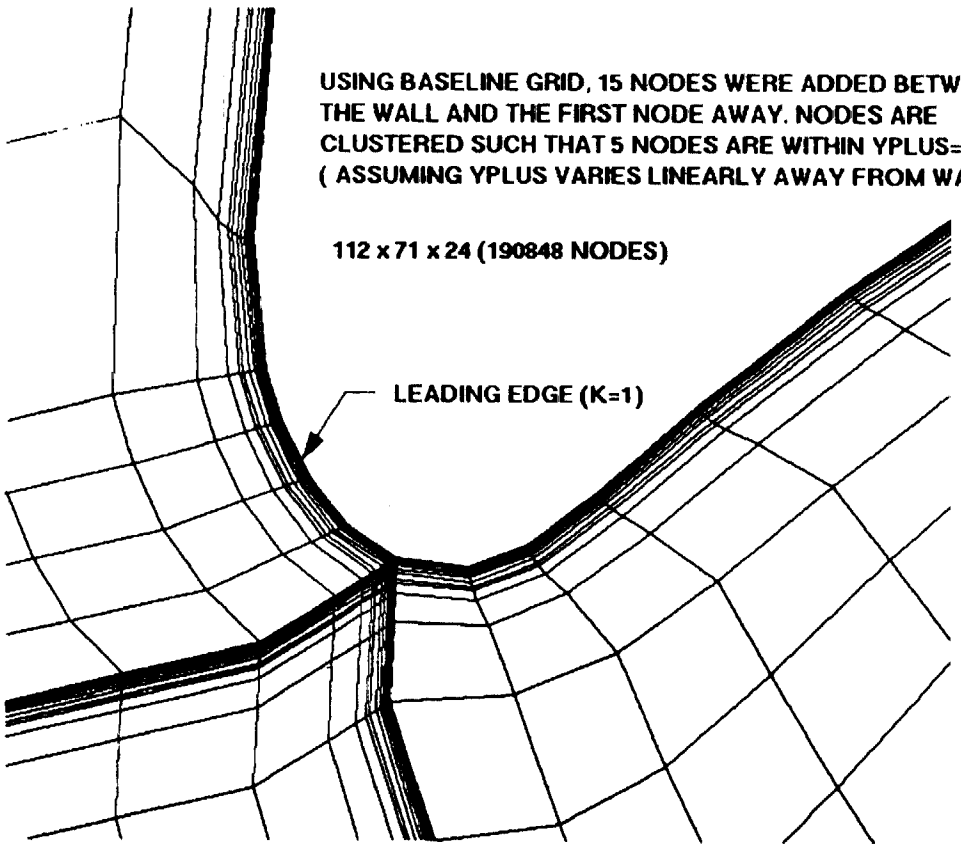

GENCORP AEROJET

GGOT TIP TREATMENT EVALUATION STUDY

Propulsion Division

IN ORDER TO QUANTIFY THE BENEFITS OF POSSIBLE TIP TREATMENTS, THE BASELINE GRID WAS RUN AT ZERO GAP AND AT A MAXIMUM GAP OF 0.030 IN. THE NODE COUNT IN THE TIP GAP FOR THE MAX CLEARANCE CASE WAS INCREASED FROM 5 TO 11 FOR A GRID DIMENSION OF 82 x 41 x 30.

CASE	CLEARANCE [IN]	PLOSS	PLOSS/PLOSS NOM.
ZERO GAP	0.	0.1572	0.8912
NOM. GAP	0.015	0.1764	1.
MAX GAP	0.030	0.1810	1.0261

AS A RESULT OF THE GRID DEPENDENCY STUDY , THE AMOUNT OF VARIATION IN PRESSURE LOSS CALCULATED WAS +/- 4 % . IN ORDER TO ADEQUATELY ASSESS DIFFERENT TIP TREATMENTS, THE FOLLOWING PROCEDURES ARE SUGGESTED:

1.) SIMILAR GRIDS FOR ASSESSING TIP TREATMENTS SHOULD BE USED, WHEN POSSIBLE.
2.) TIP TREATMENT CASES SHOULD BE FIRST EVALUATED AT THE MAXIMUM GAP (0.030 IN) IN ORDER TO MAXIMIZE DIFFERENCES BETWEEN DIFFERENT TREATMENTS. GOOD TIP TREATMENT CANDIDATES WILL THEN BE ASSESSED AT THE NOMINAL CLEARANCE.

GIVEN THE RELATIVELY LARGE SURFACE AREA AT THE BLADE TIP, A PROMISING METHOD FOR REDUCING TIP LEAKAGE MAY BE TO CREATE A POCKETED SURFACE ON THE ROTOR TIP, SIMILAR TO A LABYRINTH SEAL.

IN ORDER TO DETERMINE THE SENSITIVE PARAMETERS INVOLVED, IT IS USEFUL TO EXAMINE A LABYRINTH SEAL FLOW EQUATION. THE FOLLOWING IS A METHOD PROPOSED BY VERMES (1961) WHICH IS A MODIFICATION OF MARTIN'S FORMULA FOR LABYRINTHS:

W=5.76 * K * A * PO * BETA/[R * TO * (1-ALPHA)]**.5

W=WEIGHT FLOW [LB/SEC]
K = f(RE, L/C) - CLEARANCE FACTOR OF SINGLE ANNULAR ORIFICE
A=ANNULAR ORIFICE FLOW AREA [IN**2]
PO=UPSTREAM TOTAL PRESSURE [PSI]
TO=UPSTREAM TOTAL TEMPERATURE [DEG R]
ALPHA=8.52/[(P-L)/C+7.23] - RESIDUAL ENERGY FACTOR
P=DISTANCE BETWEEN TEETH [IN]
L=TOOTH TIP WIDTH [IN]
C=CLEARANCE [IN]
BETA={[1-(PN/PO)**2]/[N-LN(PN/PO)]}**.5 - GLAND FACTOR
PN=STATIC PRESSURE AT EXIT OF LAST TOOTH [PSI]
N=NUMBER OF TEETH
R=GAS CONSTANT FT/DEG R

GENCORP AEROJET

GGOT TIP TREATMENT EVALUATION STUDY

Propulsion Division

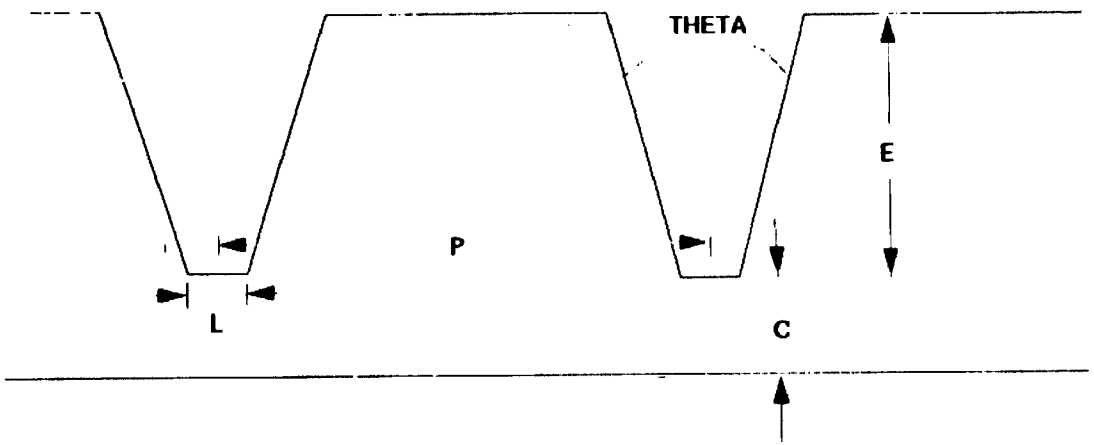

LABYRINTH GEOMETRY DEFINITION

GENCORP AEROJET

GGOT TIP TREATMENT EVALUATION STUDY

Propulsion Division

ASSUMING PRESSURES, TEMPERATURES, SEAL CLEARANCE AND TOTAL SEAL LENGTH ARE DEFINED, THE REMAINING DESIGN PARAMETERS ARE NUMBER OF TEETH AND TOOTH WIDTH. ASSUMING MINIMUM TOOTH WIDTH (DETERMINED BASED ON STRUCTURAL REQUIREMENTS), THE ONLY REMAINING PARAMETER WHICH MAY BE MODIFIED IS THE NUMBER OF TEETH

THE VERMES FORMULA MAY BE HELPFUL IN TERMS OF A 1-D APPROACH IN DETERMINING THE APPROXIMATE NUMBER OF TEETH NECESSARY AND THEIR LOCATION IN ORDER TO MINIMIZE TIP LEAKAGE AS APPLIED TO THE GGOT. DUE TO THE COMPLICATED NATURE OF THE FLOW IN THE TIP GAP WITH THE COUNTER-ROTATING ENDWALL RETARDING THE FLOW THROUGH THE GAP, THE VERMES FORMULA WOULD PROBABLY NOT BE VERY USEFUL IN PREDICTING THE ACTUAL TIP LEAKAGE.

AS AN EXAMPLE APPLIED TO THE GGOT , A TYPICAL STREAMLINE STARTING NEAR THE LEADING EDGE IS SELECTED FROM THE MAX CLEARANCE CASE. THE ASSUMED PARAMETERS ARE:

L=.030 IN C=.030 IN PO=419.5 PSI PN=197.8 TO=1261.2 LTOT=0.927 IN

NTEETH	PITCH	ALPHA	BETA	MDOT (NORM.)	
2	0.927	0.2295	0.5316	1.0	
3	0.463	0.3931	0.4553	0.9651	
4	0.309	0.5155	0.4046	0.9597	◄ OPTIMAL TOOTH NUMBER
5	0.232	0.6106	0.3677	0.9731	
6	0.185	0.6866	0.3394	1.0012	

GENCORP AEROJET

GGOT TIP TREATMENT EVALUATION STUDY

Propulsion Division

VALIDATION CASE FOR LABYRINTH SEAL BASED ON VERMES TEST DATA

FLUID: AIR

L=0.015 IN
E=0.25 IN
P=0.25 IN
C=0.030 IN
R=5 IN
THETA=14 DEG
NTEETH=10

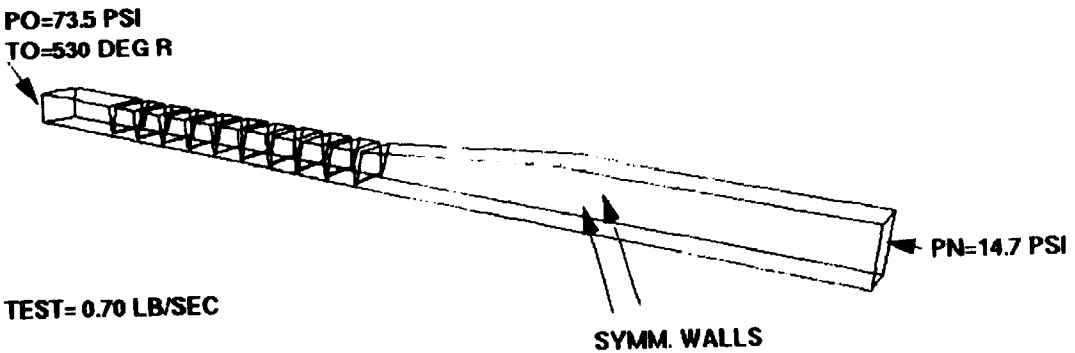

MDOT TEST= 0.70 LB/SEC

MDOT CFD = 0.91 LB/SEC

GENCORP AEROJET

GGOT TIP TREATMENT EVALUATION STUDY

Propulsion Division

VALIDATION CASE FOR LABYRINTH SEAL BASED ON VERMES TEST DATA

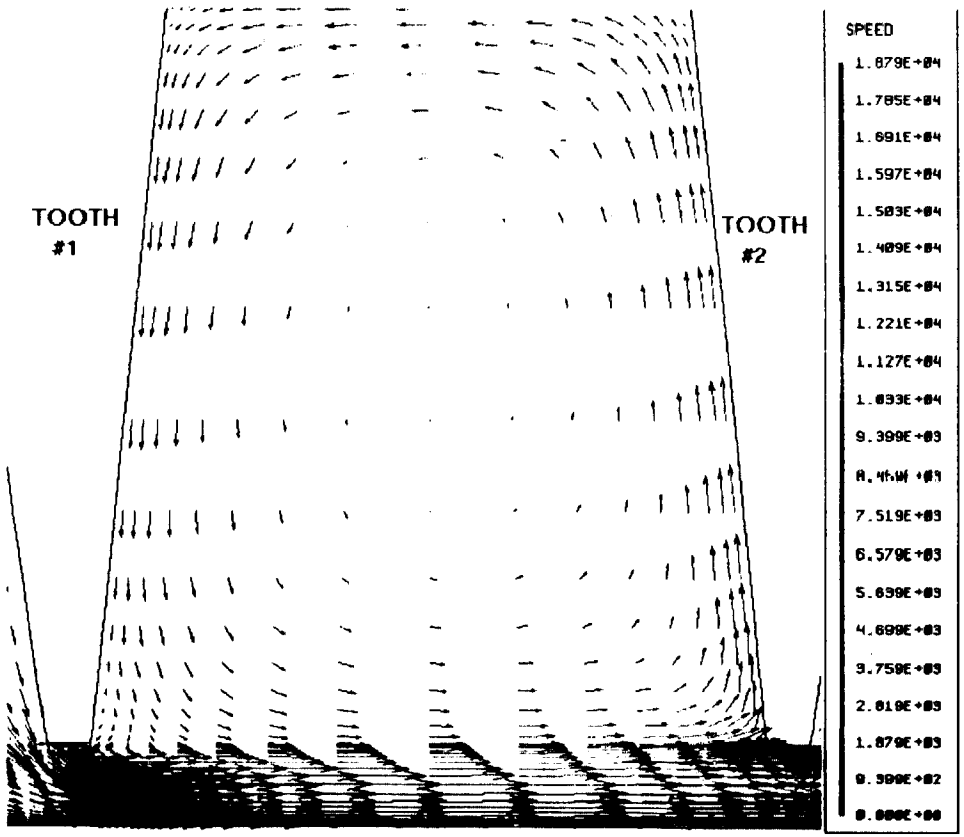

GRID SIZE = 312 x 37 x 3

FIRST CAVITY

GENCORP AEROJET

GGOT TIP TREATMENT EVALUATION STUDY

Propulsion Division

VALIDATION CASE FOR LABYRINTH SEAL BASED ON VERMES TEST DATA

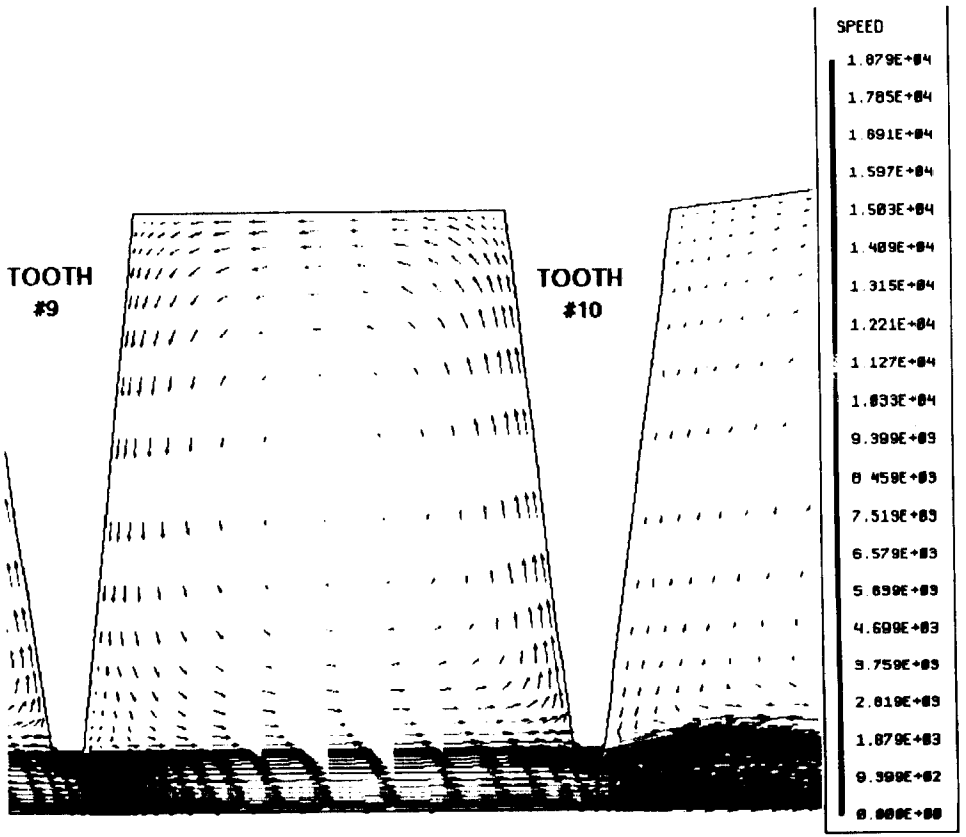

GRID SIZE = 312 x 37 x 3

LAST CAVITY

GENCORP AEROJET

GGOT TIP TREATMENT EVALUATION STUDY

Propulsion Division

CURRENT STATUS:

1.) **RUNNING HOLLOW BLADE CASE (TWO-TOOTH LABYRINTH)**

- **104 x 62 x 30 (10 NODES IN TIP GAP RADIAL DIRECTION)**
- **0.030 IN WALL THICKNESS WITH 0.030 IN TIP CLEARANCE. HOLLOW PORTION OF BLADE EXTENDS FROM MIDSPAN TO TIP.**
- **RESULTS WILL BE COMPARED WITH SOLID BLADE TO ASSESS BENEFITS IN TERMS OF LOSS REDUCTION/ REDUCED LEAKAGE.**

2.) **CONSTRUCTING ROTOR GRID FOR BASELINE MULTI-TOOTH LABYRINTH TIP SEAL (USING GRID EMBEDDING)**

- **PARAMETERICS WILL BE NECESSARY TO OPTIMIZE DESIGN**

3.) **INVESTIGATING OTHER TIP TREATMENTS WHICH MAY REDUCE RELATIVE TOTAL PRESSURE LOSSES**

- **SUCTION SIDE TRAILING EDGE SLOT TO PROVIDE FLOW GUIDANCE (TO REDUCE IMPINGEMENT ANGLE OF TIP LEAKAGE FLOW ON MAINSTREAM FLOW)**

GENCORP AEROJET

GGOT TIP TREATMENT EVALUATION STUDY

Propulsion Division

PARTIALLY HOLLOW BLADE WITH 0.030 IN WALL THICKNESS
104 x 62 x 30 (10 NODES IN TIP GAP RADIAL DIRECTION)

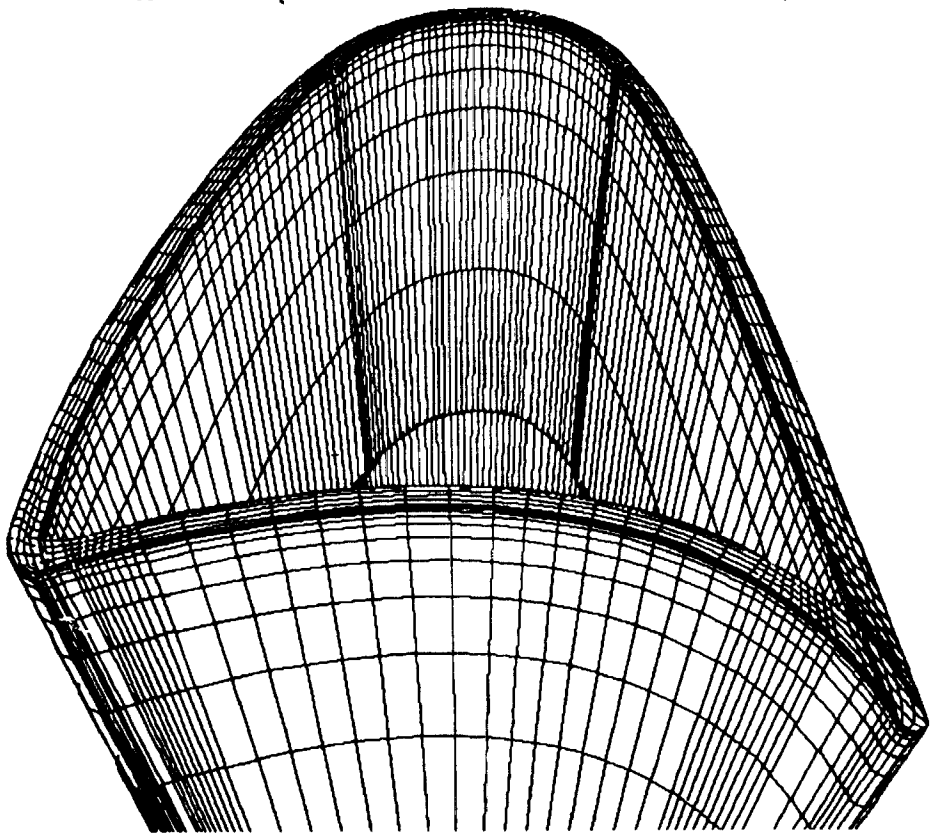

GENCORP AEROJET

GGOT TIP TREATMENT EVALUATION STUDY

Propulsion Division

ALTERNATE TIP TREATMENT METHODS - TRAILING EDGE SUCTION-SIDE SLOT

OBJECTIVE: PROVIDE FLOW GUIDANCE TO REDUCE TIP LEAKAGE IMPINGEMENT ANGLE

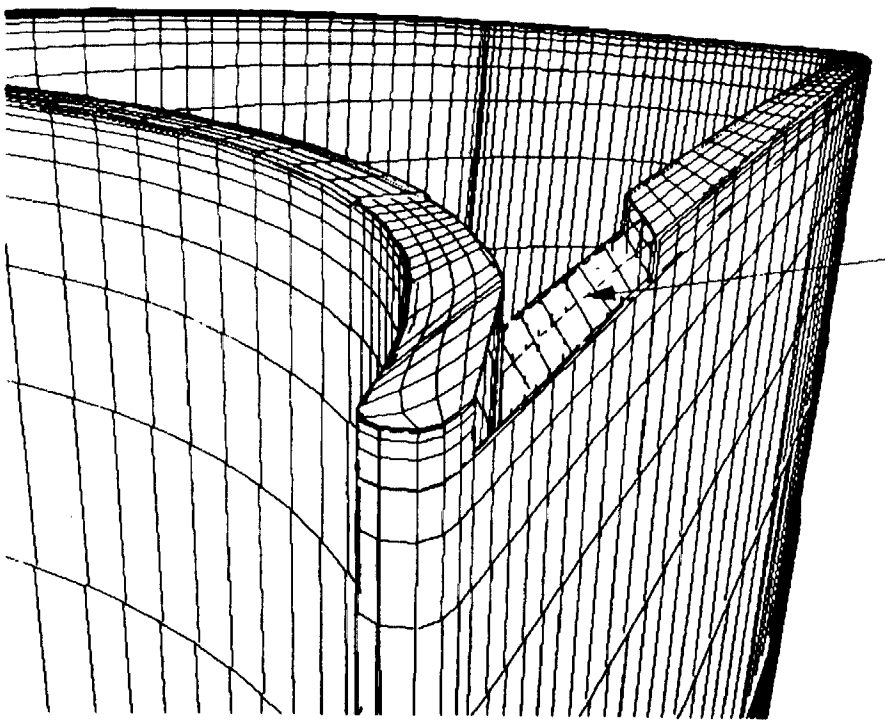

ISSUES:

1. **NEED TO MAXIMIZE SLOT ANGLE TO PROVIDE MAXIMUM GUIDANCE.**
2. **RESISTANCE PATH THOUGH SLOT SHOULD BE LESS THAN OVER TIP TO INDUCE FLOW THROUGH SLOT (FUNCTION OF FLOW AREA).**
3. **SLOT DEPTH SHOULD BE MINIMIZED TO LOCALIZE EFFECTS TO TIP REGION.**

NAVIER-STOKES ANALYSIS OF AN OXIDIZER TURBINE BLADE WITH TIP CLEARANCE WITH AND WITHOUT A MINI-SHROUD†

Tony Chan and Frederik J. de Jong
Scientific Research Associates, Inc.
Glastonbury, CT

Presented at the
Workshop for Computational Fluid Dynamics Applications
in Rocket Propulsion

April 20-22, 1993

ABSTRACT

The Gas Generator Oxidizer Turbine (GGOT) Blade is being analyzed by various investigators under the NASA MSFC-sponsored Turbine Stage Technology Team design effort. The present work concentrates on the tip clearance region flow and associated losses; however, flow details for the passage region are also obtained in the simulations. The present calculations simulate the rotor blade row in a rotating reference frame with the appropriate coriolis and centrifugal acceleration terms included in the momentum equations. The upstream computational boundary is located about one axial chord from the blade leading edge. The boundary conditions at this location have been determined by Pratt & Whitney using an Euler analysis without the vanes to obtain approximately the same flow profiles at the rotor as were obtained with the Euler stage analysis including the vanes. Inflow boundary layer profiles are then constructed assuming the skin friction coefficient at both the hub and the casing. The downstream computational boundary is located about one axial chord from the blade trailing edge, and the circumferentially averaged static pressure at this location was also obtained from the P&W Euler analysis.

Results obtained for the 3-D baseline GGOT geometry at the full scale design Reynolds number show a region of high loss in the region near the casing. Particle traces in the near tip region show vortical flow behavior of the fluid which passes through the clearance region and exits at the downstream edge of the gap. In an effort to reduce clearance flow losses, the mini-shroud concept was proposed by the Pratt & Whitney design team. Calculations were performed on the GGOT geometry with the mini-shroud. Results of these calculations indicate that the mini-shroud does not significantly affect the flow in the passage region, and although the tip clearance flow is different, the mini-shroud does not seem to prevent the above-mentioned vortical flow behavior. Since both flow distortion and total pressure losses are similar for both geometries, the addition of the mini-shroud does not seem to reduce the tip clearance flow effects.

---

† This work was supported by NASA Marshall Space Flight Center under Contract NAS8-38865.

APPROACH

UTILIZE SRA MINT CODE

- GENERAL NON-RECTANGULAR BLOCK STRUCTURE
- SINGLE GRID
- FULL NAVIER-STOKES EQUATIONS
- NO-SLIP WALL BOUNDARY EQUATIONS WITH SUBLAYER RESOLUTION
- ALGEBRAIC MIXING LENGTH TURBULENCE MODEL
- IMPLICIT LINEARIZED BLOCK SOLVER (ADI)

Scientific Research Associates

OXIDIZER TURBINE BASELINE DESIGN

FULL SCALE TURBINE FLOWPATH CLOSE-UP

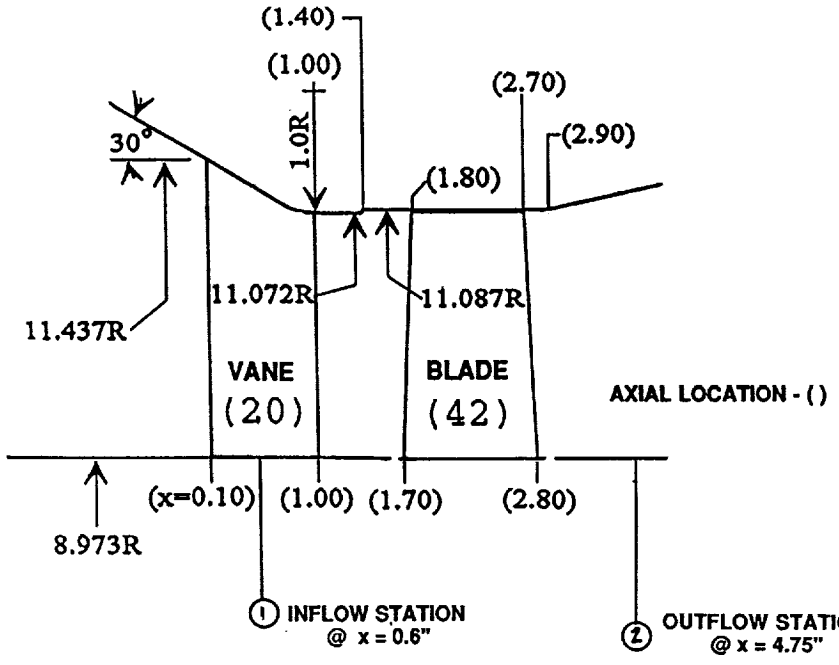

Scientific Research Associates

FLOW PARAMETERS

- SUPPLIED BY P&W DESIGN TEAM
- CIRCUMFERENTIALLY - AVERAGED SPANWISE DISTRIBUTIONS FROM EULER CODE
    - UPSTREAM AXIAL MASS FLUX
    - UPSTREAM TOTAL TEMPERATURE
    - UPSTREAM FLOW ANGLES
    - DOWNSTREAM STATIC PRESSURE
- HUB AND CASING ENDWALL BOUNDARY LAYER PROFILES CONSTRUCTED WITH ASSUMED B. L. THICKNESS δ = 0.03 IN.

Scientific Research Associates

GRID GENERATION

- "FALSE CORNER" GRID STRUCTURE
- 2-D ELLIPTIC GRIDS GENERATED WITH EAGLE

  60 x 90 POINTS IN CROSS-SECTIONAL PLANE
- 3-D GRID CONSTRUCTION

  21 BLADE CROSS-SECTIONAL PLANES

  REDISTRIBUTION IN SPANWISE DIRECTION

  28 POINTS FROM HUB TO TIP

  12 POINTS IN CLEARANCE REGION

Scientific Research Associates

BASELINE GGOT OXIDIZER TURBINE BLADE

HUB SECTION

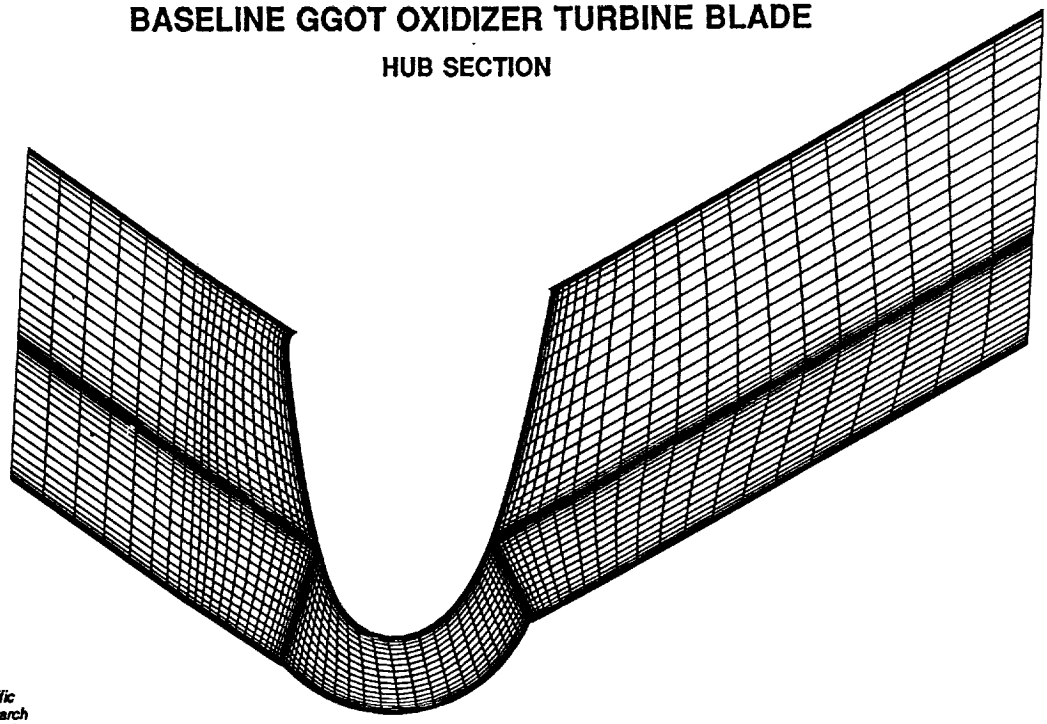

Scientific
Research
Associates

BASELINE GGOT OXIDIZER TURBINE BLADE

MID-SPAN SECTION

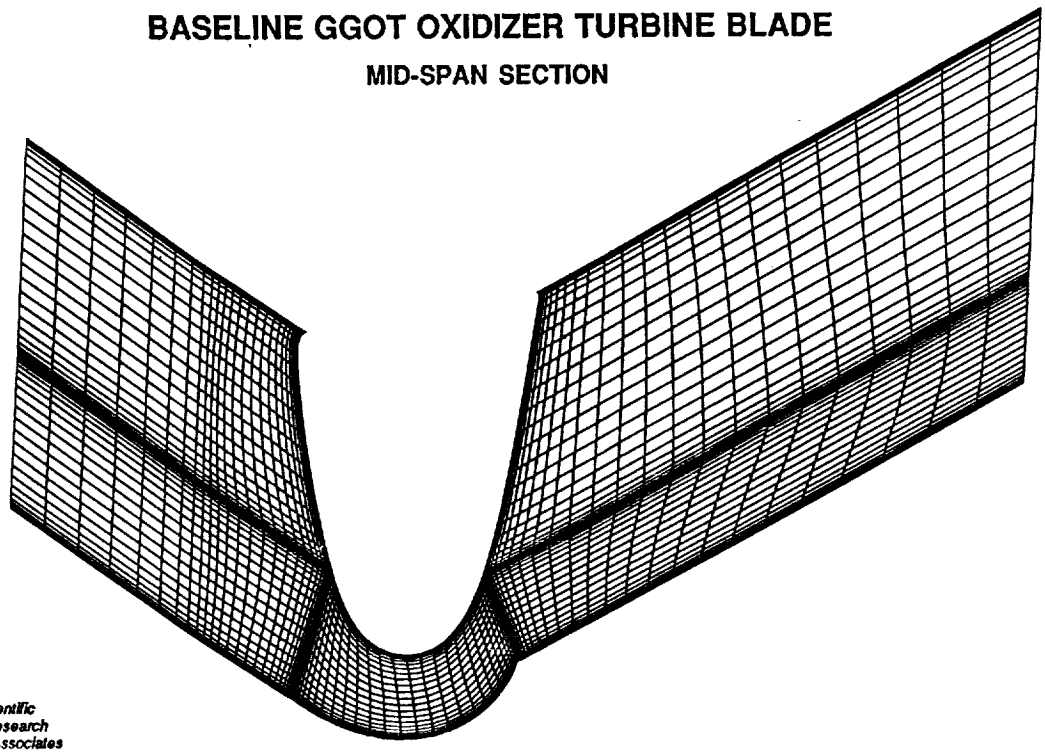

Scientific
Research
Associates

BASELINE GGOT OXIDIZER TURBINE BLADE

TIP SECTION

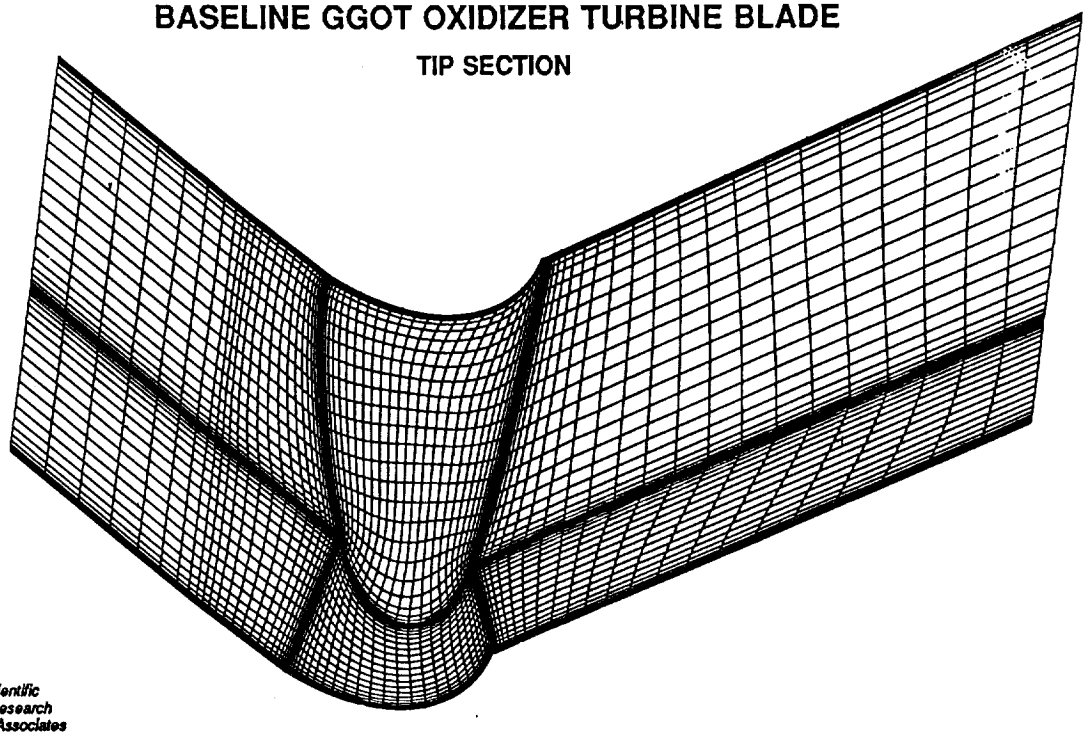

Scientific Research Associates

GGOT OXIDIZER TURBINE BLADE WITH MINI-SHROUD

TIP SECTION

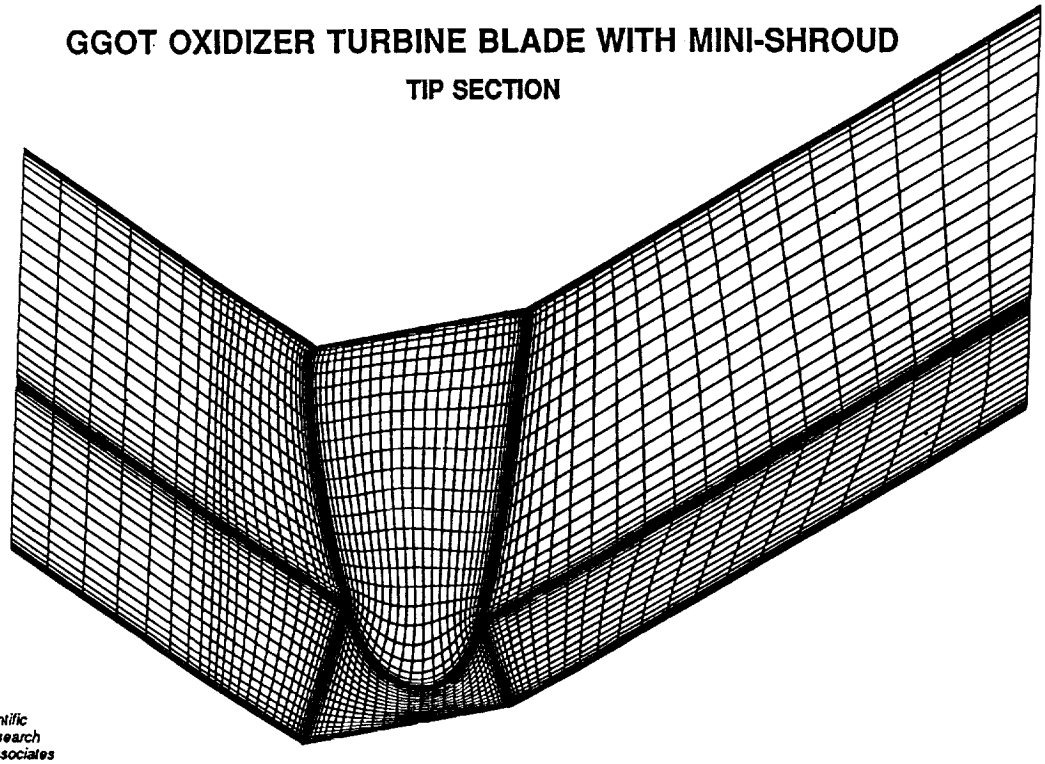

Scientific Research Associates

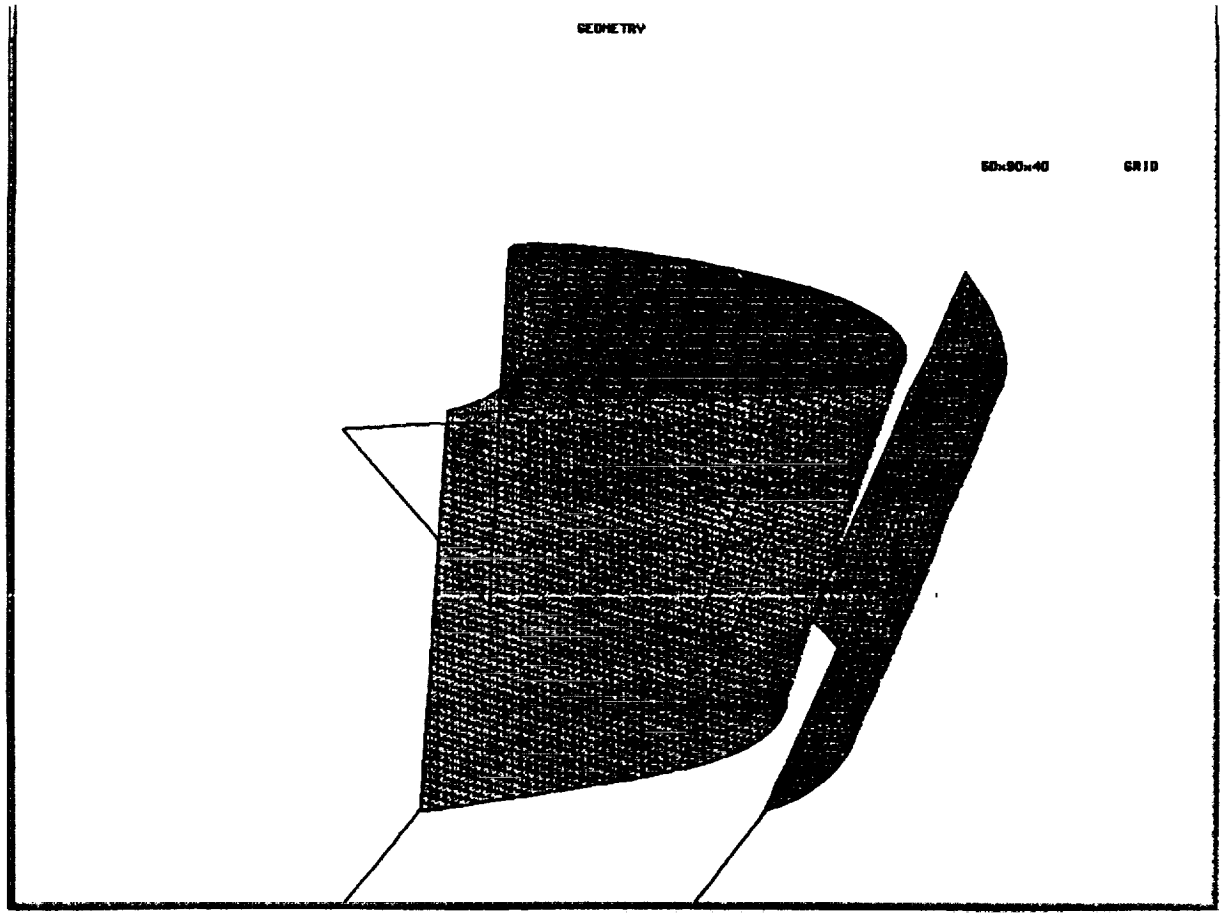
GEOMETRY
60x90x40 GRID

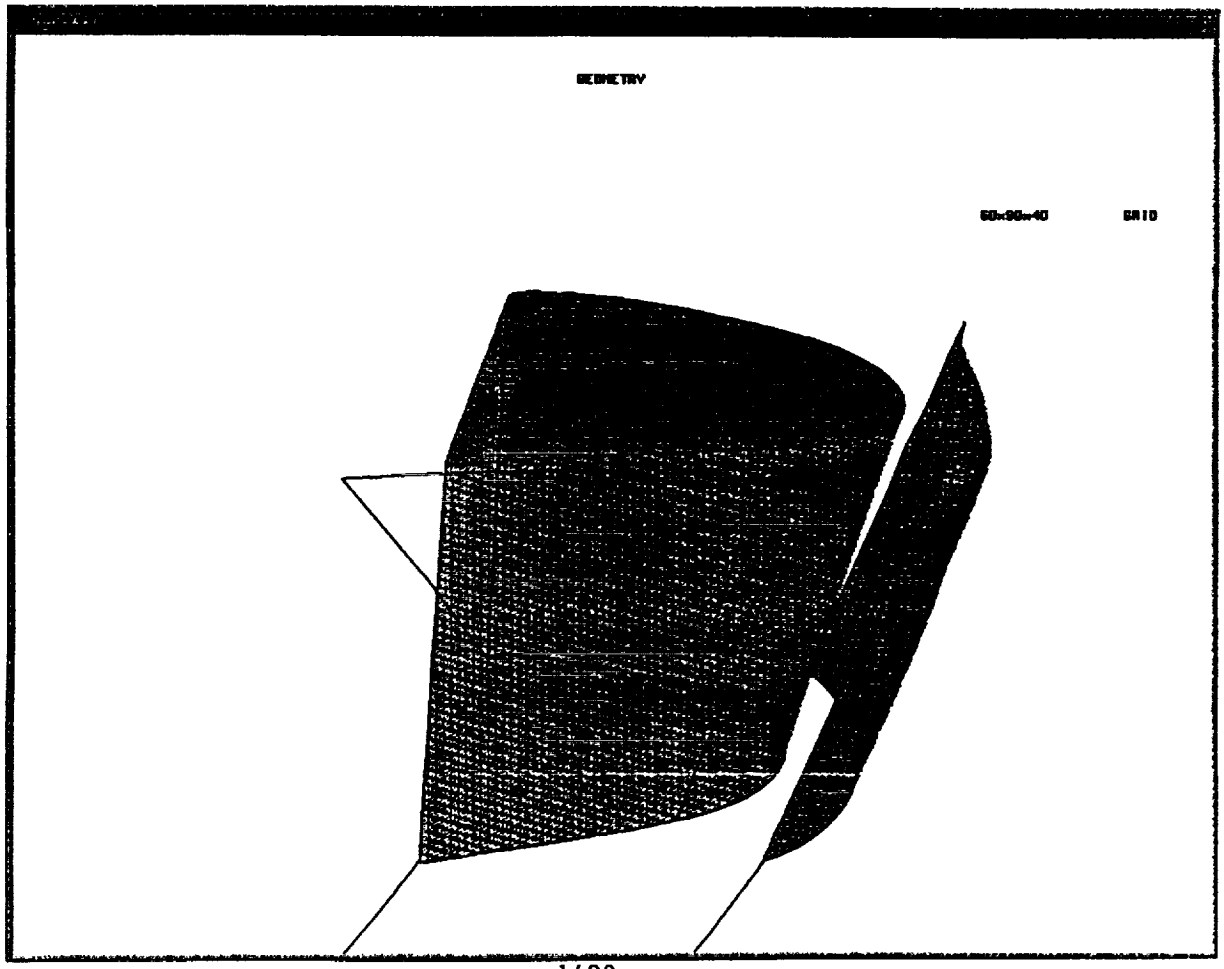
GEOMETRY
60x90x40 GRID

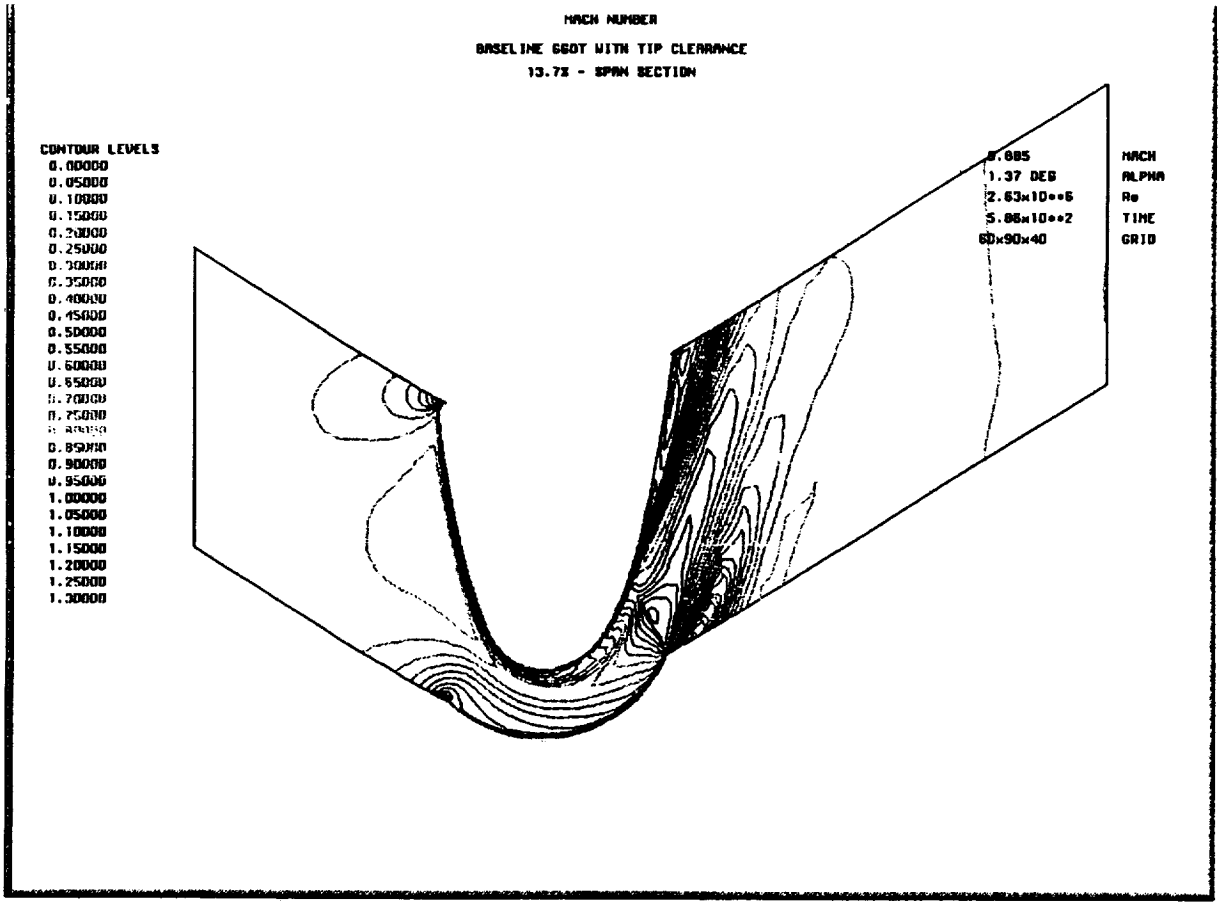

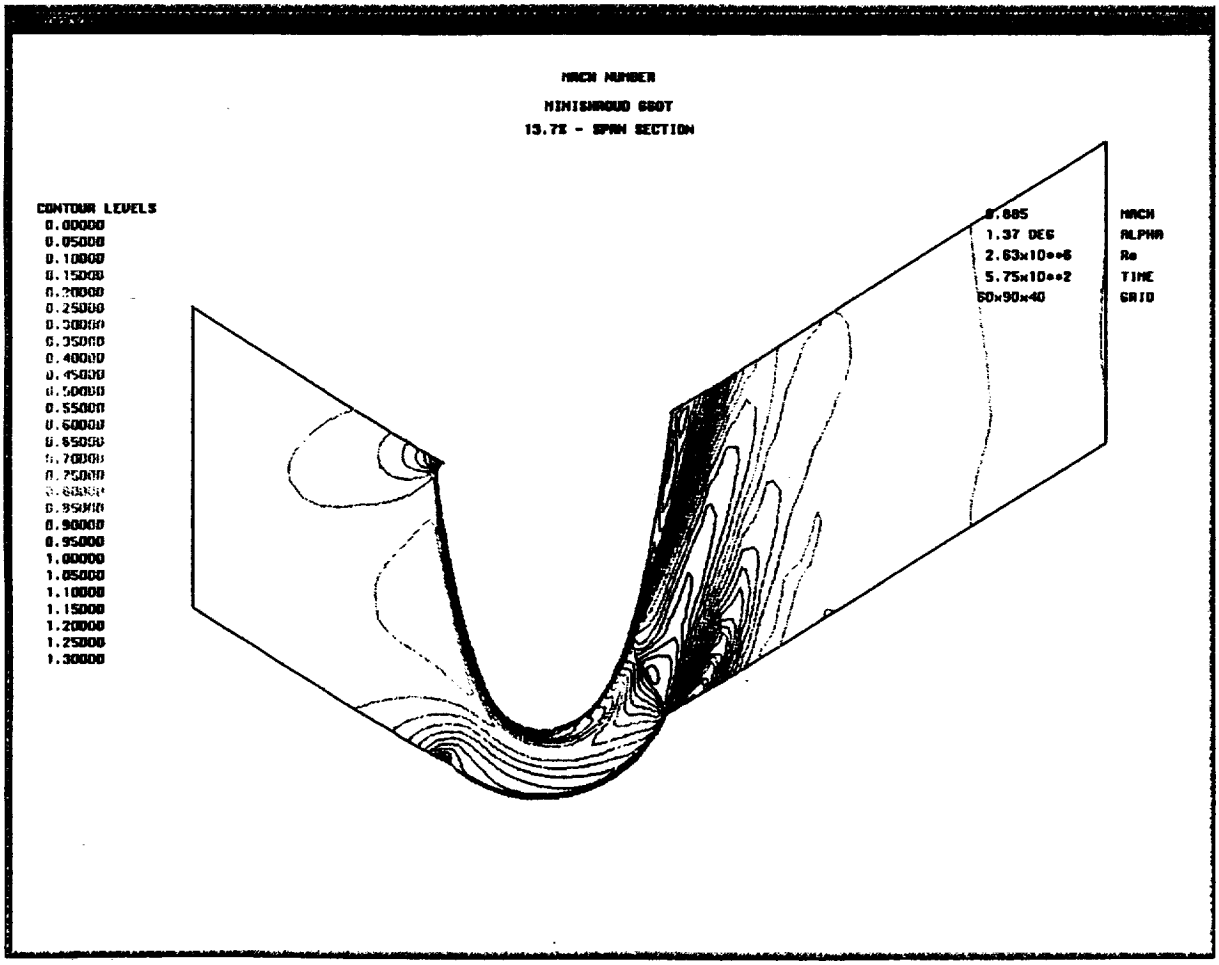

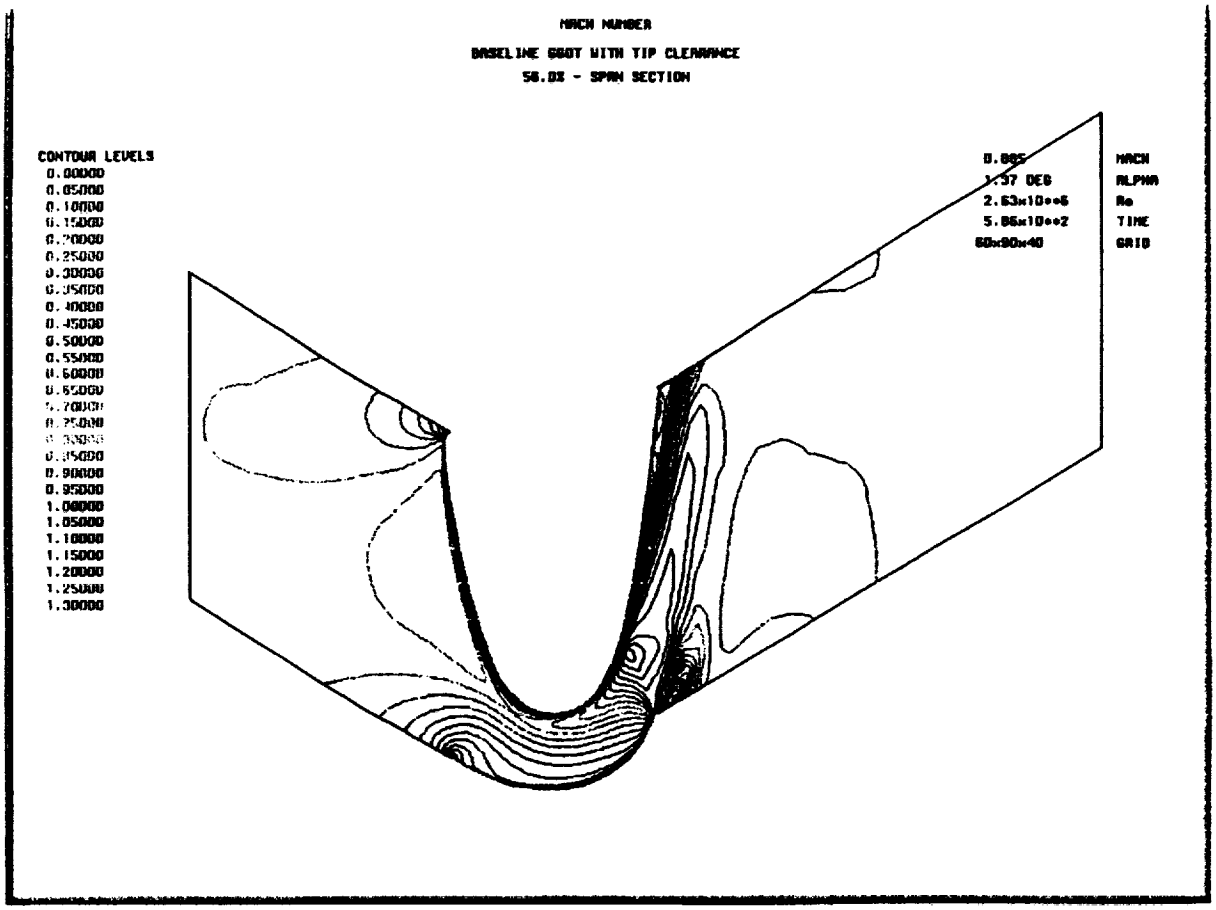

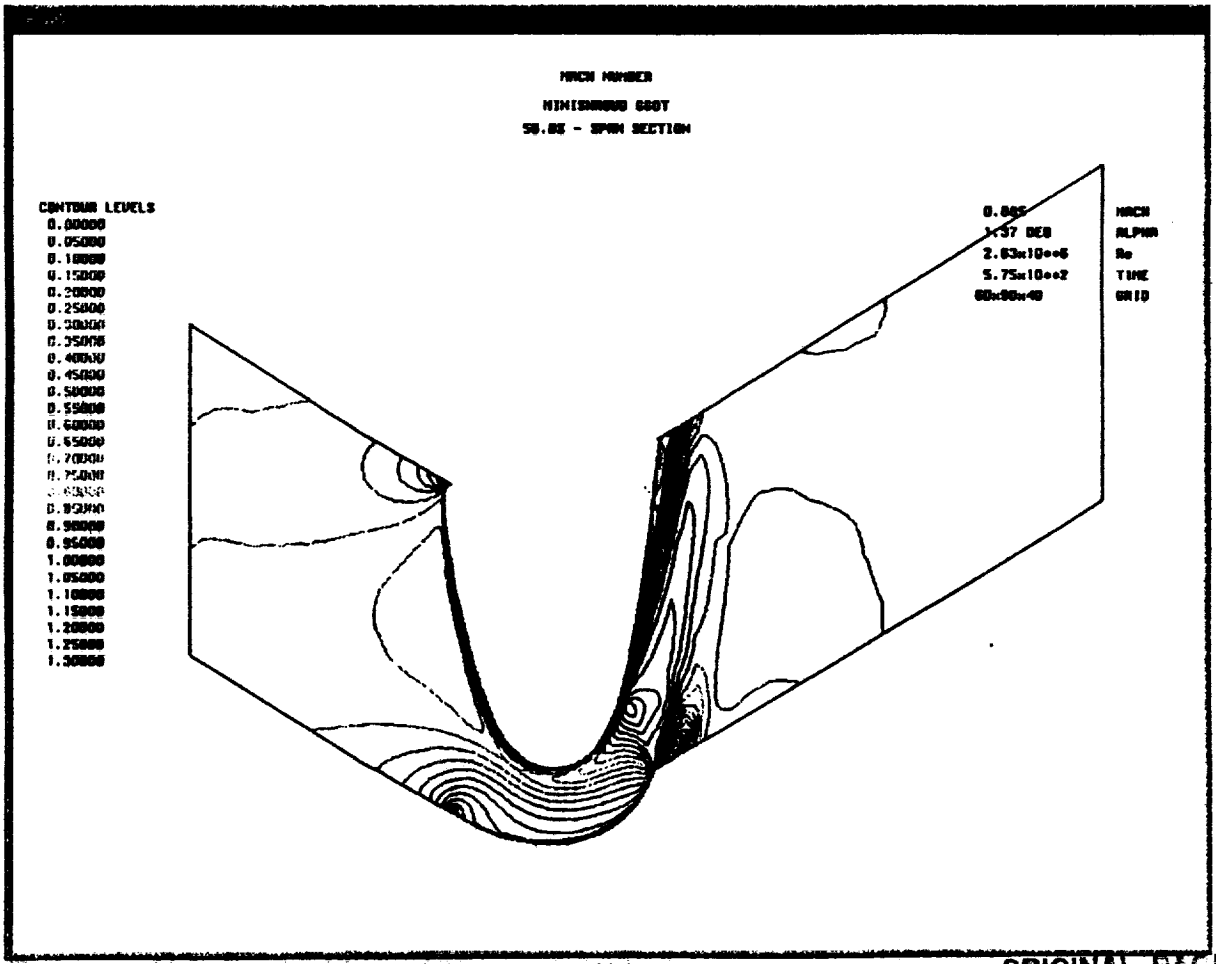

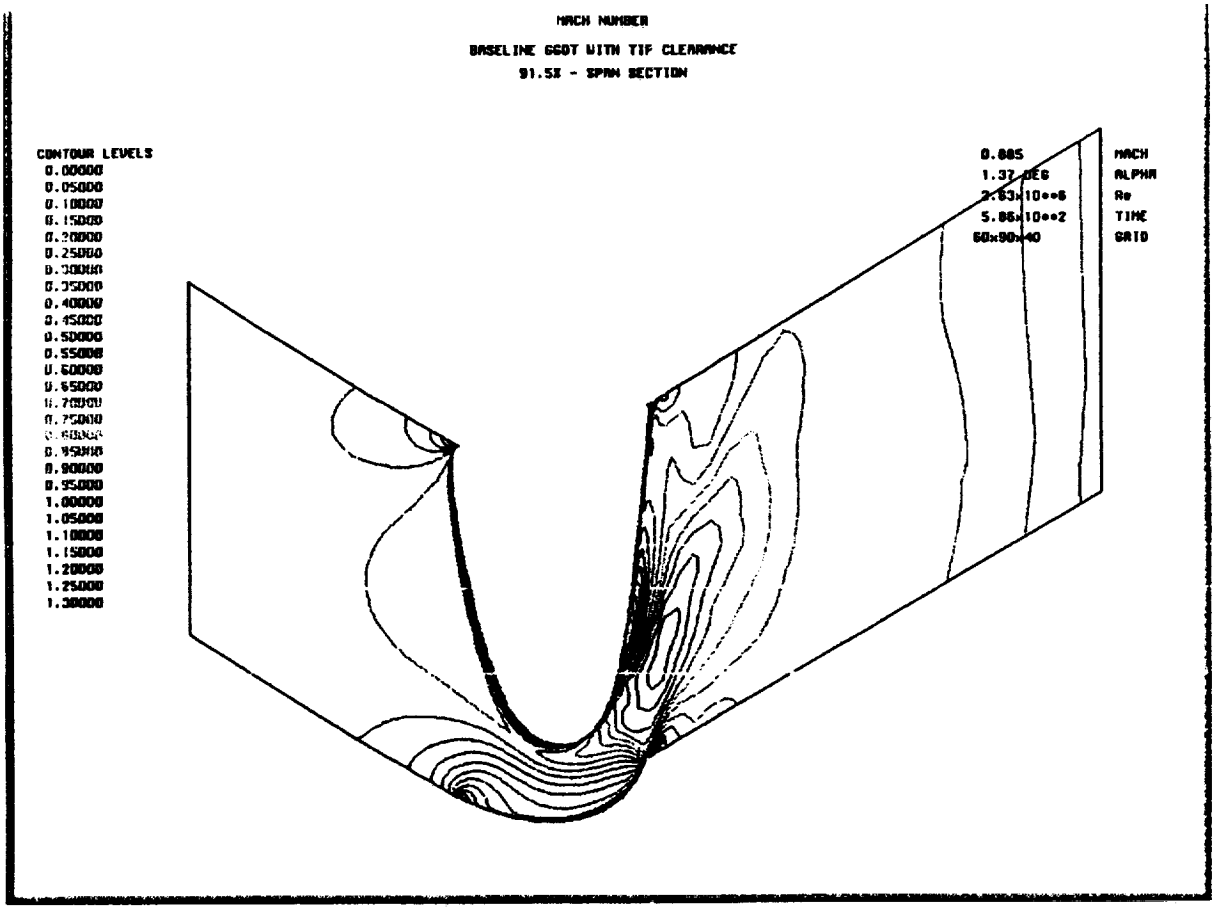

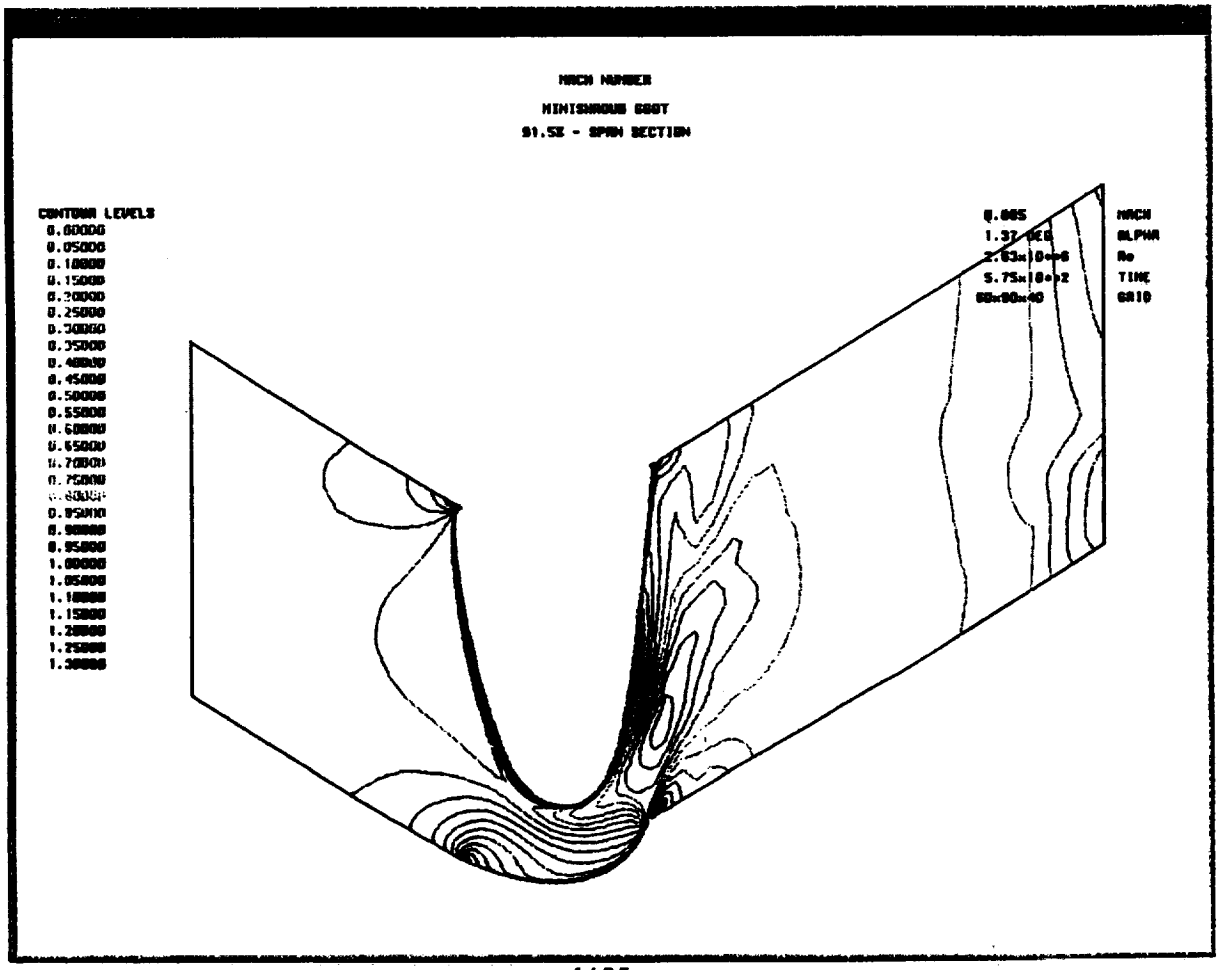

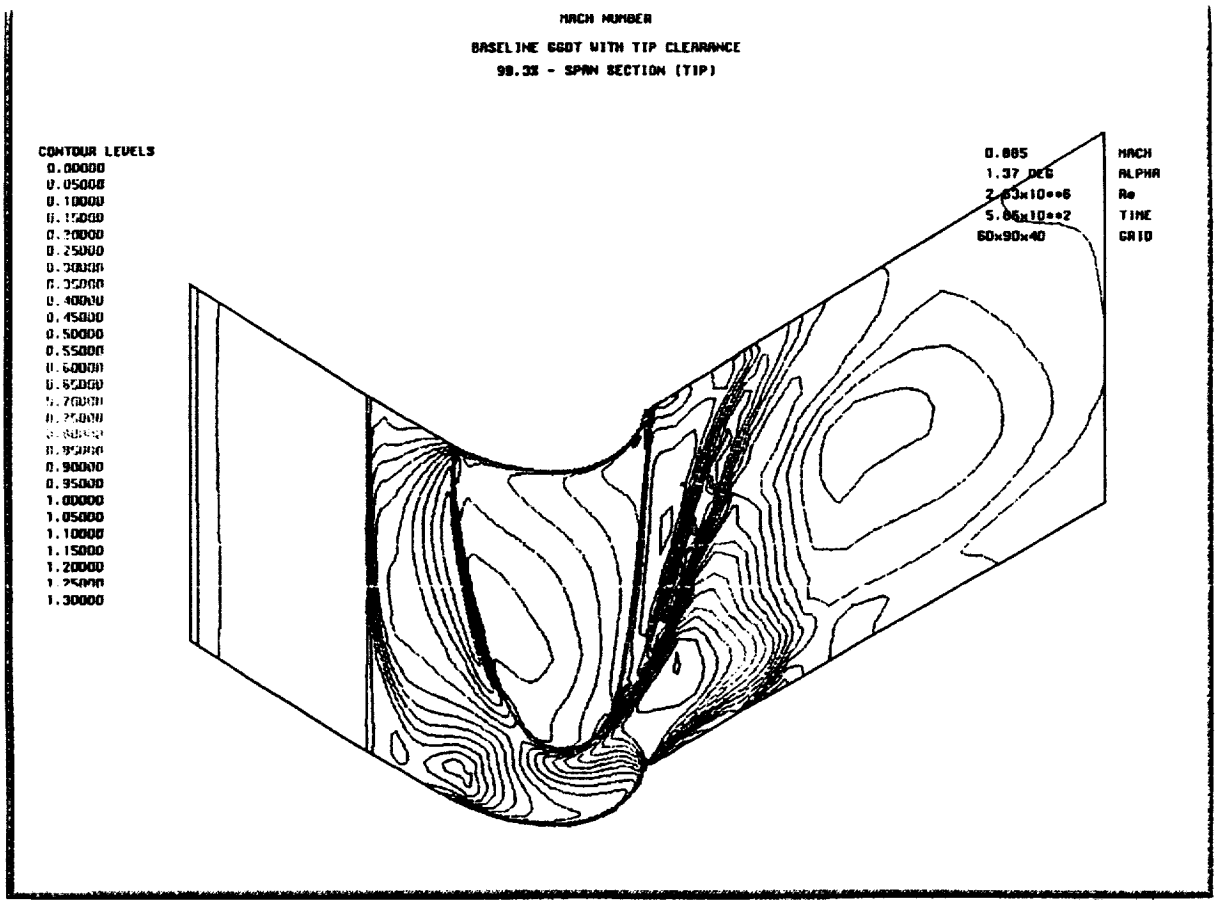

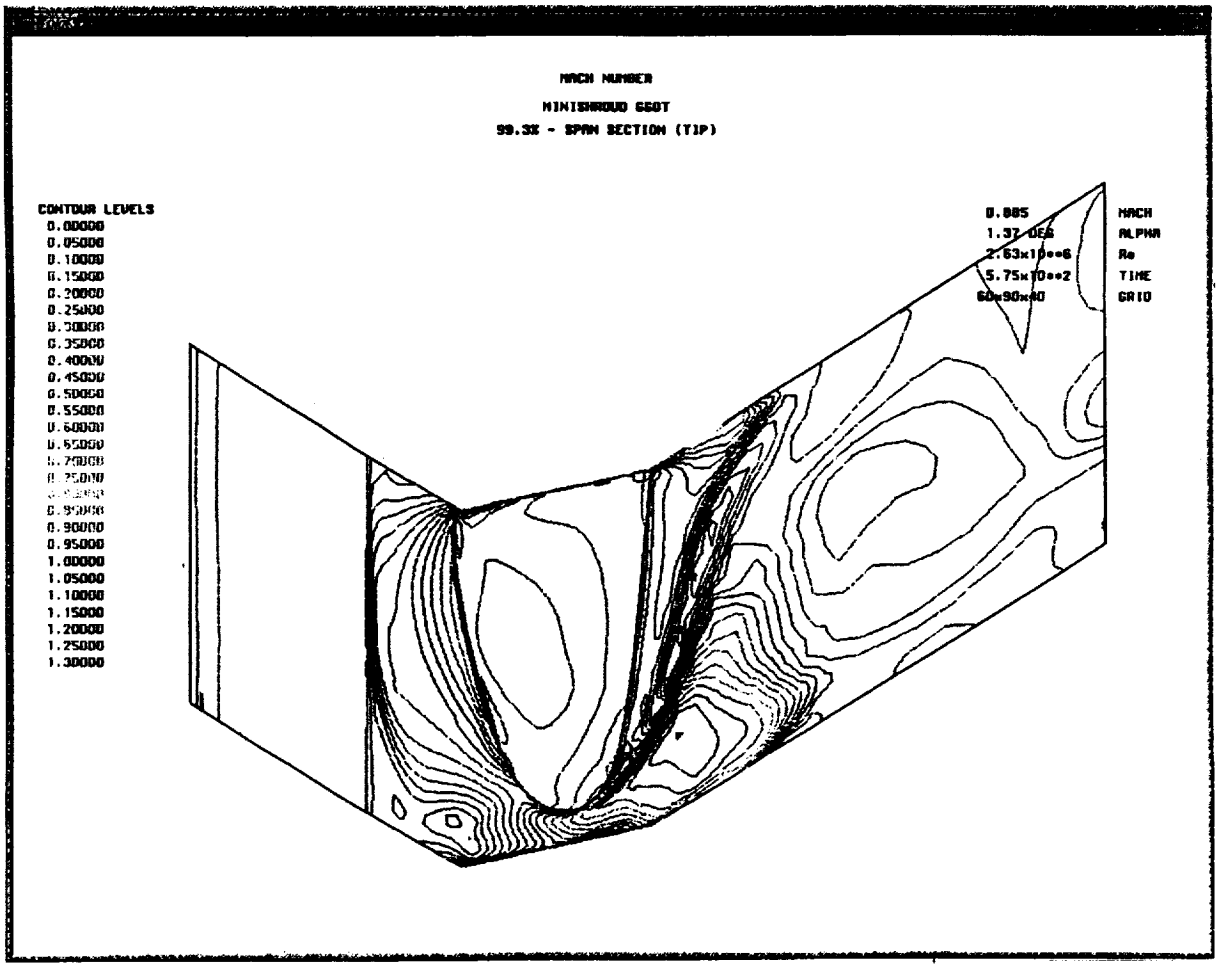

MACH NUMBER

BASELINE 6SOT WITH TIP CLEARANCE

99.65% - SPAN SECTION (MID-GAP)

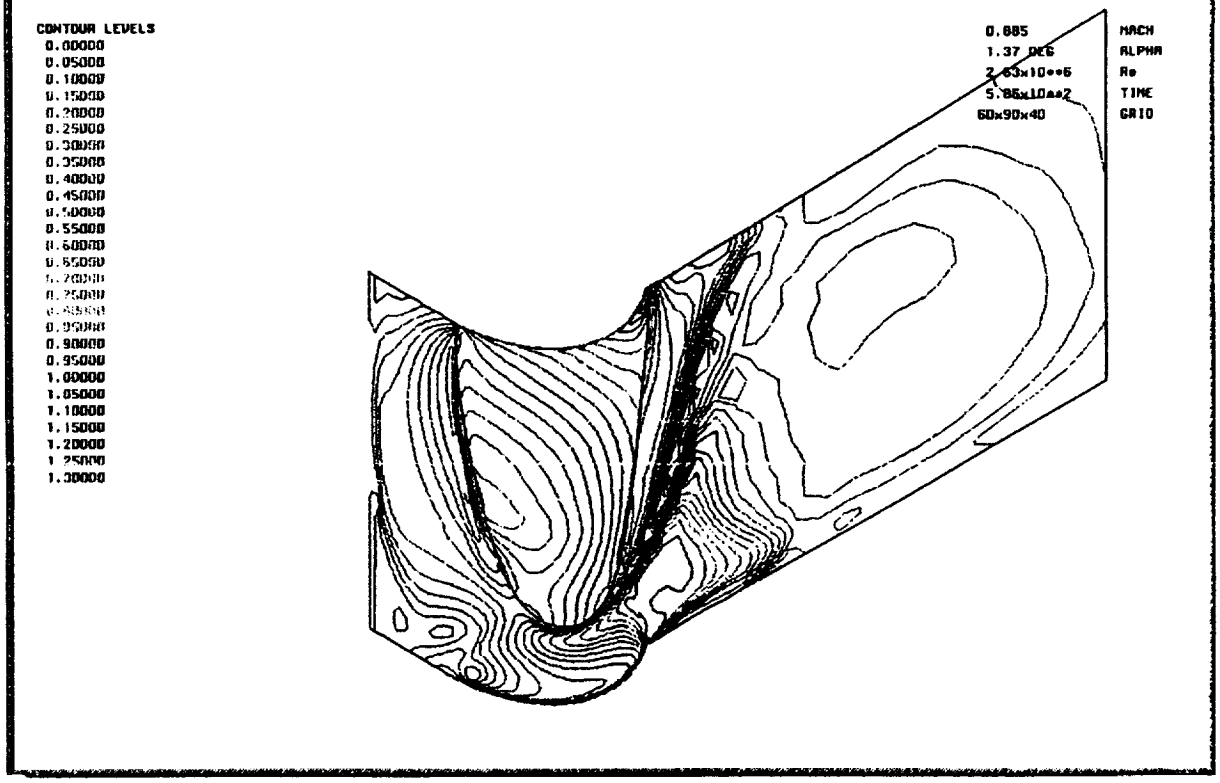

MACH NUMBER

MINISHROUD 6SOT

99.65% - SPAN SECTION (MID-GAP)

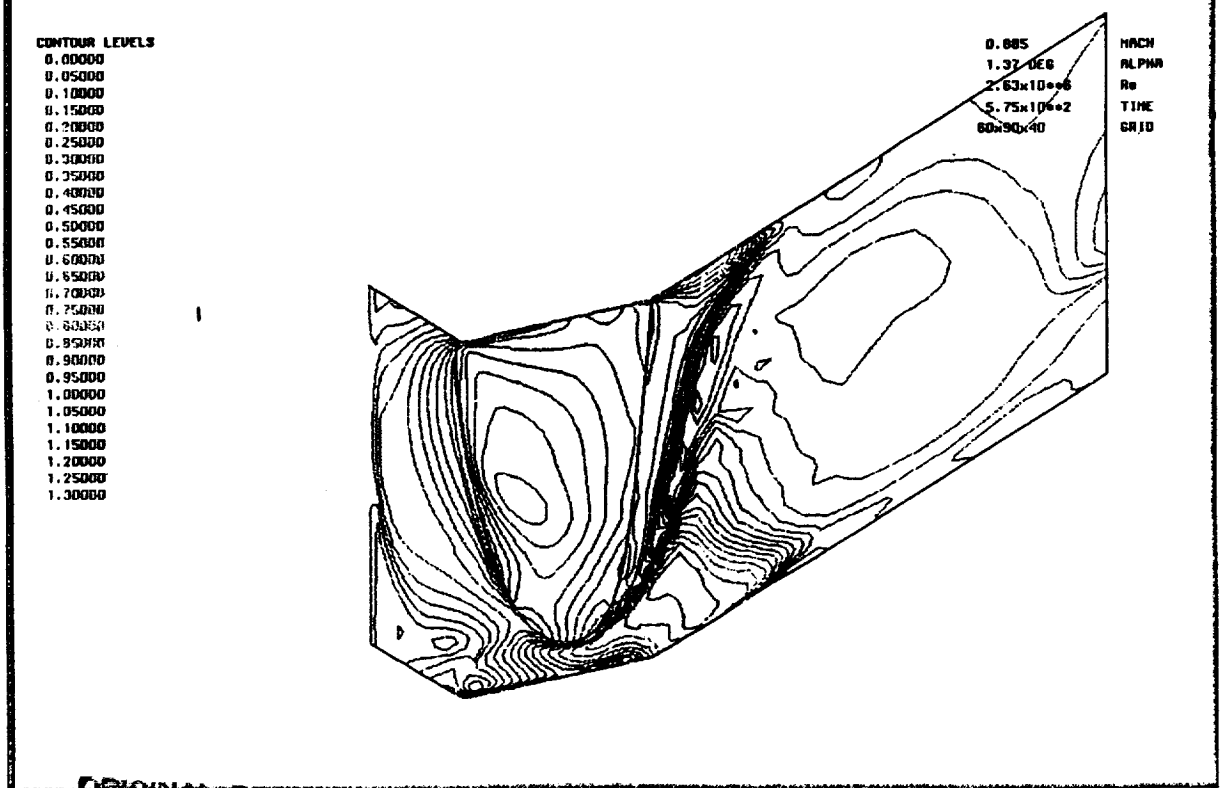

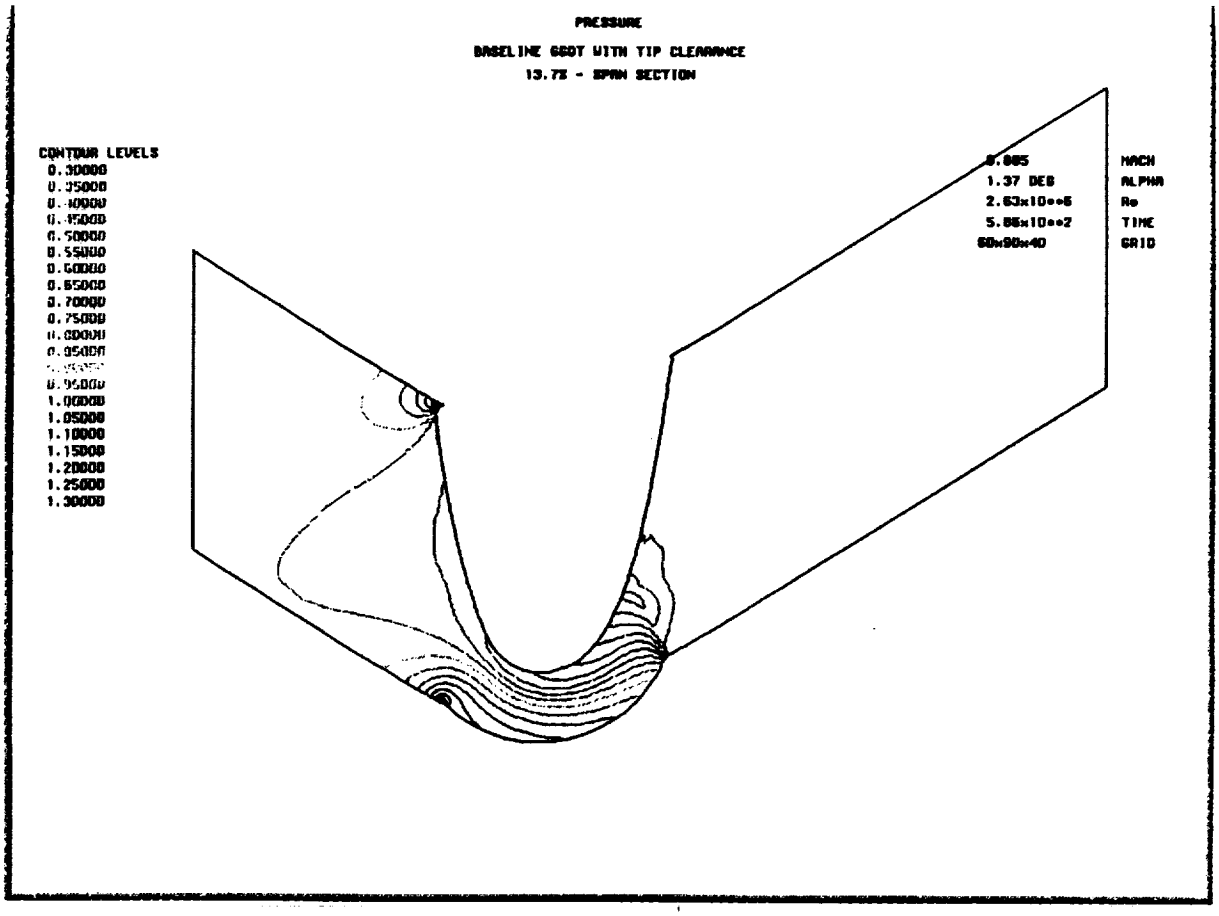

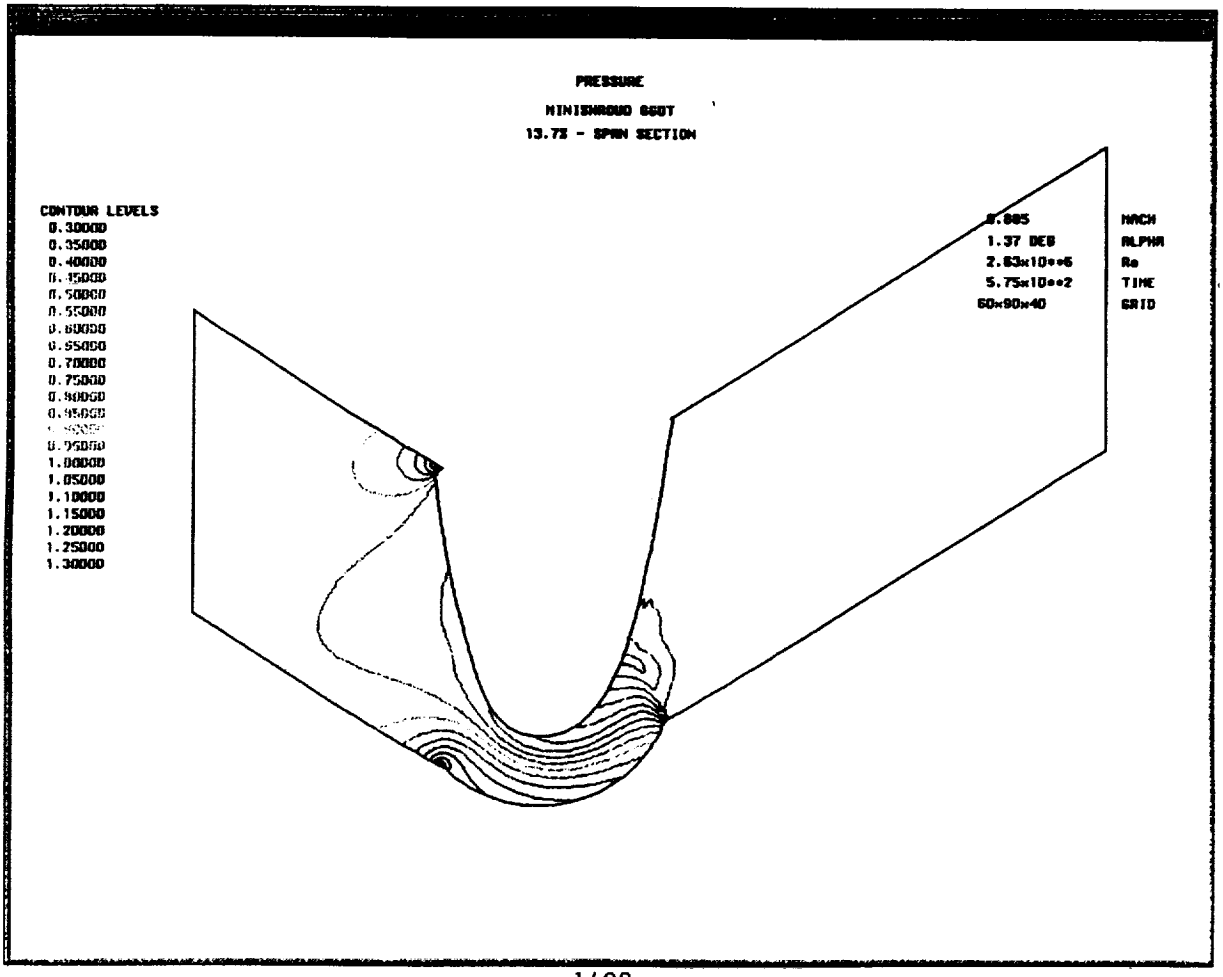

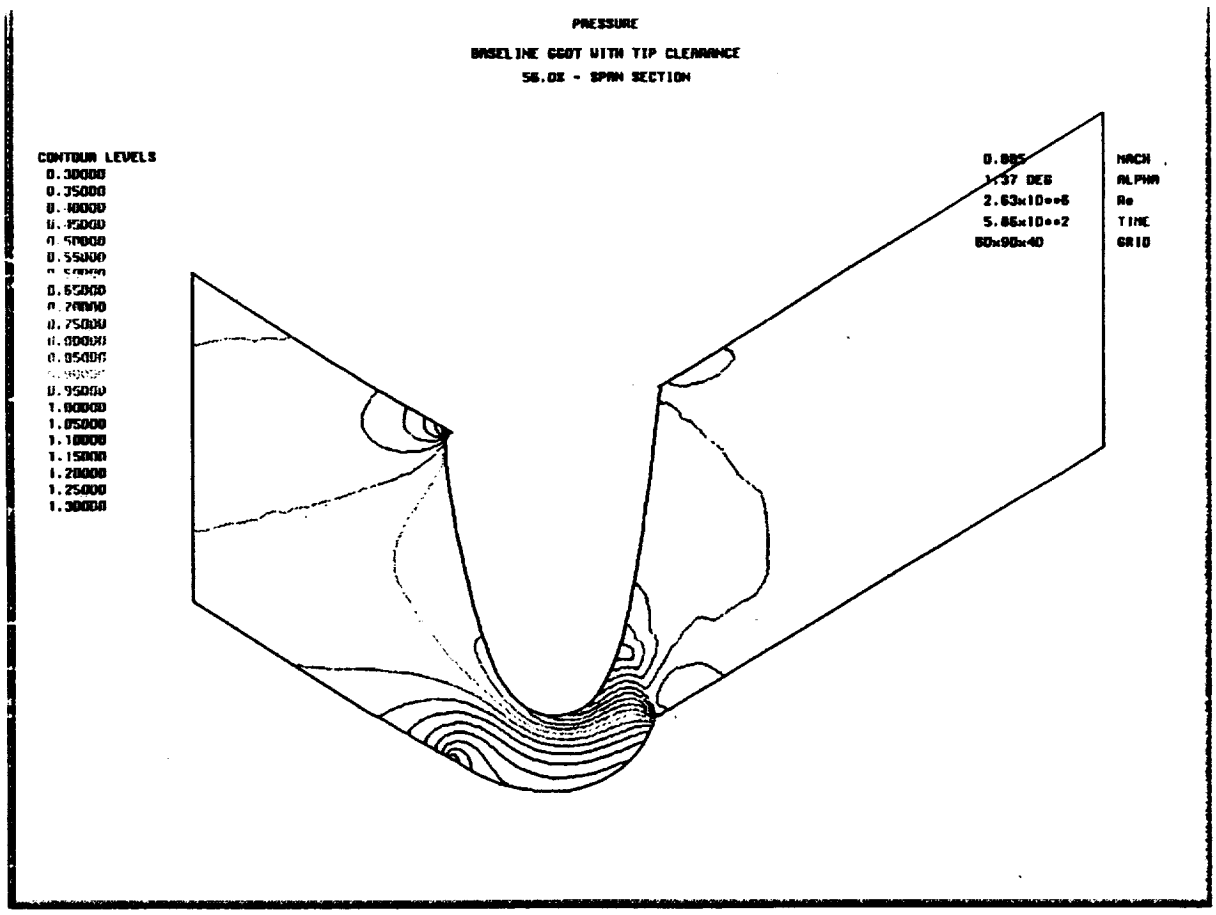

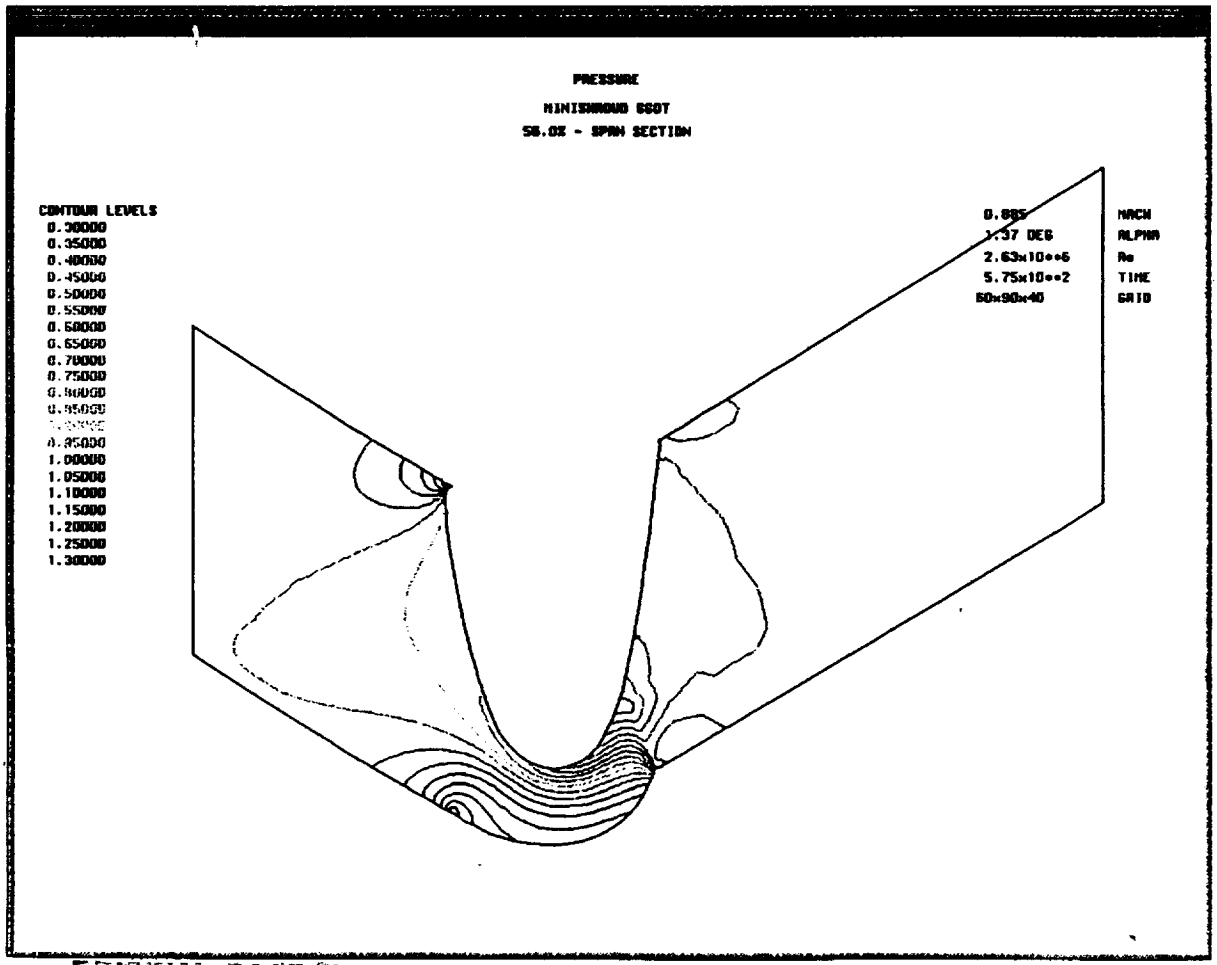

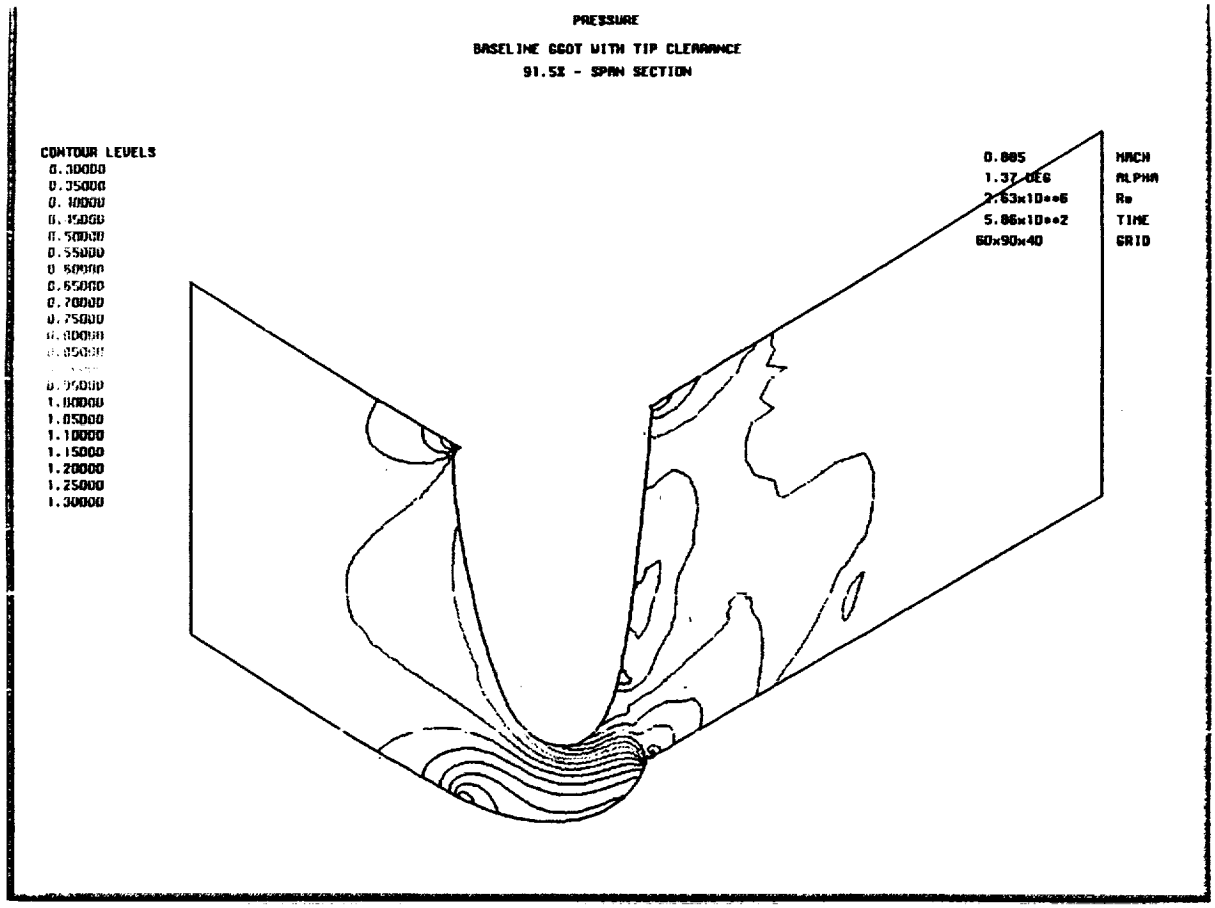

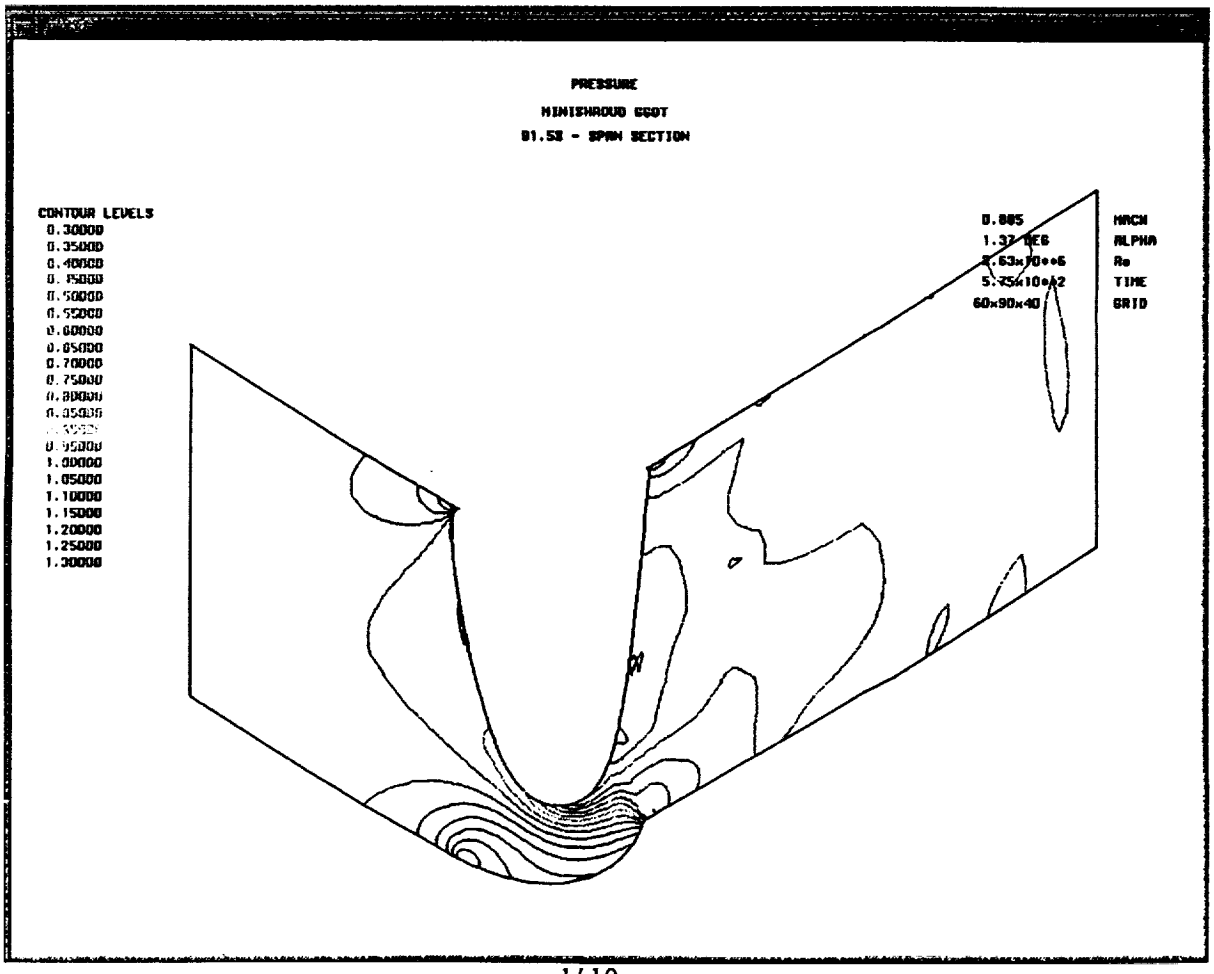

PRESSURE

BASELINE GGOT WITH TIP CLEARANCE

99.3% - SPAN SECTION (TIP)

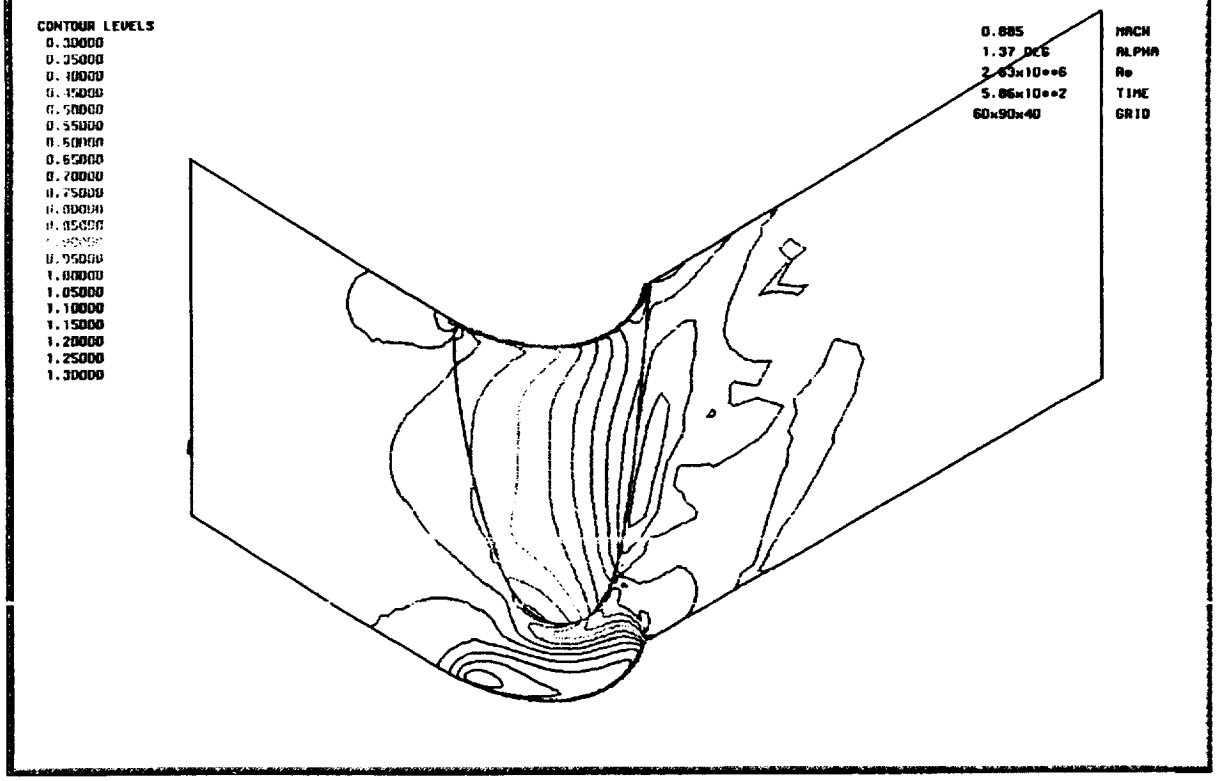

PRESSURE

MINISHROUD GGOT

99.3% - SPAN SECTION (TIP)

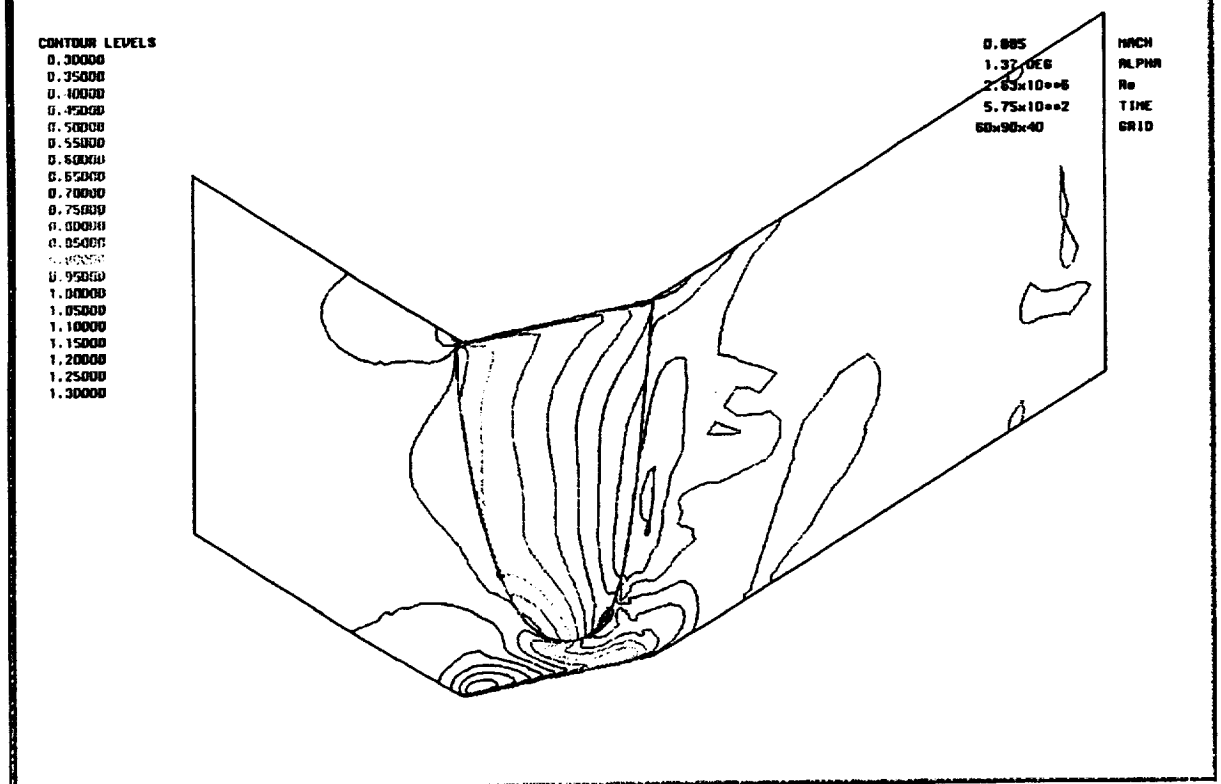

PRESSURE

BASELINE GGOT WITH TIP CLEARANCE

99.6SS - SPAN SECTION (mid-gap)

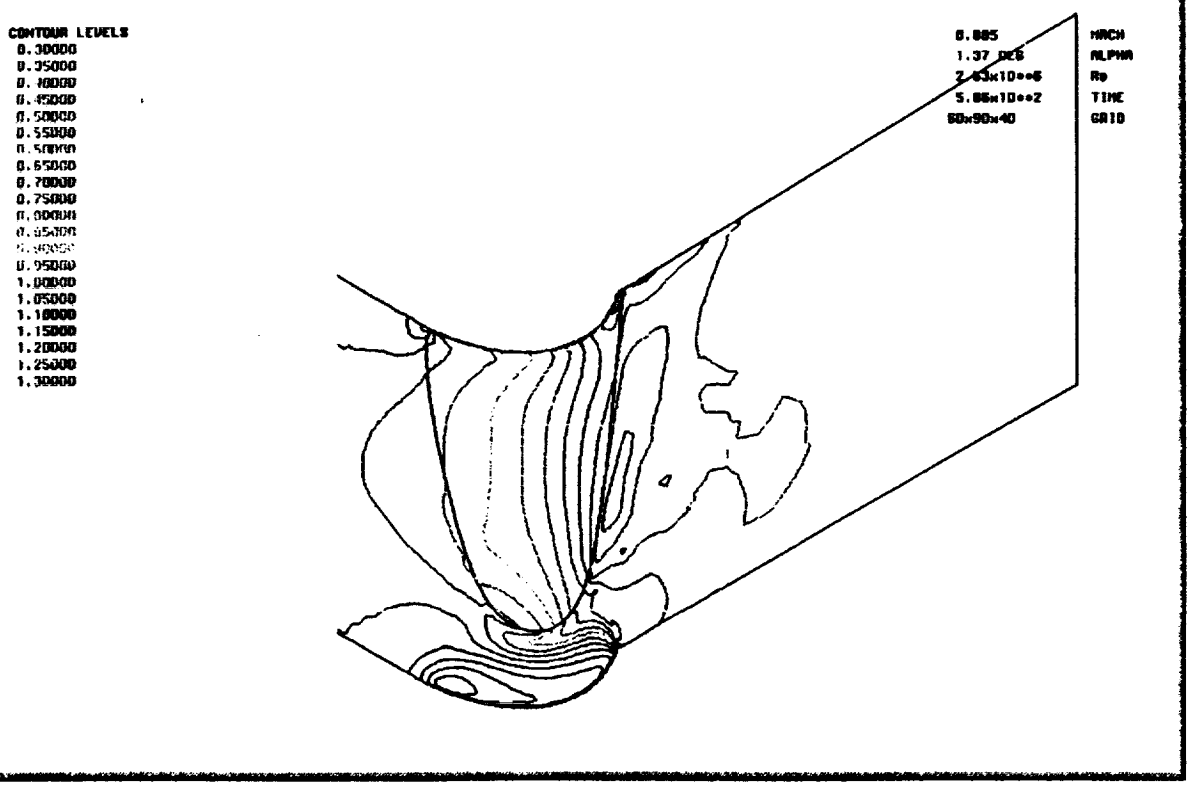

PRESSURE

MINISHROUD GGOT

99.6SS - SPAN SECTION (MID-GAP)

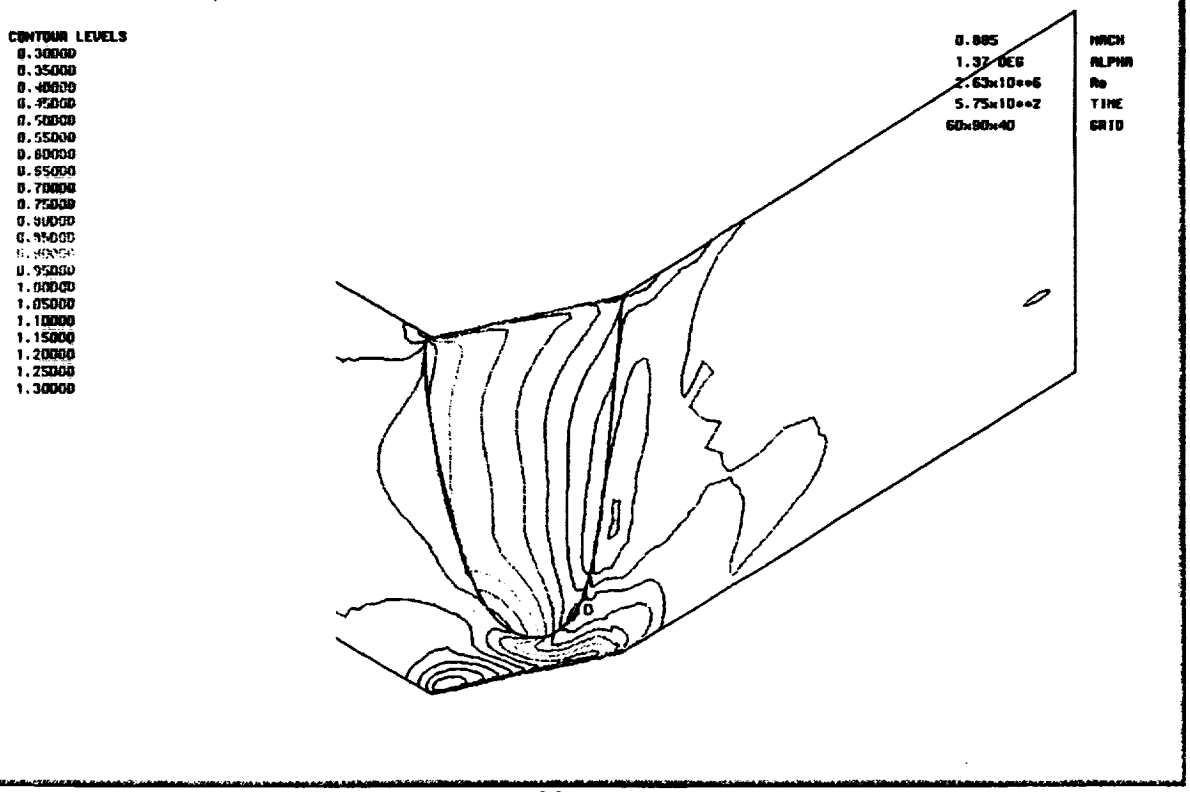

Baseline GGOT with Clearance
Blade Surface Pressure (8.1% span)
Reduced Dissipation – 60 x 90 x 40 grid

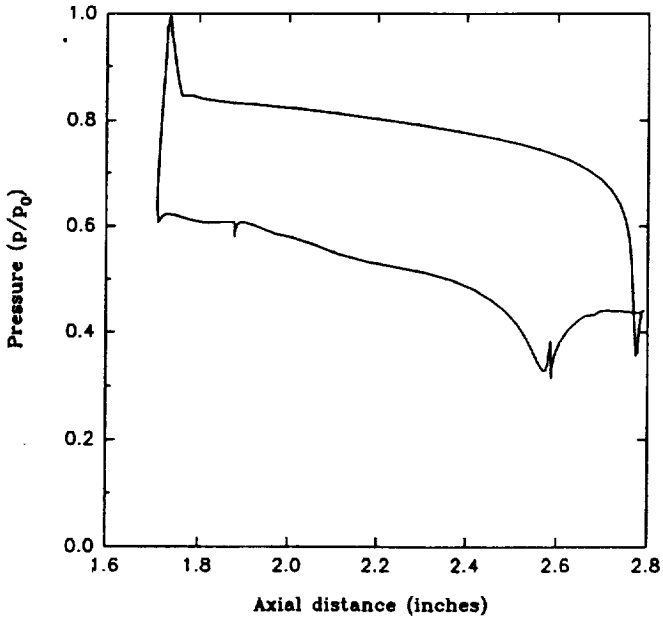

Minishroud GGOT
Blade Surface Pressure (8.1% span)
Reduced Dissipation – 60 x 90 x 40 grid

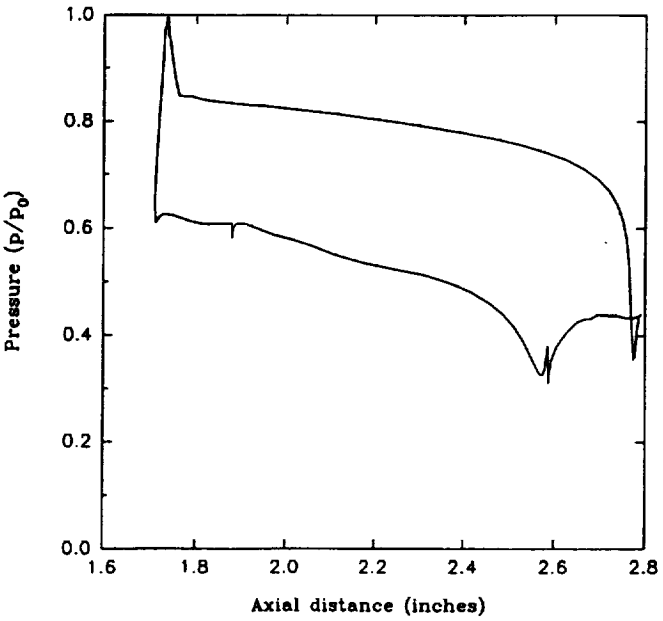

Baseline GGOT with Clearance
Blade Surface Pressure (56.4% span)

Reduced Dissipation – 60 x 90 x 40 grid

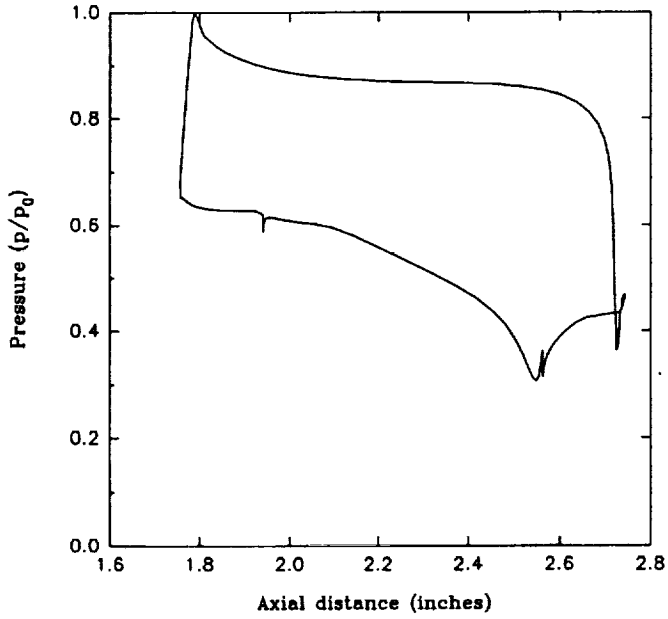

Minishroud GGOT
Blade Surface Pressure (56.4% span)

Reduced Dissipation – 60 x 90 x 40 grid

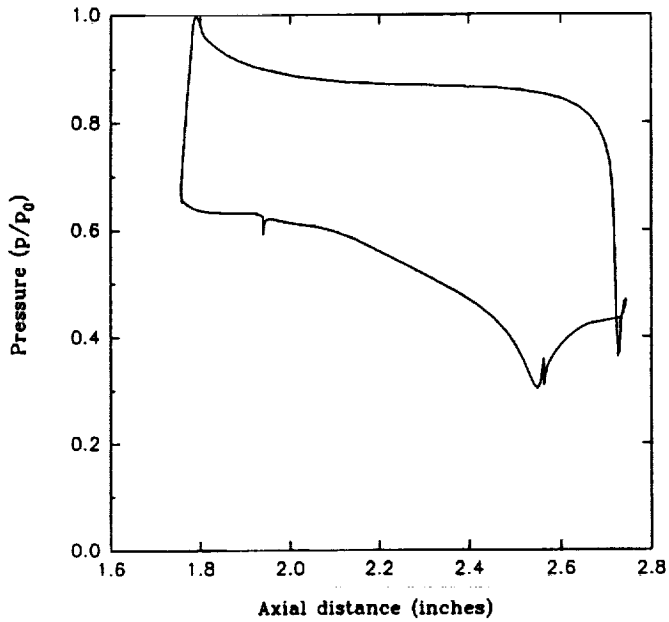

Baseline GGOT with Clearance
Blade Surface Pressure (92.2% span)

Reduced Dissipation – 60 x 90 x 40 grid

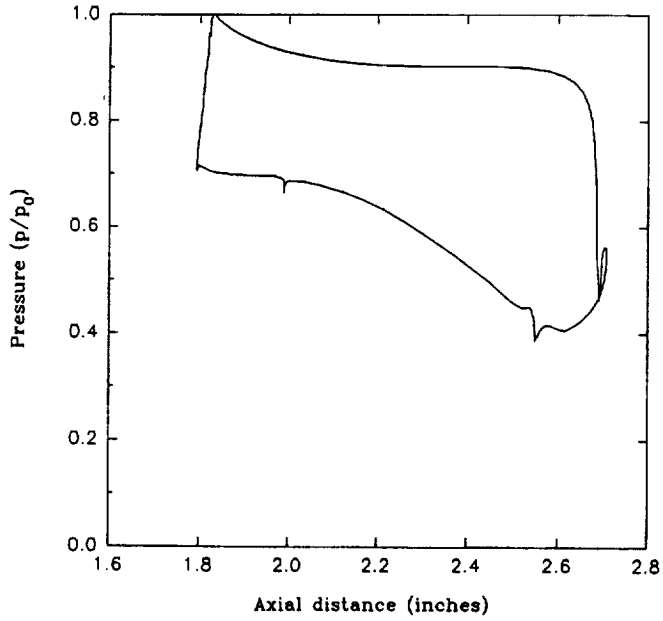

Minishroud GGOT
Blade Surface Pressure (92.2% span)

Reduced Dissipation – 60 x 90 x 40 grid

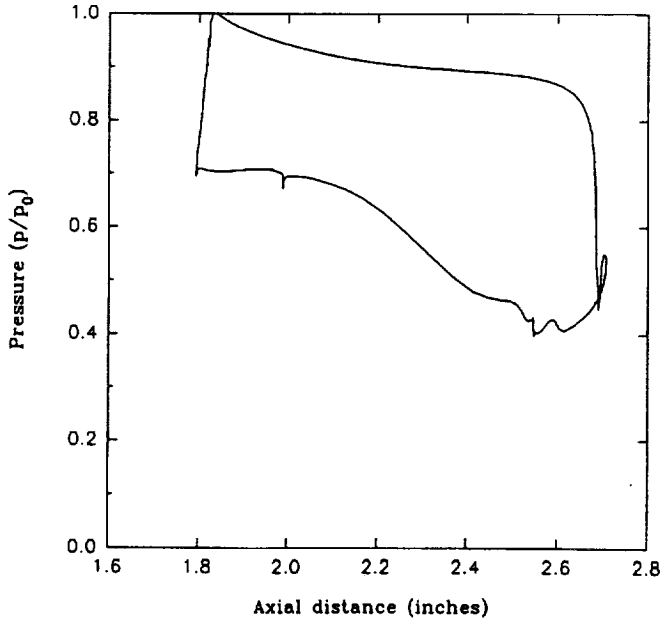

Baseline GGOT with Clearance
Blade Surface Pressure (99.6% span)

Reduced Dissipation – 60 x 90 x 40 grid

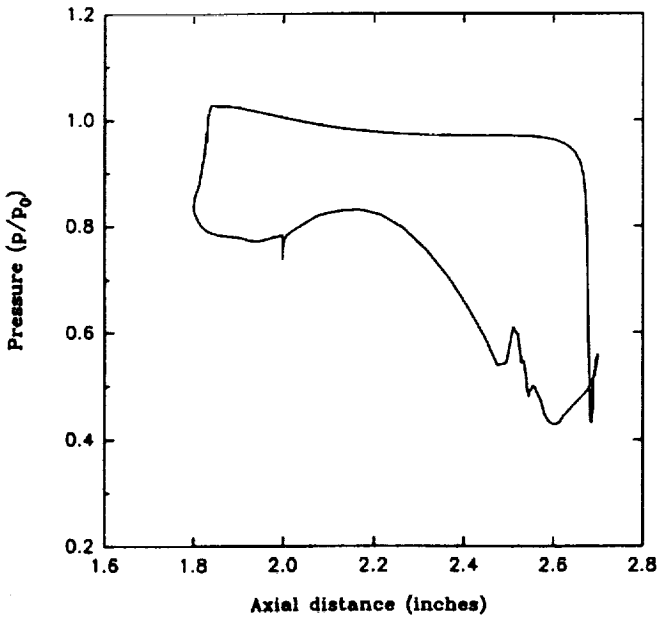

Minishroud GGOT
Blade Surface Pressure (99.6% span)

Reduced Dissipation – 60 x 90 x 40 grid

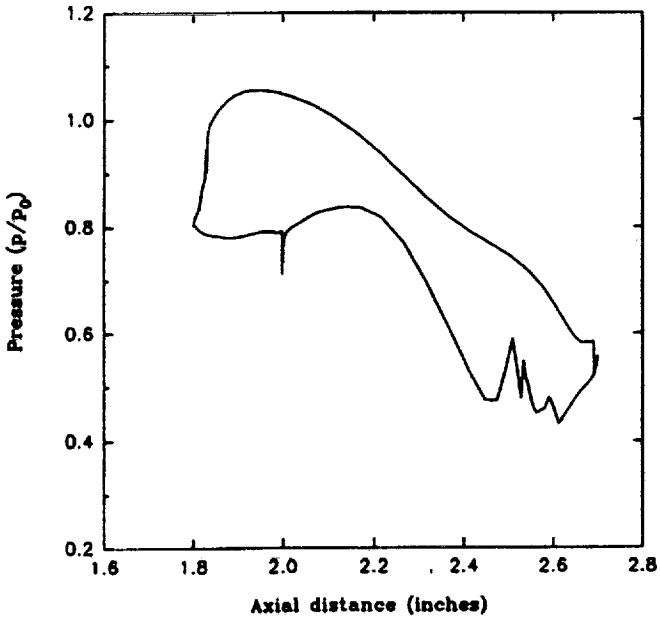

Circumferential Mass Averages
Inflow Boundary (0.6 in.)

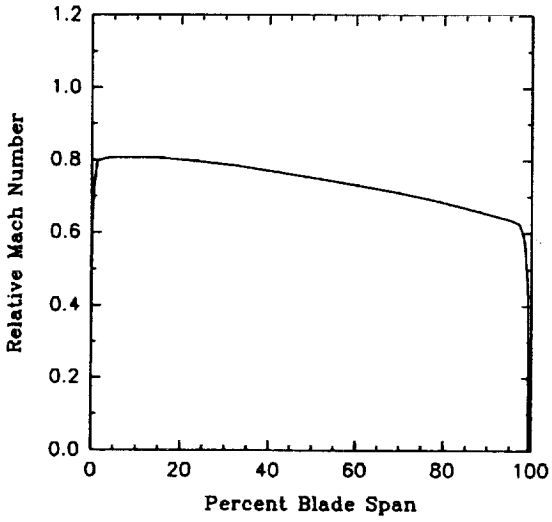

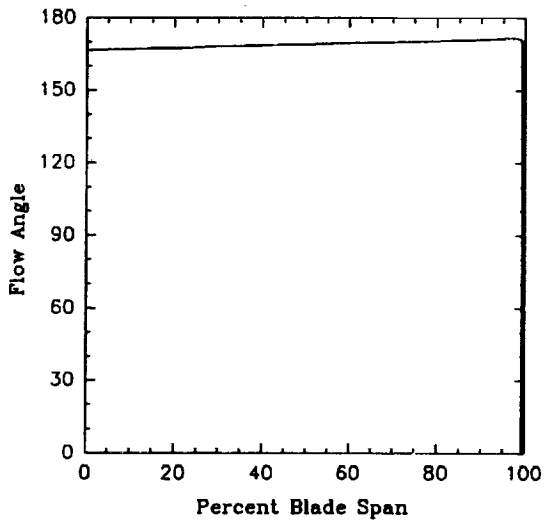

Circumferential Mass Averages
Inflow Boundary (0.6 in.)
Minishroud

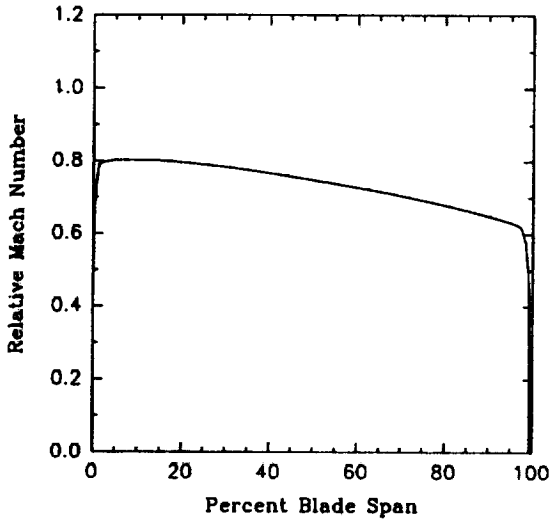

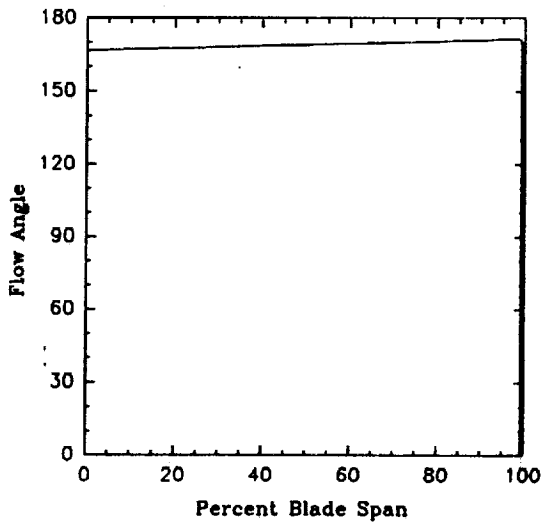

Circumferential Mass Averages
Diffuser Start Boundary (2.9 in.)

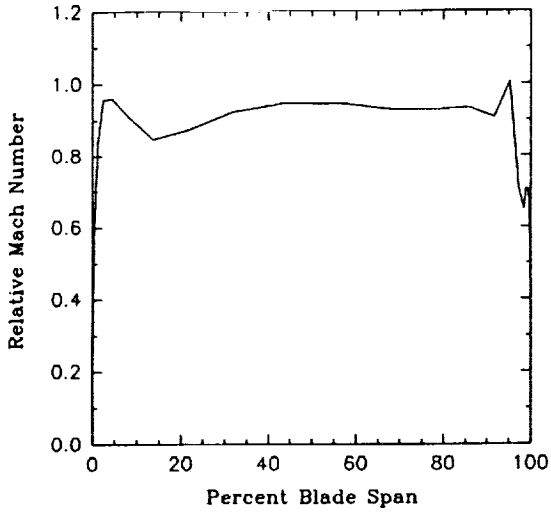

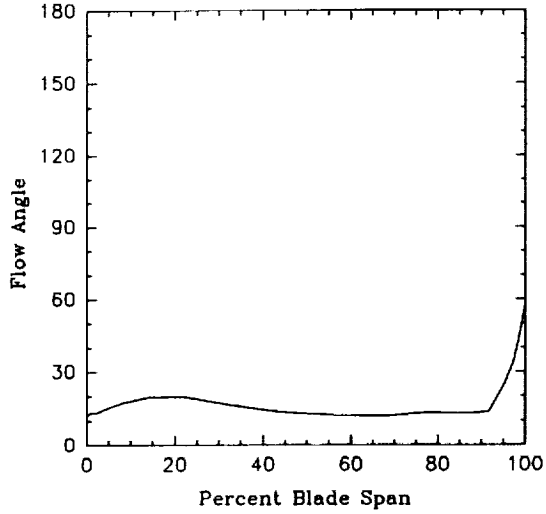

Circumferential Mass Averages
Diffuser Start Boundary (2.9 in.)
Minishroud

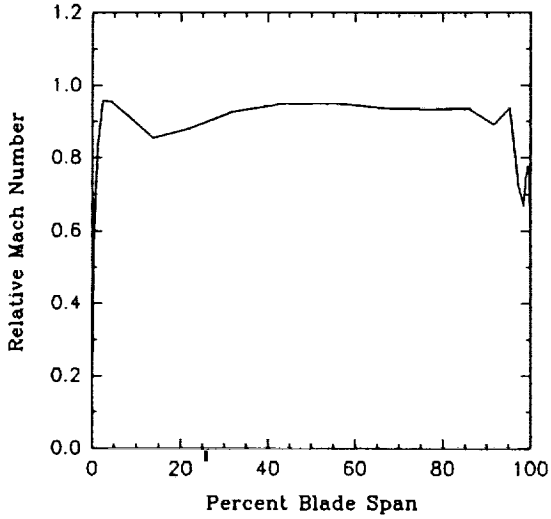

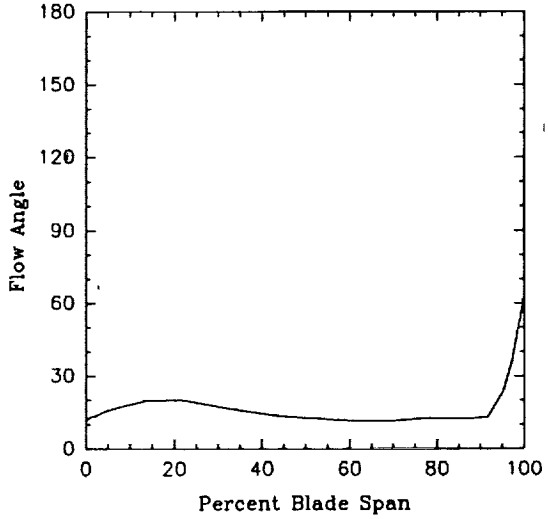

Circumferential Mass Averages
(x = 3.8 in.)

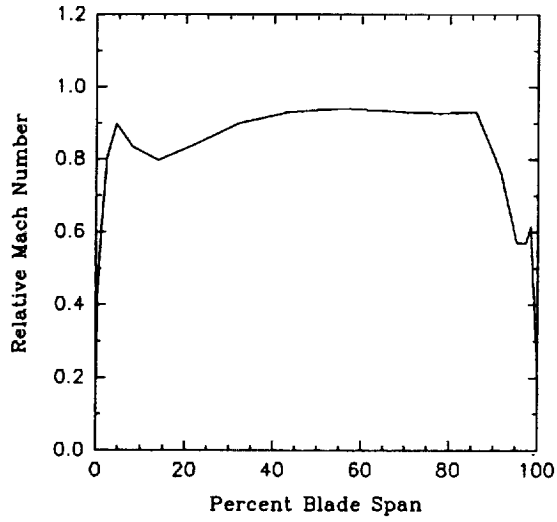

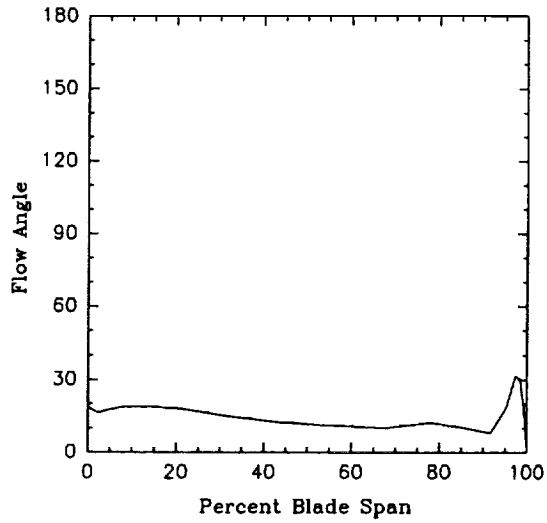

Circumferential Mass Averages
(x = 3.8 in.)
Minishroud

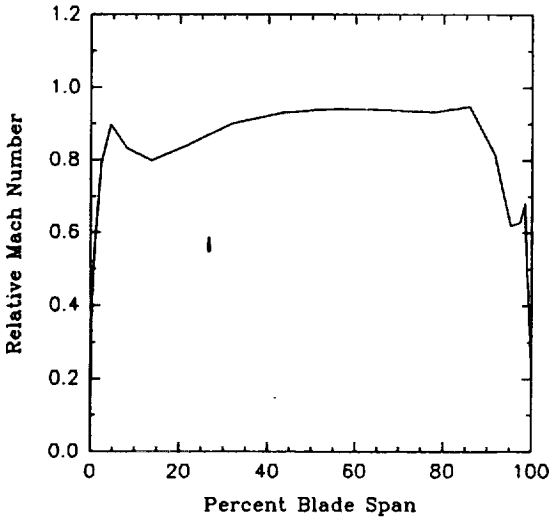

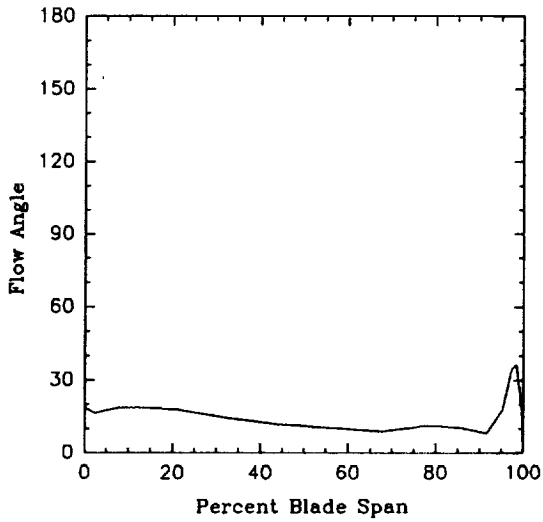

Circumferential Mass Averages
Outflow Boundary (x = 4.75 in.)

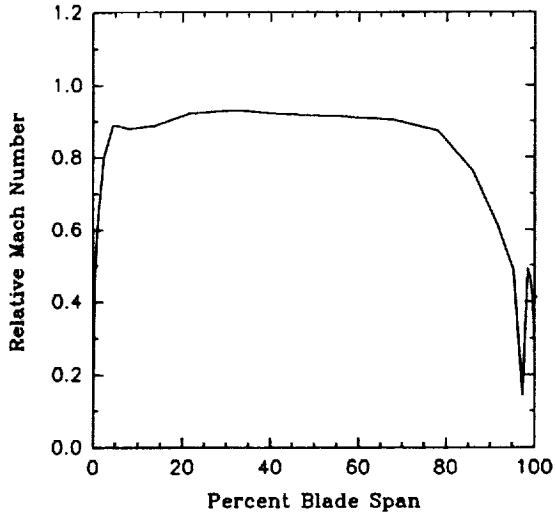

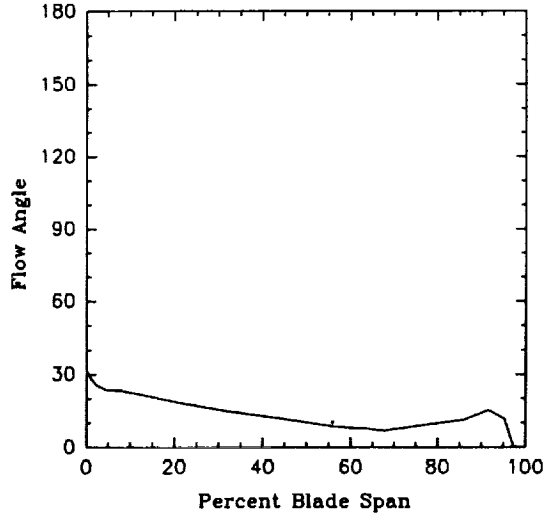

Circumferential Mass Averages
Outflow Boundary (x = 4.75 in.)
Minishroud

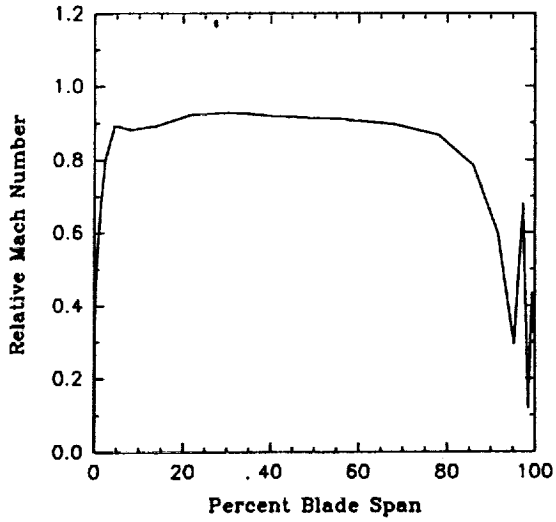

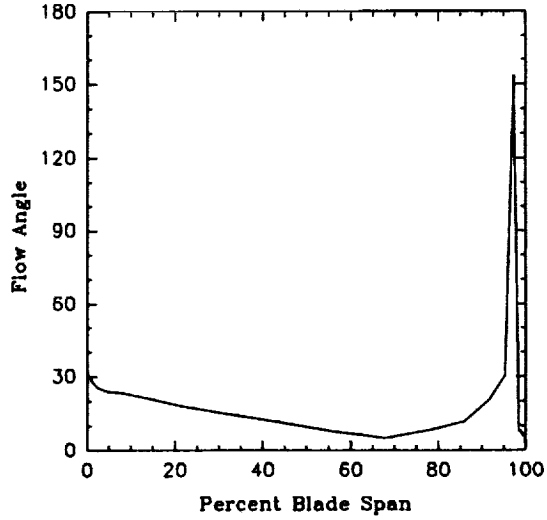

Circumferentially Mass Averaged Total Pressure Loss Across Blade

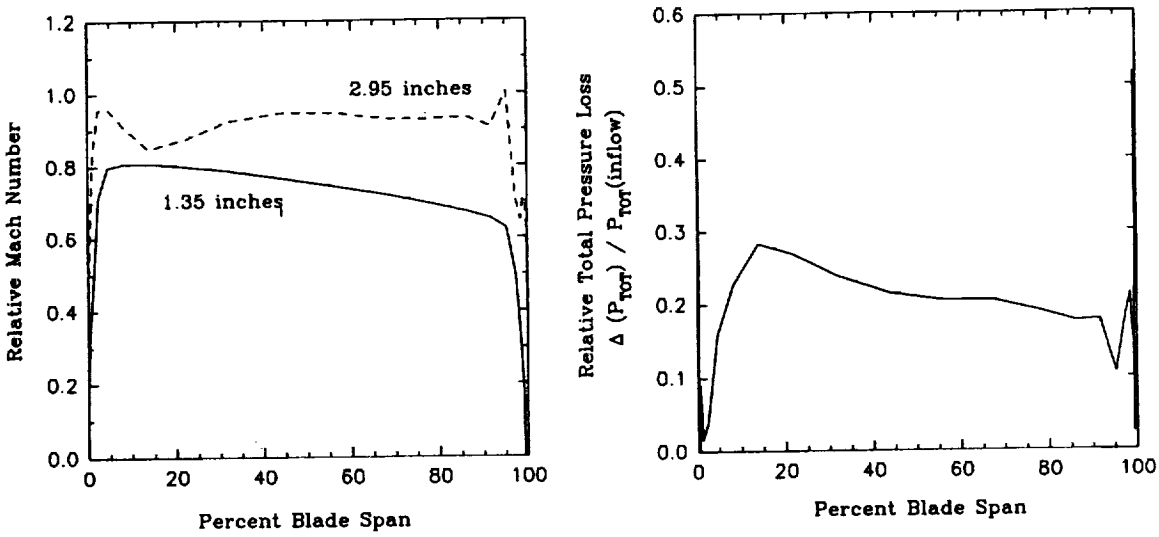

Circumferentially Mass Averaged Total Pressure Loss Across Blade

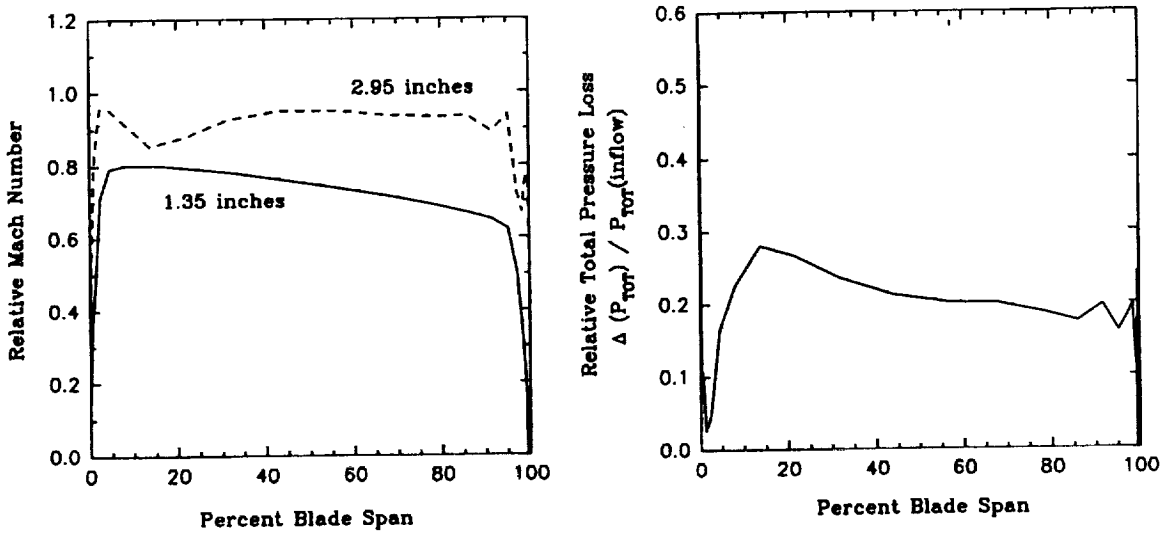

Minishroud

CONCLUSIONS

- BOTH GEOMETRIES SHOW SIMILAR VORTICAL FLOW BEHAVIOR
- TOTAL PRESSURE LOSSES ARE NOT SIGNIFICANTLY DIFFERENT
- ADDITION OF MINI-SHROUD DOES NOT REDUCE THE TIP CLEARANCE FLOW EFFECTS

Scientific Research Associates

SUPERSONIC FLOW AND SHOCK FORMATION IN TURBINE TIP GAPS

John Moore

Mechanical Engineering Department
Virginia Polytechnic Institute and State University
Blacksburg, Virginia 24061-0238

Summary

Shock formation due to overexpansion of supersonic flow at the inlet to the tip clearance gap of a turbomachine has been studied.

As the flow enters the tip gap, it accelerates around the blade pressure-side corner creating a region of minimum static pressure. The "free streamline" separates from the wall at the corner; and, for Mach numbers greater than about 1.3, it curves back to intersect the blade tip. At this point, the freestream flow is abruptly turned parallel to the surface, giving rise to an oblique shock.

The results are consistent with compressible sharp-edged orifice flow calculations found in the literature and with the theory of oblique shock wave formation in supersonic flow over a wedge. For freestream Mach numbers of 1.4 to 1.8, wave angles are 43 to 54 degrees, and turning angles are 9 to 20 degrees; as the Mach number increases, the angle of turn also increases.

It appears that in a turbine, after separating from the inlet corner, the flow reattaches on the blade tip and an oblique shock is formed at 0.4-1.4 tip gap heights into the clearance gap. The resulting shock-boundary layer interaction may contribute to further enhancement of already high heat transfer to the blade tip in this region. This in turn could lead to higher blade temperatures and adversely affect blade life and turbine efficiency.

Introduction

Tip leakage flow through the clearance gaps of unshrouded turbomachinery blades is known to cause reductions in efficiency and performance [Roelke, 1973, Hourmouziadis and Albrecht, 1987]. It is also known that enhanced heat transfer to the tips of turbine rotor blades, resulting from the separation and reattachment of the leakage flow, can be a major factor in determining blade life in high temperature gas turbines [Moore et al., 1989]. There have therefore been many recent studies of flow and heat transfer in tip gaps [Bindon, 1987, Metzger and Bunker, 1989, Metzger, Dunn, and Hah, 1991, Yaras et al., 1989]. But most of

these studies have considered only incompressible flow, and features of compressible flow such as overexpansion to high supersonic Mach numbers, shock formation within the tip gap, and shock boundary layer interaction have received little attention. It is important that this compressible flow physics be understood sufficiently well to be included in the turbine design process.

Consider, for example, turbine rotor blades in gas turbines operating with transonic flow. Around the airfoil, the flow accelerates to supersonic Mach numbers near the suction surface in regions of low static pressure. Similarly flow passing through the tip clearance gap will accelerate as the pressure falls. But its path is not as smooth as that around the airfoil profile. Efforts are made to reduce the leakage flow by using sharp corners, for example on the pressure side, and cavities. The flow may, therefore, overexpand locally and exhibit regions of supersonic flow and complex compressible flow structure.

In an attempt to shed some light on compressible flow development in tip gaps, Henry and Moore [Moore et al., 1989] made a preliminary study using a water table flow simulation. Using the hydraulic analogy between free surface liquid flow and two-dimensional compressible flow, they gained some insight into possible Mach number distributions and shock patterns to be found in turbine tip clearance gaps. It appeared that overexpansion of flow around the pressure surface corner leads to an oblique shock wave which extends from the inlet corner region to the shroud wall at about two tip gap heights into the tip gap and then reflects back to the turbine blade tip. For tip gap exit pressures corresponding to blade suction surface Mach numbers greater than 1.0, they found local maximum Mach numbers within the tip gap in the range of about 1.5 to 1.8.

Compressible Orifice Flows

Although little was found in the literature about compressible tip gap flows, much research has been done on compressible orifice flows. Benson and Pool [1965] describe early research in this area.

Benson and Pool numerically solved the equations for steady, isentropic flow of air through a two-dimensional slit. They then compared the results with Schlieren photographs and interferograms. Figure 1 shows the computed free streamlines for various back pressures. The flows range from incompressible flow $p_b/p_0 \sim 1.0$, $M \sim 0.0$, to sonic flow, $p_b/p_0 = 0.5283$, $M = 1.0$, to choked flow, $p_b/p_o = 0.0389$, $M = 2.77$.

Consider flow accelerating along the orifice wall to the sharp corner. If the back pressure is low enough to cause supersonic flow, this flow will undergo a Prandtl-Meyer expansion at the corner to the freestream Mach number. As a

result the flow turns through the corresponding expansion angle. The free streamline then continues to turn through a further ninety degrees to the point of its maximum (downward) slope. Subsequently the jet reaches a maximum width followed by a contraction (as the free streamline turns upward again).

For subsonic and sonic flow, the jet simply contracts to an asymptotic jet width. This width is $\pi/(\pi+2) = 0.61$ of the slit width for incompressible flow and 0.74 of the slit width for sonic flow, as seen in Fig. 1. With supersonic flow, the jet width contracts and then expands. At a freestream Mach number of about 1.3 ($p_b/p_0 \sim 0.36$), the maximum width of the jet is equal to the slit width. At choked flow, the maximum width is about five times the slit width.

Norwood [1961] performed a computational study similar to that of Benson and Pool. He concentrated mostly on flow near the slit. He also performed experimental work on jet reattachment in two-dimensional models of a flapper valve. The geometry of these was like that of the slit in Fig. 1 except that downstream of the minimum area a straight wall was inclined downwards at an angle of 22-1/2 degrees to the horizontal. This effectively produced a tip gap with a sharp inlet corner and a linearly increasing height. Norwood visualized the flow with shadowgraph pictures.

At low upstream stagnation pressures ($p_b/p_0 > \sim 0.23$), the jet in Norwood's models followed the horizontal wall like the subsonic and just supersonic flows in Figure 1. Further increase in the upstream pressure ($p_b/p_0 < \sim 0.23$), however, caused the jet to jump to the inclined wall. Norwood noted that in his two-dimensional models the flow jumped at a relatively constant pressure ratio. This suggested that the only characteristic parameter for the flow development was the Mach number. It also indicated that the phenomenon of reattachment on the inclined wall was, initially at least, a compressibility effect depending on the Mach number rather than a frictional effect.

In a shadowgraph picture of flow along the inclined wall, Norwood observed two features of interest in the present study. The first was "a teardrop shaped region," or "bubble," at the edge of the orifice where the flow is rapidly accelerating and the streamlines are highly curved. Norwood argued that the pressure in the bubble was very low because of the entrainment of the air inside into the main stream. The second interesting feature was an oblique shock just downstream of the throat starting on the inclined wall at the end of the bubble. This is due to the change in direction the supersonic flow encounters when it contacts the wall.

Present Contribution

The work of Moore and Elward [1992] was aimed at further understanding the mechanism of shock formation near the inlet of the tip clearance gap. The

flow structure was related to the development of compressible flow in sharp-edged orifices. Particular features of interest include the length scale of the formation process and the strength of the shocks produced. In this technical note, the findings of Moore and Elward are summarized.

Model of shock formation

Figure 2 shows the flow model postulated by Moore and Elward for the shock formation. The flow separates from the corner at the tip gap inlet. Supersonic freestream flow with a Mach number M_1 then overturns and intersects the blade tip at a distance x_i from the corner. Here the flow is abruptly turned through an angle δ, giving rise to an oblique shock wave at an angle σ-δ to the surface. This shock formation process is simply modelled as shock formation in supersonic flow over a wedge. The shock angles are then given by

$$\sin \sigma = \frac{1}{M_1} \sqrt{\frac{\frac{\rho_2}{\rho_1}}{\frac{k+1}{2} - \left[\frac{k-1}{2}\right] \frac{\rho_2}{\rho_1}}} \qquad (1)$$

and

$$\tan(\sigma-\delta) = \frac{\tan\sigma}{\frac{\rho_2}{\rho_1}} . \qquad (2)$$

Effective wall location of wave formation

Figure 3 shows the free streamlines calculated for sharp-edged orifice flows by Norwood.

From the free streamline results of Benson and Pool and of Norwood, Fig. 4 was constructed. This figure shows the distance, x_i, from the orifice entrance to the point of intersection of the free streamline with a line drawn from the orifice edge parallel to the orifice centerline, plotted against the freestream Mach number. This distance is plotted as x_i/w, or the distance in orifice half-widths. The figure shows that at higher Mach numbers, the free streamline intersects the "wall" closer

to the orifice edge. As the Mach number decreases, the free streamline intersects the wall farther and farther downstream. The free streamline becomes parallel to the wall at a pressure ratio of about 0.36 or M $\sim$ 1.3, as suggested by the results of Benson and Pool.

Figure 4 also plots the data for five water table cases against the Mach number, M_1, from Moore and Elward. Two points are plotted for each case, the location of the intersection of the line of median heights with the channel wall, denoted by the symbol m, and the location of the intersection of the line of maximum heights with the channel wall, denoted by the symbol p. The intersections for the lines of maximum height agree well with the wall locations predicted from the calculated compressible flow free streamlines. This data lies in the range x_i/w = 0.9-1.2. The trend in the data follows the predicted variation with free stream Mach number.

The angles of turn, δ, or equivalently the angles with which the free streamlines intersect the wall, are plotted against freestream Mach number in Fig. 5. The figure shows the turning angles from Moore and Elward and the free streamline angles of Benson and Pool and of Norwood. As was seen in Fig. 4, for Mach numbers above about 1.3, the free streamline intersects the wall. The angle of intersection then becomes larger as the Mach number increases.

The line of minimum Mach number required for an attached shock for a given δ is also shown on Fig. 5. It appears that the shock formation is like that of an attached shock on a wedge of half-angle, δ.

Another interpretation of the shock formation is that it is like turbulent reattachment in supersonic flow. Carriere [1970] has presented a correlation of experimental results for two-dimensional flow. Again Figure 5 shows that this is in reasonable agreement with the data, but the trend is toward somewhat lower turning angles, or later reattachment, at higher Mach numbers. This perhaps supports the argument by Norwood that the phenomenon of reattachment on his inclined wall was a compressibility effect rather than a frictional effect.

Wave formation in compressible flows

The results in Figs. 4 and 5 may be used to predict oblique shock formation in compressible flows. For example, consider a flow with a free stream Mach number of 1.8, that is, a minimum pressure p_1/p_0 = 0.174 (with k = 1.4). Figures 4 and 5 give the wave location and turning angle as x_i/w = 0.96 and δ = 18.8 degrees, respectively. Equations 1 and 2 may then be solved to get σ = 61.1 degrees and $\sigma - \delta$ = 42.3 degrees. The resulting predicted flow is shown plotted in Fig. 6.

Implications for jet engine heat transfer

The 2-D, incompressible turbulent flow calculations of Moore, et al. [1989] showed an area of enhanced heat transfer on the pressure side of a turbine blade tip as shown in Fig. 7. The heat transfer was enhanced by up to 1.8 times the downstream fully developed value in the first two to three tip gap heights. The estimated intersection of the free streamline with the sidewall of x_i/w between 0.4 and 1.4, observed in Fig. 4, would indicate a shock forming within this region of already enhanced heat transfer. The shock-boundary layer interaction could serve to further enhance the heat transfer. Increased heat transfer would lead to higher metal temperatures and increased rates of oxidation and material weight loss. This would reduce both the expected useful life of the turbine blade and the turbine efficiency.

References

Benson, R. S., and Pool, D. E., 1965, "Compressible Flow Through a Two-Dimensional Slit," *Int. J. Mech. Sci.*, Vol. 7, pp. 315-336.

Bindon, J. P., 1987, "Measurement of Tip Clearance Flow Structure on the End-Wall and within the Clearance Gap of an Axial Turbine Cascade," I. Mech. E. 1987-6, pp. 43-52, Int. Conf. on "Turbomachinery--Efficiency Prediction and Improvement," Cambridge, England.

Carriere, P., 1970, "Analyse Theorique du Decollement et du Recollement Turbulents au Bord de Fuite d'un Aubage aux Vitesses Supersoniques," Flow Research on Blading, L. S. Dzung, Ed., Elsevier Pub. Co., New York, pp. 210-242.

Elward, K. M., 1989, "Shock Formation in Overexpanded Flow--A Study Using the Hydraulic Analogy," M. S. Thesis, Virginia Polytechnic Institute and State University, Blacksburg, Virginia, April.

Hourmouziadis, J., and Albrecht, G., 1987, "An Integrated Aero/Mechanical Performance Approach to High Technology Turbine Design," AGARD Conference Proceedings No. 421 on Advanced Technology for Aero Gas Turbine Components, Paris, France.

Metzger, D. E., and Bunker, R. S., 1989, "Cavity Heat Transfer on a Transverse Grooved Wall in a Narrow Flow Channel," *ASME J. of Heat Transfer*, Vol. 111, pp. 73-79.

Metzger, D. E., Dunn, M. G., and Hah, C., 1991, "Turbine Tip and Shroud Heat Transfer," *ASME J. of Turbomachinery*, Vol. 113, pp. 502-507.

Moore, J., and K. M. Elward, 1992, "Shock Formation in Everexpanded Tip Leakage Flow," ASME Paper No. 92-GT-1.

Moore, J., Moore, J. G., Henry, G. S., and Chaudhry, U., 1989, "Flow and Heat Transfer in Turbine Tip Gaps," *ASME J. of Turbomachinery*, Vol. 111, July, pp. 301-309.

Norwood, R. E., 1961, "Two Dimensional Transonic Gas Jets," *Sc. D. Thesis*, Massachusetts Institute of Technology, Cambridge, Massachusetts, June.

Roelke, R. J., 1973, "Turbine Design and Application," Glassman, A. J., Ed., NASA SP-290, pp. 125-131.

Yaras, M., Yingkang, Z., and Sjolander, S. A., 1989, "Flow Field in the Tip Gap of a Planar Cascade of Turbine Blades," *ASME J. of Turbomachinery*, Vol. 111, No. 3, pp. 276-283.

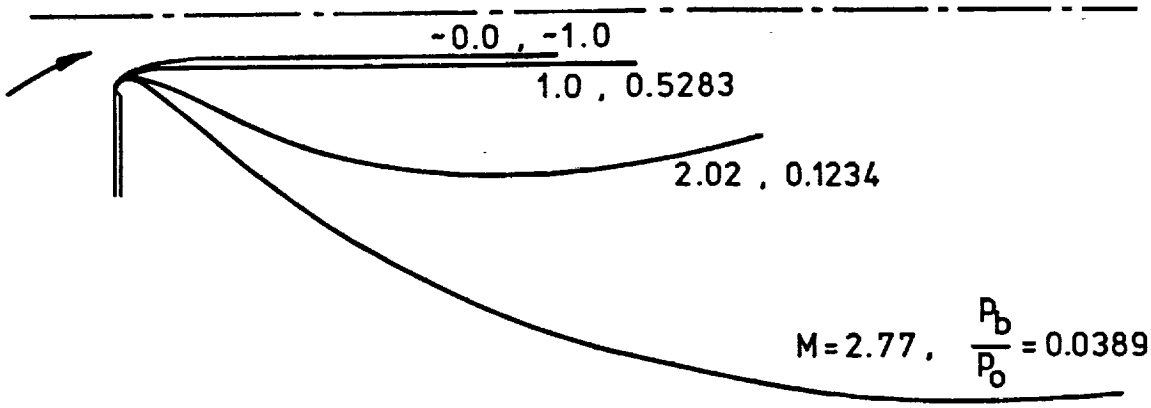

Figure 1. Free streamlines for inviscid flow of air from a half-slit with various back pressures; calculated by Benson and Pool

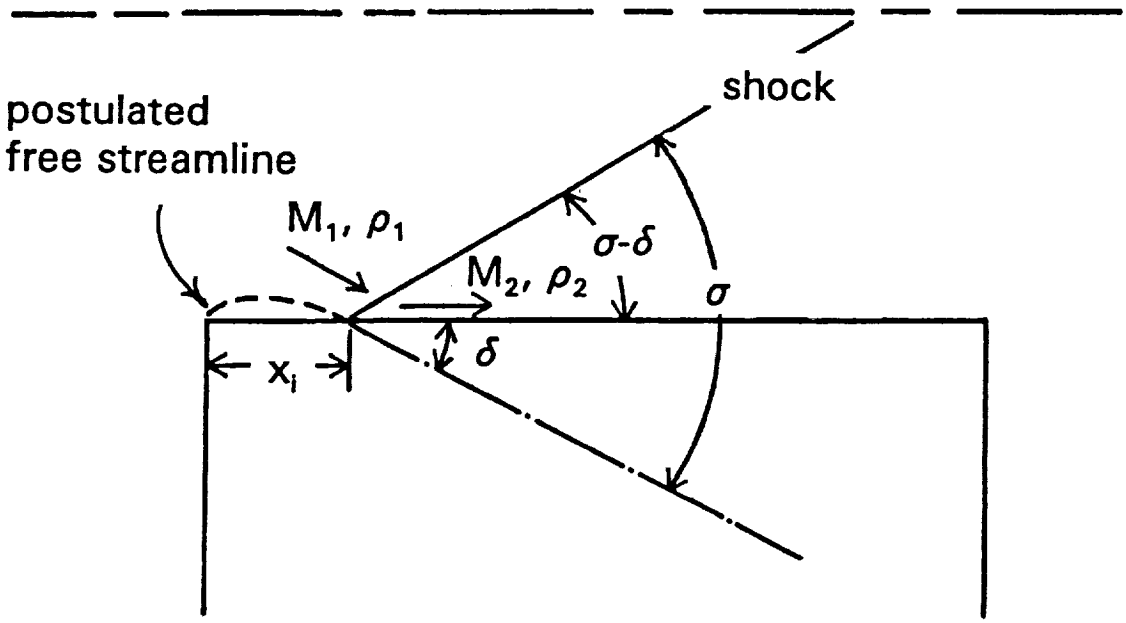

Figure 2. Model of shock formation

C-Le.

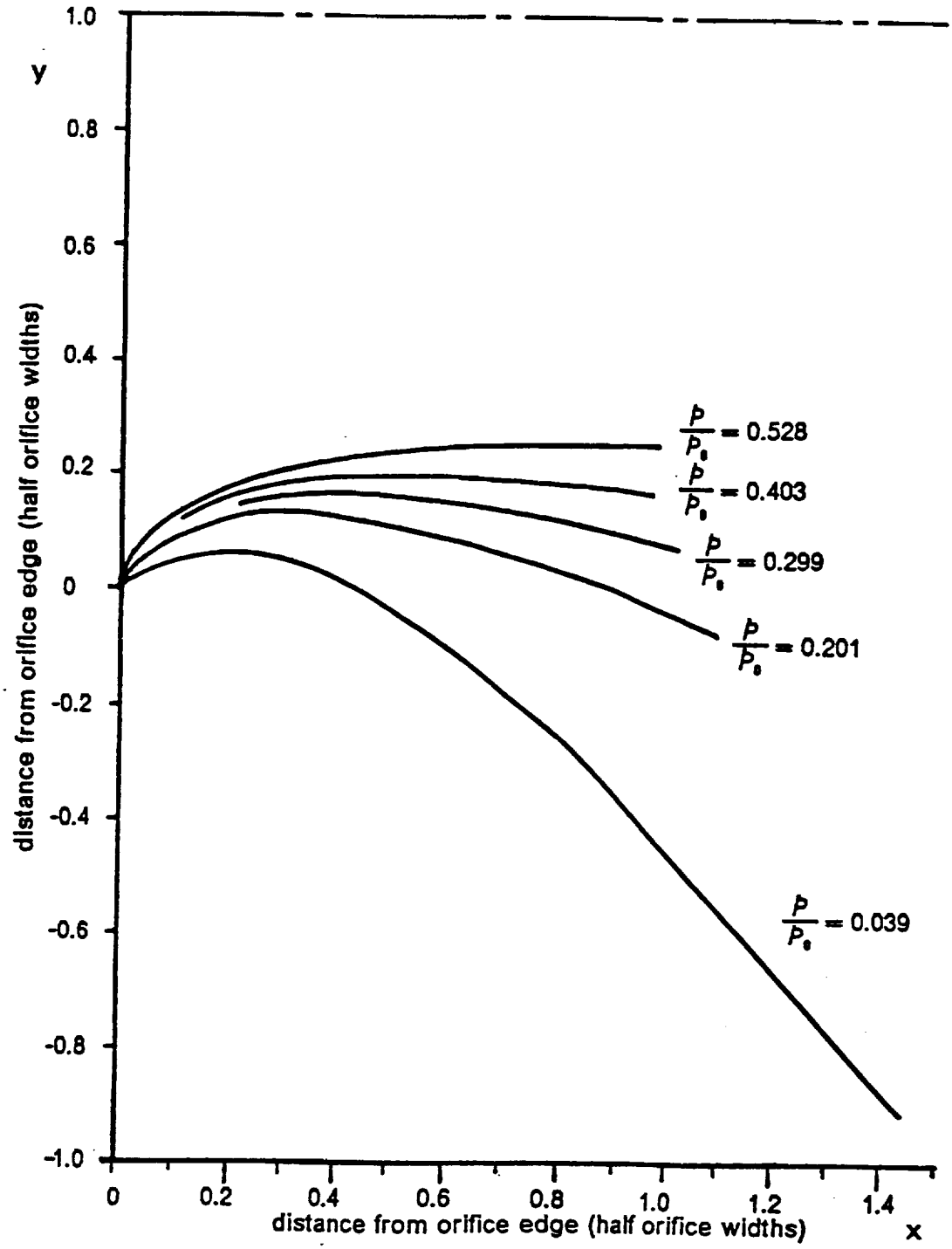

Figure 3. Norwood's calculated free streamlines from a half-slit

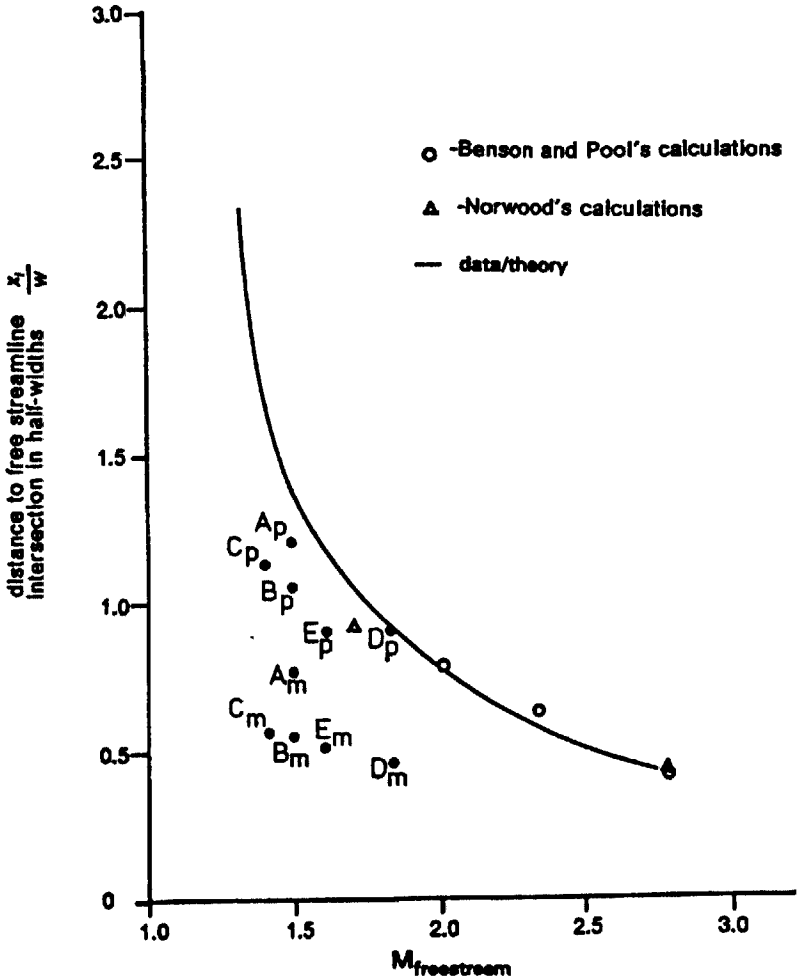

Figure 4. Comparison of free streamline intersection with channel sidewall

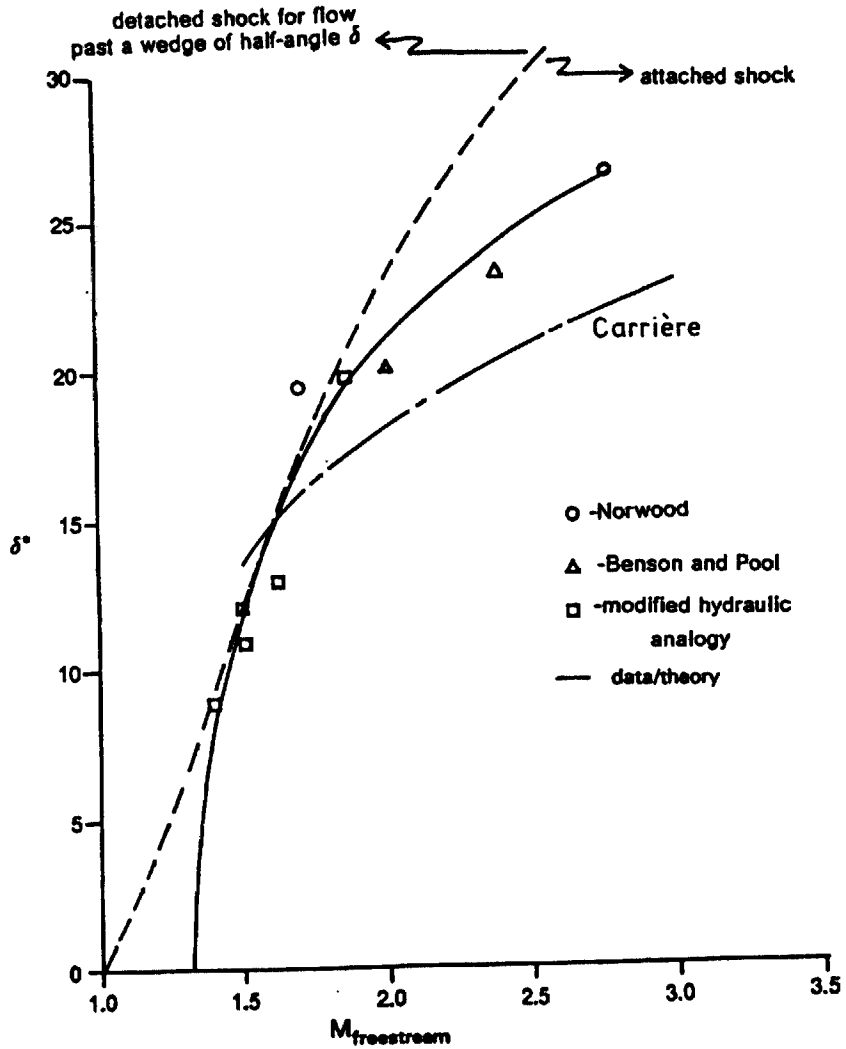

Figure 5. Compressible flow turning angles

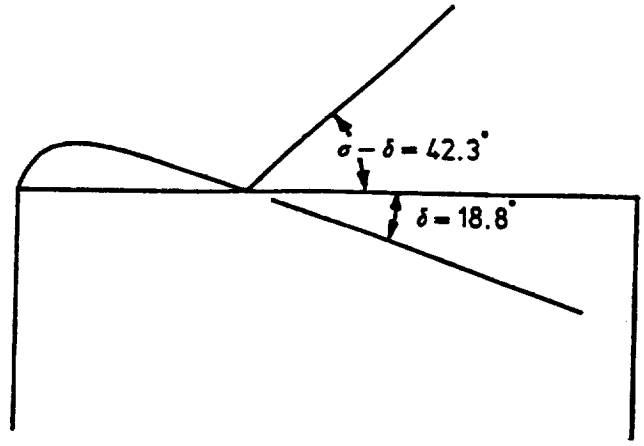

Figure 6. Predicted shock formation in compressible gas flow with $M_{freestream} = 1.8$

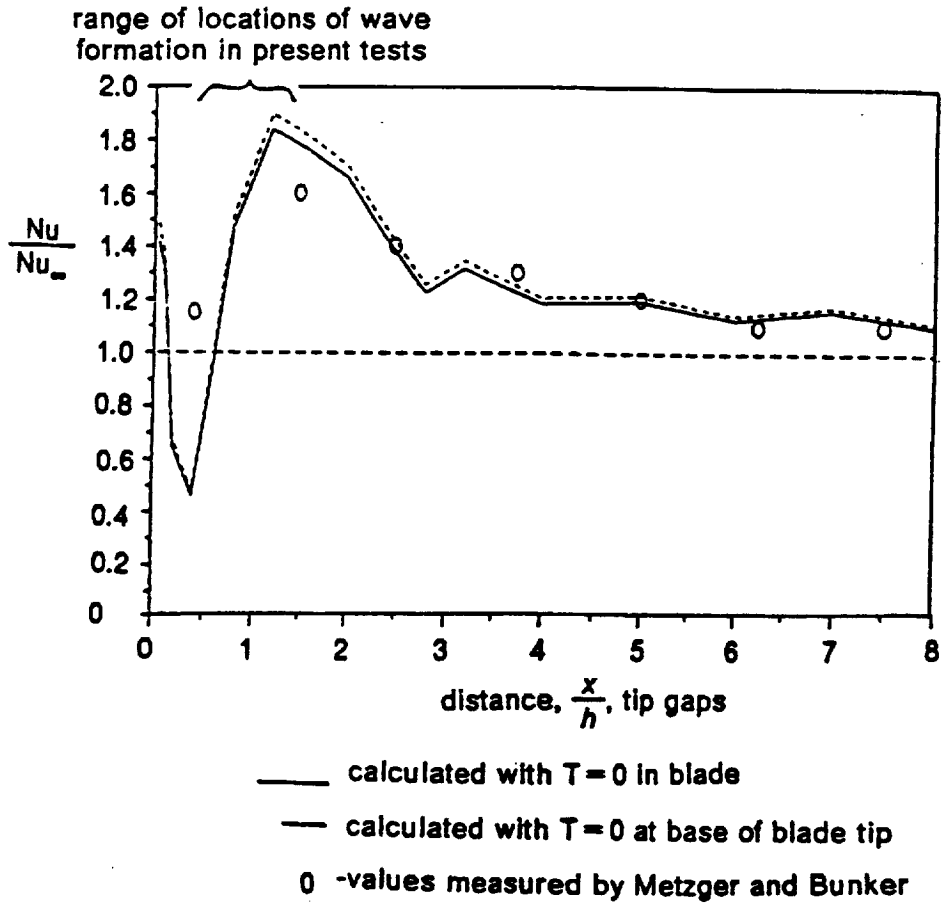

Figure 7. Enhanced heat transfer to turbine blade tip

Axisymmetric Computational Fluid Dynamics Analysis of Saturn V/S1-C/F1 Nozzle and Plume

Joseph H. Ruf
NASA/Marshall Space Flight Center
Huntsville, AL.

Abstract

An axisymmetric single engine Computational Fluid Dynamics calculation of the Saturn V/S1-C vehicle base region and F1 engine plume is described. There were two objectives of this work, the first was to calculated an axisymmetric approximation of the nozzle, plume and base region flow fields of S1-C/F1, relate/scale this to flight data and apply this scaling factor to a NLS/STME axisymmetric calculations from a parallel effort. The second was to assess the differences in F1 and STME plume shear layer development and concentration of combustible gases. This second piece of information was to be input/supporting data for assumptions made in NLS2 base temperature scaling methodology from which the vehicle base thermal environments were being generated. The F1 calculations started at the main combustion chamber faceplate and incorporated the turbine exhaust dump/nozzle film coolant. The plume and base region calculations were made for ten thousand feet and 57 thousand feet altitude at vehicle flight velocity and in stagnant freestream. FDNS was implemented with a 14 species, 28 reaction finite rate chemistry model plus a soot burning model for the RP-1/LOX chemistry. Nozzle and plume flow fields are shown, the plume shear layer constituents are compared to a STME plume. Conclusions are made about the validity and status of the analysis and NLS2 vehicle base thermal environment definition methodology.

George C. Marshall Space Flight Center
Structures and Dynamics Laboratory
Computational Fluid Dynamics Branch

NASA

Axisymmetric CFD Analysis of Saturn V/S1-C/F1 Nozzle and Plume

Joseph H. Ruf
Marshall Space Flight Center

George C. Marshall Space Flight Center
Structures and Dynamics Laboratory
Computational Fluid Dynamics Branch

NASA

Axisymmetric CFD Analysis of Saturn V/S1-C/F1 Nozzle and Plume

- BACKGROUND
- OBJECTIVE
- APPROACH
- RESULTS
- CONCLUSIONS

NASA

BACKGROUND

- STME design had hydrogen rich turbine exhaust ejected near the nozzle lip - potential recirculation to vehicle base.

- Initial NLS base heating thermal design environment severely impacted vehicle base thermal design.

- An in house CFD effort to qualitatively assess NLS/STME base heating rates was begun.
  - this included similar axisymmetric analysis of Saturn V/S1-C/F1 and NLS/STME configurations

NASA

OBJECTIVES

- Calculate an axisymmetric approximation of the nozzle, plume and base region flow fields of S1-C/F1, relate/scale this to flight data and apply this scaling factor to NLS/STME axisymmetric results.

- Assess the differences in F1 and STME plume shear layer development and concentration of combustible gases. An input/supporting data for assumptions made in NLS2 Base Temperature Scaling Methodology from which the vehicle base thermal environments were being generated.

NASA

APPROACH

- Axisymmetric model of S1-C outboard engine
  - nozzle and plumes solved separately, frozen and reacting solution obtained for all cases.

- Nozzle calculations
  - bulk flow and turbine exhaust constituents from Thermal Analysis Branch and F1 engine balance
  - nozzle extension geometry approximated, 3 equal area slots vs. 1 large and 21 smaller slots

F1 MCC and Nozzle Grid

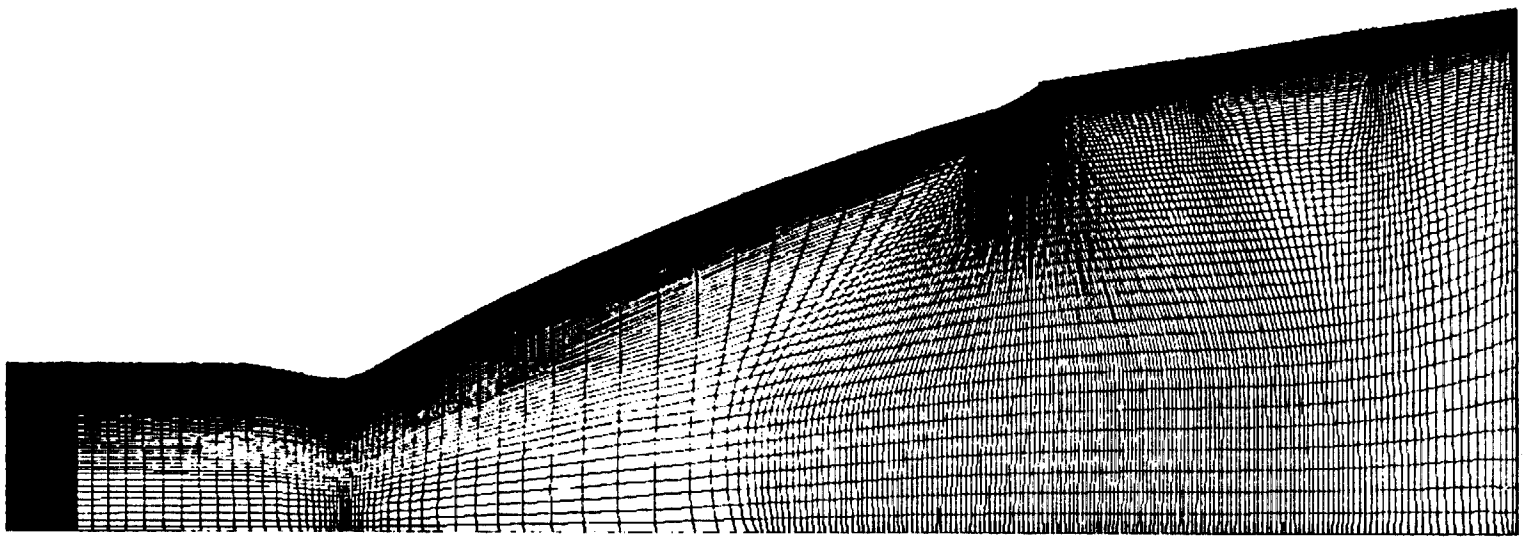

nozgrd.1.img

F1 MCC and Nozzle Grid
Nozzle Extension Detail

nozgrd.2.dsg

NASA

APPROACH, cont.

- Plume calculations
  - flow field at nozzle exit plane imposed as boundary condition
  - for base region flow, north and west boundaries initialized at flight velocities, fixed to ambient p and t
  - for plume studies, north and west boundaries specified as exits initially with zero velocity, fixed to ambient p and t
  - two altitudes solved, low - 10kft, high - 57kft

- Chemistry
  - finite rate, with 14 species and 28 reactions
  - soot modeled as solid carbon

10kft Plume Grid

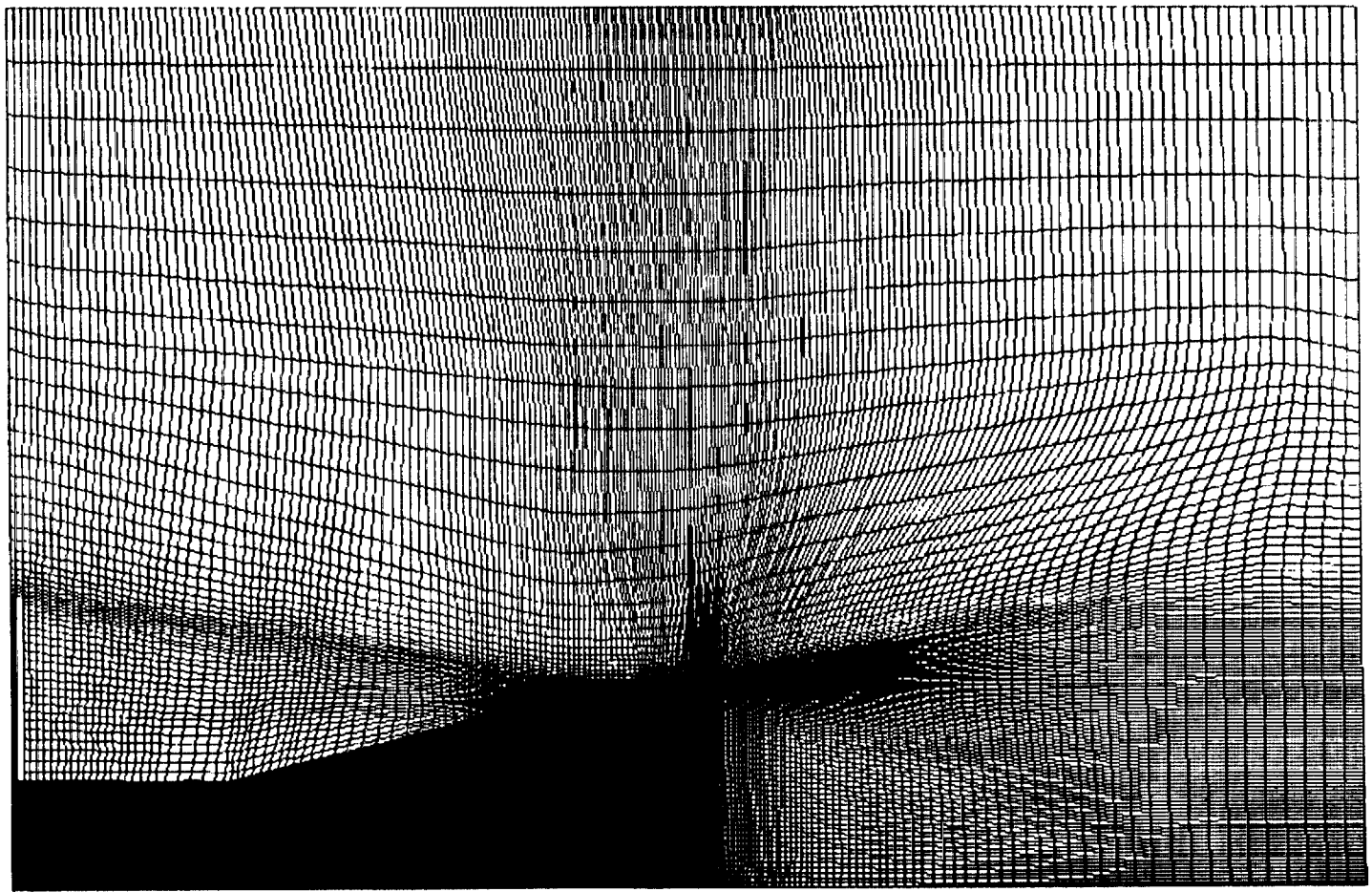

p810k.1.img

57kft Plume Grid

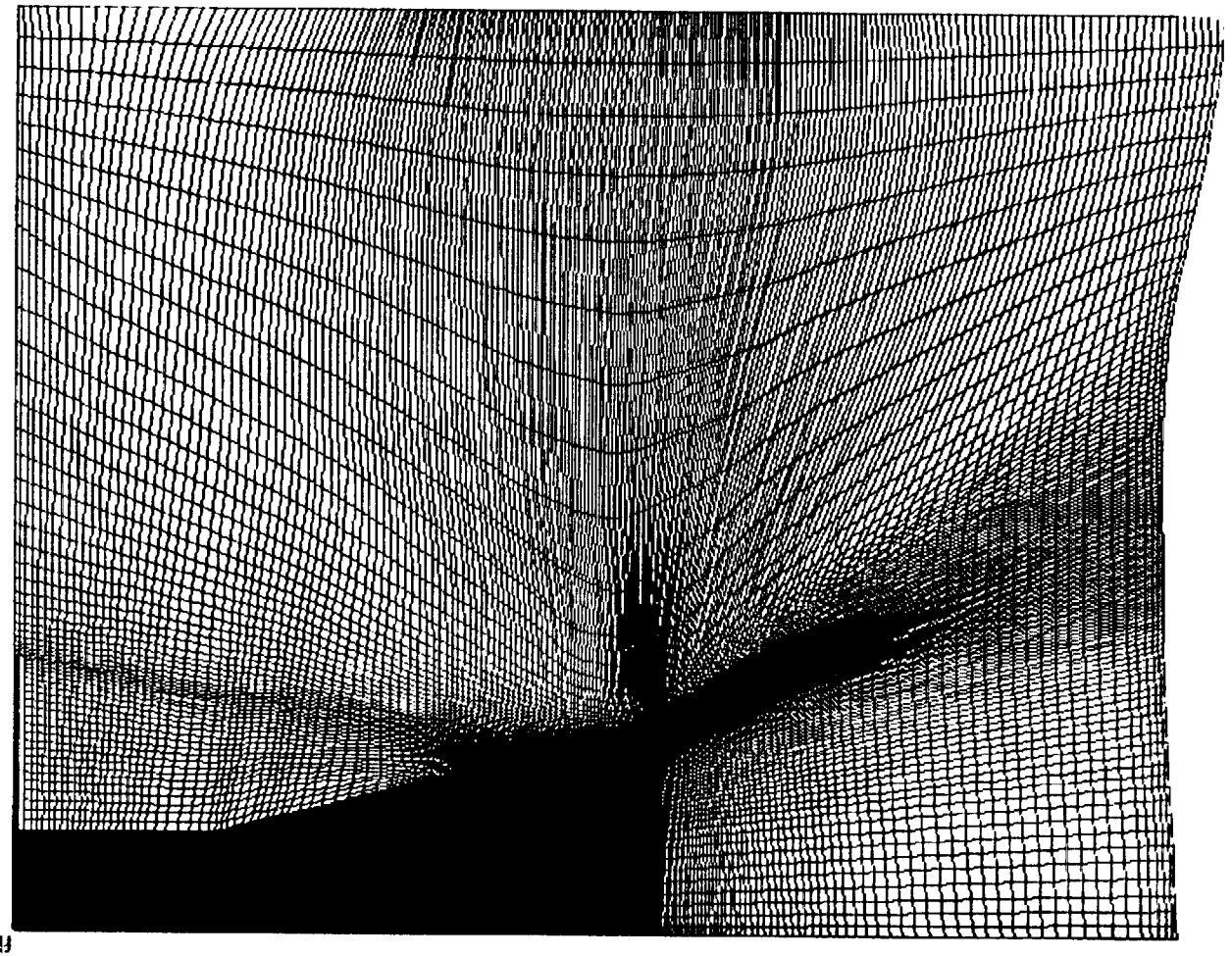

plums2.1.img

NASA

RESULTS

- Nozzle
  - effect of turbine exhaust seen well into the main flow field

  - compared to RAMP(MOC) calculation for smooth wall nozzle w/o turbine exhaust. Significant differences exist.

  - calculated thrust and Isp
    frozen flow +.5%
    finite rate +12%

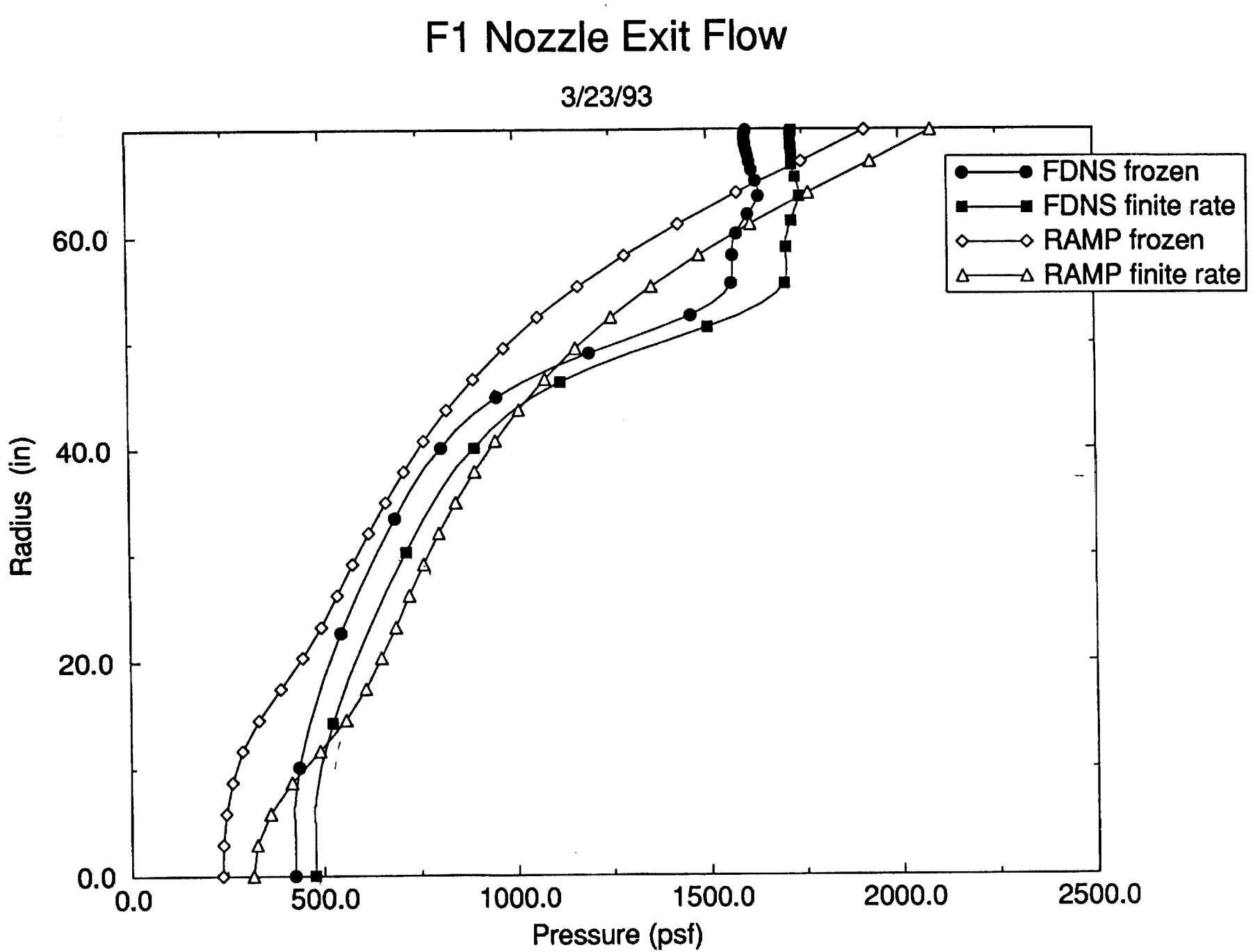
F1 Nozzle Exit Flow
3/23/93
FDNS frozen
FDNS finite rate
RAMP frozen
RAMP finite rate
Radius (in)
0.0
20.0
40.0
60.0
0.0
500.0
1000.0
1500.0
2000.0
2500.0
Pressure (psf)

NASA

RESULTS, cont.

- Plume
  - finite rate chemistry shows reduced rate of reaction at the high altitude as expected

  - significant difference in after burning of soot between the low and high altitude, soot burning at 10kft may be too vigorous

  - Combustible plume products in shear layer at high altitude in lbm/s

	nozzle radii downstream	
	1/2	1
F1	16.2	57.7
STME	29.6	53.3
ratio	1.8 to 1	.9 to 1

OH Mass Fraction
10Kft Plume

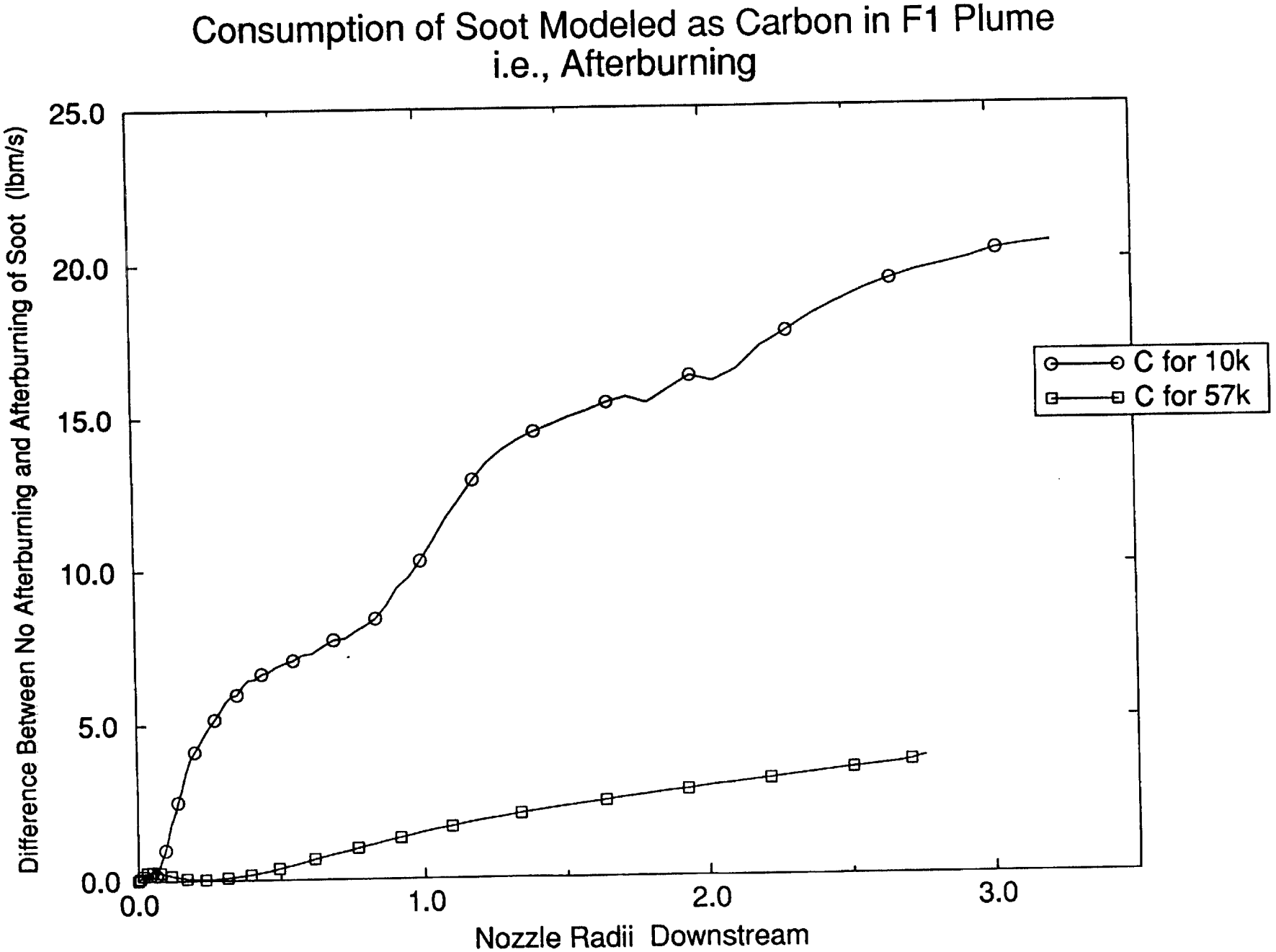
Consumption of Soot Modeled as Carbon in F1 Plume
i.e., Afterburning
Difference Between No Afterburning and Afterburning of Soot (lbm/s)
25.0
20.0
15.0
10.0
5.0
0.0
0.0
1.0
2.0
3.0
Nozzle Radii Downstream
C for 10k
C for 57k

NASA

CONCLUSIONS

- Thrust matched well for F1 with frozen flow, more work needed to get the finite rate calculation to match thrust levels.

- Need to reconcile differences between FDNS and the RAMP calculations.

- Soot burning model is too vigorous at low altitude, appears qualitative correct at high altitude.

- Recirculation to the base region was not representative of the S1-C/F1base region flow field (1st objective).

- Appears to be a significant difference in the plume shear layer development between F1 and STME (2nd objective).
  - Indicates that plume shear layer development and combustible gas concentrations are not similar, therefore, the NLS2 Base Gas Temperature Scaling Methodology may be non conservative.

Computational Fluid Dynamic (CFD) Analysis of Axisymmetric Plume and Base Flow of a Film/Dump Cooled Rocket Nozzle

P. K. Tucker
NASA/Marshall Space Flight Center (MSFC)
Marshall Space Flight Center, AL 35812

S. A. Warsi
Sverdrup Technology, Inc. (MSFC Group)
620 Discovery Drive
Huntsville, AL 35806

Film/dump cooling a rocket nozzle with fuel rich gas, as in the National Launch System (NLS) Space Transportation Main Engine (STME), adds potential complexities for integrating the engine with the vehicle. The chief concern is that once the film coolant is exhausted from the nozzle, conditions may exist during flight for the fuel-rich film gases to be recirculated to the vehicle base region. The result could be significantly higher base temperatures than would be expected from a regeneratively cooled nozzle.

CFD analyses were conduced to augment classical scaling techniques for vehicle base environments. The FDNS code with finite rate chemistry was used to simulate a single, axisymmetric STME plume and the NLS base area. Parallel calculations were made of the Saturn V S-1C/F1 plume base area flows. The objective was to characterize the plume/freestream shear layer for both vehicles as inputs for scaling the S-C/F1 flight data to NLS/STME conditions. The code was validated on high speed flows with relevant physics. This paper contains the calculations for the NLS/STME plume for the baseline nozzle and a modified nozzle. The modified nozzle was intended to reduce the fuel available for recirculation to the vehicle base region. Plumes for both nozzles were calculated at 10kFT and 50kFT.

NASA
National Aeronautics and
Space Administration

CFD ANALYSIS OF AXISYMMETRIC PLUME & BASE OF A FILM/DUMP COOLED NOZZLE

1458

Kevin Tucker
MSFC/ED32

Saif Warsi
Sverdrup Technology, Inc.

National Aeronautics and Space Administration

NLS/STME Plume and Base Region Results

OVERVIEW

- Objective
- Approach
- Results
  - 10kft/50kft Comparison
  - 50kft Baseline/Modified Comparison
- Status

National Aeronautics and Space Administration

NLS/STME Plume and Base Region Results

OBJECTIVES

- **Generate NLS/STME plume/base flows as a function of altitude**

- **Results**
  - -- Comparison of shear layer gradients
    - As a function of altitude
    - As a function of distance donwstream of nozzle
  - -- Comparison of alternate dump schemes
  - -- Comparison to S-1C for scaling Saturn flight data

- **Develop significant in-house capability for**
  - -- Reacting nozzle flows
  - -- Reacting plumes
  - -- Complex base flows

National Aeronautics and Space Administration

NLS/STME Plume and Base Region Results

APPROACH

- **Geometry**
  - -- NLS 1.5 Stage Base
  - -- 2-D/axisymmetric model of outer STME
  - -- Nozzle calculations done separately
- **Conditions**
  - -- Baseline nozzle/plume
  - -- Modified nozzle/plume
    - No dump at exit
    - Dump moved to primary injector
- **Altitudes**
  - -- 10kft
  - -- 50kft
- **Freestream**
  - -- Quiescent
  - -- Velocity at trajectory point
- **Chemistry**
  - -- Frozen
  - -- Finite rate (7 species, 9 reactions)

NASA
National Aeronautics and Space Administration

NLS/STME Plume and Base Region Results

RESULTS

10kft Grid

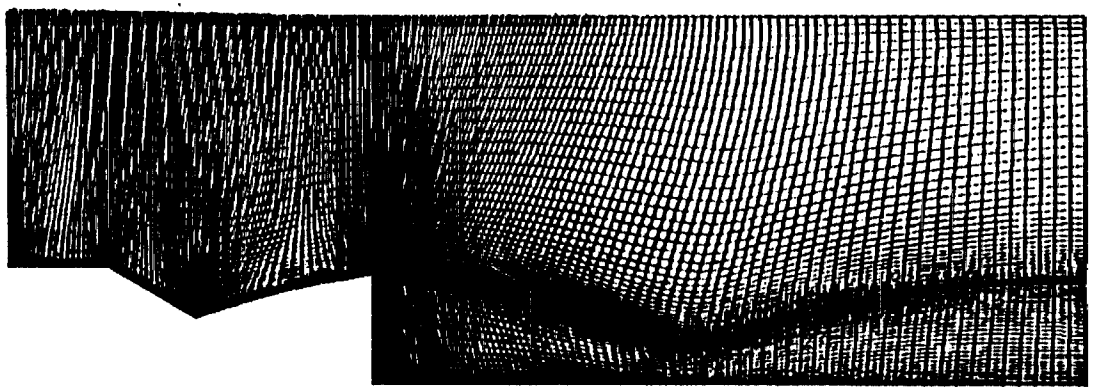

50kft Grid

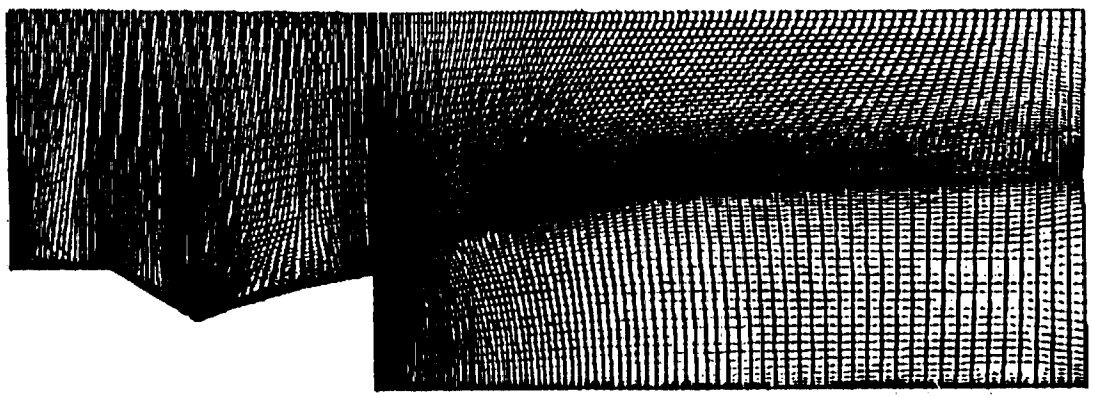

NLS/STME Plume and Base Region Results

RESULTS

10kft Baseline Reacting Flow - Quiescent Freestream (x/R = 1)

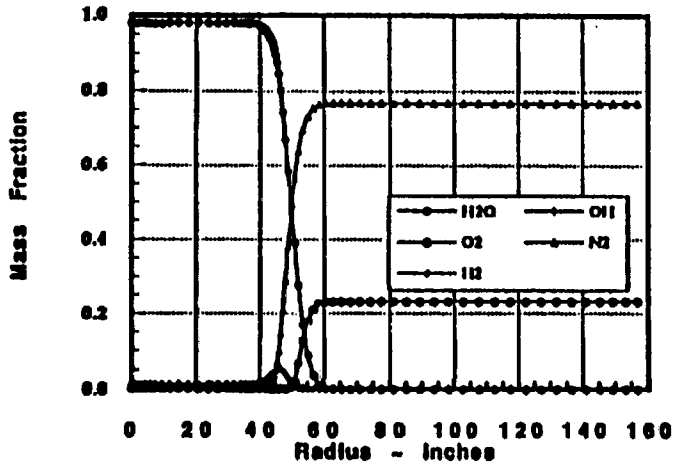

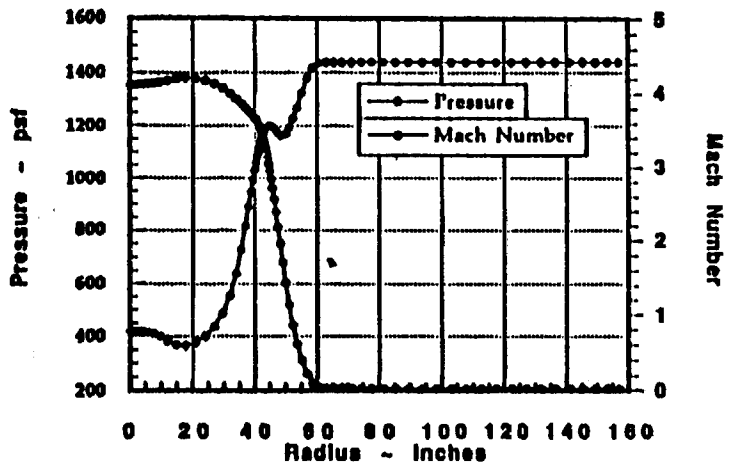

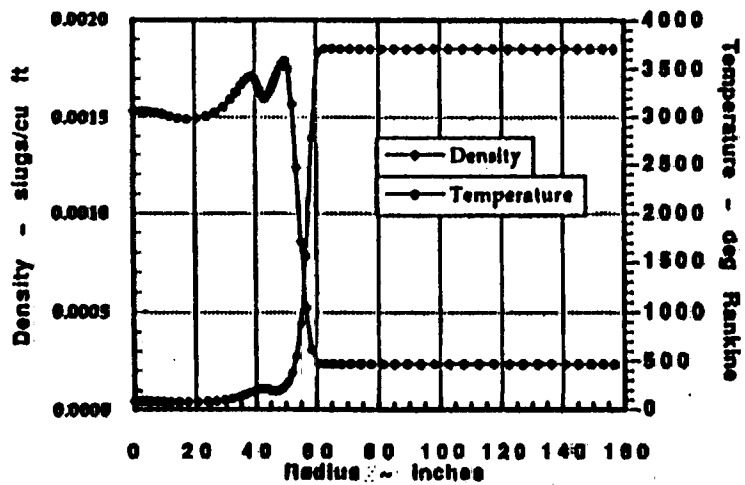

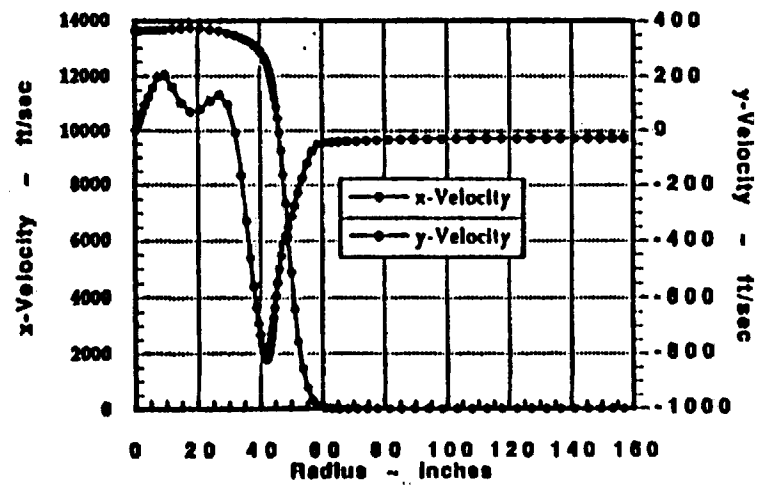

National Aeronautics and Space Administration

NLS/STME Plume and Base Region Results

Temperature (deg R)
NLS Baseline - 10kft
Reacting Flow (Quiescent)

H2 Mass Fraction
NLS Baseline - 10kft
Reacting Flow (Quiescent)

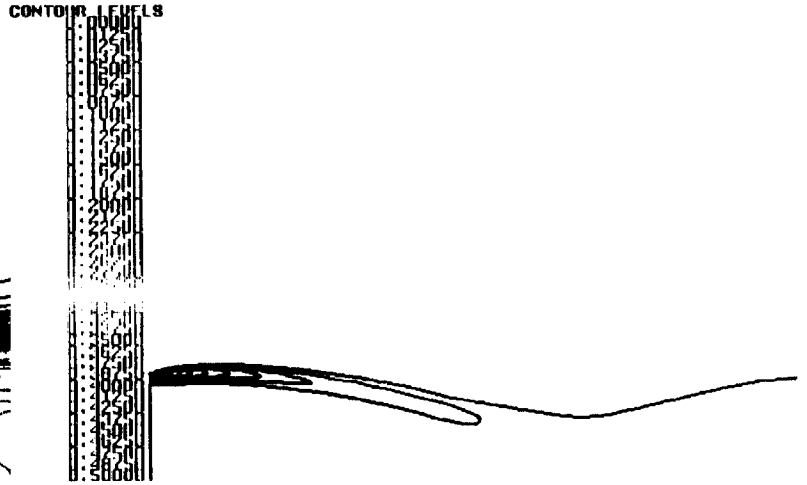

Temperature (deg R)
NLS Baseline - 50kft
Reacting Flow (Quiescent)

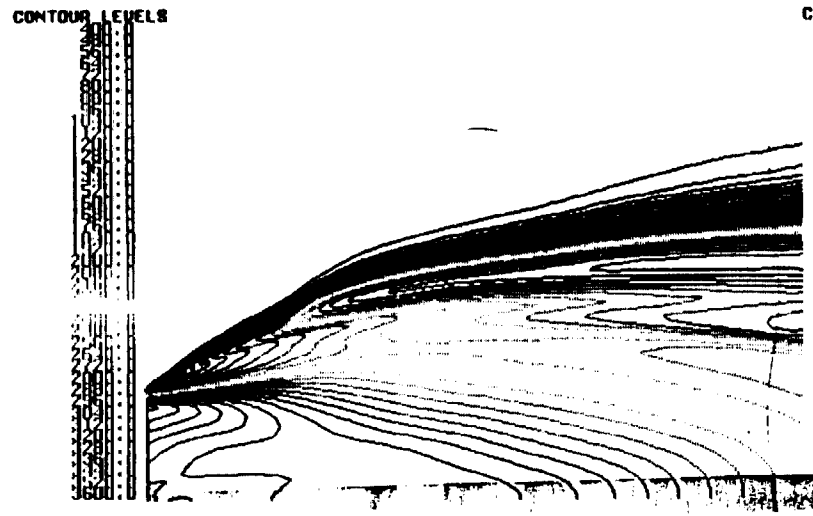

H2 Mass Fraction
NLS Baseline - 50kft
Reacting Flow (Quiescent)

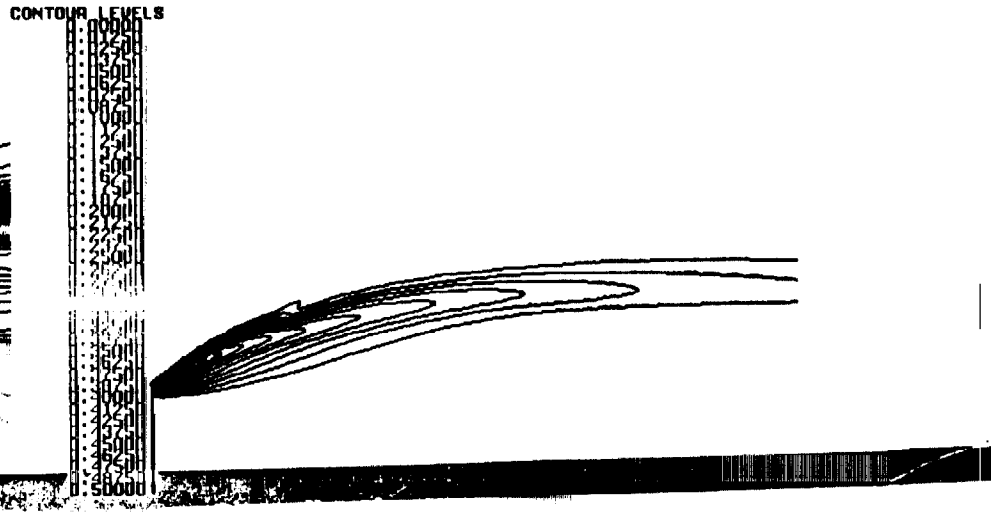

NASA
National Aeronautics and Space Administration

NLS/STME Plume and Base Region Results

RESULTS

50kft Modified Reacting Flow - Quiescent Freestream (x/R = 1)

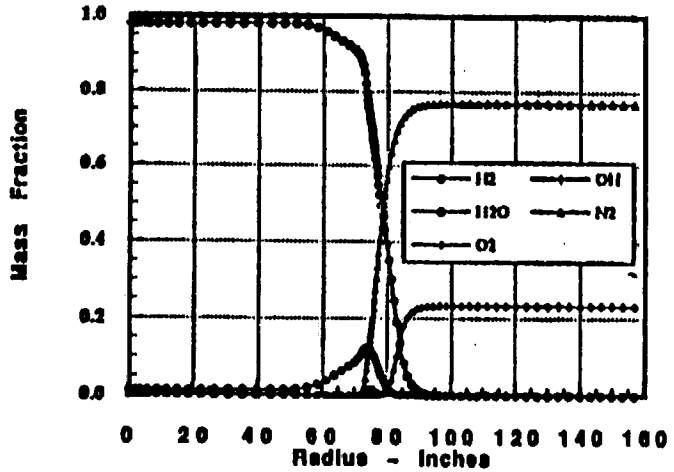

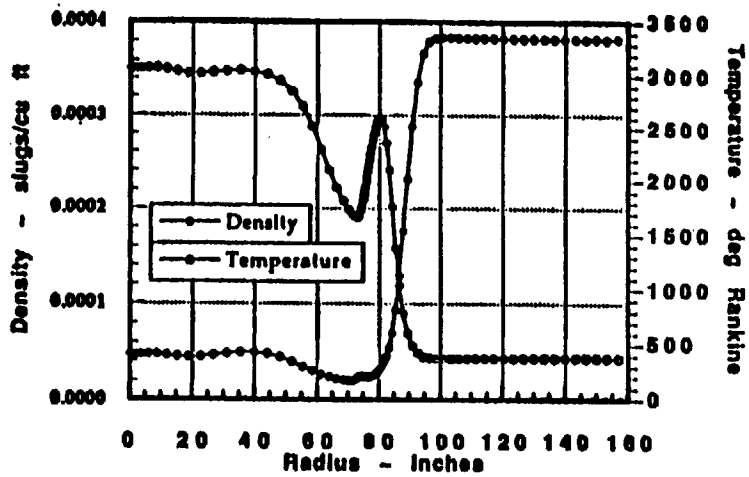

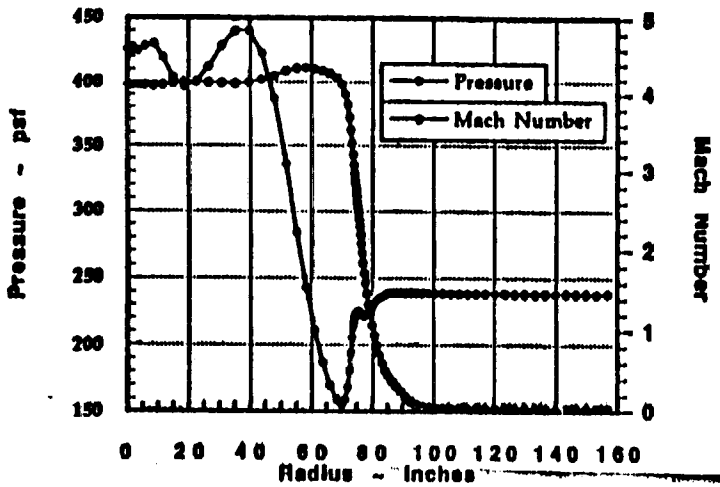

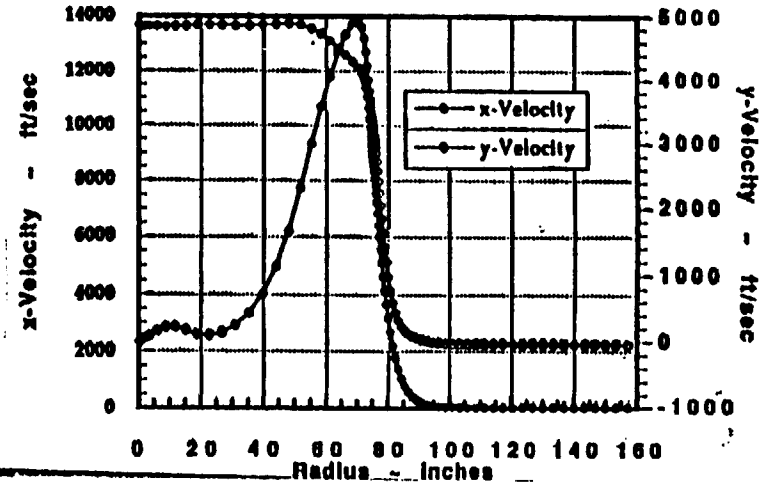

National Aeronautics and Space Administration

NLS/STME Plume and Base Region Results

OH Mass Fraction
NLS Baseline - 50kft
Reacting Flow (Quiescent)

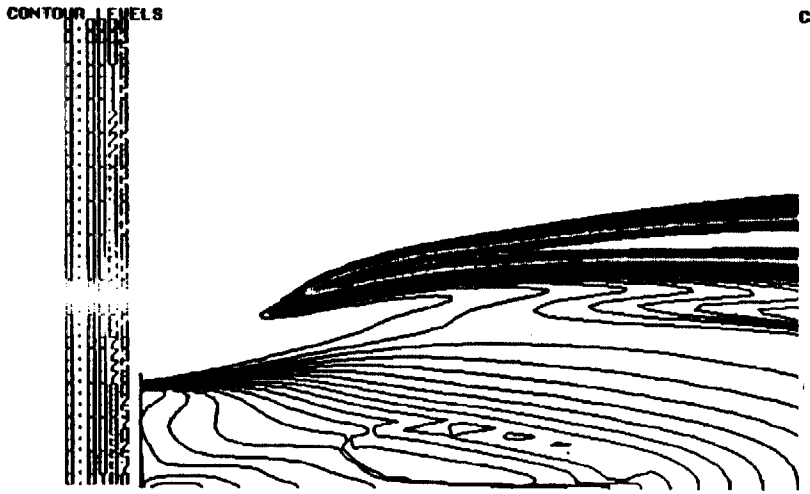

H2O Mass Fraction
NLS Baseline - 50kft
Reacting Flow (Quiescent)

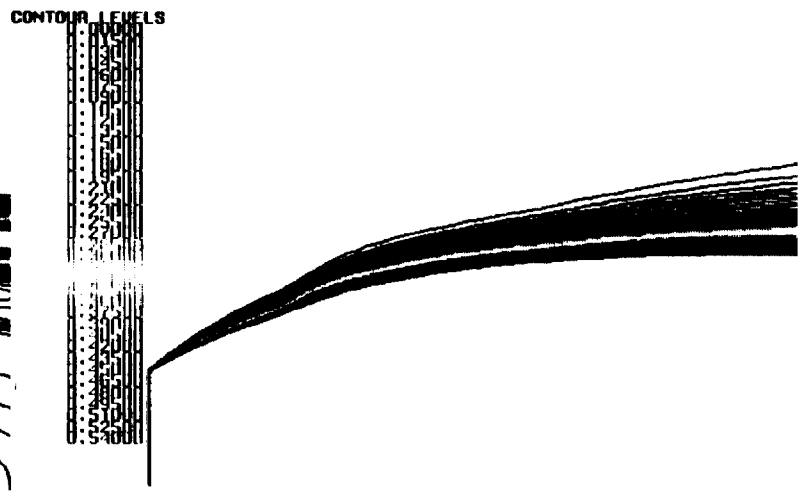

OH Mass Fraction
NLS Modified - 50kft
Reacting Flow (Quiescent)

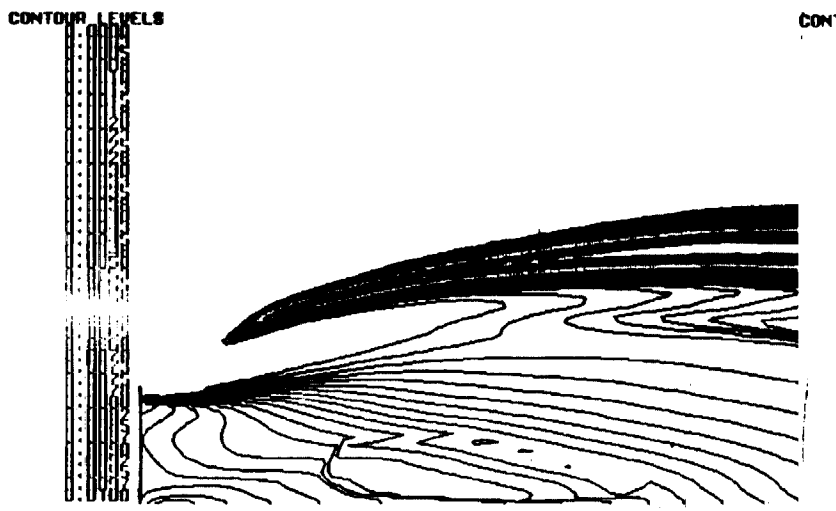

H2O Mass Fraction
NLS Modified - 50kft
Reacting Flow (Quiescent)

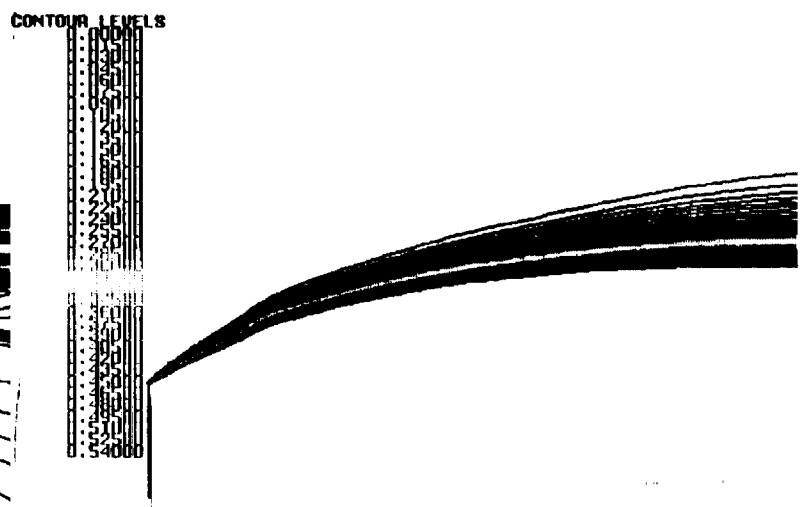

National Aeronautics and Space Administration

NLS/STME Plume and Base Region Results

APPROACH

NLS 1.5 Stage Base

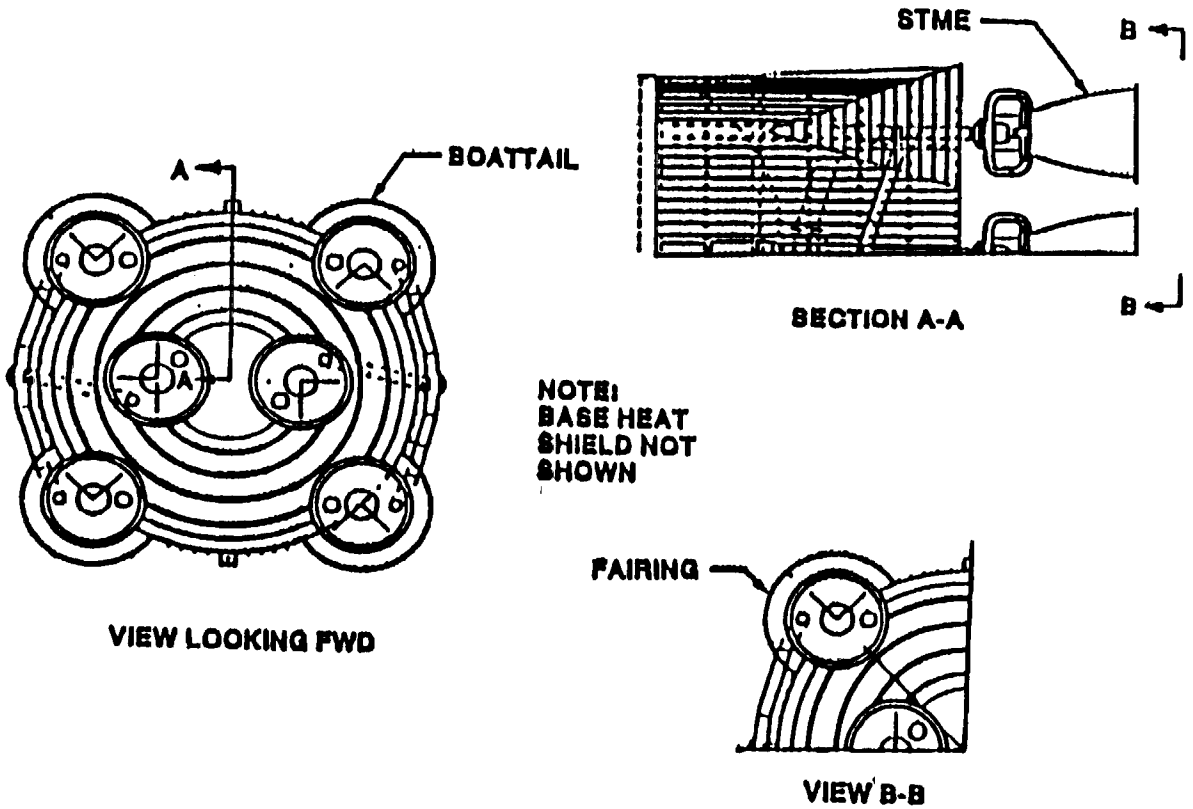

National Aeronautics and Space Administration

NLS/STME Plume and Base Region Results

APPROACH

STME Nozzle Grid

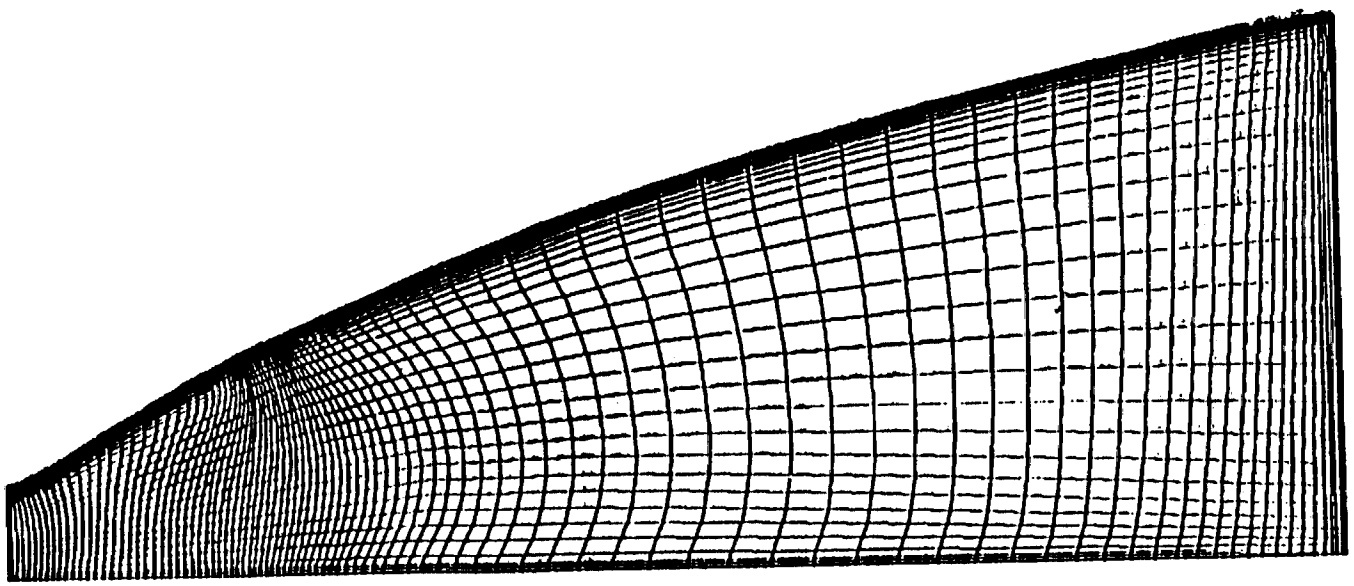

National Aeronautics and Space Administration

NLS/STME Plume and Base Region Results

TEMPERATURE

BASELINE NOZZLE

CONTOUR LEVELS
800.0
940.0
1080.0
1220.0
1360.0
1500.0
1640.0
1780.0
1920.0
2060.0
2200.0
2340.0
2480.0
2620.0
2760.0
2900.0
3040.0
3180.0
3320.0
3460.0
3600.0
3740.0
3880.0
4020.0
4160.0
4300.0
4440.0
4580.0
4720.0
4860.0
5000.0
5140.0
5280.0
5420.0
5560.0
5700.0
5840.0
5980.0
6120.0
6260.0
6400.0

1.000 MACH
0.00 DEG ALPHA
1.18x10**7 Re
100x38 . GRID

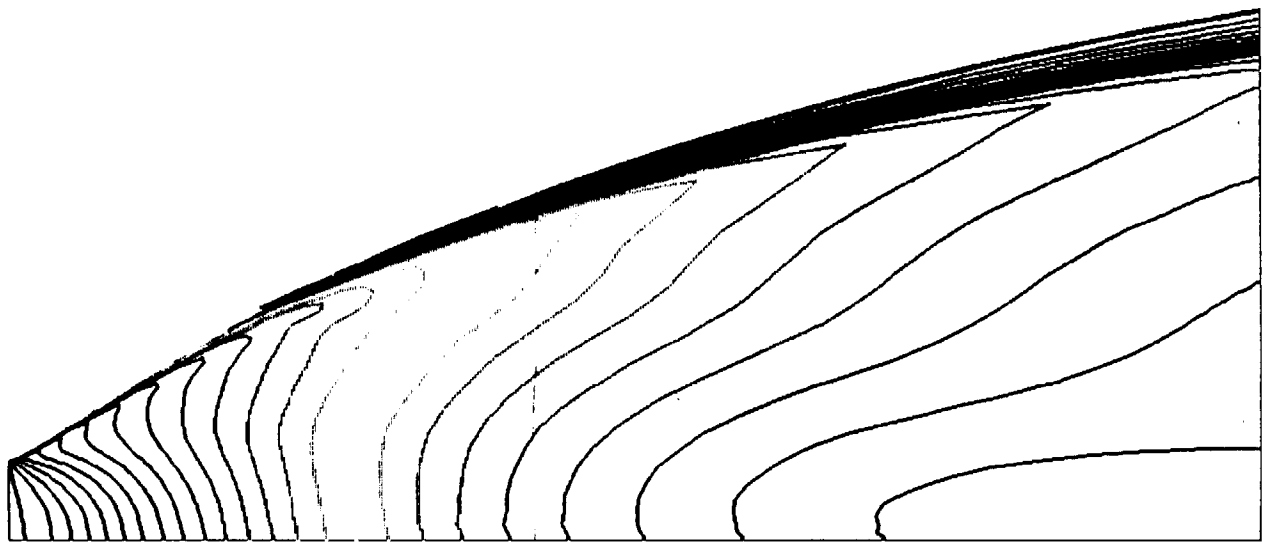

1469

National Aeronautics and Space Administration

NLS/STME Plume and Base Region Results

APPROACH

NOZZLE CASES

PLUME/BASE CASES

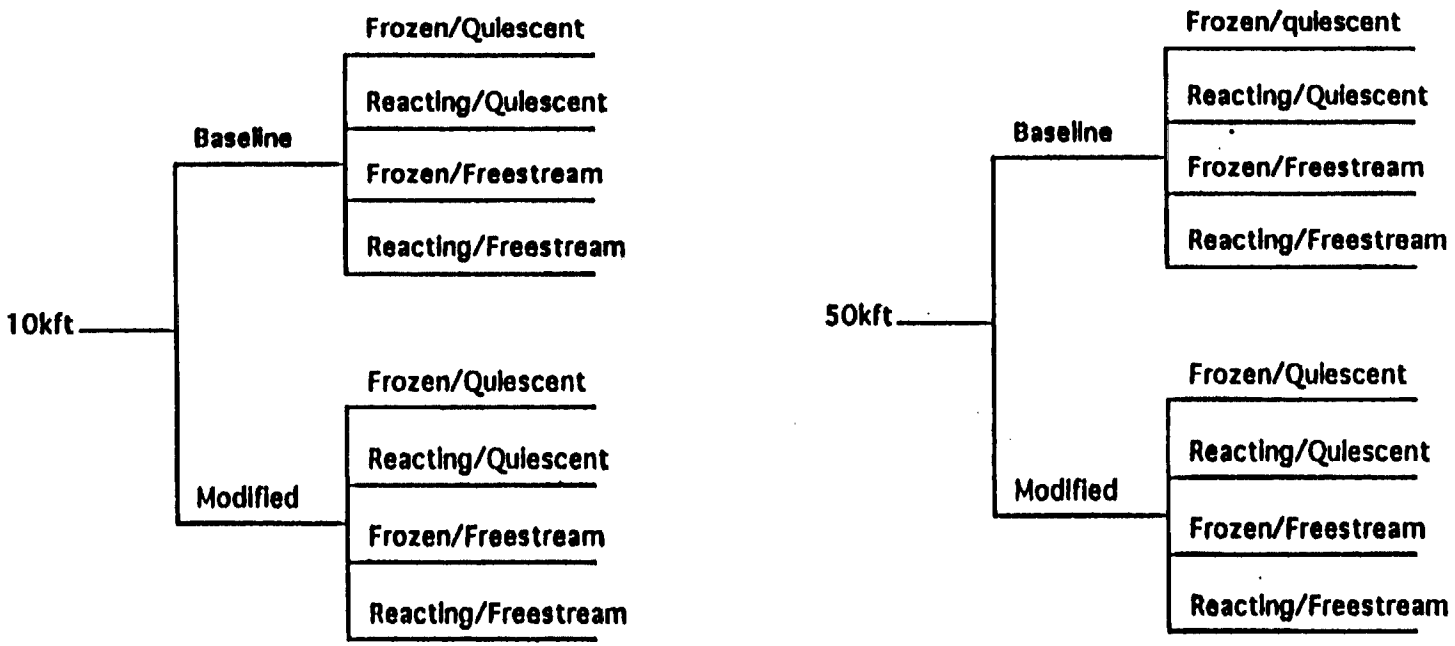

National Aeronautics and Space Administration

NLS/STME Plume and Base Region Results

RESULTS

50kft Baseline Reacting Flow - Quiescent Freestream (x/R = 1)

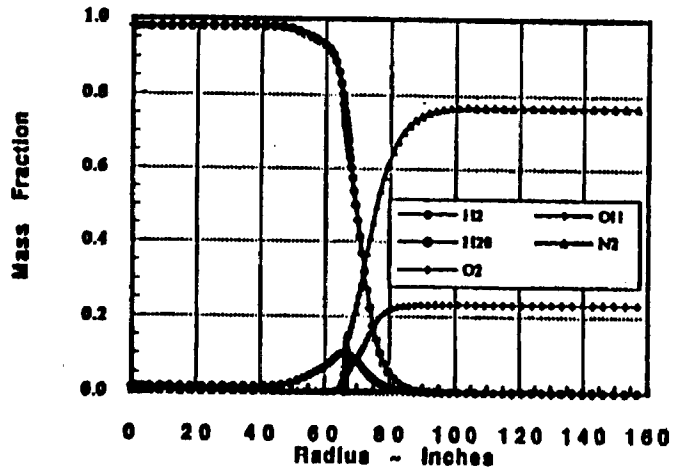

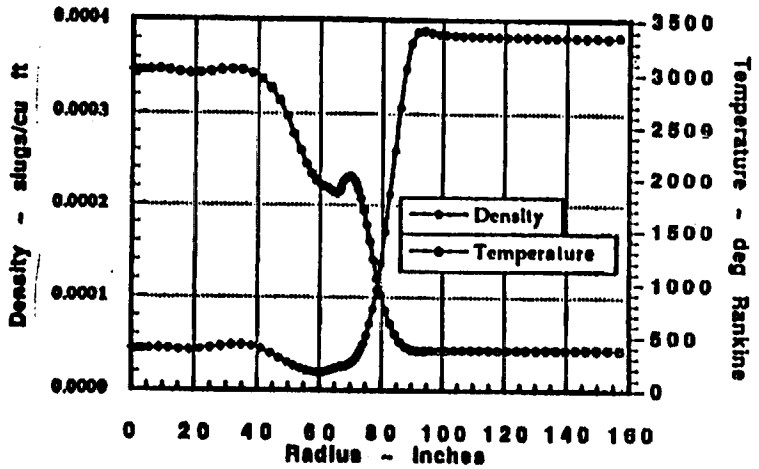

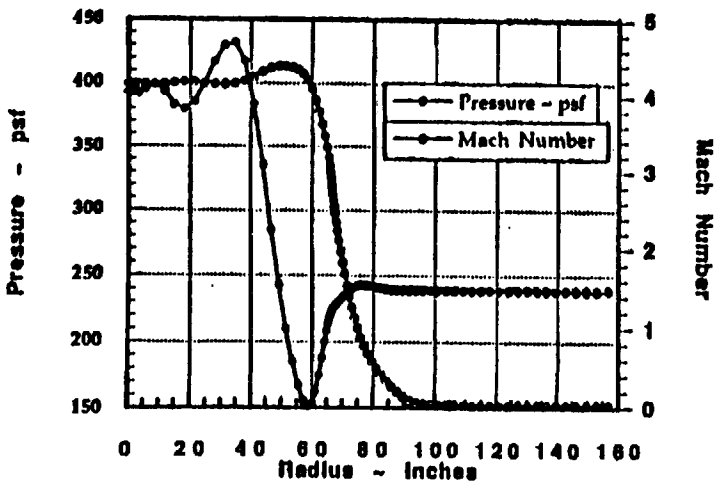

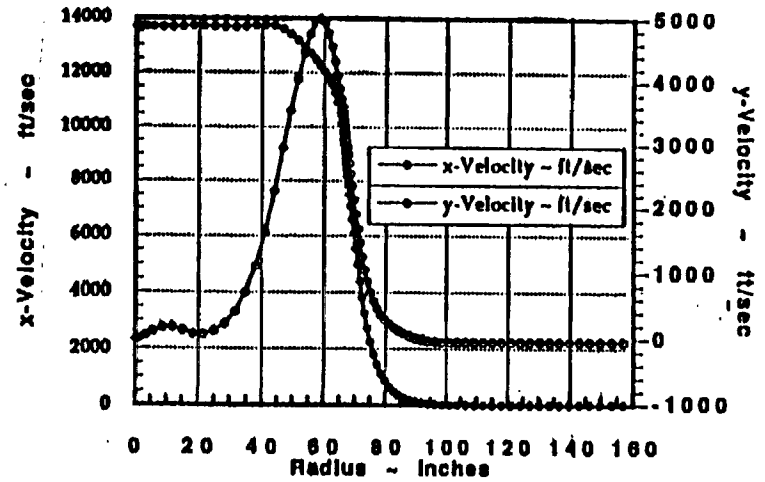

NASA
National Aeronautics and Space Administration

NLS/STME Plume and Base Region Results

RESULTS

50kft Baseline Reacting Flow - Quiescent Freestream (x/R = 1)

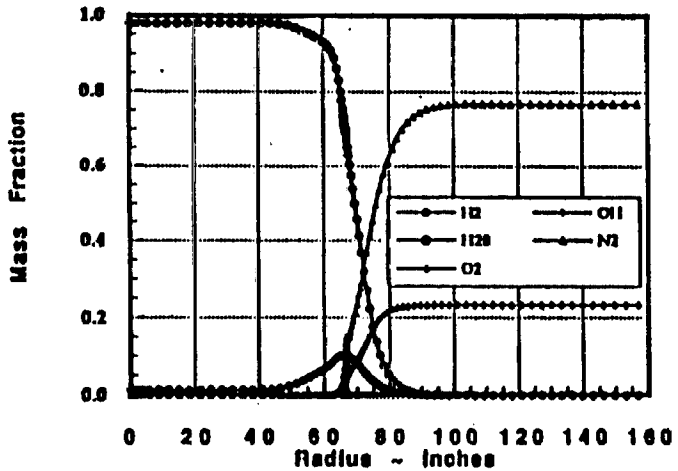

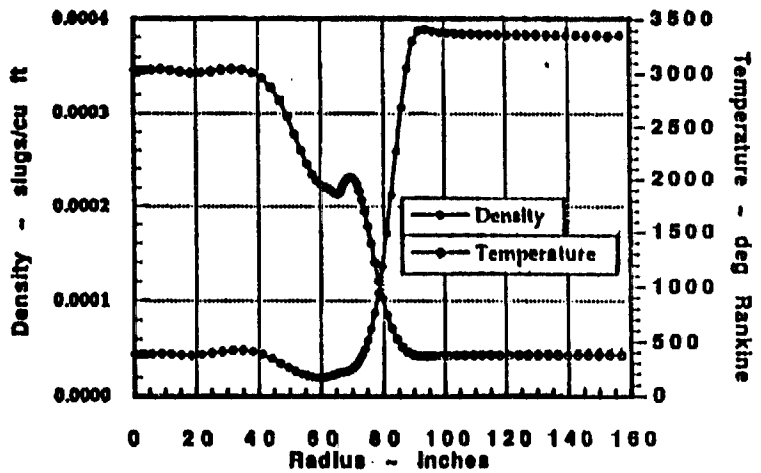

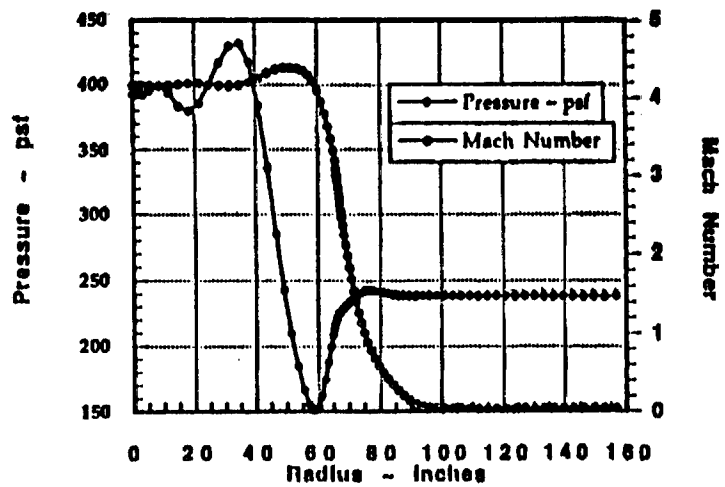

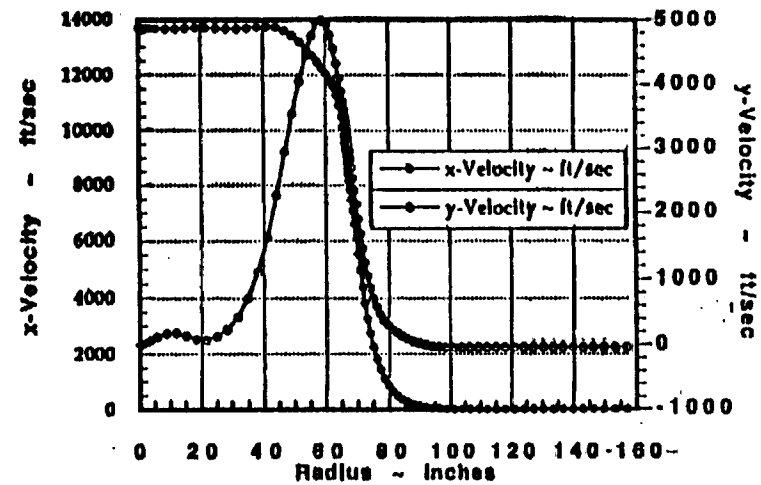

NASA
National Aeronautics and
Space Administration

STATUS/SUMMARY

- Frozen & finite rate calculations of STME plume complete for 10kft and 50kft
- Burning exhibited in plume shear layer for all cases
- Shear layer burning occurs further downstream at higher altitudes
- Shear layer burning from the modified nozzle occurs slightly upstream of baseline nozzle plume
- Shear layer gradients were delivered to ED33 for analysis & comparison to S1-C/F1
- Preliminary calculations at high altitudes indicate:
  - at 1/2 radius downstream of nozzle more combustibles (approx. 2:1) in NLS/STME shear layer
  - at 1 radius downstream of nozzle , combustible ratio is about even

NLS Base Heating CFD Analysis

Edward, P. Ascoli, Adel H. Heiba, Yann-Fu Hsu,
Ronald R. Lagnado, and Edward D. Lynch

Rockwell International, Rocketdyne Division

Workshop for Computational Fluid Dynamic
Applications in Rocket Propulsion

April 20-22, 1993
NASA Marshall Space Flight Center

Abstract

Concerns raised over possible base heating effects on the NLS 1.5 stage reference vehicle resulted in the use of CFD as a predictive analysis tool. The objective established was to obtain good engineering solutions to describe the base region flowfields at 10,000 ft. and 50,000 ft. altitudes. The Rockwell USA CFD code was employed with a zero-equation turbulence model and a four species, 1 step chemical kinetics package. Three solutions were generated for the specified altitudes on coarse and fine grids. CFD results show the base region flowfields to be highly three-dimensional in character. At the 10,000 ft. altitude, plumes contract soon after exiting the nozzles and do not interact with each other. No mechanism was identified for driving hot gas back into the base region and no significant amounts of hydrogen or water were found in the base region. Consequently, surface temperatures were all near the ambient level. At 50,000 ft., the nozzle exhaust plumes begin to interact, particularly those of the two inboard engines which are closer together. A small amount of hot gas is recirculated between the inboard nozzles near the nozzle exit plane. As a result, base region surface temperatures are slightly elevated, but still remain well within the design guideline of 1000°R.

NLS BASE HEATING CFD ANALYSIS

Edward P. Ascoli
Adel H. Heiba
Yann-Fu Hsu
Ronald R. Lagnado
Edward D. Lynch

Rockwell International, Rocketdyne Division

Workshop for Computational Fluid Dynamic
Applications in Rocket Propulsion

April 20-22, 1993
NASA Marshall Space Flight Center

ROCKETDYNE BASE HEATING CFD ANALYSIS TEAM

CFD Technology Center Management

M. Sindir, Manager — S. Barson, Project Engineer

Base Heating Analysis (Rocketdyne)

E. Ascoli*
A. Heiba*
Y. Hsu
R. Lagnado* (L)
E. Lynch
R. Ungewitter
M. Williams
R. Yang

Data Visualization and Computing (Rocketdyne)

S. Barson
M. DeCroix (L)
D. Fashena

USA Code Consulting (Rockwell Science Center)

S. Chakravarthy

Graphical Animation Consulting (NASA Ames/Sterling Software)

K. McCabe

*Full Time (L) Technical Lead

INTRODUCTION

- **CONCERNS RAISED OVER POSSIBLE BASE HEATING/BURNING EFFECTS ON NLS 1.5 STAGE REFERENCE VEHICLE**

- **UNIQUE CONFIGURATION**
  - SIX ENGINE CLUSTER
  - HYDROGEN FILM COOLANT INTERNAL TO NOZZLE WALL
  - HYDROGEN-RICH TURBINE EXHAUST USED AS COOLANT
    - DUMPED FROM NOZZLE WALL IN EXIT PLANE

- **CONCERN OVER APPLICABILITY OF EXISTING BASE HEATING DATABASE**

CFD IDENTIFIED AS ALTERNATE PREDICTIVE TOOL

APPROACH

- **OBTAIN ENGINEERING SOLUTION FOR THE 1.5 STAGE REFERENCE GEOMETRY AT 10,000 AND 50,000 FT ALTITUDES**
  - 3-D CALCULATIONS USING TWO GRIDS (638K, 212K POINTS)
  - FINE GRID JUDGED ADEQUATE FOR FLOW ENVIRONMENT DEFINITION PURPOSES (BASED ON EXPERIENCE & AXISYMMETRIC RESULTS)
  - 0-EQUATION TURBULENCE MODEL AND COMPLETE COMBUSTION CHEMISTRY MODEL
  - CONVERGENCE MONITORED THROUGH CONVENTIONAL CRITERIA (RESIDUALS) AND CHANGES IN LOCAL VALUES
  - ASSESSMENT OF KEY PARAMETERS CARRIED OUT VIA SINGLE ENGINE AXISYMMETRIC FLOW CALCULATIONS
    - GRID RESOLUTION
    - TURBULENCE MODELS
    - CHEMISTRY MODELS
  - VALIDATION DONE WITH AVAILABLE DATA ON RELEVANT 2-D & 3-D GEOMETRIES

- **ALL CALCULATIONS DONE WITH USA CODE**

NLS 1.5 STAGE GEOMETRY

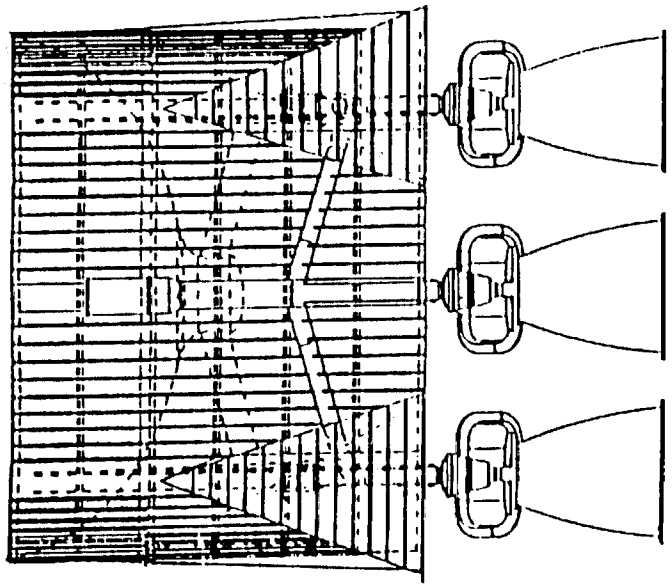

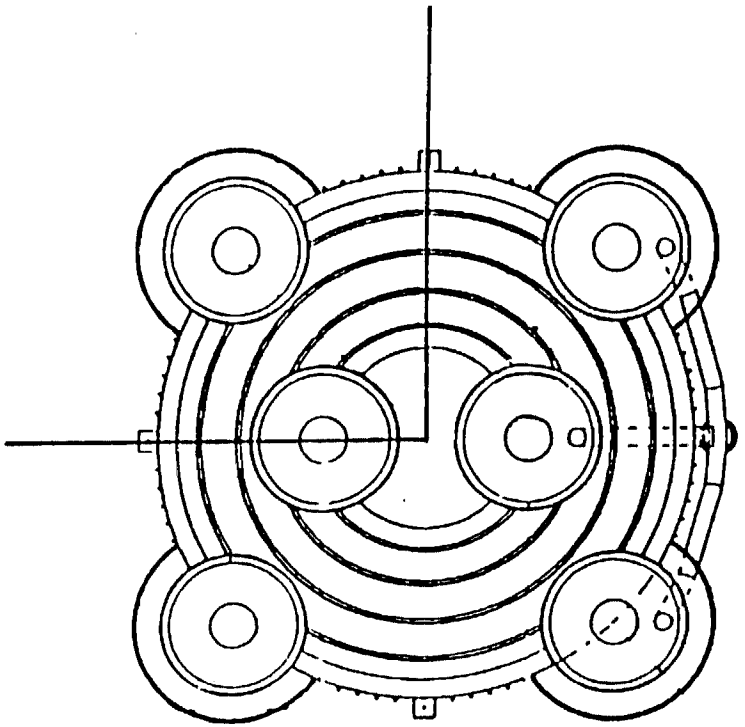

- **1.5 STAGE REFERENCE VEHICLE**
  - GRID MODELS ONE QUADRANT (TWO SYMMETRY PLANES)
  - CYCLE 0 HEAT SHIELD, BASE, FARFIELD, AND DOWNSTREAM REGIONS INCLUDED

CFD MODEL OF NLS 1.5 STAGE VEHICLE BASE AND ENGINE CLUSTER (CONT'D)

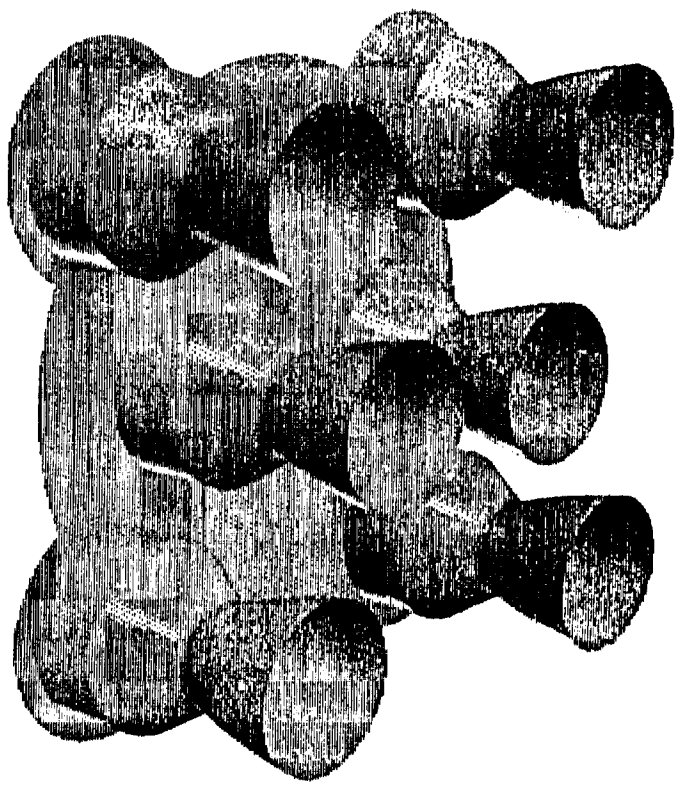

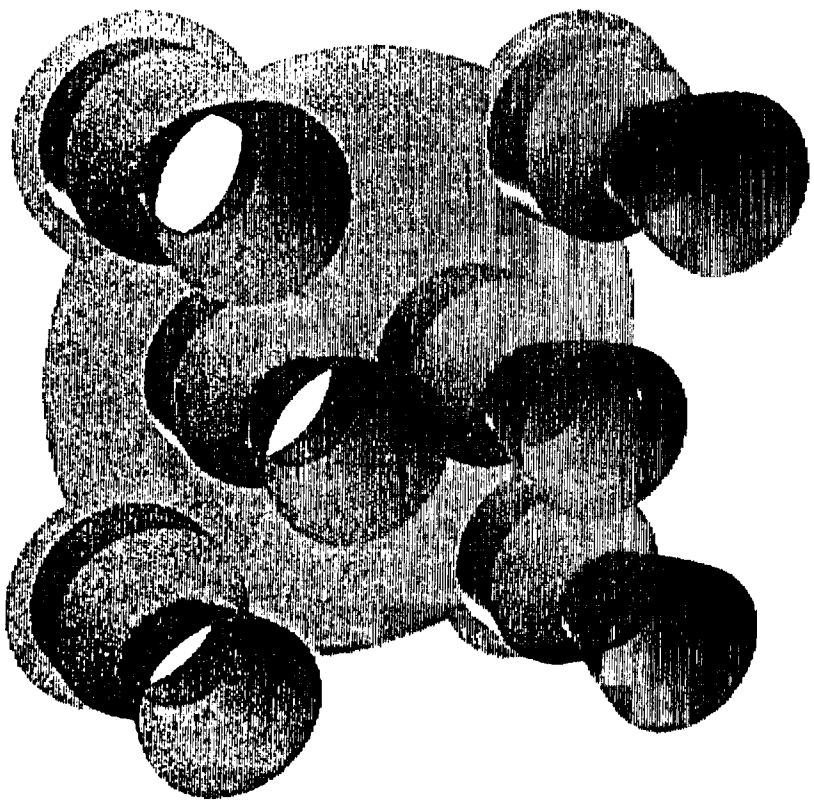

NLS 1.5 STAGE VEHICLE BASE AND ENGINE CLUSTER MODELED THROUGH SYMMETRY

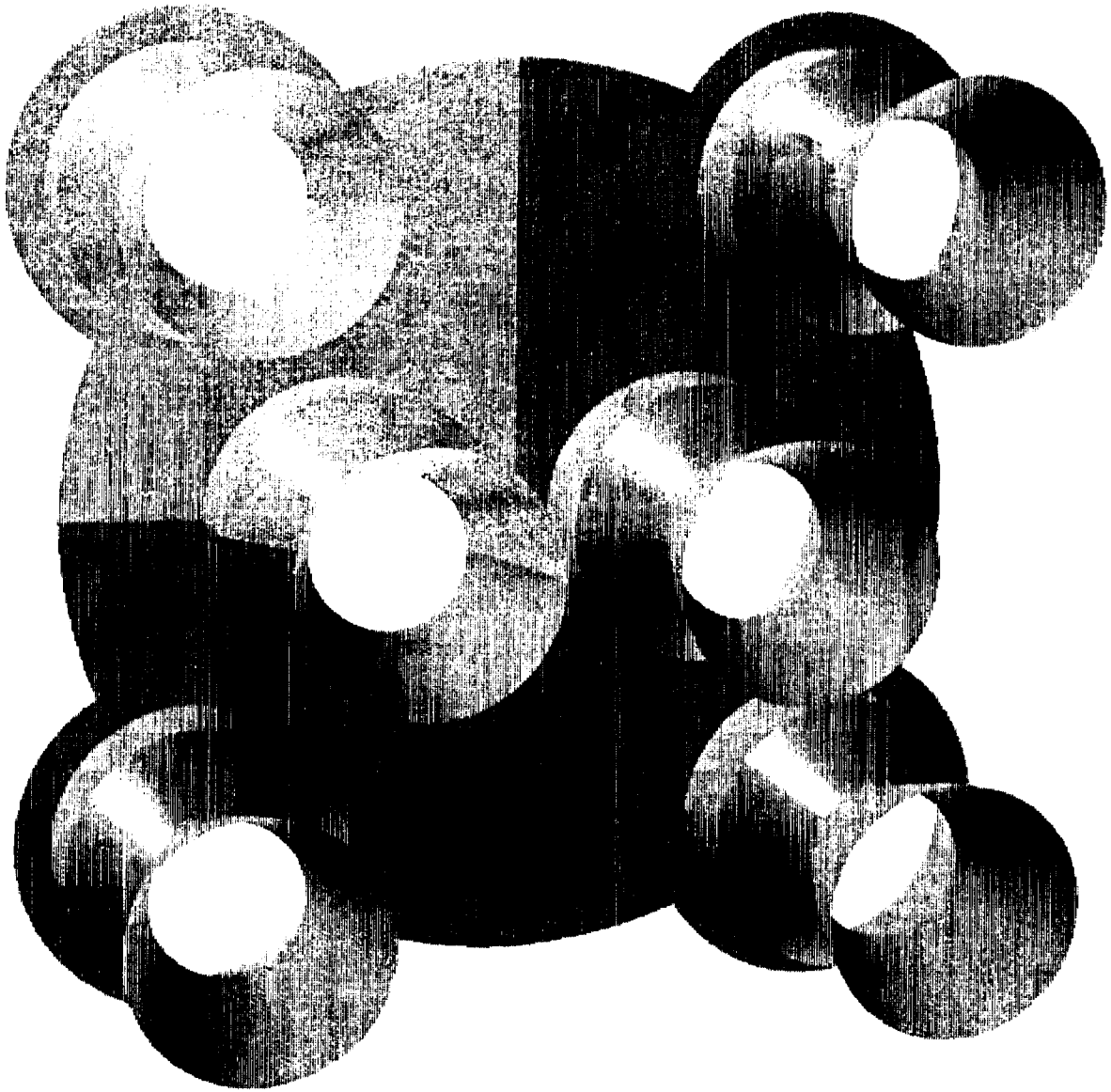

Rockwell International
Rocketdyne Division

CFD 92-042-062/D3/SLB

1.5 STAGE REFERENCE VEHICLE GRID STRUCTURE

ZONE	COLOR	I_{MAX}	J_{MAX}	K_{MAX}	NODES = $(I_{MAX}) \times (J_{MAX}) \times (K_{MAX})$	X_{MIN}	X_{MAX}	COMMENTS
1	RED	100	30	56	168,000	0	147	J = 1 IS FULL ENGINE SURFACE I = 1 IS BASE OF VEHICLE
2	BLUE	100	12	53	63,600	0	147	J = 1 IS HALF ENGINE SURFACE I = 1 IS BASE OF VEHICLE
3	YELLOW	100	13	10	13,000	0	147	I = 1 IS BASE OF VEHICLE J = 1 COMPLETES FULL ENGINE SURFACE
4	GREEN	80	30	56	134,400	147	550	EXTENDS ZONE 1
5	LAVENDER	80	12	53	50,880	147	550	EXTENDS ZONE 2
6	BLACK	80	13	10	10,400	147	550	EXTENDS ZONE 3
7	LT. BLUE	80	21	65	109,200	147	550	J = 1 IS CENTERLINE OF FULL ENGINE J = 21 IS CYLINDER MATCHING FULL ENGINE OUTFLOW CIRCLE
8	GRAY	80	21	53	89,040	147	550	AS WITH ZONE 7 BUT EXTENDS HALF ENGINE
					TOTAL = 638,520			

1.5 STAGE REFERENCE VEHICLE GRID TOPOLOGY

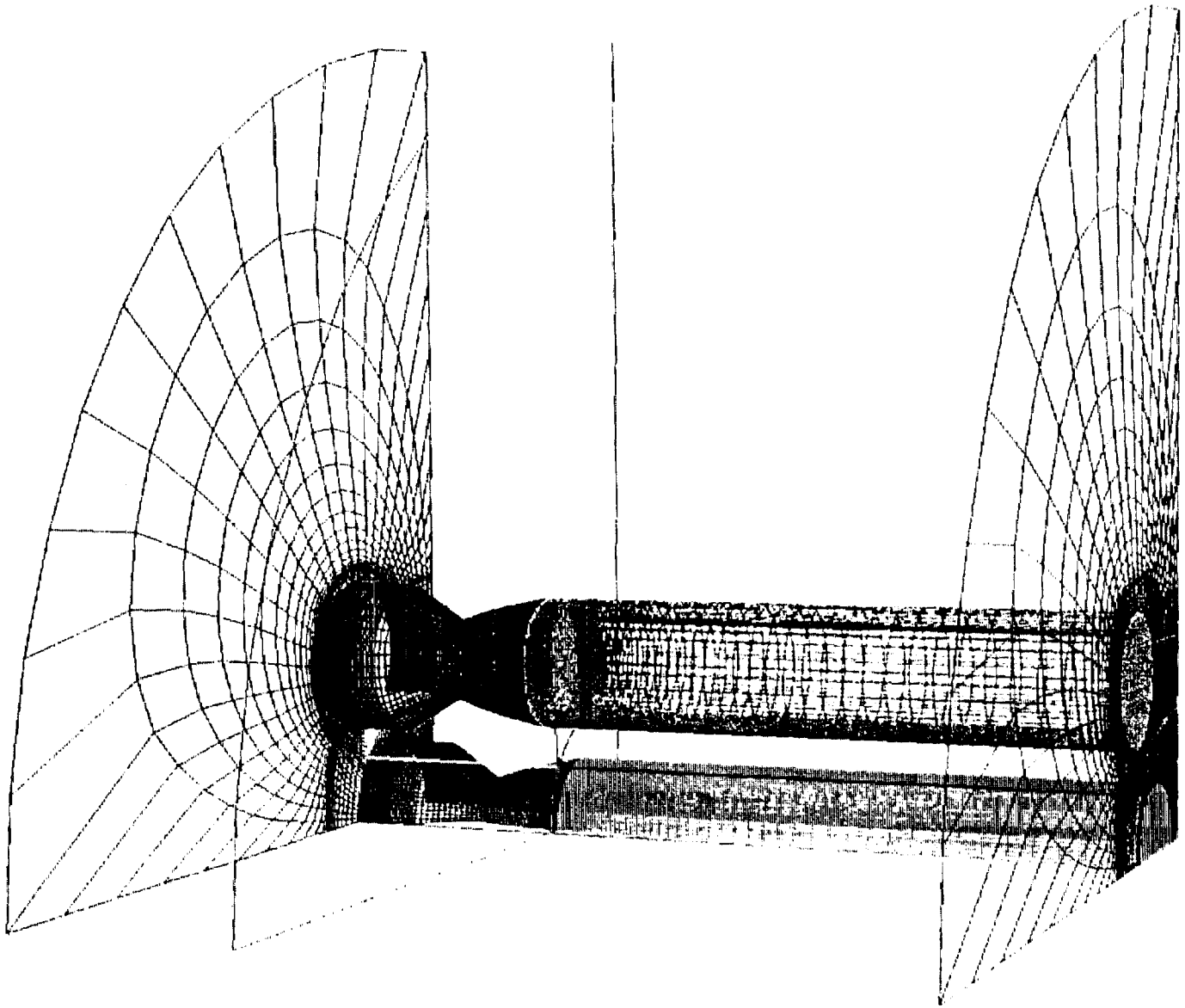

Rockwell International
Rocketdyne Division

CFD 92-042-065/D3/SLB

1.5 STAGE REFERENCE VEHICLE GRID TOPOLOGY (CONT'D)

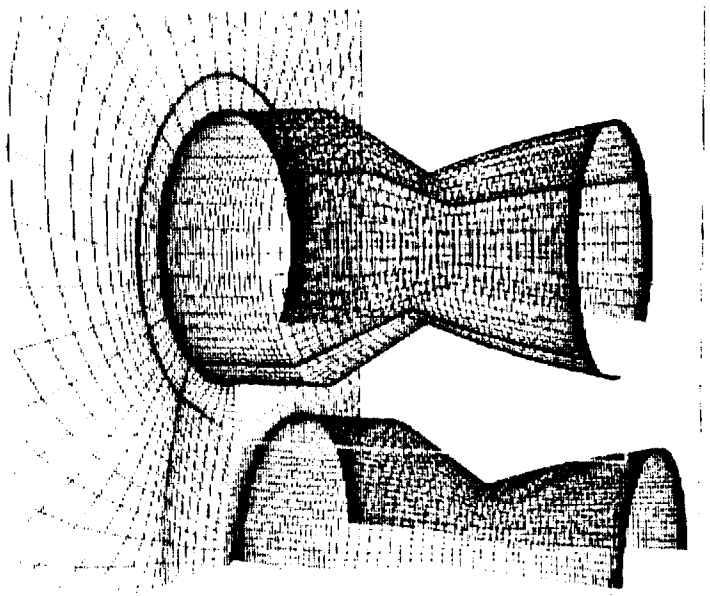

ZONES 1 - 3

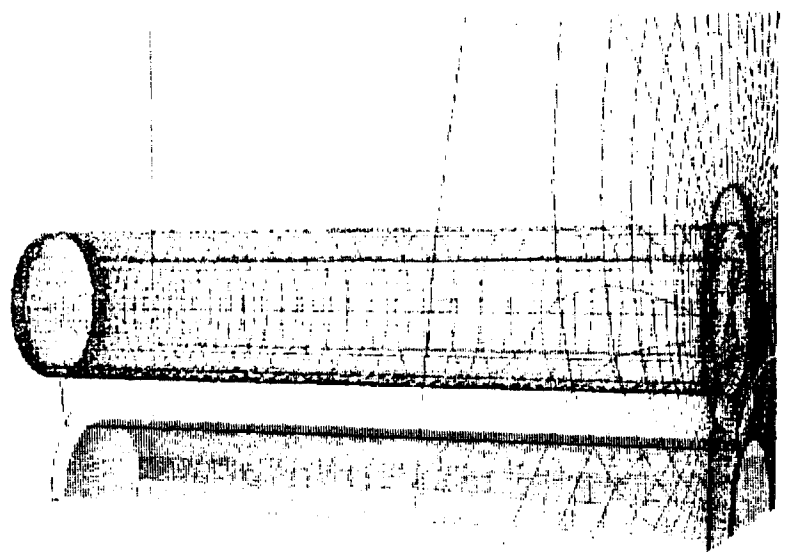

ZONES 4 - 8

BOUNDARY CONDITIONS APPLIED

BOUNDARY CONDITION	COLOR	DESCRIPTION
1	LT. BLUE	SPECIFIED VELOCITY PROFILE (FREESTREAM + B.L. PROFILE)
2	BLUE	NO-SLIP, ADIABATIC WALL
3	RED	CFD COMPUTED NOZZLE EXIT FLOW
4	YELLOW	SYMMETRY
5	GREEN	ZERO GRAIDENT/SPECIFIED BACK PRESSURE
6	TRANSPARENT	FREESTREAM

BOUNDARY CONDITIONS APPLIED (CONT'D)

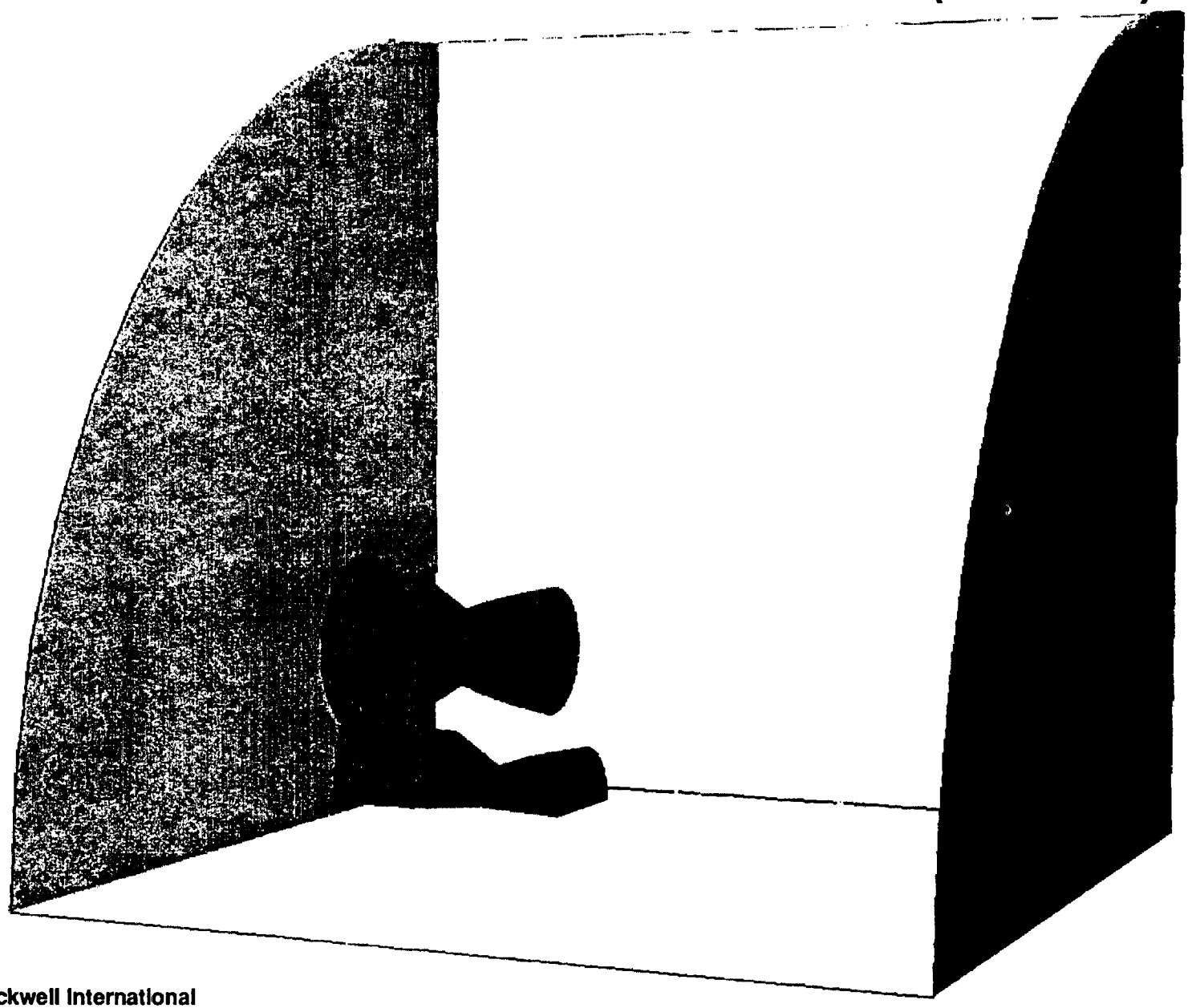

Rockwell International
Rocketdyne Division

BOUNDARY CONDITIONS APPLIED (CONT'D)

THERMAL BOUNDARY CONDITION OPTIONS

- **ADIABATIC WALL CONDITION**
  - CONSERVATIVE - PROVIDES HIGHEST TEMPERATURES
  - MORE ACCURATE FOR COARSE GRID CALCUALTIONS
  - ASSUMES ZERO HEAT FLUX BY DEFINITION

- **SPECIFIED WALL TEMPERATURE**
  - ISOTHERMAL OR SPECIFIED PROFILE
  - REQUIRES FINE GRID NEAR SURFACE
  - ALLOWS DIRECT HEAT FLUX CALCULATION

1488

PARTICLE TRACES IN BASE REGION

10,000 FOOT ALTITUDE

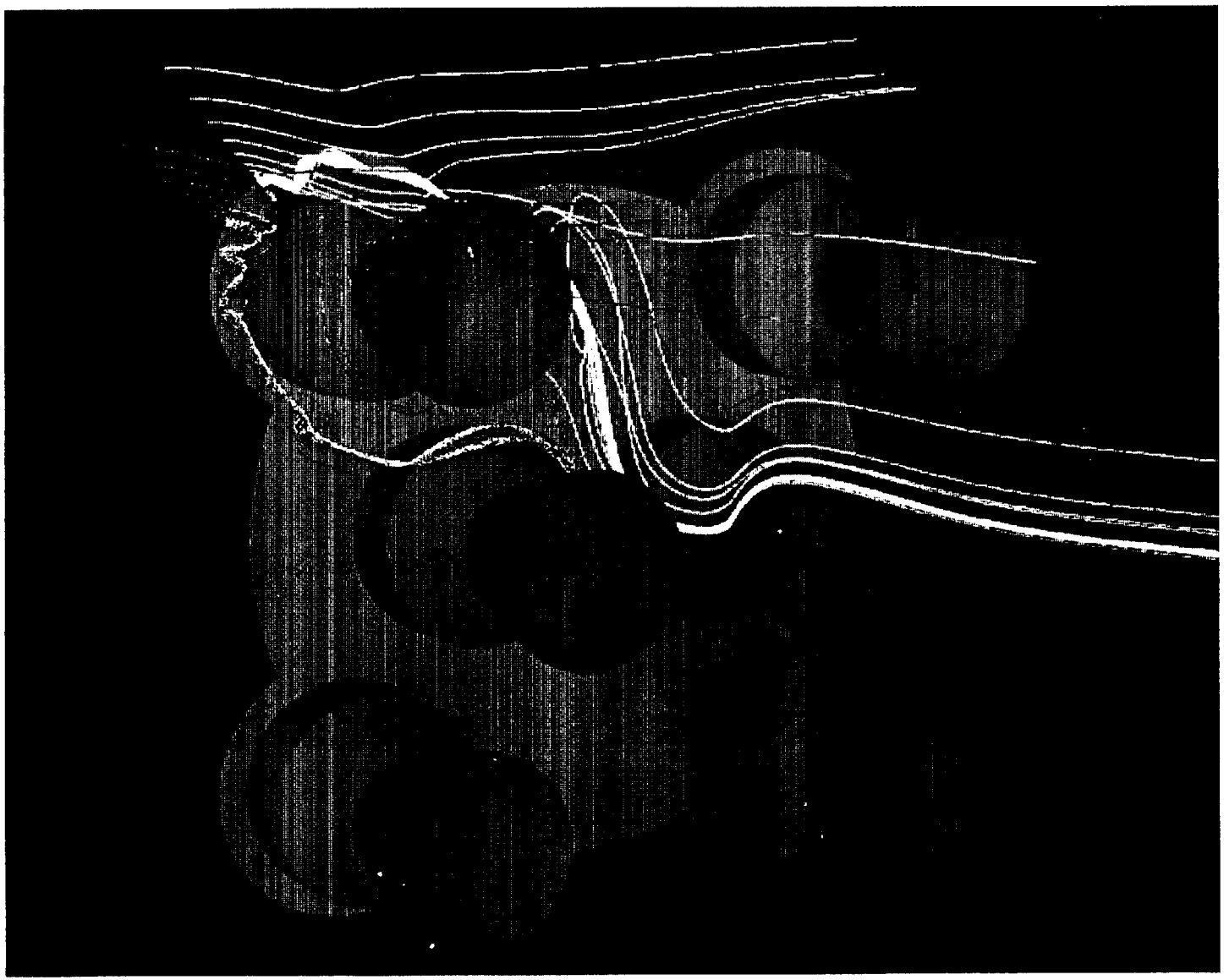

PARTICLE TRACES IN BASE REGION (CONT'D)

10,000 FOOT ALTITUDE

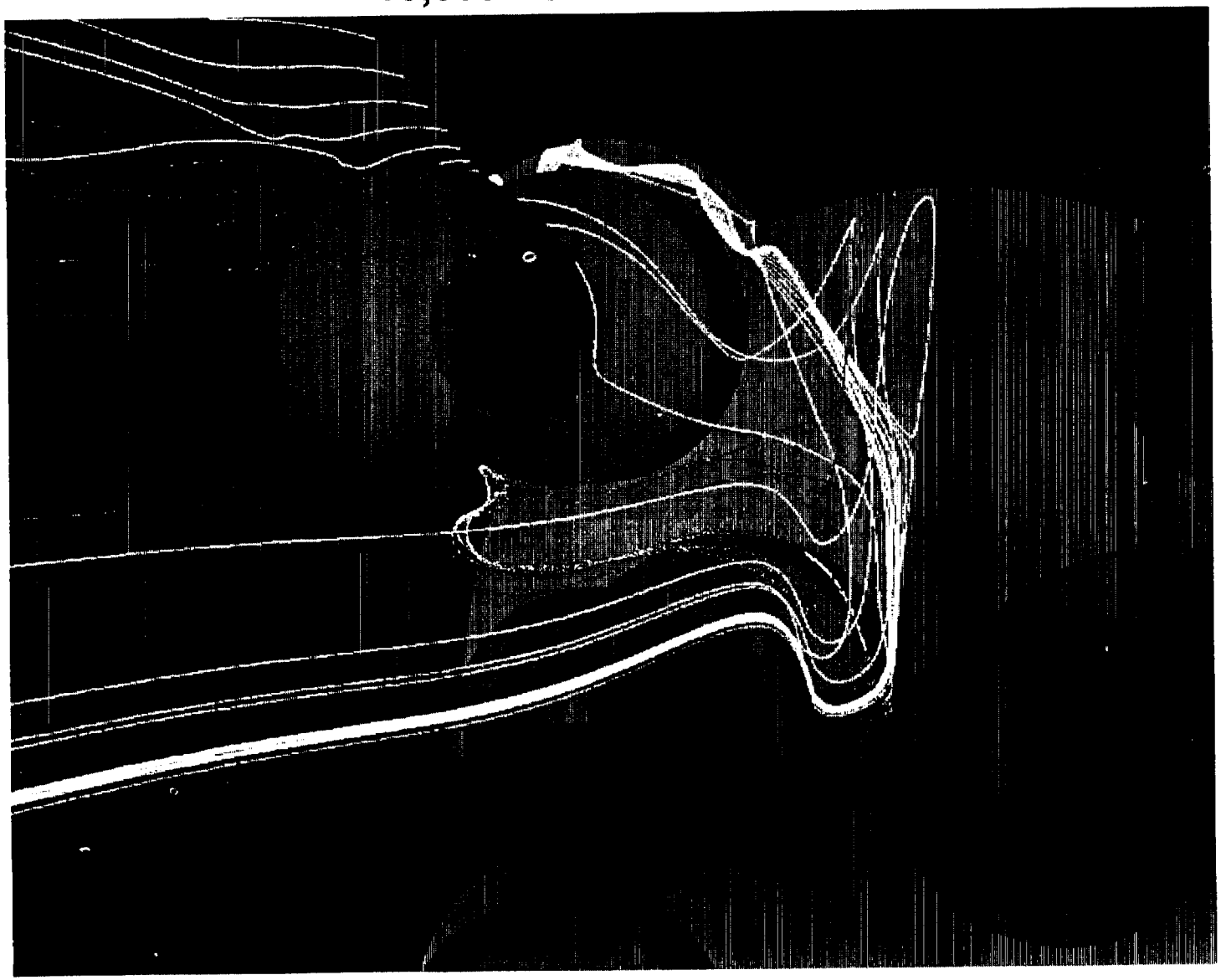

BASE REGION MACH CONTOURS (CONT'D)

10,000 FOOT ALTITUDE

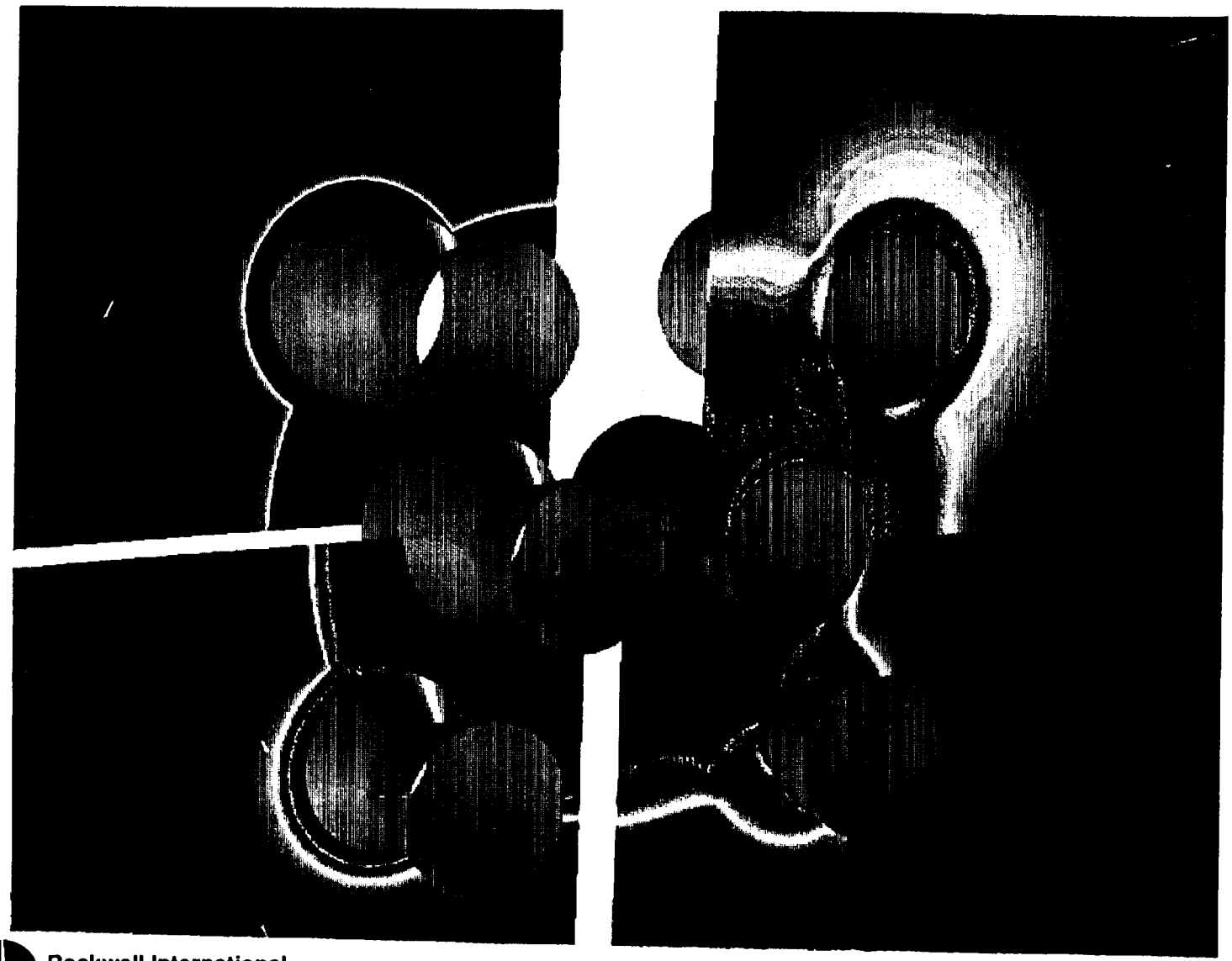

Rockwell International
Rocketdyne Division

CFD 92-042-077/D3/SLB

PLUME REGION MACH CONTOURS

10,000 FOOT ALTITUDE

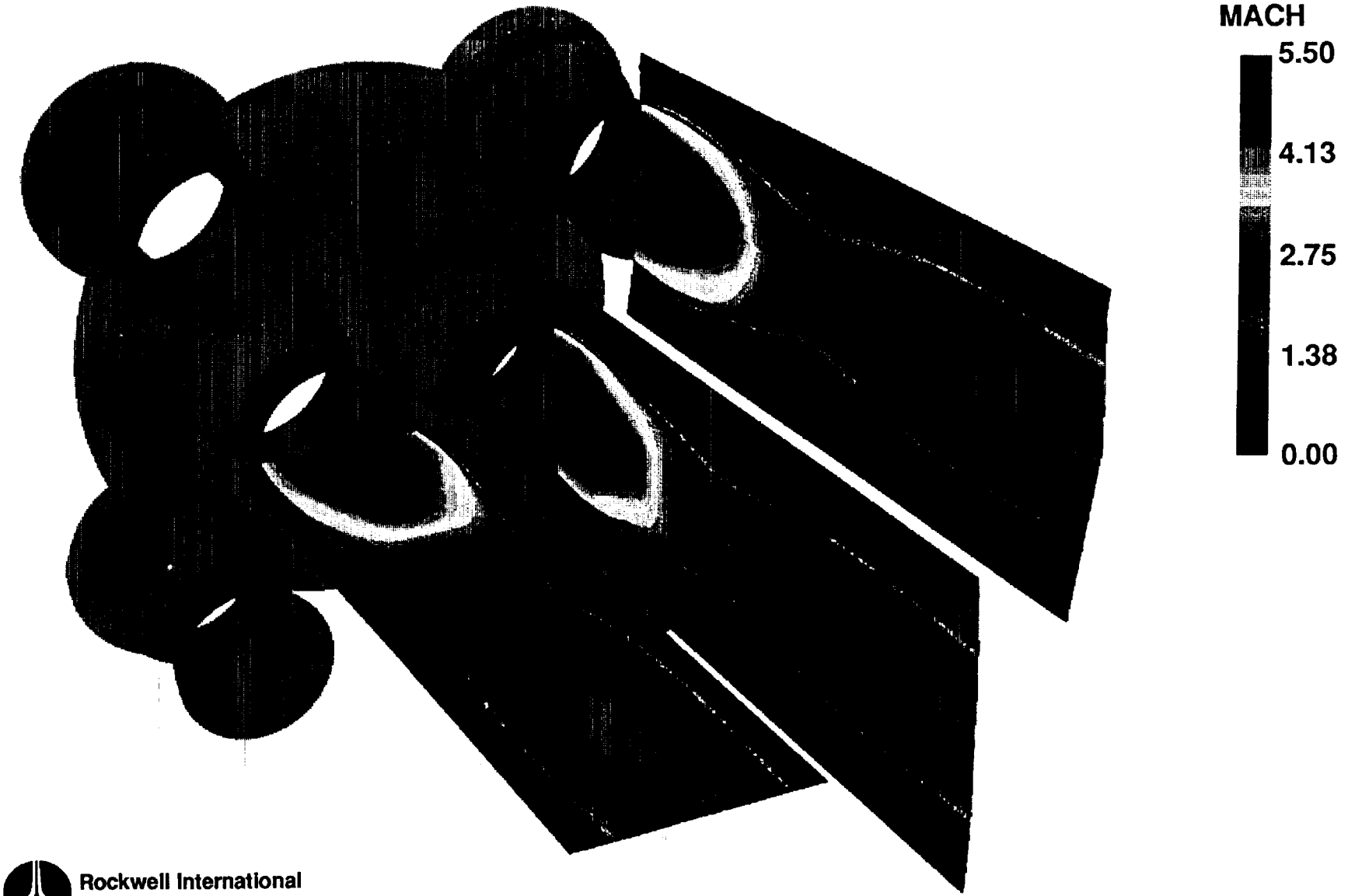

Rockwell International
Rocketdyne Division

CFD 92-042-071/D3/SLB

PARTICLE TRACES FROM NOZZLE EDGE

10,000 FOOT ALTITUDE

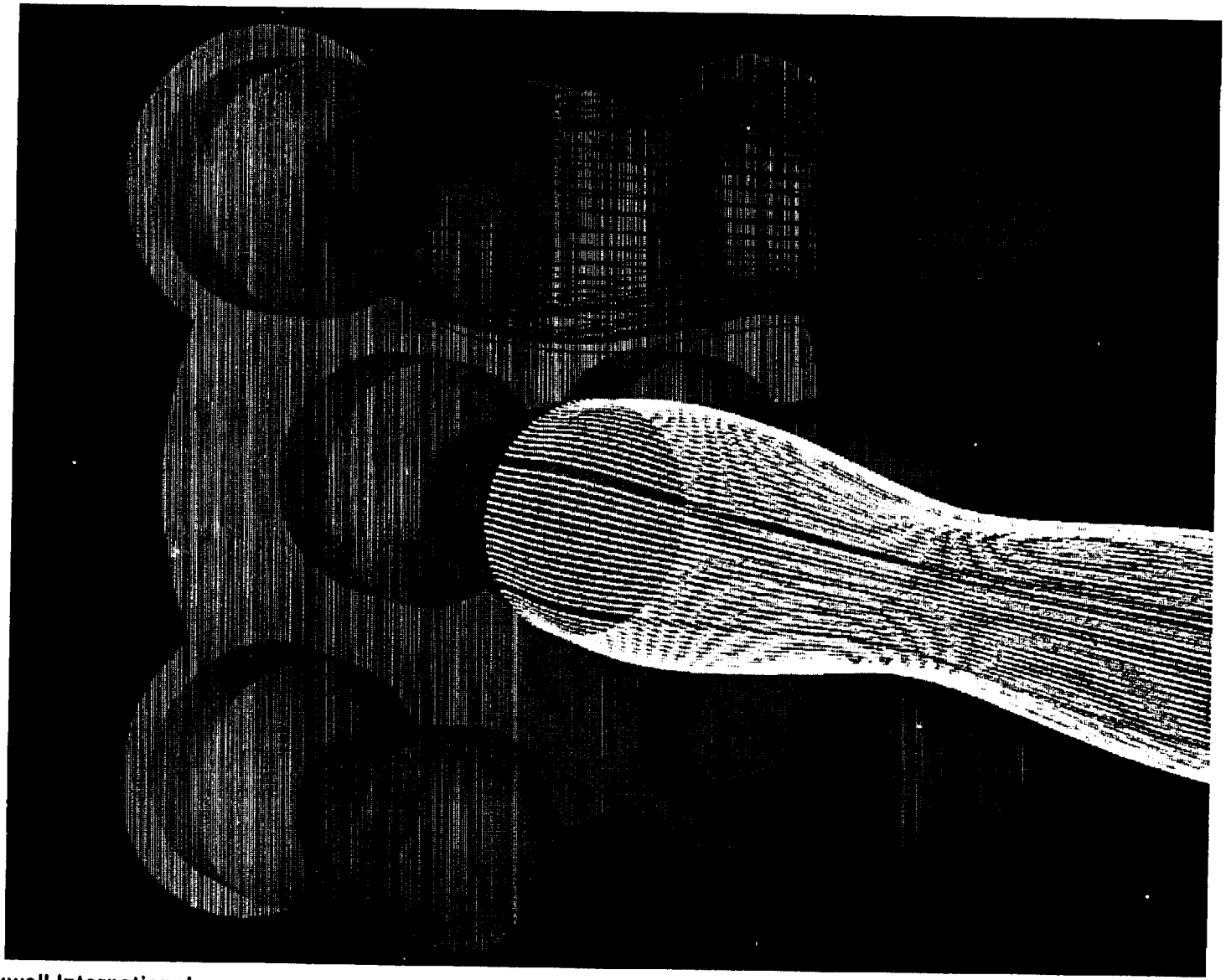

Rockwell International
Rocketdyne Division

BASE REGION H2 CONTOURS (CONT'D)

10,000 FOOT ALTITUDE

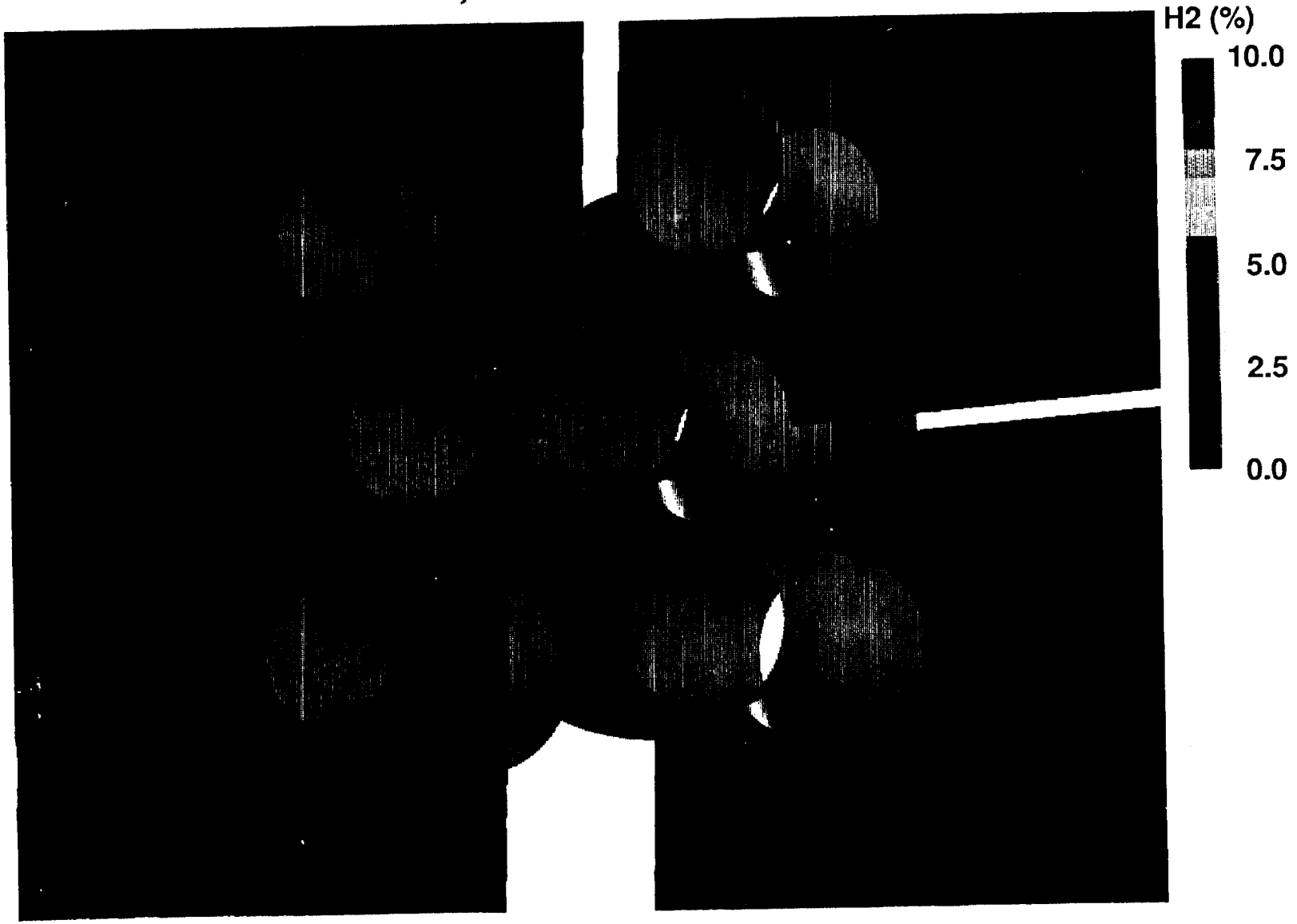

Rockwell International
Rocketdyne Division

CFD 92-042-089/D3/SLB

BASE REGION TEMPERATURE CONTOURS (CONT'D)

10,000 FOOT ALTITUDE

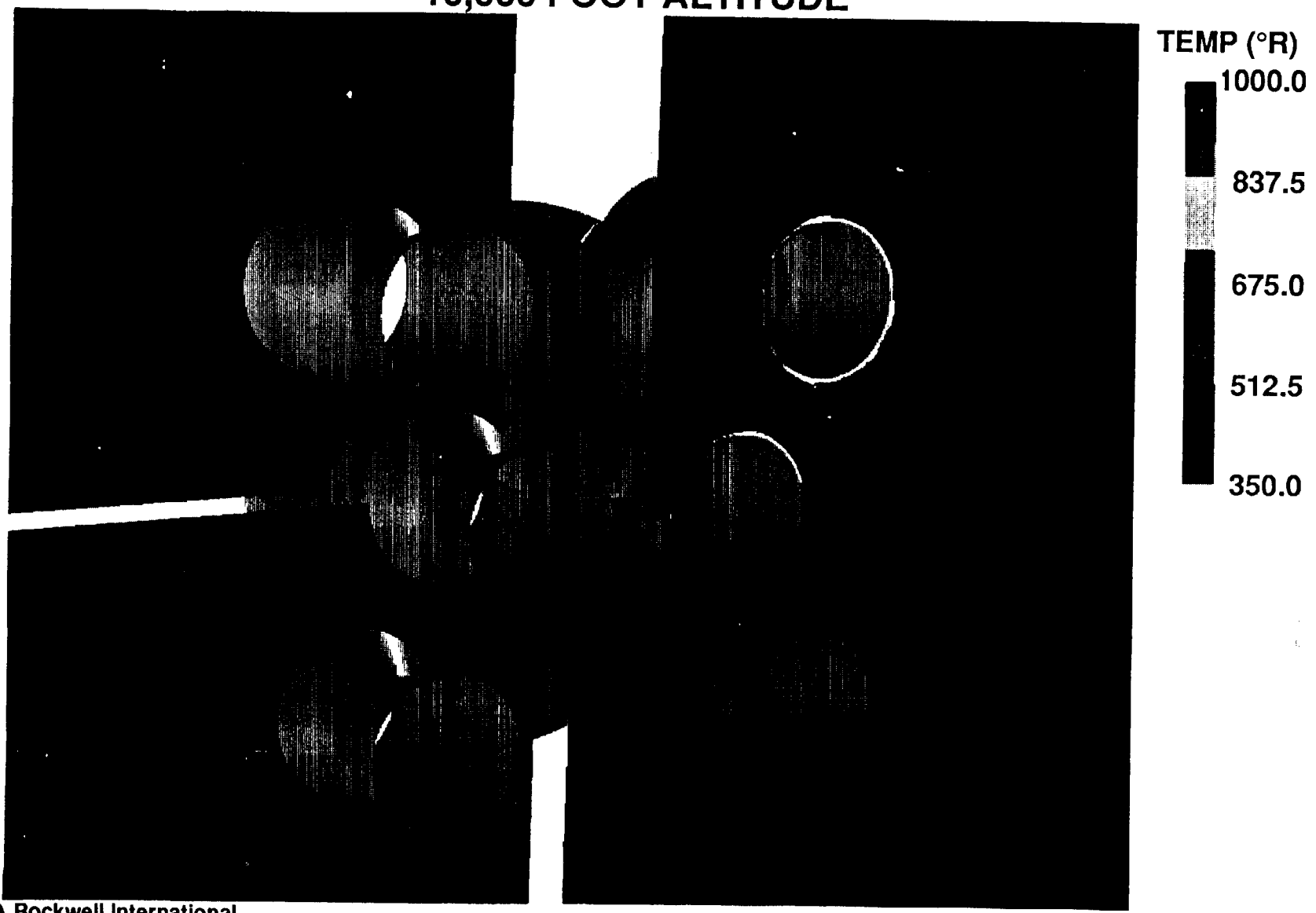

Rockwell International
Rocketdyne Division

CFD 92-042-085/D3/SLB

BASE REGION SURFACE TEMPERATURE CONTOURS

10,000 FOOT ALTITUDE

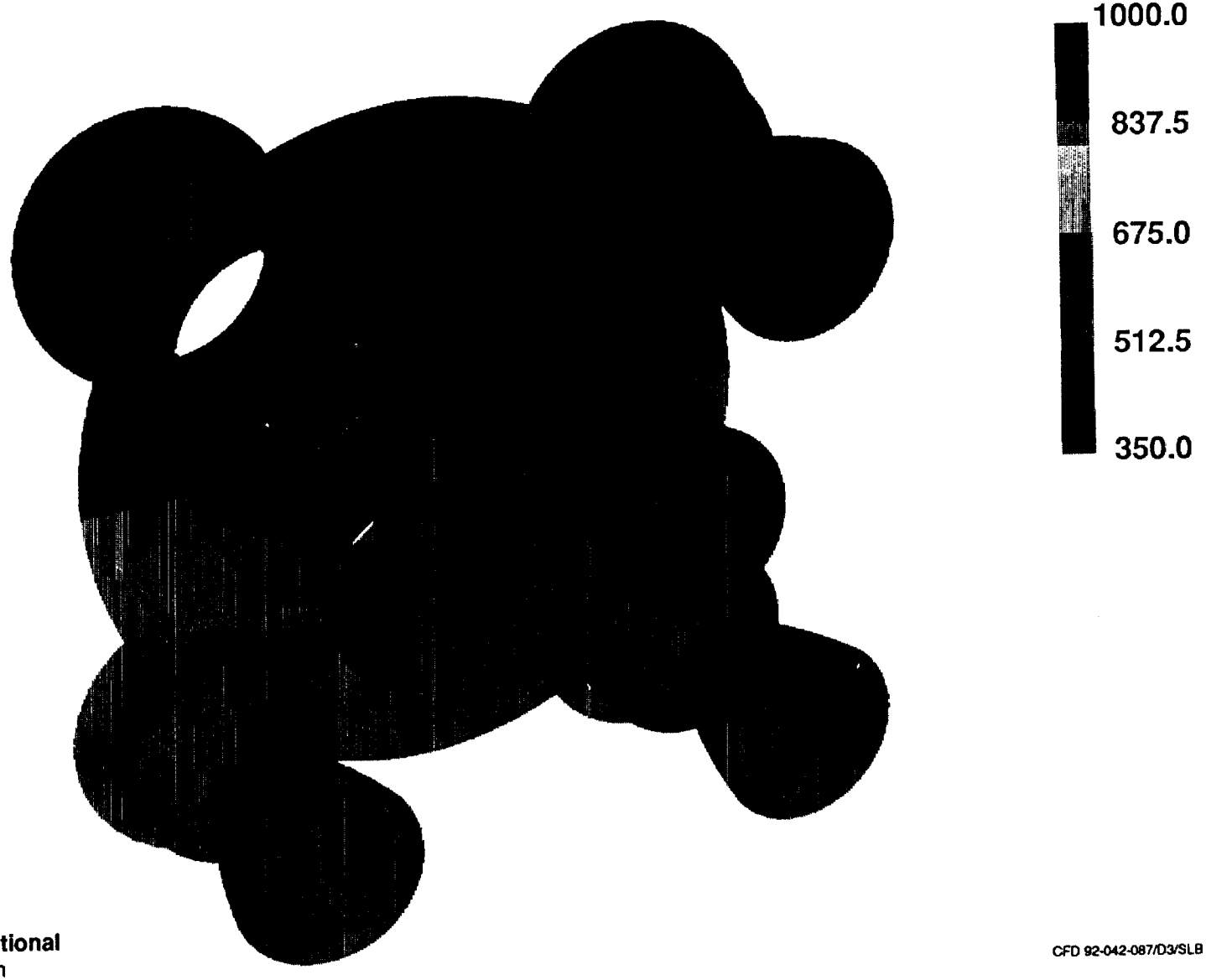

Rockwell International
Rocketdyne Division

CFD 92-042-087/D3/SLB

NOZZLE SURFACES TEMPERATURES

10,000 FOOT ALTITUDE

OUTER NOZZLE

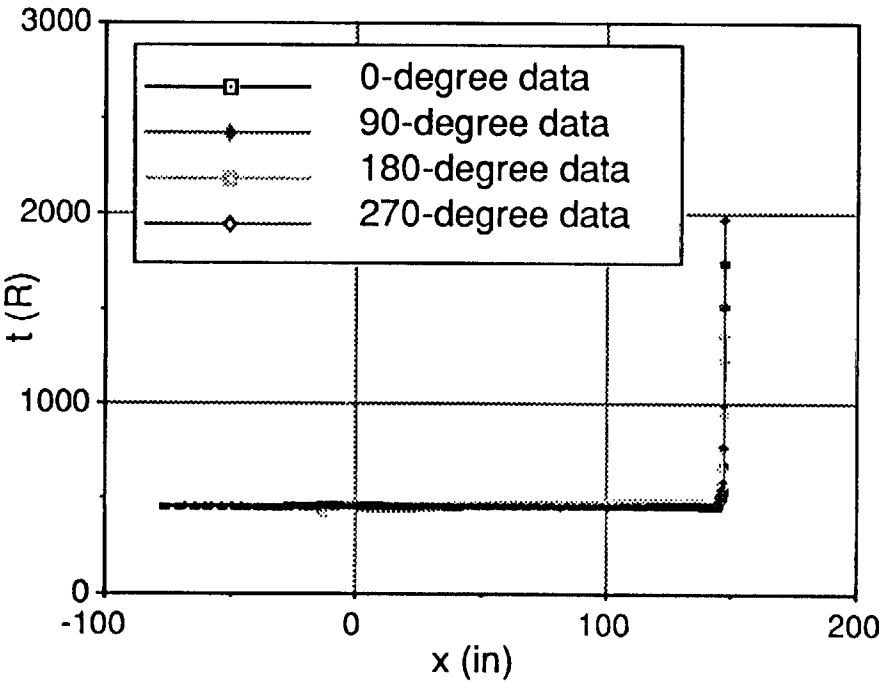

CENTER NOZZLE

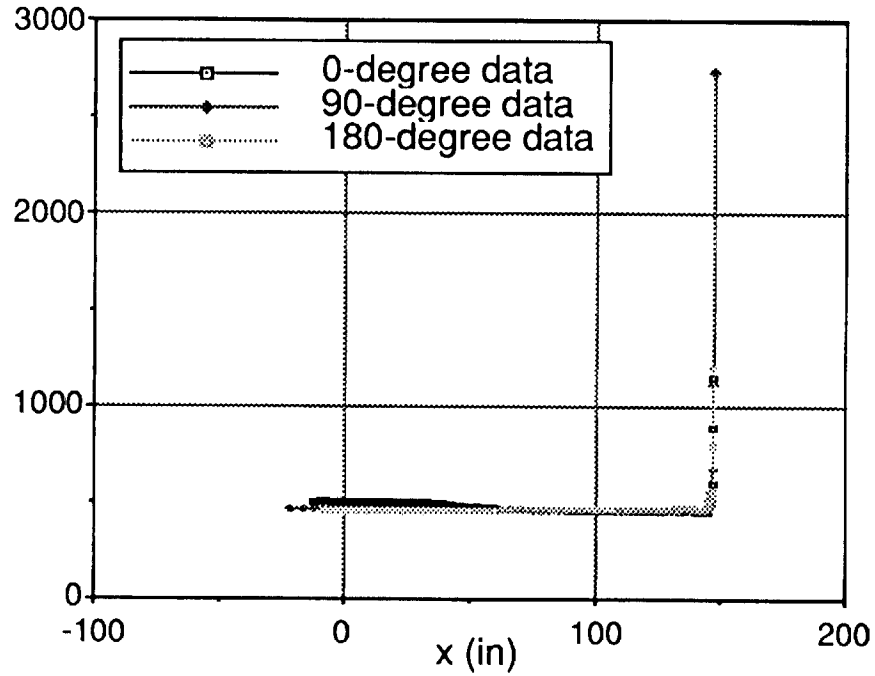

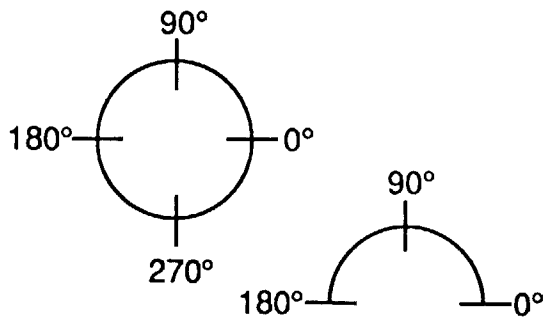

Rockwell International
Rocketdyne Division

CFD 92-042-091/D3/SLB

10,000 FOOT ALTITUDE RESULT SUMMARY

KEY FLOW FEATURES CAPTURED

- PLUME STRUCTURE DEFINED
- PLUMES DO NOT SIGNIFICANTLY INTERACT
- NO MECHANISM APPARENT TO DRIVE HOT GAS INTO BASE REGION
- NO SIGNIFICANT AMOUNT OF H_2 OR H_2O FOUND IN BASE REGION
- SURFACE TEMPERATURES WELL BELOW 1000°R
- COARSE AND FINE GRID SOLUTIONS PREDICT ESSENTIALLY SAME FLOWS

BASE REGION MACH CONTOURS (CONT'D)

50,000 FOOT ALTITUDE

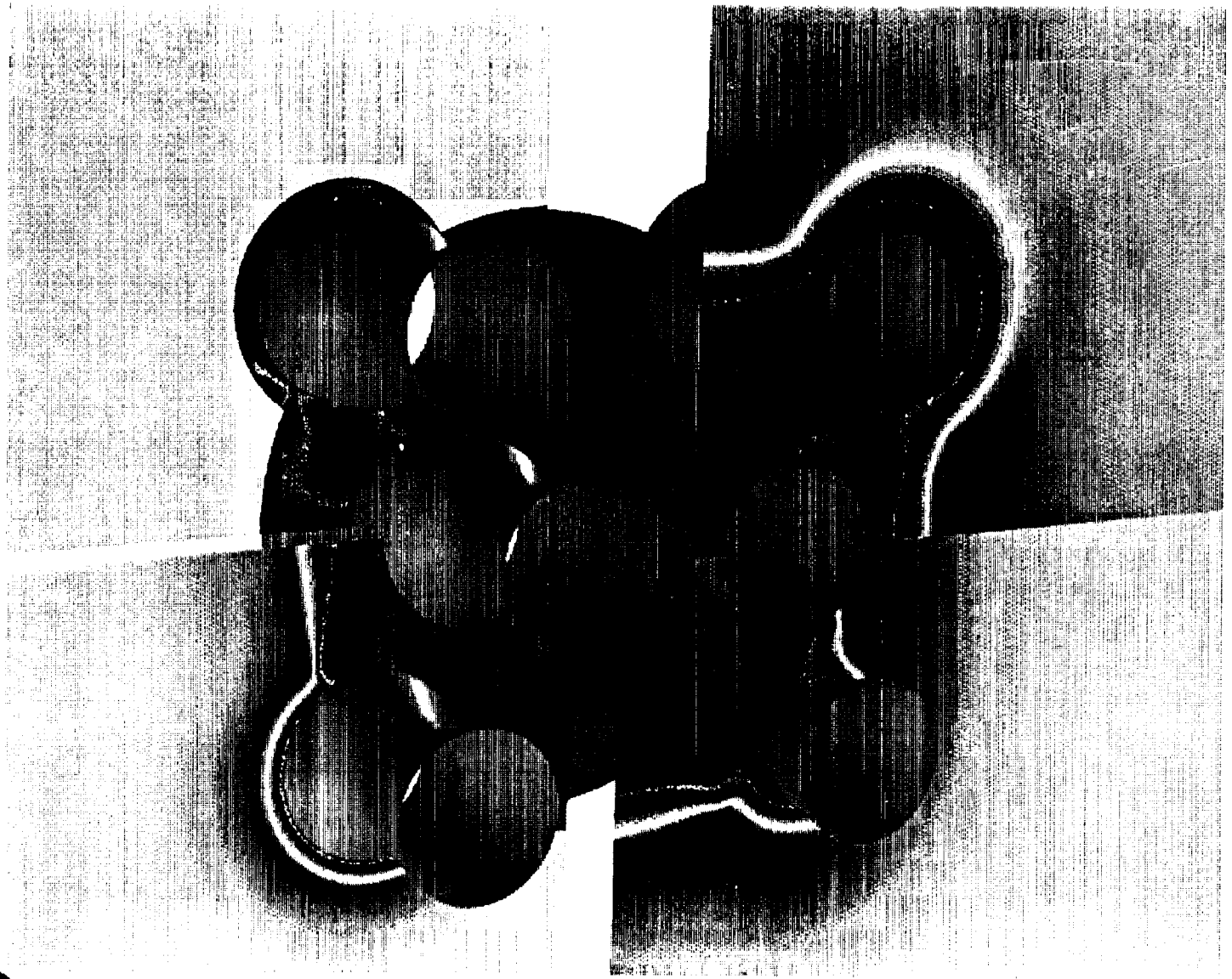

Rockwell International
Rocketdyne Division

CFD 92-042-109/D3/SLB

PARTICLE TRACES FROM NOZZLE EDGE

50,000 FOOT ALTITUDE

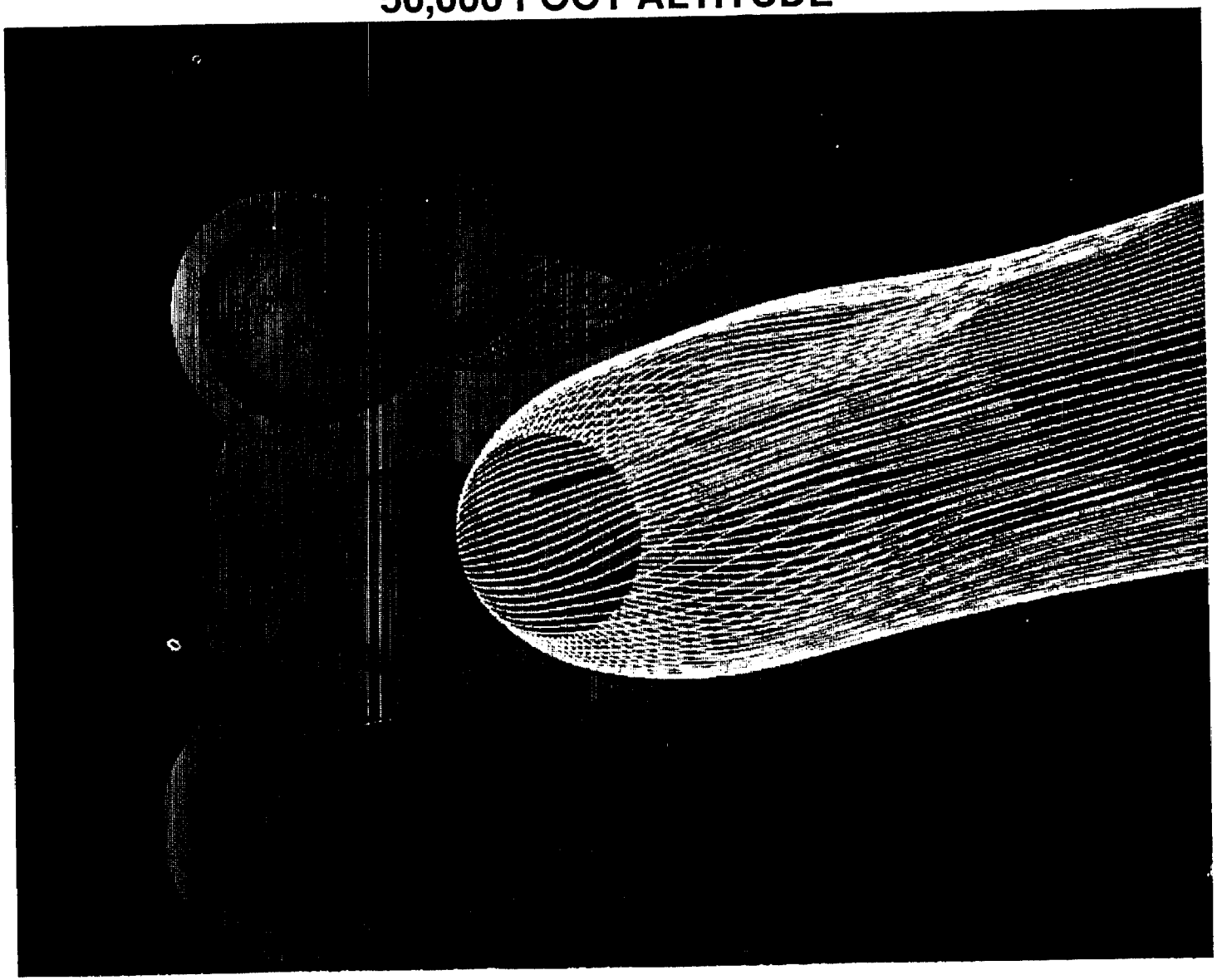

PARTICLE TRACES FROM NOZZLE EDGE (CONT'D)

50,000 FOOT ALTITUDE

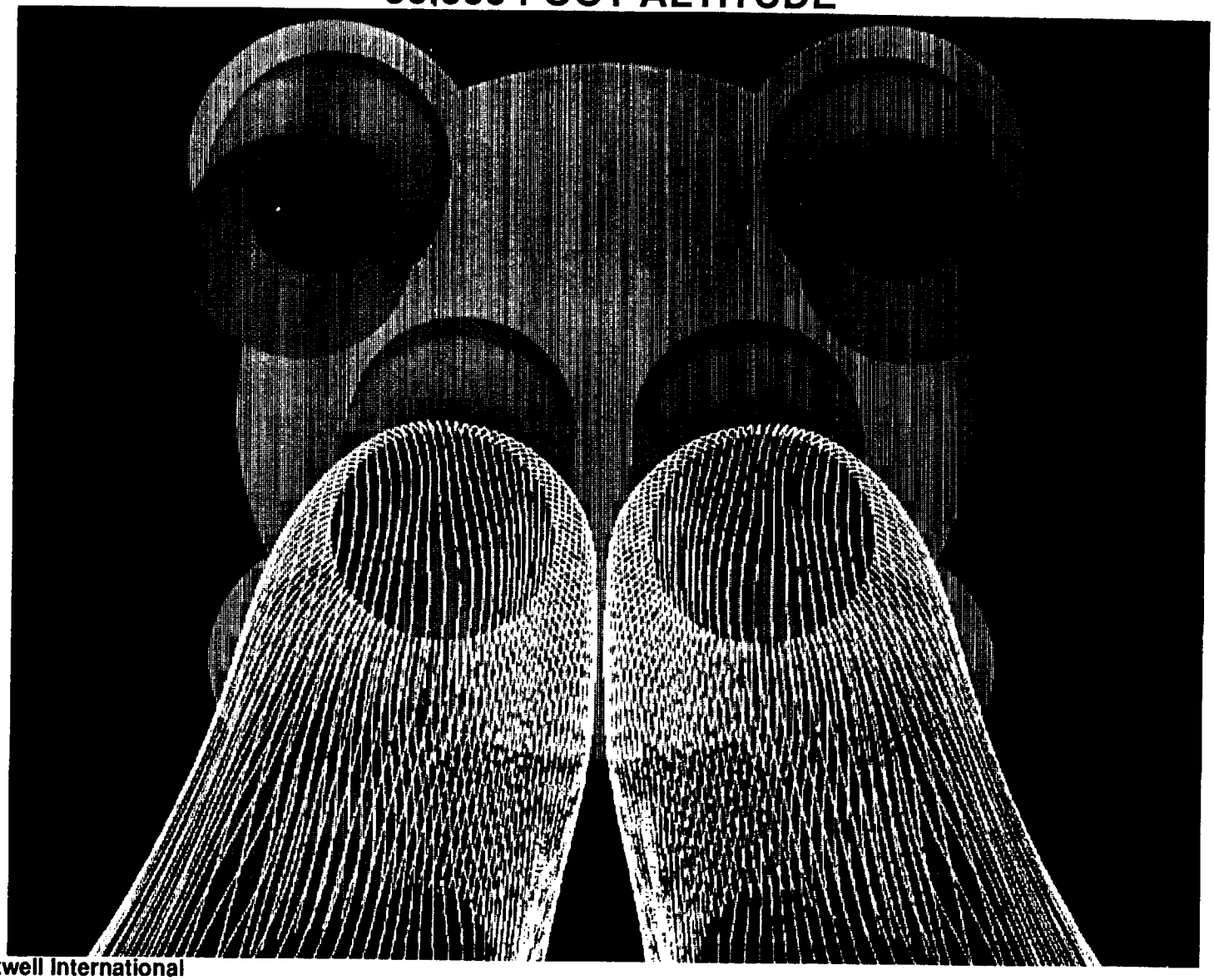

PARTICLE TRACES IN BASE REGION

50,000 FOOT ALTITUDE

Rockwell International
Rocketdyne Division

CFD 92-042-131/D3/SLB

PARTICLE TRACES IN BASE REGION (CONT'D)

50,000 FOOT ALTITUDE

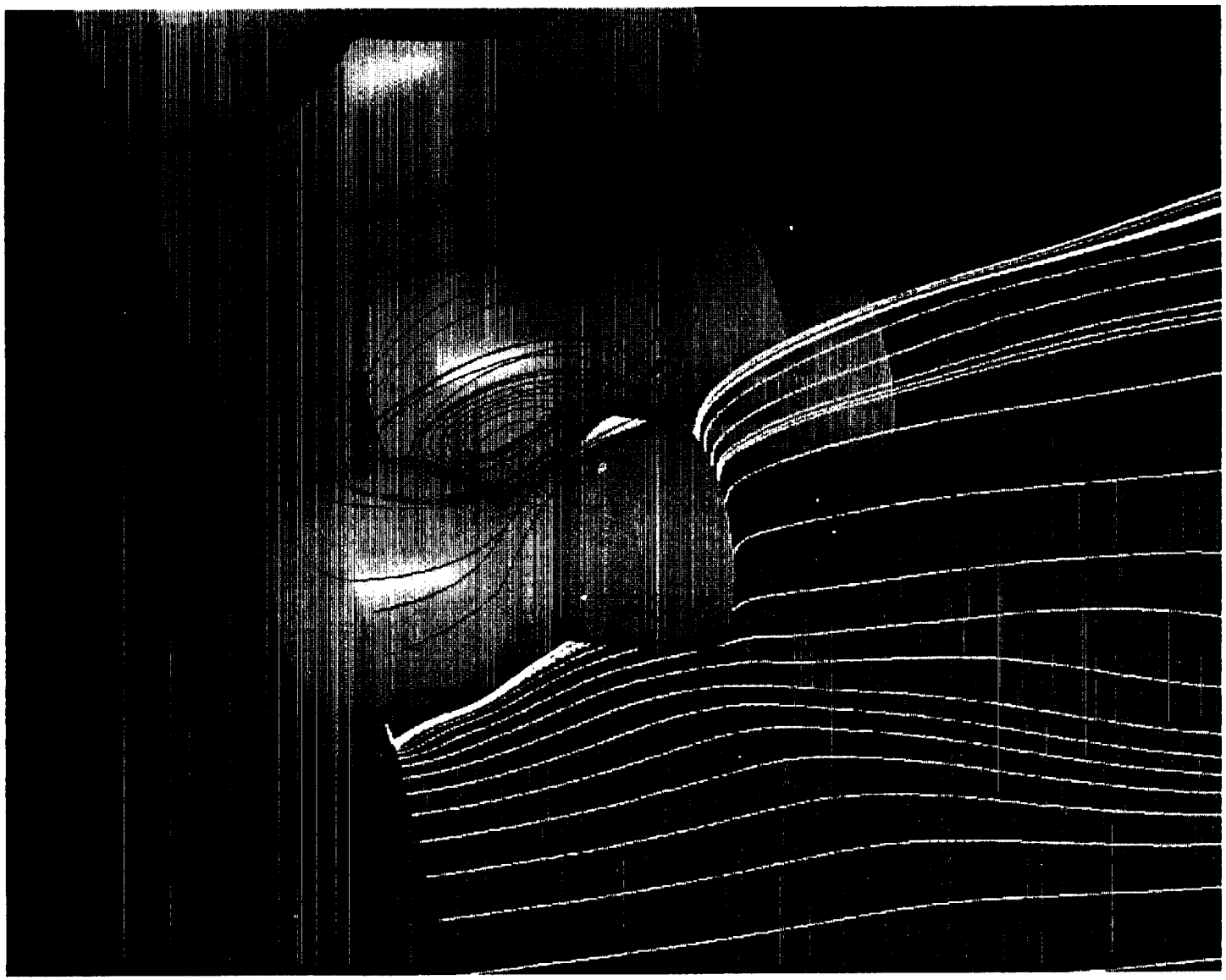

BASE REGION H2O CONTOURS (CONT'D)

50,000 FOOT ALTITUDE

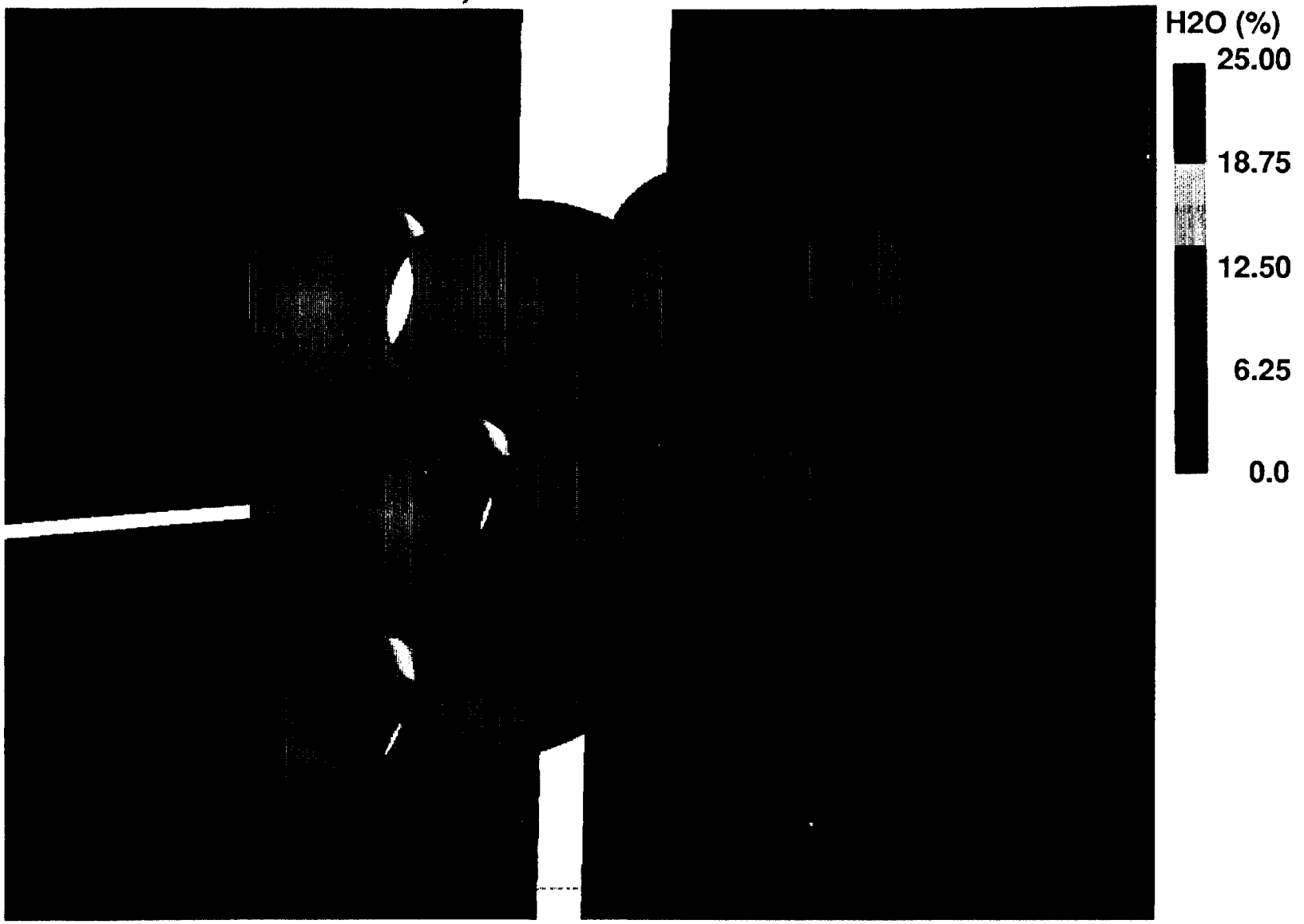

Rockwell International
Rocketdyne Division

CFD 92-042-124/D3/SLB

BASE REGION TEMPERATURE CONTOURS (CONT'D)

50,000 FOOT ALTITUDE

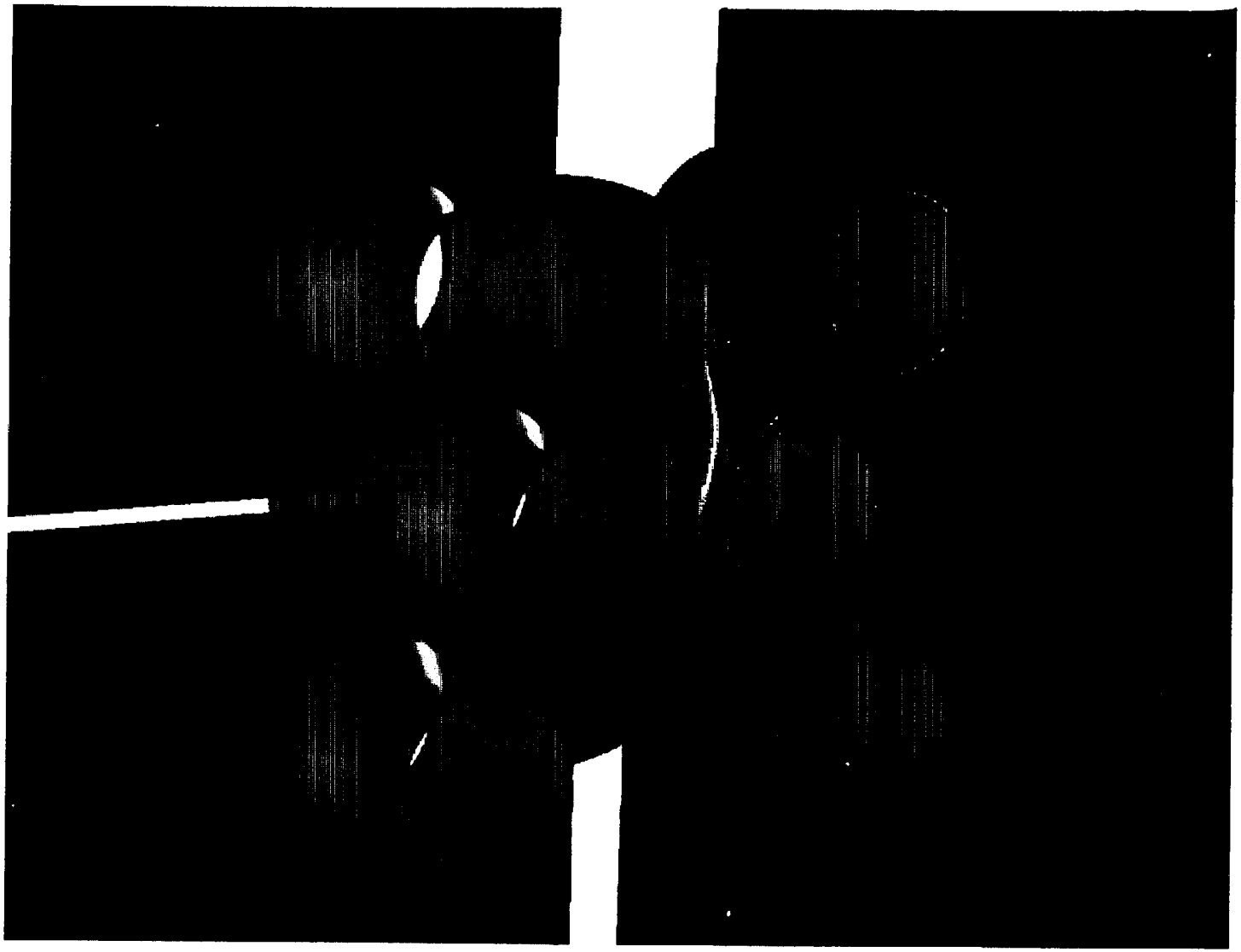

Rockwell International
Rocketdyne Division

CFD 92-042-117/D3/SLB

BASE REGION SURFACE TEMPERATURE CONTOURS

50,000 FOOT ALTITUDE

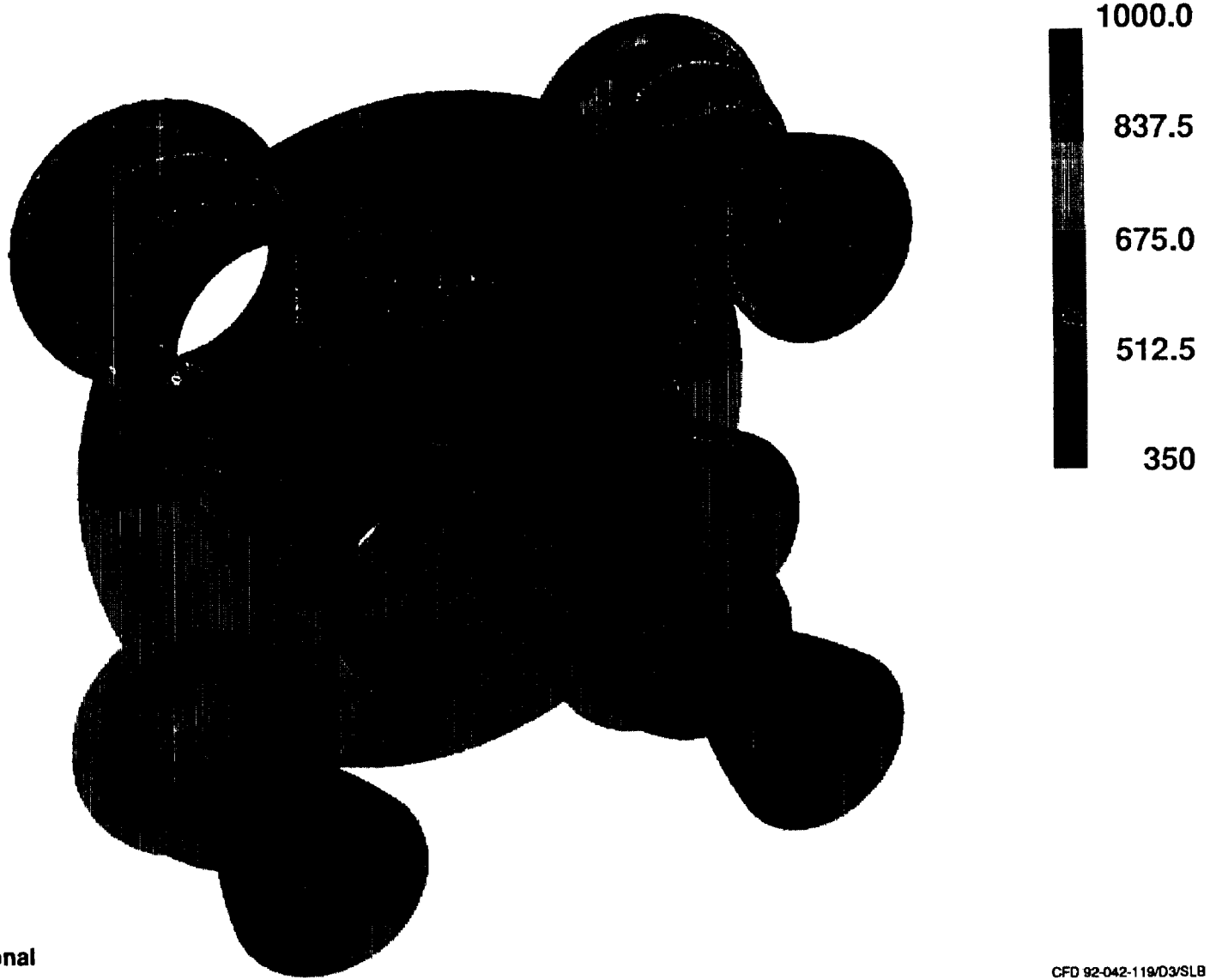

Rockwell International
Rocketdyne Division

CFD 92-042-119/D3/SLB

NOZZLE SURFACES TEMPERATURES

50,000 FOOT ALTITUDE

OUTER NOZZLE

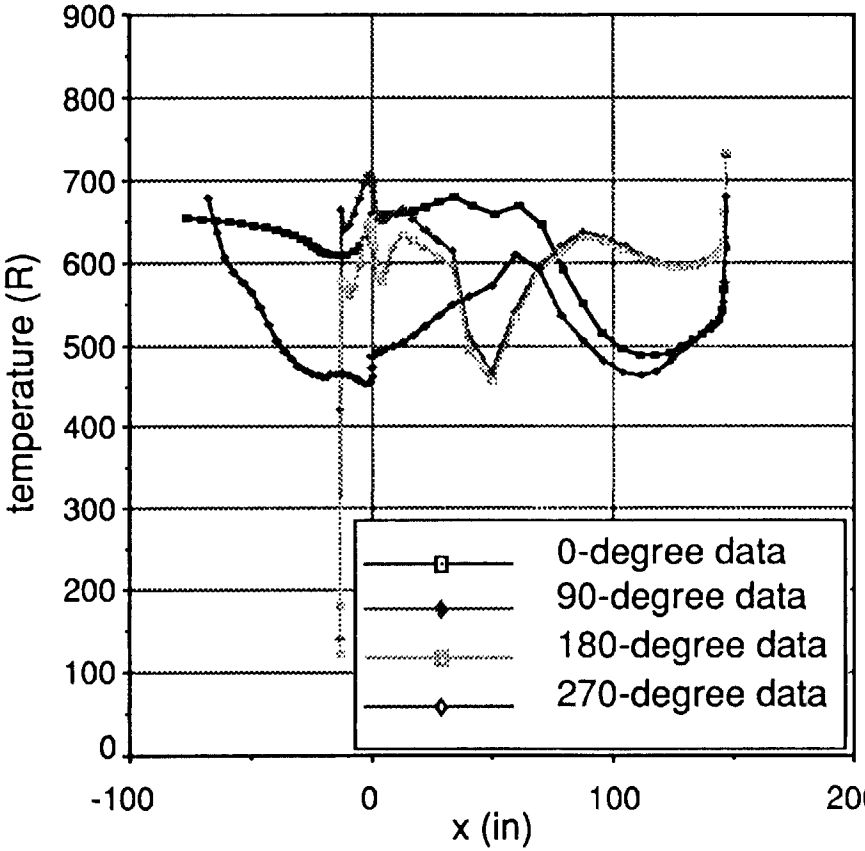

CENTER NOZZLE

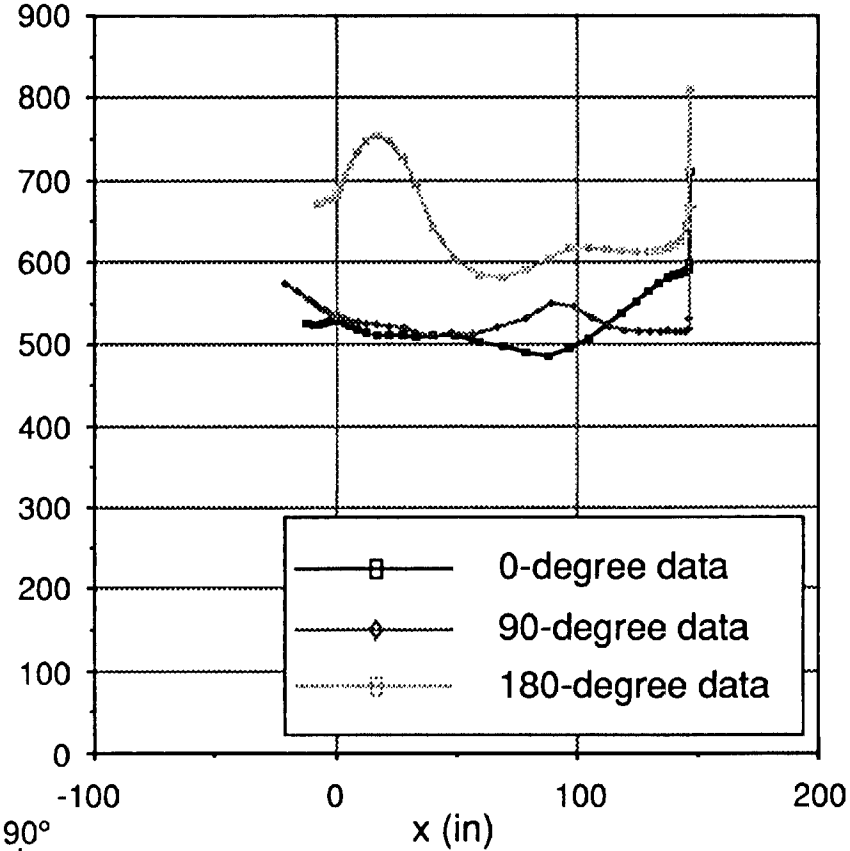

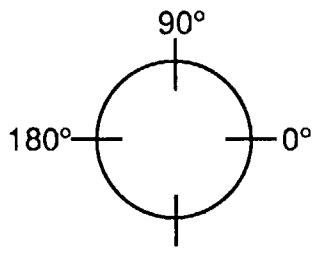

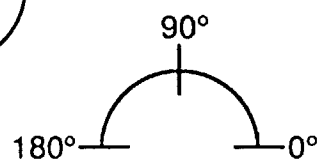

Rockwell International
Rocketdyne Division

CFD 92-042-126/D3/SLB

1507

50,000 FOOT ALTITUDE RESULT SUMMARY

- PLUME STRUCTURES DEFINED
- PLUME INTERACTION BECOMES SIGNIFICANT AT THIS ALTITUDE
- BASE GAS TEMPERATURES HIGHER THAN THOSE FOR 10,000 FOOT CASE
- NO SIGNIFICANT AMOUNT OF H2 OR H20 FOUND IN BASE REGION
- SURFACE TEMPERATURES WELL BELOW 1000°R, THOUGH WARMER THAN 10,000 FOOT CASE

SUMMARY

- BASE FLOW ENVIRONMENT DEFINED FOR NLS 1.5 STAGE REFERENCE GEOMETRY AT 10,000 AND 50,000 FT ALTITUDES
- COMPLETE PICTURE OF FLOWFIELD AVAILABLE INCLUDING VELOCITIES, PRESSURES, TEMPERATURES AND SPECIES CONCENTRATION
- SENSITIVITY OF RESULTS TO GRID RESOLUTION, TURBULENCE AND CHEMISTRY MODELS ASSESSED THROUGH SINGLE ENGINE PARAMETRICS
- VALIDATION WITH AVAILABLE TEST DATA SHOWS GOOD AGREEMENT
- RESULTS INDICATE NO BASE HEATING PROBLEM AT 10,000 FT AND 50,000 FT ALTITUDES
- STUDY DEMONSTRATES ABILITY OF CFD AS A TIME EFFECTIVE ENGINEERING TOOL TO UNDERSTAND AND ASSESS BASE HEATING PROBLEMS

ABSTRACT:

CFD Flowfield Simulation of Delta Launch Vehicles in a Power-on Configuration

Workshop for Computational Fluid Dynamic (CFD) Applications in Rocket Propulsion, George C. Marshall Space Flight Center, April 20-22, 1993

By: D. L. Pavish+, T. P. Gielda*, B. K. Soni **, J. E. Deese++, and R. K. Agarwal++

This paper summarizes recent work at McDonnell Douglas Aerospace (MDA) to develop and validate computational fluid dynamic (CFD) simulations of under expanded rocket plume external flowfields for multibody expendable launch vehicles (ELVs). Multi-engine reacting gas flowfield predictions of ELV base pressures are needed to define vehicle base drag and base heating rates for sizing external nozzle and base region insulation thicknesses. Previous ELV design programs used expensive multibody power-on wind tunnel tests that employed chamber/nozzle injected high pressure cold or hot-air. Base heating and pressure measurements were belatedly made during the first flights of past ELVs to correct estimates from semi-empirical engineering models or scale model tests.

Presently, CFD methods for use in ELV design are being jointly developed at the Space Transportation Division (MDA-STD) and New Aircraft Missiles Divison (MDA-NAMD). An explicit three dimensional, zonal, finite-volume, full Navier-Stokes (FNS) solver with finite rate hydrocarbon/air and aluminum combustion kinetics was developed to accurately compute ELV power-on flowfields. Mississippi State University's GENIE++ general purpose interactive grid generation code was chosen to create zonal, finite volume viscous grids. Axisymmetric, time dependent, turbulent CFD simulations of a Delta DSV-2A vehicle with a MB-3 liquid main engine burning RJ-1/LOX were first completed. Hydrocabon chemical kinetics and a k-ε turbulence model were employed and predictions were validated with flight measurements of base pressure and temperature. Zonal internal/external grids were created for a Delta DSV-2C vehicle with a MB-3 and three Castor-I solid motors burning and a Delta-II with an RS-27 main engine (LOX/RP-1) and 9 GEMs attached/6 burning. Cold air, time dependent FNS calculations were performed for DSV-2C during 1992. Single phase simulations that employ finite rate hyrocarbon and aluminum (solid fuel) combustion chemistry are currently in progress. Reliable and efficient Eulerian algorithms are needed to model two phase (solid-gas) momentum and energy transfer mechanisms for solid motor fuel combustion products.

+ McDonnell Douglas Aerospace-Space Transportation Division, Huntingon Beach,Ca.
++ McDonnell Douglas Aerospace-New Aircraft Missile Products Division, St. Louis, Mo.
* Presently at Ford Motor Co., Detroit, Mi.
** Mississippi State Univ. NSF/Eng. Research Center, Strarkville, Miss.

CFD FLOWFIELD SIMULATION OF DELTA LAUNCH VEHICLES IN A POWER-ON CONFIGURATION

By: D. L. Pavish *
T. P. Gielda
B. K. Soni
J. E. Deese
R. K. Agarwal

* McDonnell Douglas Aerospace - Space Transportation Division
5301 Bolsa Avenue - M.S. 12/2
Huntington Beach, California 92647
(714) 896-4383

11th Workshop for Computational Fluid Dynamic (CFD) Applications in Rocket Propulsion

PROBLEM

- CFD internal/external reacting gas (power-on) flowfield predictions are needed for engineering design of expendable launch vehicles (ELVs)

  [1] base pressure (base drag) [2] base heating rate (insulation)

- ELV cold/hot air or reacting gas wind tunnel tests require long lead times and are very expensive

- ELV base region environments often determined during initial flights

OBJECTIVE

- Utilize state of the art CFD methods to predict power-on multibody ELV flowfields

- Reduce or minimize wind tunnel testing and flight measurements of base region pressures and heating

- Reduce ELV design cycle costs and aerodynamic uncertainties

APPROACH

MDA – Space Transportation

- Apply, modify, improve existing and developing CFD techniques to predict power-on flowfields for multibody and multi-engine Delta ELVs
- Cooperative, multi-year research effort by MDA-STD, MDA-NAMPD, and Miss. State NSF/ERC
- Grid Generation

  Employ advanced GENIE^{++}, zonal, structured, grid generation code
- Navier-Stokes Flow Solver

  Time dependent, Reynolds averaged, 3D Navier-Stokes code

  Explicit Runge-Kutta integration procedure

  K-epsilon turbulence model (Jones & Launder, high Re. no. form)

  TVD dissipation scheme (Yoon and Kwak)

  Zonal, contiguous grid capability

  Finite rate combustion chemistry routines (explicit)
  hydrocarbon (RJ-1 or RP-1) and aluminum based solid motor fuel

  Robust, well validated CFD code for ELV power-off flowfields
  (see AIAA-91-1727 and AIAA-92-2681)

APPROACH (Continued)

VALIDATION

Perform a series of increasingly complex power-on simulations

(1) Single body Delta DSV-2A with MB-3 main engine burning (LOX/RJ-1) with finite rate chemistry (0° and 3° angle of attack)

(2) Delta DSV-2C with MB-3 main engine plus 3 Castor-I solids burning Hot air, single phase, finite rate reacting gas (0° angle of attack)

(3) Delta-II with RS-27 LOX/RP-1 main engine plus 9 GEMs (or Castor-IVAs) attached/6 burning

0° angle of attack to minimize grid size and computer time

Perform cold air (constant gamma) solutions before reacting gas simulations to remove grid errors

Assume single phase gas reactions w/o surface combustion

Utilize Delta launch vehicle flight measurements of base surface pressures, temperatures, heating rates

PROGRESS & RESULTS

MDA – Space Transportation

(1) AXISYMMETRIC DELTA DSV-2A POWER-ON SIMULATION (AIAA-91-3338)

Two zone overlapping viscous grid (internal and external)

Thin-layer Navier Stokes flowfield simulations

MB-3 main engine (LOX/RJ-1) with finite rate hydrocarbon combustion chemistry

Chamber temperature, pressure, mass ratios are known

Nozzle exit momentum and mass flow matched at nozzle exit

Four Mach number-trajectory points simulated (axisymmetric, 0° angle of attack)

Predicted base pressures and temperatures well validated

Demonstrated angle of attack effects on nozzle and base surface pressures

DELTA DSV FLIGHT 419 RECONSTRUCTED TRAJECTORY

MDA–Space Transportation Division

VED2955 M20DE

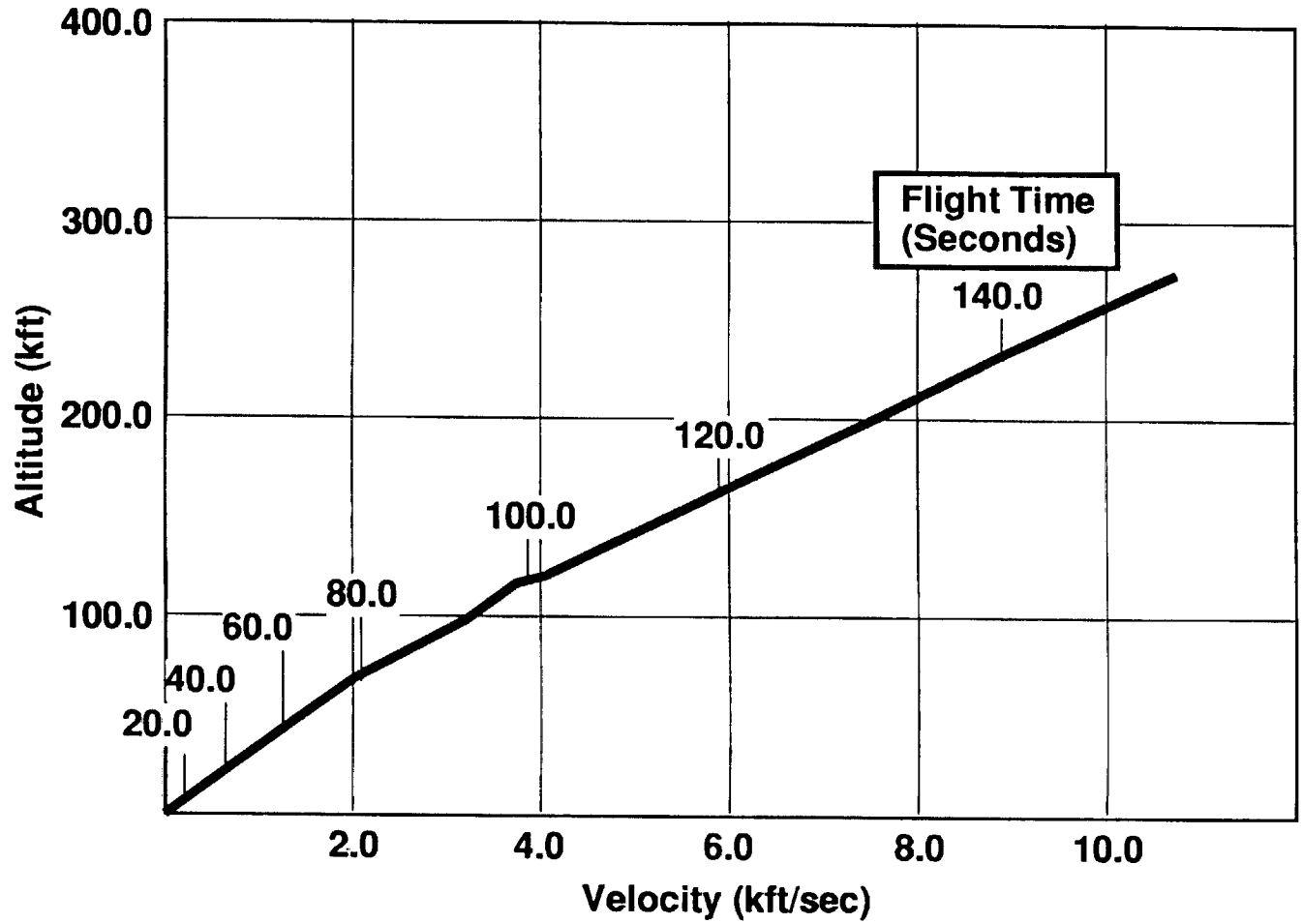

DELTA DSV-2A TWO-ZONE OVERLAPPING AXISYMMETRIC GRID

VED2949 M20DE

MDA–Space Transportation Division

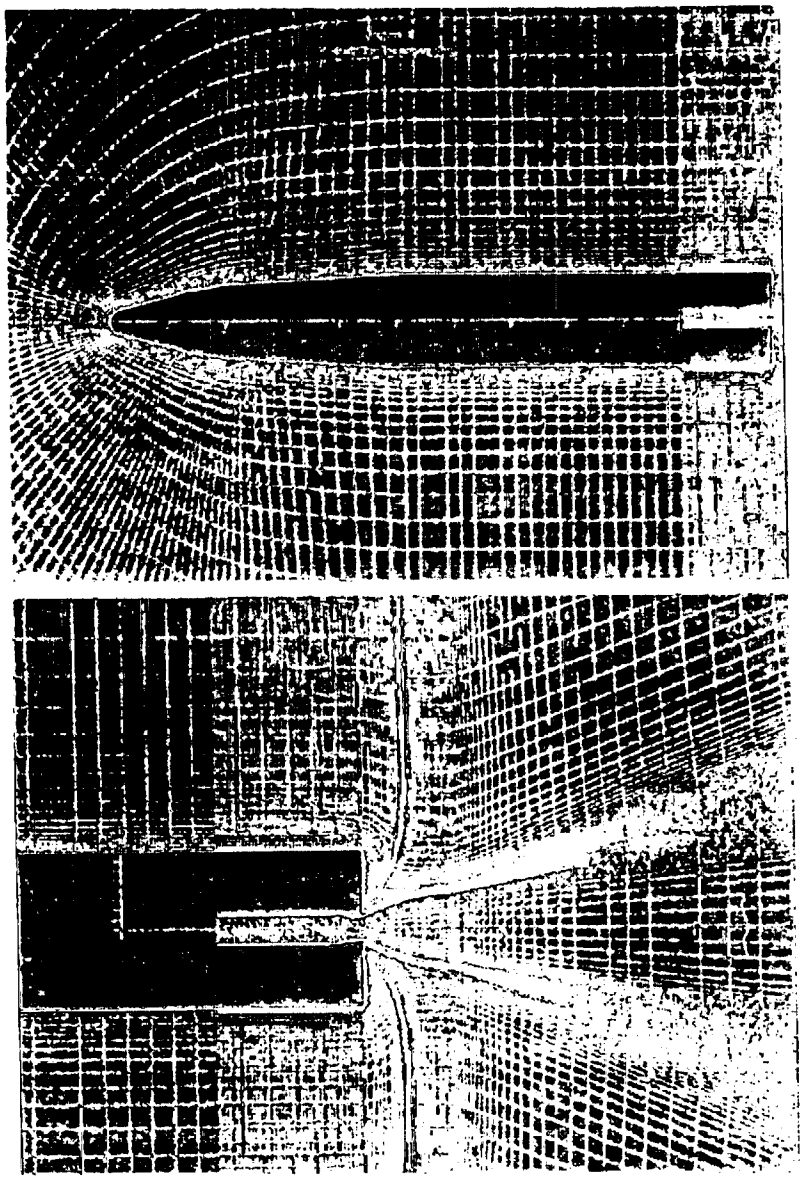

Forebody Grid

Downstream and Base Region Grid

DSV FLOWFIELD MACH NUMBER CONTOURS

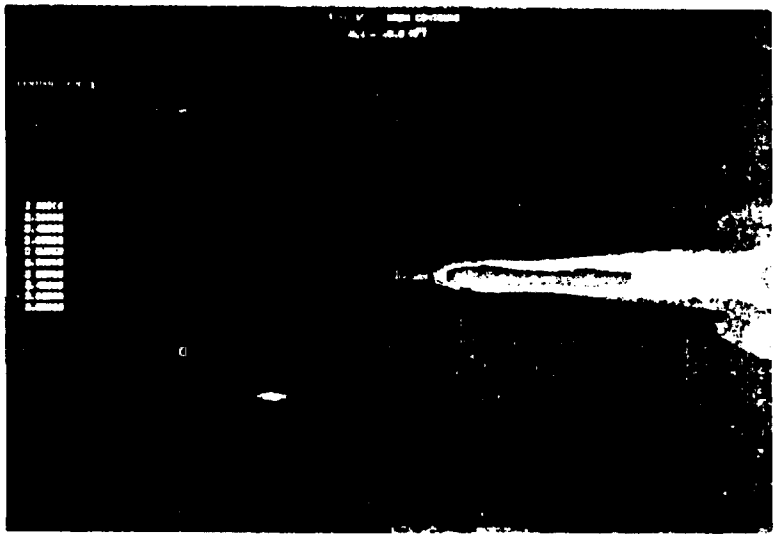

Altitude = 18 kft,
Mach Number = 1.01

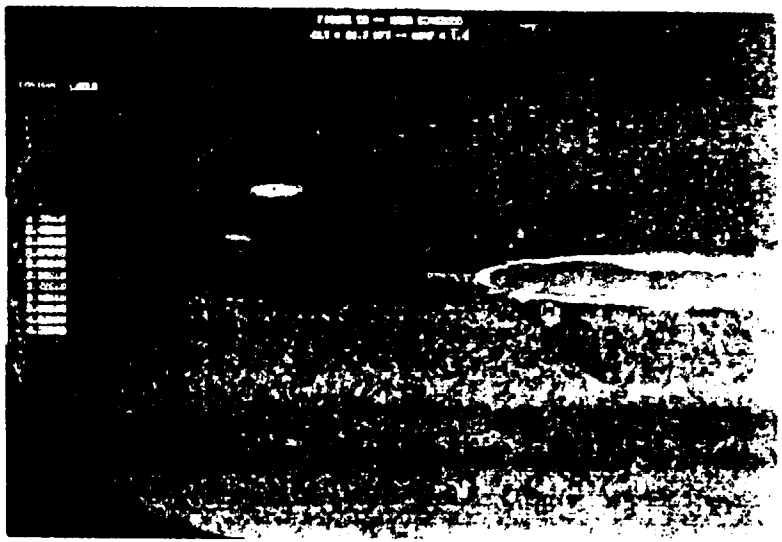

Altitude = 31.7 kft,
Mach Number = 1.4

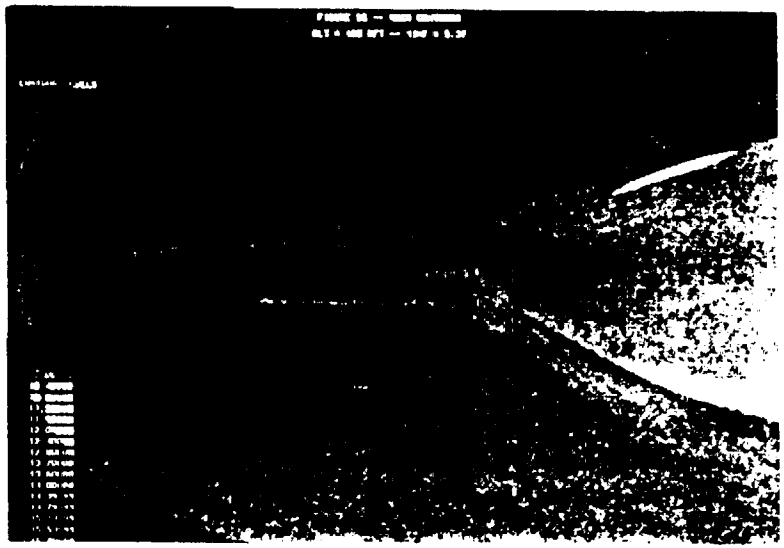

Altitude = 160 kft,
Mach Number = 5.37

DSV EXPANDED FLOWFIELD MACH NUMBER CONTOURS

VED2952 M20DE

MDA–Space Transportation Division

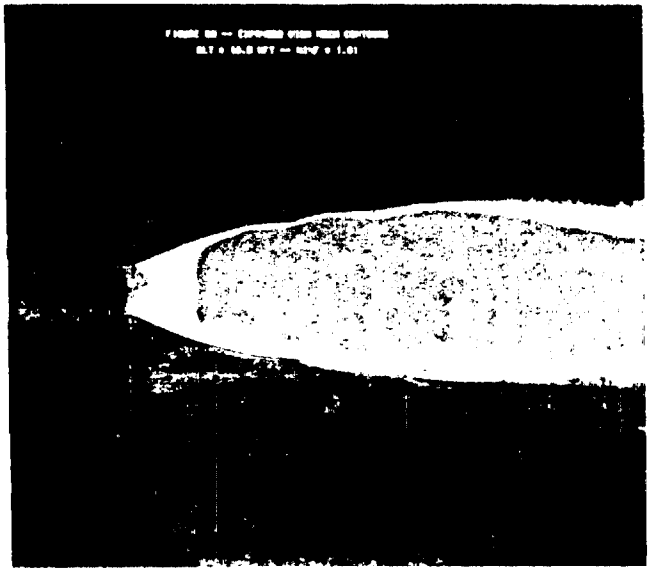

Altitude 18 kft,
Mach Number = 1.01

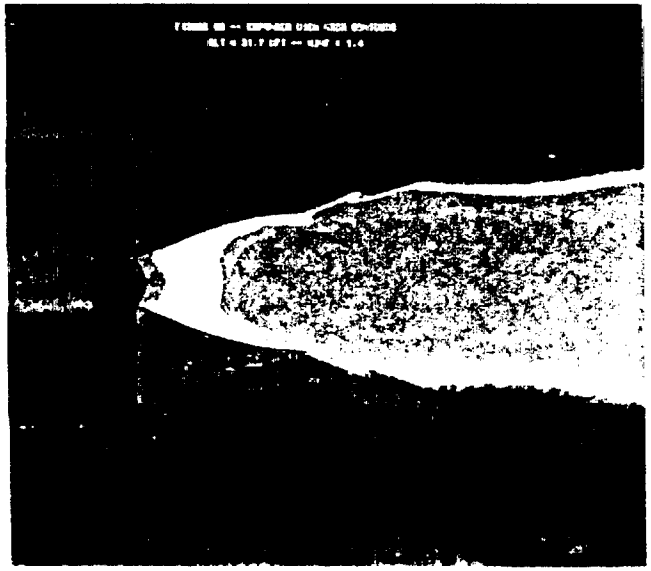

Altitude = 31.7 kft,
Mach Number = 1.4

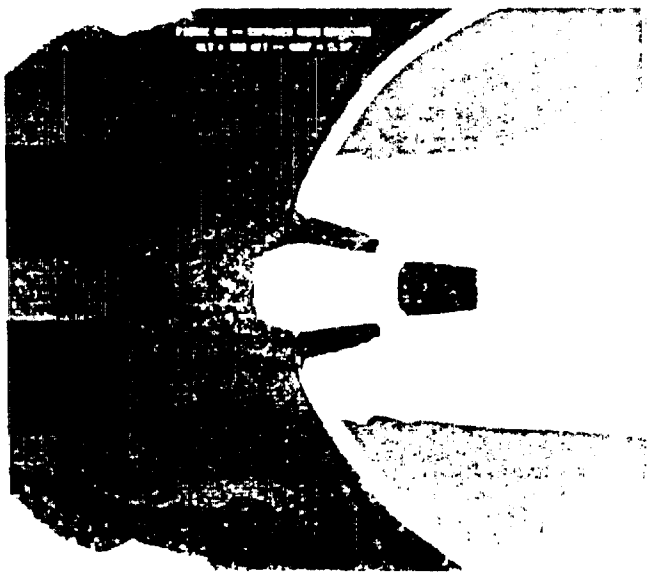

Altitude = 160 kft,
Mach Number = 5.37

DSV FLOWFIELD CO_2 MASS FRACTIONS

Altitude = 18 kft,
Mach Number = 1.01

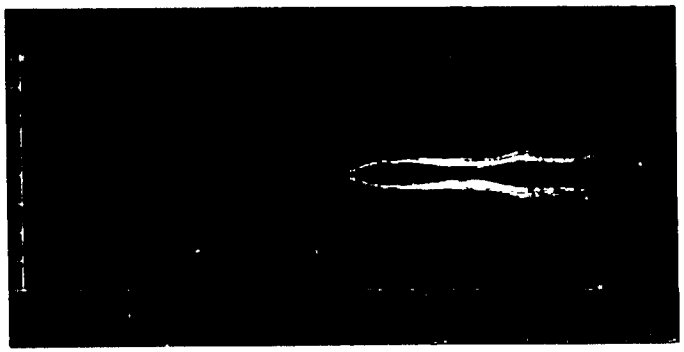

Altitude = 31.7 kft,
Mach Number = 1.4

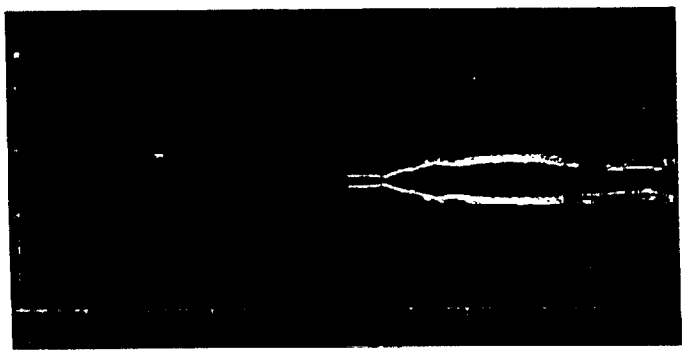

Altitude = 160 kft,
Mach Number = 5.37

DELTA DSV BASE SURFACE TEMPERATURE
COMPARISON OF CFD PREDICTION VS FLIGHT MEASUREMENTS

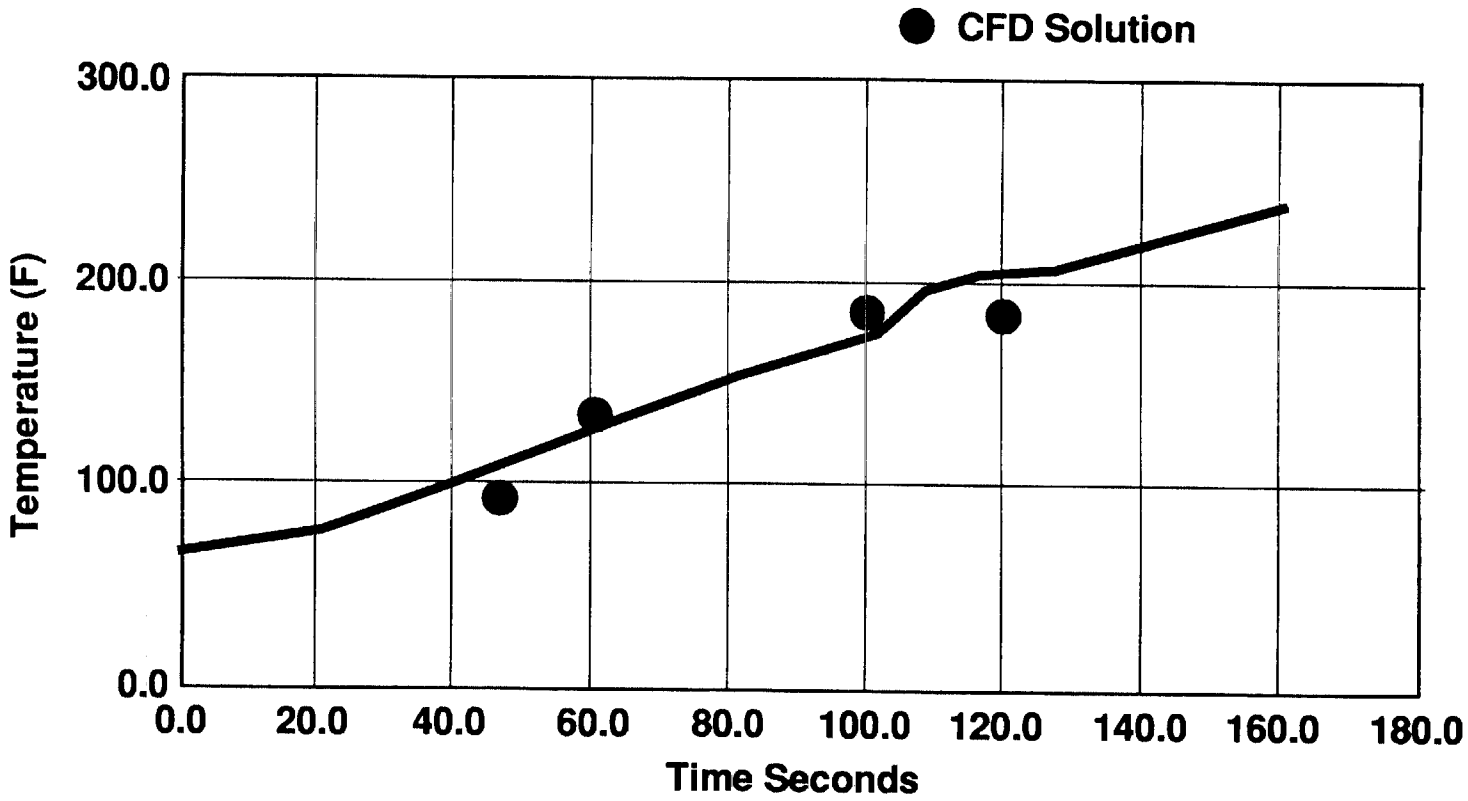

DELTA DSV BASE PRESSURE COEFFICIENTS COMPARISON OF CFD AND FLIGHT MEASUREMENTS

MDA–Space Transportation Division

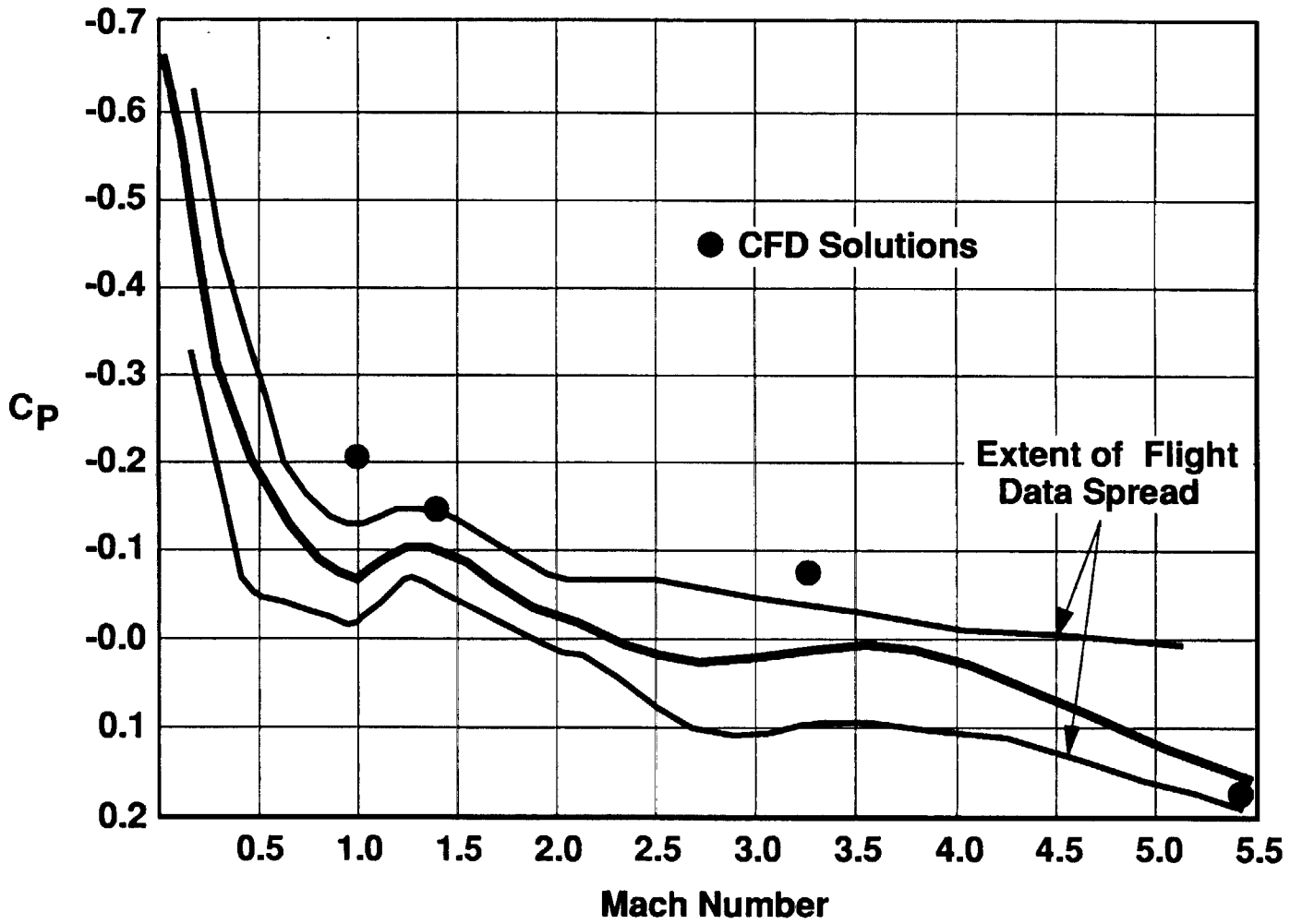

PREDICTED DELTA DSV BASE REGION SURFACE PRESSURE COEFFICIENTS

VED2956 M20DE

MDA–Space Transportation Division

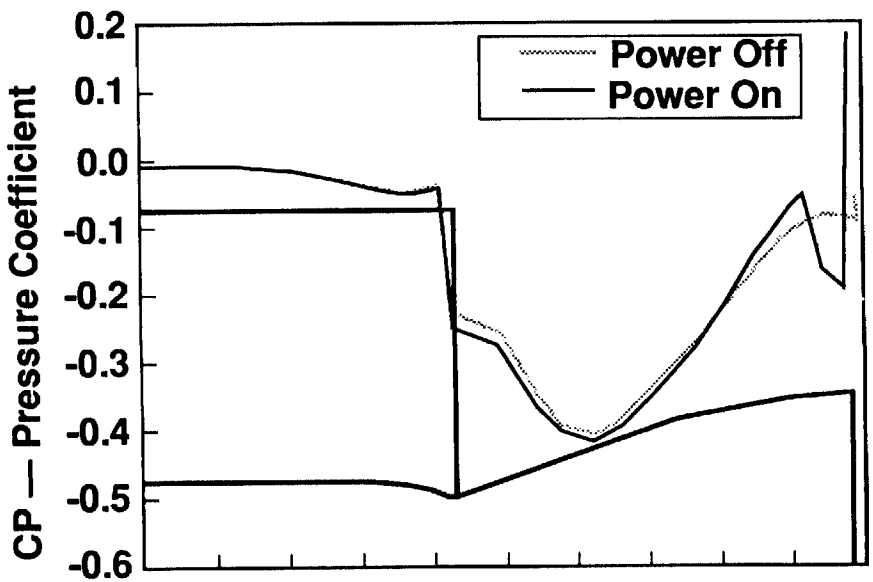

Mach Number = 1.2

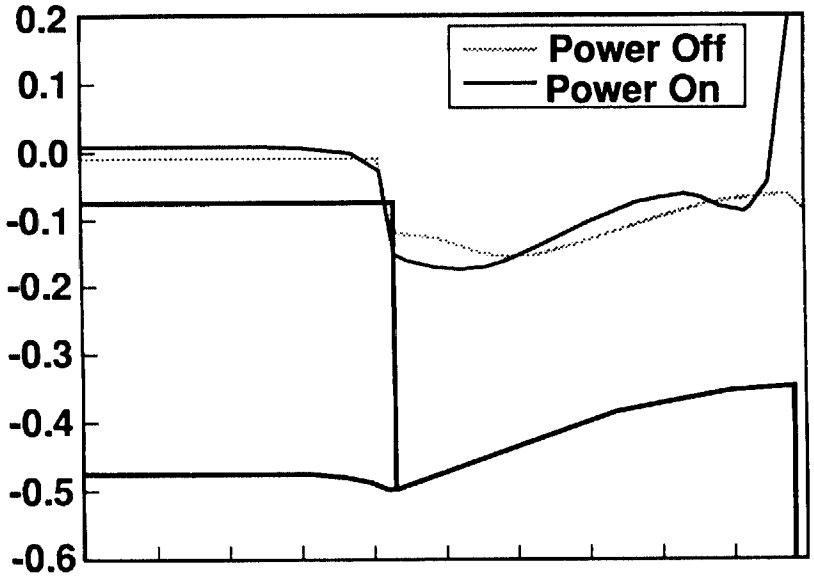

Mach Number =2.2

PREDICTIONS OF DELTA DSV AFT VEHICLE CIRCUMFERENTIAL SURFACE PRESSURE
MACH NUMBER = 1.01, ANGLE OF ATTACK = 3.0 DEGREES

MDA–Space Transportation Division

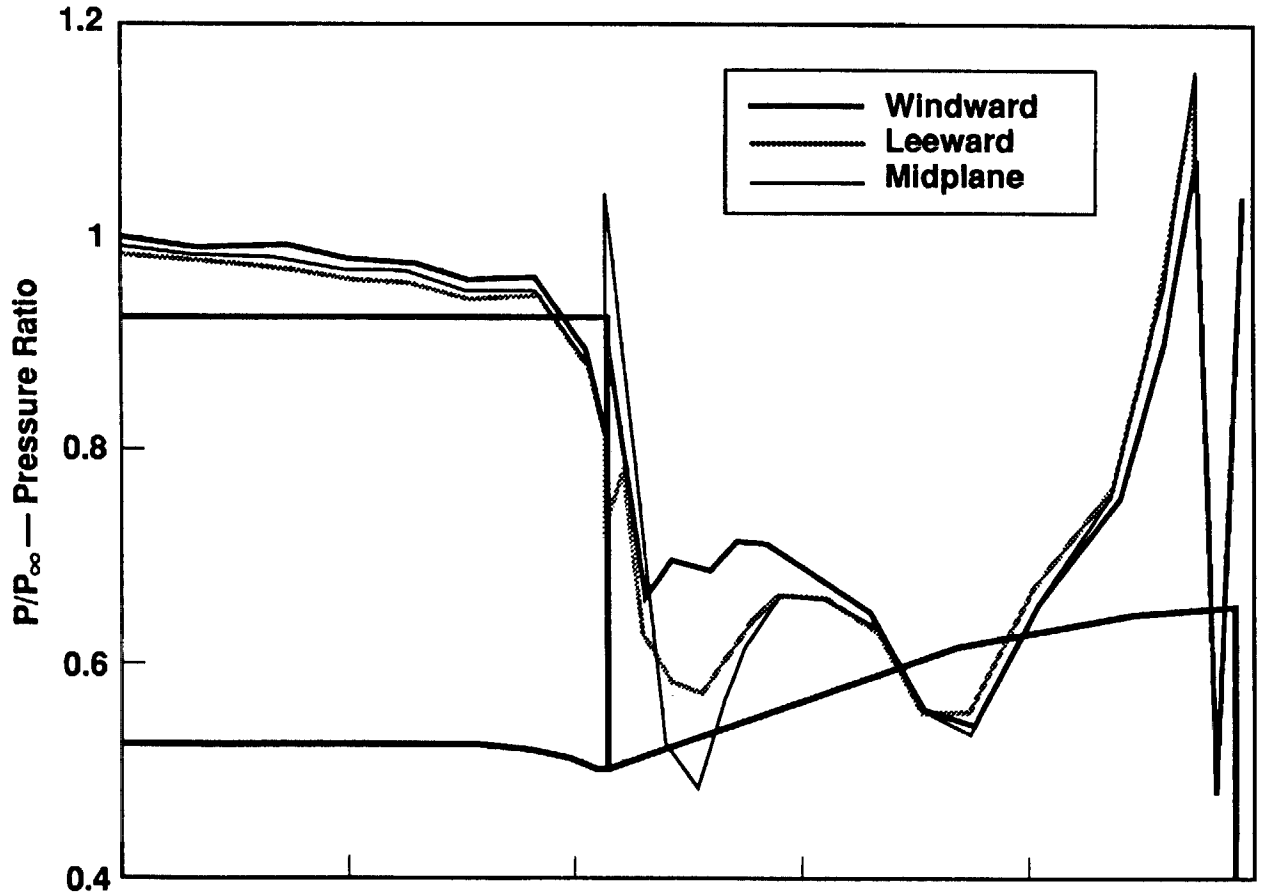

PROGRESS & RESULTS (Continued)

(2) THREE DIMENSIONAL DSV-2C POWER-ON SIMULATIONS (in progress)

160-105-40 I-J-K global grid, 8 zones (60° circumferential arc region)

Full Navier Stokes flow code simulations

Three Castor-1 solids (TP-H8038 fuel) plus MB-3 liquid main (LOX/RJ-1)

Hot gas, 0° angle of attack at Mach No. = 1.4 (completed)

Perform single phase, reacting gas simulations at 0° angle of attack (in progress)

Employ aluminum solid fuel finite rate combustion chemistry

THREE-DIMENSIONAL DELTA DSV-2C POWER-ON MULTIBODY, FLOWFIELD SIMULATION
MACH NO. = 1.4, K-E TURBULENCE MODEL, ANGLE OF ATTACK = 0 DEG

MDA–Space Transportation Division

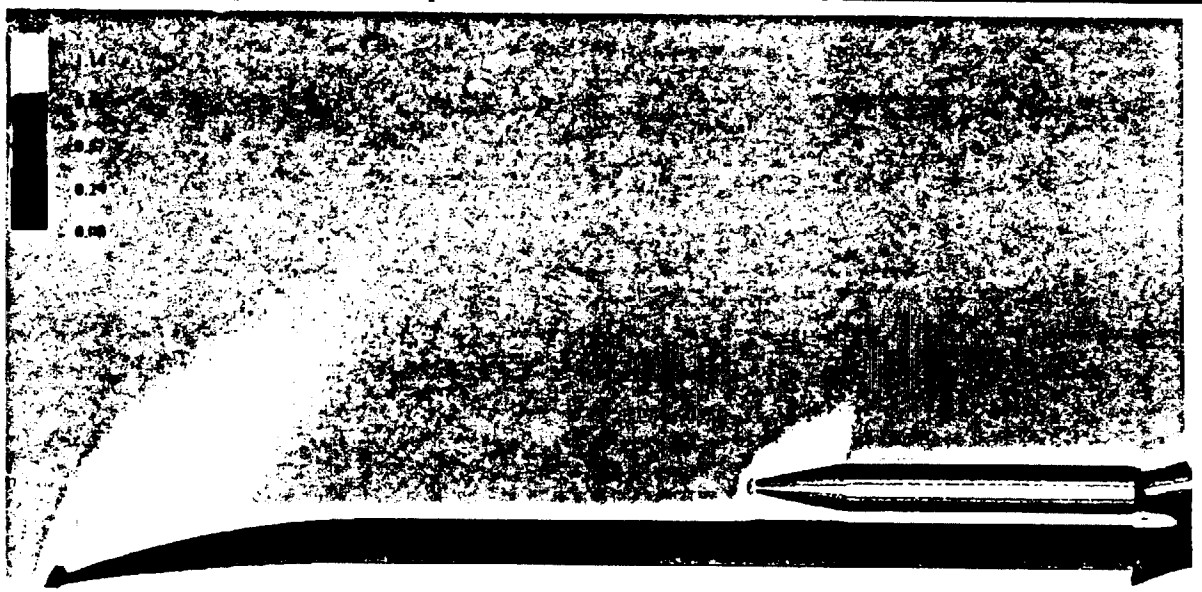

Mach Number Contours
Upstream Flowfield
Symmetry Plane

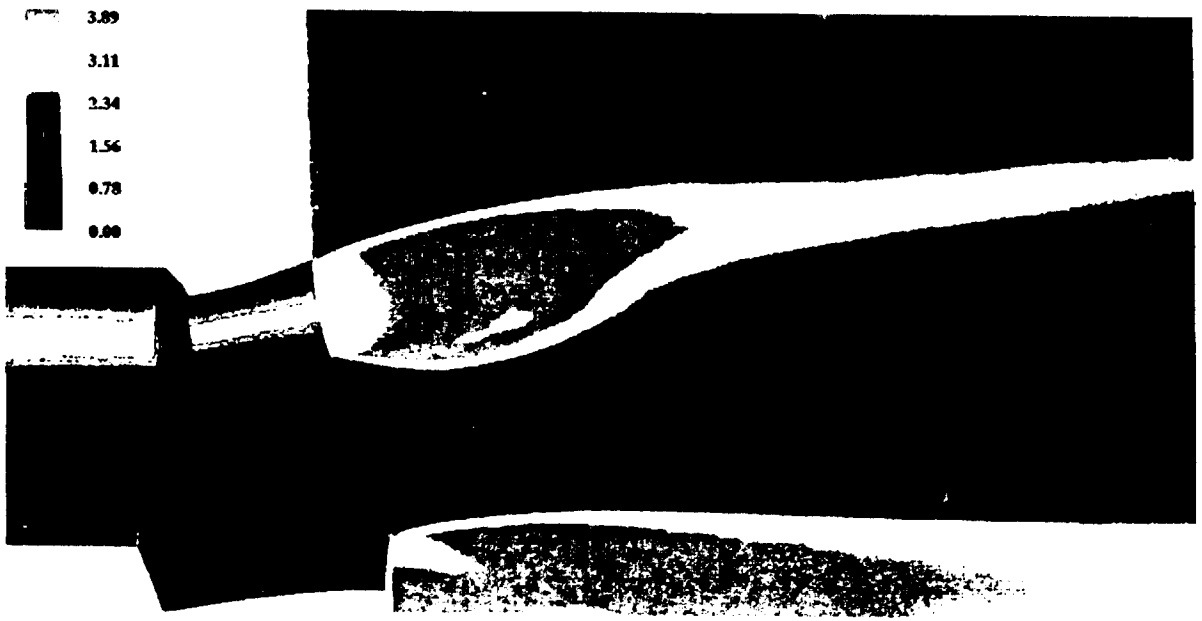

Mach Number Contours
Base Region and
Plume Flowfield

SUMMARY AND CONCLUSIONS

- Results from DSV-2A (single engine) reacting gas simulations are encouraging
- Single phase, reacting gas CFD simulations for multibody, DSV-2C and Delta-II vehicles are in progress
- Work needed to develop/modify efficient, accurate Eulerian algorithms to empirically model interaction of entrained aluminum oxide particulates

  Quantification of solid particulate and reacting gas exchange of:

Mass	(sublimation or vaporization)
Momentum	(particle drag)
Energy	(radiation, convection)

NUMERICAL STUDY OF THE SSME NOZZLE FLOW FIELDS DURING TRANSIENT OPERATIONS - A COMPARISON OF THE ANIMATED RESULTS WITH TEST

Ten-See Wang
Computational Fluid Dynamics Branch
NASA - Marshall Space Flight Center
Marshall Space Flight Center, AL 35812

Catherine Dumas
SVERDRUP Technology, Inc.
Huntsville, AL 35806

Abstract

A computational fluid dynamics (CFD) model has been applied to study the transient flow phenomena of the nozzle and exhaust plume of the Space Shuttle Main Engine (SSME), fired at sea level. The CFD model is a time accurate, pressure based, reactive flow solver. A six-species hydrogen/oxygen equilibrium chemistry is used to describe the chemical-thermodynamics. An adaptive upwinding scheme is employed for the spatial discretization, and a predictor, multiple corrector method is used for the temporal solution. Both engine start-up and shut-down processes were simulated. The elapse time is approximately five seconds for both cases. The computed results were animated and compared with the test. The images for the animation were created with PLOT3D and FAST and then animated with ABEKAS. The hysteresis effects, and the issues of free-shock separation, restricted-shock separation and the end-effects were addressed.

Numerical Study of the SSME Nozzle Flowfields during Transient Operations - A Comparison of Animated Results with Test

Ten-See Wang
Computational Fluid Dynamics Branch
NASA-Marshall Space Flight Center

Catherine Dumas
Sverdrup Technology, Inc.

11th Workshop for CFD Applications in Rocket Propulsion
Open Forum: Combustion - Nozzles/plumes - Comparison
MSFC, Alabama
April 22, 1993

Approach

Computation:

- Time accurate, axisymmetric transport equations
- Extended two-equation turbulence model
- Spatial discretization - adaptive artifical dissipation
- Six species, four equation equilibrium chemistry
- Digital transient model simulated upstream boundary conditions
- Total elapse time is approximately 5 aeconds for both start-up and shut-down transients

Animation:

- PLOT3D and FAST generated images
- ABEKAS generated animatioins

Animations

- Start-up transient animations
  - Pressure
  - Temperature
  - Mach number
- Shut-down transient animaions
  - Pressure
  - Temperature
  - Mach number
- Hot-fire test photography: from visible to IR
  - Start-up transient
  - Shut-down transient
- A comparison of computed thrust coefficients with those of measurement
  - Start-up transient
  - Shut-down transient

Summary

- The CFD animations compared well with the hot-fire test photography
- The restricted-shock separation and end-effect separation have been captured by the CFD calculation
- The computed thrust coefficient histories compared reasonably well with those of the hot-fire test data

AERODYNAMIC DESIGN AND ANALYSIS OF A HIGHLY LOADED TURBINE EXHAUST VOLUTE MANIFOLD

F.W. Huber, X.A. Montesdeoca, R.J. Rowey
Pratt & Whitney GESP
West Palm Beach, FL

The aerodynamic design and analysis of a turbine exhaust volute manifold is described. This turbine exhaust system will be used with an advanced gas generator oxidizer turbine designed for very high specific work. The elevated turbine stage loading results in increased discharge Mach number and swirl velocity, which along with the need for minimal circumferential variation of fluid properties at the turbine exit, represent challenging volute design requirements. The design approach, candidate geometries analyzed, and steady state / unsteady CFD analysis results are presented.

MSFC Turbine Stage Technology Team

- Team consisting of turbine specialists from government, industry, and universities committed to advancing the state-of-the-art of turbine design
- Effort directed at applying advanced computational fluid dynamics (CFD) codes and capability to the turbine design process
- Team focused on turbines meeting STME requirements
- Enhanced design / analysis tools available for future application

Volute Design Process Outline

Meanline Analysis

Geometry Generation

3D Flow Analysis

Baseline Volute Geometry

Turbine Team Analysis

- o Integrated Turbine/Volute Modelling
- o
- o

Advanced Concept Volute Geometry

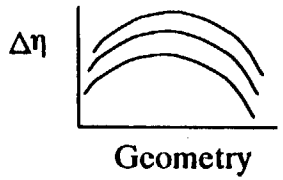

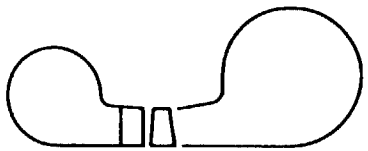

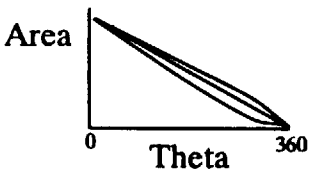

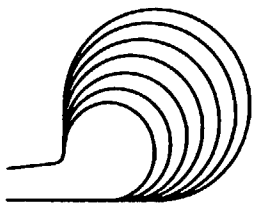

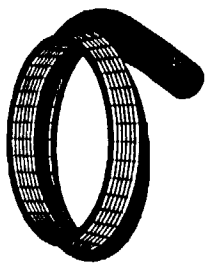

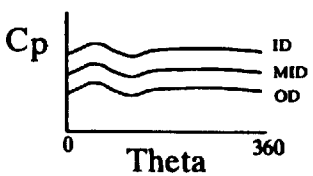

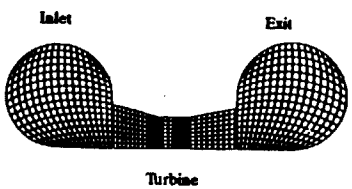

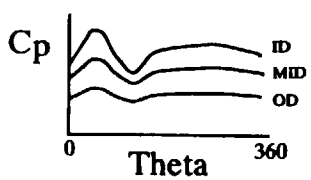

Exhaust Volute Manifold Design Requirements

HIgh Turbine Stage Loading Creates Challenging Goals

Turbine Stage Loading Summary

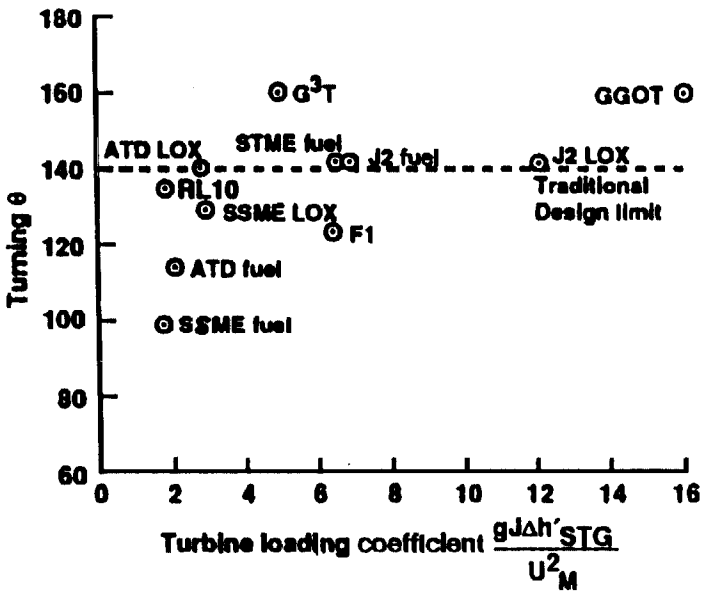

Exhaust Manifold Requirements

- Inlet Mach No. = 0.84
- Exit Mach No. = 0.3
- Minimize Transverse Press. Gradient
- Minimize Total Press. Loss

Meanline Analysis

First Pass Estimate of Geometry and Performance

- Major Geometric Features Modeled
  - Distribution of Thru-Flow Area
  - Mean Flow Path Radius
  - Inlet and Exit Flow Paths
  - Suface Roughness

- Pressure Loss Estimate
  - Wall Friction
  - Secondary Flows in a Turning Passage
  - Diffusion
  - Tongue Incidence
  - Flow Path Dump

- Parametric Studies
  - Performance Optimization and Sensitivity

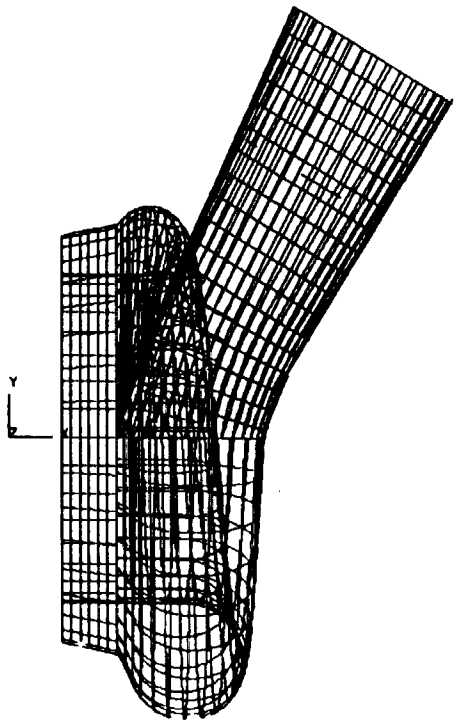

Geometry and Mesh Generation

Rules Based Design Program Used To Create Volute Geometry

INPUT:

2D Definition

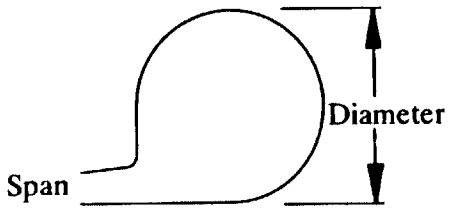

Area Distribution

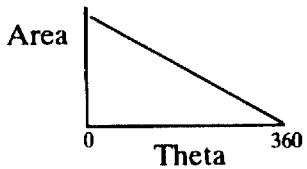

- Number of Sections Required
- CW/CCW Development

OUTPUT:

2D Contours

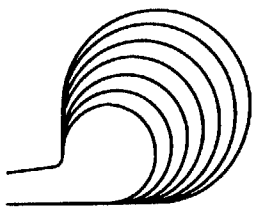

3D Surfaces

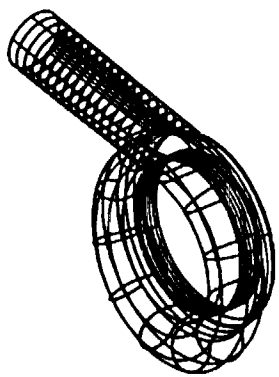

- CAD File for Geometry Enhancements
- Bulkpoint File For Mesh Generator

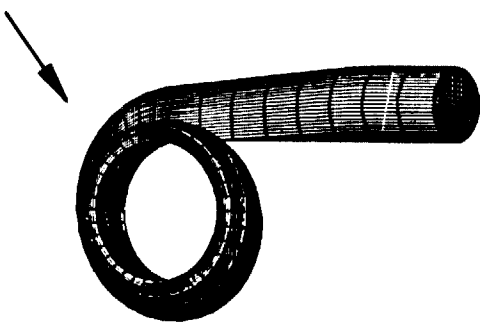

Exhaust Manifold 3D Flow Analysis
Inlet Boundary Condition Sensitivity Assessment

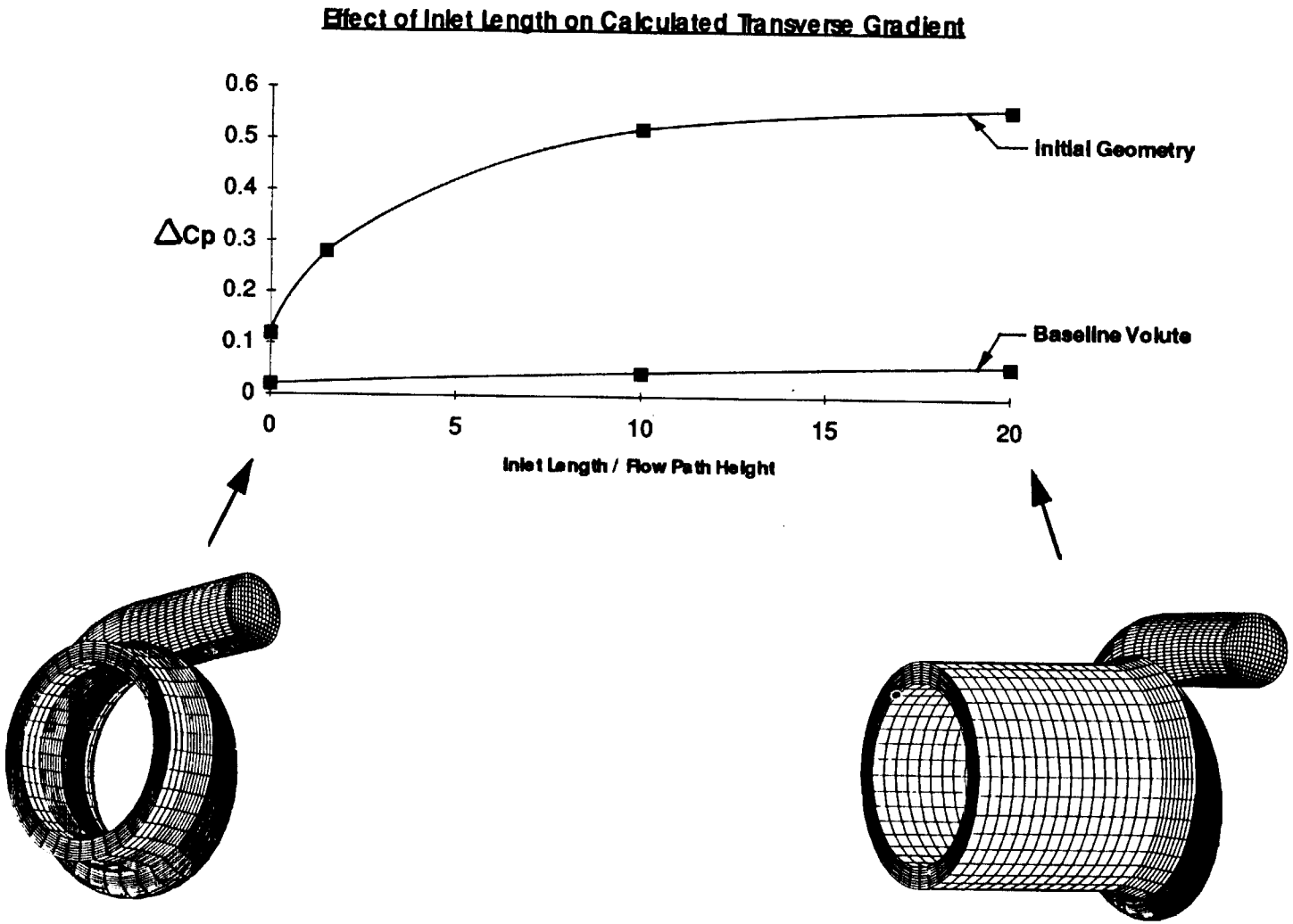

Baseline Volute 3D Flow Analysis

Circumferential Static Pressure Distribution

Steady State Model with 20:1 Inlet

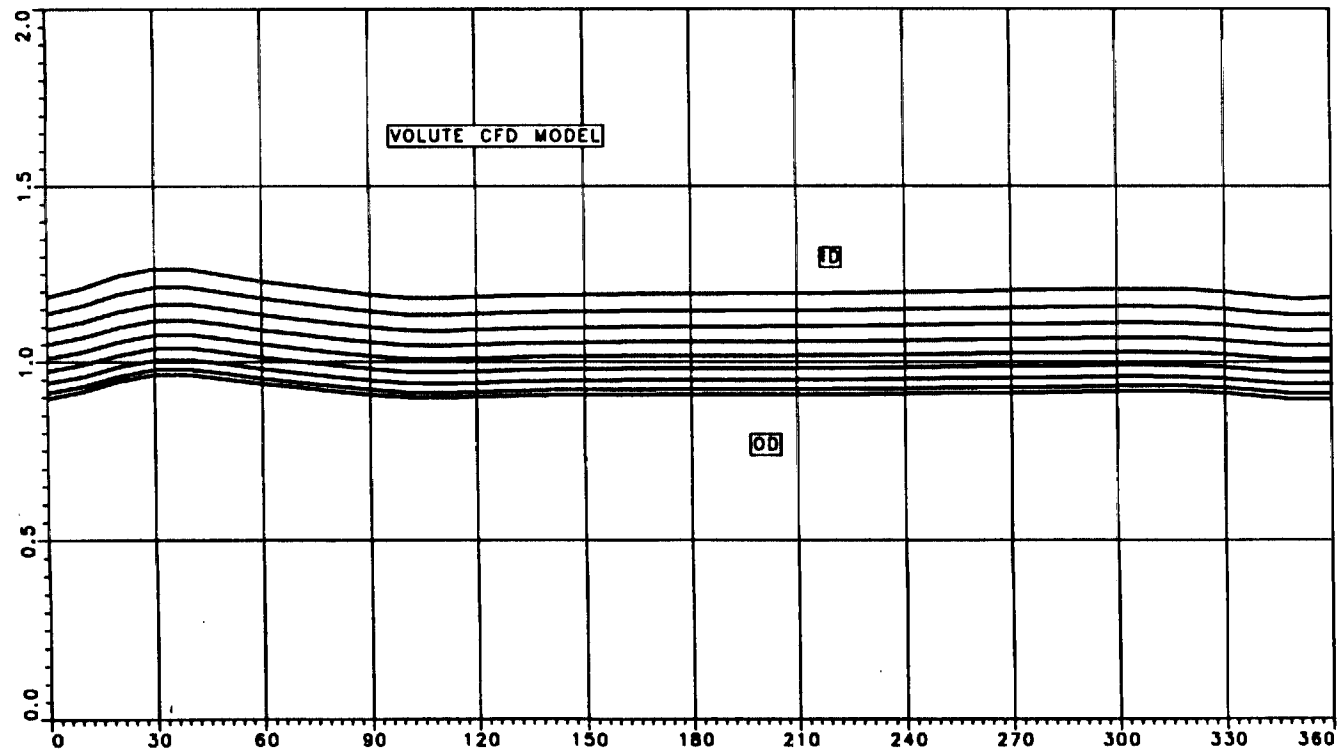

Vol Inlet Cp

Circ. Position (deg.)

Integrated CFD Modeling of Components

Circumferential Static Pressure Distribution at Turbine / Exhaust Man. Interface

Steady State Model of Inlet Volute, Turbine Stage and Exhaust Manifold

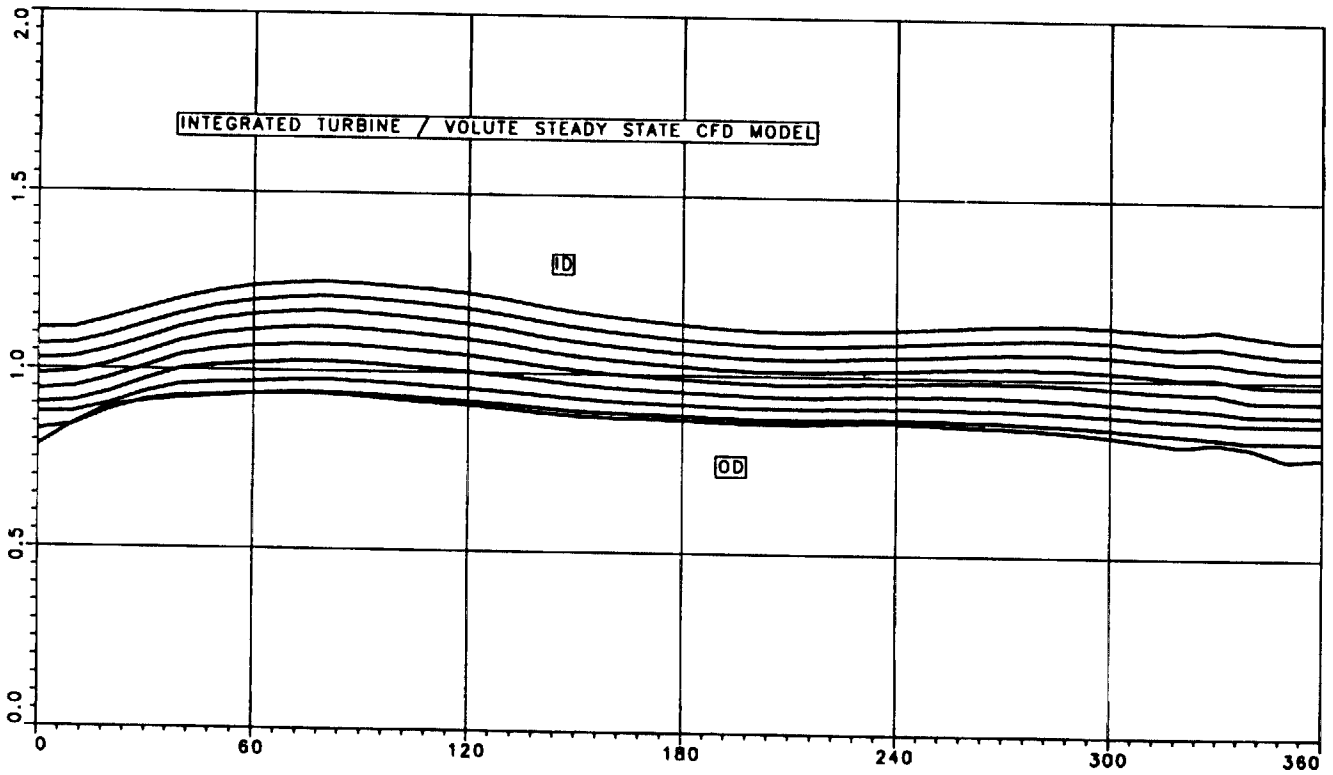

Exhaust Manifold 3D Flow Analysis

Baseline Volute Flow Vectors

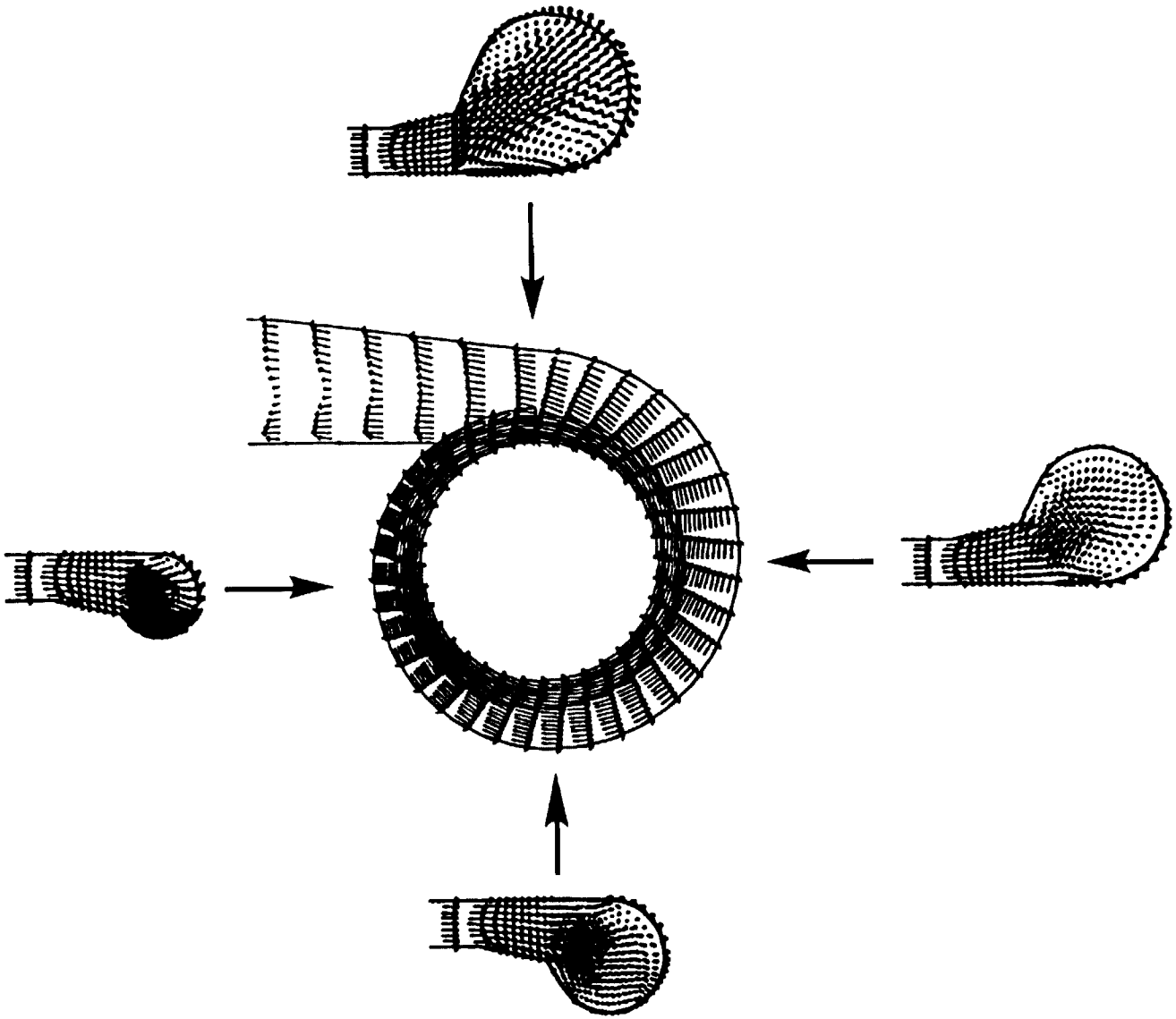

Baseline Volute

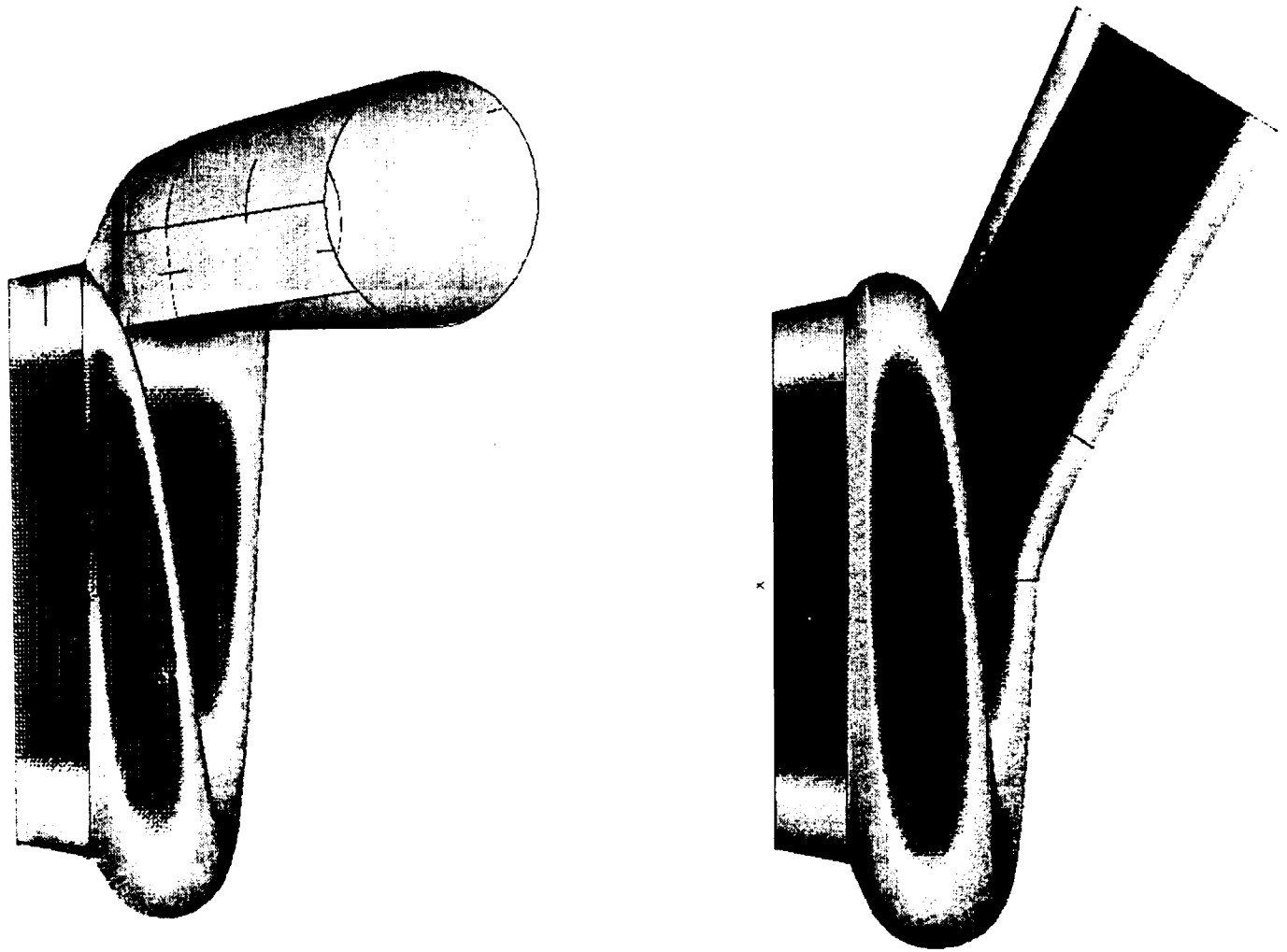

Integrated CFD Modeling of Components

Computational Mesh for Inlet Volute, Turbine Stage and Exhaust Manifold

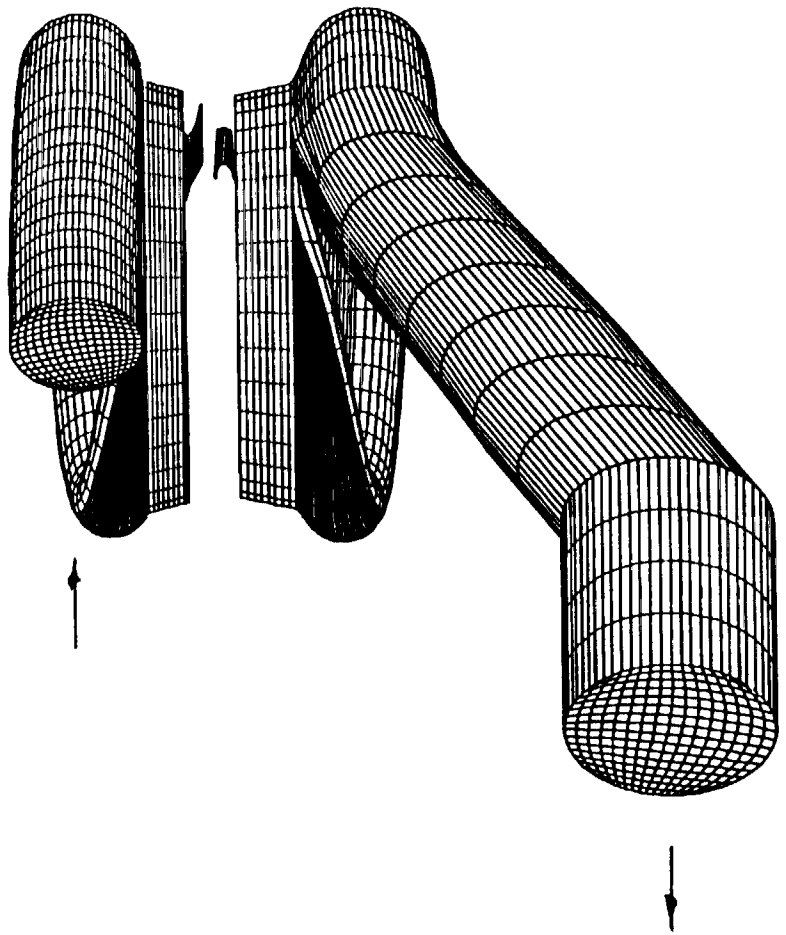

Time Accurate 3D Turbine Stage Flow Analysis
Euler (w / shear), 20 Vanes, and 42 Blades

Computational Grid

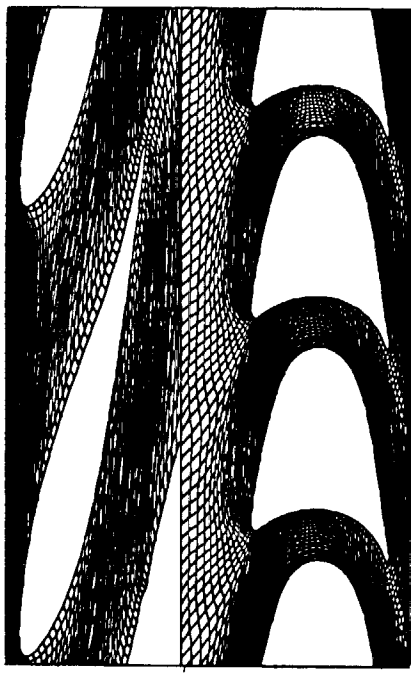

Unsteady Pressure Dist.

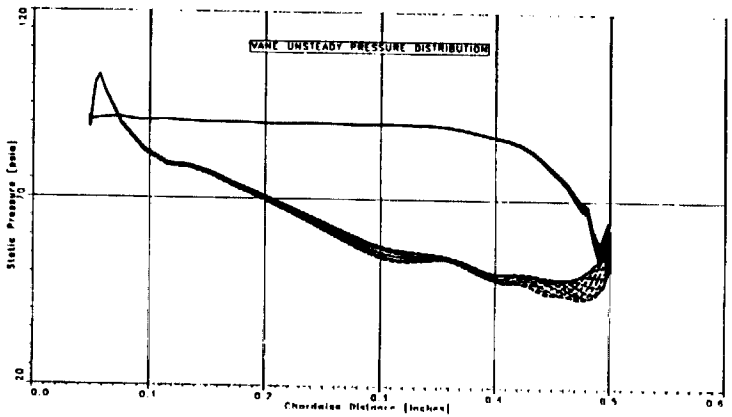

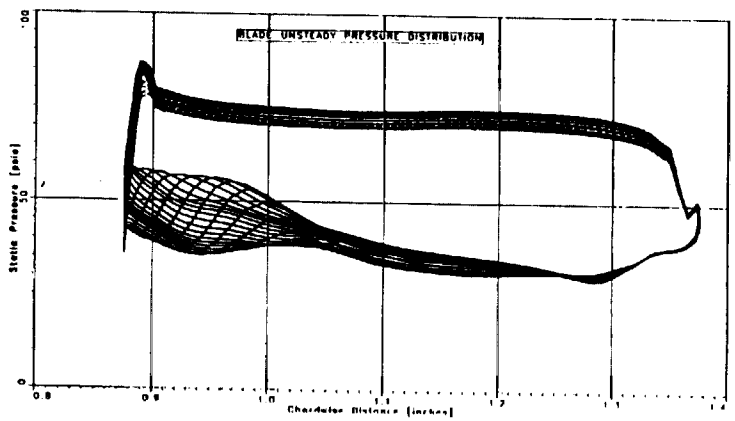

Integrated Time Accurate CFD Modeling of Components

Turbine Stage (20 Vanes, 42 Blades) and Exhaust Manifold (42 Elements)

Time Averaged Circ. Static Pressure Distribution at Turbine Exit

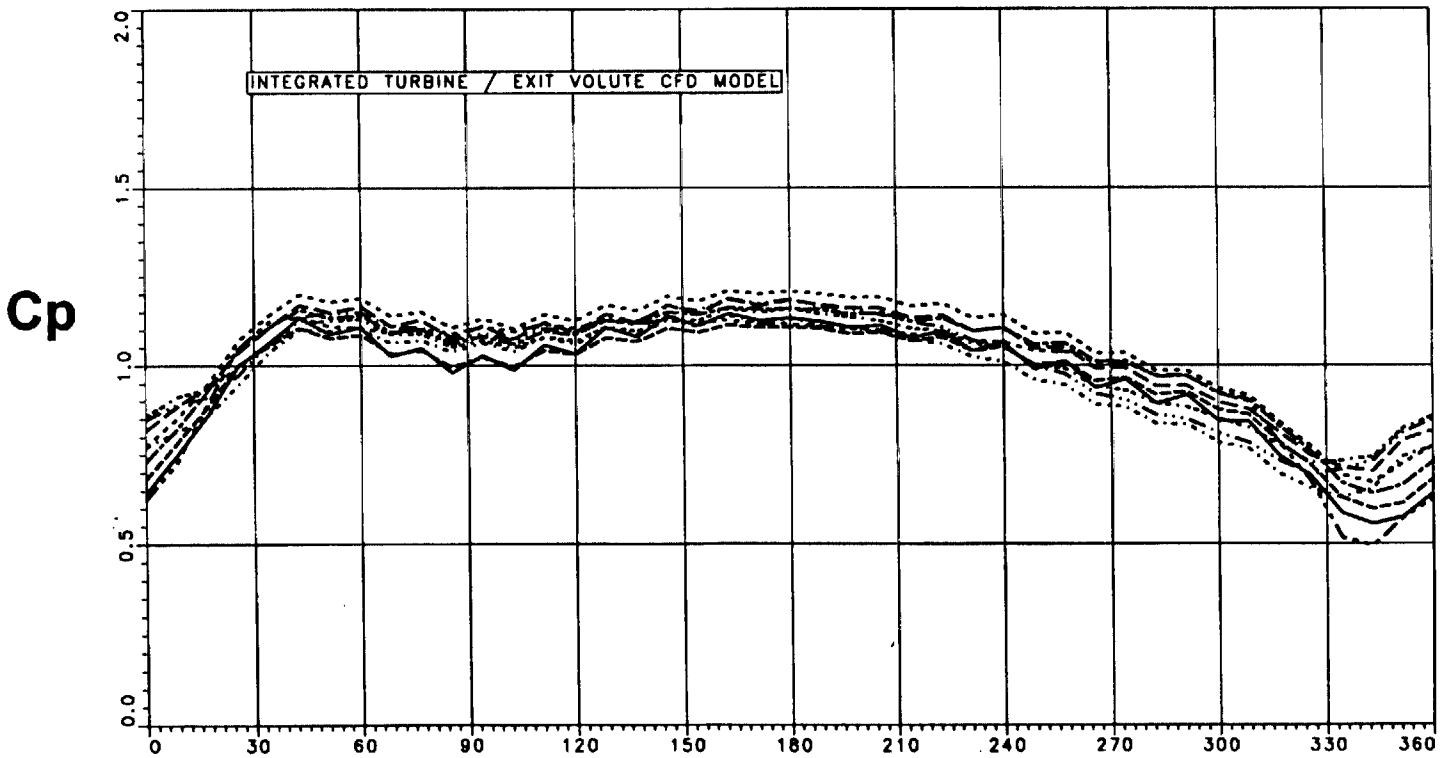

Time Accurate 3D Turbine Stage Flow Analysis

Euler (w / shear), 20 Vanes, and 42 Blades

Instantaneous Circ. Static Pressure Distribution at Turbine Exit

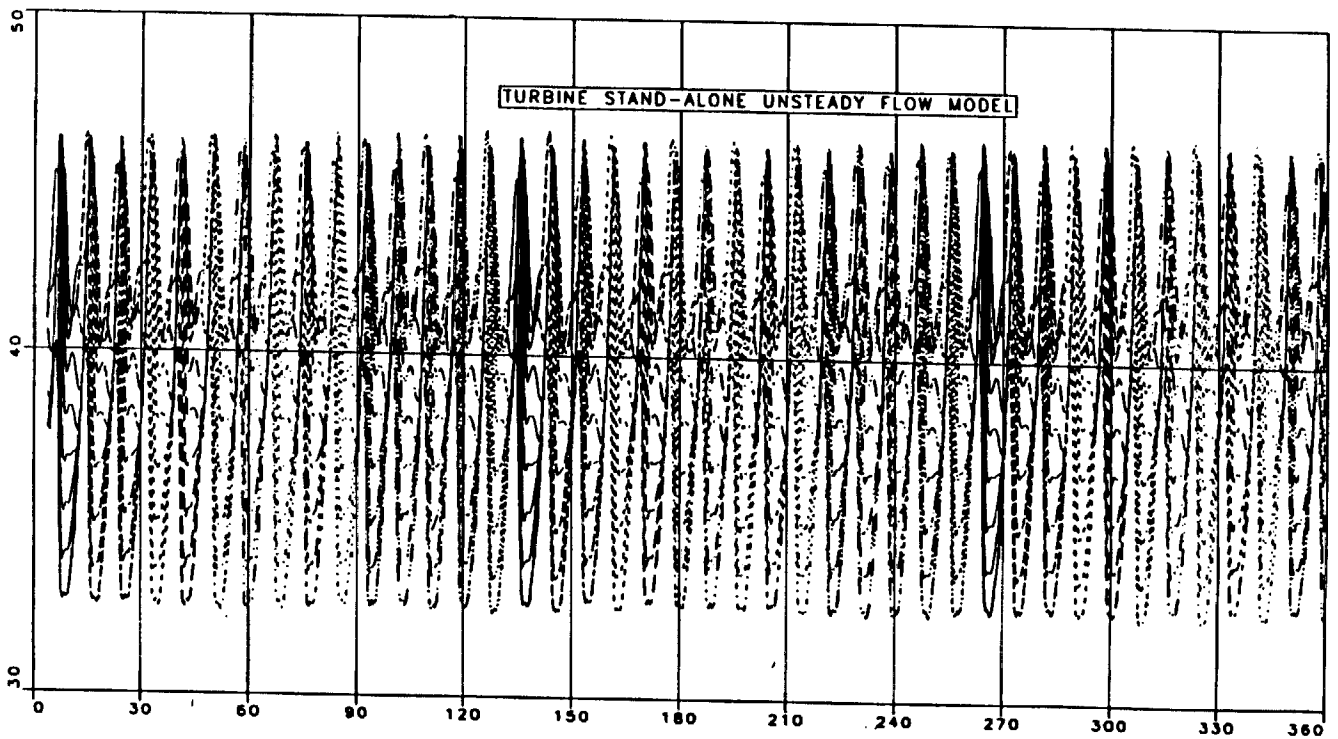

Ps (psia)

Circ. Position (deg.)

Integrated Time Accurate CFD Modeling of Components

Turbine Stage (20 Vanes, 42 Blades) and Exhaust Manifold (36 Elements)

Instantaneous Circ. Static Pressure Distribution at Turbine Exit

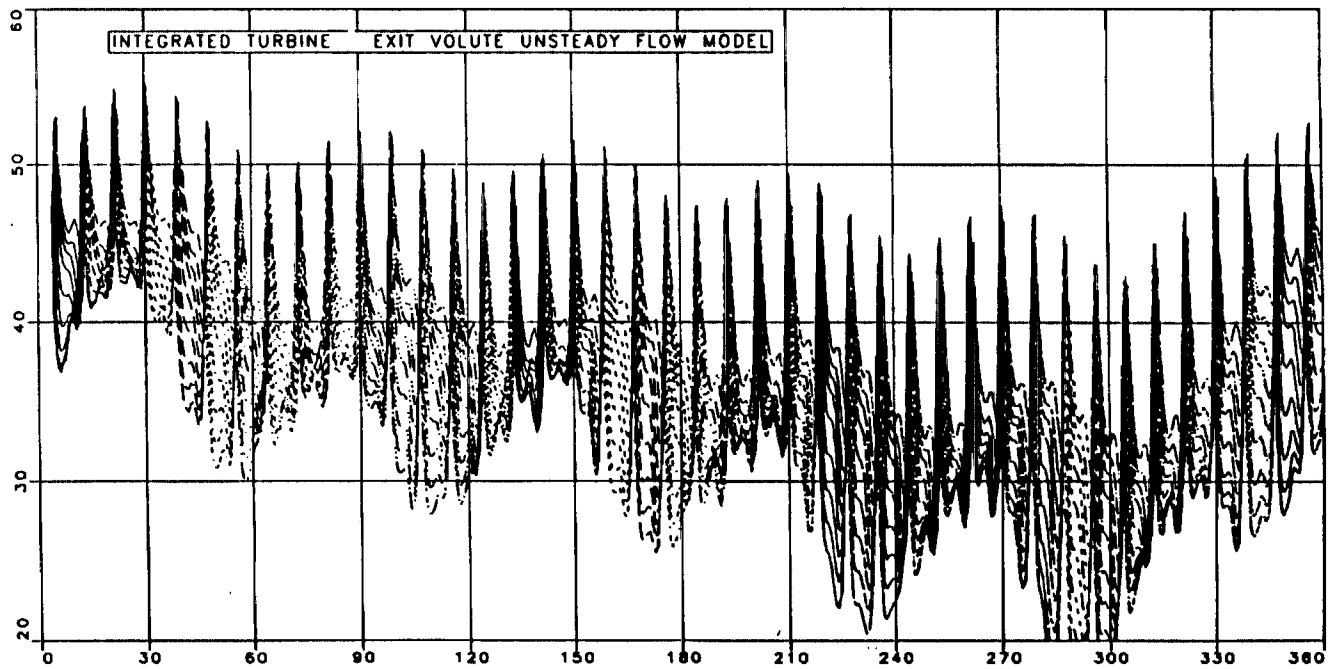

Integrated Time Accurate CFD Modeling of Components

Turbine Stage (20 Vanes, 42 Blades) and Exhaust Manifold (42 Elements)

Instantaneous Circ. Static Pressure Distribution at Turbine Exit

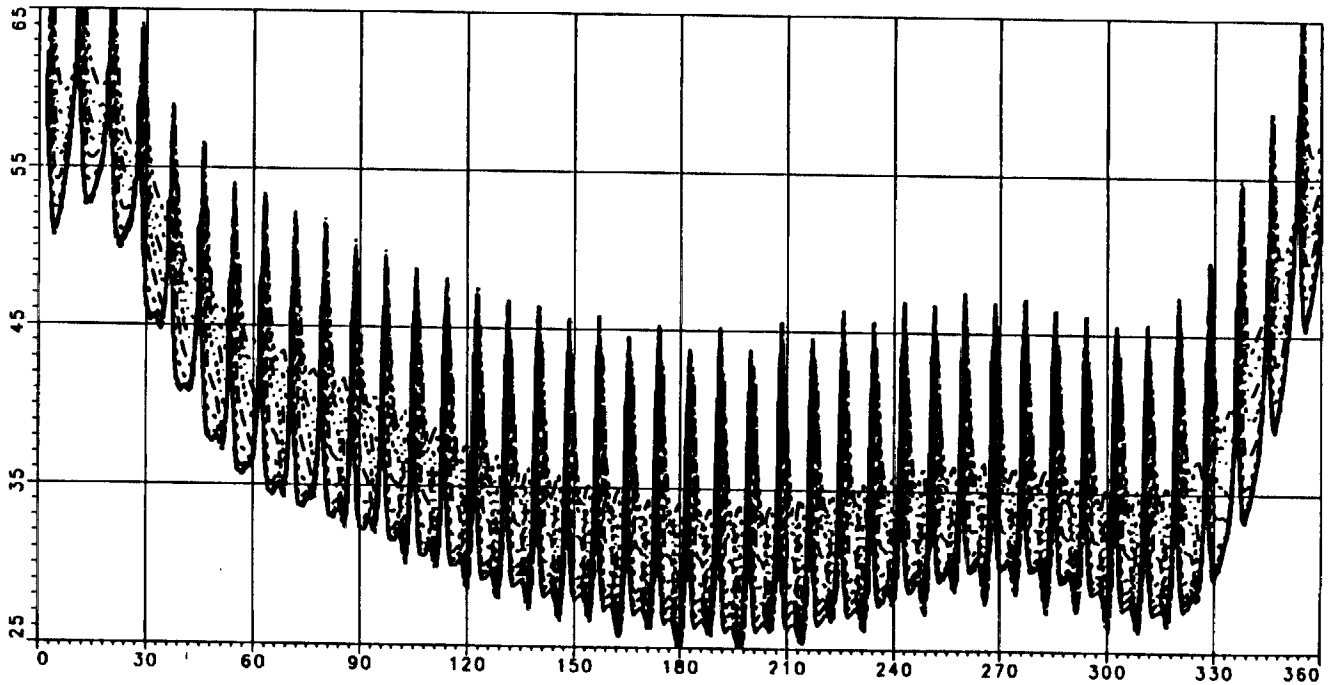

Integrated Time Accurate CFD Modeling of Components

Turbine Stage (20 Vanes, 42 Blades) and Exhaust Manifold (42 Elements)

Unsteady Pressure Distributions

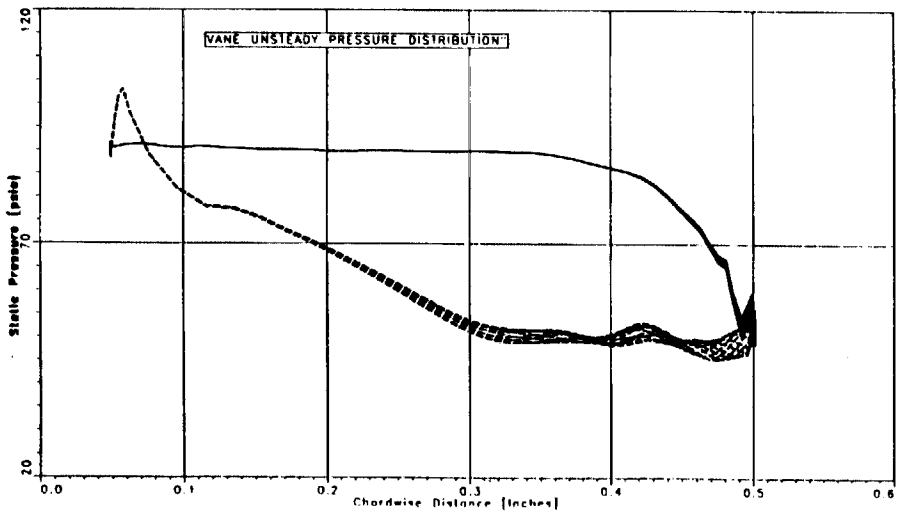

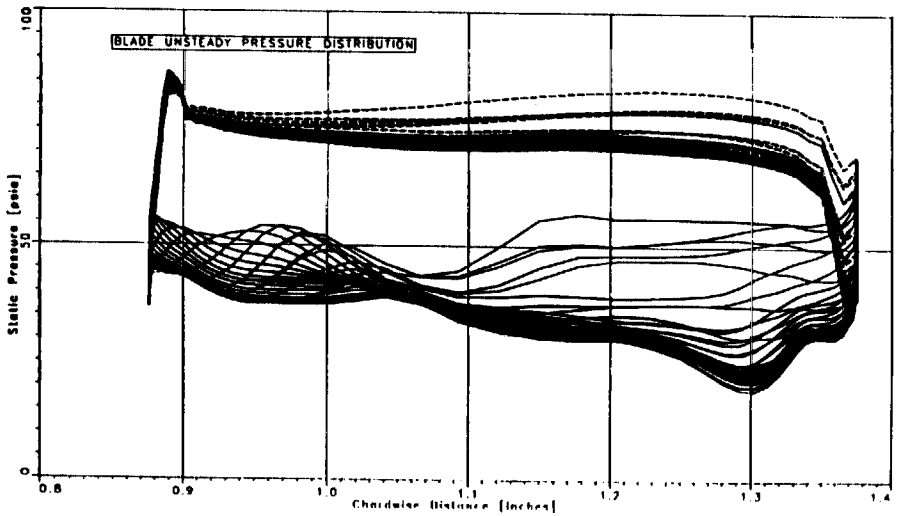

Aero Design and Analysis of a Highly Loaded Turbine Exhaust Volute Manifold

SUMMARY

- Baseline Volute Geometry Defined - Performance Evaluation at MSFC
- Efforts Now Focused on Advanced Concepts for Volute Improvement
- Time Accurate 3D CFD Model of Turbine Stage / Exh. Volute Manifold Constructed & Running
- Early Results Show Large Turbine - Volute Interaction
- Results To Be Utilized In Advanced Concept Definition

CFD Analysis of Turbopump Volutes

Edward, P. Ascoli, Daniel C. Chan, Armen Darian,
Wayne W. Hsu, and Ken Tran

Rockwell International, Rocketdyne Division

Workshop for Computational Fluid Dynamic
Applications in Rocket Propulsion

April 20-22, 1993
NASA Marshall Space Flight Center

Abstract

An effort is underway to develop a procedure for the regular use of CFD analysis in the design of turbopump volutes. Airflow data to be taken at NASA Marshall will be used to validate the CFD code and overall procedure. Initial focus has been on preprocessing (geometry creation, translation, and grid generation). Volute geometries have been acquired electronically and imported into the CATIA CAD system and RAGGS (Rockwell Automated Grid Generation System) via the IGES standard. An initial grid topology has been identified and grids have been constructed for turbine inlet and discharge volutes. For CFD analysis of volutes to be used regularly, a procedure must be defined to meet engineering design needs in a timely manner. Thus, a compromise must be established between making geometric approximations, the selection of grid topologies, and possible CFD code enhancements. While the initial grid developed approximated the volute tongue with a zero thickness, final computations should more accurately account for the geometry in this region. Additionally, grid topologies will be explored to minimize skewness and high aspect ratio cells that can affect solution accuracy and slow code convergence. Finally, as appropriate, code modifications will be made to allow for new grid topologies in an effort to expedite the overall CFD analysis process.

CFD ANALYSIS OF TURBOPUMP VOLUTES

Edward P. Ascoli
Daniel C. Chan
Armen Darian
Wayne W. Hsu
Ken Tran

Rockwell International, Rocketdyne Division

Workshop for Computational Fluid Dynamic
Applications in Rocket Propulsion

April 20-22, 1993
NASA Marshall Space Flight Center

TASK OBJECTIVES

- **DEVELOP CFD ANALYSIS PROCEDURE FOR REGULAR USE IN ENGINEERING DESIGN**

- **VALIDATE CFD CODE AND PROCEDURE WITH MSFC TURBINE AIRFLOW DATA**

- **PERFORM CFD ANALYSIS IN SUPPORT OF VOLUTE DESIGNS FOR ROCKET ENGINE TURBINES**
  - EMPHASIS ON GAS GENERATOR OXIDIZER TURBINE (GGOT) DESIGN OF TURBINE TECHNOLOGY TEAM
  - DESIGN AND OFF-DESIGN CONDITIONS

INITIAL FOCUS ON DEVELOPMENT OF PROCEDURE

- **AUTOMATE PREPROCESSING**
  - GEOMETRY CREATION AND TRANSLATION
  - GRID GENERATION
- **MODIFY/UPGRADE REACT CFD CODE AS NEEDED**
- **DEMONSTRATE PROCEDURE ON TURBINE INLET AND DISCHARGE VOLUTES**

PREPROCESSING PROCEDURE ESTABLISHED

- GEOMETRY ACQUIRED ELECTRONICALLY
- TRANSLATION VIA IGES INTO CATIA AND RAGGS
- INITIAL GRID TOPOLOGY IDENTIFIED
- INITIAL INLET AND DISCHARGE GRIDS DEVELOPED

ELECTRONIC DESIGN & GRID GENERATION TOOLS

- **CAD/CAM**
  - UNIGRAPHICS (UG) USED AT P&W
  - CATIA USED AT ROCKETDYNE
- **IGES TRANSLATOR**
  - GRAPHICS EXCHANGE STANDARD FORMAT
  - COMMON TO MOST ADVANCED GEOMETRY AND GRID GENERATION SYSTEMS
- **ROCKWELL AUTOMATED GRID GENERATION SYSTEM (RAGGS)**
  - FAMILY OF CODES FOR SURFACE DEFINITION, GRID GENERATION, AND POSTPROCESSING
  - INTERACTIVE USER INTERFACE
  - ACCEPTS IGES GEOMETRY FILES

EXTENSIVE TRANSLATION/VERIFICATION REQUIRED

- **UG IGES FILE TRANSLATED DIRECTLY TO RAGGS**
  - FILE READ SUCCESSFULLY
  - EXCESSIVE NUMBER OF PATCHES (OVER 7,000)

- **UG IGES FILE TRANSLATED TO CATIA**
  - NUMBER OF SURFACE PATCHES REDUCED
  - SURFACE ACCURACY CHECKED
  - APPROXIMATELY 340 SURFACE PATCHES USED

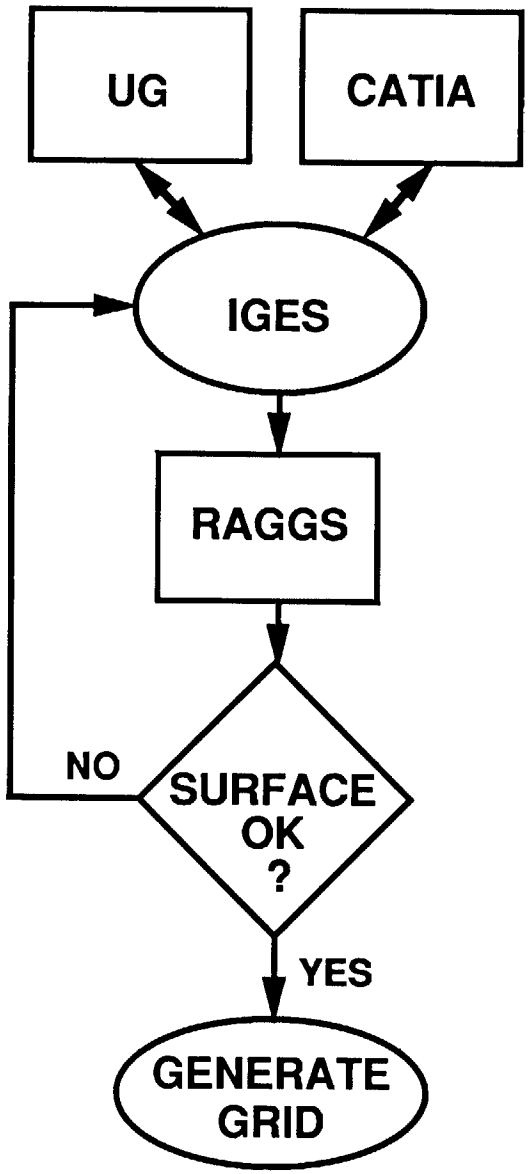

VARIETY OF TRANSLATION ISSUES ENCOUNTERED

ISSUE	SOLUTION
7249 IGES PATCHES • EXCESSIVE MEMORY REQUIREMENTS • SLOW SYSTEM RESPONSE	• INCREASED RAGGS MEMORY ALLOCATION • REDUCED NUMBER OF PATCHES VIA CATIA UTILITY
SURFACE ACCURACY INADEQUATE DUE TO PATCH NUMBER REDUCTION	ESTABLISHED BALANCE BETWEEN REDUCED NUMBER OF SURFACE PATCHES AND ACCURACY OF SURFACE

VOLUTE GEOMETRY TRANSLATED TO CATIA

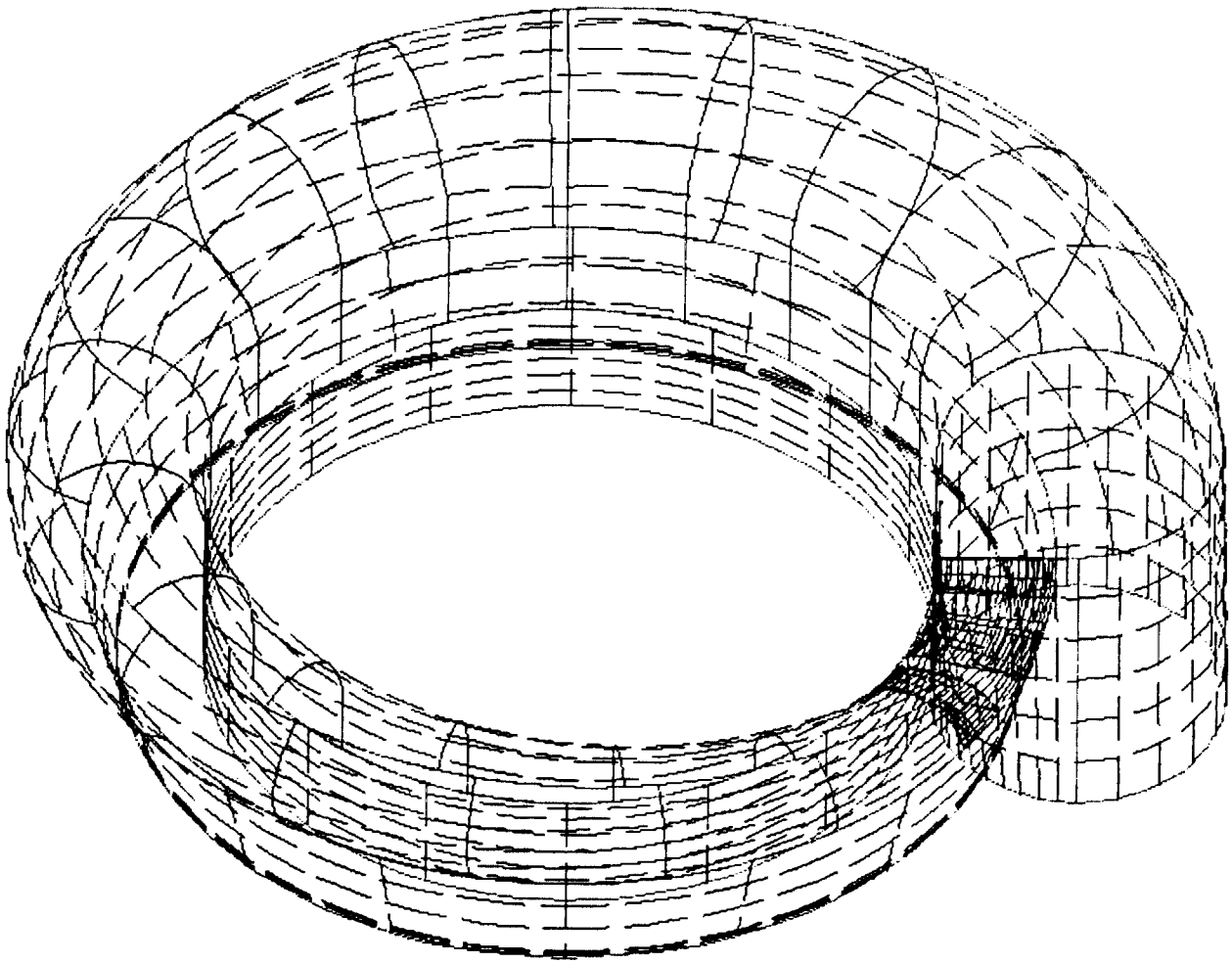

VOLUTE GEOMETRY TRANSLATED TO RAGGS

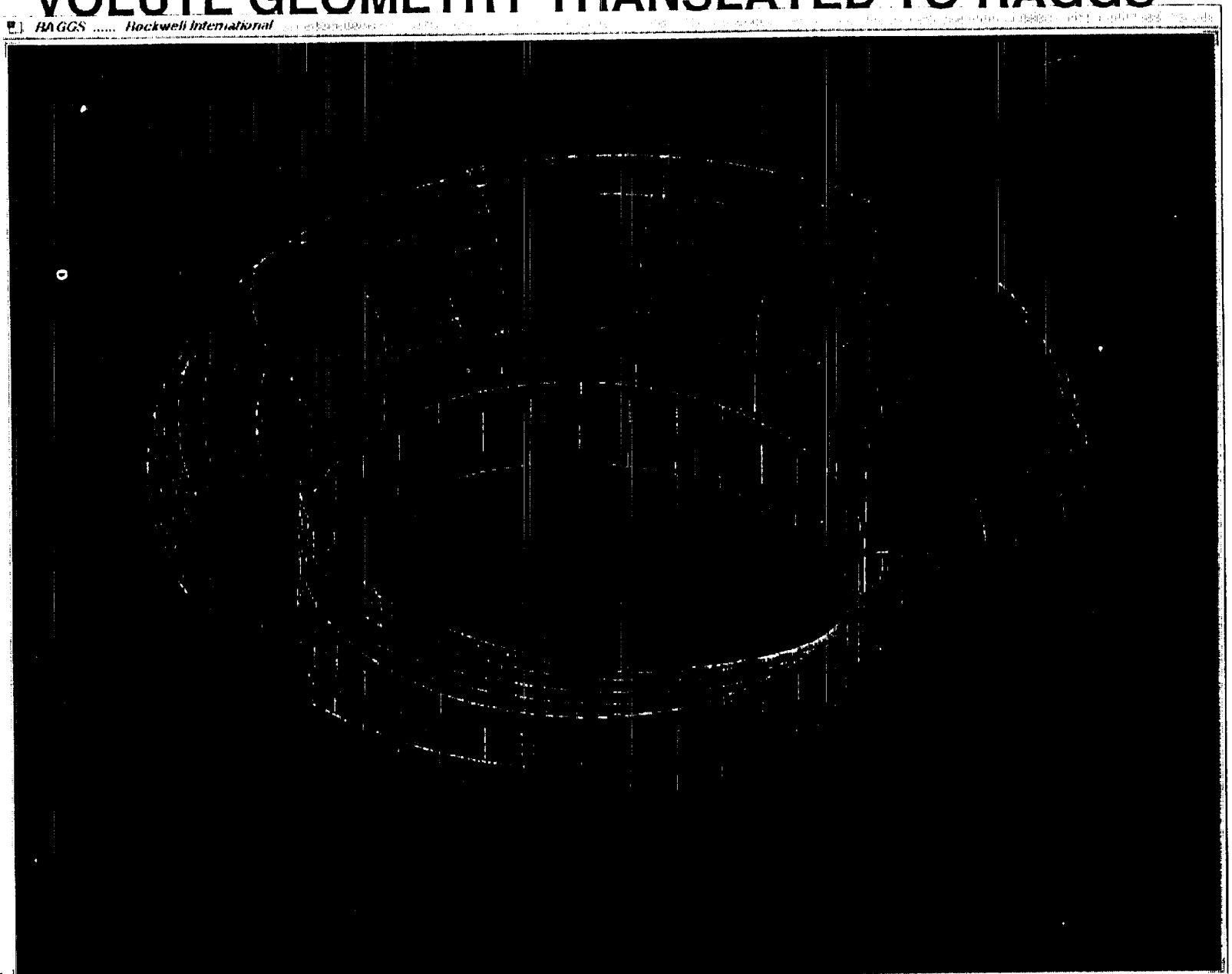

RAGGS REPRESENTATION OF VOLUTE SURFACES

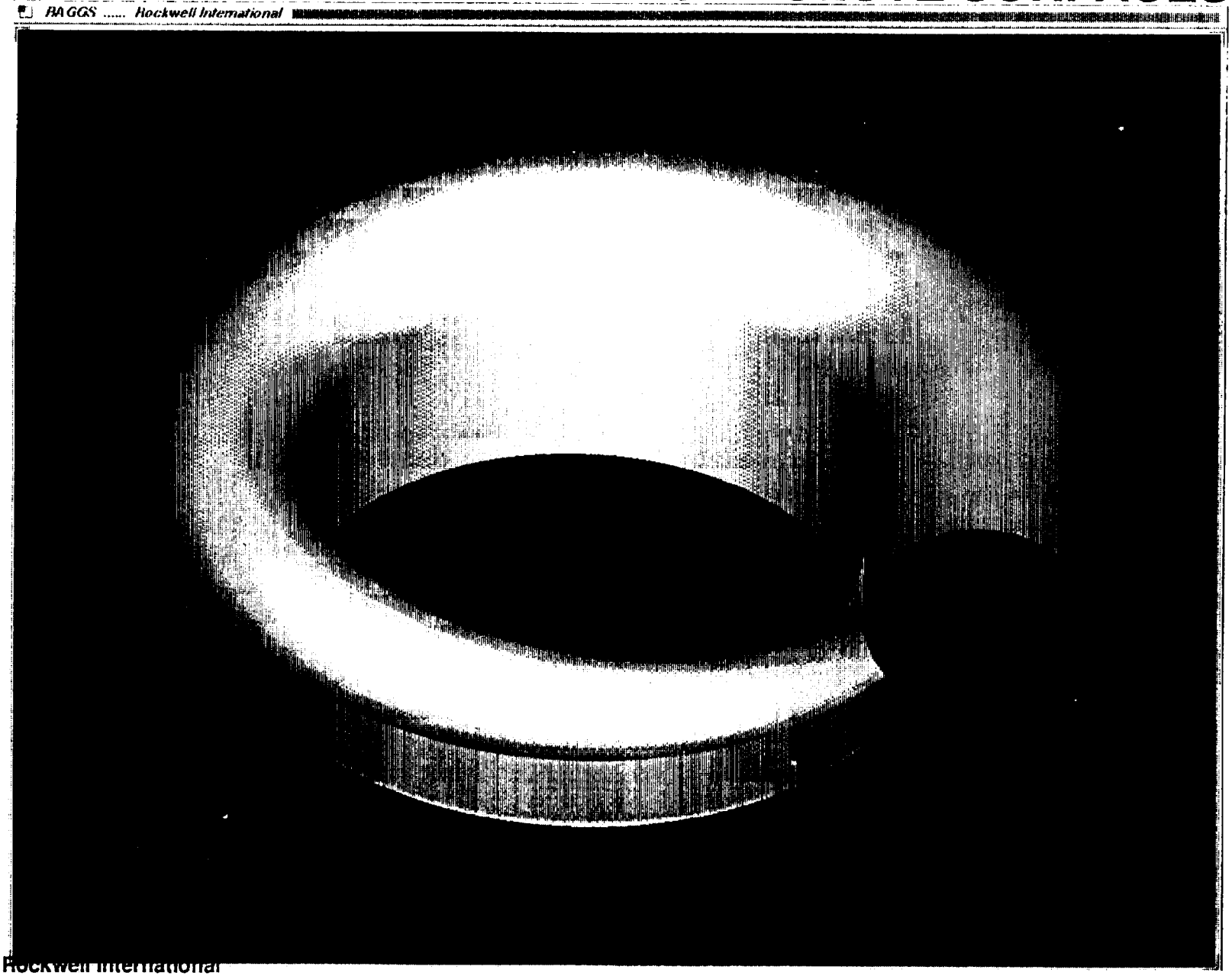

THREE ZONE GRID DEVELOPED

REGION	ZONE	COLOR	GRID POINTS
INLET	1	RED	50 X 31 X 31 = 48,050
TAPERED MANIFOLD	2	YELLOW	95 X 31 X 31 = 91,295
ANNULAR DISCHARGE	3	MAGENTA	100 X 31 X 31 = 155,000

SPACING AT WALL < 0.02" TO MAINTAIN Y + $\leq$ 1,000

THREE-ZONE VOLUTE TOPOLOGY

ZONE 1 – INLET GRID

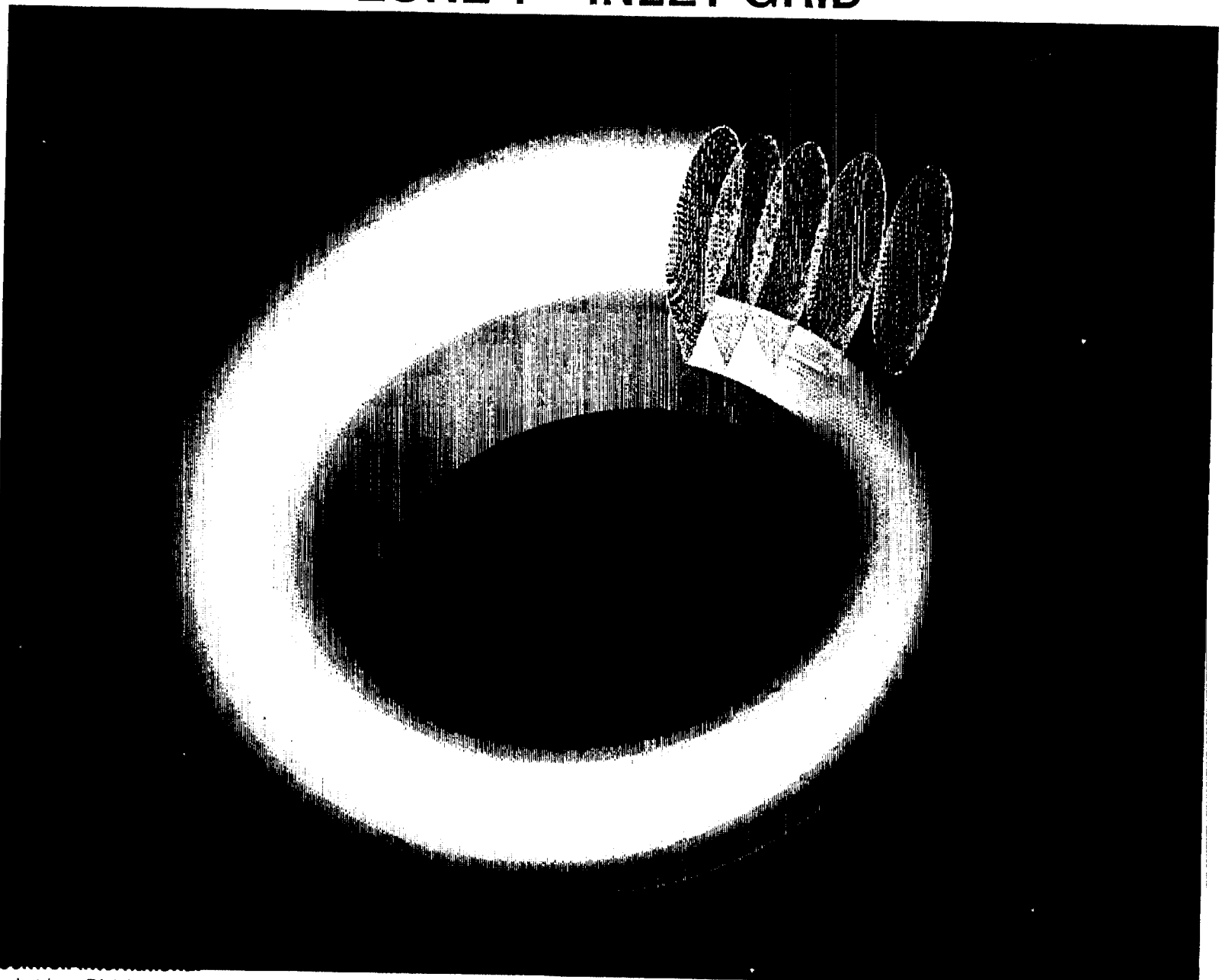

ZONE 2 – TAPERED MANIFOLD

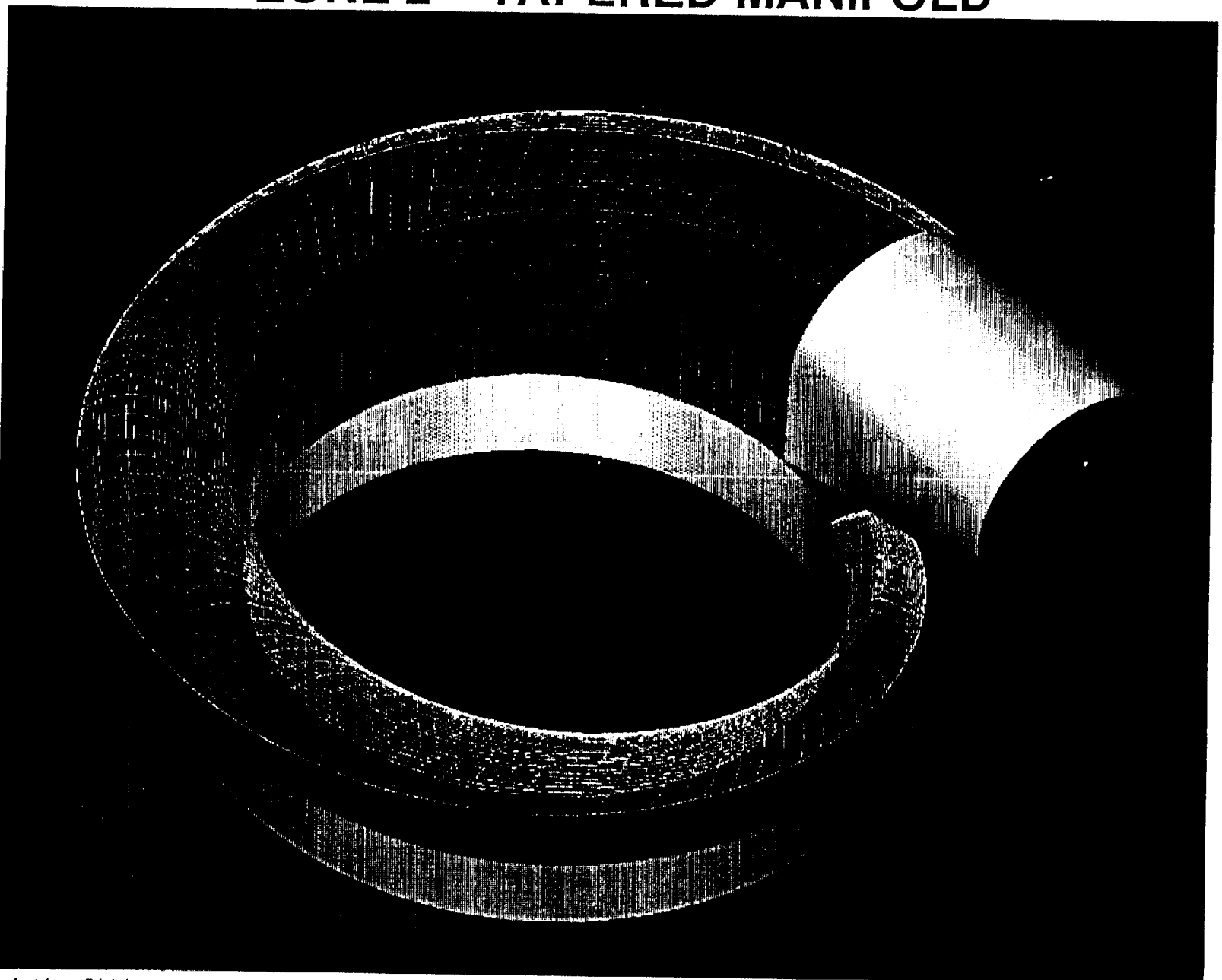

ZONE 3 – ANNUAL DISCHARGE

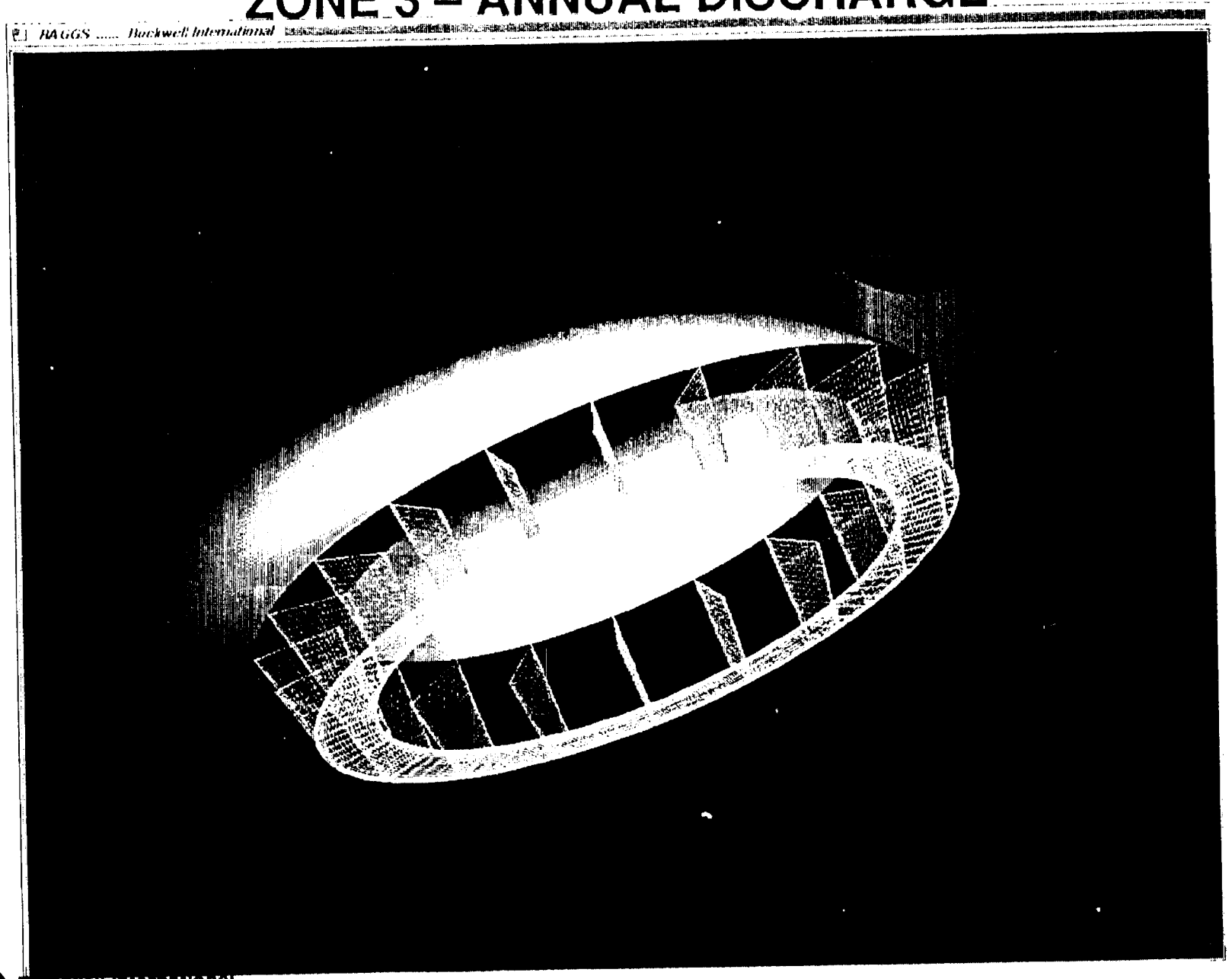

SAME TOPOLOGY USED FOR EXIT VOLUTE

ZONE	COLOR	REGION	GRID POINTS
1	RED	ANNULAR INLET	49 x 31 x 99 = 150,381
2	GREEN	MANIFOLD	31 x 31 x 95 = 91,295
3	MAGENTA	DISCHARGE	31 x 31 x 49 = 47,089
			TOTAL = 288,765

EXIT VOLUTE ZONE 1

ANNULAR INLET

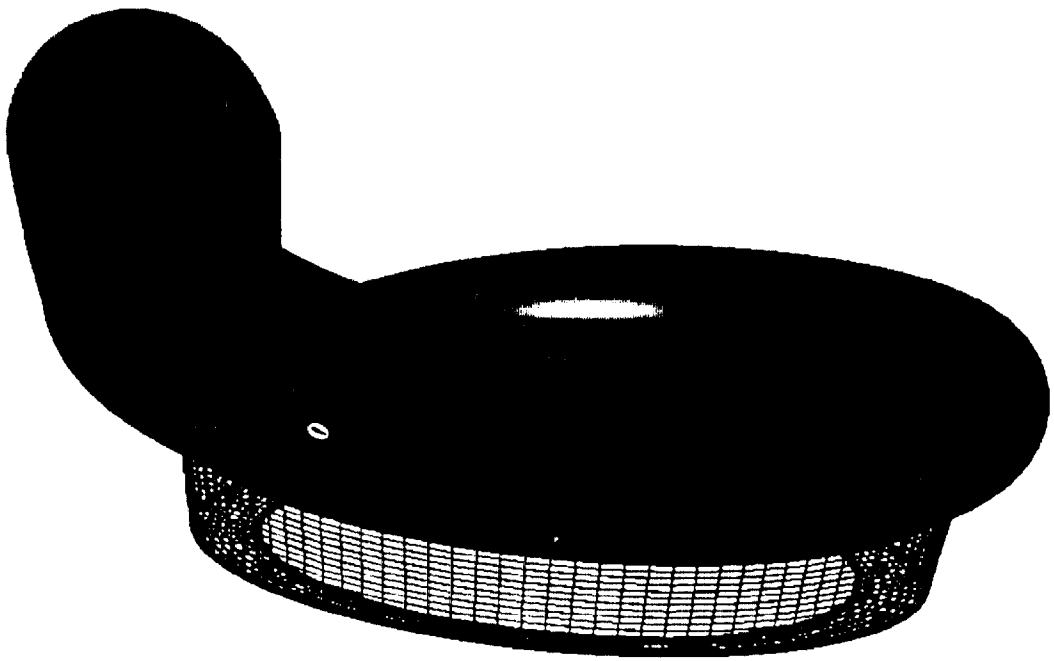

EXIT VOLUTE ZONE 2

MANIFOLD

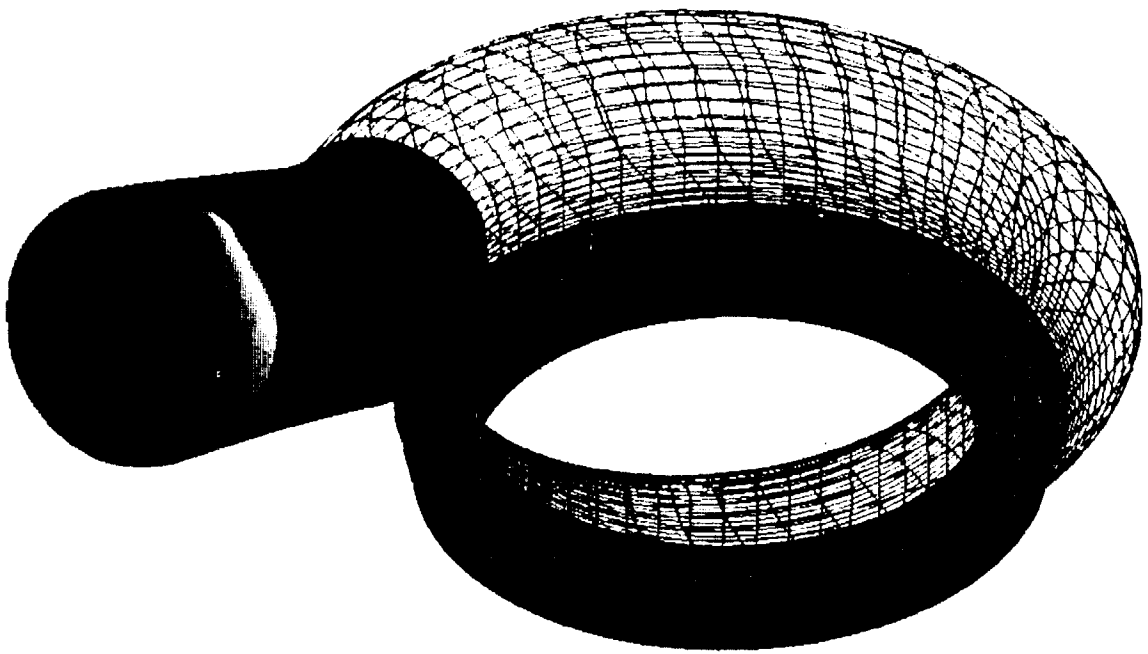

EXIT VOLUTE ZONE 3

DISCHARGE

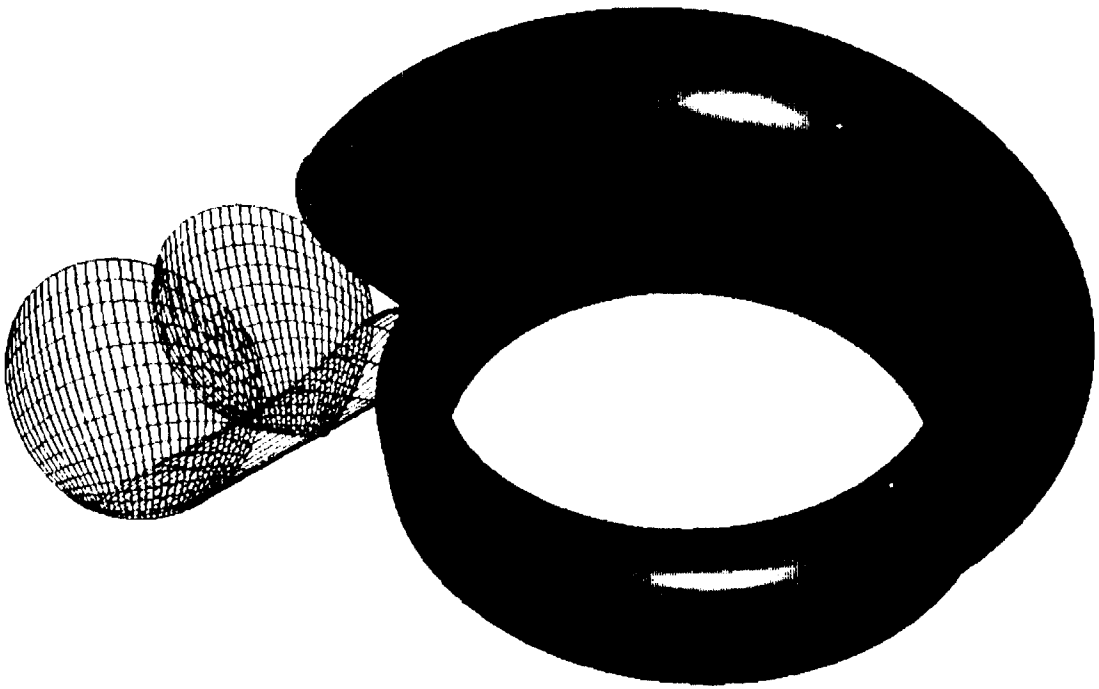

DESIGN PROCEDURE MUST MEET ENGINEERING ACCURACY, CYCLE TIME REQUIREMENTS

- **GEOMETRIC APPROXIMATIONS**
  - MAINTAIN ACCURACY IN CRITICAL AREAS
  - SIMPLIFY GRID GENERATION REQUIREMENTS
- **GRID TOPOLOGIES**
  - SATISFY CODE REQUIREMENTS
    - ASPECT RATIO
    - ORTHOGONALITY
    - ZONAL CONNECTIVITY
  - SIMPLIFY GRID GENERATION
  - GRID COINCIDENT WITH SURFACES AND REGIONS OF INTEREST
- **CODE ENHANCEMENTS AS NEEDED TO IMPROVE OVERALL PROCEDURE**

GEOMETRIC APPROXIMATIONS

- **START WITH COMPLETE DESCRIPTION AS TRANSLATED FROM CAD SYSTEM**

- **TONGUE AREA CONSIDERED CRITICAL**
  - INITIAL APPROXIMATIONS CONSIDERED INADEQUATE
    - ZERO THICKNESS
    - ALTERED MANIFOLD GEOMETRY
  - RESTORE ORIGINAL GEOMETRY

- **MANIFOLD-ANNULUS ACCURACY LESS CRITICAL**
  - CONSIDER "FILLET" INSTEAD OF SHARP CORNER
  - GRID "SMEARING" POSSIBLE WITH SOME TOPOLOGIES

GRID TOPOLOGY / CODE MODIFICATION

- **THREE-ZONE TOPOLOGY VERY NATURAL**
  - FOLLOWS GEOMETRY EXACTLY
  - SIMPLY CONNECTED ZONES
  - FORCES HIGH DEGREE OF SKEWED, HIGH ASPECT CELLS AT TAPERED END OF MANIFOLD

- **ALTERNATE TOPOLOGIES CONSIDERED**
  - PRIMARY GOAL TO MINIMIZE SKEWNESS
  - MAY "BLUR" GEOMETRY IN NONCRITICAL REGION
  - MAY REQUIRE ADDITIONAL LOGIC FOR ZONAL CONNECTIVITY
    - ALTERNATE GRID LINES REMOVED
    - ARBITRARY GRIDS

SUMMARY

- **SIGNIFICANT AUTOMATION OF PREPROCESSING**
  - CAD GEOMETRY USED DIRECTLY
  - AUTOMATED GRID GENERATION SYSTEM (RAGGS) SUCCESSFULLY APPLIED
  - SIGNIFICANT REDUCTION IN CYCLE TIME
  - INITIAL INLET AND EXIT VOLUTE GRIDS GENERATED

- **PROCEDURE BEING DEFINED TO ALLOW FOR PRODUCTIVE USE OF CFD IN DESIGN CYCLE — BEST COMPROMISE OF:**
  - GEOMETRIC APPROXIMATION
  - GRID TOPOLOGY
  - CODE ENHANCEMENTS

Three-Dimensional Viscous Flow Analysis Inside a Turbine Volute

C.Hah, J. Loellbach, and D. A. Greenwald

NASA Lewis Research Center

L. Griffin and J. Ruf

NASA Marshall Space Flight Center

A three-dimensional numerical method has been developed to analyze the complex flow field inside a turbine volute. Comparisons are made between solutions with different boundary conditions.

Three-Dimensional Viscous Flow Analysis Inside a Turbine Volute

C. Hah, O. Kwon, J. Loellbach, and D. A. Greenwald

NASA Lewis Research Center

L. Griffin and J. Ruf

NASA Marshall Space Flight Center

Consortium Turbine and Exit Volute

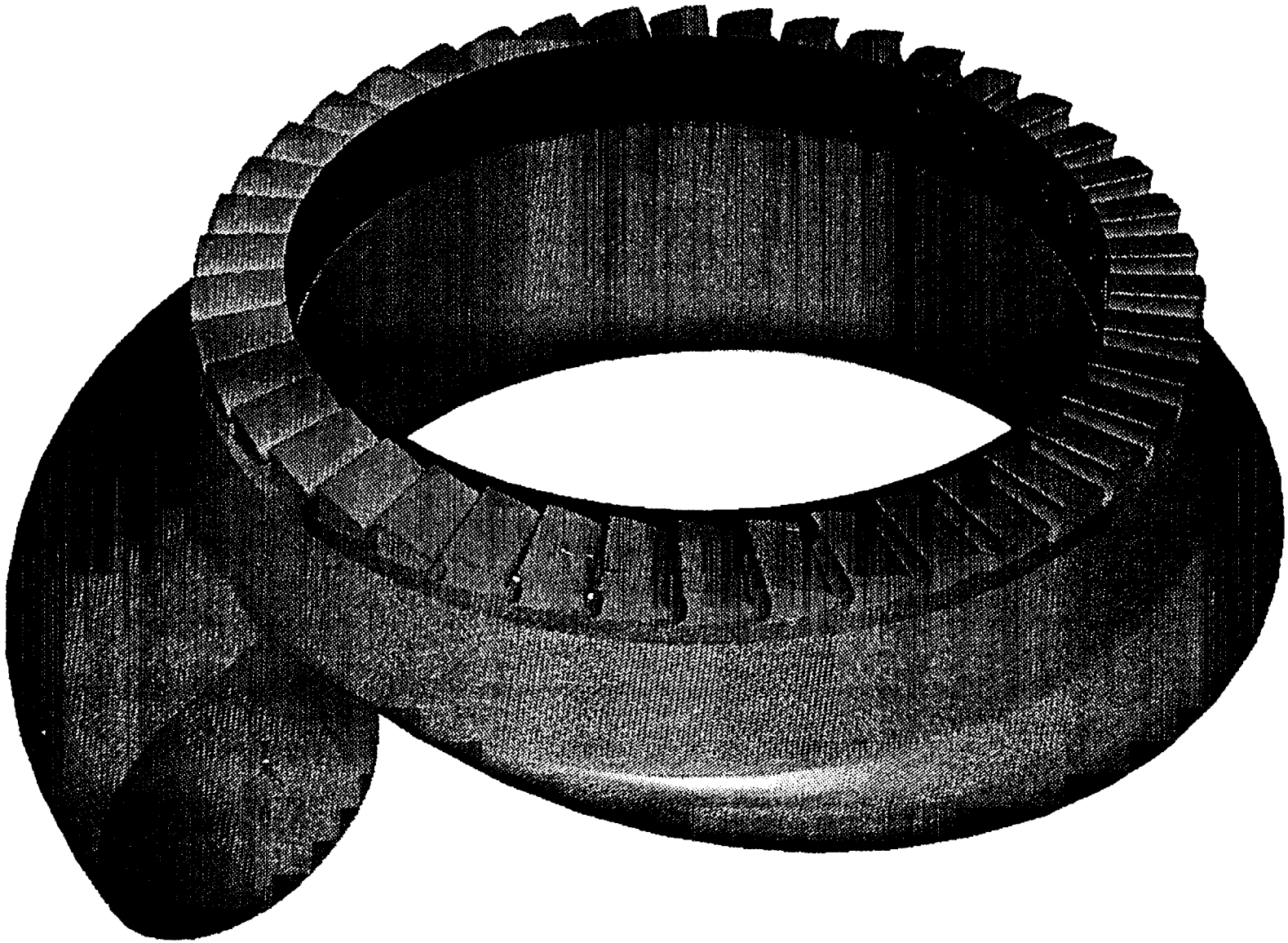

Objective

- o 3-D Turbulent Flow inside Volute
- o Integrated Analysis of Turbine Stage and Inlet & Exit Volutes

Approach

- o 3-D Navier-Stokes Code (Structured Grid)
- o 3-D Euler Code (Unstructured Grid)

TIP GRID

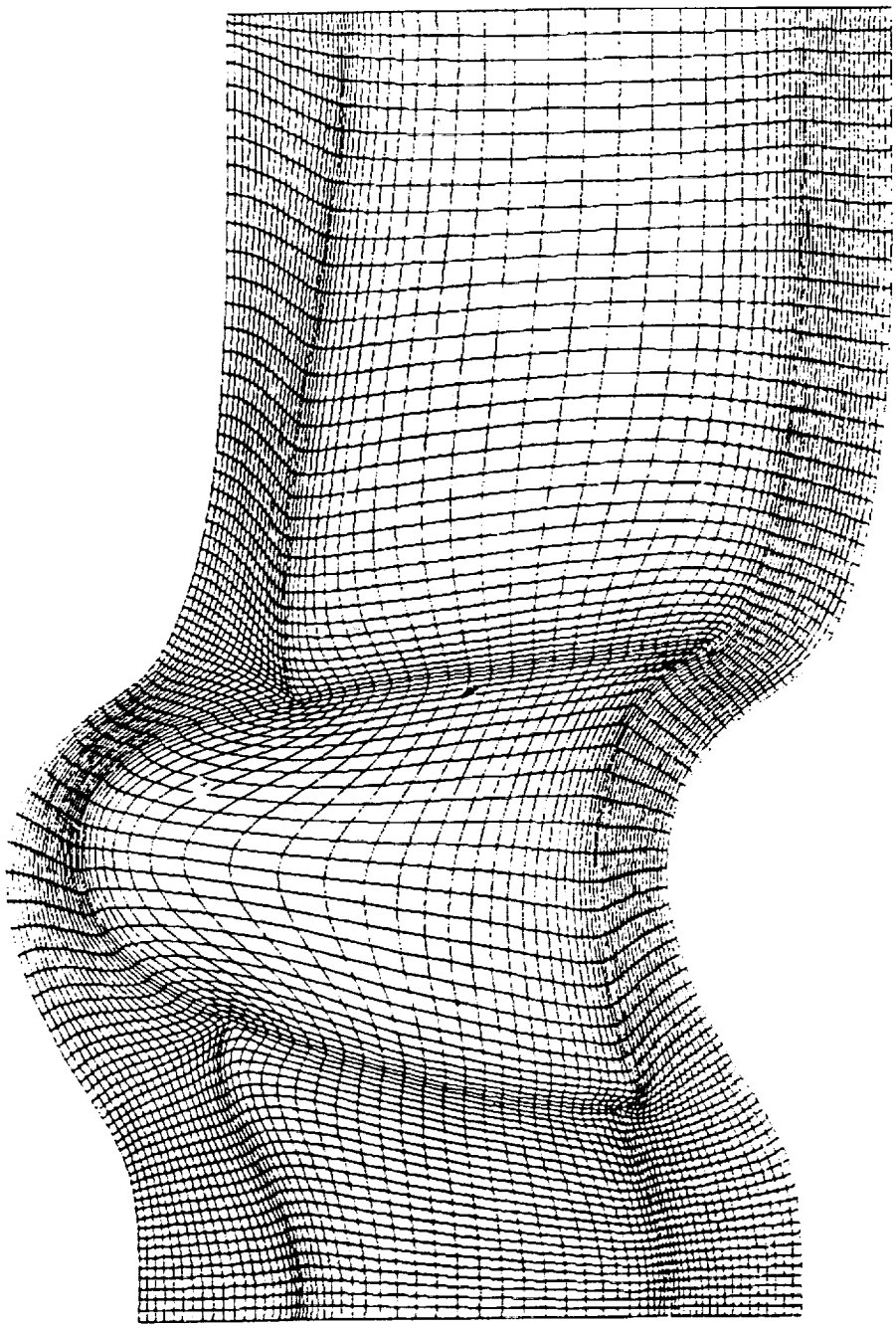

MACH-NUMBER AND VELOCITY VECTORS (MID-SPAN)

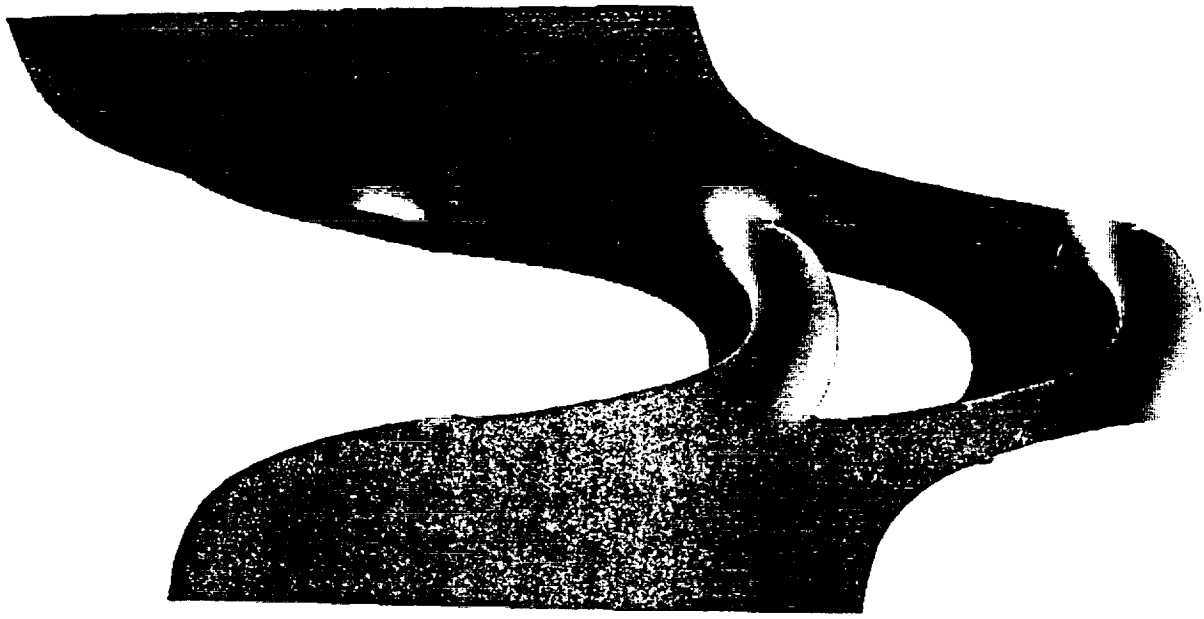

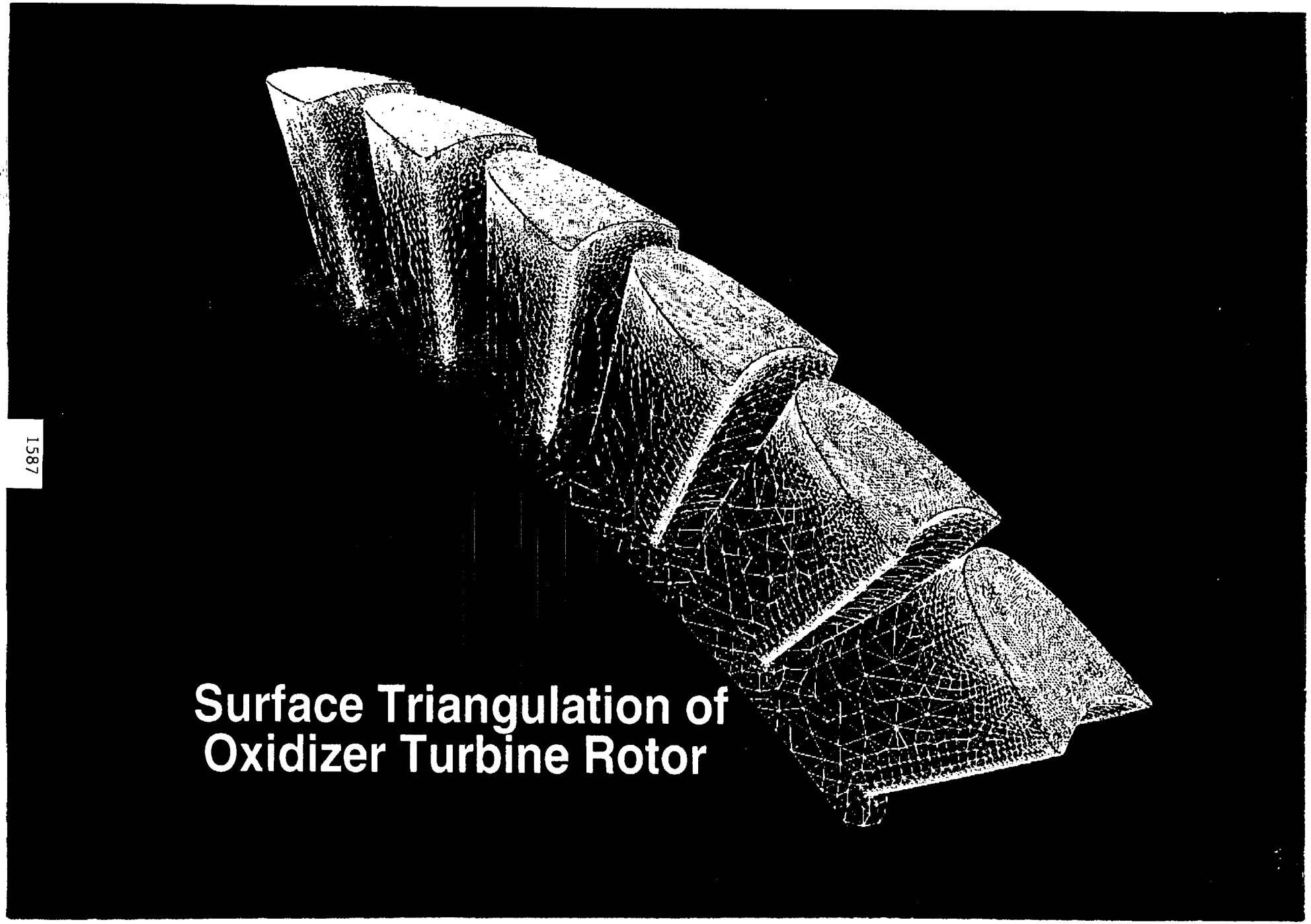

Surface Triangulation of Oxidizer Turbine Rotor

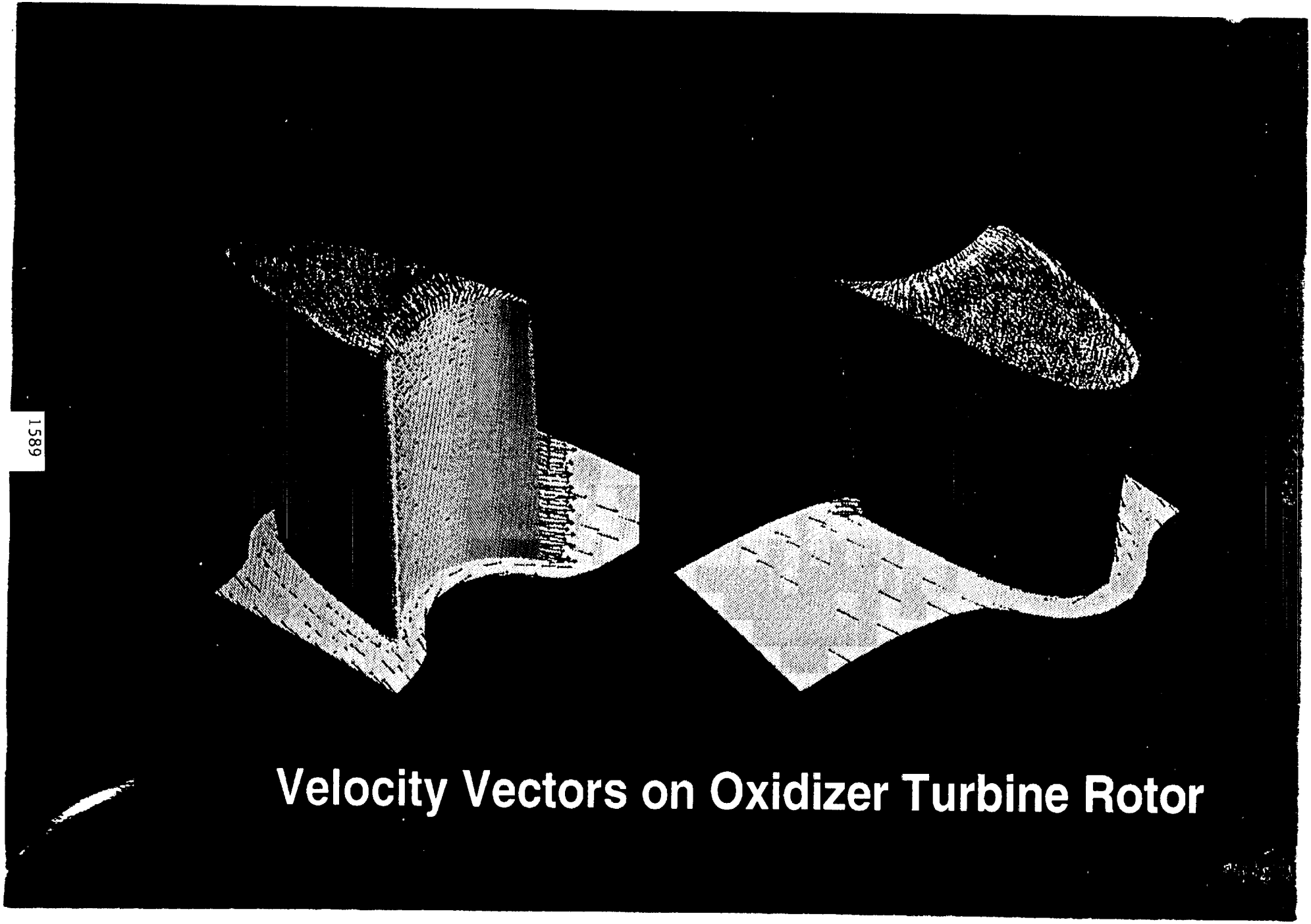

Velocity Vectors on Oxidizer Turbine Rotor

Consortium Turbine and Exit Volute

Computational grid

- o Structured Grid (I-Grid) : 51x32x46
- o Unstructured Grid : 90,000 Nodes

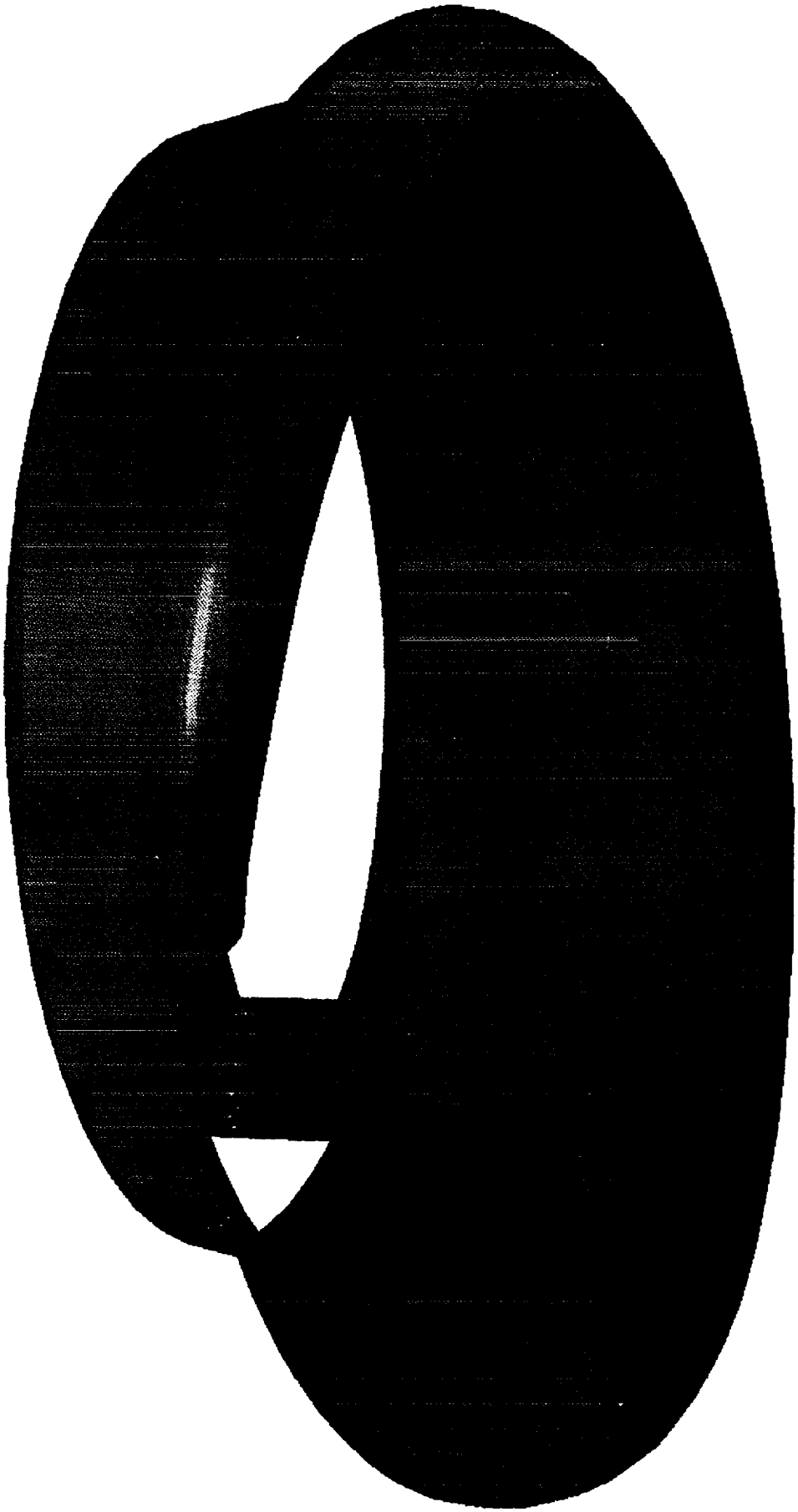

1593

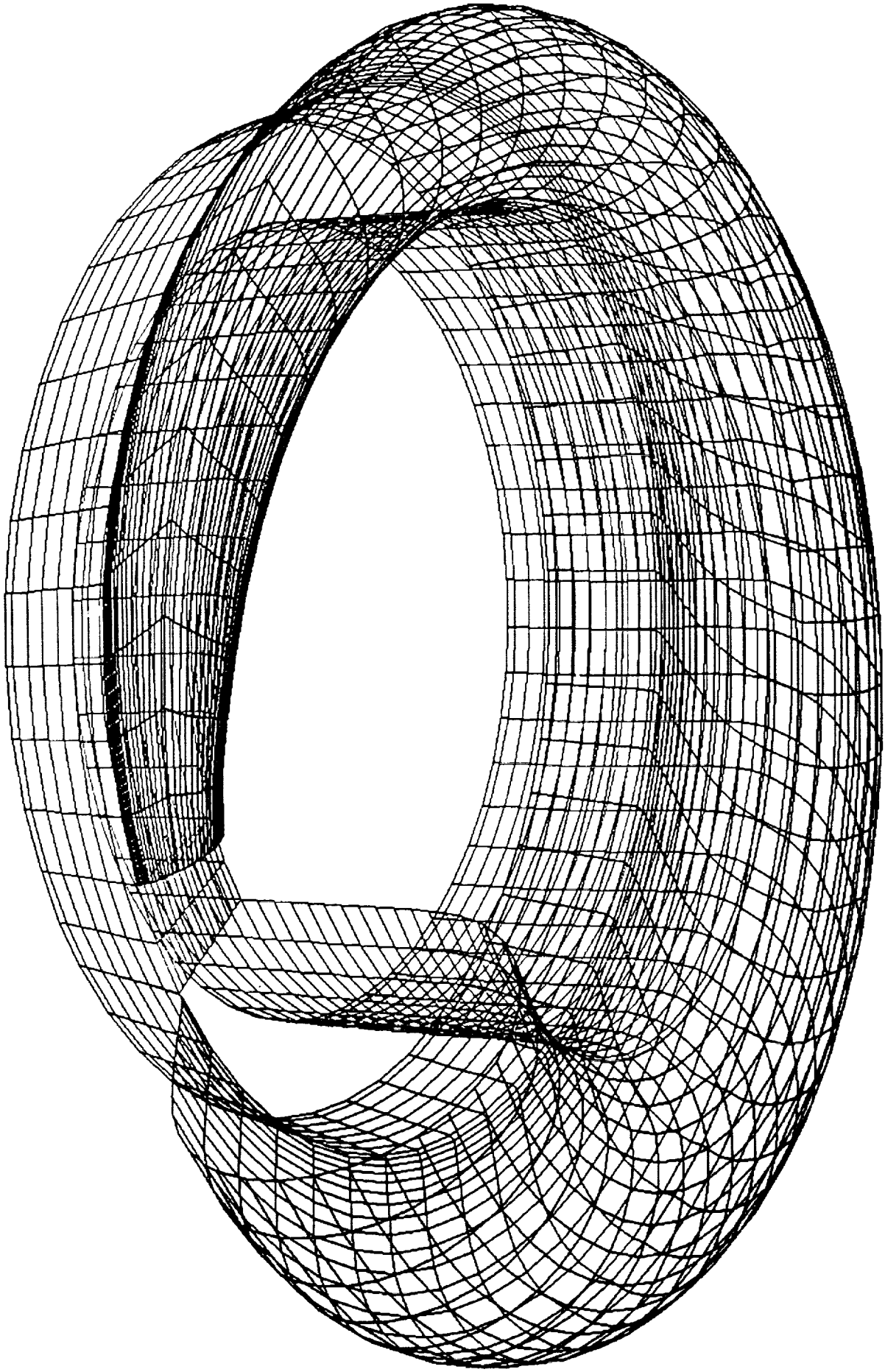

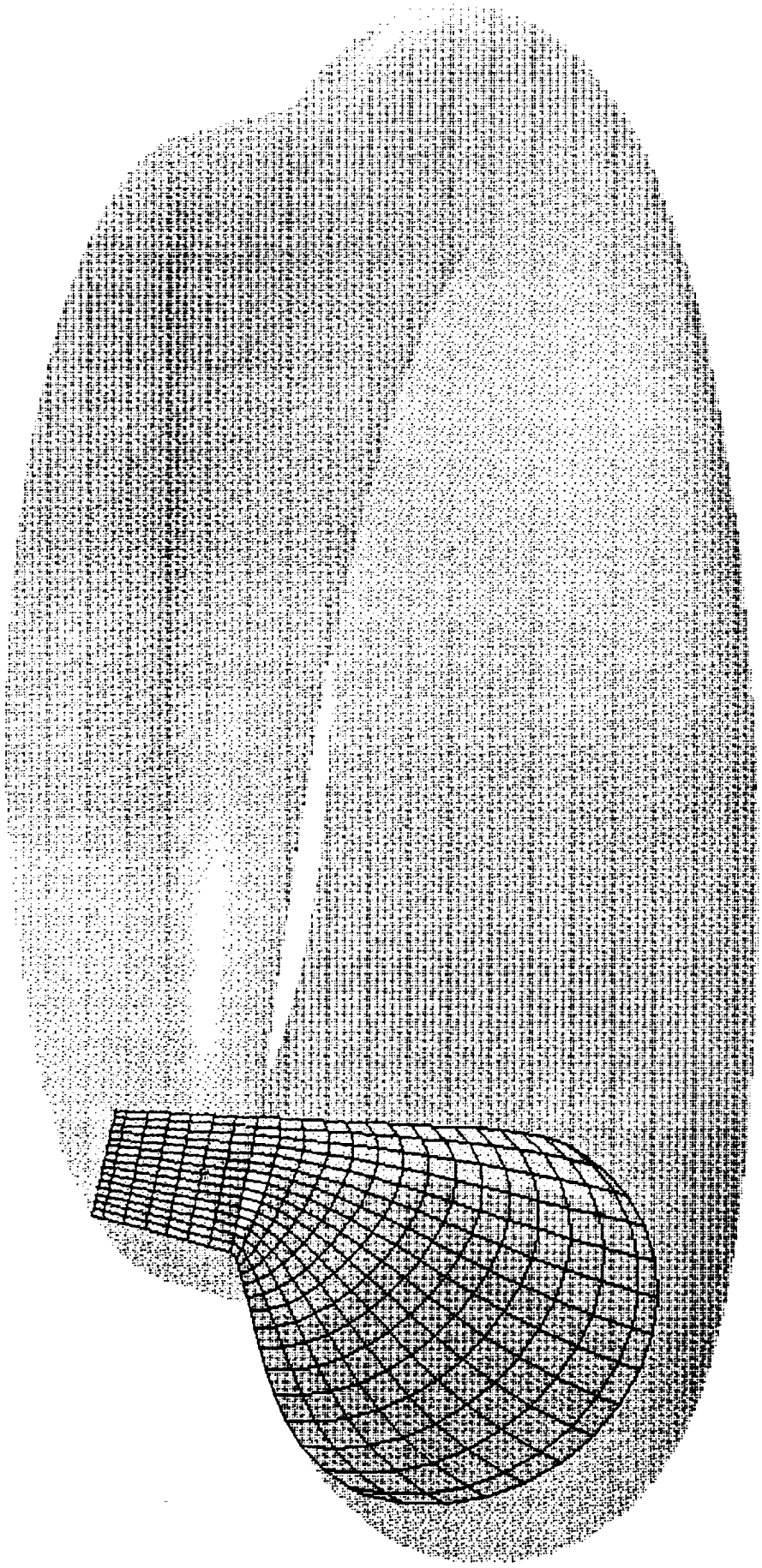

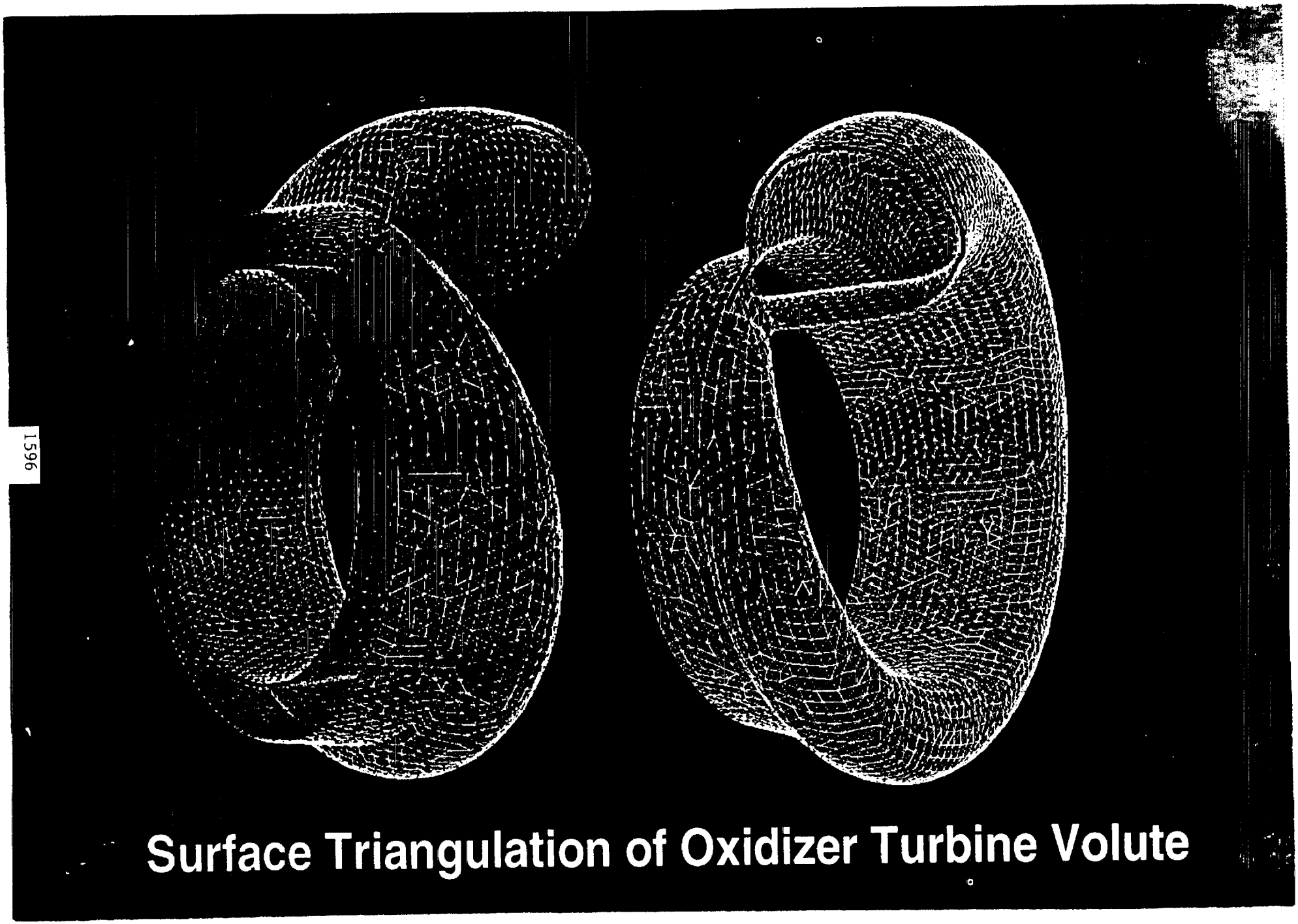

Surface Triangulation of Oxidizer Turbine Volute

BOUNDARY CONDITIONS

- Inlet
  - Total Pressure
  - Total Temperature
  - Two Velocity Components
- Exit
  - Static Pressure

HAH3D Viscous Flow Code

- o Three-Dimensional Navier-Stokes
- o Pressure-Based Control Volume
- o Two-Equation Turbulence Model with Low-Reynolds Number Extension
- o Incompressible, Transonic, Supersonic Flows
- o Tested for Wide Range of Flows

Velocity Vectors Near Inner Wall

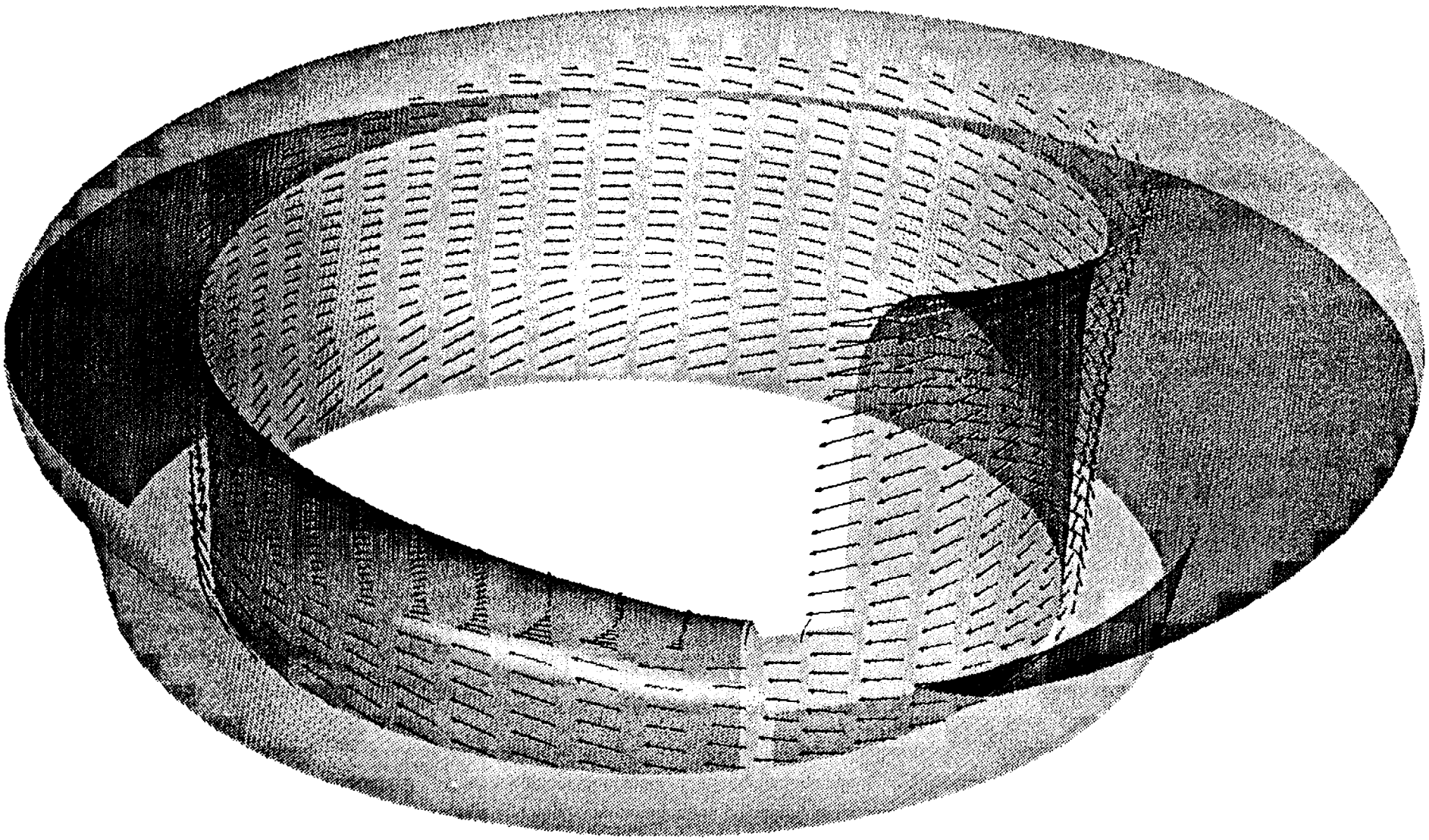

Velocity Vectors Near Outer Wall

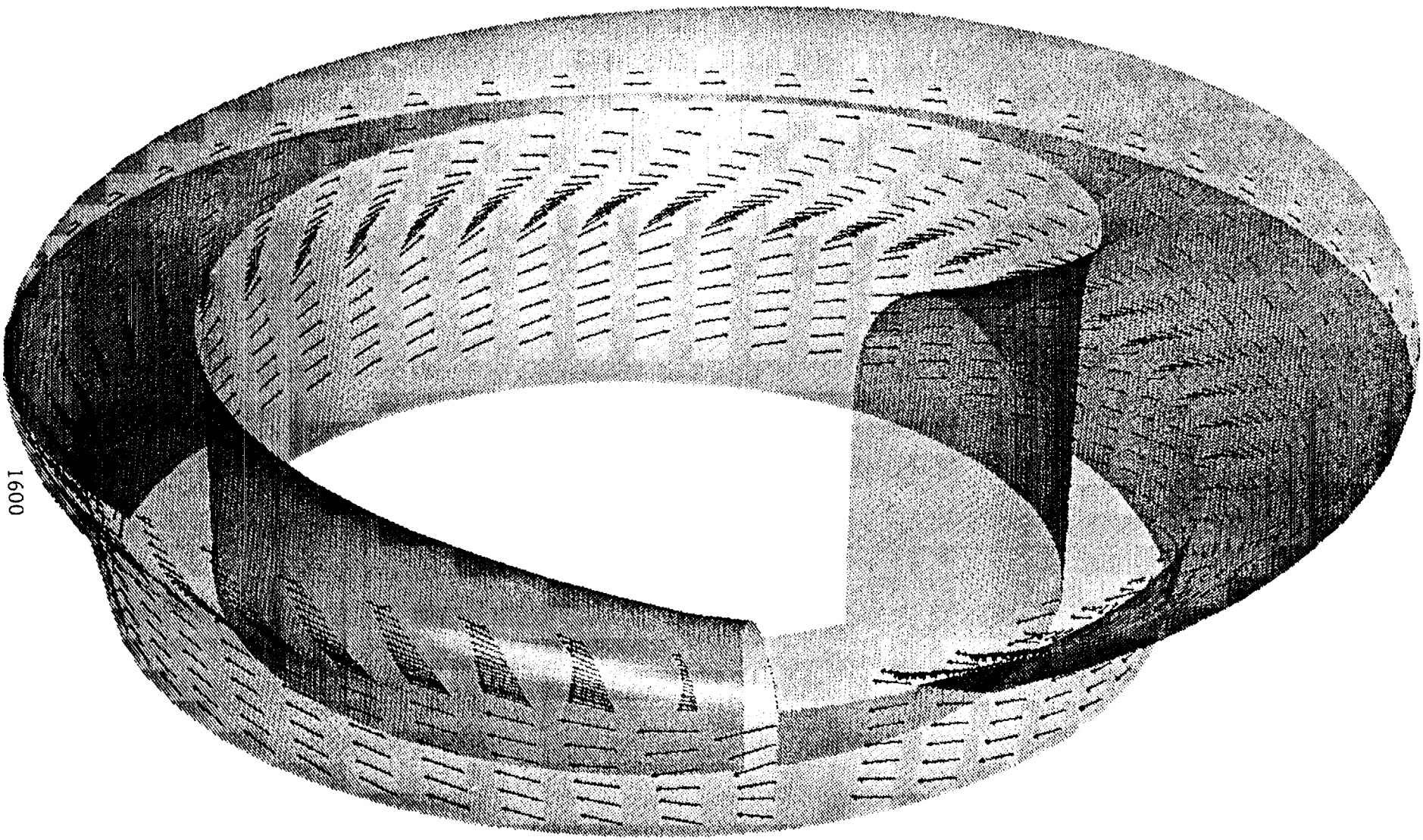

1600

Crossflow Velocity Vectors

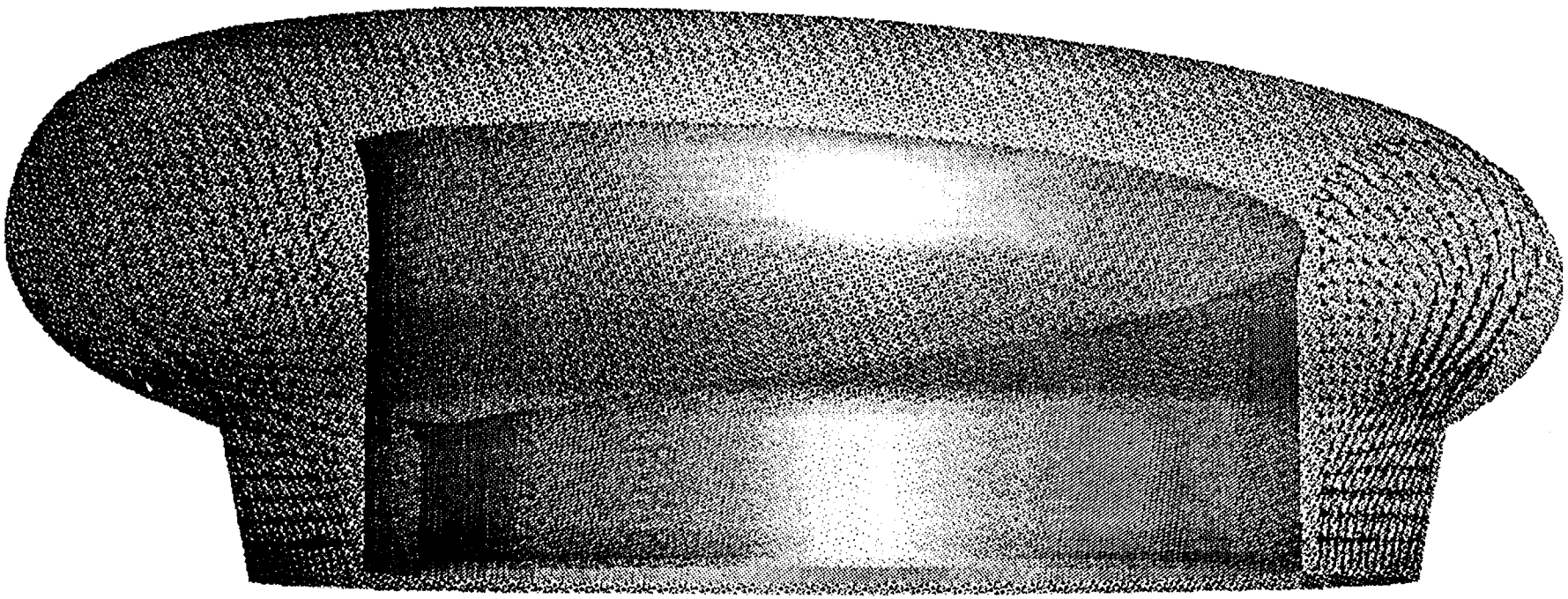

Surface Static Pressure

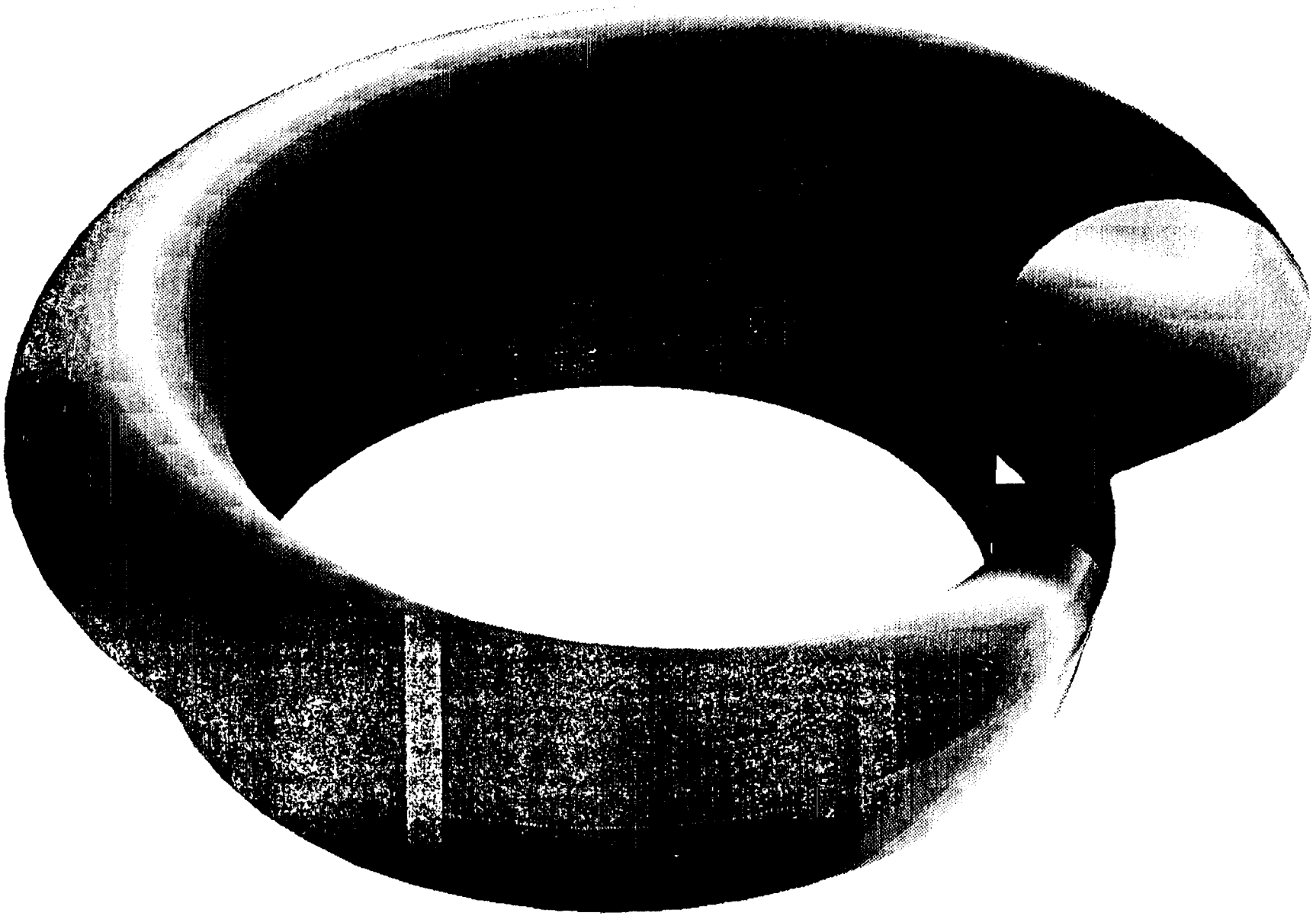

Velocity Vectors on Oxidizer Turbine Volute

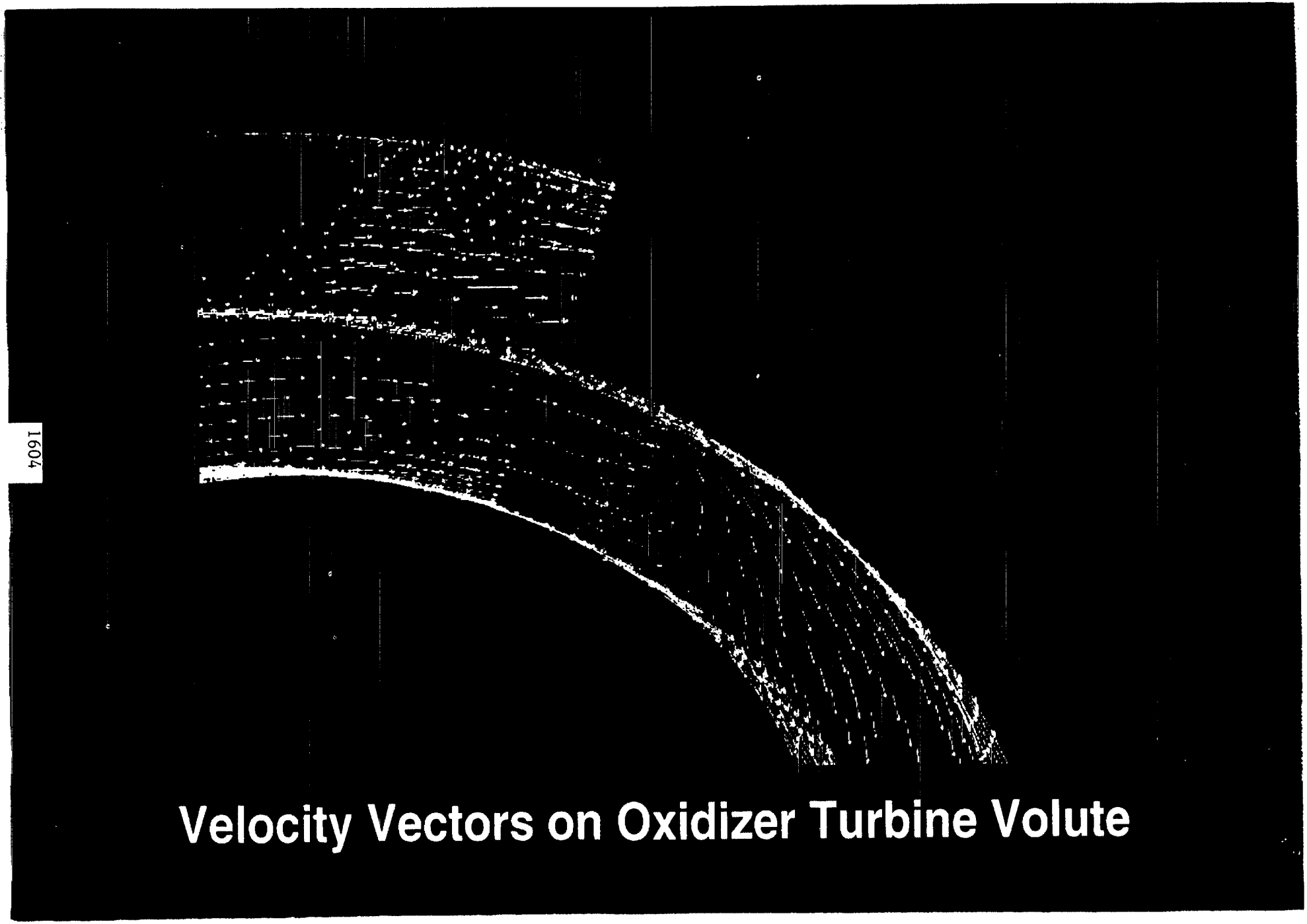

Velocity Vectors on Oxidizer Turbine Volute

Surface Pressure Contour on Oxidizer Turbine Volute

Observation and Future Study

- o Successful 3-D, N-S & Euler Flow Study for Volute Design
- o N-S & Euler Predict Different Flow features
- o Comparative Study between Structured and Unstructured Grid Methods
- o Further Verification Necessary

WORKSHOP FOR CFD APPLICATIONS IN ROCKET PROPULSION
APRIL 20-22, 1993

PHASE II HGM AIR FLOW TESTS IN SUPPORT OF HEX VANE INVESTIGATION

G. B. Cox, Jr.
L. L. Steele
D. W. Eisenhart
Pratt & Whitney/Government Engines & Space Propulsion
West Palm Beach, Fla.

Following the start of SSME certification testing for the Pratt & Whitney Alternate Turbopump Development (ATD) High Pressure Oxidizer Turbopump (HPOTP), cracking of the leading edge of the inner HEX vane was experienced. The HEX vane, at the inlet of the oxidizer bowl in the Hot Gas Manifold (HGM), accepts the HPOTP turbine discharge flow and turns it toward the Gaseous Oxidizer Heat Exchanger (GOX HEX) coil. The cracking consistently initiated over a specific circumferential region of the hex vane, with other circumferential locations appearing with increased run time. Since cracking had not to date been seen with the baseline HPOTP, a fluid-structural interaction involving the ATD HPOTP turbine exit flowfield and the HEX inner vane was suspected.

As part of NASA contract NAS8-36801, Pratt & Whitney conducted air flow tests of the ATD HPOTP turbine turnaround duct flowpath in the MSFC Phase II HGM air flow model. These tests included HEX vane strain gages and additional fluctuating pressure gages in the turnaround duct and HEX vane flowpath area. Three-dimensional flow probe measurements at two stations downstream of the turbine simulator exit plane were also made. Modifications to the HPOTP turbine simulator investigated the effects on turbine exit flow profile and velocity components, with the objective of reproducing flow conditions calculated for the actual ATD HPOTP hardware. Testing was done at the MSFC SSME Dynamic Fluid Air Flow (Dual-Leg) Facility, at air supply pressures between 50 and 250 psia. Combinations of turbine exit Mach number and pressure level were run to investigate the effect of flow regime.

Information presented includes

1) Descriptions of turbine simulator modifications to produce the desired flow environment.

2) Types and locations for instrumentation added to the flow model for improved diagnostic capability.

3) Evaluation of the effect of changes to the turbine simulator flowpath on the turbine exit flow environment.

4) Comparison of the experimental turbine exit flow environment to the environment calculated for the ATD HPOTP.

SSME ALTERNATE TURBOPUMP DEVELOPMENT PROGRAM

PHASE II HGM AIR FLOW TESTS IN SUPPORT OF HEX VANE INVESTIGATION

WORKSHOP FOR CFD APPLICATIONS IN ROCKET PROPULSION

Marshall Space Flight Center
April 20–22, 1993

G. B. Cox, Jr.
L. L. Steele
D. W. Eisenhart
Pratt & Whitney/GESP
West Palm Beach, Florida

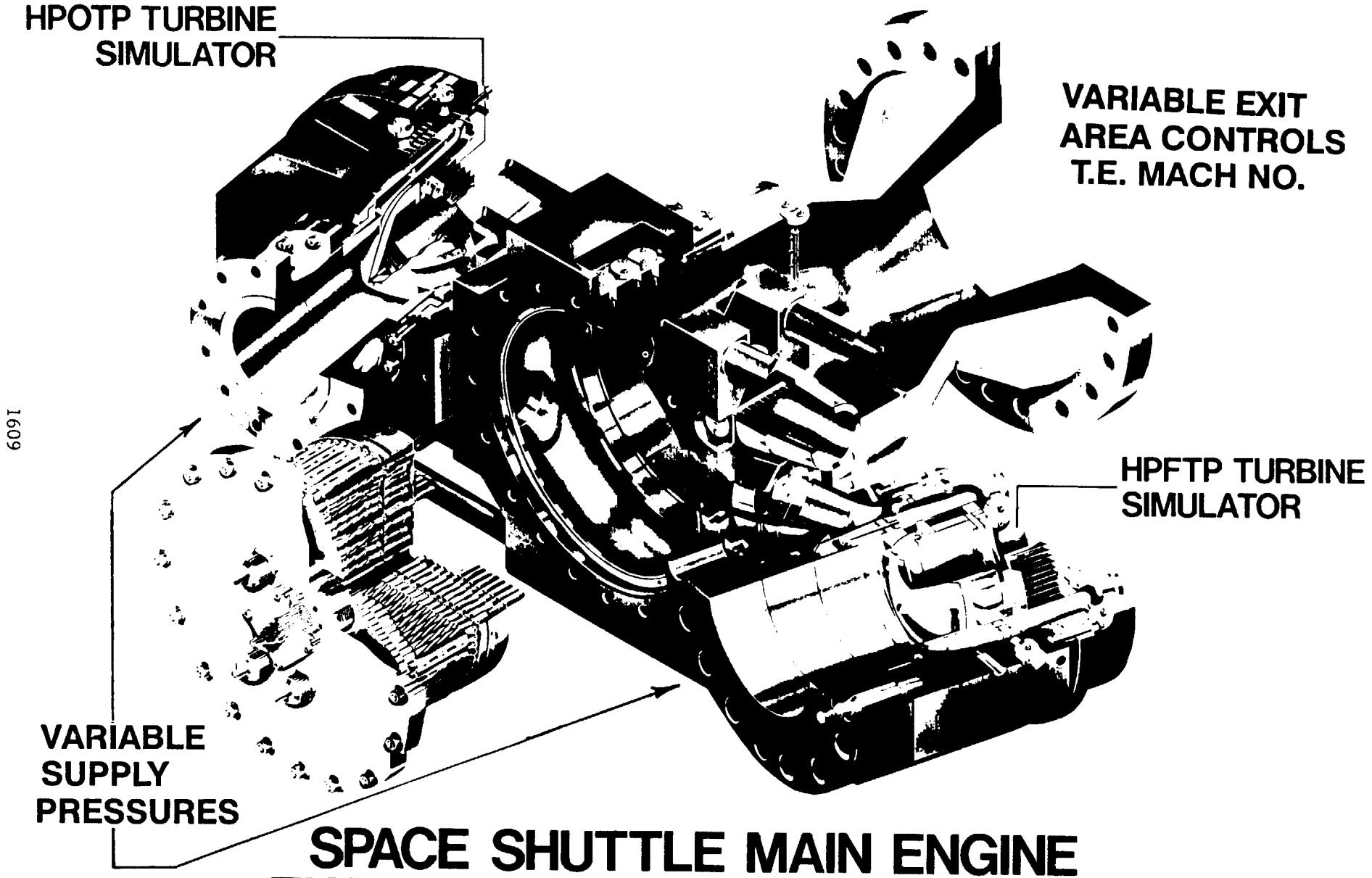

1609

SPACE SHUTTLE MAIN ENGINE EXPERIMENTAL AIR FLOW MODEL

TURBINE SIMULATOR/ORIFICE COMPARISON

BASELINE

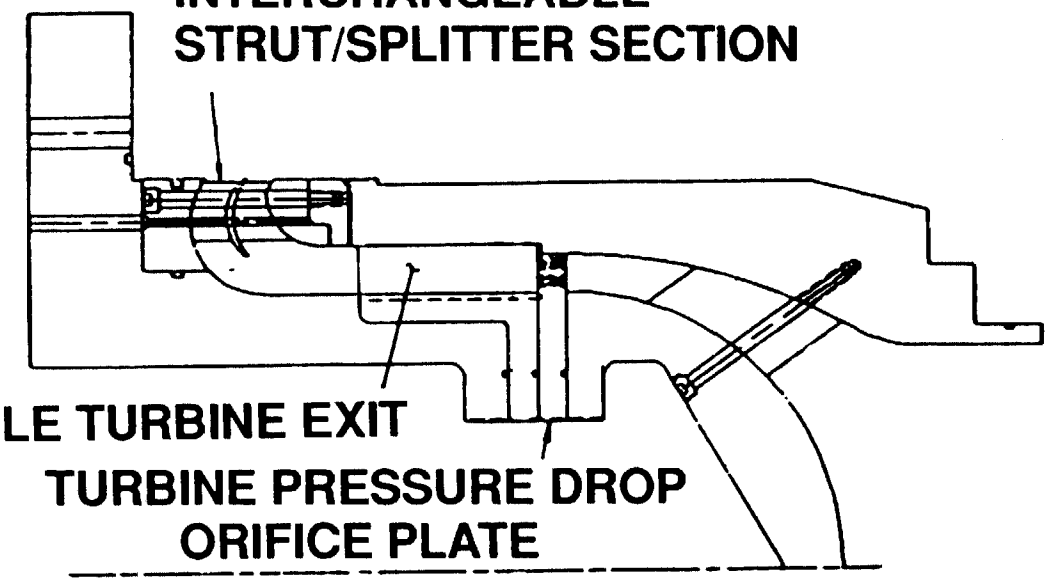

MODIFIED

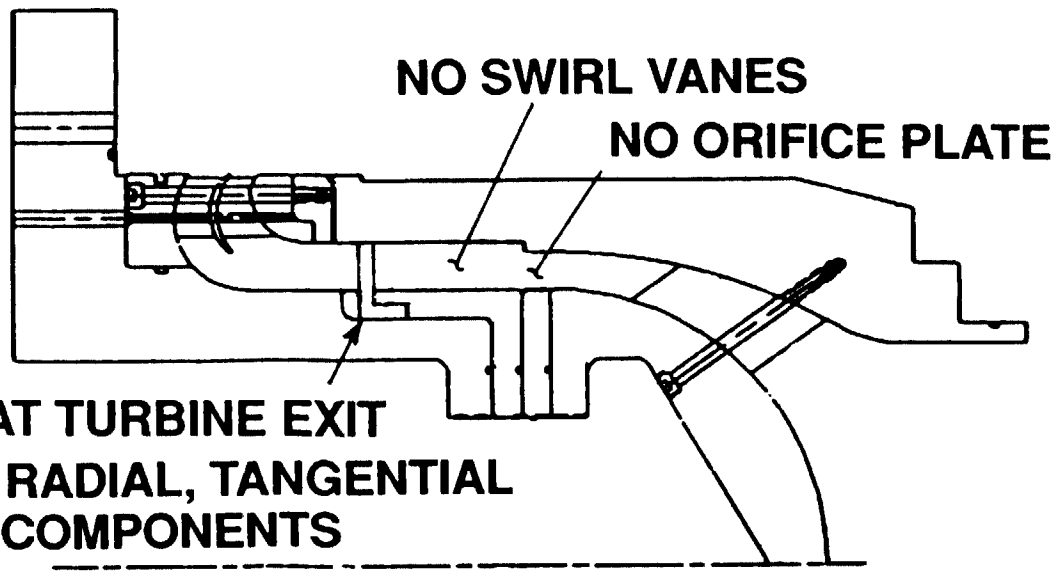

1610

FLOW MODEL/ENGINE FLOW CONDITION DIFFERENCES

Model Tests Did Not Simulate Flow Of Final Turbine Design

ENGINE	FLOW MODEL
Radial–Outward T.E. Velocity	Radial Velocity Not Matched
Low 20% Span Flow Swirl Angle	High 20% Span Flow Swirl Angle

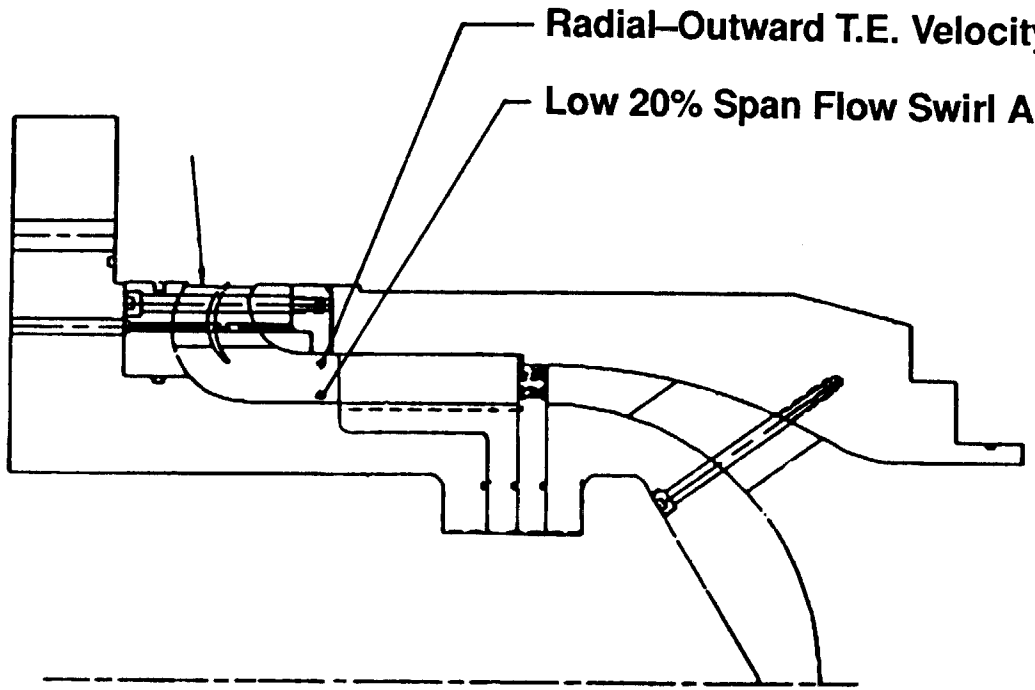

ADDITIONAL HPOTP/HGM INSTRUMENTATION

Improve Definition Of Flow Environment, HEX Vane Response

HEX VANE STRAIN GAGES
FLUCTUATING PRESSURE TRANSDUCERS

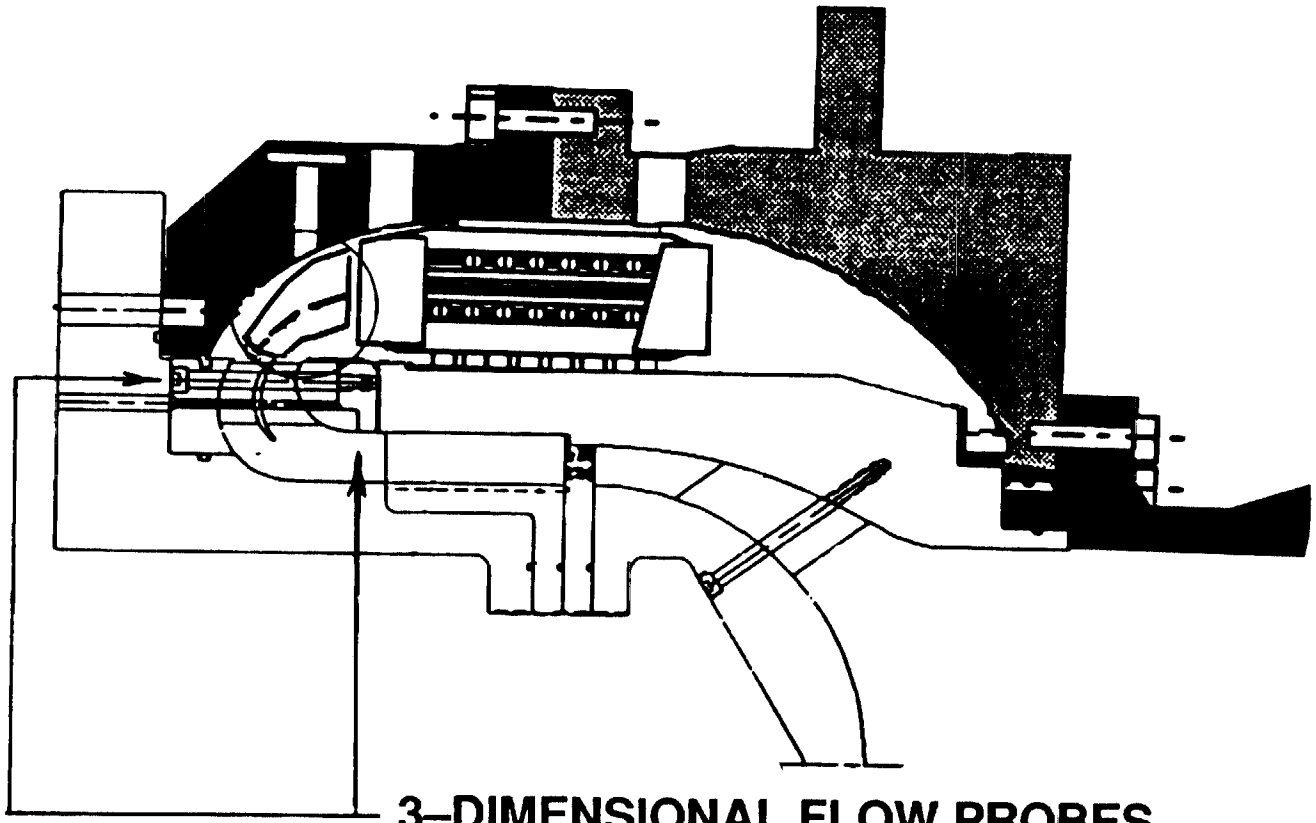

3–DIMENSIONAL FLOW PROBES

VARIATIONS OF ORIGINAL ORIFICE PLATE

Objective Was To Match ATD HPOTP Turbine Exit Flow Profile

ORIGINAL

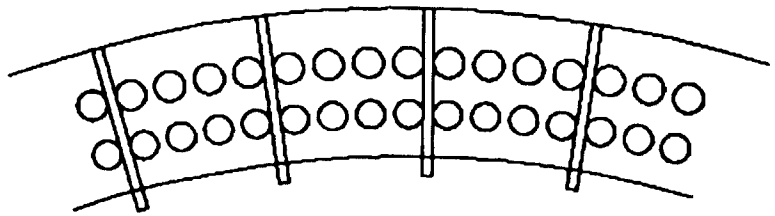

17.7% POROSITY

AXIAL FLOW

75% ORIGINAL

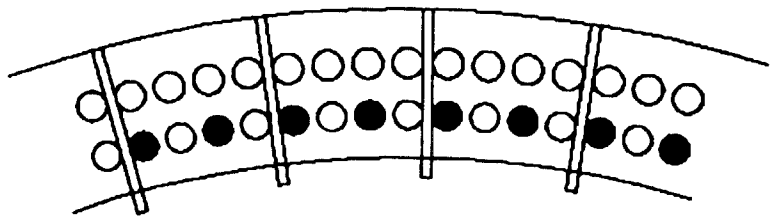

13.6% POROSITY

50% OF ID HOLES PLUGGED

LARGE AREA

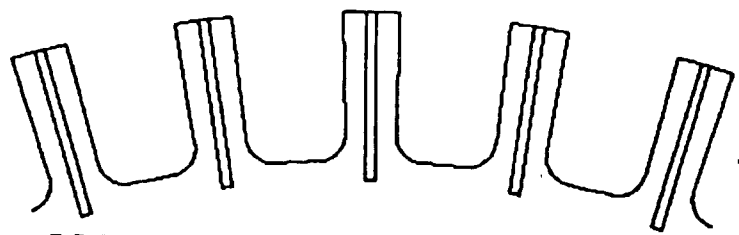

51.2% POROSITY

MATERIAL BETWEEN SWIRL VANES REMOVED

AIR FLOW MODEL TEST CONDITION MATRIX

Approx. Inlet Pressure ~PSI	Approx. Turbine Exit Mach Number							
	.04	.07	.10	.11	.13	.14	.15	.16
50			O,L			L		O,L
100			O,L			L		O,L
150			O			L		O
200			O					
250	O	O	O,7	O	O	O,7	O	O

O = Original Plate

7 = 75% Plate

L = Large–Area Plate

INITIAL ORIFICE PLATE REVISIONS RADIAL PROFILES

Significant Variation In Mass Flow Profiles Obtained

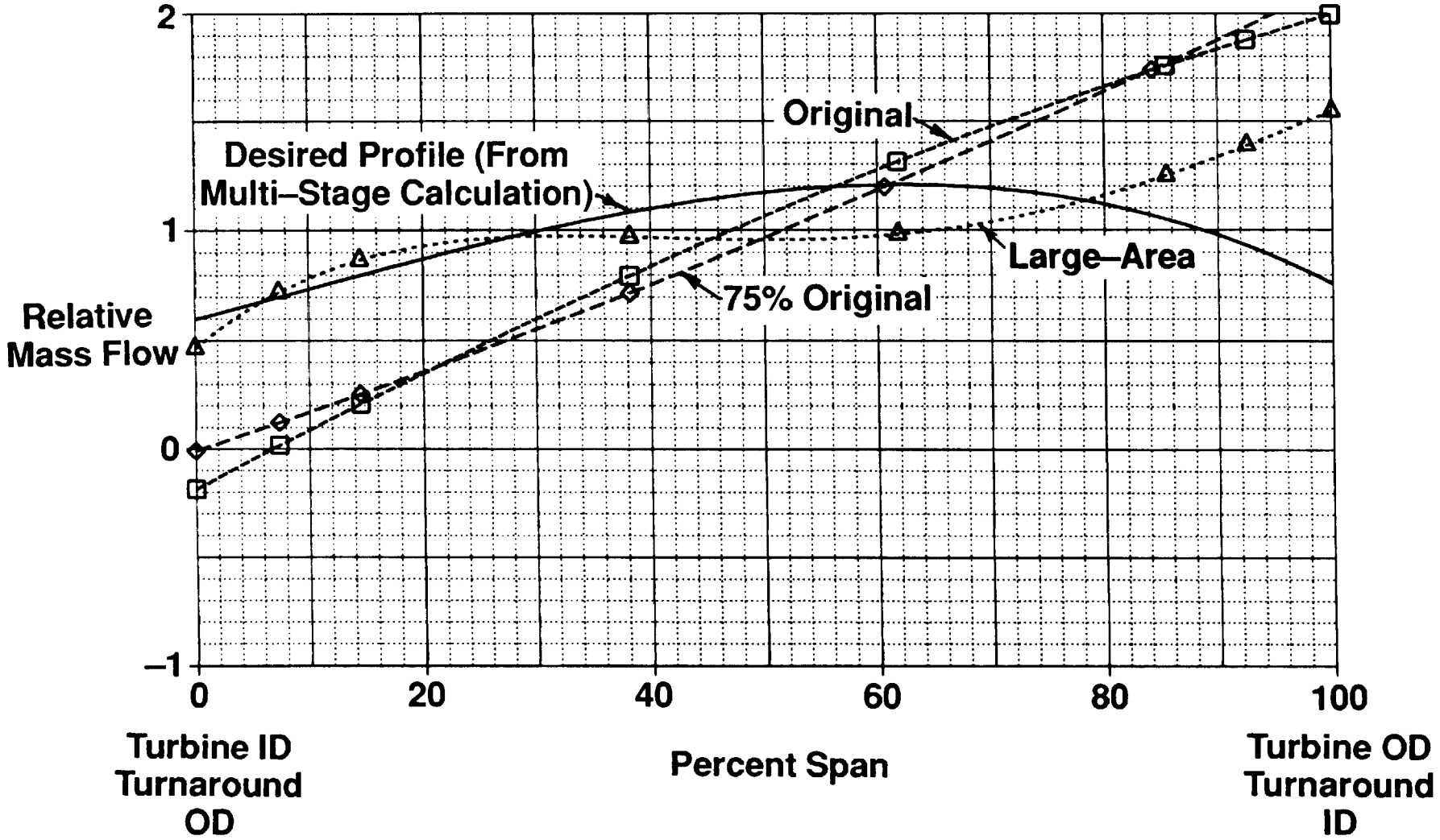

NEW ORIFICE PLATE CONFIGURATION

To Match Turbine Exit Velocity Components And Mass Profile

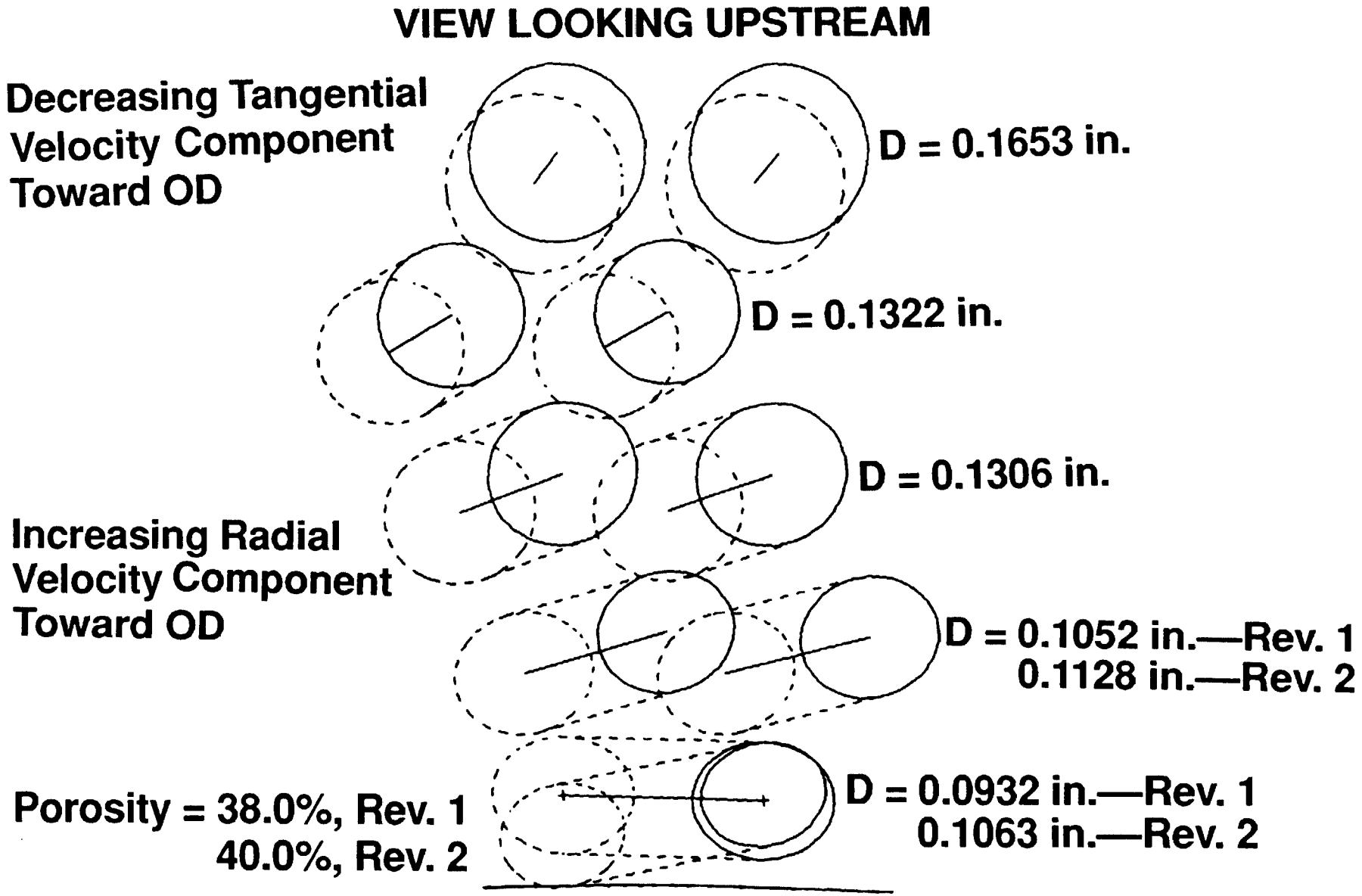

REVISED HPOTP TURBINE SIMULATOR FLOW PROFILES

Further Modification In Progress

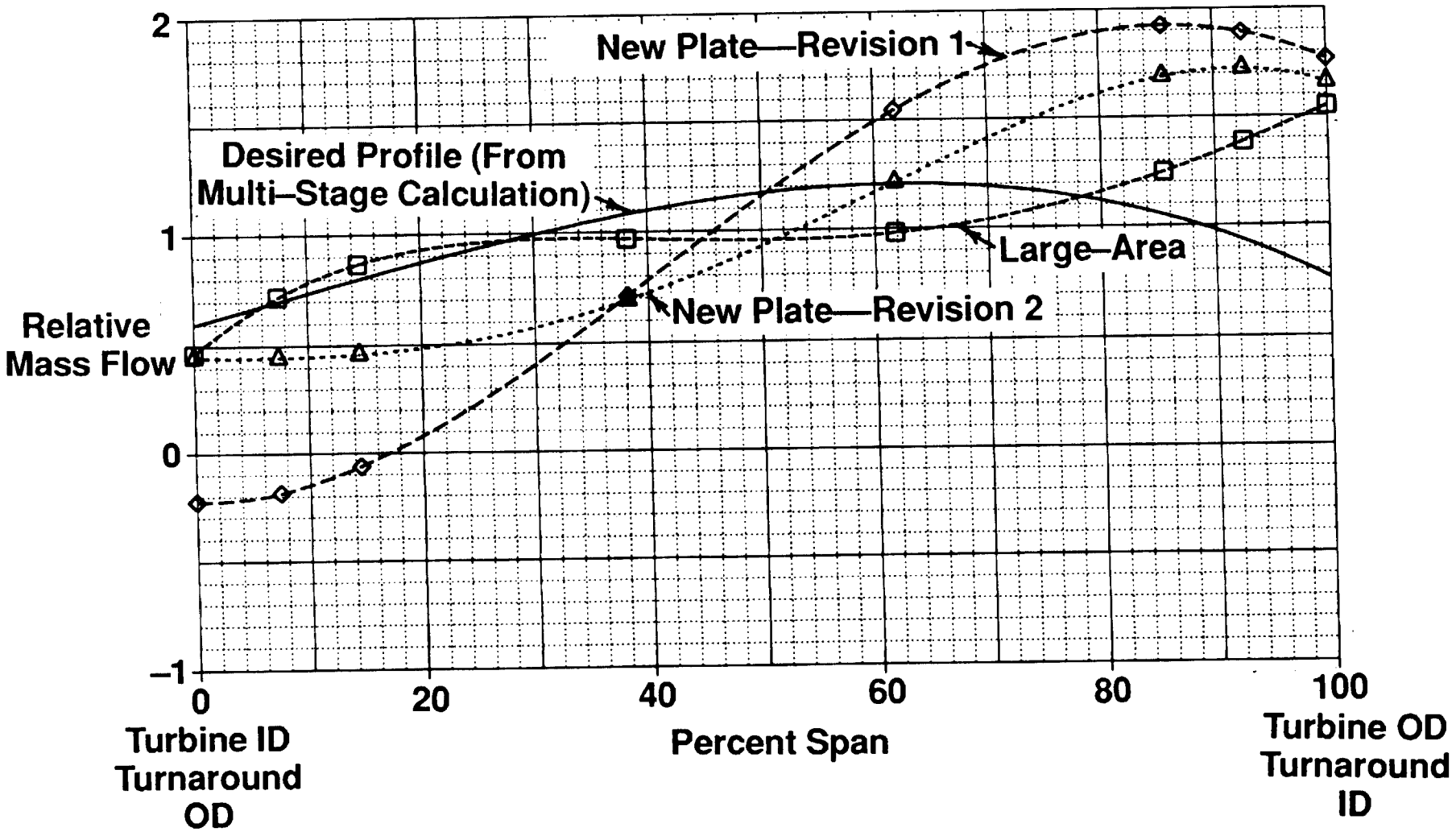

AIR FLOW TEST STATUS TO DATE

- Test Model Shows Ability To Study Complex Flow–Related Phenomena
- Contractor/Government Collaboration Vital In Rapid Response
- Accurate Evaluation Of Configuration Changes Requires Flow Conditions Closely Matching Actual Hardware
- Matching Of Flow Conditions Requires Careful Attention To Flowpath Details
- Continued Effort With Best Match Of Engine Environment
- HEX Vane Stress Level And Unsteady Pressure Analyses In Progress

NON-INTRUSIVE MEASUREMENTS IN A ROCKET ENGINE COMBUSTOR

S. Farhangi, V. T. Gylys, R. J. Jensen
Rockwell International/Rocketdyne Div.
Canoga Park, California 91303

ABSTRACT

In recent years analytical tools to characterize combustor flow have been developed in order to support design. To facilitate anchoring of combustion related physical models and the CFD codes in which they are incorporated considerable development and application of non-intrusive combustion diagnostic capabilities has occurred. Raman spectroscopy can be used to simultaneously detect all polyatomic molecules present in significant concentrations and to determine gas temperature. This is because all molecules possess a distinct temperature dependent Raman spectrum.

A multi-point diagnostic system for non-intrusive temperature and species profiling in rocket engines has been developed at Rocketdyne. In the present effort, the system has been undergoing validation for application to rocket engine component testing. A 4 inch diameter windowed combustor with a coaxial gas-gas injector was chosen for this series of validation experiments. Initially an excimer-pumped tunable dye laser and later a solid state Nd-Yag laser served as excitation sources. The Raman signal was dispersed by a monochromator and detected by a gated, intensified Charged Coupled Device (CCD) array.

Experiments were carried out prior to each series of hot fire tests to ensure that the Raman signal detected was due to a spontaneous rather than a stimulated Raman emission process. Over sixty hot fire tests were conducted during the first series of tests with the excimer/dye laser. All hot fire testing was at a mixture ratio of 0.5 and chamber pressures of ~100 and ~300 psia. The Raman spectra of hydrogen, water vapor and oxygen recorded during single element hot fire tests were reduced and analyzed. A significant achievement was the attainment of single shot Raman spectra in cold flow tests. Unfortunately, the single shot signal-to-noise ratio detoriated to an unacceptable level during the hot fire testing. Attempts to obtain temperature data from the hydrogen Q1-branch profiles obtained in hot fire tests suggest that potentially complicating factors may render the approach of averaging data on the photodiode array invalid. A second series of hot fire tests was conducted with a 4 element coaxial injector using the Nd-Yag laser. A very compact and portable diagnostics set up was assembled for ease of alignment, relocation and flexibility. Measurements were made at several regions in the chamber in order to map concentration profiles. High spatial resolution and improved signal to noise characteristics were demonstrated.

Non-intrusive Measurements in a Rocket Engine Combustor

Rocketdyne Advanced Combustion Devices

S. Farhangi, T. Gylys, and R. Jensen

Workshop for CFD Application in Rocket Propulsion

NASA MSFC

April 1993

Rockwell International
Rocketdyne Division

AGENDA

- Background / Need
- Progress (FY 92 & 93)

IMPROVEMENTS IN ROCKET INJECTOR/COMBUSTOR MODELING ARE REQUIRED

- Modeling of perfomance, durability, and stability of liquid rocket combustor systems relies heaviliy on correlations

- Advanced combustion physics modleling for CFD requires detailed experimental data for validation and anchoring.

COMBUSTOR PERFORMANCE, COMPATIBILITY KEY DESIGN ISSUES

- **Vehicle weight / cost / size & payload driven by performance**
  - ELV benchmark: $30K / incremental kilogram of payload
  - Upper stage & SSTO thrust / weight critical
- **Chamber compatibility influences life / cooling / mission**
  - Blanching related to hot wall temperature/chemistry
  - Lower heat loads may reduce pump requirements
  - Split channels affect performance of aging fleet
- **Combustion stability related to performance**
  - Spray / mixing characteristics set stability margin
  - Performance / stability margin trades

CFD CODES BEST FOR PERFORMANCE / COMPATIBILITY DESIGN ANALYSIS

- **Complete combustion physics**
  - Spray / chemistry / flowfield models
  - Models general - not specific to hardware / operating conditions
- **Detailed representation of hardware geometry / combustion**
- **Performance "data" at all locations within combustor**
  - Pressures / temperatures / species / heat loads
  - All performance parameters measurable in hot fire

Confidence in CFD limited due to lack of required detailed validation data

RAMAN WELL SUITED TO OBTAIN KEY CODE VALIDATION DATA

- **Raman spectroscopy well understood / straightforward to apply**
  - Small fraction of laser light scattered from molecules yields Raman spectrum
  - Raman light shifted in wavelength from laser / unique to each specie
- **Non Intrusive measurements with existing technology**
  - Can obtain spacial data during hot fire testing
    - Temperature
    - Species concentration

ROCKETDYNE RAMAN DIAGNOSTIC CAPABILITIES

- **Local temperature / combustion gas species concentrations**
  - Simultaneous measurements at multiple locations
  - Simultaneous species / temperature data
- **Applicable to research / development combustors**
  - CFD code validation data in research combustors
  - Performance (mixing efficiency) assessment
  - Injector / chamber compatibility evaluation

FY 92-93 RAMAN PROGRESS

- **Activated multi-point Raman system**
- **Raman species data obtained in single element combustor testing**
  - Concentration profiles reveal flame structure
  - Over 100 hot fire tests at 100 and 300 psia, MR = 0.5/various injectors
  - Ten simultaneous measurements each test
    - Data along lines at various locations downstream of the face
    - Concentrations averaged over multiple laser pulses
    - Efforts to get instantaneous data partly successful
- **Initiated assembly of multi-point "portable" Raman system**

RAMAN SYSTEM FOR RESEARCH COMBUSTOR TESTING

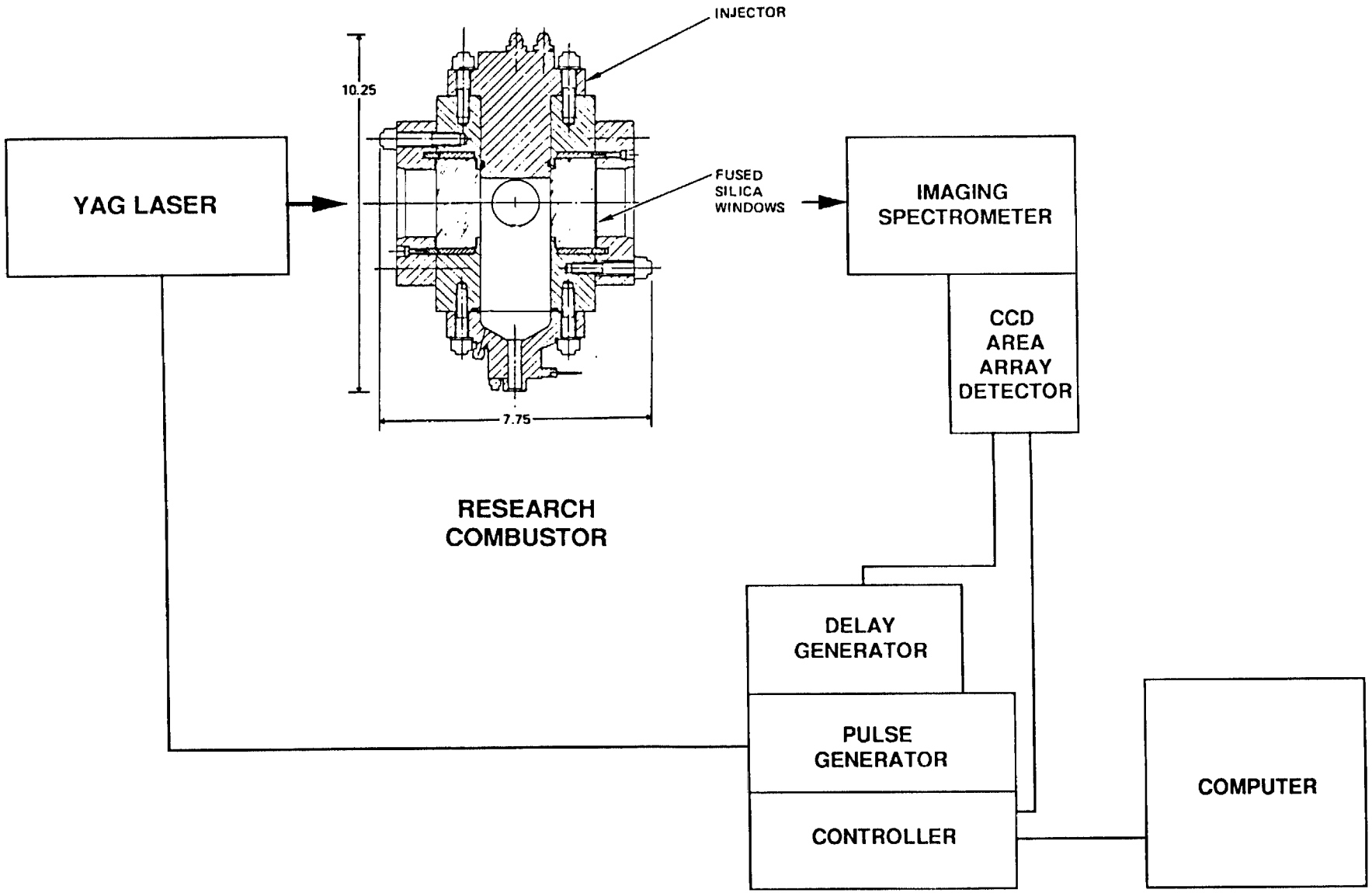

COMPLETE RAMAN SPECTRUM

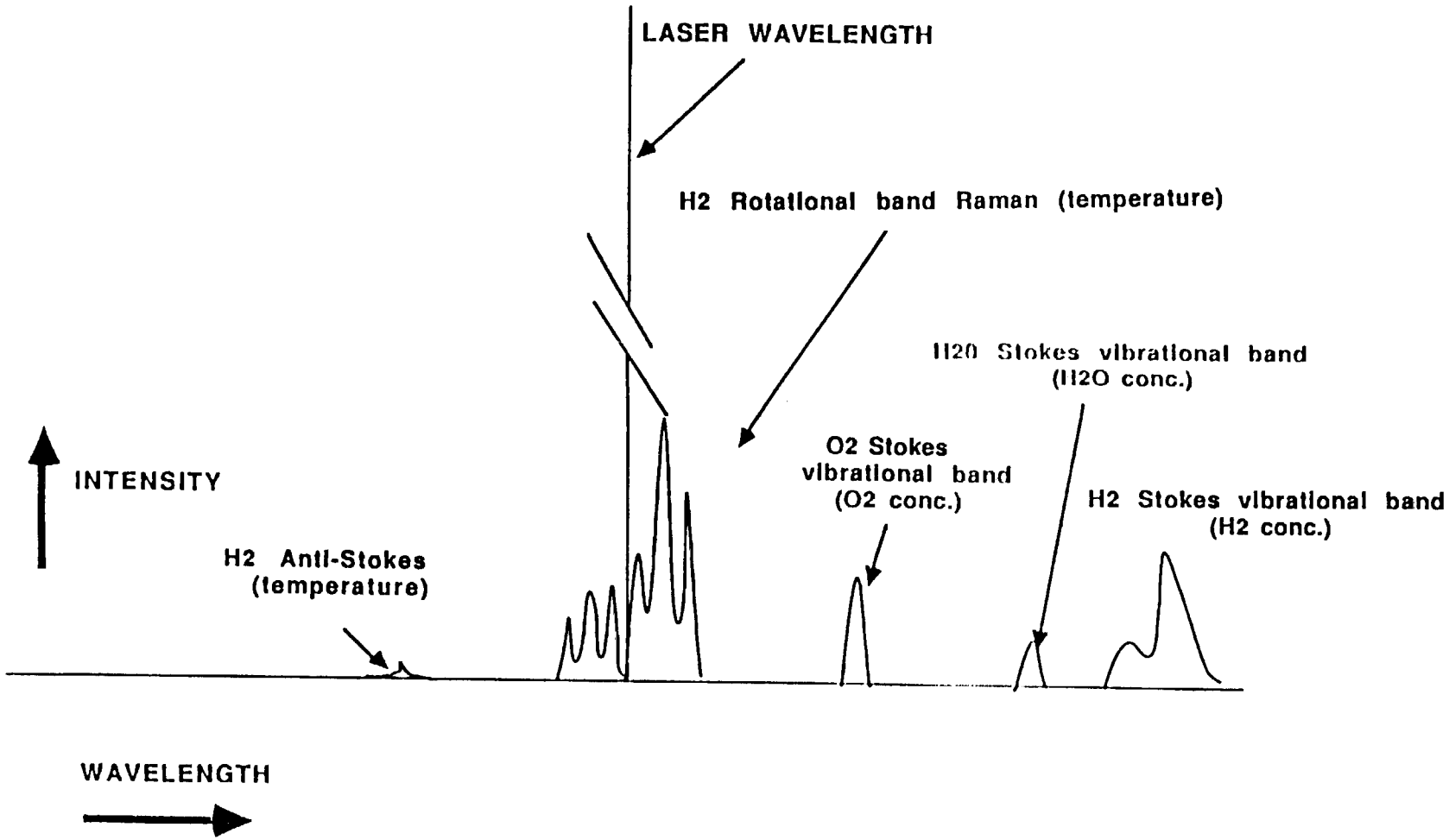

MULTI-POINT HOT FIRE RAMAN SPECTRA, 150 g/mm
(Injector Face, Pc = 100 psia, MR = 0.5)

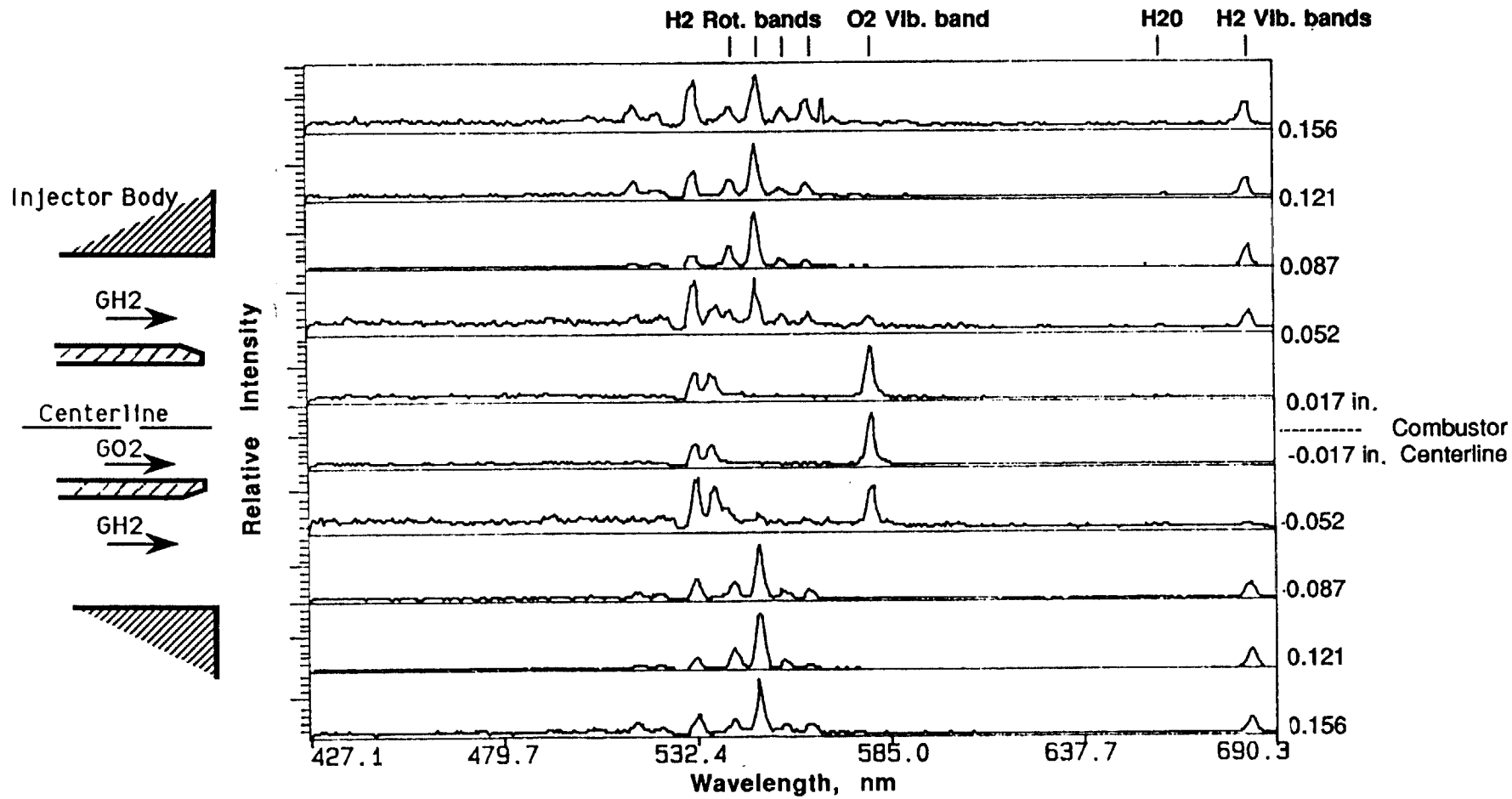

VARIATION OF SPECIES MOLE FRACTION WITH RADIAL DISRANCE

(TEST 16FR12, Injector Face, Pc = 100 psia, MR = 0.5)

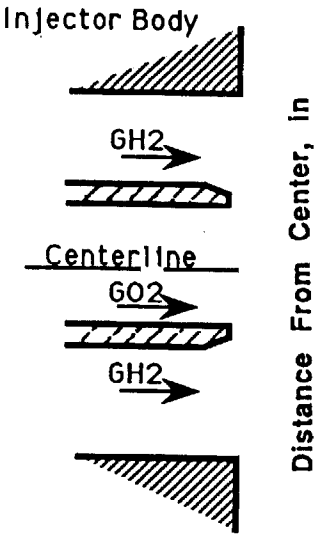

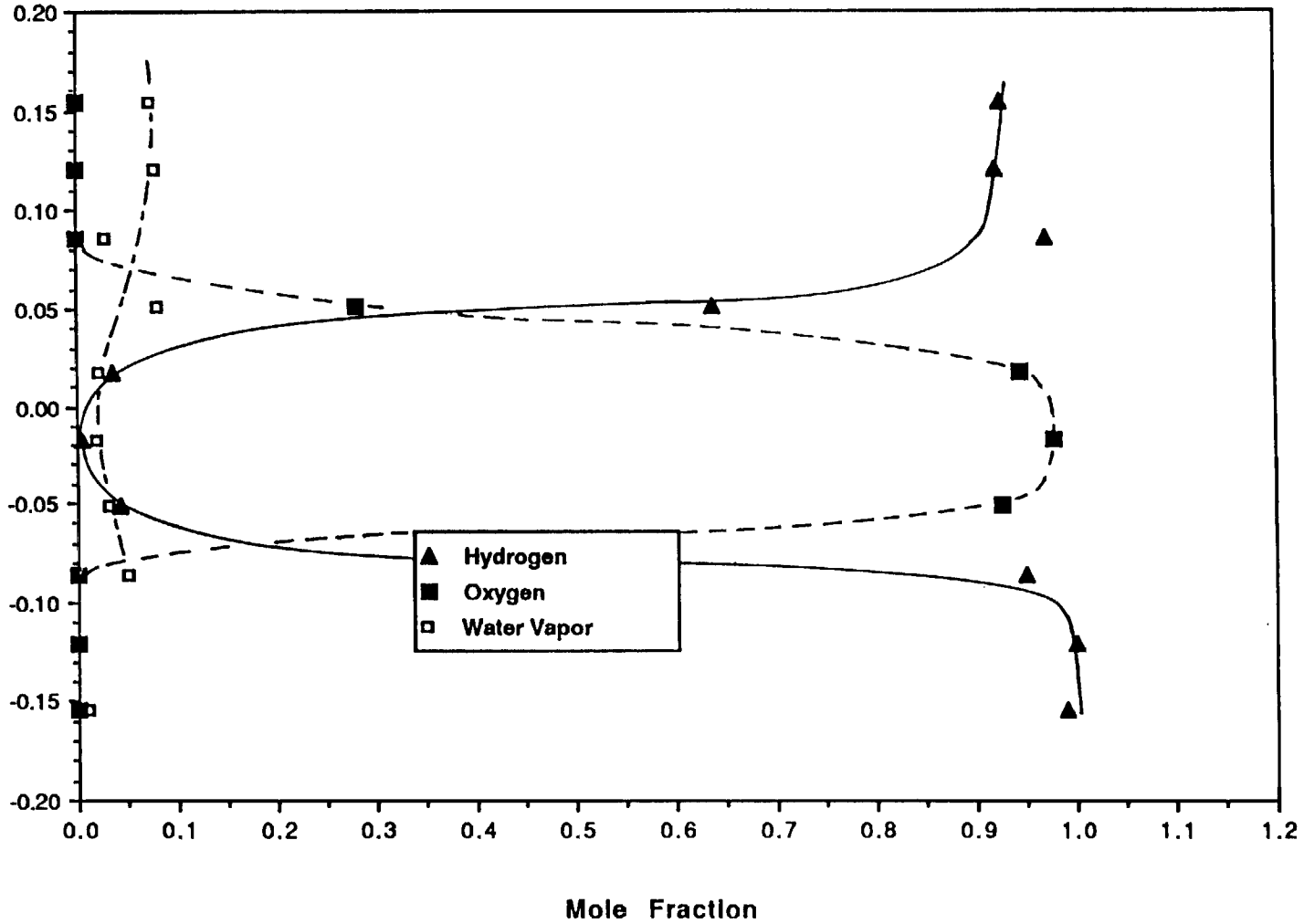

molefrac.16fr12.g2
SF 3-93

VARIATION OF SPECIES MOLE FRACTION WITH RADIAL DISRANCE
(TEST A19R70, 1.5 in. from Injector Face, Pc = 120 psia, MR = 0.5)

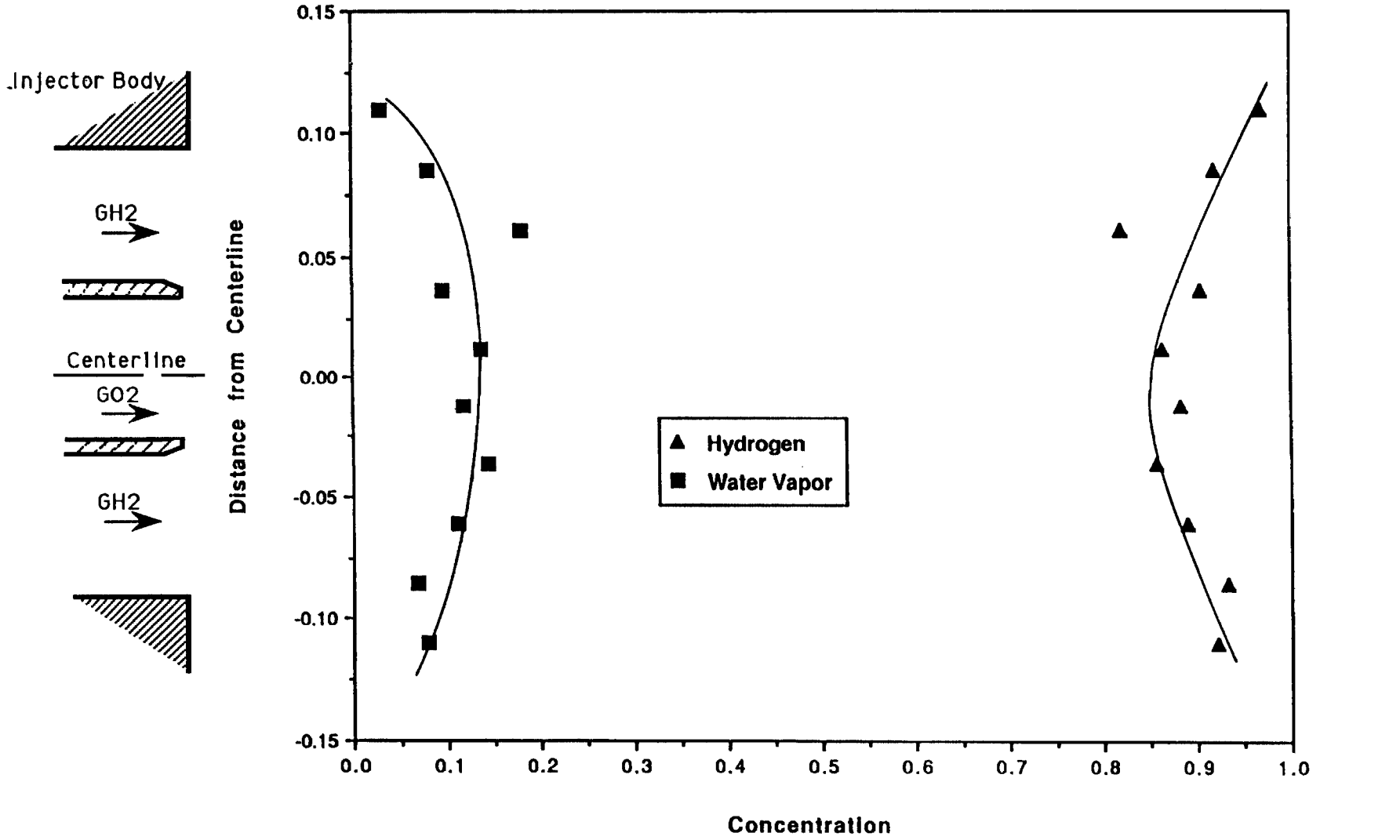

con.dist.a19r70.g3
SF 3-93

PORTABLE LASER RAMAN SYSTEM SCHEMATIC

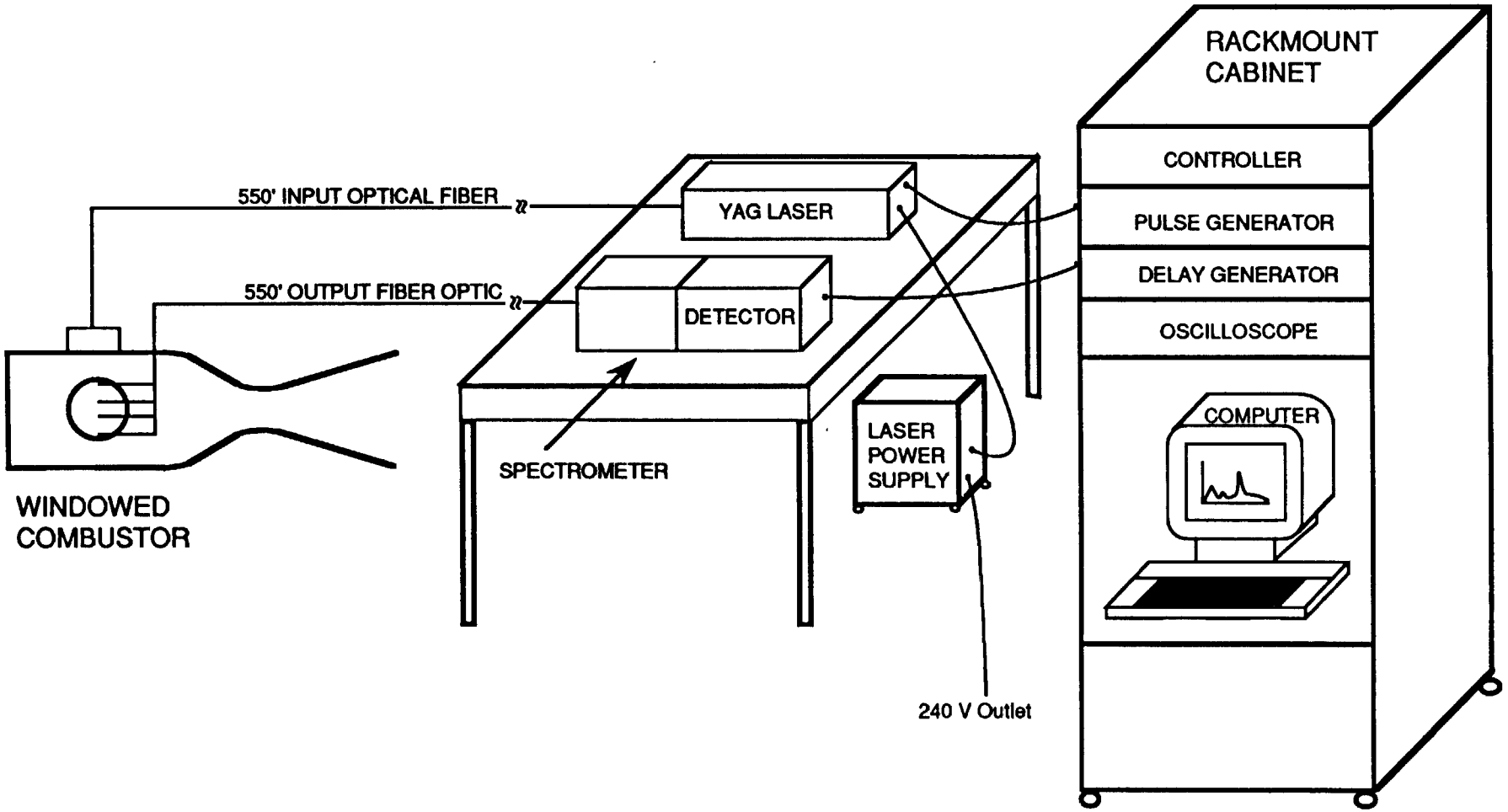

Schematic
sf 11-92

SUMMARY

- Hot fire validation of multipoint Raman diagnostic progressing
  - 10 points simultaneously
    - Species concentration (0_2, H_2 & H_20 demonstrated)
    - Temperature
  - Data collection rate of 5-10 Hz , pulse duration of ~6 ns
- Portable Raman system with fiber optics in work
- Application to code anchoring effort now feasible

IMPELLER FLOW FIELD CHARACTERIZATION WITH A LASER TWO-FOCUS VELOCIMETER

L. A. Brozowski, T. V. Ferguson, L. Rojas

Rockwell International - Rocketdyne Division
Canoga Park, California

ABSTRACT

Use of Computational Fluid Dynamics (CFD) codes, prevalent in the rocket engine turbomachinery industry, necessitates data of sufficient quality and quantity to benchmark computational codes. Existing data bases for typical rocket engine configurations, in particular impellers, are limited. In addition, traditional data acquisition methods have several limitations: typically transducer uncertainties are 0.5 percent of transducer full scale and traditional pressure probes are unable to provide flow characteristics in the circumferential (blade-to-blade) direction. Laser velocimetry circumvents these limitations by providing ± 0.5 percent uncertainty in flow velocity and ± 0.5 degree uncertainty in flow angle. The percent of uncertainty in flow velocity is based on the measured value, not full range capability. The laser electronics multiple partitioning capability allows data acquired between blades as the impeller rotates, to be analyzed separately, thus providing blade-to-blade flow characterization. Unlike some probes, the non-intrusive measurements made with the laser velocimeter does not disturb the flow.

To this end, and under Contract (NAS8-38864) to the National Aeronautics and Space Administration (NASA) at Marshall Space Flight Center (MSFC), an extensive test program was undertaken at Rocketdyne. Impellers from two different generic rocket engine pump configurations were examined. The impellers represent different spectrums of pump design: the Space Shuttle Main Engine (SSME) high pressure fuel turbopump (HPFTP) impeller was designed in the 1970's, the Consortium for CFD Application in Propulsion Technology Pump Stage Technology Team (Pump Consortium) optimized impeller was designed with the aid of modern computing techniques. The tester configuration for each of the impellers consisted of an axial inlet, an inducer, a diffuser, and a crossover discharge.

While the tested configurations were carefully chosen to be representative of generic rocket engine pumps, several features of both testers were intentionally atypical. A crossover discharge, downstream of the impeller, rather than a volute discharge was used to minimize asymmetric flow conditions that might be reflected in the impeller discharge flow data. Impeller shroud wear ring radial clearances were purposely close to minimize leakage flow, thus increasing confidence in using the inlet data as an input to CFD programs.

The empirical study extensively examined the flow fields of the two impellers via performance of laser two-focus velocimeter surveys in an axial plane upstream of the impellers and in multiple radial planes downstream of the impellers. Both studies were performed at the impeller design flow coefficients.

Inlet laser surveys that provide CFD code inlet boundary conditions were performed in one axial plane, with ten radial locations surveyed. Three wall static pressures, positioned circumferentially around the impeller inlet were used to identify asymmetrical pressure distributions in the inlet survey plane. The impeller discharge flow characterization consisted of three radial planes for the SSME HPFTP impeller and two radial planes for the Pump Consortium optimized impeller. Housing wall static pressures were placed to correspond to the radial locations surveyed with the laser velocimeter. Between five and thirteen axial stations across the discharge channel width were examined in each radial plane during the extensive flow mapping.

The largely successful empirical flow characterization of two different impellers resulted in a substantial contribution to the limited existing data base, and yielded accurate data for CFD code benchmarking.

IMPELLER FLOW FIELD CHARACTERIZATION WITH A LASER TWO-FOCUS VELOCIMETER

1636

22 April 1993

L. A. Brozowski
T. V. Ferguson
L. Rojas

Rockwell International
Rocketdyne Division

IMPELLER FLOW FIELD CHARACTERIZATION WITH A LASER TWO-FOCUS VELOCIMETER

- Background
- Test Objectives
- Nondimensionalization
- Configuration Geometry
  - Configuration - 1
  - Configuration - 2
- Test Facility and Conditions
- Laser Survey Locations
  - Impeller Inlet Survey
  - Impeller Discharge Survey
- Results Configuration - 1
- Results Configuration - 2
- Conclusion

PUMP CFD CODE VALIDATION TESTS
Background

- NASA-MSFC Contract: Advanced Design-Verification Methodology for Pump-Fed Earth-to-Orbit Propulsion Systems
  - Increasing use of CFD codes throughout rocket engine propulsion industry
  - Limited benchmark quality data available for pump CFD code validation
- Approach
  - Geometry representative of current rocket engine turbomachinery pump configurations
  - Use laser two-focus velocimeter to obtain flow characteristics (velocity and angle)
    - Non-intrusive measurement
    - Allows blade-to-blade flow characterization
    - Accuracy better than typical measurements
      - Velocity uncertainty $\pm$ 0.5 percent of measured velocity value
      - Flow angle uncertainty $\pm$ 0.5 degree

PUMP CFD CODE VALIDATION TESTS
Data Nondimensionalization

- Nondimensionalization of data allows generalization of comparison between empirical data and CFD codes
  - Length - nondimensionalized by impeller tip diameter

$$L_{nondim} = \frac{L}{D_{tip}}$$

  - Head - nondimensionalized by impeller tip speed squared

$$H_{nondim} = \frac{g*H}{U_{tip}^{2}}$$

  - Velocity - nondimensionalized by impeller tip speed

$$V_{nondim} = \frac{V}{U_{tip}}$$

PUMP CFD CODE VALIDATION TESTS
Standard Coordinate System

- Right Hand Coordinate System
  - Circumferential reference - 0 degrees at impeller trailing edge intersection with hub, positive angle increase in counterclockwise (against impeller rotation) direction
  - Axial reference - 0 at impeller leading edge intersection with shroud, negative upstream (pump inlet) positive toward pump discharge
  - Radial reference - 0 at shaft centerline
  - Data in standard plot3d (i, j, k) format
    - i-axis: meridional direction
    - j-axis: blade-to-blade direction
    - k-axis: hub-to-tip direction

1640

LAB 04/22//93

PUMP CFD CODE VALIDATION TESTS
Pictorial of Coordinate System

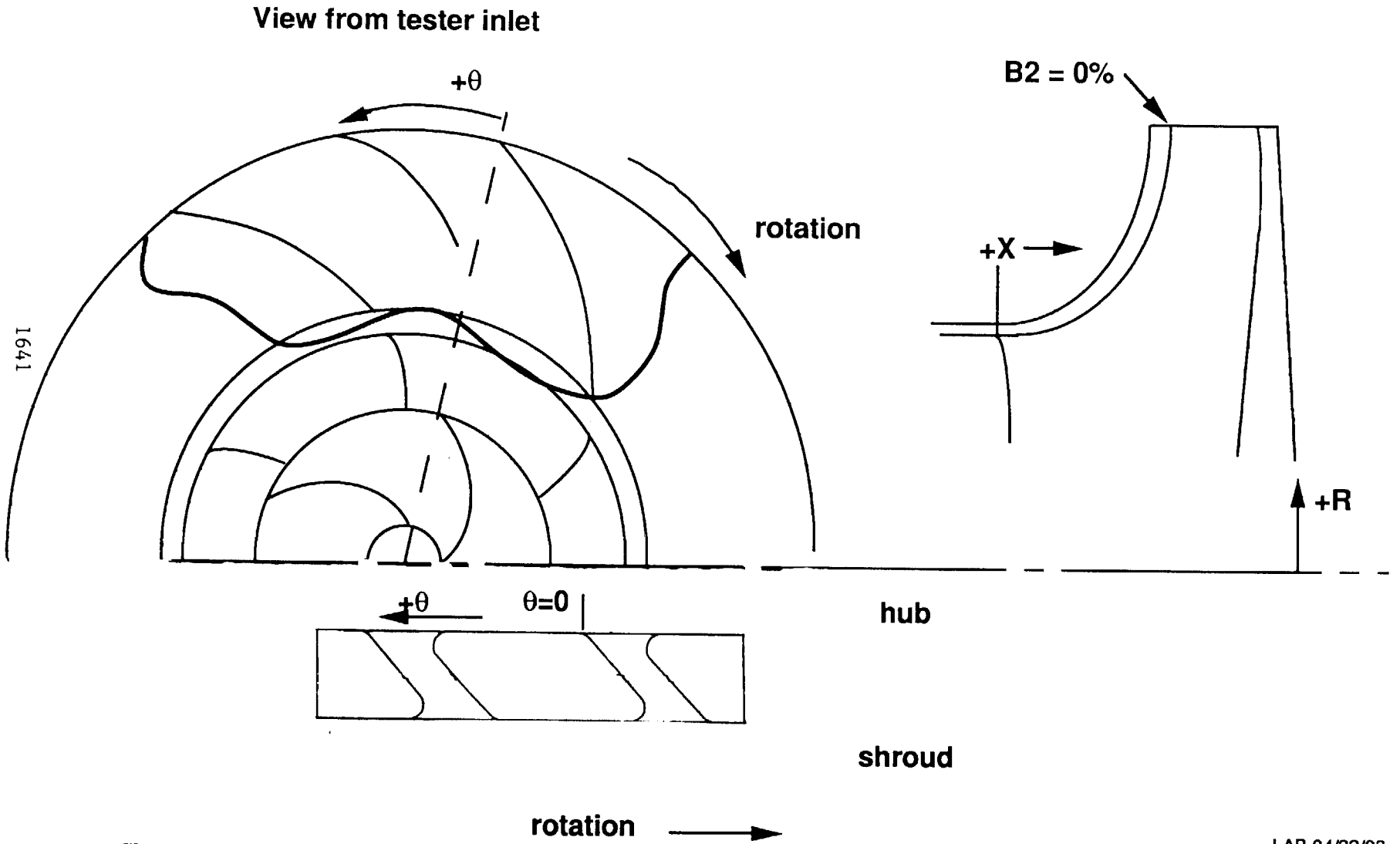

Rockwell International
Rocketdyne Division

LAB 04/22/93

PLOT3D i,j,k Convention

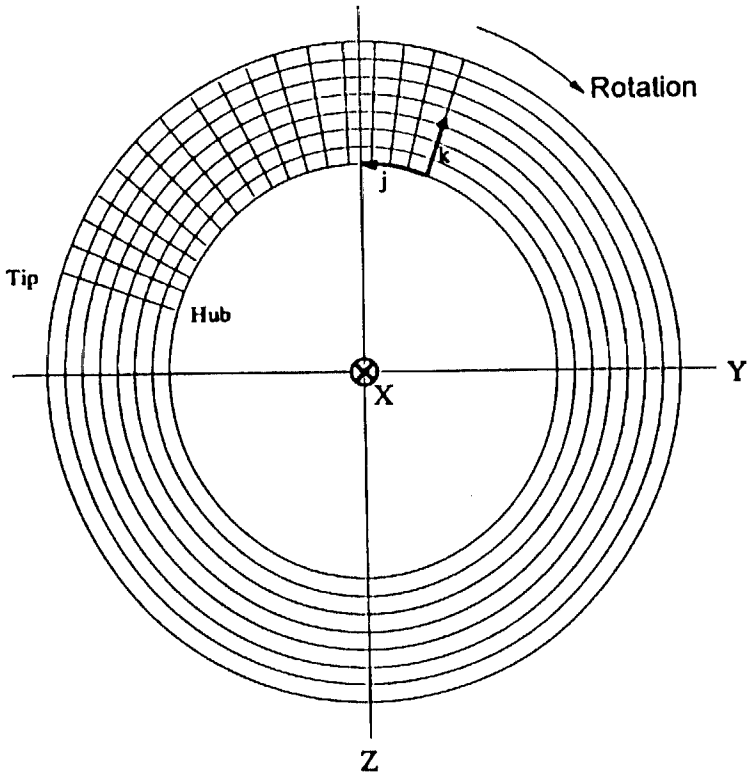

Impeller Inlet Grid

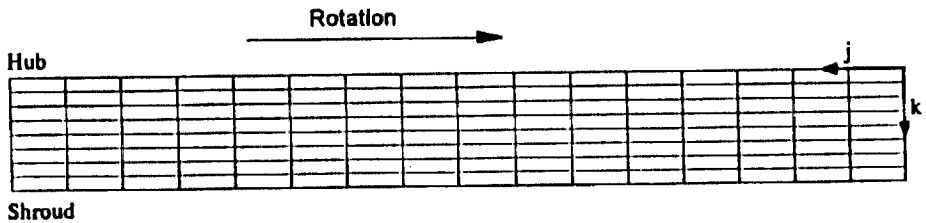

Impeller Discharge Grid

LAB 04/22/93

Rockwell International
Rocketdyne Division

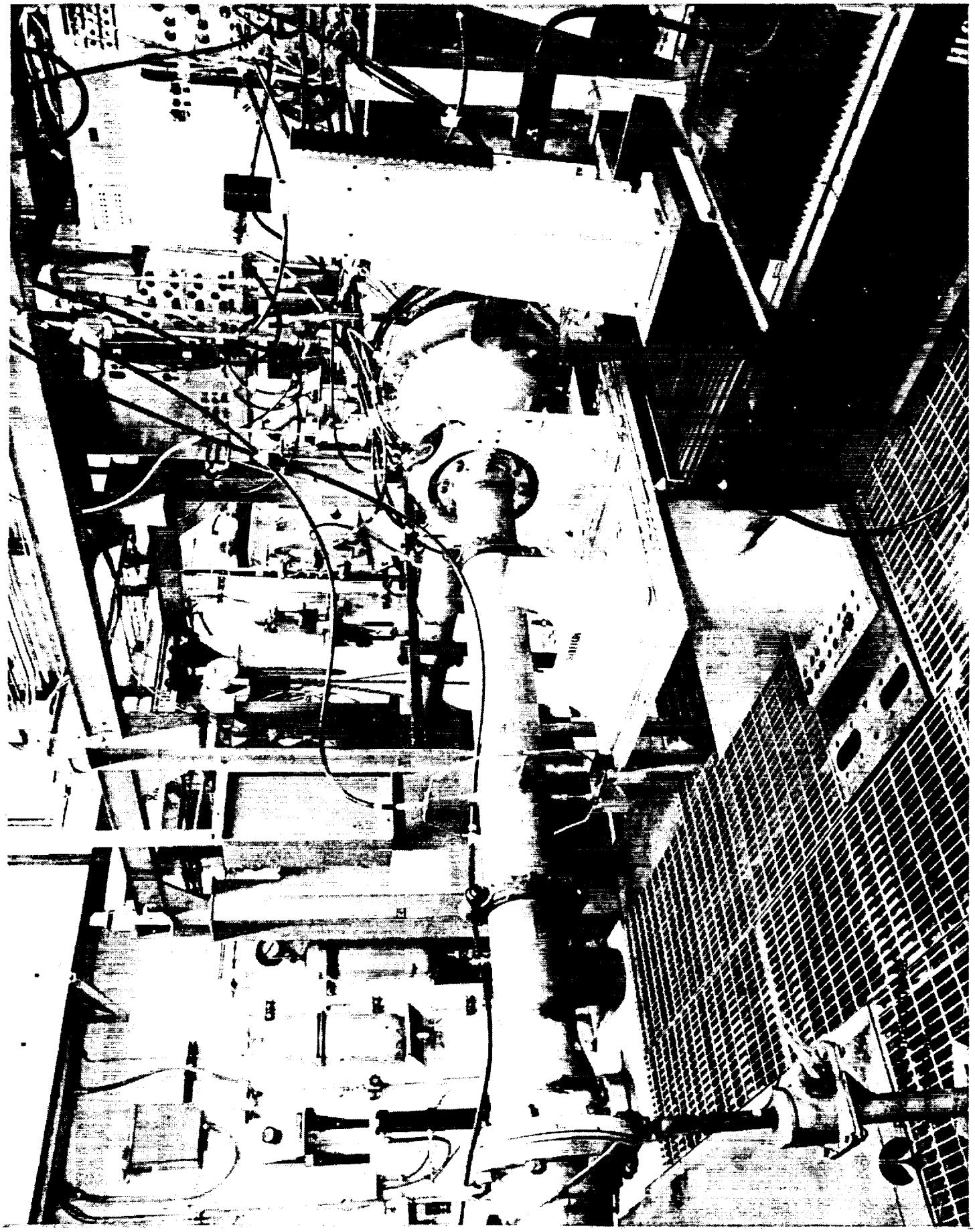

PUMP CFD CODE VALIDATION TESTS
Two Pump Configurations Tested

- Axial Inlet, Diffuser, Crossover, Volute Used in Both Configurations
  - Configuration 1 - Space Shuttle Main Engine High Pressure Fuel Turbopump
    - SSME HPFTP prototype inducer - unshrouded with six blades
    - Inducer tip nondimensional radial clearance 0.000636
    - SSME HPFTP shrouded impeller trimmed to 92 percent of original tip diameter
      - Shrouded impeller with six full blades
      - Six long partial blades, twelve short partial blades
    - Diffuser-crossover located at nondimensional radius of 0.5545
    - Impeller shroud leakage minimized wtih nondimensional shroud wear ring nominal radial clearance 0.000136

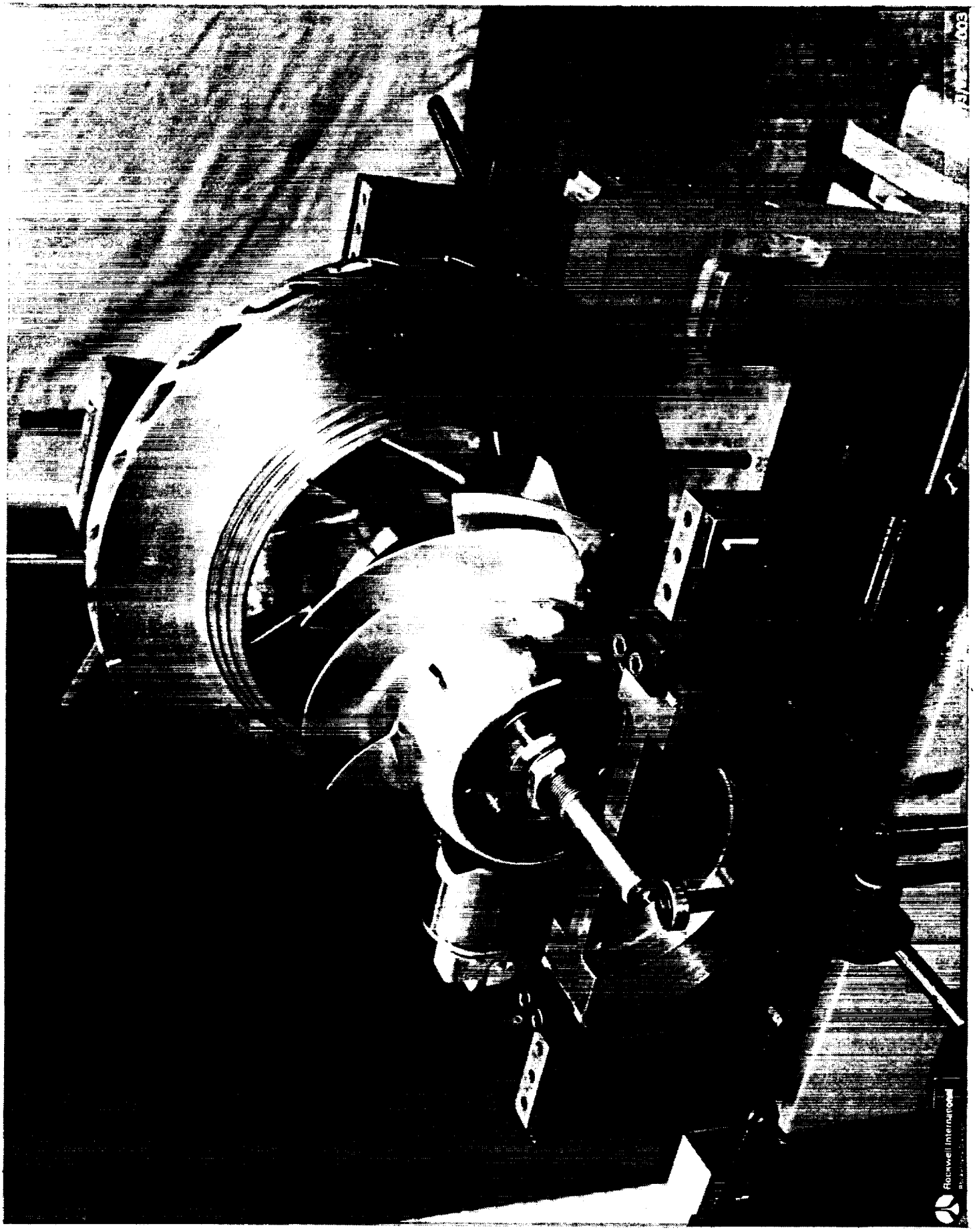

SSME HPFTP IMPELLER LASER VELOCIMETER SURVEY TESTER CROSS-SECTION

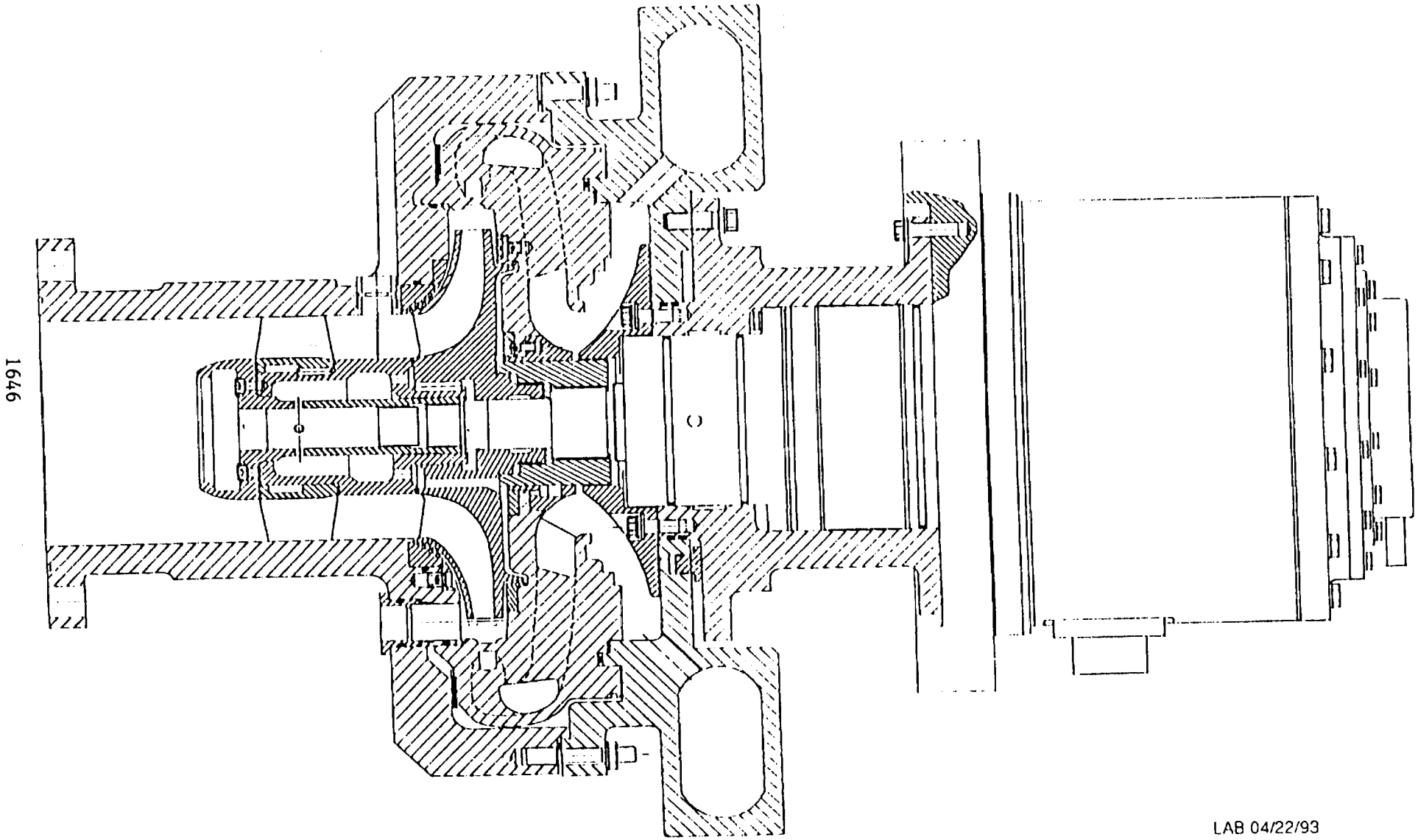

1646

LAB 04/22/93

Rockwell International
Rocketdyne Division

PUMP CFD CODE VALIDATION TESTS
Two Pump Configurations Tested

- Configuration 2 - Pump Consortium
  - Unshrouded inducer with four blades
  - Inducer tip nondimensional radial clearance 0.000967
  - Impeller design based on Consortium for CFD application in Propulsion Technology Pump Stage Technology Team requirements - Pump Consortium optimized impeller (designated Pump Consortium baseline impeller for this empirical study)
    - Shrouded impeller with six full blades, six partial blades
  - Diffuser-crossover located at nondimensional radius of 0.6711
  - Impeller shroud leakage minimized with nondimensional wear ring nominal radial clearance -0.000166

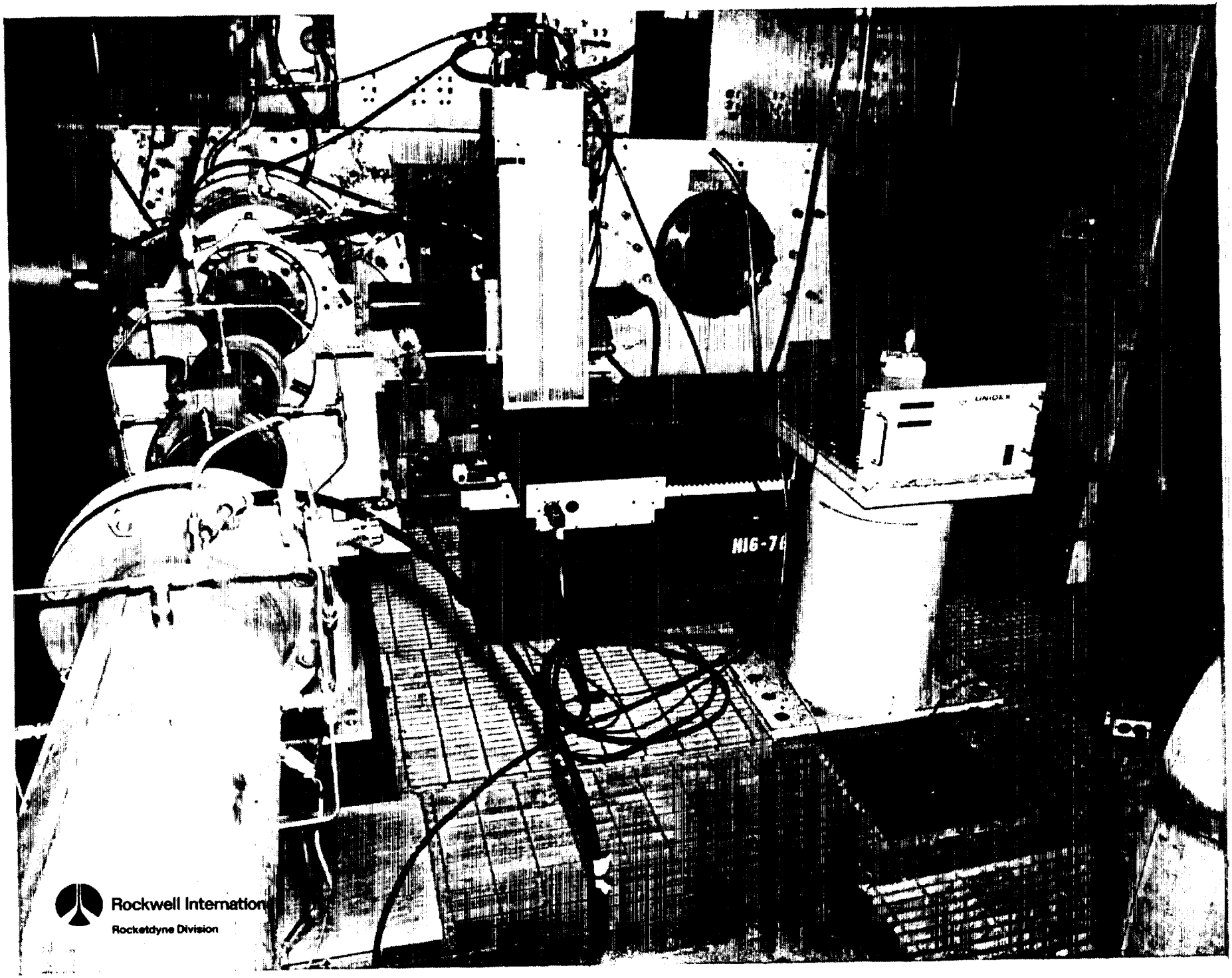
Rockwell International
Rocketdyne Division

CONSORTIUM BASELINE IMPELLER LASER VELOCIMETER SURVEY TESTER CROSS-SECTION

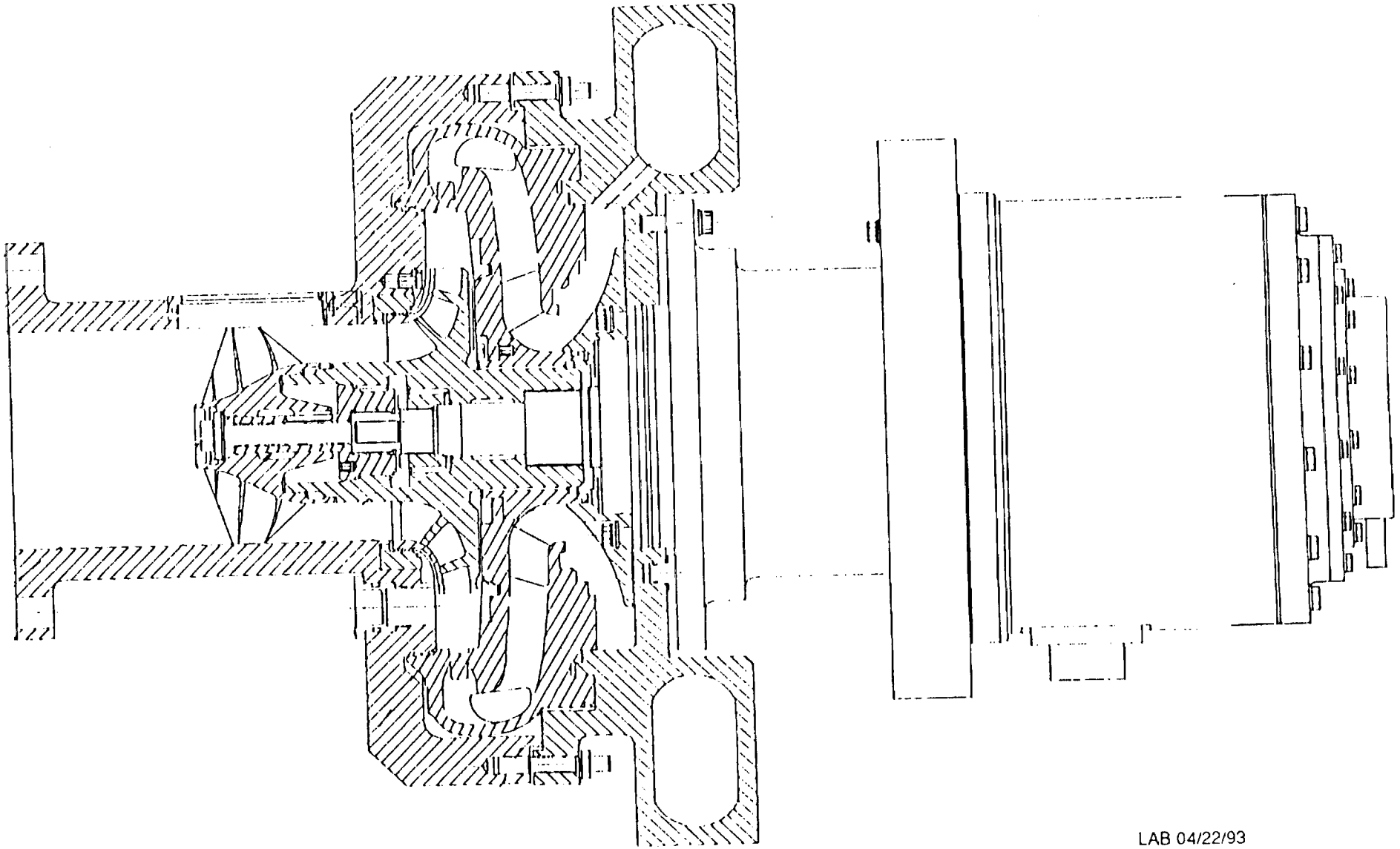

LAB 04/22/93

Rockwell International
Rocketdyne Division

PUMP CFD CODE VALIDATION TESTS
Test Facility and Test Conditions

- Rocketdyne's Engineering Development Laboratory Pump Test Facility
  - 7600 gallon closed-loop flow facility
  - 4000 HP reversible, synchronous motor
  - 128 channel static data acquisition system - 1 data sample every 6 seconds
- Both test configurations tested at 6322 rpm with ambient water
  - Configuration 1 - SSME HPFTP impeller
    - Impeller discharge tip speed = 92.487 m/s
    - Impeller inlet design flow coefficient (based on discharge tip speed) = 0.256
  - Configuration 2 - Consortium baseline impeller
    - Impeller discharge tip speed = 76.049 m/s
    - Impeller inlet design flow coefficient (based on discharge tip speed) = 0.144

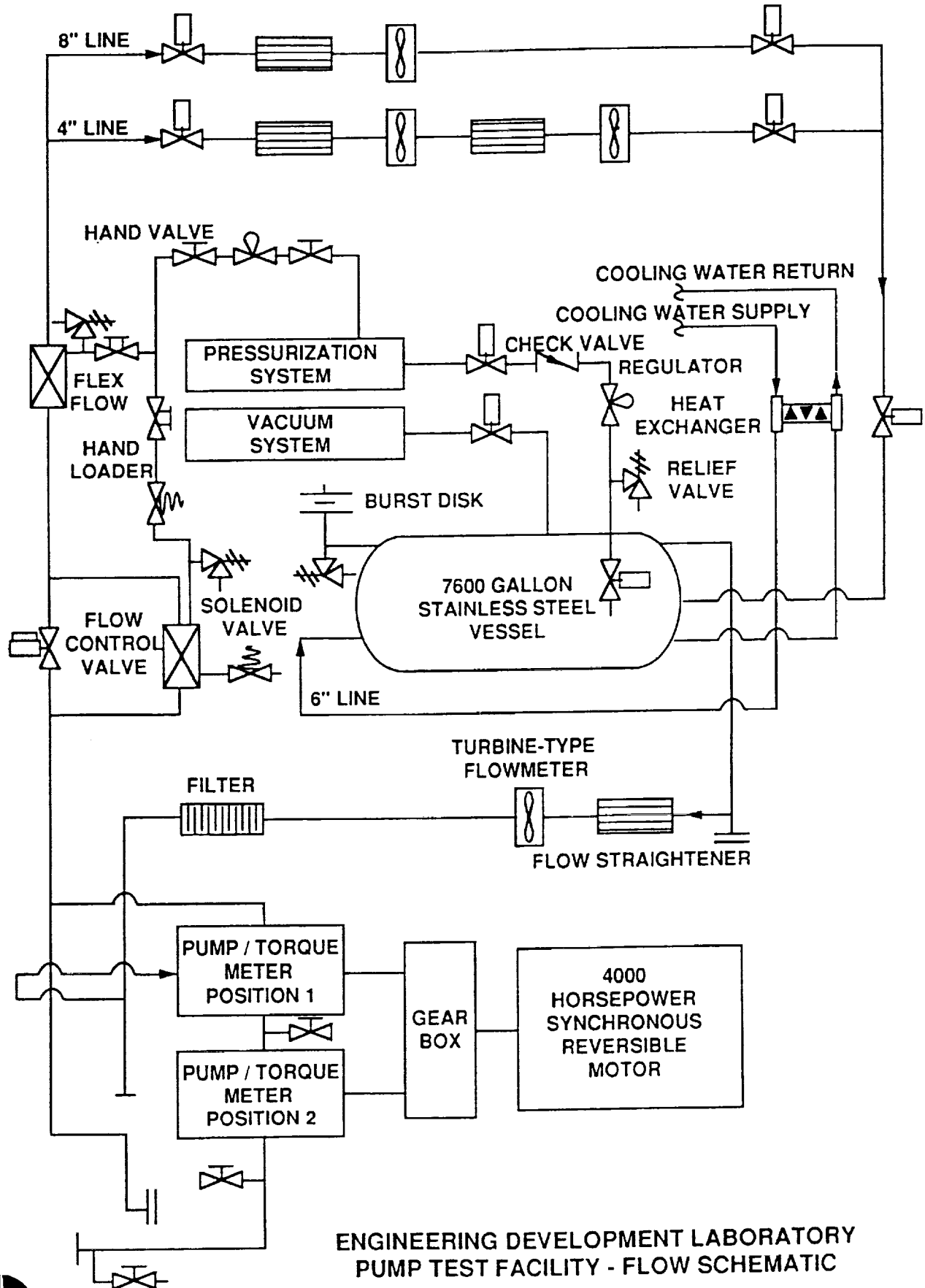

ENGINEERING DEVELOPMENT LABORATORY
PUMP TEST FACILITY - FLOW SCHEMATIC

Rockwell International
Rocketdyne Division

04/22/93

PUMP CFD CODE VALIDATION TESTS
Configurations 1 & 2 Laser Two-Focus Velocimeter Surveys

- Impeller Inlet Survey Data Locations
  - Ten radial positions (% of annulus height, 0% at hub)
    - 10, 15, 25, 35, 45, 55, 65, 75, 85, 95
    - Each radial survey referenced to impeller timing mark
      - Impeller inlet timing mark - axial projection of impeller leading edge tip
  - Configuration 1 - one axial plane located at nondimensional axial position -0.0893 (upstream of impeller leading edge tip)
  - 60 degrees blade-to-blade surveyed partitioned into 16 data windows (3.75 arc deg)
    - Data ensemble averaged over all six blade passages
  - Configuration 2 - one axial plane located at nondimensional axial position -0.1290 (upstream of impeller leading edge tip)
  - 90 degrees inducer blade-to-blade surveyed partitioned into 16 windows (5.625 arc deg)
    - Data not ensemble averaged

1653

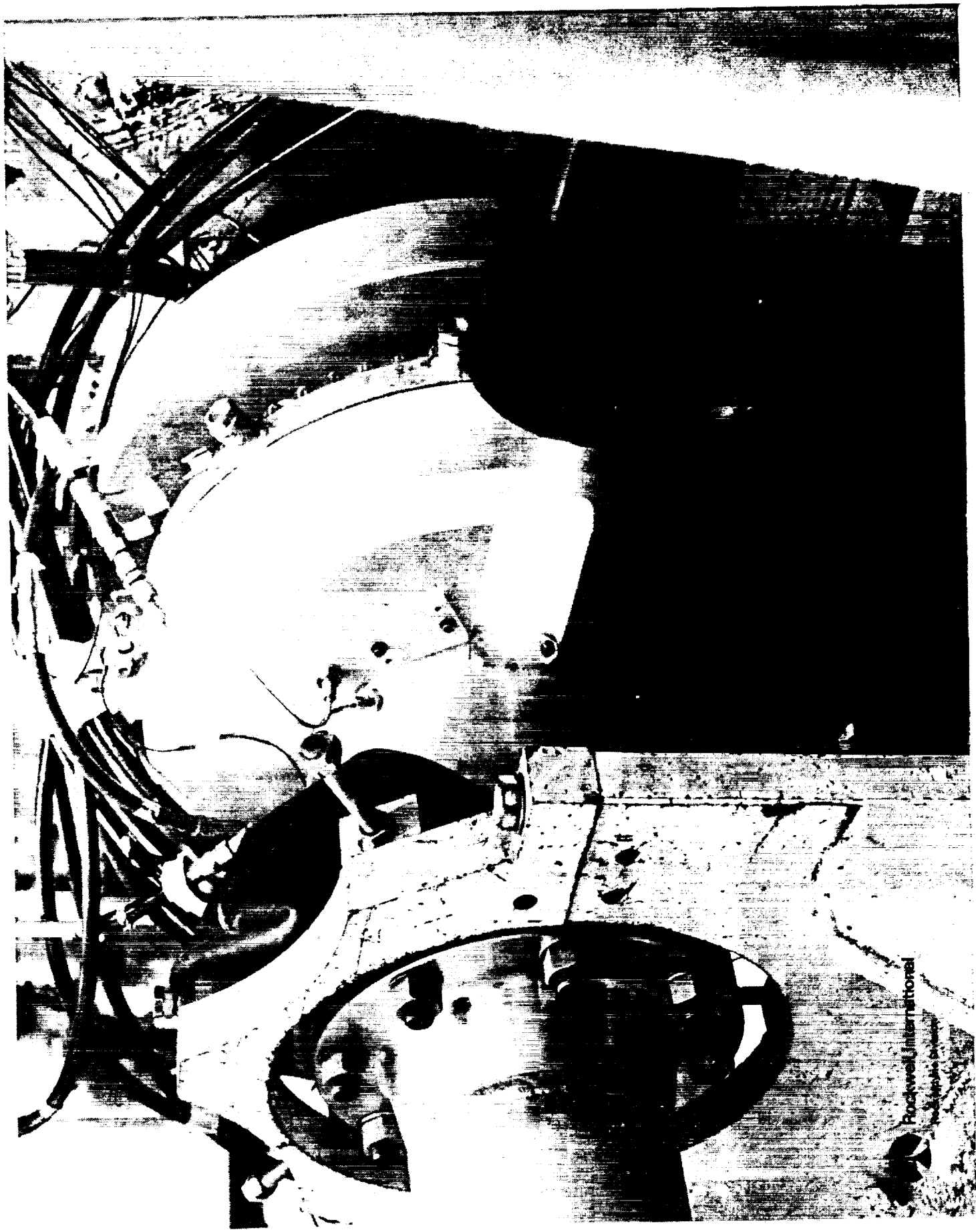
Rockwell International

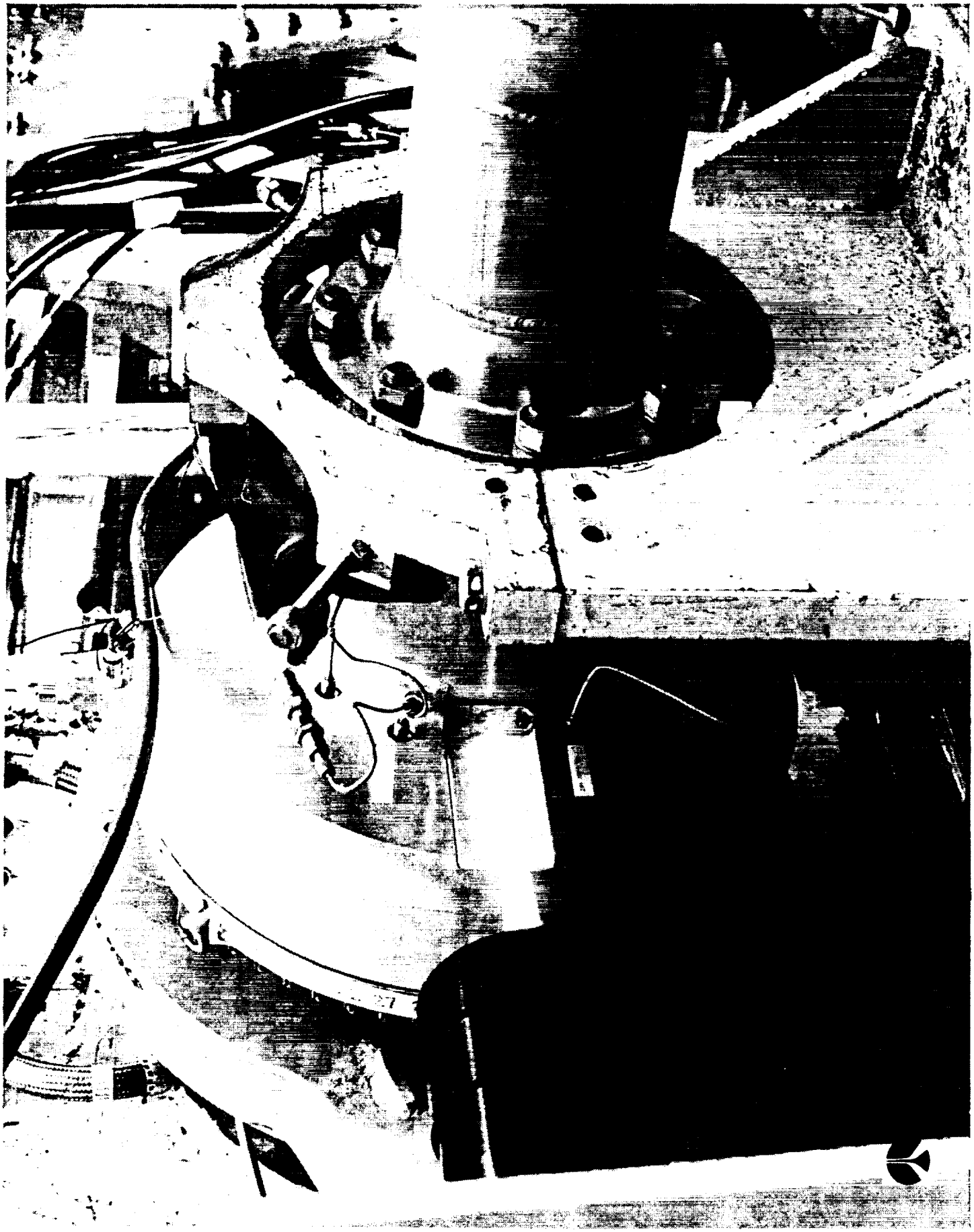

SSME HPFTP IMPELLER
LASER VELOCIMETER DATA SURVEY LOCATIONS

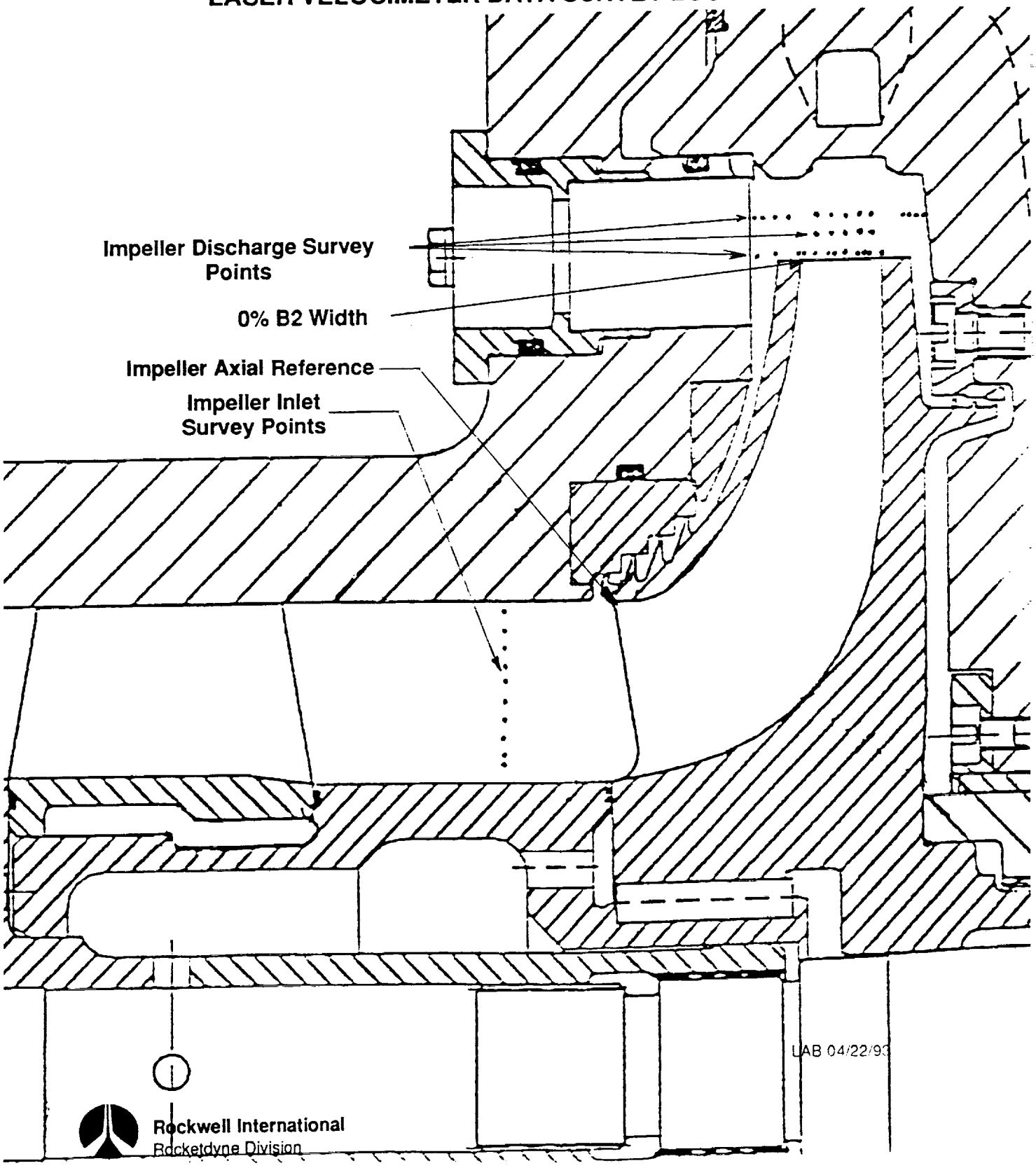

PUMP CFD CODE VALIDATION TESTS
Consortium Baseline Impeller
Laser Velocimeter Data Survey Locations

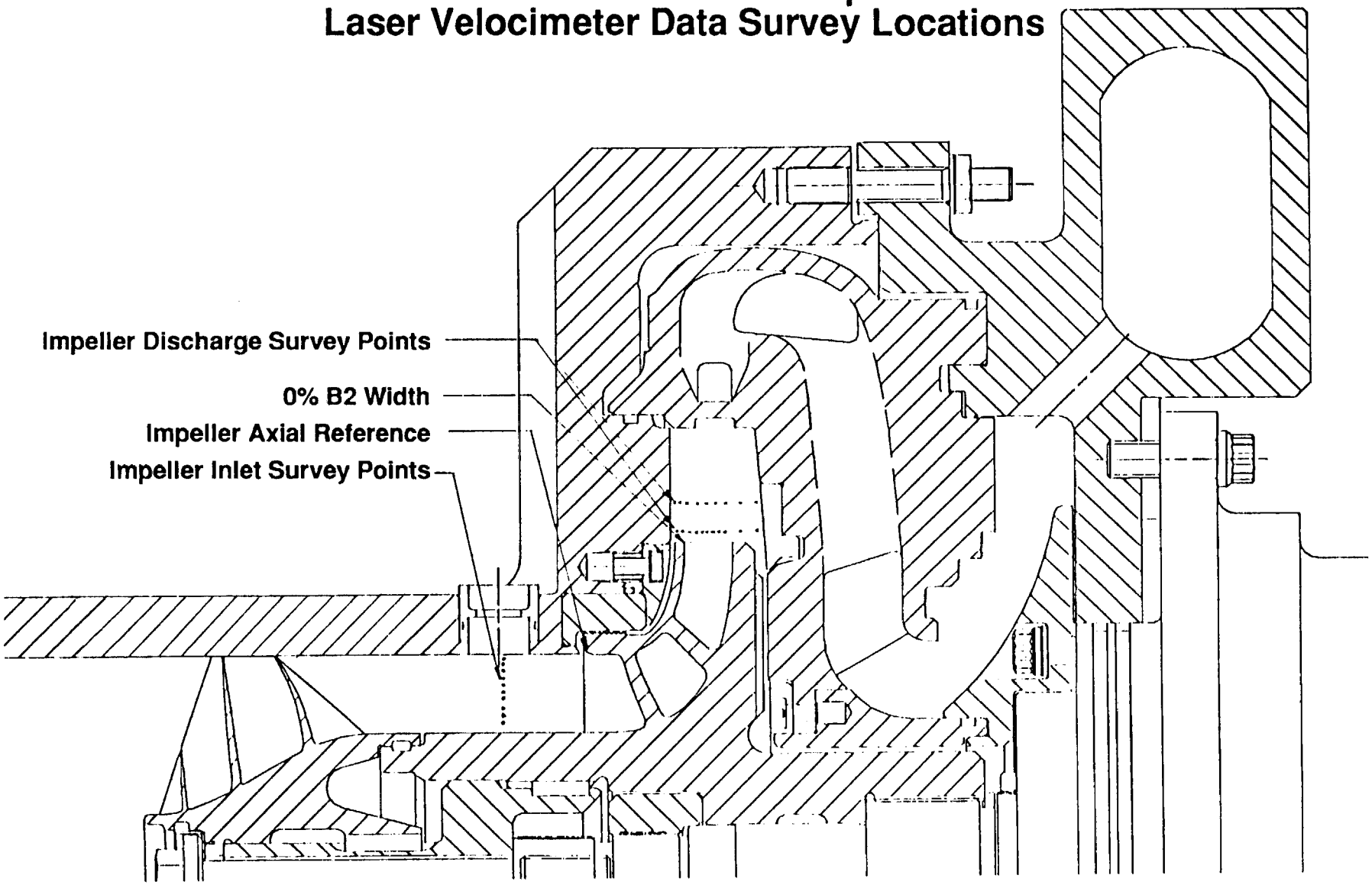

1657

LAB 04/22/93

Rockwell International
Rocketdyne Division

SSME HPFTP IMPELLER
LASER VELOCIMETER DATA SURVEY LOCATIONS

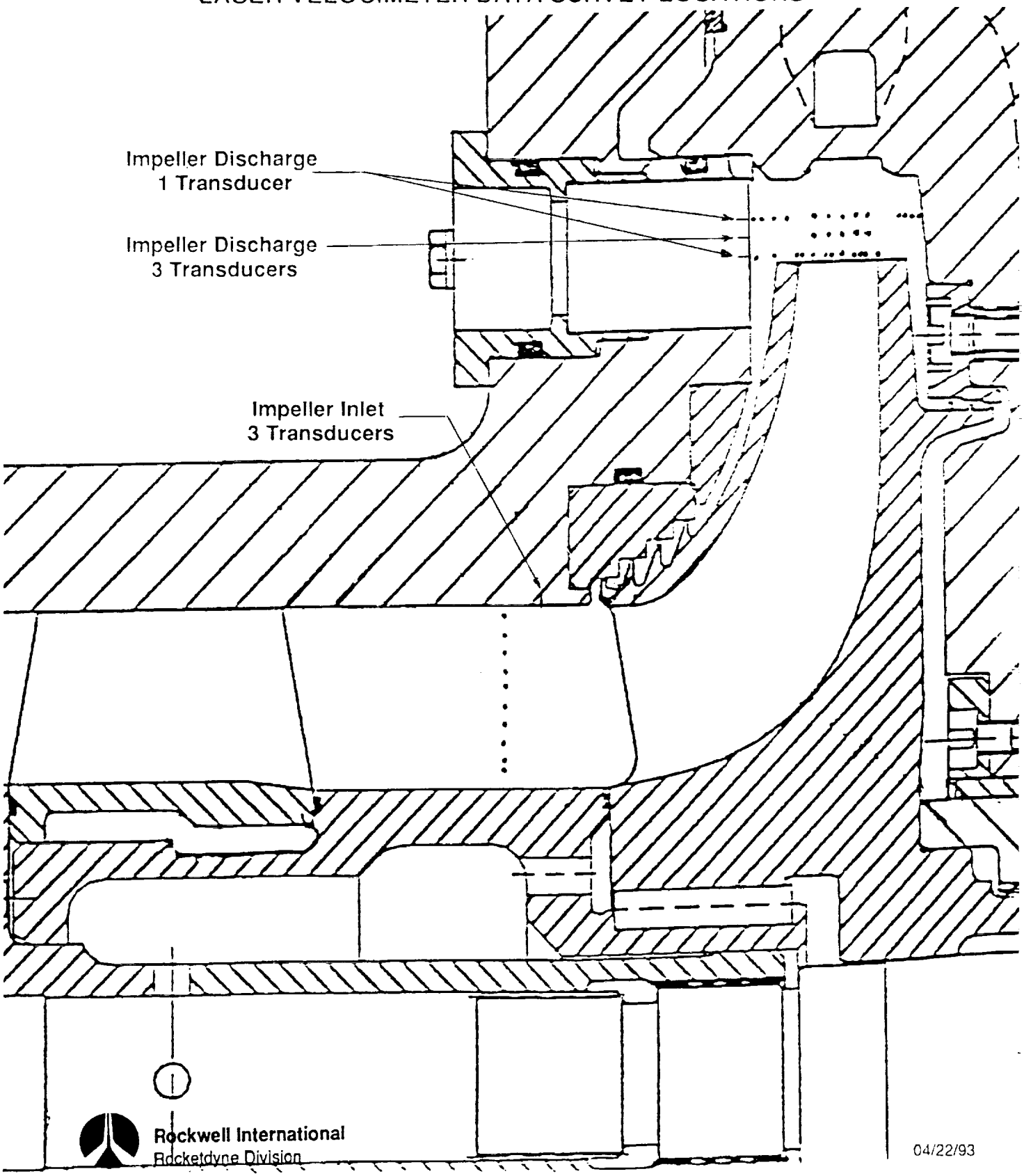

Rockwell International
Rocketdyne Division

04/22/93

CONSORTIUM BASELINE IMPELLER
WALL STATIC PRESSURE MEASUREMENT LOCATIONS

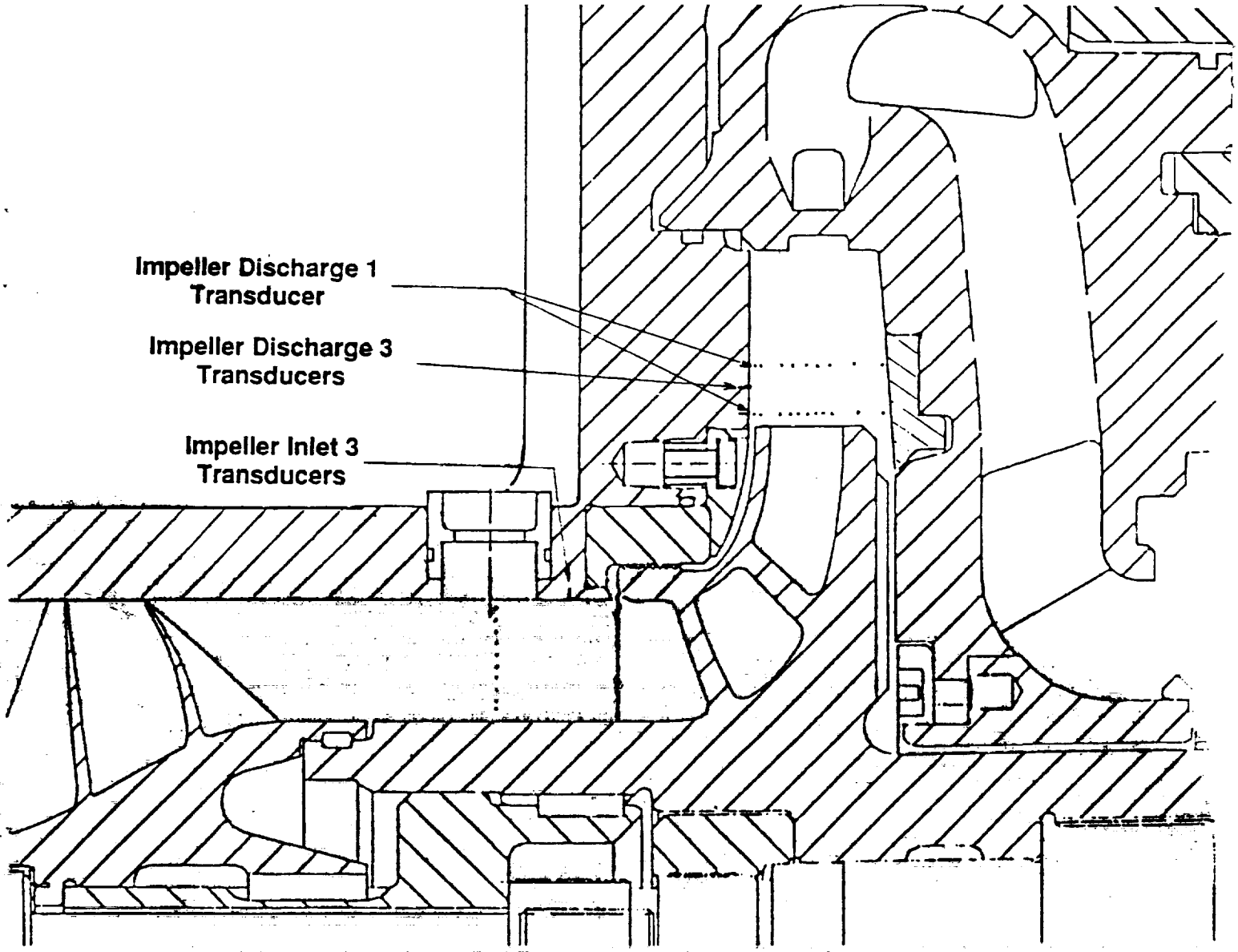

LAB 04/22/93

Rockwell International
Rocketdyne Division

PUMP CFD CODE VALIDATION TESTS
Configurations 1 & 2 Laser Two-Focus Velocimeter Surveys

- Impeller Discharge Survey Data Locations
  - 60 Circumferential full-blade-to-full-blade degrees surveyed
    - 2 Adjacent 30 degree arcs each partitioned into 16 data windows - 1.875 arc degrees
    - Each axial survey referenced circumferentially to impeller discharge timing mark
      - Timing mark between suction and pressure side of blade at impeller tip shroud
  - Data not ensemble averaged
  - Configuration 1 - three radial survey planes
    - Immediately downstream of impeller discharge - 0.5064 nondimensional radius
    - Middle discharge plane - 0.5183 nondimensional radius
    - Diffuser-side discharge plane - 0.5303 nondimensional radius
  - Configuration 2 - two radial survey planes
    - Immediately downstream of impeller discharge - 0.5138 nondimensional radius
    - Diffuser-side discharge plane - 0.5507 nondimensional radius

1660

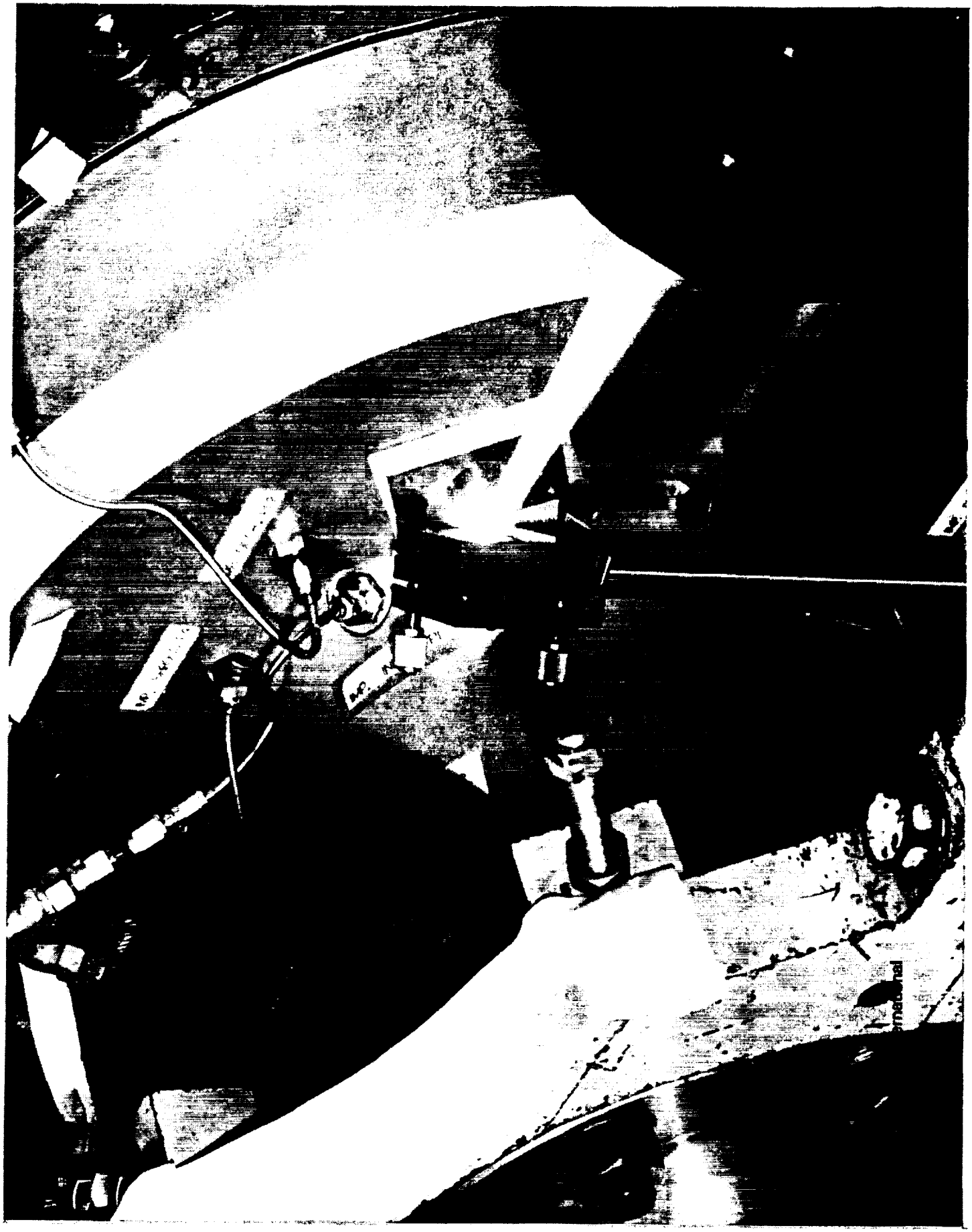


IMP. INLET P1

SSME HPFTP IMPELLER DISCHARGE
LASER VELOCIMETER DATA CIRCUMFERENTIAL REFERENCE

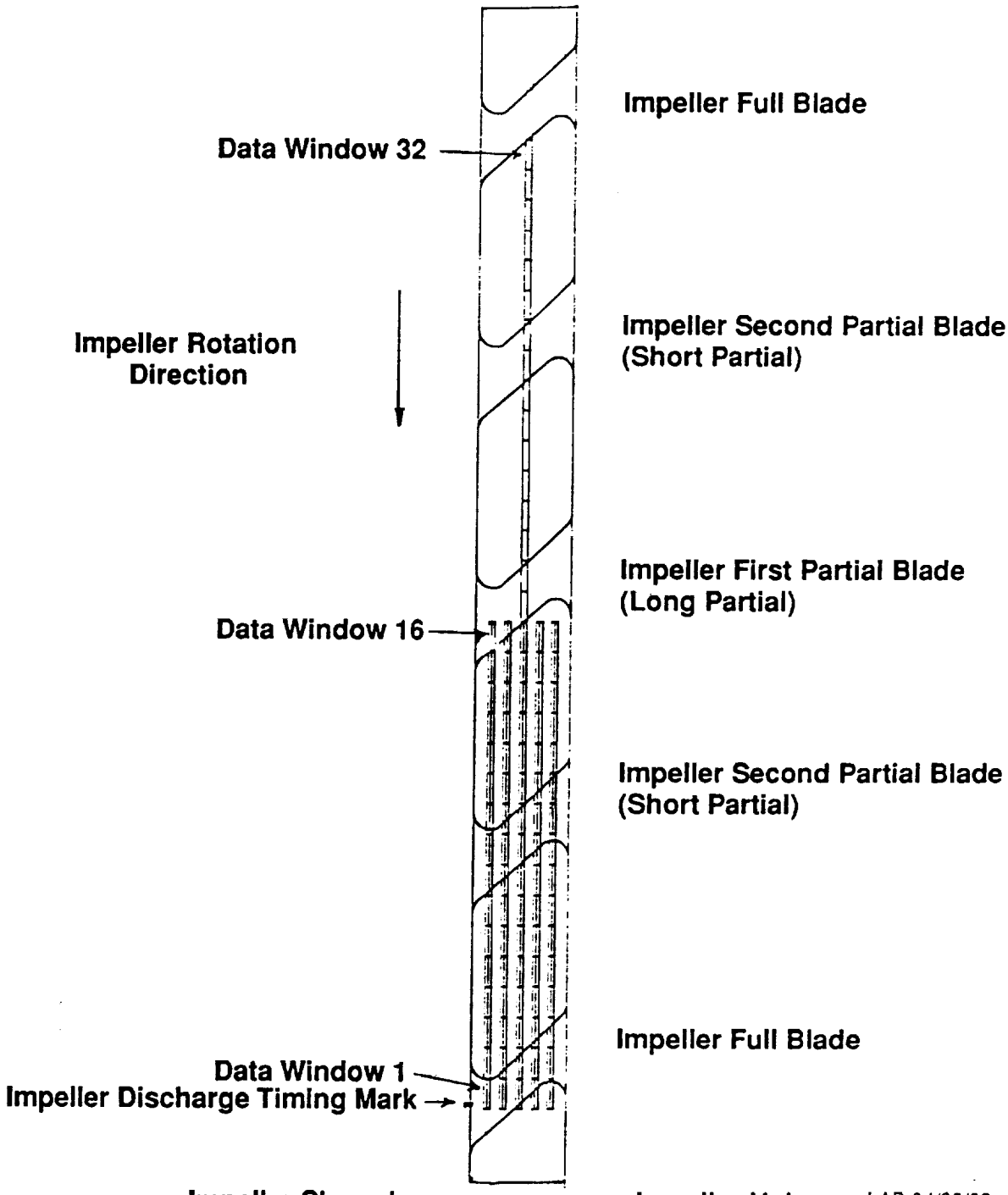

LAB 04/22/93

Rockwell International
Rocketdyne Division

CONSORTIUM BASELINE IMPELLER DISCHARGE LASER VELOCIMETER DATA CIRCUMFERENTIAL POSITIONS

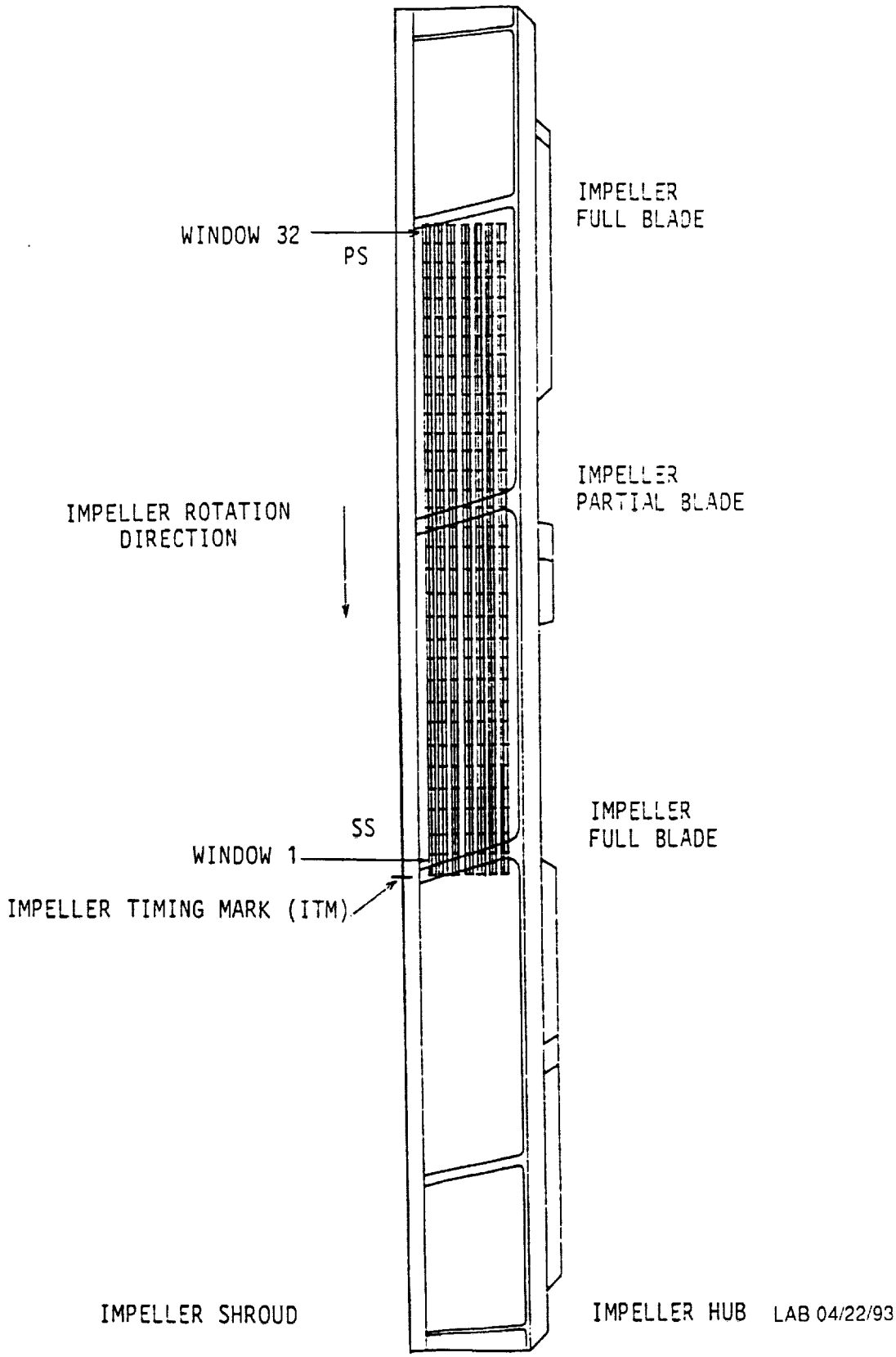

Rockwell International
Rocketdyne Division

PUMP CFD CODE VALIDATION TESTS
Configuration 1 & 2 Laser Two-Focus Velocimeter Surveys

- Axial positions chosen to adequately characterize flow
  - Configuration 1
    - Impeller discharge plane - 12 axial positions across B2 width and shroud side
    - Middle plane - 5 positions across B2 width
    - Diffuser-side plane - 13 axial positions across entire channel width
  - Configuration 2
    - Impeller discharge plane - 11 axial positions across channel, 7 within B2 width
    - Diffuser-side plane - 9 axial positions across channel, 5 within B2 width

PUMP CFD CODE VALIDATION TESTS

LASER VELOCIMETER RESULTS

CONFIGURATION 1 - SSME HPFTP IMPELLER

1666

LAB 04/22/93

Rockwell International
Rocketdyne Division

PUMP CFD CODE VALIDATION TESTS
Configuration 1 - Laser Velocimeter Survey

- Data Integrity Checks
  - Flow continuity
    - Impeller inlet plane - 98.6%
  - Circumferential variation
    - Impeller inlet circumferential pressure variations within transducer accuracy
    - Impeller discharge middle plane exhibits minimal pressure variation
    - Adjacent impeller discharge passages exhibit similar flow velocities and angles
  - Test conditions monitored over entire laser survey duration - repeatability shown

1667

PUMP CFD CODE VALIDATION TESTS
SSME HPFTP Impeller Inlet Laser Survey

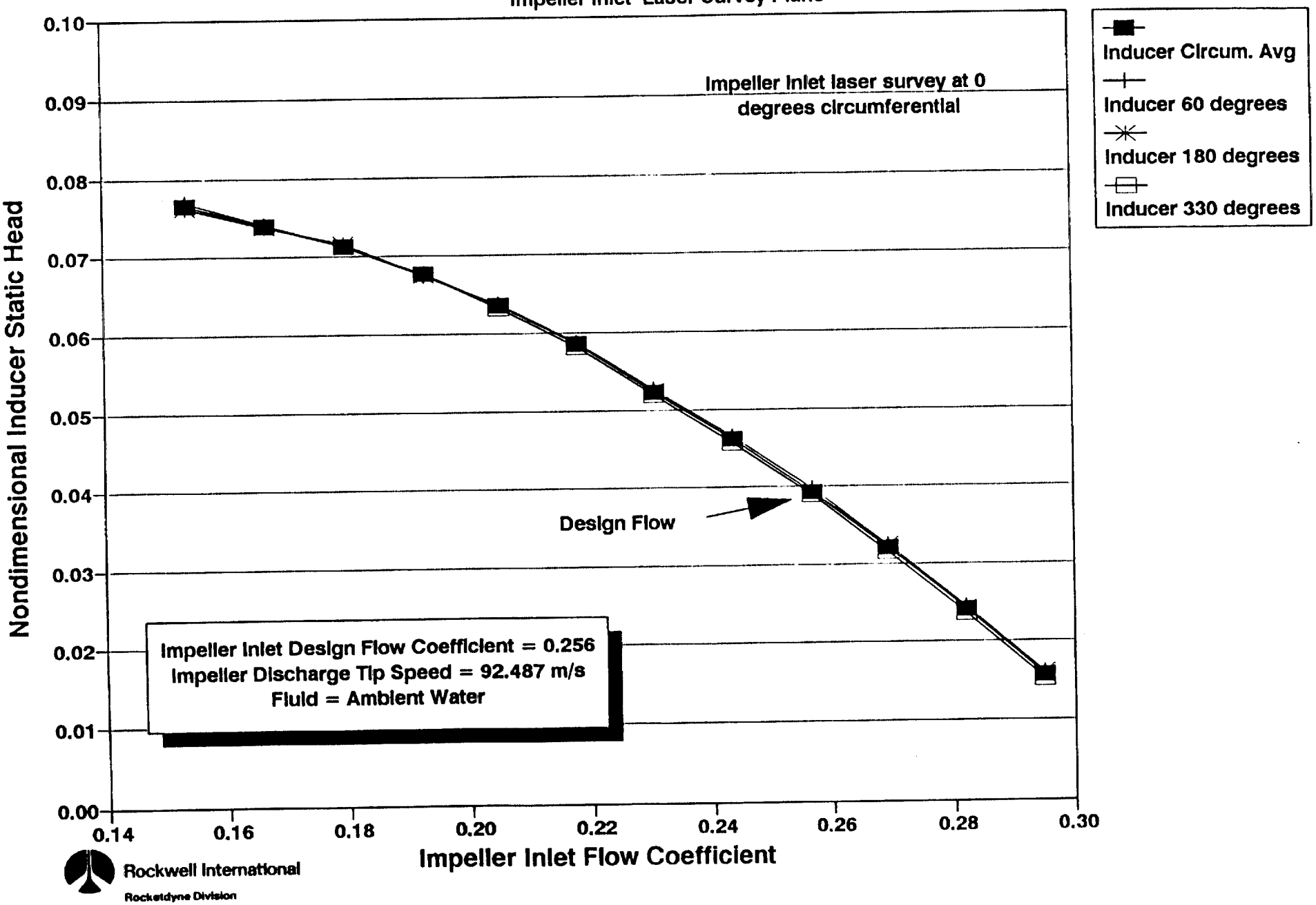

Rockwell International
Rocketdyne Division

1668

PUMP CFD CODE VALIDATION TESTS
SSME HPFTP Impeller Inlet Laser Survey

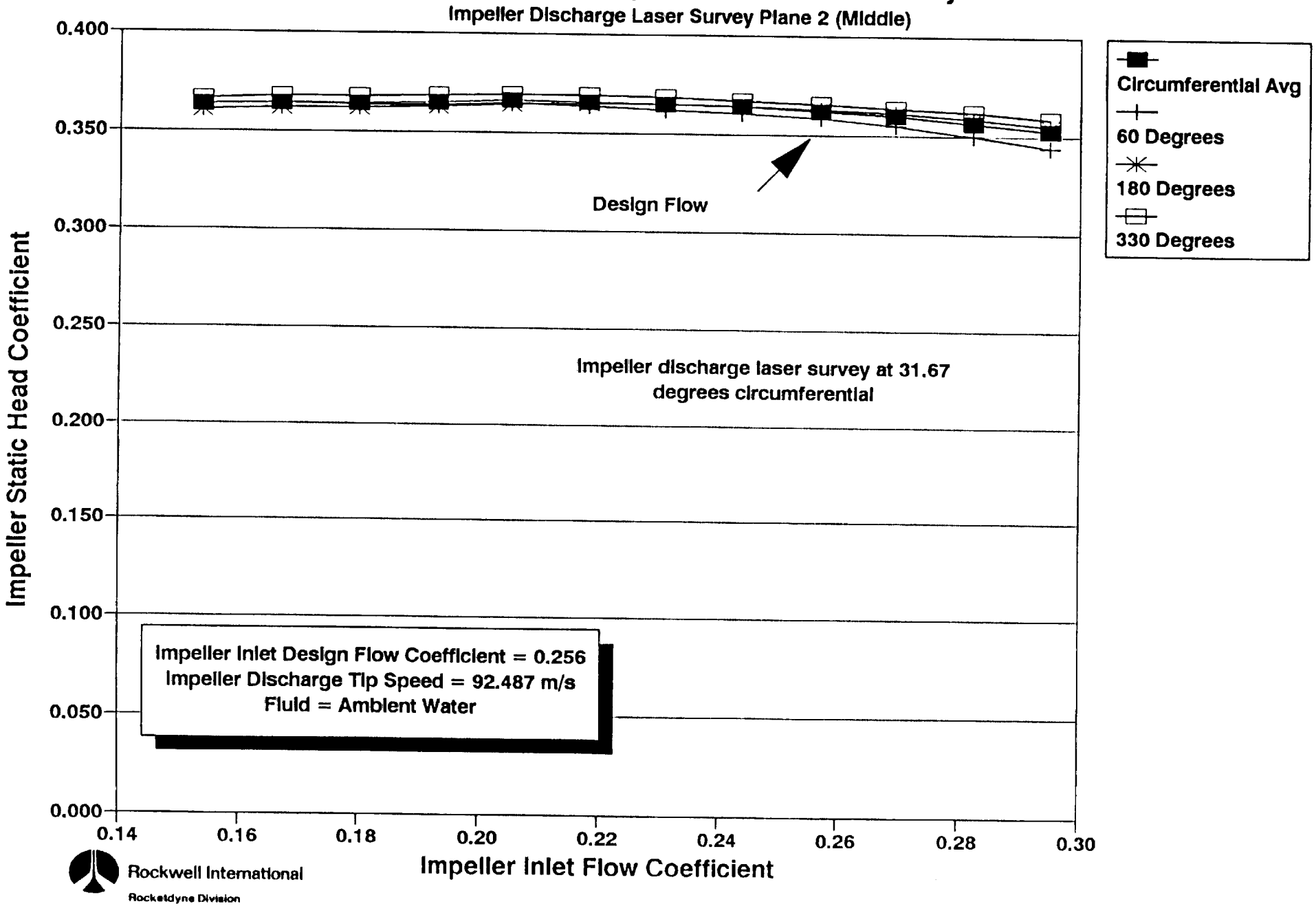

1669

PUMP CFD CODE VALIDATION TESTS
SSME HPFTP Impeller Discharge Laser Survey Plane 1 (Impeller)
Test Impeller Inlet Flow Coefficient = 0.256

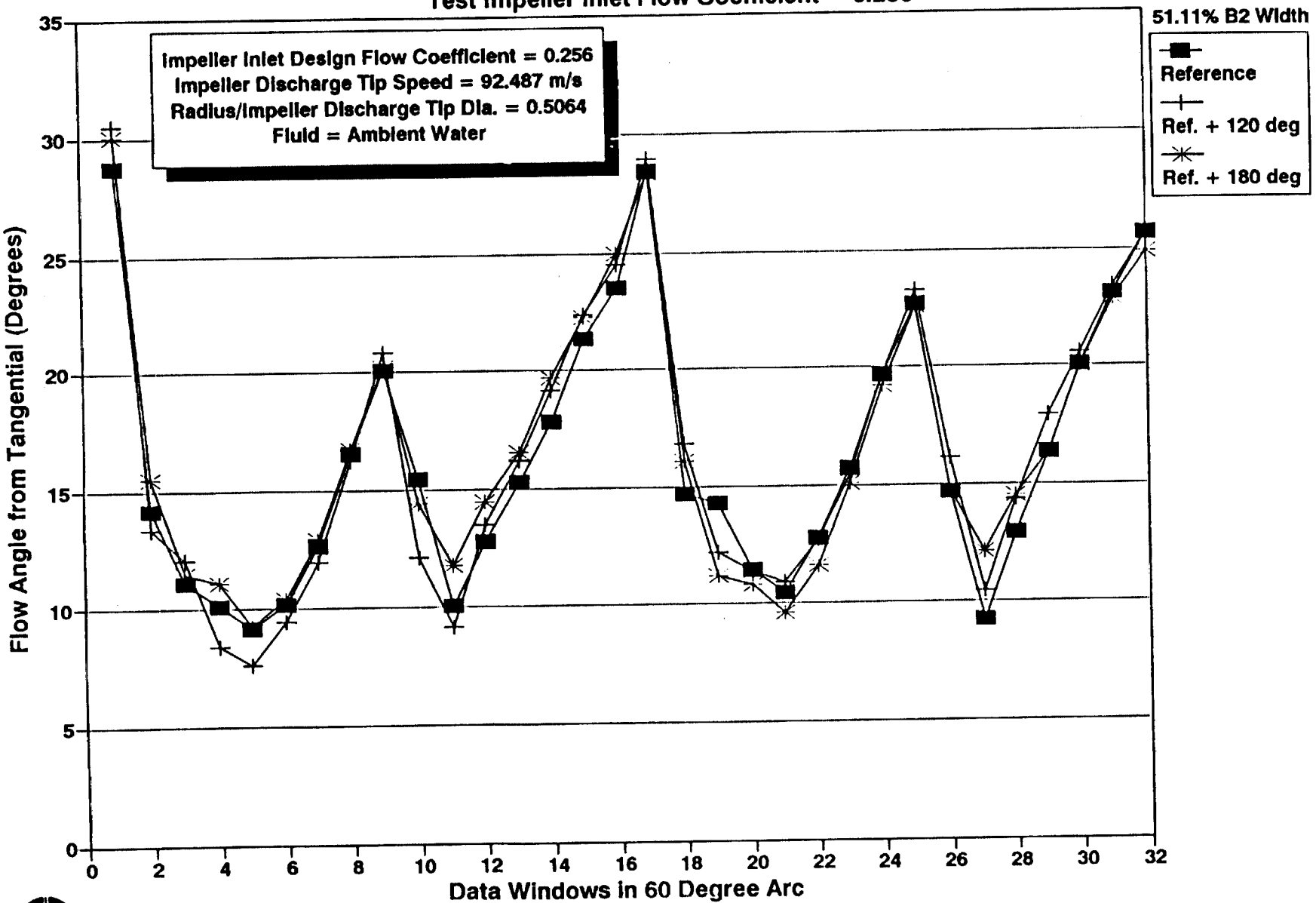

Rockwell International
Rocketdyne Division

PUMP CFD CODE VALIDATION TESTS
SSME HPFTP Impeller Discharge Laser Survey Plane 1 (Impeller)
Test Impeller Inlet Flow Coefficient = 0.256

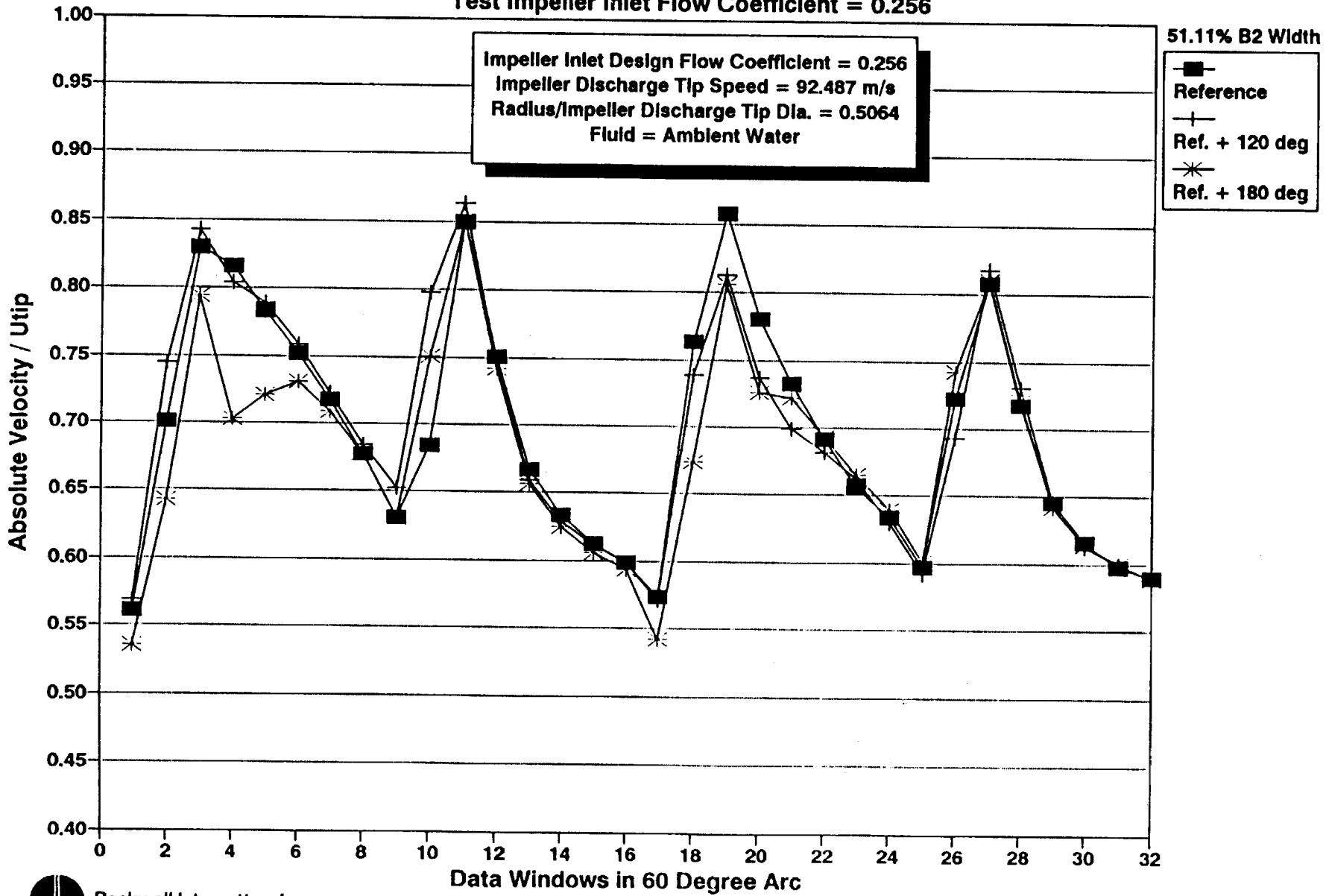

Rockwell International
Rocketdyne Division

PUMP CFD CODE VALIDATION TESTS
SSME HPFTP Impeller Inlet Laser Survey
Test Impeller Inlet Flow Coefficient = 0.256

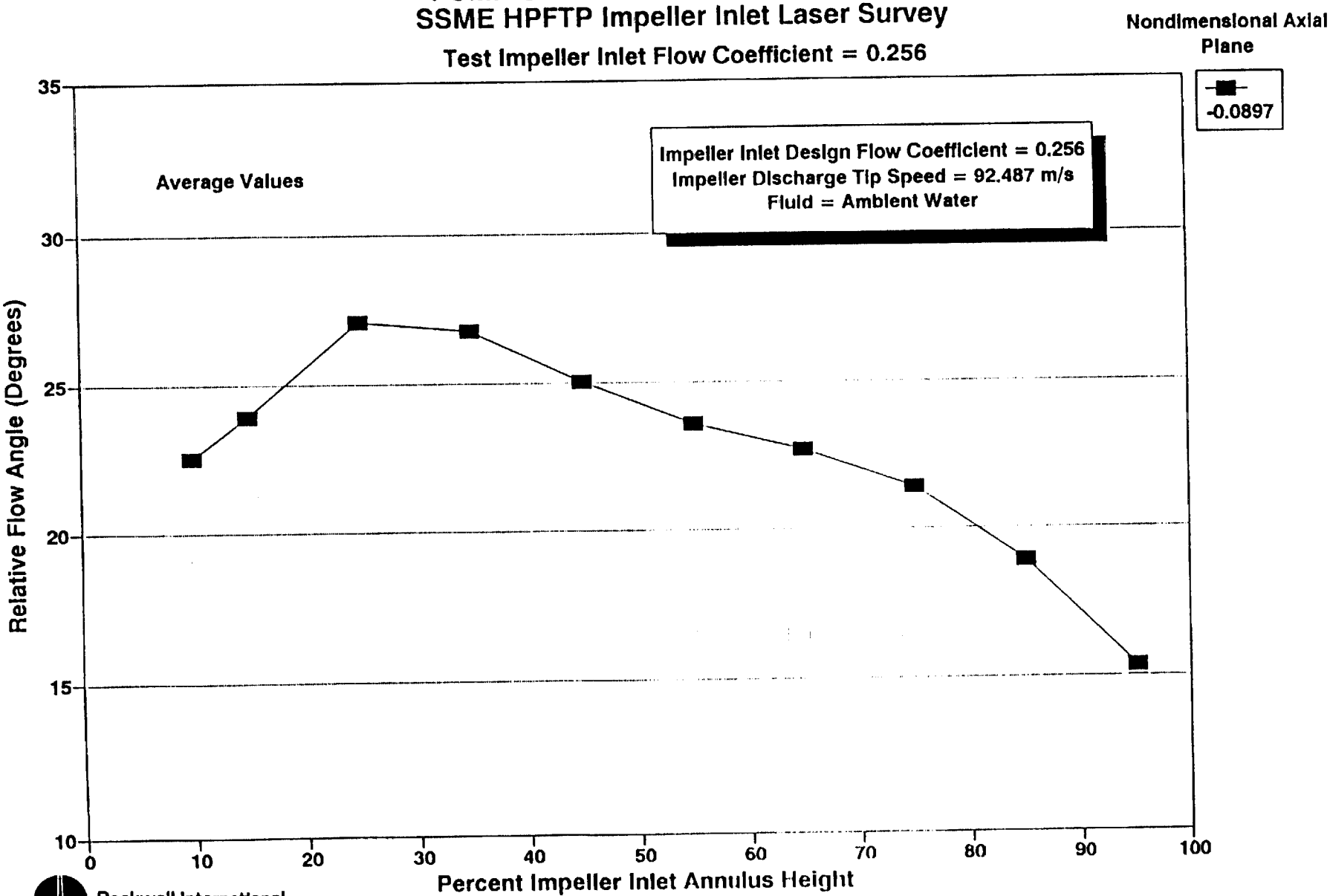

Rockwell International
Rocketdyne Division

PUMP CFD CODE VALIDATION TESTS
SSME HPFTP Impeller Inlet Laser Survey
Test Impeller Inlet Flow Coefficient = 0.256

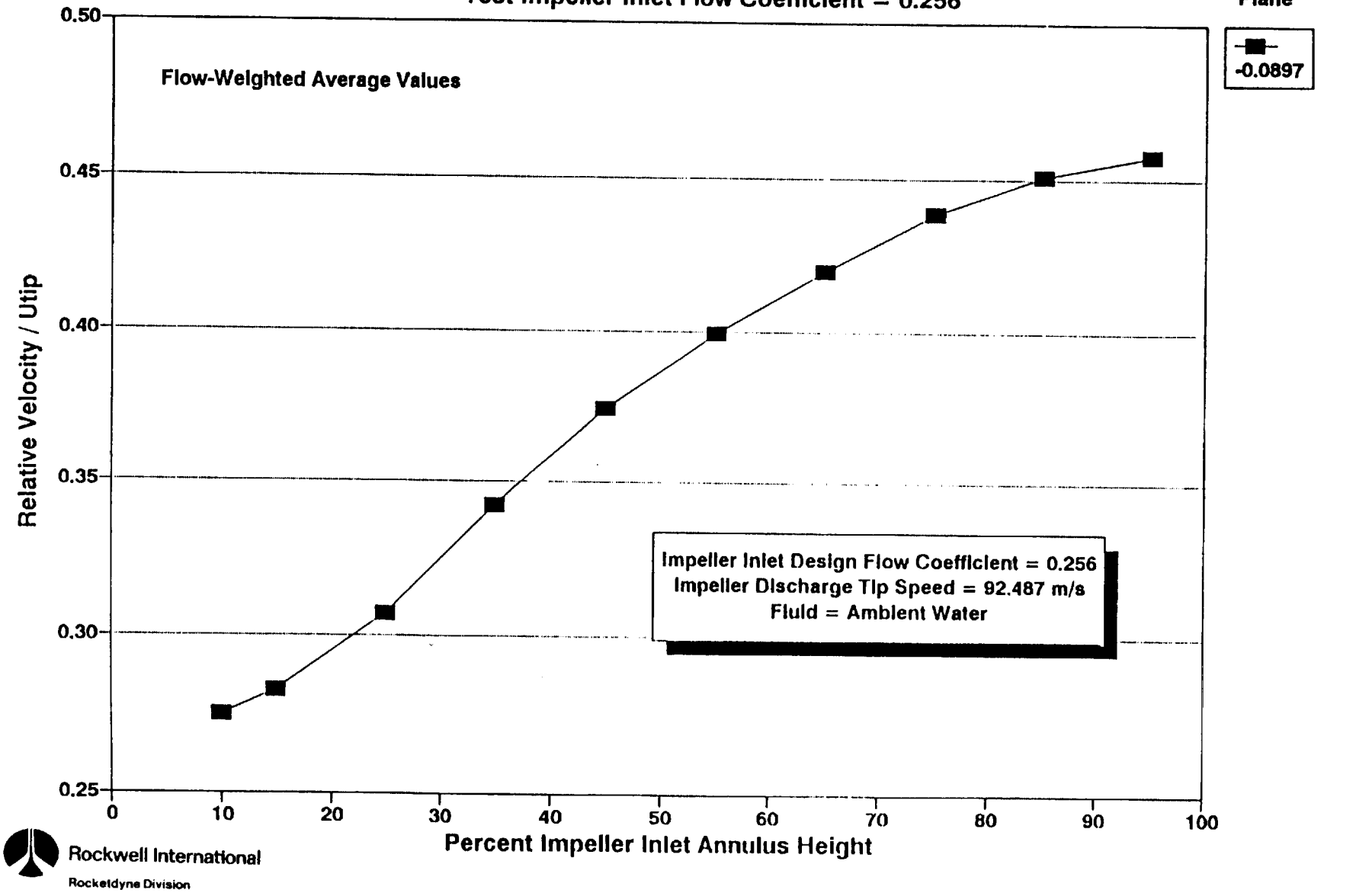

Rockwell International
Rocketdyne Division

11 INCH SSME HPFTP IMPELLER
LASER VELOCIMETER TEST DATA

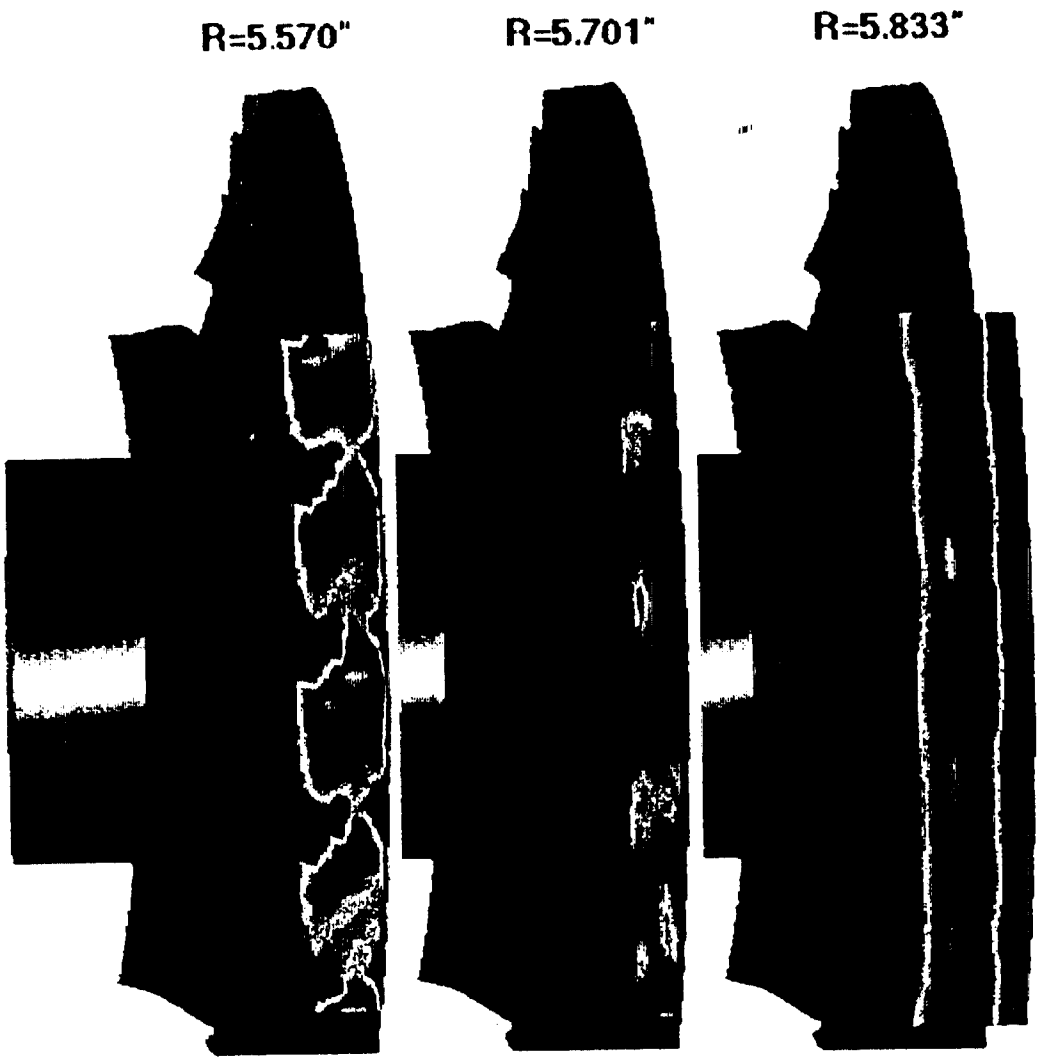

Rockwell International
Rocketdyne Division

11 INCH SSME HPFTP IMPELLER
LASER VELOCIMETER TEST DATA

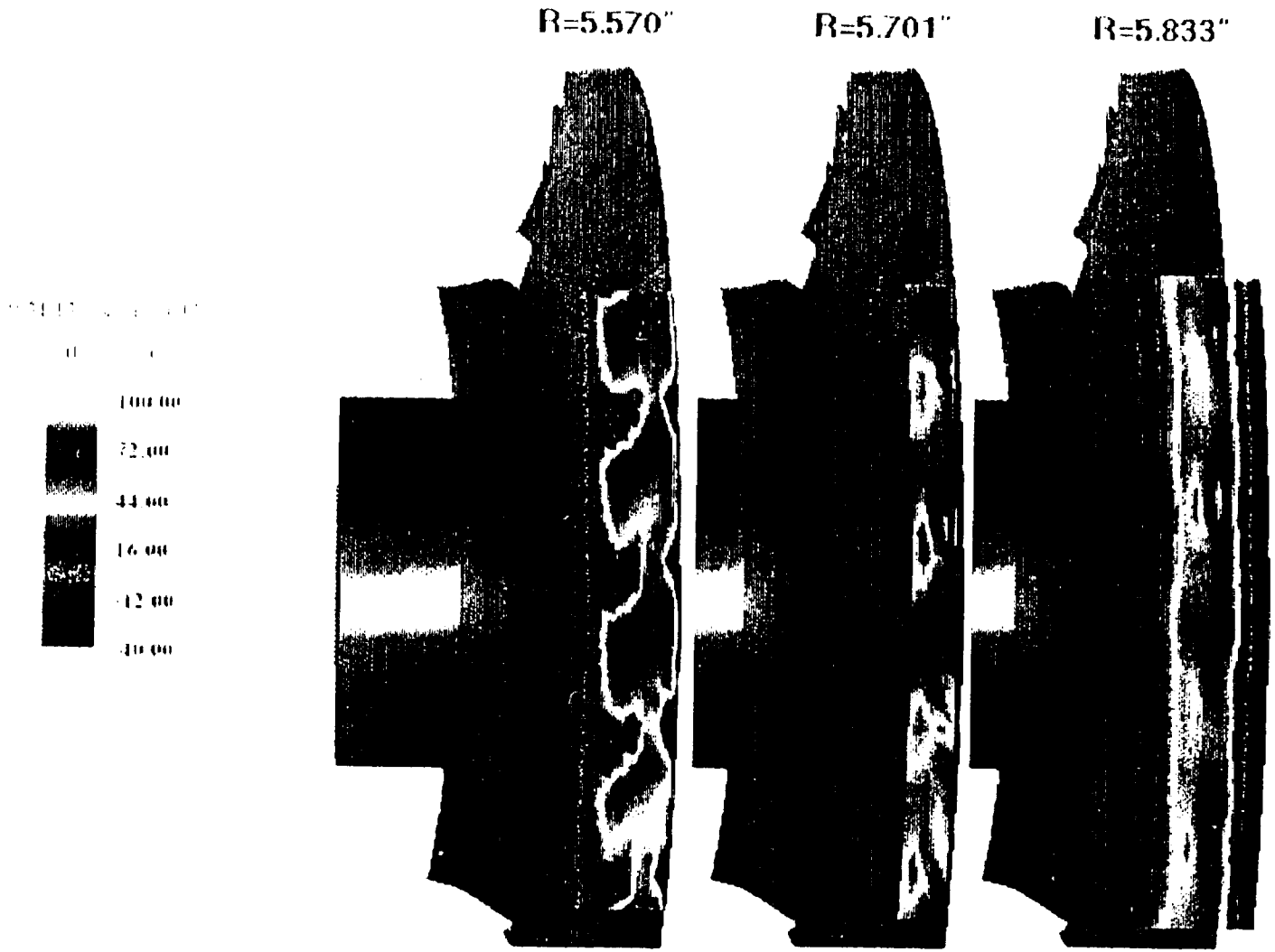

Rockwell International
Rocketdyne Division

PUMP CFD CODE VALIDATION TESTS

LASER VELOCIMETER RESULTS

CONFIGURATION 2 - PUMP CONSORTIUM BASELINE IMPELLER

1676

LAB 04/22/93

Rockwell International
Rocketdyne Division

PUMP CFD CODE VALIDATION TESTS
Configuration 2 - Laser Velocimeter Survey

- Data Integrity Checks
  - Flow continuity
    - Impeller inlet plane - 98.2%
  - Circumferential variation
    - Impeller inlet circumferential pressure variations within transducer accuracy
    - Adjacent impeller inlet passages exhibit similar flow velocities and angles
    - Impeller discharge middle plane exhibits minimal pressure variation
    - Adjacent impeller discharge passages exhibit similar flow velocities and angles
  - Test conditions monitored over entire laser survey duration - repeatability shown

PUMP CFD CODE VALIDATION TESTS
Consortium Baseline Imp. Inlet Survey
Impeller Inlet Laser Survey Plane

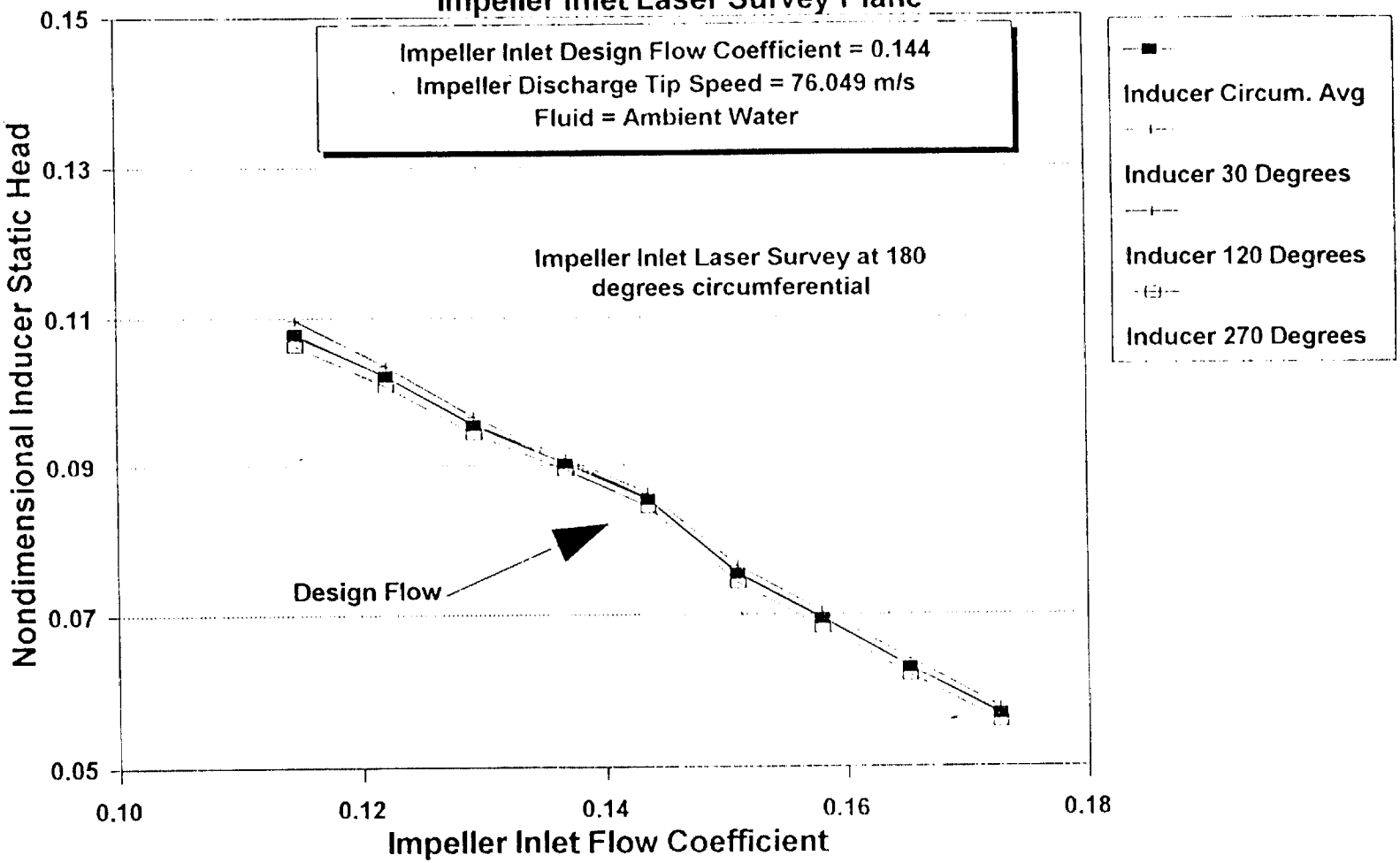

PUMP CFD CODE VALIDATION TESTS
Consortium Baseline Imp. Inlet Survey
Impeller Discharge Laser Survey Plane 2 (Middle)

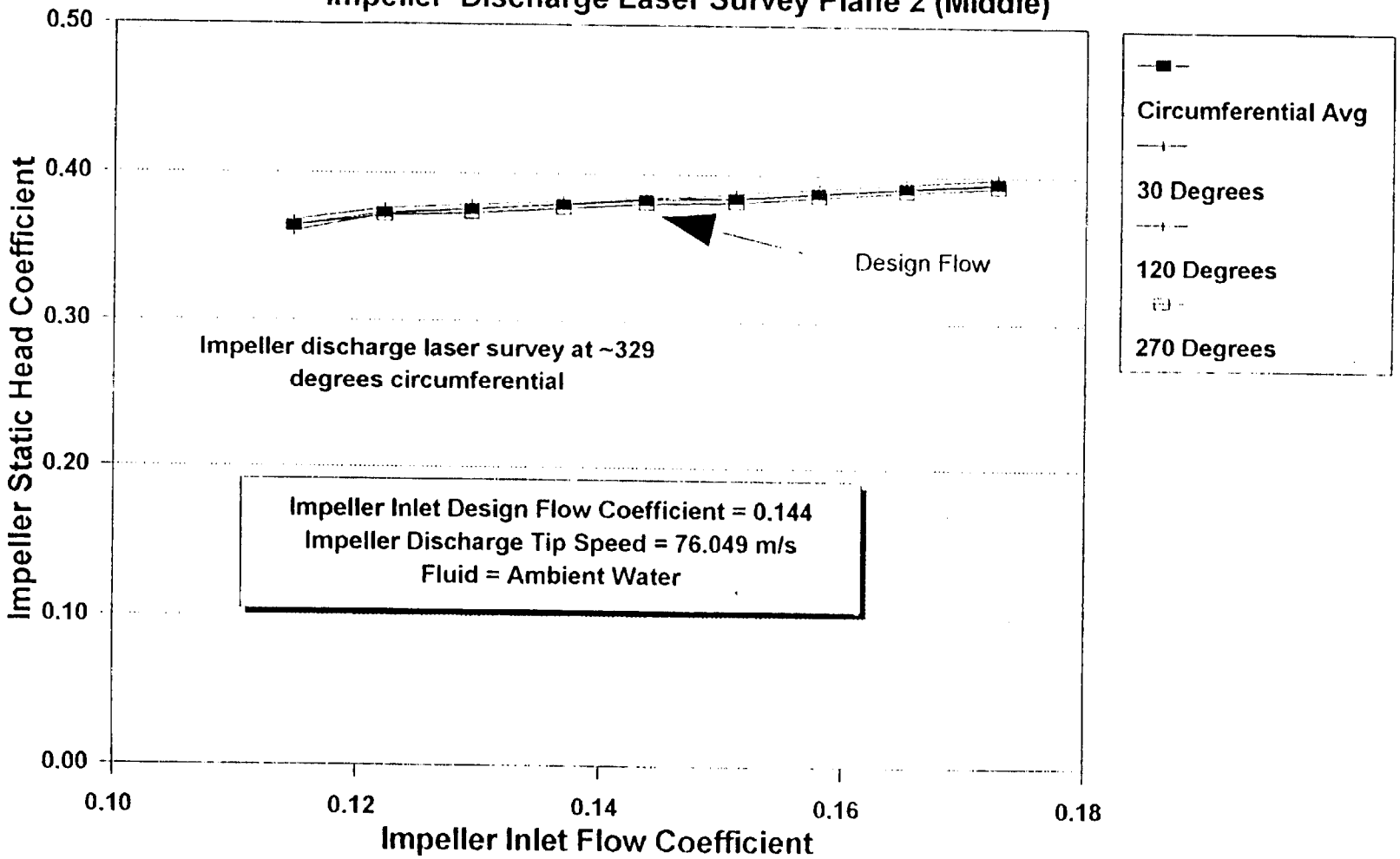

Rockwell International
Rocketdyne Division

PUMP CFD CODE VALIDATION TESTS

Consortium Baseline Imp. Inlet Survey

Test Impeller Inlet Flow Coefficient = 0.144

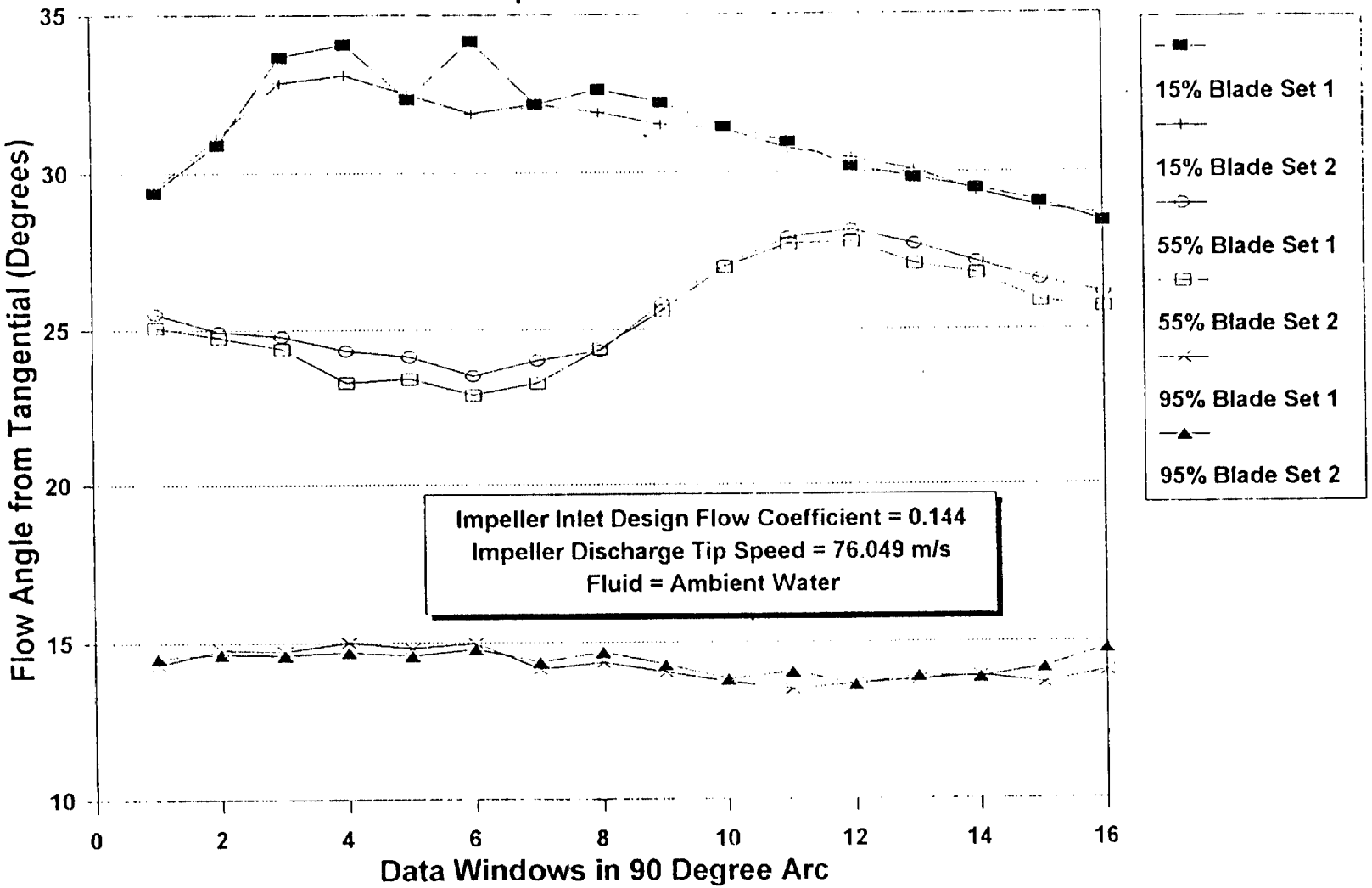

Rockwell International
Rocketdyne Division

PUMP CFD CODE VALIDATION TESTS
Consortium Baseline Imp. Inlet Survey
Test Impeller Inlet Flow Coefficient = 0.144

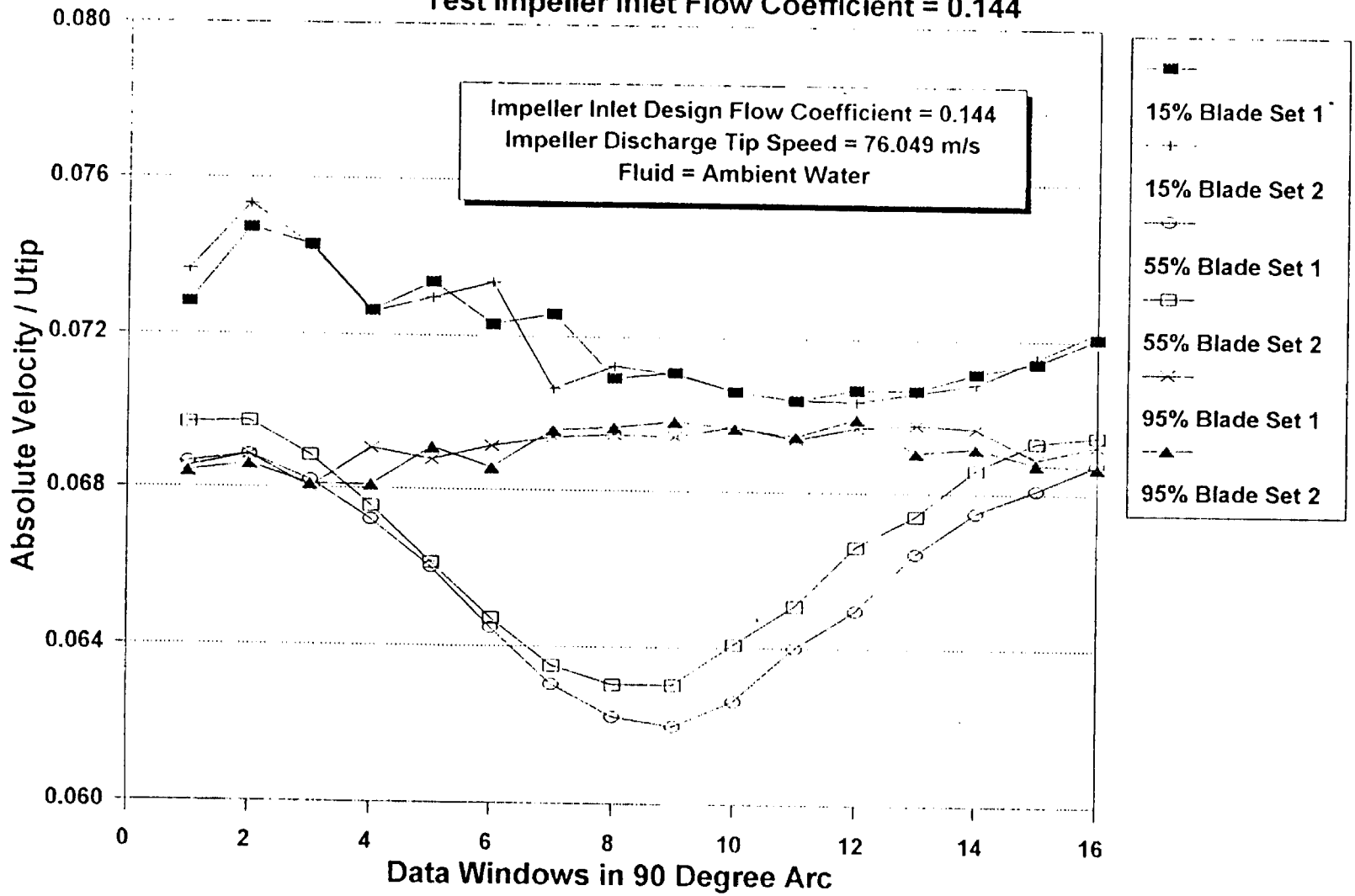

Rockwell International
Rocketdyne Division

PUMP CFD CODE VALIDATION TESTS

Consortium Baseline Imp. Discharge Laser (Impeller)

Test Impeller Inlet Flow Coefficient = 0.144

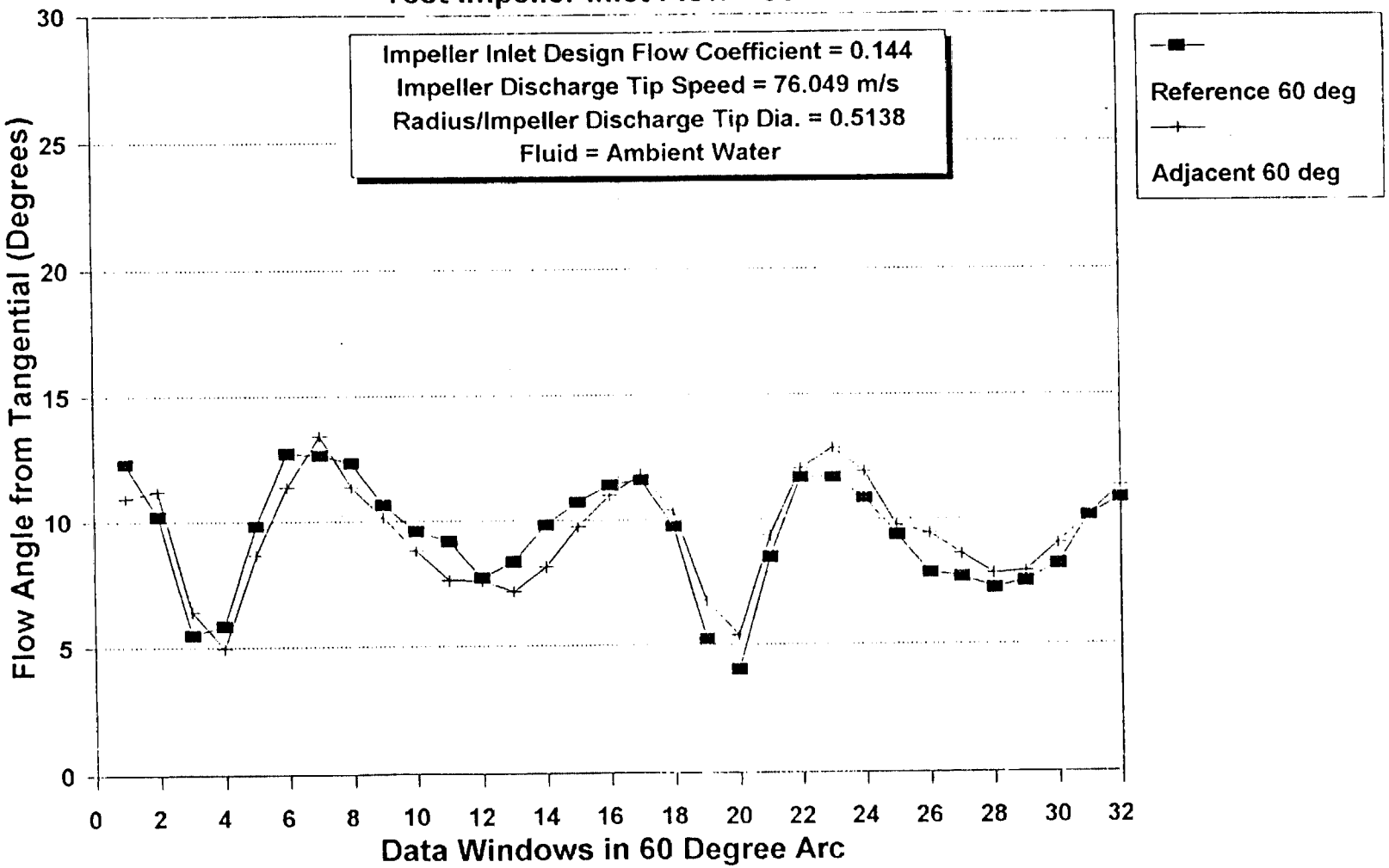

Rockwell International
Rocketdyne Division

PUMP CFD CODE VALIDATION TESTS

Consortium Baseline Imp. Discharge Survey (Impeller)

Test Impeller Inlet Flow Coefficient = 0.144

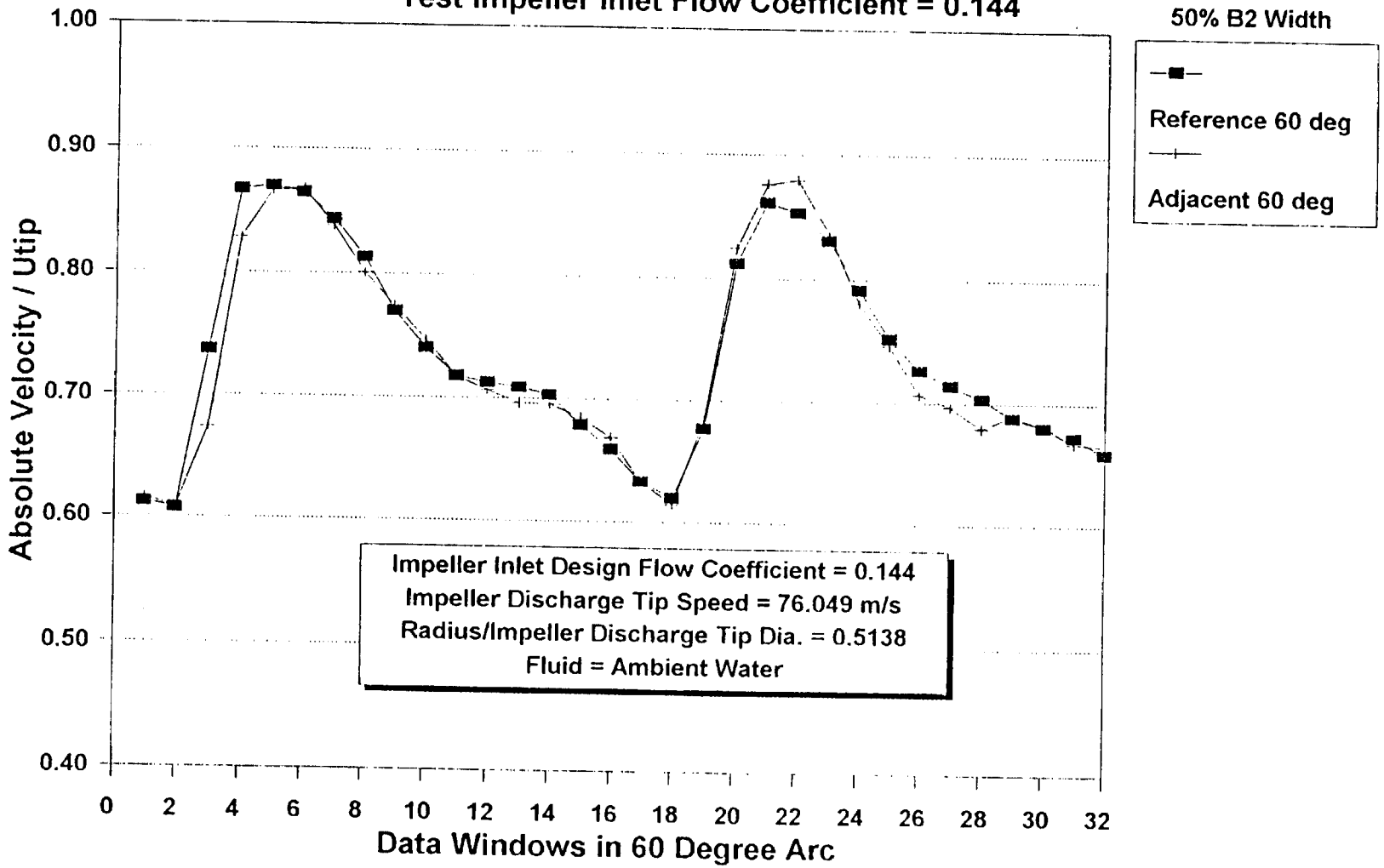

Rockwell International
Rocketdyne Division

PUMP CFD CODE VALIDATION TESTS
Consortium Baseline Imp. Inlet Survey
Test Impeller Inlet Flow Coefficient = 0.144

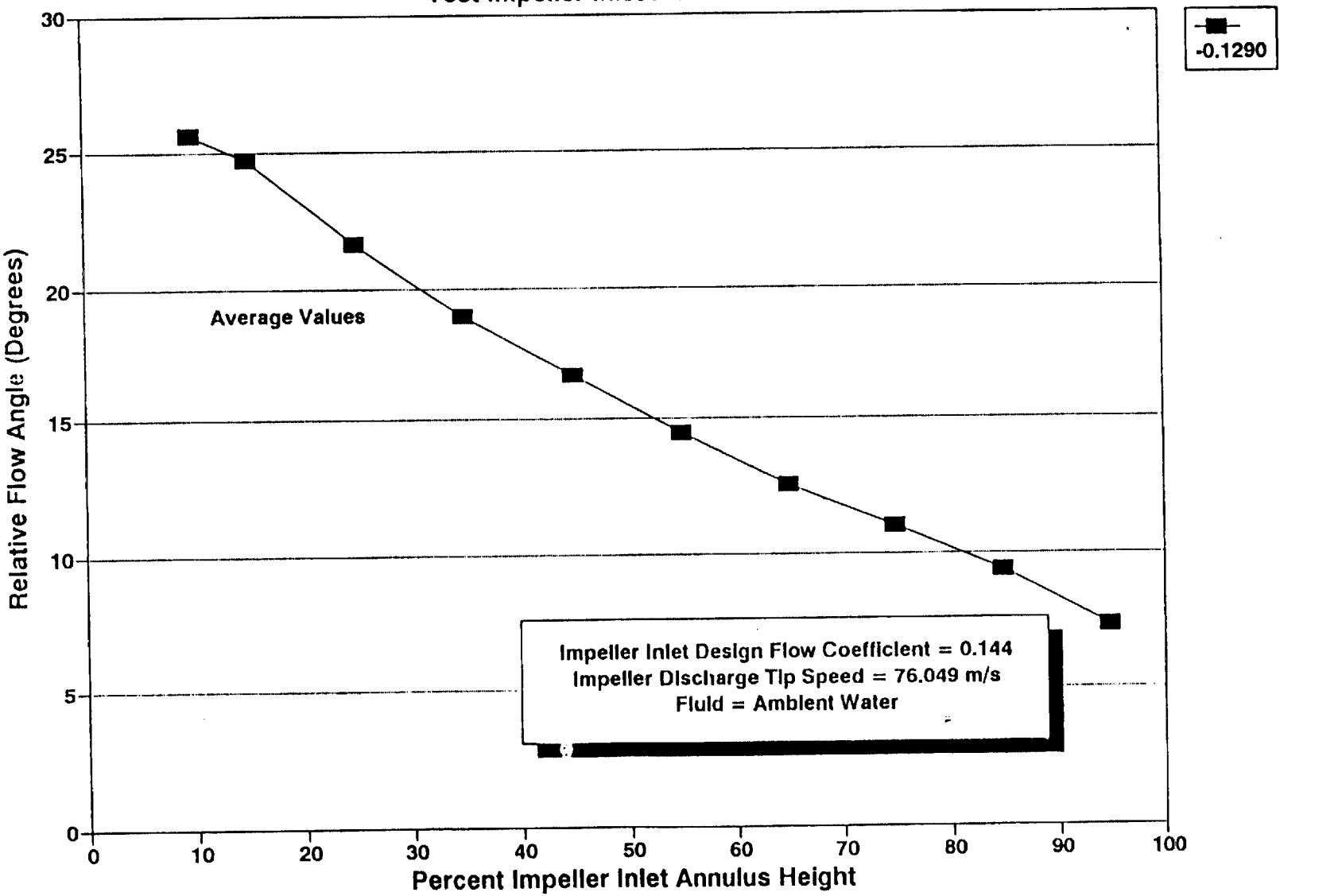

Rockwell International
Rocketdyne Division

PUMP CFD CODE VALIDATION TESTS
Consortium Baseline Imp. Inlet Survey
Test Impeller Inlet Flow Coefficient = 0.144

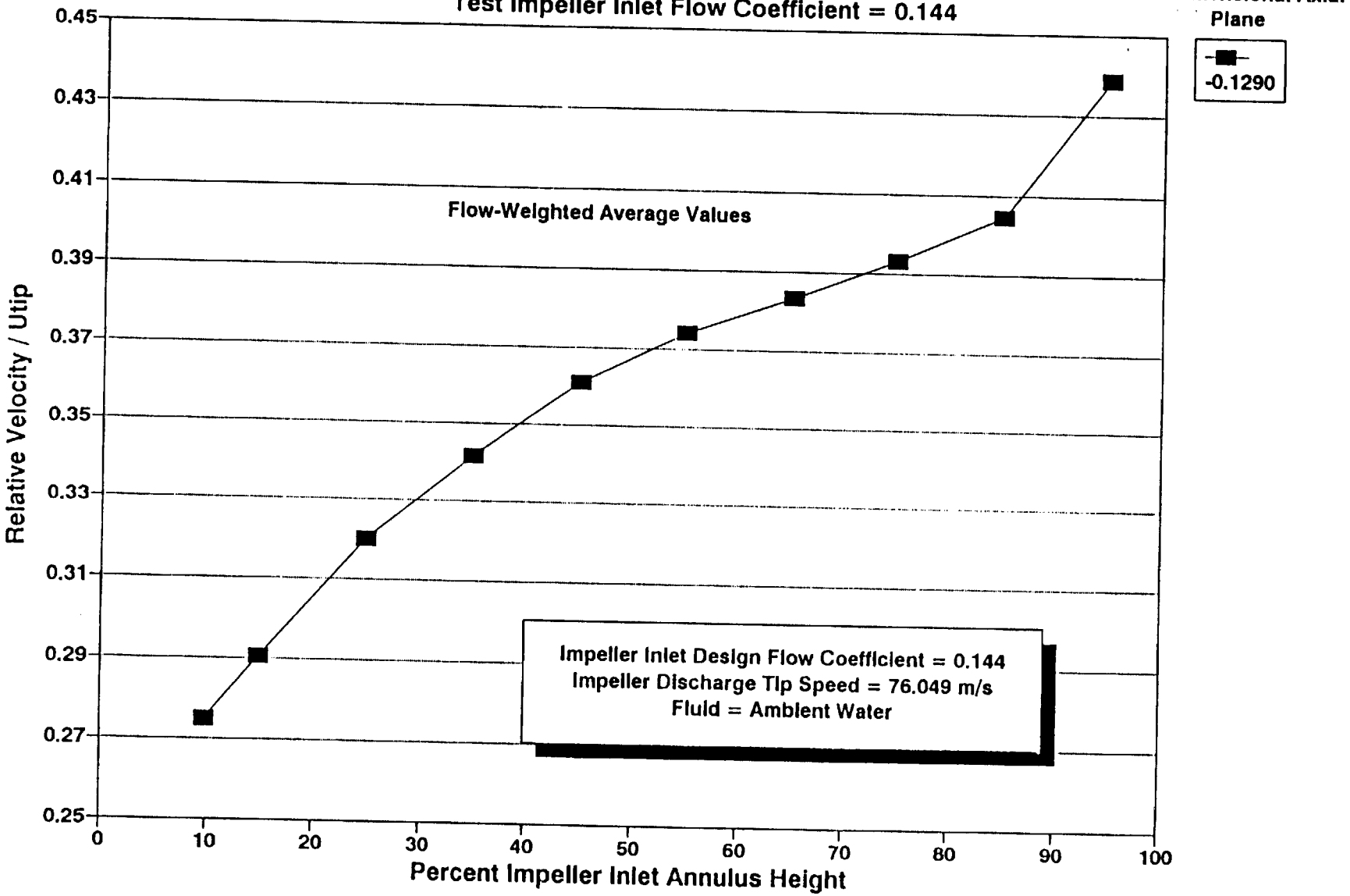

Rockwell International
Rocketdyne Division

PUMP CFD CODE VALIDATION TESTS

Consortium Baseline Impeller Discharge Laser Survey

Nondimensional Radial Planes 0.5138, 0.5597, Impeller Inlet Flow Coefficient = 0.144

Absolute Flow Angle From Tangential (Degrees)

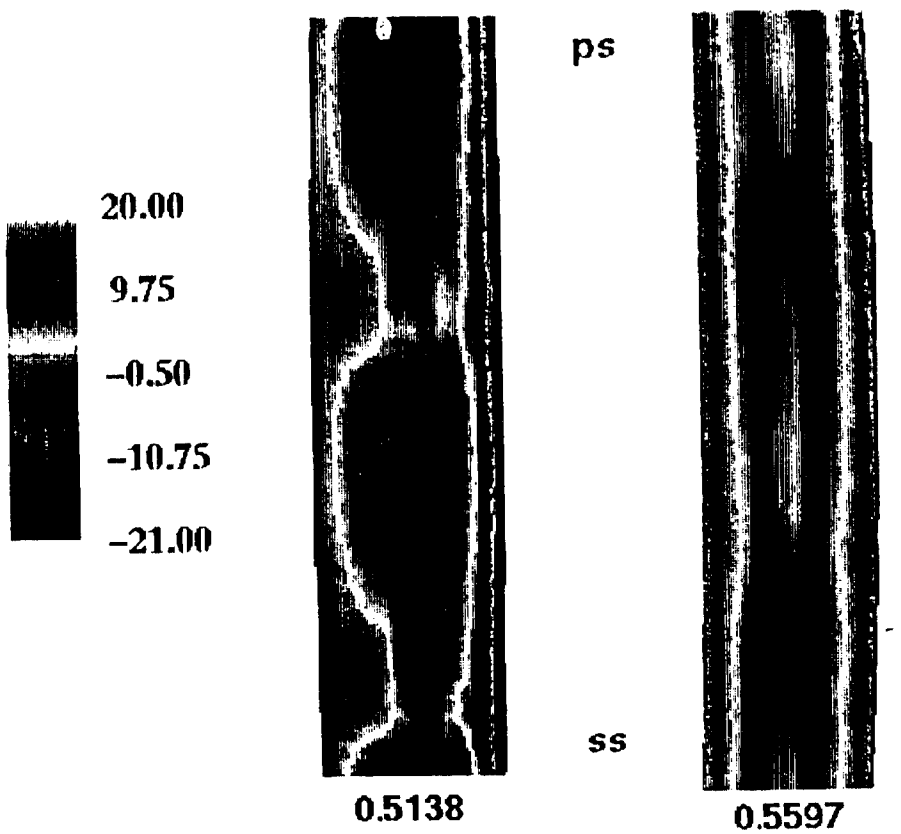

1686

Rockwell International
Rocketdyne Division

PUMP CFD CODE VALIDATION TESTS

Consortium Baseline Impeller Discharge Laser Survey

Nondimensional Radial Planes 0.5138, 0.5597, Impeller Inlet Flow Coefficient = 0.144

Nondimensional Absolute Velocity C

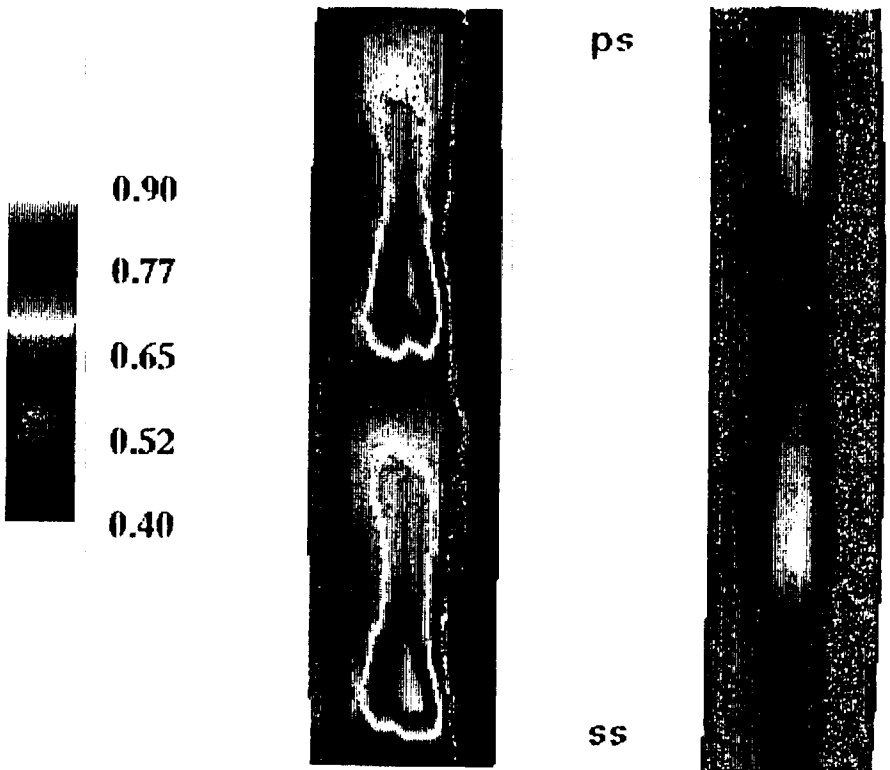

Rockwell International
Rocketdyne Division

PUMP CFD CODE VALIDATION TESTS
Conclusion

- Test Program Provides Essential Impeller Flow Data
  - Detailed blade-to-blade flow characterization obtained
  - Quality of laser velocimeter data substantiated
    - No significant impeller discharge circumferential variation
    - Test operating conditions demonstrated time independence
    - Impeller laser surveys exhibited blade passage independence
    - Impeller inlet flow continuity matches reinforces laser data accuracy
  - Data available in PLOT3D format

Detailed Measurements in the SSME High Pressure Fuel Turbine with Smooth Rotor Blades

Susan T. Hudson
NASA-Marshall Space Flight Center
ED34/Experimental Fluid Dynamics Branch
Huntsville, AL 35812

Abstract

Several tests of the Rocketdyne configuration of the Space Shuttle Main Engine (SSME) High Pressure Fuel Turbopump (HPFTP) Turbine have been completed in the Turbine Test Equipment (TTE) at Marshall Space Flight Center. The tests involved using scaled performance parameters and model measurements to predict the performance of the turbine. The overall performance has been the primary objective of the tests to date, but more detailed measurements are also of interest. During the most recent test of the Rocketdyne configuration of the HPFTP turbine with smooth rotor blades, several different measurement techniques were used to study the turbine inlet and exit velocity profiles, boundary layer thicknesses, turbulence intensities, etc. Data has been obtained using various hot film probes and three-hole cobra probes. Laser Velocimeter measurements were also made. The test plan and test data will be presented and discussed as well as lessons learned on how to obtain the various types of data.

Detailed Measurements in the SSME High Pressure Fuel Turbine with Smooth Rotor Blades

11th Workshop for Computational Fluid Dynamic Applications in Rocket Propulsion
Marshall Space Flight Center
April 20-22, 1993

Susan T. Hudson
ED34/Experimental Fluid Dynamics Branch
Marshall Space Flight Center

Outline

- Test Objectives
- Facility Description
- Model Description
- Instrumentation
- Test Plan
- Preliminary Test Results
- Conclusions

Test Objectives

- Develop and demonstrate techniques for making hot film probe, cobra probe, and laser velocimeter measurements in turbine flows
- Determine rake blockage effects on turbine performance
- Document fuel turbine acoustic environment
- Measure turbine inlet and exit velocity profiles, turbulence intensities, and boundary layer thicknesses
- Determine effect of Reynolds number on measurements

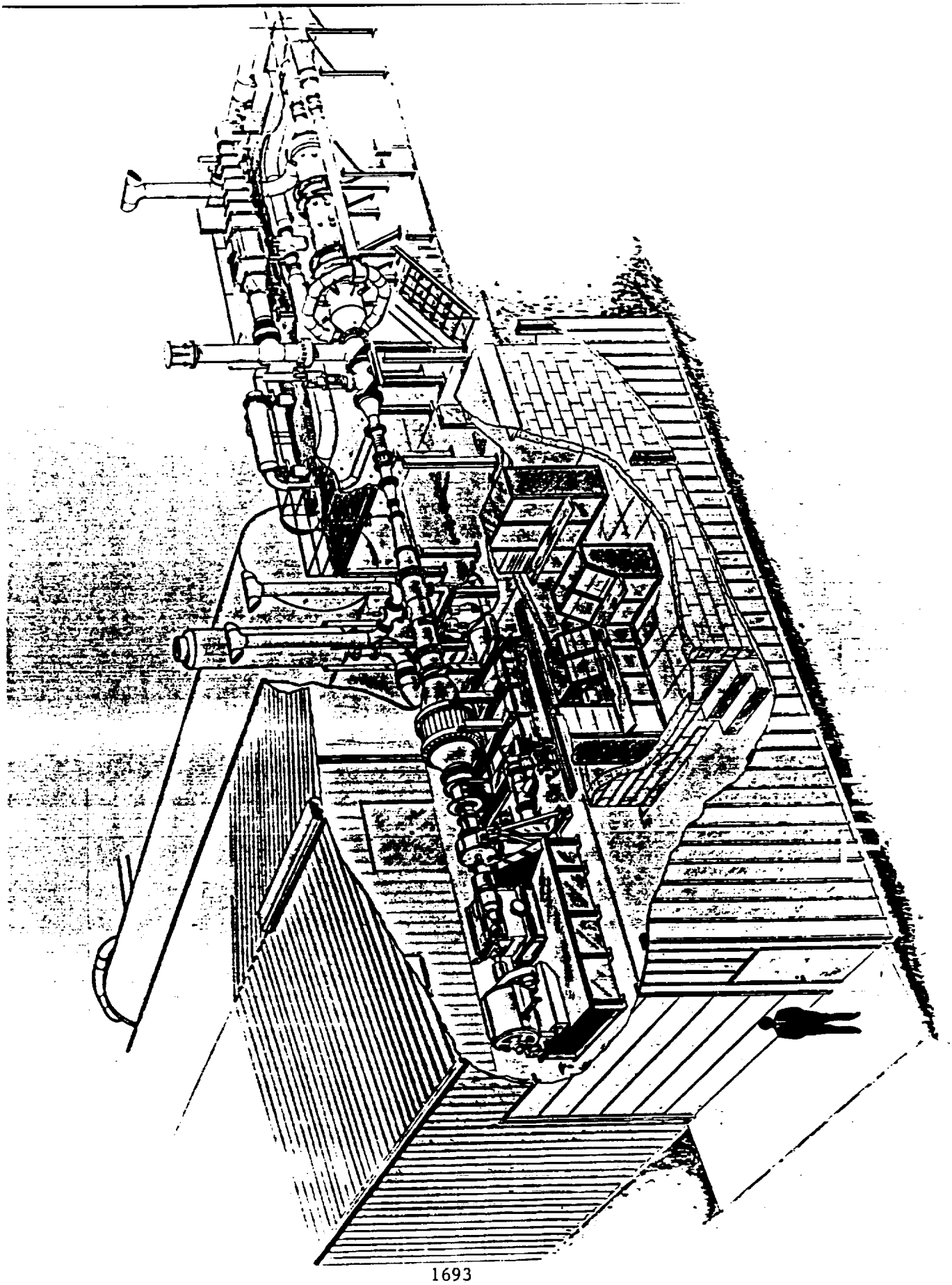

1693

TTE Facts

- Blowdown Facility (run times depend on inlet pressure)
- Regenerative Thermal Matrix Heater
- Herschel Venturi (large and small)
- Torquemeter (30, 500, 1000 ft-lb shafts)
- Gearbox (2:1, 1:1, 1:2)
- Dynamometer (600 HP continuous)
- Control Parameters -- Po, To, N, Pr
- Data Acquisition
  - Pressure Systems, Inc. (PSI) System
  - Hewlett-Packard (HP) 3852S data acquisition system
  - VAX -- database and data analysis

Phase IA Configuration

- Fully bladed two stage SSME fuel turbine test article
- Disk coolant flows not simulated
- Platform seal leakages not simulated
- Turbine exit circumferential pressure gradient not simulated
- Exit guide vanes downstream of engine position

COMPARISON OF COATED, UNCOATED, & POLISHED SSME HPFTP TURBINE BLADES

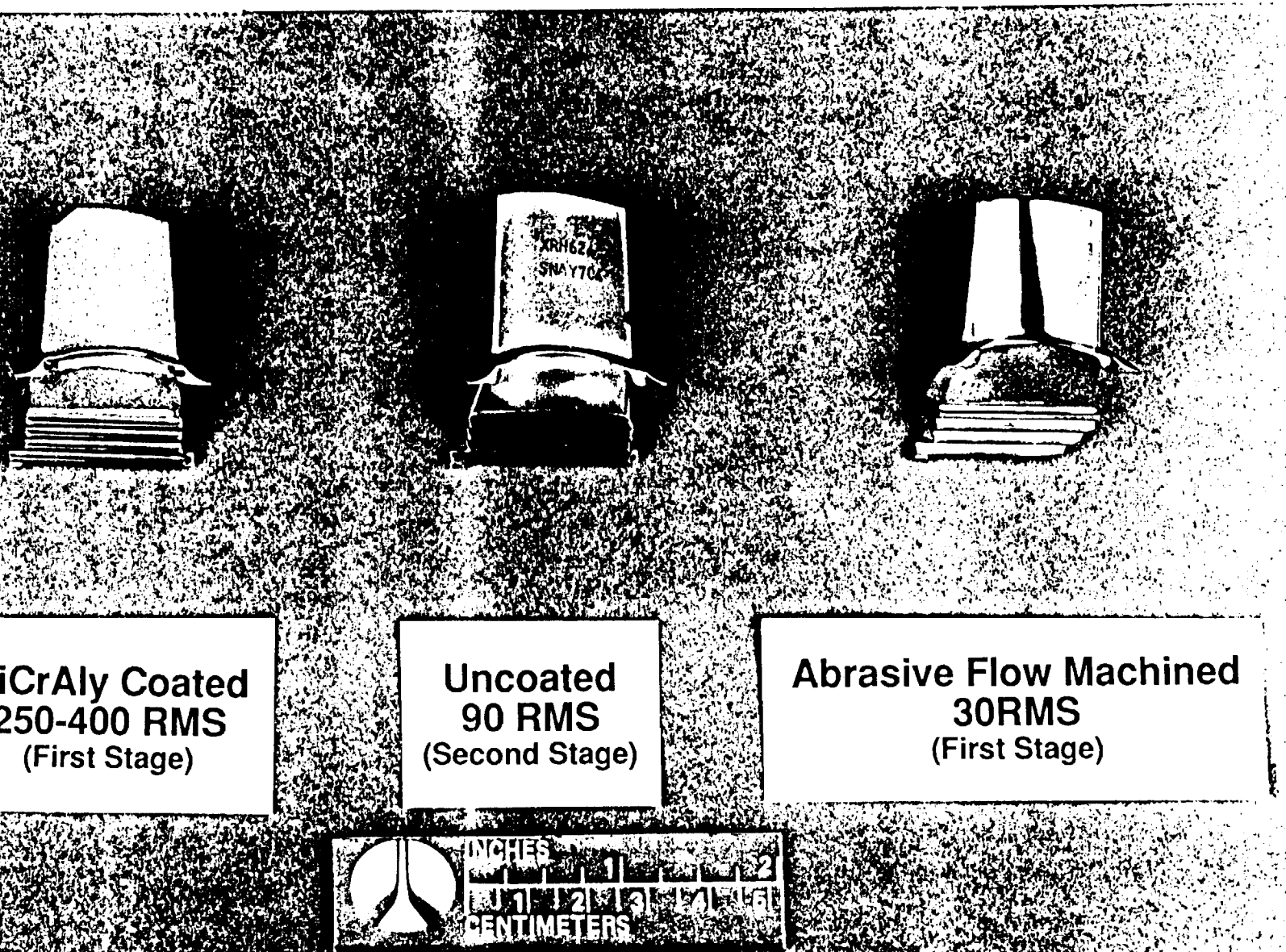

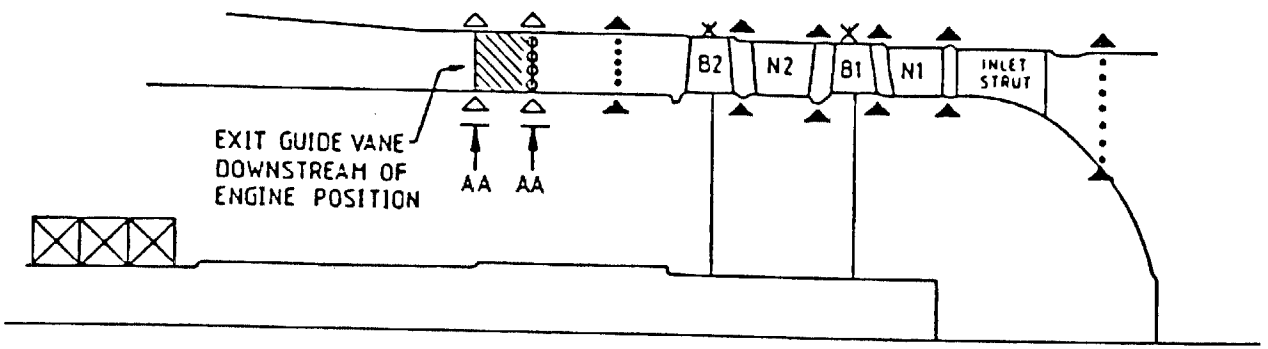

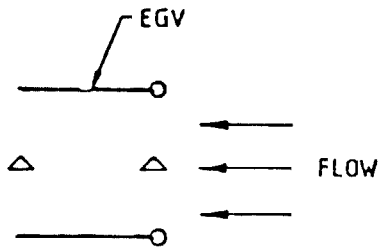

VIEW AA-AA

x Tip Clearance (3 Circumferential)
▲ Gas Path Wall (8 Circumferential)
● Rotating Ring (Continuously Variable through 90°)
o Fixed Exit (6 Circumferential)
△ Exit Static (12 Circumferential)

Phase IA Instrumentation

Instrumentation

- Inlet Spool

  Acoustic Pressure
  One Radial Actuator Tower (Cobra or Hot Film Probe)

- Turbine Inlet

  Acoustic Pressure
  Two Radial Actuator Towers (Cobra and Hot Film Probe)
  Laser Mounting Bracket
  Laser Window

- Turbine Exit

  Acoustic Pressure
  Two Radial Actuator Towers (Cobra and Hot Film Probe)
  Laser Mounting Bracket
  Laser Window

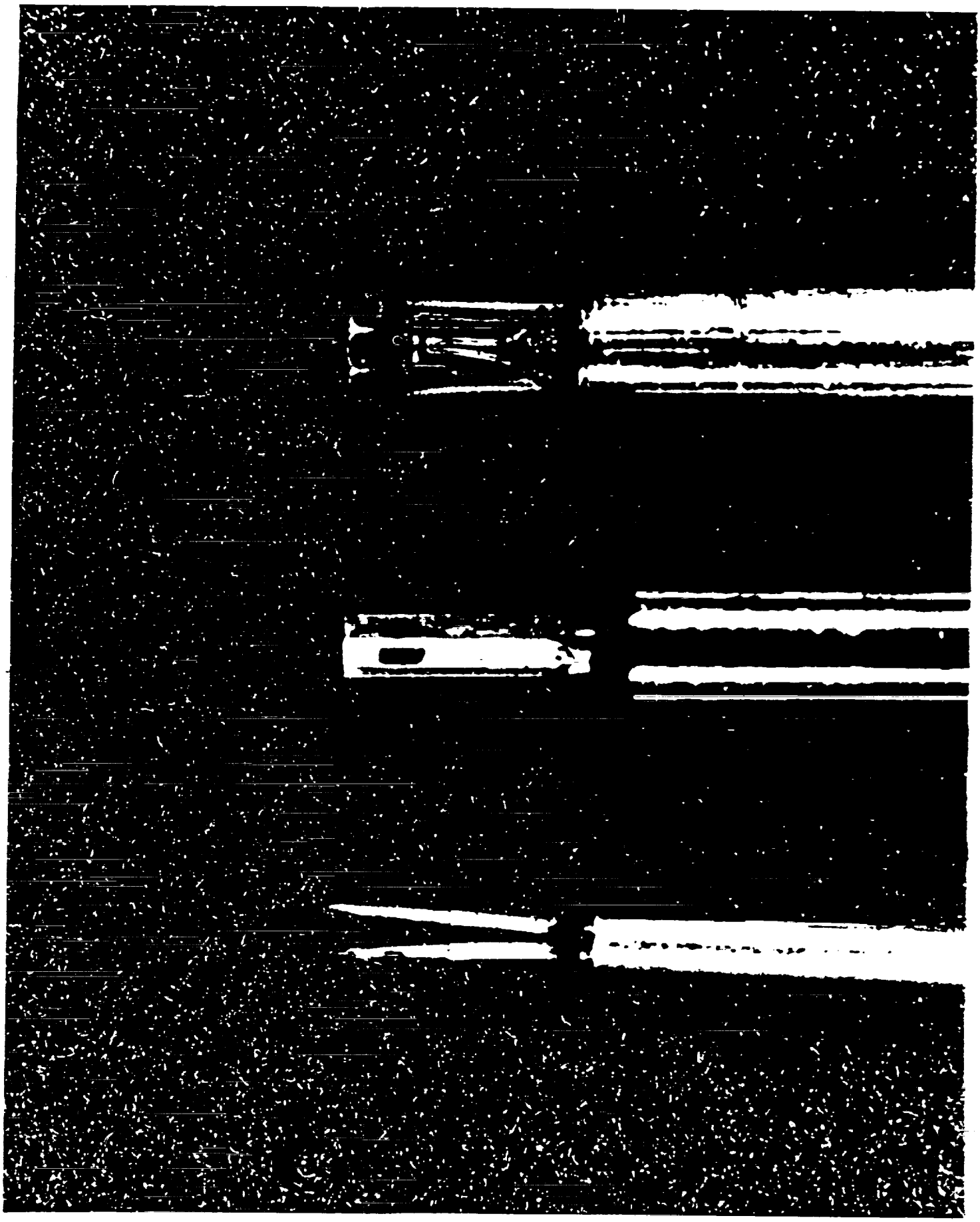

Spatial Resolution of Measurements

Instrument	Measurement Resolution		Comments
	Radially (in)	Circumferentially (in)	
Rotadata Cobra Probe	0.040	0.120	Probe head dimensions
Hot Film Probe (1260A-10)	0.001	0.050	Film diameter and width
Hot Film Probe (1234 HW)	0.040	0.040	Film diameter and width
LV Probe	0.197	0.008	Control volume size

LASER VELOCIMETER SYSTEM SCHEMATIC

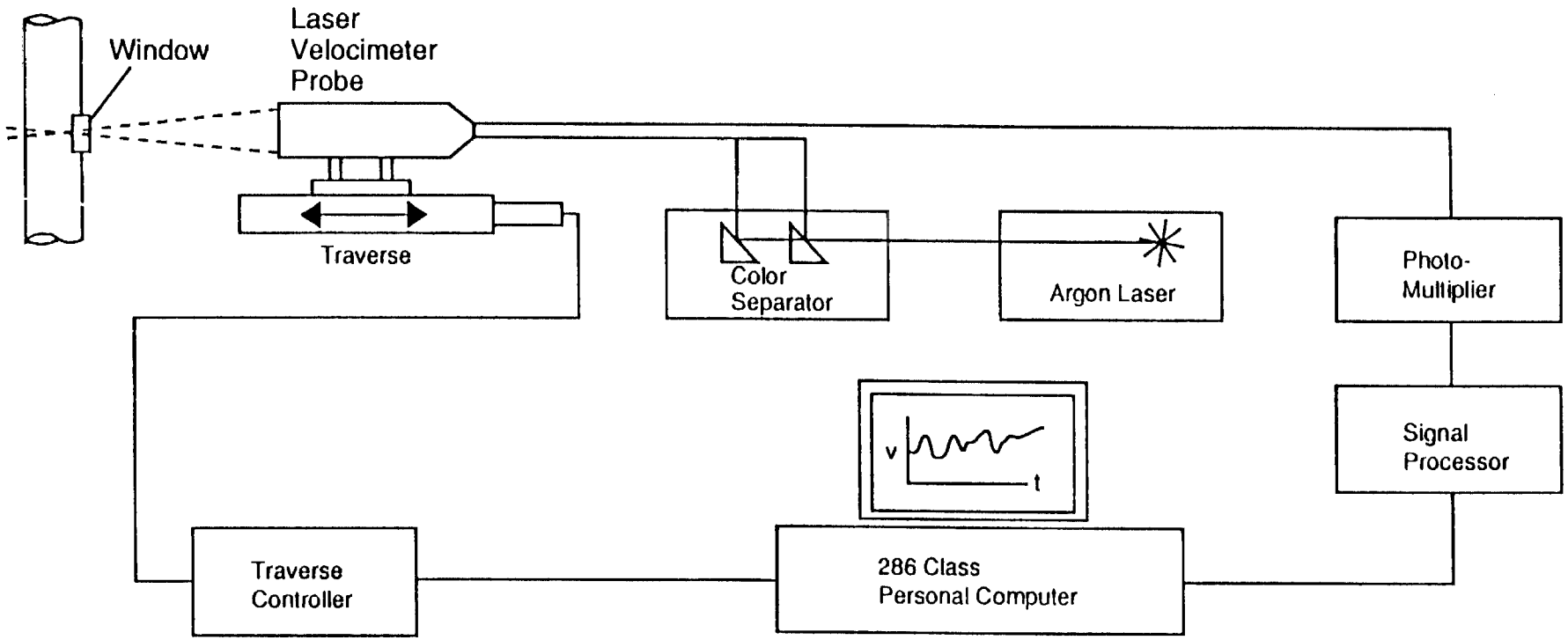

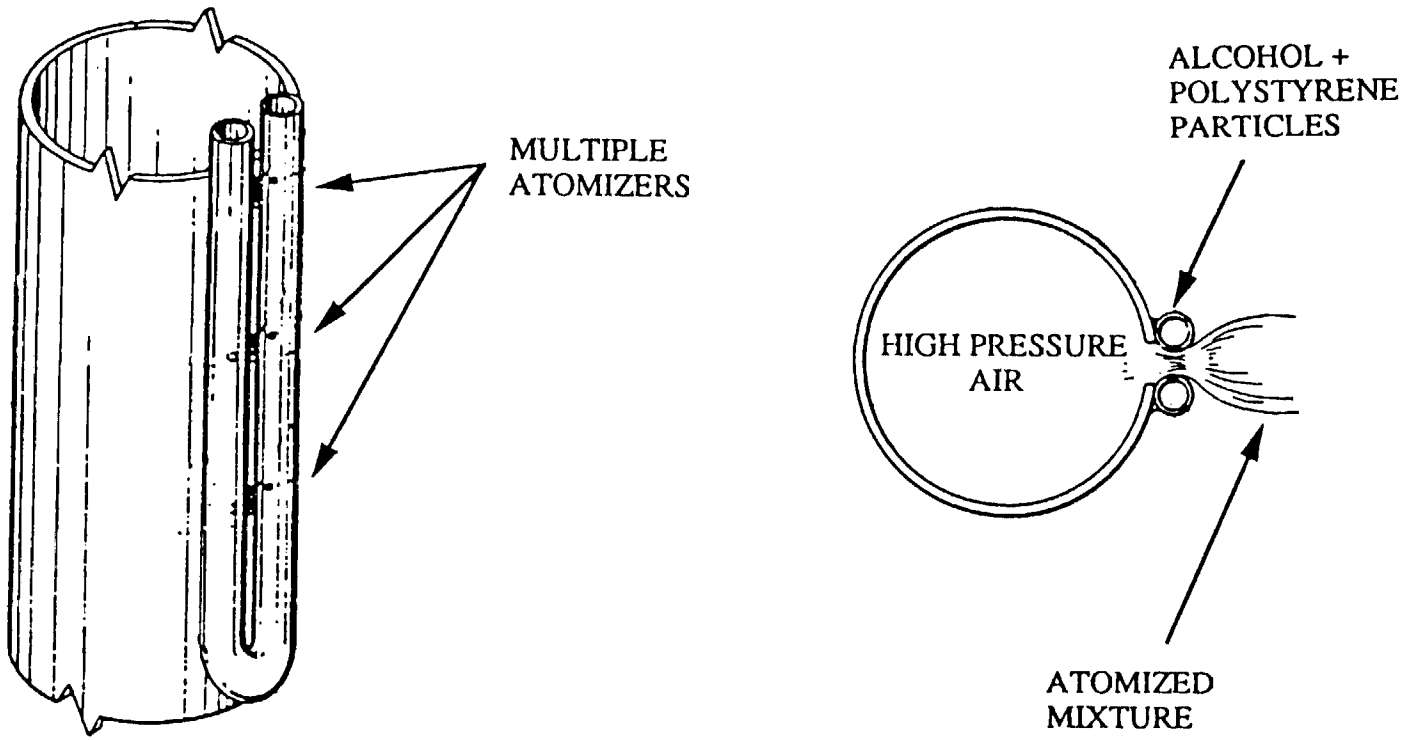

SEEGMILLER ATOMIZER

Test Plan

I. Checkout

A. Static Pressure Checks
B. Check LV Bracket Vibration
C. Reestablish Design Point (104% Power Level) Performance
D. Determine Rake Blockage Effects at Design Point
E. Prepare Acoustic Pressure Data Acquisition System

II. Develop and Demonstrate Techniques

A. Establish Hot Film Probe Insertion Technique
B. Verify use of Cobra Probes to Obtain Velocities
C. Establish LV Seeding Method and Positioning

Test Plan (continued)

III. Measurements at Design Point

A. Measure Velocity Profiles
B. Measure Turbulence Intensities
C. Measure Boundary Layer Thicknesses
D. Obtain Acoustic Pressure Data

IV. Measurement at Off-Design Points

A. Verify Rake Blockage Effects Off-Design
B. Measure Velocity Profiles
C. Measure Turbulence Intensities
D. Measure Boundary Layer Thicknesses
E. Obtain Acoustic Pressure Data

V. Determine Re Effect on Measurements

Laser Velocimeter Results

- Developed successful model/LV probe mounting design (minimal vibrations)
- Seeding successful at 50 psia with one hole seeder
- Overall poor signal to noise ratio
  - Minimize all reflections
  - Increase laser power
  - Investigate other seeding possibilities
- Separate test being planned to further improve LV measurements

SSME HPFT INLET VELOCITY PROFILE AND TURBULENCE INTENSITY

(104% POWER LEVEL--HOT FILM-CYLINDER)

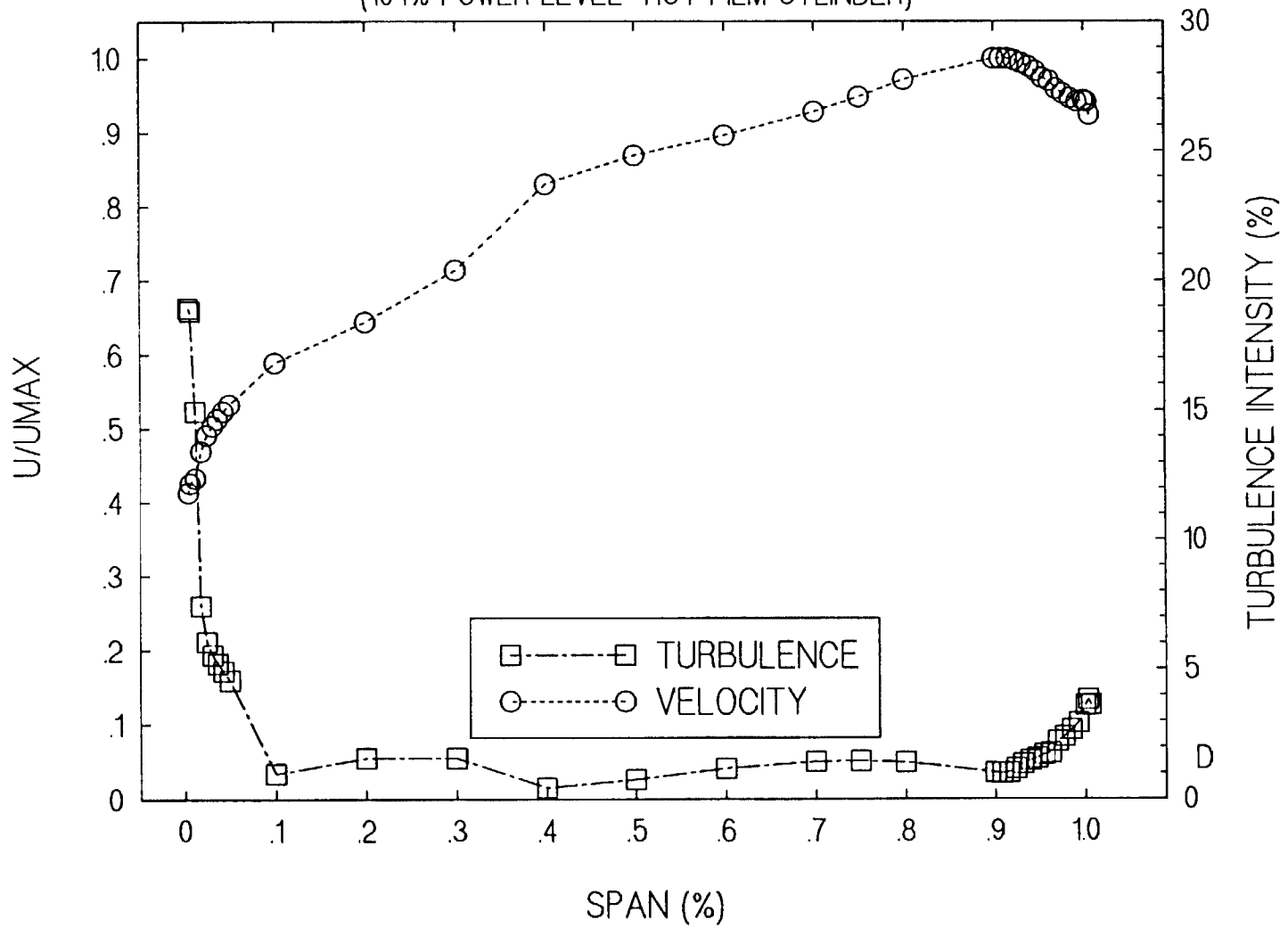

SSME HPFT EXIT VELOCITY PROFILE AND TURBULENCE INTENSITY

(104% POWER LEVEL--HOT FILM-CYLINDER)

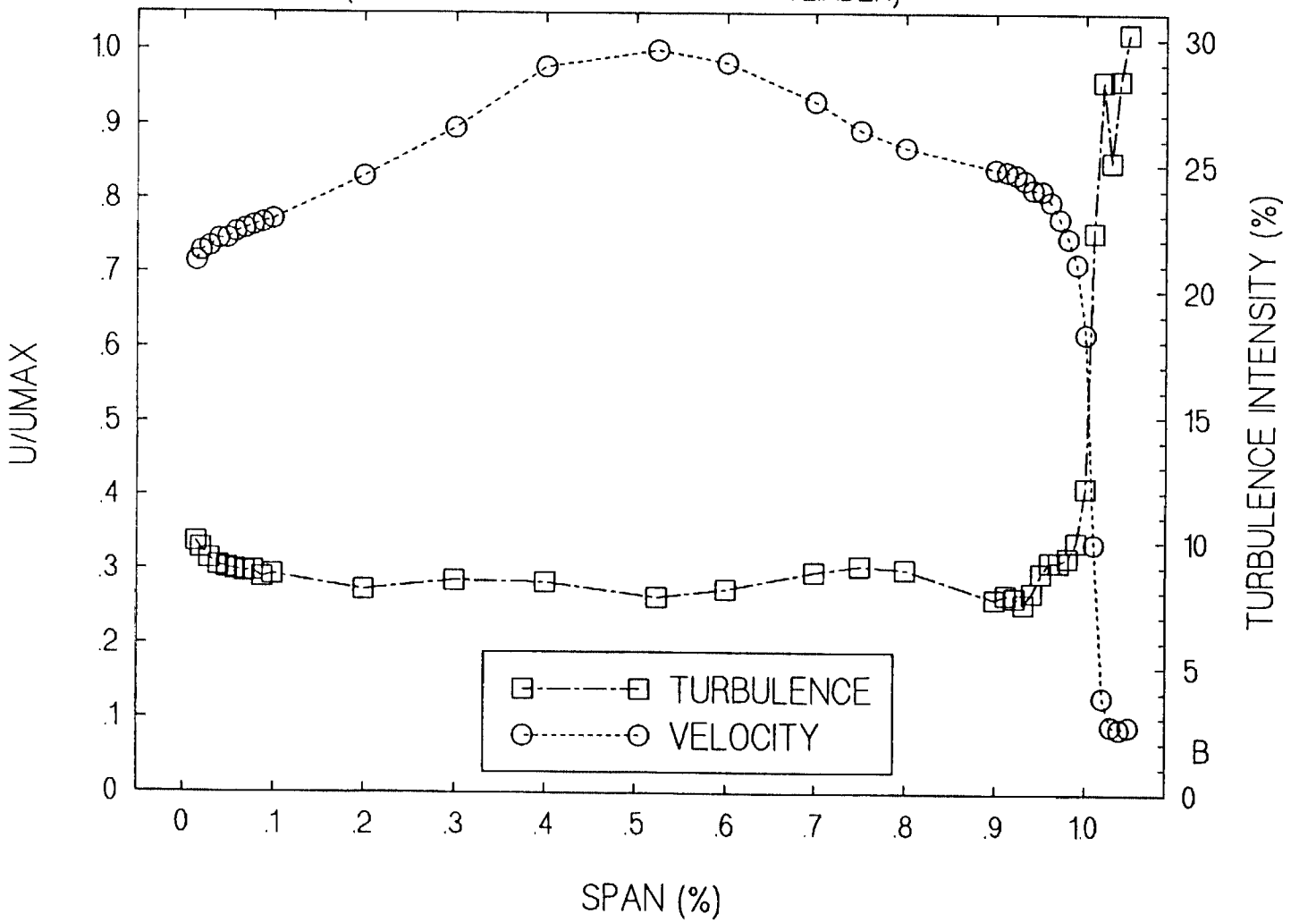

SSME HPFT EXIT VELOCITY PROFILES (104% POWER LEVEL)

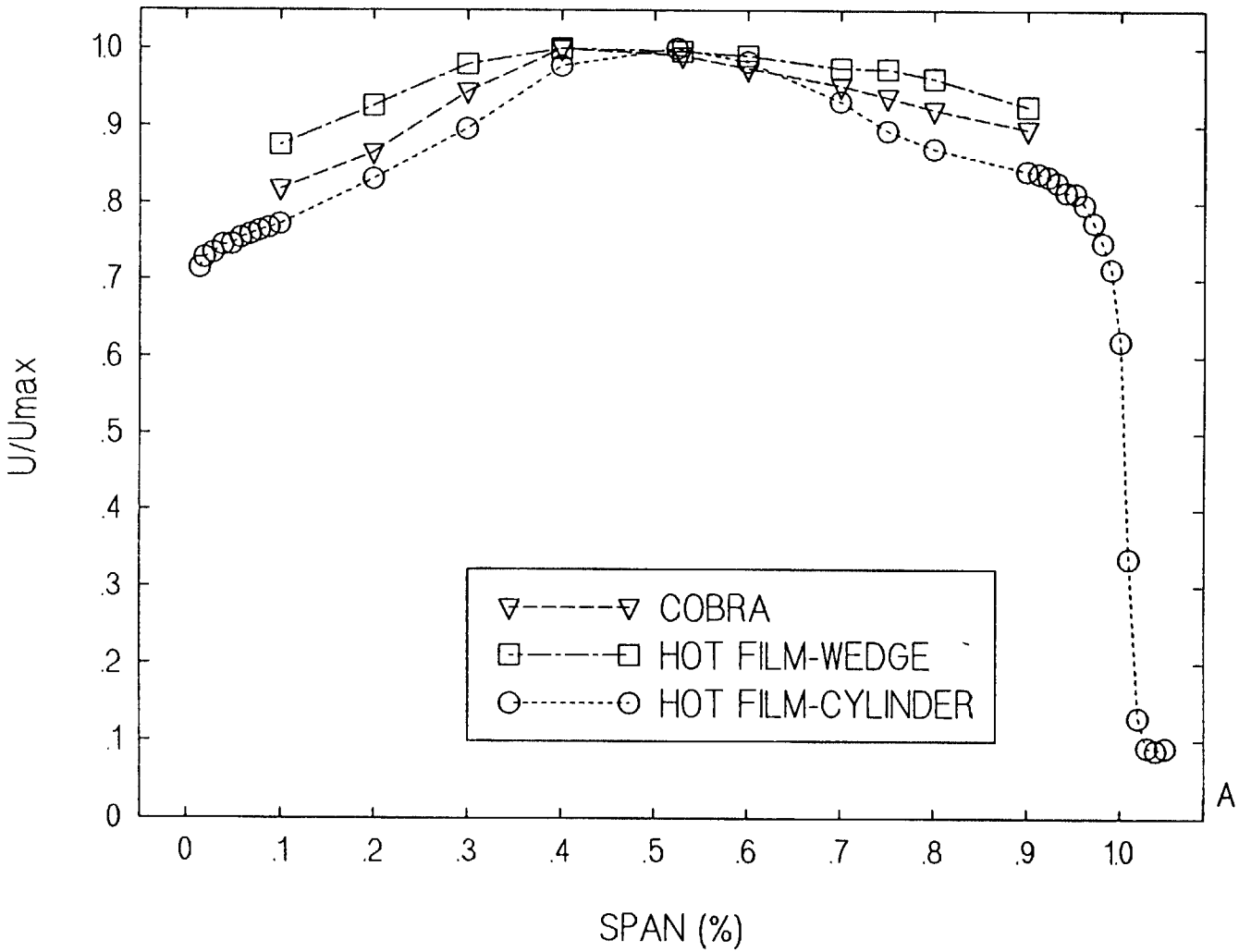

SSME HPFT Exit Swirl Versus Span and Circumferential Position (104% Power Level)

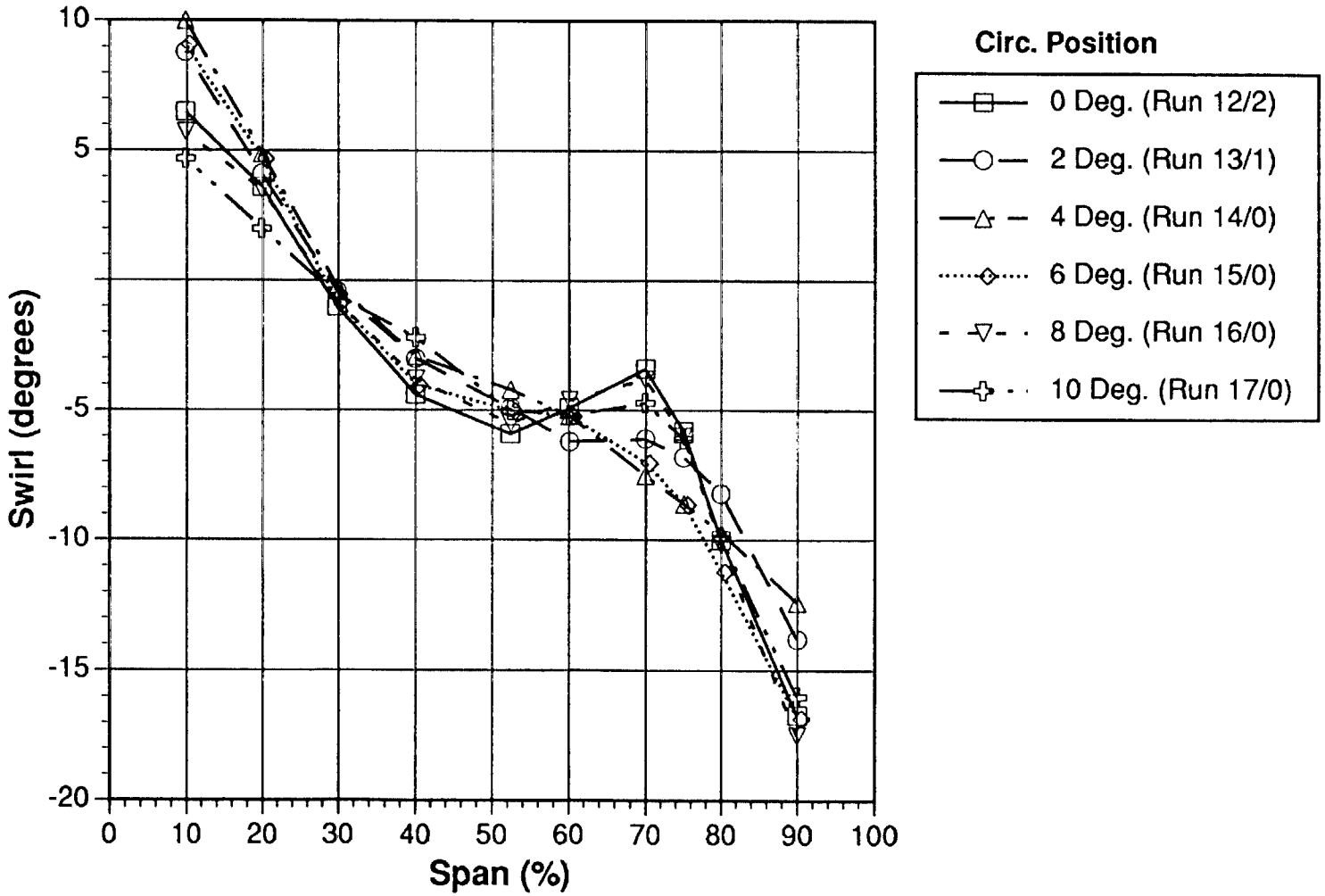

Note: Positive swirl is clockwise looking from turbine inlet to exit.

SSME HPFT Exit Velocity Versus Span and Circumferential Position (104% Power Level)

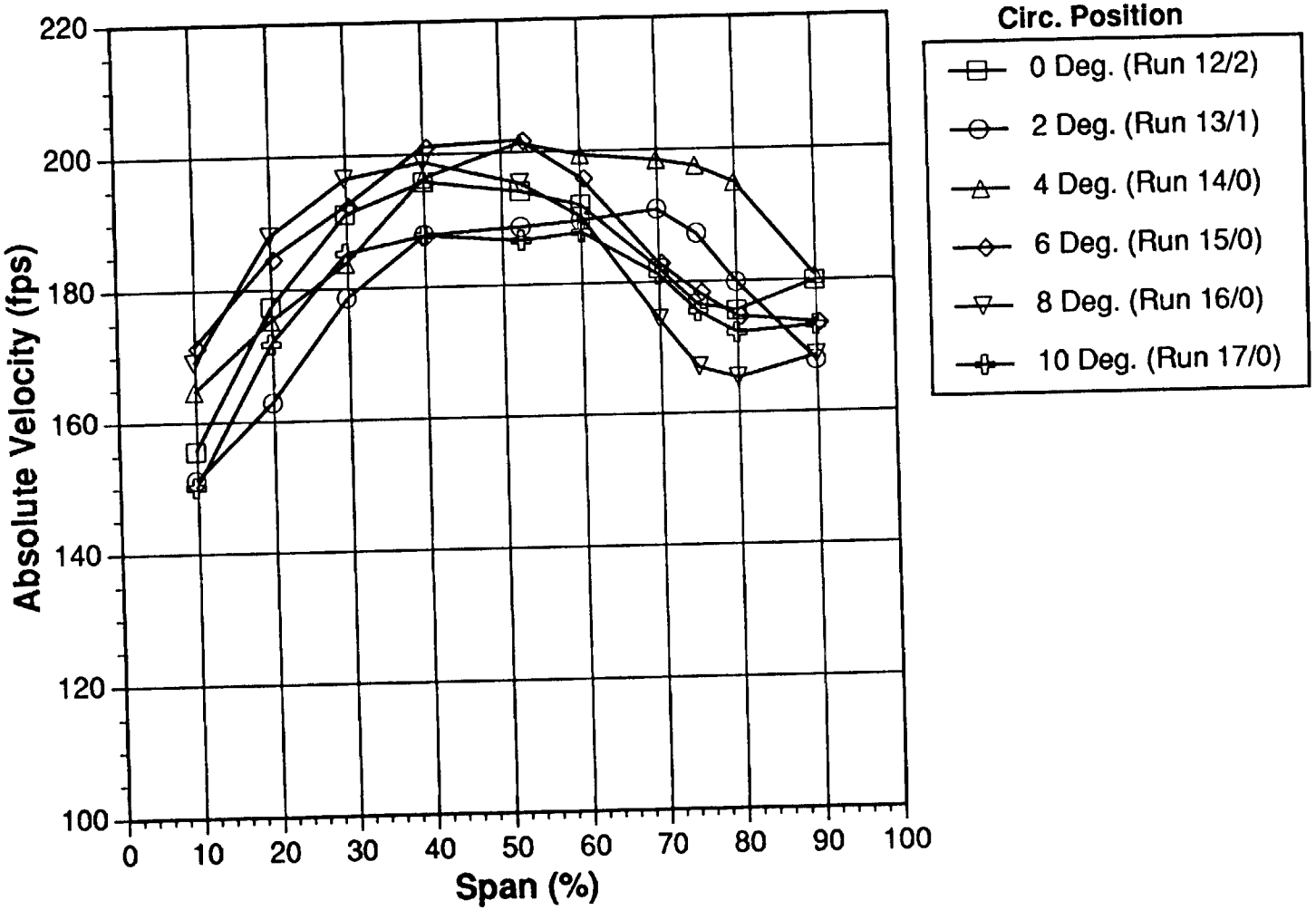

Conclusions

- Hot film probe insertion technique established
- Developed successful model/LV probe mounting design
- Seeding and LV measurements marginally successful
- Good agreement between cobra and hot film velocity profiles
- Measured turbine inlet and exit turbulence intensities (hot film)
- Measured turbine inlet and exit boundary layer thicknesses (hot film)
- Rake blockage effects appear minimal but analysis continuing
- Acoustic pressure data currently being analyzed by ED33
- Data collected to study Reynolds number effects on measurements

Development of an Algebraic Stress/Two-Layer Model for Calculating Thrust Chamber Flow Fields

By

C. P. Chen, H. M. Shang and J. Huang

Department of Chemical Engineering
University of Alabama in Huntsville
Huntsville, AL 35899

ABSTRACT

Following the consensus of a workshop in Turbulence Modeling for Liquid Rocket Thrust Chambers, the current effort was undertaken to study the effects of second-order closure on the predictions of thermochemical flow fields. To reduce the instability and computational intensity of the full second-order Reynolds Stress Model, an Algebraic Stress Model (ASM) coupled with a two-layer near wall treatment was developed. Various test problems, including the compressible boundary layer with adiabatic and cooled walls, recirculating flows, swirling flows and the entire SSME nozzle flow were studied to assess the performance of the current model. Detailed calculations for the SSME exit wall flow around the nozzle manifold were executed. As to the overall flow predictions, the ASM removes another assumption for appropriate comparison with experimental data, to account for the non-isotropic turbulence effects.

Development of an Algebraic Stress/ Two-Layer Model for Calculating Thrust Chamber Flow Fields

C. P. Chen, H. M. Shang, J. Huang
University of Alabama in Huntsville

11th Workshop for CFD Applications in Rocket Propulsion
April 20-22, 1993
NASA- Marshall Space Flight center

- **Improve Predictive Capabilities of Turbulent Transport in Thrust Chamber**
- **Non-Isotropic and Compressibility Effects are the Focus of the Study**
- **Simplified Reynolds Stress Modeling**
- **Further Modeling in Turbulent Transport of Thermal Energy and Chemical Species - $\overline{u_i' C'}$ and $\overline{u_i' T'}$ etc.**

Motivation and Objective

- Higher Order Models Are Desirable For Calculating Thrust Chamber Flow Fields
  - --- 1991 Thrust Chamber Turbulence Modeling Workshop

- To Develop a Simplified 2nd-Order Turbulence Model For Thrust Chamber Flow Calculation
  - --- Near wall treatment
  - --- Efficiency and stability

APPROACH

- PDE's for Reynolds stress $\overline{u_i u_j}$ can be derived .
  Modeling any unknown in terms of Reynolds stress, the mean strain rate etc.

- Simplifications of the Differential Reynolds stresses Equations
  — Algebraic Stress Model(ASM)

- Non-linear constitutive relations (Spezial)

APPROACH (DRS Equation)

- Differential Reynolds Stress Equation

$$\frac{D}{Dt}\overline{\rho u_i'' u_j''} = P_{ij} + D_{ij} + \pi_{ij} + C_{ij} - \varepsilon_{ij}$$

$$P_{ij} = -\bar{\rho}\left[\widetilde{u_i'' u_k''}\frac{\partial \tilde{u}_j}{\partial x_k} + \widetilde{u_j'' u_k''}\frac{\partial \tilde{u}_i}{\partial x_k}\right] \qquad \text{production}$$

$$D_{ij} = \frac{\partial}{\partial x_k}\left[\bar{\rho}\,\widetilde{u_i'' u_j'' u_k''} + \delta_{ik}\,\overline{u_j'' p'} + \delta_{jk}\,\overline{u_i'' p'} - (\mu\overline{S_{ik}u_j''} + \mu\overline{S_{jk}u_i''})\right] \qquad \text{diffusion}$$

$$\pi_{ij} = p'\left(\frac{\partial u_i''}{\partial x_j} + \frac{\partial u_j''}{\partial x_i}\right) \qquad \text{pressure-strain correlation}$$

$$C_{ij} = -\left[\widetilde{u_i''}\frac{\partial \bar{P}}{\partial x_j} + \widetilde{u_j''}\frac{\partial \bar{P}}{\partial x_i}\right] \qquad \text{compressibility}$$

$$\varepsilon_{ij} = \mu\left[S_{ik}\frac{\partial u_j''}{\partial x_k} + S_{jk}\frac{\partial u_i''}{\partial x_k}\right] \qquad \text{dissipation}$$

APPROACH --- ASM

- Similitude Principle (Mellor and Yamada)

$$P_{ij} - \frac{2}{3}\delta_{ij} P_k + \phi_{ij} + C_{ij} \cong 0$$

- Algebraic Reynolds Stress Model of Rodi

$$\frac{D}{Dt}\overline{\rho u_i'' u_j''} - D_{ij} \cong \frac{\widetilde{u_i'' u_j''}}{k}\left[\frac{Dk}{Dt} - D_k\right]$$

$$\Rightarrow \quad \left[P_{ij} + \phi_{ij} + C_{ij} - \varepsilon_{ij}\right] = \frac{\widetilde{u_i'' u_j''}}{k}\left[P_k - \varepsilon\right]$$

APPROACH ---Pressure-Strain Term

$$\pi_{ij} = \overline{p'\left(\frac{\partial u_i''}{\partial x_j} + \frac{\partial u_j''}{\partial x_i}\right)}$$

return to isotropy	$= -C_1 \frac{\varepsilon}{k} \left(\overline{\rho u_i'' u_j''} - \frac{2}{3}\delta_{ij} k\right)$	Rotta Model
rapid term	$-C_2 \left(P_{ij} - \frac{2}{3}\delta_{ij} P_k\right)$	IP Model
wall damping term	$+\pi_{ijw}$	Lumped with the two-layer model
in which	$P_k = \frac{1}{2} P_{ii}$	

- $$\frac{\overline{\rho u_i'' u_j''}}{k} = \frac{(1-C_2)(P_{ij} - \frac{2}{3}\delta_{ij}P_k) - \frac{2}{3}\delta_{ij}C_k + C_{ij}}{P_k + \varepsilon(C_1 - 1) + C_k} + \frac{2}{3}\delta_{ij}$$

where

$$P_{ij} = -\bar{\rho}\left[\widetilde{u_i'' u_k''}\frac{\partial \tilde{u}_j}{\partial x_k} + \widetilde{u_j'' u_k''}\frac{\partial \tilde{u}_i}{\partial x_k}\right]$$

$$P_k = \frac{1}{2}P_{ii}$$

k- ε Equations

- $$\frac{\partial \rho k}{\partial t} + \frac{\partial}{\partial x_j}(\rho U_j k) = \frac{\partial}{\partial x_j}\left(C_k \rho \frac{k}{\varepsilon} \overline{u_j'' u_l''} \frac{\partial k}{\partial x_l}\right) + \mu_t G - \rho\varepsilon$$

- $$\frac{\partial \rho \varepsilon}{\partial t} + \frac{\partial}{\partial x_j}(\rho U_j \varepsilon) = \frac{\partial}{\partial x_j}\left(C_\varepsilon \rho \frac{k}{\varepsilon} \overline{u_j'' u_l''} \frac{\partial \varepsilon}{\partial x_l}\right) + \frac{\varepsilon}{k}(C_{\varepsilon 1}\mu_t G - C_{\varepsilon 2}\rho\varepsilon)$$

where the production term $\mu_t G$ takes the form

$$\mu_t G = -\rho \overline{u_i'' u_j''} \frac{\partial U_i}{\partial x_j} - \frac{\mu_t}{\rho^2} \frac{\partial \rho}{\partial x_j} \frac{\partial P}{\partial x_j}$$

Turbulence model costants

$C_{\epsilon 1}$	$C_{\epsilon 2}$	C_k	C_ϵ	C_1	C_2
1.45	**1.92**	**0.22**	**0.15**	**2.5**	**0.5**

Two-Layer Wall Treatment

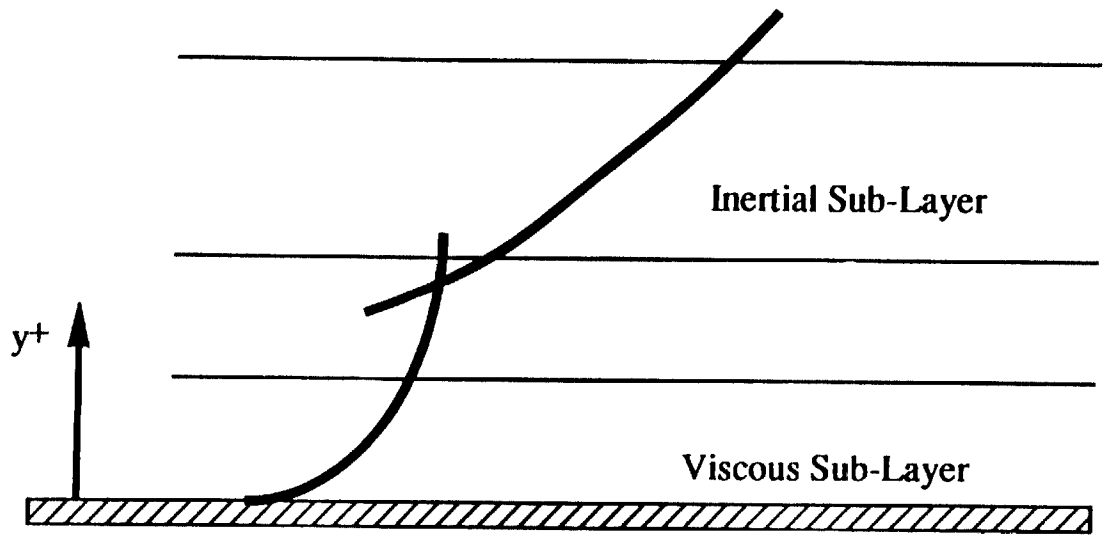

Outer Layer ---
resolved by
ASM

Inner Layer ---
Patched with a One-Equation
Model

Matching at

$$R_k = \frac{k^{1/2} y}{\mu} = 200$$

METHODOLOGIES

$$\nu_t = u' l' = C_\mu \kappa^{1/2} l_\mu = C_\mu \frac{\kappa^2}{\varepsilon} = C_\mu \frac{l_\varepsilon}{\kappa^{3/2}} \kappa^2$$

within Intertia Sublayer $\varepsilon = C_\mu^{3/4} \frac{\kappa^{3/2}}{l_\mu} = \frac{\kappa^{3/2}}{l_\varepsilon}$

$$l_\mu = C_l y \left[1 - \exp\left(-\frac{R_\kappa}{A_\mu} \right) \right] \longrightarrow \text{to be used in Eddy Viscosity}$$

$$l_\varepsilon = C_l y \left[1 - \exp\left(-\frac{R_\kappa}{A_\varepsilon} \right) \right] \longrightarrow \text{to be used in } k \text{ -equation}$$

$$C_l = \kappa C_\mu^{-3/4}$$

Matching at $R_\kappa = \frac{\kappa^{1/2} y}{\nu}$

IMPLEMENTATIONS

- Implemented into MAST-2D
- Non-Staggered Grids, Sequential Solver
- Chakravarthy-Osher TVD Scheme
- PISO-C Algorithm
- Conjugate Gradient Matrix Solver
- Time Marching

Validations

- Incompressible & Compressible Flat Plate

  Cooled & Heated Wall, Up To Mach 10

- Incompressible & Compressible Recirculating Flows

- Incompressible Swirling Flows

- Thrust Chamber Flows

Compressible Flat Plate Flow

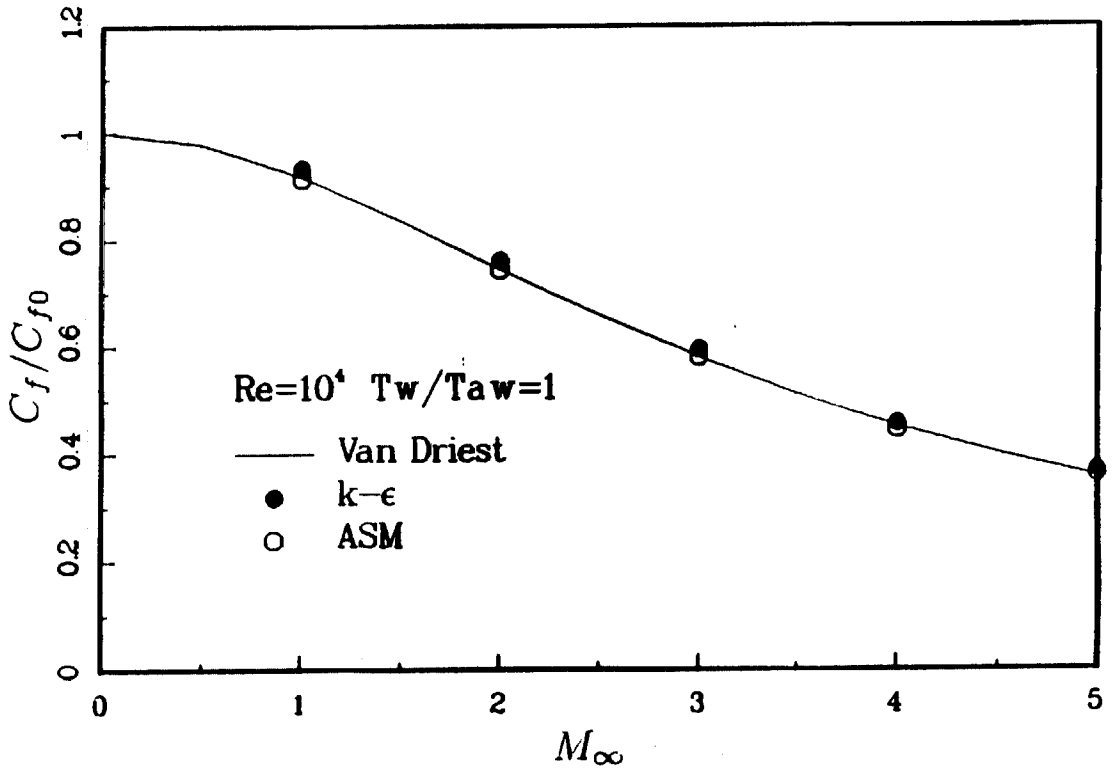

Fig. 1 Variation of C_f/C_{f0} with M_∞ for adiabatic wall boundary condition.

Compressible Flat Plate Flow

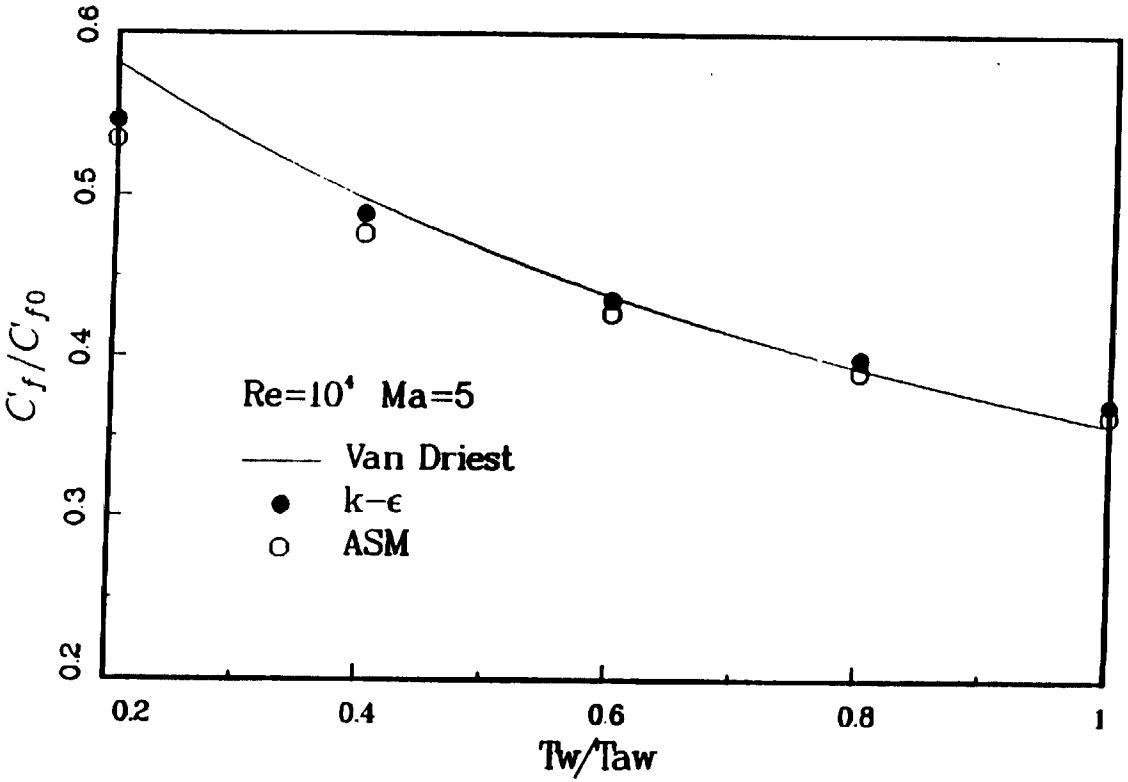

Fig. 2 Variation of C_f/C_{f0} with T_w/T_{aw} for $M_\infty = 5.0$.

Compressible Flat Plate Flow

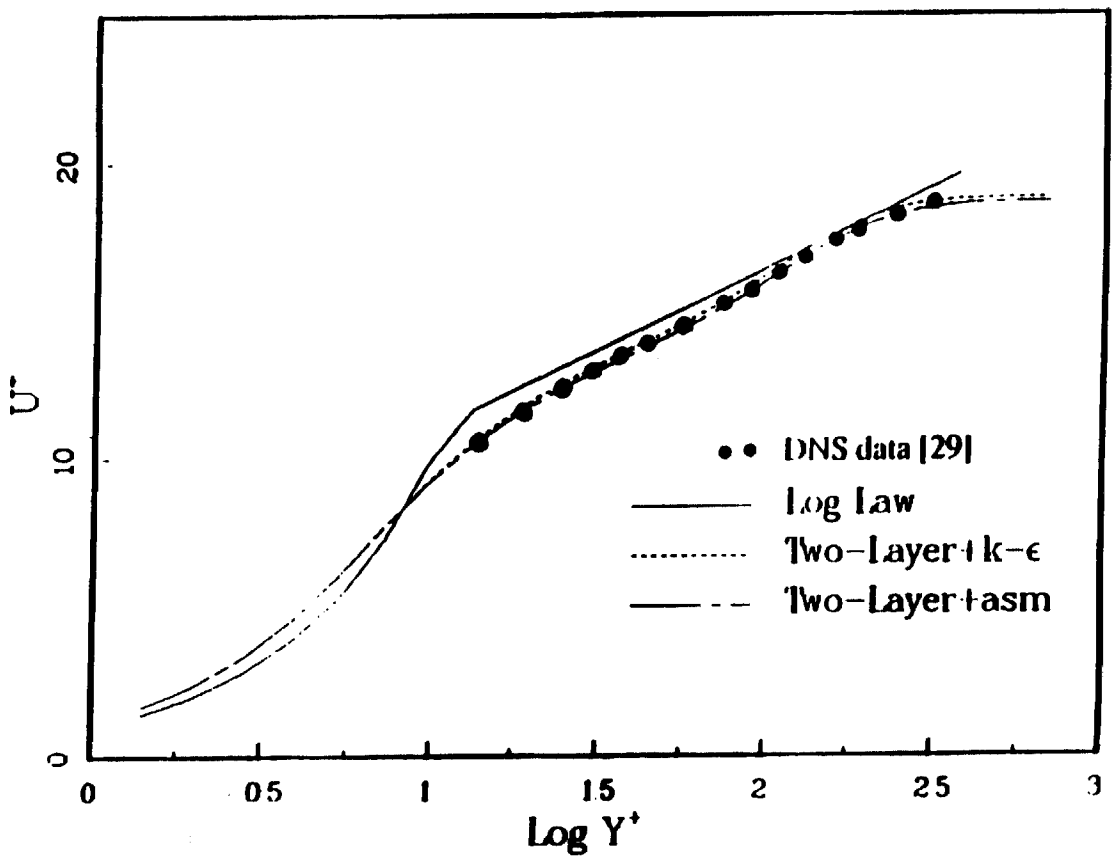

Fig. 3 Semi-log plots of u_c^+ for adiabatic wall boundary condition.

Backward Facing Step

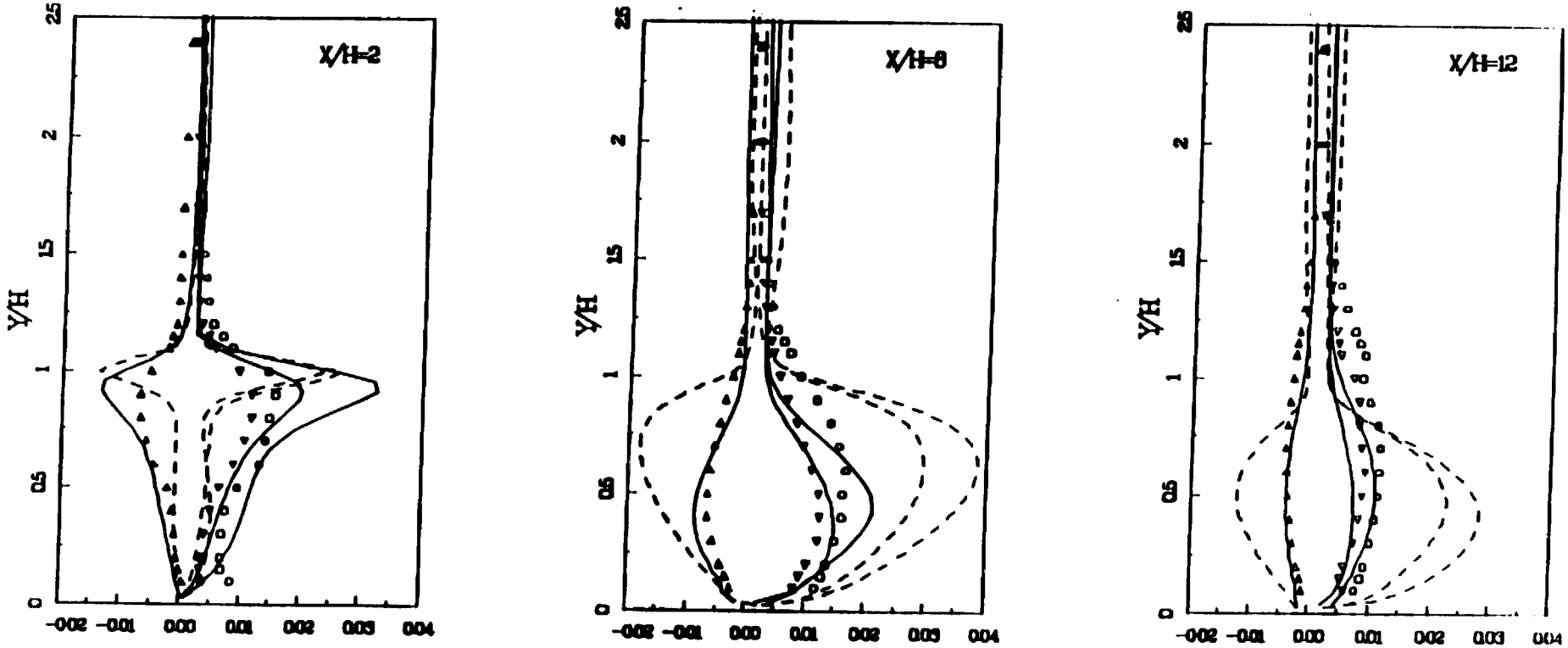

Reattachment length: k-ε 4.67H

ASM 5.94H

EXP. ~6H

---- k-ε —— k-ε/ASM data: O $\overline{u_1u_1}$ ∇ $\overline{u_2u_2}$ Δ $\overline{u_1u_2}$

Fig. 5 Reynolds stress profiles for the backward-facing step turbulent flow (9:1), with data from [31]

Confined Swirling Flows

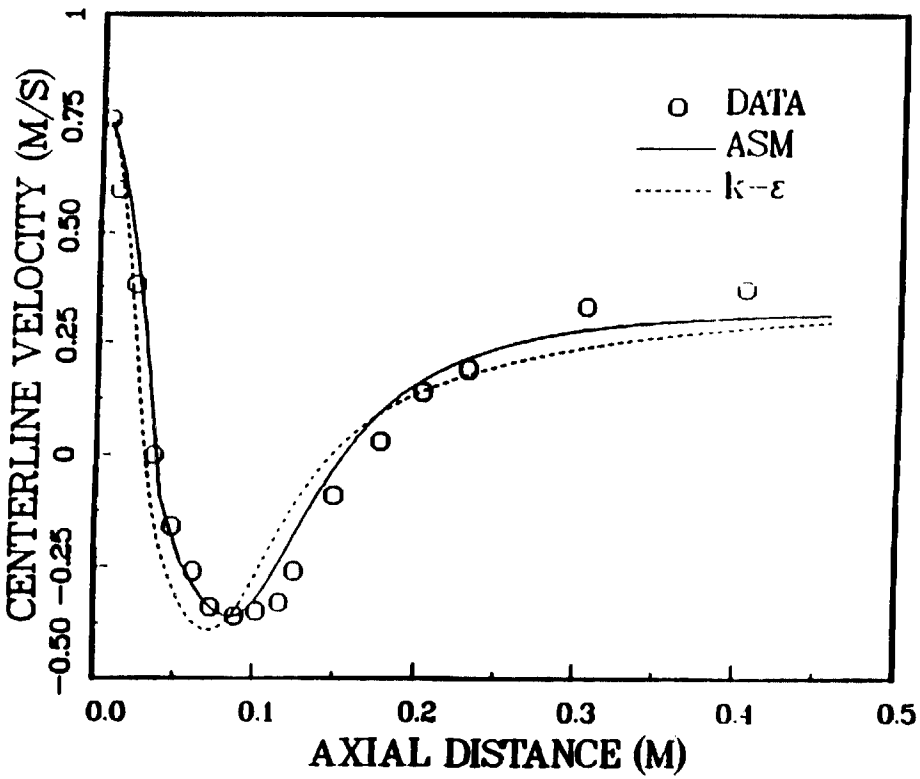

Fig. 6 Decay of mean axial centerline velocity.

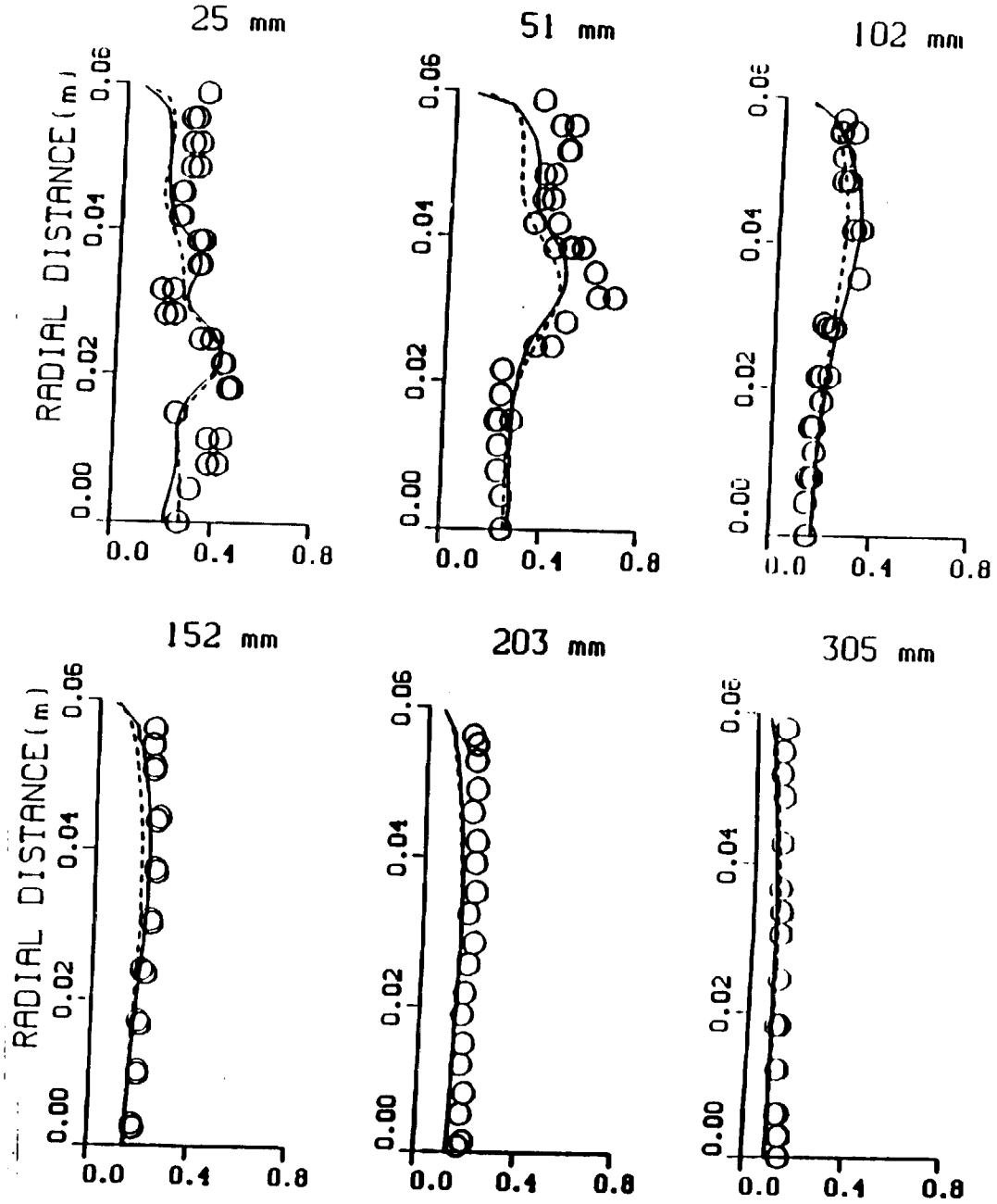

Fig. 8a Radial profiles of turbulent intensity($\sqrt{\overline{u'^2}}$)

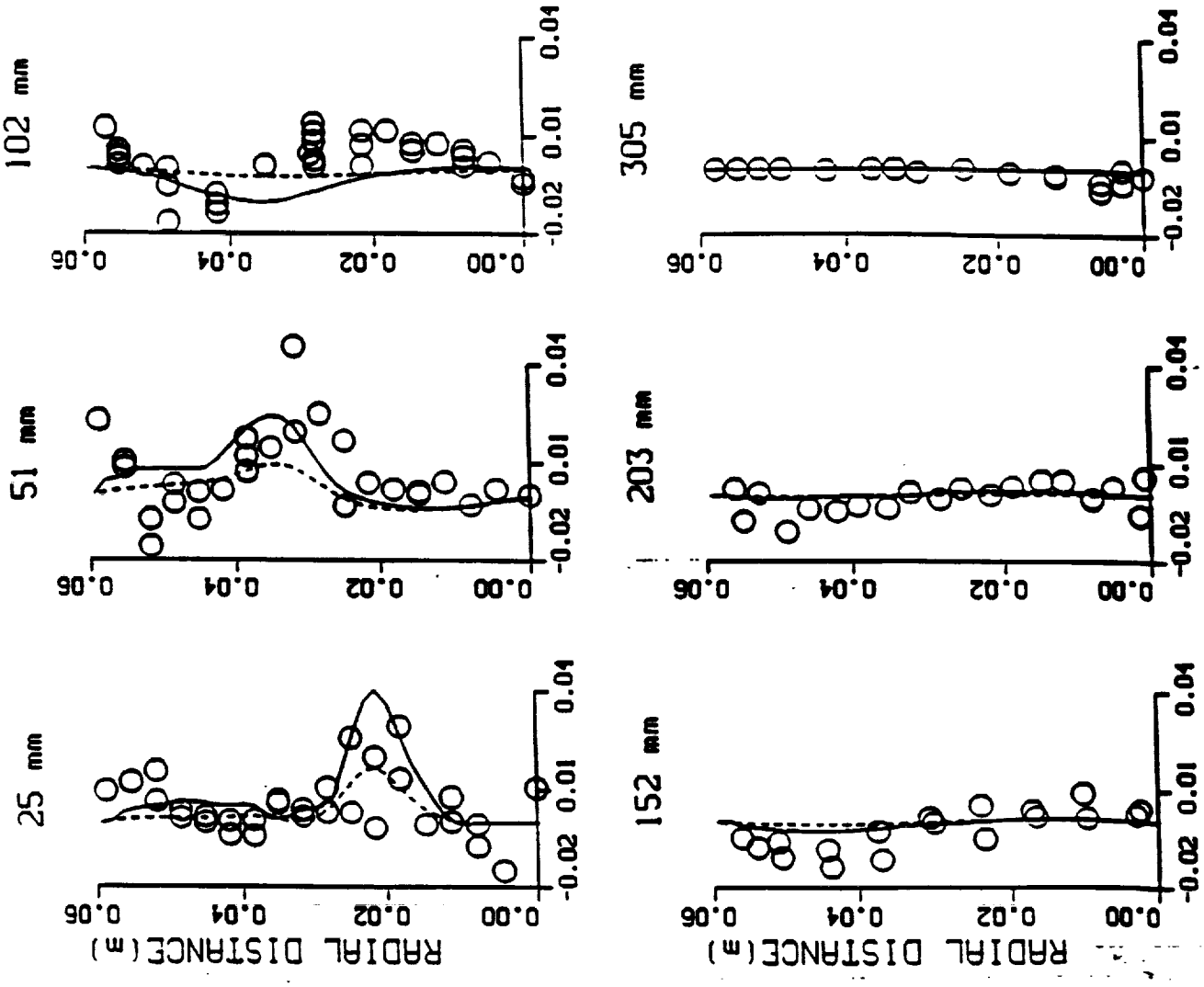

Fig. 8b Radial profiles of Reynolds stress($\overline{u'w'}$)

SSME Nozzles

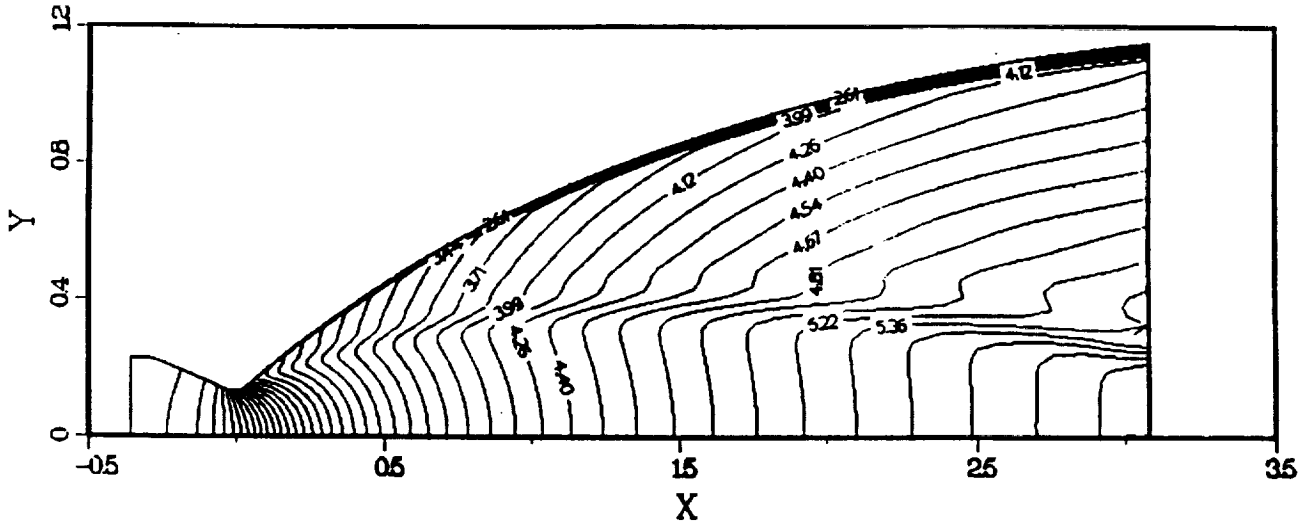

Fig. 9a Contour of Mach number for k-ϵ with two-layer model.

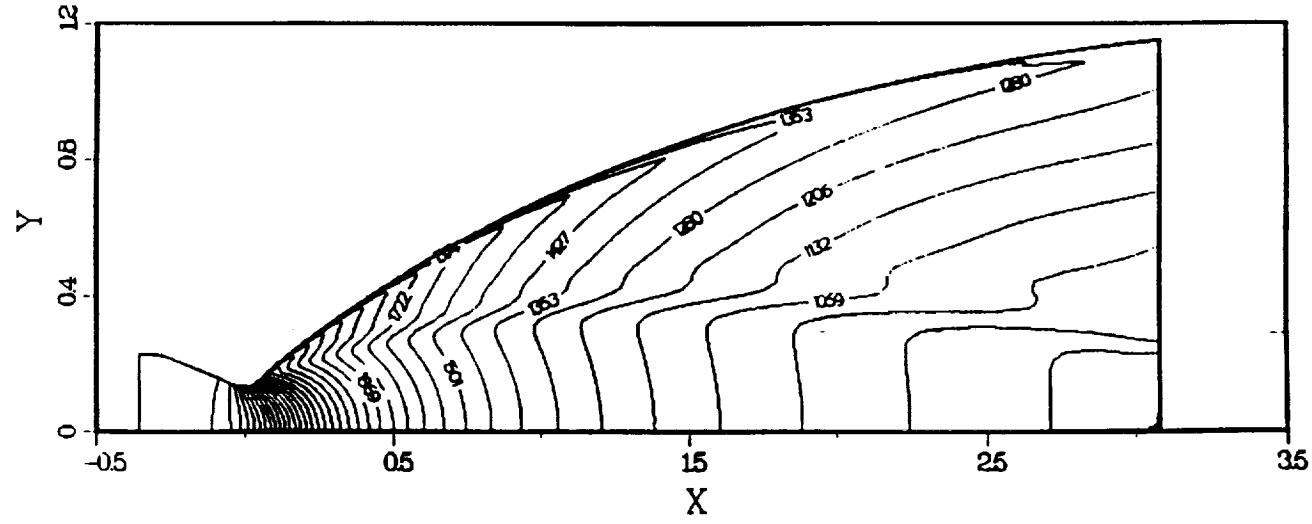

Fig. 10a Contour of temperature for k-ϵ with two-layer model.

SSME Nozzles

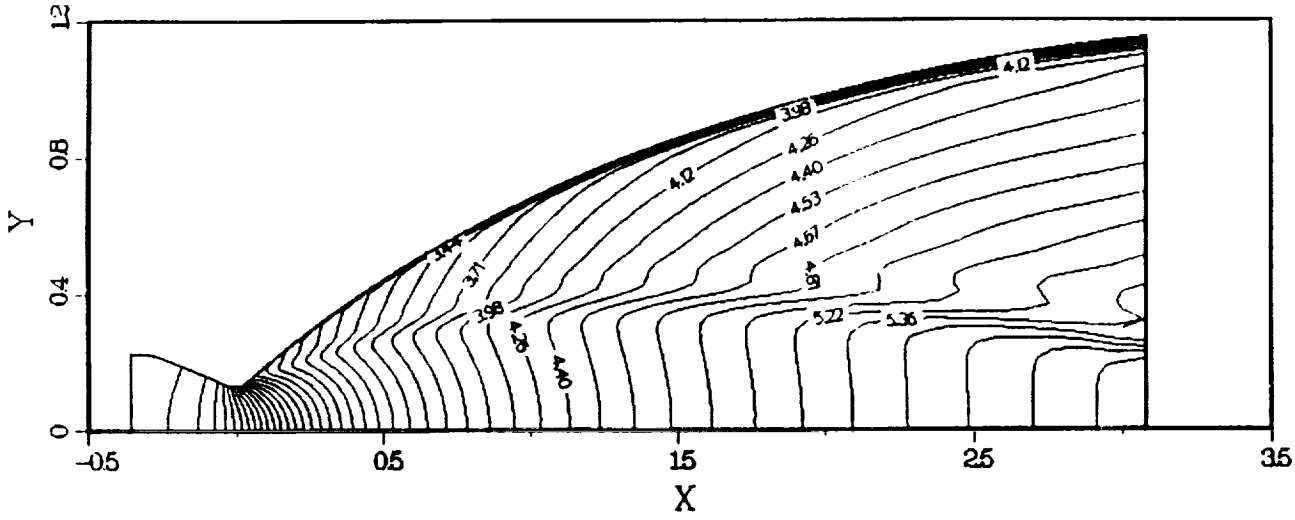

Fig. 9b Contour of Mach number for ASM with two-layer model.

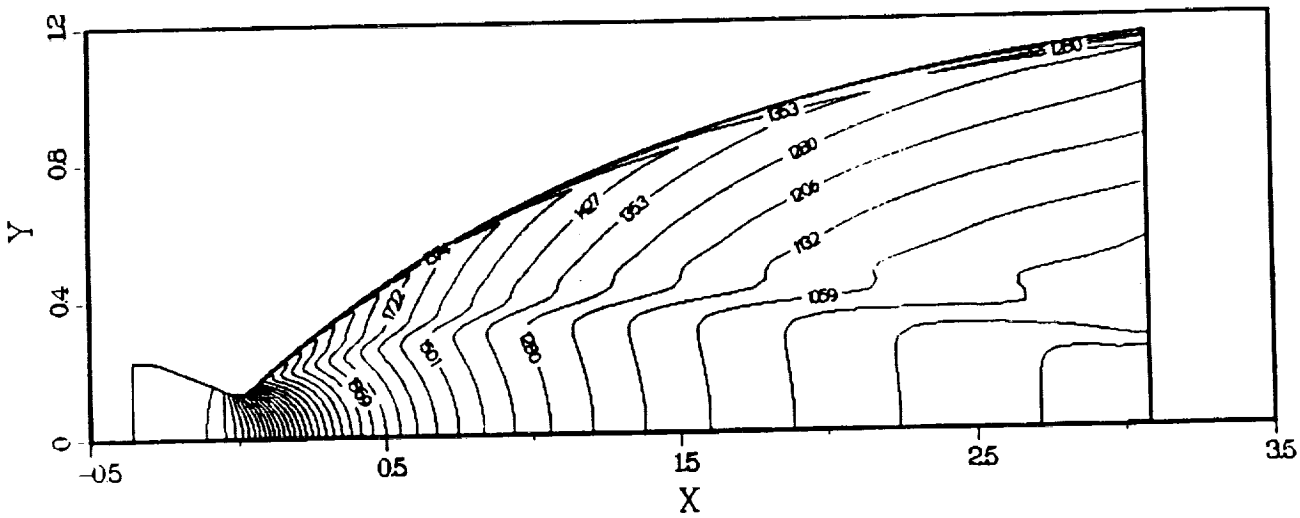

Fig. 10b Contour of temperature for ASM with two-layer model.

8 - STEP REACTIONS

		A	N	E
$M + O_2$	==== O + O	0.72000E+19	-1.0000	117908
$M + H_2$	==== H + H	0.55000E+19	-1.0000	103298
$M + H_2O$	==== H +OH	0.52000E+22	-1.5000	118000
O + H	==== OH	0.71000E+19	-1.0000	0.
$H_2O + OH$	==== $H_2O + H$	0.58000E+14	0.0000	18000
$H_2 + OH$	==== $H_2O + H$	0.20000E+14	0.0000	5166
$O_2 + H$	==== OH + O	0.22000E+15	0.0000	16800
$H_2 + O$	==== OH +H	0.75000E+14	0.0000	11099

$$k = AT^N \exp(-E/RT)$$

with k in $cm^3 \cdot mole^{-1} \cdot s^{-1}$ and E in $cal \cdot mole^{-1}$

From R.C.Rogers and Chinitz, ' Using a global hydrogen-air model in turbulent flow calcultions ', AIAA J., vol. 21, pp. 586-592, 1983.

SSME Nozzles

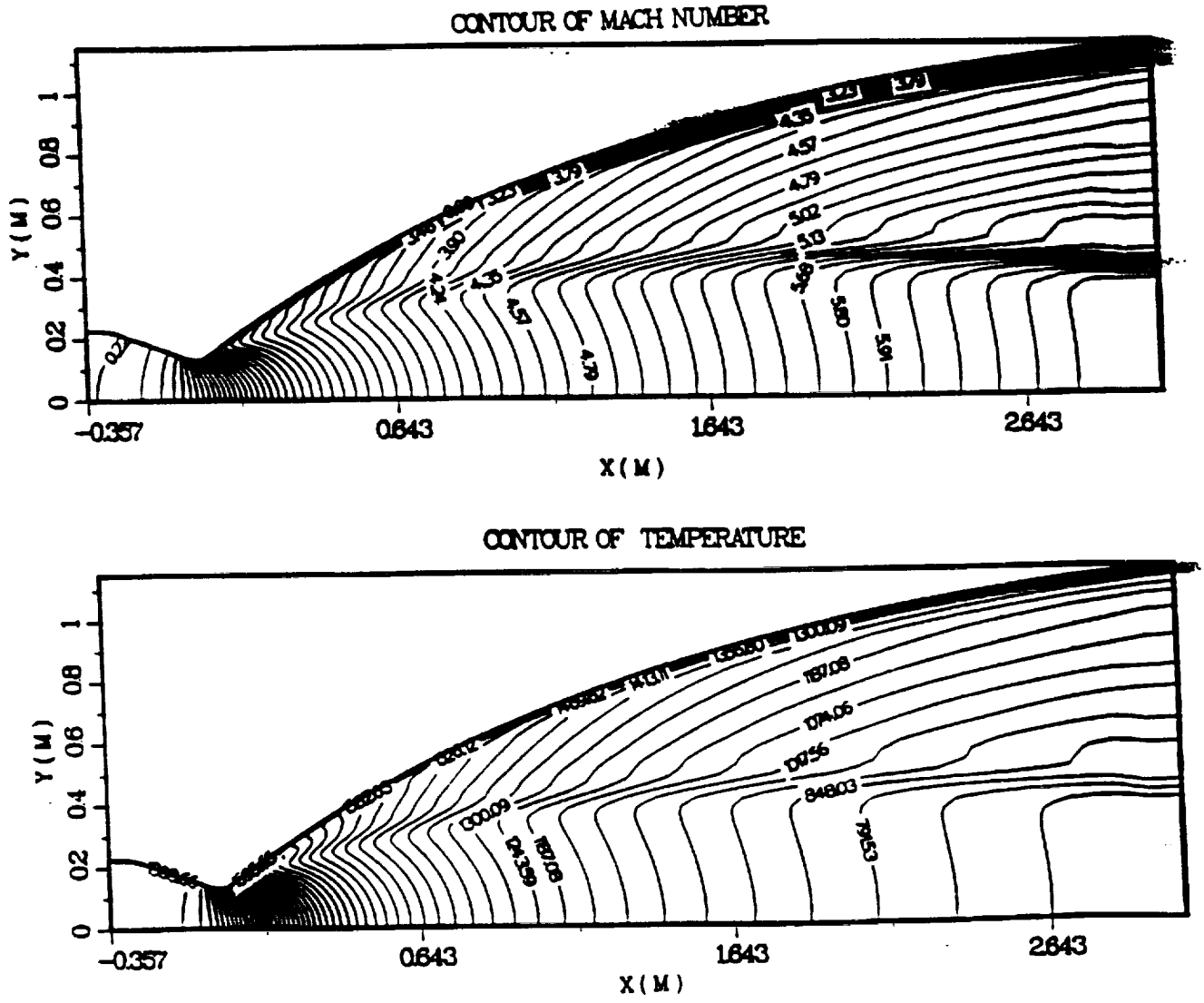

Figure A.5 Sample SSME Nozzle Flow Inputs and Results --- Turbulent, 8-Step Kinetics.
ISP = 452.78 sec. Exp. ISP=453.3sec

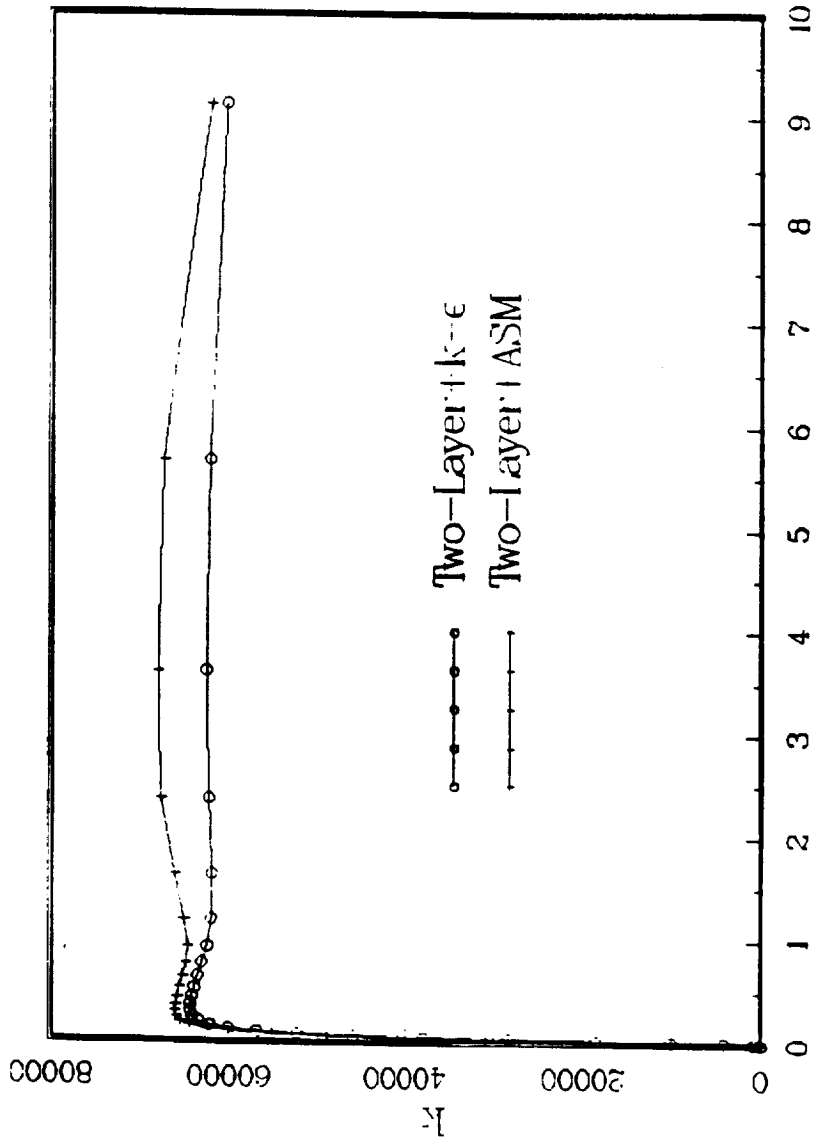

Fig. 11 Behavior of near wall TKE at nozzle exit.

George C. Marshall Space Flight Center
Science and Engineering Directorate

Propulsion Laboratory
Turbomachinery and Combustion
Devices Branch/EP62

Testbed Engine 3001 Summary Review
Combustion Devices (Tests 020-028)

National Aeronautics and
Space Administration

Nozzle Wall Static Pressure

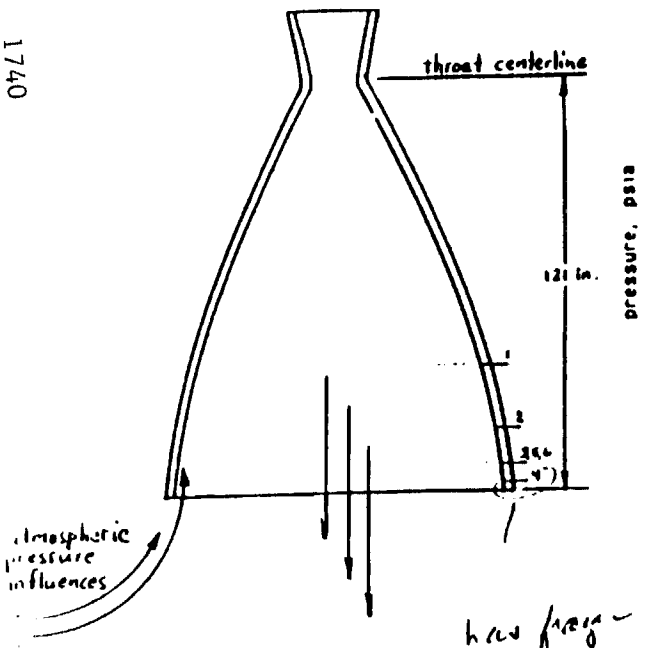

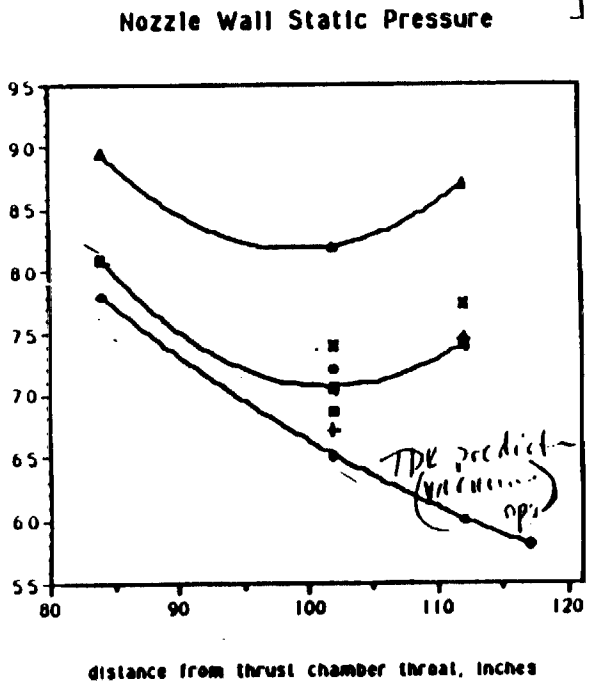

1740

Per Klem:
Increase associated w/ sea level. not expected at vacuum conds.

To run CFD calcs to compare

the location where P increase is a surprise. It is further upstream than expected

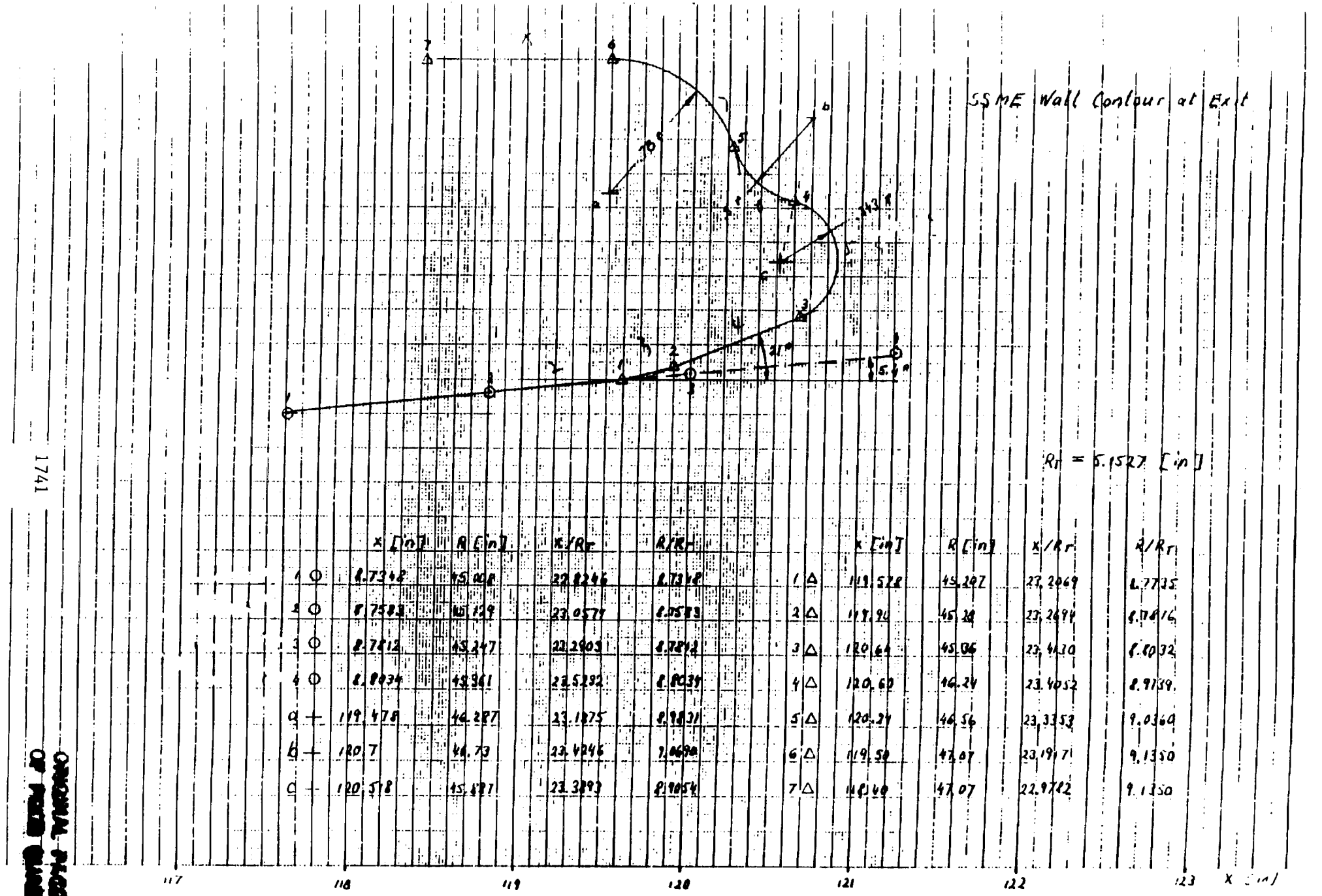

	x [in]	R [in]	x/R_T	R/R_T		x [in]	R [in]	x/R_T	R/R_T
1 ○	8.7348	45.008	22.8246	8.7348	1 △	119.528	45.207	23.2069	8.7735
2 ○	8.7583	45.129	23.0577	8.0583	2 △	119.94	45.38	23.2894	8.8016
3 ○	8.7812	45.247	23.2903	8.7812	3 △	120.64	45.06	23.4230	8.8032
4 ○	8.8034	45.361	23.5292	8.8034	4 △	120.60	46.24	23.4052	8.9139
a +	119.478	46.287	23.1875	8.9831	5 △	120.24	46.56	23.3353	9.0360
b +	120.7	46.73	23.4246	9.0690	6 △	119.58	47.07	23.1917	9.1350
c +	120.518	45.827	23.3893	8.9054	7 △	118.40	47.07	22.9782	9.1350

Fig. 12, SSME wall contour and geometry at exit

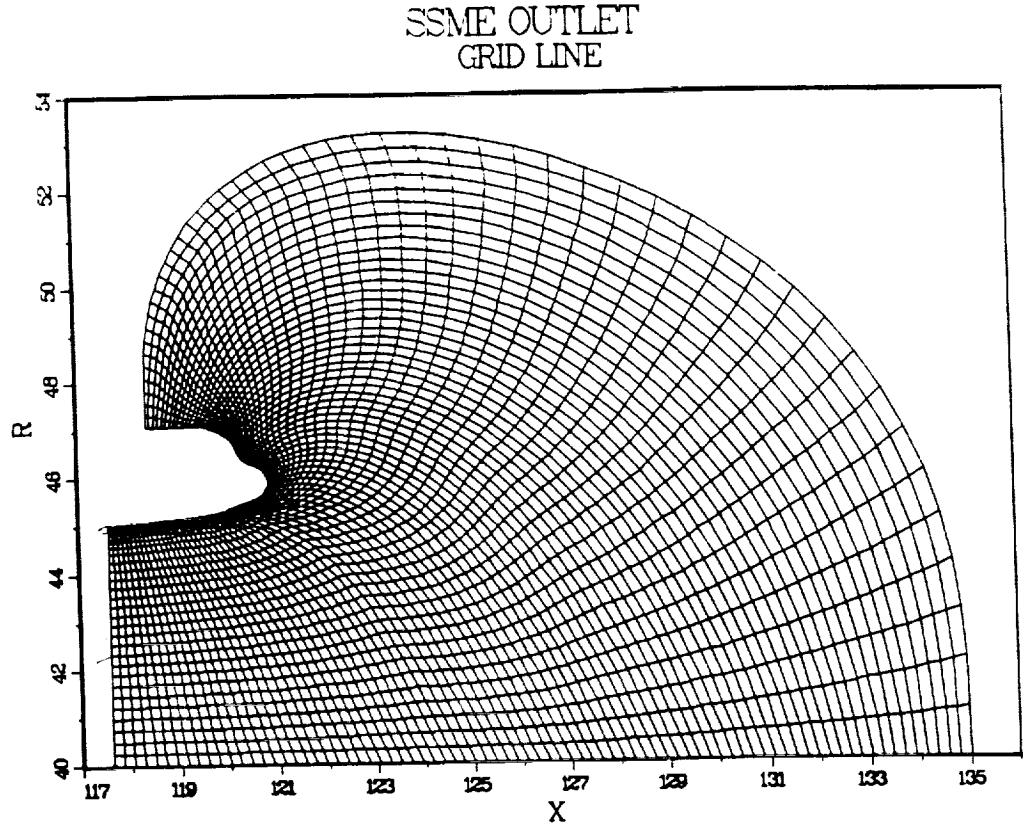

Fig. 13(a), Grid configurations for SSME nozzle exit manifold

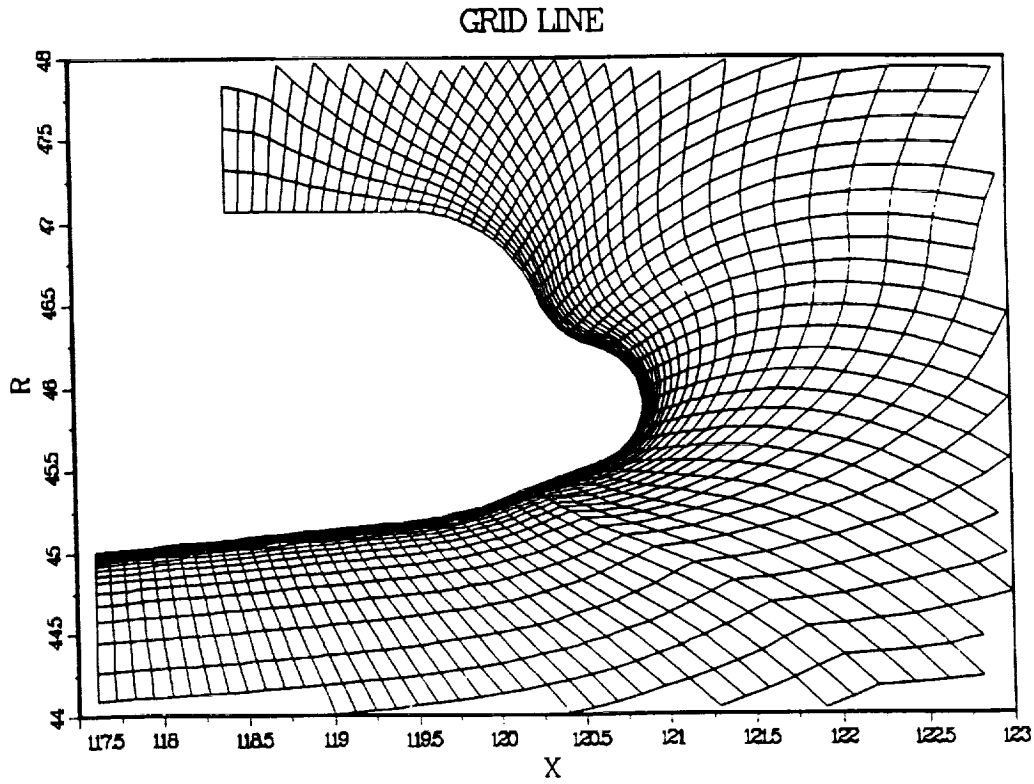

Fig. 13(b), Close-up grids for Figure 13(a)

SSME OUTLET
CONTOUR OF PRSSURE

Uncooled-Wall

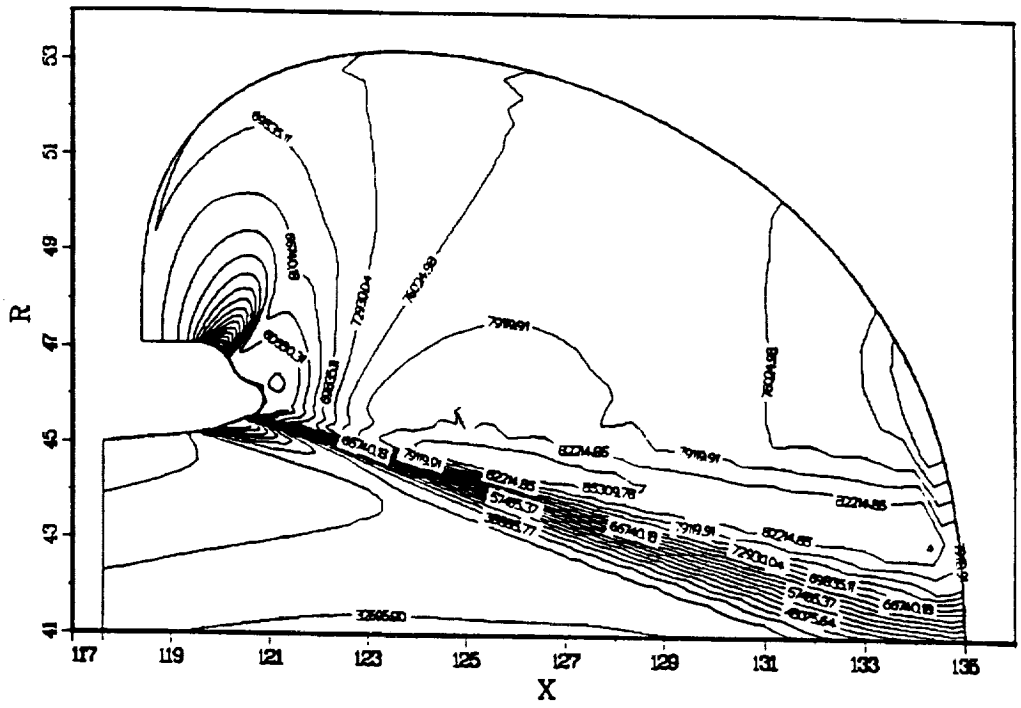

SSME OUTLET
CONTOUR OF PRSSURE

Cooled-Wall

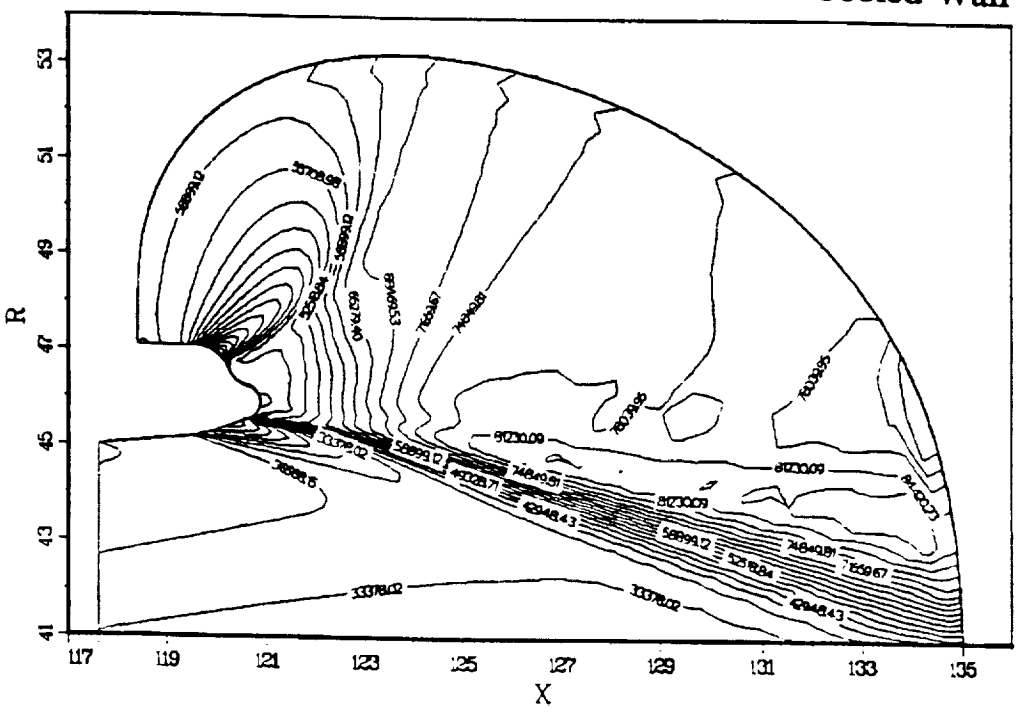

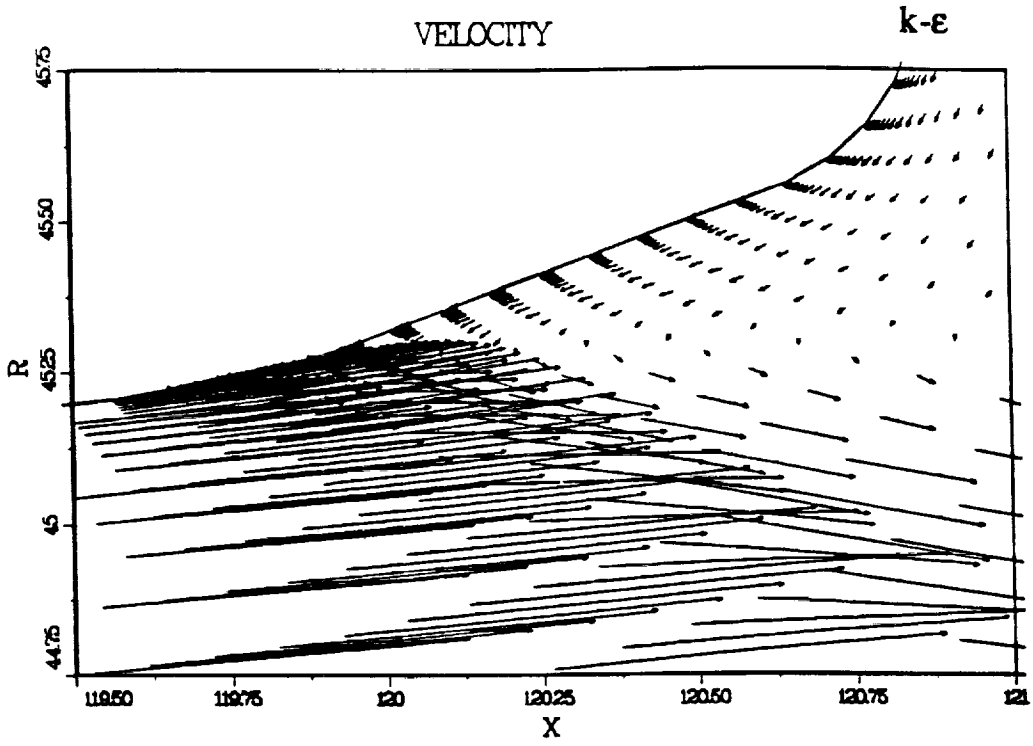
VELOCITY
k-ε
45.75
45.50
45.25
45
44.75
R
119.50
119.75
120
120.25
120.50
120.75
121
X

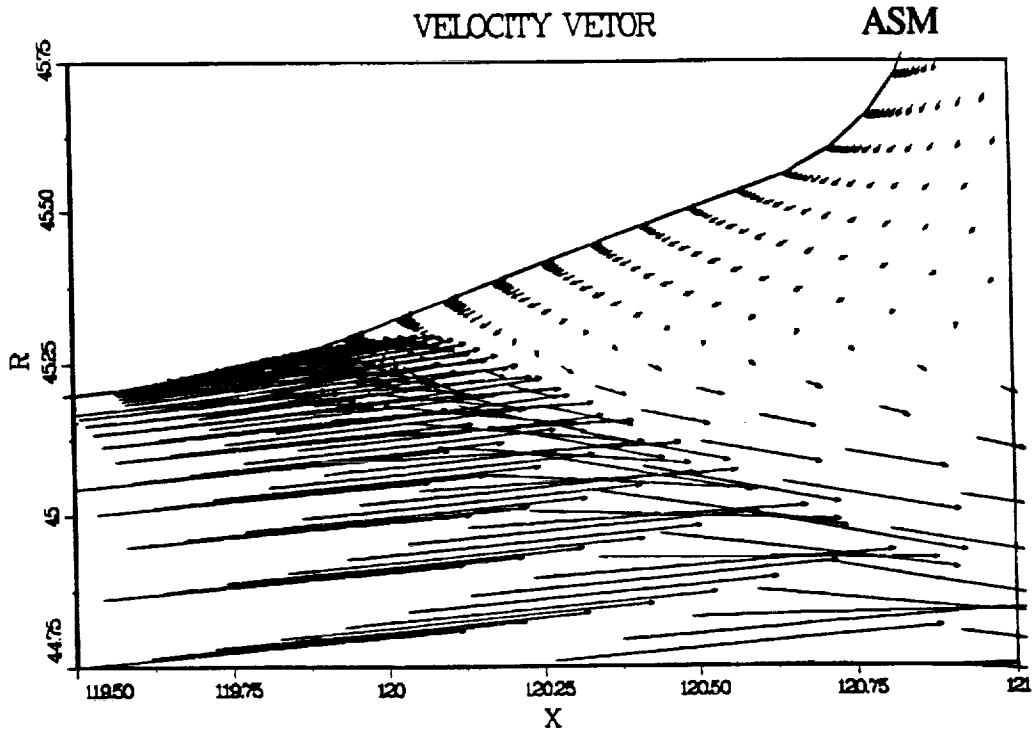
VELOCITY VETOR
ASM
45.75
45.50
45.25
45
44.75
R
119.50
119.75
120
120.25
120.50
120.75
121
X

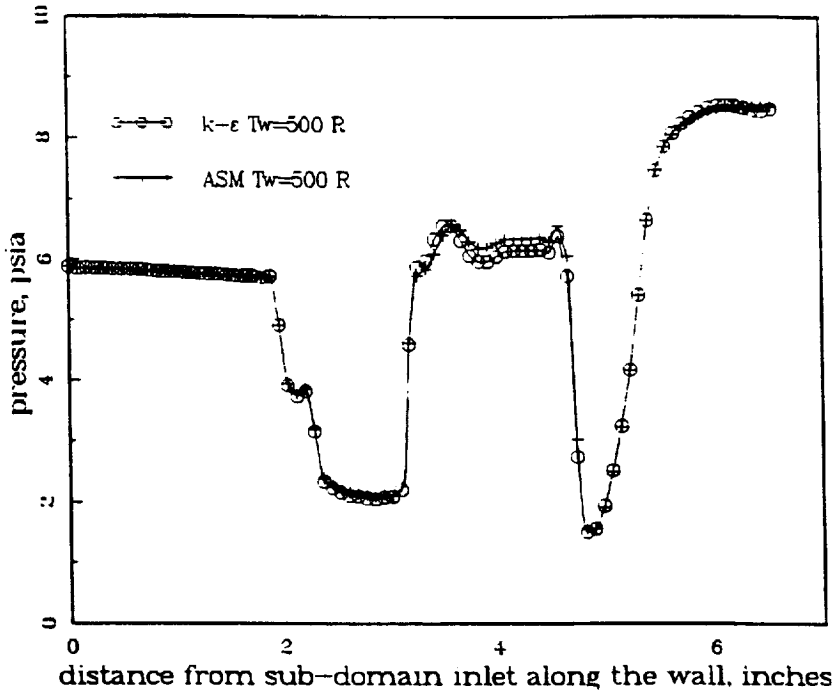

Fig. 17(a), Pressure levels along the wall near the nozzle exit using the ASM and k-ε models

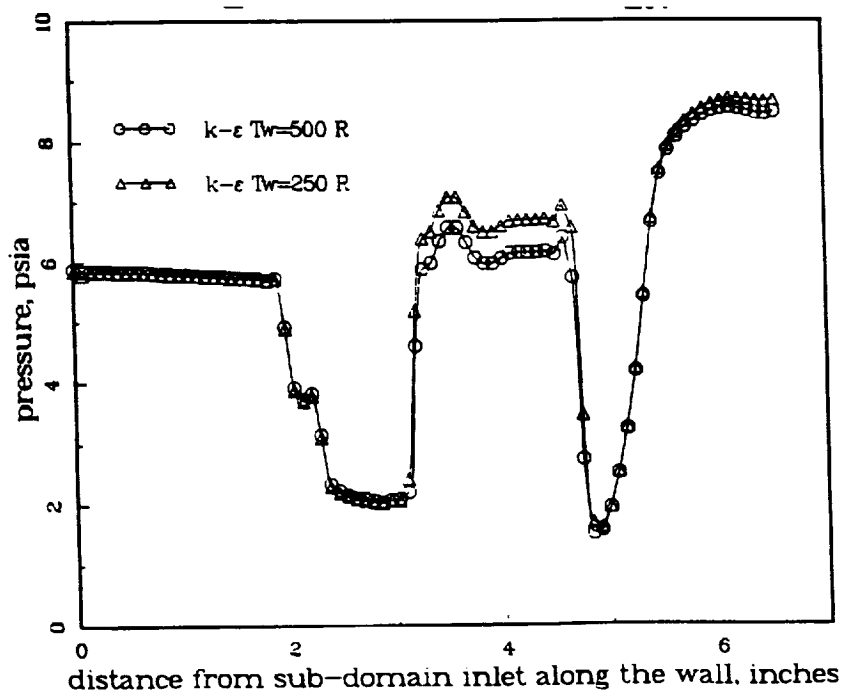

Fig. 17(b), Effects of wall temperature on the wall pressure

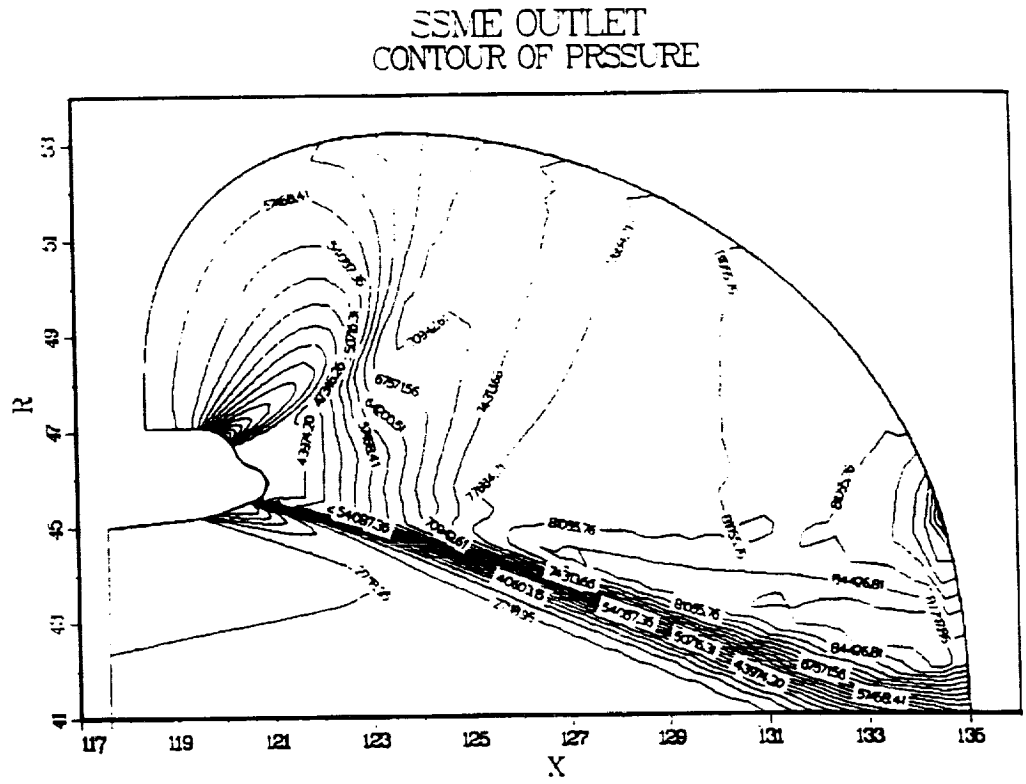

Fig. 18, Contour of pressure using 75% of the chamber pressure level

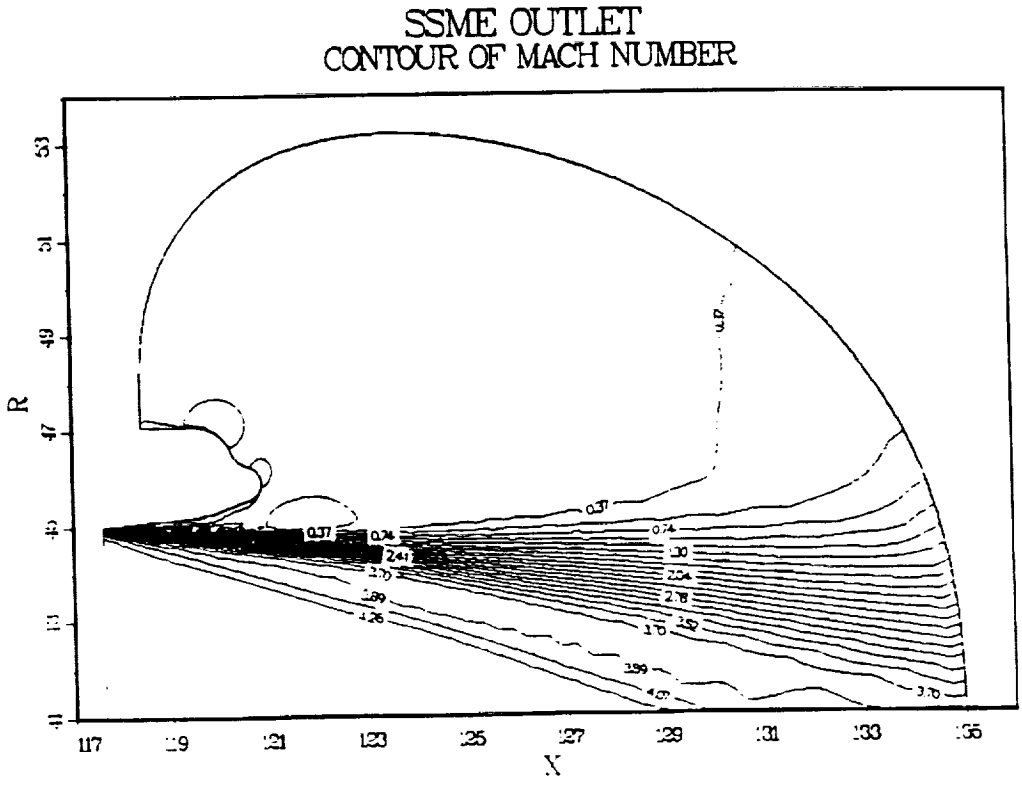

Fig. 19, Laminar flow calculations of the SSME exit flow

Summaries

- The Algebraic Stress Model Removes the Isotropic Turbulence Assumption for the Eddy Viscosity Type Models
- Improved On the Reynolds Stresses Predictions
- The ASM Does Not Improve Too Much On SSME Nozzle & Outlet Flows
  - ---RSM
  - ---Other Mechanisms
    - Shock- Boundary Layer Interactions
    - Entrainment Issues
- 3-D Calculations Are Desirable

Summaries

- The Algebraic Stress Model Removes the Isotropic Turbulence Assumption for the Eddy Viscosity Type Models
- Improved On the Reynolds Stresses Predictions
- The ASM Does Not Improve Too Much On SSME Nozzle & Outlet Flows
  - ---RSM
  - ---Other Mechanisms
    - Shock- Boundary Layer Interactions
    - Entrainment Issues
- 3-D Calculations Are Desirable

ADVANCED TURBULENCE MODELS FOR TURBOMACHINERY

Áli H. Hadid, Michele E. DeCroix, and Munir M. Sindir
Rocketdyne Division, Rockwell International

ABSTRACT

Development and assessment of the single-time-scale k-ε turbulence model with different near-wall treatments and the multi-scale k-ε turbulence model for rotating flows are presented. These turbulence models are coded as self-contained module decks that can be interfaced with a number of CFD main flow solvers. For each model, a stand-alone module deck with its own formulation, discretization scheme, solver and boundary condition implementations is presented. These satellite decks will take as input (from a main flow solver) the velocity field, grid, boundary condition specifications and will deliver turbulent quantities as output. These modules were tested as a separate entities and although many logical and programming problems were overcome only wider use and further testing can render the modules sufficiently "fool proof".

DEVELOPMENT OF A MODULAR FORMAT FOR GENERAL USE TURBULENCE MODELS

Ali H. Hadid
Michele E. DeCroix

Rockwell International, Rocketdyne Division

Workshop for Computational Fluid Dynamic Applications in Rocket Propulsion

April 20-22, 1993
NASA Marshall Space Flight Center

Rockwell International
Rocketdyne Division

STRUCTURE OF FUTURE CODES LEADS TO DEVELOPMENT OF MODULES

- **FUTURE CODES COMPOSED AT TIME OF EXECUTION**
  - INTELLIGENT DRIVERS
  - MODULES FOR PHYSICAL MODELS
- **INTEGRAL PRE- AND POSTPROCESSING TOOLS**
- **COMMON DATA BASE**

TURBULENCE MODELS TO BE ASSESSED

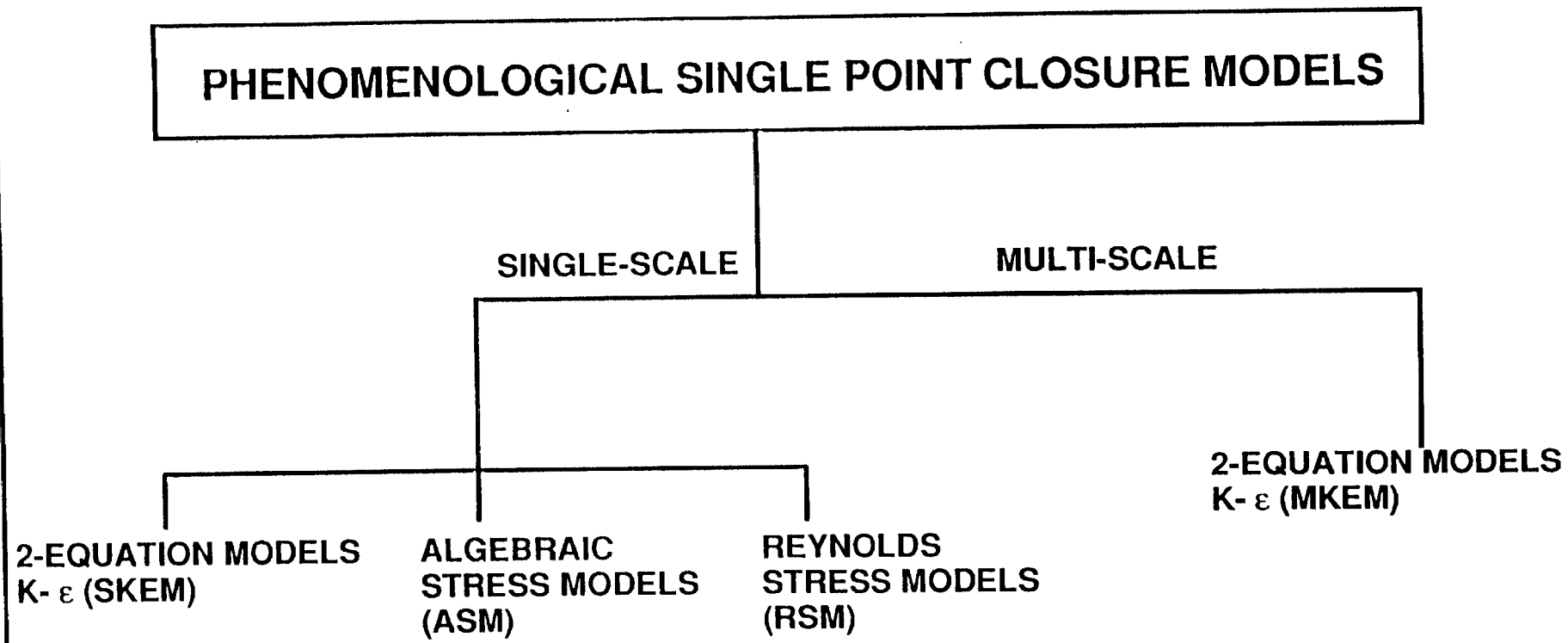

- THE 2-D/AXISYMMETRIC SINGLE-SCALE K-ε MODULE DECK (KEMOD-1) AND THE 2-D/AXISYMMETRIC MULTI-SCALE K-ε MODULE DECK (KEMOD-2) ARE COMPLETE

- NEAR-WALL TREATMENTS WILL INCLUDE (WHERE APPROPRIATE) WALL FUNCTIONS, MULTILAYER MODELS, AND LOW-REYNOLDS NUMBER APPROXIMATIONS

TURBULENCE MODEL DECK STRUCTURE AND INTEGRATION WITH NAVIER-STOKES SOLVER

- MODULES ARE BASED ON THE PHENOMENOLOGICAL SINGLE POINT TURBULENCE CLOSURE MODELS
- THEY ARE STRUCTURED BASICALLY TO ACCEPT AS INPUT THE MEAN FLOW VELOCITIES FROM A N-S SOLVER AND TO RETURN TURBULENCE QUANTITIES TO THE SOLVER

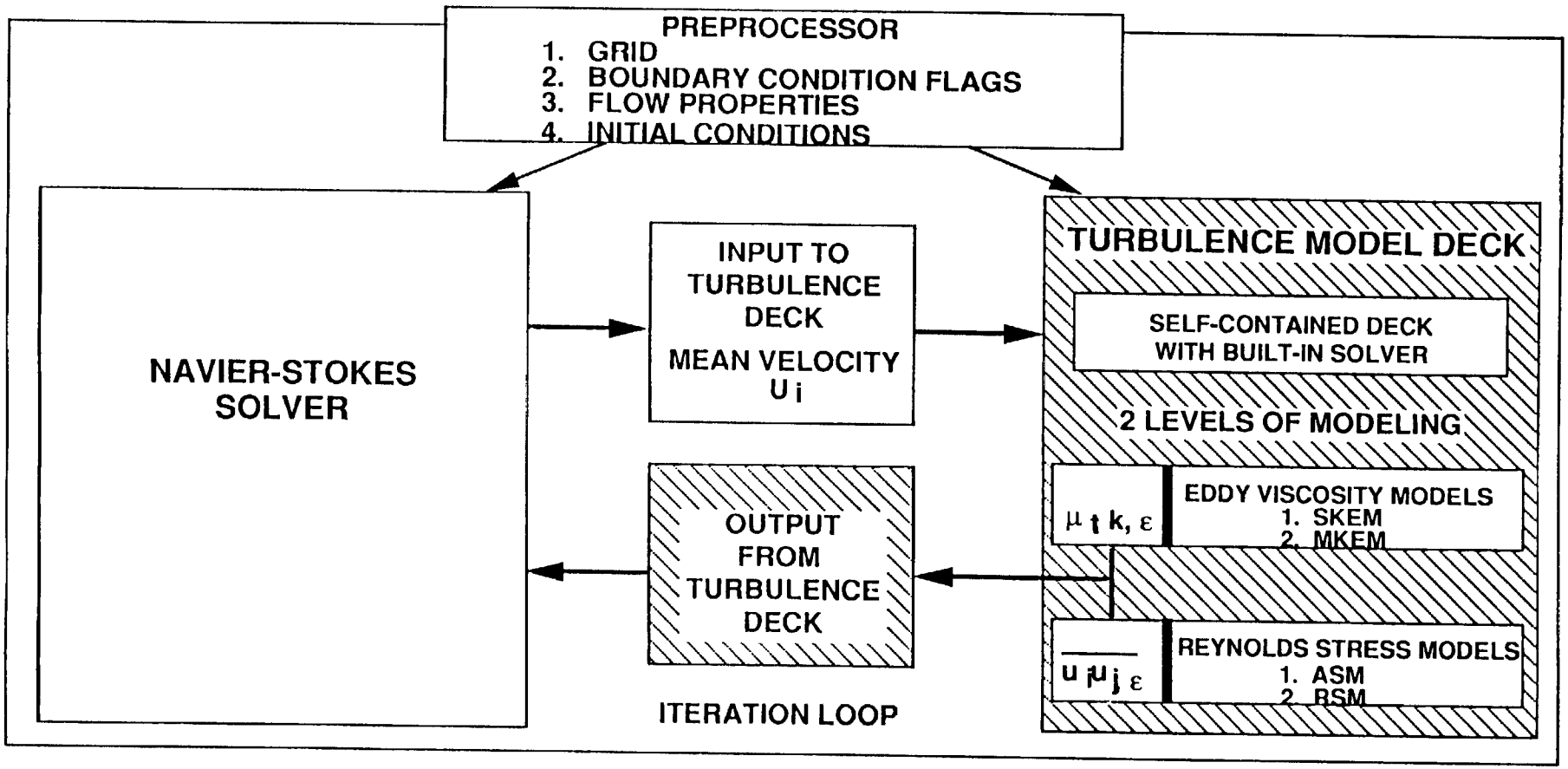

Rockwell International
Rocketdyne Division

CFD 93-013-006/D1/AHH

SINGLE-SCALE k-ε MODEL

- GENERALIZED TRANSPORT EQUATION IN 2-D/AXISYMMETRIC GEOMETRY

$$\frac{\partial(\rho u\phi)}{\partial x} + \frac{1}{r}\frac{\partial}{\partial r}(\rho r v\phi) = \frac{\partial}{\partial x}(\Gamma\phi_x \frac{\partial\phi}{\partial x}) + \frac{1}{r}\frac{\partial}{\partial r}(r\Gamma\phi_r \frac{\partial\phi}{\partial r}) + S\phi$$

- U-MOMENTUM $\quad \phi = u,\ \Gamma\phi_x = 2\mu_e,\ \Gamma\phi_r = \mu_e$

$$S_u = -\frac{\partial P}{\partial x} + \frac{1}{r}\frac{\partial}{\partial r}(\mu_e r \frac{\partial v}{\partial x})$$

- V-MOMENTUM $\quad \phi = v,\ \Gamma\phi_x = \mu_e,\ \Gamma\phi_r = 2\mu_e$

$$S_v = -\frac{\partial P}{\partial x} - \frac{\partial}{\partial r}(\mu_e r \frac{\partial u}{\partial x}) - 2\mu_e \frac{v}{r^2} + \frac{\rho w^2}{r}$$

SINGLE-SCALE k-ε MODEL (CONT'D)

- W-MOMENTUM

$$\phi = w,\ \Gamma\phi_x = \mu_e,\ \Gamma\phi_r = \mu_e$$

$$S_w = -\frac{\rho v w}{r} + \frac{w}{r^2}\frac{\partial}{\partial r}(r\mu_e)$$

- TURB. KINETIC ENERGY

$$\phi = K,\ \Gamma\phi_x = \mu + \frac{\mu_t}{\sigma_k} = \Gamma\phi_r$$

$$S_\phi = G - \rho\varepsilon$$

- TURB. ENERGY DISSIPATION

$$\phi = \varepsilon,\ \Gamma\phi_x = \mu + \frac{\mu_t}{\sigma_k} = \Gamma\phi_r$$

$$S_\phi = \frac{\varepsilon}{k}(c_1 f_1 G - c_2 f_2 \rho\varepsilon)$$

SINGLE-SCALE k-ε MODEL (CONT'D)

- $G = \mu_e \left\{ 2\left[\left(\frac{\partial u}{\partial x}\right)^2 + \left(\frac{\partial v}{\partial r}\right)^2 + \left(\frac{v}{r}\right)^2 \right] + \left(\frac{\partial u}{\partial r} + \frac{\partial v}{\partial x}\right)^2 + \left(\frac{\partial w}{\partial x}\right)^2 + \left(\frac{\partial w}{\partial r} - \frac{w}{r}\right)^2 \right\}$

- $\mu_t = C_\mu f_\mu \rho \frac{k^2}{\varepsilon}$

$\mu_e = \mu + \mu_t$

$C_\mu = 0.09,\ c_1 = 1.44,\ c_2 = 1.92,\ \sigma_k = 1.0,\ \sigma_\varepsilon = 1.0$

1756

KEMOD-1 MODULE DECK

- KEMOD-1 IS THE SINGLE-SCALE K-ε TURBULENCE MODULE DECK. IT CONSISTS OF TWO SEPARATE ROUTINES KEMOD AND MODIFY WHICH HAVE TO BE LINKED TO THE MAIN FLOW SOLVER

- KEMOD IS CALLED WITHIN THE ITERATION LOOP OF THE MAIN FLOW SOLVER

- THE MEAN VELOCITIES AND OTHER VARIABLES ARE PASSED TO THE MODULE THROUGH ITS ARGUMENT LIST (EXPLAINED IN THE USER'S MANUAL)

- A NONSTAGGERED BODY FITTED GRID ARRANGEMENT IS USED BY THE MODULE. IT USES THE MEAN FLOW VARIABLES (VELOCITIES AND MASS FLUXES) TO CONSTRUCT THE DISCRETIZED ALGEBRAIC EQUATION

- DISCRETIZED ALGEBRAIC EQUATIONS ARE SOLVED BY STONE'S STRONGLY IMPLICIT SOLVER

KEMOD-1 MODULE DECK (CONT'D)

- **SUBROUTINE GRIDG**

  READS GRID NODE LOCATIONS PASSED FROM MAIN SOLVER AND FOR THE FIRST ITERATION CALCULATES GRID RELATED QUANTITIES (CELL AREAS AND VOLUME, NORMAL DISTANCES FROM SOLID BOUNDARIES AND INTERPOLATION FACTORS)

- **SUBROUTINE CALCE**

  ASSEMBLES THE COEFFICIENTS AND SOURCE TERMS FOR THE DISCRETIZED K AND ε TRANSPORT EQUATIONS IN THE FORM

$$A_p \phi_p = \sum_{i = E, W, N, S} A_i \phi_i + S\phi$$

  THE SUBROUTINE SOLVES THE DISCRETIZED EQUATIONS AFTER MODIFYING THE SOURCES AND BOUNDARY CONDITIONS FOR THE PARTICULAR PROBLEM

KEMOD-1 MODULE DECK (CONT'D)

- SUBROUTINE TWOLAY

  CALLED IF THE TWO-LAYER OR THE LOW-REYNOLDS NUMBER MODELS ARE USED. IT CALCULATES THE COEFFICIENTS NEEDED TO DESCRIBE THE ENERGY DISSIPATION AND EDDY VISCOSITIES CLOSE TO A WALL

- SUBROUTINE SOLSIP

  SOLVES THE SYSTEM OF ALGEBRAIC K AND ε EQUATIONS USING STONE'S STRONGLY IMPLICIT METHODS

- SUBROUTINE USERM

  THIS SUBROUTINE HAS DIFFERENT ENTRY SECTIONS WHERE VARIABLES ARE UPDATED AND BOUNDARY CONDITIONS ARE SET

- SUBROUTINE MODIFY

  THIS IS THE ONLY SUBROUTINE THAT HAS TO BE CALLED FROM THE MOMENTUM EQUATION SOLVER OF THE MAIN ROUTINE. IT UPDATES THE FLUX SOURCE TERM OF THE DISCRETIZED MOMENTUM EQUATION DUE TO WALL SHEAR STRESSES

KEMOD-1 MODULE DECK (CONT'D)

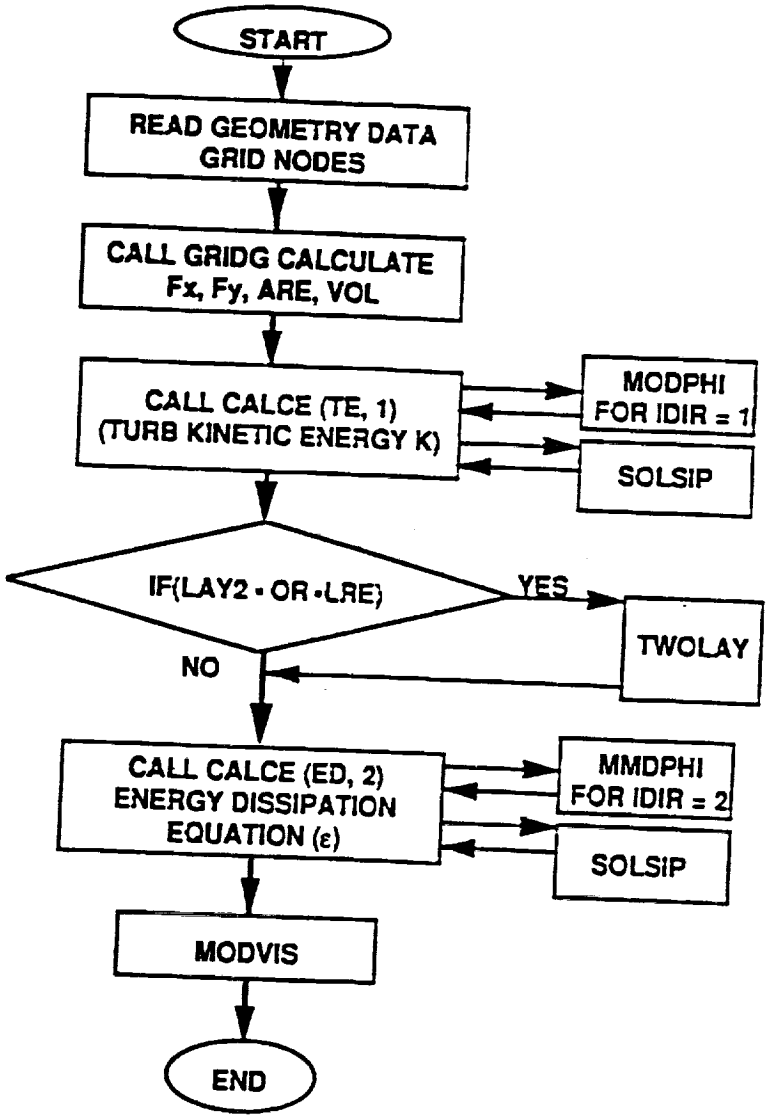

KEMOD FLOW CHART

KEMOD-1 MODULE DECK (CONT'D)

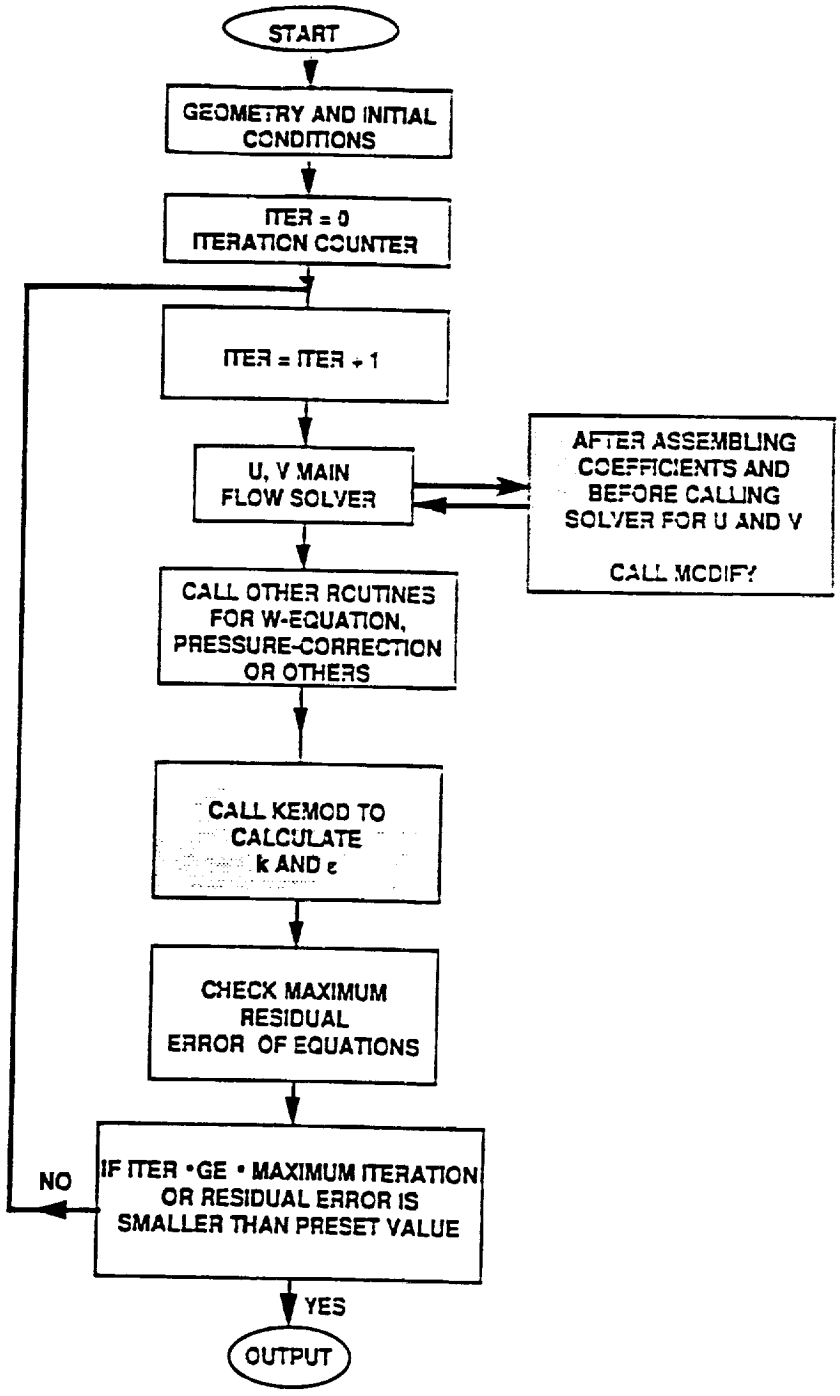

KEMOD-1 INTERFACE WITH A MAIN SOLVER

MULTI-SCALE k-ε MODEL

- DERVIED BY PARTITIONING THE TURBULENT ENERGY SPECTRUM INTO TWO SETS OF WAVE NUMBER REGIONS (PRODUCTION AND DISSIPATION RANGES) GIVING TWO EVOLUTION EQUATIONS FOR EACH REGION

- PARTITION LOCATION IS DETERMINED AS PART OF THE SOLUTION

- TURBULENT KINETIC ENERGY IN THE PRODUCTION RANGE OF THE SPECTRUM

$$\phi = k_p, \Gamma_{\phi x} = \Gamma_{\phi r} = \mu + \frac{\mu_t}{\sigma k_p}$$

$$S_{k_p} = G - \rho\varepsilon_p$$

MULTI-SCALE k-ε MODEL (CONT'D)

- **ENERGY TRANSFER RATE IN THE PRODUCTION RANGE OF THE SPECTRUM**

$$\phi = \varepsilon_p, \quad \Gamma_{\phi x} = \Gamma_{\phi r} = \frac{\mu_t}{\sigma k_p}$$

$$S_{\varepsilon p} = \frac{1}{\rho} C_{p1} \frac{G^2}{K_p} + C_{p2} \frac{G\varepsilon_p}{k_p} - \rho C_{p3} \frac{\varepsilon_p^2}{k_p}$$

- **TURBULENT KINETIC ENERGY IN THE DISSIPATION RANGE OF THE SPECTRUM**

$$\phi = k_t, \quad \Gamma_{\phi x} = \Gamma_{\phi r} = \frac{\mu_t}{\sigma k_t}$$

$$S_{kt} = \rho\varepsilon_p - \rho\varepsilon_t$$

MULTI-SCALE k-ε MODEL (CONT'D)

- **ENERGY DISSIPATION RATE IN THE DISSIPATION RANGE**

$$\phi = \varepsilon_t, \Gamma_{\phi x} = \Gamma_{\phi r} = \mu + \frac{\mu_t}{\sigma_{\varepsilon t}}$$

and

$$S_{\varepsilon t} = \rho C_{t1} \frac{\varepsilon_p^2}{k_t} + \rho C_{t2} \frac{\varepsilon_t \varepsilon_p}{k_t} - \rho C_{t3} \frac{\varepsilon_t^2}{k_t}$$

- **MODEL IS SIMILAR TO THAT USED BY KIM AND CHEN WITH CONSTANTS**

$$\sigma_{kp} = 0.75,\ \sigma_{\varepsilon p} = 1.15,\ \sigma_{kt} = 0.75,\ \sigma_{\varepsilon t} = 1.15$$

$$C_{p1} = 0.21,\ C_{p2} = 1.24,\ C_{p3} = 1.84,\ C_{t1} = 0.29$$

$$C_{t2} = 1.28,\ C_{t3} = 1.66 \text{ and } C_\mu = 0.09$$

KEMOD-2 MODULE DECK

- KEMOD-2 IS A MULTI-TIME SCALE K-ε TURBULENCE MODULE DECK. IT CONSISTS OF TWO MAIN ROUTINES KEMOD AND MODIFY

- KEMOD IS CALLED WITHIN THE ITERATION LOOP OF THE MAIN FLOW SOLVER

- MEAN VELOCITIES AND OTHER VARIABLES ARE PASSED TO THE MODULE THROUGH ITS ARGUMENT LIST (EXPLAINED IN THE USER'S MANUAL

- THE MODULE IS STRUCTURED IN A SIMILAR WAY TO KEMOD-1 AND SUBROUTINE CALCE ASSEMBLES THE COEFFICIENTS AND SOURCE TERMS FOR THE DISCRETIZED K_p, ε_p, K_t, ε_t TRANSPORT EQUATIONS

KEMOD-2 MODULE DECK (CONT'D)

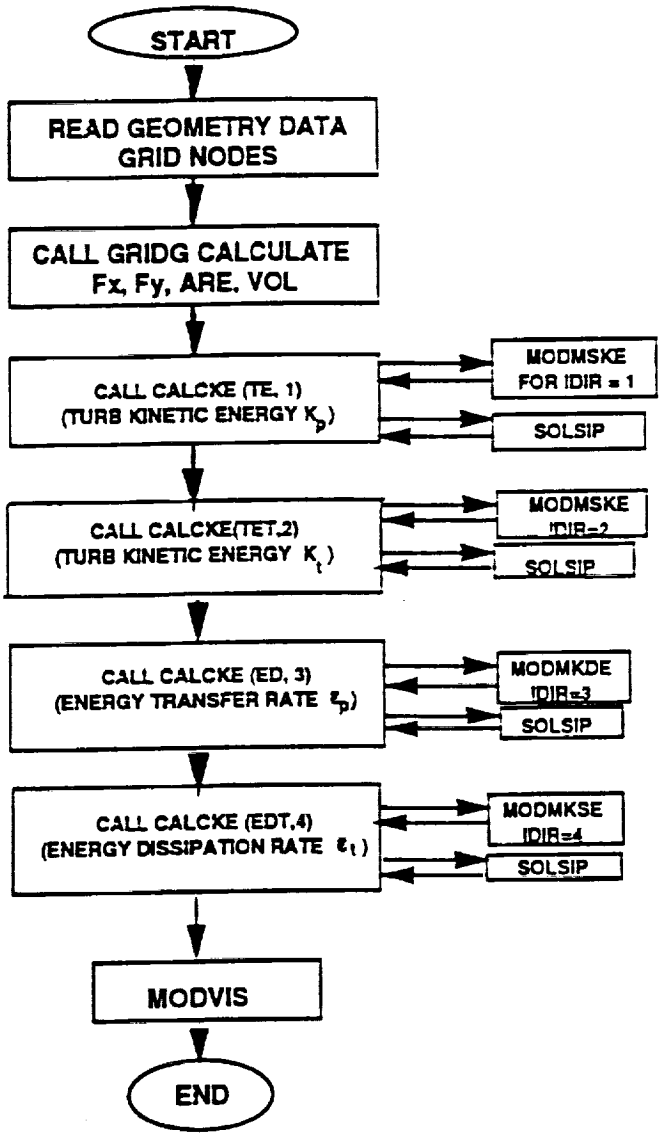

KEMOD-2 FLOW CHART

KEMOD-2 MODULE DECK (CONT'D)

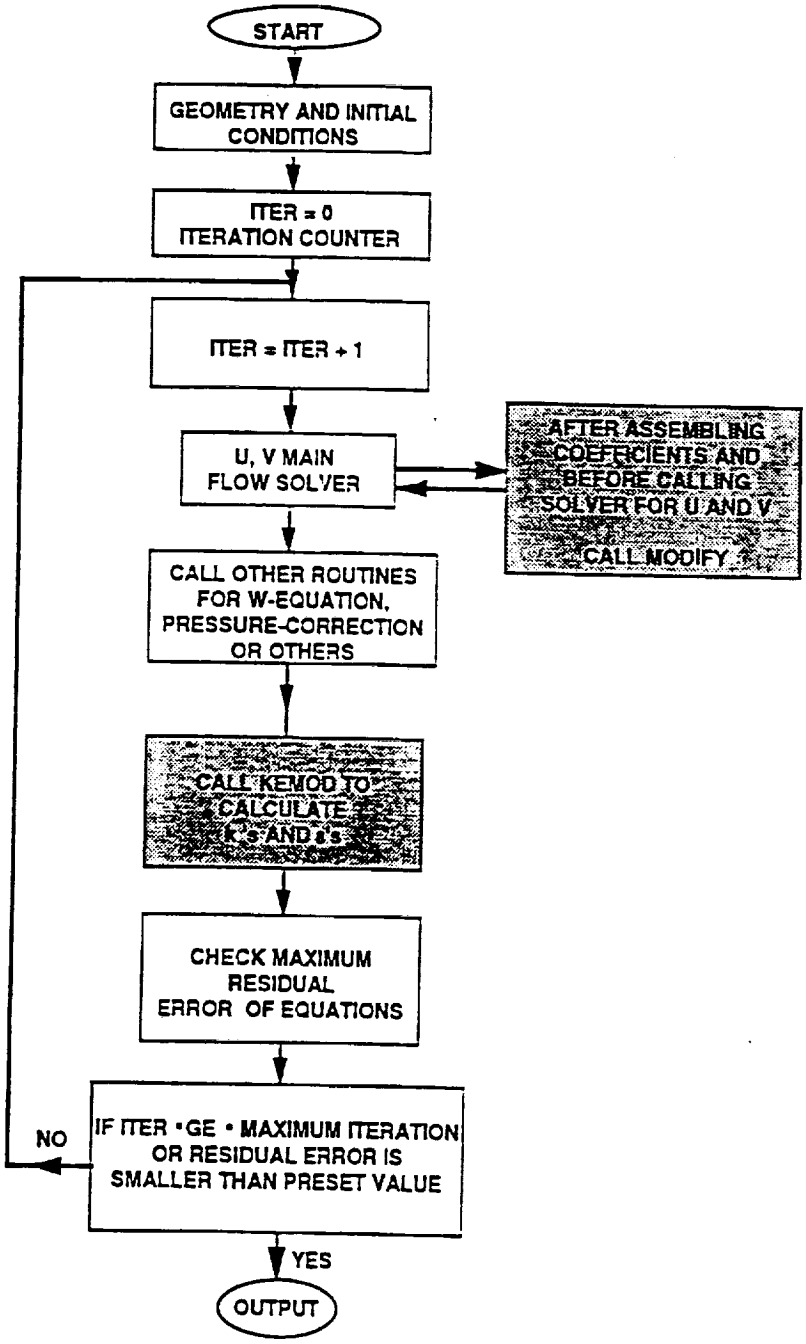

KEMOD-2 INTERFACE WITH MAIN SOLVER

ROBACK AND JOHNSON – SWIRLING COAXIAL JETS DISCHARGING INTO AN EXPANDED DUCT

R. ROBACK AND B. JOHNSON, "MASS AND MOMENTUM TURBULENT TRANSPORT EXPERIMENT WITH CONFINED SWIRLING COAXIAL JETS," NASA CR-168252, 1983

GEOMETRY

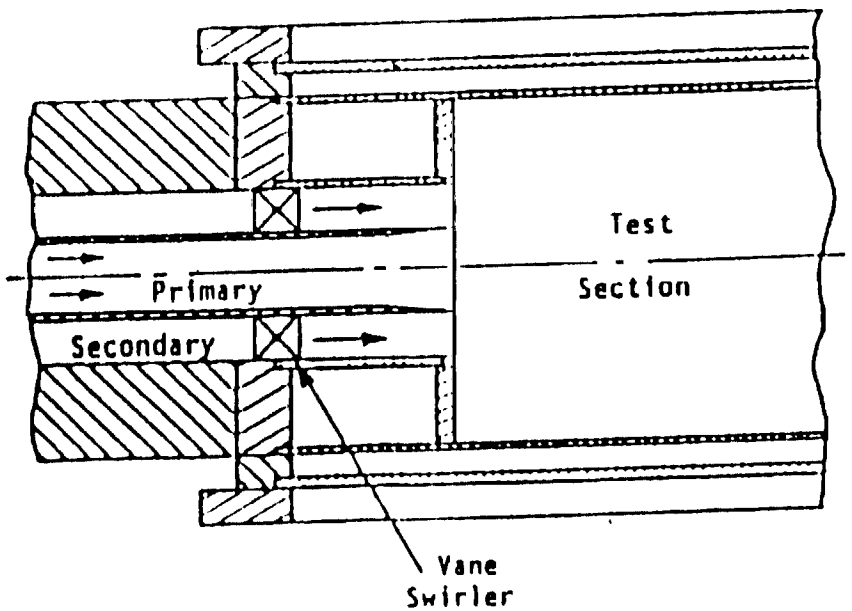

ROBACK AND JOHNSON RESULTS
VELOCITY VECTORS

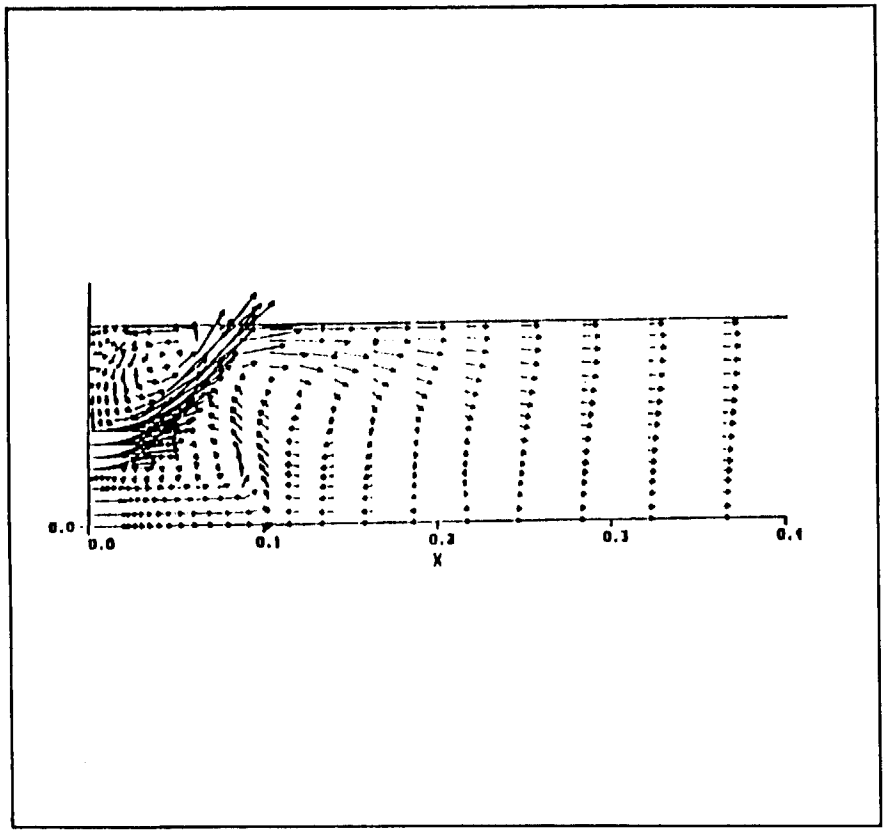

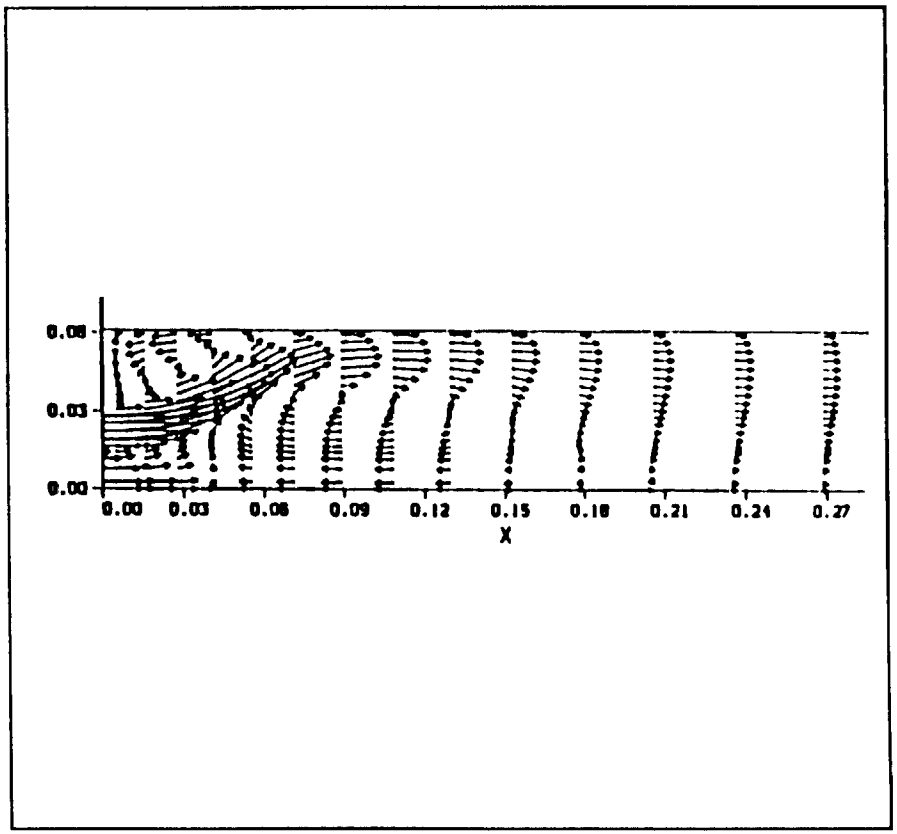

SINGLE-SCALE K-ε MODEL

MULTI-SCALE K-ε MODEL

Rockwell International
Rocketdyne Division

CFD 92-032-020/D3/MMS

1769

ROBACK AND JOHNSON RESULTS
TANGENTIAL VELOCITY PREDICTIONS AT X = 0.025 M

□ DATA
——— WALL FUNCTION
— — — LOW-REYNOLDS NO. MODEL
– · – · – 2-LAYER MODEL

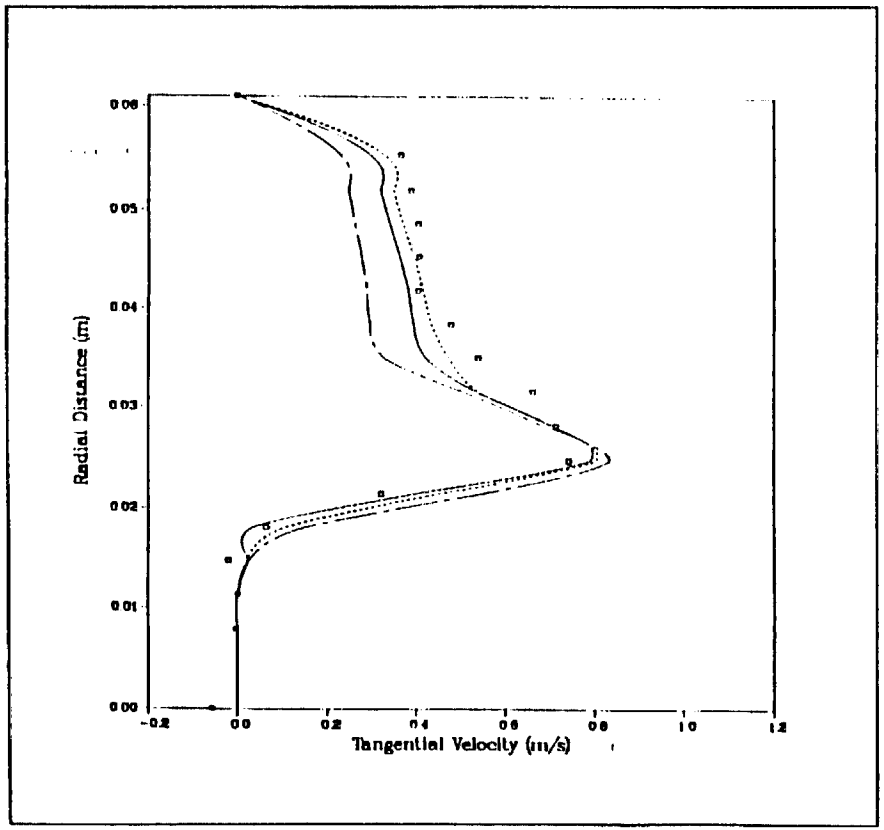

□ DATA
——— SINGLE-SCALE K-ε MODEL
— — — MULTI-TIME SCALE K-ε MODEL

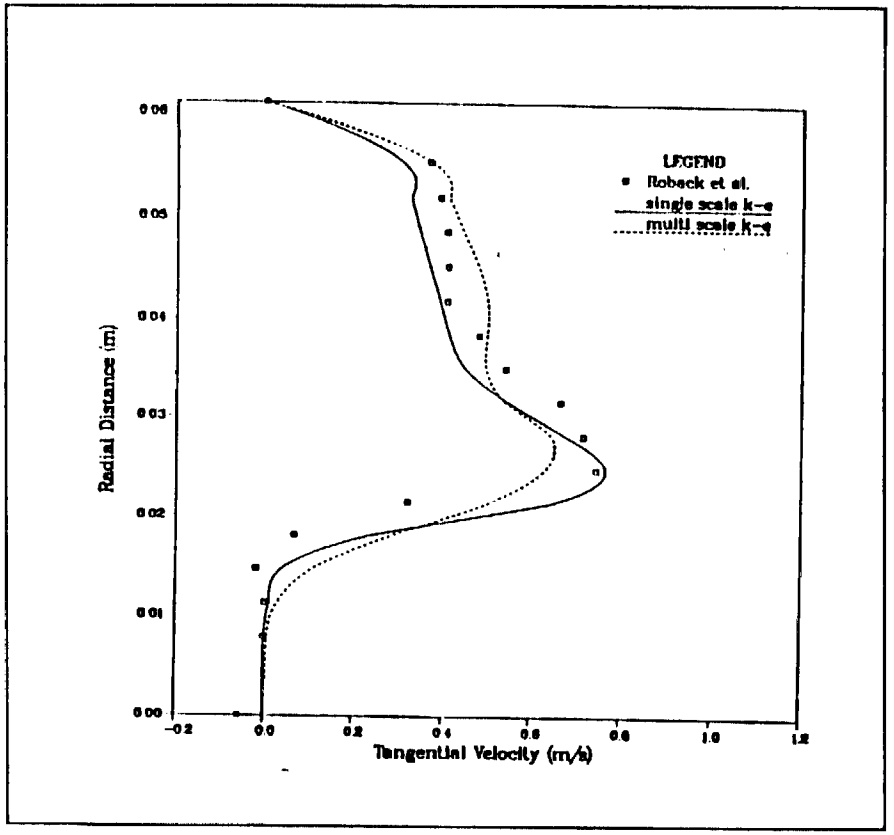

SINGLE-SCALE K-ε

SUMMARY

- **KEMOD-1 (2-D)**
  - SINGLE SCALE k-ε TURBULENCE MODULE COMPLETE
  - TESTED USING REACT AND USA CODES
- **KEMOD-2 (2-D)**
  - MULTISCALE k-ε TURBULENCE MODULE COMPLETE
  - TESTED USING REACT CODE
- **DEVELOPMENT OF MODULES FOR FULL AND ALGEBRAIC REYNOLDS STRESS MODELS IN PROGRESS**
- **WORK ON 3-D MODULES TO BEGIN AS SCHEDULED (FY '94)**

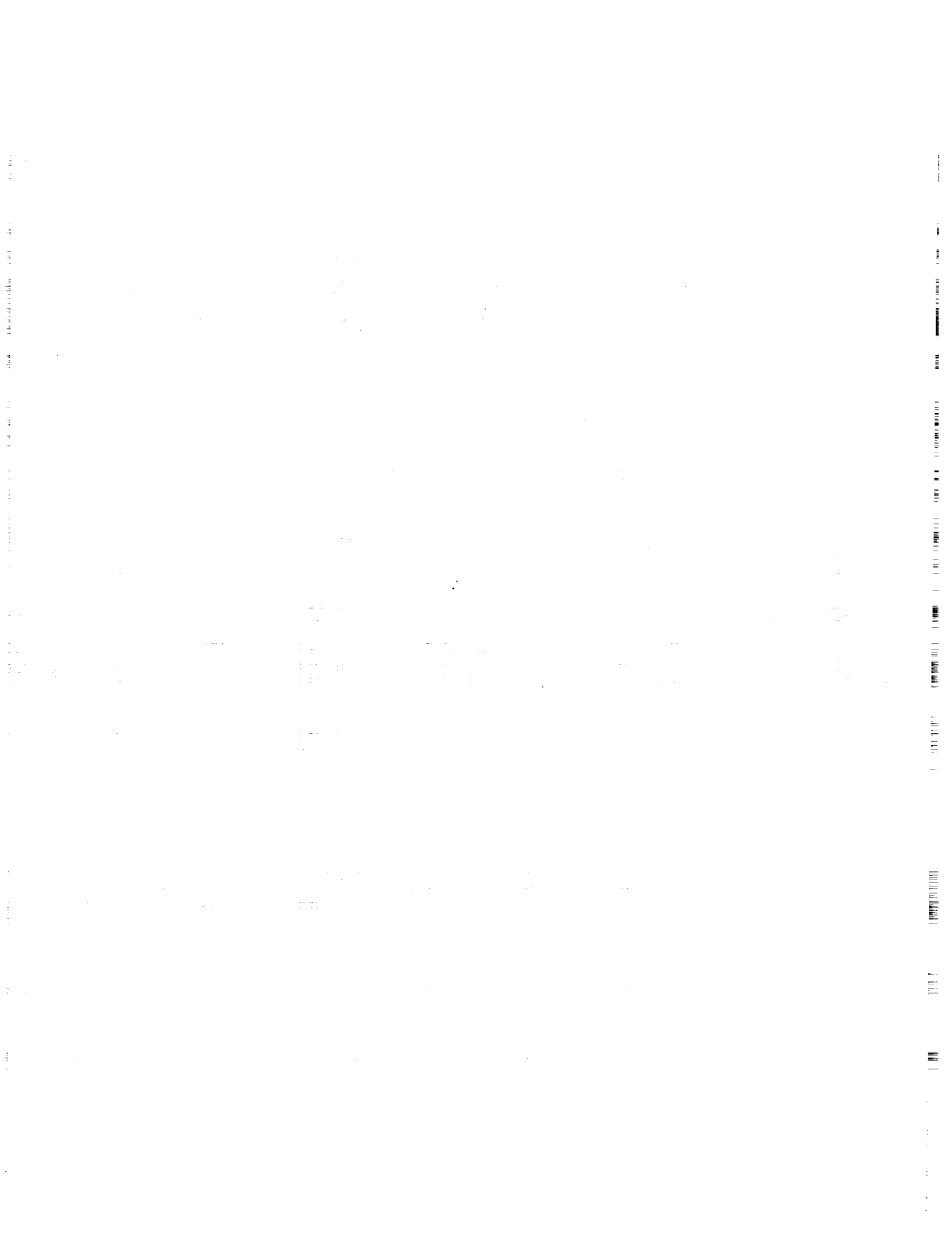

NUMERICAL COMPUTATION OF AERODYNAMICS AND HEAT TRANSFER IN A TURBINE CASCADE AND A TURN-AROUND DUCT USING ADVANCED TURBULENCE MODELS

B. LAKSHMINARAYANA AND J. LUO

The Pennsylvania State University
Department of Aerospace Engineering
University Park, PA 16802

The objective of this research is to develop turbulence models to predict the flow and heat transfer fields dominated by the curvature effect such as those encountered in turbine cascades and turn-around ducts.

A Navier-Stokes code has been developed using an explicit Runge-Kutta method with a two layer k-ε/ARSM (Algebraic Reynolds Stress Model), Chien's Low Reynolds Number (LRN) k-ε model and Coakley's LRN q-ω model. The near wall pressure strain correlation term was included in the ARSM. The formulation is applied to Favre-averaged N-S equations and no thin-layer approximations are made in either the mean flow or turbulence transport equations. Anisotropic scaling of artificial dissipation terms was used. Locally variable timestep was also used to improve convergence. Detailed comparisons were made between computations and data measured in a turbine cascade by Arts et al. at Von Karman Institute. The surface pressure distributions and wake profiles were predicted well by all the models. The blade heat transfer is predicted well by k-ε/ARSM model, as well as the k-ε model. It's found that the onset of boundary layer transition on both surfaces is highly dependent upon the level of local freestream turbulence intensity, which is strongly influenced by the streamline curvature.

Detailed computation of the flow in the turn around duct has been carried out and validated against the data by Monson as well as Sandborn. The computed results at various streamwise locations both on the concave and convex sides are compared with flow and turbulence data including the separation zone on the inner well. The k-ε/ARSM model yielded relatively better results that the two-equation turbulence models. A detailed assessment of the turbulence models has been made with regard to their applicability to curved flows.

NUMERICAL COMPUTATION OF AERODYNAMICS AND HEAT TRANSFER IN A TURBINE CASCADE AND A TURN-AROUND DUCT USING ADVANCED TURBULENCE MODELS*

B. Lakshminarayana and J. Luo

The Pennsylvania State University
Department of Aerospace Engineering
University Park, Pennsylvania

OBJECTIVE:

TO DEVELOP TURBULENCE MODELS TO PREDICT FLOW AND HEAT TRANSFER FIELDS IN TURBOMACHINERY INCLUDING CURVATURE, ROTATION AND HIGH TEMPERATURE EFFECTS

OUTLINE:

- **INTRODUCTION**
- **NUMERICAL TECHNIQUE**
- **TURBULENCE MODELS**
- **FLOW AND HEAT TRANSFER FIELD IN A HIGH MACH NUMBER TRANSONIC TURBINE CASCADE**
- **FLOW FIELD IN A TURN-AROUND DUCT**
- **CONCLUSIONS**

*SPONSORED BY NASA HUNTSVILLE WITH LISA GRIFFIN AS THE TECHNICAL MONITOR

GOVERNING EQUATIONS
(Cartesian)

$$\frac{\partial Q}{\partial t} = -\left(\frac{\partial E}{\partial x} + \frac{\partial F}{\partial y} + \frac{\partial G}{\partial z}\right) + \left(\frac{\partial E_v}{\partial x} + \frac{\partial F_v}{\partial y} + \frac{\partial G_v}{\partial z}\right) + S$$

$$Q = \begin{pmatrix} \rho \\ \rho u \\ \rho v \\ \rho w \\ \rho e_0 \\ \rho k \\ \rho \varepsilon \end{pmatrix}, E = \begin{pmatrix} \rho u \\ \rho uu + p \\ \rho uv \\ \rho uw \\ (\rho e_0 + p)u \\ \rho uk \\ \rho u\varepsilon \end{pmatrix}, F = \begin{pmatrix} \rho v \\ \rho uv \\ \rho vv + p \\ \rho vw \\ (\rho e_0 + p)v \\ \rho vk \\ \rho v\varepsilon \end{pmatrix}, G = \begin{pmatrix} \rho w \\ \rho uw \\ \rho vw \\ \rho ww + p \\ (\rho e_0 + p)w \\ \rho wk \\ \rho w\varepsilon \end{pmatrix},$$

$$E_v = \begin{pmatrix} 0 \\ \tau_{xx} \\ \tau_{xy} \\ \tau_{xz} \\ u\tau_{xx}+v\tau_{xy}+w\tau_{xz}-q_x \\ \left(\mu_l + \frac{\mu_l}{Pr_k}\right)\frac{\partial k}{\partial x} \\ \left(\mu_l + \frac{\mu_l}{Pr_\varepsilon}\right)\frac{\partial \varepsilon}{\partial x} \end{pmatrix}, F_v = \begin{pmatrix} 0 \\ \tau_{yx} \\ \tau_{yy} \\ \tau_{yz} \\ u\tau_{yx}+v\tau_{yy}+w\tau_{yz}-q_y \\ \left(\mu_l + \frac{\mu_l}{Pr_k}\right)\frac{\partial k}{\partial y} \\ \left(\mu_l + \frac{\mu_l}{Pr_\varepsilon}\right)\frac{\partial \varepsilon}{\partial y} \end{pmatrix}, G_v = \begin{pmatrix} 0 \\ \tau_{zx} \\ \tau_{zy} \\ \tau_{zz} \\ u\tau_{zx}+v\tau_{zy}+w\tau_{zz}-q_z \\ \left(\mu_l + \frac{\mu_l}{Pr_k}\right)\frac{\partial k}{\partial z} \\ \left(\mu_l + \frac{\mu_l}{Pr_\varepsilon}\right)\frac{\partial \varepsilon}{\partial z} \end{pmatrix}, S = \begin{pmatrix} 0 \\ 0 \\ \rho(\omega^2 y + 2\omega w) \\ \rho(\omega^2 z - 2\omega v) \\ 0 \\ P - \rho\varepsilon + \mathfrak{D} \\ (C_1 P - C_2 \rho\varepsilon)\frac{\varepsilon}{k} + \mathfrak{E} \end{pmatrix}$$

- Relative velocities, constant rotation rate about x axis, ω. Averaged quantities.
- Energy, $e_0 = \varepsilon + \frac{q^2}{2} - \frac{\omega^2 r^2}{2}$, rothalpy constant along streamlines for inviscid steady state.

TECHNIQUES

1. RK2D code :

* 2-D Navier-Stokes code, Conservative, compressible formulation

* Favre-Averaged Mean and Turbulence equations

* 4-stage explicit Runge-Kutta scheme

* 2nd and 4th order artificial dissipation (with eigenvalue and local velocity scaling)

* Coupled with compressible Low-Reynolds number K-ε model , q-ω model , ARSM , NLSM (Nonlinear -stress model) , AHFM(Algebraic Heat Flux model)

* Characteristic boundary conditions, H grids (generated by a combined algebraic and elliptic method to keep smoothness and orthogonality near the wall)

2. TEXSTAN code

* 2-D boundary layer code developed by Crawford

* Extension of STAN 5, Patankar-Spalding numerical scheme

* Include 7 differential two-equation turbulence models (Jones-Launder, Chien,Lam- Bremhorst , etc.) and mixing length model

RSM (Reynolds Stress Model)
(Gibson & Launder 1978)

Reynolds stresss transport equation :

$$U_k \frac{\partial \overline{u_i u_j}}{\partial x_k} = -\overline{u_i u_k} U_{j,k} - \overline{u_j u_k} U_{i,k} + \overline{\frac{p}{\rho}(u_{i,j} + u_{j,i})}$$

$$-\frac{\partial}{\partial x_k}\left[\overline{u_i u_j u_k} + \frac{\overline{p u_j}}{\rho}\delta_{ik} + \frac{\overline{p u_i}}{\rho}\delta_{jk} - \nu\frac{\partial \overline{u_i u_j}}{\partial x_k}\right] - 2\nu\overline{\frac{\partial u_i}{\partial x_k}\frac{\partial u_j}{\partial x_k}}$$

i.e., $C_{ij} - D_{ij} = P_{ij} + \phi_{ij} - \varepsilon_{ij}$

where $\varepsilon_{ij} = \frac{2}{3}\varepsilon$ (Dissipation)

$\phi_{ij} = \phi_{ij1} + \phi_{ij2} + \phi_{ij1,w} + \phi_{ij2,w}$ (Pressure-strain correlation)

$\phi_{ij1} = -C_1 \frac{\varepsilon}{k}(\overline{u_i u_j} - \frac{2}{3}k\delta_{ij})$ (Return-to-isotropy part)

$\phi_{ij2} = -C_2(P_{ij} - \frac{2}{3}P_k\delta_{ij})$ (Rapid part)

$$\phi_{ijw,1} = c_1' \frac{\varepsilon}{k}(\overline{u_k u_m} n_k n_m \delta_{ij} - \frac{3}{2}\overline{u_i u_k} n_k n_j - \frac{3}{2}\overline{u_j u_k} n_k n_i) f_n$$

(Near-wall term)

$$\phi_{ijw,2} = c_2'(\phi_{km,2} n_k n_m \delta_{ij} - \frac{3}{2}\phi_{ik,2} n_k n_j - \frac{3}{2}\phi_{jk,2} n_k n_i) f_n$$

(Near-wall term)

$f_n = k^{3/2}/(2.55 x_n \varepsilon)$ (x_n is the distance normal to the wall)

Constants : c_1=1.8, c_2=0.6, c_1' =0.5, c_2' =0.3

ARSM (Algebraic Reynolds Stress Model)

ARSM assumption:

$$C_{ij} - D_{ij} = \frac{\overline{u_i u_j}}{k}(C_k - D_k) = \frac{\overline{u_i u_j}}{k}(P_k - \varepsilon)$$

$$\Rightarrow C_{ij} - D_{ij} = \frac{\overline{u_i u_j}}{k}(C_k - D_k) = \frac{\overline{u_i u_j}}{k}(P_k - \varepsilon)$$

$$\Rightarrow C_{ij} - D_{ij} = \frac{\overline{u_i u_j}}{k}(C_k - D_k) = \frac{\overline{u_i u_j}}{k}(P_k - \varepsilon)$$

where

$$P_k = -\overline{u_i u_j} U_{i,j}$$

$$P_{ij} = -\overline{u_i u_k} U_{j,k} - \overline{u_j u_k} U_{i,k}$$

$\phi_{ij1,w}$ and $\phi_{ij2,w}$ as in RSM

NLSM (Nonlinear Stress Model)
(Shih , Zhu & Lumley 1992)

Reynolds stress :

$$\overline{u_i u_j} = \frac{2}{3}k\delta_{ij} - \nu_t(U_{i,j} + U_{j,i}) + \frac{C_{\tau 1}}{A_2 + \eta^3}\frac{k^3}{\varepsilon^2}(U_{i,k}U_{k,j} + U_{j,k}U_{k,i} - \frac{2}{3}\pi\delta_{ij}) + \frac{C_{\tau 2}}{A_2 + \eta^3}\frac{k^3}{\varepsilon^2}(U_{i,k}U_{j,k} - \frac{1}{3}\tilde{\pi}\delta_{ij}) + \frac{C_{\tau 3}}{A_2 + \eta^3}\frac{k^3}{\varepsilon^2}(U_{k,i}U_{k,j} - \frac{1}{3}\tilde{\pi}\delta_{ij})$$

where

$$\pi = U_{i,j}U_{j,i}$$

$$\tilde{\pi} = U_{i,j}U_{i,j}$$

$$\nu_t = C_\mu \frac{k^2}{\varepsilon}$$

$$C_\mu = \frac{2/3}{A_1 + \eta + \alpha\xi}$$

$$\xi = \frac{k}{\varepsilon}\Omega$$

$$\Omega = (2\Omega^*_{ij}\Omega^*_{ij})^{\frac{1}{2}}$$

$$\Omega^*_{ij} = (U_{i,j} - U_{j,i})/2$$

$$\eta = \frac{k}{\varepsilon}S$$

$$S = (2S_{ij}S_{ij})^{\frac{1}{2}}$$

$$S_{ij} = (U_{i,j} + U_{j,i})/2$$

Constants:

$C_{\tau 1}$	$C_{\tau 2}$	$C_{\tau 2}$	A_1	α	A_2
-4	13	-2	1.25	0.9	1000

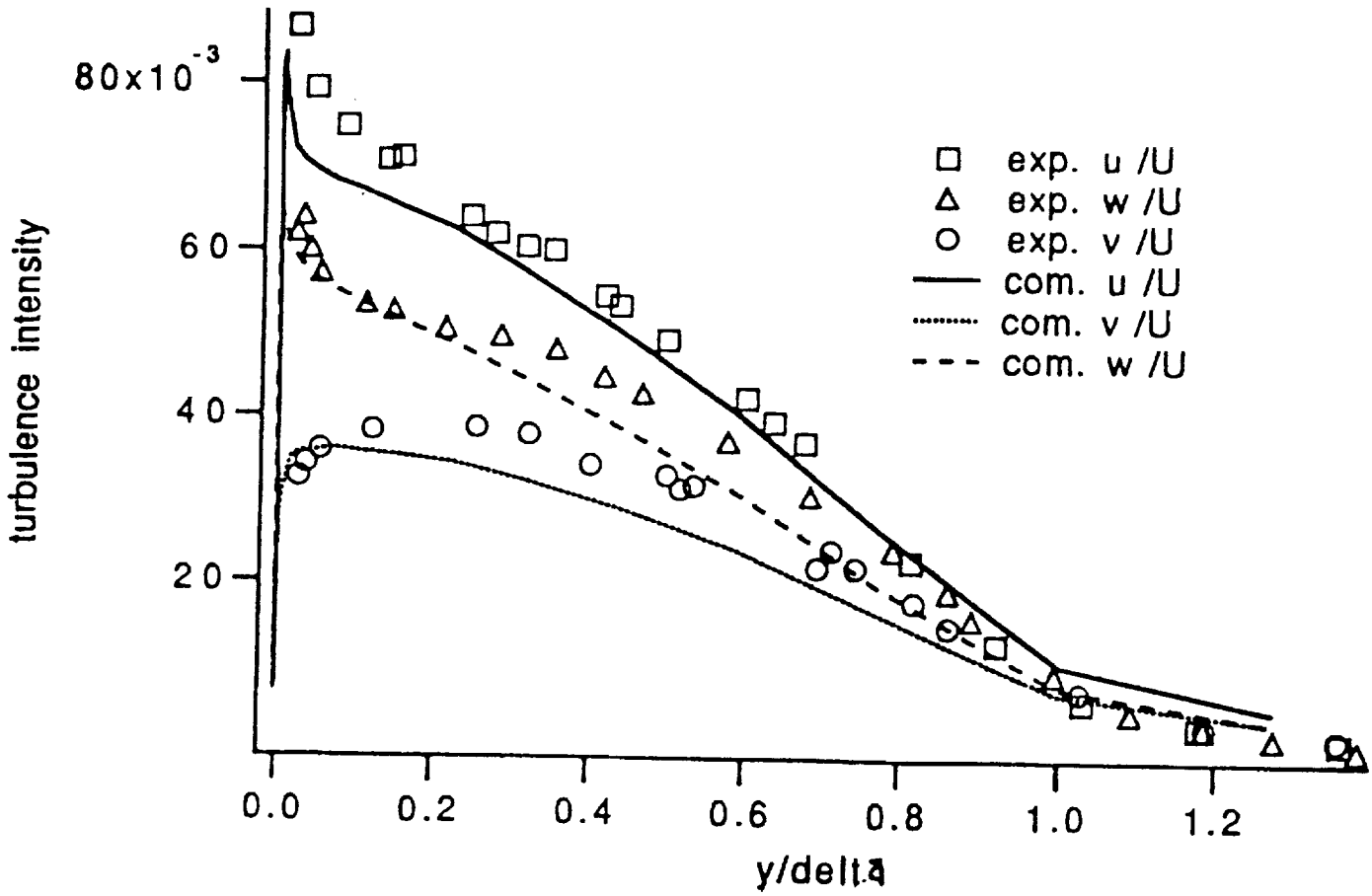

Fig. Validation of the ARSM model: Turbulence intensity profile in the flat-plate turbulent boundary layer : experiment by Klebanoff; computation by ARSM

180-degree TURN AROUND DUCT(TAD)

Geometry & Grid :

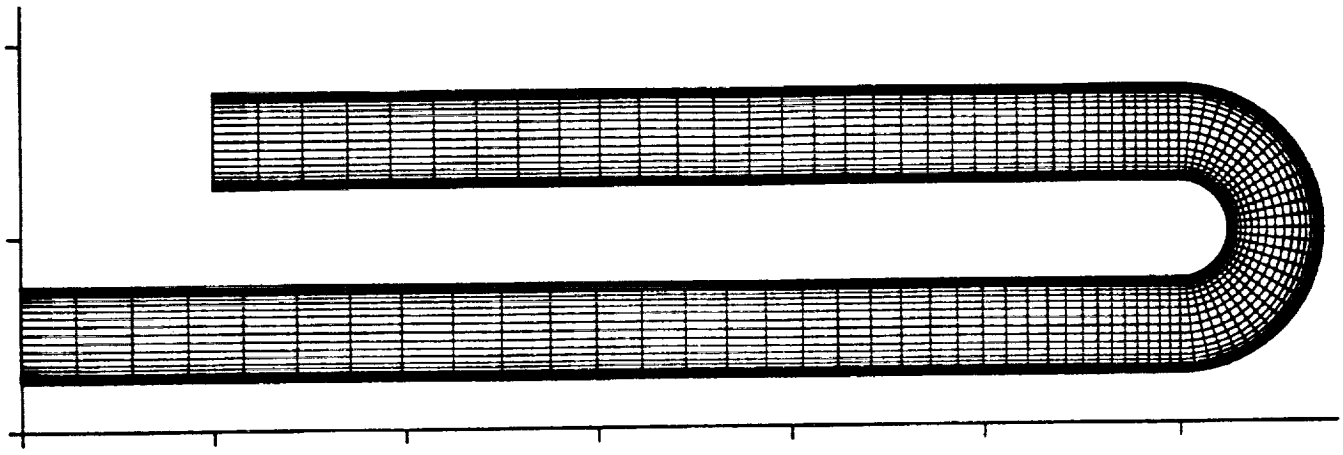

EARLIER RESEARCH ON TAD FLOW

- Measurements:

*Sandborn (1988), Sandborn and Shin (1989) (Water flow, Re=7×10^4- $5*10^5$ (Re based on duct height and bulk velocity)

*Monson, Seegmiller , McConnaughey & Chen (1989,1990) (Air flow, Re=10^5,10^6)

*Sharma etal (1987) (Axisymmetric TAD air flow, Re=10^5)

- Earlier Computations:

*Chen and Sandborn (1986) (K-ε and curvature-corrected K-ε)

*Monson, Seegmiller & McConnaughey (1989,1990) (mixing-length & K-ε with curvature-correction)

*Avva etal (1990) (High Re and Low-Re K-ε)

*Gallardo & Lakshminarayana (1993) (curvature-modified K-ε)

- Agreement in above computations are not satisfactory.

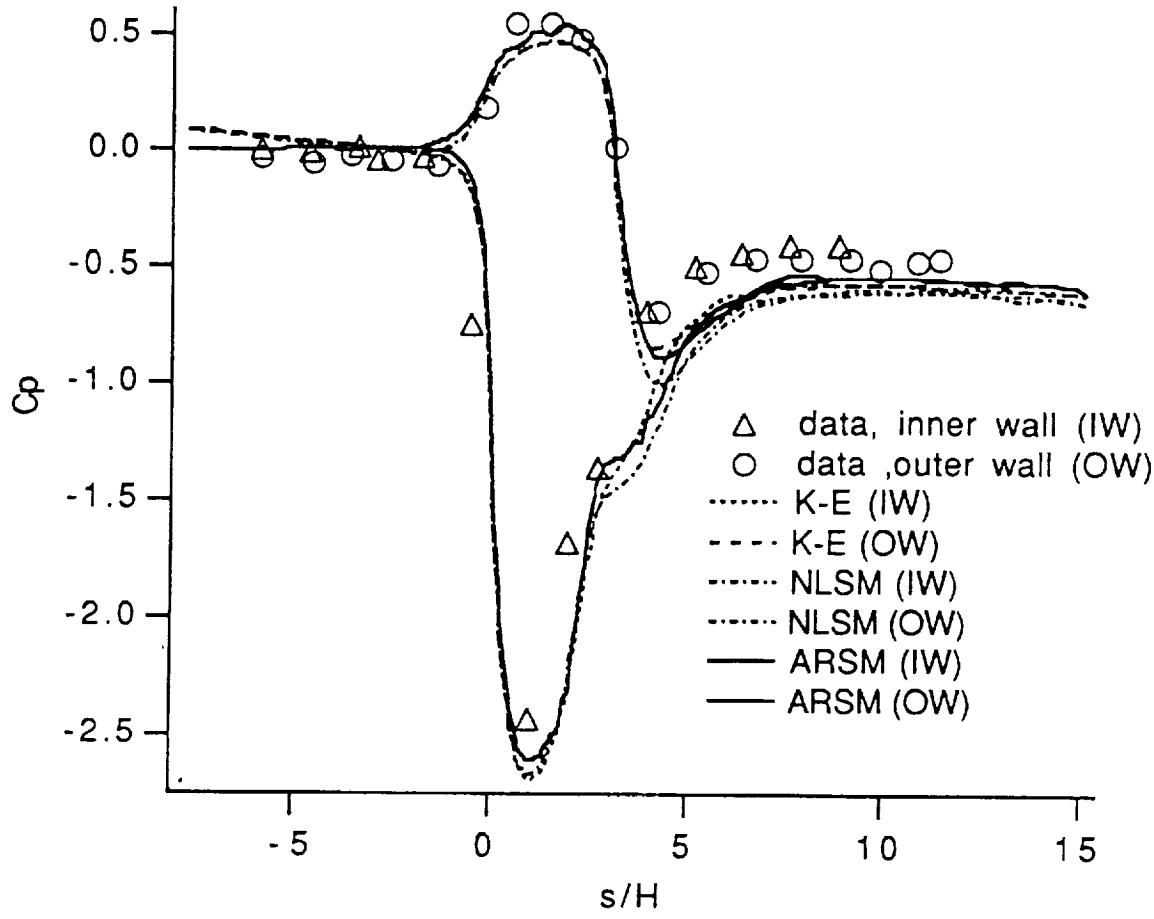

Fig.1 Static pressure coefficient on turnaround duct inner and outer walls

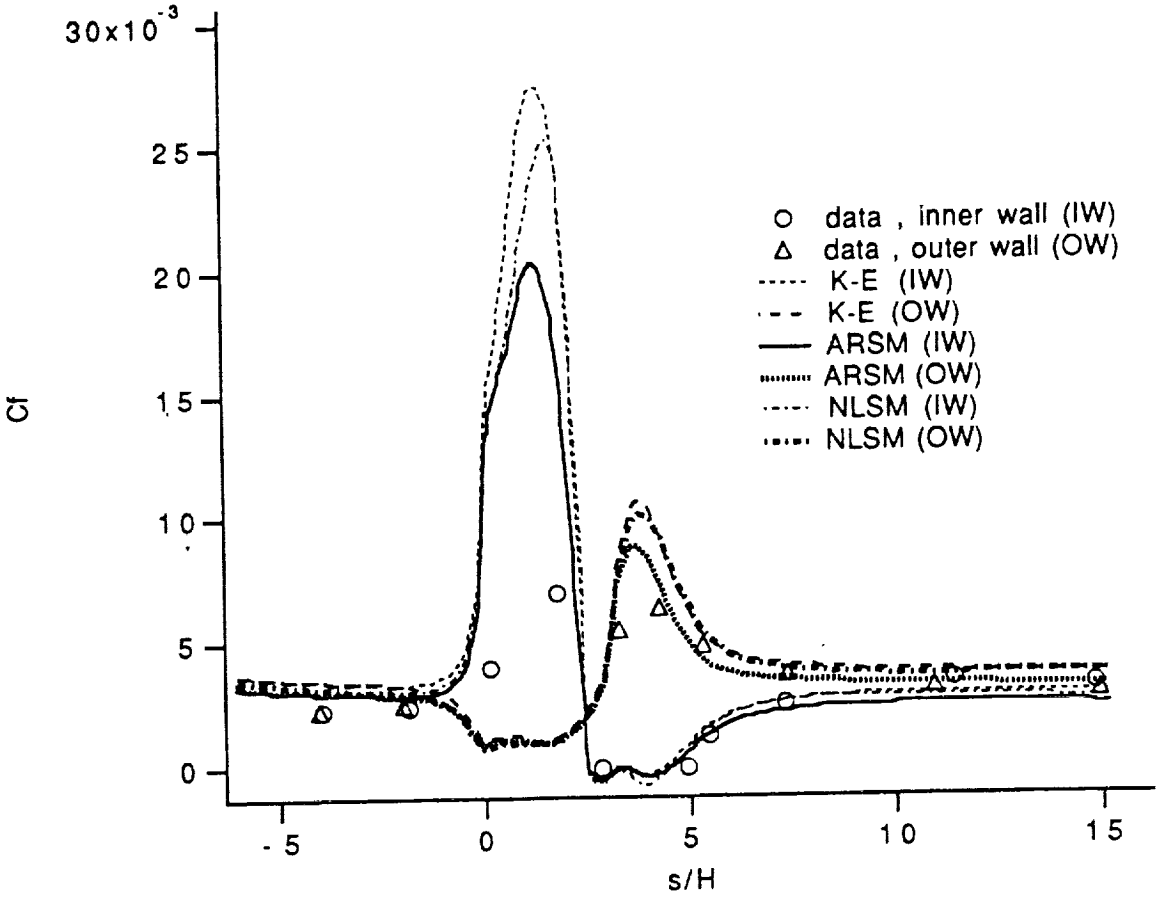

Fig. 2 Skin friction coefficient on turnaround duct inner and outer walls

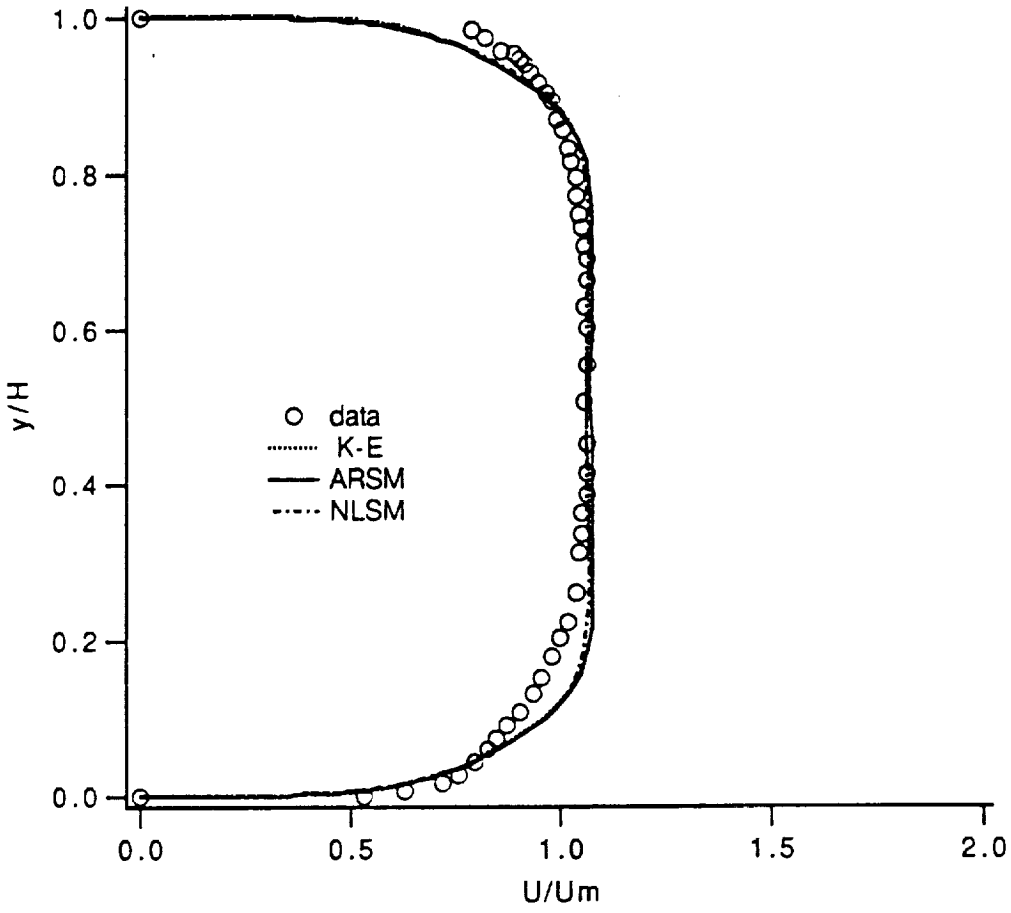

Fig.3 (a) Longitudinal velocity in turnaround duct, x/H=-4

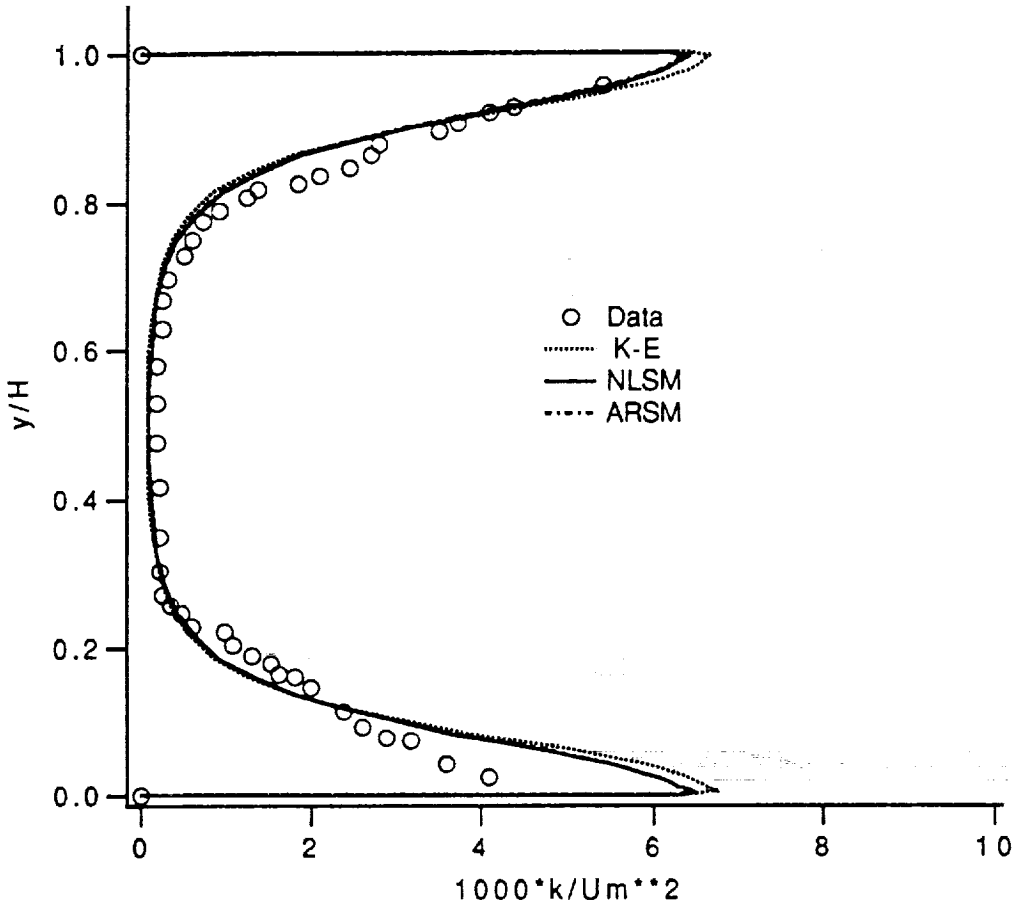

Fig.3(b) Turbulent kinetic energy profile

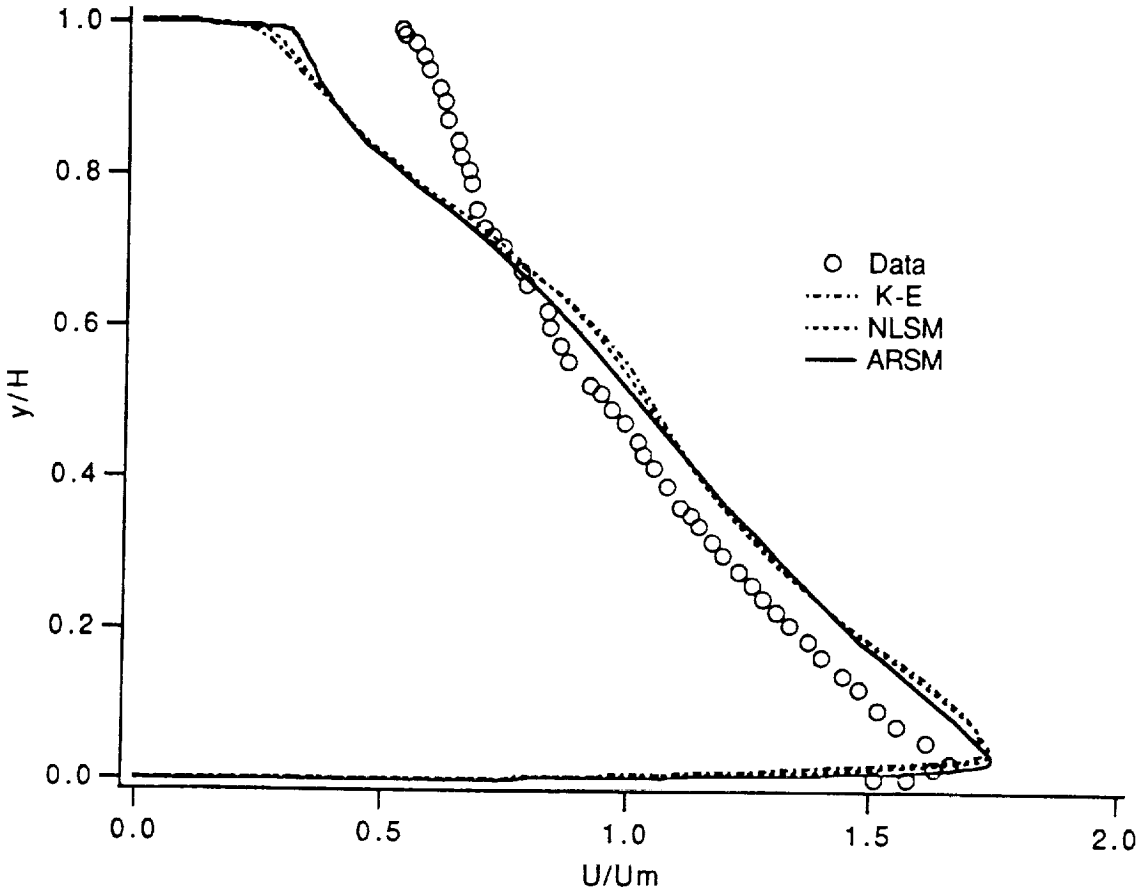

Fig.5(b) Longitudinal velocity in turnaround duct, theta=90 deg.

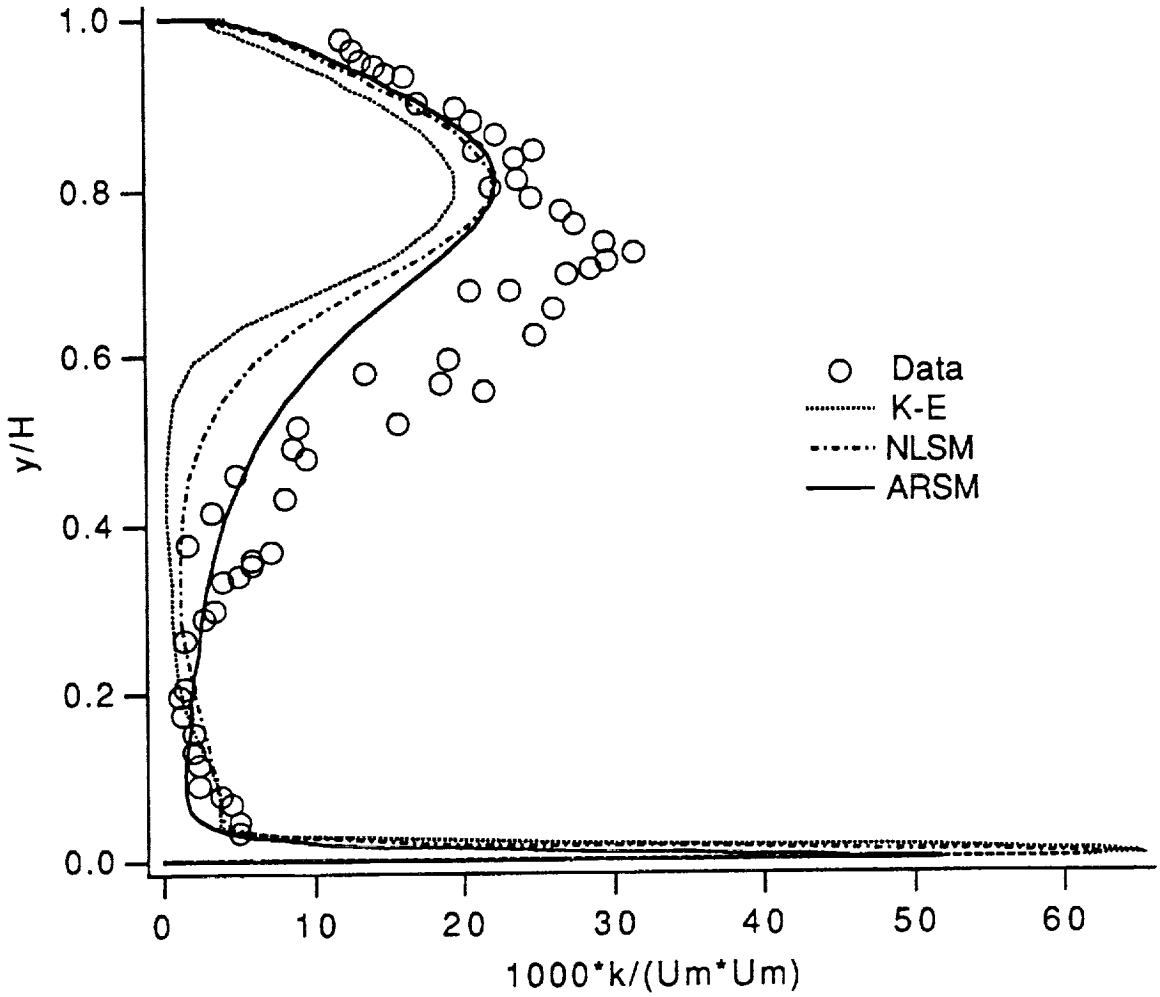

Fig.5(c) Turbulent kinetic energy

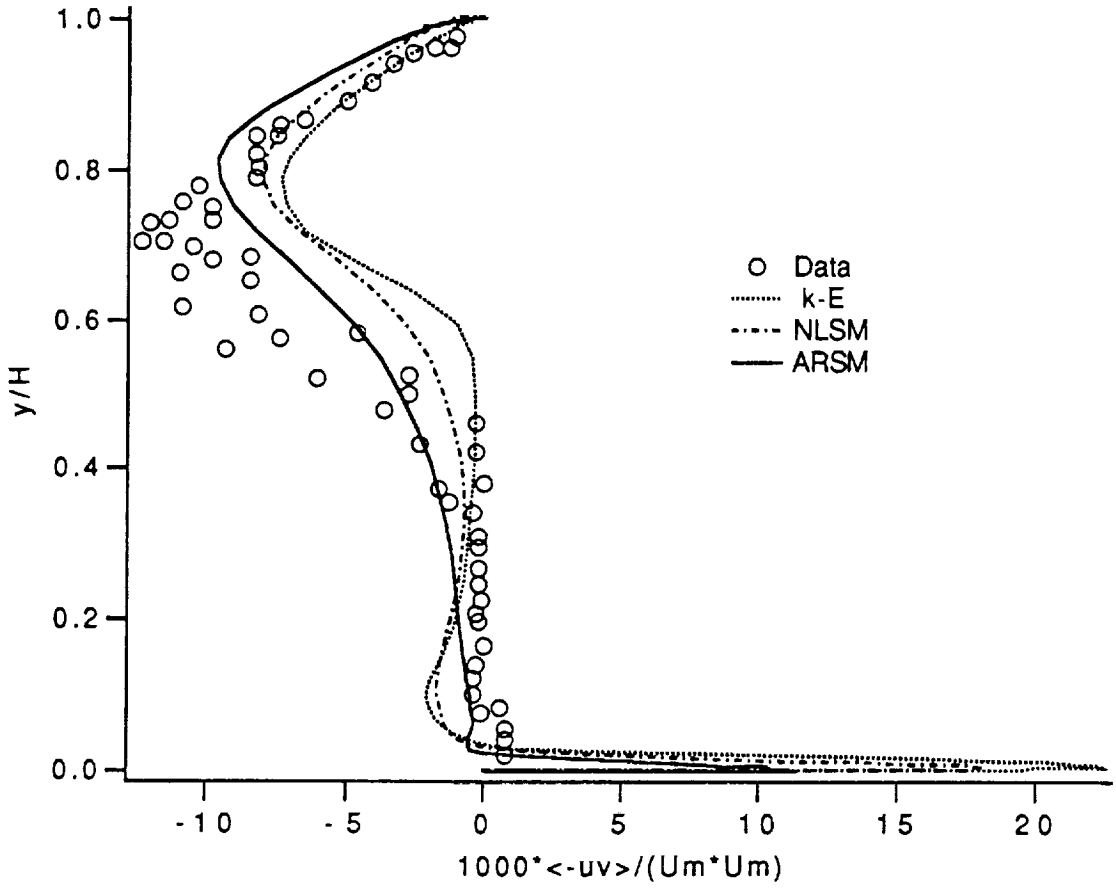

Fig.5(d) Turbulent shear stress

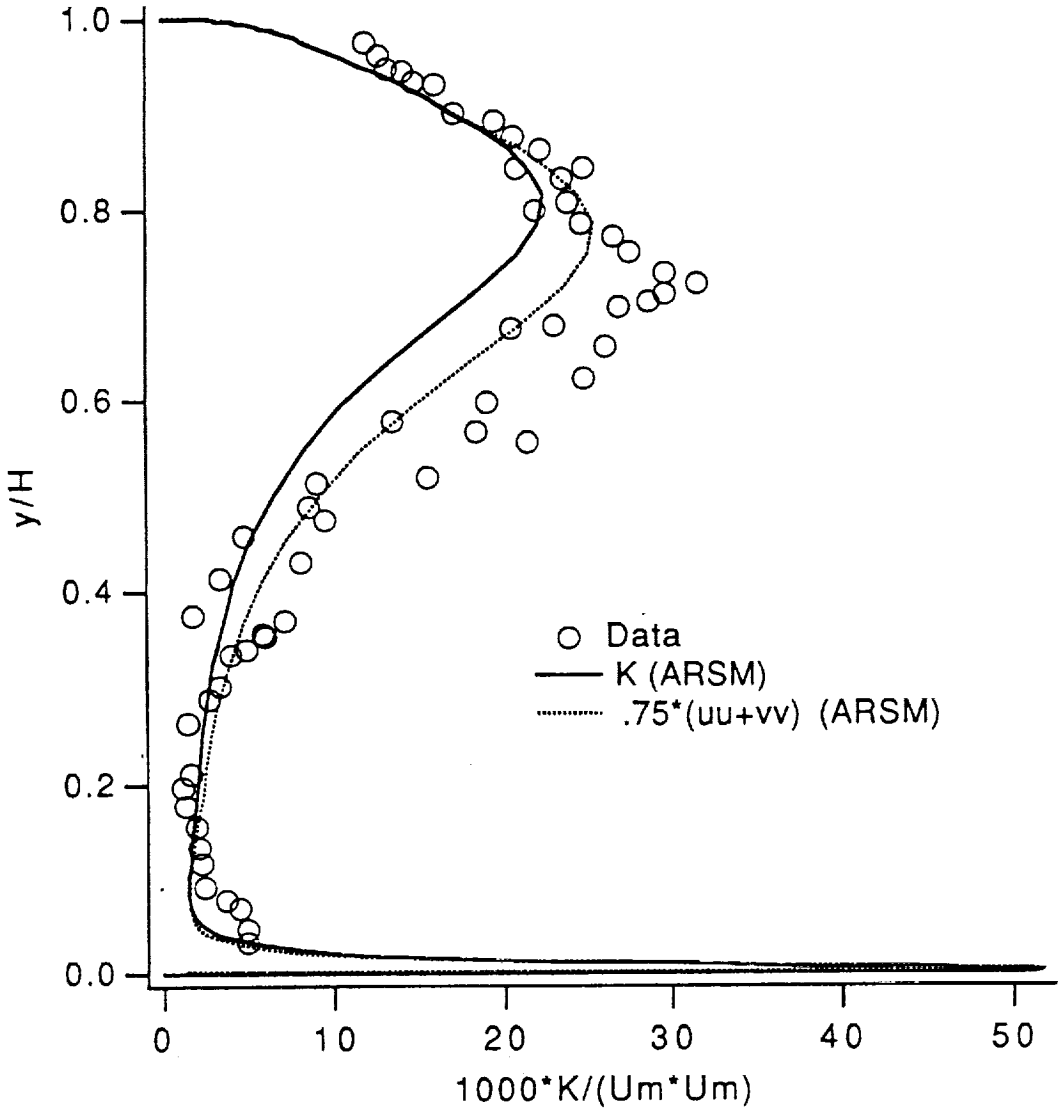

Fig.5 (e) Comparison of K and 0.75*(uu+vv)

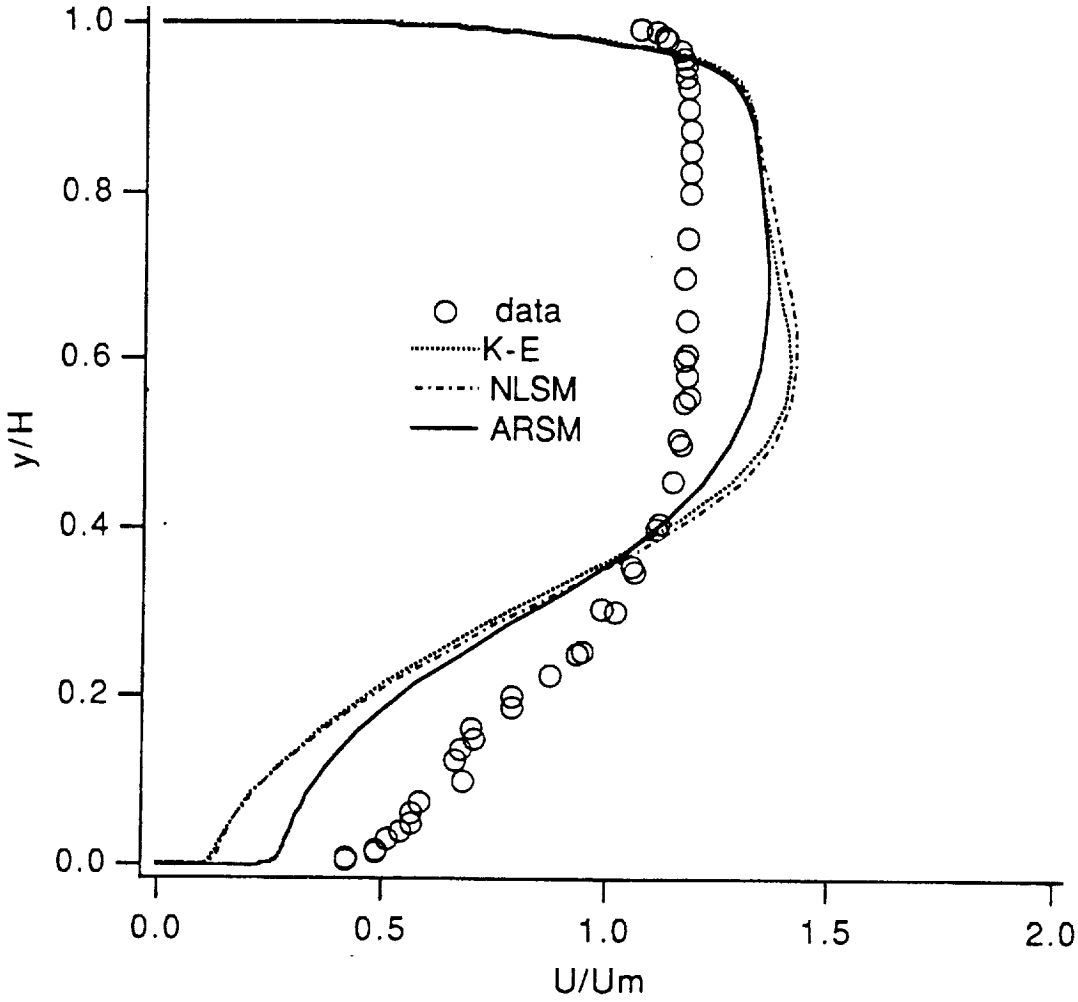

Fig.7(a) Longitudinal velocity in turnaround duct, x/H = 2 (downstream of turn)

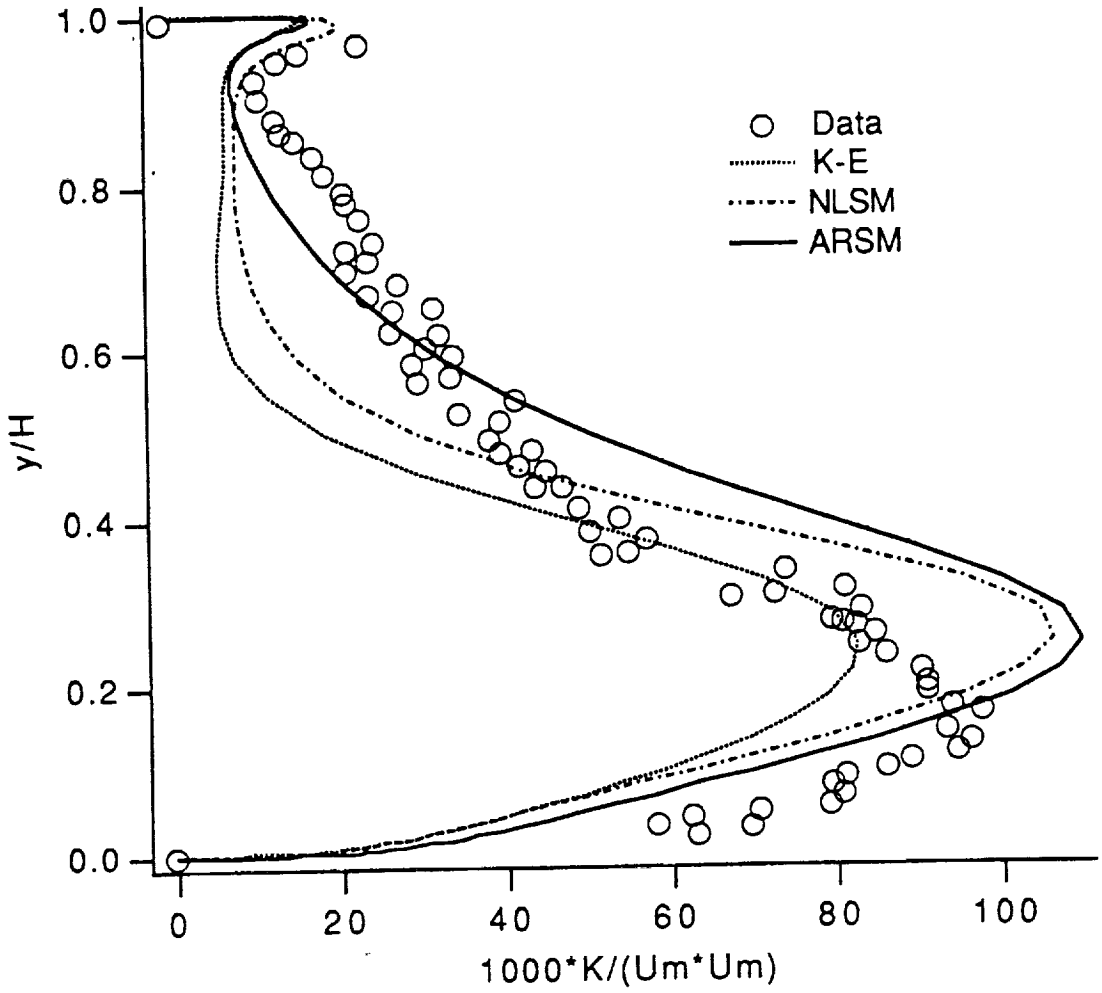

Fig.7(b) Turbulent kinetic energy

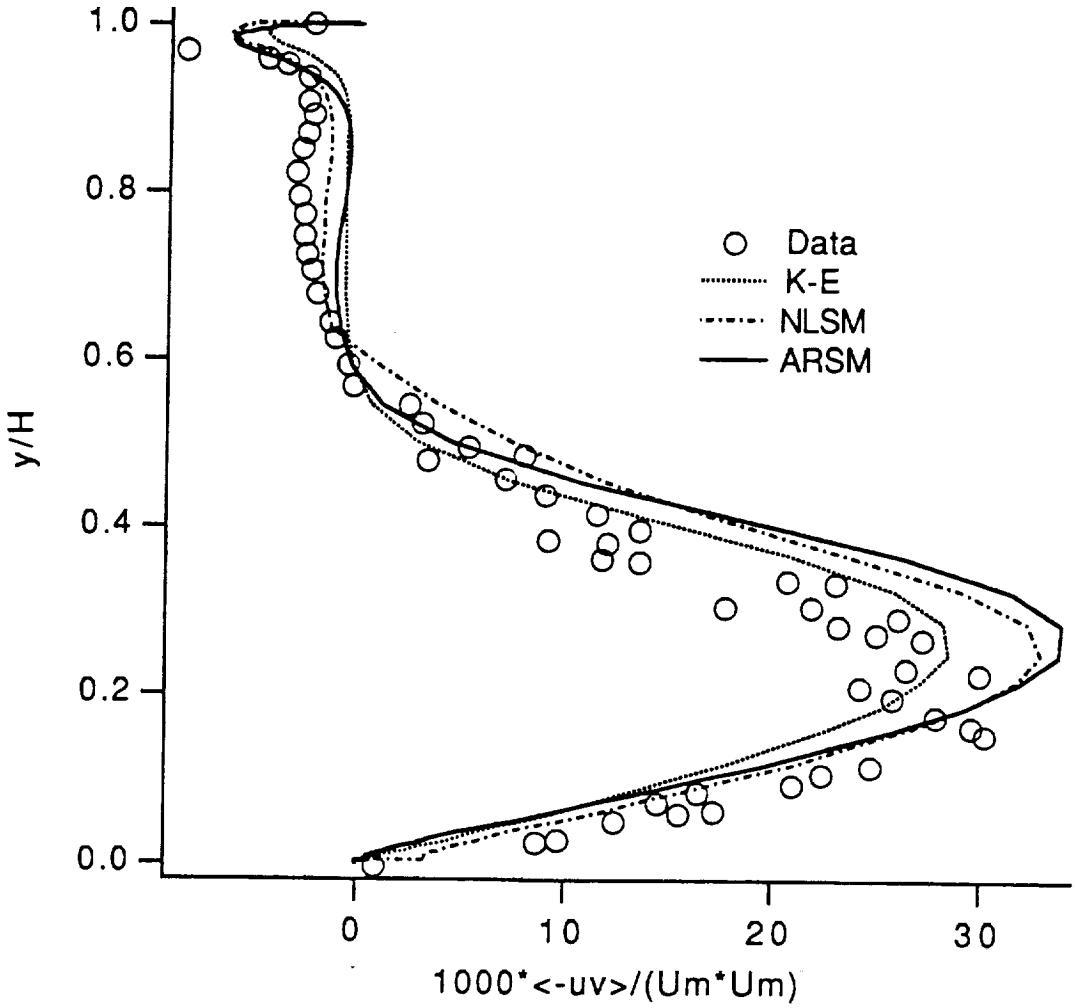

Fig. 7(c) Turbulent shear stress

VKI Turbine Nozzle Guide Vane Cascade

* Measurement by Arts etal (1990) at Von Karman Institute

* M(inlet)=0.15, M(outlet)=0.7 to 1.11, Re=0.5 - 2 x 10^6 , To=415k, T(wall) = 300k

* Geometry and grid

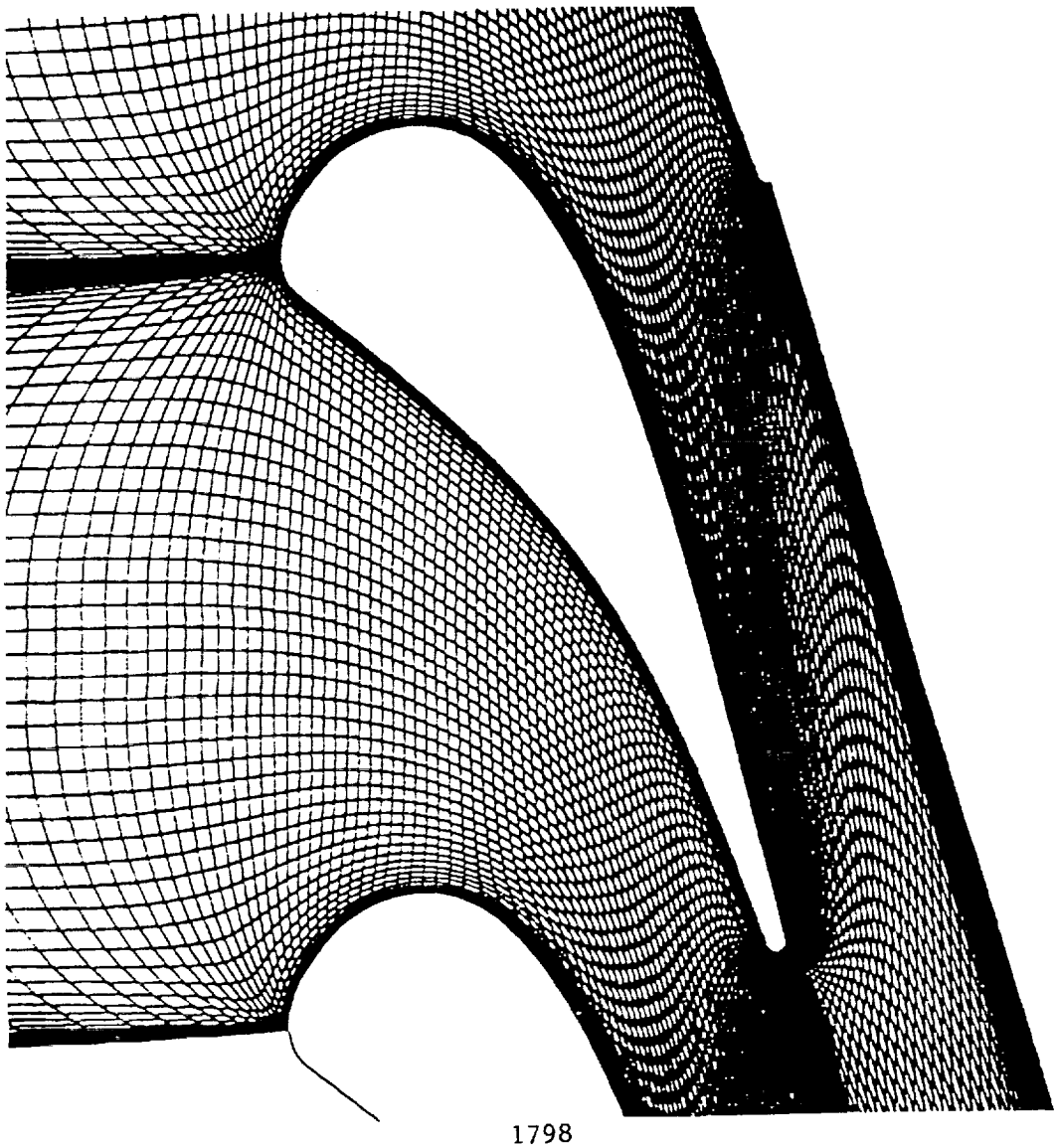

3. Smoothing: Typical values for 2nd and 4th order dissipation taken as 2%-3% and 3%-4% for the turbine cascade computations.

4. Table: Computed cases :

cases	Mur228	Mur224	Mur239
P_{o1}(bar)	0.915	0.909	3.387
T_{o1} (K)	403	403	412
$Re_{,2}$	0.6E+6	0.6E+6	2.1 E+6
Tu_{in}(%)	1	6	6

T(wall) = 300k for all these cases.

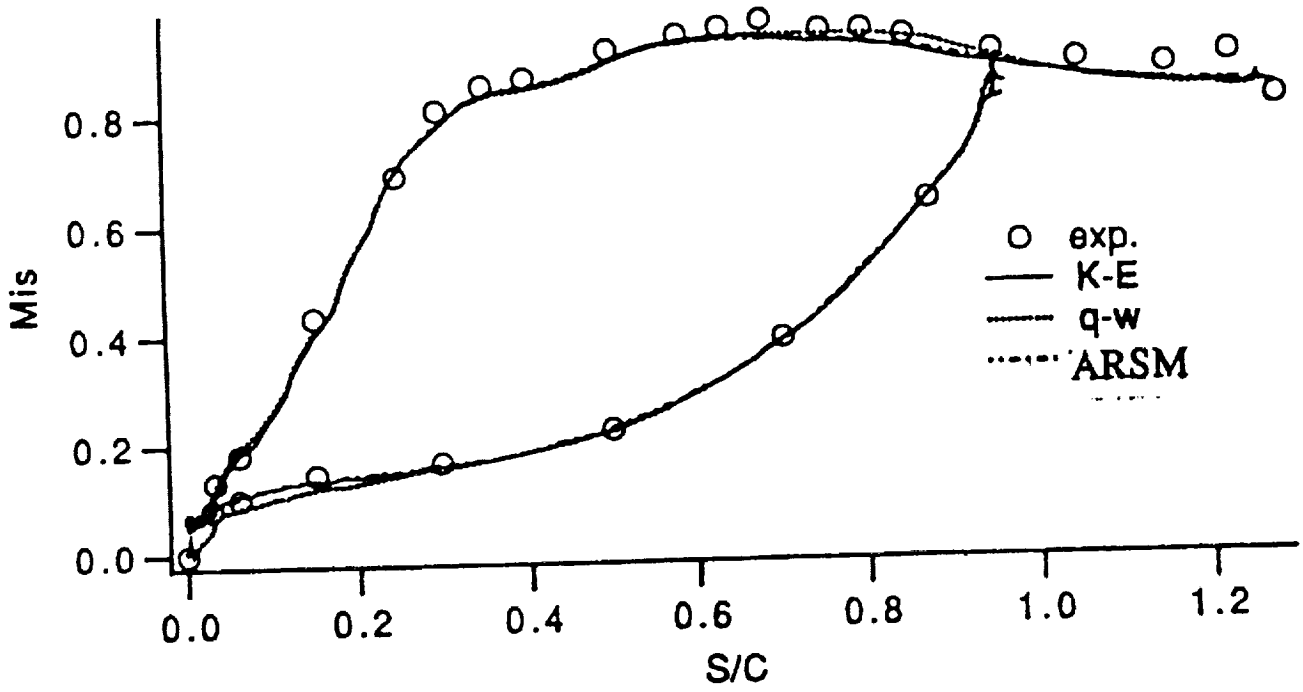

Fig. 9 Blade isentropic Mach number distribuition for Mur043 (P_{o1} =1.435 bar, M_2^{is} =0.93, Tu (inlet) =1%)

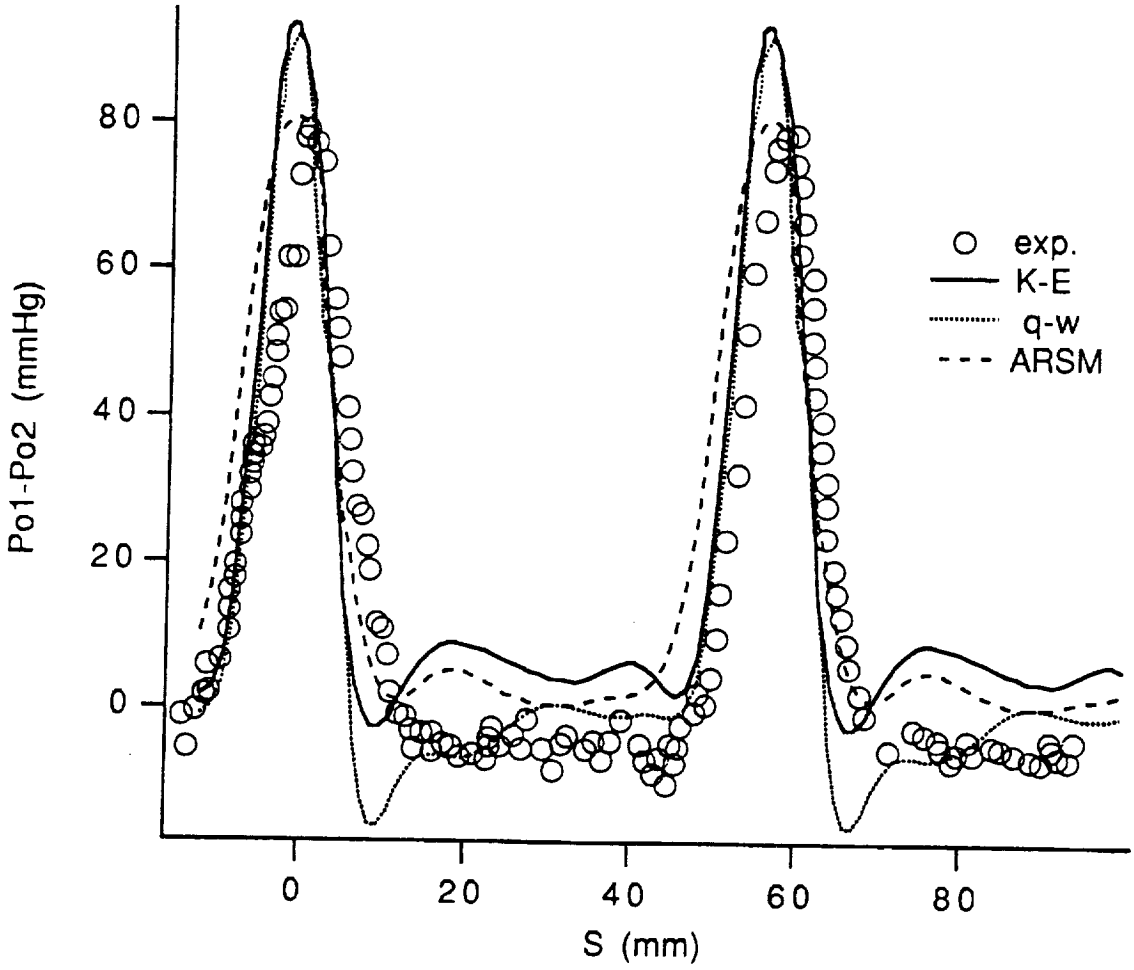

Fig.10 Computed and measured wakes for mur043

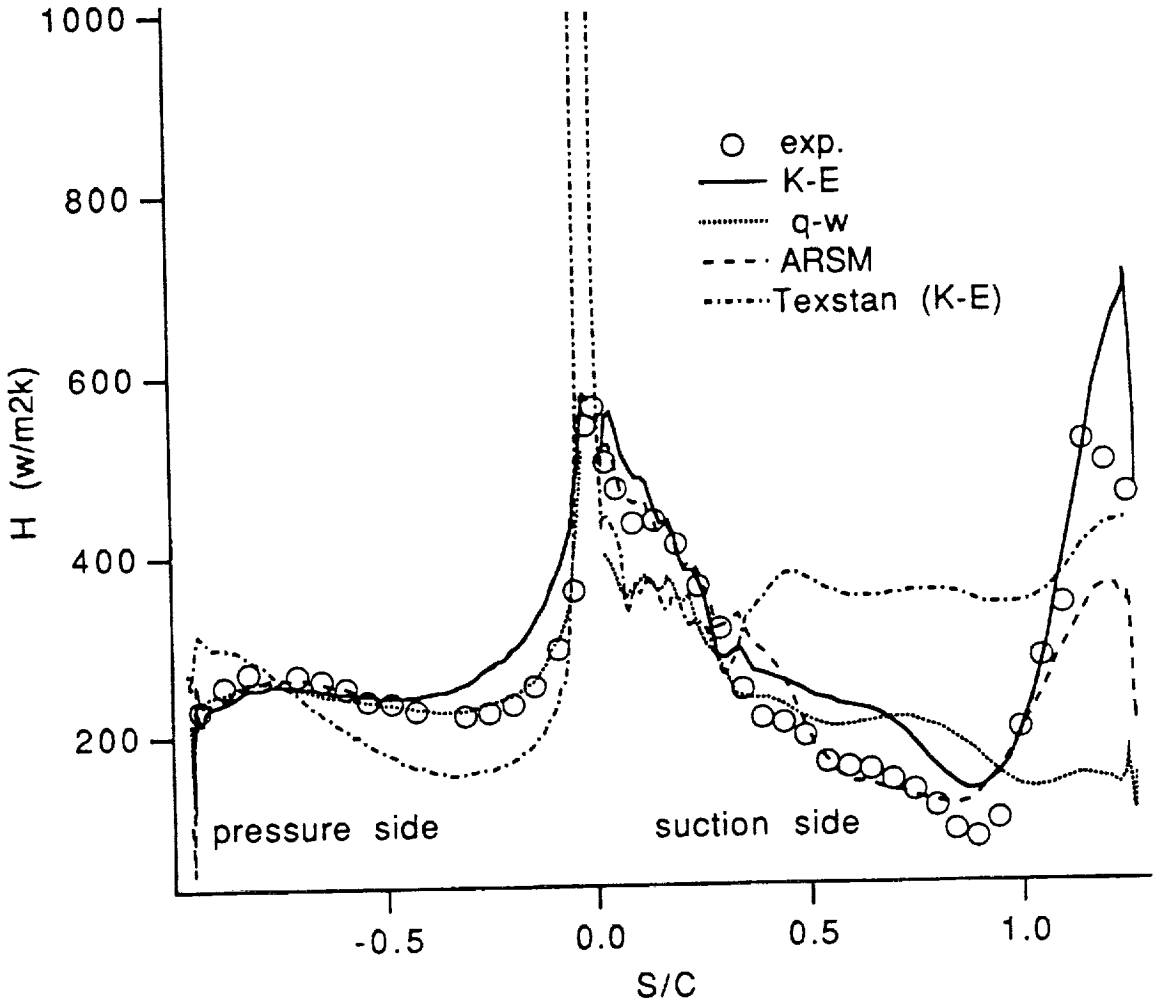

Fig. 11 Heat Transfer Prediction for Mur224

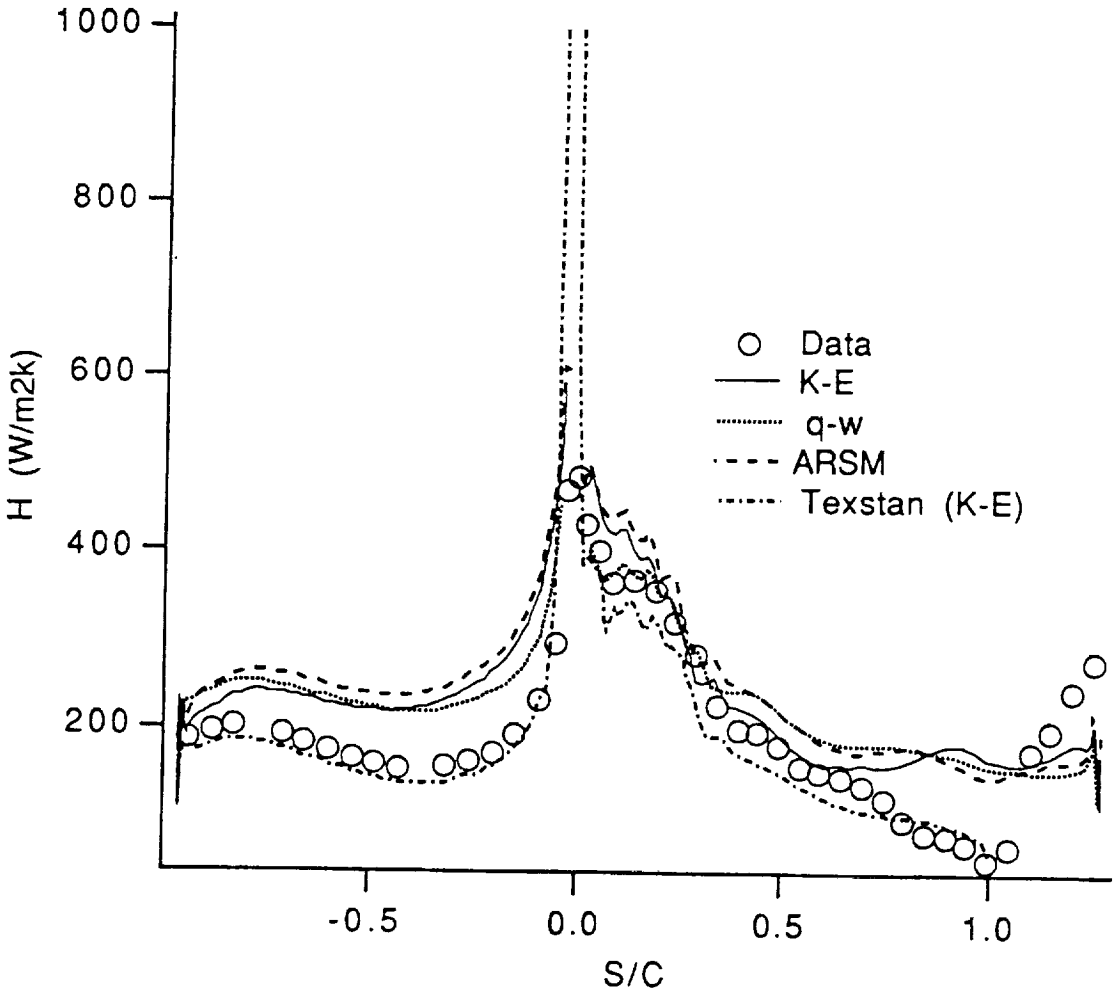

Fig. 12 Heat transfer prediction for Mur228

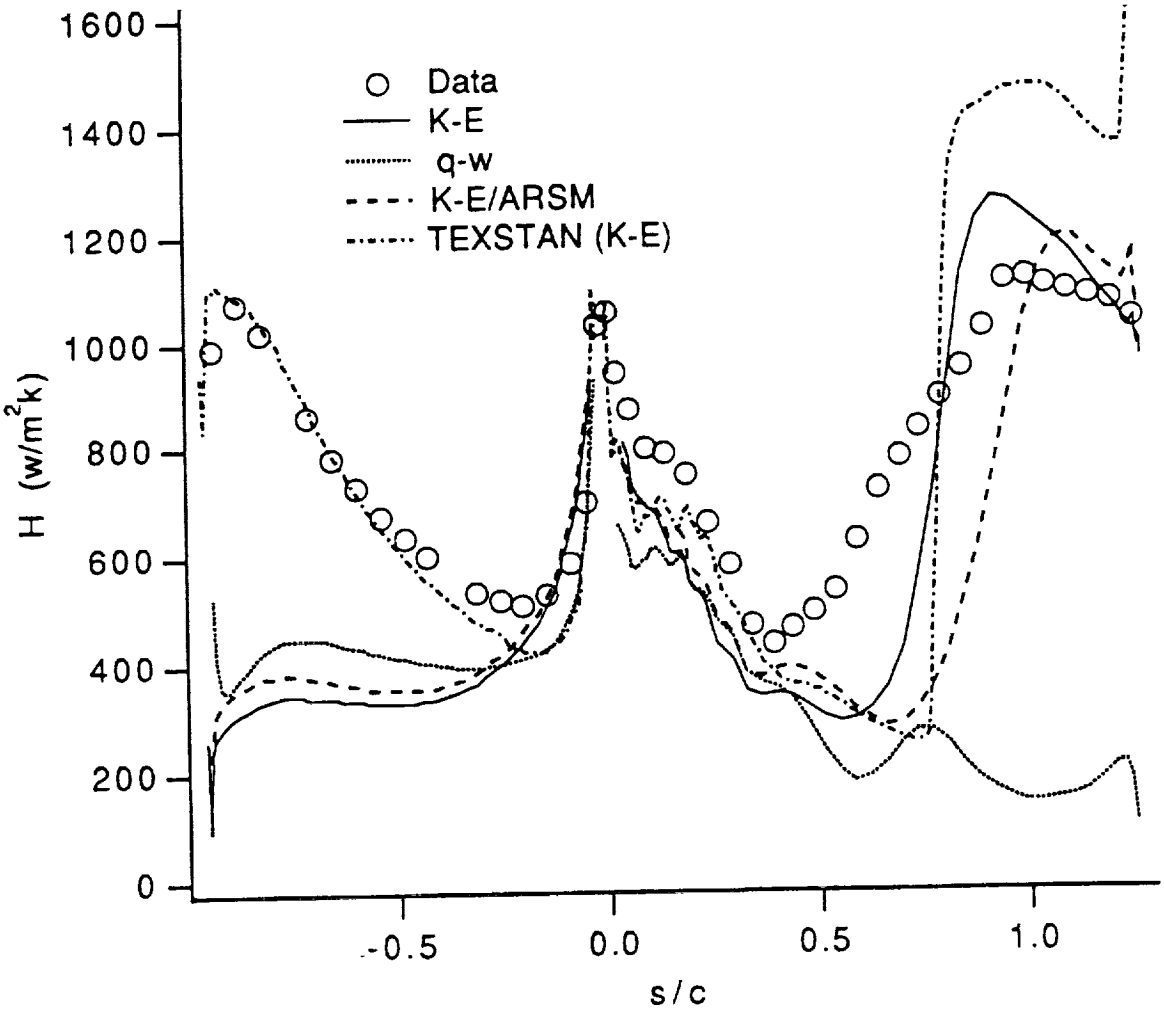

Fig.13 Heat Transfer for Mur239

CONCLUSIONS

*A two-dimensional Navier-Stokes code has been developed using an explicit Runge-Kutta method incorporating the ARSM model, NLSM model , Chien's LRN k-ε model and Coakley's LRN q-ω model.

*The surface pressure distributions and wake profiles of a transonic turbine cascade were predicted well by the k-ε , ARSM and q-ω models. The heat transfer on suction surfaces were predicted well by the k-ε and ARSM models.

*The heat transfer on pressure side for one case (MUR239) was underpredicted. This was caused by the underprediction of mainstream turbulence level , which strongly influences the transition location.

*The boundary layer code predicts the heat transfer on pressure surface well, but it

does not capture the transition on suction surfaces for all the 3 cases.

*The wall damping function (f_μ) in Chien's model was modified to yield improved prediction for flow under adverse pressure gradient.

*For TAD flow, good predictions have been obtained for the surface pressure distribution and skin friction coefficients. The ARSM model yields better prediction than NLSM and k-ε models, for both the mean and the turbulence quantities.

*The near wall "echo" term ϕ_{ijw} is not correctly modelled for strongly curved flows, especially near the concave surface.

*For more accurate prediction of strongly curved TAD flows, it may be necessary to use existing RSM, including the modeling for the wall region.

Liquid Propellant Rocket Engine Combustion Simulation with a Time-Accurate CFD Method

Y.S. Chen, H.M. Shang and Paul Liaw
Engineering Sciences, Inc.
Huntsville, Alabama

and

J. Hutt
NASA George C. Marshall Space Flight Center
NASA/MSFC, Alabama

ABSTRACT

Time-accurate computational fluid dynamics (CFD) algorithms are among the basic requirements as an engineering or research tool for realistic simulations of transient combustion phenomena, such as combustion instability, transient start-up, etc., inside the rocket engine combustion chamber. A time-accurate pressure based method is employed in the FDNS code for combustion model development. This is in connection with other program development activities such as spray combustion model development and efficient finite-rate chemistry solution method implementation. In the present study, a second-order time-accurate time-marching scheme is employed. For better spatial resolutions near discontinuities (e.g. shocks, contact discontinuities), a 3rd-order accurate TVD scheme for modeling the convection terms is implemented in the FDNS code. Necessary modification to the predictor/multi-corrector solution algorithm in order to maintain time-accurate wave propagation is also investigated. Benchmark 1-D and multi-dimensional test cases, which include the classical shock tube wave propagation problems, resonant pipe test case, unsteady flow development of a blast tube test case, and H2/O2 rocket engine chamber combustion start-up transient simulation, etc., are investigated to validate and demonstrate the accuracy and robustness of the present numerical scheme and solution algorithm.

LIQUID PROPELLANT ROCKET ENGINE COMBUSTION SIMULATION WITH A TIME-ACCURATE CFD METHOD

Y.S. Chen, H.M. Shang and Paul Liaw
Engineering Sciences, Inc.
Huntsville, Alabama

and

J. Hutt
NASA Marshall Space Flight Center

NASA Contract NAS8-39832

Presented at

THE 11TH WORKSHOP FOR COMPUTATIONAL FLUID DYNAMICS APPLICATIONS IN ROCKET PROPULSION

APRIL 20-22, 1993

ESI Engineering Sciences, Inc.

OVERVIEW

- BACKGROUND
- APPROACH
- NUMERICAL METHOD
- BENCHMARK VALIDATION CASES
- SUMMARY AND FUTURE PLAN

BACKGROUND

- A CONTINUING RESEARCH EFFORT TO DEVELOP A ROBUST AND ACCURATE PRESSURE-BASED CFD CODE FOR COMPLEX COMBUSTION FLOW APPLICATIONS

- HIGH-ORDER, TIME-ACCURATE AND EFFICIENT NUMERICAL SCHEMES ARE ESSENTIAL FOR TRANSIENT REACTING FLOW COMPUTATIONS

- INTEGRATION OF REALISTIC SPRAY AND REACTION MODELS FOR STEADY-STATE AND TRANSIENT FLOW APPLICATIONS IS THE FINAL GOAL

BASIC BUILDING BLOCKS

- TIME ACCURATE CFD CODES FOR ALL SPEED RANGE (FDNS, MAST, ETC.)
- GENERAL AND ROBUST TURBULENCE MODELS --TWO-EQUATION TURBULENCE MODELS OR HIGHER-ORDER ONES
- EFFICIENT TIME-ACCURATE FINITE-RATE CHEMISTRY SOLUTION METHODS
- REALISTIC TWO-PHASE FLOW MODELS FOR SPRAY COMBUSTION

GOVERNING EQUATIONS

- COMPRESSIBLE FLOW CONSERVATION EQUATIONS
- CONTINUITY, MOMENTUM, ENERGY (STATIC ENTHALPY) TURBULENCE MODELS AND SPECIES TRANSPORT EQUATIONS
- EDDY VISCOSITY TYPE TURBULENCE MODELING
- MULTIPLE SPECIES FORMULATION WITH FINITE-RATE CHEMISTRY
- MOMENTUM AND ENERGY EQUATIONS INCLUDE MULTIPLE PHASE SOURCE TERMS

GAS PHASE GOVERNING EQUATIONS

$$\frac{\partial \rho U}{\partial t} + \frac{\partial}{\partial x_i}\left(\rho u_i U + \mu_e \frac{\partial U}{\partial x_i} \right) = S_U$$

where $U = \left(1, u, v, w, h, k, \varepsilon \text{ and } \alpha_n\right)$

$$S_U = \begin{Bmatrix} 0 \\ -\frac{\partial P}{\partial x_i} + \frac{\partial}{\partial x_j}\left(\mu_e \frac{\partial u_i}{\partial x_j} \right) - \frac{2}{3}\frac{\partial}{\partial x_j}\left(\mu_e \frac{\partial u_i}{\partial x_j} \right) + D_i + M_p u_p \\ \frac{DP}{Dt} + \Phi + Q_t + H_p + M_p\left(hv + \frac{1}{2}u_r^2 \right) \\ \rho\left(P_r - \varepsilon \right) \\ \rho \frac{\varepsilon}{k}\left[\left(C_1 + C_3 P_r / \varepsilon \right) P_r - C_2 \varepsilon \right] \\ \omega_n, \quad n = 1, \ldots\ldots N \end{Bmatrix}$$

NUMERICAL METHOD

- PRESSURE BASED FINITE DIFFERENCE NAVIER-STOKES FLOW SOLVER (BASED ON THE FDNS CODE)
- SECOND-ORDER TIME-ACCURATE (CRANK-NICHOLSON) DELTA-FORM FORMULATIONS
- CHARKRAVARTHY-OSHER THIRD-ORDER TVD FLUX LIMITER EMPLOYED FOR THE CONVECTION TERMS AS OPPOSED TO THE ORIGINAL CENTRAL PLUS ADAPTIVE DAMPING SCHEME)
- MULTIPLE-ZONE GENERAL COORDINATES MESH SYSTEMS

CHARKRAVARTHY-OSHER TVD FLUXES

$$\frac{\partial F}{\partial \xi} = f_{i+1/2} - f_{i-1/2} + h_{i+1/2} - h_{i-1/2}$$

where f and h represent first-order fluxes and TVD flux limiters respectively.

$$f_{i+1/2} = \max\left\{0, (\rho U)_{i+1/2}\right\}\phi_i + \max\left\{0, -(\rho U)_{i+1/2}\right\}\phi_{i+1}$$

$$h_{i+1/2} = \begin{cases} \frac{1}{4}|\rho U|_{i+1/2}\left\{d\phi^{+}_{i+1/2} + d\phi^{-}_{i-1/2} + \alpha\left(d\phi^{+}_{i+1/2} - d\phi^{-}_{i-1/2}\right)\right\}, U \geq 0 \\ \frac{1}{4}|\rho U|_{i+1/2}\left\{d\phi^{-}_{i+1/2} + d\phi^{+}_{i+3/2} + \alpha\left(d\phi^{-}_{i+1/2} - d\phi^{+}_{i+3/2}\right)\right\}, U < 0 \end{cases}$$

BENCHMARK VALIDATION CASES

- CLASSICAL SHOCK TUBE
  (1-D WITH 160 GRID AND 0.005 TIME STEP SIZE)

- RESONANT PIPE PRESSURE OSCILLATIONS
  (1-D WITH 100 GRID AND 0.005 TIME STEP SIZE)

- A BLAST TUBE FLOW FIELD SIMULATION
  (2-D WITH 7000 GRID AND 0.01 TIME STEP SIZE)

- A H2/O2 ROCKET ENGINE CHAMBER START-UP TRANSIENT SIMULATION
  (2-D WITH 6000 GRID AND 0.0001 TIME STEP SIZE OR 0.1 μsec)

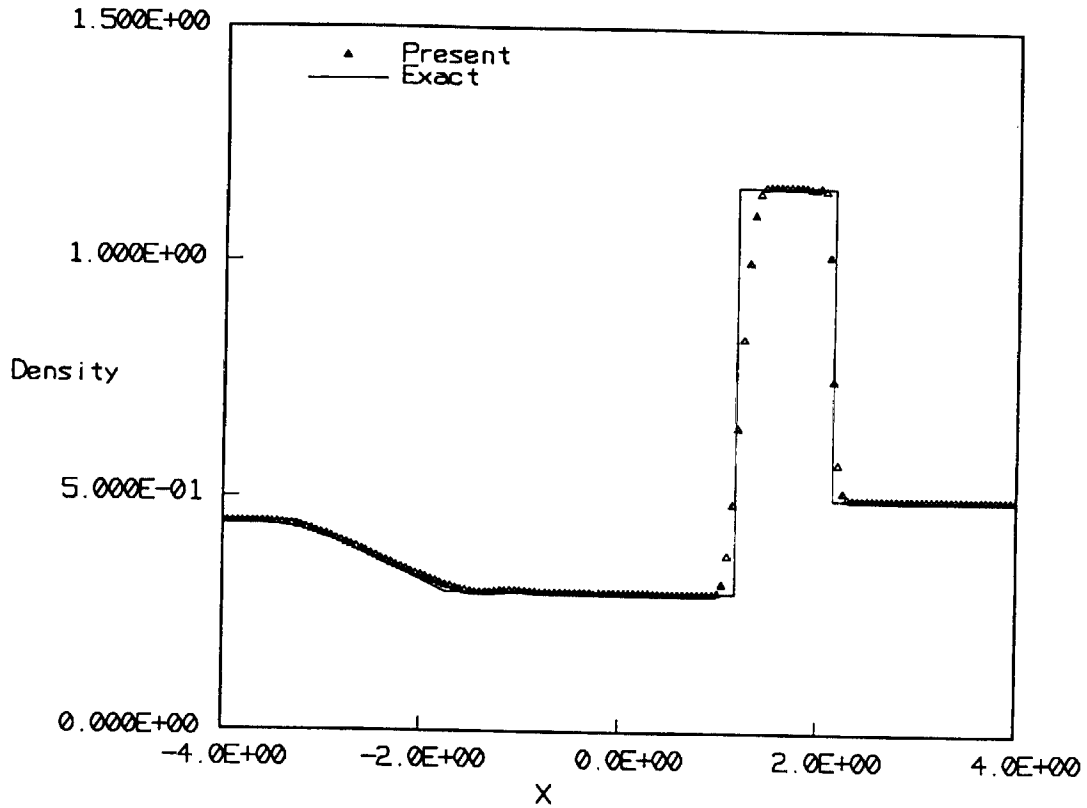

Figure 1 (a). Closed shock tube test case. (t = 0.95)

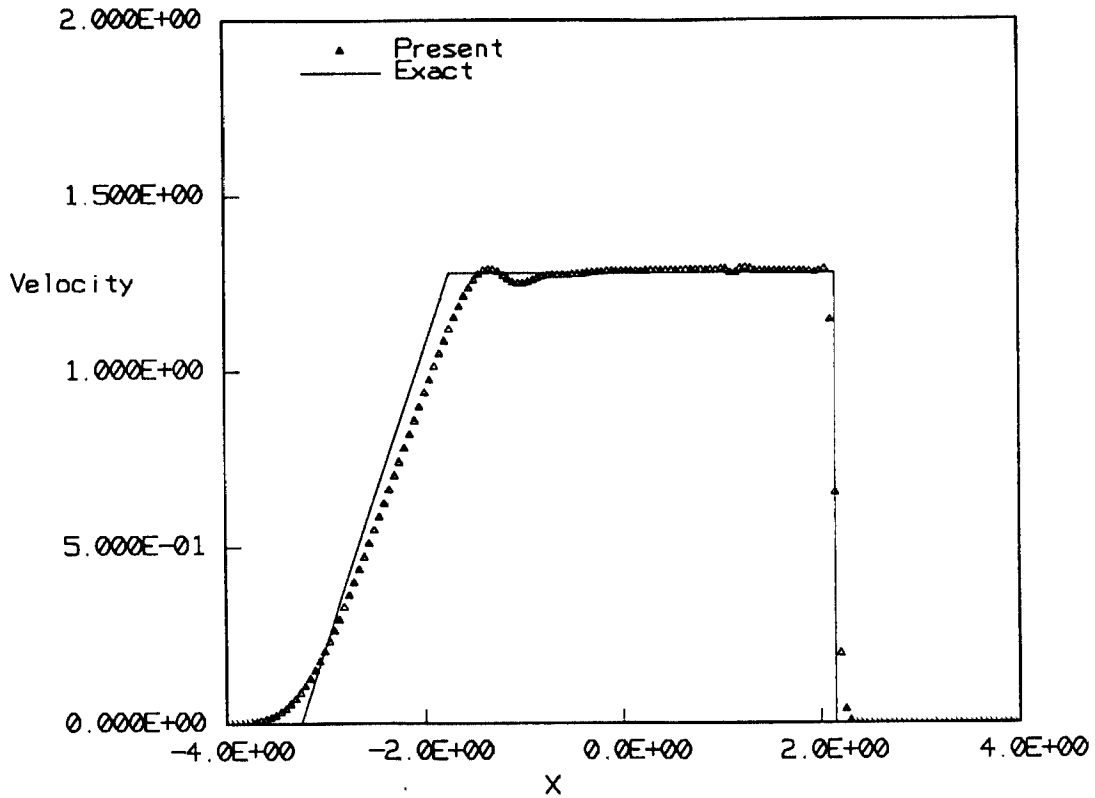

Figure 1 (b). Closed shock tube test case. (t = 0.95)

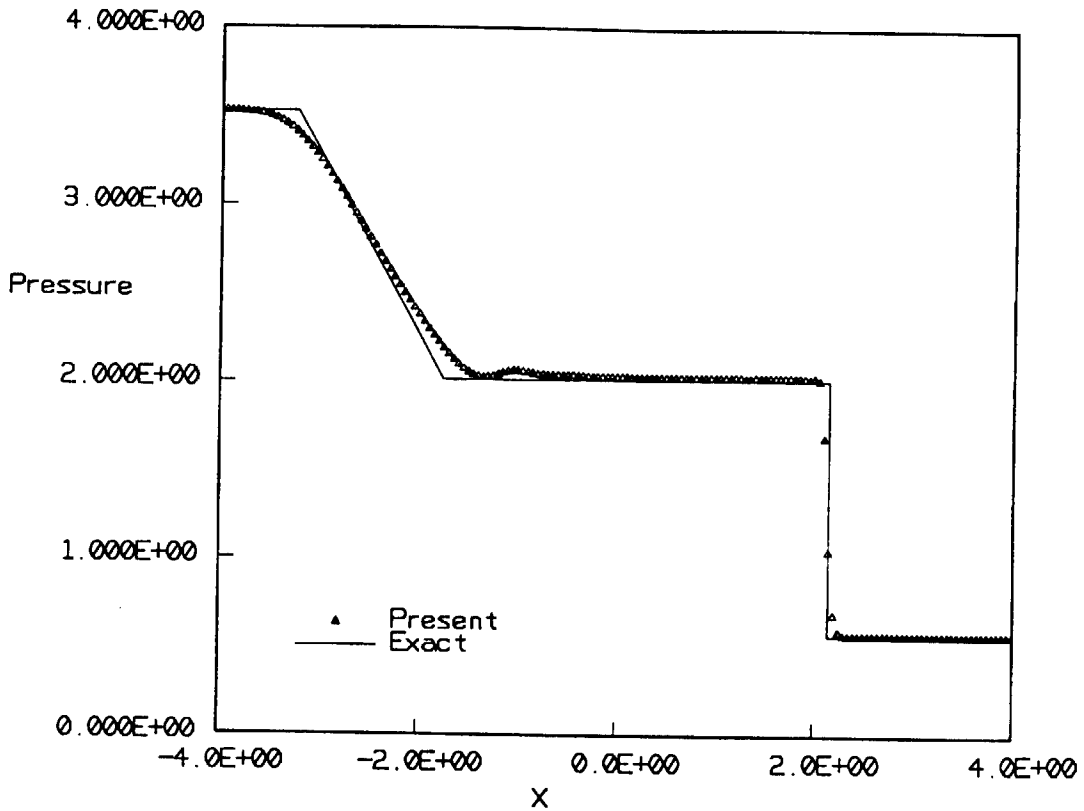

Figure 1 (c). Closed shock tube test case. (t = 0.95)

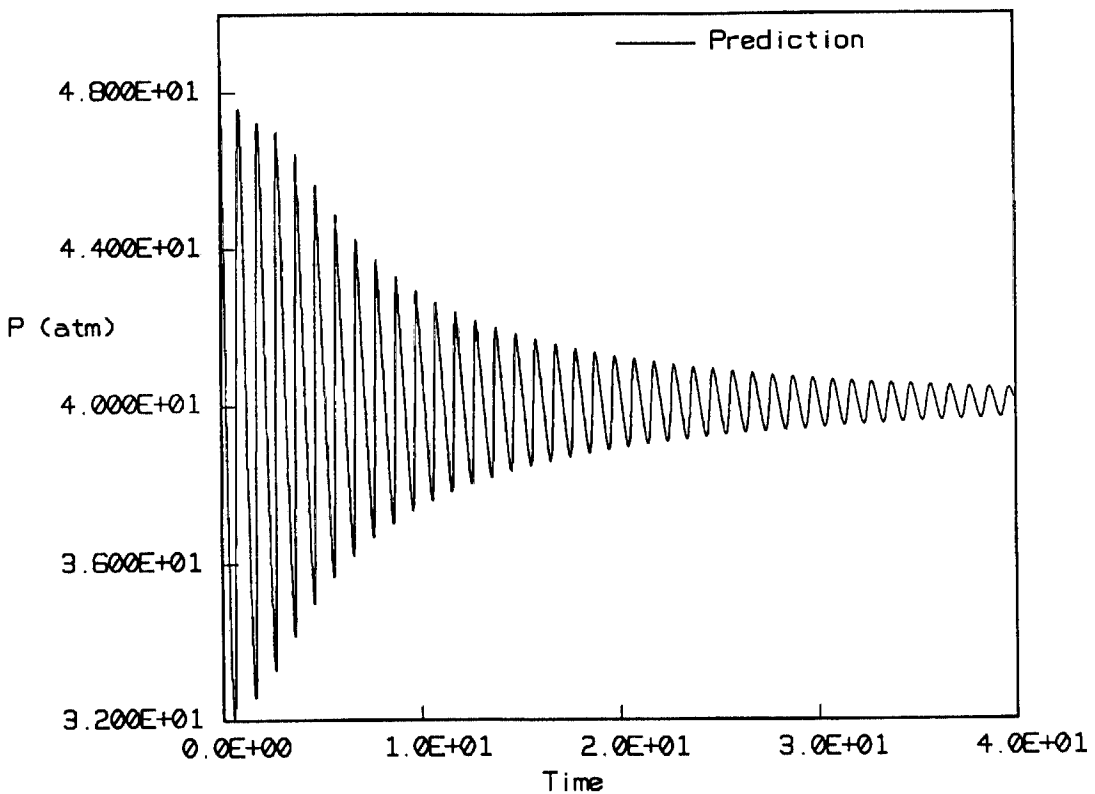

Figure 2. Resonant pipe pressure time-history.

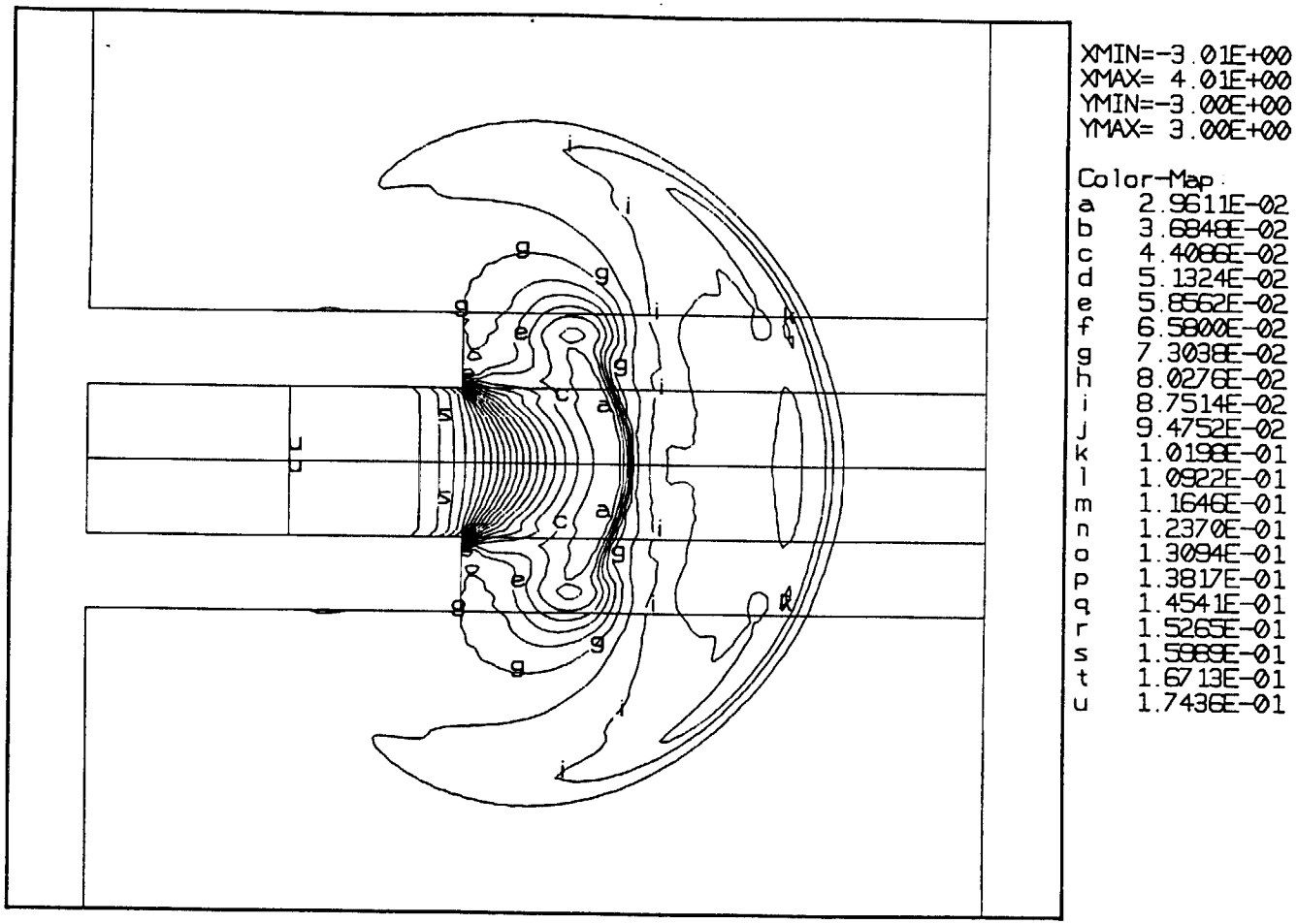

Fig. 3. Blast tube flow field simulation. (a) Density contours.

ESI

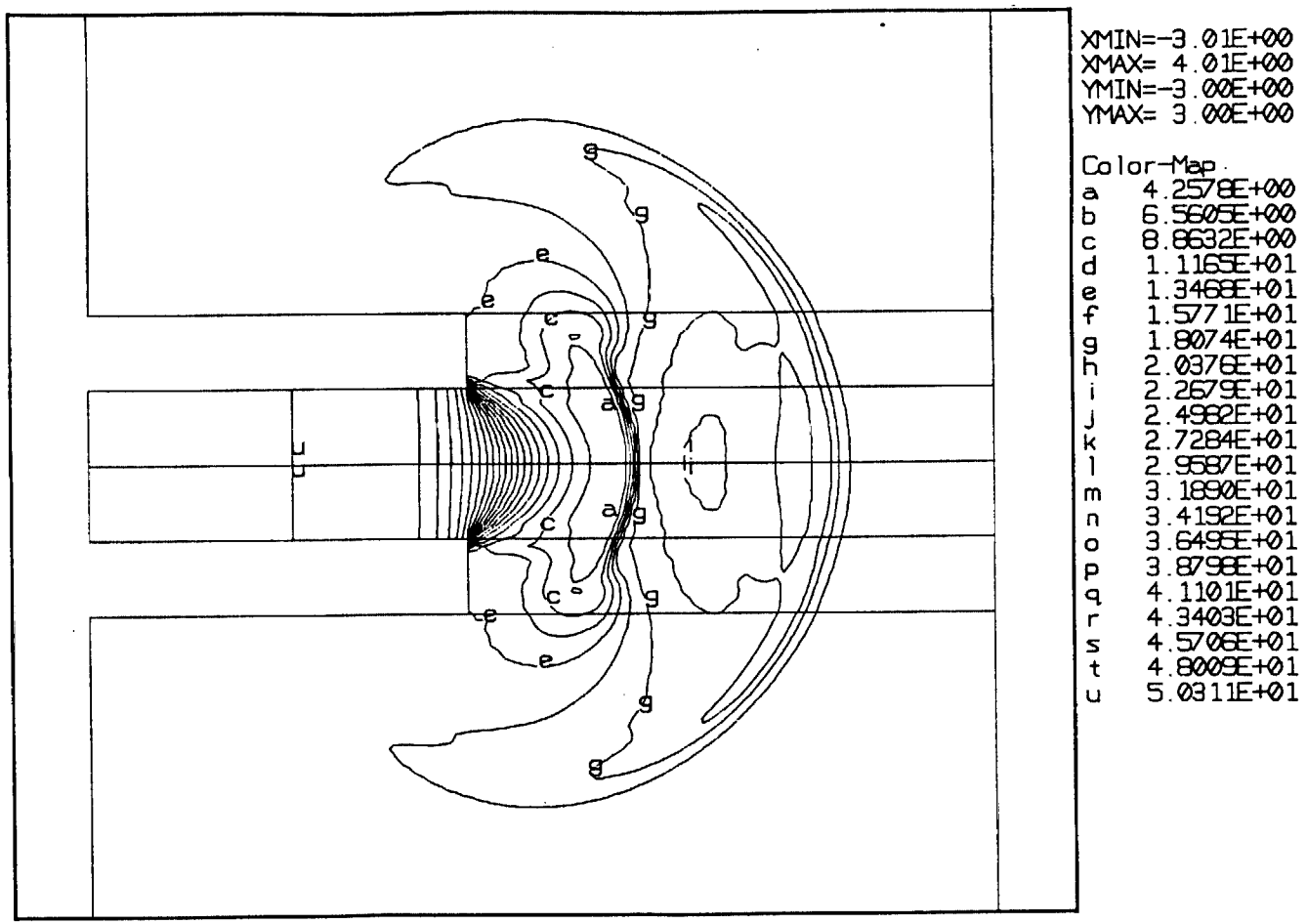

Fig. 3. Blast tube flow field simulation. (b) Pressure contours. (Time = 0.75 ms)

ESI

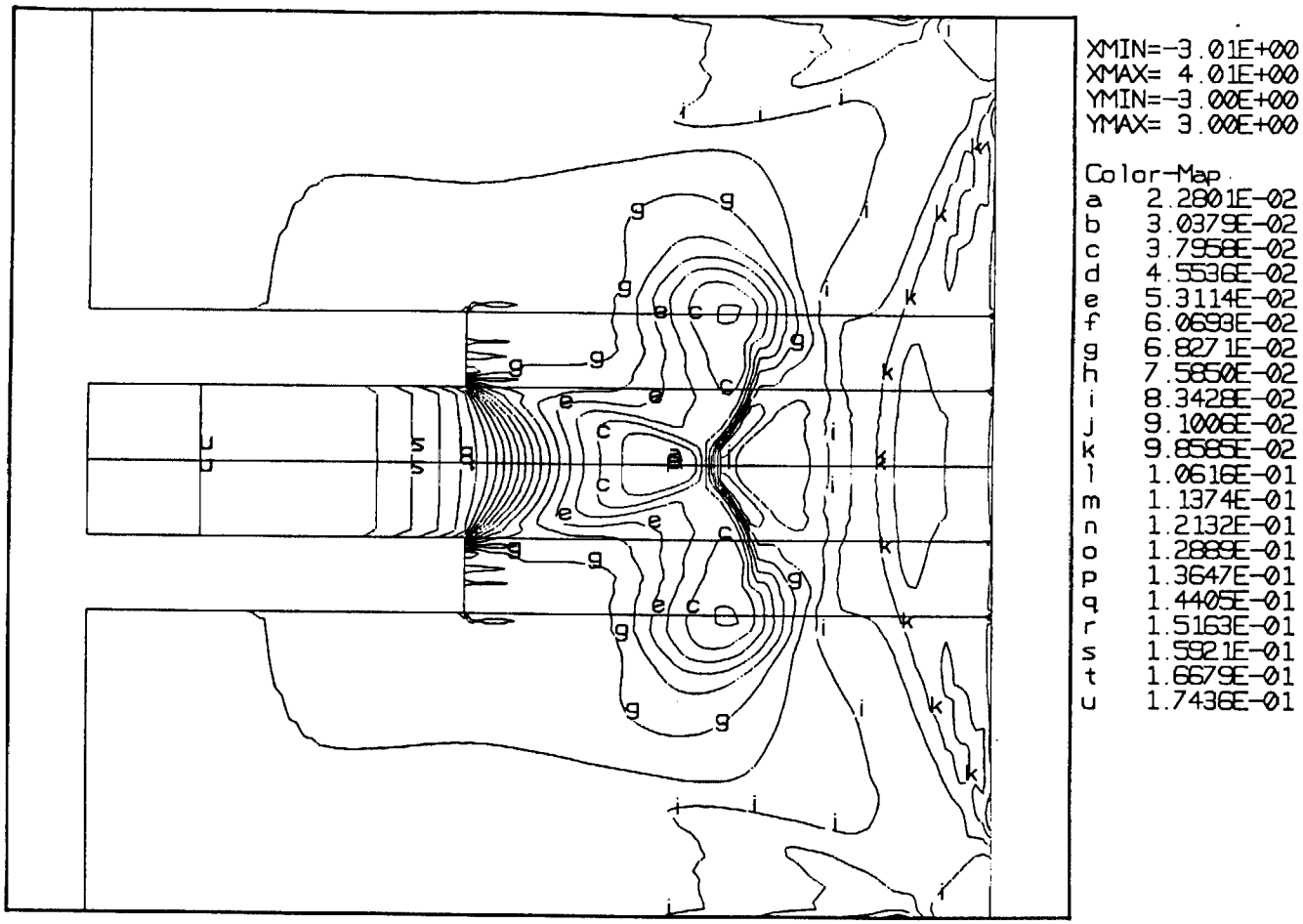

Fig. 4. Blast tube flow field simulation. (a) Density contours. (Time = 1.50 ms)

ESI

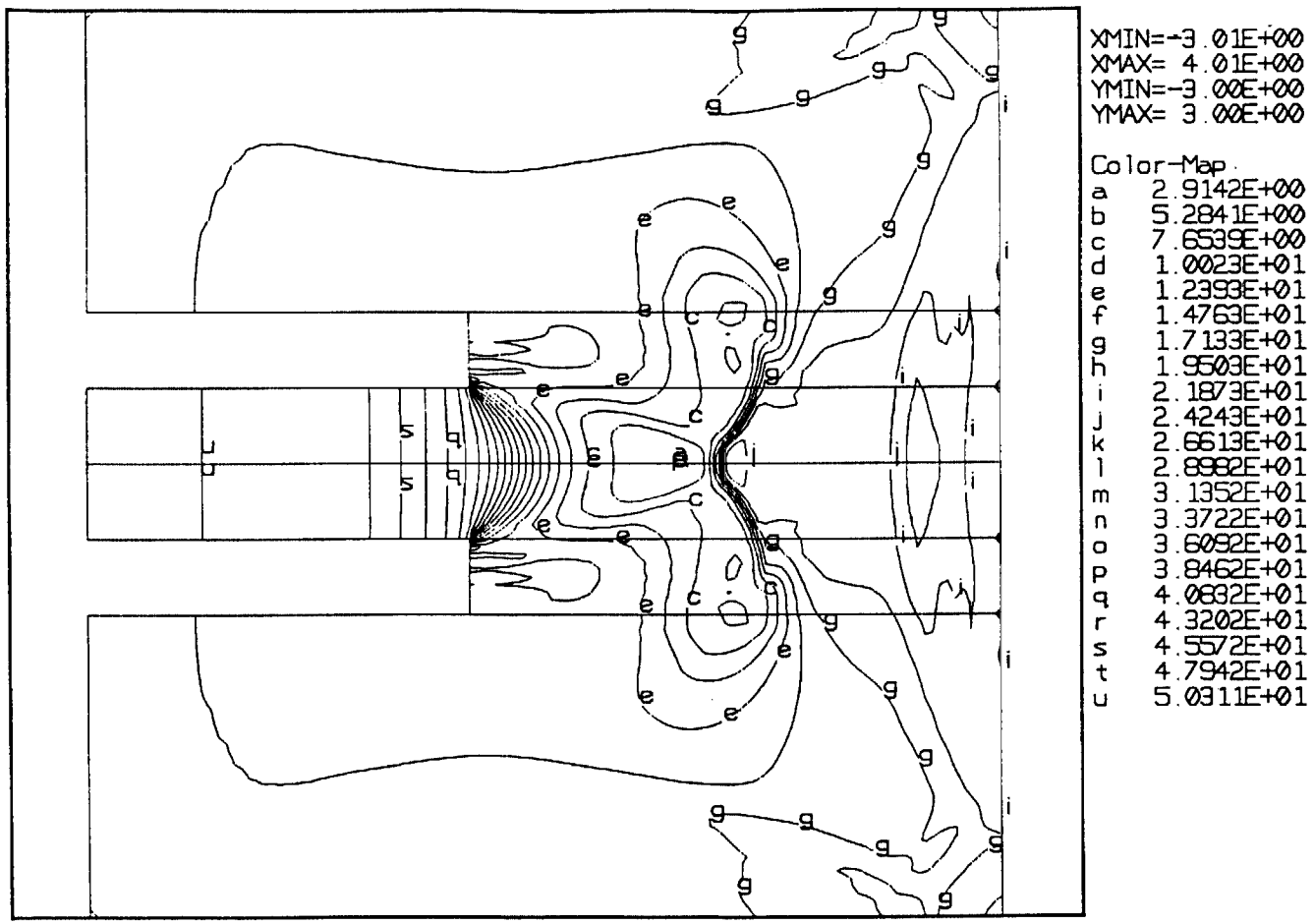

Fig. 4. Blast tube flow field simulation. (b) Pressure contours. (Time = 1.50 ms)

ESI

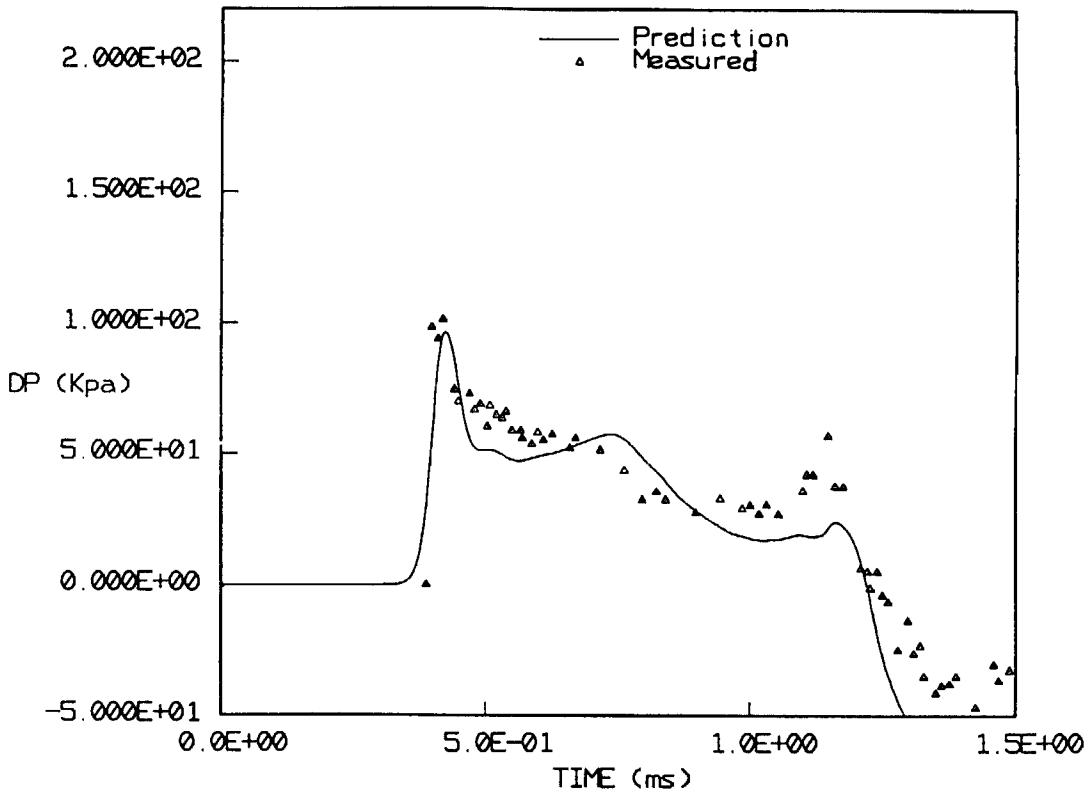

Fig. 5. Comparison of overpressure time history.
(at X/D = 1.51)

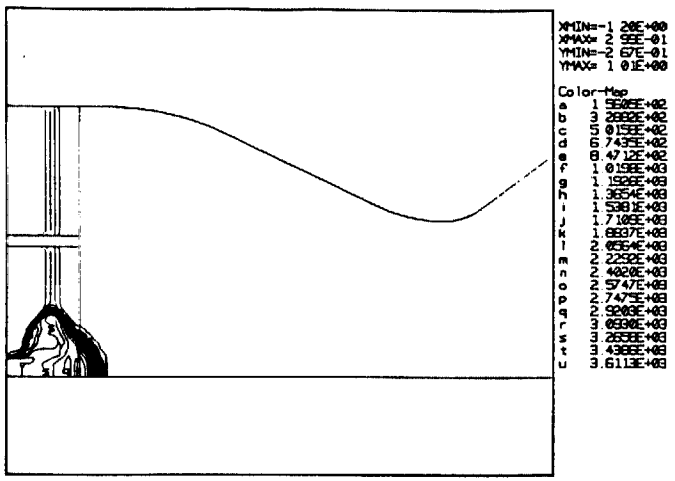

Fig. 6. SSME main combustion chamber test case. (Temp. Contours)
(a) Time = 0.03 ms.

ESI

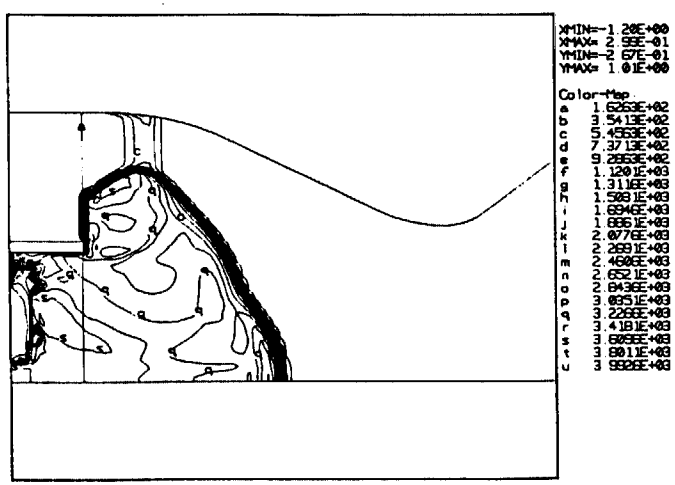

Fig. 6. SSME main combustion chamber test case. (Temp. Contours)
(b) Time = 0.10 ms.

ESI

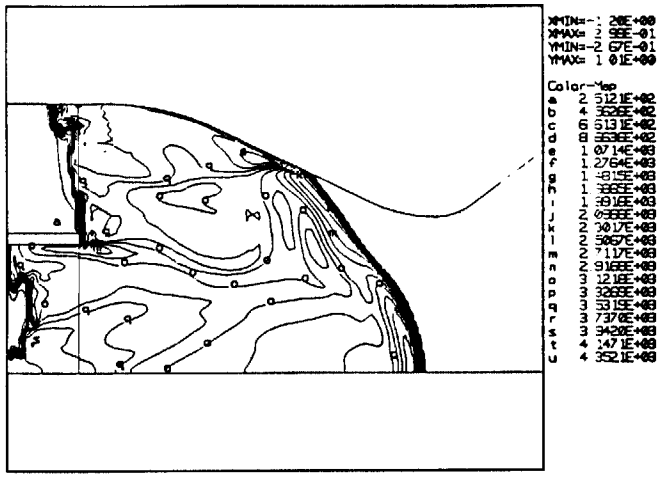

Fig. 6. SSME main combustion chamber test case. (Temp. Contours)
(c) Time = 0.15 ms.

ESI

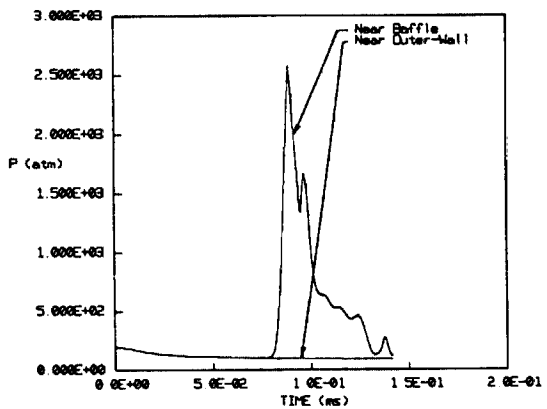

Fig. 7 Chamber pressure time-history during start-up

SUMMARY AND FUTURE WORK

- TIME-ACCURACY OF THE 3RD-ORDER C-O TVD SCHEME AND PREDICTOR/CORRECTOR SOLUTION ALGORITHM OF THE FDNS CODE HAS BEEN VALIDATED AND DEMONSTRATED IN THE PRESENT STUDY

- LARGE PRESSURE OSCILLATIONS CAN BE EXPECTED DURING H2/O2 ROCKET ENGINE START-UP TRANSIENT (THE MAGNITUDE CAN BE REDUCED WITH CORRECT O/F RATIO DISTRIBUTIONS AND START-UP SEQUENCE)

- SPRAY COMBUSTION MODEL WILL BE INCLUDED IN FUTURE STUDY

Convergence Acceleration of Implicit Schemes in the Presence of High Aspect Ratio Grid Cells

P. E. O. Buelow, S. Venkateswaran and C. L. Merkle
Propulsion Engineering Research Center
The Department of Mechanical Engineering
The Pennsylvania State University
University Park, PA 16802.

The performance of Navier-Stokes codes are influenced by several phenomena. For example, the robustness of the code may be compromised by the lack of grid resolution, by a need for more precise initial conditions or because all or part of the flowfield lies outside the flow regime in which the algorithm converges efficiently. A primary example of the latter effect is the presence of extended low Mach number and/or low Reynolds number regions which cause convergence deterioration of time marching algorithms. Recent research into this problem by several workers including the present authors has largely negated this difficulty through the introduction of time-derivative preconditioning. In the present paper, we employ the preconditioned algorithm to address convergence difficulties arising from sensitivity to grid stretching and high aspect ratio grid cells.

Strong grid stretching is particularly characteristic of turbulent flow calculations where the grid must be refined very tightly in the dimension normal to the wall, without a similar refinement in the tangential direction. High aspect ratio grid cells also arise in problems that involve high aspect ratio domains such as combustor coolant channels. In both situations, the high aspect ratio cells can lead to extreme deterioration in convergence. It is the purpose of the present paper to address the reasons for this adverse response to grid stretching and to suggest methods for enhancing convergence under such circumstances.

Numerical algorithms typically possess a maximum allowable or optimum value for the time step size, expressed in non-dimensional terms as a CFL number or von-Neumann number (VNN). In the presence of high aspect ratio cells, the smallest dimension of the grid cell controls the time step size causing it to be extremely small, which in turn results in the deterioration of convergence behaviour. For explicit schemes, this time step limitation cannot be exceeded without violating stability restrictions of the scheme. On the other hand, for implicit schemes, which are typically unconditionally stable, there appears to be room for improvement through careful tailoring of the time-step definition based on results of linear stability analyses. In the present paper, we focus on the central-differenced alternating direction implicit (ADI) scheme. The understanding garnered from this analyses can then be applied to other implicit schemes.

In order to systematically study the effects of aspect ratio and the methods of mitigating the associated problems, we use a two pronged approach. We use stability analyses as a tool for predicting numerical convergence behavior and numerical experiments on simple model problems to verify predicted trends. Based on these analyses, we determine that efficient convergence may be obtained at all aspect ratios by getting a combination of things right. Primary among these are the proper definition of the time step size, proper selection of viscous preconditioner and the precise treatment of boundary conditions. These algorithmic improvements are then applied to a variety of test cases to demonstrate uniform convergence at all aspect ratios.

Convergence Acceleration of Implicit Schemes In the Presence of High Aspect Ratio Grid Cells

P. E. O. Buelow, S. Venkateswaran, C. L. Merkle

Propulsion Engineering Research Center
The Pennsylvania State University
University Park, PA 16802

11th Workshop for Computational Fluid Dynamic
Applications in Rocket Propulsion
April 20-22, 1993
Marshall Space Flight Center, Alabama

Philosophy of Grid Aspect Ratio Study

- Assessment of High Aspect Ratio Problem
  - — Disparate propagation speeds in X and Y
- Stability Theory
  - — Scalar Convection-Diffusion Equation
  - — Euler Equations
  - — Navier-Stokes Equations
- Numerical Convergence Studies
  - — Simple Model Problems
  - — Realistic Flow Problems
- Improved Algorithm to Provide Aspect Ratio Control
  - — Precise Time-Step Definition
  - — Viscous Preconditioning
  - — Boundary Condition Implementation

The Navier-Stokes Equations

$$\Gamma \frac{\partial Q_v}{\partial t} + \frac{\partial E}{\partial x} + \frac{\partial F}{\partial y} = H + L(Q_v)$$

- Solution Vector

$$Q_v = (\ p,\ u,\ v,\ T\ )^T$$

- Preconditioning Matrix

$$\Gamma = \begin{pmatrix} 1/\epsilon c^2 & 0 & 0 & 0 \\ u/\epsilon c^2 & \rho & 0 & 0 \\ v/\epsilon c^2 & 0 & \rho & 0 \\ \frac{h+\frac{1}{2}(u^2+v^2)}{\epsilon c^2} - 1 & \rho u & \rho v & \rho C_p \end{pmatrix}$$

- Parameter ϵ
  - — Activates Inviscid and Viscous Preconditioning
  - — Value Depends on Local Mach Number and Cell Reynolds Number

Numerical Solution Procedure

- Central-Differenced *ADI* Algorithm

$$\left[S + \frac{\partial A}{\partial x} - \frac{\partial}{\partial x} R_{xx}\right] S^{-1} \left[S + \frac{\partial B}{\partial y} - \frac{\partial}{\partial y} R_{yy}\right] \Delta Q_v = -\mathcal{R}^n$$

- Approximate factorization errors control convergence behavior.

- Optimum CFL_{u+c} is typically between 1 and 10.
  - — Other inviscid and viscous time scales are optimized by the preconditioning matrix.

Time-Step Definition

- Local Time-Stepping or Constant CFL Condition

$$Max\ (\ CFL_x,\ CFL_y\ ) = CFL$$

- For high aspect ratios, CFL_x and CFL_y become disparate

$$CFL_y = CFL, \qquad CFL_x = CFL/AR$$

Euler Stability Analysis

- Aspect Ratio (AR) of Unity

$CFL = 1$

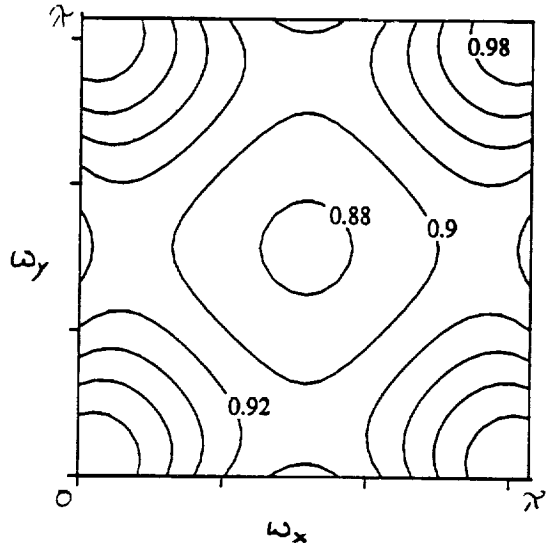

$CFL = 10$

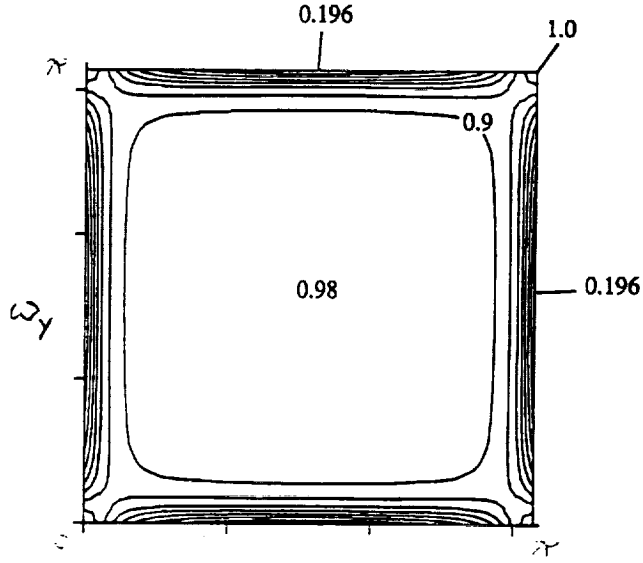

Euler Stability Analysis

- Aspect Ratio (AR) of 100

$CFL_y = 1$

$CFL_x = 0.01$

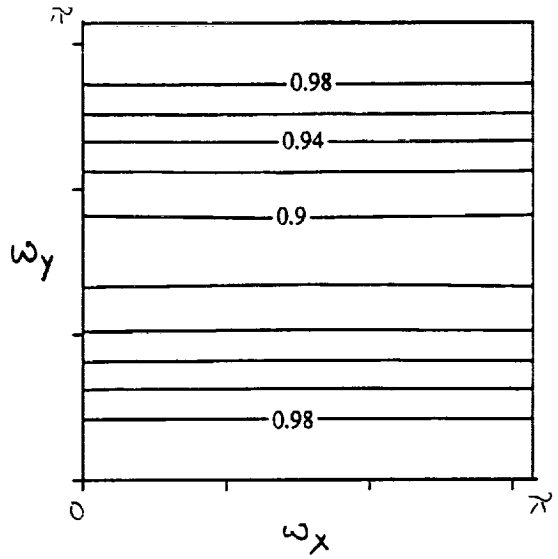

$CFL_y = 10$

$CFL_x = 0.1$

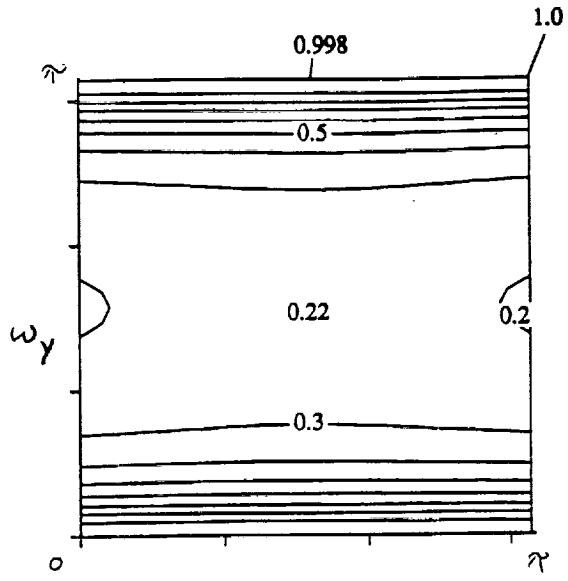

Euler Stability Analysis

- Aspect Ratio (AR) of 100

$CFL_y = 100$

$CFLx = 1$

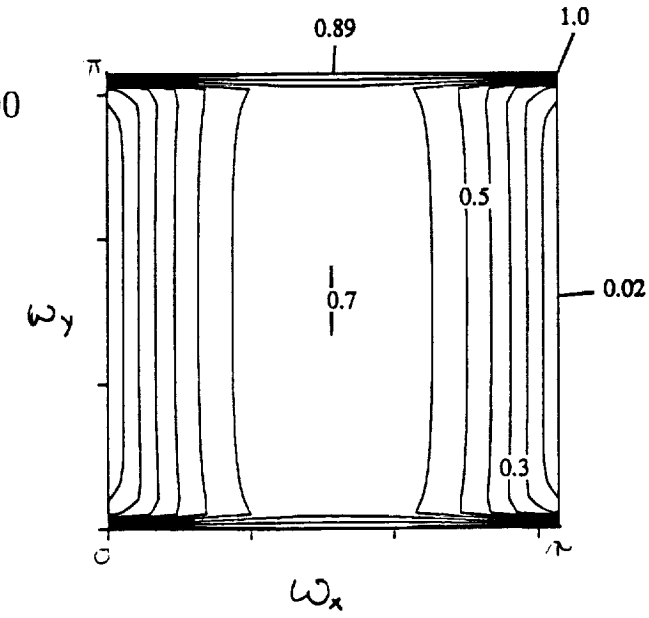

$CFL_y = 1000$

$CFL_x = 10.$

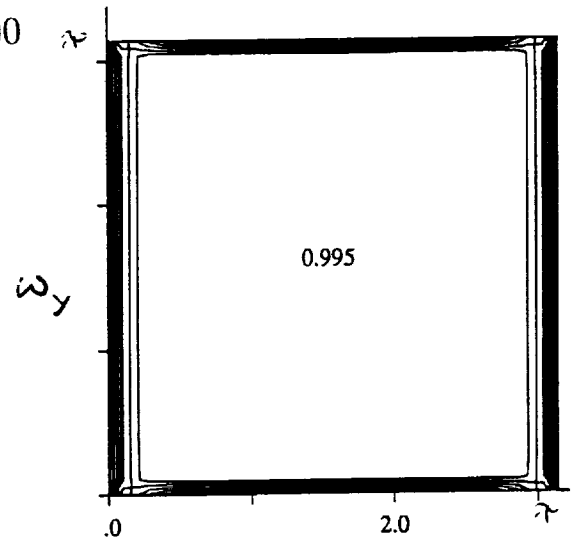

New Time-Step Definition

- Conclusions from Stability Analysis:
  - — Min-CFL Preferable to Max-CFL
  - — Efficient Convergence at all AR
- Minimum-CFL Definition

$$Min\ (\ CFL_x,\ CFL_y\ ) = CFL$$

- For high aspect ratios,

$$CFL_y = CFL * AR, \qquad CFL_x = CFL$$

Implementation of Boundary Conditions

- Extrapolation vs Characteristic
  - — Both work well for small CFL's
  - — Characteristics usually superior at high CFL's
- Proper MOC Implementation:
  - — Implicit procedures
  - — Boundary conditions applied before approximate factorization
  - — Consistent order of accuracy: LHS / RHS

High Aspect Ratio Convergence—Inviscid Duct

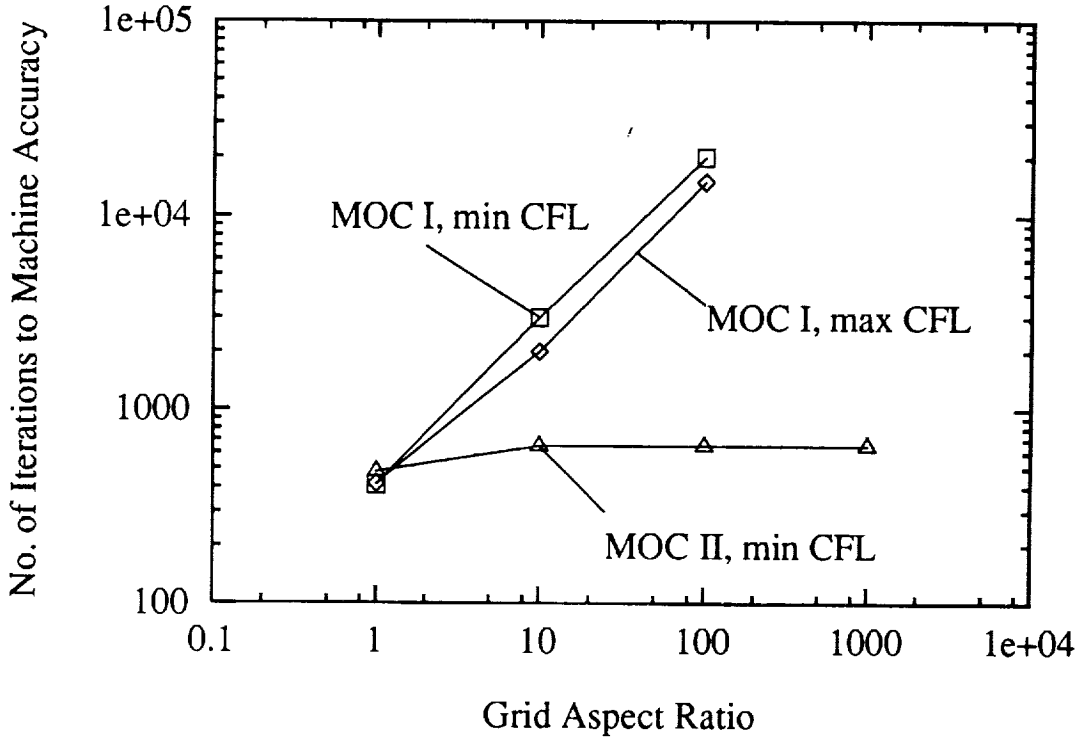

Navier-Stokes Analysis

- Parameter ϵ controls low Re number convergence
  - — Viscous terms limit time step at high AR
  - — ϵ chosen to optimize inviscid and viscous modes simultaneously
- Obvious choice: $\epsilon = f$ (Max-CFL, Max-VNN)
- Scalar Stability Results: $\epsilon = f$ (Min-CFL, Min-VNN)

Navier-Stokes Analysis

- Min-CFL, Min-VNN Stability Result

$AR = 1000$

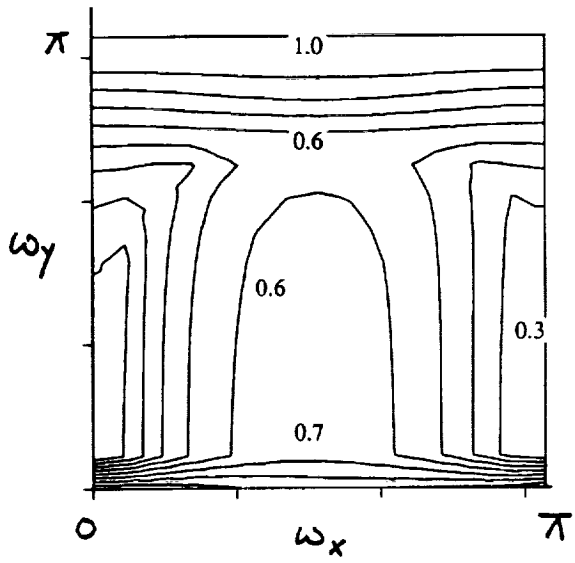

$CFL_x = 1,\ CFL_y = 1000$

$VNN_x = 1,\ VNN_y = 1 \times 10^6$

Navier-Stokes Analysis

- Conclusions from Stability Results:
  - — Vector system different from scalar equation
  - — Approximate factorization error $CFL_x * VNN_y$ limits convergence
- Viscous preconditioner, $\epsilon = f$ (Min-CFL,Max-VNN)
  - — Maintains Min-CFL for 'inviscid' modes
  - — Uses traditional Max-VNN definition for 'viscous' modes

Navier-Stokes Analysis

- Min-CFL, Max-VNN Stability Result

$AR = 1000$

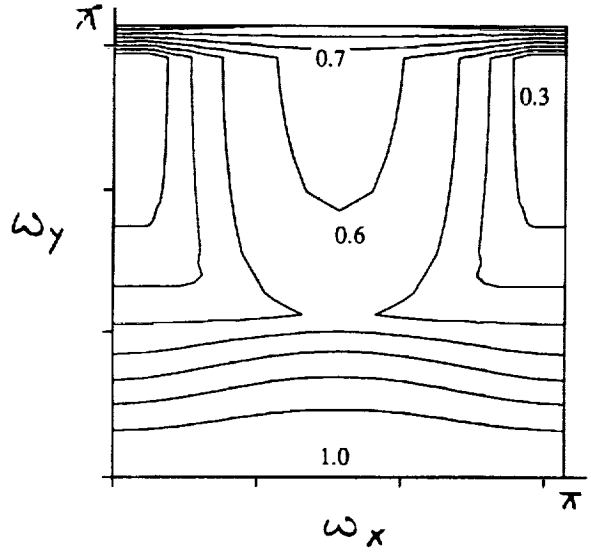

$CFL_x = 1,\ CFL_y = 1000$

$VNN_x = 1 \times 10^{-6},\ VNN_y = 1$

High Aspect Ratio Convergence—Viscous Duct

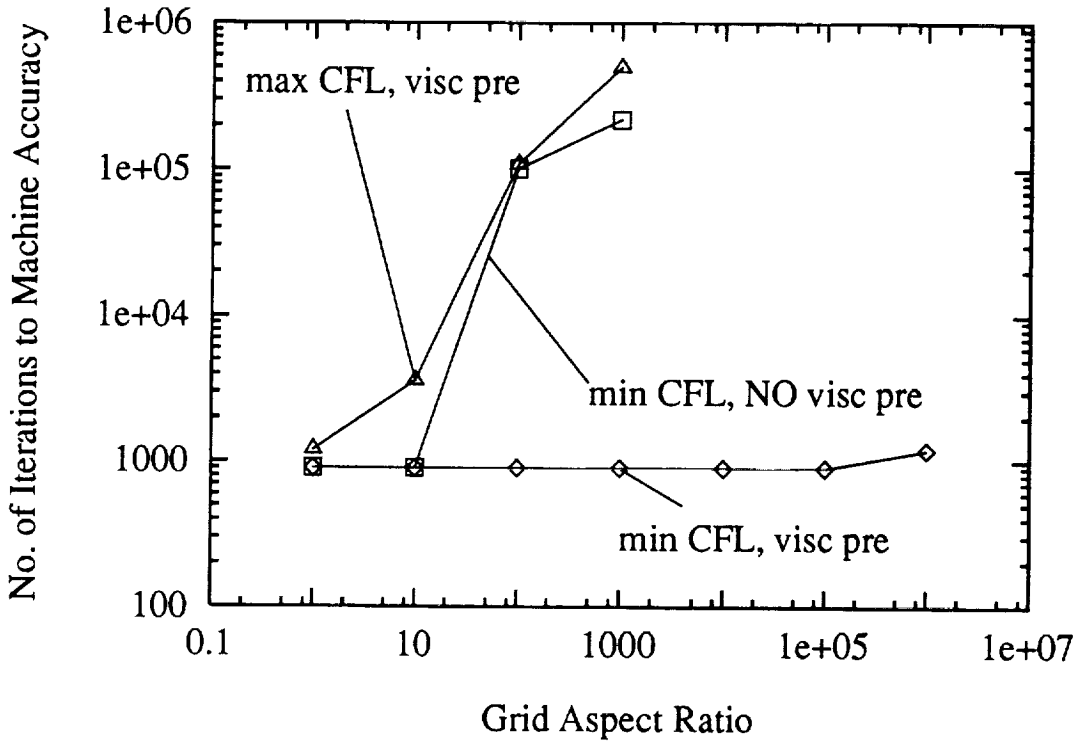

Hydrogen/Oxygen Shear-Layer Stretched Grid and Solution

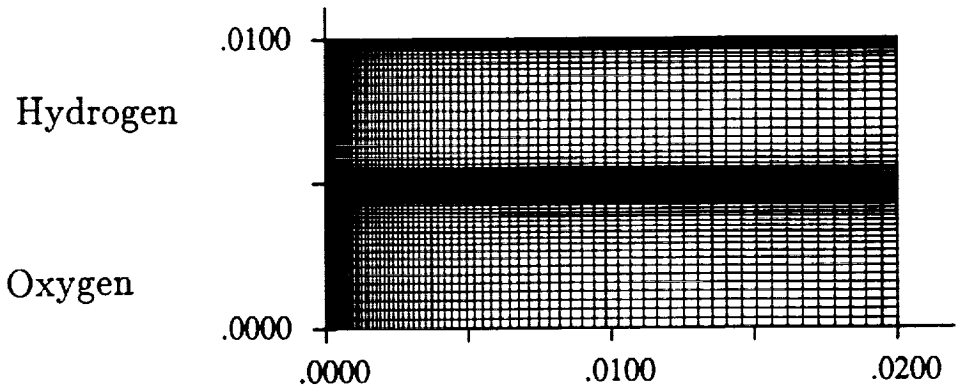

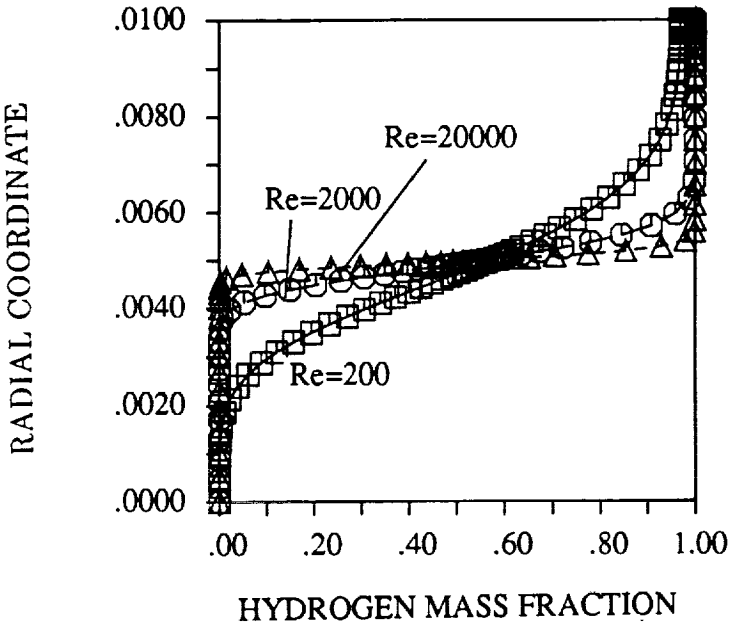

Hydrogen/Oxygen Shear-Layer Convergence

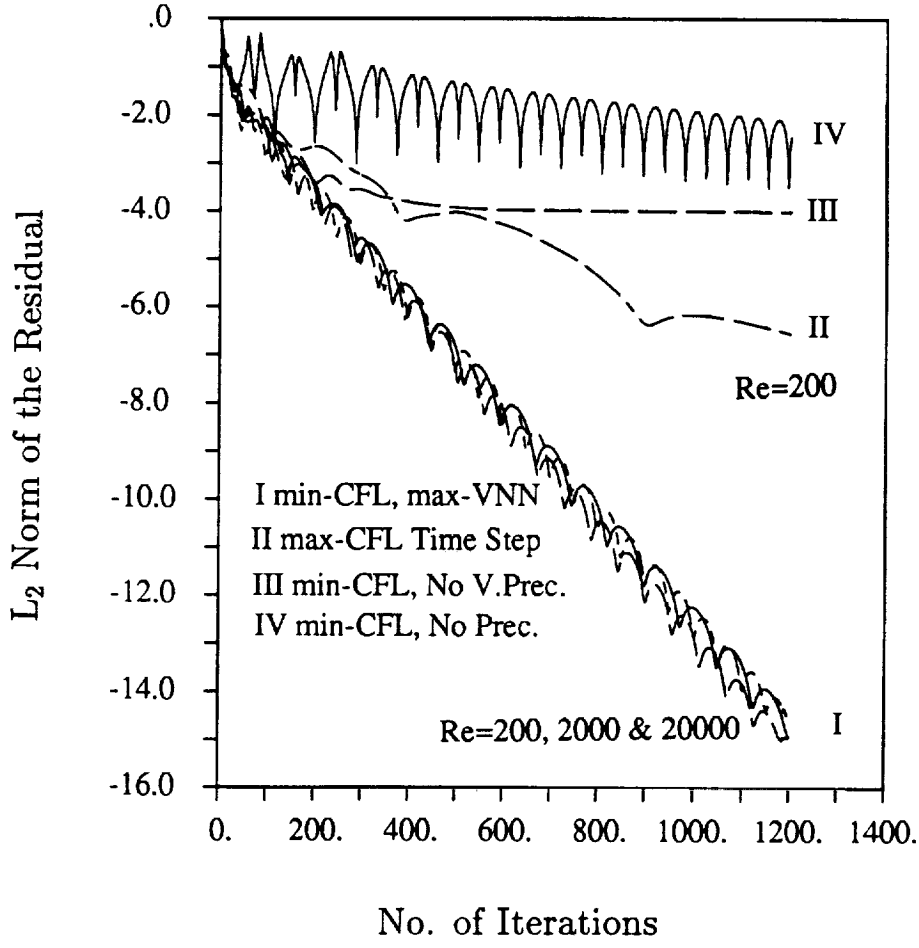

High Reynolds Number Boundary Layer Convergence—Stretched Grid

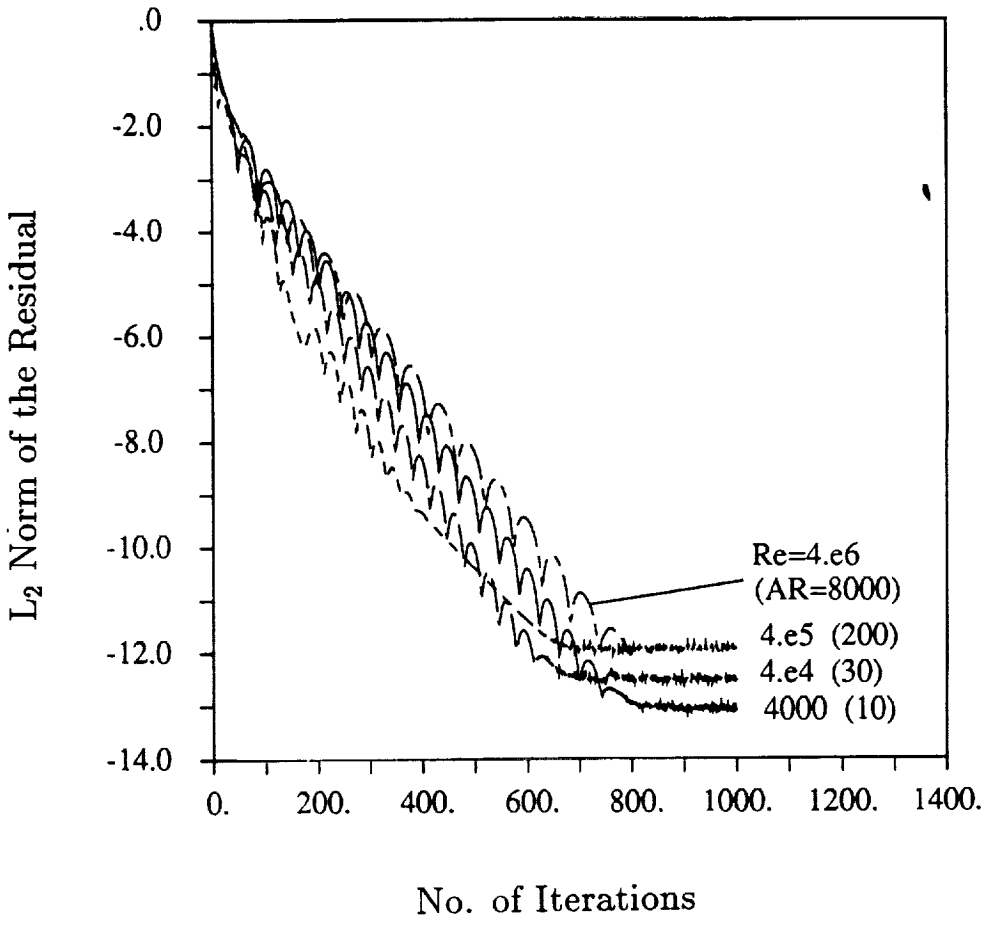

High Reynolds Number Boundary Layer Blasius Solution

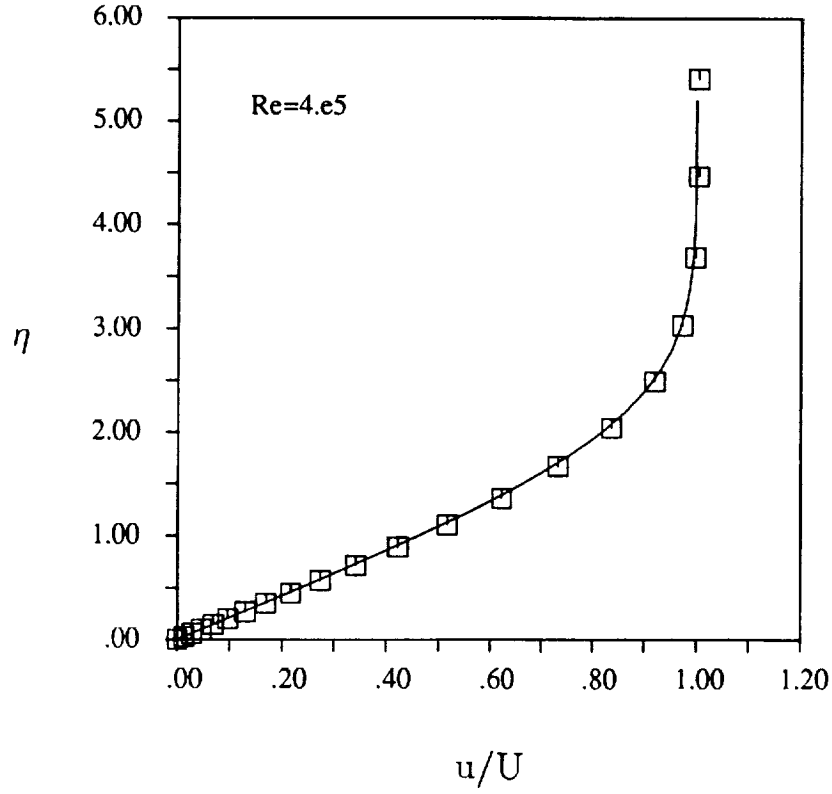

High Reynolds Number Boundary Layer Turbulent Velocity Profile

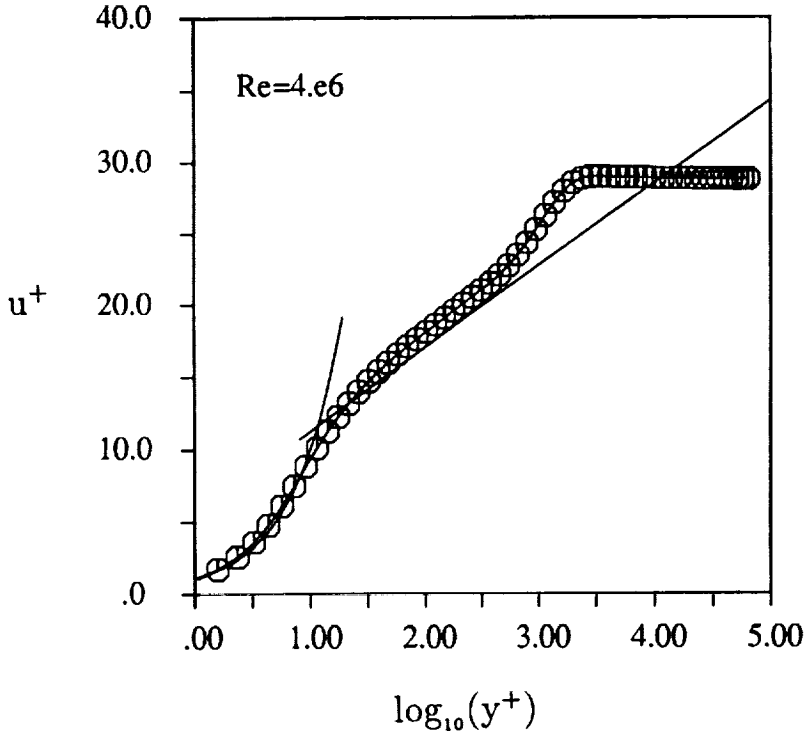

Turbulent Nozzle Computation
Stretched Grid and Solution

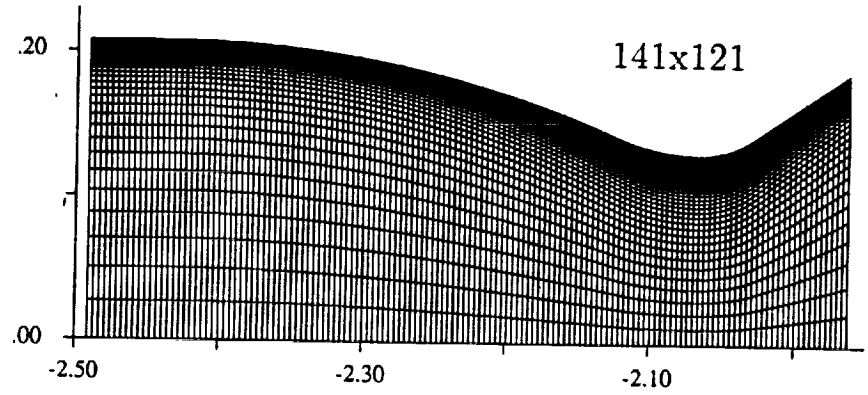

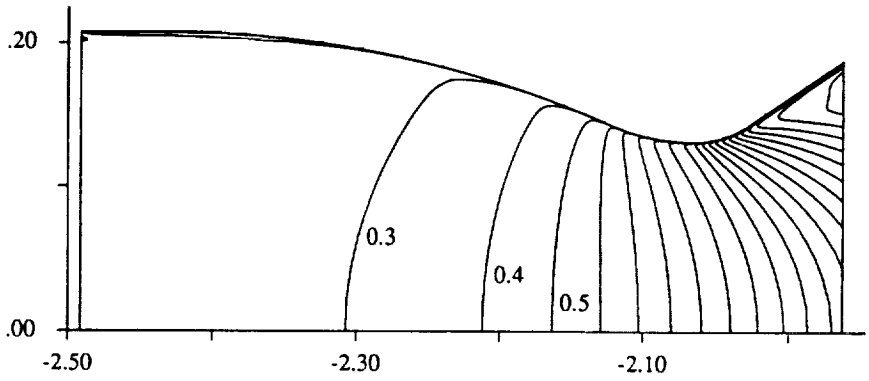

Turbulent Nozzle Computation
Convergence

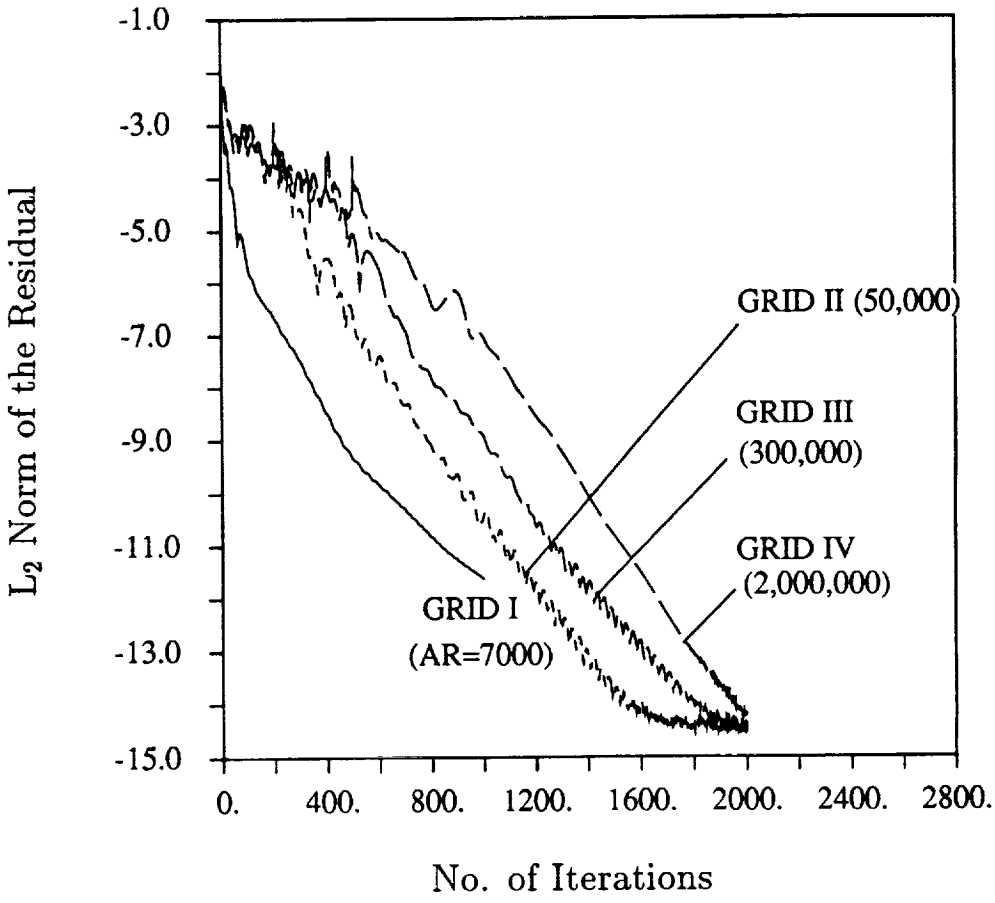

Turbulent Nozzle Computation
Wall Heat Flux

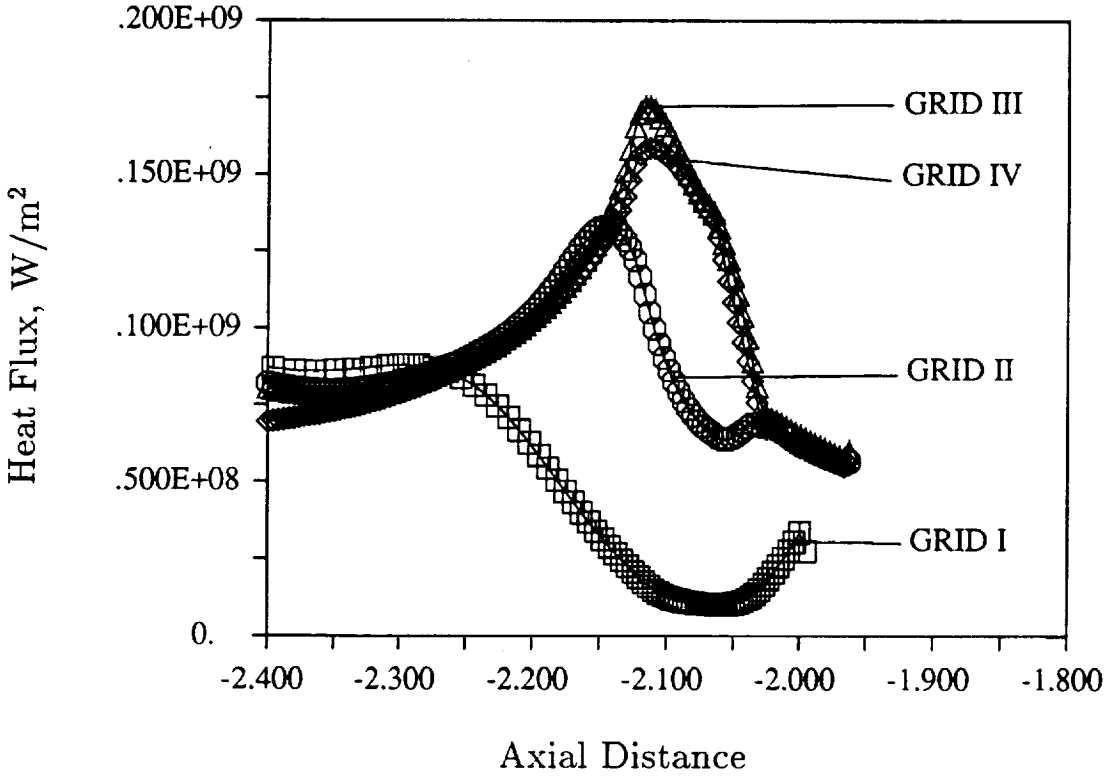

Conclusions—High Aspect Ratio Study

- High Aspect Ratio Analysis
  - — Stability Theory
  - — Numerical Convergence Studies
- Convergence Control:
  - — Min-CFL Time Step
  - — Max-VNN Viscous Preconditioner
  - — Correct implementation of boundary conditions
- Uniform Convergence Demonstrated for All AR's
  - — Above issues addressed in combination
  - — Efficient convergence for variety of test cases

Conclusions (Contd.)

- Present results are for two-dimensional central-differenced *ADI* scheme
- Explicit Schemes:
  - — Optimum time step causes poor convergence at high *AR*'s
- Upwind Schemes Also Suffer at High *AR*'s
  - — Present improvements may be incorporated
  - — Rich variety of approximate factorization methods
- Three-dimensional computations:
  - — *ADI* scheme is conditionally stable
  - — Two kinds of high aspect ratio grids
  - — Algorithmic improvements appear promising

A TIME-ACCURATE FINITE VOLUME METHOD VALID AT ALL FLOW VELOCITIES

S.-W. Kim
Resident Research Associate
CFD for Space Branch,
NASA Lewis Research Center, MS 5-11,
Cleveland, Ohio 44135

A finite volume method to solve the Navier-Stokes equations at all flow velocities (e.g., incompressible, subsonic, transonic, supersonic and hypersonic flows) is presented. The numerical method is based on a finite volume method that incorporates a pressure-staggered mesh and an incremental pressure equation for the conservation of mass. Comparison of three generally accepted time-advancing schemes, i.e., Simplified Marker-and-Cell (SMAC), Pressure-Implicit-Splitting of Operators (PISO), and Iterative-Time-Advancing (ITA) scheme, are made by solving a lid-driven polar cavity flow and self-sustained oscillatory flows over circular and square cylinders. Calculated results show that the ITA is the most stable numerically and yields the most accurate results. The SMAC is the most efficient computationally and is as stable as the ITA. It is shown that the PISO is the most weakly convergent and it exhibits an undesirable strong dependence on the time-step size. The degenerated numerical results obtained using the PISO is attributed to its second corrector step that cause the numerical results to deviate further from a divergence free velocity field. The accurate numerical results obtained using the ITA is attributed to its capability to resolve the nonlinearity of the Navier-Stokes equations.

The present numerical method that incorporates the ITA is used to solve an unsteady transitional flow over an oscillating airfoil and a chemically reacting flow of hydrogen in a vitiated supersonic airstream. The turbulence fields in these flow cases are described using multiple-time-scale turbulence equations.

For the unsteady transitional over an oscillating airfoil, the fluid flow is described using ensemble-averaged Navier-Stokes equations defined on the Lagrangian-Eulerian coordinates. It is shown that the numerical method successfully predicts the large dynamic stall vortex (DSV) and the trailing edge vortex (TEV) that are periodically generated by the oscillating airfoil. The calculated streaklines are in very good comparison with the experimentally obtained smoke picture. The calculated turbulent viscosity contours show that the transition from laminar to turbulent state and the relaminarization occur widely in space as well as in time. The ensemble-averaged velocity profiles are also in good agreement with the measured data and the good comparison indicates that the numerical method as well as the multiple-time-scale turbulence equations successfully predict the unsteady transitional turbulence field.

The chemical reactions for the hydrogen in the vitiated supersonic airstream are described using 9 chemical species and 48 reaction-steps. Consider that a fast chemistry can not be used to describe the fine details (such as the instability) of chemically reacting flows while a reduced chemical kinetics can not be used confidently due to the uncertainty contained in the reaction mechanisms. However, the use of a detailed finite rate chemistry may make it difficult to obtain a fully converged solution due to the coupling between the large number of flow, turbulence, and chemical equations. The numerical results obtained in the present study are in good agreement with the measured data. The good comparison is attributed to the numerical method that can yield strongly converged results for the reacting flow and to the use of the multiple-time-scale turbulence equations that can accurately describe the mixing of the fuel and the oxidant.

A TIME-ACCURATE FINITE VOLUME METHOD VALID AT ALL FLOW VELOCITIES

S.-W. Kim*
CFD for Space Branch,
NASA Lewis Research Center, MS 5-11,
Cleveland, Ohio 44135

* Resident Research Associate

CONTENTS

INTRODUCTION

Fluid flow inside Space Propulsion Systems includes all flow velocities, i.e.,

Incompressible Flows ($M < \varepsilon$),
Low Mach Number Flows,
Transonic Flows,
Supersonic Flows, and
Hypersonic Flows.

A number of numerical methods to solve flows (mostly steady flows) at all flow velocities have been proposed in recent years.

Establish a numerical method that will yield accurate numerical results for flows at all velocities that include:

i. steady and unsteady flows*,
ii. lamianr, transitional, and turbulent flows,*
iii. chemically reacting flows*

* Need to identify a best time-integration scheme among many available methods.

** Multiple-time-scale turbulence equations are used in the present unsteady transitional flow and the chemically reacting flow calculations.

Comparison of Unsteady Flow Solution Techniques*

Iterative Time-Advancing Scheme (ITA).

Simplified Marker and Cell (SMAC).

Pressure-Implicit Splitting of Operators (PISO).

* Kim & Benson, Computers and Fluids, vol. 21, pp. 435-454, 1992

1. Iteartive Time-Advancing Scheme (ITA)

Solve momentum equation.

$$(\rho C_1+A_i^*)u_i^{**}=\sum_{nb} A_k^* u_k^{**} + S_i^* - \frac{\partial p^*}{\partial x_i} + \rho C_2 u_i^{n-1} - \rho C_3 u_i^{n-2} \quad (1)$$

Correct the velocity field to be divergence free

Incremental pressure equation

$$\frac{\partial}{\partial x_j}\left\{\frac{1}{(\rho C_1+A_j^*)}\frac{\partial p'}{\partial x_j}\right\} = \frac{\partial u_j^{**}}{\partial x_j} \quad (2)$$

Incremental velocity equation

$$u_i' = \frac{1}{(\rho C_1+A_i^*)}\frac{\partial p'}{\partial x_i} \quad (3)$$

Velocity and pressure corrections

$$u_i^{***} = u_i^{**} + u'_i \quad (4)$$

$$p^{**} = p^{*} + p' \qquad (5)$$

Solve eqs. (1-5) iteratively until all flow variables converge for each time-level.

The ITA can account for the nonlinearity in each component of the momentum equations and the nonlinear coupling of u- and v-velocity.

2. Simplified Marker and Cell (SMAC)

Predictor Step: Solve momentum equation.

$$(\rho C_1 + A_i^{n-1})u_i^* = \sum_{nb} A_k^{n-1} u_k^* + S_i^{n-1} - \frac{\partial p^{n-1}}{\partial x_i} + \rho C_2 u_i^{n-1} - \rho C_3 u_i^{n-2} \quad (1)$$

Corrector Step: Correct the velocity field to be divergence free

Auxiliary pressure potential equation

$$\frac{\partial}{\partial x_j}\left(\frac{\partial \phi}{\partial x_j}\right) = \frac{\partial u_j^*}{\partial x_j} \quad (2)$$

Update velocity

$$u_i^n = u_i^* - \frac{\partial \phi}{\partial x_i} \quad (3)$$

Consistent pressure field

$$p^n = p^{n-1} + \rho C_1 \phi \quad (4)$$

Solve eqs. (1-4) for each time-level.The velocity field strongly satisfy the conservation of mass.

Conservation of momentum is achieved by obtaining a consistent pressure field.

3. Pressure-Implicit Splitting of Operators

Predictor Step: Solve momentum equation.

$$(\rho C_1 + A_i^{n-1}) u_i^* = H_i^* - \frac{\partial p^{n-1}}{\partial x_i} + \rho C_2 u_i^{n-1} - \rho C_3 u_i^{n-2} \qquad (1)$$

where

$$H_i^* = \sum_{nb} A_k^{n-1} u_k^* + S_i^{n-1}$$

First Corrector Step: Correct velocity and pressure for mass imbalance

Incremental pressure equation

$$\frac{\partial}{\partial x_j}\left(\frac{1}{(\rho C_1 + A_j^{n-1})} \frac{\partial p'}{\partial x_j}\right) = \frac{\partial u_j^*}{\partial x_j} \qquad (2)$$

Correct velocity and pressure

$$u_i' = - \frac{1}{(\rho C_1 + A_i^{n-1})} \frac{\partial p'}{\partial x_i} \qquad (3)$$

$$u_i^{**} = u_i^{*} + u'_i \tag{4}$$

$$p^{**} = p^{*} + p' \tag{5}$$

Second Corrector Step: Correct velocity and pressure for momentum imbalance

Incremental pressure equation

$$\frac{\partial}{\partial x_j}\left(\frac{1}{(\rho C_1 + A_j^{**})}\frac{\partial p''}{\partial x_j}\right) = \frac{\partial}{\partial x_j}\left\{\frac{1}{(\rho C_1 + A_j^{**})}(H_j^{**} - H_j^{*})\right\} \tag{6}$$

where

$$H_i^{**} = \sum_{nb} A_k^{**} u_k^{**} + S_i^{**}$$

Correct velocity and pressure

$$(\rho C_1 + A_i^{**})u_i'' = H_i^{**} - H_i^{*} - \frac{\partial p''}{\partial x_i} \tag{7}$$

$$u_i^n = u_i^{**} + u''_i \tag{8}$$

$$p^n = p^* + p'' \tag{9}$$

Solve eqs. (1-9) for each time-level.

In the 2nd corrector step, the velocity and pressure are driven by the momentum imbalance.

The velocity field may not satisfy the conservation of mass accurately.

Consequently, the conservation of momentum can not be satisfied accurately if a large mass imbalance occur.

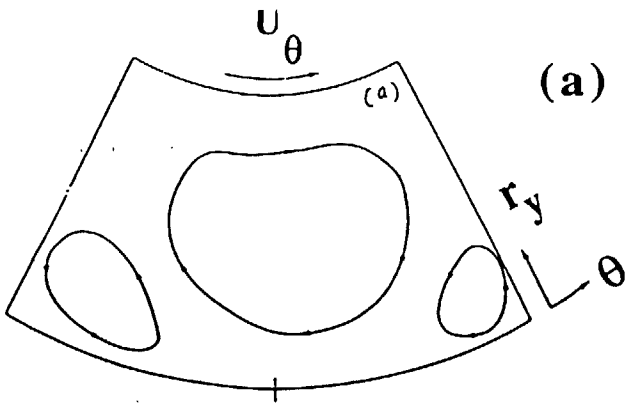

(a) nomenclature

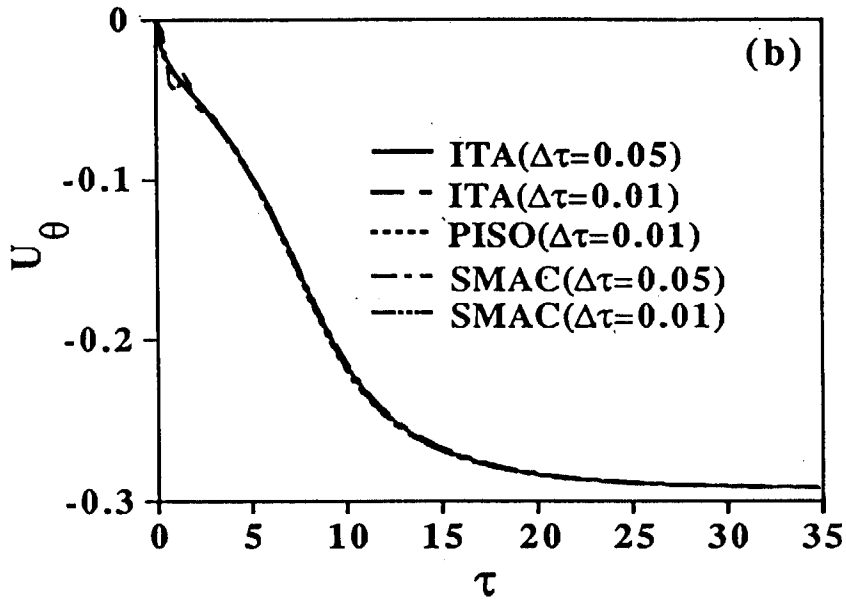

(b) evolution of u_Θ at $(r_y,\Theta)=(0.246, 0.)$

Polar cavity flow starting from rest

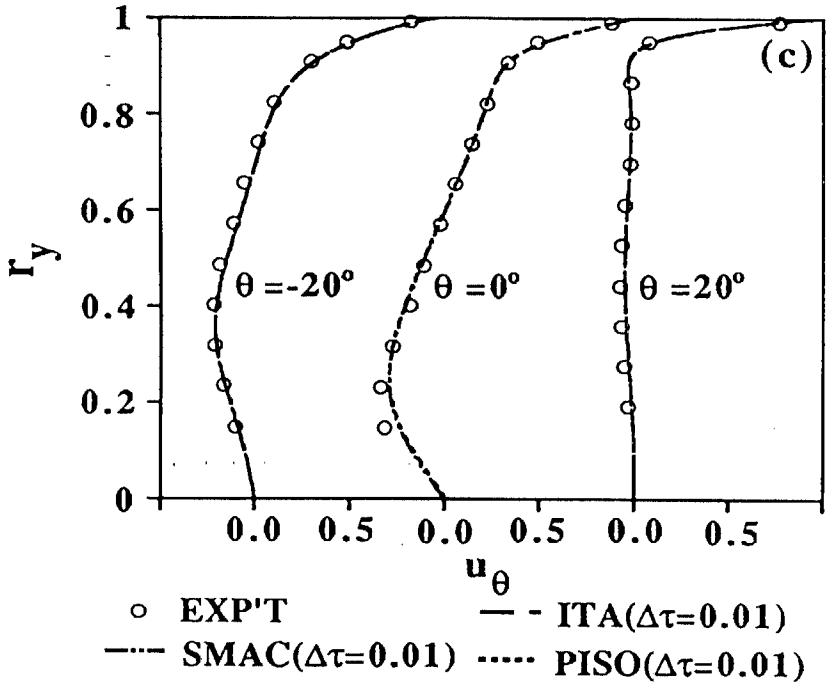

(c) u_Θ velocity profiles

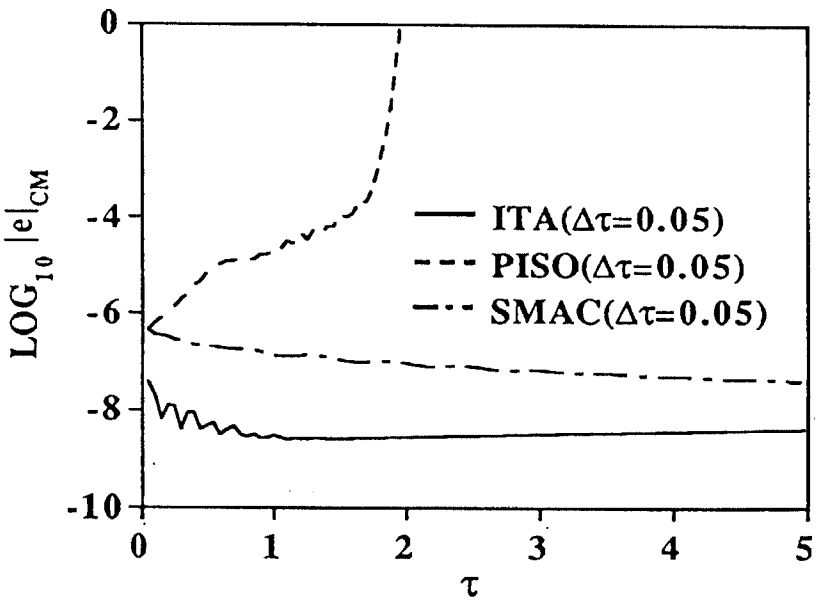

(d) mass imbalance

Polar cavity flow starting from rest

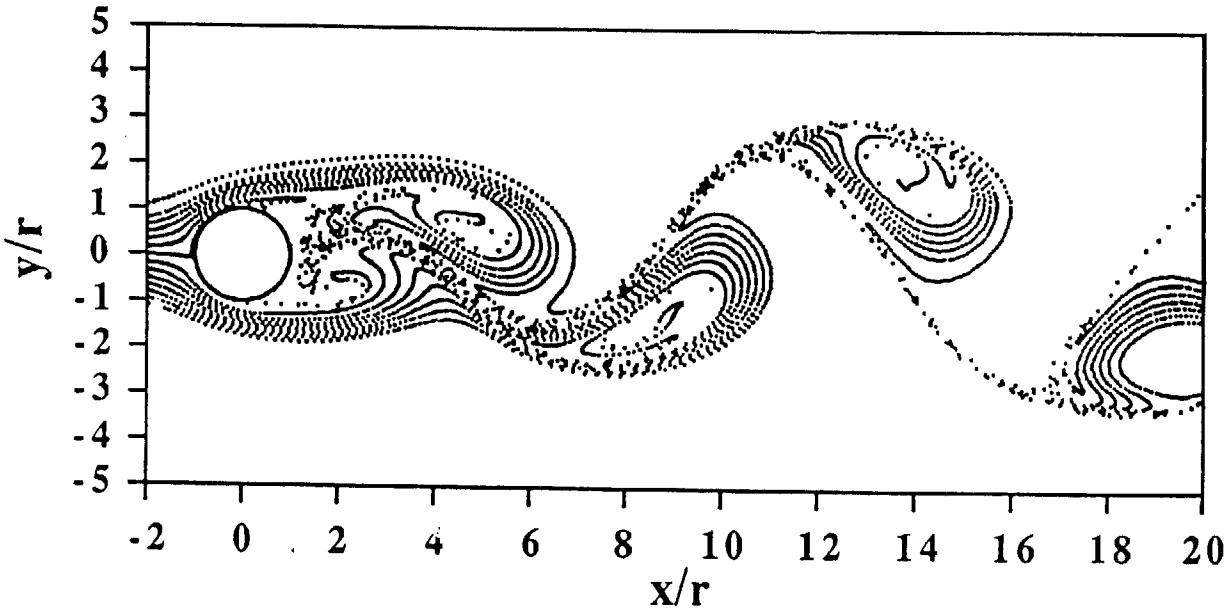

Streaklines for flow over a circular cylinder.

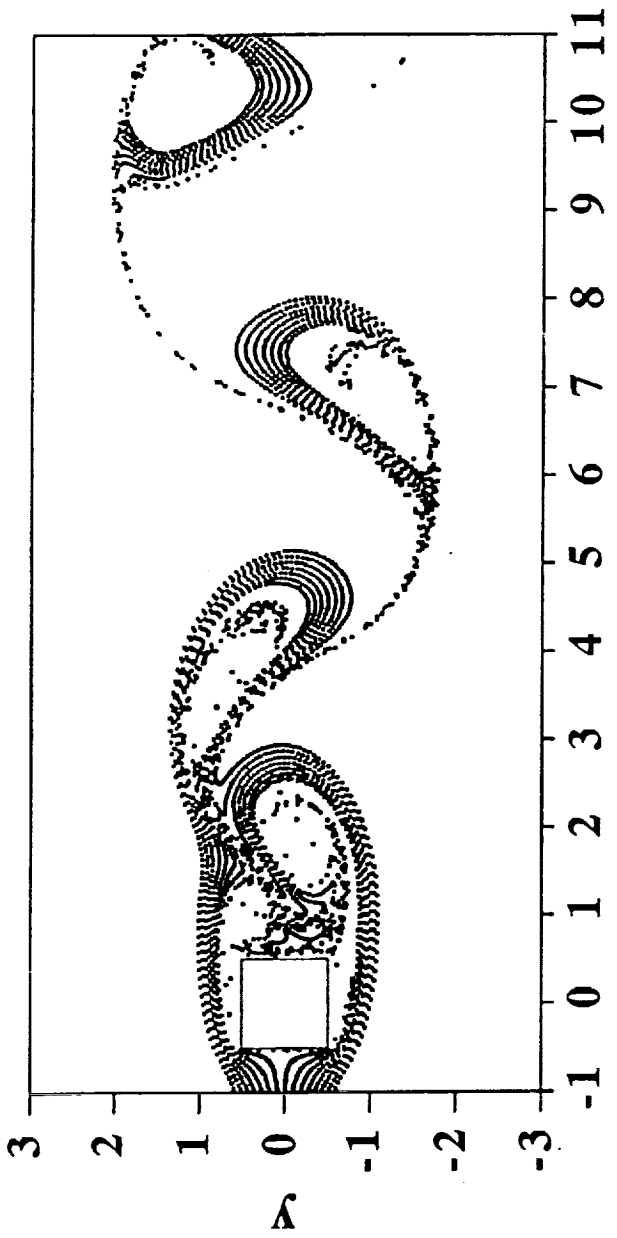

Streaklines for flow over a square cylinder.

Strouhal Numbers ($S_t = 2fr/U_o$) for Flow over a Circular Cylinder

	ITA	SMAC		PISO		Ref. [2]	Ref. [14]	Exp't
$\Delta\tau$	0.05	0.05	0.01	0.05	0.01	0.01	—	—
S_t	0.158	0.155	0.157	0.164	0.160	0.16	0.147	0.16

Ref. [2]: Braza, Chassing, Ha Minh, JFM 1986,
Ref. [14]: Eaton, JFM 1987.

Calculation of Unsteady Transitional Flow over Oscillating Airfoil*

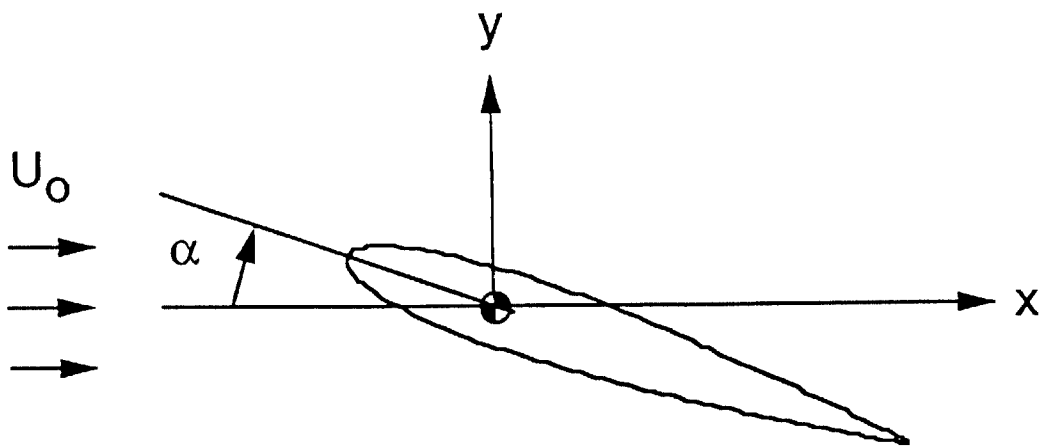

$$\alpha = \alpha_o + \alpha_A \sin(\omega t)$$

α: angle of attack

α_o: mean angle of attack (=15°)

α_A: amplitude of oscillation (=10°)

ω: angular velocity (=2πf, f=3.924Hz)

* Kim, Zaman, and Panda, To be presented in the ASME Fluid Engineering Conference, Washington D.C., June 20-24, 1993.

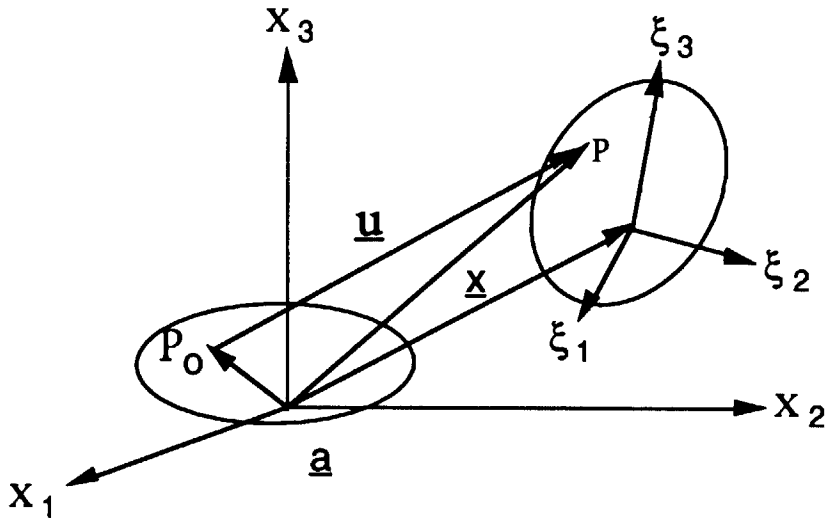

Lagrangian-Eulerian coordinates

x: fixed reference coordinates

ξ: moving coordinates

$J = |\partial \xi_j / \partial a_j|$

Conservation of mass equation

$$\frac{\partial}{\partial t}(\rho J) = J\frac{\partial}{\partial x_j}\left\{\rho\left(u_j^g - u_j\right)\right\} \quad (1)$$

Conservation of linear momentum equation

$$\frac{\partial}{\partial t}(\rho u_i J) = J\frac{\partial}{\partial x_j}\left\{\rho u_i\left(u_j^g - u_j\right)\right\} + J\frac{\partial \tau_{ij}}{\partial x_j} - J\frac{\partial p}{\partial x_i} \quad (2)$$

Convection-diffusion equation for scalar variables (i.e., $\phi = \left\{k_p, \varepsilon_p, k_t, \varepsilon_t, \text{etc.}\right\}$

$$\frac{\partial}{\partial t}(\rho \phi J) = J\frac{\partial}{\partial x_j}\left\{\rho\phi\left(u_j^g - u_j\right)\right\} + J\left\{\mu_e\frac{\partial \phi}{\partial x_j}\right\} - J\rho f(\phi)$$

Ensemble average

$$\overline{u}(x_o,t_o) = \lim_{N\to\infty}\left\{\frac{1}{N}\sum_{n=1}^{N} u(x_o,t_o)\right\}$$

Aside: Time average

$$u = \overline{u} + u'$$

$$\overline{u} = \lim_{T\to\infty}\left\{\frac{1}{T}\int_{t_o}^{t_o+T} u\,dt\right\}$$

Hence $\frac{\partial \overline{u}}{\partial t} = 0$, and the time-average is useful for steady flows only.

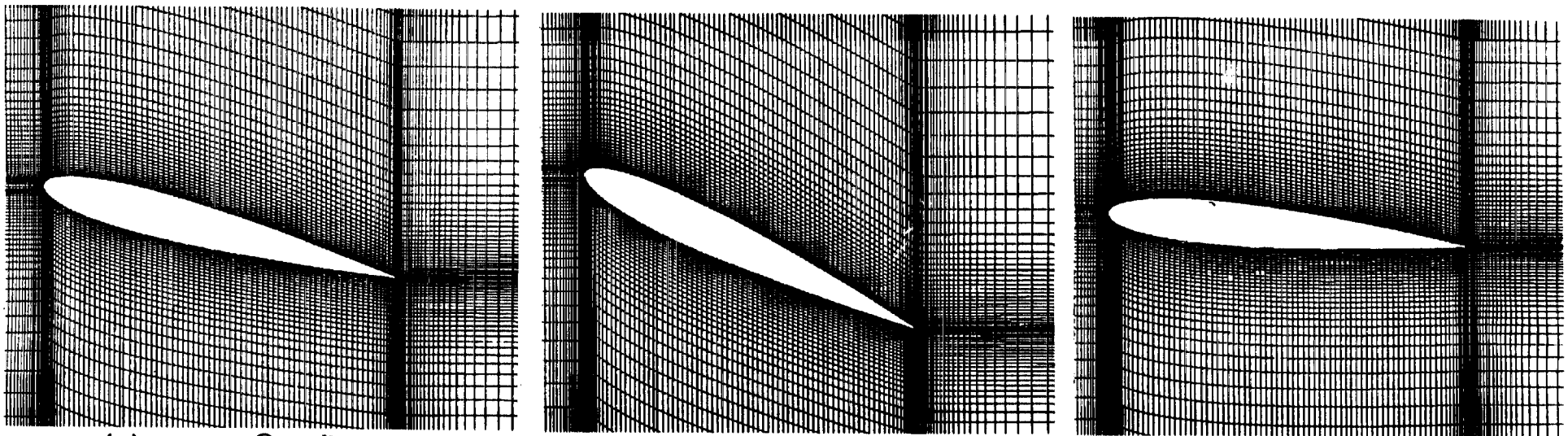

(a) $\alpha = 15^{o}$, $t/T = 0.0$ (b) $\alpha = 25^{o}$, $t/T = \pi/2$ (c) $\alpha = 5^{o}$, $t/T = 3/2\ \pi$

Oscillating airfoil and moving mesh

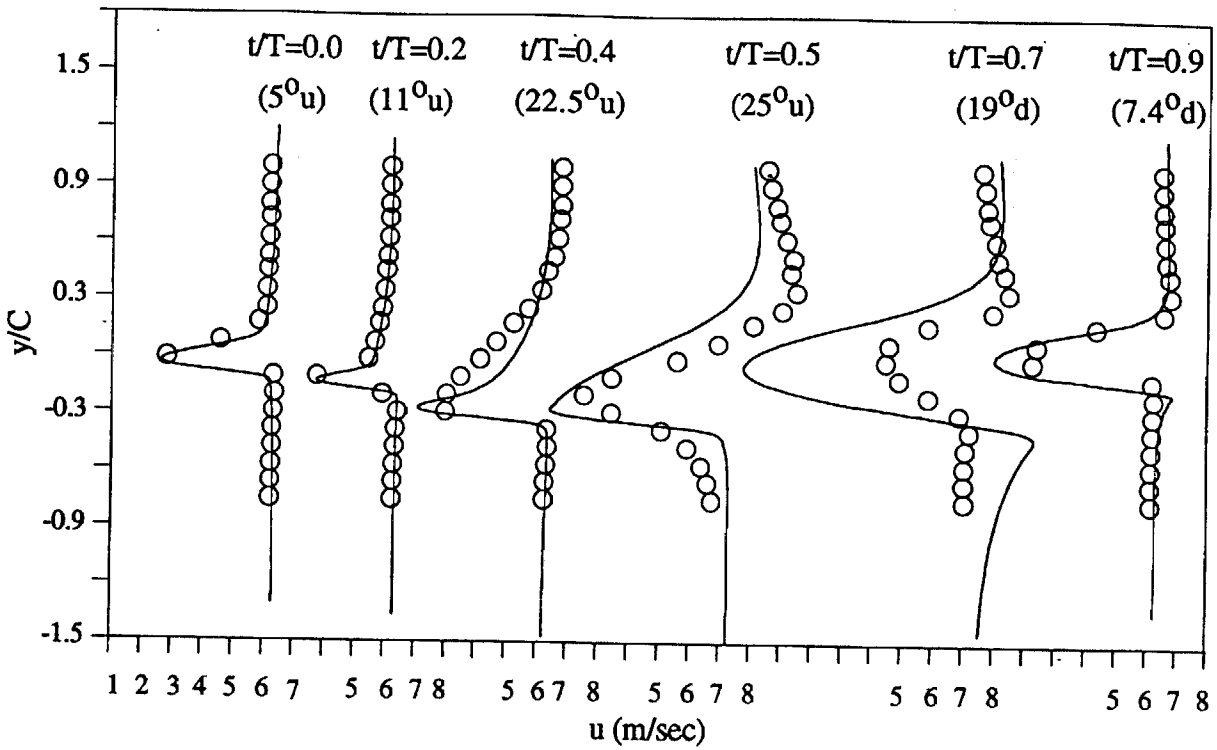

Ensenble-averaged velocity profiles at x/c=1.0

The deteriorated comparison at $\alpha \approx 19^{o}$d

(i) The hot wire can not accurately measure the velocity components when the flow is misaligned more than approximately 30^{o} from the hot wire axis.

(ii) The interaction between the DSV and the TEV occurs in a relatively coarse mesh region and the numerical method yields somewhat deteriorated results.

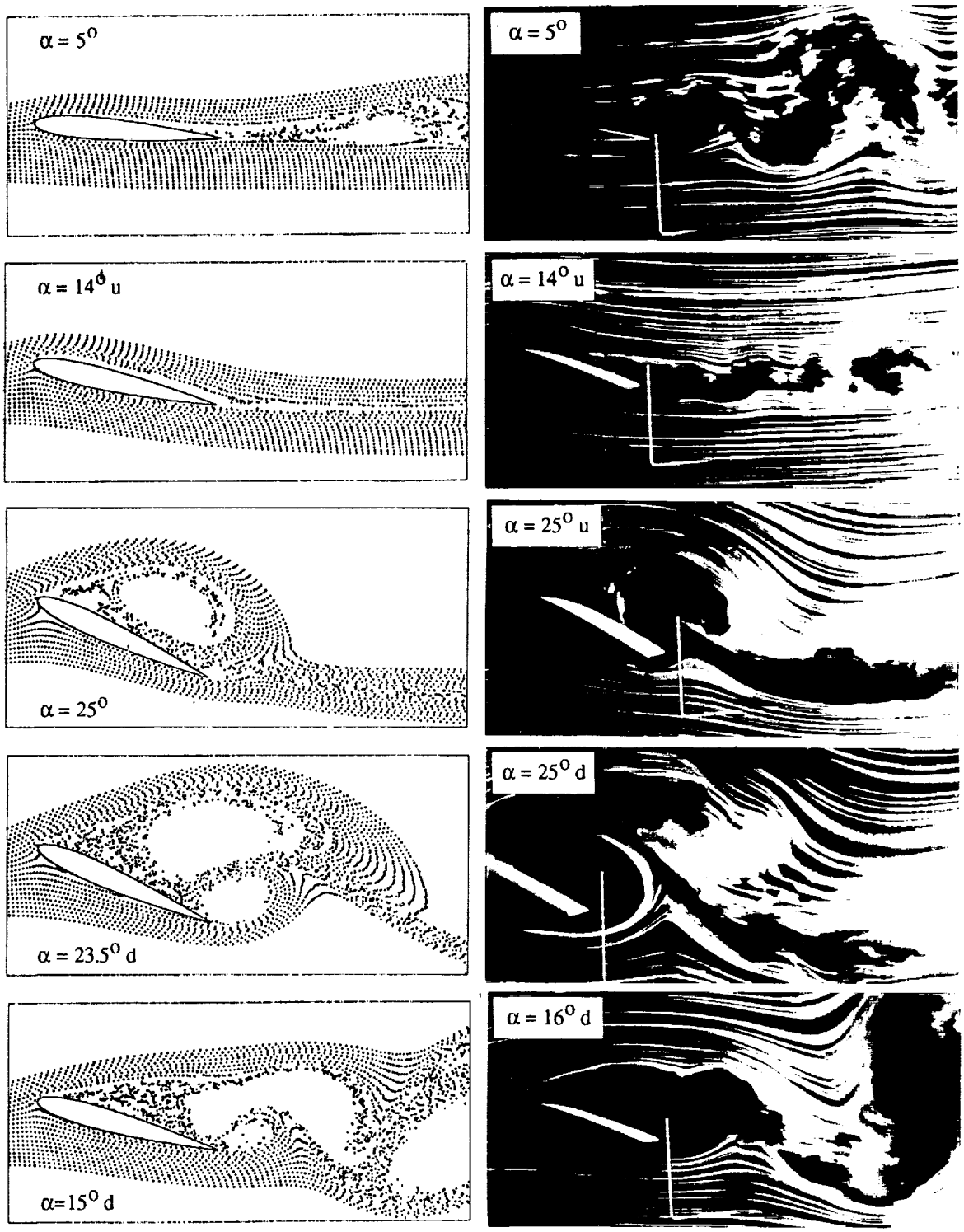

Comparison of calculated streaklines with smoke picture.

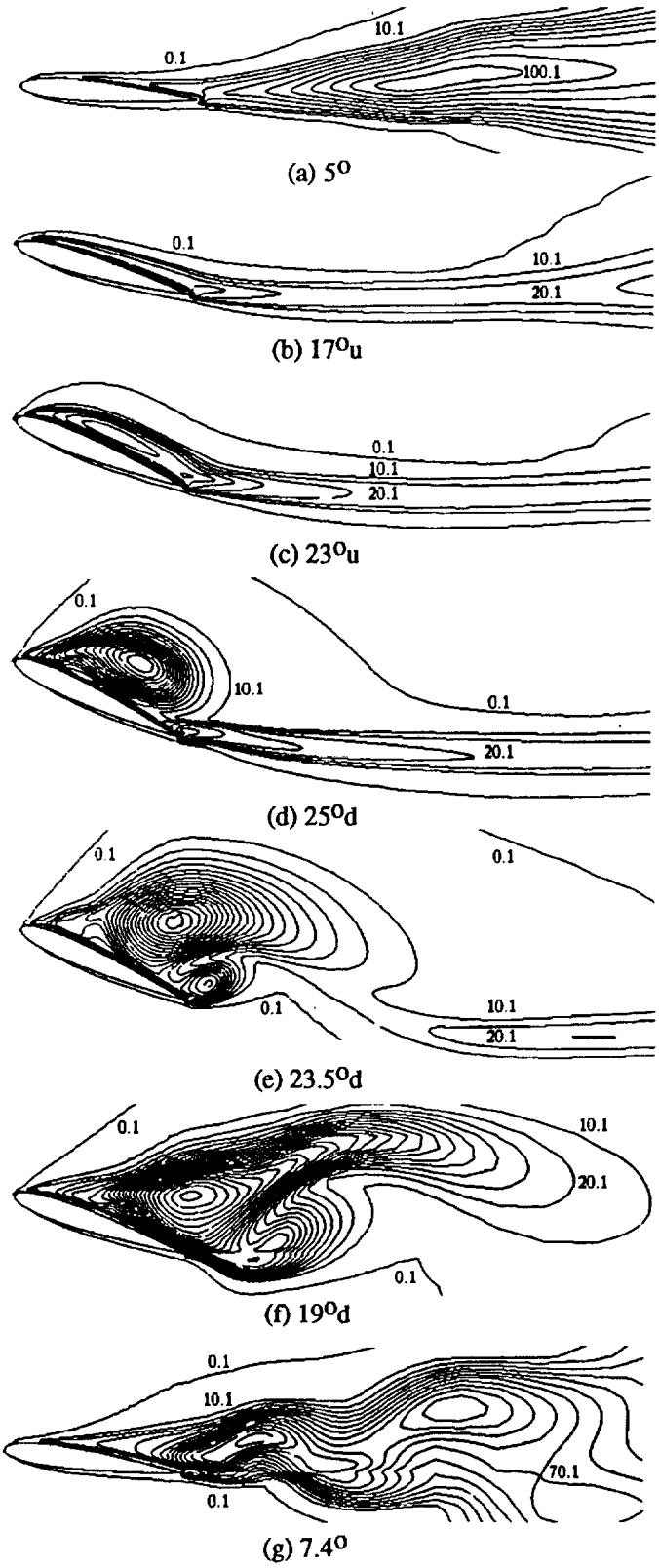

Turbulent viscosity contour ($\Delta\mu/\mu_t = 10$)

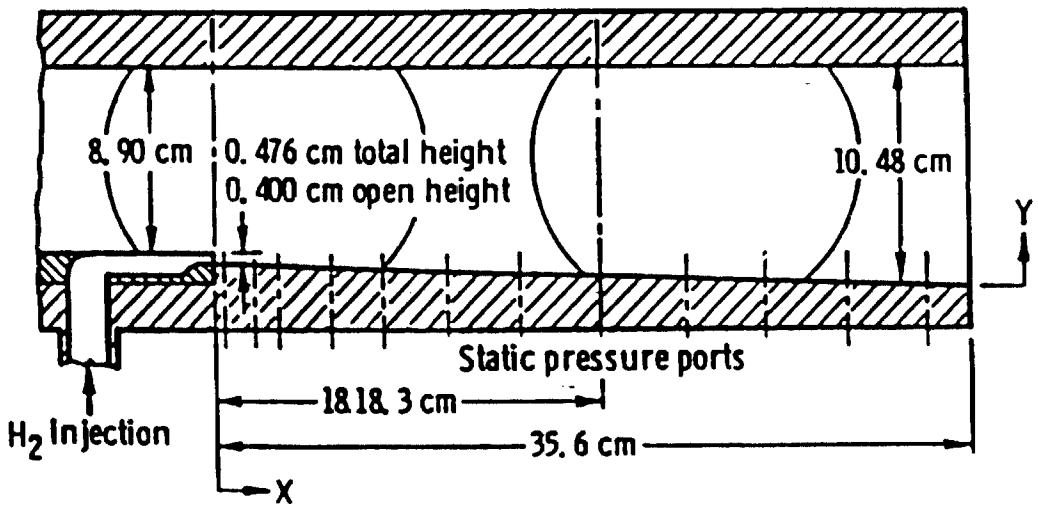

Combustion of H_2 in vitiated supersonic airstream (Burrows and Kurkov, 1973)

Chemical species concentration equation

$$\frac{\partial}{\partial t}\left(\rho Y_i\right) + \nabla\cdot\left\{\rho Y_i\left(v + V_i\right)\right\} = \dot{w}_i$$

where the diffusion velocity, V_i, is approximated using the Fick's law given as

$$Y_i V_i = -\left(D_{i,l} + D_{i,t}\right)\nabla Y_i$$

The production rate of the *i*-th species, $\dot{w}_i$, is given as

$$\dot{w}_i = \sum_{k=1}^{N_r} M_i\left(n''_{i,k} - n'_{i,k}\right) w_k$$

where

$$\omega_k = k_{f,k}\prod_{j=1}^{N_s} c_j^{\nu'_{j,k}} - k_{b,k}\prod_{j=1}^{N_s} c_j^{\nu''_{j,k}}$$

Chemical reactions for the combustion of H_2 in a vitiated supersonic airstream are described using 9 chemical species (H_2, O_2, H_2O, OH, O, H, HO_2, H_2O_2, and N_2) and 48 reaction-steps (Burks and Oran, 1981; Kumar, 1989).

A fast chemistry can not be used to describe the fine details (such as the instability) of chemically reacting flows.

A reduced chemical kinetics can not be used confidently due to the uncertainty contained in the reaction mechanisms.

The use of a detailed finite rate chemistry may make it difficult to obtain a fully converged solution due to the coupling between the large number of flow, turbulence, and chemical equations. The numerical method needs to be strongly convergent. Accuracy also depends on the capability of turbulence equations used.

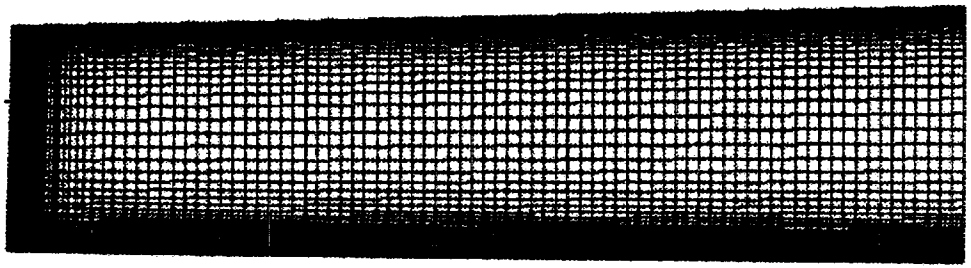

127 x 124 mesh

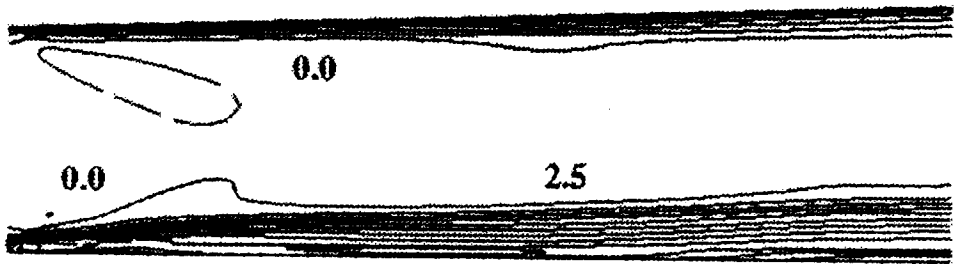

mach number contour (dM=0.2)

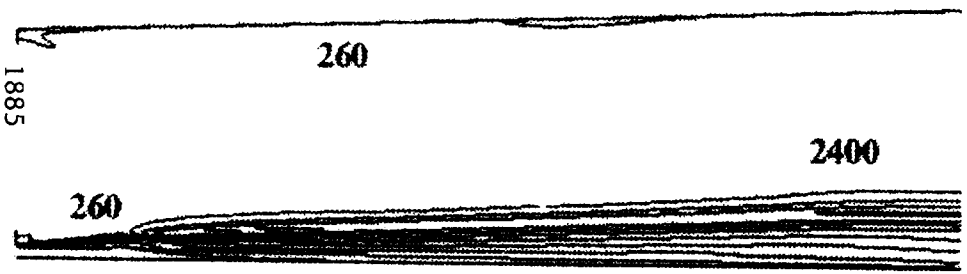

temperature contour (dT=200)

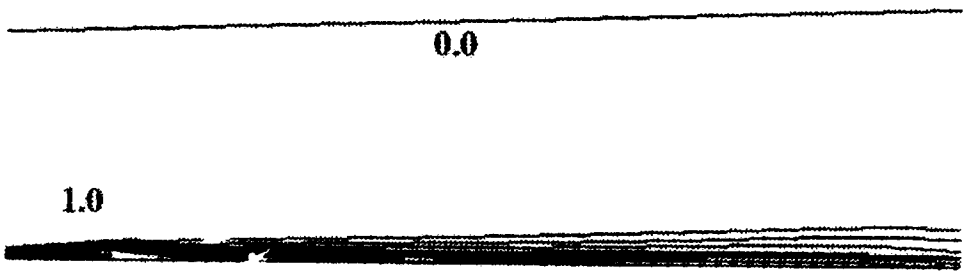

H2 mass fraction (dY=0.1)

Combustion of H_2 in vitiated supersonic airstream

CONCLUSIONS AND DISCUSSION

On comparison of SMAC, PISO, and ITA

1. The SMAC is the most efficient computationally and yields accurate numerical results.

   Calculation of steady flows using an unsteady flow solver.

   * No unsteady flow solver is more efficient than steady flow solvers to solve steady flows (Jang et al., *Numer. Heat Transfer*, 1986.)

   * Only the SMAC can compete with steady flow solvers (ITA with $\Delta\tau=\infty$) to solve steady flows.

2. The 2nd corrector step of PISO.

   Velocity and pressure are driven by momentum imbalance.
   Thus the velocity field is not divergence free.
   Large amount of mass imbalance can cause divergence.

3. The ITA can best resolve the nonlinearity of the Navier-Stokes Equations.

CONCLUSIONS AND DISCUSSION

Calculations of
incompressible and compressible flows,
steady and unsteady flows,
lamianr, transitional, and turbulent flows,
chemically reacting flows
are presented.

Calculations of
chemically reacting flows with spray combustion
Hypersonic Flows.
are in progress.

The accurate numerical results are attributed to the capability of

(i) the ITA that can best resolve the nonlinearity of the Navier-Stokes equations,
(ii) the new pressure correction algorithm that can strongly enforce the conservation of mass, and
(iii) the Multiple-time-scale turbulence equations that can resolve the inequilibrium turbulence field.

A CONTROLLED VARIATION SCHEME FOR CONVECTION TREATMENT IN PRESSURE–BASED ALGORITHM

Wei Shyy, Siddharth Thakur and Kevin Tucker

Department of Aerospace Engineering, Mechanics & Engineering Science,
University of Florida

and
NASA Marshall Space Flight Center

Convection effect and source terms are two primary sources of difficulties in computing turbulent reacting flows typically encountered in propulsion devices. The present work intends to elucidate the individual as well as the collective roles of convection and source terms in the fluid flow equations, and to devise appropriate treatments and implementations to improve our current capability of predicting such flows. A controlled variation scheme (CVS) has been under development in the context of a pressure–based algorithm, which has the characteristics of adaptively regulating the amount of numerical diffusivity, relative to central difference scheme, according to the variation in *local* flow field. Both the basic concepts and a pragmatic assessment will be presented to highlight the status of this work.

A CONTROLLED VARIATION SCHEME FOR CONVECTION TERM TREATMENT IN PRESSURE-BASED ALGORITHM

Wei Shyy
Siddarth Thacker
University of Florida

Kevin Tucker
MSFC/ED32

Overview of Algorithm

- Handle Different Physics & Varying Number of Unknowns: u, v, w, p, ϱ, T, k, ε, etc. Without Reformulating the Algorithm
- Suitable for Incompressible & Compressible Flows
- Suitable for Steady & Unsteady *Flows at All Speeds*
- Modern Concepts, e.g., Modern Discretization Schemes, Multigrid, Composite Grids, etc. Should be Implementable, in Principle

▶ Pressure–Based Sequential Solver

Treatment of Convection

- **Convection terms:** Strong Nonlinearity

- **Critical Situations**
  - High Local Cell Peclet Numbers (Convection Dominates Diffusion)
  - Sharp Gradients in Flowfield
  - Recirculation
  - Interaction of Convection with Turbulence, Chemical Reactions, etc.
  - Presence of Source Terms

- **Flows with Sharp Gradients, e.g., Shocks**
  - Any First–Order Scheme → too diffusive
  - Any Linear Second–Order Scheme → spurious oscillations near sharp gradients
  - **Remedy** → Nonlinear Second–Order TVD (Total Variation Diminishing) Schemes

- **Source Terms:** Cause Numerical Difficulties Due to Different Length and Time Scales

Present Approach

- **Sequential Solver**
- **Explicit Control of Numerical Viscosity**
  - Based on Total Variation Diminshing (TVD) Concept
  - Controlled Variation Scheme (CVS)
- **Cases Studied**
  - Compressible Shock Tube Flows
  - Longitudinal Combustion Instability
  - Incompressible Recirculating Flows (Laminar and Turbulent)

Harten's Implicit TVD Scheme

- **Scalar Conservation Law**

$$\frac{\partial w}{\partial t} + \frac{\partial f(w)}{\partial x} = 0$$

- **Implicit TVD Scheme**

$$w_i^{n+1} + \left(\tilde{f}_{i+1/2}^{n+1} - \tilde{f}_{i-1/2}^{n+1}\right) = w_i^n$$

- **Numerical Flux**

$$\tilde{f}_{i+1/2}^{n+1} = \frac{1}{2}\Big[\; f_i + f_{i+1} + g_i + g_{i+1} - Q\left(a_{i+1/2} + \gamma_{i+1/2}\right)\Delta_{i+1/2} w \;\Big]$$

Central Diff. Flux	Anti–diffusion Flux	Numerical Dissipation Flux
$\overline{F}$	$\overline{G}$	$\overline{Q}$

Model Problem I

- **Linear Steady Burgers' Equation**

$$\alpha\phi_x = \beta\phi_{xx} \qquad \alpha,\ \beta = constants > 0$$

$$\phi(0) = 0\ , \quad \phi(1) = 1$$

- **Cell Peclet Number (P)**

$$P = \frac{\alpha}{\left[\frac{\beta}{h}\right]} = local\left[\frac{convection}{diffusion}\right]$$

- **Central Difference Scheme**

$$(2 - P)\,\phi_{i+1} - 4\phi_i + (2 + P)\,\phi_{i-1} = 0$$

Critical Value : $|P| > 2$

Effective Cell Peclet Number of CVS

- **Ratio of Local Convection to Diffusion Strength**

Diffusion (CVS) = Physical + Numerical

$$P_{cvs} = \frac{\alpha}{\left[\frac{\beta}{h} + \alpha \left\{ \frac{\overline{Q}_{i+1/2} - \overline{G}_{i+1/2}}{\Delta_{i+1/2}\phi} \right\} \right]}$$

- **Normalized Viscosity**

$$Q^* - G^* = \frac{\alpha \left\{ \frac{\overline{Q}_{i+1/2} - \overline{G}_{i+1/2}}{\Delta_{i+1/2}\phi} \right\}}{\beta/h}$$

Model Problem II

- **Linear Steady Burgers' Equation With Source**

$$\alpha\phi_x = \beta\phi_{xx} + \alpha\psi(x)$$

$$\phi(0) = 0$$

Right Boundary Condition:

Neumann: $(\phi_x)_{x=L} = 0$

Dirichlet : $\phi(L) = 0$

- **Source Term ψ(x)**

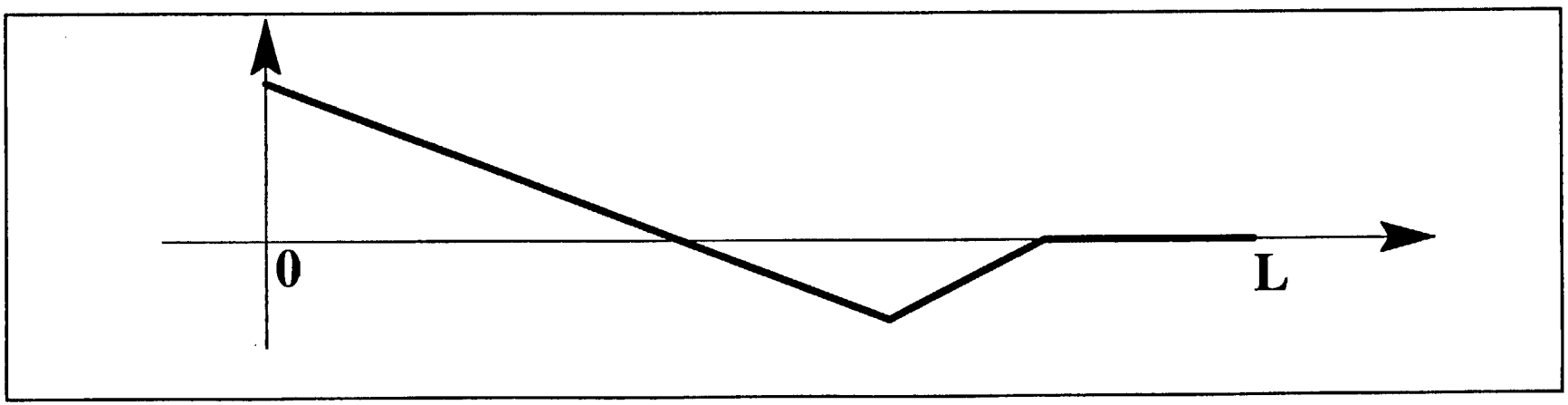

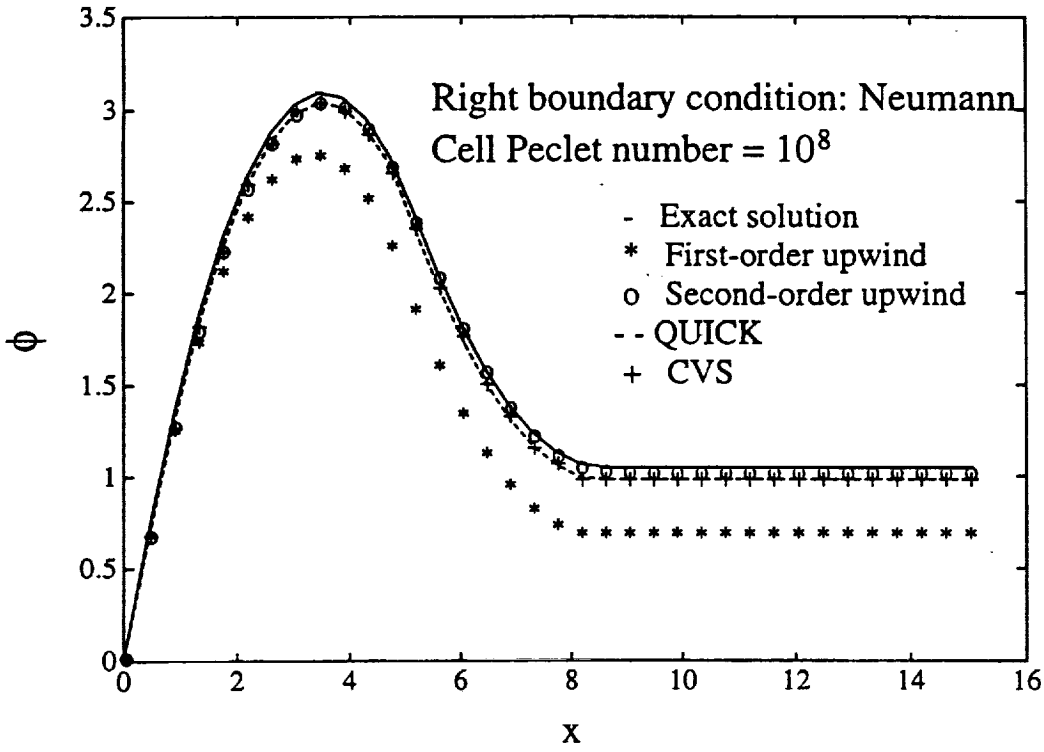

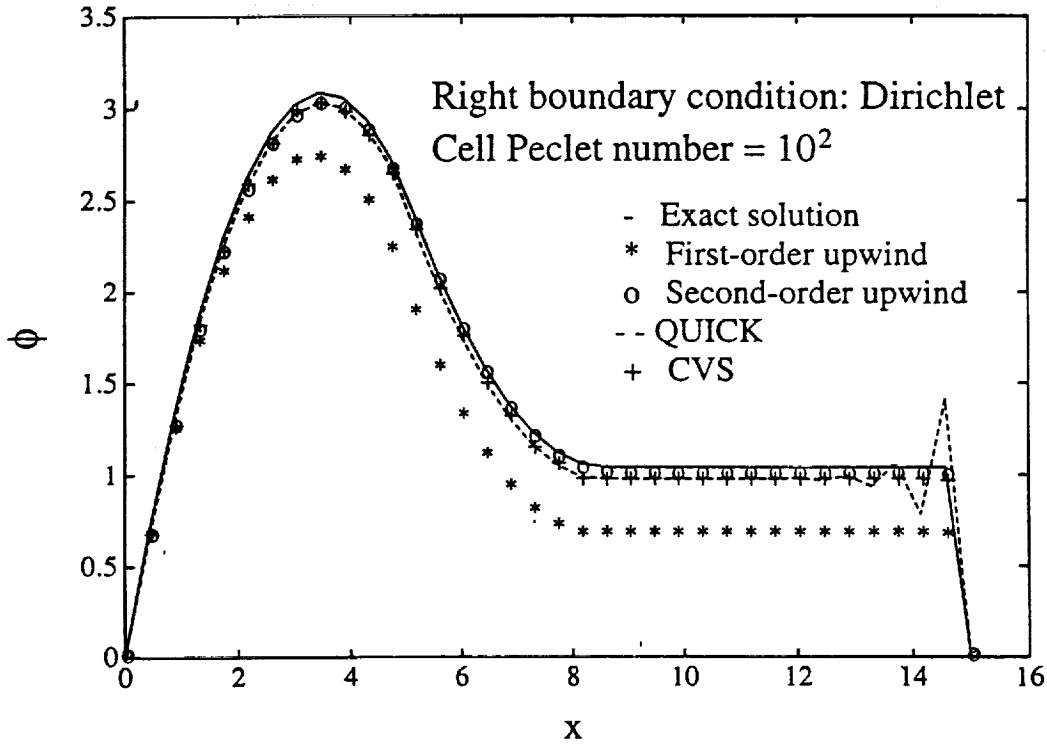

Model Problem II: Different Schemes

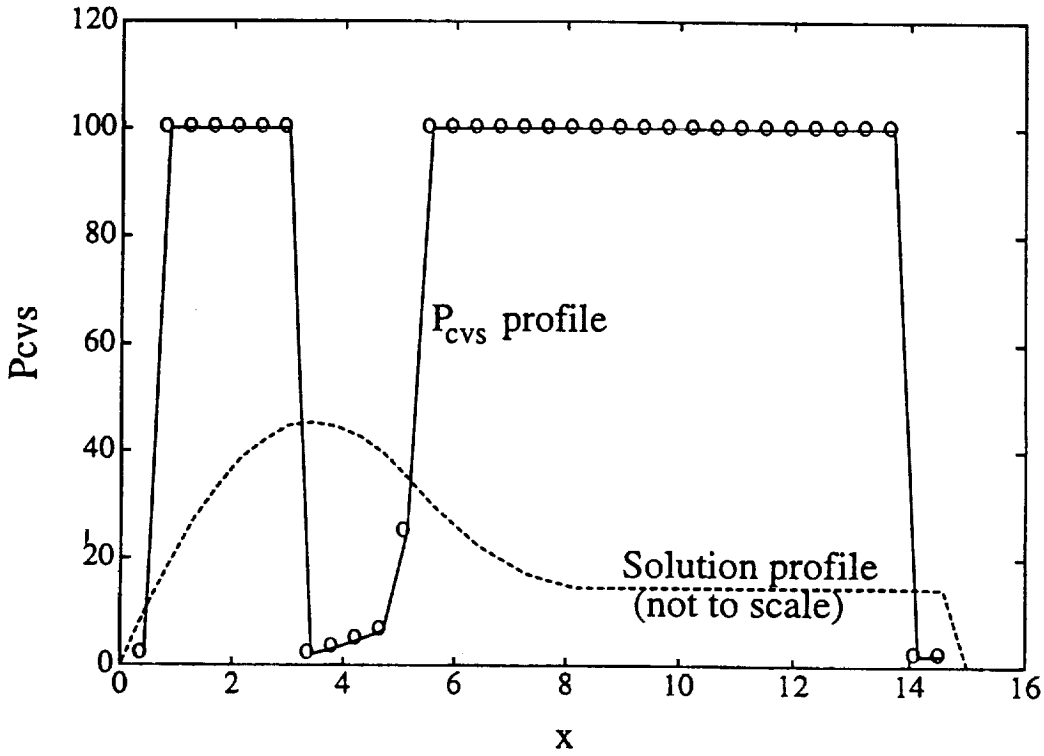

Model Problem II: Dirichlet B.C., P=100
Effective Cell Peclet Number

i	x	P_{cvs}
2	0.42	1.96
9	3.42	1.96
10	3.85	3.15
11	4.28	4.66
12	4.71	6.32
13	5.14	24.85
34	14.14	1.97
35	14.57	1.96
Remaining i	Remaining x	100.00

Treatment of Source Terms

- Using TVD Type Sequential Solver
- Special Techniques :
  MacCormack's Predictor–Corrector
  Strang's Operator–Splitting
- 1–D Longitudinal Combustion Instability Problem

TREATMENT OF SOURCE TERMS: A LONGITUDINAL COMBUSTION INSTABILITY PROBLEM

Besides convection terms, source terms (if present) in the Navier–Stokes equations can be strong enough to cause numerical difficulties such as a loss of accuracy in the form of spurious oscillations in the solution profiles or numerical instability. This is so because strong source terms can be sufficiently stiff and the time and length scales imposed by them may not be commensurate with those imposed by convection, for example. Thus, due attention has to be paid to the source terms and not just to the convection terms.

A one–dimensional longitudinal combustion instability problem is chosen which has a strong heat release source term. The high accuracy TVD type of convection treatment in a sequential solver (second fig. clockwise: top right) is seen to provide higher accuracy than the first–order upwind scheme (first figure: top left), as evident from the amplitudes of the ten pressure modeshapes shown in the viewgraph. However, the TVD type of convection treatment without any special source term treatment yields spurious oscillations in modehapes numbered 5, 6 and 7 (second figure clockwise). From the corresponding heat release modeshapes (third fig. clockwise), it is clear that modes 5, 6 and 7 are the modes of maximum heat release, thus demonstrating that when source terms become stiff enough they may lead to spurious oscillations. This can be resolved by increasing the amount of numerical dissipation in the scheme (by varying δ) but this is accompanied by an overall smearing of solution profiles. However, special source term treatment such as MacCormack's predictor–corrector method or Strang's time–splitting method (here, the latter) can resolve the problem by suppressing any spurious oscillations without the need of any extra numerical damping. This is clearly evident from the bottom left plot (fourth fig. clockwise).

Special Source Term Treatment

- Conservation law with a source term

$$w_t + f(w)_x = \psi(w)$$

- **Treatment**

a) MacCormack's Predictor-Corrector Method

b) Operator Splitting (Strang's Time-Splitting)

$$W^{n+1} = S_\psi(\Delta t/2)\ S_f(\Delta t)\ S_\psi(\Delta t/2)\ W^n$$

where S_f represents the numerical solution operator for

$$w_t + f(w)_x = 0$$

and S_ψ is the numerical solution operator for the ODE

$$w_t = \psi(w)$$

1–D Combusting Flow in a Duct

- To illustrate the effect of a strong source term (heat release) on numerical accurcay
- To demonstrate the efficacy of special source term treatment for a strong source term

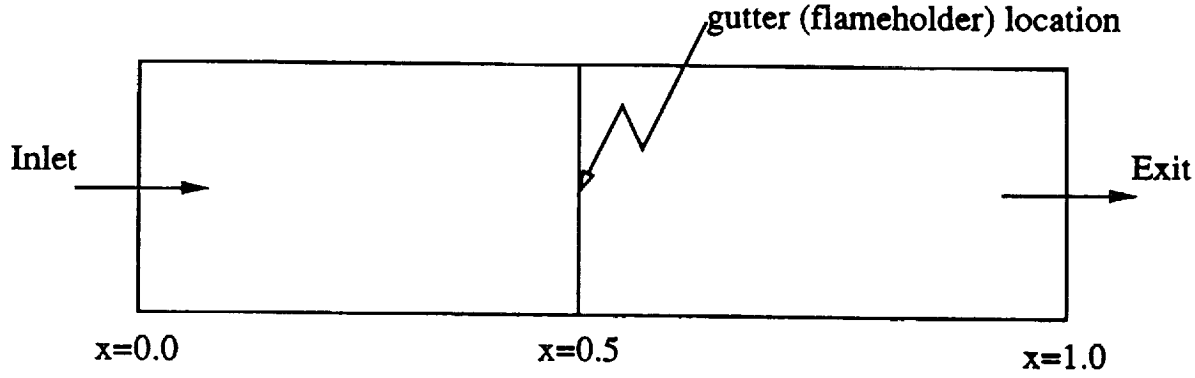

Basic Equations

$$\frac{\partial \rho}{\partial t} + \frac{\partial (\rho u)}{\partial x} = 0$$

$$\frac{\partial m}{\partial t} + \frac{\partial (mu)}{\partial x} = -\frac{\partial p}{\partial x} + \frac{1}{Re_\infty}\frac{\partial \tau_{11}}{\partial x}$$

$$\frac{\partial E}{\partial t} + \frac{\partial (Eu)}{\partial x} = -\frac{\partial (pu)}{\partial x} + \frac{1}{Re_\infty}\left[\frac{1}{Pr_\infty}\frac{\partial}{\partial x}\left(\frac{\partial h}{\partial x}\right) + \frac{\partial}{\partial x}(u\tau_{11})\right] + Q(x,t)$$

Combustion Instability Problem : Mode Shapes

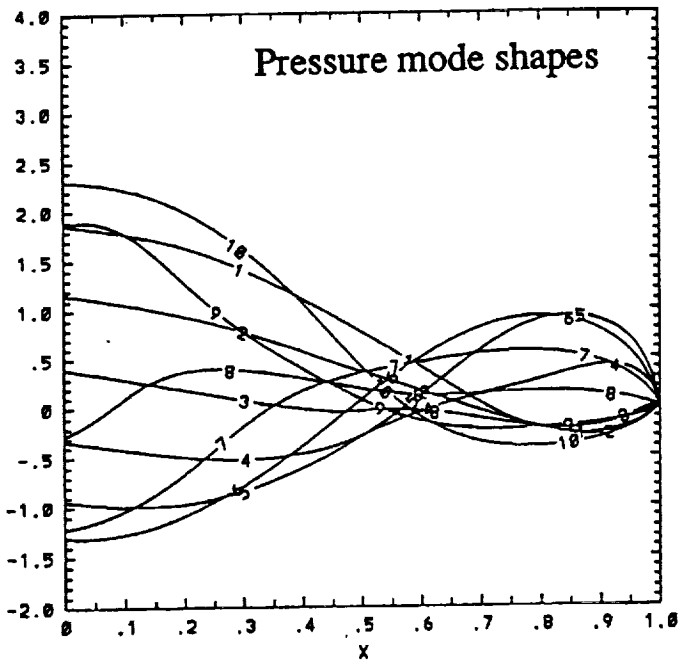

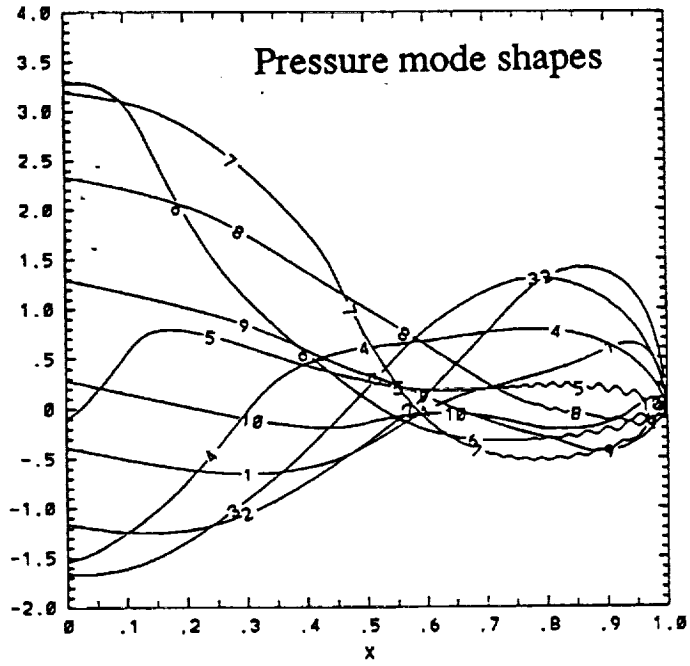

First-Order Upwind Scheme

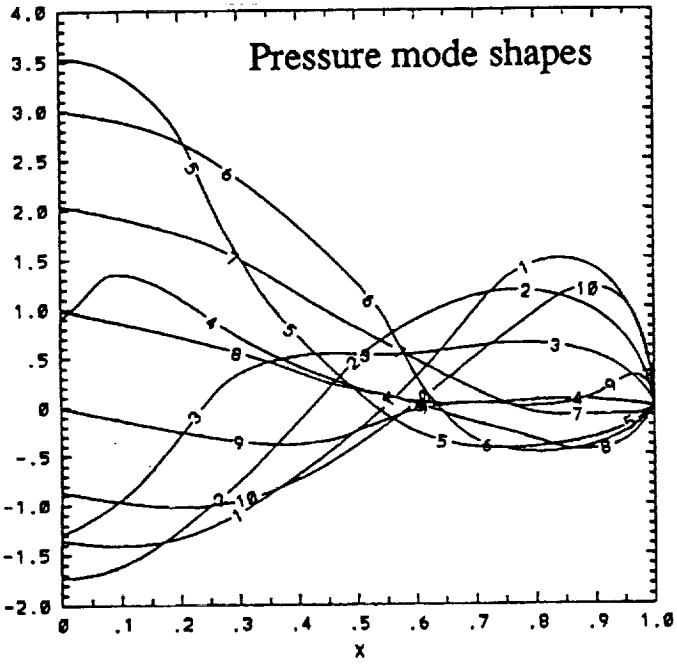

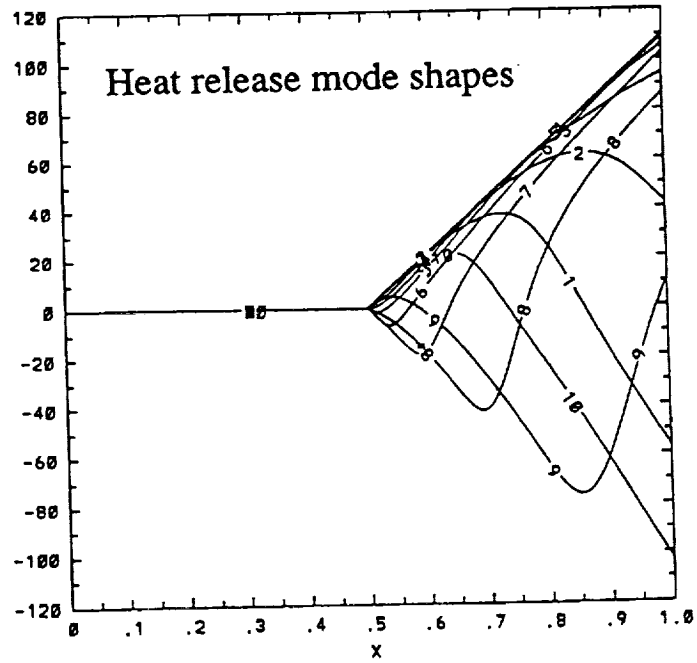

TVD Scheme; Source Treatment

$\delta = 0$

TVD Scheme; No Source Treatment

$\delta = 0$

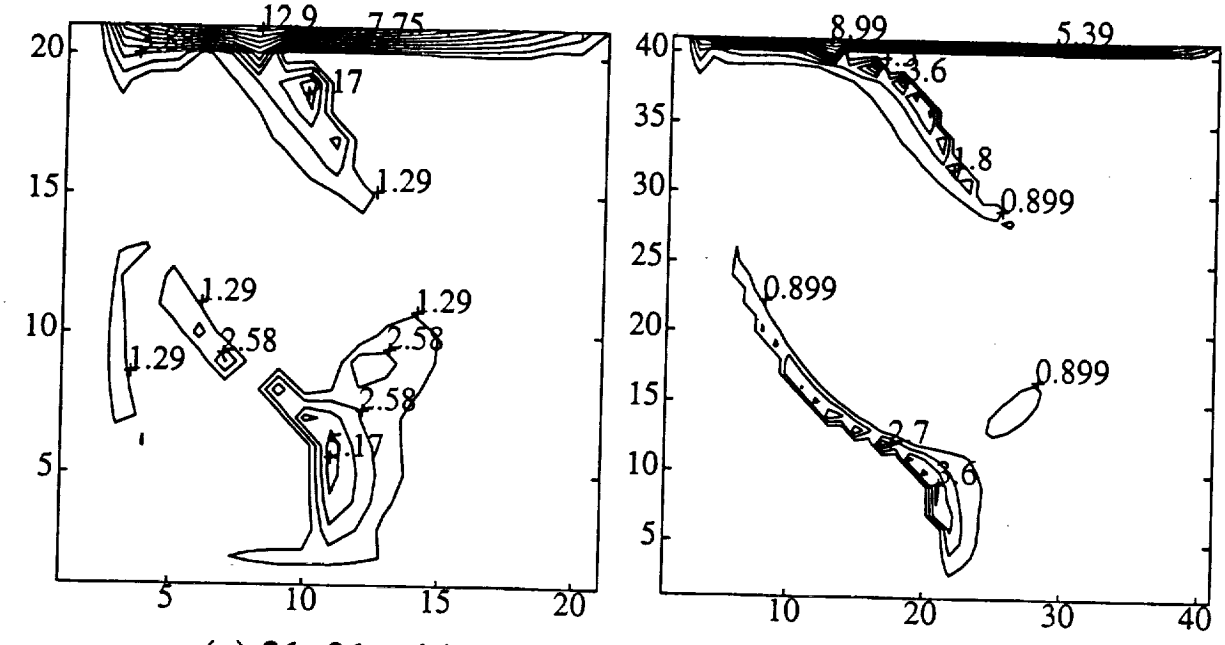

(a) 21x21 grid

(b) 41x41 grid

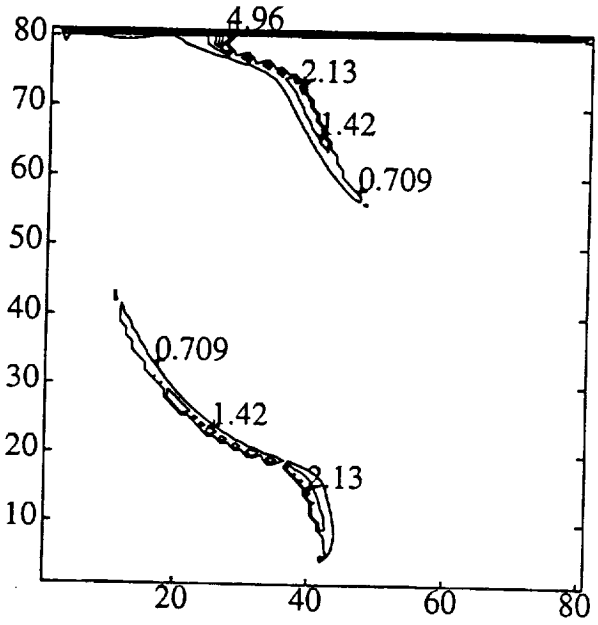

(c) 81x81 grid

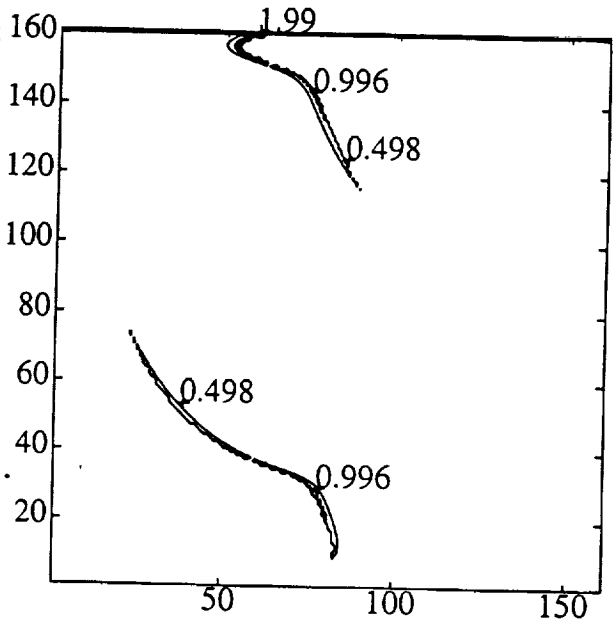

(d) 161x161 grid

Normalized Viscosity (Q* - G*)

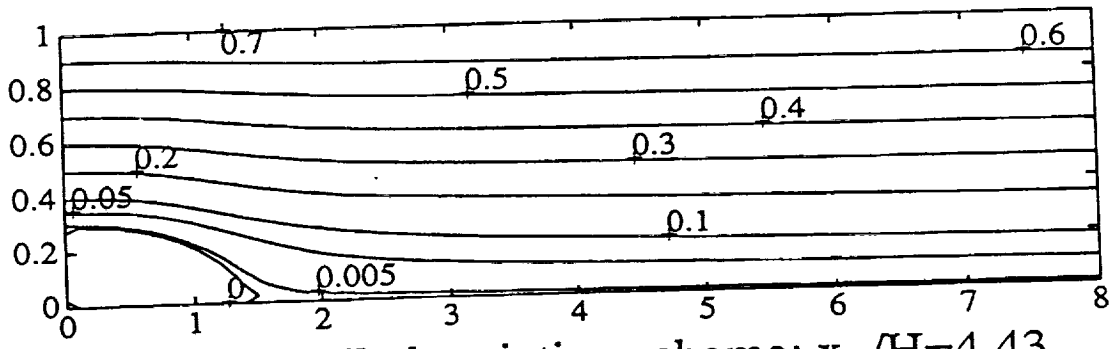

(d) Controlled variation scheme; $x_R/H=4.43$

Streamfunction: Backward-Step, Turbulent Flow

Re = 132,000

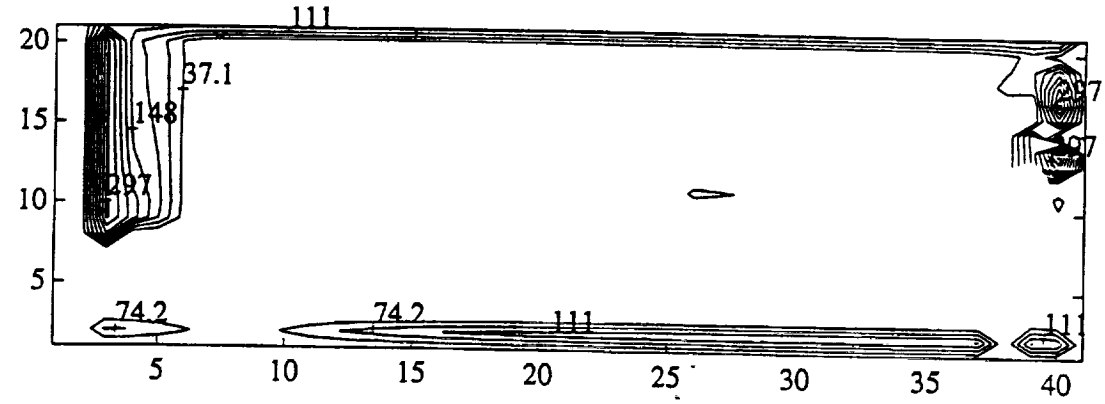

(a) 41x21 Grid

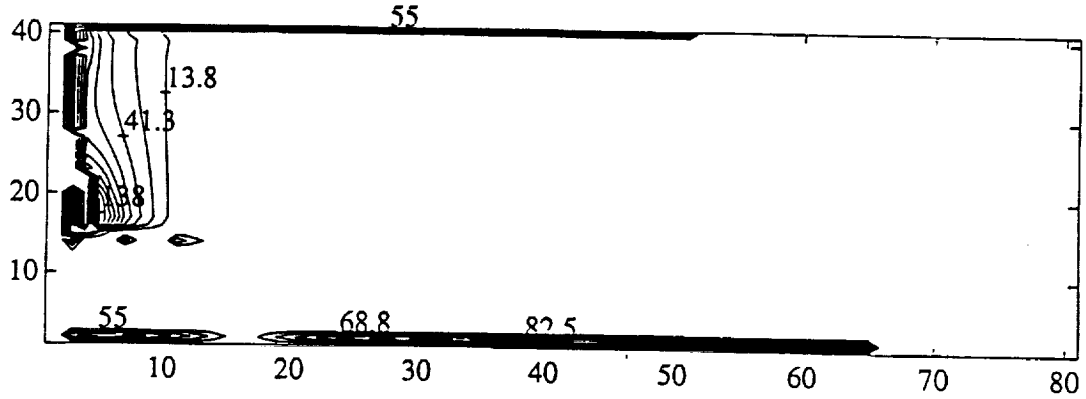

(b) 81x41 Grid

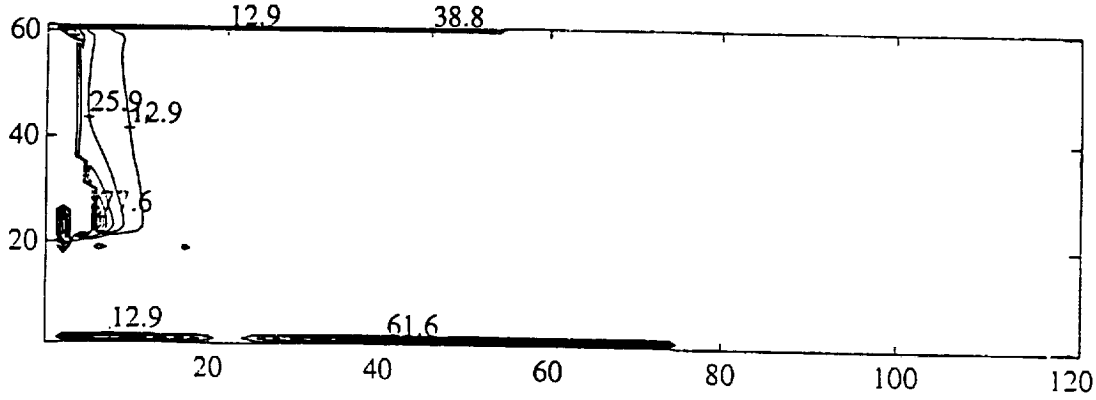

(c) 121x61 Grid

Q*-G* on Various Grids

CVS: Conclusions

- TVD Schemes can be Effectively Extended to Sequential Solvers
- CVS Effective for High Cell Peclet Number (Convection–Dominated) Recirculating Flows
- Mechanism → Reduces Effective Local Cell Peclet Number Via Controlled Numerical Dissipation
- Numerical Dissipation Decreases Monotonically With Grid Refinement
- CVS Truly Useful When Central Difference Fails, e.g., Turbulent Flows → Enforces Physical Realizability

REPORT DOCUMENTATION PAGE

Form Approved
OMB No. 0704-0188

1. AGENCY USE ONLY *(Leave blank)*	2. REPORT DATE	3. REPORT TYPE AND DATES COVERED
	July 1993	Conference Publication

4. TITLE AND SUBTITLE

Eleventh Workshop for Computational Fluid Dynamic Applications in Rocket Propulsion—Part II

5. FUNDING NUMBERS

6. AUTHOR(S)

R.W. Williams, Compiler

7. PERFORMING ORGANIZATION NAME(S) AND ADDRESS(ES)

George C. Marshall Space Flight Center
Marshall Space Flight Center, Alabama 35812

8. PERFORMING ORGANIZATION REPORT NUMBER

M-726

9. SPONSORING/MONITORING AGENCY NAME(S) AND ADDRESS(ES)

National Aeronautics and Space Administration
Washington, DC 20546

10. SPONSORING/MONITORING AGENCY REPORT NUMBER

NASA CP-3221

11. SUPPLEMENTARY NOTES

Prepared by Structures and Dynamics Laboratory, Science and Engineering Directorate.

12a. DISTRIBUTION/AVAILABILITY STATEMENT

Subject Category: 34
Unclassified—Unlimited

12b. DISTRIBUTION CODE

13. ABSTRACT *(Maximum 200 words)*

Conference publication includes 79 abstracts and presentations and 3 invited presentations given at the Eleventh Workshop for Computational Fluid Dynamic Applications in Rocket Propulsion held at George C. Marshall Space Flight Center, April 20–22, 1993. The purpose of the workshop is to discuss experimental and computational fluid dynamic activities in rocket propulsion. The workshop is an open meeting for government, industry, and academia. A broad number of topics are discussed including computational fluid dynamic methodology, liquid and solid rocket propulsion, turbomachinery, combustion, heat transfer, and grid generation.

14. SUBJECT TERMS spray, injector, computational fluid dynamics, rocket propulsion, liquid rocket, solid rocket, turbopump, turbomachinery, combustion, methodology, impeller, inducer, heat transfer, grid generation, nozzle, plume

15. NUMBER OF PAGES 955

16. PRICE CODE A99

17. SECURITY CLASSIFICATION OF REPORT	18. SECURITY CLASSIFICATION OF THIS PAGE	19. SECURITY CLASSIFICATION OF ABSTRACT	20. LIMITATION OF ABSTRACT
Unclassified	Unclassified	Unclassified	Unlimited